The McGraw·Hill Companies

3rd Edition

Control Systems

Principles and Design

About the Author

M Gopal is presently **Professor**, Department of Electrical Engineering, Indian Institute of Technology, Delhi. His teaching and research stints span over three decades at prestigious institutes.

Dr Gopal is the author/co-author of six books. His Video Course on Control Engineering is being transmitted periodically through *EKLAVYA Technology Channel* of the IITs. He is author of an interactive web compatible multimedia course on Control Engineering, available on the site: nptel@iitm.ac.in

Dr Gopal has a large number of research publications to his credit. His currentresearch interests are in the areas of **Machine Learning, Soft-Computing Technologies,** and **Intelligent Control.**

The McGraw-Hill Companies

Control Systems

Principles and Design

Third Edition

M Gopal

Professor
Department of Electrical Engineering
Indian Institute of Technology
New Delhi

Tata McGraw-Hill Publishing Company Limited
NEW DELHI

McGraw-Hill Offices

New Delhi New York St Louis San Francisco Auckland Bogotá Caracas
Kuala Lumpur Lisbon London Madrid Mexico City Milan Montreal
San Juan Santiago Singapore Sydney Tokyo Toronto

The McGraw-Hill Companies

Tata McGraw-Hill

Published by Tata McGraw-Hill Publishing Company Limited,
7 West Patel Nagar, New Delhi 110 008.

This edition can be exported from India only by the publishers,
Tata McGraw-Hill Publishing Company Limited.

ISBN (13 digits): 978-0-07-066879-9
ISBN (10 digits): 0-07-066879-5

Managing Director: *Ajay Shukla*

General Manager: Publishing—SEM & Tech Ed: *Vibha Mahajan*
Sponsoring Editor: *Shukti Mukherjee*
Editorial Executive: *Suman Sen*
Executive—Editorial Services: *Sohini Mukherjee*
Senior Production Manager: *P L Pandita*

General Manager: Marketing—Higher Education & School: *Michael J. Cruz*
Product Manager: SEM & Tech Ed: *Biju Ganesan*

Controller—Production: *Rajender P Ghansela*
Asst. General Manager—Production: *B L Dogra*

Typeset at Script Makers, 19, A1-B, DDA Market, Paschim Vihar, New Delhi 110 063, and printed at Rashtriya Printer, M-135, Panchsheel Garden, Naveen Shahdara, Delhi 110032.

Cover: Rashtriya

DQXACRCXDDCXR

The McGraw-Hill Companies

To
my

Lakshmi

Contents

Preface to the Third Edition

This text provides an integrated treatment of all those aspects of control systems engineering that prepare the student for early productivity upon entering industrial practice. Important aspects of the subject that help realize this objective are:

- Knowledge of the basic control configurations that have been devised, and the characteristic performance features of each. This helps one in initially selecting one or more alternative configurations that have a potential for success.
- Knowledge of the tools of 'control system design toolbox' comprising time-tested design procedures; a particular application needs intelligent selection of tools from this box.
- Familiarity with available hardware so that commercially available components to implement the design can be selected.
- Competence in modelling of physical systems using judicious assumptions.

This text attempts to provide a detailed description of basic control configurations since this storehouse is what one draws on when conceiving a design for a new application. The vast majority of practical systems are designed in this way rather than by some mathematical synthesis procedure. The list of topics includes fundamental control modes: proportional, integral, derivative; and specialized control schemes: cascade control, minor-loop feedback control, state variable feedback.

The 'control system design toolbox' comprises a collection of results based on the so-called 'classical' and 'modern' control concepts. The *classical control theory* is characterized by frequency-domain methods developed during the period of about twenty years—from the early 1940s through the early 1960s. This theory is still going strong; it provides an efficient framework for the design of feedback controls in all areas of applications, though the term 'classical control' appears to suggest that it is out of date. In fact classical design methods have been greatly enhanced by the availability of low-cost computers for system analysis and simulation. The graphical tools of classical design can now be more easily used with computer graphics and the effects of nonlinearities and model approximations evaluated by computer simulation. The classical control theory today provides useful design tools in the hands of practising control engineers.

The *modern control theory* (which is not so modern any longer) refers to a collection of state-space based methods developed in the late 1950s and early 1960s, which deals with matrix methods, eigen analysis, and applications of optimization methods. Modern control methods initially enjoyed a great deal of success in academic circles, but they did not perform very well in many areas of application. Modern control, however, provided a lot of insight into system structure and properties. Today, one does not need to make a choice: both the classical control methods and modern control methods are useful and complement each other. In

this text, major emphasis is on frequency-domain design methods based on transfer function representation of systems. A modest investment has been made on state-space methods based on differential equation representations of systems. A conscious and persistent effort has been made to relate these topics to their proper role in the larger scene of engineering design.

The practice of using digital hardware for controller implementation has been widely accepted. However, it does not mean that control theory and practice is now concerned with sampled-data system theory, microcomputer programming and electronic design of interface hardware. Digital control, in fact, contributes relatively few basic control concepts of its own to the control system design toolbox. The vast majority of digital systems in operation today are implementing well-known design principles, conceived before digital computers were used in control system practice. Most of these principles were actually used in analog systems. In this book, a modest investment in digital methods has been made so that the control engineer can work well in the increasingly digital environment.

Real-life control engineering practice requires extensive knowledge in instrumentation and process dynamics in addition to the knowledge in control systems design. The process dynamics which may vary greatly from one process to another, can only be effectively mastered during practice; the coverage to the topic in this textbook is limited to basic principles for modelling simple mechanical, electrical, fluid, and thermal systems. In-depth coverage of instrumentation is also not possible in a control text. Nevertheless, an exposure to commercially available hardware is important. In this book, innumerable realistic (but simple) application examples are included to develop familiarity with available hardware.

Many known and unknown uncertainties are involved in development of models for designing linear control systems. If the design performs well for substantial variations in the dynamics of the plant from that used in design, we say the design is robust. *Robust-control design methods* consider the robustness requirement as the primary aim of design. Quantitatively specified relations between the amount of uncertainties and the properties to be attained dominate the design process.

Control design methods developed in this book presuppose that sufficiently accurate model of the process to be controlled is available; meeting the specifications on steady-state accuracy, transient-response characteristics, and disturbance rejection is the primary aim of design. In these design methods, the treatment of model uncertainties appears only qualitatively through simulation of the closed-loop system. This limitation of our presentation will, however, not severely limit the applications of these methods. In fact, the design of most industrial control systems is based on the methods presented here, wherein we cash on the feedback property that all feedback-control designs are robust to certain extent because feedback reduces sensitivity of the closed-loop system with respect to uncertainties in the plant model on which the design is based. Building of uncertainty model (*i.e.*, quantifying uncertainties) itself is subject to uncertainties; the industry, by and large, continue to rely on the conventional linear control design methods.

With the desire to use linear control design methods (general methods for nonlinear systems do not exist), we neglect some of the *nonlinearities.* Investigation of the effects of this approximation on the performance of the system is a part of the design cycle. In general, simulation of the closed-loop system with nonlinearities included in the loop, is the only tool in our 'control system design toolbox'. However, for specific classes of nonlinear systems, some classical methods of analysis are available. These analysis methods help improve the design of the closed-loop system. The subject of nonlinear systems analysis has been given reasonable space in this book.

A modern development that is significant to practical design is the wide availability and low cost of Computer-Aided-Design (CAD) software. Attempts have been made to integrate learning of control system analysis and design with learning of how to compute the answers with MATLAB—the most widely used CAD software package in universities. Some instructors believe that to use CAD software packages effectively, the student must first understand the basics of the method being used so that the results from the

computer can be evaluated and checked for reasonableness by independent analysis. They feel that it is mandatory that the student retain the ability to compute simple answers by hand. Instructors, who believe in preparing the student for industrial practice at an early stage, ignore the hand-computation grill and encourage the use of CAD software package right from day 1 of the course delivery. They feel that need-based self-learning is an on-going process in industrial practice.

Whatever be the mechanism of integration, the requirement of supplementing learning of automatic control theory with the learning of a suitable CAD software package is not in dispute. We have given MATLAB and Simulink support in such a way that the main flow of the text is not MATLAB based. This will hopefully make the book useful for both the modes of course delivery; emphasis on hand-computation or emphasis on MATLAB computation.

A CORE COURSE ON CONTROL SYSTEMS

For students with no background in control, the first ten chapters present a thorough treatment of continuous-time systems, beginning with an introduction to Laplace transform, and ending with in-depth account of frequency-domain design methods. This, in fact, is the core of 'essentials' for industrial practice. This coverage could form a one-semester course on control systems.

However some flexibility must be in-built in a teaching package, to enable the instructor to tune the course material as per the specific background and needs of the students. Different useful course configurations will emerge when tuning is done as per the following guidelines:

- Most first-course students will have some background in dynamics and Laplace transforms. Therefore, the corresponding course contents may be covered as a review.
- Coverage of industrial control devices has always been a difficult issue under the constraint of available time for course delivery. Covering only motors and position/speed control systems will not convey the full power of control theory. Both the motion control and process control systems should be covered (The time-constants in a process control loop are generally much higher than those in a motion control loop). To realize this objective, the minimum input on control hardware includes: potentiometers, dc servomotors, dc tachogenerator; pneumatic control valves, and electropneumatic transducer. To present additional examples of closed-loop control, some or all of the devices: synchros, LVDT, ac servomotors, ac tachogenerator, hydraulic actuators, eletrohydraulic servo valves; should be covered.

  With a desire to cover a wide range of applications, some authors show pictures of feedback control systems and then directly give block diagram description with models; without giving details of development of models. This 'black box' approach is not helpful in preparing the student for industrial practice. This book follows 'grey box' approach wherein details of development of models of devices used in feedback loops are given. With the knowledge of the approximations made in models used to design a controller, the robustness properties of the final design can be studied.

  The criticism of the proposed approach could be that the students may not be able to keep the perspective as they plow through detailed description of lot of devices. Based on the background of the students, a judicious selection by the instructor will make the course delivery effective.
- The options include dropping of signal flow graph analysis without loss of continuity (CAD software available today (Simulink, for example) provides powerful tools for analysis without the need for block diagram reduction), and leaving controller tuning as a self-reading exercise for the students.
- We recognize that robustness properties are better preserved for design carried out in frequency domain; therefore frequency-domain design should be given more space, with root-locus plots helping the analysis of this design.

- The design of PI/PD/PID controller is a simpler search problem with 2 to 3 trial parameters. The filtering and other signal conditioning may be independently designed. The lag/lead/lag-lead compensator design involves 3 to 5 parameters. The student should be exposed to the total parametric search problem. Again, a careful selection may be made by the instructor so that perspective of the student is not lost.
- Recognition of the fact that increasingly controllers are implemented using op amps and embedded computers, leads to deletion of passive circuits from the course profile; the emphasis should be on op amps/computers. A modest investment in digital control (Sections 11.1-11.6 of the book), without using the *z*-transforms, will serve this objective well.

ELECTIVE COURSE ON CONTROL SYSTEMS

It is not realistic to try to cover the entire book in one semester. There are, however, two 'one-semester books' within the book. While chapters 1–10 give the material for the core course on control systems, chapters 11–14 provide a reasonable coverage of advanced control system analysis and design techniques: digital control systems, state variable methods for control system analysis and design, nonlinear systems analysis. The subject matter can't be given a comprehensive treatment in the available space, but the emphasis is clearly outlined and logically linked to the rest of the book. These chapters form a supplement to the presentation in earlier chapters, and could form a one-semester elective course on control systems. Though the core course provides the essentials of control systems engineering for industrial practice, the elective will bring the student at a higher knowledge platform; more effective and productive for industrial practice.

WEBSITE URL

The book includes a wealth of supplements available in the dedicated website:
http://www.mhhe.com/gopal/cs3e
It includes:

For Students

- Source codes of the MATLAB problems given in Appendix A, and a set of 164 multiple-choice questions on control theory for self-appraisal;

For Instructors

- Provides the faculty with the Solution Manual for the exercise problems given at the end of all chapters in the book. The instructor part of the website is password protected and will be available to the instructors who adopt this text.
  This request can be sent to the local sales representative.

M. GOPAL
mgopal@ee.iitd.ac.in

Preface to the First Edition

This text provides an integrated treatment of all those aspects of control systems engineering that prepare the student for early productivity upon entering industrial practice. Important aspects of the subject that help realise this objective are:

(a) Knowledge of the basic control configurations that have been devised and the characteristic performance features of each. This helps one in initially selecting one or more alternative configurations that have potential for success.
(b) Knowledge of the tools of 'control system design tool box' comprising time-tested design procedures; a particular application needs intelligent selection of tools from this box.
(c) Familiarity with available hardware so that commercially available components to implement the design can be selected.
(d) Competence in modelling of physical systems using judicious assumptions.

This text attempts to provide detailed description of basic control configurations since this storehouse is what one draws on when conceiving a design for a new application. The vast majority of practical systems are designed in this way rather than by some mathematical synthesis procedure. The list of topics includes fundamental control modes: on-off, proportional, integral, derivative, phase-lead, phase-lag; and specialised control schemes: command and disturbance feedforward, cascade control, state-variable feedback.

The 'control system design tool box' comprises extensive collection of results based on the so-called 'classical' and 'modern' control concepts. The *classical control theory* is characterised by frequency-domain methods developed during the period of about twenty years—from the early 1940s through the early 1960s. It has a large body of use-tested knowledge covering linear, nonlinear and sampled-data systems. This theory is still going strong; it provides an efficient framework for the design of feedback controls in all areas of applications, though the term 'classical control' appears to suggest that it is out-of-date. In fact classical design methods have been greatly enhanced by the availability of low-cost computers for system analysis and simulation. The graphical tools of classical design can now be more easily used with computer graphics and the effects of nonlinearities and model approximations evaluated by computer simulation. Coupled with hardware developments such as microprocessors and electro-optic measurement schemes, the classical control theory today provides useful design tools in the hands of practising control engineers.

The *modern control theory* (which is not so modern any longer) refers to a collection of state-space based methods developed in the late 1950s and early 1960s, which deals with matrix methods, eigen analysis, and applications of optimisation methods such as calculus of variations. Modern control methods initially enjoyed a great deal of success in academic circles, but they did not perform very well in many areas of

application. Modern control provided a lot of insight into system structure and properties, but it masked other important feedback properties that could be studied and manipulated using classical control. During the past two decades, a body of methods, which is a combination of modern state-space methods and classical frequency-domain methods, has emerged. These techniques are commonly known as *robust control.*

In this text, major emphasis is on frequency-domain design methods based on transfer function representation of systems. State-space based design methods (eigenstructure assignment, optimal control) and the advanced robust control methods are beyond the scope of the book. A conscious and persistent effort has, however, been made to relate these topics to their proper role in the larger scene of engineering design.

Compared to transfer functions, the response of state variable equations is easy to programme. For this reason, many computer-aided design packages use state-space and matrix notation, and therefore it is helpful for control engineers to be familiar with it. An adequate coverage of state variable representation, and its relationship with transfer function representation is within the scope of the book. This limited augmentation of the frequency-domain methods will also provide a smooth transition to the study of advanced control system design techniques.

The practice of using digital hardware for controller implementation has been widely accepted. However, it does not mean that control theory and practice is now concerned with sampled-data system theory, microcomputer programming and electronic design of interface hardware. Digital control, in fact, contributes relatively few basic control concepts of its own to the control system design tool box. The vast majority of digital systems in operation today are implementing well-known design principles, conceived before digital computers were used in control system practice. Most of these principles were actually used in analog systems. Digital control theory adds little to one's expertise in the initial conceptual phase of design. An introductory course in control systems engineering, therefore, must provide an adequate coverage of various analog methods of control system analysis and design. Investment in digital methods is also required so that the control engineer can work well in the increasingly digital environment. Depending upon the availability of curriculum space, the objective of preparing the student for practical control system design in industry may be realised through modest investment in digital methods in an introductory course or a substantial investment in a second course. This spirit has guided the preparation of this text.

Real-life control engineering practice requires extensive knowledge in instrumentation and process dynamics in addition to the knowledge in control systems design. The process dynamics which may vary greatly from one process to another, can only be effectively mastered during practice; the coverage to the topic in this textbook is limited to basic principles for modelling simple mechanical, electrical, fluid, and thermal systems. In-depth coverage of instrumentation physics is also not possible in a control text. This, however, is not a major problem as the required instrumentation knowledge can be readily acquired in practice from experienced engineers or through vendor courses. Nevertheless, an exposure to commercially available hardware is important. In this book, innumerable realistic (but simple) application examples are included to develop familiarity with available hardware.

A modern development that is singnificant to practical design is the wide availability and low cost of Computer-Aided-Design (CAD) software. Although a practical designer is handicapped without access to such tools, and students definitely benefit from their hands-on use, the text has been designed in such a way that personal access to CAD software facility is not essential. It is advisable to first create a firm knowledgebase of the fundamental results of feedback control theory withourt any diversion to other domains of learning; this knowledge can then be supplemented by CAD facility to solve practical design problems wherein it is desirable to vary several parameters during the design stage to investigate effect on the system performancee. Some problems for computer solution may be assigned to familiarise the students with CAD tools. This book offers computer-aided learning environment with any commercially available CAD software.

Acknowledgements

I would like to acknowledge the contributions of faculty and students across the country, whose suggestions through previous editions have made a positive impact on this new edition. I wish to acknowledge with thanks the considerable help and education I have received from my students and colleagues at Indian Institute of Technology, Delhi. Additional contribution made by the students M Arunkumar, CMC Krishnan, N N Apte, and E Hassan, in software development and other professional tasks needed to give shape to the final product, deserves sincere appreciation.

I also express my appreciation to the following reviewers who offered valuable suggestions for this third edition. The prepublication reviews have had a great impact on the revision project.

Anil Dixit	Bansal Institute of Science and Technology, Bhopal
J S Saini	DBCR University of Science and Technology, Sonepat
K K Gupta	Birla Institute of Technology and Science, Pilani
Hari Om Bansal	Birla Institute of Technology and Science, Pilani
Shahida Khatoon	Department of Electrical Engineering, Faculty of Engineering and Technology, Jamia Millia Islamia, New Delhi
M K Ghosh	Netaji Subash Engineering College, Kolkata
Sanjoy Mandal	Department of Electrical Engineering, College of Engineering and Management, East Midnapore, West Bengal
Sudipta Chakrabarty	Department of Electrical Engineering, BP Poddar Institute of Technology and Management, Kolkata
Anish Deb	Department of Applied Physics, University College of Science and Technology, Kolkata
D N Sonawane	Department of Instrumentation, COEP's Pune Institute of Engineering and Technology, Pune
Uma Maheswari	College of Engineering Guindy, Anna University, Chennai

Finally, I would like to thank The Tata McGraw-Hill Publishing Company, and its executives for providing professional support for this project through all phases of its development. Specifically, Vibha Mahajan, Suman Sen, Sohini Mukherjee and P L Pandita deserve due recognition for their contributions.

M. Gopal

The material in the book has been class-tested. The sequencing and internal organisation of various chapters is such that it permits flexibility of adaptation to the variations in students' prior training and curricula. A judicious selection of a set of case studies from innumerable application examples given in the book, makes the book comprehensible for all engineering disciplines that have control courses as part of their curricula. Practical flavour with careful and complete explanations makes the book appealing for self-study by practising engineers. The book should also serve as a guide for applying design techniques to industrial control problems.

There are twelve chapters in the book. Chapter 1 gives an overview of all the important application areas and all the basic categories of control systems. A brief account of major historical landmarks in the development of the fascinating area of control systems engineering is also given. The chapter concludes with an outline of scope and organisation of the book.

Chapters 2-11 are devoted to hardware familiarity, concepts of feedback control theory, and the frequency-domain tools of control system design. The material in these chapters forms the core of the introductory course in control engineering. Depending upon the curriculum time and plan of the follow-up courses, additional material from Chapter 12 may be used.

The familiarity with the theory of functions of a complex variable, the Fourier transforms, the Laplace transforms, and elementary matrix algebra is helpful but not necessary; these mathematical techniques are reviewed at appropriate places to the extent needed in the book.

Generous participation of instructors, students, and practising engineers to eliminate errors in the text and to refine the presentation, will be gratefully acknowledged.

M. GOPAL

1 Introduction to the Control Problem

1.1 CONTROL SYSTEMS: TERMINOLOGY AND BASIC STRUCTURE

In recent years, control systems have assumed an increasingly important role in the development and advancement of modern civilization and technology. Practically every aspect of our day-to-day activities is affected by some type of control system. A bathroom toilet tank is a control system. A home-heating system, a refrigerator, an air-conditioner, and an automobile are all control systems. Control systems are indispensable in modern industrial processes. We find control systems in all sectors of the industry, such as quality control of manufactured products, automatic assembly line, machine-tool control, space technology and weapon systems, transportation systems, power systems, robotics, and many others. Even such problems as inventory control, and socio-economic systems control, may be approached from the theory of feedback control. In this book we will deal with the control of *engineering systems* that are governed by the laws of physics and are therefore called *physical systems*.

In control parlance, the system to be controlled is given various names: *process*, *plant*, and *controlled system* being perhaps the most common. In the so-called process industries (chemicals, petroleum, steam power, fuel, etc.), one repeatedly encounters the need to control temperature, flow rate, liquid-level in vessels, pressure, humidity, chemical composition, and the like; such applications are generally considered *process control* applications. Historically, the wide practical application of control first took place in the process area. Most of the basic concepts were developed and brought to successful realization by the intuitive and experimentally-oriented engineering methods typical of the 1900 to 1940 era.

Around the time of the Second World War, the technical needs of military systems—automatic airplane pilots, gun-positioning systems, radar antenna control systems, and the like—led to more scientific approaches in the control engineering field. A comprehensive mathematical theory—the theory of *servomechanism*[1]—aimed mainly at applications wherein the need is to control mechanical motions (position, velocity, or acceleration), was developed around 1940 to 1950. Since this time, the design methods of the process-control area, and the servomechanism area have gradually converged. The terminology of the two areas is also converging. The word 'process' is now in use for all types of controlled systems. Also, irrespective of the area of application, the word 'servomechanism' (or *servo system*) is used for a *command following system* wherein the controlled attribute of the system is required to follow a given command.

[1]The word servomechanism originated from the words servant (or slave) and mechanism.

Figure 1.1 shows the input–output configuration of a process (or plant). Process *outputs* are the response variables which we require to behave in some specified fashion. Process *inputs* are flows of energy and/or material that cause the process to react or respond. The inputs are classified into *manipulated inputs* (subject to our control) and *disturbance inputs* (undesirable and unavoidable effects beyond our control, generated from outside process-environment, and from within). The presence of the disturbance is one of the main reasons of using the control. Clever management of manipulated variables so as to counteract the effects of disturbances is the primary role of the *controller*. Figure 1.2 shows the input–output configuration of a *control system*.

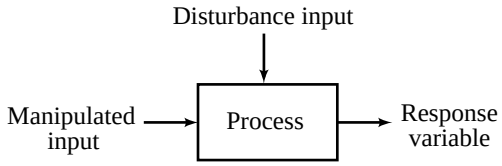

Fig. 1.1 Process input–output configuration

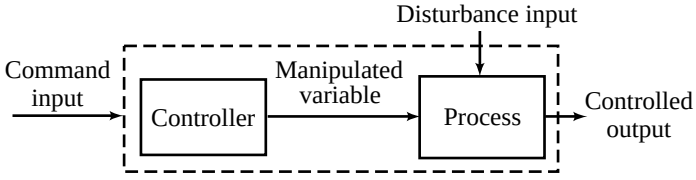

Fig. 1.2 Input–output configuration of a control system

When the desired value of the controlled output is more or less fixed and the main problem is to reject disturbance effects, the control system is sometimes called a *regulator*. The command input for a regulator becomes a constant and is called a *set-point*, which corresponds to the desired value of the controlled output. The set-point may however be changed in time from one constant value to another, and the need for the control of manipulated variables arises from the requirements of both the set-point changes and the disturbance rejection. The control problem is then called *resetting control problem*.

In the *follow-up* or *tracking system*, the controlled output is required to follow or track a time-varying command input. For such systems, the need for the control of manipulated variables arises from the requirements of command-following as well as disturbance rejection.

In the configuration of Fig. 1.3, the controller receives information about the desired value of the controlled output and uses this information as a means of control of the manipulated variables. In contrast to this configuration, the configuration of Fig. 1.4 utilizes measurement of the controlled output in order to compare the actual output with the desired output response. The controller then uses this difference as a means of control of manipulated variables. The configuration of Fig. 1.3 is that of an *open-loop control system* while that of Fig. 1.4 is that of a *closed-loop control system* or *feedback control system*.

To make these definitions more concrete, let us consider some familiar examples of control systems.

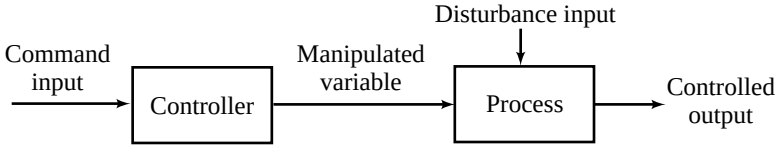

Fig. 1.3 Input–output configuration of an open-loop control system

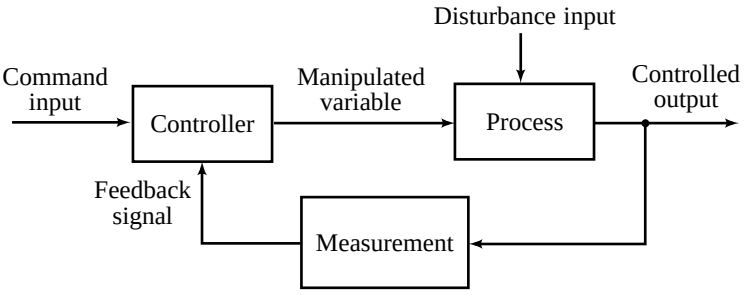

Fig. 1.4 Input–output configuration of a closed-loop control system

Example 1.1 Automobile Driving System

The system to be controlled has two inputs (steering and acceleration/braking) and two controlled outputs (heading and speed). The two command inputs are the direction of the highway and speed limits with traffic signals. A block diagram of this two-input, two-output system is shown in Fig. 1.5.

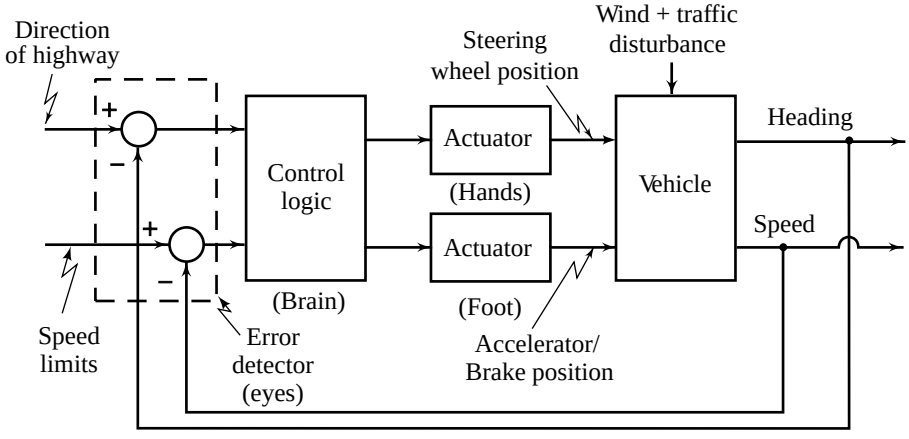

Fig. 1.5 Automobile driving control system

Systems with more than one controlled output and command input are called *multivariable* or *multi-input*, *multi-output* (MIMO) systems. On the other hand, in *single-input*, *single-output* (SISO) systems, a single output is controlled by a single input. In multivariable systems, an input that is meant to control a particular output also affects the other controlled outputs. This coupling is called *interaction*.

The automobile-driving system is a MIMO system. We can *decouple* this system into two SISO systems for the purpose of design because the interaction is negligible. Steering control affects the heading and not speed, and the accelerator control affects the speed and not the heading. However, braking of the vehicle for speed control decreases the side forces at the tyre-road interface for directional control, and with locked wheels the directional control is completely lost. If we consider this interaction negligible, we can consider the vehicle-heading control system as a decoupled SISO system, with no interaction with the vehicle-speed control system.

The command inputs for an automobile on the road cannot be constant set-points. These inputs depend on the traffic and road conditions and vary in an uncontrolled manner. The actual signal inputs to the system are derived by the driver from the actual road and traffic conditions. The human operator sub-system will therefore be a component in the overall control system of the automobile, as shown in Fig. 1.5. The desired course and speed are compared with a measurement of the actual course and speed in order to generate a measurement of the error. The human operator then controls the manipulated variables (steering wheel position, accelerator/brake position) in a manner (control logic) which reduces the absolute error.

Example 1.2 Residential Heating System

In this system, the indoor temperature is the response variable of interest, and it is affected by the main disturbance input—the outdoor temperature. In the scheme of Fig. 1.6, the desired temperature, which is the command-input temperature, is set on a calibrated dial. This positions the valve that admits the steam for circulation through the radiator. The valve dial is calibrated when the environment temperature has a certain value. When this value changes significantly, the controlled temperature will deviate from the desired value by a large error and hence precise control will not be realized. The open-loop scheme of Fig. 1.6 is used when performance requirements for heating of a residential building are not very stringent.

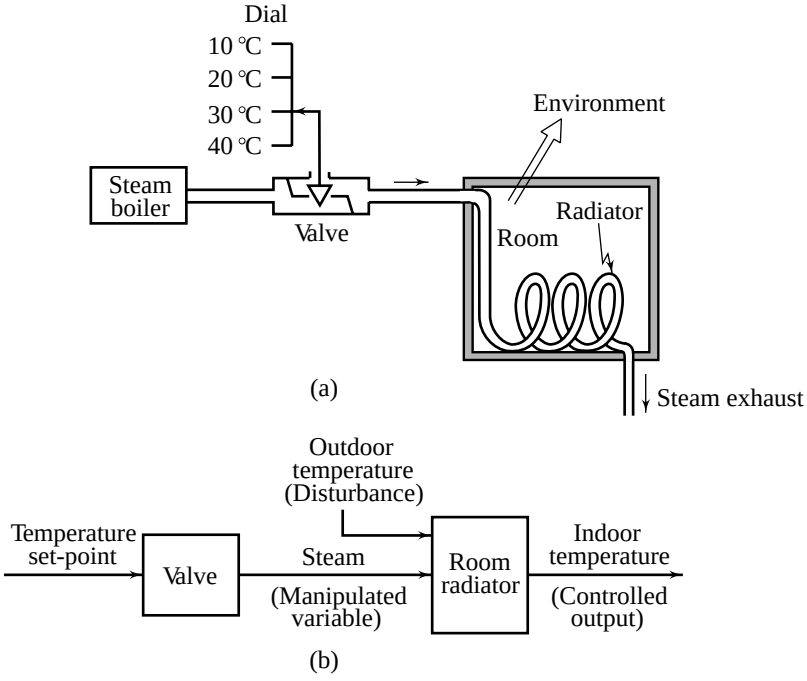

Fig. 1.6 Open-loop temperature control system

In an open-loop system, there is no automatic adjustment of any errors in output temperature that may occur. If there is any error, it must be spotted by the heating-system operator and then the required alteration must be done manually. In open-loop control, we must reset the controller input values or live with the consequences—overheated rooms, excessive use of energy, etc. The way to rectify this is to *inform* the controller on-line about what is going wrong. The sensor can detect the temperature level,

and this information can be passed electronically to the controller, which can then alter the input power setting. By doing this, we are *feeding back* information from the current situation to the temperature controller; we are *closing the loop*.

The open-loop control system of Fig. 1.6 can be converted to a closed-loop system by adding the functions of measurement of the controlled temperature, comparison of measured and desired values of the controlled temperature, and control logic to make changes in the heating rate when the desired and measured values differ.

Most residential heating (or cooling) systems utilize one form or another of the on–off control. For example, a thermostat with a bimetallic temperature-sensor and a snap-action switch to control a simple solenoid-actuated steam valve is often used for this purpose. In a thermostat, two materials with grossly different thermal expansion coefficients are bonded together. When heated, the different expansion rates cause the assembly curve shown in Fig. 1.7a. This effect is used to control the power supply to the solenoid (Fig. 1.7b). When the solenoid coil is energized, the plunger becomes magnetized and mutual attraction takes place between the coil and the plunger. If the force required by the load on the plunger does not exceed the force developed by the solenoid, the plunger will pull in. In the temperature control scheme of Fig. 1.7b, position 1 of the switch corresponds to the opening of the steam valve, and position 2 corresponds to the closing of the valve.

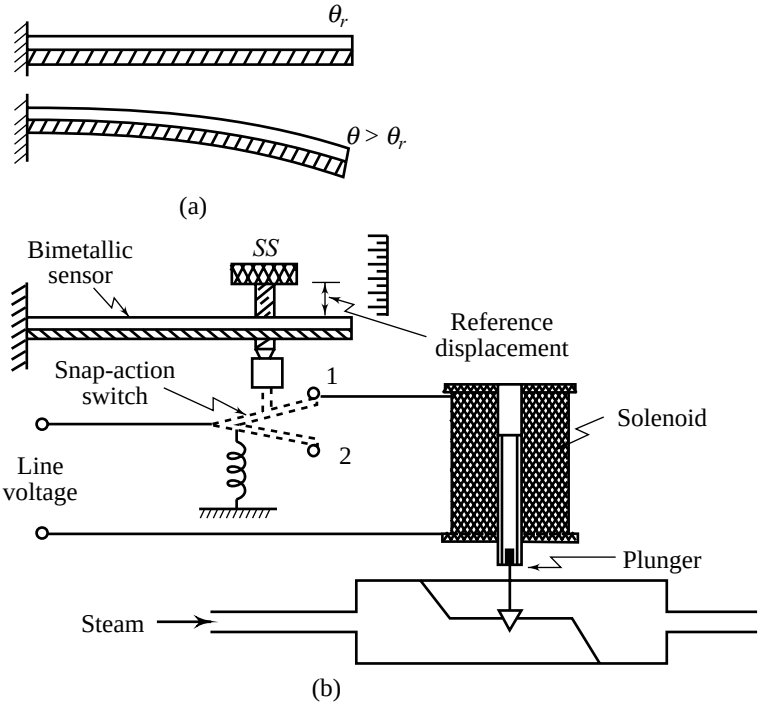

Fig. 1.7 Closed-loop temperature control system

The position of the set-screw *SS* (reference displacement) determines the desired temperature θ_r. The principle of operation of the temperature control system is that the actuator (solenoid + steam valve) is made to operate according to the sequence in which one of the two possible situations specified below has come about at a given time.

- *Situation* 1: The controlled variable θ assumes a value below the desired temperature θ_r, or in other words, the error $e = (\theta_r - \theta)$ is positive. In this situation, the snap-action switch is in position 1, the solenoid is in the energized state, and the steam valve is open. The controlled variable θ gradually increases (with the error e decreasing).
- *Situation* 2: The controlled variable θ assumes a value above the desired temperature θ_r, i.e., the error e is negative. In this situation, the bimetallic strip curls, the snap-action switch is thrown to position 2, the solenoid is de-energized, and the steam valve is closed. The controlled variable θ is gradually decreasing (the absolute error is also decreasing) due to the heat transfer from the room to colder surroundings.

Figure 1.8 shows the functional block diagram of the closed-loop temperature control system. Note that the control signal can assume only two values corresponding to the two states of the snap-action switch. The thermostat is serving as the sensing element as well as the controller—it performs the task of automatic reduction of the error to zero, irrespective of the situation created by the disturbance. Further study of the system will be taken up in Chapter 2.

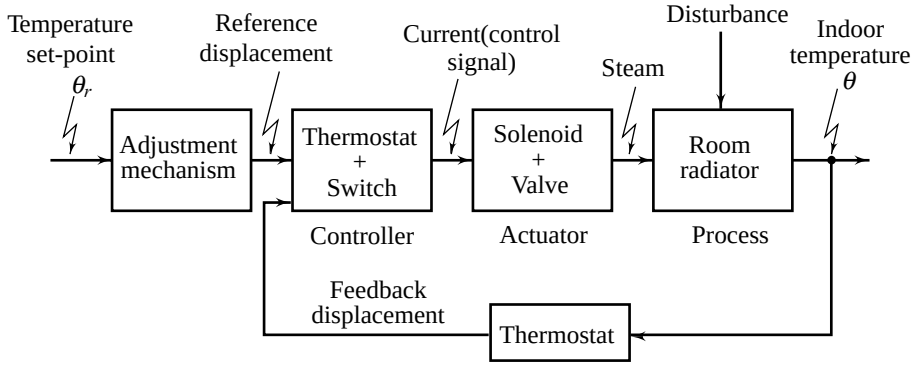

Fig. 1.8 Functional block diagram of the system of Fig. 1.7

Comparison of Figs 1.5 and 1.8 gives many common features of the two closed-loop systems. However, the two systems differ clearly in one aspect. In Fig. 1.5, both the feedback of the controlled outputs (actual course, and speed of travel) for comparison with command inputs (desired course, and speed of travel), and the control actions (rotation of steering wheel, and acceleration/braking) take place through the human operator. In Fig. 1.8, the human operator has been replaced by automatic error-detecting and correcting devices; both feedback of the controlled output (actual indoor temperature), and the correcting action (control of the valve position) take place without the need of a human operator. Such systems, therefore, are *automatic closed-loop control systems*. The systems with human operators included into the closed-loop are *man-machine control systems*.

Basic Structure of a Feedback Control System

The familiar examples of feedback control cited earlier, fit into the basic structure shown in Fig. 1.9.

To understand Fig. 1.9, we begin with the *command signal* y_r—the desired value of the *controlled variable* y. This signal has the same units as the controlled variable, but may or may not exist as an actual physical quantity. For example in the residential heating system of Fig. 1.8, y_r is the desired room temperature, but this is not an actual measurable temperature; it exists only 'mathematically' as the numbers printed on the thermostat dial. In fact, the actual physical input to the control system is a displacement of the

set-screw, which is *reference input r* for the residential heating system. The functional block of *reference input elements* represents conversion of the command signal to the reference input signal. The reference input element can, when necessary, perform a more sophisticated function such as noise filtering (y_r might be voltage signal contaminated by high-frequency noise).

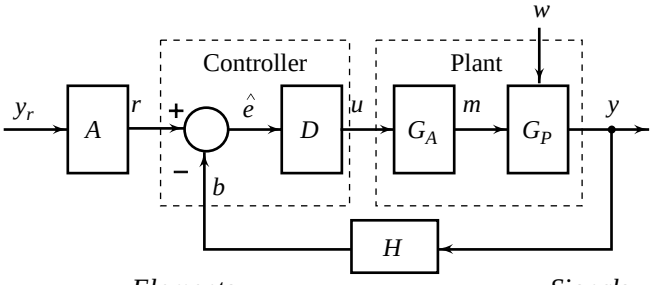

Elements

A	: Reference input elements	D	: Control logic elements
G_A	: Actuator elements (Final control elements)	G_P	: Controlled system elements
H	: Feedback elements		

Signals

b	: Feedback signal	y	: Controlled variable (output)
w	: Disturbance input	$\hat{e}$	: Actuating error signal
u	: Control signal	m	: Manipulated variable
r	: Reference input	y_r	: Command input

Fig. 1.9 Basic structure of a feedback control system

The *summing junction* is a symbol for the *error detector* which compares the reference input r with the *feedback signal* b and generates a signal $\hat{e} = (r - b)$. The *feedback elements block* is often a sensor for measuring y, but since its functions sometimes include more than simple measurement (e.g., noise filtering), the name *feedback element* rather than *sensing element* has been chosen. The signal $\hat{e}$ defines the *actuating error signal*, and not the *system error signal*, which is logically defined as $e = (y_r - y)$. Note that r, b and $\hat{e}$ always have exactly the same dimensions.

The *control logic elements block* produces the *control signal u* which has the knowledge about the desired control action. The *controller* is generally thought of as a system that compares the reference input with the feedback signal and is also responsible for a suitable control action. In general, the control signal is a function of the error signal, which in turn is a function of the command input y_r and controlled output y; the functional relationship may therefore be expressed as $u = f(y_r, y)$. The primary objective set for this book is to study this functional relationship.

The *actuator elements block* (*final control elements*) consists of devices that develop enough torque, pressure, heat, etc. (*manipulated variable m*), to influence the objects under control. Thus, the actuator elements are the 'muscle' of a control system while the control logic elements are the 'brain'.

Disturbance inputs w are the variables over which the designer has no control, and perhaps little information is available on their magnitude, functional form, or time of occurrence. The controlled variable y is influenced by both the manipulated variable m and disturbance w.

The structure shown in Fig. 1.9 defines the basic types of signals and components necessary for the description of any feedback control system; however, it must be adapted to the needs of each specific design. Alternative feedback structures will be introduced in Section 1.3.

1.2 THE GENESIS AND ESSENCE OF THE FEEDBACK CONTROL THEORY

From the simple and familiar examples of automatic control systems presented in Section 1.1, conclusions can be derived regarding the characteristics common to these systems, notwithstanding their manifestable heterogeneity. Automatic control systems share the following general features:

1. The principle of operation of the system uses the feedback idea, i.e., there exists a closed loop: error → manipulated variable → controlled variable → error.
2. The primary objective of the system is error self-nulling.

In all practical control systems, the objective of error self-nulling is required to be realized with a prescribed accuracy (steady-state errors, speed of response, etc.). A demand on accuracy, as we shall shortly see, may result in the loss of *stability*.[2] The reconciliation of the requirements of satisfactory accuracy and adequate stability margin is the principal accomplishment of the feedback control theory. Detailed quantitative study of the effects of feedback on control system performance will be taken up in Chapter 4. The objective of the brief qualitative study in this section is to introduce the basic principles of the feedback control theory.

A brief consideration of the origins of the feedback control theory will be in order here. Examples of feedback control systems have been identified dating back to the third century BC. Ktesibios, a Greek living in Alexandria, is credited with building a self-regulating flow device for use in water clocks. Several examples of feedback control systems appear in windmill designs used by the Dutch in the fifteenth century.

The arrival of the machine age was accompanied by a large increase in the number of control system designs. The development of the steam engine led to the requirement for a speed control device to maintain constant speed in the presence of changes in load torque or steam pressure. In 1788, James Watt of Glasgow developed his now famous flyball governor for this purpose. The principle of the flyball governor is still used for speed control applications.

Analytical tools for control problems were first developed by J. C. Maxwell in 1868. Maxwell utilized a linear differential equation approach and derived stability conditions for a third-order system. In 1876, Edward John Routh was able to determine the stability conditions for higher-order systems. A solution to the stability problem was also obtained by Adolf Hurwitz and reported in 1895. Routh and Hurwitz were unaware of each other's work. In 1911, equivalence of the Routh and Hurwitz criteria was established.

From 1900 to 1940, significant developments occurred in large-scale power generation, aeronautics, chemical industries, and electronics. The development of the vacuum-tube amplifier, in particular, resulted in many analytical techniques for the design of feedback systems.

One of the key problems in electronics, especially since its application to long-distance telephony, was to develop amplifiers with good gain stability. The difficulty stemmed from the considerable scattering of characteristics in the mass-produced electronic tubes and from changes in characteristics taking place in time (e.g., due to emission loss). In 1927, Harold S. Black discovered the negative feedback amplifier as a solution to this problem. Figure 1.10a shows the idea of operation. A potential-dividing resistor delivers a part of the amplifier's output voltage y to the amplifier's input, where it is subtracted from input voltage r. Figure 1.10b gives the equivalent block diagram of the system. It follows from this diagram that:

$$y = G(r - Hy)$$

The closed-loop gain:

$$M = \frac{y}{r} = \frac{1}{\frac{1}{G} + H}$$

[2] Stability is a notion that describes whether the system will be able to follow the input command (Chapter 5). In anonrigorous sense, a system is said to be unstable if its output is out of control or increases without bound.

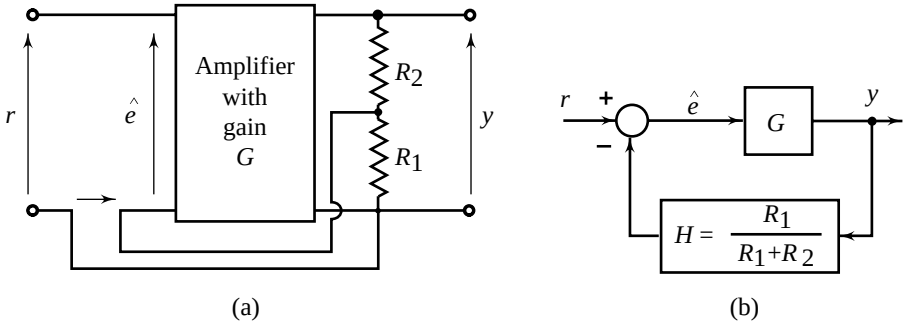

Fig. 1.10 Amplifier with feedback

This equation, specifying the relationship between the closed-loop gain M, the open-loop gain G, and the feedback gain H, is crucial for the feedback theory which was developed in electronics (the studies of Harry Nyquist and Hendrik W. Bode in the 1930s) and which relied heavily on the then widely-fostered frequency methods of analysis. The most important observation from this equation which determines feedback performance is that:

$$M \cong \frac{1}{H} = \frac{R_1 + R_2}{R_1} \text{ for } \frac{1}{G} << H \quad \text{or} \quad GH >> 1$$

where GH denotes the feedback-loop gain. It follows that under the conditions of strong feedback ($GH >> 1$), the closed-loop gain M does not depend upon the open-loop gain G; it depends only on the potential-dividing resistor. The gain M is practically constant even if gain G varies to a considerable extent, as long as it remains sufficiently high. Thus, by making use of feedback, it has become possible to convert an amplifier with very high but unsteady gain into an amplifier with a lower but steady gain. Furthermore, the higher the gain G, the more steady is M. On the other hand, an excessive increase of G results in the loss of stability. The reconciliation of the requirements of satisfactory performance and adequate stability margins was first the central problem and later the principal accomplishment of the feedback control theory.

During World War II, electronics engineers noticed an analogy between the feedback amplifier and the servomechanism of a radar command post, both in structure and principle of operation, and also with respect to the goal and the basic problem, i.e., reconciliation of the requirements of accuracy and stability. The feedback theory was then successfully applied to the design of servomechanisms, becoming more advanced in the process, and, in this way the *theory* of *servomechanisms* came into being.

The application of the theory of servomechanisms to the process industry led to the *feedback control theory*. At about the same time, Norbert Wiener founded *cybernetics* as the new field of study which transplanted elements of the feedback theory to economics, biology and other sciences.

Frequency-response methods have dominated the control systems area since the late 1940s as analysis and design tools. The Nyquist and Bode diagrams became indispensable for assessing the closed-loop stability of feedback control systems. Evans' root-locus method brought the complex variable based approach to a fully developed state by 1948. A mature *classical* control systems engineering area thus evolved.

Further advances in control systems engineering resulted from the space programme and associated challenges—launching, manoeuvring, guidance, and tracking of space vehicles. The emergence of a *modern* control theory based on state-space ideas is generally traced back to the early 1960s.

After this brief consideration of the origins of the feedback control theory, let us focus our attention on the requirement of reconciling accuracy and stability, which makes the existence of a uniform feedback control theory fully justifiable. We have already considered one example—the electronic amplifier, wherein

strong feedback results in insensitivity to variations in parameters of the electronic tube. There is, however, an upper limit on the improvement of performance beyond which stability suffers. In the following we consider more examples.

Example 1.3 Servomechanism for Steering of Antenna

One of the earliest applications of radar tracking was for anti-aircraft fire control; first with guns and later with missiles. Today many civilian applications exist as well, such as satellite-tracking radars, navigation-aiding radars, etc.

The radar scene includes the radar itself, a target, and the transmitted waveform that travels to the target and back. Information about the target's spatial position is first obtained by measuring the changes in the back-scattered waveform relative to the transmitted waveform. The time-shift provides information about the target's range, the frequency-shift provides information about the target's radial velocity, and the received voltage magnitude and phase provide information about the target's angle[3] [1,2].

In a typical radar application, it is necessary to point the radar antenna towards the target and follow its movements. The radar sensor detects the error between the antenna axis and the target, and directs the antenna to follow the target. The servomechanism for steering the antenna in response to commands from radar sensor is considered here. The antenna is designed for two independent angular motions, one about the vertical axis in which the azimuth angle is varied, and the other about the horizontal axis in which the elevation angle is varied (Fig. 1.11). The servomechanism for steering the antenna is described by two controlled variables—the azimuth angle β, and the elevation angle α. The desired values or commands are the azimuth angle β_r, and the elevation angle α_r, of the target. The feedback control problem involves error self-nulling, under conditions of disturbances beyond our control (such as wind power).

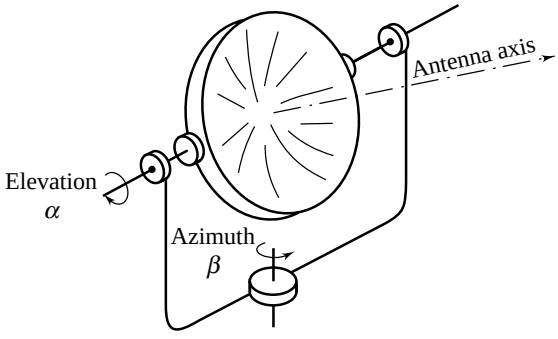

Fig. 1.11 Antenna configuration

The control system for steering of the antenna can be treated as two independent systems—the azimuth-angle servomechanism, and the elevation-angle servomechanism. This is because the interaction effects are usually small. The operational diagram of the azimuth-angle servomechanism is shown in Fig. 1.12. The steering command from the radar sensor which corresponds to the target azimuth angle is compared with the azimuth angle of the antenna axis. The occurrence of the azimuth-angle error causes an error signal to pass through the amplifier, which increases the angular velocity of the servomotor in a direction towards an error reduction. In the scheme of Fig. 1.12, the measurement and processing of signals (calculation of control signal) is digital in nature and is based on proportional control logic. Figure 1.13a gives the functional block diagram of the control system. A simple model of the load (antenna) on the motor is shown in Fig. 1.13b. The moment of inertia J and the viscous friction coefficient B are the parameters of the assumed model. The nominal load is included in the plant model for the control design. The main disturbance input is the deviation of the load from the nominal estimated value as a result of uncertainty in our estimate, effect of wind power, etc.

[3]The bracketed numbers are keyed to the list of references given at the end of the book.

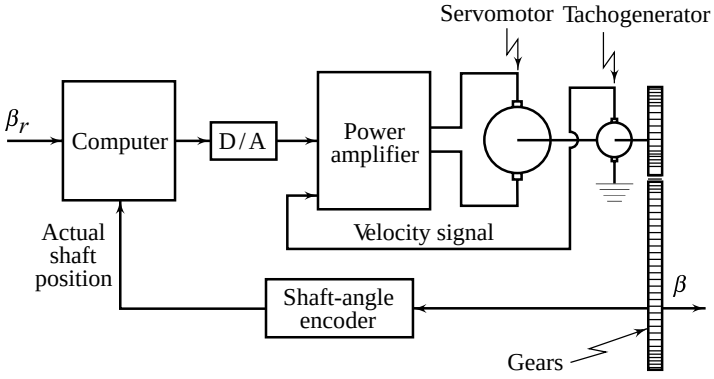

Fig. 1.12 Azimuthal servomechanism for steering of antenna

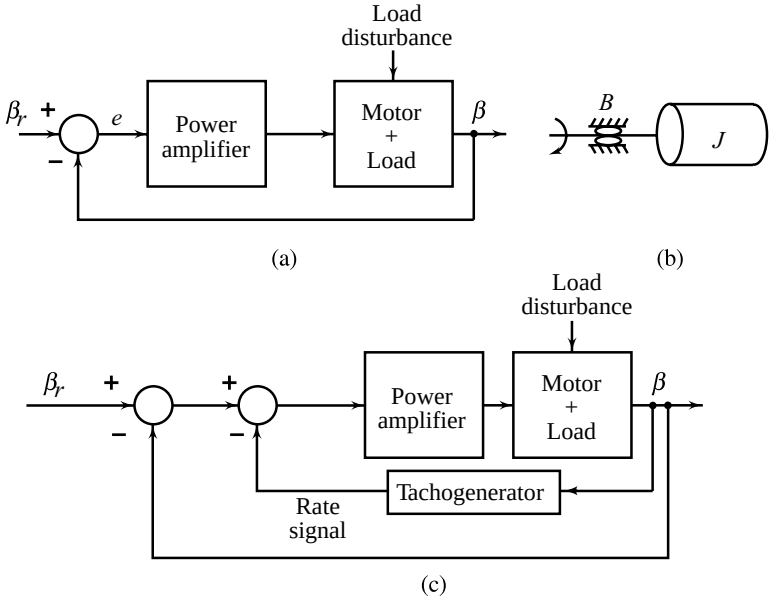

Fig. 1.13 Functional block diagram of azimuthal servomechanism

In the tracking system of Fig. 1.13a, the occurrence of error causes the motor to rotate in a direction favouring the dissolution of error. Note that the components of our system cannot respond instantaneously because any real-world system cannot go from one energy level to another in zero time. Thus, in any real-world system, there is some kind of dynamic lagging behaviour between the input and the output. In the servosystem of Fig. 1.13a, the control action on the occurrence of the deviation of the controlled output from the desired value (the occurrence of error), will be delayed by the cumulative dynamic lags of the shaft-angle encoder, digital computer and digital-to-analog converter, power amplifier, and the servomotor with load. Eventually, however, the trend of the controlled variable deviation from the desired value will be reversed by the action of the amplifier output on the rotation of the motor, returning the controlled variable towards the desired value. Now, if a strong correction (high amplifier gain) is applied (which is desirable from the point of view of the control system performance, e.g., strong correction improves the speed of response (Chapter 4)), the controlled variable overshoots

the desired value (the 'run-out' of the motor towards an error with the opposite rotation), causing a reversal in the algebraic sign of the system error. Unfortunately, because of the system dynamic lags, a reversal of correction does not occur immediately and the amplifier output (acting on 'old' information) is now actually driving the controlled variable in the same direction as it is already going, rather than opposing its excursions, leading to a larger deviation. Eventually, the reversed error does cause a reversed correction, but the controlled variable overshoots the desired value in the opposite direction and the correction is again in the wrong direction. The controlled variable is thus driven alternatively in opposite directions before it settles to an equilibrium condition. This oscillatory state is unacceptable as the behaviour of the antenna-steering servomechanism. The considerable amplifier gain, which is necessary if high accuracies are to be obtained, aggravates the described unfavourable phenomenon.

The occurrence of these oscillatory effects can be controlled by the application of special compensation feedback. When a signal proportional to the motor's angular velocity (called the rate signal) is subtracted from the error signal (Fig. 1.13c), the braking process starts sooner before the error reaches a zero value. The 'loop within a loop' (velocity feedback system embedded within a position feedback system) configuration utilized in this application is a classical scheme called *cascade control* in the process field and *minor-loop feedback* in servomechanisms.[4]

Example 1.4 Variable Speed dc Drive

Many industrial applications require variable speed drives. For example, variable speed drives are used for pumping duty to vary flow rate or pumping pressure, rolling mills, harbour cranes, rail traction, etc. [3–5].

The variable speed dc drive is the most versatile drive available. The silicon controlled rectifiers (SCR) are almost universally used to control the speed of dc motors because of the considerable benefits that accrue from the compact static controllers supplied directly from the ac mains.

Basically all the dc systems involving the SCR controllers are similar but with different configurations of the devices, different characteristics may be obtained from the controller. Figure 1.14 shows a dc motor driven by a full-wave rectified supply. Armature current of the dc motor is controlled by an SCR which is in turn controlled by the pulses applied by the SCR trigger control circuit.

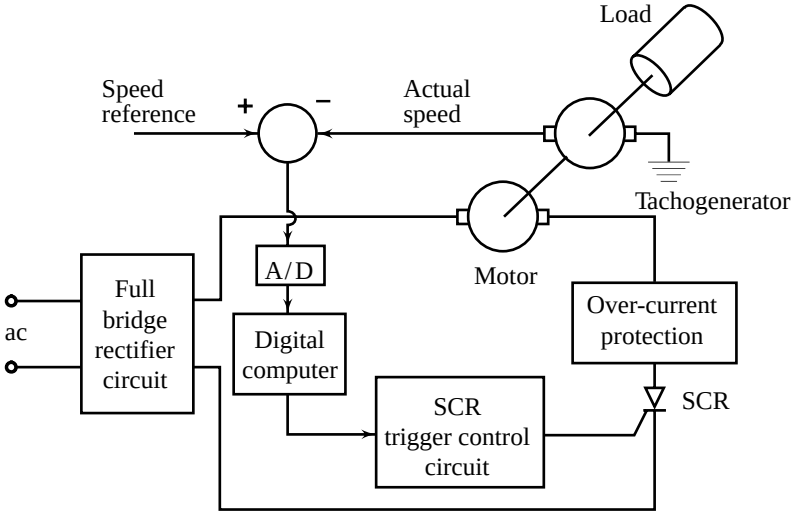

Fig. 1.14 Variable speed dc drive

[4]This, and other compensation schemes will be discussed in later chapters.

Firing angle of the SCR controls the average armature current which in turn controls the speed of the dc motor. The average armature current (speed) increases as the trigger circuit reduces the delay angle of firing of the SCR, and the average armature current (speed) reduces as the delay angle of firing of the SCR is increased.

In the scheme of Fig. 1.14, the reference voltage which corresponds to the desired speed of the dc motor, is compared with the output voltage of the tachogenerator corresponding to the actual speed of the motor. The occurrence of the error in speed causes an error signal to pass through the trigger circuit which controls the firing angle of the SCR in a direction towards an error reduction. When the processing of the error signal (calculation of the control signal) is based on the proportional control logic, a steady-state error between the actual speed and the desired speed exists (Chapter 4). The occurrence of the steady-state error can be eliminated by generating the control signal with two components: one component proportional to the error signal, and the other proportional to the integral of the error signal. This proportional-integral control logic will be examined in detail in Chapter 4.

A point which needs a special mention here is that the presence of disturbances is the main reason for using feedback control. Without disturbances, there is probably no need for feedback control. Table 1.1 gives the details of commonly occurring disturbances in the control system examples considered earlier.

Table 1.1 Disturbances in specific feedback control systems

Feedback control system	*Disturbance in controlled system*	*Measurement noise*
Residential heating system	Ambient temperature	Mechanical vibrations of bimetallic strip
Servomechanism for steering of antenna	Wind power	Target surface fluctuations
Variable speed dc drive	Variations in load on dc motor	Mechanical vibrations

Other disturbances which affect the performance of control systems are:

(i) uncertainty in our estimate of the hardware parameters of the process and other components of the control system (the estimates of the parameters are used for the design of controller); and

(ii) changes in the parameters taking place in time (due to wear, ageing, environmental effects, etc.), thereby affecting the dynamic characteristics of the system.

As we shall see later in this book, feedback control systems:

(i) greatly reduce the effect on the controlled variable of all external disturbances except those associated with the sensor (measurement system); and

(ii) are tolerant of variations in hardware parameters other than those of the sensor.

The feedback signal coming from the sensor of controlled variable contains useful information related to disturbances (external disturbances and variations in hardware parameters), which is usually of a relatively low frequency. It may often include high frequency 'noise' introduced by the measurement sensors. Such noise signals are too fast for the control system to correct; *low-pass filtering* is often needed to allow good control performance.

1.3 FEEDFORWARD-FEEDBACK CONTROL STRUCTURE

This section presents the principle of one of the most profitable control schemes: *feedforward control*. In earlier sections, we studied the principle of feedback control; a very simple technique that compensates for any disturbance affecting the controlled variable. When a disturbance enters the process, the controlled variable deviates from its desired value (set-point) and, on sensing the error, the feedback controller manipulates the process input in a way favouring the dissolution of error. The main limitation of a feedback control system is that in order for it to compensate for disturbances, the controlled variable must first deviate from its desired value. Feedback control acts upon an error between the set-point and the controlled variable. This means that once a disturbance enters a process, it must propagate through the process and force the controlled variable to deviate from the set-point before corrective action can be taken.

Feedforward control compensates for disturbances before they affect the controlled variable. In this scheme, the disturbances are measured before they enter the process and required value of the manipulated variable to maintain the controlled variable at its desired value is calculated; implementation of such a control results in undisturbed controlled variable. The design of this type of control scheme does not generally require any specialized control theory; basic system dynamics are sufficient in most cases. Success of *disturbance feedforward* control schemes depends on our ability to:

(i) measure the disturbance; and

(ii) estimate the effect of the disturbance on the controlled variable, so that we can compensate for it.

Let us consider an example of disturbance-feedforward.

Example 1.5 Heat Exchanger

The schematic diagram of a heat exchanger is shown in Fig. 1.15. The process fluid flows inside the tubes of the heat exchanger and is heated by the steam condensing on the outside of the tubes. The objective is to control the outlet temperature θ of the process fluid in the presence of variations[5] in the process fluid flow Q and its inlet temperature θ_i. The objective of controlling the outlet temperature in the presence of disturbances can be accomplished by setting up a feedback control loop as shown in Fig. 1.15a. The flow controller consists of an electronic amplifier and an electropneumatic transducer, which converts the voltage corresponding to the error between the controlled temperature and its set-point value to a pneumatic pressure variable (based on proportional control logic). The error voltage is derived from the output voltage of the temperature sensor (corresponding to the output temperature θ) and the set-point voltage corresponding to the desired temperature. The pneumatic pressure actuates a pneumatic valve[6], whose essential features are shown in Fig. 1.15b. The actuator section of the valve comprises of a diaphragm whose position is set by the balance between the force exerted by a spring and the controller output pressure on the diaphragm.

In the control scheme of Fig. 1.15a, the feedback controller, which manipulates the heat input to the heat exchanger, will not act until an error has developed. If the system involves large time lags, it will take some time before any corrective action takes place.

[5]In a typical application, the heat exchanger is a part of the overall system; disturbances in Q and θ_i are caused by other processing operations taking place in the system (in the next section, we will study a distillation system wherein the heat exchanger is a sub-system).

[6]By far, the most common form of valve used in process control is the pneumatic actuating valve which can provide large power output. Pneumatic systems use a readily available working medium—compressed air supplies, and are commonly used in process industry because of their explosion-proof characteristics, simplicity and ease of maintenance.

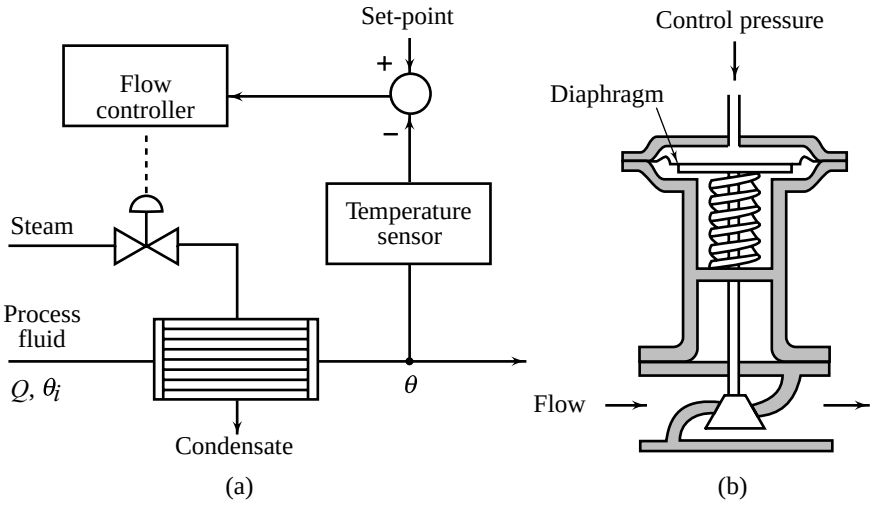

Fig. 1.15 Feedback control loop for heat exchanger

If feedforward control is provided in such a system, then as soon as a change in Q and/or θ_i occurs, a corrective measure will be taken simultaneously by manipulating the heat input to the heat exchanger. Fig. 1.16 shows the disturbance-feedforward control scheme.

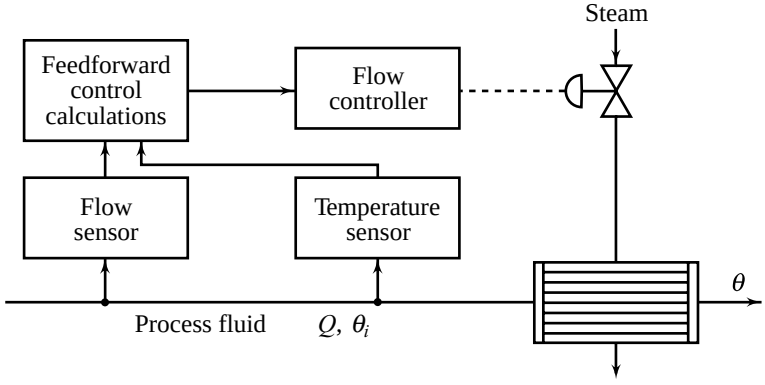

Fig. 1.16 Disturbance compensated open-loop system

Feedforward control can minimize the transient error. However, since it is an open-loop control, there are limitations to its functional accuracy. Feedforward control will not cancel the effects of unmeasurable disturbances. It is therefore necessary that a feedforward control system include a feedback loop as shown in Fig. 1.17. Essentially, the feedforward control minimizes the transient error caused by measurable disturbances, while the feedback loop compensates for any imperfections in the functioning of the feedforward control and provides corrections for unmeasurable disturbances.

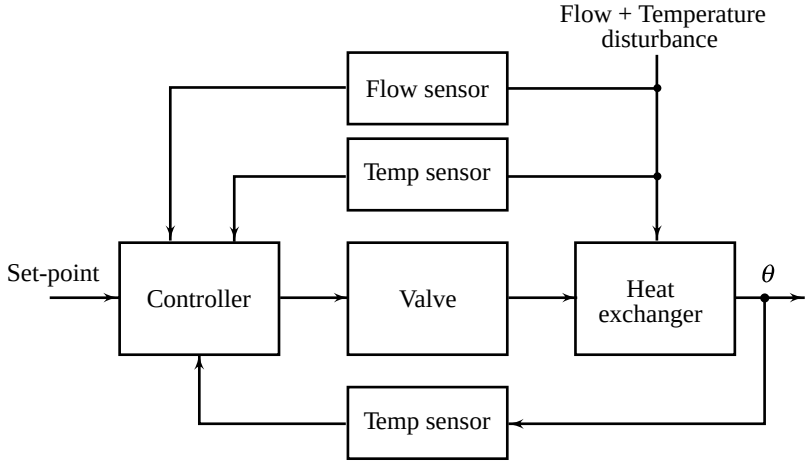

Fig. 1.17 Feedforward–feedback control structure for the heat exchanger

Another control scheme using the feedforward concept is the *command-feedforward* in combination with feedback loop (Fig. 1.18). Here, based on the knowledge of process characteristics, the command is augmented by command-compensator to produce improved performance. Command-feedforward has been used in several ways for servo applications. In the next section, we will give a combined feedforward-feedback scheme employing command feedforward for the angular motion control of a robot manipulator.

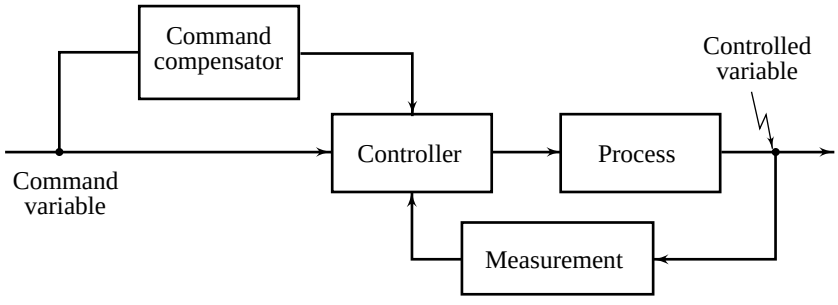

Fig. 1.18 A control scheme employing command feedforward

1.4 MULTIVARIABLE CONTROL SYSTEMS

Complex processes and machines often have several variables (outputs) that we wish to control, and several manipulated inputs available to provide this control. Sometimes the control situation is simple; one input affects primarily one output and has only weak effect on the other outputs. In such situations, it is possible to ignore weak *interactions* (*coupling*) and design controllers under the assumption that one input affects only one output. Input–output pairing to minimize the effect of interactions and application of SISO control schemes to obtain separate controllers for each input–output pair, results in an acceptable performance. This, in fact, amounts to considering the multivariable system as consisting of an appropriate number of separate SISO systems. Coupling effects are considered as disturbances to the separate control systems and may not cause significant degradation in their performance if the coupling is weak. We have already discussed

examples of the multivariable systems of this nature—the automobile driving system (Example 1.1), and the antenna stabilization system (Example 1.3).

A multivariable system is said to have strong interactions (coupling) if one input affects more than one output appreciably. There are two approaches for the design of controllers for such systems.

1. Design a *decoupling controller* to cancel the interactions inherent in the system. Consider the resulting multivariable system as consisting of an appropriate number of SISO systems, and design a controller for each system.
2. Design a single controller for the multivariable system, taking interactions into account.

In this section, we give examples of multivariable systems with strong interactions. These and many other important applications are difficult to present convincingly in an introductory text since their dynamic modelling is too complex to be accommodated. We will therefore only highlight the salient features of these control systems. Selected titles for detailed study are [119–122].

Example 1.6 Distillation System

The purification of materials is a prominent operation of the chemical industry. There is scarcely any chemical process which does not require preliminary purification of raw materials or final separation of products from by-products. The towers of a modern petroleum refinery are the evidence of the important role played by these separations in a processing plant.

Figure 1.19 is a schematic diagram of a bubble-cup tray tower used for distillation [13].

Distillation is a method of separating the components of a liquid mixture by the repeated systematic application of vaporization and condensation. For example, if a liquid solution of ammonia and water is partially vaporized by heating, it is found that the newly created vapour phase and residual liquid both contain ammonia and water, but in proportions which at equilibrium are different for the two phases and different from those in the original solution. The vapour phase is richer in the more volatile component (ammonia) and the residual liquid is richer in the less volatile component (water), compared to the original solution. If the vapour and the liquid are separated from each other and the vapour condensed, two solutions, one richer in ammonia and the other richer in water, are obtained. If the process of vaporization and condensation is continued over a number of stages, it eventually produces a product with a very high degree of purity in the more volatile component.

The thermal efficiency of this staged operation can be greatly improved if the energy released when the vapour is condensed in one stage is used to vaporize the liquid in an adjacent stage. If the heat required to vaporize one mole (a mole of a substance is defined as the amount of substance whose mass numerically equals its molecular weight) of liquid is equal to the heat that is released when one mole of vapour condenses and is independent of composition, then it is evident that a heat source and sink are needed only at the ends of the cascade.

In the distillation column, the necessary heat transfer is accomplished by the direct contact between vapour and liquid by trays (perforated plates) which are designed so that vapour stream bubbles directly through the liquid as illustrated in Fig. 1.19. The feed (multicomponent, in general) is introduced into a vertical cascade of stages close to its centre. The feed mixes with the 'downcoming' liquid. The liquid at every stage is stripped of the more volatile component by the rising vapour, originally produced at the bottom by partial vaporization of the bottom liquid in the reboiler. The liquid residue at the bottom is rich in the less volatile component and is removed. The rising vapour gets progressively enriched in the more volatile component. It is condensed and stored in the reflux accumulator. The material returned at the top of the tower is the reflux and the material removed from the reflux accumulator is the distillate which is rich in the more volatile component.

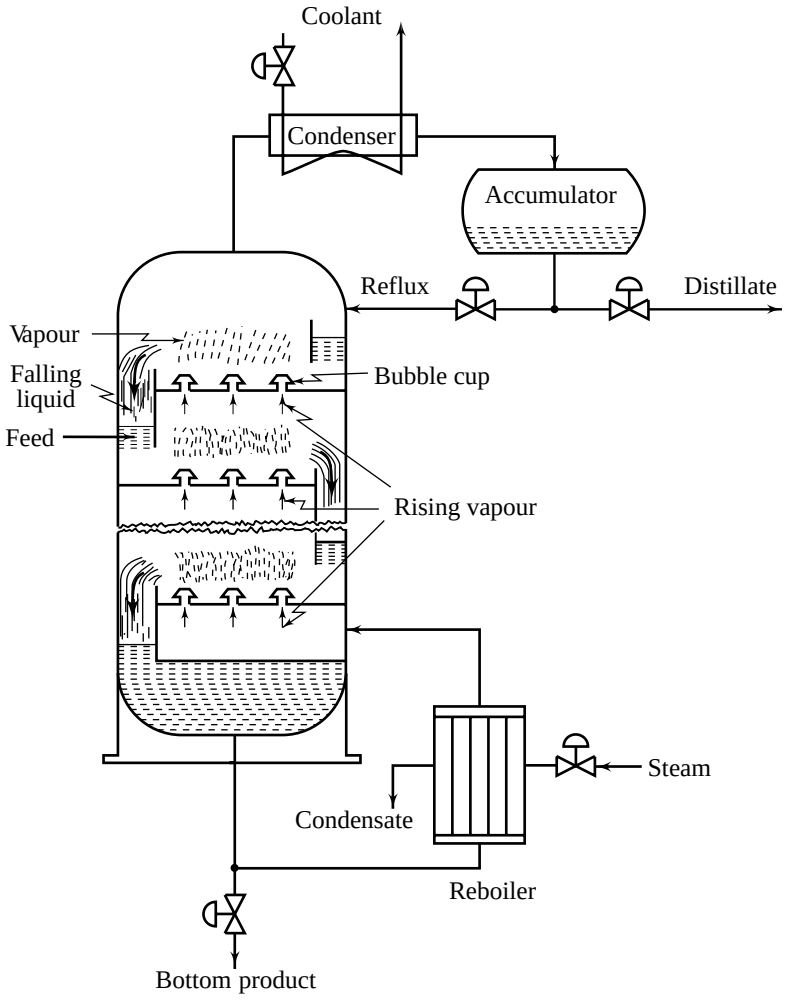

Fig. 1.19 A distillation column with five primary controlled variables: two compositions, two levels, and pressure

Let us now consider a simple control scheme for the distillation system. The two main objectives of the control are to maintain two product compositions, x_D (overhead (distillate) product composition) and x_B (bottom product composition), at their set points. The three secondary objectives are to maintain the vapour balance by controlling the column pressure and the liquid balances by controlling the levels in the reflux accumulator and the column bottom.

In the control scheme shown in Figs 1.20–1.21, the distillate rate is manipulated to control the level of the reflux accumulator, and the bottom rate is manipulated to control the bottom level. The two variables do not affect the operation of the column directly; the level control systems may therefore be treated as independent SISO systems.

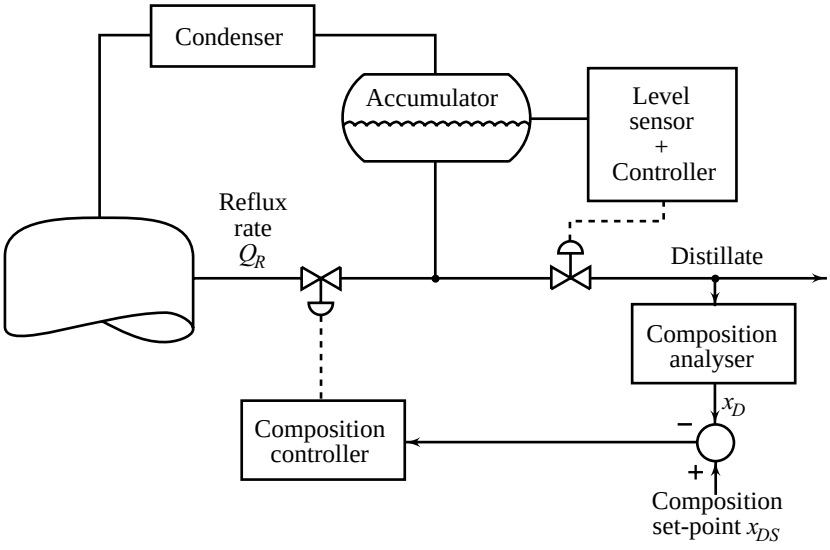

Fig. 1.20 Distillation-column reflux

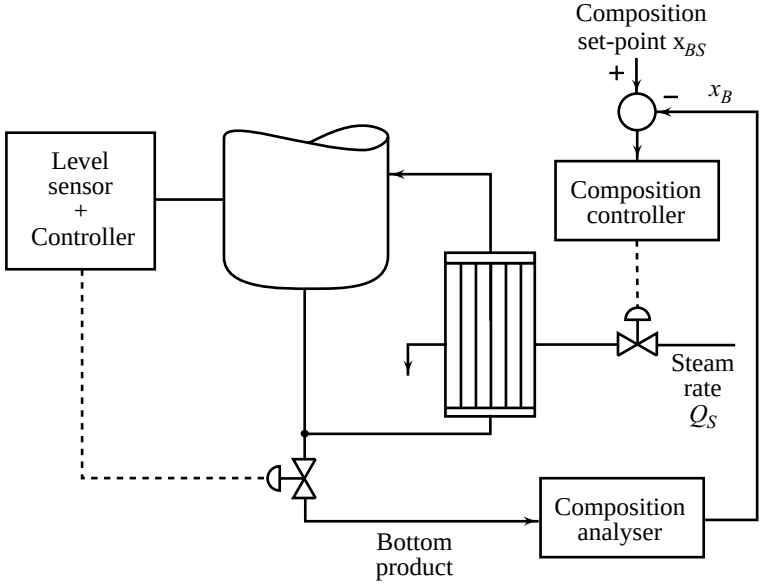

Fig. 1.21 Distillation-column reboiler

In a column, the pressure is determined solely by the heat balance. If heat is supplied in the reboiler at a higher rate than it is removed in the condenser, the pressure in the column rises with time. Column pressure can be controlled by manipulating the reboiler heating rate or the condenser cooling rate. We will assume that the pressure controller manipulates the condenser cooling rate and results in a non-interacting control loop (not shown in the figures).

This reduces the problem to a two-by-two multivariable control problem: the manipulated variables are steam rate Q_S and reflux rate Q_R, and the controlled variables are the bottom product composition x_B

and the distillate composition x_D. Figure 1.22 shows a block diagram representation of the resulting two-input, two-output system. Changes in the input variable Q_R cause responses in both the outputs, x_D and x_B. Similarly, input variable Q_S affects x_B as well as x_D.

In this book we will consider many examples of liquid-level, and temperature, control systems. SISO design techniques will provide control logic in a large number of cases.

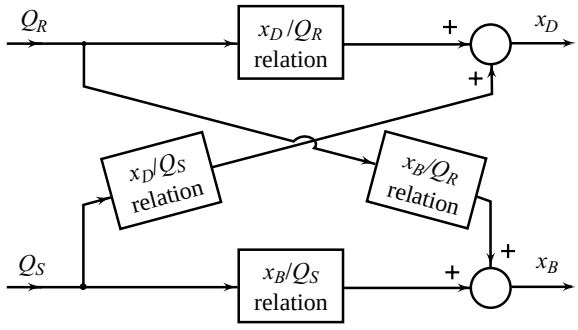

Fig. 1.22 Block diagram representation of the multivariable control of a distillation column

Example 1.7 Aircraft Stability and Control

Aircraft control is one of the most important applications through which the control system techniques have developed. In aircraft control systems, the 'airframe' acts as a 'plant'; the behaviour of which is to be controlled. Main parts of an airframe include (Fig. 1.23):

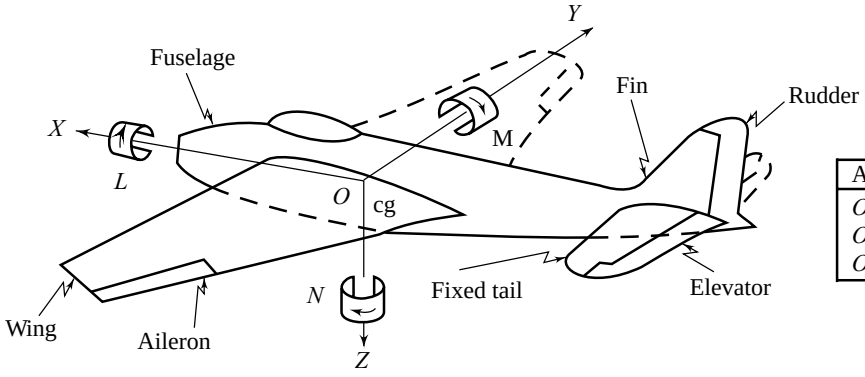

Axis	Moment
OX	*Rolling L*
OY	*Pitching M*
OZ	*Yawing N*

Fig. 1.23 Control surfaces of an airframe

(i) fuselage or mainbody; (ii) wings with ailerons;
(iii) horizontal tail plane with elevator; and (iv) fin or vertical tail plane with rudder.

Ailerons, elevator and rudder are the control surfaces. A control surface is a movable (hinged) flap which forms a portion of the fixed aerodynamic surface (wing, horizontal tail, vertical tail) and which is employed to vary the lift coefficient of the surface. Figure 1.24 shows aileron deflection; the aileron angle δ_a is defined as the mean value of the angular displacements of the two ailerons. The other two controls which can be manipulated by the pilot are the elevator deflection δ_e and rudder deflection δ_r.

In examining the stability and control of a rigid aircraft, it is customary to separate the six degrees of freedom into two groups of three each. One group describes the longitudinal dynamics of the aircraft and comprises the translational motions along the *OX*-and *OZ*-axes, and the pitching motion. The other group describes the lateral dynamics of the aircraft and comprises the remaining three degrees of freedom, namely, the translational motion along the *OY*-axis, and the yawing and rolling motions. The elevator control forces and the throttle, affect the longitudinal motion, whereas the aileron and rudder primarily affect the lateral motion. It has been found that for the preliminary design work, the coupling of the lateral motion into longitudinal motion can be ignored.

In general, a control functions by causing a change in the pressure distribution on a surface, which results in a change in the lift coefficient of the surface. This change in the lift coefficient causes a change in the moment balance of the aeroplane and results in the angular moment about one or more of the axes. The principal control actions of the three control surfaces are:

(i) the rudder controls yawing, i.e., motion about the *OZ*-axis;

(ii) the ailerons control rolling, i.e., motion about the *OX*-axis; and

(iii) the elevator controls pitching, i.e., motion about the *OY*-axis.

The actual positioning of the control surfaces is obtained by electric or hydraulic motors which are controlled by the pilot.

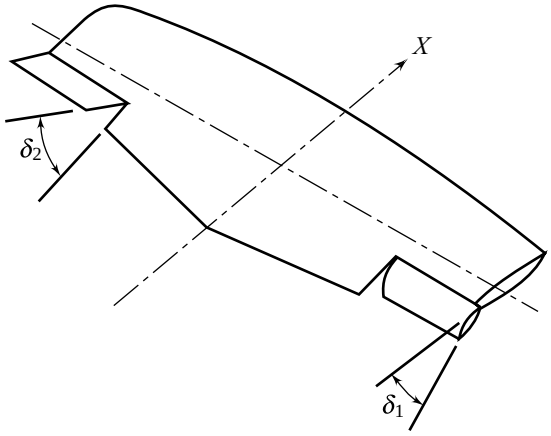

Fig. 1.24 Aileron deflection

Later in this book we shall analyse aircraft motions (SISO systems) under assumptions which neglect many details but preserve the essential nature of the problem. Mathematical modelling of aircraft dynamics is beyond the scope of this book. References [14–16] give a good treatment of the subject.

Example 1.8 Robotic Control System

Machines that automatically load and unload, cut, weld or cast, are used by the industry in order to obtain accuracy, safety, economy, and productivity. Programmable computers integrated with machines that often substitute for human labour in specific repeated tasks, are the modern *robots*.[7] Such devices even have anthropomorphic mechanisms, including what we might recognize as mechanical arms, wrists, and hands.

A *robot manipulator* is made of several links connected usually in series by the joints to form an arm. A link is revolute or prismatic depending upon the type of motion caused by the actuator attached to its joint. When the actuator of a joint causes rotational motion, the link is *revolute*, and when the actuator produces translational motion, the link is called *prismatic*. A gripper, which is referred to as a hand or an end-effector, is attached to the arm by means of wrist joints. The function of the wrist is to orient the end-effector properly.

The motion of a manipulator end-effector is caused by the movements of the actuators driving the joints. The joint actuators are electric or hydraulic motors, or pneumatically driven devices. The positions of the joints determine the *configuration of the arm*, which places the end-effector at a specific location in the environment. The motion of the joints produced by the actuators determines the position and orientation of the end-effector at any time. Transducers such as encoders and tachometers can be used to provide information for determining the position and orientation of the end-effector, and to control the manipulator motion.

The set of all points that can be reached by the end-effector of a manipulator arm forms the *workspace* of the manipulator. A particular position of the end-effector is specified by three independent coordinates, which represent three degrees-of-freedom. Similarly, a specific orientation of the end-effector is determined by three independent variables. Thus, six independent variables are needed to describe the

[7]The word robot seems to originate from the Czech language: robota means compulsory service.

position and orientation of the end-effector. Commercially available robots have typically six joints, giving six degrees-of-freedom. However, robots with less than six joints, designed for specific tasks, are also available. Figure 1.25 shows a picture of the PUMA (Programmable Universal Manipulator for Assembly), a revolute manipulator.

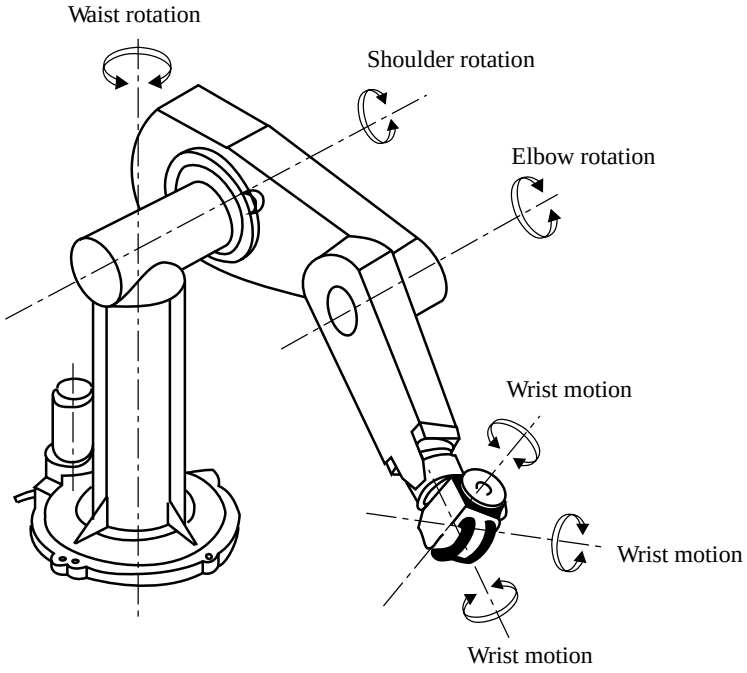

Fig. 1.25 An industrial robot: PUMA

The objective in providing the position control for a robot manipulator is to design an appropriate controller for the robot motors, so that the position and the orientation of the end-effector follow the desired trajectory with no errors even in the presence of disturbances. A multi-link manipulator is a highly complex system—each link of the robot arm has varying inertia and exerts varying torques on all the other links as the configuration of the robot arm changes. The equations of motion for a multi-link manipulator describe a MIMO system; the equations are coupled representing the effects of interactions of the joints (This MIMO system can't be considered as consisting of an appropriate number of separate SISO systems). For a six-joint robot, joint positions θ_i; $i = 1, \ldots, 6$ (represented by the position vector $\boldsymbol{\theta}$ in Fig. 1.26) are the controlled outputs, and actuator torques u_i; $i = 1, \ldots, 6$ (represented by the input vector $\mathbf{u}$ in Fig. 1.26) are the manipulated variables. $\boldsymbol{\theta}_r$ is the position vector corresponding to the desired trajectory.

Perfect tracking can be achieved by a scheme employing command feedforward. Let $\boldsymbol{\theta}_r(t)$ be the input to a feedforward controller with dynamics which are inverse of the dynamics of the manipulator. When

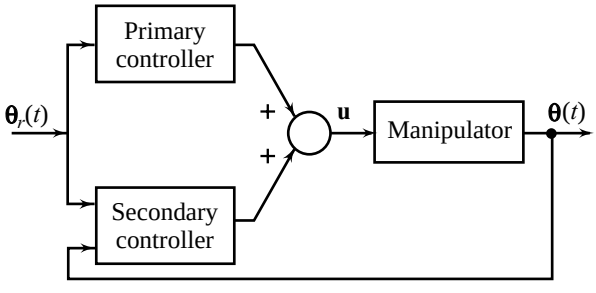

Fig. 1.26 Manipulator system with primary and secondary controllers

the manipulator is driven by the output of such a controller, we get $\boldsymbol{\theta}(t) = \boldsymbol{\theta}_r(t)$. The command-tracking based on this *inverse dynamics* concept can be perfect only if we can exactly determine the dynamic model of the manipulator.

The robotic system is too complex to allow exact identification of the dynamic model. Also, the system is subject to unmeasurable disturbances. Undesirable deviations of the actual motion of the manipulator from the desired trajectory can be corrected by means of feedback control. A block diagram showing the total control system (primary controller (feedforward) and secondary controller (feedback)) is displayed in Fig. 1.26.

The problem of control of the multi-link manipulator is too complex to be included in this introductory text. To bring robot application into our range, we will consider the problem of control of a single-link manipulator (SISO system). The problem of control of a two-link manipulator has been examined in the companion book [155]. Selected titles for further reading are [17–19].

1.5 SCOPE AND ORGANIZATION OF THE BOOK

This text is mainly concerned with basic concepts of feedback control theory, frequency-domain design tools, and analog/digital implementation of design. We do not intend to solve all the control problems that can be posed under the defined category. In fact, we primarily study a special class of control systems, namely linear, time-invariant, lumped, and deterministic systems. For this class of systems, a fairly complete treatment of the control problem has been given in this book. The development of the material has been influenced by several existing books mentioned in the references given at the end of this text.

In each chapter of the book, analysis/design examples are interspersed to illustrate the concepts involved. At the end of each chapter, there are a number of review examples and questions; some of these also serve the purpose of extending the text material. The same approach is followed in unsolved problems. Answers have been given to inspire confidence in the reader.

The examples we have considered in this book are generally low-order systems. Such a selection of examples helps in conveying the fundamental concepts of feedback control without the distraction of large amounts of computations inherent in high-order systems. Many of the real-life design problems are more complex than the ones discussed in this book; high-order systems are common and, in addition, several parameters are to be varied during the design stage to investigate their effect on the system performance. Computer-Aided-Design (CAD) tools are extremely useful for complex control problems. Several software packages with computer graphics are available commercially for CAD of control systems [151–154]. Access to the CAD software is helpful, but not necessary, to solve the control problems discussed in this book. Let us now go through the organization of the chapters in sequence.

Chapter 2 combines some mathematical background with physical system modelling. Basic principles for modelling simple, mechanical, electrical (Op Amp based networks for implementation of compensators), hydraulic and thermal systems are treated, and transfer function and state variable models are derived. The analysis of transfer function models is also given. The analysis of state variable models, and their relationship to transfer functions are deferred to Chapter 12. References for Chapter 2 are [29, 31, 34–40].

Chapter 3 covers the mathematical models of different devices currently in use in industrial control practice. Models of typical industrial control systems are also included. The choice of examples is based on a desire to cover as many different application areas as possible. Devices used in computer-based control systems are covered later in Chapter 11. References for Chapter 3 are [41–51].

Chapter 4 introduces the basic modes of feedback control—proportional (P), integral (I), and derivative (D). A suitable combination of the three basic modes can improve all aspects of system performance.

The material on stability has been progressively built in this book at several places. Chapter 5 introduces the two basic concepts of stability—BIBO (bounded-input, bounded-output) stability and asymptotic

stability, as applied to linear time-invariant systems and presents the Routh stability criterion for stability analysis. More on stability analysis appears later in Chapters 8,12 and 14.

Chapter 6 gives control system performance specifications in time-domain. A number of performance measures for the speed of response, relative stability, and steady-state accuracy; and robusteness issues are introduced.

The practice of selecting a certain class of controller (P, PI, PID) based on past experience with certain classes of processes (pressure, flow, liquid-level, temperature, etc.) and then setting controller parameters by experiment once the controller is installed, has come to be known as *controller tuning*. Chapter 6 also includes this 'experimental' design method. References for process control are [6–13].

Control system design has always relied heavily on graphical methods. Chapter 7 develops the root-locus method. Although computer programs are readily available for generating these plots, designers must be able to sketch them first, at least roughly, in order to use the programs efficiently and interpret the results. The material in Chapter 7 has been organized in this spirit. This chapter also uses the root-locus method for compensation; lead/lag, and PID compensation are covered in detail.

Chapter 8 describes the Nyquist stability criterion. Robust stability measures—the gain margin and the phase margin—are introduced in this chapter.

Chapter 9 gives control system performance specifications in the frequency-domain. Correlation between time- and frequency-response is also established.

Chapter 10 uses frequency-response plots—Bode plot, and Nichols chart, for compensator design. Lead/lag and PID compensation are covered in detail.

References for the material in Chapters 4–10 are [58–79].

A brief account of digital control systems, state-space techniques and nonlinear systems, in Chapters 11–14, completes the text. Although these chapters can be used as an introduction for students who will be continuing their study of control systems engineering, they are useful as a supplement to the discussion of analysis and design in the previous chapters. The subject matter could not be given comprehensive treatment for want of space (detailed account is available in the companion book [155]), but the emphasis is clearly outlined and logically linked to the rest of the book.

Chapter 11 addresses how one 'digitizes' the control systems developed in Chapters 6 – 10, how the analysis of sampled-data systems requires another analysis tool—the z-transform, and how direct digital control design in carried out in the z-transform domain. References for Chapter 11 are [80 – 98].

In Chapters 12 and 13, we introduce alternative techniques for realizing the control objectives, first identified in Chapter 6 and realized in Chapters 7 and 10 using, respectively, the root-locus plots and frequency-response plots. The state variable methods discussed in Chapters 12 and 13 are alternative means to the same end. All these approaches are fundamentally complimentary and each needs to be understood to achieve the most effective control systems design.

Chapter 12 presents basic material for the state-space analysis of control systems. The solution of the time-invariant state equation is derived and concepts of controllability and observability are discussed. Chapter 13 treats the design of control systems in state space. This chapter begins with the pole-placement problems, followed by the design of state observers. Finally, quadratic optimal control problem is introduced. References for Chapters 12 and 13 are [99-108].

Many practical systems are sufficiently nonlinear so that the important features of their performance may be completely overlooked if they are analyzed and designed through linear techniques as such. Chapter 14, the final chapter, introduces some commonly used analysis techniques (describing function, phase plane & Lyapunov stability) which take account of system nonlinearities. References for Chapter 14 are [125-129].

Appendix A provides MATLAB and Simulink support for computer-aided control system design. MATLAB problems included in the appendix and all the chapters, give the student practice with problem solving, using computers. Multiple-choice questions given in Appendix B serve the purpose of self-appraisal review of the control theory.

Dynamical Systems Modelling and Response: The Transfer Function

2

2.1 INTRODUCTION

The most important task confronting the control system analyst is developing a mathematical model of the process of interest. In many situations, the essence of the analytical design problem is in the modelling; once that is done, the rest of the analysis falls quickly into place.

The control system engineer is often required to deal with a system having a number of sub-systems, the physical principles of which depend on entirely different types of physical laws. A chemical process, for example, may comprise a chemical reactor, the dynamics of which are the subject of chemical kinetic theory, a heat exchanger which is governed by thermodynamic principles, and various valves and motors, the dynamics of which depend on the physics of the mechanical and electrical systems. The control of a typical aircraft entails an understanding of the interaction between the airframe, governed by principles of aerodynamics and structural dynamics, the actuators which are frequently hydraulic or electrical, and the sensors (gyroscopes and accelerometers) which operate under the laws of rigid body dynamics.

One of the attractions of control system engineering is its interdisciplinary content. The control system engineer sees the 'big picture' in the challenge to harmonize the operation of a number of interconnected systems, each of which operates under a different set of laws.

The analyst needs *mathematical models* of the processes in the system under study—equations and formulae that predict how the various devices will behave in response to the inputs to these devices. From the viewpoint of system analyst, each device is the proverbial "black box" whose operation is governed by appropriate mathematical models. The behaviour of the overall process is studied and controlled by studying the interaction of these black boxes.

The present chapter reviews the basic laws of physics used to develop mathematical models of mechanical, electrical, hydraulic, and thermal systems that are commonly encountered in control systems as plant models or as models of control logic elements. The next chapter deals with the models of actuators, measurement sensors, and error detectors. The models of overall control systems are then developed by considering the interaction of these devices. Models of digital devices used in automatic control systems are discussed in Chapter 11.

An alternative approach of modelling is to regard the physical system as merely a 'black box', into which one can inject inputs and from which one can obtain measurements of the corresponding outputs. We then use this data to obtain a mathematical model of the system which produces the same outputs from the given inputs. This approach of modelling is known in the literature as *system identification*. Some simple identification methods will appear in later chapters. The companion book [155] has more details.

System models are classified according to the types of equations used to describe them. The family tree shown in Fig. 2.1 illustrates the major system classifications. The dashed lines in the figure indicate the existence of subdivisions similar to the others shown at the same level.

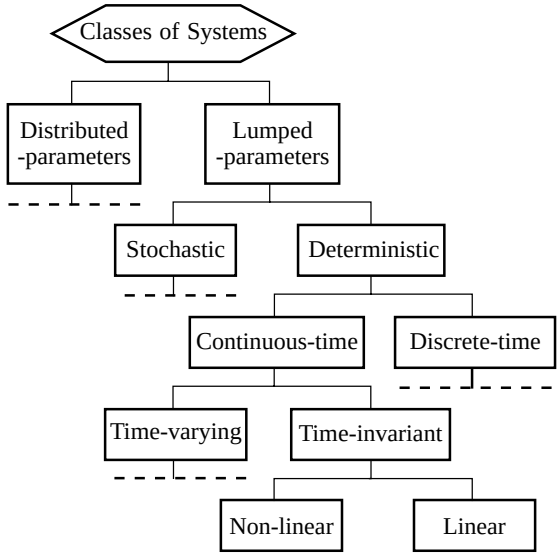

Fig. 2.1 Major classes of system equations

The significant variables in a system are distributed in space and they vary with spatial coordinates and time. The resulting dynamic models, called *distributed-parameter models*, consist of partial differential equations with time and space coordinates as independent variables. In *lumped-parameter models*, the matter is assumed to be lumped at some discrete points of the space, or the space is sub-divided into cells and the matter is assumed to be lumped at these cells. The resulting dynamic models are ordinary differential equations with time as the only independent variable. For example, the assumption that a solid is a rigid body permits lumping of all its mass at its mass centre, resulting in lumped-parameter models of dynamics. Considerable simplification is achieved in mathematical models when lumped-parameter models are used. In this book, we employ lumped-parameter models for control system design.

In physical systems, every signal (inputs, external disturbances, measured outputs) has associated with it certain amount of randomness (usually referred to by the generic term 'noise'). These uncertainties are inconsequential in many practical cases, and we proceed as though all signals are known functions of time. This assumption gives us a *deterministic model* of the system. When signals must be treated as random functions of time, *stochastic models* are used to characterize the system behaviour. In this book, we will make the assumption of deterministic signals.

If all the elemental equations are defined for all time, then the system is a *continuous-time system*. If, as in sampled-data systems, some elemental equations are defined or used only at discrete points in time, a *discrete-time system* is the result. Continuous-time systems are governed by differential equations and discrete-time systems by difference equations. The primary focus in this book is on continuous-time systems. Chapter 11 provides an introduction to discrete-time systems.

A classification between large-scale and small-scale systems could be made in terms of *multi-input multi-output* (MIMO) and *single-input single-output* (SISO) systems. Our emphasis in this book will be on SISO models with scalar input $r(t)$ and scalar output $y(t)$.

If we set a system going at some time t_0 and apply the input $r(t)$; $t \in (t_0, \infty)$, monitoring the corresponding output $y(t)$; $t \in (t_0, \infty)$, the output, in general, is not uniquely determinable and one way of associating a unique y with each r consists in including the information on total energy stored within the system at time t_0

before application of the external input. This information may be given in terms of characterizing variables whose value at time t_0 gives the stored-energy status of the system at that time. Therefore a complete mathematical model of a system includes *initial conditions* at the time of application of external input. The initial conditions of the model at t_0 give the energy status of the system at that time.

The output of a system at time $t_1 > t_0$ is uniquely determined by its initial conditions at t_0 and the input $r(t)$; $t \in (t_0, t_1]$. The input after t_1 has no effect on the system output at t_1; the system cannot foresee the future and responds only to inputs it has already received. This condition is called the *causality condition; causality is an intrinsic property of every physical system*.

A system is said to be *relaxed* at time t_0 if the energy stored at time t_0 is zero. This implies that initial conditions of the model at t_0 are zero and the output $y(t)$; $t \in (t_0, \infty)$ is uniquely determined by the input $r(t)$; $t \in (t_0, \infty)$.

If one or more parameters, or the very form of an elemental equation, vary in a known fashion with time, the system is said to be *time-varying*. For example, in the guidance and control of a rocket, the mass of the rocket changes with time due to the depletion of fuel, and also the aerodynamic damping can change with time as the air density changes with altitude. The complexity of the control system design increases considerably when the parameters are time-varying. In this book, we shall concern ourselves with those applications where the *time-invariance* assumption can safely be made, and therefore the models we use will have constant parameters.

Assume that a time-invariant system is relaxed and the input is applied at $t = t_0$. As long as relaxedness assumption is satisfied, a delay in the application of input by time τ will have no effect on the waveform of the output except for a corresponding delay by time τ. In general, as long as we start in the same energy state, any delay in application of input shifts the response correspondingly without affecting the magnitude. This suggests that in the study of time-invariant systems, the time origin t_0 is not important. For convenience, we can shift the origin to $t = 0$.

Consider a system to have input r and output y; suppose further that with the system at rest (relaxed system) at $t = 0$, we apply the input $r_1(t)$; $t \geq 0$, and observe the output $y_1(t)$; $t > 0$. After restoring the system to rest, we apply a second input $r_2(t)$; $t \geq 0$ and again observe the output, which we will call $y_2(t)$; $t > 0$. Then we form a composite input $r(t) = \alpha_1 r_1(t) + \alpha_2 r_2(t)$; $t \geq 0$, where α_1 and α_2 are real numbers. If *superposition* applies, then the response of the relaxed system to input $r(t)$ will be $y(t) = \alpha_1 y_1(t) + \alpha_2 y_2(t)$; $t \geq 0$. Superposition will apply if and only if the system is *linear*. Linear systems have the *decomposition* property which says that the response of a system to the input r starting in an energy state given by a set of initial conditions at $t = 0$ is identical with the *zero-input* response ($r = 0$) of the system starting in the given energy state plus the *zero-state response* (system at rest at $t = 0$) of the system to input r. A sufficient condition for linearity is that both the components of the response satisfy superposition property.

Powerful mathematical tools that provide general methods of analysis and design are available for linear systems. For *nonlinear* systems, general methods are not available and each system must be studied as one of a kind. Practically none of the systems is completely linear, but a linear model is often appropriate over certain ranges of operation. Linearization over desired ranges of operation is usually possible and we will mostly employ linear models for systems with nonlinearities. For situations where this approximation becomes too crude to be employed and/or nonlinearities are deliberately introduced, mathematical tools such as Lyapunov stability analysis, describing function method and the phase-plane method may be employed (refer Chapter 14).

In this book, we will be mainly concerned with linear, time-invariant, lumped systems. Application of physical laws to such a system, as we shall see in this chapter, results in a set of ordinary differential equations which directly provide us with the rates of change of significant variables characterizing the dynamics of the system. These differential equations when rearranged in the form of a set of first-order differential equations,

are called *state equations*. Laplace transformation of these differential equations with zero initial conditions gives us *transfer function* representation.

Through the examples given in this chapter, it will become clear that to obtain a transfer function model, one first writes the state equations of the system which 'naturally' arise from the application of physical laws. State variable modelling is thus a 'natural' step required for transfer function modelling.

State variable analysis and design methods use the matrix theory and are, to some extent, different from those based on transfer function models. We have separated state variable methods from those based on transfer functions. State variable methods are covered in Chapters 12 – 13 while the rest of the book uses the transfer function approach.

The presence of disturbances is one of the main reasons for using feedback control. Without disturbances, there is probably no need for feedback control. The character of the disturbances imposes fundamental limitations on the performance of a control system.

The disturbances may be classified as load disturbances, measurement errors, and parameter variations. *Load disturbances* are external disturbances from the process environment which influence the process variables. *Measurement errors* enter through the measuring instruments (sensors). Disturbances also enter in the form of *variations in the parameters* due to wear and tear, ageing, environmental effects, etc., or due to unmodelled dynamics. In Chapter 4, we will study the effects of these disturbances on control system performance.

In the present chapter, simple yet effective models of load disturbances are given. Transfer functions of disturbance variables (uncontrolled inputs) on the output variables of industrial plants have been derived for commonly occurring load disturbances.

A review of the study of dynamic response of linear time-invariant systems using Laplace transforms has also been given in this chapter.

2.2 STATE VARIABLE MODELS

In this and the next five sections, three different forms of mathematical models for linear time-invariant lumped systems will be introduced. Depending upon the requirements of analysis or the design techniques used, one form of model might be preferable to another in describing the same system. Since we study only time-invariant systems, we shall assume, without loss of generality, that the initial time is zero ($t_0 = 0$) and that the time interval of interest is $[0, \infty)$, i.e., $\{0 \le t < \infty\}$.

Consider the resistance-inductance-capacitance (RLC) network shown in Fig. 2.2. The input is a voltage source. The desired output information is usually the voltages and currents associated with various elements of the network. This information at time t can be obtained if the voltage across the capacitor and the current through the inductor of the network at that time are known, in addition to the values of the input. The voltage $e(t)$ across the capacitor and the current $i(t)$ through the inductor thus constitute a set of *characterizing variables* of the network. The selection of characterizing variables is linked with the energy concept. At time t, energy stored in the capacitor is $\frac{1}{2} Ce^2(t)$ and energy stored in the inductor is $\frac{1}{2} Li^2(t)$. Dynamical changes in characterizing variables are caused by the redistribution of energy within the network. The number of independent energy storage possibilities thus equals the number of characterizing variables of the network. The values of the characterizing variables at time t describe the *state* of the network at that time; these variables are therefore called *state variables* of the network.

Network analysis usually requires setting up of dynamical equations (using Kirchhoff's voltage and current laws) in terms of rates of change of capacitor voltages and inductor currents. The solution of these equations describes the state of the network at time t. The desired output information is then obtained from the state using an algebraic relation.

Let us set up dynamical equations for the RLC network of Fig. 2.2, by using Kirchhoff's voltage law. The governing equations of the system are

$$R\,i(t) + e(t) + L\,\frac{di(t)}{dt} = e_i(t);\; C\,\frac{de(t)}{dt} = i(t)$$

Rearrangement of these equations gives the rates of change of capacitor voltage and inductor current.

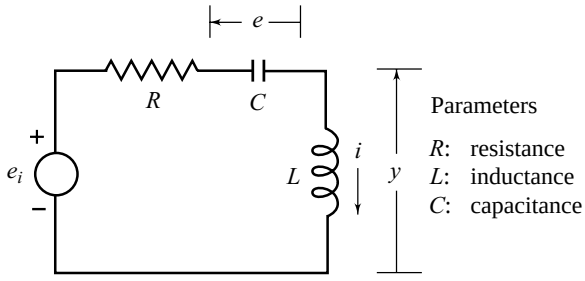

Fig. 2.2 An RLC network

$$\left.\begin{aligned}\frac{de(t)}{dt} &= \frac{1}{C}\,i(t)\\ \frac{di(t)}{dt} &= -\frac{1}{L}\,e(t) - \frac{R}{L}\,i(t) + \frac{1}{L}\,e_i(t)\end{aligned}\right\} \tag{2.1a}$$

The solution of these equations for the given input $e_i(t)$ applied at $t = 0^+$, and the given initial state $\{e(0), i(0)\}$ yields the state $\{e(t), i(t)\}$, $t > 0$. If $y(t)$ shown in Fig. 2.2 is the desired output information, we have the following algebraic relation to obtain $y(t)$:

$$y(t) = -e(t) - R\,i(t) + e_i(t) \tag{2.1b}$$

Equations (2.1a) give the rates of change of state variables (capacitor voltage $e(t)$, and inductor current $i(t)$) in terms of the state variables and the input. These equations are called the *state equations*. Equation (2.1b) is an instantaneous relation, reading output $y(t)$ from the state variables $\{e(t), i(t)\}$ and the input $e_i(t)$. This equation is called the *output equation*.

It may be noted that the state of a system is not uniquely specified. For the network of Fig. 2.2, the charge $q(t)$ deposited on the capacitor is given by

$$q(t) = C\,e(t)$$

Therefore, the variables $q(t)$ and $i(t)$ also qualify as state variables for this network.

In terms of these state variables, the state and output equations are given below:

$$\left.\begin{aligned}\frac{dq(t)}{dt} &= i(t)\\ \frac{di(t)}{dt} &= -\frac{1}{LC}\,q(t) - \frac{R}{L}\,i(t) + \frac{1}{L}\,e_i(t)\end{aligned}\right\} \tag{2.2a}$$

$$y(t) = -\frac{1}{C}\,q(t) - R\,i(t) + e_i(t) \tag{2.2b}$$

In mass-spring-damper systems, we are usually interested in the displacements, velocities, and forces associated with various elements of the systems. Normally, an independent set of displacements and velocities of the masses, and displacements of the springs constitutes a set of state variables of the system. The values of these variables at time t describe the status of energy storage elements at that time, and also ensure that the desired output information can be 'read' from the state variables.

For the mass-spring-damper system of Fig. 2.3a, the displacement $x(t)$ and velocity $v(t)$ are state variables. A systematic way of setting up dynamical equations for mass-spring-damper systems is to draw a free-body diagram. In a free-body diagram, each mass is isolated from the rest of the system; forces acting on each free-body are due to the rest of the system, including external forces. The free-body mass moves under the

action of the resultant force. By applying Newton's law of motion to each free-body, we get the force equations describing the dynamics of the system.

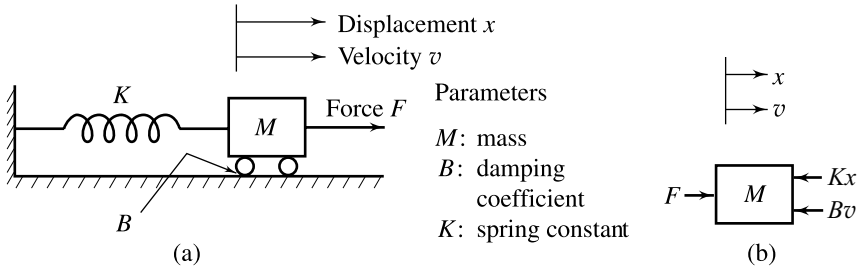

Fig. 2.3 (a) A mass-spring-damper system (b) Free-body diagram

Figure 2.3b shows the free-body diagram of the system of Fig. 2.3a. Applying Newton's law of motion, the force equation can be written as

$$F(t) - B\,v(t) - K\,x(t) = M\,\frac{dv(t)}{dt}$$

Since $v(t) \triangleq \dfrac{dx(t)}{dt}$, we have

$$M\frac{d^2x(t)}{dt^2} + B\frac{dx(t)}{dt} + K\,x(t) = F(t)$$

Rearrangement of these equations gives the rates of change of displacement $x(t)$ and velocity $v(t)$:

$$\left.\begin{aligned} \frac{dx(t)}{dt} &= v(t) \\ \frac{dv(t)}{dt} &= -\frac{K}{M}x(t) - \frac{B}{M}v(t) + \frac{1}{M}F(t) \end{aligned}\right\} \qquad (2.3a)$$

The solution of these equations for given input (force $F(t)$) applied at $t = 0^+$ and given initial state $\{x(0), v(0)\}$ yields the state $\{x(t), v(t)\}$, $t > 0$. If displacement of the mass is the desired output $y(t)$, we have the output equation

$$y(t) = x(t) \qquad (2.3b)$$

Consider now the general SISO system shown in the block diagram of Fig. 2.4a. We will denote the system *state* by *n state variables* $\{x_1(t), x_2(t), \ldots, x_n(t)\}$. In compact notation, this information may be represented by the *state vector*

$$\mathbf{x}(t) \triangleq \begin{bmatrix} x_1(t) \\ x_2(t) \\ \vdots \\ x_n(t) \end{bmatrix}$$

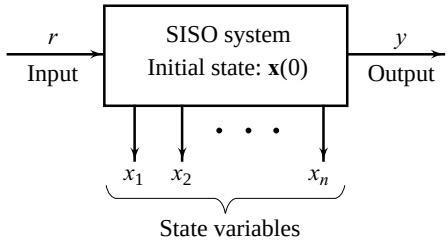

Fig. 2.4a A SISO system

The dimension of the state vector defines the *order of the system*.

The set of equations that describe the relationship among input, output, and the state variables, is called the *state variable model*. For *n*th-order linear time-invariant system, the state variable model takes the form (refer Eqns. (2.1), (2.2), (2.3)):

$$\left.\begin{aligned}
\dot{x}_1(t) \triangleq \frac{dx_1(t)}{dt} &= a_{11}\,x_1(t) + a_{12}\,x_2(t) + \cdots + a_{1n}\,x_n(t) + b_1\,r(t)\\
\dot{x}_2(t) \triangleq \frac{dx_2(t)}{dt} &= a_{21}\,x_1(t) + a_{22}\,x_2(t) + \cdots + a_{2n}\,x_n(t) + b_2\,r(t)\\
&\vdots\\
\dot{x}_n(t) \triangleq \frac{dx_n(t)}{dt} &= a_{n1}\,x_1(t) + a_{n2}\,x_2(t) + \cdots + a_{nn}\,x_n(t) + b_n\,r(t)\\
y(t) &= c_1\,x_1(t) + c_2\,x_2(t) + \cdots + c_n\,x_n(t) + d\,r(t)
\end{aligned}\right\}$$

or in vector-matrix[1] form

$$\dot{\mathbf{x}}(t) = \mathbf{A}\mathbf{x}(t) + \mathbf{b}\,r(t) : \textit{state equation} \tag{2.4a}$$

$$y(t) = \mathbf{c}\mathbf{x}(t) + d\,r(t) : \textit{output equation} \tag{2.4b}$$

with

$$\mathbf{x}(t) = \begin{bmatrix} x_1(t) \\ x_2(t) \\ \vdots \\ x_n(t) \end{bmatrix};\ \mathbf{A} = \begin{bmatrix} a_{11} & a_{12} & \cdots & a_{1n} \\ a_{21} & a_{22} & \cdots & a_{2n} \\ \vdots & \vdots & & \vdots \\ a_{n1} & a_{n2} & \cdots & a_{nn} \end{bmatrix};\ \mathbf{b} = \begin{bmatrix} b_1 \\ b_2 \\ \vdots \\ b_n \end{bmatrix};\ \mathbf{c} = [c_1\ c_2\ \cdots\ c_n]$$

where $\mathbf{x}(t)$, $r(t)$ and $y(t)$ are, respectively, the state, the input and the output of a system; $\mathbf{A}$ is $n \times n$ constant matrix; $\mathbf{b}$ is $n \times 1$ constant column vector; $\mathbf{c}$ is $1 \times n$ constant row vector; and d is a constant scalar representing direct coupling between input and output.

Equations (2.4a) are n first-order differential equations expressing time derivatives of each of the components of the state vector $\mathbf{x}(t)$ as a linear combination of system states and input. The solution of these equations for given input $r(t)$ applied at $t = 0^+$, and given initial state $\mathbf{x}(0)$ yields the system state $\mathbf{x}(t)$, $t > 0$. The output $y(t)$ (Eqn. (2.4b)) is a linear combination of system states and input.

Equations (2.4a) and (2.4b) together provide the input-output-state description of a dynamic system, represented diagrammatically in Fig. 2.4b. Note that in this model structure, the dynamic evolution of system state in response to initial state $\mathbf{x}(0)$ and input $r(t)$ is obtained; desired output information $y(t)$ is then 'read' from $\mathbf{x}(t)$.

The general MIMO system is shown in the block diagram of Fig. 2.5. Time functions, r_1, r_2, ..., r_p are the input variables, and y_1, y_2, ..., y_q are the output variables. The state, as in the case of SISO systems, is represented by the variables x_1, x_2, ..., x_n. For notational economy, the different

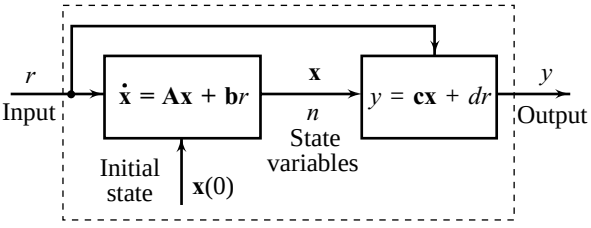

Fig. 2.4b Input-output-state description

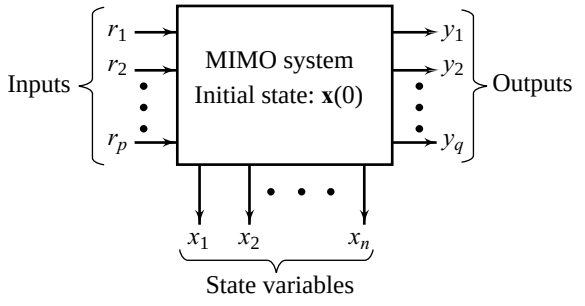

Fig. 2.5 A MIMO system

[1] We will use lower case bold letters to represent vectors, and upper case bold letters to represent matrices.

variables may be represented by the input vector $\mathbf{r}(t)$, the output vector $\mathbf{y}(t)$, and the state vector $\mathbf{x}(t)$, where

$$\mathbf{r}(t) = \begin{bmatrix} r_1(t) \\ r_2(t) \\ \vdots \\ r_p(t) \end{bmatrix}; \mathbf{y}(t) = \begin{bmatrix} y_1(t) \\ y_2(t) \\ \vdots \\ y_q(t) \end{bmatrix}; \mathbf{x}(t) = \begin{bmatrix} x_1(t) \\ x_2(t) \\ \vdots \\ x_n(t) \end{bmatrix}$$

For MIMO systems, the derivative of each state variable becomes a linear combination of system states $x_1, x_2, \ldots, x_n$, and the inputs $r_1, r_2, \ldots, r_p$. Also, each output variable at time t is a linear combination of the states and the inputs at time t. The state variable model for MIMO systems takes the following form:

$$\dot{\mathbf{x}}(t) = \mathbf{A}\mathbf{x}(t) + \mathbf{B}\mathbf{r}(t) : \textit{state equation} \tag{2.5a}$$

$$\mathbf{y}(t) = \mathbf{C}\mathbf{x}(t) + \mathbf{D}\mathbf{r}(t) : \textit{output equation} \tag{2.5b}$$

with

$$\mathbf{A} = \begin{bmatrix} a_{11} & a_{12} & \cdots & a_{1n} \\ a_{21} & a_{22} & \cdots & a_{2n} \\ \vdots & \vdots & & \vdots \\ a_{n1} & a_{n2} & \cdots & a_{nn} \end{bmatrix}; \mathbf{B} = \begin{bmatrix} b_{11} & b_{12} & \cdots & b_{1p} \\ b_{21} & b_{22} & \cdots & b_{2p} \\ \vdots & \vdots & & \vdots \\ b_{n1} & b_{n2} & \cdots & b_{np} \end{bmatrix}; \mathbf{C} = \begin{bmatrix} c_{11} & c_{12} & \cdots & c_{1n} \\ c_{21} & c_{22} & \cdots & c_{2n} \\ \vdots & \vdots & & \vdots \\ c_{q1} & c_{q2} & \cdots & c_{qn} \end{bmatrix}; \mathbf{D} = \begin{bmatrix} d_{11} & d_{12} & \cdots & d_{1p} \\ d_{21} & d_{22} & \cdots & d_{2p} \\ \vdots & \vdots & & \vdots \\ d_{q1} & d_{q2} & \cdots & d_{qp} \end{bmatrix}$$

A, **B**, **C** and **D** are respectively. $n \times n$, $n \times p$, $q \times n$ and $q \times p$ constant matrices.

Since every real-world system has some nonlinearity, a mathematical model of the form (2.5) is always an approximation to reality. Many real-world nonlinearities involve a 'smooth' curvilinear relation between an independent variable x and a dependent variable y:

$$y = f(x) \tag{2.6a}$$

A linear approximation to the curve, accurate in the neighbourhood of selected operating point x_0, is the tangent line to the curve at that point. This approximation is given conveniently by the first two terms of the Taylor series expansion of $f(x)$:

$$y = f(x_0) + \left[\frac{df}{dx}\bigg|_{x=x_0}\right](x - x_0) + \left[\frac{d^2 f}{dx^2}\bigg|_{x=x_0}\right]\frac{(x - x_0)^2}{2!} + \cdots$$

The linear approximation is

$$y \cong f(x_0) + \left[\frac{df}{dx}\bigg|_{x=x_0}\right](x - x_0) \tag{2.6b}$$

When a dependent variable y is related nonlinearly to several independent variables x_1, x_2, x_3, etc., according to

$$y = f(x_1, x_2, x_3, \ldots) \tag{2.6c}$$

we may linearize using the multivariable form of the Taylor series:

$$y \cong f(x_{10}, x_{20}, \ldots) + \left[\frac{\partial f}{\partial x_1}\bigg|_{x_{10}, x_{20}, \ldots}\right](x_1 - x_{10}) + \left[\frac{\partial f}{\partial x_2}\bigg|_{x_{10}, x_{20}, \ldots}\right](x_2 - x_{20}) + \cdots \tag{2.6d}$$

We will use the linearizing approximations in developing linear state variable models of the form (2.5) from nonlinear relationships of the form given below:

$$\left.\begin{aligned}
\dot{x}_1(t) &= f_1(x_1(t), x_2(t), \ldots, x_n(t), r_1(t), \ldots, r_p(t)) \\
\dot{x}_2(t) &= f_2(x_1(t), x_2(t), \ldots, x_n(t), r_1(t), \ldots, r_p(t)) \\
&\vdots \\
\dot{x}_n(t) &= f_n(x_1(t), x_2(t), \ldots, x_n(t), r_1(t), \ldots, r_p(t))
\end{aligned}\right\} \quad (2.7a)$$

$$\left.\begin{aligned}
y_1(t) &= g_1(x_1(t), x_2(t), \ldots, x_n(t), r_1(t), \ldots, r_p(t)) \\
&\vdots \\
y_q(t) &= g_q(x_1(t), x_2(t), \ldots, x_n(t), r_1(t), \ldots, r_p(t))
\end{aligned}\right\} \quad (2.7b)$$

where $f_i(\cdot)$, $i = 1, 2, \ldots, n$ are nonlinear functions describing state equations,
and $g_j(\cdot)$, $j = 1,2, \ldots, q$ are nonlinear functions describing output equations.

2.3 IMPULSE RESPONSE MODELS

Consider the SISO system of Fig. 2.3. The system is excited by two types of inputs; the external input $r(t)$, and the initial state $\mathbf{x}(0)$ representing initial energy storage in the system. The response variables are the state variables $x_1(t), x_2(t), \ldots, x_n(t)$, and the output variable $y(t)$.

In this section, we derive a mathematical model based on the following assumptions/requirements (Fig. 2.6):

(i) Initial state $\mathbf{x}(0) = \mathbf{0}$, i.e., the output $y(t)$ is solely and uniquely excited by the input $r(t)$ for $t \geq 0$.
A system is said to be *relaxed*[2] at $t_0 = 0$, if $\mathbf{x}(0) = \mathbf{0}$.

(ii) We are interested only in the input–output relation; dynamic evolution of the state $\mathbf{x}(t)$ is not required.

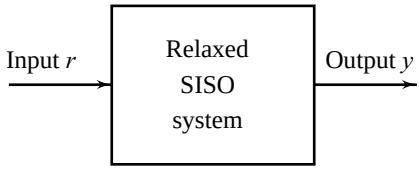

Fig. 2.6 Input–output description

The input $r(t)$ and the output $y(t)$ of any linear time-invariant system that is initially relaxed at $t_0 = 0$, can be described by an equation of the form

$$y(t) = \int_0^t g(t-\tau)\, r(\tau)\, d\tau = \int_0^t g(\tau)\, r(t-\tau)\, d\tau \quad (2.8)$$

This is called a *convolution integral*. The second integration is obtained from the first by substituting $\tau' = t - \tau$, and then changing the dummy variable τ' to τ. The function $g(t)$ is defined only for $t \geq 0$ and is called the *impulse response* of the system. In order to derive Eqn. (2.8) and give an interpretation of $g(t)$, we need the concept of impulse function.

A rectangular elementary *pulse function* is defined as

$$p_T(t) = \begin{cases} 1 & \text{for } 0 < t < T \\ 0 & \text{otherwise} \end{cases} \quad (2.9a)$$

Figure 2.7 gives the graphical representation of pulse functions.

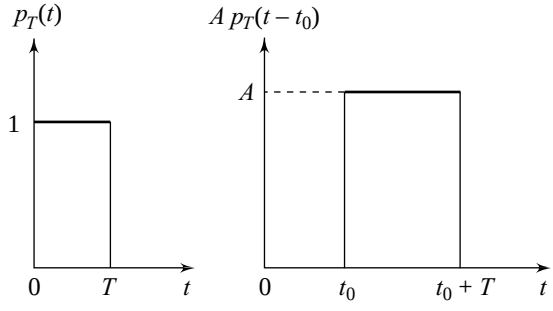

Fig. 2.7 Pulse functions

[2]The case of zero initial conditions is common in control system design because the signals are usually defined as deviations from some initial steady-state. When this is done, the initial value of the perturbation is, by definition, zero.

$A\,p_T(t-t_0)$ is a pulse of height A and duration T occurring at $t = t_0$:

$$A\,p_T(t-t_0) = \begin{cases} A & \text{for } 0 < (t-t_0)\,t < T \\ 0 & \text{otherwise} \end{cases} \tag{2.9b}$$

Consider the *unit pulse function* $\delta_\Delta(t) = \dfrac{1}{\Delta}\,p_\Delta(t)$ (2.10)

It is a pulse of height $\dfrac{1}{\Delta}$ and duration Δ (i.e., of unit 'area') occurring at $t = 0$.

The properties of $\delta_\Delta(t)$ are such that its height increases whenever its duration decreases, but in such a way that its 'area' thereby remains constant and is equal to unity.

As $\Delta \to 0$, we obtain the limiting 'function'

$$\delta(t) \triangleq \lim_{\Delta\to 0} \delta_\Delta(t) \tag{2.11}$$

which is called the *unit impulse function* or *δ-function*.

Properties of the δ-function are:

$$\delta(t) = \lim_{\Delta\to 0} \delta_\Delta(t) = \begin{cases} 0 & for\ t \neq 0 \\ \infty & for\ t = 0 \end{cases} \tag{2.12a}$$

$$\int_{-\infty}^{\infty} \delta(t)dt = \int_{-\infty}^{\infty} \lim_{\Delta\to 0} \delta_\Delta(t)dt = 1 \tag{2.12b}$$

From these properties it follows that $\delta(t)$ is not an ordinary function as we cannot assign a value to the dependent variable for each value of the independent variable. The quantitative characteristic of $\delta(t)$ does not lie in its amplitudes but is given solely by its 'area'. Consequently, $\delta(t)$ is not defined in the ordinary sense but $\int_{-\infty}^{\infty} \delta(t)dt$ is defined; $\delta(t)f(t)$ is not defined but $\int_{-\infty}^{\infty} \delta(t)f(t)dt$ is defined:

$$\int_{-\infty}^{\infty} \delta(t)f(t)dt = \int_{-\infty}^{\infty} \lim_{\Delta\to 0} \delta_\Delta(t)f(t)dt = \lim_{\Delta\to 0} \int_{-\infty}^{\infty} \frac{1}{\Delta}\,p_\Delta(t)f(t)dt = \lim_{\Delta\to 0} \frac{1}{\Delta} \int_0^{\Delta} f(t)dt$$

$$= f(0), \text{ assuming } f(t) \text{ is continuous at } t = 0 \tag{2.13}$$

Figure 2.8 gives the graphical representation of impulse functions. The definition of impulse $\delta(t - t_0)$ occurring at $t = t_0$ is based on the following properties.

$$\left.\begin{aligned} &\text{(i)} \quad \int_{-\infty}^{\infty} \delta(t-t_0)dt = 1 \\ &\text{(ii)} \quad \int_{-\infty}^{\infty} f(t)\delta(t-t_0)dt = f(t_0), \\ &\quad \text{for any } f(t) \text{ that is continuous at } t = t_0 \end{aligned}\right\} \tag{2.14}$$

$A\delta(t - t_0)$ is an impulse of 'area' A (strength A) occurring at $t = t_0$.

We can now derive Eqn. (2.8). An input function $r(t)$ can easily be approximated by a train of pulses as shown

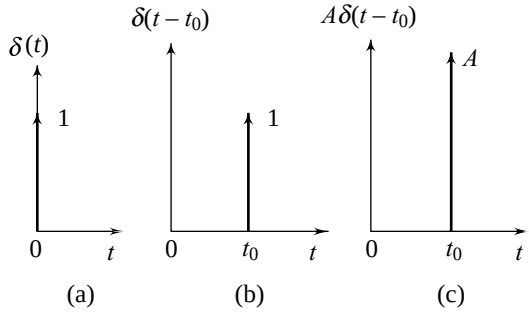

Fig. 2.8 Impulse functions

in Fig. 2.9. It is convenient to take a uniform pulse width Δ for the pulse train. In the light of description of a pulse given by Eqns. (2.9)–(2.10), we can express $r(t)$ as

$$r(t) \cong \sum_{i=0}^{\infty} r(i\Delta)\, p_\Delta(t - i\Delta) \cong \sum_{i=0}^{\infty} r(i\Delta)\, \delta_\Delta(t - i\Delta)\Delta \tag{2.15}$$

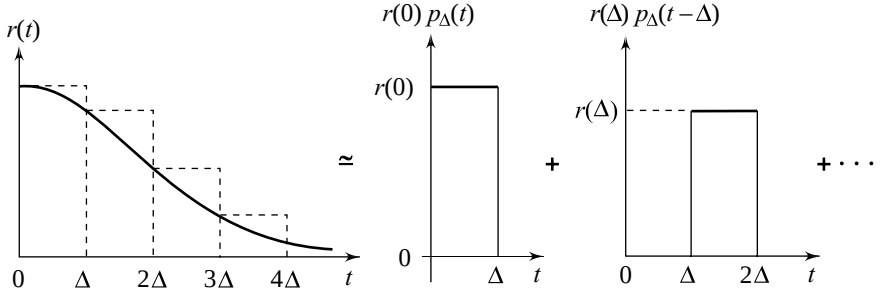

Fig. 2.9 Resolution of a function

Now if the output of the linear time-invariant system due to the input $\delta_\Delta(t)$ is denoted by $g_\Delta(t)$, then the properties of linearity and time-invariance imply that the output of the system due to $r(t)$ is given by

$$y(t) \cong \sum_{i=0}^{\infty} r(i\Delta) g_\Delta(t - i\Delta)\Delta \tag{2.16}$$

As we allow $\Delta \to 0$, the pulse function becomes an impulse function, number of impulses grow so that $(i\Delta)$ becomes a continuous variable τ, and the sum in Eqn. (2.16) approaches an integral. The output $y(t)$ resulting from an input $r(t)$ is thus

$$y(t) = \int_0^{\infty} r(\tau)\, g(t - \tau) d\tau \tag{2.17}$$

where

$$g(t) \overset{\Delta}{=} \lim_{\Delta \to 0} g_\Delta(t) \tag{2.18}$$

is the response of the system to unit impulse input applied at $t = 0$.

Hence the function $g(t)$ is called the *impulse response* of the system. Since $g(t - \tau)$ is the response due to an input applied at $t = \tau$, it is not defined for $t < \tau$;

$$g(t - \tau) = 0, \text{ for } t < \tau \tag{2.19}$$

On the basis of this property, Eqn. (2.17) reduces to

$$y(t) = \int_0^{t} g(t - \tau) r(\tau) d\tau$$

Equation (2.8) is thus proved.

A very important property of the impulse response model is that it can be obtained from the input and output terminals of a system even if the system's internal structure is not known. If the system is known to be linear, time-invariant, and relaxed at $t = 0$, then by applying $\delta_\Delta(t)$ function at the input terminal, the response at the output terminal gives us immediately the impulse response (approximate one; goodness of approximation is dependent on Δ) of the system. If the impulse response is known, the output of the system due to any input can be computed from Eqn. (2.8).

We now transform $r(t)$ and $g(t)$ using the mapping[3]

$$f(t) \rightarrow F(s) \tag{2.20}$$

where

$$F(s) \triangleq \int_0^\infty f(t)e^{-st}\,dt\,;t>0,\ s = \text{a complex variable} = \sigma + j\omega;\ j \triangleq \sqrt{-1} \tag{2.21}$$

The application of this mapping to Eqn. (2.8) yields

$$Y(s) = \int_0^\infty y(t)e^{-st}dt = \int_0^\infty \left[\int_0^t g(t-\tau)r(\tau)d\tau\right]e^{-st}dt \tag{2.22}$$

Since $g(t-\tau) = 0$ for $\tau > t$ as implied by Eqn. (2.19), the upper limit of t in Eqn.(2.22) can be set at ∞:

$$Y(s) = \int_0^\infty \left[\int_0^\infty g(t-\tau)r(\tau)d\tau\right]e^{-st}dt$$

Changing the order of integrations, gives

$$Y(s) = \int_0^\infty \left[\int_0^\infty g(t-\tau)e^{-st}dt\right]r(\tau)d\tau = \int_0^\infty \left[\int_0^\infty g(t-\tau)e^{-s(t-\tau)}dt\right]e^{-s\tau}r(\tau)d\tau$$

which, if we substitute $\theta = t - \tau$, can be expressed as

$$Y(s) = \int_0^\infty \left[\int_{-\tau}^\infty g(\theta)e^{-s\theta}d\theta\right]e^{-s\tau}r(\tau)d\tau$$

Using the fact that $g(\theta) = 0$ for $\theta < 0$, we obtain

$$Y(s) = \int_0^\infty \left[\int_0^\infty g(\theta)e^{-s\theta}d\theta\right]e^{-s\tau}r(\tau)d\tau = \left[\int_0^\infty g(\theta)e^{-s\theta}d\theta\right]\left[\int_0^\infty r(\tau)e^{-s\tau}d\tau\right] = G(s)\,R(s) \tag{2.23}$$

where

$$R(s) = \int_0^\infty r(t)e^{-st}\,dt \text{ and } G(s) = \int_0^\infty g(t)e^{-st}\,dt$$

We see that by applying the mapping (2.21), a convolution integral is transformed into an algebraic equation.

The mapping (2.21) is, in fact, the definition of *Laplace transform*[4].

2.4 THE LAPLACE TRANSFORM

The Laplace transform is a technique of expressing a signal $f(t)$ as a continuous sum of exponential functions of the form e^{st} with $s = \sigma + j\omega; j \triangleq \sqrt{-1}$.

Recall the mapping (2.21) introduced in the previous section:

[3]It is conventional to use capital letters for s-functions and lower case for t-functions. Our notation mostly follows this convention.

[4]We assume that the reader has had a previous introduction to the theory of Laplace transforms. The next section provides a brief review of the Laplace transform techniques, adequate for the purposes of this text.

$$f(t) \rightarrow F(s); f(t) = 0 \text{ for } t < 0$$

where
$$F(s) = \int_0^\infty f(t)e^{-st}dt;\ t > 0 \tag{2.24}$$

This mapping, in fact, defines the Laplace transform of $f(t)$, denoted by $\mathscr{L}[f(t)]$ or $F(s)$, provided the integral exists[64].

The Laplace transform has proven to be a natural and powerful means of analyzing linear time-invariant systems. Most of the physical systems are nonlinear and time-varying in nature; however many of these nonlinear systems have regions of operation in which their behaviour is 'reasonably' linear. Also, their characteristics change very slowly in relation to variations in the inputs. A linear time-invariant model is often appropriate for many physical systems, making them amenable to analysis by techniques such as the Laplace transform. This is fortunate because the analysis techniques available for linear time-invariant systems are much more powerful and general than those that apply to nonlinear/time-varying systems. Thus, being able to make the assumption that a system is linear and time-invariant is crucial.

The class of linear time-invariant systems, as we shall see later in this chapter, can be represented by ordinary differential equations with constant, real coefficients. Application of the Laplace transform turns a differential equation into an algebraic equation that is much easier to manipulate and interpret. The resulting Laplace transforms are ratios of polynomials in s with constant, real coefficients. The benefits of this representation will become clear in subsequent chapters where it leads to graphical techniques for designing compensation (controllers) for systems with feedback.

The condition of existence of integral in Eqn. (2.24) does not turn out to be a matter of great concern because the class of functions that arise in the analysis of linear time-invariant control systems are well behaved and the transform analysis exists. The brief introduction to the theory of Laplace transforms given in this chapter provides the working tools adequate for the purposes of this text.

Before proceeding, it is worth making sure that the nature of the mapping (2.24) is fully understood. The Laplace transform variable s is a complex variable:

$$\text{Re}(s) + j\ \text{Im}(s) = s = \sigma + j\omega;\ j \triangleq \sqrt{-1} \tag{2.25}$$

For a fixed value of σ, the locus of s is a vertical line in the complex s-plane (Fig. 2.10a). The vertical line corresponding to $\sigma = 0$ in the complex s-plane (Fig. 2.10b) will be of specific interest to us. This line is the *imaginary axis* of the s-plane.

Very often, Laplace transforms given by (2.24) work out as the ratio of two constant-coefficient polynomials of the form:

$$F(s) = \frac{b_0 s^m + b_1 s^{m-1} + \cdots + b_m}{s^n + a_1 s^{n-1} + \cdots + a_n};\ m \le n \tag{2.26a}$$

where all the a_i, and b_j are real.

The Laplace transform *zeros* are the values of s for which the transform is zero. The zeros are found by setting the numerator polynomial to 0 and solving the resulting equation. The Laplace transform *poles* are the values of s for which the transform is infinite. The poles are found by setting the denominator polynomial to 0 and solving the resulting equation. The *degree* of denominator polynomial is given by integer n, and that of the numerator is given by integer m.

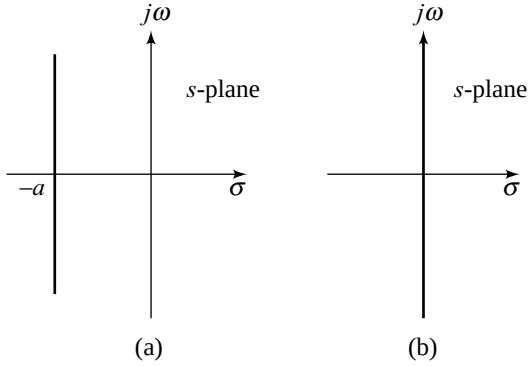

Fig 2.10 The complex s-plane

The fact that the coefficients a_i, and b_j are real guarantees that the roots of the denominator and numerator polynomials of $F(s)$ will be either real or complex-conjugate pairs. Under these conditions, we can write

$$F(s) = \frac{K\prod_{i=1}^{m}(s+z_i)}{\prod_{i=1}^{n}(s+p_i)}\ ;\ m \le n \tag{2.26b}$$

where zeros $s = -z_i$ and poles $s = -p_i$ are either real or complex-conjugate pairs; K is a constant.

To see the nature of mapping (2.24), we consider the function

$$f(t) = \begin{cases} e^{-at} & \text{for } t \ge 0 \\ 0 & \text{for } t < 0 \end{cases} \tag{2.27}$$

For this function,

$$F(s) = \int_0^\infty e^{-at}\, e^{-st} dt = \int_0^\infty e^{-(s+a)}\, dt = \frac{-1}{s+a}\left[e^{-(s+a)t}\right]_{t=0}^{t=\infty} = \frac{1}{s+a}\left[1 - \lim_{t\to\infty} e^{-(s+a)t}\right] \tag{2.28a}$$

$$\lim_{t\to\infty} e^{-(s+a)t} = \lim_{t\to\infty} e^{-(\sigma+j\omega+a)t} = \lim_{t\to\infty} e^{-(\sigma+a)t}\, e^{-j\omega t} \tag{2.28b}$$

The term

$$e^{-j\omega t} = \cos\omega t - j\sin\omega t$$

will not approach a limit as $t \to \infty$. Therefore for the limit in (2.28b) to exit, the term $e^{-(\sigma+a)t}$ must approach the limit zero as $t \to \infty$. This will be true only if

$$-(\sigma + a) < 0$$

or equivalently

$$\sigma > -a \tag{2.29a}$$

Thus for $\sigma > -a$, Eqn. (2.28a) gives

$$F(s) = \frac{1}{s+a} \tag{2.29b}$$

The regions of convergence for both $a > 0$ and $a < 0$ are shown in Fig. 2.11. The region is an infinite half plane that lies strictly to the right of the vertical line through $s = -a$. The same result holds if a is complex. For $a = \alpha + j\beta$, the region of convergence is an infinite half plane to the right of the vertical line through $s = -\alpha$.

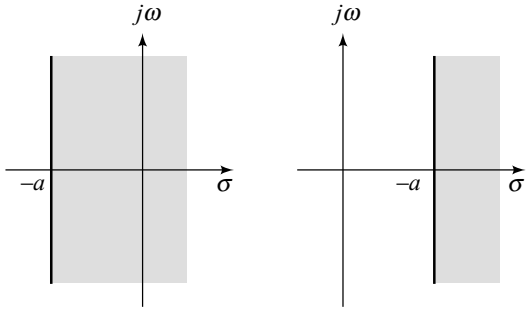

(a) $a > 0$ (b) $a < 0$

Fig 2.11 Region of convergence

2.5 LAPLACE TRANSFORMS OF SIGNALS USEFUL FOR CONTROL SYSTEM ANALYSIS

To motivate the discussion in a control systems context, we revisit the generalized functional block diagram of Fig. 1.9. There are two inputs (external excitations) applied to a control system; a command input $y_r(t)$ (or reference input $r(t)$), and a disturbance input $w(t)$. We will first talk of disturbances.

2.5.1 Simple Models of Disturbances

External disturbances, $w(t)$, are typically the uncontrolled variations in the load on a control system. In systems controlling mechanical motions, load disturbances may represent forces/torques, e.g., wind gusts on

a stabilized antenna (refer Example 1.3), variation in payload of a robot (refer Example 1.8), etc. In voltage regulating systems, variations in electrical load are a major source of disturbances. In thermal systems, the load disturbances may be caused by variations in surrounding temperature (refer Example 1.2). In fluidic systems, the load disturbances may result from variations in feed flow or variations in demanded flow (refer Example 1.5).

Disturbances which are erratic, uncertain signals having no distinguishing waveform properties, are commonly referred to as *noise*. The accommodation of noise in a control problem is best handled by treating the noise as a *stochastic* or *random process*. The general theory of stochastic processes is quite complex, and is beyond the scope of this book.

In this book we consider load disturbances which typically vary slowly. Such disturbances are normally well behaved uncertain signals having distinguishing waveform properties. As we shall see in Chapter 4, the errors due to load disturbances tend to be corrected by proper design of feedback control.

In the following, we consider simple, yet effective, models that characterize commonly occurring disturbances.

Impulse Function The impulse is a simple idealization of sudden disturbances of short duration. A *unit impulse function* is defined as (refer Eqns (2.12)–(2.14))

$$\left.\begin{aligned} \delta(t) &= \begin{cases} 0 & \text{for } t \neq 0 \\ \infty & \text{for } t = 0 \end{cases} \\ \int_{-\infty}^{\infty} \delta(t)\,dt &= 1 \\ \int_{-\infty}^{\infty} f(t)\,\delta(t)\,dt &= f(0) \end{aligned}\right\} \tag{2.30a}$$

It may be symbolically shown as in Fig. 2.12a.

Applying the definition of the Laplace transform yields (refer Eqns (2.9)–(2.11)).

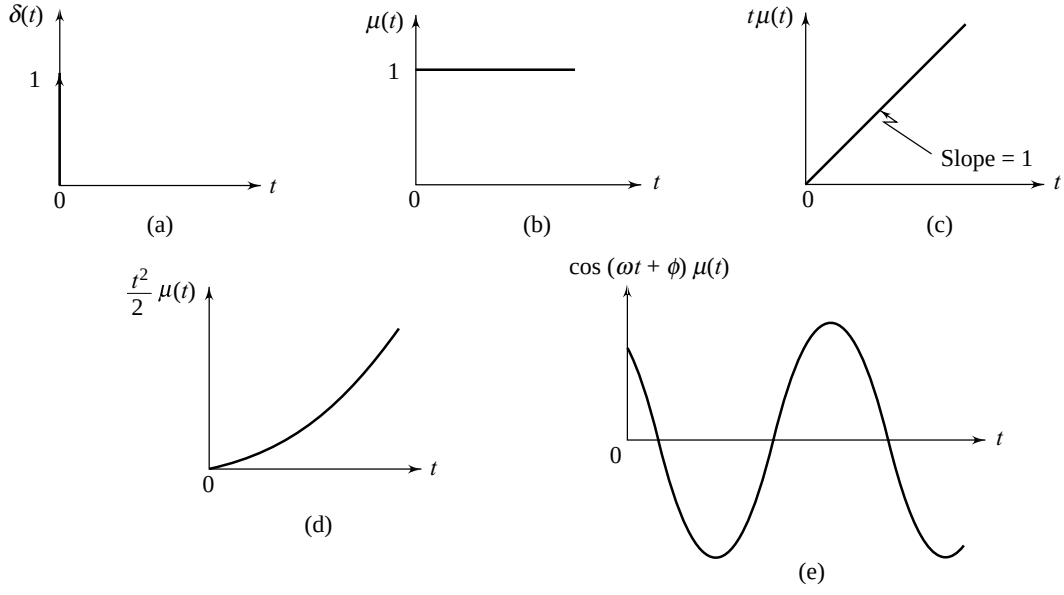

Fig. 2.12 Simple models of disturbances

$$\mathscr{L}[\delta(t)] = \int_0^{\infty} \delta(t)e^{-st}dt = \lim_{\Delta\to 0}\int_0^{\Delta} \frac{1}{\Delta}e^{-st}dt = \lim_{\Delta\to 0}\frac{-1}{\Delta s}\left[e^{-st}\right]\Big|_{t=0}^{t=\Delta} = \lim_{\Delta\to 0}\frac{1-e^{-\Delta s}}{\Delta s}$$

This expression can be evaluated by treating numerator and denominator as functions of Δ and applying L Hospital's rule to obtain:

$$\lim_{\Delta\to 0}\frac{1-e^{-\Delta s}}{\Delta s} = \lim_{\Delta\to 0}\frac{\frac{d}{d\Delta}(1-e^{-\Delta s})}{\frac{d}{d\Delta}(\Delta s)} = \lim_{\Delta\to 0}\frac{se^{-\Delta s}}{s} = 1$$

Therefore

$$\mathscr{L}[\delta(t)] = 1 \tag{2.30b}$$

Step Function A step signal is another prototype for a disturbance. It is typically used to represent a sudden jump in the magnitude of otherwise constant (slowly varying) disturbances. A *unit step function*[5] (Fig. 2.12b)

$$\mu(t) = \begin{cases} 1 & \text{for } t > 0 \\ 0 & \text{otherwise} \end{cases} \tag{2.31a}$$

Applying the Laplace transform to the unit step yields

$$\mathscr{L}[\mu(t)] = \int_0^{\infty} e^{-st}dt = \frac{-1}{s}\left[e^{-st}\right]\Big|_{t=0}^{t=\infty} = \frac{1}{s}\left[1-\lim_{t\to\infty}e^{-st}\right] = \frac{1}{s} \tag{2.31b}$$

where $\lim_{t\to\infty} e^{-st} = 0$ if $\mathrm{Re}(s) = \sigma > 0$. Thus, the region of convergence is the open half plane to the right of the $j\omega$ axis (refer Fig. 2.11).

Ramp Function *A unit ramp function* (Fig. 2.12c) is defined as

$$w(t) = \begin{cases} t & \text{for } t > 0 \\ 0 & \text{otherwise} \end{cases} \tag{2.32a}$$

or simply

$$w(t) = t\mu(t) \tag{2.32b}$$

Given that the Laplace transform of $f(t)$ is known, it is easy to find the transform of $tf(t)$:

$$\frac{d}{ds}F(s) = \frac{d}{ds}\int_0^{\infty} f(t)e^{-st}\,dt = \int_0^{\infty}\frac{d}{ds}[f(t)e^{-st}]dt = -\int_0^{\infty} tf(t)e^{-st}dt = -\mathscr{L}[tf(t)]$$

Therefore

$$\mathscr{L}[tf(t)] = -\frac{d}{ds}(F(s)) \tag{2.33}$$

Using this result, the Laplace transform of ramp function is easily obtained.

$$\mathscr{L}[t\mu(t)] = -\frac{d}{ds}\left(\frac{1}{s}\right) = \frac{1}{s^2} \tag{2.34}$$

The region of convergence is given by $\mathrm{Re}(s) > 0$.

A ramp function is used to represent disturbances that suddenly start to drift away. In practice, the disturbances are often bounded; however, the ramp is a useful idealization.

[5]Unit step function is generally denoted as $u(t)$ in system theory. However, in control theory, $u(t)$ is commonly used to represent control signal. In this book we will use $u(t)$ for control signal representation, and $\mu(t)$ for unit step function.

Parabolic Function A parabolic function is one degree faster than the ramp function (in practice, we seldom find it necessary to use a signal faster than a parabolic function).

A *unit parabolic function* (Fig. 2.12d) is defined as

$$w(t) = \begin{cases} \dfrac{t^2}{2} & \text{for } t > 0 \\ 0 & \text{othewise} \end{cases} \tag{2.35a}$$

or simply

$$w(t) = \frac{t^2}{2}\,\mu(t) \tag{2.35b}$$

Using the result (2.33), we obtain

$$\mathscr{L}\left[\frac{t^2}{2}\mu(t)\right] = \frac{1}{2}\mathscr{L}[t\{t\mu(t)\}] = -\frac{1}{2}\frac{d}{ds}\left(\frac{1}{s^2}\right) = \frac{1}{s^3} \tag{2.35c}$$

The region of convergence is given by $\mathrm{Re}(s) > 0$.

Note that in deriving this result, we have used the following property of Laplace transforms.

$$\mathscr{L}[k\,f(t)] = k\,\mathscr{L}[\,f(t)]\;;\; k \text{ is a constant} \tag{2.36}$$

Sinusoidal Function The sine wave is a prototype for a periodic disturbance—for example, waves in ship control systems.

Consider a sine wave of unity amplitude and frequency ω (Fig. 2.12*e*):

$$w(t) = \begin{cases} \cos(\omega t + \phi) \text{ for } t \geq 0 \\ 0 \qquad\qquad \text{otherwise} \end{cases} \tag{2.37a}$$

or simply

$$w(t) = \cos(\omega t + \phi\,)\,\mu(t) \tag{2.37b}$$

The transform of sinusoids can be found by expanding the function into complex exponential components.

$$w(t) = \frac{e^{j(\omega t+\phi)} + e^{-j(\omega t+\phi)}}{2};\; j \triangleq \sqrt{-1}$$

To obtain Laplace transform of this function, we will use linearity property of Laplace transforms.

$$\mathscr{L}[k_1 f_1(t) \pm k_2 f_2(t)] = k_1\mathscr{L}[\,f_1(t)] \pm k_2\,\mathscr{L}[\,f_2(t)]; \tag{2.38}$$

k_1 and k_2 are constants.

$$\mathscr{L}[w(t)] = \frac{1}{2}e^{j\phi}\mathscr{L}[e^{j\omega t}] + \frac{1}{2}e^{-j\phi}\mathscr{L}[e^{-j\omega t}] = \frac{\frac{1}{2}e^{j\phi}}{s - j\omega} + \frac{\frac{1}{2}e^{-j\phi}}{s + j\omega} = \frac{s\cos\phi - \omega\sin\phi}{s^2 + \omega^2};\; \mathrm{Re}(s) > 0 \tag{2.39}$$

Given the Laplace transform of $\cos(\omega t + \phi\,)$, we can obtain Laplace transform of $e^{-at}\cos(\omega t + \phi\,)$ as follows.

$$\mathscr{L}[e^{-at} f(t)] = \int_0^\infty e^{-at} f(t) e^{-st} dt = \int_0^\infty f(t) e^{-(s+a)t}\, dt = F(s + a) \tag{2.40}$$

Noting that

$$\mathscr{L}[\cos(\omega t + \phi\,)] = \frac{\frac{1}{2}e^{j\phi}}{s - j\omega} + \frac{\frac{1}{2}e^{-j\phi}}{s + j\omega}$$

we substitute $(s + a)$ for s to obtain the Laplace transform of $e^{-at}\cos(\omega t + \phi)$ as follows:

$$\mathscr{L}[e^{-at}\cos(\omega t + \phi)] = \frac{\frac{1}{2}e^{j\phi}}{s + a - j\omega} + \frac{\frac{1}{2}e^{-j\phi}}{s + a + j\omega} = \frac{(s + a)\cos\phi - \omega\sin\phi}{(s + a)^2 + \omega^2}\ ;\ \mathrm{Re}(s) > -a \qquad (2.41)$$

2.5.2 Standard Test Signals

In addition to the disturbance input, the other excitation signal to a control system is the command input (Fig. 1.9). The command (or reference) signals of some control systems are known to the designer. For example, the command signal of a residential heating system (Example 1.2) is a step function, whose magnitude is the desired temperature. If an antenna is used to track a communication satellite (refer Example 1.3), then the command signal is very close to a ramp function.

In many control systems, however, the command signals are not known fully ahead of time. For instance, in a radar tracking system for military applications (refer Example 1.3), the position and speed of the target to be tracked vary in an unpredictable manner; it is thus difficult to express the actual input signals mathematically by simple functions. The characteristics of actual signals which severely strain a control system are

(i) a sudden shock (modelled by impulse function),
(ii) a sudden change (modelled by step function),
(iii) a linear change with time (modelled by ramp function), and
(iv) faster changes with time (a parabolic function is one degree faster than a ramp function).

System dynamic behaviour can be adequately judged and compared under the application of standard test signals—an impulse input, a step input, a ramp input, and a parabolic input.

Another standard test signal of great importance is the sinusoidal signal. When the response of a linear time-invariant system is analysed in frequency domain, a sinusoidal function with variable frequency is used as input function. Input frequency is swept from zero to beyond the significant range of system characteristics; curves in terms of amplitude ratio and phase between input and output are drawn as functions of frequency. It is possible to predict the time-domain behaviour of the system from the frequency-domain characteristics. We will take up this aspect of control system analysis in Chapters 8 and 9.

We summarize the Laplace transforms we have derived to this point plus some additional transforms in Table 2.1. All the transforms listed in the table can easily be derived from the first principles. It may be noted that in this transform table, regions of convergence have not been specified. In our applications of systems analysis, which involve transformation from time-domain to s-domain and inverse transformation, the variable s acts as a dummy operator. If transform pairs for functions of interest to us are available, we are not concerned with the region of convergence.

2.5.3 Laplace Transform Inversion

A convenient method for obtaining the *inverse Laplace transform of* $Y(s)$ is to use the method of "partial fraction expansion". The idea of this method is to expand $Y(s)$ as a sum of partial fractions, and then find $y(t)$ as the sum of the inverse transforms of the individual members of the partial fraction expansion. The reason this works well is that the Laplace transforms that frequently arise in the study of control systems are ratios of polynomials in s with real coefficients (refer Eqns (2.26)). The fact that the coefficients are real is crucial because it guarantees that the roots of the numerator and denominator polynomials will be either real or complex-conjugate pairs.

This, in turn, means that the individual terms in the partial fraction expansion of the transform will be simple in form. The transform pairs encountered using the partial fraction expansion technique will usually be those found in Table 2.1 (Those not found in the table can easily be derived by using basic properties of

Laplace transformation); thus inverse transform of each term in the expansion is known. As a consequence, with some practice, it is possible to do the inverse transformation by inspection.

Later in this chapter, we will illustrate the partial fraction expansion method by examples.

Table 2.1 Abbreviated table of Laplace transforms

$f(t);\ t \geq 0$	$F(s)$	$f(t);\ t \geq 0$	$F(s)$
$\delta(t)$: unit impulse	1	$1-e^{-at}$	$\dfrac{1}{s(s+a)}$
$\mu(t)$: unit step	$\dfrac{1}{s}$	$\sin \omega t$	$\dfrac{\omega}{s^2+\omega^2}$
t	$\dfrac{1}{s^2}$	$\cos \omega t$	$\dfrac{s}{s^2+\omega^2}$
$\dfrac{t^2}{2}$	$\dfrac{1}{s^3}$	$e^{-at}\sin \omega t$	$\dfrac{\omega}{(s+a)^2+\omega^2}$
e^{-at}	$\dfrac{1}{s+a}$	$e^{-at}\cos \omega t$	$\dfrac{s+a}{(s+a)^2+\omega^2}$
te^{-at}	$\dfrac{1}{(s+a)^2}$		

2.6 LAPLACE TRANSFORMS FOR SIMPLE SYSTEMS

When we begin to use Laplace transforms to analyze systems and their controllers, we will need to manipulate the transforms of signals and their time derivatives. We are required to know only a handful of useful properties and formulae, and some practice will soon ensure a good familiarity with their use.

Differentiator We can find the Laplace transform of the derivative of a signal $y(t)$ by using the relationship

$$\mathscr{L}\left[\frac{dy}{dt}\right] = sY(s) - y(0) \tag{2.42a}$$

where $y(0)$ is the initial value of $y(t)$, evaluated at $t = 0$.

We can prove this relationship using integration by parts as follows:

$$\int udv = uv - \int vdu$$

Setting $u = e^{-st}$ and $dv = \dfrac{dy}{dt}$, we get

$$\int_0^\infty e^{-st}\left(\frac{dy}{dt}\right)dt = [e^{-st}y(t)]\Big|_{t=0}^{t=\infty} - \int_0^\infty y(t)(-se^{-st})dt = -y(0) + s\int_0^\infty y(t)e^{-st}dt = sY(s) - y(0)$$

If the signal $y(t)$ has zero initial condition, then the result becomes

$$\mathscr{L}\left[\frac{dy}{dt}\right] = sY(s); \tag{2.42b}$$

a derivative operating on a signal can be represented as multiplying its Laplace transform by s. We see this in the block diagram for differentiator in the Fig. 2.13a.

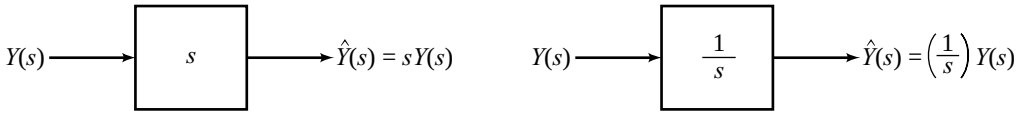

Fig. 2.13 Block diagram representation of (a) differentator (b) integrator in transform domain

Having found the Laplace transform of the first derivative of a signal, it is an easy matter to extend this result to higher derivatives.

$$\mathscr{L}\left[\frac{d^2y}{dt^2}\right] = s[sY(s)-y(0)] - \left.\frac{dy}{dt}\right|_{t=0} = s^2Y(s) - sy(0) - \dot{y}(0) \tag{2.42c}$$

where the initial conditions are $\dot{y}(0)$ and $\dot{y}(0)$. If the initial conditions are defined as zero,

$$\mathscr{L}\left[\frac{d^2y}{dt^2}\right] = s^2F(s) \tag{2.42d}$$

Repeated application of this result will yield the general formula:

$$\mathscr{L}\left[\frac{d^ny(t)}{dt^n}\right] = s^nY(s) - \sum_{i=0}^{n-1} s^{n-1-i}\left.\frac{d^iy(t)}{dt^i}\right|_{t=0} ;n>0, \frac{d^0y(t)}{dt^0} \triangleq y(t) \tag{2.43}$$

Integrator The Laplace transform of the integral of a signal $y(t)$ results in the relation

$$\mathscr{L}\left[\int_0^t y(\tau)d\tau\right] = \left(\frac{1}{s}\right)Y(s) \tag{2.44}$$

We can prove this relationship using integration by parts $\left(\int udv = uv - \int vdu\right)$. Setting $u = \int_0^t y(\tau)d\tau$ and $dv = e^{-st}$, we obtain

$$\int_0^\infty \left(\int_0^t y(\tau)d\tau\right)e^{-st}\,dt = \left(\int_0^t y(\tau)d\tau\right)\left(-\frac{1}{s}e^{-st}\right)\Big|_{t=0}^{t=\infty} - \int_0^\infty \left(-\frac{1}{s}e^{-st}\right)y(t)dt = 0 + \frac{1}{s}\int_0^\infty y(t)e^{-st}\,dt = \left(\frac{1}{s}\right)Y(s)$$

Thus an integrator operating on a signal can be represented as multiplying its Laplace transform by $(1/s)$. We see this in the block diagram for integrator in Fig. 2.13b.

Final Value Theorem The final value theorem is frequently used in the study of control systems to quickly assess the final, steady-state value of the time response of a linear system. We will illustrate the use of this theorem in the next section. In the following, we state and prove the theorem.

The final value theorem is concerned with the evaluation of $y(t)$ as $t \to \infty$ assuming, of course, that $y(t)$ does approach a limit. Using partial fraction expansion for inverting Laplace transforms, it is simple to show that $y(t)$ approaches a limit as $t \to \infty$ if all the poles of $Y(s)$ lie in the left half of complex plane ($\mathrm{Re}(s) < 0$ in Fig.2.10). The imaginary-axis boundary is however excluded except for a single pole at $s = 0$. This is because purely sinusoidal signals, whose transforms will have poles on the imaginary axis, do not settle to a constant value as $t \to \infty$. Multiple poles at $s = 0$ are also excluded because, as we have already seen in the table of Laplace transforms, these correspond to unbounded signals like ramps. A more compact way of phrasing these conditions is to say that $sY(s)$ must be *analytic* on the boundary and the right half of the complex s-plane. The final value theorem states that when this condition on $sY(s)$ is satisfied, then

$$\lim_{t\to\infty} y(t) = \lim_{s\to 0} sY(s) \tag{2.45}$$

The proof is as follows:

$$\mathscr{L}\left[\frac{dy}{dt}\right] = \int_0^\infty \frac{dy}{dt} e^{-st}\, dt = sY(s) - y(0)$$

However,

$$\lim_{s\to 0} \int_0^\infty \frac{dy}{dt} e^{-st}\, dt = \int_0^\infty \frac{dy}{dt}\, dt = \lim_{t\to\infty} [y(t)] - y(0)$$

These two equations yield

$$\lim_{t\to\infty} [y(t)] - y(0) = \lim_{s\to 0} [sY(s)] - y(0)$$

or

$$\lim_{t\to\infty} y(t) = \lim_{s\to 0} [sY(s)]$$

Dead-time/ Transportation Lag One modelling feature which we would include in our collection of simple models in this book is the feature known as *dead-time* or *transportation lag*. Figure 2.14 shows modelling of the dead-time process. The Laplace transform of the dead-time model is given by

$$\mathscr{L}[y(t-\tau_D)] = e^{-s\tau_D} Y(s) \tag{2.46}$$

We can prove this relationship as follows.

$$\mathscr{L}[y(t)] = Y(s) = \int_0^\infty y(\tau) e^{-s\tau} d\tau = \int_0^\infty [y(\tau)\mu(\tau)] e^{-s\tau} d\tau$$

Changing the variable of integration by setting $\tau = t - \tau_D$ yields

$$Y(s) = \int_{\tau_D}^\infty y(t-\tau_D)\mu(t-\tau_D) e^{-s(t-\tau_D)} dt = e^{s\tau_D} \int_{\tau_D}^\infty y(t-\tau_D)\,\mu(t-\tau_D) e^{-st}\, dt$$

Since the function

$$\mu(t-\tau_D) = \begin{cases} 1 & \text{for } t > \tau_D \\ 0 & \text{otherwise} \end{cases}$$

we can write

$$Y(s) = e^{s\tau_D} \int_0^\infty y(t-\tau_D) e^{-st} dt = e^{s\tau_D}\, \mathscr{L}[y(t-\tau_D)]$$

It is worth noting that Eqn. (2.46) results in a Laplace transform that is not a simple ratio of polynomials in s because variable s occurs in the argument of the exponential function. In the analysis of control systems using linear polynomial representations, it is sometimes inconvenient to use this exponential representation for the dead-time.

There are several approximations to the dead-time. The simplest is the Taylor series approximation. That is

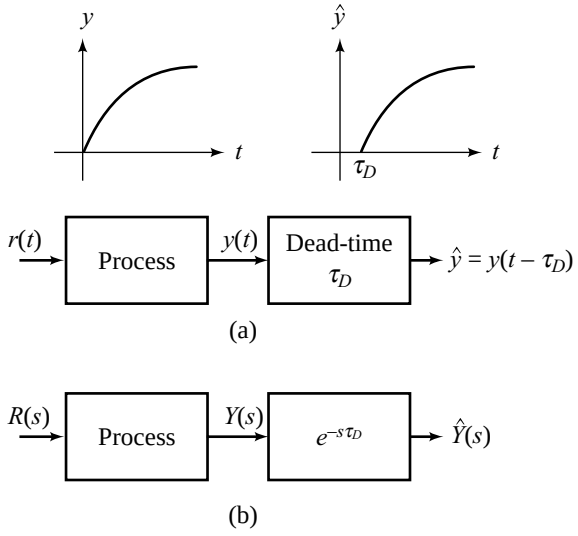

Fig. 2.14 Behaviour of a dead-time element

$$e^{-s\tau_D} = \left[e^{-s\tau_D}\right]_{s=0} + \left[\frac{d}{ds}e^{-s\tau_D}\right]_{s=0} s + \text{higher-order terms}$$
$$= 1 - \tau_D s + \text{higher-order terms}$$
$$\simeq 1 - \tau_D s \qquad (2.47)$$

Another is

$$e^{-s\tau_D} \simeq \frac{1}{1+\tau_D s} = 1 - \tau_D s + \text{higher-order terms} \qquad (2.48)$$

The Pade approximants [73] provide a family of approximations of increasing accuracy and complexity. These approximations are based on frequency-response comparisons; the simplest one being the first-order approximation:

$$e^{-s\tau_D} \simeq \frac{1-\tau_D s/2}{1+\tau_D s/2} \qquad (2.49)$$

Having catalogued the possible approximations for the dead-time, we would like to point out here that approximations of dead-time are not always necessary; some of the design techniques, as we will see later, are just as easy to work out using $e^{-s\tau_D}$ itself, as it is using any of these approximations.

2.7 TRANSFER FUNCTION MODELS

The very first step in the analytical study of a system is to set up mathematical equations to describe the system. Because of different analytical methods used, or because of different questions asked, we may often set up different mathematical models to describe the same system.

We have seen earlier in Section 2.3 (Eqn.(2.8)) that the input $r(t)$ and the output $y(t)$ of any linear time-invariant system that is initially relaxed at t =0,can be described by an equation of the form

$$y(t) = \int_0^t g(t-\tau)r(\tau)d\tau \qquad (2.50)$$

The function $g(t)$ is called the *impulse response* of the system.

The application of Laplace transform to Eqn. (2.50) gives us an extremely useful mathematical description of a linear time-invariant system (refer Eqn. (2.23)).

$$Y(s) = \mathscr{L}[y(t)] = G(s)R(s) \qquad (2.51)$$

where $R(s) \triangleq \mathscr{L}[r(t)]$ and $G(s) \triangleq \mathscr{L}[g(t)]$

The function $G(s)$ is called the *transfer function* of the system.

The transfer function of a linear time-invariant system is, by definition, the Laplace transform of the impulse response of the system.

The Laplace transform variable s in a transfer function $G(s)$, as will be seen later, can be associated with frequency. Hence the transfer function description of a system is often referred to as in *frequency-domain*, whereas the impulse response description is said to be in time-domain.

In this book, the major emphasis is on frequency-domain design methods. Providing more space for discussion on transfer functions will be in order here.

Later in this chapter and in the next chapter, we will use the basic laws of physics to develop mathematical models of mechanical, electrical, hydraulic and thermal systems that are commonly encountered in control systems. As we shall see, the application of physical laws to these systems, under the assumption of linearity

and time-invariance, results in a set of ordinary linear differential equations with real constant coefficients. These differential equations when rearranged in the form of a set of first-order differential equations, result in *state variable model*. Laplace transformation of these differential equations with zero initial conditions gives us *transfer function*, as we will shortly see. Thus, to obtain a transfer function model, one first writes the differential equations governing the dynamics of the system, which 'naturally' arise from the application of physical laws.

Consider the general form of differential equations, given below.

$$\frac{d^n y}{dt^n} + a_1 \frac{d^{n-1} y}{dt^{n-1}} + \cdots + a_{n-1} \frac{dy}{dt} + a_n y = b_0 \frac{d^m r}{dt^m} + b_1 \frac{d^{m-1} r}{dt^{m-1}} + \cdots + b_{m-1} \frac{dr}{dt} + b_m r \tag{2.52}$$

The coefficients a_i and b_j are real constants; m and n are integers with $m \leq n$; $r = r(t)$ (the input) is the known time function, and $y = y(t)$ (the output) is the unknown solution of the equation; and n is called the *order* of the differential equation.

The coefficient of the highest derivative of y is assumed to be one. If it is not, it can be made one by dividing both sides of the equation by the original value of the coefficient.

To completely specify the problem so that a *unique solution* $y(t)$ can be obtained, a set of n *initial conditions* for $y(t)$ and its first $n - 1$ derivatives must be specified. The set of initial conditions is

$$\left\{ y(0), \left.\frac{dy}{dt}\right|_{t=0}, \ldots, \left.\frac{d^{n-1} y}{dt^{n-1}}\right|_{t=0} \right\}$$

If a system is *relaxed* (*i.e.*, at rest) when the input $r(t)$ is switched on at $t = 0^+$, then the initial conditions for the differential equation model of the system are all zero. The implication of the relaxedness assumption is that the response depends only on the input $r(t)$. The input is applied at $t = 0^+$; $r(t)$ and its derivatives are zero at $t = 0$.

Applying the Laplace transform to Eqn. (2.52) under the assumption of zero initial conditions, yields (refer Eqn. (2.43))

$$s^n Y(s) + a_1 s^{n-1} Y(s) + \cdots + a_{n-1} s Y(s) + a_n Y(s) = b_0 s^m R(s) + b_1 s^{m-1} R(s) + \cdots + b_{m-1} s R(s) + b_m R(s)$$

Solving for $Y(s)$:

$$Y(s) = \frac{b_0 s^m + b_1 s^{m-1} + \cdots + b_{m-1} s + b_m}{s^n + a_1 s^{n-1} + \cdots + a_{n-1} s + a_n} R(s)$$

Comparing with Eqn. (2.51), we see that the ratio of polynomials in complex variable s is the transfer function $G(s)$ of the system.

$$G(s) = \frac{b_0 s^m + b_1 s^{m-1} + \cdots + b_{m-1} s + b_m}{s^n + a_1 s^{n-1} + \cdots + a_{n-1} s + a_n} = \frac{Y(s)}{R(s)}; \; m \leq n \tag{2.53}$$

Thus the *transfer function of a linear time-invariant system is the ratio of the Laplace transforms of its output and input variables, assuming zero initial conditions*.

$$G(s) = \left.\frac{\mathscr{L}[y(t)]}{\mathscr{L}[r(t)]}\right|_{\substack{\text{system relaxed} \\ \text{at } t_0 = 0}} = \left.\frac{Y(s)}{R(s)}\right|_{\substack{\text{system relaxed} \\ \text{at } t_0 = 0}} \tag{2.54}$$

where $Y(s)$ = Laplace transform of the output variable $y(t)$,
$R(s)$ = Laplace transform of the input variable $r(t)$, and
$G(s)$ = transfer function of the system.

Figure 2.15 gives a block diagram of a SISO system in transform domain.

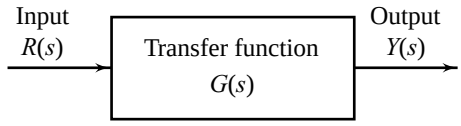

Fig. 2.15 Description of a SISO system in transform domain

Note that whenever a transfer function is used to describe a system, the system is always implicitly assumed to be linear, time-invariant, and relaxed at $t_0 = 0$.

There are two different ways in which transfer function models are usually obtained.

(i) For lumped linear time-invariant systems, mathematical model building based on physical laws normally results in a set of (first-order, and second-order) differential equations. Applying Laplace transform to the differential equations results in a transfer function model of the system.

We will be mostly concerned with this approach. A number of examples of mechanical, electrical, hydraulic and thermal systems will be taken to illustrate the modelling procedure. One important feature will clearly emerge from these examples—application of physical laws to a system results in a set of differential equations which directly provide us with the rates of change of state variables of the system. State variable formulation is thus a 'natural' representation of the system dynamics. We, in fact, first obtain the state variable formulation by applying physical laws and therefrom derive the transfer function model by Laplace transformation.

(ii) The transfer function model of a system can be identified from experimentally obtained input-output data. Generally the identification methods can be considered to be a type of curve-fitting, where the assumed transfer function is fitted to the available data in some optimal manner. The methods may be based on frequency response (sinusoidal input), step response (step input), impulse response (pulse input; pulse of small width approximating an impulse), or the response to more general inputs.[6]

Identification methods have not been covered in this book. Only simple methods based on step response and frequency response are given in later chapters. Refer [155] for more details on identification methods.

Example 2.1 Consider the mass-spring-damper system shown in Fig. 2.3.

Application of Newton's law results in the following equation (refer Fig. 2.3b).

with

$$\left.\begin{aligned} M\frac{dv(t)}{dt} &= F(t) - Bv(t) - K\,x(t) \\ \frac{dx(t)}{dt} &= v(t) \end{aligned}\right\} \tag{2.55}$$

$x(t)$ is the displacement of the mass, $v(t)$ is the velocity, $F(t)$ is the applied force; M, B and K are the parameters of the system.

Equations (2.55), as recognized earlier in Section 2.2, are in fact the state equations of the mechanical system. We can express these two first-order differential equations in terms of a single second-order differential equation:

$$M\frac{d^2x(t)}{dt^2} + B\frac{dx(t)}{dt} + K\,x(t) = F(t) \tag{2.56}$$

Laplace transformation of either Eqns (2.55) or Eqn. (2.56) will give us the transfer function model of the system.

[6] In Chapter 12, methods of deriving *canonical* (special) state variable models from a given transfer function will be presented. This is called the *realization problem*.

Laplace transformation of differential equations of the first and second-order, will require following results (refer Eqn. (2.43)):

$$\mathscr{L}\left[\frac{dx(t)}{dt}\right] = sX(s) - x(0);$$

$$\mathscr{L}\left[\frac{d^2x(t)}{dt^2}\right] = s^2X(s) - sx(0) - \frac{dx}{dt}(0)$$

Taking the Laplace transform of all the terms of Eqn. (2.56), under the assumption of zero initial conditions, we obtain

$$M[s^2\,X(s)] + B[sX(s)] + KX(s) = F(s)$$

where $X(s) \triangleq \mathscr{L}[x(t)]$; $F(s) \triangleq \mathscr{L}[F(t)]$.

Solving for $X(s)$:

$$X(s) = \frac{F(s)}{Ms^2 + Bs + K}$$

Therefore, the transfer function $G(s)$ of the mass-spring-damper system is

$$G(s) = \frac{X(s)}{F(s)} = \frac{1}{Ms^2 + Bs + K} \tag{2.57}$$

The highest power of the complex variable s in the denominator polynomial of a transfer function determines the *order of the transfer function*. The mechanical system under consideration is thus described by the second-order transfer function given by Eqn. (2.57). Note that differential Eqn. (2.56) or the state equation model (2.55), governing the behaviour of the mechanical system, is also of second-order.

Example 2.2 Consider the electrical network of Fig. 2.2. Application of Kirchhoff's voltage law results in the following equation

with

$$\left.\begin{aligned} L\frac{di(t)}{dt} + Ri(t) + e(t) &= e_i(t) \\ C\frac{de(t)}{dt} &= i(t) \end{aligned}\right\} \tag{2.58}$$

$e(t)$ is the voltage across the capacitor, $i(t)$ is the current through the inductor, $e_i(t)$ is the voltage source and R, L, and C are the parameters of the system.

Equations (2.58), as recognized earlier in Section 2.2, are in fact state equations of the electrical network. Taking the Laplace transform of all the terms of these equations, under the assumption of zero initial conditions, we obtain

$$C[sE(s)] = I(s);\ L[sI(s)] + R\,I(s) + E(s) = E_i(s)$$

where

$$E_i(s) \triangleq \mathscr{L}[e_i(t)];\ E(s) \triangleq \mathscr{L}[e(t)];\ I(s) \triangleq \mathscr{L}[i(t)]$$

Eliminating $E(s)$ from these equations, we get

$$\left(R + sL + \frac{1}{sC}\right)I(s) = E_i(s) \tag{2.59a}$$

The output (refer Fig. 2.2)

$$y(t) = L\frac{di}{dt}$$

or under the assumption of zero initial conditions,

$$Y(s) = sL\, I(s) \tag{2.59b}$$

The transfer function $G(s)$ of the RLC network (obtained from Eqns. (2.59a) and (2.59b)) is

$$G(s) = \frac{Y(s)}{E_i(s)} = \frac{s^2}{s^2 + \frac{R}{L}s + \frac{1}{LC}} \tag{2.60}$$

Since the highest power of s in the denominator polynomial of $G(s)$ is two, the transfer function model of the RLC network is of second-order. Note that state equation model of this network is also of second-order.

Impedance approach is useful for developing transfer functions of electrical circuits. Impedance $Z(s)$ of a passive circuit is the ratio of the Laplace transform of the voltage across the circuit to the Laplace transform of the current through the circuit under the assumption of zero initial conditions. For impedances in series, the equivalent impedance is equal to the sum of the individual impedances. For impedances in parallel, the reciprocal of the equivalent impedance is equal to the sum of the reciprocals of the individual impedances.

Let us derive the transfer function of the circuit of Fig. 2.2 using impedance approach. In transform domain, the RLC-series circuit appears as shown in Fig. 2.16.

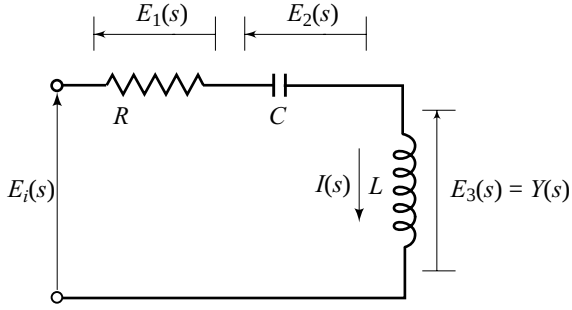

Fig. 2.16 RLC-series circuit in transform domain

For the resistor,

$$e_1(t) = Ri(t);\ Z_1(s) = \frac{E_1(s)}{I(s)} = R$$

For the capacitor,

$$i(t) = C\frac{de_2(t)}{dt};\ Z_2(s) = \frac{E_2(s)}{I(s)} = \frac{1}{sC}$$

For the inductor,

$$e_3(t) = L\frac{di(t)}{dt};\ Z_3(s) = \frac{E_3(s)}{I(s)} = sL$$

Total impedance of the circuit

$$Z(s) = Z_1(s) + Z_2(s) + Z_3(s) = R + \frac{1}{sC} + sL$$

The circuit obeys the relation $E_i(s) = Z(s)\, I(s) = \left(R + \frac{1}{sC} + sL\right) I(s)$

This equation is same as Eqn. (2.59a), which was derived by Laplace transformation of the state equations.

Since $G(s)$ is a rational function of a complex variable, we use the terminology of the theory of complex variables. Consider a general transfer function model

$$G(s) = \frac{Y(s)}{R(s)} = \frac{b_0 s^m + b_1 s^{m-1} + \cdots + b_{m-1}s + b_m}{s^n + a_1 s^{n-1} + \cdots + a_{n-1}s + a_n} ; \; m \le n \tag{2.61}$$

where a_i and b_j are constant parameters of the model of the system with input $r(t)$ and output $y(t)$. As seen from Eqns (2.57) and (2.60), a_i and b_j are given by physical parameters of the system.

$G(s)$ is a rational function of s, i.e., a quotient of two polynomials of s. For $m \le n$, $G(s)$ is a *proper rational function*, and for $m < n$, $G(s)$ is a *strictly proper rational function*.

We will represent the numerator polynomial of $G(s)$ by $N(s)$, and the denominator polynomial by $\Delta(s)$:

$$G(s) = \frac{N(s)}{\Delta(s)} \tag{2.62}$$

where

$$N(s) = b_0 s^m + b_1 s^{m-1} + \cdots + b_{m-1}s + b_m$$
$$\Delta(s) = s^n + a_1 s^{n-1} + \cdots + a_{n-1}s + a_n$$

Note that there is no loss in generality to assume that the coefficient of s^n in the polynomial $\Delta(s)$ is unity (i.e., the denominator polynomial $\Delta(s)$ is assumed to be *monic*[7]).

The highest power of the complex variable s in the denominator polynomial $\Delta(s)$ of the transfer function $G(s)$ determines the *order of the transfer function model.* The denominator polynomial $\Delta(s)$ is called the *characteristic polynomial*.

The roots of the equation

$$\Delta(s) = 0 \tag{2.63a}$$

are called the *poles* of the transfer function $G(s)$, and roots of the equation

$$N(s) = 0 \tag{2.63b}$$

are called the *zeros*.

Equation (2.63a) is called the *characteristic equation*; the poles are the *characteristic roots*.

The transfer function $G(s)$ given by Eqn. (2.61) can be expressed in the *pole-zero form* as

$$G(s) = \frac{K(s+z_1)(s+z_2)\cdots(s+z_m)}{(s+p_1)(s+p_2)\cdots(s+p_n)} ; \; m \le n \tag{2.64a}$$

where K, p_i and z_j are constants; $K = b_0$ is the *gain constant* of the transfer function, $-p_1, -p_2, \ldots, -p_n$ are the n poles (real or complex) of the transfer function (n roots of the characteristic equation (2.63a)), and $-z_1$, $-z_2, \ldots, -z_m$ are the m finite zeros (real or complex) of the transfer function (m roots of Eqn. (2.63b)).

In the representation of $G(s)$ in pole-zero form given by Eqn. (2.64a), it has been assumed that the poles and zeros are *distinct* (*simple*). If a pole, say at $s = -p_1$, is *multiple* (repeated) with multiplicity v, the corresponding transfer function in pole-zero form becomes

$$G(s) = \frac{K(s+z_1)(s+z_2)\cdots(s+z_m)}{(s+p_1)^v (s+p_{v+1})\cdots(s+p_n)} ; \; m \le n \tag{2.64b}$$

Multiple zeros may also appear in a transfer function model.

We have so far considered SISO systems. Complex processes and machines often have several variables (outputs) we wish to control, and several manipulated inputs to provide this control (refer Eqns. (2.5)). Systems with same number of input variables as the number of output variables are quite common in industry.

[7]A monic polynomial has a leading coefficient equal to unity.

Consider a system with p output variables $y_1, y_2, \ldots, y_p$ and p input variables $r_1, r_2, \ldots, r_p$. A mathematical model of this system is, therefore, $p \times p$ *transfer function matrix* defined below:

$$\begin{bmatrix} Y_1(s) \\ Y_2(s) \\ \vdots \\ Y_p(s) \end{bmatrix} = \begin{bmatrix} G_{11}(s) & G_{12}(s) & \cdots & G_{1p}(s) \\ G_{21}(s) & G_{22}(s) & \cdots & G_{2p}(s) \\ \vdots & \vdots & & \vdots \\ G_{p1}(s) & G_{p2}(s) & \cdots & G_{pp}(s) \end{bmatrix} \begin{bmatrix} R_1(s) \\ R_2(s) \\ \vdots \\ R_p(s) \end{bmatrix} \tag{2.65a}$$

An important general property of such systems (and a major source of design difficulties) is *interaction* (or *coupling*) between inputs r_i and outputs y_j in the sense that any input r_i; $1 \leq i \leq p$, will have a dynamic effect on all the outputs y_j; $1 \leq j \leq p$. If each input r_i has a dynamic effect only on y_i, the system is said to be *non-interacting* (or *decoupled*). For a non-interacting system, the transfer function matrix in Eqn. (2.65a) becomes a diagonal matrix:

$$\begin{bmatrix} Y_1(s) \\ Y_2(s) \\ \vdots \\ Y_p(s) \end{bmatrix} = \begin{bmatrix} G_1(s) & 0 & \cdots & 0 \\ 0 & G_2(s) & \cdots & 0 \\ \vdots & \vdots & & \vdots \\ 0 & 0 & \cdots & G_p(s) \end{bmatrix} \begin{bmatrix} R_1(s) \\ R_2(s) \\ \vdots \\ R_p(s) \end{bmatrix} \tag{2.65b}$$

Thus our 'multivariable' system consists of p independent SISO systems. It is self-evident that each of these systems can be individually controlled by SISO feedback loops.

In simple control situations, it is possible to ignore *weak interactions* and design controllers under the assumptions that one input affects only one output. Interaction effects are considered as disturbances to the separate control systems and may not cause significant degradation in their performance if coupling is weak. Our focus in this book is on SISO systems; multivariable systems with weak coupling will also be considered.

In this book, the major emphasis is on frequency-domain design methods. Hence we mostly deal with transfer functions (Chapters 2–11).

The frequency-domain design methods have been greatly enhanced by the availability of low-cost computers for system analysis and simulation. The use of state variable formulation, introduced earlier in Section 2.2, has become widespread in CAD packages. In this introductory book, modest investment in state variable methods is therefore necessary. In Chapter 12, we give an adequate coverage of state variable representation and its relationship with transfer function representation. Chapter 13 provides an introduction to control system design using state variable methods.

2.7.1 Dynamic Response

This sub-section is concerned with the dynamic response of linear time-invariant systems to disturbance signals and standard test signals. We will study the response of a system from its transfer function model; therefore the system is implicitly assumed to be initially relaxed.

Basically four steps are involved in the computation of $y(t)$ from

$$Y(s) = G(s)\, R(s)$$

1. Find the Laplace transform of $r(t)$ using results of Section 2.5 or transform pairs given in Table 2.1.
2. Compute the poles of $G(s)\, R(s)$.
3. Expand $Y(s)$ into partial fractions.
4. Obtain $y(t)$ by taking inverse Laplace transform of $Y(s)$ using transform pairs listed in the Table 2.1.

In the following, we give an example to illustrate the procedure.

Example 2.3 Given the transfer function

$$G(s) = \frac{Y(s)}{R(s)} = \frac{1}{s^2 + 3s + 2};$$

find the response y(t) to the input

(i) $r(t) = 5\,\mu(t)$; (ii) $r(t) = 5t\,\mu(t)$

Solution

(i) For the given step input, $R(s) = \frac{5}{s}$.

Therefore,

$$Y(s) = \frac{1}{s^2 + 3s + 2} R(s) = \frac{1}{(s+1)(s+2)}\left(\frac{5}{s}\right)$$

Expanding $Y(s)$ into partial fractions, gives

$$Y(s) = \frac{5}{s(s+1)(s+2)} = \frac{A_1}{s} + \frac{A_2}{s+1} + \frac{A_3}{s+2}$$

$$A_1 = \lim_{s\to 0}\left[(s)\frac{5}{s(s+1)(s+2)}\right] = \frac{5}{2}$$

$$A_2 = \lim_{s\to -1}\left[(s+1)\frac{5}{s(s+1)(s+2)}\right] = -5$$

$$A_3 = \lim_{s\to -2}\left[(s+2)\frac{5}{s(s+1)(s+2)}\right] = \frac{5}{2}$$

or

$$Y(s) = \underbrace{\frac{5/2}{s}}_{\text{Excitation pole}} \underbrace{- \frac{5}{s+1} + \frac{5/2}{s+2}}_{\text{System poles}}$$

Inverting $Y(s)$, we obtain the time response

$$y(t) = \underbrace{\left[\frac{5}{2}\right.}_{\text{Steady-state response}} \underbrace{\left. - 5e^{-t} + \frac{5}{2}e^{-2t}\right]}_{\text{Transient response}} \mu(t) \qquad (2.66)$$

The transient response terms correspond to system poles excited by the input. These terms vanish as $t \to \infty$.

The second response term arises due to the excitation pole, and has the same nature as the input itself except for a modification in magnitude caused by the system's behaviour to the specified input. Since the input exists as $t \to \infty$, the second response term does not vanish and is called the *steady-state response* of the system. Figure 2.17a shows the response to the given step input.

The steady-state response can be quickly obtained without doing the complete inverse Laplace transform, by use of the *final value theorem* (Eqn. (2.45)), since $sY(s)$ has no poles on the imaginary axis and in the right half s-plane.

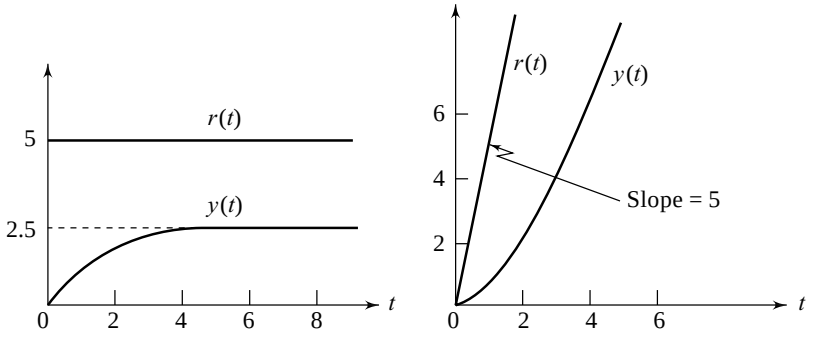

Fig. 2.17 (a) Step response; (b) Ramp response

(ii) For the given ramp input, $R(s) = \dfrac{5}{s^2}$.

Therefore, $$Y(s) = \frac{5}{s^2(s+1)(s+2)}$$

Expanding $Y(s)$ in partial fractions, gives

$$Y(s) = \frac{A_1}{s^2} + \frac{A_2}{s} + \frac{A_3}{s+1} + \frac{A_4}{s+2}$$

$$A_1 = \lim_{s\to 0}\left[(s^2)\frac{5}{s^2(s+1)(s+2)}\right] = \frac{5}{2}$$

$$A_2 = \lim_{s\to 0}\frac{d}{ds}\left[(s^2)\frac{5}{s^2(s+1)(s+2)}\right] = \lim_{s\to 0}\left[\frac{-5(2s+3)}{(s^2+3s+2)^2}\right] = \frac{-15}{4}$$

$$A_3 = \lim_{s\to -1}\left[(s+1)\frac{5}{s^2(s+1)(s+2)}\right] = 5$$

$$A_4 = \lim_{s\to -2}\left[(s+2)\frac{5}{s^2(s+1)(s+2)}\right] = \frac{-5}{4}$$

or $$Y(s) = \frac{5/2}{s^2} - \frac{15/4}{s} + \frac{5}{s+1} - \frac{5/4}{s+2}$$

Inverting $Y(s)$, we obtain the time response

$$y(t) = \left(\frac{-15}{4} + \frac{5}{2}t + 5e^{-t} - \frac{5}{4}e^{-2t}\right)\mu(t) \qquad (2.67a)$$

The ramp response is composed of three types of terms—constant, ramp, and exponentials. The exponentials (transient component) decay leaving behind the steady-state response

$$y_{ss}(t) = \frac{5}{2}t - \frac{15}{4} \qquad (2.67b)$$

Figure 2.17b shows the response to given ramp input. The response diverges from the ramp input as t increases.

Note that final value theorem is not applicable in this case.

2.7.2 Computer Simulation

The Laplace transform approach of investigating the dynamics of a linear system results in *closed form response* (refer Example 2.3)—the response variable y is given by a mathematical expression in terms of independent variable t. The method works well if the system model is relatively of low-order, with relatively simple input functions[8]. If the model does not have these characteristics, we have to resort to numerical solution methods (*digital simulation*). The disadvantage of this type of solution is that generality is lost; the numerical values of the input functions, coefficients of the model, etc., must be specified [151–154]. However, often there is no alternative.[9]

2.8 CHARACTERISTIC PARAMETERS OF FIRST- AND SECOND-ORDER MODELS

In this book, we will frequently come across first- and second-order transfer function models. Special emphasis on the characteristics of these models is justified.

2.8.1 First-Order Models

We consider here a first-order model which can be represented by the first-order differential equation:

$$\frac{dy(t)}{dt} + ay(t) = br(t) \tag{2.68}$$

where $y(t)$ represents output of the system; $r(t)$ represents input; a and b represent model parameters (they depend on physical parameters of the system).

The transfer function of this first-order model becomes

$$\frac{Y(s)}{R(s)} = G(s) = \frac{b}{s+a}$$

A more common notation for first-order transfer function is

$$\frac{Y(s)}{R(s)} = G(s) = \frac{K}{\tau s+1} \tag{2.69}$$

since the physical meaning can be given to both K and τ.

In the following, we obtain the time response from Eqn. (2.69) to a unit-step signal. From the characteristics of the time response, the physical meaning of the parameters K and τ will become clear.

For a unit-step input, $R(s) = 1/s$. Therefore

$$Y(s) = \frac{K}{s(\tau s+1)} = K\left[\frac{1}{s} - \frac{\tau}{\tau s+1}\right] \tag{2.70a}$$

$$y(t) = K(1-e^{-t/\tau});\ t \geq 0 = \underbrace{K}_{\text{Steady-state response}} - \underbrace{Ke^{-t/\tau}}_{\text{Transient response}} \tag{2.70b}$$

This solution is now investigated in detail. The step response as given by Eqns (2.70) is plotted in Fig. 2.18; the two components of the response are plotted separately along with the complete response. Note that the exponentially decaying transient term has an initial slope of K/τ, i.e.,

[8]Most of the models used in the following chapters are of first-, second-, and third-order with simple input functions. Computer simulation is therefore not essential. However CAD facility, if available, can provide a better feel of how control system design is done in practice.

[9]The analog computer simulation provides another way of investigating system dynamics. This method is rarely used now because of the advantages of digital simulation (Appendix A). However, it still provides an excellent means of developing control system prototypes (refer Section 2.13).

$$\frac{d}{dt}(-Ke^{-t/\tau})\Big|_{t=0} = \frac{K}{\tau}e^{-t/\tau}\Big|_{t=0} = \frac{K}{\tau}$$

Mathematically, the transient term does not decay to zero in a finite length of time. However, if the term continued to decay at its initial rate, the term would reach a value of zero in time $t = \tau$. The parameter τ is called the system *time constant*. It has units of time (seconds, minutes, etc.). This can be verified from the units of parameters of the physical system represented by the model (2.69).

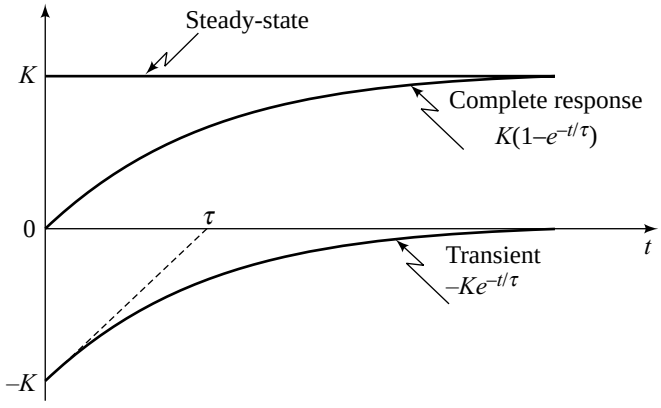

Fig. 2.18 Step-response of a first-order system

The decay of the transient term is illustrated in Table 2.2 as a function of time-constant τ. We observe that the transient term has decayed to less than five per cent of its initial value in three time-constants, and to less than two per cent of its initial value in four time-constants. In a practical sense, we consider the transient term to have decayed to zero in three to four time-constants. Therefore, the time-constant is related to the speed of response of the system. The slower the system responds to input, the larger the value of τ.

Table 2.2

t	$e^{-t/\tau}$
τ	$e^{-1} = 0.3679$
2τ	$e^{-2} = 0.1353$
3τ	$e^{-3} = 0.0498$
4τ	$e^{-4} = 0.0183$
5τ	$e^{-5} = 0.0067$

Figure 2.19 shows unit-step responses $y(t)$ of the following three systems:

(i) $G_1(s) = \dfrac{10}{s+1}$; (ii) $G_2(s) = \dfrac{10}{2s+1}$; (iii) $G_3(s) = \dfrac{10}{5s+1}$

The time-constants of the system transfer functions are given by $\tau_1 = 1$, $\tau_2 = 2$, $\tau_3 = 5$.

The time-constant represents the time taken for the output to rise to 63.2% of the change in output. In the plots of Fig. 2.19, the output changes from zero to a steady-state value $y_{ss} = 10$. We insert a line at $0.632y_{ss}$ on the graph so that the time-constants are identified. As τ increases, the response becomes slower, i.e., it takes longer to reach 63.2% of the final output.

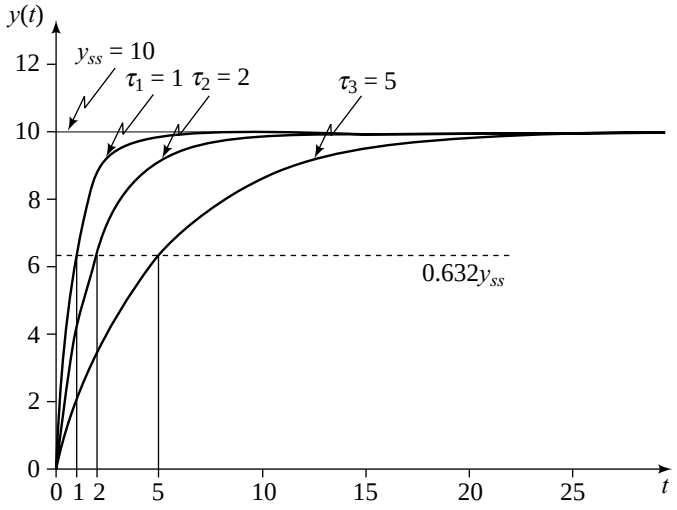

Fig. 2.19 Speed of response for different time-constants

Another important parameter encountered in Eqns (2.70) is K. Note that

$$\lim_{t\to\infty} y(t) = K$$

The parameter K is the *system gain*, which tells us how much the output variable will change at steady-state in response to a unit change in the input variable.

The gain K and time-constant τ are the two parameters which describe the 'personality' of the first-order system. These parameters may be obtained from the physical parameters of the system or experimentally by conducting the step-response test/sinusoidal-response test (described later in Chapters 6 and 8).

The transfer function

$$G(s) = \frac{K}{\tau s + 1} \tag{2.71}$$

is called the *time-constant form* for first-order transfer functions and will be encountered in all types of systems—electrical, mechanical, thermal, hydraulic, etc. A process described by this form of transfer functions is called a *first-order lag* or a *simple lag*.

2.8.2 Second-Order Models

We consider here a second-order model which can be represented by the second-order differential equation:

$$\frac{d^2y(t)}{dt^2} + a_1\frac{dy(t)}{dt} + a_2y(t) = br(t) \tag{2.72}$$

where $y(t)$ represents the output of the system; $r(t)$ represents input; a_1, a_2 and b represent model parameters (they depend on the physical parameters of the system).

The transfer function of this second-order model becomes

$$\frac{Y(s)}{R(s)} = G(s) = \frac{b}{s^2 + a_1 s + a_2} \tag{2.73}$$

A more common notation for second-order transfer functions is

$$\frac{Y(s)}{R(s)} = G(s) = \frac{K}{\frac{1}{\omega_n^2}s^2 + \frac{2\zeta}{\omega_n}s + 1} = \frac{K\omega_n^2}{s^2 + 2\zeta\omega_n s + \omega_n^2} \tag{2.74}$$

since physical meaning can be given to the three parameters K, ζ and ω_n.

In the following, we obtain the time response from Eqn. (2.74) to a unit-step signal ($R(s) = 1/s$). From the characteristics of the time response, the physical meaning of the parameters K, ζ, and ω_n will become clear.

The response of the second-order transfer function (2.74) is dependent on the two poles of the transfer function, which are the roots of the characteristic equation

$$s^2 + 2\zeta\omega_n s + \omega_n^2 = (s + \zeta\omega_n + j\omega_n\sqrt{1-\zeta^2})(s + \zeta\omega_n - j\omega_n\sqrt{1-\zeta^2}) = 0 \tag{2.75}$$

The unit-step response of the transfer function (2.74) with the parameter $\zeta = 0$, is given by

$$Y(s) = \frac{K\omega_n^2}{s\left(s^2 + \omega_n^2\right)} = K\left[\frac{1}{s} - \frac{s}{s^2 + \omega_n^2}\right]$$

$$y(t) = K(1 - \cos\omega_n t);\ t \geq 0 \tag{2.76}$$

The output oscillates indefinitely about the steady-state value K; there is no decay in the magnitude of the oscillations. We will shortly see that the outputs of transfer functions with the parameter $\zeta > 0$ exhibit *damped oscillations*. This provides the physical significance of the parameter ζ, called the *damping ratio*. It is an indicator of the type of transient behaviour expected in a system's response. The damping ratio is a dimensionless parameter. This can be verified from the units of parameters of the physical system represented by the model (2.74).

All physical systems have some damping ($\zeta > 0$). If there were no damping ($\zeta = 0$) in the system, the output response would contain oscillations that did not decay. The frequency ω_n of these oscillations would be the *natural frequency* (sometimes referred to as the *undamped natural frequency)* of the system. The parameter ω_n has the dimension of reciprocal time, and its unit is rad/sec. This can be verified from the units of parameters of the physical system represented by the model (2.74).

We can classify second-order systems depending on the value of its damping ratio parameter ζ:

If $0 < \zeta < 1$, then the system is *underdamped.*

If $\zeta = 1$, then the system is *critically damped.*

If $\zeta > 1$, then the system is *overdamped.*

Underdamped systems (0<ζ<1) Underdamped transfer function models have complex conjugate poles in the left-half of s-plane (refer Eqn. (2.75)). The unit-step response is given by

$$Y(s) = \frac{K\omega_n^2}{s\left(s^2 + 2\zeta\omega_n s + \omega_n^2\right)}$$

$$= K\left[\frac{1}{s} - \frac{s + \zeta\omega_n}{(s + \zeta\omega_n)^2 + \omega_d^2} - \frac{\zeta\omega_n}{(s + \zeta\omega_n)^2 + \omega_d^2}\right] \tag{2.77}$$

where

$$\omega_d = \omega_n\sqrt{1-\zeta^2}\ . \tag{2.78}$$

Using the table of transform pairs (Table 2.1), we get

$$y(t) = K\left[1 - e^{-\zeta\omega_n t}\left(\cos\omega_d t + \frac{\zeta}{\sqrt{1-\zeta^2}}\sin\omega_d t\right)\right] = K\left[1 - \frac{e^{-\zeta\omega_n t}}{\sqrt{1-\zeta^2}}\sin\left(\omega_d t + \tan^{-1}\frac{\sqrt{1-\zeta^2}}{\zeta}\right)\right]; t \geq 0 \quad (2.79)$$

The step response as given by Eqn. (2.79) is plotted in Fig. 2.20 for various values of ζ, and fixed ω_n. For $0<\zeta<1$, the system response exhibits decaying oscillations of frequency $\omega_d = \omega_n\sqrt{1-\zeta^2}$. ω_d is called the *damped natural frequency*. With ζ approaching zero, ω_d approaches ω_n, and the system response exhibits continuous oscillations (refer Eqn.(2.76)). With ζ approaching one, the system response approaches the final value without overshooting it and consequently there are no oscillations (this will be proved shortly). Systems with $0<\zeta<1$ are called underdamped systems.

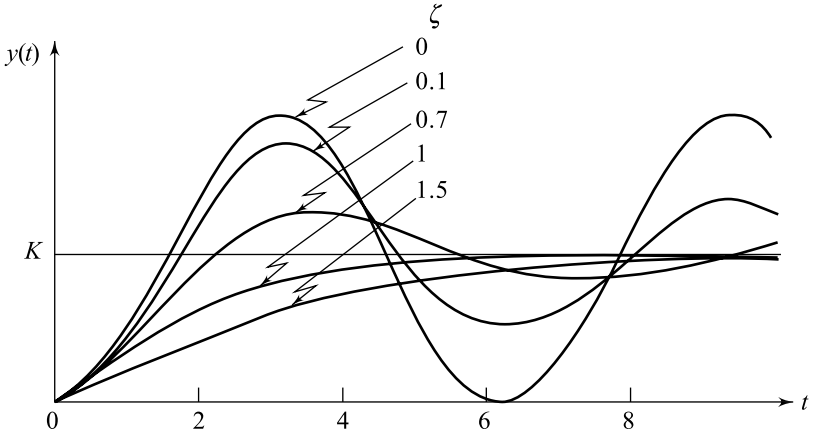

Fig. 2.20 Step-response curves of a second-order system (ω_n = 1)

The curves

$$K\left[1 \pm \frac{e^{-\zeta\omega_n t}}{\sqrt{1-\zeta^2}}\right] \quad (2.80a)$$

are the envelope curves for the step response. The response curve $y(t)$ always remains within this pair of envelope curves as shown in Fig. 2.21. The time-constant of these envelope curves is $1/\zeta\omega_n$. The speed of decay of the transient response depends on the value of the time-constant

$$\tau = \frac{1}{\zeta\omega_n} \quad (2.80b)$$

Critically damped systems (ζ=1) Critically damped transfer function models have two real and equal poles in the left-half of s-plane (refer Eqn. (2.75)). The unit-step response is given by

$$Y(s) = \frac{K\omega_n^2}{s\left(s^2 + 2\omega_n s + \omega_n^2\right)} = K\left[\frac{1}{s} - \frac{\omega_n}{(s+\omega_n)^2} - \frac{1}{(s+\omega_n)}\right]$$

$$y(t) = K[1 - e^{-\omega_n t} - \omega_n t e^{-\omega_n t}]; t \geq 0 \quad (2.81)$$

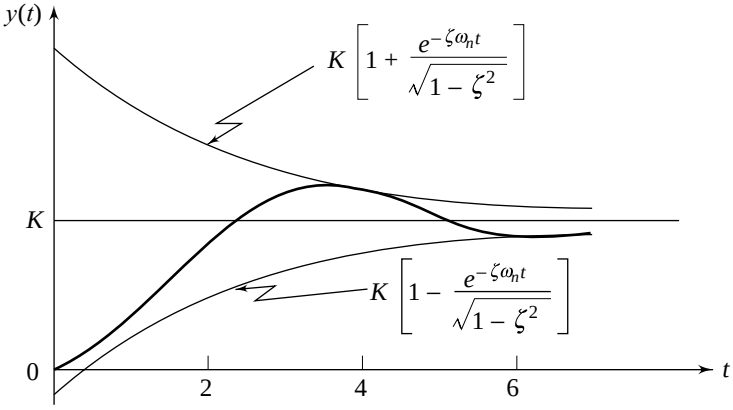

Fig. 2.21 Envelope curves for the step response of a second-order system ($\omega_n = 1$, $\zeta = 0.7$)

The curve corresponding to $\zeta = 1$ in Fig. 2.20 follows Eqn. (2.81). The response for $\zeta = 1$ approaches the final value without overshooting it, and consequently there are no oscillations. For $\zeta < 1$, the system response exhibits oscillations. Systems with $\zeta = 1$ are called critically damped systems.

Overdamped systems ($\zeta > 1$) Overdamped transfer function models have two real and unequal poles in the left-half of s-plane (refer Eqn. (2.75)). The unit-step response is given by

$$Y(s) = \frac{K\omega_n^2}{s(s^2 + 2\zeta\omega_n s + \omega_n^2)} = \frac{K\omega_n^2}{s(s + \zeta\omega_n + \omega_n\sqrt{\zeta^2 - 1})(s + \zeta\omega_n - \omega_n\sqrt{\zeta^2 - 1})}$$

$$= K\left[\frac{1}{s} + \frac{1}{2\sqrt{\zeta^2 - 1}(\zeta + \sqrt{\zeta^2 - 1})}\left(\frac{1}{s + \zeta\omega_n + \omega_n\sqrt{\zeta^2 - 1}}\right)\right] - \frac{1}{2\sqrt{\zeta^2 - 1}(\zeta - \sqrt{\zeta^2 - 1})}\left(\frac{1}{s + \zeta\omega_n - \omega_n\sqrt{\zeta^2 - 1}}\right)$$

$$y(t) = K\left[1 + \frac{1}{2\sqrt{\zeta^2 - 1}(\zeta + \sqrt{\zeta^2 - 1})} e^{-(\zeta + \sqrt{\zeta^2 - 1})\omega_n t} - \frac{1}{2\sqrt{\zeta^2 - 1}(\zeta - \sqrt{\zeta^2 - 1})} e^{-(\zeta - \sqrt{\zeta^2 - 1})\omega_n t}\right]; t \geq 0 \qquad (2.82)$$

Representative response curve for $\zeta > 1$ is shown in Fig. 2.20. The effect of increasing damping beyond its critical value is to make the response sluggish. Systems with $\zeta > 1$ are called overdamped systems.

The parameters K, ζ and ω_n describe the 'personality' of a second-order system. These parameters may be obtained from the physical parameters of a system or experimentally by conducting the sinusoidal response test (described later is Chapter 8).

The transfer function

$$G(s) = \frac{K}{\frac{1}{\omega_n^2}s^2 + \frac{2\zeta}{\omega_n}s + 1} \qquad (2.83)$$

is the standard form for second-order transfer functions, and will be encountered in all types of systems—electrical, mechanical, thermal, hydraulic, etc. It is called a *second-order lag* or a *quadratic lag*. For $\zeta > 1$, the system no longer has a quadratic lag; it is then a cascade of two simple lags.

2.9 SINUSOIDAL TRANSFER FUNCTIONS

Consider the transfer function (refer Eqn. (2.64a))

$$G(s) = \frac{Y(s)}{R(s)} = \frac{K\prod_{i=1}^{m}(s+z_i)}{\prod_{i=1}^{n}(s+p_i)} \tag{2.84}$$

where m and n are integers with $m \le n$; $s = -z_i$ are the zeros of the transfer function, and $s = -p_i$ are the poles. The poles are strictly in the left half of the s-plane. We will assume, without any loss of generality, that the poles are real and distinct.

Let the input $r(t) = R_0 \sin \omega_0 t \mu(t)$; R_0 is a constant and ω_0 is sinusoidal frequency. The Laplace transform of $r(t)$ is

$$R(s) = \frac{R_0\omega_0}{s^2 + \omega_0^2} \tag{2.85}$$

For this sinusoidal input, the Laplace transform of the output can be written as

$$Y(s) = \frac{A}{s - j\omega_0} + \frac{A^*}{s + j\omega_0} + F(s); j \triangleq \sqrt{-1} \tag{2.86}$$

where the residue A^* is the conjugate of the residue A, and

$$F(s) = \sum_{i=1}^{n} \frac{A_i}{s + p_i}$$

with

$$A_i = [(s + p_i)Y(s)]|_{s=-p_i} = [(s + p_i)G(s)R(s)]|_{s=-p_i}$$

The inverse Laplace transform of $F(s)$ is

$$f(t) = \sum_{i=1}^{n} A_i e^{-p_i t}$$

If we are interested in the steady-state response, we need not solve for the residues A_i; when all the $p_i > 0$, the time function in $f(t)$ will decay to zero as $t \to \infty$. We need the residue A because it is a part of the steady-state response.

$$A = [(s - j\omega_0)Y(s)]|_{s=j\omega_0} = \left[(s - j\omega_0)\frac{R_0\omega_0}{s^2 + \omega_0^2}G(s)\right]\Bigg|_{s=j\omega_0} = \frac{R_0}{2j}G(j\omega_0) = \frac{R_0}{2j}|G(j\omega_0)|e^{j\phi}\ ;\phi = \angle G(j\omega_0) \tag{2.87}$$

The output $y(t)$ is the inverse Laplace transform of the right-hand side of Eqn. (2.86):

$$y(t) = \mathscr{L}^{-1}[Y(s)] = \mathscr{L}^{-1}\left[\frac{A}{s - j\omega_0} + \frac{A^*}{s + j\omega_0} + F(s)\right]$$

$$= R_0|G(j\omega_0)|\left[\mathscr{L}^{-1}\left\{\frac{e^{j\phi}}{2j(s - j\omega_0)}\right\} + \mathscr{L}^{-1}\left\{-\frac{e^{-j\phi}}{2j(s + j\omega_0)}\right\}\right] + \mathscr{L}^{-1}\left\{\sum_{i=1}^{n}\frac{A_i}{s + p_i}\right\}$$

$$= R_0|G(j\omega_0)|\left\{\frac{e^{j(\omega_0 t + \phi)} - e^{-j(\omega_0 t + \phi)}}{2j}\right\} + \sum_{i=1}^{n} A_i e^{-p_i t} = R_0|G(j\omega_0)|\sin(\omega_0 t + \phi) + \sum_{i=1}^{n} A_i e^{-p_i t}$$

The steady-state response is

$$\lim_{t\to\infty} y(t) \triangleq y_{ss}(t) = R_0|G(j\omega_0)|\sin(\omega_0 t + \phi) \tag{2.88}$$

The steady-state response remains the same when we relax the assumption of all poles being real and distinct, and allow all types of poles but restricted to left half of s-plane (this will be established quantitatively in Chapter 5).

Thus, if a sinusoidal input is applied to a system $G(s)$, all of whose poles have a negative real part, the steady-state response is a scaled, phase-shifted version of the input. The scaling factor is $|G(j\omega_0)|$, and the phase shift ϕ is the phase of $G(j\omega_0)$.

The sinusoidal steady-state that results after the transient component dies out, is by definition, the *frequency response* of the system. For an input $r(t) = R_0 \sin \omega_0 t$, the output is of the form $Y_0 \sin(\omega_0 t + \phi) = R_0|G(j\omega_0)| \sin(\omega_0 t + \phi)$; both the amplitude ratio $Y_0/R_0 = |G(j\omega_0)|$ and the phase angle $\phi = \angle G(j\omega_0)$ change when we use different frequency ω_0, and our desired results are graphs of these two quantities against frequency, the so-called *frequency response curves.*

For obtaining frequency response, we need not resort to a complete solution for a given sinusoidal input. *Sinusoidal transfer function* provides a much better method. It can be shown that if we replace s by $j\omega (j \triangleq \sqrt{-1}\,;\ \omega \triangleq$ sinusoidal frequency, radian/sec), in $G(s)$ to obtain $G(j\omega)$, we get a complex number $M\angle\theta$ where $M = |G(j\omega)|$ will be the amplitude ratio Y/R and $\theta = \angle G(j\omega)$ will be the angle by which the output sine wave leads the input sine wave (negative θ means the output sine wave lags the input sine wave). $G(j\omega)$ is called the sinusoidal transfer function.

The concept of frequency response is especially relevant to those systems that exhibit frequency-selective characteristics, meaning that very selectively pass or reject a band of frequencies. A *lowpass filter,* for example, is a frequency-selective system which passes without appreciable change only 'low' frequencies, while severely diminishing the output amplitude at 'high' frequencies. Similarly, one can speak of *highpass* and *bandpass* filters.

Ideally, a filter should totally reject all frequencies outside its passband, and therefore an ideal filter would have a clearly defined *bandwidth.* However, unfortunately, such filters are physically unrealizable, although they may be closely approximated. Real filters have more or less a gradual transition between passband and rejection, and defining the bandwidth of a real filter becomes somewhat arbitrary. A commonly used convention is to take the bandwidth as that range of positive frequencies over which the amplitude ratio drops not lower than $1/\sqrt{2} = 0.707$ times the maximum value in the passband. Figure 2.22a shows the gain and phase characteristics of the ideal lowpass filter that has a sharp cut-off at ω_{BW}; therefore ω_{BW} defines the bandwidth of the ideal filter. Figure 2.22b shows the characteristics of a real lowpass filter:

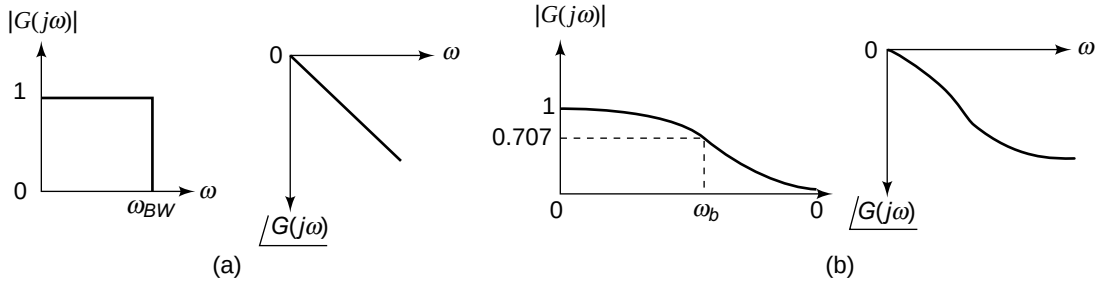

Fig. 2.22 Frequency-response curves

$$|G(j\omega)|_{\max} = |G(j0)| = 1 \tag{2.89a}$$

$$|G(j\omega_b)| = 0.707 \tag{2.89b}$$

ω_b defines the bandwidth of the real filter.

Frequency-response curves form the basis of many important analysis and design methods. These methods will be discussed in later chapters of the book.

2.10 MODELS OF MECHANICAL SYSTEMS

The present and the next three sections are concerned with the modelling of simple physical systems. In these sections, the presentation of the basic material from the system dynamics area is, for reasons of space, limited to essentials. Readers interested in more details are referred to other literature [34–40].

In the analysis of mechanical systems, it is convenient to make use of three idealized elements—the mass, the spring and the dashpot. These elements represent three essential phenomena which occur in various ways in mechanical systems.

2.10.1 Mechanics of Translation

The ideal mass element represents a particle of mass which is the lumped approximation of the mass of a body concentrated at the centre of the mass.

The concept of the elastic deformation of a body is symbolized by the ideal element shown as a helical spring.

Friction exists in physical systems whenever mechanical surfaces are operated in sliding contact. Friction encountered in physical systems may be of many types.

1. *Coulomb friction force*: It is the force of sliding friction between dry surfaces. This force is substantially constant.
2. *Viscous friction force*: It is the force of friction between moving surfaces separated by viscous fluid, or the force between a solid body and a fluid medium. This force is approximately linearly proportional to velocity over a certain limited velocity range.
3. *Stiction*: It is the force required to initiate motion between two contacting surfaces (which is obviously more than the force required to maintain them in relative motion).

In many situations of interest, viscous friction predominates. Our models of mechanical systems are based on this assumption. Refer Chapter 14 for situations where this approximation is not valid.

Sometimes it may even be necessary to introduce viscous friction intentionally to improve the dynamic response of a system. A *dashpot* is a device that provides viscous friction or damping. It consists of a piston and an oil-filled cylinder with a narrow annular passage between the piston and the cylinder (Fig. 2.23). Any relative motion between the piston and the cylinder is resisted by oil.

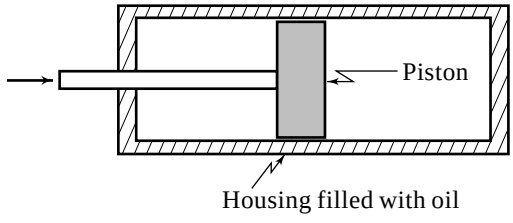

Fig. 2.23 Dashpot

Mechanical translational systems consisting of the three parameters M, B, and K are components of many control systems. As an example, consider the system for machining a work piece on a lathe. The tool movement of such a system is shown in Fig 2.24a. The carriage is moved at a constant speed and the control of the tool position is in the direction of the cross slide. The load on the hydraulic actuator consists of mass M, and viscous friction with coefficient B. The disturbance acting on the actuator is the thrust force on the tool required to machine the work piece.

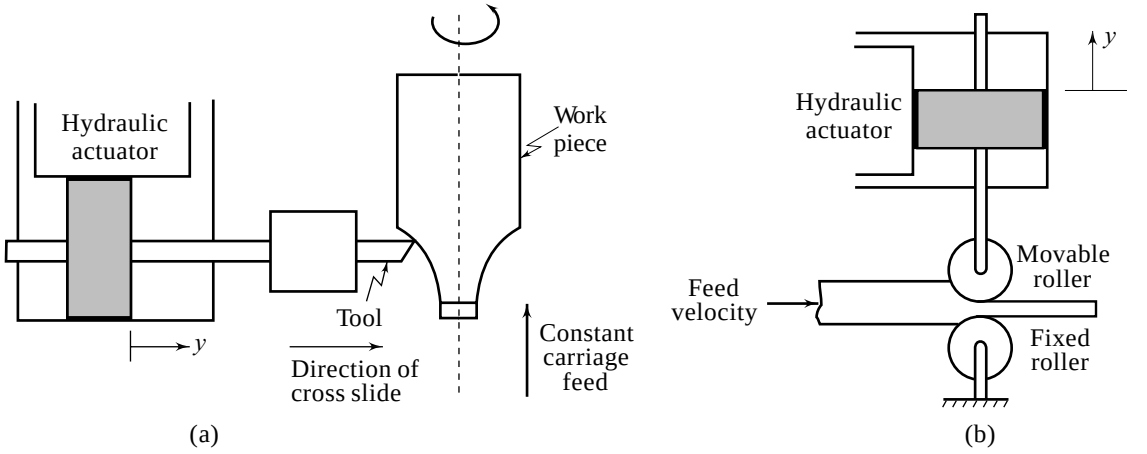

Fig. 2.24 (a) Machining control system; (b) System for controlling the thickness of rolled steel

Another example of mass-spring-damper systems is shown in Fig. 2.24b. The system controls the thickness of the rolled steel in a steel mill. The rolls are driven at a constant speed by drive motors. The translational motion of the movable roll is controlled by the hydraulic actuator. The load on the hydraulic actuator consists of mass M, and viscous friction with coefficient B. The disturbance acting on the actuator is the upward force on the roll which is quite significant when the slabs enter the rolls or leave the rolls.

Feedback control schemes for the applications referred above will be discussed in the next chapter.

The mass-spring-damper system shown in Fig. 2.25a is thus a useful model of the load on the actuator in industrial control systems. The viscous friction has been indicated by a stylized dashpot and F_w represents the load disturbance. Let us obtain the transfer function model of this system. In order to obtain a linear model, we will assume that the friction force of the dashpot is proportional to $\dot{y}$ (true for small velocities). Also the spring is considered a linear device; the spring force is proportional to y (true for small displacements).

Figure 2.25b shows the free-body diagram of the system. Applying Newton's law of motion, the force equation can be written as

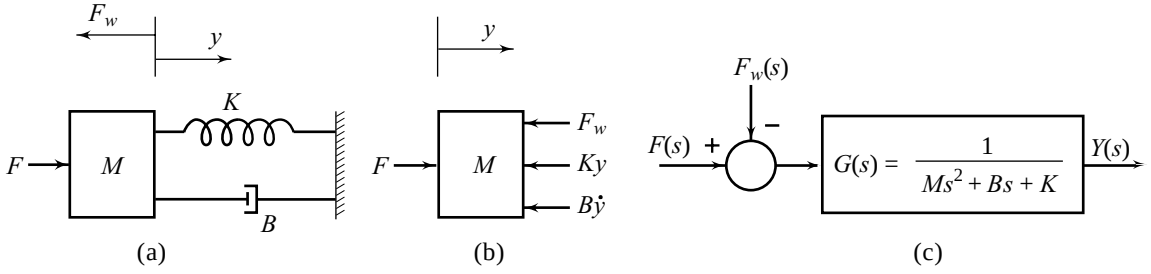

Fig. 2.25 A mass-spring-damper system

$$F(t) - F_w(t) - B\frac{dy(t)}{dt} - Ky(t) = M\frac{d^2y(t)}{dt^2}$$

or
$$M\frac{d^2y(t)}{dt^2} + B\frac{dy(t)}{dt} + Ky(t) = F(t) - F_w(t) \tag{2.90}$$

This is a linear, constant-coefficient differential equation of second-order.

Taking the Laplace transform of each term of this equation (assuming zero initial conditions), we obtain

$$Ms^2Y(s) + BsY(s) + KY(s) = F(s) - F_w(s)$$

where

$$Y(s) \triangleq \mathscr{L}[y(t)];\ F(s) \triangleq \mathscr{L}[F(t)];\ F_w(s) \triangleq \mathscr{L}[F_w(t)]$$

Therefore,

$$Y(s) = \frac{1}{Ms^2 + Bs + K} F(s) - \frac{1}{Ms^2 + Bs + K} F_w(s) \tag{2.91a}$$

Figure 2.25c gives the block diagram representation of the system.

$$G(s) = \frac{1}{Ms^2 + Bs + K} = \frac{1/K}{\frac{M}{K}s^2 + \frac{B}{K}s + 1} = \frac{1/K}{\frac{1}{\omega_n^2}s^2 + \frac{2\zeta}{\omega_n}s + 1} \tag{2.91b}$$

is a quadratic lag; the parameters of the standard form (2.74) of a quadratic lag can easily be obtained from the physical parameters M, B, and K.

The metric system of units for mechanical translational systems is given in Table 2.3.

2.10.2 Fixed-Axis Rotation

Mechanical systems involving fixed-axis rotation occur in the study of machinery of many types and are very important. The modelling procedure is very close to that used in translation. In these systems, the variables of interest are the torque and the angular velocity (or angular displacement). The three basic components for the rotational systems are moment of inertia, torsional spring, and viscous friction.

In low-power servos, the driving and driven shafts can be treated as having negligible elasticity; these rotational systems can therefore be modelled using two components: the moment of inertia J, and the viscous friction with coefficient B. High-power servos, however, may require three components: moment of inertia J, viscous friction with coefficient B, and torsional spring with spring constant K.

To cite an example of rotational load, we revisit the servomechanism for steering of an antenna, shown in Fig. 1.13a. A simple model of the load (antenna) is the moment of inertia–damper system shown in Fig. 1.13b. This model is resketched in Fig. 2.26a; J is the moment of inertia of the antenna, and B represents the viscous friction introduced by bearings and other sources. Torque $T(t)$ is the controlled input generated by the motor, angular displacement $\theta(t)$ of the antenna is the output, and $T_w(t)$ represents the uncontrolled load disturbance torque (due to wind, for example).

The free-body diagram is shown in Fig. 2.26b. The torque equation is

$$T(t) - B\frac{d\theta(t)}{dt} - T_w(t) = J\frac{d^2\theta(t)}{dt^2}$$

or

$$J\frac{d^2\theta(t)}{dt^2} + B\frac{d\theta(t)}{dt} = T(t) - T_w(t) \tag{2.92}$$

This is a linear, constant-coefficient differential equation of second-order.

Taking the Laplace transform of each term of this equation (assuming zero initial conditions), we obtain

$$Js^2\theta(s) + Bs\theta(s) = T(s) - T_w(s)$$

where

$$\theta(s) \triangleq \mathscr{L}[\theta(t)];\ T(s) \triangleq \mathscr{L}[T(t)];\ T_w(s) \triangleq \mathscr{L}[T_w(t)]$$

Therefore,

$$\theta(s) = \frac{1}{Js^2 + Bs} T(s) - \frac{1}{Js^2 + Bs} T_w(s) \tag{2.93a}$$

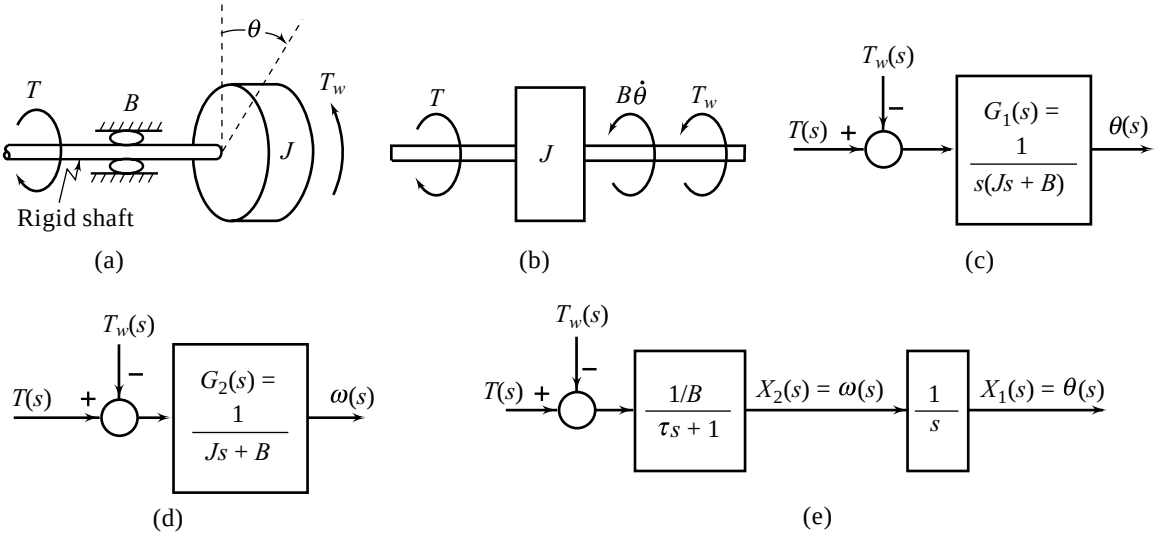

Fig. 2.26 An inertia-damper system

Figure 2.26c gives the block diagram representation of the system.

$$G_1(s) = \frac{1}{s(Js + B)} = \frac{1/B}{s\left(\frac{J}{B}s + 1\right)} = \frac{1/B}{s(\tau s + 1)} \tag{2.93b}$$

where $\tau = J/B$.

If we assume that angular velocity $\omega(t) = \dfrac{d\theta(t)}{dt}$ is the output, then the differential equation of the system becomes

$$J\frac{d\omega(t)}{dt} + B\omega(t) = T(t) - T_w(t) \tag{2.94}$$

This is a linear constant-coefficient differential equation of first-order.

The Laplace transformation of Eqn. (2.94) under the assumption of zero initial conditions, gives

$$(Js + B)\omega(s) = T(s) - T_w(s)$$

where

$$\omega(s) \triangleq \mathscr{L}[\omega(t)].$$

Therefore,

$$\omega(s) = \frac{1}{Js + B}T(s) - \frac{1}{Js + B}T_w(s) \tag{2.95a}$$

Fig. 2.26d shows the corresponding block diagram.

$$G_2(s) = \frac{1}{Js + B} = \frac{1/B}{\frac{J}{B}s + 1} = \frac{1/B}{\tau s + 1} \tag{2.95b}$$

where τ is the time-constant of the simple lag.

The differential equations obtained by applying physical laws to mechanical rotational systems are, in fact, the state equations[10] of the system. Only some rearrangement of these equations is required to obtain state variable model in the standard format given in Eqns (2.4).

A selection of the state variables and corresponding state equations are given below.

$$x_1(t) = \theta(t); x_2(t) = \omega(t) = \dot{\theta}(t)$$
$$\dot{x}_1(t) = x_2(t)$$
$$\dot{x}_2(t) = -\frac{B}{J}x_2(t) + \frac{1}{J}(T(t) - T_w(t))$$

Taking the Laplace transform on both sides of the state equations (assuming zero initial conditions), we obtain

$$sX_1(s) = X_2(s)$$
$$sX_2(s) = -\frac{B}{J}X_2(s) + \frac{1}{J}[T(s) - T_w(s)]$$
$$X_1(s) \triangleq \mathscr{L}[x_1(t)]; X_2(s) \triangleq \mathscr{L}[x_2(t)]$$

The corresponding block diagram representation is shown in Fig. 2.26e. It consists of two blocks; the first block is a simple lag with speed $\omega(s)$ as the output, and the second block is an integrator whose output is displacement $\theta(s)$.

The metric system of units for mechanical rotational systems is summarized in Table 2.3.

Table 2.3 Mechanical symbols and units

Quantity	*Metric units*	*Quantity*	*Metric units*
Force (F)	Newtons or kg-m/sec^2	Torque (T)	Newton-m
Displacement (y)	Metres (m)	Angle (θ)	Radians (rad)
Velocity (v)	m/sec	Angular velocity (ω)	rad/sec
Acceleration ($\dot{v}$)	m/sec^2	Angular accele–ration ($\dot{\omega}$)	rad/sec^2
Mass (M)	kg	Moment of inertia(J)	Newton-m/(rad/sec^2) or kg-m^2
Spring constant(K)	Newtons/m	Torsional spring constant (K)	Newton-m/rad
Damping coeffi-cient (B)	Newtons/(m/sec)	Damping coeffi-cient (B)	Newton-m/(rad /sec)

Example 2.4 Consider the mechanical system shown in Fig. 2.27a. This system represents a *Shaker Table* which can be set to vibrate and then used to calibrate measuring instruments or to test the resilience of manufactured products[63].

Consider that an object, for example a camera, is placed on a shaker table and the input force $F(t)$ applied through a solenoid valve:

$$F(t) = K_s i(t) \tag{2.96}$$

[10]In mechanical rotational systems with inertia, torsional spring, and damper elements, normally an independent set of angular velocities and displacements associated with inertia elements, and angular displacements associated with torsional spring elements constitutes a state vector.

where K_s (Newtons/ amp) is gain parameter of the solenoid. The input force is resisted by the spring (K) and the damping element (B). The net effect of these forces is the vertical displacement, $y(t)$, of the combined shaker table and camera.

The displacement $y(t)$ is considered with respect to position of the shaker table under the loaded condition. The gravitational forces, therefore, do not appear in the model being formulated.

Figure 2.27b shows the free-body diagram for the system. From this figure, we have the following differential equation describing the dynamics of the system.

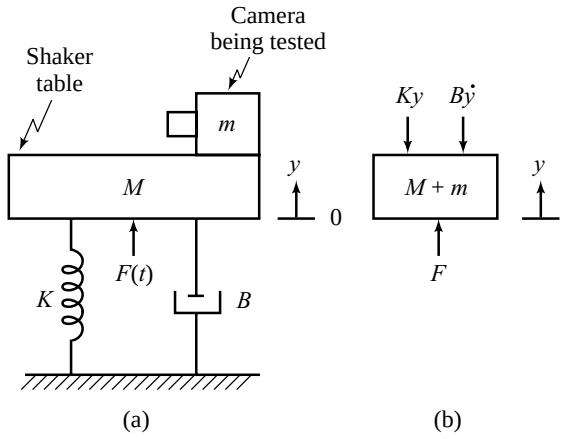

Fig. 2.27 Shaker table with camera being tested

$$(M + m)\,\ddot{y}\,(t) = F(t) - K\,y(t) - B\,\dot{y}\,(t)$$

Taking the Laplace transform of this equation, assuming zero initial conditions, we obtain

$$(M + m)s^2Y(s) = F(s) - KY(s) - BsY(s) \tag{2.97}$$

Suppose that a transfer function is described between $I(s)$ and $Y(s)$; i.e., between the current input to the solenoid and the resulting displacement of the shaker table. From Eqns. (2.96) and (2.97) we obtain

$$\frac{Y(s)}{I(s)} = \frac{K_s / K}{\frac{M+m}{K}s^2 + \frac{B}{K}s + 1} \tag{2.98}$$

With the parameters:

$M = 2.5$ kg; $m = 250$ g; $K = 1.1\times10^7$ Newtons/m;

$B = 1100$ Newtons /(m/sec); K_s=275 Newtons/amp;

the transfer function becomes

$$\frac{Y(s)}{I(s)} = \frac{2.5\times10^{-5}}{2.5\times10^{-7}\,s^2 + 1.0\times10^{-4}\,s + 1} = G_1(s) \tag{2.99}$$

The system poles are the roots of the equation

$$2.5\times10^{-7}\,s^2 + 1.0\times10^{-4}\,s + 1 = 0$$

or

$$(s + 2\times10^3 + j1.99\times10^3)(s + 2\times10^3 - j1.99\times10^3) = 0$$

The poles are complex conjugate:

$$s_{1,2} = -\zeta\omega_n \pm j\omega_d = -2\times10^3 \pm j1.99\times10^3$$

These poles will give rise to a transient response: a damped sinusoid with damped natural frequency $\omega_d = 1.99\times10^3$ rad/sec. The response will decay to zero as $t \to \infty$. The steady-state response is due to excitation poles. If we inject a sinusoidal input signal

$i(t) = A \sin \omega_F t\, \mu(t)$; ω_F is the forcing frequency,

the steady-state response (refer Eqn. (2.99))

$$y_{ss}(t) = A|G_1(j\omega_F)|\sin(\omega_F t + \phi_1);\ \phi_1 = \angle G_1(j\omega_F) \tag{2.100}$$

where

$$G_1(j\omega) = \frac{2.5\times10^{-5}}{\left[1-\left(\frac{\omega}{\omega_n}\right)^2\right] + j\,10^{-4}\times\omega};\ \omega_n = \sqrt{\frac{1}{2.5\times10^{-7}}}$$

The shaker table thus vibrates with an amplitude $A|G_1(j\omega_F)|$. The vibrations become violent as the frequency ω_F approaches ω_n— the natural frequency of the system, resulting in high dynamic stresses on the table.

The table is designed to oscillate and test the resilience of the object (camera) on the table at different frequencies to determine how it responds when stimulated (stimulation = mass m × acceleration y_{Ass}; $(Y_A(s) = s^2Y(s))$).

2.10.3 Analogous Systems

If two systems are described by dynamical equations of identical form, these are said to be *analogs* of each other. For example, the electric *analog* of the mechanical system of Fig. 2.3 is the RLC circuit shown in Fig. 2.28. This can be established as follows.

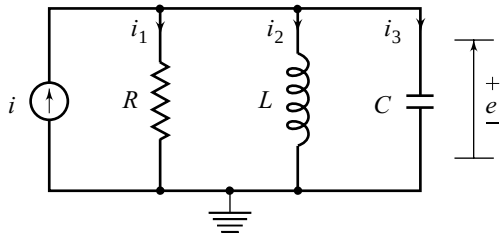

Fig.2.28 An RLC circuit

The mechanical system of Fig. 2.3 is governed by the differential equation (refer Eqn. (2.56))

$$M\frac{d^2x(t)}{dt^2} + B\frac{dx(t)}{dt} + Kx(t) = F(t) \tag{2.101}$$

Rewriting this equation in terms of velocity variable $v(t) = \dot{x}(t)$ results in the following integro-differential equation.

$$M\frac{dv(t)}{dt} + Bv(t) + K\int_{-\infty}^{t} v(\tau)\,d\tau = F(t) \tag{2.102}$$

The electric circuit of Fig.2.28 obeys the relation

$$I(s) = \frac{E(s)}{Z(s)}$$

where

$I(s) \triangleq \mathscr{L}[i(t)]; E(s) \triangleq \mathscr{L}[e(t)]$; and impedance $Z(s)$ of the RLC-parallel circuit is given by

$$\frac{1}{Z(s)} = \frac{1}{R} + \frac{1}{sL} + \frac{1}{1/sC}$$

Inverse Laplace transform of the equation

$$I(s) = \frac{E(s)}{R} + \frac{E(s)}{sL} + sCE(s)$$

results in the following integro-differential equation.

$$C\frac{de(t)}{dt} + \frac{1}{R}e(t) + \frac{1}{L}\int_{-\infty}^{t} e(\tau)\,d\tau = i(t)$$

Comparing this equation with Eqn. (2.102), we at once observe their mathematical similarity with respect to the following analogous pairs:

$$F(t) \leftrightarrow i(t);\ v(t) \leftrightarrow e(t) \tag{2.103}$$
$$M \leftrightarrow C;\ K \leftrightarrow 1/L;B \leftrightarrow 1/R$$

The commonly-used characterizing variables in an electrical system—the voltage and the current—are respectively called *across* and *through* variables of the system. By analogy, velocity and force are, respectively, the across and through variables of mechanical systems. The analogous variables and element pairs in (2.103) are appropriately called the *force-current analogy*.[11]

The variables and basic elements of mechanical rotational systems with their electrical analogs (*torque-current analogy*) are listed below.

$$T(t) \leftrightarrow i(t);\ \omega(t) \leftrightarrow e(t)$$
$$J \leftrightarrow C;\ K \leftrightarrow 1/L;\ B \leftrightarrow 1/R \tag{2.104}$$

The concept of analogous systems is a useful technique for the study of various systems such as electrical, mechanical, thermal, liquid level, etc. Generally it is convenient to study a non-electrical system in terms of its electrical analog as electrical systems are more easily amenable to experimental study.

The principle of analogy is the basic principle behind the use of analog computers for investigating system behaviour—an analog to the physical system can be developed from the components of an analog computer. An analog computer provides an excellent means for developing control system prototypes.

The metric system of units for electrical systems is summarized in Table 2.4.

Table 2.4 Electrical symbols and units

Quantity	*Metric units*
Voltage (e)	Volts
Current (i)	Amperes
Inductance (L)	Henrys
Capacitance (C)	Farads
Resistance (R)	Ohms

2.11 MODELS OF THERMAL SYSTEMS

The basic requirement for the representation of thermal systems by lumped-parameter models is that the temperature of the medium be considered uniform. When the medium is small, this approximation is valid. Also when the medium consists of a body of air or liquid, the temperature can be considered uniform if there is perfect mixing of the fluid. When a single temperature does not accurately represent the thermal state of the entire medium, i.e., there is complex temperature distribution throughout the medium, the problem becomes one of the distributed parameters, requiring the use of partial differential equations. Here, however, in order to simplify the analysis, uniformity of temperature is assumed and thereby the systems are represented by lumped-parameter models.

Heat flow rate h (through variable; analogous to current), and temperature θ (across variable; analogous to voltage) are the commonly used characterizing variables of thermal systems for the purpose of modelling.

[11] Another possible analogy between mechanical and electrical systems is the *force-voltage analogy*. The corresponding analogous electrical system for the mechanical system of Fig. 2.3 will be an RLC-series circuit excited by a voltage source.

Thermal resistance and capacitance are the two basic elements. The resistance that we have encountered so far has been an element that dissipates energy and converts it into heat (damper in mechanical systems, and resistor in electrical systems). Thermal resistance is not an element that dissipates energy; it is a consequence of the fact that a temperature difference is required to cause heat to flow. Thermal capacitance is an energy storage element; a parameter representing internal thermal energy (determined by molecular activity) of the substance.

2.11.1 Heat-Transfer Systems without Carrier Fluids

The flow of heat through a solid material occurs by conduction. The basic equation for one-dimensional heat conduction through a plane wall of surface area $A(\text{m}^2)$ and thickness $l(\text{m})$ is

$$h = \sigma A\left(\frac{\theta_1 - \theta_2}{l}\right) \tag{2.105}$$

where h = heat flow rate, Joules/sec;

$\Delta\theta = \theta_1 - \theta_2$ = temperature drop along the direction of heat flow, °C; and

σ = thermal conductivity of the material, Joules/(°C) (m) (sec).

Many solids interface with fluids. A simple model for convective heat transfer mechanism at solid–fluid interface is given by the relation

$$h = UA(\theta_S - \theta_F) \tag{2.106}$$

where h = heat flow rate, Joules/sec (negative sign of h will indicate flow of heat from fluid to solid);

A = area of the surface (solid–fluid interface), m^2;

θ_S = temperature of the solid, °C;

θ_F = temperature of the fluid, °C; and

U = film coefficient of the solid–fluid interface, Joules/(m^2) (°C) (sec).

Using Eqns (2.105)–(2.106), we define *thermal resistance* as follows:

$$R_{CD} = \text{conductive thermal resistance} = \frac{l}{\sigma A}\text{, °C/(Joules/sec)} \tag{2.107a}$$

$$R_{CV} = \text{convective thermal resistance} = \frac{1}{UA}\text{, °C/(Joules/sec)} \tag{2.107b}$$

The rate of heat storage (in the form of internal energy) in a substance is governed by the relation

$$h_1 - h_2 = Mc\frac{d\theta}{dt} \tag{2.108}$$

where h_1 = heat-input rate, Joules/sec;

h_2 = heat-output rate, Joules/sec;

M = mass of the substance, kg;

c = specific heat of the substance, Joules/(kg) (°C); and

θ = temperature of the substance, °C.

Using Eqn. (2.108), we define *thermal capacitance* as follows:

$$C = Mc, \text{ Joules/°C} \tag{2.109}$$

2.11.2 Heat-Transfer Systems with Carrier Fluids

When large quantities of heat are to be transported over considerable distances, it can be best done by the flowing fluid as a carrier of thermal energy. In such systems, there exist many energy storage effects, in

addition to storage of energy in the form of internal thermal energy—storage in a gravity field, storage due to compressibility of the fluid, storage due to change in the volume of the container, storage due to inertia of the fluid flowing through a pipe, etc.

We first consider the case where the changes in internal thermal energies outweigh the changes in the mechanical energies associated with the fluid. The extreme opposite case will be taken up in the next section where it will be assumed that the changes in mechanical energies outweigh the changes in the internal thermal energy. There are many important practical examples where none of these two approximations is sufficiently accurate for dynamic modelling. These are characterized by strong mechanical–thermal interactions. Fuel flow in turbines and rockets are specific examples. These areas are somewhat specialized; we shall give examples from only the two simple categories mentioned above.

In the following we define important parameters of heat-transfer systems with carrier fluids, under the assumption that the changes in the internal thermal energy outweigh the changes in mechanical energies.

Thermal capacitance of the carrier fluid is defined as follows:

$$C = V\rho c, \text{ Joules/°C} \tag{2.110}$$

where

V = volume of the fluid chamber, m^3

ρ = fluid density, kg/m^3; and

c = specific heat of the fluid, Joules/(kg) (°C).

Carrier fluid-flow into a chamber is a source of thermal-energy input. Also, the outflowing fluid takes away thermal energy from the chamber. Carrier flow heat-input rate and heat-output rate depend upon the temperatures of the inflowing and outflowing fluids, respectively.

Let θ_i (°C) be the temperature of the inflowing fluid into a chamber and θ_0(°C) be the temperature of the outflowing fluid. Flow rate $Q(m^3/sec)$ and density ρ (kg/m^3) are assumed constant.

Heat-input rate, $h_1 = Q\rho\, c\theta_i$, Joules/sec

Heat-output rate, $h_2 = Q\rho\, c\theta_0$, Joules/sec

Net change in transportation of heat is given by

$$h_1 - h_2 = Q\rho\, c(\theta_i - \theta_0) \tag{2.111}$$

From this equation, we define the *thermal resistance* due to carrier fluid-flow as

$$R = \frac{1}{Q\rho c}, \text{ °C/(Joules/sec)} \tag{2.112}$$

Table 2.5 summarizes the metric system of units for thermal systems.

Table 2.5 Thermal symbols and units

Quantity	*Metric units*
Rate of heat flow (h)	Joules/sec
Temperature (θ)	°C
Thermal capacitance (C)	Joules/°C
Thermal resistance (R)	°C/(Joules/sec)

Example 2.5 As an illustration of a heat transfer system, consider the room heating system discussed earlier in Example 1.2 (Figs. 1.6–1.8). The indoor temperature is controlled by the steam circulating through the radiator coils; the heat released for heating the room is the latent heat of condensation. The indoor temperature is also affected by the external environmental changes. The control of steam flow is

performed by a thermostat which produces an on–off signal depending on the size of the incoming error signal. This is accomplished by a relay. We set a desired temperature on the thermostat. This value is compared with the measured value of the indoor temperature. If the indoor temperature is low, the error is positive and when the error value increases above a threshold, the thermostat switches on the heating system. When the indoor error reduces below a threshold value, the thermostat switches off the heating system. Note that the thermostat essentially contains a temperature transducer and an on–off controller.

To obtain a lumped-parameter model for the system, assume that the state of air in the room can be described by a single temperature. Definitions of system parameters and variables are as follows:

Q = steam flow rate, kg/sec
λ = latent heat of condensation , Joules /kg
V = volume of the room, m^3
ρ_a = air density, kg/m^3
c_p = specific heat, Joules /(kg)(°C)
θ_i = indoor temperature, °C
θ_0 = outdoor temperature, °C
R = thermal resistance for heat transfer between the room and its surroundings (convective heat transfer at fluid-solid interface between the air and inside of the room walls + conductive thermal resistance for conduction through the room walls + convective thermal resistance between the outside of the room walls and its surroundings), °C/Joules/sec)

We assume the heat capacity of the radiator to be negligible compared to that of the room air. Heat balance equation for the room air is

$$V\rho_a c_p \frac{d\theta_i(t)}{dt} = Q(t)\lambda - \frac{\theta_i(t) - \theta_0(t)}{R} \tag{2.113}$$

Manipulating this equation gives

$$V\rho_a c_p R \frac{d\theta_i(t)}{dt} = \lambda R Q(t) - (\theta_i(t) + \theta_0(t))$$

or

$$V\rho_a c_p R \frac{d\theta_i(t)}{dt} + \theta_i(t) = \lambda R Q(t) + \theta_0(t) \tag{2.114}$$

This is a first-order differential equation with constant coefficients.

Taking Lapalce transform on both sides of Eqn. (2.114), assuming zero initial conditions, we obtain

$$s(V\rho_a c_p R)\theta_i(s) + \theta_i(s) = \lambda R Q(s) + \theta_0(s) \tag{2.115}$$

where

$$Q(s) \triangleq \mathcal{L}\,[Q(t)]; \theta_i(s) \triangleq \mathcal{L}\,[\theta_i(t)]; \theta_0(s) \triangleq \mathcal{L}\,[\theta_0(t)]$$

Solving for $\theta_i(s)$ from Eqn. (2.115), we get

$$\theta_i(s) = \frac{K}{\tau s + 1} Q(s) + \frac{1}{\tau s + 1}\theta_0(s) \tag{2.116}$$

where

$$\tau = V\rho_a c_p R, \text{ and } K = \lambda R$$

This equation shows that the indoor temperature is affected by both the heat input due to the heating system and the outdoor temperature. This is shown in the block diagram form in Fig. 2.29 (Refer Chapter 14 for the characteristics of on–off control systems).

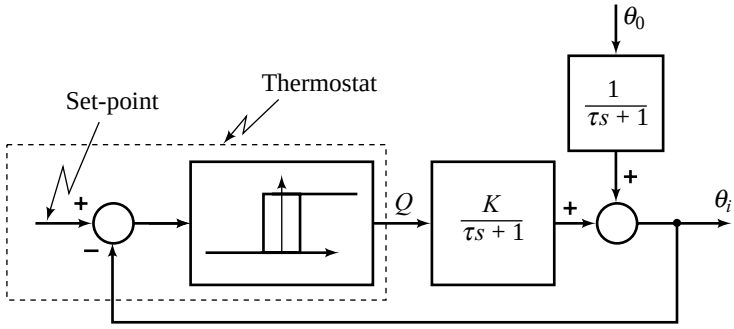

Fig.2.29 Block diagram representation of the system of Fig. 1.8

Example 2.6 Continuously Stirred Tank Heater

The continuously stirred tank sketched in Fig. 2.30 is used to heat a process stream so that its premixed components achieve a uniform composition. Temperature control is important because high temperature tends to decompose the product while a low temperature results in incomplete mixing. The tank is heated by a heater.

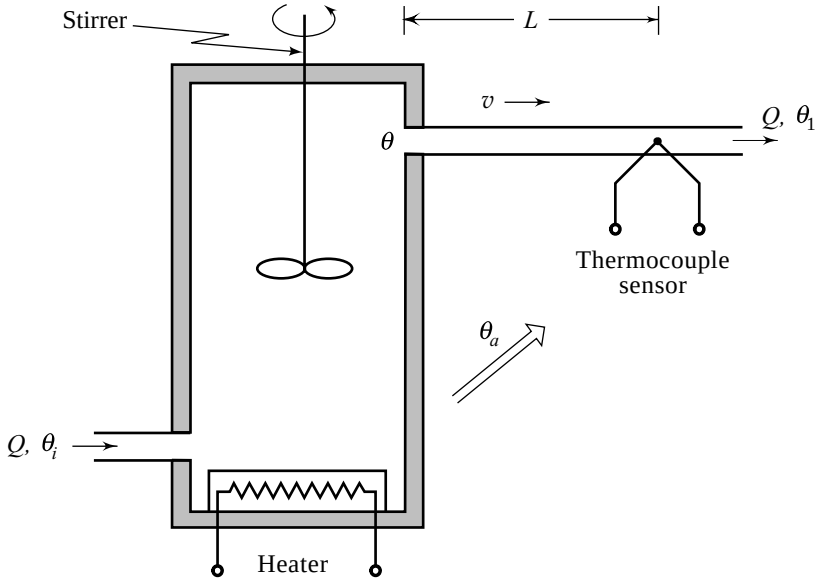

Fig.2.30 A thermal process with dead-time element

In the following we develop the model of the process. The temperature control problem will be studied in the next and later chapters.

Definitions of system parameters and variables are as follows:

V= volume of the liquid in the tank, m^3
ρ = density of the liquid, kg/m^3
c = specific heat of the liquid, Joules/(kg)(°C)
Q = flow rate of liquid (constant), m^3/sec

θ = perturbation in temperature (°C) of liquid in the tank from the nominal point of operation, in response to perturbation h (Joules/sec) in the heat flow rate from the heater, and perturbation θ_i(°C) in inflowing-liquid temperature (θ_i is uncontrolled and hence is disturbance input for the process).

The following assumptions are made for simplified analysis:

1. The liquid inflow and outflow rates for the tank are equal so that the liquid level in the tank is maintained constant during the operation.
2. The tank is kept at a uniform temperature by perfect mixing with the help of a stirrer. Thus, a single temperature is used to describe the thermal state of the entire liquid. The temperature inside the tank = temperature of the outflowing liquid.
3. The tank is well insulated so that the heat loss through its walls is negligible.
4. The heat storage capacity of the heater mass and the tank walls is negligible.

The heat-balance equation for the tank liquid:

$$V\rho c\frac{d\theta(t)}{dt} = h(t) + Q\rho c(\theta_i(t) - \theta(t)) \tag{2.117}$$

Taking the Laplace transform on both sides of the Eqn. (2.117), assuming zero initial conditions, we obtain

$$s(V\rho c)\theta(s) = H(s) + Q\rho c\theta_i(s) - Q\rho c\theta(s)$$

where

$$H(s) \triangleq \mathcal{L}\ \{h(t)\}; \theta(s) \triangleq \mathcal{L}\ [\theta(t)]; \theta_i(s) \triangleq \mathcal{L}\ [\theta_i(t)]$$

Manipulating this equation gives

$$(s\tau + 1)\theta(s) = KH(s) + \theta_i(s) \tag{2.118}$$

where $\tau = \dfrac{V}{Q}$ = process time-constant, and gain $K = 1/Q\rho c$.

Solving for $\theta(s)$ from Eqn. (2.118), we get

$$\theta(s) = \frac{K}{\tau s + 1}H(s) + \frac{1}{\tau s + 1}\theta_i(s) \tag{2.119}$$

The process shown in Fig.2.30 includes a sensor (measuring device) to measure the outlet temperature $\theta(t)$. Any change in the inlet temperature θ_i will change the outlet temperature θ, and this information is needed by control logic elements in a feedback control scheme to take suitable corrective action (feedback control scheme for thermal process of Fig.2.30 will be discussed in the next chapter). We have used thermocouple temperature sensor to measure $\theta(t)$.

Although we generally prefer to measure the controlled variable (outlet temperature θ) as directly as possible, the location of the thermocouple temperature sensor (output is a few millivolts) in the tank encounters problems of vibrations caused by tank stirrer; thus we locate it in the pipeline downstream of the tank. Under this situation, the measured response $\theta_1(t)$ to the disturbances $\theta_i(t)$ will be the same as actual response $\theta(t)$ except that it will be delayed by some amount of time. The time delay thus introduced is referred to as *dead-time* or *transportation lag* to distinguish it from the delay associated with the time-constant of a simple lag. We will see in later chapters that the presence of such delays tends to cause oscillations and makes the system less stable. Dead-time should be avoided to the extent possible.

Figure 2.30 defines the behaviour of the dead-time element (pipe). The input $\theta(t)$ and the output $\theta_1(t)$ are related by

$$\theta_1 = \theta(t - \tau_D);\ t > \tau_D$$

where

$$\tau_D = \text{dead-time} = \frac{\text{distance}}{\text{velocity}} = \frac{L}{v} = \frac{L}{Q / A_p} \text{ sec};$$

L = length of pipe, m;

A_p = cross-sectional area of pipe, m^2; and

Q = flow rate, m^3/sec.

The transfer function of the dead-time element becomes

$$\frac{\theta_1(s)}{\theta(s)} = e^{-s\tau_D} \tag{2.120}$$

Figure 2.31 is the block diagram representation of the system. $H(s)$ is the controlled input, and $\theta_i(s)$ is uncontrolled disturbance.

We have made three simplifying assumptions (stated earlier) to derive the model. Before concluding this example, we study the effects of relaxing these assumptions.

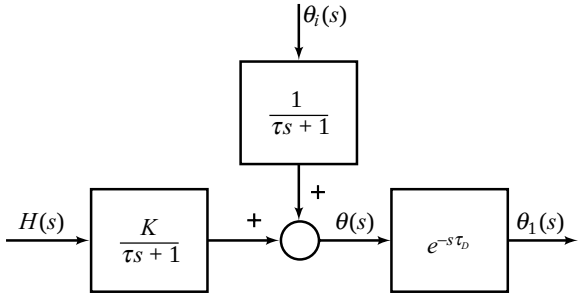

Fig.2.31 Block diagram model of the system of Fig. 2.30

1. Relaxing assumption 1 (inflow and outflow rates are different) will lead to a change in the level of the liquid in the tank. This amounts to a change in energy in the gravity field. We are considering only those cases where the change in energy is due to the change in internal thermal energy only. Modelling of mechanical–thermal energy interactions is not covered.
2. Relaxing assumption 2 (state of the tank cannot be described by a single temperature) will lead to a distributed-parameter system, requiring partial differential equations to describe the system.
3. Relaxing assumption 3 (heat loss through the walls of the tank is not negligible) will require consideration of convective heat transfer at the tank wall–air interface (Eqn. (2.106)). The heat-balance Eqn. (2.117) will get modified; perturbation θ_a in ambient temperature will be included as uncontrolled input.
4. Relaxing assumption 4 (heat storage capacity of the heater mass and the tank walls is not negligible) will add two more energy storage elements; the order of the model will therefore increase by two.

In control systems, we frequently come across situations where there is unavoidable time delay in the signal flow between sub-systems or components. The delay usually results from physical separation of the components and typically occurs as a delay between the change in the manipulated variable and its effect on the plant, or a delay in the measurement of the output. Dead-time elements are needed for accurate modelling of such systems. Digital computers in control systems also introduce the necessity of dead-time elements to model computational delay inherent in these systems.

In the process-control field (control of pressure, flow, liquid-level, temperature, etc.) systems are relatively slow and complex, and in most cases, the time delay in signal flow between sub-systems results in dead-time effects. Even where a pure dead-time element is not present, the complexity of the process (which

will typically contain several first-order lags) will often result in a response which has the appearance of a pure dead-time element. Modelling of such complex systems is a very difficult task. However, many years of experience has proved that the controllers based on approximate process models are quite versatile. The common form of model used to characterize a process is the following:

$$G(s) = \frac{Ke^{-s\tau_D}}{\tau s + 1} \tag{2.121}$$

K = the process steady-state gain;
τ_D = the effective process dead-time; and
τ = the effective process time-constant.

This model characterizes the process by three parameters: the gain K, the dead-time τ_D and the time-constant τ. These parameters can be experimentally determined by performing a step test.

The crudity of such a model precludes the use of sophisticated design techniques which have been formulated in recent years. These models are useful in the simple 'experimental design' approach called *controller tuning* where a controller based on approximate process characterization is first installed, and then controller parameters are tuned by experiment. We will study controller tuning and step testing methods in Chapter 6.

2.12 MODELS OF HYDRAULIC SYSTEMS

The hydraulic systems of interest to control engineers may be classified into two main types:

1. *Liquid-level systems* consisting of storage tanks and connecting pipes. Liquid height in tanks and flow rate in pipes are the variables to be controlled. The driving force is the relative difference in the liquid-heights in the tanks.
2. *Hydraulic devices* using an incompressible oil as their working medium. These devices are used for controlling the forces and motions. The driving force is the high pressure oil supplied by the hydraulic pumps.

Liquids are slightly compressible at high pressures. However, approximate dynamic models based on the assumption of incompressibility of liquids are usually sufficiently accurate. Simple models developed in this book use this approximation.

Volumetric flow rate q (through variable; analogous to current) and pressure p (across variable; analogous to voltage) are the commonly used characterizing variables of hydraulic systems. The three basic elements of hydraulic systems are the resistance, the capacitance, and the inertance. The inertance represents fluid inertia and is derived from the inertia forces required to accelerate a fluid in a pipe. It is an energy-storing element. Another energy-storing element is the capacitance which, as we shall see, represents storage in a gravity field. In most applications of interest to us, energy storage due to the inertance element is negligible compared to that due to the capacitance element.

The tank shown in Fig. 2.32 illustrates the concept of hydraulic capacitance. A (m^2) is the surface area of the tank's bottom, and tank's sides are vertical. If $\bar{Q}_i$ (m^3/sec) represents the steady-state inflow rate, $\bar{Q}$ (m^3/sec) represents the steady-state outflow rate,

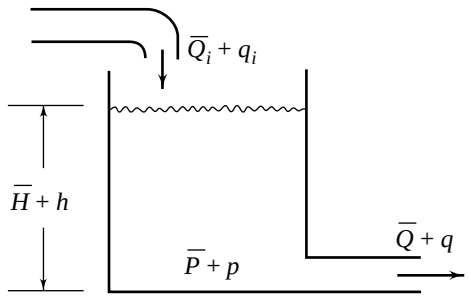

Fig. 2.32 Capacitance of a storage tank

and $\bar{H}$ (m) represents the steady-state height of the liquid in the tank, then the volume-balance at steady-state gives

$$\bar{Q}_i = \bar{Q}\ ;\ \bar{H} = \text{constant}$$

The hydrostatic pressure due to height $\bar{H}$ is

$$\bar{P} = \rho g \bar{H}\ , \text{Newtons/m}^2$$

where ρ = density of the liquid, kg/m^3; and
g = acceleration due to gravity, m/sec^2.

The standard unit of pressure is *pascal* (Pa): 1 Pa of pressure is defined as the force of 1 Newton applied over an area of 1 m^2. Industrial pressures are often measured in pounds per square inch (psi). Pascals can be obtained by multiplying psi by 6.8948×10^3.

The atmospheric pressure is 14.70 psi (101 kPa) at sea level. *Gauge pressure* is referenced to atmospheric pressure, and *absolute pressure* is referenced to perfect vacuum. Gauge pressure can be obtained by subtracting the ambient atmospheric value from the absolute value. Likewise, absolute pressure can be found by adding the ambient pressure to the gauge pressure. Letters *g* or *a* may be suffixed to the pressure units to clearly denote gauge pressure or absolute pressure (e.g., psig, psia). The pressure variables in our discussion represent gauge pressures. The atmospheric pressure has been taken as zero gauge pressure.

In the system of Fig. 2.32, the perturbation $q_i(t)$ in the inflow rate will change the height of the liquid in the tank by $h(t)$, the pressure across the pipe by $p(t)$ and the outflow rate by $q(t)$. The volume-balance equation becomes

$$\bar{Q}_i + q_i(t) = A \frac{d}{dt}(\bar{H} + h(t)) + \bar{Q} + q(t)$$

Perturbation from steady-state is described by the equation

$$q_i(t) = A \frac{dh(t)}{dt} + q(t) \tag{2.122}$$

Since

$$p(t) = \rho g\, h(t), \tag{2.123}$$

it follows that

$$q_i(t) - q(t) = \frac{A}{\rho g} \frac{dp(t)}{dt} \tag{2.124}$$

The *hydraulic capacitance* due to storage in gravity field is defined as

$$C = \frac{A}{\rho g}\ , \text{cub-m/(Newtons/m}^2) \tag{2.125}$$

In terms of hydraulic capacitance, Eqn. (2.124) may be written as

$$q_i(t) - q(t) = C \frac{dp(t)}{dt} \tag{2.126}$$

With reference to Fig. 2.32, the outflow $q(t)$ should obviously depend on $p(t)$ somehow. The greater the pressure $p(t)$, the greater the outflow rate. The concept of hydraulic resistance introduced below will help in establishing a relationship between $q(t)$ and $p(t)$.

Liquid trying to flow out of a container, as in Fig. 2.32, can meet with resistance in several ways. If the outlet is simply a hole, the liquid meets resistance merely because it cannot easily flow through the hole. This is known as *orifice flow*. If the outlet is a pipe, the friction between the liquid and the pipe walls produces

resistance to flow. The presence of a component such as valve in the pipe increases the resistance. Components such as elbow bends, couplings of pipes of different diameters, etc., also resist the flow.

Symbolic representation of an obstruction to flow is shown in Fig. 2.33a. A controllable obstruction, such as a hydraulic valve with an adjustable opening, may be represented as in Fig. 2.33b. The upstream pressure is P_1 and the back pressure achieved downstream is P_2. The flow rate Q depends on the pressure difference $\Delta P = (P_1 - P_2)$. This relationship is usually nonlinear; it can be obtained either experimentally or analytically.

Suppose that an experimental curve relating the flow rate Q to the pressure drop ΔP is available for an obstruction. A typical curve is shown in Fig. 2.33c. Let the slope of the curve at the equilibrium point $(\bar{Q}, \Delta\bar{P})$ be denoted by k. Then, for a small deviation from equilibrium, we obtain

$$q(t) = k(\Delta p(t)) \tag{2.127}$$

From this equation, *hydraulic resistance* is defined as

$$R = \frac{1}{k}, \left(\frac{\text{Newtons}/\text{m}^2}{\text{m}^3/\text{sec}}\right) \tag{2.128}$$

The value of R depends on the steady-state condition chosen for linearization.

When an equation relating the flow to the pressure drop is available, the resistance can be obtained analytically. The following flow-pressure relationship models the orifice flow.

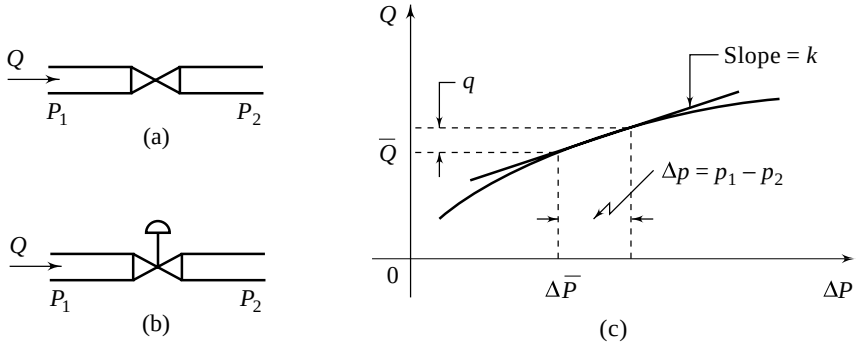

Fig. 2.33 (a) Flow obstruction; (b) Adjustable obstruction; (c) Steady-state operating point

$$Q = C_0 A_0 \sqrt{\frac{2(P_1 - P_2)}{\rho}} \tag{2.129}$$

where

A_0 = orifice area;
C_0 = the experimentally determined number, called the orifice coefficient;
ρ = density of the fluid;
$P_1 - P_2 = \Delta P$ = pressure difference across the orifice.

The orifice coefficient is dependent on the geometric configuration of the orifice and to some extent upon the flow velocity. For sharp-edged orifices, it normally ranges from 0.6 to 0.8.

For incompressible fluids, ρ is constant and therefore Q is a function of pressure difference ΔP:

$$Q = f(\Delta P) \tag{2.130a}$$

This equation may be linearized about an equilibrium point using Taylor series expansion (refer Eqns (2.6)).

The flow rate through a valve with adjustable opening is a function of both the pressure difference ΔP across the valve and the adjustable area A_0, or equivalently the adjustable valve opening x_v:

$$Q = f(x_v, \Delta P) \tag{2.130b}$$

Table 2.6 summarizes the metric system of units for hydraulic systems.

Table 2.6 Hydraulic symbols and units

Quantity	*Metric units*
Volume flow rate(q)	m^3/sec
Pressure (p)	Newtons/m^2
Hydraulic capacitance (C)	m^3/(Newtons/m^2)
Hydraulic resistance (R)	$\frac{\text{Newtons/m}^2}{\text{m}^3/\text{sec}}$

The concepts of hydraulic capacitance and hydraulic resistance will now be used to develop models of hydraulic systems. In the following, we develop a model for a liquid-level system. Models of hydraulic devices for controlling forces and motions will be developed in the next chapter.

Example 2.7 We consider here the two-tank system shown in Fig. 2.34. $q_i(t)$ is the input and $h_1(t)$ is the output of tank 1, and $q_1(t)$ is the input and $h_2(t)$ is the output of tank 2.

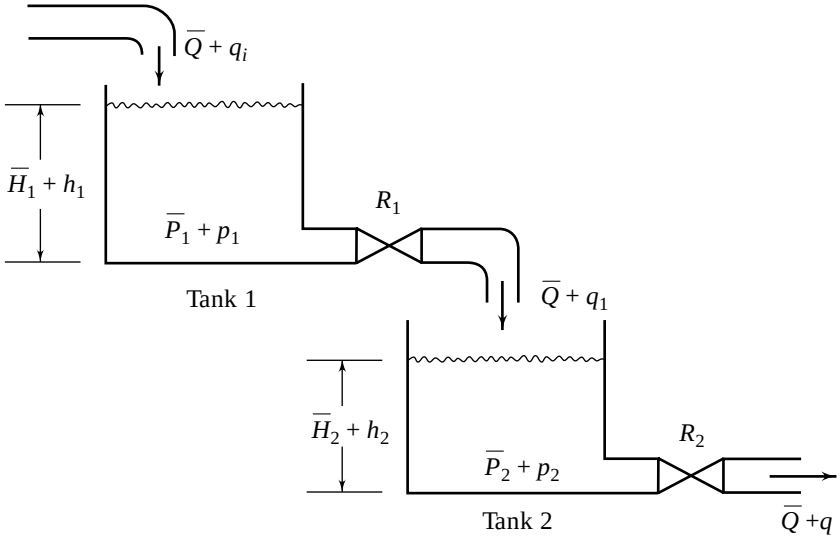

Fig. 2.34 A non-loading two-tank system

The flow-balance equation for tank 1 is

$$q_i(t) = C_1 \frac{dp_1(t)}{dt} + q_1(t); p_1(t) = \rho g h_1(t) \tag{2.131a}$$

The flow $q_1(t)$ through resistance R_1 is given by

$$q_1(t) = \frac{p_1(t)}{R_1} \tag{2.131b}$$

Definitions of various parameters and variables of the hydraulic system are obvious.
Transfer function model of tank 1, obtained from Eqns (2.131) is

$$\frac{H_1(s)}{Q_i(s)} = \frac{R_1/\rho g}{\tau_1 s + 1};\ \tau_1 = R_1 C_1 \tag{2.132}$$

Similarly, the transfer function model of tank 2 is given by

$$\frac{H_2(s)}{Q_1(s)} = \frac{R_2/\rho g}{\tau_2 s + 1};\ \tau_2 = R_2 C_2$$

Substituting for Q_1(s) from Eqns (2.131), we obtain

$$\frac{H_2(s)}{H_1(s)} = \frac{R_2/R_1}{\tau_2 s + 1} \tag{2.133}$$

The block diagram of Fig. 2.35a is developed by 'chaining' Eqns (2.132) and (2.133). This diagram shows that the inlet flow $q_i(t)$ initially affects the level $h_1(t)$ in tank 1. A change in this level then affects the level $h_2(t)$ in tank 2. The level of the first tank affects the level of the second tank, but this level does not in turn affect the level of the first tank. The overall transfer function in such cases where there is no loading due to sub-system interconnection, is obtained by multiplying together the individual transfer functions. The block diagram of Fig. 2.35a can be reduced to that of Fig. 2.35b. The overall transfer function of the two-tank system of Fig. 2.34 is given by

$$\frac{H_2(s)}{Q_i(s)} = \frac{R_2/\rho g}{\tau_1\tau_2 s^2 + (\tau_1 + \tau_2)s + 1} \tag{2.134}$$

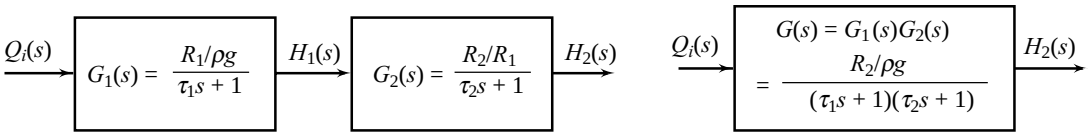

Fig. 2.35 Block diagram models of the system of Fig. 2.34

We now connect the two tanks as shown in Fig. 2.36. Loading is now present and Eqn. (2.134) is not a valid transfer function model for this system as explained below.

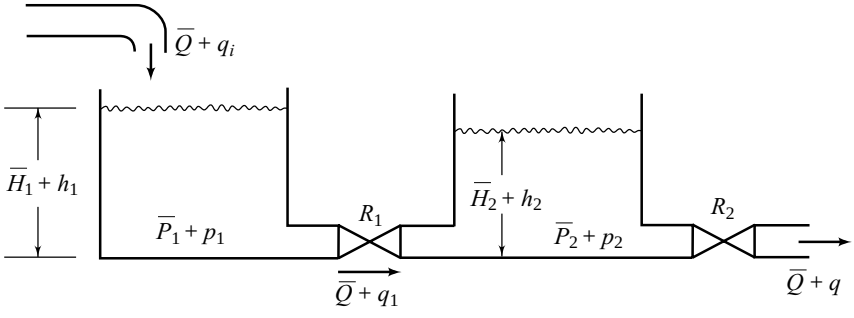

Fig. 2.36 Loading effect in a two-tank system

The flow-balance equation for tank 1 is

$$q_i(t) = C_1 \frac{dp_1(t)}{dt} + q_1(t)$$

Similarly, for tank 2

$$q_1(t) = C_2 \frac{dp_2(t)}{dt} + q(t)$$

The flow $q_1(t)$ through resistance R_1 is governed by the equation

$$q_1(t) = \frac{p_1(t) - p_2(t)}{R_1}$$

and the flow $q(t)$ through resistance R_2 is given by

$$q(t) = \frac{p_2(t)}{R_2}$$

If $h_2(t)$ is considered the output and $q_i(t)$ the input, the transfer function of the system becomes

$$\frac{H_2(s)}{Q_i(s)} = \frac{R_2/\rho g}{\tau_1\tau_2 s^2 + \left(\tau_1 + \tau_2 + \frac{R_2}{R_1}\tau_1\right)s + 1} \qquad (2.135)$$

Note that the transfer function is not equal to that given by Eqn. (2.134). The difference is due to the presence of the loading effect; the level $h_2(t)$ of tank 2 now affects the level $h_1(t)$ of tank 1. The degree to which the overall transfer function is modified from the product of the individual transfer functions depends upon the amount of loading.

In general, loading effects occur because when analysing an isolated sub-system, we assume that no power is being withdrawn at its output location. When we later decide to attach another sub-system to the output of the first, this second sub-system does withdraw some power violating our earlier assumption and thereby invalidating the analysis based on this assumption.

One way to reduce loading effects to negligible proportions is to interpose *buffer amplifiers* between the sub-systems. These devices, which may be electrical, hydraulic, pneumatic, or the like, to suit the physical nature of the connected sub-systems, have their own internal power supplies and can thus supply power to a 'downstream' sub-system without withdrawing their power from the 'upstream' sub-system. That is, such amplifiers have high input impedance and low output impedance (op amp is one example (Section 2.13)).

When we model chains of sub-systems by simple multiplication of their individual transfer functions later in the text, the assumption will always be that the interconnection of various sub-systems is non-loading; loading effects are either not present, have been proven negligible, or have been made negligible by the use of buffer amplifiers.

2.13 MODELS OF OPERATIONAL-AMPLIFIER CIRCUITS FOR IMPLEMENTING PROPORTIONAL-INTEGRAL-DERIVATIVE MODES OF CONTROL

The central theme of the book is to modify a system's behaviour by adding feedback, and by applying some control logic (refer Fig.1.9). A mathematical model of the control logic, as we shall see later in the book, is usually a transfer function $D(s)$. Therefore, it is important to know how these transfer functions can be constructed. In control theory terminology, we will refer to the control logic transfer function as 'compensator', and the construction of the transfer function as 'realization of the compensator'.

We have earlier defined the 'control-logic block + error-detector block'as controller (Fig. 1.9). The term 'controller' is also in use for only the control logic. We will therefore not make distinction between the terms 'compensator' and 'controller'; the two will carry the same meaning at the design stage. Appropriate additional functions will be added at the implementation stage.

Passive (no internal power source) electric networks made up of resistors and capacitors (inductor is a very bulky component at low frequencies) is a common form of implementation of compensators. Condition for realizability of transfer function $D(s)$ with passive resistor-capacitor (RC) networks is that all finite poles of $D(s)$ must be simple and lie on the negative real axis; the zeros of $D(s)$ may be anywhere in the s-plane [39]. By connecting an op amp (operational amplifier) on to the output of a passive RC network, it is possible to realize a specified gain of the compensator. The op amp also serves to reduce loading effects.

With the ever-increasing reliability of integrated circuits, active electric networks made up of resistors, capacitors, and op amps have generally replaced the passive networks for implementation of compensators. Every proper transfer function is realizable using active RC networks[39]; therefore, compensators with complex-conjugate poles can also be implemented. Even in situations where passive RC network realization is possible, an op amp based realization permits the use of reasonable-valued resistors and capacitors (passive RC networks at low frequencies can become rather bulky because of capacitor sizes). The primary advantage of active compensators is their small size and weight for low-frequency applications and their ruggedness. There are, of course, problems like offsets, noise, etc., which are introduced because of op amp usage. An alert designer can, however, take care of these aspects while doing a practical design. Technological advancements are providing a big relief to the designer from these considerations.

Today, most complex industrial processes are under computer control. A complete computer-based installation, in a multi-level viewpoint of control strategy, handles the design tasks at plant management level, production scheduling and control level, and supervisory level, in addition to controlling individual process units at the lowest level in the hierarchy[155]. It is common to delegate process control functions at the lowest level to the special individual control units, connected to the higher levels through computer system. Op amp control units are in use to serve these functions.

PID or *three-term control logic* is widely used in industry. The PID name comprises the first letters of the three terms which make up this controller.

P stands for the **P**roportional term in the controller.

I stands for the **I**ntegral term in the controller.

D stands for the **D**erivative term in the controller.

In the mid-1900s, several technological and analysis concepts came together to make PID widely accepted as an effective control logic. Figure 2.37a shows the three links for the PID control:

$$U(s) = \left[K_P + \frac{K_I}{s} + K_D s \right] E(s) \tag{2.136a}$$

or

$$u(t) = K_P e(t) + K_I \int_0^t e(\tau) d\tau + K_D \frac{de(t)}{dt} \tag{2.136b}$$

where K_P is the *proportional gain*, K_I is the *integral gain*, K_D is the *derivative gain*; the controller operates on the error signal $e(t)$ to provide control signal $u(t)$.

The time-constant form of PID control (Fig. 2.37b) is as follows:

$$u(t) = K_c \left[e(t) + \frac{1}{T_I} \int_0^t e(\tau) d\tau + T_D \frac{de(t)}{dt} \right] \tag{2.137a}$$

or

$$U(s) = K_c\left[1 + \frac{1}{T_I s} + T_D s\right]E(s) \tag{2.137b}$$

where K_c is the *controller gain*, T_I is the *integral* or *reset time*, and T_D is the *derivative* or *rate time*.

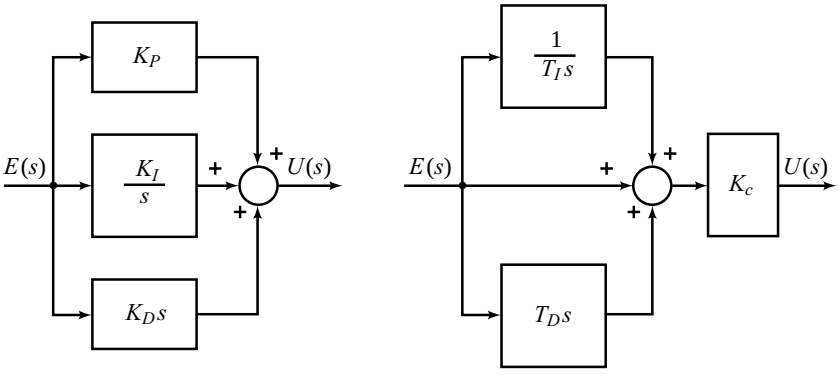

Fig.2.37 PID controller blocks

If we look at real control applications, we find that the feedback signal is the sum of measured output(controlled) signal and a measurement noise component. The error signal $e(t)$ thus contains a corrupting high-frequency noise signal. This noise component has important implications for the use of the derivative term in PID controllers, as is seen below.

$$D(s) = \frac{U(s)}{E(s)} = K_P + \frac{K_I}{s} + K_D s$$

$$D(j\omega) = K_P + \frac{K_I}{j\omega} + K_D \times j\omega \tag{2.138}$$

The derivative term produces amplification of high-frequency signals. The consequence of the possibility of measurement noise being present within the feedback loop is that we do not, in practical applications, apply the derivative directly to the measured output of the process. Instead, we introduce a *low-pass filter* in the D-term. A low-pass filter has the effect of attenuating high-frequency signals.

We incorporate a low-pass filter of the form $1/(\tau_D s + 1)$ into the derivative term as follows:

$$D(s) = K_c\left[1 + \frac{1}{T_I s} + \frac{T_D}{\tau_D s + 1}\right] \tag{2.139}$$

This introduces one additional design parameter τ_D. In some of the process control applications, the design procedure is carried out for three parameters: K_c, T_I and T_D; with the filter term $\tau_D = T_D/N$, and the value of N is usually selected to be in the range $5 \le N \le 20$. This amounts to handling the control design and filter design problems independently.

In the following, we present some simple and useful op amp (operational amplifier) circuit models for implementation of the three types of control logic—proportional (P), integral (I) and derivative (D); and the composite logic—PI, PD, and PID. The reader may want to digest the subject in several smaller bites; the presentation that follows in this section may be skipped and referred back later when specific compensator designs are encountered.

2.13.1 Simple Op Amp Circuit Models

The circuit symbol for an operational amplifier (op amp) is shown in Fig. 2.38a. Two input terminals marked '+' and '–' are shown. These polarity signs refer to the phase relationship between the individual input signals and the output signal; the output signal is in phase with the signal applied to the input pin marked '+', known as the *non-inverting input*, and is in antiphase to the signal applied to the pin marked '–', known as the *inverting input*. The power supply connections are labelled V^+ for the positive voltage and V^- for the negative voltage. The op amp is usually shown as in Fig. 2.38b, without the power supply connections.

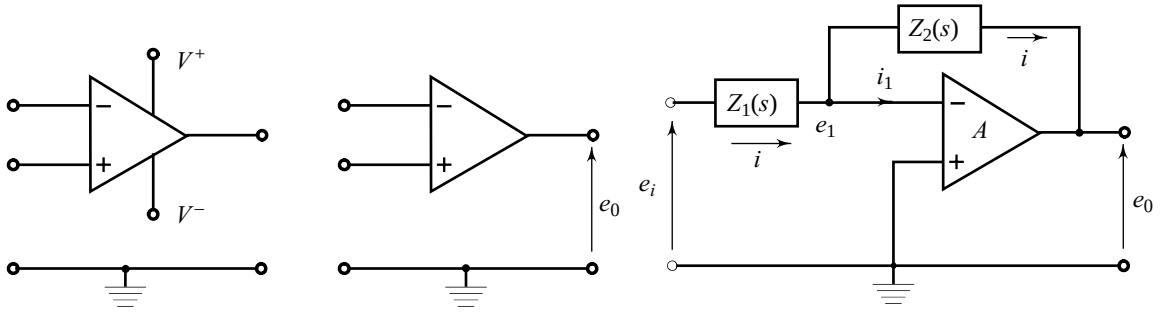

Fig. 2.38 (a) Circuit symbol for an op amp (b) Simplified symbol (c) Op amp circuit building block

Characteristics of an *ideal amplifier* are listed below.

1. Infinite input impedance; an ideal amplifier can be connected to any signal source with no loading effects.
2. Infinite gain.
3. Zero output impedance; an ideal amplifier is capable of driving any load.
4. Infinite bandwidth; an ideal amplifier can amplify any signal frequency.

Op amps approach the first three characteristics closely. The 741 op amp has an input impedance of 6 MΩ, gain of the order of 10^5, and can supply at least 5 mA to a load of 2000 Ω.

The gain of 741 op amp is 10^5 at frequencies between zero (dc) and 10 Hz. Beyond this value of frequency, the gain reduces considerably. Therefore, the op amps approach the ideal amplifier for dc and low frequency signals.

Analysis of op amp circuits becomes simple under the assumption of ideal characteristics. Consider, for example, the circuit of Fig. 2.38c.

1. Since gain A is infinite and output e_0 is finite, the voltage e_1 is virtually zero.
2. Input impedance is infinite; therefore $i_1 = 0$.

For the circuit of Fig. 2.38c (under the second assumption),

$$I(s) = \frac{E_i(s) - E_1(s)}{Z_1(s)} = \frac{E_1(s) - E_0(s)}{Z_2(s)}$$

Since $E_1(s) = 0$ as per first assumption, we get

$$I(s) = \frac{E_i(s)}{Z_1(s)} = -\frac{E_0(s)}{Z_2(s)}$$

or

$$\frac{E_0(s)}{E_i(s)} = -\frac{Z_2(s)}{Z_1(s)} \qquad (2.140)$$

where

$Z_1(s)$ = impedance connected to the input of the amplifier, and

$Z_2(s)$ = impedance connected between output and input of the amplifier.

By choosing proper values of $Z_1(s)$ and $Z_2(s)$, operational amplifiers can be used for various purposes.

Example 2.8 Figure 2.39 shows seven simple op amp circuits. In the following, we derive transfer function for each circuit. From the transfer function models, it will become obvious that these circuits are used for amplification, integration, and differentiation of a given signal.

Figure 2.39*a*

$$\frac{E_0(s)}{E_i(s)} = -\frac{R_2}{R_1} \tag{2.141a}$$

The circuit is thus a constant gain amplifier. The gain can be made adjustable by using a potentiometer for one of the resistances.

Note the phase relationship between input and output; the circuit of Fig. 2.39a is called an *inverting amplifier*.

Figure 2.39*b*

A circuit with $R_1 = R_2$ is an *inverter*; it simply inverts the sign of the input voltage without changing its magnitude. It can be used in cascade with other elements to maintain proper sign relations, as shown in *Figure* 2.39b. For this circuit,

$$\frac{E_0(s)}{E_i(s)} = \frac{R_2}{R_1} \tag{2.141b}$$

Figure 2.39*c*

$$\frac{E_0(s)}{E_i(s)} = -\frac{1/sC}{R} = -\frac{1}{RCs} \tag{2.142a}$$

The circuit is thus an *integrator*.

Equation (2.142a) is true if the initial voltage on the capacitor is zero. Inverse Laplace transformation of this equation gives

$$e_0(t) = -\frac{1}{RC}\int_0^t e_i(\tau)d\tau \tag{2.142b}$$

Figure 2.39*d*

$$\frac{E_0(s)}{E_i(s)} = -\frac{R_2 + 1/sC}{R_1} = -\frac{R_2}{R_1} - \frac{1}{R_1Cs} \tag{2.143a}$$

$$e_0(t) = -\frac{R_2}{R_1}e_i(t) - \frac{1}{R_1C}\int_0^t e_i(\tau)d\tau \tag{2.143b}$$

The circuit thus processes the input signal by 'proportional + integral' action.

Figure 2.39*e*

$$\frac{E_0(s)}{E_i(s)} = -\frac{R}{1/sC} = -RCs \tag{2.144a}$$

$$e_0(t) = -RC\frac{de_i(t)}{dt} \tag{2.144b}$$

The circuit is thus a *differentiator*.

Figure 2.39*f*

$$\frac{E_0(s)}{E_i(s)} = -\frac{R_2}{\dfrac{R_1(1/sC)}{R_1 + 1/sC}} = -\frac{R_2}{R_1}(R_1Cs + 1) \tag{2.145a}$$

$$e_0(t) = -\frac{R_2}{R_1}e_i(t) - R_2C\frac{de_i(t)}{dt} \tag{2.145b}$$

The circuit thus processes the input signal by 'proportional + derivative' action.

Figure 2.39*g*

$$\frac{E_0(s)}{E_i(s)} = -\frac{R_2 + 1/sC_2}{\dfrac{R_1(1/sC_1)}{R_1 + 1/sC_1}} = -\frac{(R_2C_2s + 1)(R_1C_1s + 1)}{R_1C_2s} = -\left[\frac{R_2C_2R_1C_1s^2 + R_2C_2s + R_1C_1s + 1}{R_1C_2s}\right]$$

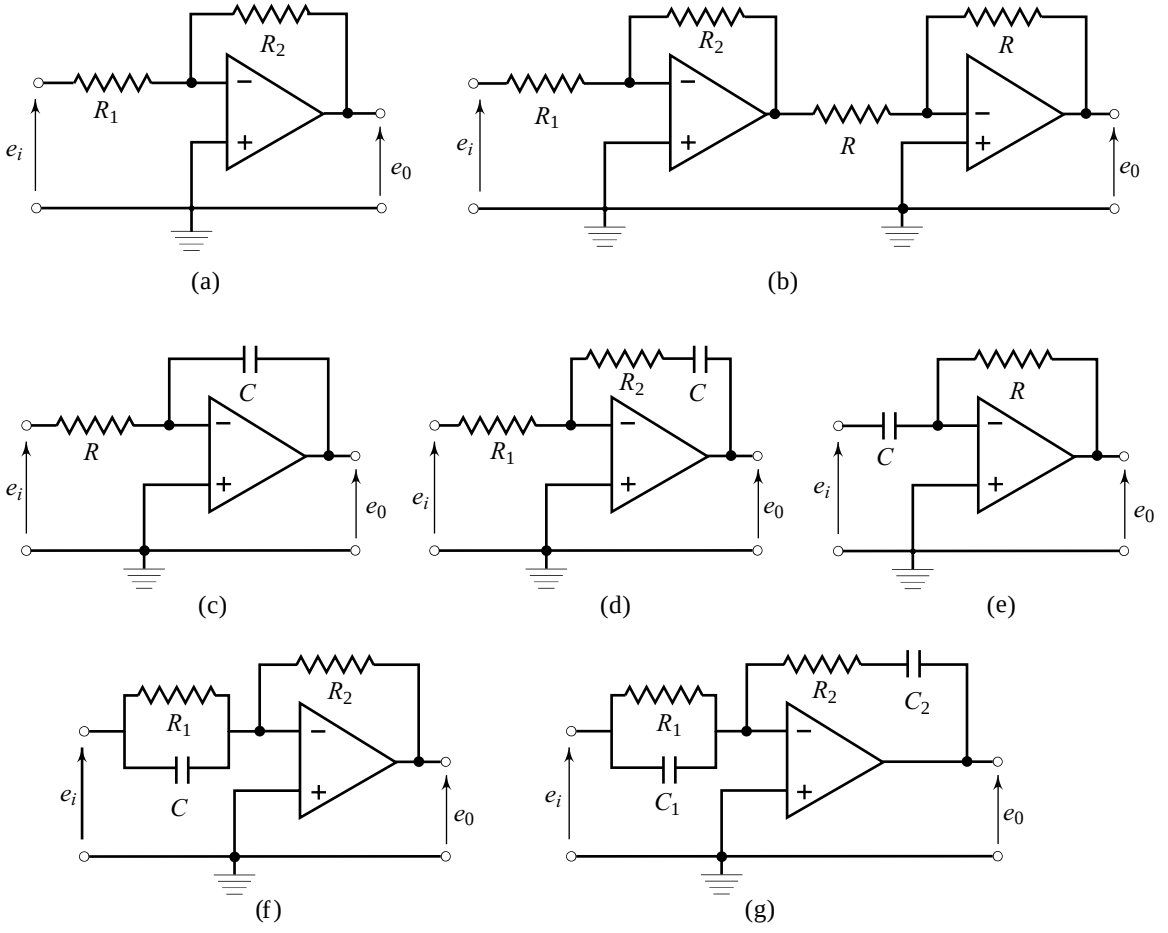

Fig. 2.39 Commonly used op amp circuits

$$= -\left[\frac{R_1C_1 + R_2C_2}{R_1C_2} + \frac{1}{R_1C_2 s} + R_2C_1 s\right] \tag{2.146a}$$

$$e_0(t) = -\frac{R_1C_1 + R_2C_2}{R_1C_2} e_i(t) - \frac{1}{R_1C_2}\int_0^t e_i(\tau)d\tau - R_2C_1\frac{de_i(t)}{dt} \tag{2.146b}$$

The circuit thus processes the input signal by 'proportional + integral + derivative' action.

2.13.2 Practical Op Amp Circuits

In the following, we outline the limitations of some of the circuits of Fig. 2.39, and give 'practical' circuits used in implementing compensator transfer functions of feedback control systems [44].

Gain-limited Integrator Figure 2.39c is the ideal op amp implementation of an integrator. The transfer function of this circuit is given by Eqn. (2.142a), and is reproduced below.

$$\frac{E_0(s)}{E_i(s)} = -\frac{1}{RCs} \tag{2.147}$$

The ideal integrator has infinite dc (zero frequency) gain. For applications requiring finite dc gain (In Chapter 7, we will discuss feedback-control applications), resistor R_1 connected in parallel with the capacitor C is used. Figure 2.40a shows this implementation. The resistor R_1 in conjunction with resistor R limits the maximum gain of the integrator.

The integrator gain now becomes

$$\frac{E_0(s)}{E_i(s)} = \frac{R_1/R}{R_1Cs + 1} \tag{2.148}$$

This (low frequency) gain-limited integrator can be thought of as a low-pass filter with a dc gain equal to R_1/R and a time-constant of R_1C.

In Fig. 2.40a, one amplifier is set up as an integrator with an output which is of opposite polarity to that of the input. To reverse the inverted signal, another amplifier has been added. The two amplifiers form a noninverting integrator, resulting in a positive output for a positive input.

Bandwidth-limited Differentiator Figure 2.39e is the ideal op amp implementation of a differentiator. The transfer function of the circuit is given by Eqn. (2.144a), and is reproduced below.

$$\frac{E_0(s)}{E_i(s)} = -RCs \tag{2.149}$$

The ideal differentiator has gain that increases with an increase in frequency and becomes infinite as frequency approaches infinity.

A significant amount of noise that occupies the high end of the frequency spectrum, gets superimposed on the sensor feedback signal which is processed by a PID controller. Since the gain of the derivative term increases linearly with frequency, the noise signal tends to be greatly amplified. To reduce the controller sensitivity to noise, amplifier gain needs to be limited. Without using a complex filtering scheme, it can be achieved by adding a resistor in series with the input capacitor. This network changes the amplifier characteristics, resulting in a limited high-frequency gain.

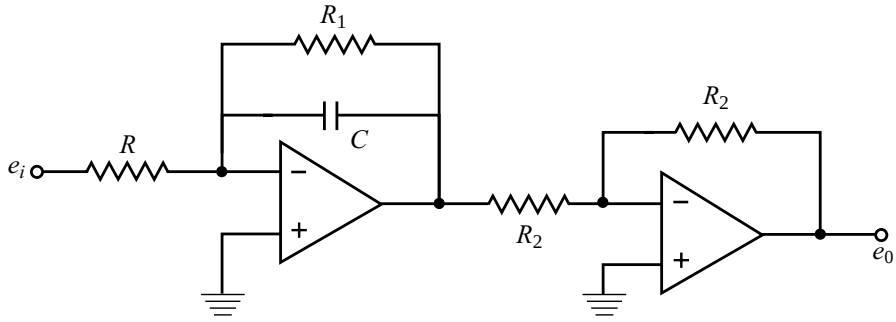

(a) Gain-limited integrator

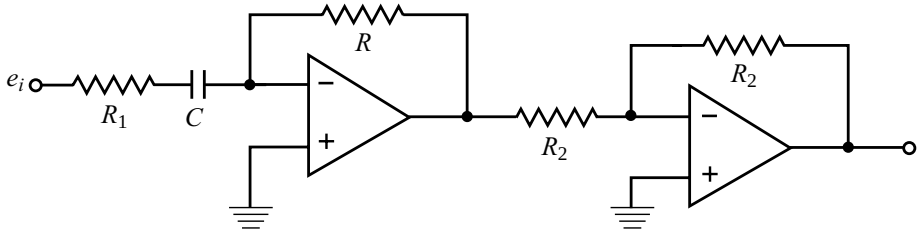

(b) Gain-limited differentiator

Fig. 2.40

A schematic diagram of the modified differentiator is shown in Fig. 2.40b. Resistor R_1 in conjunction with resistor R, limits the maximum amplifier gain. As the frequency increases, the impedance of the input capacitor becomes smaller. Because the amplifier gain is controlled by the ratio of the feedback and input impedances, with the input impedance becoming smaller with an increase in frequency, the amplifier gain continues to increase. The resistor R_1 in series with the capacitor sets a limit on the minimum value of input impedance.

The derivative gain now becomes

$$\frac{E_0(s)}{E_i(s)} = \frac{RCs}{R_1Cs+1} \tag{2.150}$$

This practical differentiator can be thought of as a derivative block followed by a low-pass filter with a time-constant equal to R_1C. The result is a bandwidth-limited derivative action.

Summing Amplifier The error detector in the general block diagram of a feedback control system shown in Fig.1.9 represents an operation of algebraic summation of reference and feedback signals. This operation can be implemented using an op amp circuit of Fig. 2.41. In this figure, two inputs are reference e_r and feedback e_b in volts. The output of the circuit

$$e_0 = \frac{R_f}{R}(e_r - e_b) \tag{2.151}$$

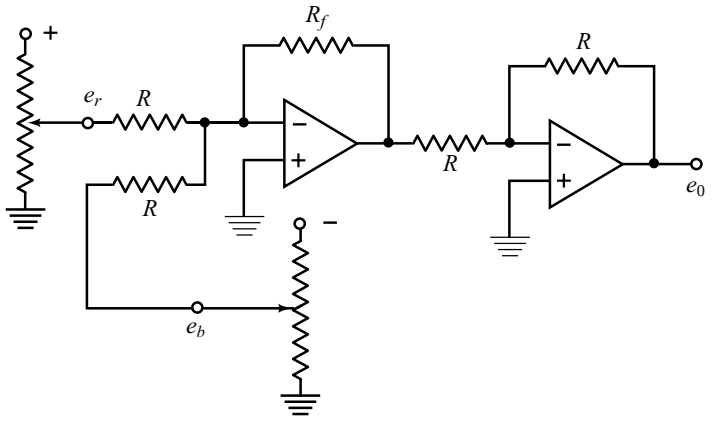

Fig. 2.41 A summing amplifier

Example 2.9 Consider the network shown in Fig. 2.42. The transfer function for this network can be obtained as follows.

The equivalent impedance of R_1 and C_1 is

$$Z_1(s) = \frac{R_1}{R_1C_1s + 1}$$

The equivalent impedance of R_2 and C_2 is

$$Z_2(s) = \frac{R_2}{R_2C_2s + 1}$$

The transfer function between the output $E_2(s)$ and the input $E_1(s)$ is

$$\frac{E_2(s)}{E_1(s)} = -\frac{Z_2(s)}{Z_1(s)} = -\frac{R_2}{R_1}\left(\frac{R_1C_1s + 1}{R_2C_2s + 1}\right) \quad (2.152)$$

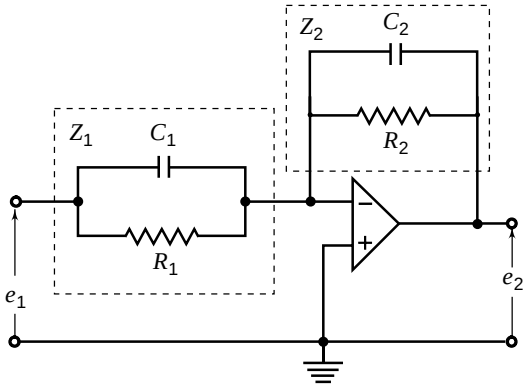

Fig. 2.42 Operational amplifier circuit

Notice that the transfer function in Eqn. (2.152) contains a minus sign. If this sign is not acceptable in the actual application, a sign inverter may be connected to either the input or the output of the network in Fig. 2.42. An example is shown in Fig. 2.43. The sign inverter has the transfer function

$$\frac{E_3(s)}{E_2(s)} = -\frac{R_4}{R_3}$$

Hence, the network shown in Fig. 2.43 has the following transfer function.

$$\frac{E_3(s)}{E_1(s)} = \frac{R_2R_4}{R_1R_3}\left(\frac{R_1C_1s + 1}{R_2C_2s + 1}\right) = \frac{R_4C_1}{R_3C_2}\left(\frac{s + \dfrac{1}{R_1C_1}}{s + \dfrac{1}{R_2C_2}}\right) \quad (2.153)$$

Controllers (also called compensators) are sometimes formulated with a transfer function of the form (this form, as we shall see in later chapters, effectively realizes PD control logic and is called *lead compensator*)

$$D(s) = K\left(\frac{s + 1/\tau}{s + 1/\alpha\tau}\right);\ \alpha < 1,\ K > 0,\ \tau > 0 \quad (2.154)$$

The network of Fig. 2.43 realizes a lead compensator if $R_1C_1 > R_2C_2$, as seen from Eqn. (2.153).

$$R_1C_1 = 1/\tau;\ R_2C_2 = 1/\alpha\tau;\ \frac{R_4C_1}{R_3C_2} = K$$

For given values of K, τ, and α; there are six op amp circuit parameters: R_1, R_2, R_3, R_4, C_1, and C_2; which are required for realization of the compensator. The values of the six circuit parameters are determined from the three compensator parameters using the three equations given above. There is an additional degree of freedom in the choice of the values of the circuit parameters which is used to set the impedance level of the network.

Another common formulation of compensators is of the form (this form, as we shall see in later chapters, effectively realizes PI control logic and is called *lag compensator*)

$$D(s) = K\left(\frac{s+1/\tau}{s+1/\beta\tau}\right);\ \beta > 1,\ K > 0,\ \tau > 0 \qquad (2.155)$$

The network of Fig. 2.43 realizes a lag compensator if $R_1C_1 < R_2C_2$, as seen from Eqn. (2.153).

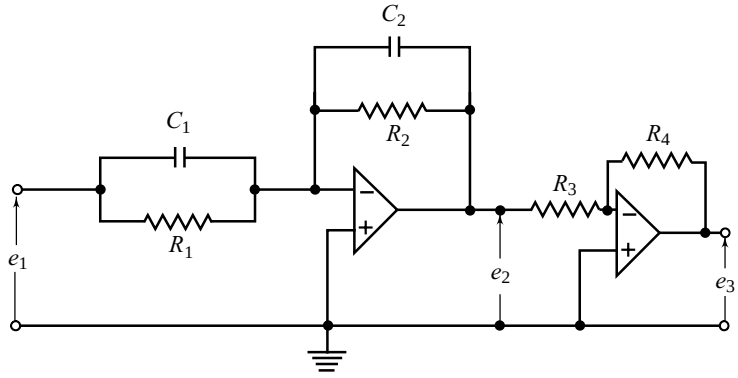

Fig. 2.43 Operational amplifier circuit used as a lead or a lag compensator

A *lag-lead compensator* (we shall encounter such designs in later chapters)

$$D(s) = K\left(\frac{s+1/\tau_2}{s+1/\beta\tau_2}\right)\left(\frac{s+1/\tau_1}{s+1/\alpha\tau_1}\right);\ \beta > 1,\ \alpha < 1,\ K > 0,\ \tau_1 > 0,\ \tau_2 > 0 \qquad (2.156)$$

may be realized by cascading two active networks as shown in Fig.2.44.

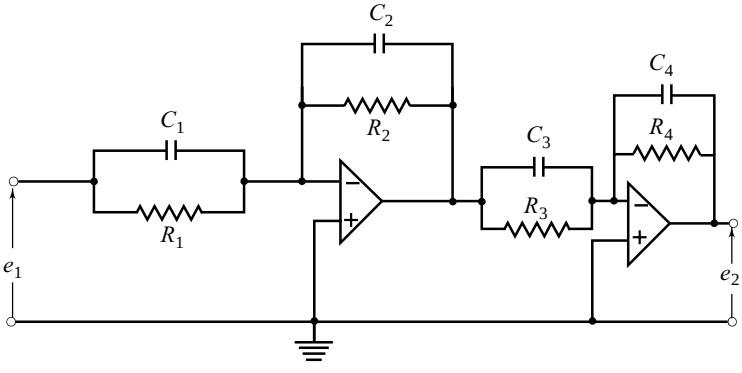

Fig. 2.44 Operational amplifier circuit used as a lag-lead compensator

In addition to realizing a given compensator transfer function, the impedance level of the op amp circuit is required to be set to acceptable values to reduce the loading effects in feedback loop.

It should be noted that many alternative circuit designs for a given compensation requirement are possible. Some practical circuits [44] are given in Problems 2.17-2.22. Choosing an optimal design is an important task for the control engineer (The topic of Operational-Amplifier circuit design is not covered in this book.)

Review Examples

Review Example 2.1 Consider a second-order system described by the transfer function

$$\frac{Y(s)}{R(s)} = \frac{K}{\frac{1}{\omega_n^2}s^2 + \frac{2\zeta}{\omega_n}s + 1}$$

where ω_n = undamped natural frequency, and ζ = damping ratio.
For an underdamped system, $0 < \zeta < 1$.
Assume that this system is excited by a unit ramp input

$$R(s) = \frac{1}{s^2}$$

This gives

$$Y(s) = \frac{K\omega_n^2}{s^2(s^2 + 2\zeta\omega_n s + \omega_n^2)} = K\left[\frac{1}{s^2} - \frac{2\zeta/\omega_n}{s} + \frac{2\zeta}{\omega_n}\frac{s + \zeta\omega_n}{(s + \zeta\omega_n)^2 + \omega_d^2} + \frac{2\zeta^2 - 1}{(s + \zeta\omega_n)^2 + \omega_d^2}\right]$$

where $\omega_d = \omega_n\sqrt{1-\zeta^2}$.

Using the table of transform pairs given in Table 2.1, we get

$$\begin{aligned} y(t) &= K\left[t - \frac{2\zeta}{\omega_n} + \frac{2\zeta}{\omega_n}e^{-\zeta\omega_n t}\cos\omega_d t + \frac{(2\zeta^2 - 1)}{\omega_d}e^{-\zeta\omega_n t}\sin\omega_d t\right] \\ &= K\left[t - \frac{2\zeta}{\omega_n} + \frac{e^{-\zeta\omega_n t}}{\omega_d}\left\{2\zeta\sqrt{1-\zeta^2}\cos\omega_d t + (2\zeta^2 - 1)\sin\omega_d t\right\}\right] \\ &= Kt - \frac{2\zeta}{\omega_n}K + \frac{Ke^{-\zeta\omega_n t}}{\omega_n\sqrt{1-\zeta^2}}\sin\left(\omega_d t + 2\tan^{-1}\frac{\sqrt{1-\zeta^2}}{\zeta}\right) \end{aligned} \tag{2.157}$$

The last term in this expression is the transient response term, which decays to zero with increasing time. Its rate of decay is dictated by the time-constant $1/\zeta\omega_n$. The steady-state component of the response to unit ramp input $r(t) = t$ is

$$y_{ss} = K\left(t - \frac{2\zeta}{\omega_n}\right) \tag{2.158}$$

which is also a ramp function.

Note that the steady-state ramp output is nothing but Kt delayed by $2\zeta/\omega_n$ as shown in Fig. 2.45. The damped oscillations contributed by the transient component of the response are centred on the ramp. If K does not equal 1, the response diverges from the unit ramp input as t increases.

By similar analysis, it can easily be established that the critically damped and overdamped responses ($\zeta \geq 1$) are characterized by the exponential rise toward the steady-state ramp output $K\left(t - \dfrac{2\zeta}{\omega_n}\right)$.

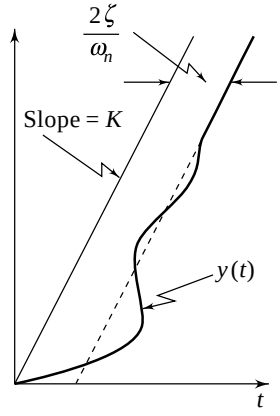

Fig. 2.45 Ramp response of second-order underdamped systems

Review Example 2.2 Consider the mechanical system shown in Fig. 2.46a. This system is a simplified 'one-wheeled' model of an automobile suspension system with M_1: the mass of the automobile, B: the shock absorbers, K_1: the springs, M_2: the mass of the wheels, and K_2: the elasticity of the tyres. The system objective is to reduce vibrations $y_1(t)$ due to disturbance force $F_w(t)$.

The displacements $y_1(t)$ and $y_2(t)$ are considered with respect to positions of the vehicle and the wheels on a level road under the loaded condition. The gravitational forces, therefore, do not appear in the model being formulated.

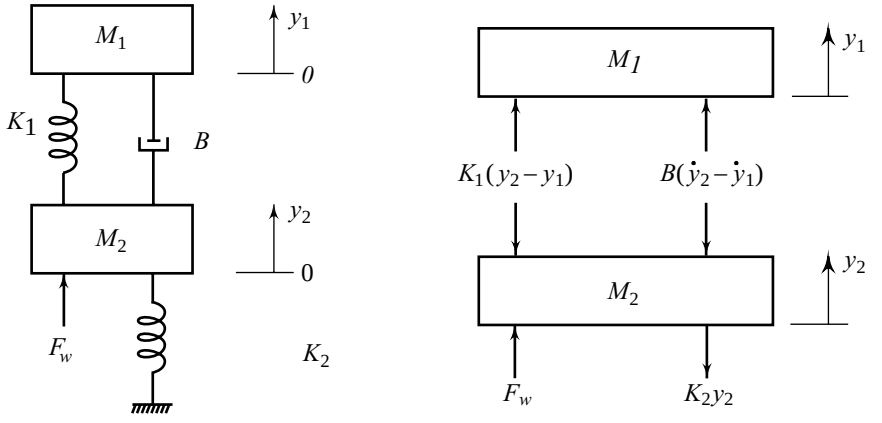

Fig. 2.46

Figure 2.46b shows the free-body diagram for the system. From this figure, we have the following differential equations describing the dynamics of the system.

$$M_1 \ddot{y}_1(t) = K_1(y_2(t) - y_1(t)) + B(\dot{y}_2(t) - \dot{y}_1(t)) \quad (2.159a)$$

$$M_2 \ddot{y}_2(t) = F_w(t) - K_1(y_2(t) - y_1(t)) - B(\dot{y}_2(t) - \dot{y}_1(t)) - K_2 y_2(t) \quad (2.159b)$$

Taking the Laplace transform of these equations, assuming zero initial conditions, we obtain

$$M_1 s^2 Y_1(s) + B(sY_1(s) - sY_2(s)) + K_1(Y_1(s) - Y_2(s)) = 0 \quad (2.160a)$$

$$M_2 s^2 Y_2(s) + B(sY_2(s) - sY_1(s)) + K_1(Y_2(s) - Y_1(s)) + K_2 Y_2(s) = F_w(s) \quad (2.160b)$$

Suppose that a transfer function is desired between $F_w(s)$ and $Y_1(s)$, i.e., between the disturbance force applied to the wheels and the resulting displacement of the automobile. This transfer function can be found by eliminating $Y_2(s)$ in Eqns (2.160). Solving Eqn. (2.160a) for $Y_1(s)$, we obtain

$$Y_1(s) = \frac{Bs + K_1}{M_1 s^2 + Bs + K_1} Y_2(s)$$

Now Eqn. (2.160b) can be solved for $Y_2(s)$:

$$Y_2(s) = \frac{1}{M_2 s^2 + Bs + K_1 + K_2} F_w(s) + \frac{Bs + K_1}{M_2 s^2 + Bs + K_1 + K_2} Y_1(s)$$

Eliminating $Y_2(s)$ from these equations, gives

$$G(s) = \frac{Y_1(s)}{F_w(s)}$$

$$= \frac{Bs + K_1}{[M_1 M_2 s^4 + B(M_1 + M_2)s^3 + (K_1 M_2 + K_1 M_1 + K_2 M_1)s^2 + K_2 Bs + K_1 K_2]}$$

The dynamics of the mechanical system are completely described by this transfer function. Given the mass of the automobile, the mass of the wheels, and the elasticity of the tyres, the smoothness of the ride is determined by the parameters of the shock absorber and the springs. These parameters are used to tune the system to give a good response. As a physical shock absorber deteriorates, the value of the parameter B changes the transfer function and quality of the ride.

A spring-mass-damper system may be schematically represented as a network by showing the mass as a two-terminal component; one terminal is free and has associated with it the motional variable v, and the other terminal represents a reference (commonly earth) with respect to which the motional variable of the free terminal is measured. As an example, the mechanical system of Fig. 2.46a is redrawn in Fig. 2.47 which may be referred to as the *mechanical network*.

The dynamical equations of the system of Fig. 2.46a could also be obtained by writing nodal equations for the mechanical network of Fig. 2.47 (with force and velocity analogous to current and voltage, respectively; the algebraic sum of all the forces at a node is zero).
The result is

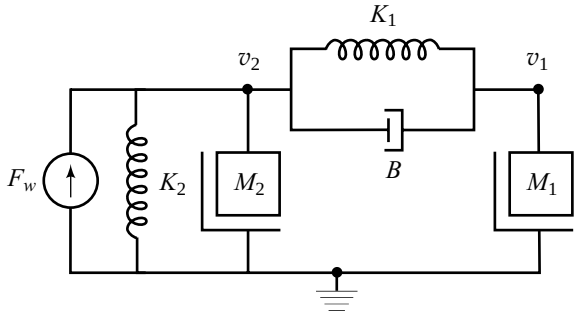

Fig.2.47 Mechanical network for the system of Fig. 2.46a

$$M_1 \dot{v}_1 + B(v_1 - v_2) + K_1 \int_{-\infty}^{t} (v_1 - v_2)dt = 0$$

$$M_2 \dot{v}_2 + K_2 \int_{-\infty}^{t} v_2 dt + B(v_2 - v_1) + K_1 \int_{-\infty}^{t} (v_2 - v_1)dt = F_w$$

Since $\int_{-\infty}^{t} v dt = y$, we can write these equations as

$$M_1 \dot{v}_1 + B(v_1 - v_2) + K_1(y_1 - y_2) = 0$$

$$M_2 \dot{v}_2 + K_2 y_2 + B(v_2 - v_1) + K_1(y_2 - y_1) = F_w$$

The result is the same as obtained earlier in Eqns (2.159) using the free-body diagram approach.

Review Questions

2.1 Define a linear time-invariant system. Explain superposition and decomposition properties which linear systems obey.

2.2 Dynamic behaviour of control systems can be adequately judged and compared under application of standard test signals. Describe various standard test signals commonly used in control system design. Give time-domain and *s*-domain representations of the signals.

2.3 State and prove the final value theorem of the Laplace transform. What is the condition under which the theorem is valid?

2.4 Explain the reasons for dead-time element in process control loops. Show that dead-time can be represented by the transfer function $e^{-s\tau_D}$. How do you approximate this transfer function by a rational function?

2.5 What is the definition of "transfer function"? What are the properties of systems whose responses can be described by transfer functions?

2.6 (a) Interconnection of various sub-systems in a feedback control system is required to be non-loading. Why ?

(b) Explain the use of op amp interposed as buffer amplifier between the sub-systems to reduce loading effects.

2.7 Sketch op amp circuits capable of providing outputs which approximate to

(a) proportional plus integral of the input;

(b) proportional plus derivative of the input; and

(c) proportional plus integral plus derivative of the input.

Problems

2.1 (a) The transfer function of a first-order process is given by

$$\frac{Y(s)}{R(s)} = G(s) = \frac{K}{\tau s + 1}$$

(i) Find the impulse response to an impulse of strength A.

(ii) Find the step response to a step of strength A.

(iii) Find the ramp response to a ramp function with slope A.

(iv) Find the response to sinusoidal input $A \sin \omega t$.

Identify the steady-state and transient components of the response in each case.

(b) Consider a second-order model

$$\frac{Y(s)}{R(s)} = G(s) = \frac{\omega_n^2}{s^2 + 2\zeta\omega_n s + \omega_n^2}\ ;\ 0 < \zeta < 1$$

Find the response $y(t)$ to the input

(i) $r(t) = \mu(t)$, a unit step function (ii) $r(t) = t\mu(t)$, a unit ramp function

Find the steady-state component y_{ss} of $y(t)$ in each case.

Will the final value theorem give the correct value of y_{ss} in each case? Why?

2.2(a) Find the response of the system

$$\frac{Y(s)}{R(s)} = \frac{K}{\tau s + 1}$$

to a unit-step input $r(t)$, and discuss the effects of variations in parameters K and τ on transient behaviour.

(b) Find the response of the system

$$\frac{Y(s)}{R(s)} = \frac{K\omega_n^2}{s^2 + 2\zeta\omega_n s + \omega_n^2}$$

to a unit-step input $r(t)$, and discuss the effects of variations in parameters K, ζ and ω_n on transient behaviour.

MATLAB Exercise Using Control System Toolbox, obtain step-response plots for a range of parameter sets, and therefrom give your analysis of the effects of variations in parameters.

2.3 (a) A system with impulse response

$$g(t) = e^{-t}(1 - \sin t)$$

is subjected to unit-step input. Find the transfer function, and therefrom obtain the steady-state value of the output.

MATLAB Exercise Use Symbolic Math Toolbox to find the Laplace transform of $g(t)$.

(b) Determine unit-ramp response of a system having the transfer function

$$G(s) = \frac{s+1}{s+2}$$

What is the steady-state value of the response?

MATLAB Exercise Use Symbolic Math Toolbox to find the inverse Laplace transform of $G(s)\,R(s)$. Also using Control System Toolbox (**lsim** command), plot the ramp response.

2.4 A second-order transfer function model is given by

$$\frac{Y(s)}{R(s)} = \frac{10000}{s^2 + 600s + 10000}$$

and the input is $r(t) = 25t\,\mu(t)$.

Show that the response is able to track the input with a steady-state delay of 60 msec. What is the value of steady-state error: $\lim_{t\to\infty}(r(t) - y(t))$?

2.5 The parameters of the mechanical system of Fig. P2.5 are

M = 1,000 kg; B = 10,000 N/(m/sec); and

K = 100,000 N/m

A step force of 1000 Newtons is applied to the mass at $t = 0$.

The initial conditions are $y(0) = \dot{y}(0) = 0$.

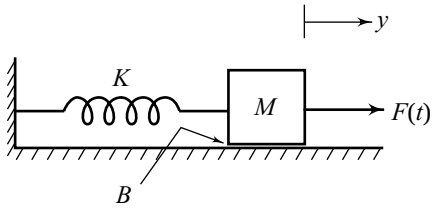

Fig. P2.5

From the physical parameters of the system, obtain the parameters: damping ratio ζ, undamped natural frequency ω_n, and damped natural frequency ω_d, which describe the dynamical behaviour of the system. Also obtain the step response.

MATLAB Exercise Use Symbolic Math Toolbox to find the inverse Laplace transform of $Y(s)$. Also using Control System Toolbox, plot the step response.

2.6 (a) Prove that the steady-state output of a system having transfer function $G(s)$ with all the poles in the left-half of s-plane, and input $r(t) = R_0 \cos(\omega_0 t)$ is given by

$$y_{ss}(t) = R_0|Gj\omega_0)|\cos(\omega_0 t + \phi); \phi = \angle G(j\omega_0)$$

(b) A sinusoidal input $r(t) = 2 \sin 2t$ is applied to a system with transfer function

$$G(s) = \frac{2}{s(s+2)}$$

Determine the steady-state output $y_{ss}(t)$.

2.7 Consider a system described by the differential equation

$$\ddot{y}(t) + 7\dot{y}(t) + 10\, y(t) = \dot{r}(t) + 3\, r(t)$$

(a) Find the system response to an input $e^{-t}\mu(t)$ assuming zero initial conditions.

(b) Find the system response to an input $e^{-t}\mu(t)$ when the initial conditions are $y(0) = 1$, $\dot{y}(0) = 1/2$.

MATLAB Exercise Use Symbolic Math Toolbox to find the inverse Laplace transform of $Y(s)$.

2.8 Consider the system of Fig. P2.8a, where an ac motor designed to run at a constant speed is mounted on a cantilever system. The rotating part of the motor has an eccentricity; this gives rise to an exciting force of frequency ω_F; $F(t) = A \sin \omega_F t$.
A lumped -parameter model of the system of Fig. P2.8a is of the form shown in Fig. P2.8b. Show that the sinusoidal transfer function of the model is

$$G(j\omega) = \frac{Y(j\omega)}{F(j\omega)} = \frac{1/K}{1 - \left(\frac{\omega}{\omega_n}\right)^2}; \omega_n = \sqrt{K/M}$$

Find the steady-state response of the system to an input $F(t) = A \sin \omega_F t$; therefrom show that the machine vibrates, and the vibrations become violent as the forcing frequency ω_F approaches ω_n.

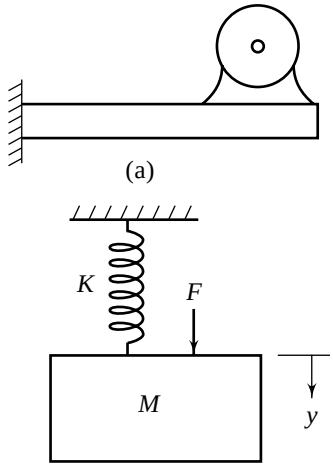

Fig. P2.8

2.9 Measurements made on vehicles travelling on typical roads have shown that some construction techniques result in sinusoidal wave patterns in the road surface; a representative wavelength λ is 15 m, and a representative road-surface peak amplitude is 7.5 cm. The forcing frequency of road patterns on a vehicle travelling with a speed of v m/sec is $\omega = 2\pi v/\lambda$ rad/sec.

A simplified representation of a vehicle's front wheel system consisting of a tyre of mass M and a shock absorber of damping coefficient B is shown in Fig. P2.9. Spring K_1 represents the elasticity of the tyre, while K represents that of shock absorber. We assume that the inertia of the car body is so large that the body can be considered as a fixed support.

Determine the transfer function $X(s)/Y(s)$ and therefrom obtain the peak amplitude of the tyre displacement x when the car speed is 100 km/hr.

Given: M = 15 kg, B = 5.25 kN/(m/sec), K_1 = 175 kN/m, and K = 35 kN/m.

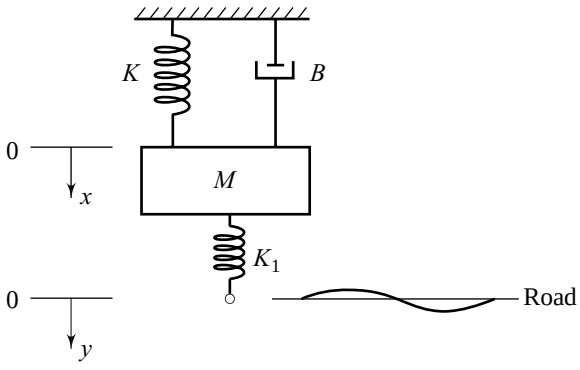

Fig. P2.9

2.10 Figure P2.10a shows a machine of mass M mounted on a foundation using a spring of stiffness K with a damper of coefficient B in parallel.

(a) The machine generates a disturbing force $F(t) = A \sin \omega t$. Find the force transmitted to the foundation at steady-state.

(b) With reference to Fig. P2.10b, determine the machine vibration $x(t)$ due to the foundation vibration $y(t) = A \sin \gamma t$.

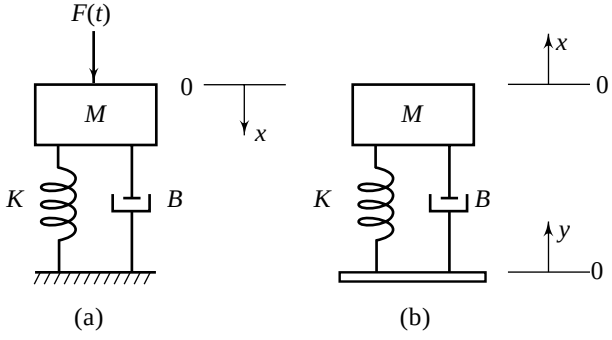

Fig. P2.10

2.11 A dynamic absorber is shown in Fig. P2.11. This system is representative of many situations involving the vibration of machines containing unbalanced components. The parameters M_2, K_2 and B_2 may be chosen so that the main mass M_1 does not vibrate in response to foundation vibration. Obtain a set of differential equations describing the dynamics of the system.

2.12 The stirred tank sketched in Fig. P2.12 is used to heat a process stream by steam condensing inside a coil.

Given:

λ = latent heat of condensation of saturated steam = 2247×10^3 Joules/kg

C_1 = thermal capacitance of the coil mass = 503×10^3 J/°C

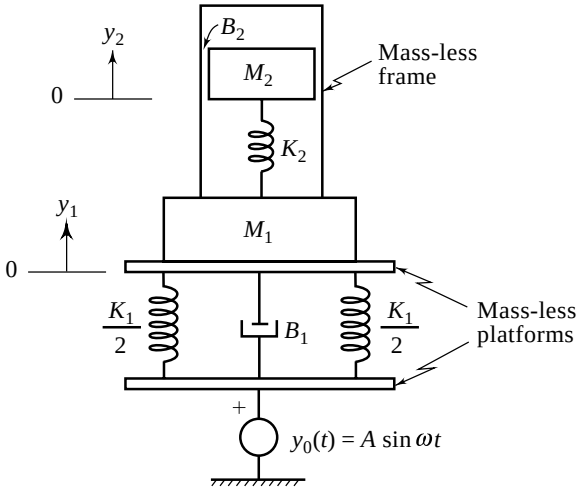

Fig. P2.11

U = overall convective heat transfer coefficient at the coil-liquid interface
= 42.97×10^3 J/(min) (m^2) (°C)

A = heat transfer area = 22.57 m^2

Q = feed flow rate = 0.425 m^3/min

ρ = density of the feed = 1090 kg/m^3

c = heat capacity of the feed = 3350 J/(kg) (°C)

V = volume of the liquid in the tank = 3.4 m^3

θ_1, θ_2 : perturbations (°C) of the temperature of coil mass and liquid in the tank, respectively, in response to perturbation q_m (kg/min) in the steam flow rate.

θ_i = perturbation of the temperature of the feed (disturbance input).

Derive the transfer function models $\left.\frac{\theta_2(s)}{Q_m(s)}\right|_{\theta_i=0}$, and $\left.\frac{\theta_2(s)}{\theta_i(s)}\right|_{q_m=0}$.

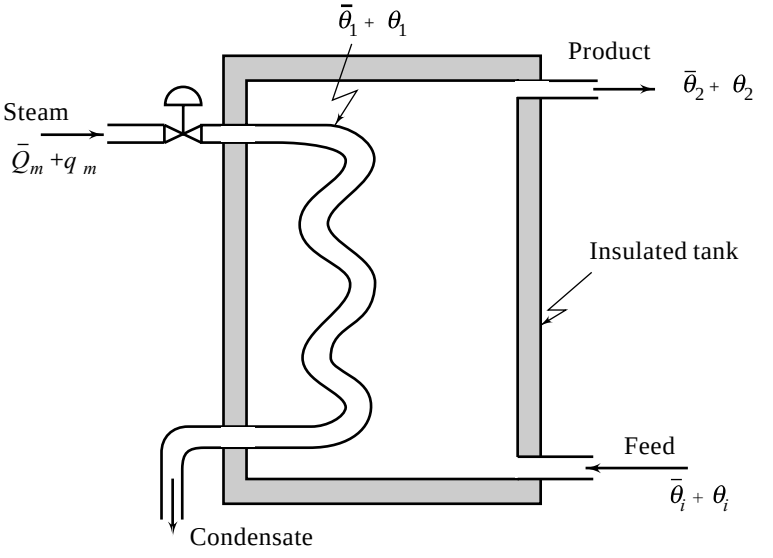

Fig. P2.12

2.13 Reconsider the stirred tank of Problem 2.12 (Fig. P2.12). At the steady-state, the temperature of the feed is $\bar{\theta}_i$ = 55°C, and the temperature of the liquid in the tank is $\bar{\theta}_2$ = 80 °C. Find the steady-state mass flow rate $\bar{Q}_m$ of steam through the control valve.

2.14 Figure P2.14 shows a process consisting of two interconnected tanks with surface areas A_1 and A_2. h_1 and h_2 are the deviations in tank levels from equilibrium values. q_1 is the deviation in inflow rate from equilibrium value, and R_0, R_1 and R_2 are linearized valve resistance values (R = incremental change in pressure across the valve/incremental change in flow through the valve). The flow rate q_1 into the tank is controlled by the signal x_1 via valve and actuator, and is modelled by the linear equation

$$q_1 = K_1 x_1$$

We are interested in knowing how the tank levels will respond to changes in x_1. Develop suitable transfer function models for the system.

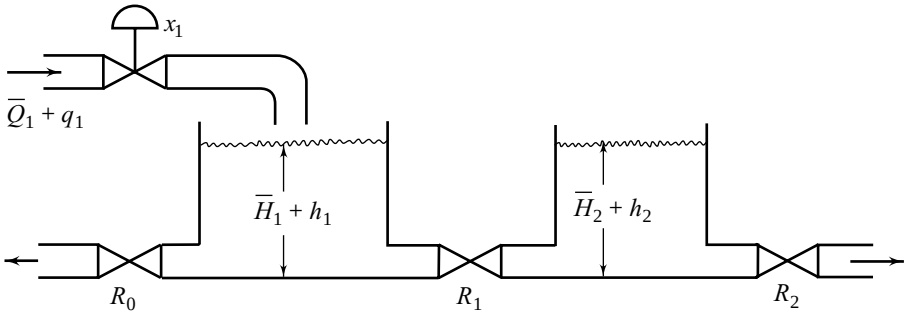

Fig. P2.14

Given: $A_1 = 1, A_2 = 0.5, K_1 = 1, R_0/\rho g = 1, R_1/\rho g = 0.5, R_2/\rho g = 2$
ρ = density of the liquid, and g = acceleration due to gravity

2.15 The scheme of Fig. P2.15 describes a simple liquid-level control process. h and q_i are, respectively, deviations in tank level and inflow rate from equilibrium values; A is the surface area of the tank and R is linearized valve resistance value (R=incremental change in pressure across the valve/incremental change in flow through the valve). The flow rate q_i is controlled by the signal x, and is modelled by $q_i = K_v x$.

We are interested in knowing how the tank level will respond to changes in x under the following disturbances: (i) Liquid is drawn off from the tank (to be used elsewhere in the processing operation) by a variable displacement pump. q_w is the disturbance flow rate (ii) The tank of Fig. P2.15 is connected to another tank in the processing operation; there is a variable back pressure p_w at the orifice outlet.

Develop a differential equation model for the system.

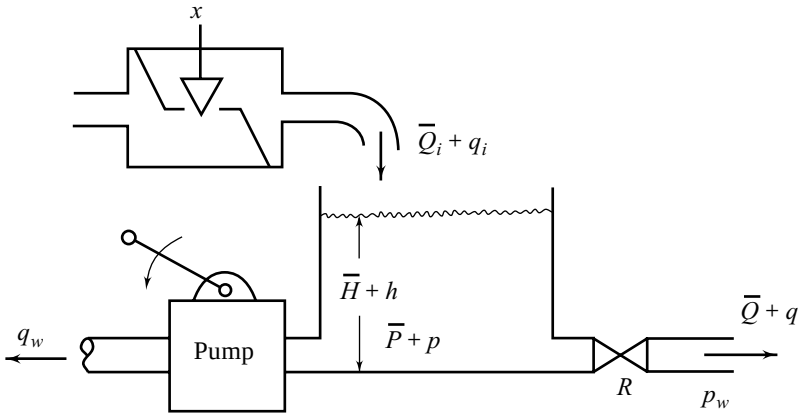

Fig. P2.15

2.16 The transfer function of a dead-time element $e^{-\tau_D s}$ may be approximated by a rational function. Two often-used approximations are given below:

(i) $e^{-\tau_D s} = \dfrac{1 - \tau_D s/2}{1 + \tau_D s/2}$ (ii) $e^{-\tau_D s} = \dfrac{1 - \tau_D s/2 + \tau_D^2 s^2/12}{1 + \tau_D s/2 + \tau_D^2 s^2/12}$

Prove that the first approximation is correct through the first three terms, and the second approximation is correct through the first five terms of the Taylor series expansion of $e^{-\tau_D s}$.

2.17 Show that the parallel arrangement of 'constant gain amplifier' and 'differentiator' op amp circuits shown in Fig. P2.17 is a realization of the transfer function

$$D(s) = K_P + K_D s$$

of a 'proportional + derivative' compensator. Determine the parameters K_P and K_D in terms of the parameters of the circuit.

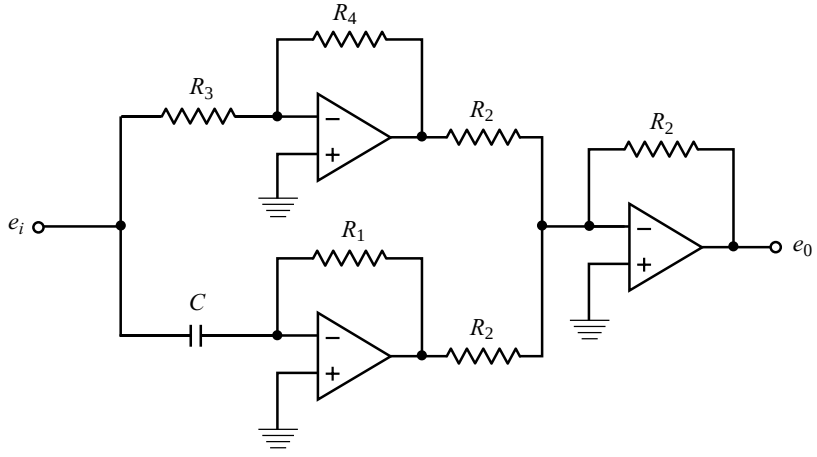

Fig. P2.17

2.18 Show that the parallel arrangement of 'constant gain amplifier' and 'integrator' op amp circuits shown in Fig. P2.18 is a realization of the transfer function

$$D(s) = K_P + K_1/s$$

of a 'proportional + integral' compensator.
Determine the parameters K_P and K_I in terms of the parameters of the circuit.

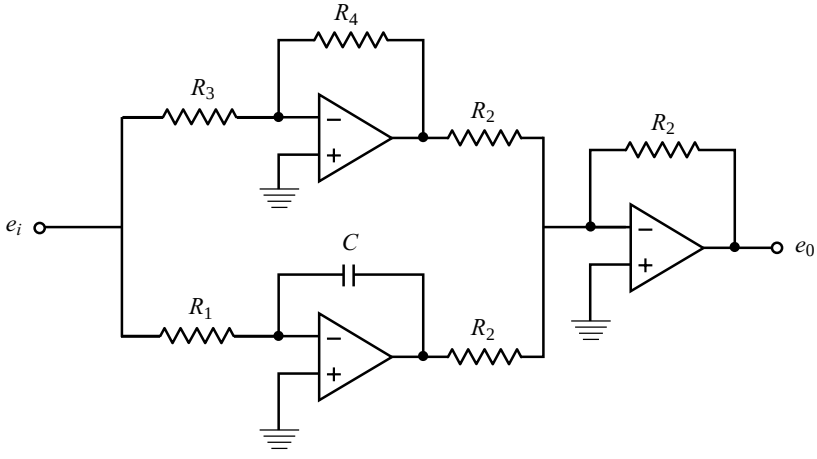

Fig. P2.18

2.19 Consider the PD circuit (TF : $K_2 + K_d s$) of Fig. P2.17, cascaded with the PI circuit (TF : $K_1 + K_i/s$) of Fig. P2.18 (In principle, it makes no difference whether the PD element or the PI element comes first). The cascaded circuit is shown in Fig. P2.19. Show that it realizes the transfer function

$$D(s) = K_P + K_I/s + K_D s$$

of a 'proportional + integral + derivative' compensator.
Determine K_P, K_I and K_D in terms of K_2, K_d, K_1 and K_i.

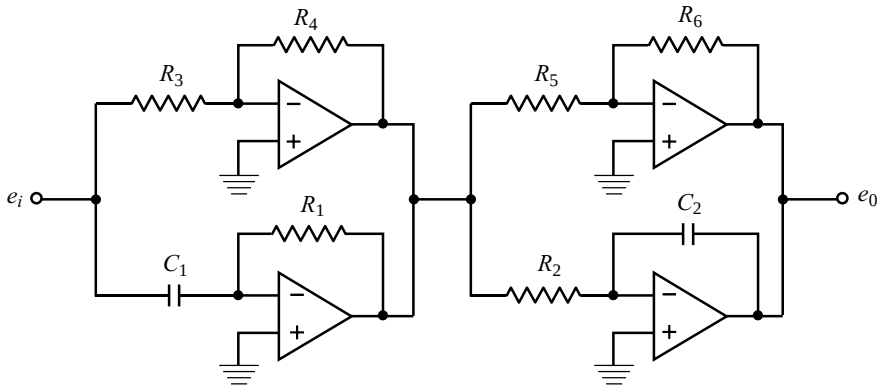

Fig. P2.19

2.20 (a) Show that the parallel arrangement of 'constant gain amplifier' and 'bandwidth-limited differentiator' op-amp circuits shown in Fig. P2.20 is a realization of the transfer function

$$D(s) = K_2 + \frac{K_1 s}{\tau_1 s + 1}$$

of a 'proportional + bandwidth-limited derivative' compensator.
Determine the parameters K_2, K_1, and τ_1 in terms of the parameters of the circuit.

(b) Compensators are sometimes formulated with a transfer function of the form (called *lead compensator*)

$$D(s) = K_c \left(\frac{\tau s + 1}{\alpha \tau s + 1} \right) \; ; \; \alpha < 1, K_c > 0, \; \tau > 0$$

Prove that this transfer function can be obtained with the parallel arrangement of op amp circuits shown in Fig. P2.20. Determine K_c, τ and α in terms of K_2, K_1, and τ_1.

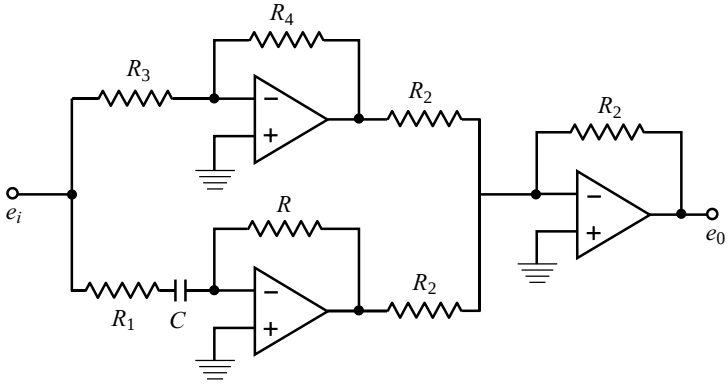

Fig. P2.20

2.21 (a) Show that the parallel arrangement of 'constant gain amplifier and gain-limited integrator' op amp circuits shown in Fig. P2.21 is a realization of the transfer function

$$D(s) = K_2 + \frac{K_1}{\tau_1 s + 1}$$

of a 'proportional + gain-limited integral' compensator.

Determine the parameters K_2, K_1, and τ_1 in terms of the parameters of the circuit.

(b) Compensators are sometimes formulated with a transfer function of the form (called *lag compensator*)

$$D(s) = K_c\left(\frac{\tau s + 1}{\beta\tau s + 1}\right);\ \beta > 1,\ K_c > 0,\ \tau > 0$$

Prove that this transfer function can be obtained with the parallel arrangement of op amp circuits shown in Fig. P2.21. Determine K_c, τ and β in terms of K_2, K_1 and τ_1.

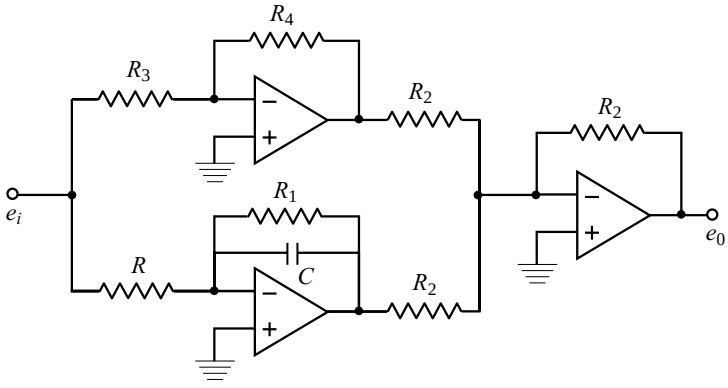

Fig. P2.21

2.22 Show that the circuit of Fig. P2.22 (cascade of 'proportional + bandwidth-limited derivative', and 'proportional + gain-limited integral') realizes the transfer function.

$$D(s) = K_c\left(\frac{\tau_1 s + 1}{\alpha\tau_1 s + 1}\right)\left(\frac{\tau_2 s + 1}{\beta\tau_2 s + 1}\right);\ \alpha < 1,\ \beta > 1,\ K_c > 0,\ \tau_1 > 0,\ \tau_2 > 0$$

of a lag-lead compensator.

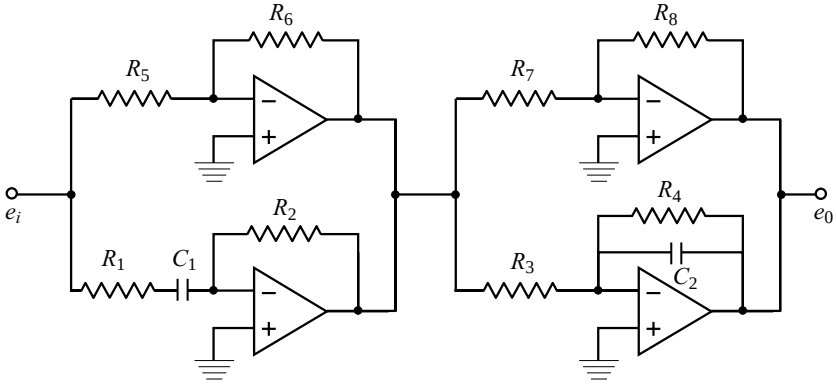

Fig. P2.22

3 Models of Industrial Control Devices and Systems

3.1 INTRODUCTION

Control engineering is an exciting and challenging field within the engineering sciences, because by its very nature it is a multidisciplinary subject and it plays a critical role in many practical technical applications. To be more specific, control theory brings together such different fields as electrical, mechanical and chemical engineering and applied mathematics. It plays a major role in engineering applications of all kinds of complexity. This may be a dc motor, a robot arm, an aircraft, a satellite, a power plant or a plant for chemical industries such as a distillation column.

The most fundamental idea of control theory is to change the dynamical behaviour of a plant by a controller such that the dynamics gets certain desired properties. In almost all cases, the controller design is done by building a mathematical model, which can be emulated on a computer and serves as the basis for controller synthesis. It is obvious that the model represents the real system only to a certain degree of accuracy. Despite this, the controller has to work for the real system as well as the model; in other words, it has to be "robust" against errors in the mathematical model.

Building a mathematical model for a plant, actuator, or sensor means that physical laws have to be applied to find the differential equations which govern the dynamics of the system. A decision has to be made on the level of detail to which the mathematical model has to be developed. This requires good engineering judgement and some experience. Once the differential equations which govern the system are found, a computer simulation is built for analysis. This may be done by using a simulation tool such as MATLAB/SIMULINK (Appendix A). There is no simple recipe for model building which is applicable to any thinkable situation.

Our discussion in this chapter is limited to the widely used control devices and systems for control of speed or position of an inertia load, and for control of temperature, or pressure of a process fluid. The objective is to show the reader how the mathematical models that we shall be dealing with in the remainder of the book arise from physical systems.

Control configurations and control laws employed in our examples represent only the conceptual designs of control systems for given control problems. In most of our examples, we have used a simple proportional control law realized by an amplifier. It should be understood that these conceptual designs may not be the

final designs to be adopted. It may be necessary to modify a conceptual design after completing a detailed analysis of its mathematical model. In some cases, the entire conceptual design may have to be discarded as unsuitable in favour of another design. This chapter meets the limited objective of deriving a mathematical model of a control system for a given conceptual design. Several of the examples given in this chapter will be reconsidered later for detailed analysis and design.

3.2 GENERALIZED BLOCK DIAGRAM OF A FEEDBACK SYSTEM

We have already used block diagrams to represent the input–output behaviour of a linear system; the signal into the *block* represents the input, the signal out of the block represents the output, while the block itself stands for the transfer function of the linear system (Fig. 3.1a). The flow of information (signal) is unidirectional from the input to the output, with the output being equal to the input multiplied by the transfer function of the block. A complex system comprising of several non-loading elements is represented by the interconnection of the blocks for the individual elements. The blocks are connected by lines and arrows indicating the unidirectional flow of information from the output of one block to the input of the other (Fig. 3.1b). In addition to this, a *summing junction* (Fig. 3.1c) in a block diagram represents the dynamic summation of signals, and a *branch point* (Fig. 3.1d) is a take-off point at which the information branches out and goes concurrently to other blocks or summing junctions.

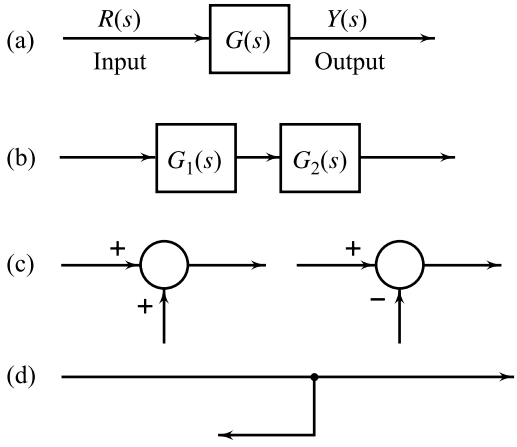

Fig. 3.1 Elements of a block diagram

Various feedback control configurations were described in Chapter 1 using block diagrams of general functional nature. With the transfer function concept introduced in Chapter 2, we are now equipped to consider *operational block diagrams* necessary for design and analysis. We begin with the block diagram shown in Fig. 3.2. It represents the basic structure of feedback control systems (refer Fig. 1.9). Not all systems can be forced into this format, but it serves as a reference for discussion.

In Fig. 3.2, the variable $y(t)$ is the *controlled variable* of the system. The desired value of the controlled variable is $y_r(t)$; the *command input* $y_r(t)$ and $y(t)$ have the same units. In this chapter, we will discuss many motion control systems with speed or position of an inertia load as controlled variable. Process control examples with temperature, or pressure of a process fluid as controlled variable will also appear.

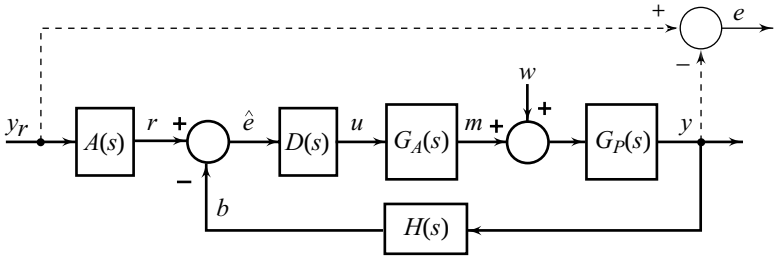

Fig. 3.2 Generalized operational block diagram of a feedback system

The *feedback elements* with transfer function $H(s)$ are system components that act on the controlled variable $y(t)$ to produce the *feedback signal* $b(t)$. $H(s)$ typically represents the sensor action to convert the controlled variable $y(t)$ to an electrical sensor output signal $b(t)$.

The *reference input elements* with transfer function $A(s)$ convert the command signal $y_r(t)$ into a form compatible with the feedback signal $b(t)$. The transformed command signal is the actual physical input to the system. This actual signal input is defined as the *reference input*.

The comparison device (*error detector*) of the system compares the reference input $r(t)$ with the feedback signal $b(t)$ and generates the *actuating error signal* $\hat{e}(t)$. The signals $r(t)$, $b(t)$ and $\hat{e}(t)$ have the same units. The *controller* with transfer function $D(s)$ acts on the actuating error signal to produce the *control signal* $u(t)$.

The control signal $u(t)$ has the knowledge about the desired control action. The power level of this signal is relatively low. The *actuator elements* with transfer function $G_A(s)$ are the system components that act on the control signal $u(t)$ and develop enough torque, pressure, heat, etc. (*manipulated variable* $m(t)$), to influence the *controlled system*. $G_P(s)$ is the transfer function of the controlled system.

The *disturbance* $w(t)$ represents the undesired signals that tend to affect the controlled system. The disturbances may be introduced into the system at more than one location.

The dashed-line portion of Fig. 3.2 shows the *system error* $e(t) = y_r(t) - y(t)$. Note that the actuating error signal $\hat{e}(t)$ and the system error $e(t)$ are two different variables.

Figure 3.2 defines the basic types of signals and components necessary for the description of any feedback control system; however it must be adopted to the needs of each specific design. A large number of motion and process control examples given later in this chapter will surely help in better appreciation of what has been said in this section.

3.3 BLOCK DIAGRAM MANIPULATIONS

The basic feedback system block diagram of Fig. 3.2 is shown in an abridged form in Fig. 3.3. The output $Y(s)$ is influenced by the control signal $U(s)$ and the disturbance signal $W(s)$ as per the following relation:

$$Y(s) = G_P(s)G_A(s)U(s) + G_P(s)W(s) \tag{3.1a}$$

$$= G(s)U(s) + N(s)W(s) \tag{3.1b}$$

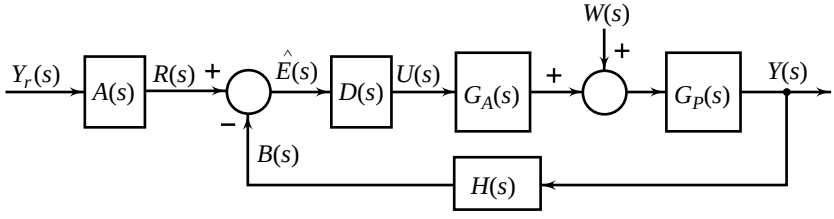

Fig. 3.3 A general linear feedback system

where $G(s)$ is the transfer function from the control signal $U(s)$ to the output $Y(s)$, and $N(s)$ is the transfer function from the disturbance input $W(s)$ to the output $Y(s)$. Using Eqns (3.1a) and (3.1b), we can modify the block diagram of Fig. 3.3 to the form shown in Fig. 3.4. Note that in the block diagram model of Fig. 3.4, the plant includes the actuator elements.

The *open-loop transfer function* of the feedback system of Fig. 3.4 is $D(s)G(s)H(s)$ (it is the transfer function between $R(s)$ and $B(s)$ if the feedback loop is broken at the summing point).

$$\text{Open-loop transfer function} \triangleq D(s)G(s)H(s) \tag{3.1c}$$

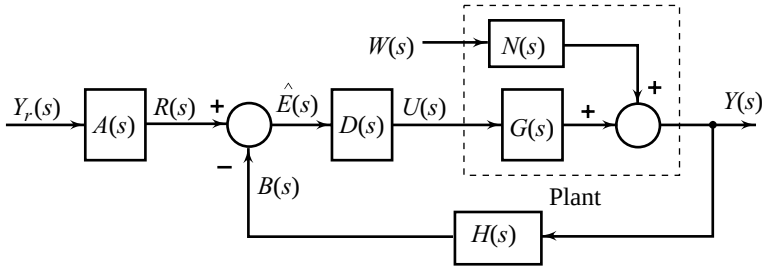

Fig. 3.4 Equivalent representation of the block diagram of Fig. 3.3

Note that for the closed-loop system, $D(s)G(s)H(s)$ is the transfer function product around the entire feedback loop. We call it *loop gain*, and denote it by $L(s)$:

$$L(s) \triangleq D(s)G(s)H(s) \tag{3.1d}$$

The actuating error signal

$$\hat{E}(s) = R(s) - B(s) = A(s)Y_r(s) - H(s)Y(s)$$

The control signal

$$U(s) = D(s)A(s)Y_r(s) - D(s)H(s)Y(s) \tag{3.2a}$$

$$= D(s)H(s)\left[\frac{A(s)}{H(s)}Y_r(s) - Y(s)\right] \tag{3.2b}$$

Using Eqns (3.2), we can simplify Fig. 3.4 to obtain the structure shown in Fig. 3.5.

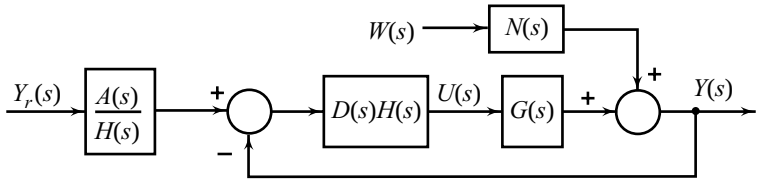

Fig. 3.5 Simplification of the block diagram of Fig. 3.4

A further simplification of Fig. 3.5 is possible if $H = A$. In this case, which is quite common, we can model the system as the *unity feedback system* as shown in Fig. 3.6, and take advantage of the fact that now the actuating signal is the system error $e(t)$.

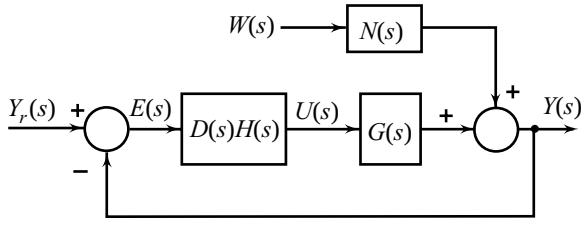

Fig. 3.6 Unity feedback system

The block diagrams in Figs 3.4–3.6, as we shall see later, are very useful for the purpose of system design. However, it should be clear that these block diagrams have lost the physical significance. For example, the block in Fig. 3.5 with transfer function $A(s)/H(s)$, does not refer to any physical portion of the original system. Rather, it represents the result of manipulating Eqn. (3.2a) into the form given by Eqn. (3.2b).

Thus, the reader is advised to think in terms of the *equations* that the block diagrams represent, rather than to attach any special significance to block diagrams themselves. For example, a unity-feedback block diagram does not convey that the sensor gain in necessarily unity. The only role played by a block diagram is that it is a convenient means of representing the various system equations, rather than writing them out explicitly. *Block diagram manipulation* is nothing more than the manipulation of a set of algebraic transform equations.

For the analysis of a feedback system, we require the transfer function between the input—either reference or disturbance—and the output. We can use block diagram manipulations to eliminate all the signals except the input and the output. The reduced block diagram leads to the desired result.

Consider the block diagram of Fig. 3.7. This feedback system has two inputs. We shall use superposition to treat each input separately.

When the disturbance input is set to zero, the single-input system of Fig. 3.8 results. The transfer function between the input $R(s)$ and the output $Y(s)$ is referred to as the *reference transfer function* and will be denoted by $M(s)$. To solve for $M(s)$, we write the pair of transform equations

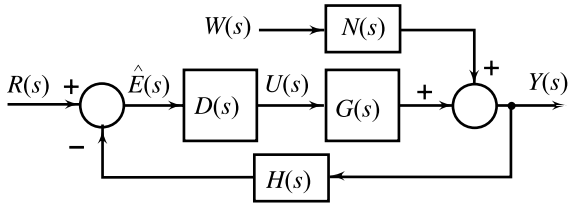

Fig. 3.7 A typical feedback system with two inputs

$$\hat{E}(s) = R(s) - H(s)Y(s);\ Y(s) = G(s)U(s) = G(s)D(s)\hat{E}(s)$$

and then eliminate $\hat{E}(s)$ to obtain

$$[1 + D(s)G(s)H(s)]Y(s) = D(s)G(s)R(s)$$

which leads to the desired result:

$$M(s) = \left.\frac{Y(s)}{R(s)}\right|_{W(s)=0} = \frac{D(s)G(s)}{1 + D(s)G(s)H(s)} \tag{3.3}$$

Similarly, we obtain the *disturbance transfer function* $M_w(s)$ by setting the reference input to zero in Fig. 3.7 yielding Fig. 3.9, and then solving for $Y(s)/W(s)$. From the revised block diagram,

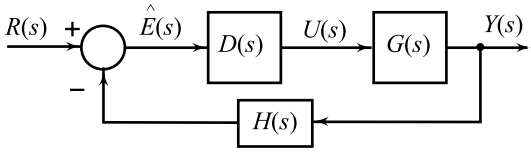

Fig. 3.8 Block diagram without disturbance input

$$\hat{E}(s) = -H(s)Y(s)$$

$$Y(s) = G(s)D(s)\hat{E}(s) + N(s)W(s)$$

from which $\hat{E}(s)$ can be eliminated to give

$$M_w(s) = \left.\frac{Y(s)}{W(s)}\right|_{R(s)=0} = \frac{N(s)}{1 + D(s)G(s)H(s)} \tag{3.4}$$

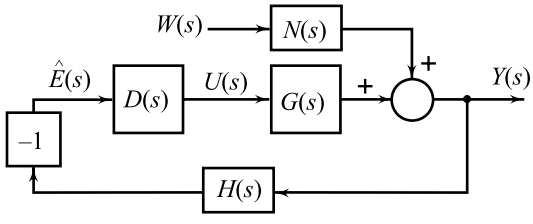

Fig. 3.9 Block diagram without reference input

The response to the simultaneous application of $R(s)$ and $W(s)$ is given by

$$Y(s) = M(s)R(s) + M_w(s)W(s) \tag{3.5}$$

Figure 3.10 shows the reduced block diagram model of the given feedback system.

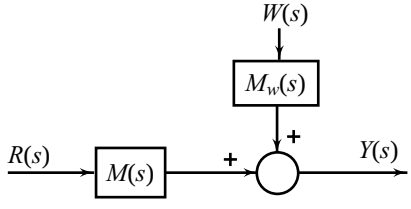

Fig. 3.10 Reduced block diagram model for system of Fig. 3.7

The transfer functions given by Eqns (3.3) and (3.4) are referred to as *closed-loop transfer functions*. Looking at Eqn. (3.3), we notice that the numerator is the multiplication of the transfer functions in the *forward path* between the two variables $R(s)$ and $Y(s)$. The denominator of this equation has the term $D(s)G(s)H(s)$ which is the *loop gain*. An inspection of Eqn. (3.4) shows that the numerator is again the multiplication of the transfer functions in the forward path between $W(s)$ and $Y(s)$. The denominator is the same as in the case of Eqn. (3.3).

From the examples of block diagram manipulations given above, we observe that there are two different objectives which may motivate one to manipulate a block diagram. The most obvious is to obtain the overall transfer function for the purpose of analysis (the block diagram of Fig. 3.7 was manipulated to obtain the one given in Fig. 3.10. The reader should, however, note that the CAD software available today (Simulink, for example (Appendix A), provides powerful tools for analysis without the need for block diagram reduction). The other objective is to manipulate a block diagram into a simpler form which is more convenient in the design process (the block diagram of Fig. 3.3 was manipulated to obtain the one given in Fig. 3.6).

The process by which we have manipulated the block diagrams is nothing more than the manipulation of a set of algebraic transform equations. We can, in fact, manipulate a complex block diagram directly by using the simple rules of block diagram reduction. The most commonly encountered block diagram operations are summarized in Table 3.1.

Table 3.1 Rules of block diagram algebra

Rule	Original diagram	Equivalent diagram
1	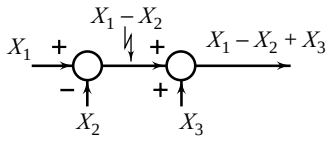	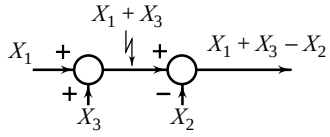
2	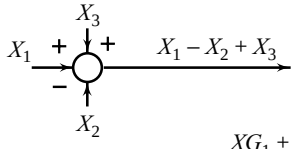	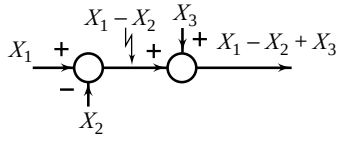
3	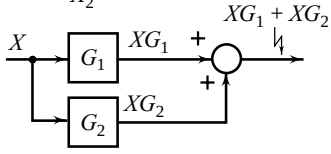	
4	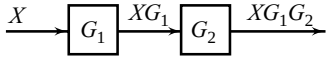	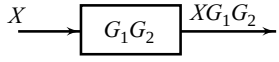
5	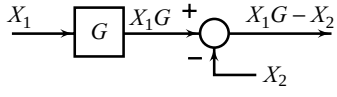	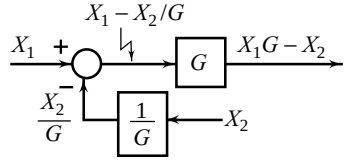
6	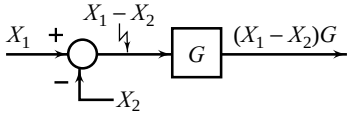	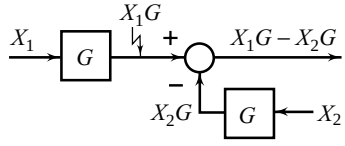
7	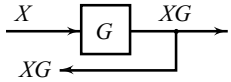	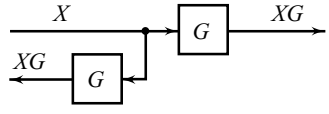

(*Contd*)

Table 3.1 (*Contd*)

Rule	Original diagram	Equivalent diagram
8	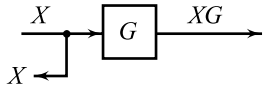	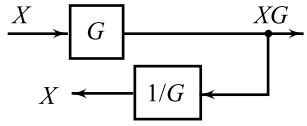
9	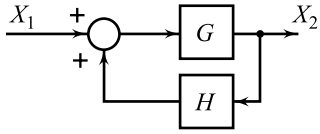	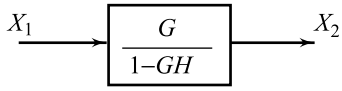
10	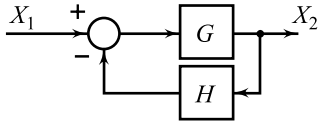	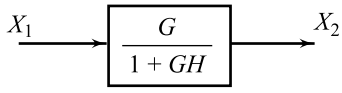

Example 3.1 As we shall see later in this chapter, often a feedback system will have more than one feedback path resulting in a multiple-loop configuration. The block diagram of a typical multiple-loop feedback control system is shown in Fig. 3.11 (Note that the loop $G_3(s)G_4(s)H_1(s)$ is a positive-feedback loop). Let us obtain the closed-loop transfer function of this system using block diagram manipulation rules given in Table 3.1.

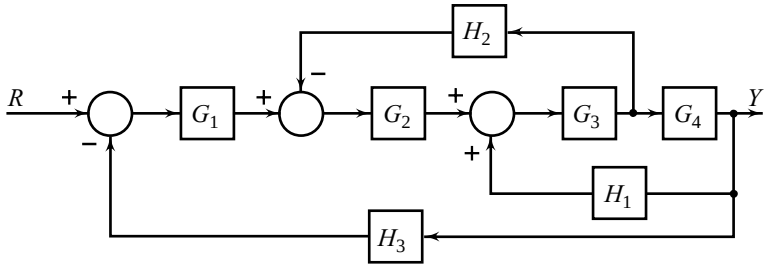

Fig. 3.11 A multiple-loop feedback control system

The block diagram reduction procedure is based on the utilization of rules 9 and 10, which eliminate feedback loops. The other rules are used to transform the diagram to the form ready for eliminating feedback loops. First, in order to eliminate the loop $G_3G_4H_1$, we move H_2 behind block G_4 by using rules 8 and 4 and obtain Fig. 3.12a. Eliminating the loop $G_3G_4H_1$ by rules 4 and 9, we obtain Fig. 3.12b. Then eliminating the inner loop containing H_2/G_4 by rules 4 and 10, we obtain Fig. 3.12c. Finally, by reducing the loop containing H_3, we obtain the closed-loop transfer function as shown in Fig. 3.12d.

An alternate approach is to move the summing point of the positive feedback loop containing H_1, outside the negative feedback loop containing H_2. Application of rules 5, 4 and 1 results in Fig. 3.13a. Eliminating the feedback loop containing H_2, we get Fig. 3.13b. Then, the elimination of loop containing H_1/G_2 gives Fig. 3.13c. Finally, eliminating the loop containing H_3 results in Fig. 3.13d.

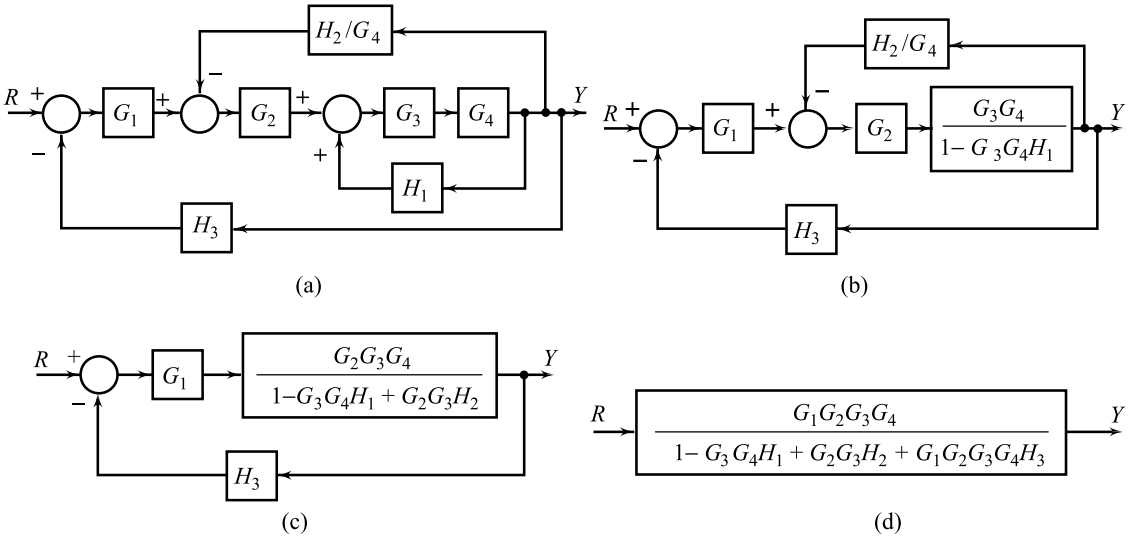

Fig. 3.12 Block diagram reduction of the system of Fig. 3.11

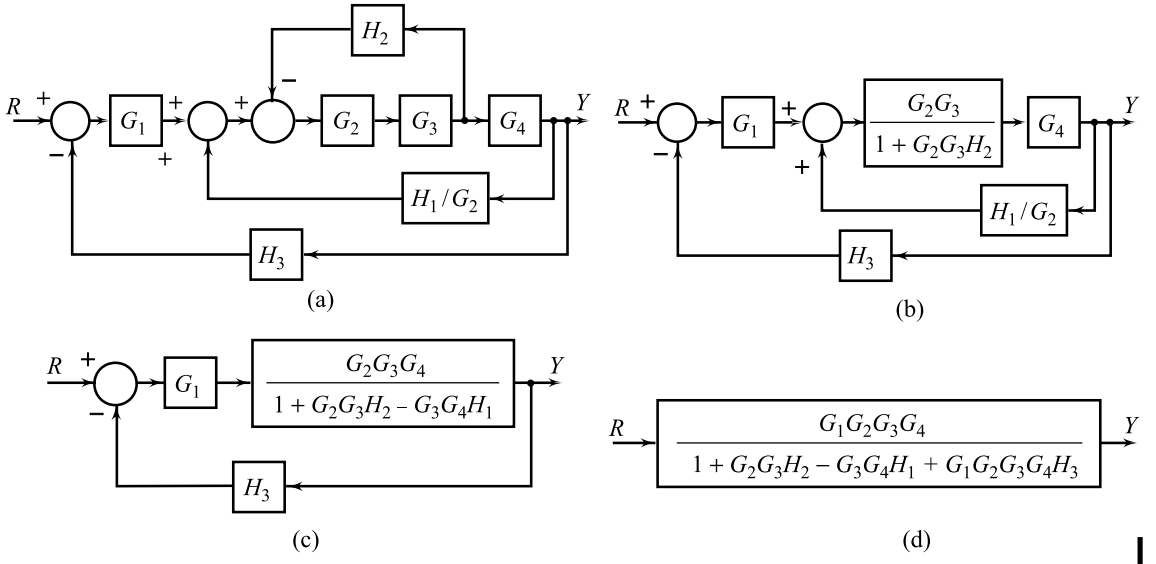

Fig. 3.13 Block diagram reduction of the system of Fig. 3.11

3.4 SIGNAL FLOW GRAPHS AND THE MASON'S GAIN RULE

Block diagrams are adequate for the representation of the inter-relationships of the variables of a control system. However, for a system with reasonably complex inter-relationships, the block diagram reduction procedure is cumbersome and often quite difficult to complete. An alternative method for determining the relationship between system variables, called the *signal flow graph* method, is based on a representation of the system by line segments. The advantage of this method is the availability of a *gain rule*, which provides

the relation between system variables without requiring any reduction procedure or manipulation of the signal flow graph.

3.4.1 Signal Flow Graph Terminology

The basic element of a signal flow graph is a unidirectional line segment called a *branch*, which relates the dependency of an input and an output variable in a manner equivalent to a block of a block diagram. The input and output points of the branch, called *nodes*, represent the input and output variables; the branch transmits the input-node signal to the output node through a gain, called the *transmittance* of the branch.

In the signal flow graph of Fig. 3.14, the branch is directed from node X_1 to node X_2, representing the dependence of the variable X_2 upon X_1. The signal X_1 travelling from the node X_1 along the branch is multiplied by the transmittance G of the branch so that a signal GX_1 is delivered at node X_2; $X_2 = GX_1$.

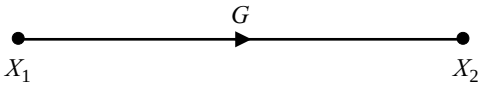

Fig. 3.14 Signal flow graph of $X_2 = GX_1$

In a signal flow graph with several nodes and branches, each node variable is the algebraic sum of all incoming signals; and all outgoing signals from any node equal the node variable and do not affect it. As an illustrative example, consider a system described by the following set of algebraic equations:

$$X_2 = G_{12}X_1 + G_{32}X_3 + G_{42}X_4 + G_{52}X_5;\ X_3 = G_{23}X_2;\ X_4 = G_{34}X_3 + G_{44}X_4;\ X_5 = G_{35}X_3 + G_{45}X_4 \quad (3.6)$$

where X_1 is the input variable and X_5 is the output variable.

The signal flow graph for this system is constructed as shown in Fig. 3.15, although the indicated sequence of steps is not unique.

The nodes representing the variables X_1, X_2, X_3, X_4 and X_5 are located in order from left to right (Fig. 3.15a). The first equation in the set (3.6) states that X_2 depends upon four signals; its signal flow graph is shown in Fig. 3.15b. Similarly, the signal flow graphs of the remaining three equations in the set (3.6) are shown in Figs 3.15c, 3.15d, and 3.15e, respectively, giving the complete signal flow graph of Fig. 3.15f.

Let us now precisely define the various terms used in connection with signal flow graphs.

(i) *Node:* It represents a system variable which is equal to the sum of all incoming signals at the node. All outgoing signals from the node are equal to the node variable and do not affect the value of the node variable.
For example, X_1, X_2, X_3, X_4 and X_5 are nodes of Fig. 3.15f.

(ii) *Branch:* A signal travels along a branch from one node to another in the direction indicated by the branch arrow and in the process gets multiplied by the gain or transmittance of the branch. The branch operator (gain/transmittance) is written on the signal flow graph near the branch arrow.
For example, in Fig. 3.15f, the signal reaching node X_3 from node X_2 is given by $G_{23}X_2$ where G_{23} is the transmittance from node X_2 to node X_3.

(iii) *Input node or source:* It is a node with only outgoing branches (X_1 in Fig. 3.15f).

(iv) *Output node or sink:* It is a node with only incoming branches.
Node X_5 in Fig. 3.15f has an outgoing branch, but after introducing an additional branch with unit transmittance as shown in Fig. 3.15g, the added node becomes an output node. This operation is equivalent to adding an equation

$$X_5 = X_5$$

in the set (3.6).
However, we cannot convert a non-input node into an input node by a similar operation.

(v) *Path*: It is the traversal of connected branches in the direction of the branch arrows such that no node is traversed more than once.

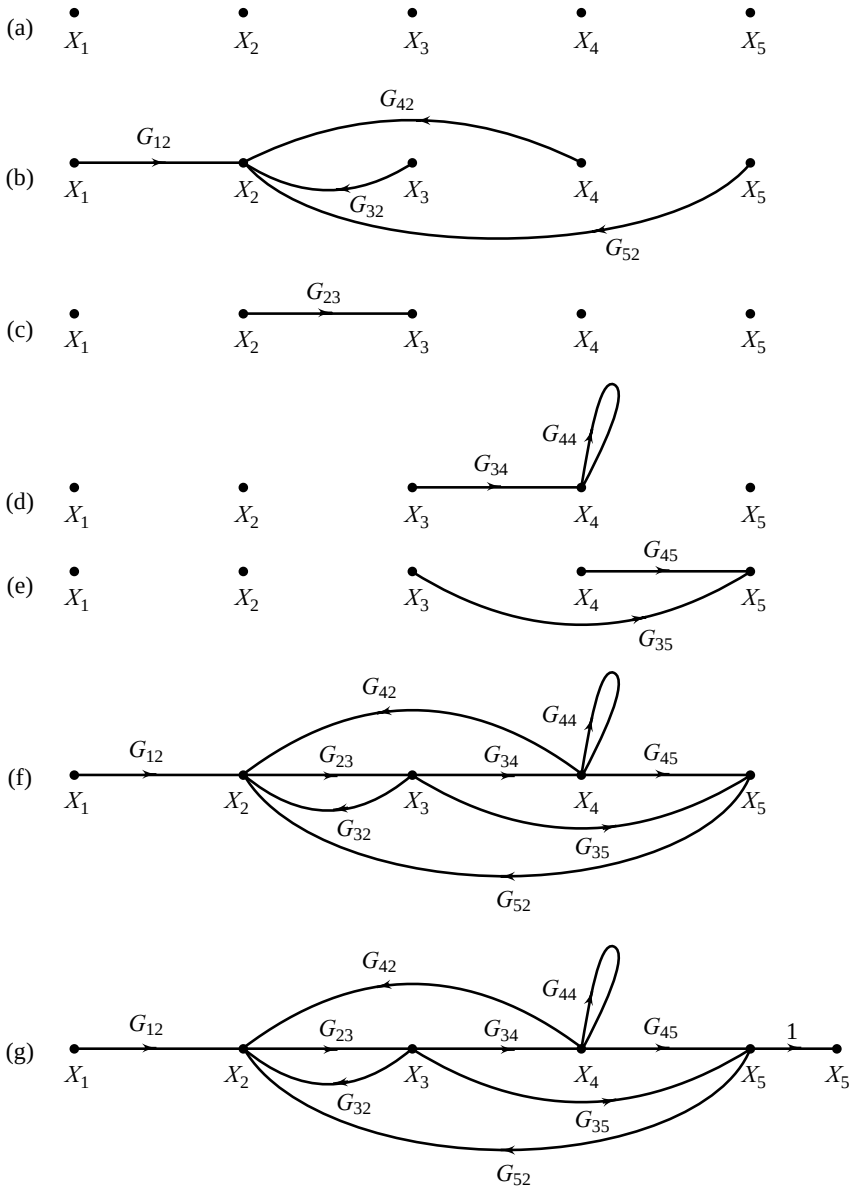

Fig. 3.15 Construction of signal flow graph for Eqns (3.6)

(vi) *Forward path:* It is a path from the input node to the output node.
For the signal flow graph of Fig. 3.15g, there are two forward paths shown in Figs 3.16a and 3.16b.

(vii) *Loop:* It is a path which originates and terminates at the same node. The flow graph of Fig. 3.15g has five loops shown in Figs 3.16c to 3.16g.

(viii) *Nontouching loops:* Loops are said to be nontouching if they do not possess any common node. The flow graph of Fig. 3.15g has two possible combinations of two non-touching loops. These are shown in Figs 3.16h and 3.16i. This flow graph does not have combinations of more than two nontouching loops.

(ix) *Forward path gain:* It is the product of the branch gain encountered in traversing a forward path. The two forward paths of Figs 3.16a and 3.16b have the path gains $(G_{12}G_{23}G_{34}G_{45})$ and $(G_{12}G_{23}G_{35})$, respectively.

(x) *Loop gain:* It is the product of the branch gains encountered in traversing a loop. The five individual loops of Figs 3.16c to 3.16g have loop gains $(G_{23}G_{32})$, $(G_{23}G_{34}G_{42})$, G_{44}, $(G_{23}G_{34}G_{45}G_{52})$, and $(G_{23}G_{35}G_{52})$, respectively.

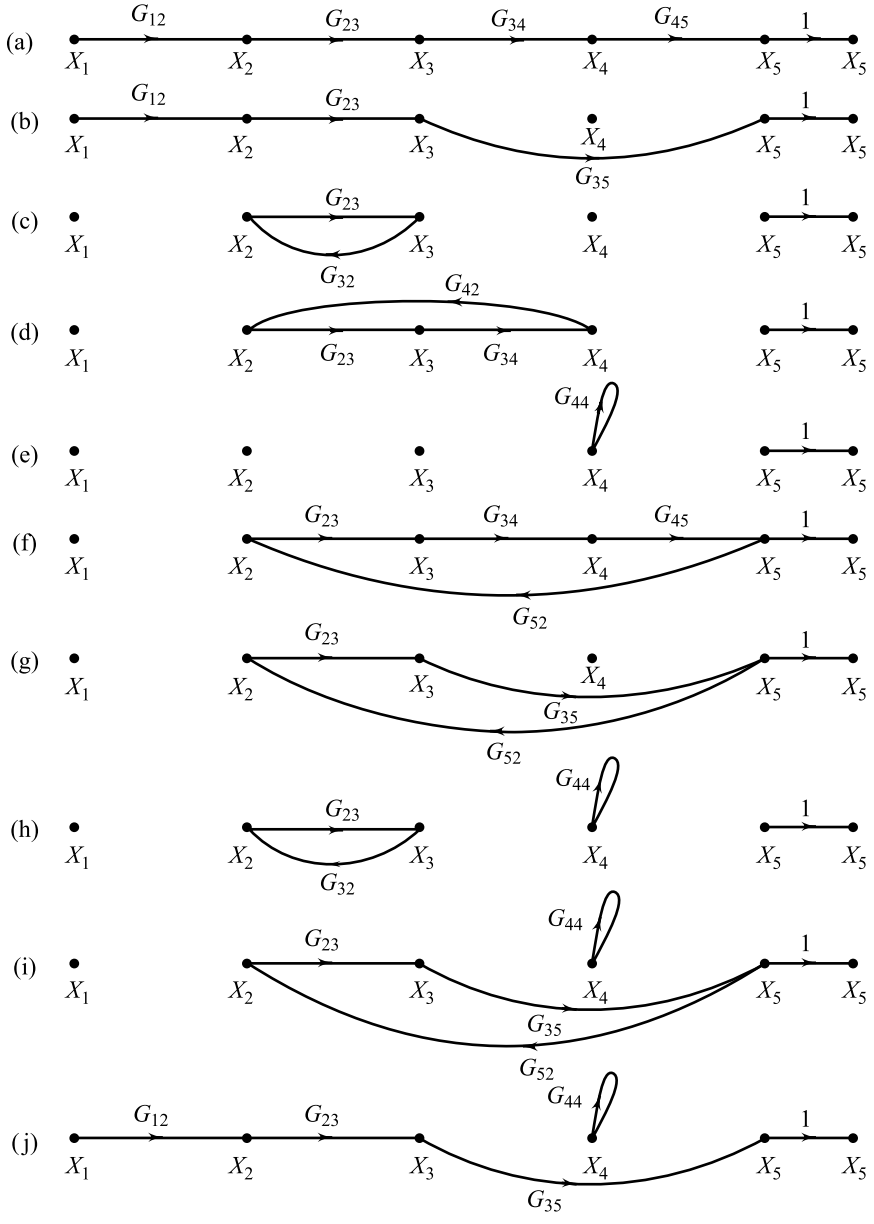

Fig. 3.16 Application of Mason's gain rule to the signal flow graph of Fig. 3.15g

3.4.2 The Mason's Gain Rule

The relationship between an input variable and an output variable of a signal flow graph is given by the net gain between the input and the output nodes and is known as the overall gain of the system. Mason's gain rule[1] for the determination of the overall system gain is given below.

$$M = \frac{1}{\Delta}\sum_{k=1}^{N} P_k \Delta_k = \frac{X_{out}}{X_{in}} \tag{3.7a}$$

where M = gain between X_{in} and X_{out}
X_{out} = output node variable
X_{in} = input node variable
N = total number of forward paths
P_k = path gain of the kth forward path
Δ = 1– (sum of loop gains of all individual loops) + (sum of gain products of all possible combinations of two nontouching loops) – (sum of gain products of all possible combinations of three nontouching loops) + ⋯

$$= 1 - \sum_m P_{m1} + \sum_m P_{m2} - \sum_m P_{m3} + \cdots \tag{3.7b}$$

P_{mr} = gain product of the mth possible combination of r nontouching loops.
Δ_k = the value of Δ for that part of the graph not touching the kth forward path.

Let us illustrate the use of Mason's gain rule by finding the overall gain of the signal flow graph shown in Fig. 3.15g. The following conclusions are drawn by inspection of this signal flow graph.

(i) There are two forward paths with path gains

$$P_1 = G_{12}G_{23}G_{34}G_{45} \quad \text{(Fig. 3.16a)}$$

$$P_2 = G_{12}G_{23}G_{35} \quad \text{(Fig. 3.16b)}$$

(ii) There are five individual loops with loop gains

$$P_{11} = G_{23}G_{32} \quad \text{(Fig. 3.16c)}$$

$$P_{21} = G_{23}G_{34}G_{42} \quad \text{(Fig. 3.16d)}$$

$$P_{31} = G_{44} \quad \text{(Fig. 3.16e)}$$

$$P_{41} = G_{23}G_{34}G_{45}G_{52} \quad \text{(Fig. 3.16f)}$$

$$P_{51} = G_{23}G_{35}G_{52} \quad \text{(Fig. 3.16g)}$$

(iii) There are two possible combinations of two nontouching loops with loop gain products

$$P_{12} = G_{23}G_{32}G_{44} \quad \text{(Fig. 3.16h)}$$

$$P_{22} = G_{23}G_{35}G_{52}G_{44} \quad \text{(Fig. 3.16i)}$$

(iv) There are no combinations of three nontouching loops, four nontouching loops, etc. Therefore

$$P_{m3} = P_{m4} = \cdots = 0$$

Hence from Eqn. (3.7b),

$$\Delta = 1 - (G_{23}G_{32} + G_{23}G_{34}G_{42} + G_{44} + G_{23}G_{34}G_{45}G_{52} + G_{23}G_{35}G_{52}) + (G_{23}G_{32}G_{44} + G_{23}G_{35}G_{52}G_{44})$$

(v) The first forward path is in touch with all the loops. Therefore $\Delta_1 = 1$. The second forward path is not in touch with one loop (Fig. 3.16j). Therefore, $\Delta_2 = 1 - G_{44}$.

[1]For the derivation, based on Cramer's rule for solving linear equations by determinants, the papers of Mason [41, 42] should be consulted.

From Eqn. (3.7a), the overall gain is

$$M = \frac{X_5}{X_1} = \frac{P_1\Delta_1 + P_2\Delta_2}{\Delta} = \frac{G_{12}G_{23}G_{34}G_{45} + G_{12}G_{23}G_{35}(1 - G_{44})}{\left[1 - (G_{23}G_{32} + G_{23}G_{34}G_{42} + G_{44} + G_{23}G_{34}G_{45}G_{52} + G_{23}G_{35}G_{52}) + G_{23}G_{32}G_{44} + G_{23}G_{35}G_{52}G_{44}\right]}$$

3.4.3 Block Diagram Reduction Using The Mason's Gain Rule

Due to the similarity between block diagrams and signal flow graphs, the Mason's gain rule can be used to determine the input-output relationships of either. In general, given a block diagram of a linear system, we apply the gain rule directly to it. However, in order to be able to identify all the loops and non-touching parts clearly, it may sometimes be helpful if an equivalent signal flow graph for the given block diagram is drawn before applying the gain rule.

Example 3.2 Consider the block diagram shown in Fig. 3.17a. The equivalent signal flow graph is drawn in Fig. 3.17b. Note that since a node on the signal flow graph is interpreted as a summing point of all incoming signals to the node, the negative feedbacks on the block diagram are represented by assigning negative gains to the feedback paths on the signal flow graph.

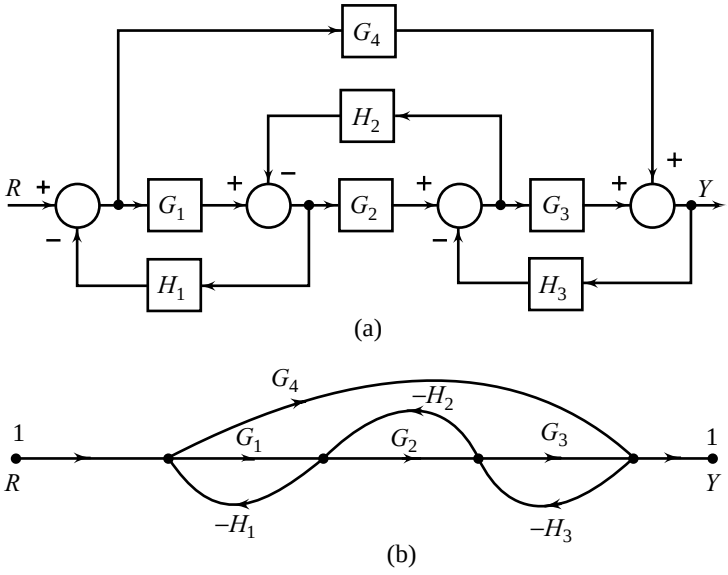

Fig. 3.17 (a) Block diagram of a control system (b) Equivalent signal flow graph

There are two forward paths with path gains

$$P_1 = G_1G_2G_3;\ P_2 = G_4$$

There are four individual loops with loop gains

$$P_{11} = -G_1H_1;\ P_{21} = -G_2H_2;\ P_{31} = -G_3H_3;\ P_{41} = -G_4H_3H_2H_1$$

There is one combination of two nontouching loops with loop gain product

$$P_{12} = G_1H_1G_3H_3$$

There are no combinations of more than two nontouching loops.
Hence from Eqn. (3.7b),

$$\Delta = 1 - (-G_1H_1 - G_2H_2 - G_3H_3 - G_4H_3H_2H_1) + G_1H_1G_3H_3$$

The first forward path is in touch with all the loops. Therefore $\Delta_1 = 1$. The second forward path is not in touch with one loop (Fig. 3.17b). Therefore $\Delta_2 = 1 - (-G_2H_2)$.
From Eqn. (3.7a), the overall gain is

$$M = \frac{Y}{R} = \frac{P_1\Delta_1 + P_2\Delta_2}{\Delta} = \frac{G_1G_2G_3 + G_4 + G_4G_2H_2}{1 + G_1H_1 + G_2H_2 + G_3H_3 + G_4H_3H_2H_1 + G_1H_1G_3H_3}$$

Example 3.3 Consider another typical block diagram shown in Fig. 3.18. This feedback system has two inputs. We shall use the superposition to treat each input separately. The Mason's gain rule may be applied directly to the block diagram without transforming it into an equivalent signal flow graph.

When the disturbance input $W(s)$ is zero, the resulting block diagram has one forward path and two loops. The two loops touch each other and the forward path touches both the loops. By Mason's gain rule (Eqns (3.7))

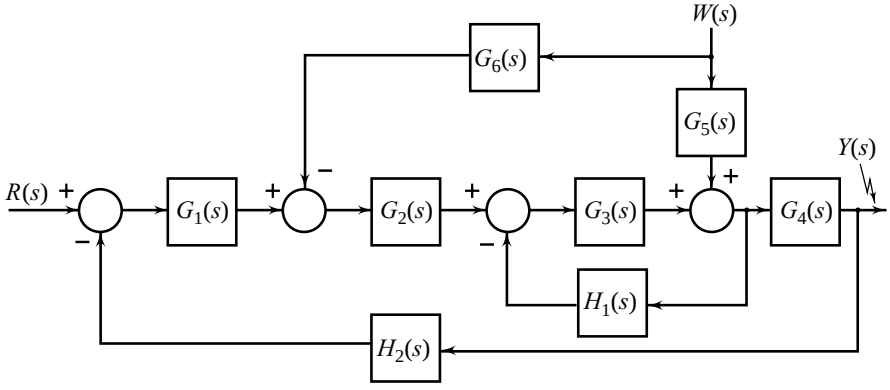

Fig. 3.18 Block diagram of a control system

$$M(s) = \left.\frac{Y(s)}{R(s)}\right|_{W(s)=0} = \frac{G_1(s)G_2(s)G_3(s)G_4(s)}{1 + G_3(s)H_1(s) + G_1(s)G_2(s)G_3(s)G_4(s)H_2(s)}$$

With $R(s) = 0$, the block diagram has two forward paths and two loops. The two loops touch each other and both the forward paths touch both the loops. By Mason's gain rule,

$$M_w(s) = \left.\frac{Y(s)}{W(s)}\right|_{R(s)=0} = \frac{G_5(s)G_4(s) - G_6(s)G_2(s)G_3(s)G_4(s)}{1 + G_3(s)H_1(s) + G_1(s)G_2(s)G_3(s)G_4(s)H_2(s)}$$

The response to the simultaneous application of $R(s)$ and $W(s)$ is given by

$$Y(s) = M(s)R(s) + M_w(s)W(s)$$

3.5 DC MOTOR SPEED CONTROL

Manufacturing systems use some form of motor to actuate a process; for example, for accurate positioning in robotic welding, and for accurate velocity in conveyor systems. We will develop, in this chapter, simple models of motor *speed control* and *position control* systems.

The applications of control systems developed in this chapter are not limited to manufacturing floors. We use feedback to control inertia load. The inertia load may consist of a small object such as a precision instrument in a manufacturing system, or a very large, massive object such as a radar antenna, a rigid satellite or control surfaces of an aircraft. There are numerous applications wherein one encounters the need to control mechanical motions.

The dc motor has been a workhorse in industry for the better part of the century. It has survived because it provides good torque at all speeds and can be manufactured easily and inexpensively. It is being replaced, to some extent, by brushless dc motors and ac induction motors. However, commutator dc motors are still manufactured in great quantities because for many applications, they are still the best solution. In the following we consider the dc motor speed control systems, and the components that make up these systems.

3.5.1 DC Servomotors

A sketch of the basic components of a dc motor is given in Fig. 3.19. The non-turning part (called the *stator*) has magnets which establish a field across the turning part (called the *rotor*). The magnets may be electromagnets or, for small motors, permanent magnets. In an electromagnet motor, the stator is wound with wire and current is forced through this winding (called the *field winding*). For a constant field current i_f, the magnetic flux ϕ is constant; the magnetic flux may be varied by varying the field current.

The rotor is wound with wire and through this winding (called the *armature winding*) a current i_a is forced through the (stationary) brushes and the (rotating) commutator. The reaction of the magnetic flux ϕ with the armature current i_a produces a torque T_M that forces the armature to rotate. The relationship among the developed torque T_M (newton-m), flux ϕ (webers) and current i_a (amps) is

$$T_M = K_{M1}\, \phi\, i_a \tag{3.8a}$$

where K_{M1} is a constant.

In servo applications, a wound-field dc motor is generally used in the linear range of magnetization; the flux ϕ is therefore proportional to field current i_f, and

$$T_M = K_{M2}\, i_f\, i_a \tag{3.8b}$$

where K_{M2} is a constant.

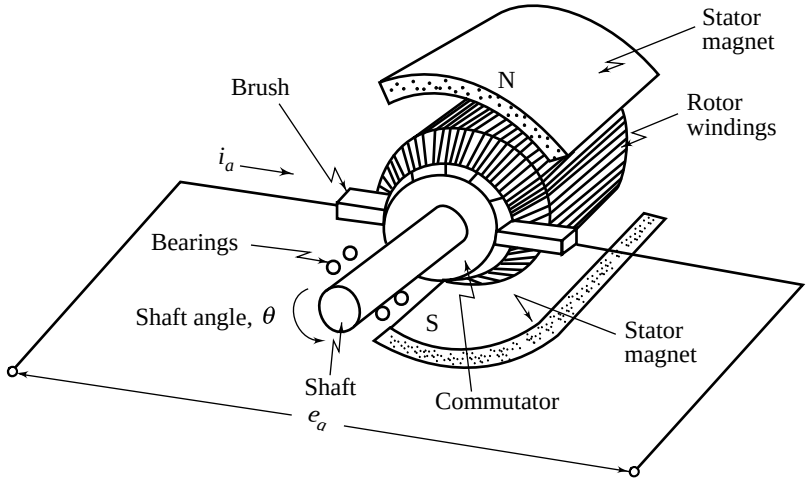

Fig. 3.19 Sketch of a dc motor

As the armature rotates in the magnetic field, a voltage is induced into the armature winding. This voltage is 180° out of phase with the applied armature voltage and is therefore called *back emf*. The relationship among the back emf e_b (volts), rotor velocity ω (rad/sec) and flux ϕ (webers) is

$$e_b = K_{m1}\,\phi\,\omega \tag{3.9a}$$

where K_{m1} is a constant.

For the wound-field motor,

$$e_b = K_{m2}\,i_f\,\omega \tag{3.9b}$$

where K_{m2} is a constant.

Equations (3.8) and (3.9) form the basis of dc motor operation.

In a permanent-magnet (PM) motor, the flux ϕ is constant; the torque T_M exerted on the motor rotor can therefore be controlled by varying the armature current (refer Eqn. (3.8a)). If the direction of the armature current is reversed, the direction of the torque is reversed.

In a wound-field motor, the torque may be controlled by varying the armature current and/or the field current (refer Eqn. (3.8b)). Generally, one of these is varied to control the torque while the other is held constant. In the *armature control* mode of operation, the field current is held constant and armature current is varied to control the torque. In the *field-control* mode, the armature current is maintained constant and field current controls the torque; a reversal in the direction of field current reverses the direction of the torque.

In servo applications, a dc motor is required to produce rapid accelerations from standstill. Therefore, the physical requirements of such a motor are low inertia and high starting torque. Low inertia is attained with reduced armature diameter; with a consequent increase in armature length such that the desired power output is achieved. Thus, except for minor differences in constructional features, a dc servomotor is essentially an ordinary dc motor.

Armature-Controlled dc Motor The symbolic representation of armature-controlled dc motor as a control system component is shown in Fig. 3.20. Under consideration is a wound-field motor. An external dc source supplies a constant current i_f to the field winding. The armature circuit consists of the armature resistance R_a and the armature inductance L_a; both are due to the total armature winding which makes an electrical contact with the brushes of the commutator. e_a is the applied armature voltage which controls the motor operation, and e_b is the back emf.

On the mechanical side, the motor rotor and the attached load can be treated as inertia and viscous friction; J and B are the corresponding parameters. T_w is the disturbance load torque. The torque T_M developed by the motor drives the load with angular velocity ω.

Let us summarize the variables and parameters in the dc motor model of Fig. 3.20:

R = armature winding resistance (ohms);
L_a = armature winding inductance (henrys);
i_a = armature current (amps);
i_f = field current (amps) = a constant;
e_a = applied armature voltage (volts);
e_b = back emf (volts);
ω = angular velocity of the motor rotor (rad/sec);

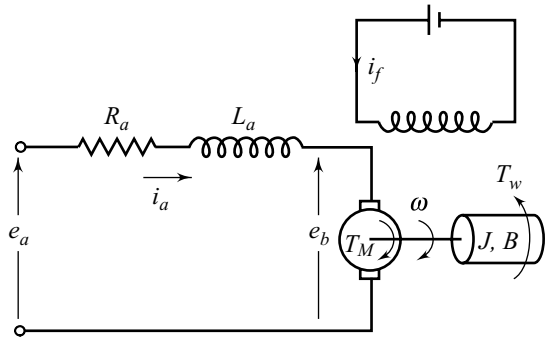

Fig. 3.20 Armature-controlled dc motor with load

θ = angular displacement of the motor rotor (rad);
T_M = torque developed by the motor (newton-m);
J = moment of inertia of the motor rotor with attached mechanical load (kg-m^2 or (newton-m)/(rad/sec^2));
B = viscous-friction coefficient of the motor rotor with attached mechanical load ((newton-m)/(rad/sec)); and
T_w = disturbance load torque (newton-m).

Since the field current is kept constant in the armature-control mode of operation, Eqns (3.8b) and (3.9b) become

$$T_M = K_T\, i_a \tag{3.10a}$$

$$e_b = K_b\, \omega \tag{3.10b}$$

where

$K_T \triangleq$ torque constant; $K_b \triangleq$ back emf constant

The differential equation of the armature circuit is

$$L_a \frac{di_a}{dt} + R_a\, i_a + e_b = e_a \tag{3.11}$$

The torque equation is

$$J\, \frac{d\omega}{dt} + B\omega + T_w = T_M \tag{3.12}$$

Taking the Laplace transform of Eqns (3.10) – (3.12), assuming zero initial conditions, we get

$$T_M(s) = K_T\, I_a(s) \tag{3.13a}$$

$$E_b(s) = K_b \omega(s) \tag{3.13b}$$

$$(L_a s + R_a)\, I_a(s) = E_a(s) - E_b(s) \tag{3.13c}$$

$$(Js + B)\, \omega(s) = T_M(s) - T_w(s) \tag{3.13d}$$

Figure 3.21 shows a block diagram representation of the dc motor system. The block diagram gives a clear picture of the cause and effect relationships in the physical system of Fig. 3.20. The voltage applied to the armature circuit is $E_a(s)$ which is opposed by the back emf $E_b(s)$. The net voltage $(E_a(s) - E_b(s))$ acts on a linear circuit comprised of resistance and inductance in series, having the transfer function $1/(sL_a + R_a)$. The result is an armature current $I_a(s)$. For the fixed field, the torque developed by the motor is $K_T I_a(s)$. The torque rotates the load at a speed $\omega(s)$ against the disturbance $T_w(s)$; the load having moment of inertia J and viscous friction with coefficient B has the transfer function $1/(Js + B)$. The back emf signal $E_b(s) = K_b\omega(s)$ is taken off from the shaft speed and fedback negatively to the summing point. Note that although a dc motor by itself is basically an open-loop system, it has a 'built in' feedback loop caused by the back emf.

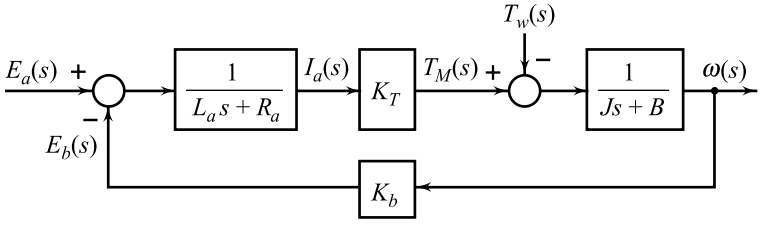

Fig. 3.21 Block diagram of a dc motor (armature-controlled) system

The transfer function between the motor velocity $\omega(s)$ and the input voltage $E_a(s)$ obtained from the block diagram is

$$\frac{\omega(s)}{E_a(s)} = \frac{K_T}{(L_a s + R_a)(Js + B) + K_T K_b} \tag{3.14}$$

The inductance L_a in the armature circuit is usually small and may be neglected. If L_a is neglected, then the transfer function given by Eqn. (3.14) reduces to

$$\frac{\omega(s)}{E_a(s)} = \frac{K_T / R_a}{Js + B + K_T K_b / R_a} \tag{3.15}$$

The back emf constant K_b represents an added term to the viscous friction coefficient B. Therefore, the back emf effect is equivalent to an 'electric friction' which tends to improve the stability of the dc motor system.

The transfer function given by Eqn. (3.15) may be written in the form given below.

$$\frac{\omega(s)}{E_a(s)} = \frac{K_m}{\tau_m s + 1} \tag{3.16}$$

where $$K_m = \frac{K_T}{R_a B + K_T K_b} = \text{motor gain constant}$$

and $$\tau_m = \frac{R_a J}{R_a B + K_T K_b} = \text{motor time-constant}$$

When the motor is used to control shaft position θ, rather than the speed ω, we get the block diagram model shown in Fig. 3.22. The transfer function between the shaft position $\theta(s)$ and the input voltage $E_a(s)$ becomes

$$\frac{\theta(s)}{E_a(s)} = \frac{K_m}{s(\tau_m s + 1)} \tag{3.17}$$

The significance of this transfer function is that the dc motor is essentially an integrating device between the input voltage and the shaft position. This is expected since if e_a is a constant input, the motor displacement will behave as the output of an integrator; that is, it will increase linearly with time. We shall see later that the integrating effect $1/s$ in Eqn. (3.17) gives a feedback position control system a better steady-state behaviour than the corresponding speed control system.

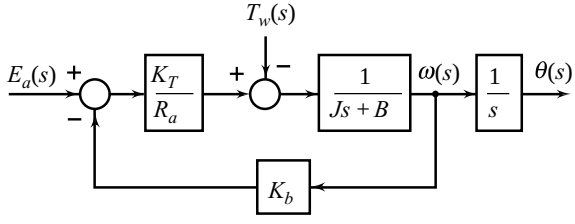

Fig. 3.22 The dc motor (armature-controlled) model with displacement as output

The motor torque and back emf constants are inter-related. Their relationship is deduced below.

Power developed in the armature is

$$P = e_b(t)\, i_a(t) \text{ [(volts) (amps) = watts]}$$

$$= K_b\, \omega(t)\, i_a(t) \left[\left(\frac{\text{volts}}{\text{rad/sec}} \right) (\text{rad/sec})(\text{amp}) \right]$$

In terms of torque and angular velocity,

$$P = T_M(t)\omega(t) \text{ [(newton-m) (rad/sec) = watts]}$$

$$= K_T\, i_a(t)\omega(t)\left[\left(\frac{\text{(newton-m)}}{\text{amp}}\right)(\text{amp})(\text{rad/sec})\right]$$

Therefore,

$$K_b\ (\text{volts/(rad/sec)}) = K_T\ (\text{newton-m/amp}) \tag{3.18}$$

This result can be used to advantage in practice as K_b can be measured more easily and with greater accuracy than K_T.

In a PM motor, the field winding is absent and a constant magnetic flux is provided by the permanent magnet. Since in the preceding development, the magnetic flux is a constant, Eqns (3.14) – (3.18) are also valid for a PM motor.

The torque-speed curves of a dc motor describe the static torque-producing capability of the motor with respect to the applied voltage and motor speed. With reference to Fig. 3.21, in the steady-state the effect of the inductance is zero, and the torque equation of the motor is

$$T_M = \frac{K_T}{R_a}(E_a - K_b\omega) = -\frac{K_T K_b}{R_a}\omega + \frac{K_T}{R_a}E_a$$

where T_M, E_a, and ω represent the steady-state values of the motor torque, applied voltage and speed, respectively.

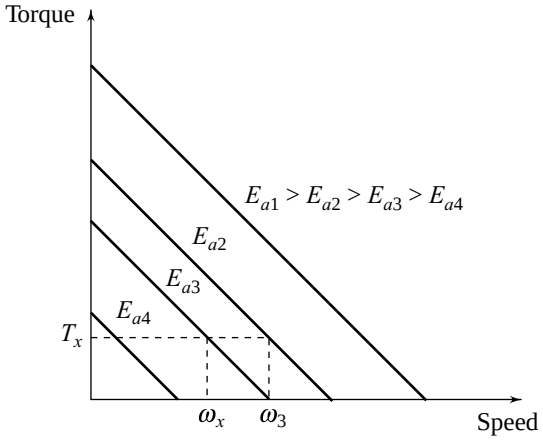

Fig. 3.23 Typical torque-speed curves of an armature-controlled dc motor

Figure 3.23 shows a typical set of torque-speed curves (experimentally obtained/supplied by the manufacturer) of a dc motor for various constant armature voltages.

The no-load point on the torque-speed characteristic corresponding to armature voltage E_{a3} is defined by the coordinates (ω_3, 0) in Fig. 3.23. If a load T_x is applied to the motor shaft, the operating point of the motor shifts from the point (ω_3, 0) to the point (ω_x, T_x) as shown in the figure.

Thus, the applied torque reduces the motor speed. The reduction in speed results in a lower back emf and, for a constant armature voltage E_{a3}, reduction in back emf causes an increase in armature current. The increase in armature current is responsible for an increase in motor-generated torque to accommodate the applied load T_x. If the new steady-state speed ω_x is too low and the original speed ω_3 must be restored, the armature voltage must be increased. This is illustrated in Fig. 3.23; the increase in armature voltage from E_{a3} to E_{a2} restores the original no-load speed ω_3 with the load T_x applied.

In a dc motor system, there may be a significant nonlinear friction due to the rubbing contact between the brushes and the commutator. Also, torque saturation may occur because of the limitation of the maximum current that the motor can handle due to the heat-dissipation rating of the motor. Refer Chapter 14 for methods for analysis of control systems with nonlinearities in the closed loop. Also see Appendix A wherein Simulink tool has been employed.

Field-Controlled dc Motor The schematic diagram of a field-controlled dc motor is shown in Fig. 3.24. In this system,

R_f = field winding resistance (ohms);
L_f = field winding inductance (henrys);
i_f = field current (amps);
i_a = armature current (amps) = a constant;
e_f = applied field voltage (volts);
ω = angular velocity of the motor rotor (rad/sec);
θ = angular displacement of the motor rotor (rad);
T_M = torque developed by the motor (newton-m);
J = moment of inertia of the motor rotor with attached mechanical load (kg-m^2 or (newton-m)/(rad/sec^2));
B = viscous-friction coefficient of the motor rotor with attached mechanical load ((newton-m)/(rad/sec)); and
T_w = disturbance load torque (newton-m).

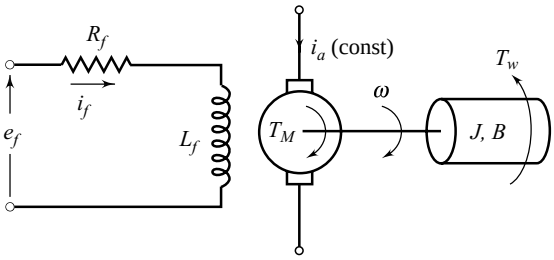

Fig. 3.24 Field-controlled dc motor with load

The following assumptions are made in the derivation of the transfer function of field-controlled motor:
(a) a constant current i_a is fed into the armature;
(b) the air gap flux ϕ is proportional to field current i_f; and
(c) the torque developed by the motor is proportional to field current;

$$T_M = K_T' i_f;\ K_T' \triangleq \text{torque constant.}$$

The voltage applied to the field circuit is $E_f(s)$ which acts on a linear circuit comprising of resistance and inductance in series, having the transfer function $1/(L_f s + R_f)$. The result is a field current $I_f(s)$. For fixed armature current, the torque developed by the motor is $K'_T I_f(s)$. This torque rotates the load at a speed $\omega(s)$ against the disturbance $T_w(s)$; the load having moment of inertia J and viscous-friction coefficient B has the transfer function $1/(Js + B)$. These cause and effect relationships are described by the block diagram of Fig. 3.25. The transfer function between the motor displacement $\theta(s)$ and the input voltage $E_f(s)$, obtained from the block diagram, is

$$\frac{\theta(s)}{E_f(s)} = \frac{K_T'}{s(L_f s + R_f)(Js + B)} = \frac{K_m'}{s(\tau_f s + 1)(\tau_m s + 1)} \tag{3.19}$$

where

$K'_m = K'_T/(R_f B)$ = motor gain constant;
$\tau_f = L_f/R_f$ = time-constant of the field circuit; and
$\tau_m = J/B$ = mechanical time-constant.

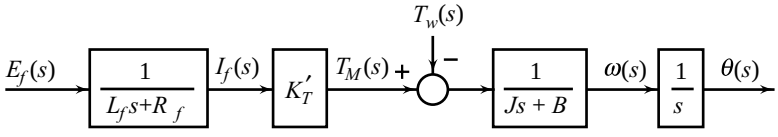

Fig. 3.25 Block diagram of a field-controlled dc motor

For small-size motors, field control is advantageous because only a low power servo amplifier is required while the constant armature current, which is not large, can be supplied from an inexpensive constant voltage source. This control scheme poses great practical difficulties in medium- and large-size motors; because of large back emf of the motor, the armature current cannot be kept constant by supplying a constant voltage to the armature. The assumption of constant armature current leads to the linear equations representing the

operation of the motor. However, if instead, a constant voltage source is applied to the armature, the equation of the motor becomes nonlinear and cannot be handled by linear analysis methods. For this reason, it is normal practice to have a fixed excitation and control the armature current.

3.5.2 Electronic Amplifiers

Broadly speaking, there are two types of electronic amplifiers used in control systems:

(a) A *small signal amplifier* is one which linearly amplifies a small signal (usually voltage) and is suitable for sensor circuits to amplify weak measured signals. The operational amplifier (usually called the op amp) is in common use.

From the block diagram of Fig. 3.2, we see that a control signal in a feedback loop is a function of the error signal. The functional dependence is given by the controller transfer function $D(s)$. Mechanization of $D(s)$, as we shall see in the next chapter, usually requires amplification of the error signal, and generation of the derivative and the integral of the error signal. Op amp circuits (refer Section 2.13) are now commonly used for mechanization of the controller transfer function $D(s)$.

(b) A *power amplifier* is one which controls a large amount of power, and is therefore suitable for actuating devices.

Power amplifiers are available in three major types: the smooth transistor, the switching transistor (pulse-width modulated (PWM)), and the silicon control rectifier (SCR). Smooth transistor amplifiers use the transistors in a smooth modulating fashion and produce an output voltage that is high-power copy of the input. These amplifiers are used mainly below 1 kW applications. Switching (PWM) amplifiers use the transistors as on–off switches; the output voltage is a constant-frequency, fixed-amplitude waveform whose duty cycle is smoothly varied with input voltage. Switching amplifiers are economical in the 25 W to 5 kW range. In SCR amplifiers, the input voltage smoothly modulates the point in each power-line cycle at which the SCR (this term arises from the device as controlled rectifier is constructed from silicon), also known as the *thyristor*, is made to conduct. These amplifiers are often used in high power applications.

To be precise, the transfer function of an electronic amplifier is of the form

$$G(s) = \frac{K_A}{\tau_A s + 1} \tag{3.20}$$

However, usually the time constant τ_A is negligibly small compared to the dynamics of the plant; the transfer function can therefore be approximated as

$$G(s) = K_A \tag{3.21}$$

where K_A is the proportional gain of the amplifier.

In addition to neglecting 'fast' dynamics, the model (3.21) of the amplifier further differs from reality because of its perfect linearity which assumes no limit on the magnitude of the input signal. Actually the amplifier, like other devices, exhibits saturation, limiting its output when input becomes too large (refer Chapter 14.)

Discussion on hardware aspects of various types of electronic amplifiers is beyond the scope of this book [50].

3.5.3 DC Tachogenerator

We are interested in measuring the rotational velocity of the drive shafts for feedback control. Optical encoders are often used in manufacturing and robotics to provide a measurement of the angular movement (angular velocity/angular position). The encoder is mounted on the drive shaft and rotates at the same velocity as the shaft. The output of the encoder is a series of electrical pulses, directly proportional to the shaft

velocity/position. Interfacing an encoder with a computer is straightforward (discussed later in Chapter 11). We consider here a transducer that produces continuous-time electrical signal proportional to velocity. Such a transducer facilitates interfacing with an op amp comparator/control circuit.

A tachogenerator is an electromechanical device which produces an output voltage that is proportional to its shaft speed. Figure 3.26 shows the schematic diagram of a dc tachogenerator. It comprises a stator (nonrotating part) with a permanent-magnet field, a rotating armature circuit, and a commutator and brush assembly. The rotor is connected to the shaft to be measured. The output voltage of the tachogenerator is proportional to the angular velocity of the shaft. The polarity of the output voltage is dependent on the direction of rotation of the shaft. Dynamics of a dc tachogenerator can be represented by the equation

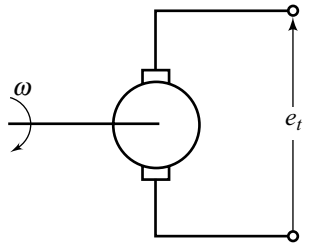

Fig 3.26 Schematic diagram of a dc tachogenerator

$$e_t(t) = K_t \omega(t) \tag{3.22}$$

where e_t is the output voltage (volts), ω is the rotor velocity (rad/sec), and K_t is the sensitivity of the tachogenerator (volts per rad/sec).

The transfer function from $\omega(t)$ to $e_t(t)$ of a dc tachogenerator is of the form

$$\frac{E_t(s)}{\omega(s)} = K_t \tag{3.23}$$

3.5.4 A Speed Control System

Basic structure of speed control systems will remain the same irrespective of the application. We consider here conveyor systems in a manufacturing process to transport goods from different areas of the production facility. A typical conveyor system may use a belt on rollers to carry products. The rollers are driven by motors(Fig. 3.27). If the *load* (conveyor belt and products) presented a constant torque to the motor shaft, then no control would be required. But the load does change, and as a result, control is required if the motor is to achieve its purpose. A typical conveyor system may require the motor to achieve and maintain a constant speed (*set-point*) while working against a load of varying torque (*disturbance*).

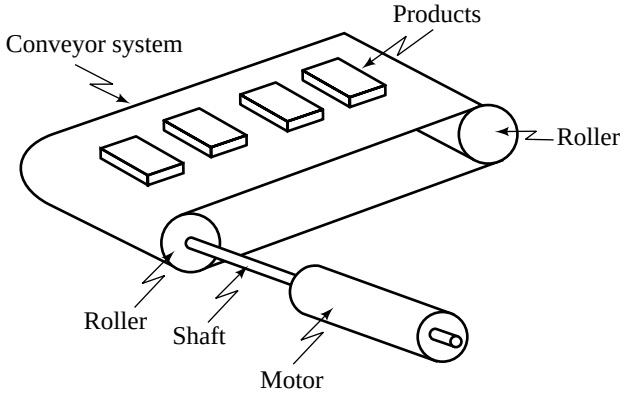

Fig 3.27 Conveyor belt system in a manufacturing process

To meet the manufacturing requirements, it is imperative that the conveyor belt operates at a constant speed; and has acceptable transient performance in moving from one speed setting to the next. We know that we have made several approximations while deriving models of the components that make up a speed control system. For example, nonlinear frictional effects due to brushes and commutator in dc machines have been ignored. Also we have assumed that the dc machines will be operating in the linear range of magnetization. We have neglected the inductance of the armature circuit. The tachogenerator and power amplifier models are of zero-order; we have assumed that the time-constants of these devices are much smaller than that of the process, and can be neglected. Also

the numerical values of the parameters of the models are obtained from the design manuals of the equipment, which are usually not very precise on the parametric values. One may argue that one should attempt to take all these factors into account to develop a model. This approach will not be cost effective; the time and money spent on modelling is already much higher than that spent on developing a control design. In addition, a complex mathematical model will not necessarily lead to a better control design. The design toolkit is well developed for linear systems; but for nonlinear systems we have limited results. Robustness provided by feedback loop against external disturbances T_w and the model uncertainties, is a well-tested solution to the control problem.

Figure 3.28 shows a closed-loop block diagram for the speed control system. We have introduced a scaling block with transfer function K_t in the forward path to allow us to compare the command input with controlled output of the system. (Reference voltage e_r is calculated from the command input, ω_r (set-point), using the relation $e_r = K_t\ \omega_r$, and this value is then fed to the system through a potentiometer setting (Fig. 3.29)). Here K_b is the back emf constant of the motor, R_a is the armature resistance (armature inductance is assumed negligible), K_T is the torque constant of the moter; J and B are, respectively, moment of intertia and viscous-friction coefficient on motor shaft, and T_w is the disturbance torque on motor shaft (refer Eqns (3.10)–(3.13), and Fig. 3.22).

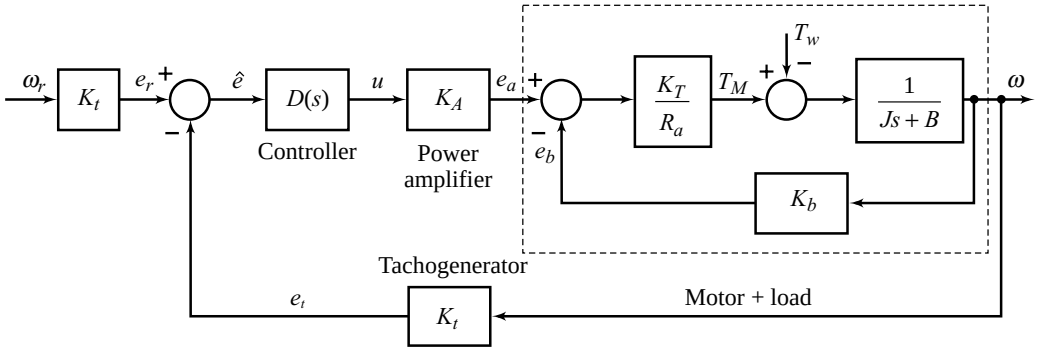

Fig. 3.28 Closed-loop block diagram for speed control system

Figure 3.29 shows schematic diagram for speed control using proportional control logic. The feedback voltage e_t from the tachogenerator of sensitivity K_t volts/(rad/sec) represents the actual speed ω of the motor. The reference-input voltage e_r represents the desired motor speed ω_r. An op amp circuit amplifies the error $(e_r - e_t)$ between the reference and feedback voltage signals and supplies a voltage u to a power amplifier. The output e_a of the power amplifier drives the armature-controlled dc motor which rotates in the direction to reduce the error $(e_r - e_t)$ as a consequence of the negative feedback. Reduction in $(e_r - e_t)$ results in reduction in the difference between the desired motor speed and actual motor speed. Reversal in the polarity of e_r reverses the direction of rotation of the motor.

It is seen that the control law is

$$u = \frac{R_f}{R}(e_r - e_t)$$

i.e., the control signal is proportional to the error. It will be seen in later chapters that the speed control system of Fig. 3.29 has poor disturbance-rejection property with a proportional control law. The performance of the control system can be improved by introducing an appropriately designed controller[2] $D(s)$ in the forward path of the loop (refer Fig. 3.28).

[2]The objective set for this chapter is the control hardware familiarity. In almost all the control system examples in this chapter, we will use an amplifier (proportional control law) as a controller, knowing very well that it may not satisfy the control requirements. The problem of design of controllers will be discussed in the next and later chapters.

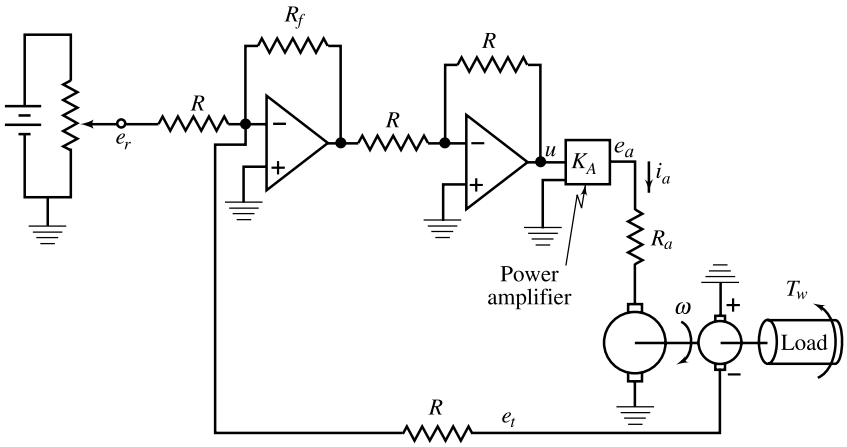

Fig.3.29 Schematic diagram of a speed control system

3.6 DC MOTOR POSITION CONTROL

In the following, we consider the position control systems, and the components that make up these systems.

3.6.1 Geared Drives

Electrical motors generally produce their maximum power at high speed. In other words, generally electrical motors exert rather small torques while rotating at high speeds (power = torque × angular velocity). In consequence, appropriate gearing is necessary for the electrical motors in order for these systems to drive large loads (requiring large torques) at low speeds. For example, robot arms are usually moved at low speeds, less than 1 revolution/sec, while required maximum torques range from a few newton-m to several hundred newton-m. A large gear reduction is typically required for standard servomotors.

Figure 3.30 shows a motor driving a load through a gear train which consists of two gears coupled together. The gear with N_1 teeth is called the primary gear and the gear with N_2 teeth is called the secondary gear. Angular displacements of shafts 1 and 2 are denoted by θ_1 and θ_2 respectively, with their positive directions as indicated in the figure. The moment of inertia and viscous friction of motor and gear 1 are denoted by J_1 and B_1 respectively, and those of gear 2 and load are denoted by J_2 and B_2 respectively. T_M is the torque developed by the motor and T_w is the disturbance torque on the load. Elasticity of the gear teeth and shafts is assumed negligible.

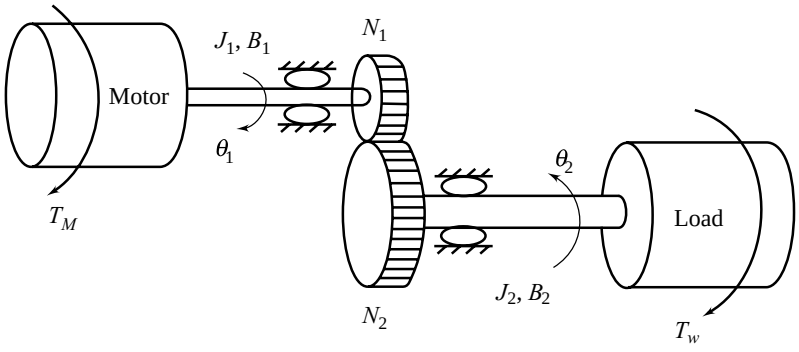

Fig. 3.30 Motor driving a load through gearing

A free-body diagram is shown in Fig. 3.31. T_{12} is the torque exerted on gear 1 by gear 2, and T_{21} is the torque transmitted to gear 2 through gear 1. For the motor shaft, the differential equation is

$$J_1 \ddot{\theta}_1 + B_1 \dot{\theta}_1 + T_{12} = T_M \tag{3.24}$$

For the load shaft,

$$J_2 \ddot{\theta}_2 + B_2 \dot{\theta}_2 + T_w = T_{21} \tag{3.25}$$

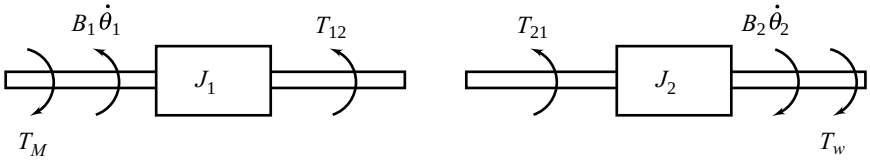

Fig. 3.31 Free-body diagram for system of Fig. 3.30

Idealized characteristic of the gear train is given by the relationship $\theta_2 = (N_1/N_2)\,\theta_1$. In reality, there is always a certain amount of backlash (free play) between coupled gears. Keeping the backlash small will inevitably increase the friction between the teeth, and wear out the teeth faster. On the other hand, an excessive amount of backlash may cause sustained oscillations or chattering phenomenon in control systems (refer Chapter 14). The assumption of zero backlash is reasonable for high quality, well-adjusted gear boxes.

Let r_1 be the radius of gear 1 and r_2 be the radius of gear 2. Since the linear distance travelled along the surface of each gear is the same, $\theta_1 r_1 = \theta_2 r_2$. The number of teeth on a gear surface being proportional to gear radius, we have $(N_1 / r_1) = (N_2 / r_2)$. The linear forces developed at the contact point of both the gears are equal, hence $(T_{12} / r_1) = (T_{21} / r_2)$. By combining these equalities, we obtain

$$\frac{T_{12}}{T_{21}} = \frac{N_1}{N_2} = \frac{\theta_2}{\theta_1} \tag{3.26}$$

Differentiating this equation twice, we have the following relation for speed and acceleration:

$$\frac{\ddot{\theta}_2}{\ddot{\theta}_1} = \frac{\dot{\theta}_2}{\dot{\theta}_1} = \frac{N_1}{N_2} \tag{3.27}$$

From Eqns (3.26) and (3.27), it is observed that with $(N_1 / N_2) < 1$, the gear train provides torque magnification and speed reduction. By proper selection of N_1 / N_2, gear trains can be used to attain mechanical matching of motor to load: a servomotor operating at high speed and generating low torque is matched to a load to be moved at low speed but requiring high torque.

Eliminating T_{12} and T_{21} from Eqns (3.24) and (3.25) with the help of Eqn. (3.26), we obtain

$$J_1 \ddot{\theta}_1 + B_1 \dot{\theta}_1 + \frac{N_1}{N_2}\,(J_2 \ddot{\theta}_2 + B_2\, \dot{\theta}_2 + T_w) = T_M \tag{3.28}$$

Elimination of θ_2 from Eqn. (3.28) with the help of Eqn. (3.27), yields

$$\left[J_1 + \left(\frac{N_1}{N_2}\right)^2 J_2\right]\ddot{\theta}_1 + \left[B_1 + \left(\frac{N_1}{N_2}\right)^2 B_2\right]\dot{\theta}_1 + \frac{N_1}{N_2}\,T_w = T_M \tag{3.29}$$

Note that the load inertia J_2 is reflected on the motor shaft as $(N_1 / N_2)^2\, J_2$, load viscous-friction B_2 is reflected on the motor shaft as $(N_1 / N_2)^2\, B_2$, and the load disturbance T_w is reflected on the motor shaft as $(N_1 / N_2)\, T_w$.

Equation (3.29) suggests that the geared system of Fig. 3.30 is equivalent to non-geared (direct drive) system of Fig. 3.32 with equivalent moment of inertia

$$J_{1eq} = J_1 + \left(\frac{N_1}{N_2}\right)^2 J_2, \tag{3.30a}$$

equivalent friction

$$B_{1eq} = B_1 + \left(\frac{N_1}{N_2}\right)^2 B_2 \tag{3.30b}$$

and equivalent disturbance torque

$$T_{weq} = \left(\frac{N_1}{N_2}\right) T_w \tag{3.30c}$$

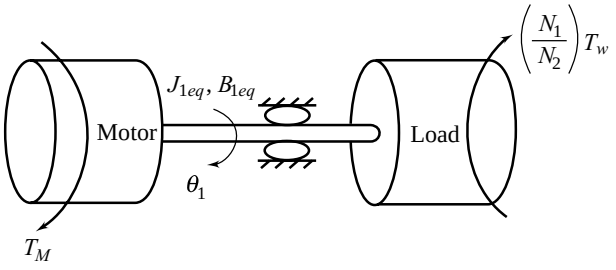

Fig. 3.32 Equivalent direct-drive system for the geared system of Fig. 3.30

The problems that the mechanical gearing unavoidably possess (backlash, friction, etc.), can be solved completely using the *direct-drive technology*. An order of magnitude larger torque can be generated by direct-drive motors in a compact and light-weight body. The dc torque motors are capable of exerting much larger torque compared with regular dc motors. These motors are designed in such a way that the output torque rather than power is maximized (refer [19] for details).

3.6.2 Potentiometers

For conversion of a linear or an angular displacement into voltage, a potentiometer is probably the simplest device. Potentiometric transducers are relatively inexpensive and easy to apply. However, they have some limitations. The resolution (minimum change in output voltage obtained by moving the wiper, expressed as a percentage of the total applied voltage) of precision wire-wound potentiometers (constructed by winding resistance wire on a form) ranges from 0.001 to 0.5 percent. This discontinuous output voltage contributes to servo inaccuracy. Potentiometers are temperature-sensitive, a characteristic that affects their accuracy. The wiper contact is another limiting factor, being subject to wear and dirt and potentially producing electrical noise.

In a large number of control systems, the low-amplitude high-frequency noise generated by the potentiometer does not create problems. This is because the plant usually acts as a low-pass filter. However, if the potentiometer output is differentiated to obtain a measure of velocity, the resulting signal will be completely useless.[3]

A non-wire potentiometer (constructed by depositing conductive plastic resistance material on a form) is stepless and therefore resolution is better. However, values less than 1000 Ω and hard to obtain with non-wire type of potentiometers, while wire-wound potentiometers can be made with very low values.

3.6.3 A Position Control System

The basic structure of position control systems will remain the same irrespective of the application. We consider here a robot manipulator in a manufacturing process for load and unload operations. The motion of load gripper in a typical robot system is caused by the movements of dc motors driving the joints. Positions of the joints at any time determine the location of the gripper in the environment at that time (refer Example 1.8.).

[3]Differentiation of the signal sin t contaminated by low-magnitude high-frequency noise 0.01 sin$10^3 t$ gives (cos$t$ + 10 cos$10^3 t$); noise becomes the dominant term after differentiation.

In the following, we investigate the linear position control of a single-link robot manipulator, which consists of a single rigid link attached to a joint (Fig. 3.33). The joint can move the link and the gripper in two-dimensional space. The manipulator is driven by an armature controlled dc motor through a gear train.

We model the manipulator link and its payload (the object picked up by the gripper) as a lumped parameter system with moment of inertia J_L and viscous damping factor B_L. In response to motor torque T_M, the link will rotate; the angular position of the link is designated by θ_L. It may be noted that the moment of inertia will not necessarily be constant because during the course of an operation, the robot may pick up different objects with its gripper. The variation in the payload will change the effective moment of inertia of the link. In robotic applications, J_L is usually constant during each task; however it may vary from task to task.

Consider a conceptual design of a position control system, shown in the schematic diagram of Fig. 3.34a.

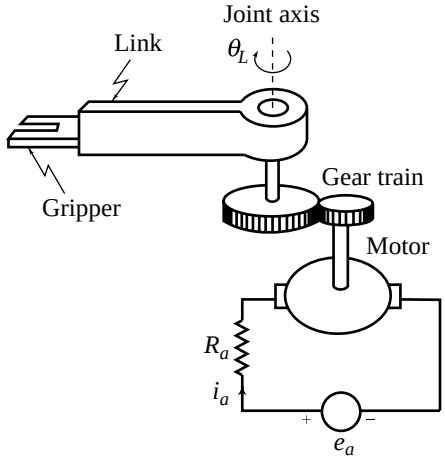

Fig. 3.33 A single-link robot manipulator

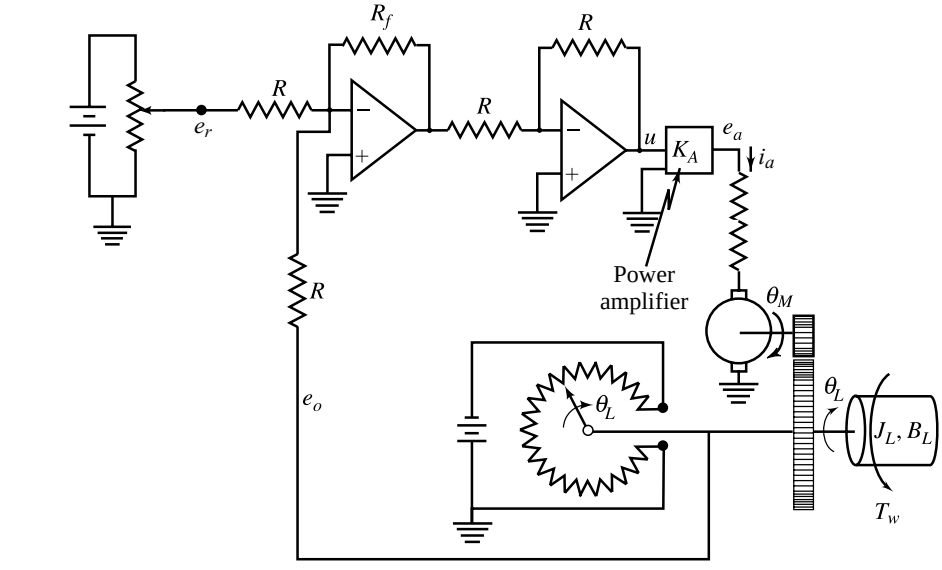

Fig. 3.34 Closed-loop position control system (a) Schematic diagram (b) block diagram

The operation of the system is as follows. The load with an inertia J_L and viscous friction with coefficient B_L is to be positioned at some desired angle θ_R (T_w represents the load torque disturbance). The feedback potentiometer, whose wiper arm is mechanically coupled to the load shaft, produces a voltage e_o which represents the actual load position θ_L.

The feedback velotage

$$e_o = K_P \theta_L \tag{3.31}$$

where K_P = sensitivity of the potentiometer in volts/deg.

The reference voltage e_r is calculated from the command input, θ_R (set-point), using the relation $e_r = K_P \theta_R$, and this value is then fed to the system through a potentiometer setting.

The error voltage $(e_r - e_o)$ is amplified by an op amp circuit that supplies a voltage u to a power amplifier. The output e_a of the power amplifier drives the armature-controlled dc motor (reversal in the polarity of e_r reverses the direction of rotation of the motor). The torque developed by the motor is transmitted to the load shaft through a gear train. The transmitted torque rotates the load shaft in the direction to reduce the error $(e_r - e_o)$ as a consequence of the negative feedback. When $e_r = e_o$, the motor stops, as its drive is cut off. This must necessarily occur when $\theta_R = \theta_L$ because feedback voltage is $e_o = K_P \theta_L$, and the reference voltage (by calculation) is $e_r = K_P \theta_R$.

A change in the load position caused by disturbances in the system (internal or external) causes the error signal $(e_r - e_o)$ to reappear, which after amplification acts on the motor; the motor torque transmitted to the load shaft forces the load to return to its original position.

A block diagram of the system is shown in Fig. 3.34b (refer Eqns (3.10)–(3.13), (3.30), and Fig. 3.22). Here K_b is the back emf constant of the motor, R_a is the armature resistance (armature inductance is assumed negligible), K_T is the torque constant of the motor, n is the gear ratio (n = load shaft speed $\dot{\theta}_L$ /motor shaft speed $\dot{\theta}_M$), J and B are, respectively, equivalent moment of inertia and viscous-friction coefficient on motor shaft, and nT_w is the equivalent disturbance torque on motor shaft.

It will be seen in the next chapter that the performance of position control system of Fig. 3.34 can be improved by introducing minor-loop feedback (refer Figs 1.12 and 1.13). A signal proportional to motor/load angular velocity, generated by a tachogenerator is fedback. Since tachogenerators tend to be noisy at low speeds, in a geared system one usually puts the tacho on the motor, rather than the load.

3.7 AC (CARRIER) CONTROL SYSTEMS[4]

The ac servomotors possess many virtues in comparison to dc servomotors. These include significantly lower costs, weight and inertia, higher efficiency, and fewer maintenance requirements because of no commutator and brushes. However, as we shall see later, the characteristics of ac motors are quite nonlinear and these motors are more difficult to control, especially for positioning applications. The ac motors are best suited for low-power applications such as in instrument servos (e.g., control of pen in X-Y recorders) and computer-related equipment (e.g., disk drives, tape drives, printers, etc).

The dc motors are expensive because of brushes and commutators. These motors have relatively lower torque-to-volume, and torque-to-inertia ratios. However, the characteristics of dc motors are quite linear and these motors are easier to control. The dc motors have been generally used for large-power applications such as in machine tools and robotics.

Developments in technology are opening new applications for both ac and dc motors. Today, with the development of the rare-earth magnet, dc motors with very high torque-to-volume ratio at reasonable costs

[4]This section and the related problems in the book which involve ac devices, may be skipped if a course plan so demands.

have become possible. Furthermore, the advances made in brush-and-commutator technology have made these wearable parts practically maintenance-free. The advancements made in power electronics have made brushless dc motors quite popular in high-performance control systems [51]. Advanced manufacturing techniques have also produced dc motors with rotors of very low inertia, thus achieving very high torque-to-inertia ratios. These properties have made it possible to use dc motors in many low-power control applications that formerly used ac motors. On the other hand, three-phase induction motors with pulse-width modulated power amplifiers are currently gaining popularity in high-power control applications.

In the following, we describe the basic characteristics of an ac servomotor, and the related components commonly used in position control systems.

3.7.1 AC Servomotor

An ac servomotor is basically a two-phase induction motor except for certain special design features. Consider a typical set of curves of speed versus torque, shown in Fig. 3.35. For an induction motor used in power applications, the rotor resistance is low in order to obtain high maximum torque (Curve *A*, Fig. 3.35). However, this type of characteristic is not suitable for feedback control systems, mainly because of the positive slope on part of the curve. We will shortly see that a negative slope on the torque-speed curve is essential for stability (The dc motors inherently exhibit the desired torque-speed characteristic, Fig. 3.23). In order to obtain the desired type of characteristic, induction motors for servo applications are designed to have high rotor resistance (Curve *B*, Fig. 3.35). It should be noted that the required characteristic is purchased at a price of power which is dissipated as heat in the high rotor resistance. This decreases the efficiency of the motor and also limits its maximum power rating since the temperature rise in the motor becomes excessive for motors with high power rating.

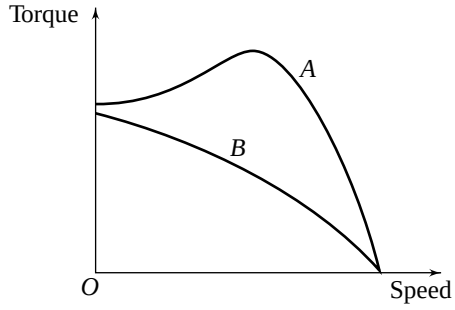

Fig. 3.35 Torque-speed characteristics of ac motors

In servo applications, an induction motor is required to produce rapid accelerations from standstill. Therefore, low inertia is a physical requirement of a servomotor. Thus, except for minor differences in constructional features (rotor has high resistance and low inertia), an ac servomotor is essentially a two-phase induction motor.

The stationary part (stator) of an ac motor is slotted to accommodate two field windings with their axes 90^{o} apart. A two-phase excitation voltage is supplied to the stator windings. The resultant currents produce a rotating magnetic field which, by transformer action, induces voltages in the conductors in the rotating part of the machine (rotor); thereby producing currents in the short-circuited paths of rotor conductors. Interaction of the magnetic field with these currents produces a torque on the rotor.

In the dc motor, current for armature (rotor) conductors is supplied conductively by connection to a voltage source through brush and commutator. In the ac motor, the current for rotor conductors is supplied inductively by the magnetic field. Since no external connections are made to the rotor circuit, the motor can be made very robust and requires little maintenance.

Elementary analysis of the ac motor is more complex than that of the dc motor. So, rather than give the details of production of magnetic field and derivation of motor-torque equation using these details, we use the experimental data of the motor in the form of a set of torque-speed curves to obtain a model.

The symbolic representation of an ac servomotor as a control system component is shown in Fig. 3.36. One phase, designated as the *reference phase*, is excited by a constant voltage source, the frequency of which is usually 50/60, 400, or 1000 Hz. By using frequencies of 400 Hz or higher, the system can be made less susceptible to low-frequency noise. Due to this feature, ac devices are extensively used in aircraft and missile control systems in which noise and disturbance often create problems.

The second phase of the servomotor, designated as the *control phase*, is excited by a voltage of variable magnitude and polarity. The control signal of the servo loop dictates the magnitude and polarity of this voltage.

The control signals in a servo loop are usually of low frequency, in the range of 0 to 20 Hz. For production of rotating magnetic field, the control-phase voltage must be of the same frequency as the reference-phase voltage, and in addition, the two voltages must be in time quadrature. The arrangement shown in Fig. 3.36 meets these requirements. The input signal $e_c(t)$ is applied to the control phase after modulation; the carrier frequency of the modulation process is equal to the frequency of the reference-phase supply. The 90° phase difference between the control-phase and reference-phase voltages is obtained by the insertion of a capacitor (Note that a single-phase power supply is required to run the motor).

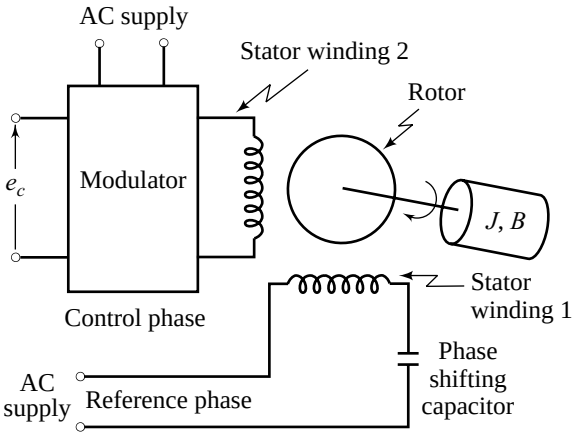

Fig. 3.36 Symbolic representation of an ac servomotor

Figure 3.37 shows the waveforms of a typical input signal $e_c(t)$, the carrier signal cos $\omega_c t$ and the *suppressed-carrier modulated signal* $e_{cm}(t) = e_c(t)$ cos $\omega_c t$. Note that the envelope of the modulated signal e_{cm} is identical to the low-frequency signal e_c. The polarity of e_c dictates the phase of e_{cm} with respect to that of cos $\omega_c t$. If e_c is positive, then e_{cm} and cos $\omega_c t$ have the same phase; otherwise they have 180° phase difference:

$$\begin{aligned} e_{cm}(t) &= |\, e_c(t)| \cos\, \omega_c t \qquad \text{for } e_c(t) > 0 \\ &= |\, e_c(t)|\, \cos(\omega_c t + \pi) \quad \text{for } e_c(t) < 0 \end{aligned} \tag{3.32}$$

This means that a reversal in phase of e_{cm} occurs whenever the signal e_c crosses the zero-magnitude axis. This reversal in phase causes a reversal in the direction of rotation of the magnetic field and hence a reversal in the direction of rotation of the motor shaft.

The modulator in Fig. 3.36 transforms the signal e_c into the signal e_{cm}. If we consider e_c as the input and e_{cm} in Eqn. (3.32) as the output, then the

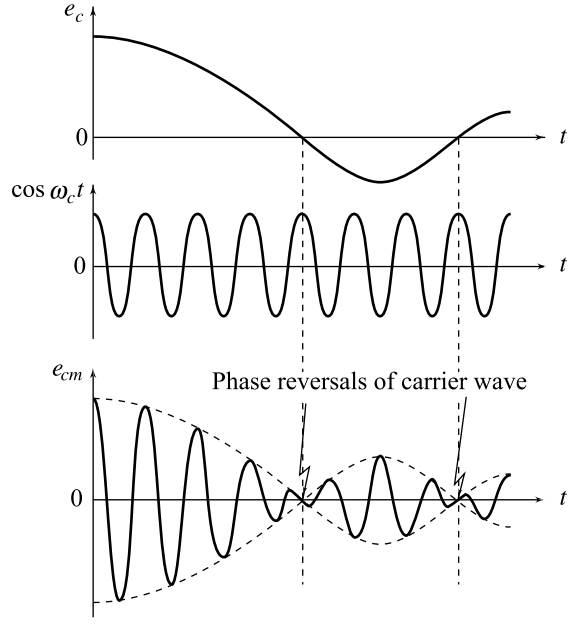

Fig. 3.37 Input–output waveforms of a modulator

mathematical description of the modulator will be rather complicated. Recall that the reason for the introduction of e_{cm} is to match the operational frequency ranges; therefore the information is not stored in e_{cm}, but rather in its envelope. Hence, we should consider e_c as the input and the envelope of e_{cm} as the output of the modulator. Therefore, the transfer function of the modulator is just equal to 1, for the envelope of e_{cm} is identical to e_c.

The torque-speed curves of a typical ac servomotor plotted for fixed reference-phase voltage $E_r \cos \omega_c t$ and different values of constant input voltages $e_c \leq E_r$ are shown in Fig. 3.38. All these curves have negative slope. (Note that the curve for $e_c = 0$ goes through the origin; this means that when the control-phase voltage becomes zero, the motor develops a decelerating torque, causing it to stop). The curves show a large torque at zero speed. This is a requirement for a servomotor in order to provide rapid acceleration.

It is seen that the torque-speed curves of an ac servomotor are nonlinear except in the low-speed region. In order to derive a transfer function for the motor, some linearizing approximations are necessary. A servomotor seldom operates at high speeds; therefore, the linear portions of the torque-speed curves can be extended out to the high speed region, as shown in Fig. 3.38 by use of dashed lines. But even with this approximation, the resultant curves are still not parallel to each other. This means that for constant speeds, except near-zero speed, the torque does not vary linearly with respect to input voltage e_c. The curves in Fig. 3.39 illustrate this effect.

For speeds near zero, all the curves are straight lines parallel to the characteristic at rated input voltage ($e_c = E_r$), and are equally spaced for equal increments of the input voltage. Under this assumption, the torque T_M generated by the motor is represented by the equation

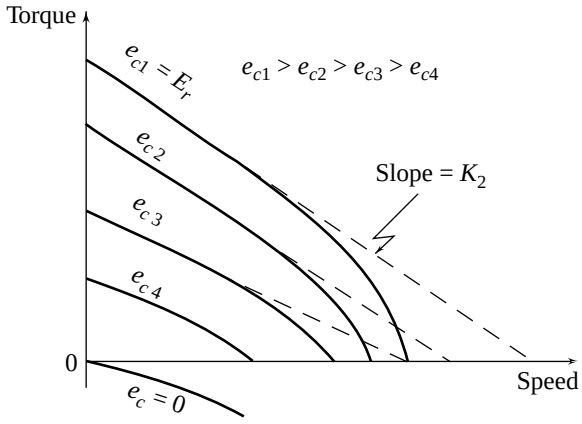

Fig. 3.38 Torque-speed curves of an ac servomotor

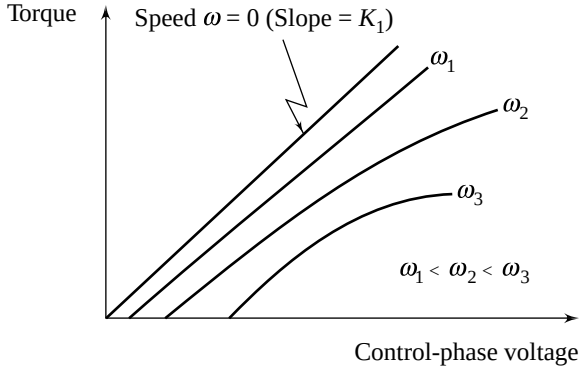

Fig. 3.39 Torque vs control voltage curves of an ac servomotor

$$T_M = K_1 e_c - K_2 \dot{\theta} \tag{3.33}$$

where K_1 and K_2 are the slopes defined in Figs 3.38 and 3.39. Note that both K_1 and K_2 are positive numbers.

If we consider that the moment of inertia of the motor rotor with attached mechanical load is J, the viscous-friction coefficient of the motor rotor with attached mechanical load is B, and the disturbance load torque is T_w, then we have

$$T_M = K_1 e_c - K_2 \dot{\theta} = J\ddot{\theta} + B\dot{\theta} + T_w \tag{3.34}$$

Figure 3.40 shows a block diagram representation of the ac motor system. The transfer function between the shaft position $\theta(s)$ and the input voltage $E_c(s)$, obtained from the block diagram, is

$$\frac{\theta(s)}{E_c(s)} = \frac{K_1}{s(Js + B + K_2)} = \frac{K_m}{s(\tau_m s + 1)} \tag{3.35}$$

where $K_m = \dfrac{K_1}{B + K_2}$ = motor gain constant and $\tau_m = \dfrac{J}{B + K_2}$ = motor time-constant

Since K_2 is a positive number, the above equations show that the effect of the slope of the torque-speed curve is to add more friction to the motor, which does improve the damping of the motor. However, if K_2 is a negative number, for $|K_2| > B$, negative damping occurs and the motor becomes unstable. This verifies the statement made previously that the conventional induction motors are not suitable for servo applications.

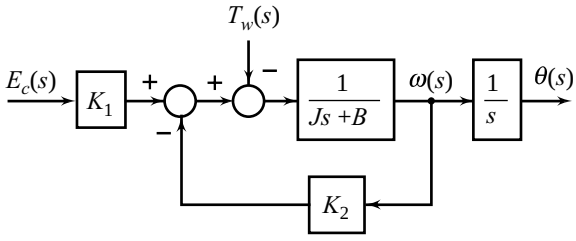

Fig. 3.40 Block diagram of an ac motor system

It must be noted that the modulation process for running the ac servomotor is not necessary if the control signal in the servo loop is an ac signal of frequency equal to that of reference phase supply. The transfer function model given by Eqn. (3.35) is applicable in these situations also, with the only difference that the input variable for the model is not the control-phase voltage itself but rather its envelope. This is in order as the information about the required control action is stored in the envelope of the control-phase voltage; the frequency of the voltage is governed only by the operational frequency range of the servomotor.

3.7.2 AC Tachogenerator

The ac tachogenerator resembles a two-phase induction motor in that it comprises two stator windings arranged in space quadrature, and a rotor which is not conductively connected to any external circuit. A sinusoidal voltage

$$e_r(t) = E_r \sin \omega_c t$$

is applied to the *excitation* (*reference*) *winding* (refer Fig. 3.41b). When the rotor is stationary ($\dot{\theta} = 0$), no emf is induced in the *output winding* and therefore the output voltage will be zero. When the motor turns, a voltage at the reference frequency ω_c is induced in the output winding. The magnitude of the output voltage is proportional to the rotational speed. A change in the direction of shaft rotation causes a 180° phase shift in the output voltage. When the output voltage is in phase with the reference, the direction of rotation is said to be *positive*, and when the output voltage is 180° out of phase, the direction is said to be *negative.*

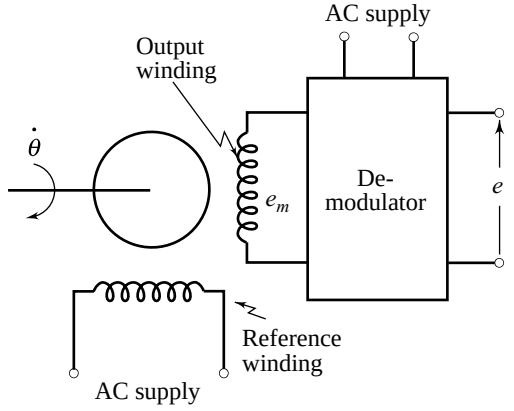

Fig. 3.41 Schematic diagram of an ac tachogenerator

The output voltage of an ac tachogenerator is, thus, in a modulated form. A typical waveform of the output voltage $e_m(t)$ is shown in Fig. 3.42. It can be mathematically represented as

$$e_m(t) = e(t) \sin \omega_c t$$

In the measurement system shown in Fig. 3.41, we have used a *demodulator* for signal conditioning. The input to the demodulator is $e_m(t)$ and its output is $e(t)$. Since the information about shaft speed is stored not in $e_m(t)$ itself but rather in its envelope, we should consider the envelope of $e_m(t)$ as the input of the demodulator. Therefore, the transfer function of the demodulator is just equal to 1, for the envelope of $e_m(t)$ is identical to the output $e(t)$. The output voltage of an ac tachogenerator (with signal conditioning) is therefore of the same form as that for a dc tachogenerator (refer Eqn. (3.22)), i.e.,

$$e(t) = K_t \frac{d\theta(t)}{dt} \tag{3.36a}$$

where K_t is the sensitivity of the tachogenerator (volts per rad/sec).

The transfer function from $\theta(t)$ to $e(t)$ of an ac tachogenerator is of the form

$$\frac{E(s)}{\theta(s)} = s\,K_t \tag{3.36b}$$

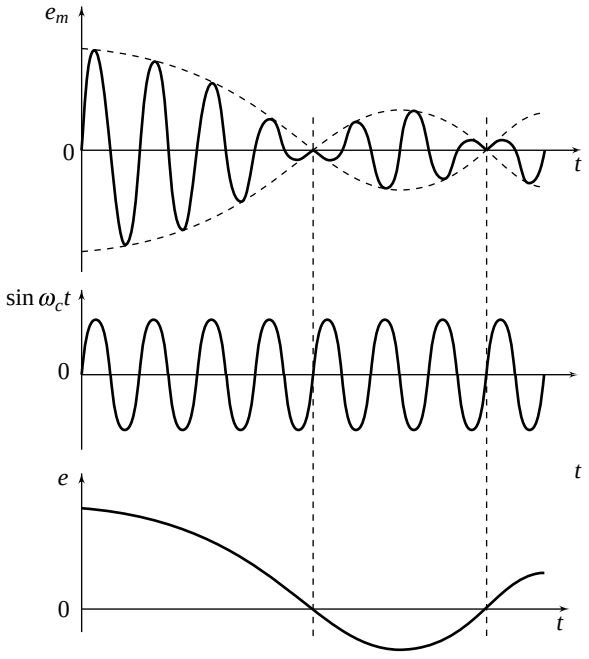

Fig. 3.42 Waveforms illustrating the operation of a demodulator

3.7.3 Synchros

A synchro system, formed by interconnection of the devices called the *synchro transmitter* and the *synchro control transformer*, is perhaps the most widely used error detector in feedback control systems. It measures and compares two angular displacements, and its output voltage is approximately linear with angular difference. Our discussion on synchro devices will be limited to the basic features of the synchro transmitter and the synchro control transformer.

The constructional features, electrical circuit, and a schematic symbol of a synchro transmitter are shown in Fig. 3.43. The stationary part of the machine (stator) is slotted to accommodate three Y connected coils, wound with their axes 120° apart. The stator windings are not directly connected to the ac power source. Their excitation is supplied by the ac magnetic field produced by the rotating part of the machine (rotor).

The rotor is of a dumb-bell construction with a single winding. A single-phase excitation voltage is applied to the rotor through two slip rings. The resultant current produces a magnetic field and, by the transformer action, induces voltages in the stator coils. The effective voltage induced in any stator coil depends upon the angular position of the coil's axis with respect to the rotor axis.

Let the ac voltage applied to the rotor be

$$e_r(t) = E_r \sin \omega_c t \tag{3.37}$$

When the rotor is in the position corresponding to $\theta = 0$ in Fig. 3.43b, the voltage induced across the stator winding S_2 and the neutral is maximum and is written as

$$e_{S_2 n} = KE_r \sin \omega_c t$$

where K is a proportional constant.

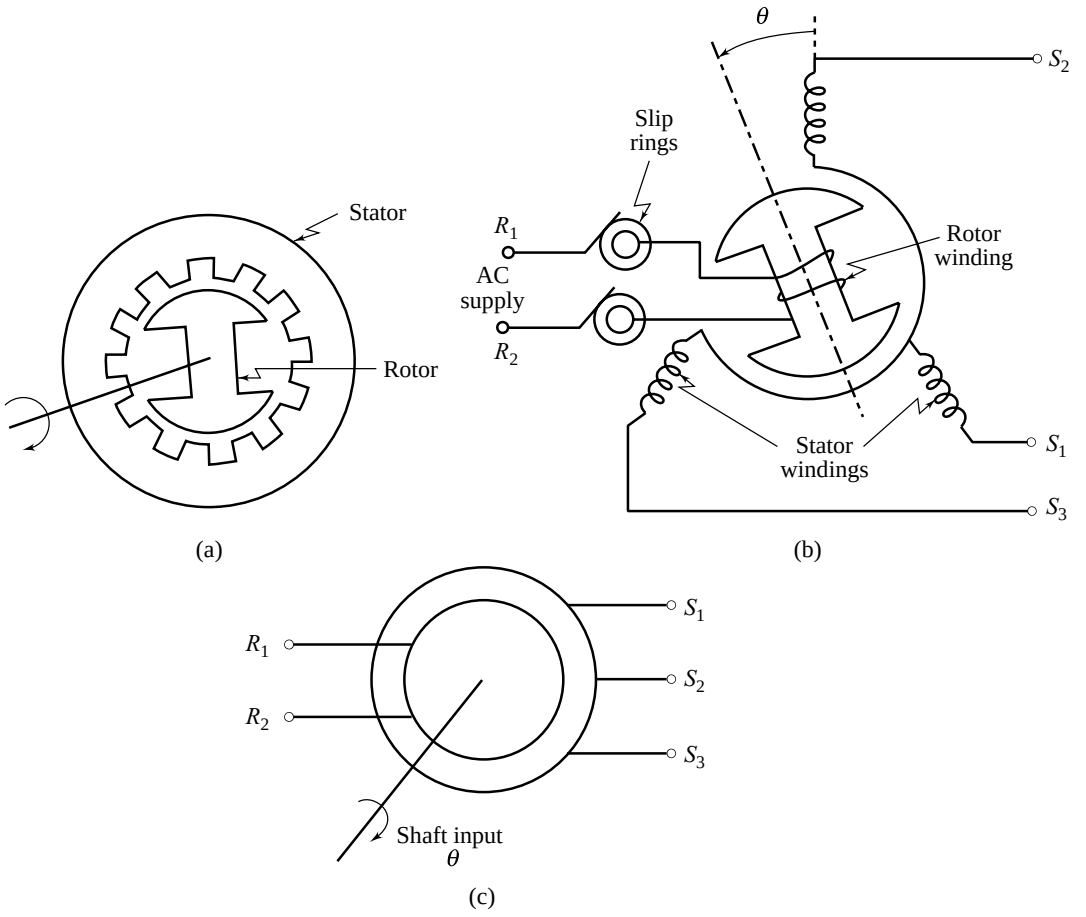

Fig. 3.43 (a) Constructional features, (b) electrical circuit, and (c) schematic symbol of a synchro transmitter

When the rotor is in position corresponding to $\theta = 90°$ in Fig. 3.43b, the voltage e_{S_2n} is zero. Therefore when $\theta = 0$, the coupling coefficient between the rotor winding and the stator winding S_2 is 1, and when $\theta = 90°$, the coupling coefficient equals 0. In fact, in general, the coupling coefficient between S_2 winding and rotor winding is equal to cos θ for any position of the rotor:

$$e_{S_2n} = KE_r \cos\theta \sin\omega_c t$$

When the rotor is at 0° position with respect to the S_2 winding, it is at $-120°$ position with respect to the S_3 winding; that is, positive (counter clockwise) rotation of 120° is required to move the rotor from the first position to the second position. Thus, if S_2 winding is taken as a reference,

$$e_{S_3n} = KE_r \cos(\theta - 120) \sin\omega_c t$$

In the same way,

$$e_{S_1n} = KE_r \cos(\theta - 240) \sin\omega_c t$$

The three terminal voltages of the stator are

$$e_{S_1S_2} = e_{S_1n} + e_{nS_2} = \sqrt{3}\, KE_r \sin(\theta + 240) \sin\omega_c t \qquad (3.38a)$$

$$e_{S_2S_3} = e_{S_2n} + e_{nS_3} = \sqrt{3}\, KE_r \sin(\theta + 120) \sin\omega_c t \qquad (3.38b)$$

$$e_{S_3S_1} = e_{S_3n} + e_{nS_1} = \sqrt{3}\, KE_r \sin\theta \sin\omega_c t \tag{3.38c}$$

When $\theta = 0°$, maximum voltage is induced in winding S_2, and it follows from Eqn. (3.38c) that the terminal voltage $e_{S_3S_1}$ is zero. This position of the rotor is defined as the *electrical zero* of the transmitter and is used as reference for specifying the angular position of the rotor.

It should be noted that the synchro is not a three-phase machine. In a three-phase machine, there are three voltages equal in magnitude, displaced from each other by 120 electrical degrees. With the synchro, which is a single-phase device, the three stator voltages vary in magnitude, and one stator coil is in phase or 180° out of phase with another coil.

It is seen that the input to the synchro transmitter is the angular position of its rotor shaft and the output is a set of three stator coil-to-coil voltages (common connection between the stator coils is not accessible) given by Eqns (3.38). By measuring and identifying the set of voltages at the stator terminals, it is possible to identify the angular position of the rotor.[5]

Our interest here is in synchro error detector formed by interconnection of two synchro devices—the transmitter and the control transformer. A typical arrangement of a synchro error detector in servo applications is to connect the stator leads of the transmitter to the stator leads of the control transformer. A servo loop using the synchro error detector is shown in Fig. 3.44. Basically, the principle of operation of a synchro control transformer is identical to that of the synchro transmitter, except that the rotor is cylindrically shaped so that the air-gap flux is uniformly distributed around the rotor. This feature of the control transformer minimizes the change in the rotor impedance with the rotation of the shaft; the signal conditioning circuit, therefore, sees a constant impedance.

Referring to the arrangement shown in Fig. 3.44, the voltages given in Eqns (3.38a)–(3.38c) are impressed across the corresponding stator terminals of the control transformer. Due to the similarity in the magnetic construction, the flux patterns produced in the two synchros will be the same if all losses are neglected. For example, if the rotor of the transmitter is in its electrical zero position, the fluxes produced in the transmitter and in the control transformer are as shown in Fig. 3.45. When the rotor of the control transformer is in the position shown in the figure, the induced voltage at its rotor winding terminals is zero; the shafts of the two synchros are considered to be in alignment, and the control transformer is said to be in *null position*. Thus the null position of a control transformer in a servo loop is that position of its rotor for which the output voltage on the rotor winding is zero with the transmitter in its electrical zero position.

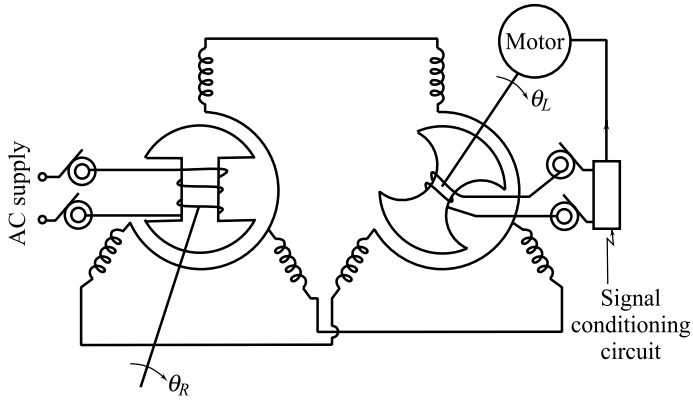

Fig. 3.44 Servo loop using synchro error detector

[5]A synchro/digital (S/D) converter accepts the three ac voltages from the synchro as input and gives out a digital output which is a measure of the magnitude and direction of rotor movement (refer [72] for details). There also exists a digital/synchro (D/S) transmitter to convert digital data to synchro format voltages.

Let the rotor of the transmitter rotate through an angle θ from its electrical zero position, and let the rotor of the control transformer rotate in the same direction through an angle α from its null position (refer Fig. 3.45); the net angular separation of the two rotors is then $(90 - \theta + \alpha)$ and the voltage induced in the control transformer is proportional to the cosine of this angle:

$$e_m(t) = K'E_r \cos(90 - \theta + \alpha) \sin \omega_c t$$
$$= K'E_r \sin(\theta - \alpha) \sin \omega_c t$$

where K' is a proportional constant.

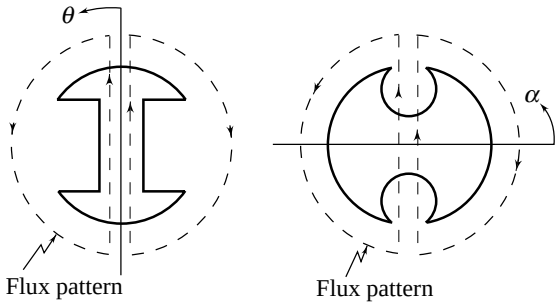

Fig. 3.45 Rotor positions and flux patterns

For small values of $\phi(t) = \theta(t) - \alpha(t)$, $e_m(t) = K'E_r \phi(t) \sin \omega_c t$

The output voltage of the synchro error detector is thus a modulated signal with the carrier frequency ω_c equal to the frequency of the ac supply to the rotor winding of the synchro transmitter. The magnitude of the modulated carrier wave is proportional to $\phi(t) = \theta(t) - \alpha(t)$, and the phase reversals of the modulated wave depend on the sign of $\phi(t)$ (refer Fig. 3.42).

Signal conditioning of the modulated output of the synchro error detector by an amplifier and a demodulator gives an output voltage

$$e(t) = K_s \phi(t) \tag{3.39}$$

where K_s = sensitivity of the synchro error detector in volts/deg.

The transfer function of the synchro error detector is, therefore, of the form

$$\frac{E(s)}{\phi(s)} = K_s \tag{3.40}$$

It must be noted that the signal-conditioning circuit will not include the demodulation process if the synchro-output signal is connected to an ac device (e.g., ac servomotor). The transfer function model given by Eqn. (3.40) is applicable in these situations also, with the only difference that the output variable of the model is not the synchro-output voltage itself but rather its envelope. This is in order as the information about the angular separation of the two shafts is stored in the envelope of the synchro-output voltage; the frequency of the voltage is governed only by the operational frequency range of the synchro device.

Compared with potentiometers, the synchros offer higher sensitivity, longer life, ruggedness, and continuous rotation capability.

3.7.4 A Carrier Control System

A heavy telephoto camera can be controlled by the system shown in Fig. 3.46a. The camera is driven by an ac motor through a gear train and is designed to follow the movement of the spotting scope. This system employs ac components and all the signals other than the input and output shaft positions are suppressed-carrier modulated signals. Such systems are known as *carrier control systems* and are designed so that the signal cut-off frequency is much less than the carrier frequency. It is then sufficiently accurate to analyze these systems on the basis of modulating signals only.

In the system of Fig. 3.46a, a pair of synchros with sensitivity K_s is used as an error detector to generate the error signal $e = K_s(\theta_R - \theta_L)$. An ac amplifier of gain K_A is used to amplify this signal. The output e_c of the amplifier drives the ac servomotor. The torque developed by the motor is transmitted to the load shaft through a gear train with gear ratio n ($n = N_1/N_2$ = load shaft speed $\dot{\theta}_L$ /motor shaft speed $\dot{\theta}_M$).

The two-phase motor develops a torque in accordance with the equation (refer Eqn. (3.33))

$$T_M = K_1\, e_c - K_2\, \dot{\theta}_M$$

where the constants K_1 and K_2 are given by torque-speed characteristics of the motor.

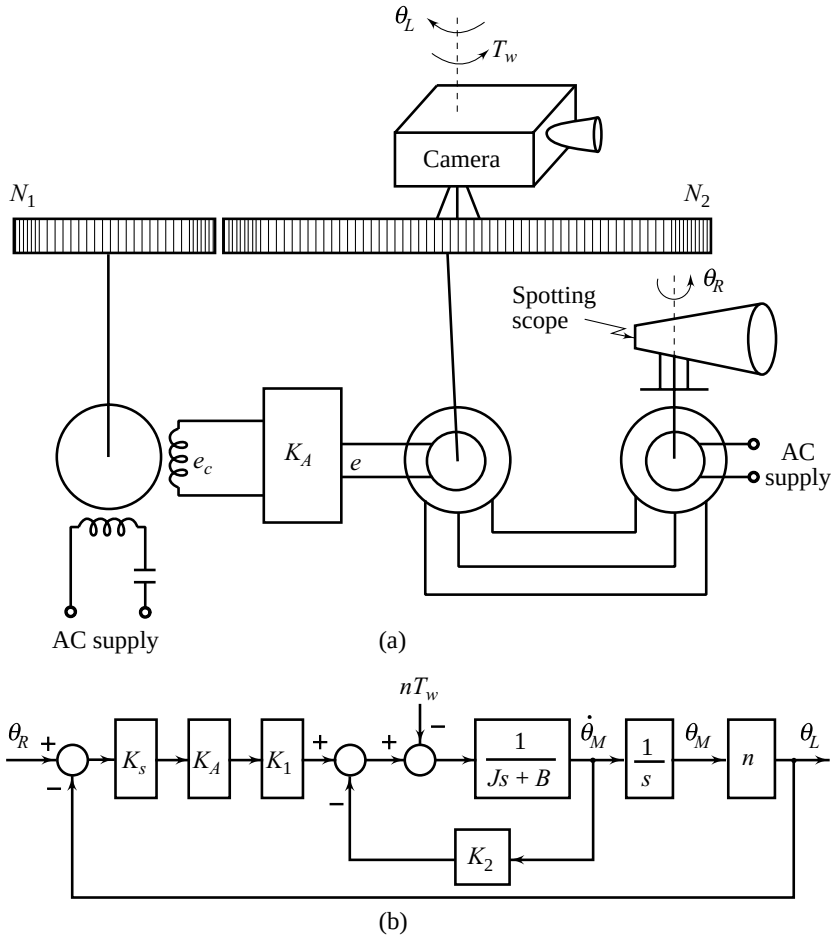

Fig. 3.46 An ac (carrier) control system (a) schematic diagram (b) block diagram

This torque drives the load (camera) of moment of inertia J_L and viscous-friction with coefficient B_L, against the disturbance load torque T_w. Assume that the moment of inertia and viscous-friction of the motor are represented by J_M and B_M, respectively. The equivalent moment of inertia of the motor-load combination reflected on the motor shaft is given by (refer Eqns (3.30))

$$J = J_M + n^2\, J_L$$

and the equivalent viscous-friction coefficient

$$B = B_M + n^2\, B_L$$

nT_w is the equivalent disturbance torque on the motor shaft.

In terms of these parameters, the torque equation of the system becomes

$$T_M = J\ddot{\theta}_M + B\dot{\theta}_M + nT_w$$

A block diagram of the system is shown in Fig. 3.46b.

The output of the synchro error detector in Fig. 3.46, is a carrier-modulated signal. The information about the misalignment of the two shaft positions is carried by the envelope of this signal. As we shall see in the next chapter, generation of the control signal requires processing on the information signal, i.e., the envelope of the synchro-output signal. For example, we may require a derivative and/or an integration of the information signals in addition to amplification. A demodulator provides the necessary interface between the synchro error detector and the op amp circuit for generating the control signal. The low-frequency control signal can drive a dc motor after power amplification. Alternatively, the control signal may be modulated to drive an ac motor.

3.8 HYDRAULIC DEVICES FOR MOTION CONTROL

Hydraulically operated devices are frequently used in control systems. In these devices, power is transmitted through fluid flow under pressure. The fluid used is relatively incompressible such as petroleum-based oils or certain non-inflammable synthetic oils.

When both high speed and high power are required, hydraulic systems may be mandatory or desirable. Common hydraulic control applications are power steering and brakes in automobiles, steering mechanism of ships, aircraft control surface actuators, control of large machine tools, servo systems for cranes and hoists, robots, and rolling mills, etc.

Some of the important hydraulic devices are discussed in this section.

3.8.1 Hydraulic Actuators

The hydraulic output devices used in control systems are generally of two types—those intended to produce rotary motion and those whose output is translational. The first type is known as the hydraulic motors and the second ones known as the hydraulic linear actuators.

The hydraulic linear actuator shown in Fig. 3.47 consists of a pilot valve and a power cylinder. The piston inside the power cylinder divides the cylinder into two chambers. The pilot valve—known as *spool valve* because of its shape—controls the flow rate of the hydraulic fluid to the power cylinder. It is a four-port valve: one port is connected to the hydraulic fluid supply at constant pressure, two control ports are connected to each chamber of the cylinder, and the drain port (the two drain ports are joined) is connected to the reservoir. The valve spool has two lands.

When the spool is in the neutral position ($x = 0$), the fluid flow in the power cylinder is blocked completely and the position of the piston, which moves the load, is $y = 0$. As the spool is moved to the right (x positive), the right-chamber port of the power cylinder is opened to the supply pressure P_s whereas the left-chamber port is opened to pressure P_r, which is slightly above the atmospheric pressure but we approximate it as zero gauge pressure in our model. Right-chamber pressure P_1 thus rises (while left-chamber pressure P_2 falls), producing an accelerating force on the load that moves to the left (y positive). If the spool is moved to the left (x negative), the left-chamber port of the power cylinder is opened to the supply pressure P_s, whereas the right-chamber port is opened to P_r. The direction of the fluid flow in the cylinder and hence the direction of displacement y of the load is reversed. This hydromechanical system acts as a power amplifier since the power (force × velocity) applied to position the valve is much smaller than that developed at the load.

[6]This section and the related problems in the book which involve hydraulic actuator, may be skipped if a course plan so demands.

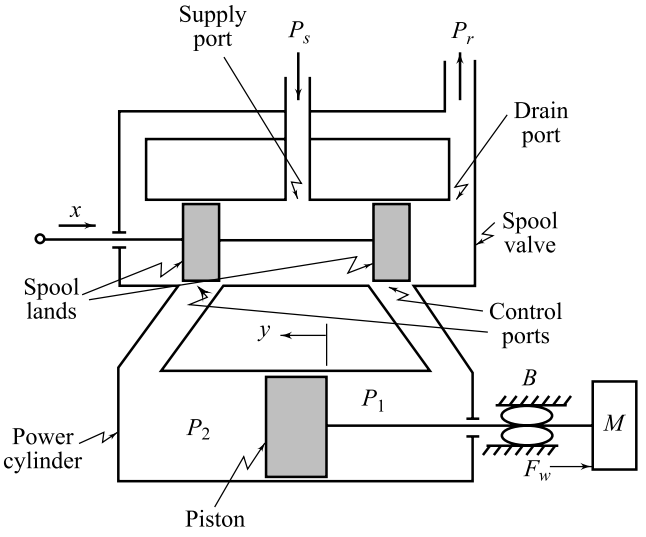

Fig. 3.47 Hydraulic linear actuator with a load

Note that when the valve spool is in its neutral position, the flow area of the control ports is not in general zero. This is because spool lands and ports cannot be manufactured with perfectly sharp edges. Thus, a real valve will either be underlapped or overlapped (Fig. 3.48). Since an overlapped valve causes a dead zone for small spool motions (which is undesirable in control systems (refer Chapter 14), underlapped valves are often preferred.

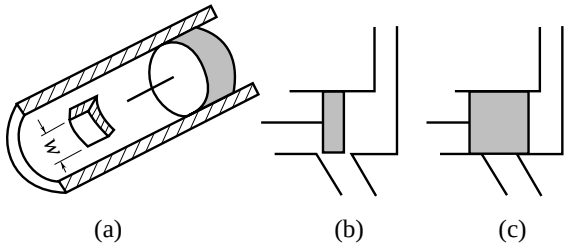

Fig. 3.48 (a) Spool valve construction
(b) underlapped valve
(c) overlapped valve

With an underlapped valve in the neutral position, the cylinder pressures P_1 and P_2 will approach half the supply pressure P_s. This can be explained as follows.

The fluid flow through the valve ports is similar to the flow through an orifice; the orifice flow relation (2.129) can therefore be applied. Let ΔP_v be the pressure drop across a valve port. Then

$$q = C_o A_o \sqrt{\frac{2(\Delta P_v)}{\rho}} \tag{3.41}$$

where

q = volume flow rate through the port; C_o = discharge coefficient;
A_o = uncovered area of the port; ρ = density of the fluid.

The area A_o is equal to $w \times x$, where w is the width of the port (refer Fig. 3.48a). Since C_o, ρ (compressibility assumed negligible), and w are constant, the flow q is a function of x and ΔP_v.

Let us now examine the neutral position of the spool valve. In this position, the fluid leakage into the right chamber of the cylinder is at the rate proportional to $(P_s - P_1)^{1/2}$, and the leakage out of the right chamber is at the rate proportional to $(P_1 - P_r)^{1/2}$. Equilibrium of leakage in and out of the right chamber of the cylinder will be achieved when $P_1 = P_s/2$. Similarly, equilibrium of leakage in and out of the left chamber will be achieved when $P_2 = P_s/2$. This situation will be taken as the equilibrium point.

The movement of the spool from its neutral position and the load-induced pressure on the power piston will disturb the system from its equilibrium position. Assume that the load changes the right-chamber pressure to $P_1 = (P_s/2) + p_1$, and the left-chamber pressure to $P_2 = (P_s/2) + p_2$; the load-induced pressure

$$\Delta p = P_1 - P_2 = p_1 - p_2$$

The pressure drop from the supply to the reservoir, $P_s - P_r$, must equal the sum of the drops across both the control ports and the power piston. That is

$$P_s - P_r = 2\Delta P_v + \Delta p$$

where the drop across a control port is $\Delta P_v = P_s - P_1 = P_2 - P_r$, and the drop across the piston is

$$\Delta p = P_1 - P_2$$

Therefore,

$$\Delta P_v = \frac{1}{2}[P_s - P_r - \Delta p]$$

Since P_s = constant and $P_r = 0$, we see that ΔP_v varies only if Δp changes. Thus the variables x and Δp determine the volume flow rate:

$$q = f(x, \Delta p) \tag{3.42}$$

This relation is nonlinear. Linearization about the equilibrium point ($x = 0$, $\Delta p = 0$, $q = 0$) gives

$$q = K_1 x - K_2 \Delta p \tag{3.43}$$

where $K_1 \triangleq \left.\dfrac{\partial f}{\partial x}\right|_{x=\Delta p=0} > 0$, is the flow gain; and $K_2 \triangleq \left.\dfrac{\partial f}{\partial \Delta p}\right|_{x=\Delta p=0} > 0$, is the pressure coefficient.

Figure 3.49 shows this linearized relationship among q, x, and Δp. The straight lines shown are the linearized characteristic curves of the hydraulic actuator. Note that the region near the origin is most important because system operation usually occurs near this point. The flow gain K_1 and the pressure coefficient K_2 can be estimated theoretically from Eqn. (3.41), or more accurately from the experimental tests once the valve has been built.

Referring to Fig. 3.47, we see that the rate of fluid flow into the power cylinder is proportional to the rate at which the piston moves, i.e.,

$$K_1 x - K_2 \Delta p = A\,\dot{y} \tag{3.44}$$

where A is the area of the piston.

Notice that because of high force levels and pressure differentials, there may be leakage from one chamber of the power cylinder to the other. However, translational actuators usually have piston rings that are essentially leak free. Equation (3.44) is true under the assumption of zero leakage around the piston.

The force developed by the power piston is equal to the pressure difference Δp times the piston area A. Assume that the power piston moves a load consisting of a mass M, and viscous friction with coefficient B. Then

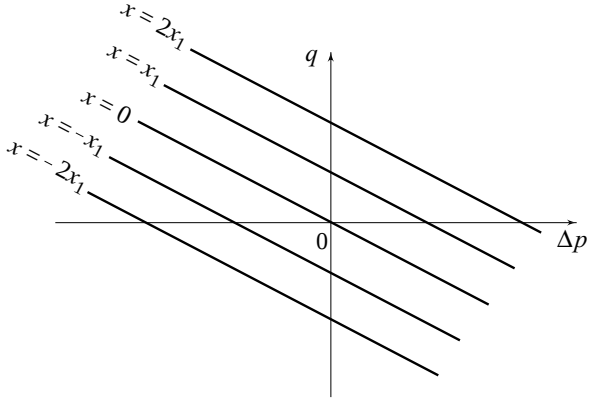

Fig. 3.49 Linearized characteristic curves of a hydraulic actuator

$$A\,\Delta p = M\ddot{y} + B\dot{y} + F_w \qquad (3.45)$$

where F_w represents the load disturbance.

Figure 3.50 shows a block diagram representation of the hydraulic system. The transfer function between the load displacement y and the spool displacement x, obtained from the block diagram, is

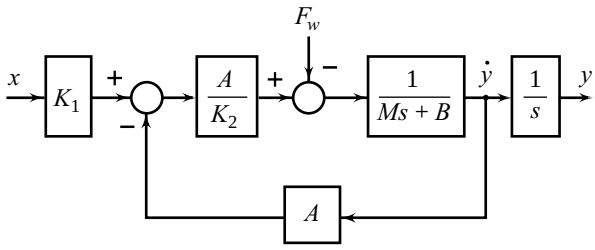

Fig. 3.50 Block diagram of the hydraulic system of Fig. 3.47

$$\frac{Y(s)}{X(s)} = \frac{K}{s(\tau s + 1)} \qquad (3.46)$$

where $K = \dfrac{AK_1}{BK_2 + A^2}$ = gain constant of the actuator; and $\tau = \dfrac{MK_2}{BK_2 + A^2}$ = time-constant of the actuator.

The controlled fluid power from a spool valve can be converted into rotating mechanical power by a hydraulic motor (refer [49, 53]).

3.8.2 Electrohydraulic Servovalves

The key to harnessing the power developed by hydraulic actuators and controlling them with analog electronic devices/digital computers, is the electrohydraulic servovalve. In its simplest form, an electrohydraulic servovalve is a spool valve with a spool positioned by solenoid-type magnetic actuators. These valves are called *single-stage valves.*

For a large flow rating, the forces required to rapidly and accurately position the spool are beyond the capabilities of solenoid-type electromagnetic positioners. Large electrohydraulic servovalves have an electromechanical first stage and a hydromechanical second stage.

Electrohydraulic valves of different sizes and constructional features are commercially available. The basic principle of operation of these valves is illustrated by the schematic diagram in Fig. 3.51. A magnetic torque motor activates this *two-stage valve*. The armature of the torque motor, which acts as a flapper, extends into the airgaps of the magnetic flux provided by a permanent magnet. The armature (flapper) is pivoted and its one end is positioned between two nozzles. The armature is wound with wire and current is forced through this armature winding. The reaction of the magnetic flux with armature current produces a torque that forces the armature to rotate.

In Fig. 3.51, the armature winding is energized by a balanced amplifier which has the input e. When the input is zero, the currents i_1 and i_2 are equal. Since they flow in opposite directions, the net torque is zero and the flapper is stationary at its central position between the two nozzles. If e is not zero, one of the currents increases and the other decreases in proportion to the magnitude of e. The resulting torque is proportional to the magnitude of e and its direction depends on the polarity of e.

The developed torque, balanced by the torsional spring at the pivot, moves the flapper to the right or left. If the flapper moves to the right, the back pressure of the right-hand nozzle rises while that of the left-hand nozzle falls. A differential pressure between the nozzles is created which produces a force on the spool. This force, balanced by springs, results in spool displacement to the left.

A servovalve model is given by the equation

$$x = Ke \qquad (3.47)$$

where x = spool displacement; e = input voltage; and K = valve gain.

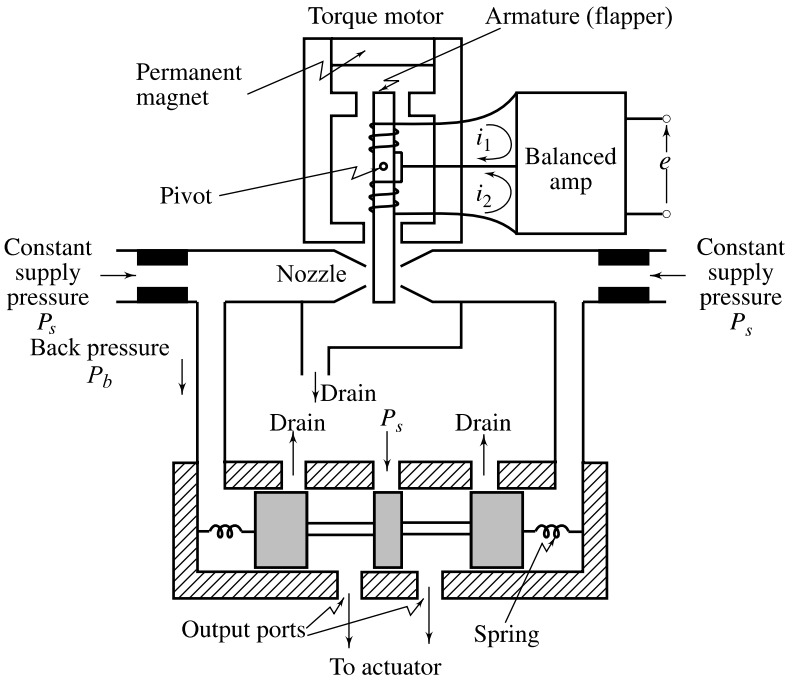

Fig. 3.51 An electrohydraulic servovalve

This approximate model is adequate since the dynamics relating x to e is generally quite fast relative to the time-constants of the hydraulic actuator interfaced to the servovalve.

3.8.3 Linear Variable Differential Transformer

A linear variable differential transformer (LVDT) measures a linear displacement. The schematic diagram of an LVDT is shown in Fig. 3.52. A primary coil is wound between two secondary coils on a hollow cylindrical form. A movable core is positioned inside the coil form. The primary is excited by an ac source. When the core is in its exact centre position ($y = 0$), the two secondaries are linked by an equal number of flux lines; the emf induced in secondary 1 will be the same as the emf induced in secondary 2. The two secondaries are so connected that their induced voltages oppose each other, and the output voltage will be zero corresponding to $y = 0$. When the core is moved to the right, fewer lines of flux link secondary 1 than secondary 2. Thus a greater emf is induced in secondary 2 than in

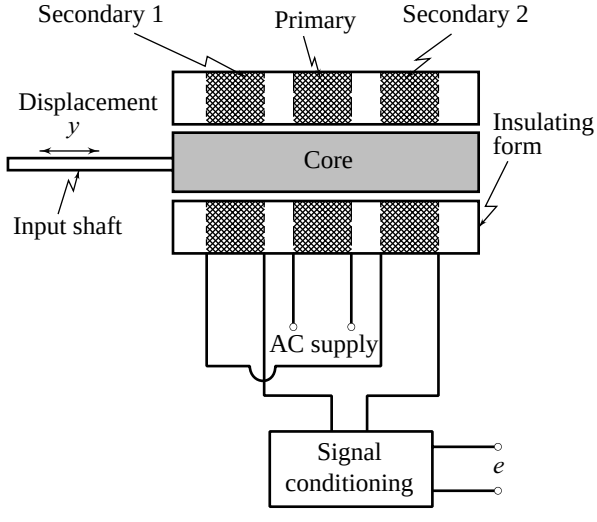

Fig. 3.52 Linear variable differential transformer (LVDT)

secondary 1 and a net voltage appears at the output. When the core is moved to the left, a net voltage will again appear at the output, but it is in anti-phase to that for an equivalent displacement to the right.

The output voltage of LVDT is in a modulated form, i.e.,

$$e_m(t) = K\, y(t) \sin \omega_c t$$

where ω_c, the carrier frequency, is the same as the frequency of ac supply. The magnitude of the modulated carrier wave is proportional to the core displacement $y(t)$ with K as the constant of proportionality, and the phase reversals of the modulated carrier wave depend on the sign of $y(t)$ (refer Fig. 3.42).

Signal conditioning by a demodulator and an amplifier gives an output voltage

$$e(t) = K_s\, y(t) \tag{3.48}$$

where K_s = sensitivity of the displacement transducer in volts/mm.

Compared with potentiometer, the LVDT offers higher sensitivity, longer life, ruggedness, and continuous motion capability.

3.8.4 A Hydraulic Servomechanism

A hydraulic servo system used to control the transverse feed of a machine tool is shown in Fig. 3.53a. The cutting tool is powerfully positioned by the hydraulic cylinder fed by the spool valve. The load on the power piston may be assumed to consist of mass M and viscous friction with coefficient B. The disturbance acting on the power piston is the thrust force F_w on the tool.

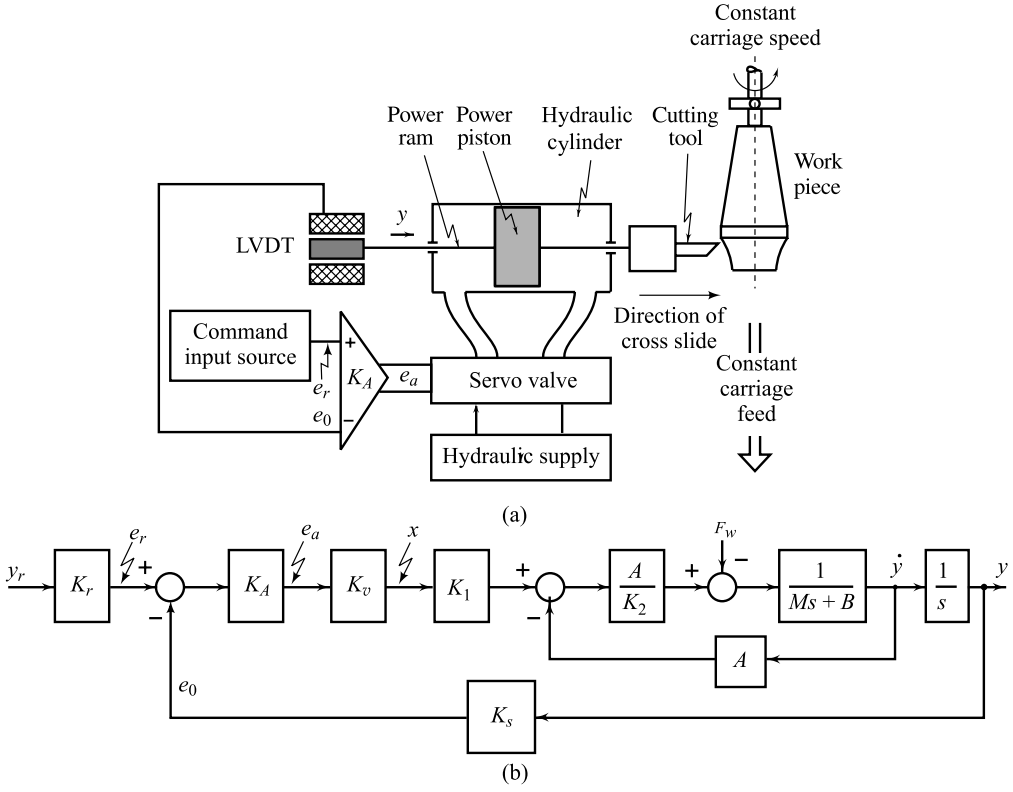

Fig. 3.53 An electrohydraulic servomechanism; (a) schematic diagram, (b) block diagram

The actual tool position $y(t)$ is required to follow a time-varying command input position $y_r(t)$. The command input $y_r(t)$ may be generated by a punched tape reader (or a digital computer for computer-controlled hydraulic servo system (refer Chapter 11)). The command input device produces a voltage $e_r=K_r y_r$. The carriage is moved at a constant speed and the control of the tool position is in the direction of cross slide. The LVDT produces a feedback voltage $e_0(t)$ proportional to the actual tool position ($e_0(t)=K_s\, y(t)$; K_s is a constant). The error ($e_r–e_0$) is amplified by an amplifier of gain K_A volts/volt. The servo valve regulates the spool displacement and hence controls port opening x; $x = K_v\, e_a$, where K_v is the valve gain. The rate of oil flow in the power cylinder is $q = K_1x–K_2\Delta p$, where Δp is the differential pressure across the piston of area A, and K_1 and K_2 are constants.

All variables are deviations from an equilibrium position corresponding to a rest position of the load; the spool lands completely cover the control ports.

A block diagram of the system is shown in Fig. 3.53b (refer Eqns (3.42–3.46), and Fig. 3.50).

3.9 PNEUMATIC DEVICES FOR PROCESS CONTROL

While hydraulic devices use an incompressible fluid (oil), the working medium in a pneumatic device is a compressible fluid, generally air. It is primarily the different properties of the fluids involved that characterize the differences between the two types of devices.

Many factors bear on the electric/hydraulic/pneumatic decision for those applications where all are technically feasible. Some of these factors are initial cost, maintenance, the nonlinear and other complex characteristics involved, etc.

Pneumatic devices are widely used in process systems used to control temperature, pressure, flow rate, liquid level, and the like. These systems have long time-constants; the response time of pneumatic devices is adequate for their control. Some of the important devices used in process control systems are discussed in this section.

3.9.1 Flow Control Valve

In a large number of process control systems, the final actuator controls the flow of some fluid—liquid, gas, or steam—using flow control valves. All control valves operate by inserting a variable restriction in the flow path. The plug valve (Fig. 3.54) operates by moving a tapered plug, thereby varying the gap between the plug and the valve seat. The flow is controlled by the linear movement of the valve stem.

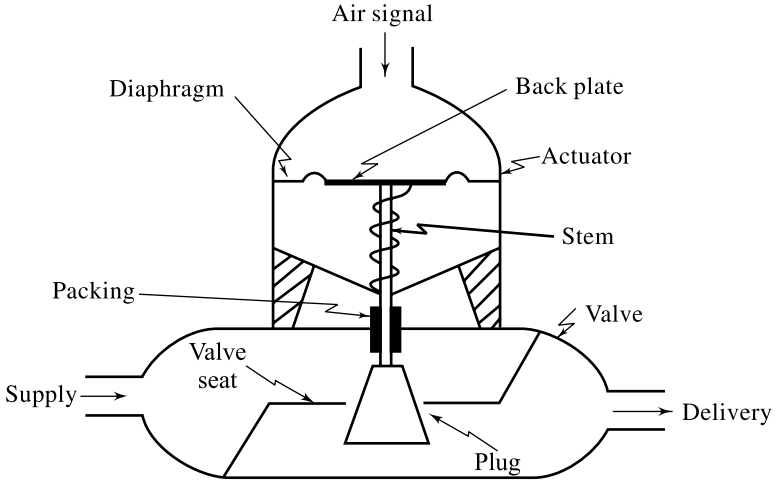

Fig. 3.54 A pneumatic control value

Pneumatic actuation of the control valves is most common in the process industries. When a valve is supplied by a manufacturer, the pneumatic actuator and the valve are usually attached to each other to form one unit. Figure 3.54 shows a unit where the pneumatic device controls the reciprocating stem of the valve as the pressure on the spring-loaded diaphragm changes[7]. The stem positions a plug in the orifice of the valve body.

An increase in the signal pressure above the diaphragm exerts a force on the diaphragm and the back plate which causes the stem to move down until the force from the now more compressed spring balances the force on the stem. This results in an increase in the cross-sectional area for flow between the plug and the seat, thereby increasing the flow.

In general, the flow rate of fluid through the valve depends upon the upstream and downstream fluid pressures and the size of the opening through the valve. If all components (including the process) in a feedback control system are essentially linear, then the control valve flow characteristic (relationship between flow through the valve and valve stem position) should also be linear, since the system performance (stability, speed of response, etc.) will be uniform over all system operating conditions. If other system components (usually the process) exhibit significant nonlinearities, then we can choose a valve characteristic that is the inverse of the process nonlinearity, thereby linearizing the overall system and gaining the benefits of uniform performance [49].

Control valves with linear flow characteristics are commonly used in processes where the pressure drop across the valve is fairly constant. In our process control examples, we will use control valves with the following characteristics:

(i) the flow through the valve is proportional to valve stem position; and
(ii) the valve stem position is proportional to input signal pressure.

3.9.2 Electropneumatic Transducer

The key to harnessing the power developed by pneumatic actuators and controlling them with analog electronic devices/digital computers, is the electropneumatic transducer. It receives an electrical signal and transmits a proportional output pressure.

Electropneumatic transducers of different sizes and constructional features are commercially available. The basic principle of operation of these devices is illustrated by the schematic diagram in Fig. 3.55. A magnetic torque motor activates the transducer. The armature of the torque motor, which acts as a flapper, extends into the airgaps of magnetic flux provided by a permanent magnet. The signal current is passed through four coils, wired as shown, and causes a rotary torque on the armature (flapper arm). The torque is proportional to the signal current and causes a change in the flapper/nozzle gap.

Assume that an increase in signal current develops a torque that moves the flapper downwards at the nozzle end. The resulting restriction produces an increased pressure in the nozzle and in the upper chamber of the pneumatic relay. The relay responds to the increase in pressure by closing the exhaust port and opening the supply port, thereby increasing the output pressure to the control valve.

When a decreasing signal current is received, the armature rotates to uncover the nozzle, resulting in a decrease in the pressure in the nozzle and the relay. The relay diaphragm moves upward and the exhaust port opens to bleed the output pressure to atmosphere, thereby reducing the pressure applied to the control valve.

Figure 3.55 shows that the electropneumatic transducer is also itself a complete feedback system; thus it must be properly designed for stability and accuracy. If we are users (rather than designers) of such a device, we are concerned only with its overall dynamics from input current i to output pressure p. The dynamics relating p to i is generally quite fast compared to other time-constants in the process control loop; so we model the electropneumatic transducer as a zero-order system with p proportional to i.

[7]Electromechanical actuation of a control valve having rotating stem is another popular choice. A dc motor is configured as the position control actuator. The shaft of the motor is coupled to the rotating stem of the valve through gearing. The motor and the reduction gears provide an incremental control of fluid flow.

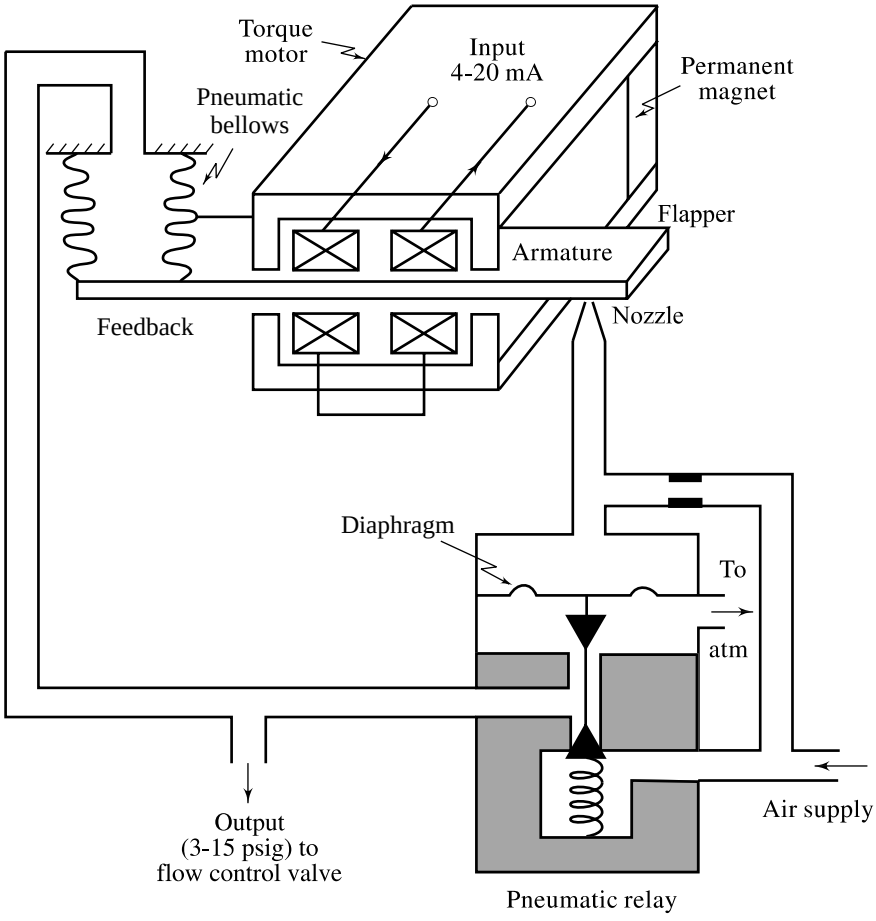

Fig. 3.55 Current to pressure converter

3.9.3 A Temperature Control System

The stirred tank in Fig. 3.56 is used to heat a process stream so that its pre-mixed components achieve a uniform composition. Temperature control is important because a high temperature tends to decompose the product while a low temperature results in incomplete mixing. The tank is heated by the steam condensing inside a coil. The temperature in the tank is controlled by manipulating the steam valve position.

The control hardware required to control the temperature of a process stream leaving a continuously stirred tank reactor (CSTR) is shown in Fig. 3.56. This hardware, available from manufacturers of process-control equipment, consists of the components listed below along with their respective conversions:

- sensor (temperature to current);
- transducer (current to pressure);
- controller (current to current);
- control valve (pressure to flow rate).

A thermocouple is used to measure the temperature; the signal from the thermocouple is sent to the signal-conditioning circuit, which produces an output in the range of 4–20 mA (the industrial standard current range), which is a linear function of the input. The output of the sensor is compared with the set-point to produce an error signal. The controller converts the error to an output in the range of 4 – 20 mA according to the control law. The only control law we have considered so far has been proportional. In the next chapter,

other control laws will be described. The output of the controller enters the electropneumatic transducer, which produces an output in the range of 3 – 15 psig (the industrial standard pressure range), which is a linear function of the input. Finally, the output of the electropneumatic transducer is sent to the top of the pneumatic control valve, which adjusts the flow of the steam to the coil in the stirred tank. We will assume that the valve is linear.

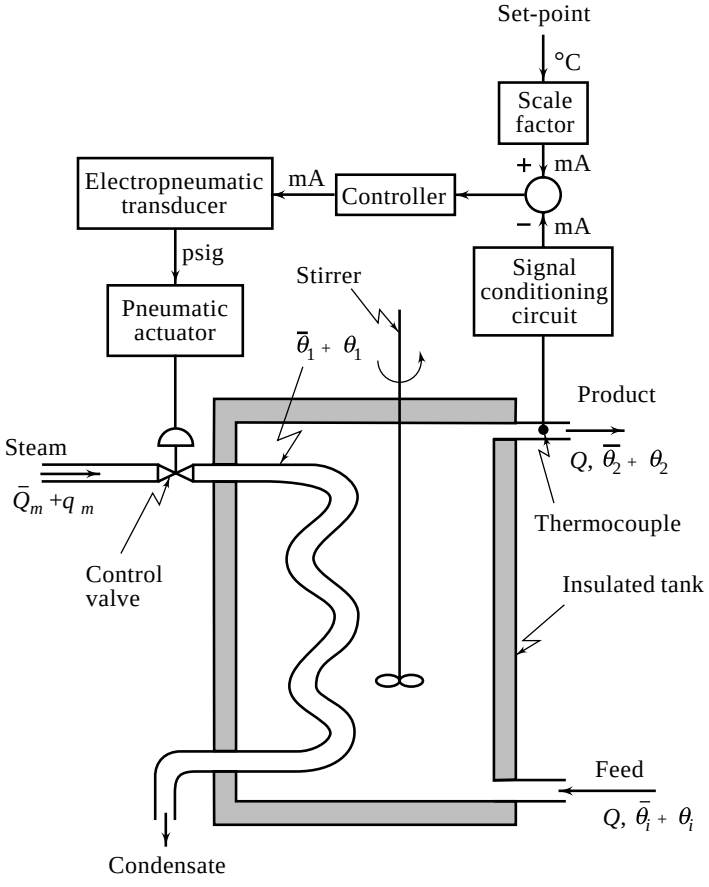

Fig. 3.56 Temperature control of a continuously stirred tank reactor

Simplifying assumptions:

1. The liquid inflow and outflow rates for the tank are equal so that the liquid level in the tank is maintained constant during the operation.
2. The liquid in the tank is well-stirred so that its state can be described by the temperature of the outflowing liquid.
3. The tank is well-insulated so that the heat loss through its walls is negligible. Also, the heat storage capacity of the tank walls is negligible.

We consider here a CSTR where the process feed has a density ρ of 1090 kg/m^3 and a heat capacity c of 3350 Joules/kg-°C. The volume V of the liquid in the reactor is maintained constant at 3.4 m^3 by a constant feed rate Q of 0.425 m^3/min. Thermal capacitance C_1 of the coil mass is 503×10^3 Joules/°C. The heat transfer area A is 22.57 m^2 and the heat transfer coefficient U is 42.97×10^3 Joules/min-m^2-°C. The steam is saturated; it can be assumed that its latent heat of condensation λ is constant at 2247×10^3 Joules/kg.

At steady state, the temperature of the feed $\bar{\theta}_i$ is 55 °C. Assume that the design requirement is to maintain the tank liquid at a temperature $\bar{\theta}_2$ of 80 °C. Possible perturbations from the steady state are caused by the desired change θ_r in the temperature of the tank liquid, and the change θ_i in the feed temperature (a disturbance). These perturbation signals give rise to perturbations θ_1 and θ_2 in the temperatures of the coil mass and the tank liquid, respectively, from their steady-state values $\bar{\theta}_1$ and $\bar{\theta}_2$.

The heat balance for the coil mass:

$$C_1 \frac{d}{dt}(\bar{\theta}_1 + \theta_1) = (\bar{Q}_m + q_m)\lambda - UA\,[\bar{\theta}_1 + \theta_1 - (\bar{\theta}_2 + \theta_2)] \tag{3.49}$$

where

$\bar{Q}_m$ = steam flow rate (kg/min) at steady state, and
q_m = manipulation of the steam flow rate.

The heat balance for the tank liquid:

$$V\rho c \frac{d}{dt}(\bar{\theta}_2 + \theta_2) = Q\rho c\,[\bar{\theta}_i + \theta_i] + UA\,[\bar{\theta}_1 + \theta_1 - (\bar{\theta}_2 + \theta_2)] - Q\rho c\,[\bar{\theta}_2 + \theta_2] \tag{3.50}$$

The process steady state is described by the following equations:

$$\bar{Q}_m\,\lambda - UA(\bar{\theta}_1 - \bar{\theta}_2) = 0$$

$$Q\rho c\,\bar{\theta}_i + UA(\bar{\theta}_1 - \bar{\theta}_2) - Q\rho c\,\bar{\theta}_2 = 0$$

This gives

$$Q\,\rho\,c(\bar{\theta}_i - \bar{\theta}_2) + \bar{Q}_m\,\lambda = 0$$

Since $\bar{\theta}_i = 55$ °C and $\bar{\theta}_2 = 80$ °C, the steady-state mass flow rate of steam through the coil is

$$\bar{Q}_m = \frac{0.425 \times 1090 \times 3350 \times (80 - 55)}{2247 \times 10^3} = 17.27 \text{ kg/min}$$

At steady state, the error signal in the control configuration of Fig. 3.56 is zero. The necessary steam flow rate $\bar{Q}_m$ can be achieved with the zero error signal because the electropneumatic transducer has a zero adjustment which allows pressure to be at the middle (9 psig) of its 3–15 psig range when the input to the transducer is zero, and the valve actuator has a zero adjustment which allows the valve opening to be put anywhere desired with its input pressure at 9 psig.

Let us now derive the process model that describes perturbation dynamics about the steady state.

From Eqns (3.49) and (3.50), we obtain

$$C_1 \frac{d\theta_1}{dt} = q_m \lambda - UA(\theta_1 - \theta_2)$$

$$V\rho c \frac{d\theta_2}{dt} = Q\rho c(\theta_i - \theta_2) + UA(\theta_1 - \theta_2)$$

By Laplace transformation and manipulation of these equations, we obtain

$$(\tau_1 s + 1)\,\theta_1(s) = \theta_2(s) + K_1 Q_m(s)$$

$$(\tau_2 s + 1)\,\theta_2(s) = K_2\theta_1(s) + K_3\theta_i(s)$$

where

$$\tau_1 = \frac{C_1}{UA}; \tau_2 = \frac{V\rho c}{UA + Q\rho c}: K_1 = \frac{\lambda}{UA};$$

$$K_2 = \frac{UA}{UA + Q\rho c}; K_3 = \frac{Q\rho c}{UA + Q\rho c}$$

Block-diagram representation of these equations is shown in Fig. 3.57a.

Substituting the numerical values of various parameters, we obtain

$\tau_1 = 0.52$ min, $\tau_2 = 4.92$ min, $K_1 = 2.32$ °C/kg-min

$K_2 = 0.385$ °C/ °C, $K_3 = 0.615$ °C/ °C

Manipulation of the block diagram of Fig. 3.57a, with the above numerical values for various parameters, gives

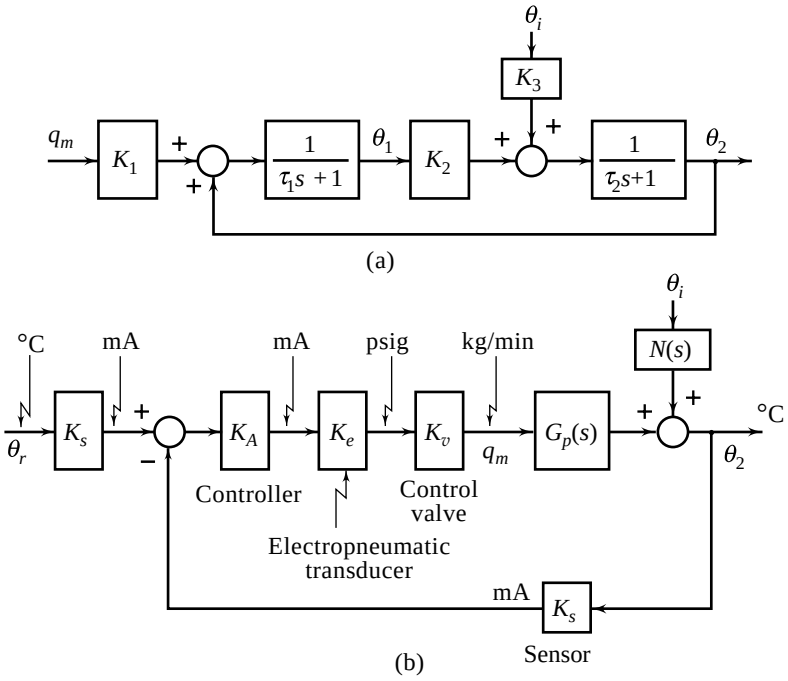

Fig. 3.57 Block diagrams for the system of Fig. 3.56

$$\theta_2(s) = G_p(s)\, Q_m(s) + N(s)\theta_i(s)$$

where

$$G_p(s) = \frac{0.35}{s^2 + 2.13s + 0.24}; N(s) = \frac{0.24(0.52s + 1)}{s^2 + 2.13s + 0.24}$$

The dynamics of the other components of the feedback system—the temperature sensor, the controller (amplifier), the electropneumatic transducer and the pneumatic control valve—are negligible, relative to the process time-constants. All these components are fast enough to be treated as zero-order systems. Figure 3.57b shows a block-diagram representation of the temperature control loop.

3.9.4 A Liquid-Level Control System

There are two basic purposes for liquid-level control. The first is to hold level as closely as possible to its optimum operating point. An example would be the level of water in a boiler drum: if too high, some water

would be carried over with the steam; if too low, evaporating tubes may be overheated. Its second purpose is to close material or energy balance, so that inflow and outflow are equal in steady state. In many of these situations, the actual level in the vessel may have no particular significance. An example is the reactor in Fig. 3.56, which is designed to operate under conditions of constant feed rate and withdrawal of product. Examples of liquid-level control in distillation column were earlier in Chapter 1 (Figs 1.20 – 1.21).

Figure 3.58 show a tank containing liquid. We are interested in regulating the level of the liquid in the tank. The flow of liquid into the tank is controlled by an electropneumatic valve. The measurement of the head of the liquid in the tank is done by employing a pressure sensor. A diaphragm in the sensor converts pressure information into a physical displacement which is further converted into proportional electrical signal by signal conditioning circuits. Integrated circuit manufactures have developed composite pressure sensors employing a semiconductor diaphragm onto which a semiconductor strain gauge has been grown. Appropriate signal conditioning is included in integrated circuit form, providing a dc voltage or current, linearly proportional to the pressure (head), over a specified range.

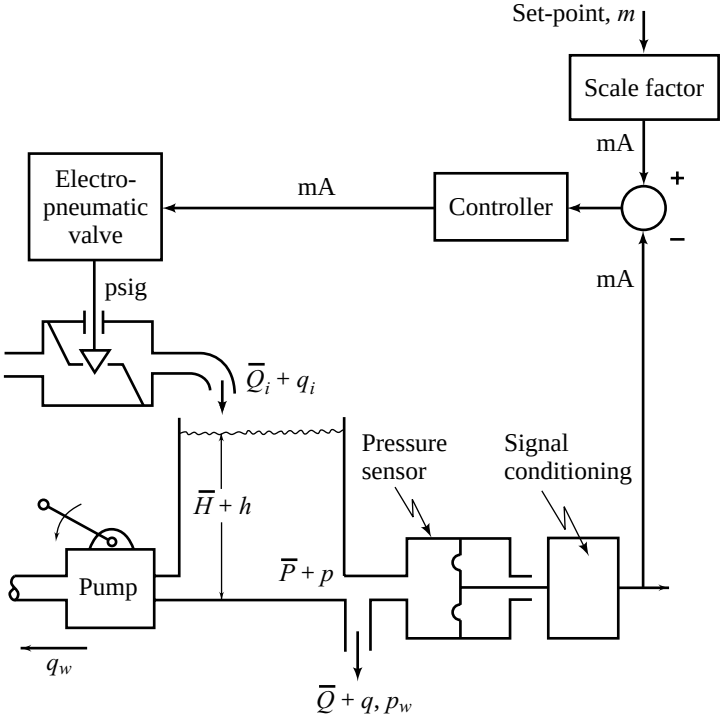

Fig. 3.58 A liquid-level control system

For steady-state equilibrium flow, steady-state inflow rate $\bar{Q}_i$ = steady-state outflow rate $\bar{Q}$, and the liquid height $\bar{H}$ = constant.

Let $q_i(t), q(t)$ and $h(t)$ be the deviations about this equilibrium. The equation governing the change in liquid volume is:

$$\frac{d}{dt}(Ah(t)) = q_i(t) - q(t) \tag{3.51}$$

where A is the constant cross-sectional area of the tank.

The flow through the outlet pipe restriction is governed by the equation (refer Eqns (2.123), (2.127) – (2.128))

$$q(t) = k\rho g\, h(t)$$

$$= \frac{1}{R} h(t) \tag{3.52}$$

where R (m/(m^3/sec)) is a parameter representing flow resistance through outlet pipe.
Eliminating $q(t)$ form Eqns (3.51) and (3.52), we obtain

$$A\frac{dh(t)}{dt} + \frac{1}{R} h(t) = q_i(t)$$

Defining time-constant $\tau = AR$, we get

$$\tau\frac{dh(t)}{dt} + h(t) = Rq_i(t) \tag{3.53}$$

We have the following system parameters:

Radius of the tank = 2 m (Area A = 12.56 m^2)

ρ = 1000 kg/m^3; g = 9.81 m/sec^2

Experimentally obtained exit-pipe restriction parameter

R = 140 m/(m^3/sec)

We can work out the value of τ:

$\tau = 12.56 \times 140 = 1758$ sec = 29.3 min

In developing this model, we have not considered disturbances in the process. Disturbances may enter in the model in the following ways:

1. Liquid may be drawn off from the tank (to be used elsewhere in the processing operation) by a variable displacement pump. q_w (m^3/sec) is the disturbance flow rate.
2. If the tank of Fig. 3.58 is connected to another tank in the processing operation, there will be a variable back pressure $\{p_w(t)\}$ at the orifice outlet ; $h_w = \frac{1}{\rho g} p_w$ is the resulting disturbance in the liquid head.

The volume balance equation now becomes

$$A\frac{dh(t)}{dt} + \frac{1}{R}(h(t) - h_w(t)) = q_i(t) - q_w(t) \tag{3.54}$$

Taking the Laplace transform on both sides of this equation (assuming zero initial conditions), we obtain

$$H(s) = \frac{R}{\tau s + 1} Q_i(s) + \frac{1/\rho g}{\tau s + 1} P_w(s) - \frac{R}{\tau s + 1} Q_w(s) \tag{3.55}$$

where

$$H(s) \triangleq \mathscr{L}[h(t)]; Q_i(s) \triangleq \mathscr{L}[q_i(t)]; P_w(s) \triangleq \mathscr{L}[p_w(t)]; Q_w(s) \triangleq \mathscr{L}[q_w(t)]$$

With the given system parameters, this equation becomes

$$H(s) = \frac{140}{29.3s + 1} Q_i(s) + \frac{1.02 \times 10^{-4}}{29.3s + 1} P_w(s) - \frac{140}{29.3s + 1} Q_w(s) \tag{3.56}$$

The system response to the controlled inflow has a gain of 140 m/(m^3/sec), and a time-constant of 29.3 min. The response to pressure disturbance at the outlet has a gain of 1.02×10^{-4} m/(newton/m^2), and to disturbance flow the gain is 140 m/(m^3/sec).

We take the output signal range of pressure sensor as 4–20 mA (the industrial standard current range). The tank of our liquid-level control system is of 4 m height with a maximum fill level of 3 m.

$$\text{Sensor gain} = \frac{16\text{ mA}}{3\text{ m}} = 5.33\text{ mA/m} \tag{3.57}$$

The time-constant of the sensor is very small compared to process time-constant τ; the gain 5.33 mA/m, thus, is the transfer function of the sensor.

The control valve in our system of Fig. 3.58 has a maximum capacity of 200 m^3/hr. The nominal pressure of the valve is 3 to 15 psig (the industrial standard pressure range).

$$\text{Valve gain} = \frac{0.056(\text{m}^3/\text{sec})}{12(\text{psig})} \times \frac{12(\text{psig})}{16(\text{mA})} = 0.0035\ (\text{m}^3/\text{sec})/\text{mA} \tag{3.58}$$

Again the dynamics of the control valve are much faster than that of the process, and the valve could be treated as a zero-order system.

The block diagram of the liquid-level control loop is shown in Fig. 3.59; h_r is the change in the set-point value from the initial setting.

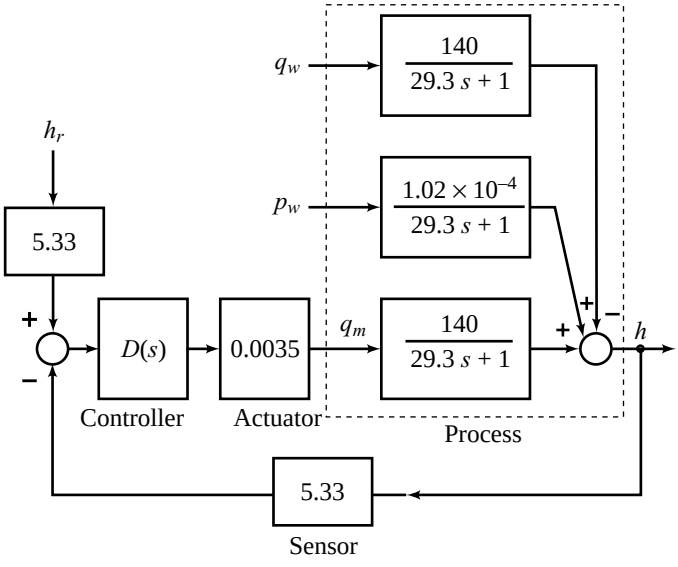

Fig. 3.59 Block diagram for the system of Fig. 3.58

Review Examples

Review Example 3.1 Consider the temperature control system of Fig. 3.60 which is set up to produce a steady process stream at a controlled temperature. The temperature θ (°C) of the outflowing liquid is measured by a thermocouple which produces an output voltage e_t(volts) proportional to θ ($e_t = K_t\,\theta$). This voltage is subtracted from the reference voltage e_r to generate the error signal $e = (e_r - e_t)$, which in turn regulates the heating rate h by means of an SCR amplifier [5]. Basically a solid state

switch, the SCR amplifier controls the heating rate by varying the point in the ac power cycle at which the heater is connected to (or disconnected from) the power line (see Fig. 3.61). As the line frequency (50 Hz) is very high relative to the thermal system frequency response, we take h to mean the *average* power over the cycle, rather than the instantaneous electrical power, and assume that h follows the amplifier input voltage e instantly. The nonlinear steady-state relation (static calibration curve) between e and h can be linearized at any chosen operating point, giving heater gain K_h; $h = K_h e$ watts. Simplifying assumptions:

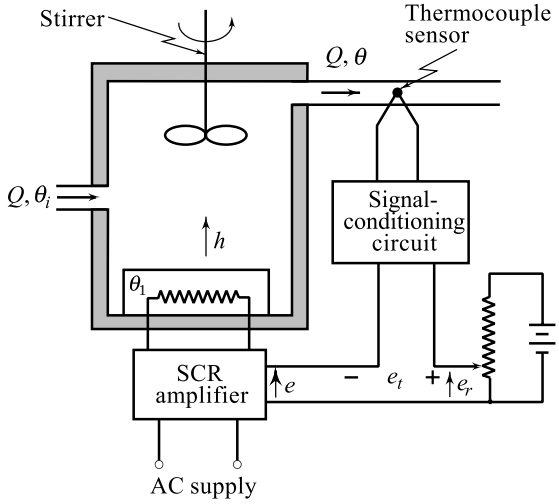

Fig. 3.60 A temperature control system

1. The liquid inflow and outflow rates for the tank are equal (Q m^3/sec) so that the liquid level in the tank is maintained constant (volume V m^3 of the liquid in the tank is therefore constant).
2. The liquid in the tank is well stirred so that its state can be described by the temperature θ of the outflowing liquid.
3. The tank is well insulated so that the heat loss through its walls is negligible. Also the heat storage capacity of the tank walls is negligible.
4. The heat storage capacity of the heater mass is negligible.

Assuming an initial equilibrium point and taking all the variables as perturbations, we obtain the following heat-balance equation.

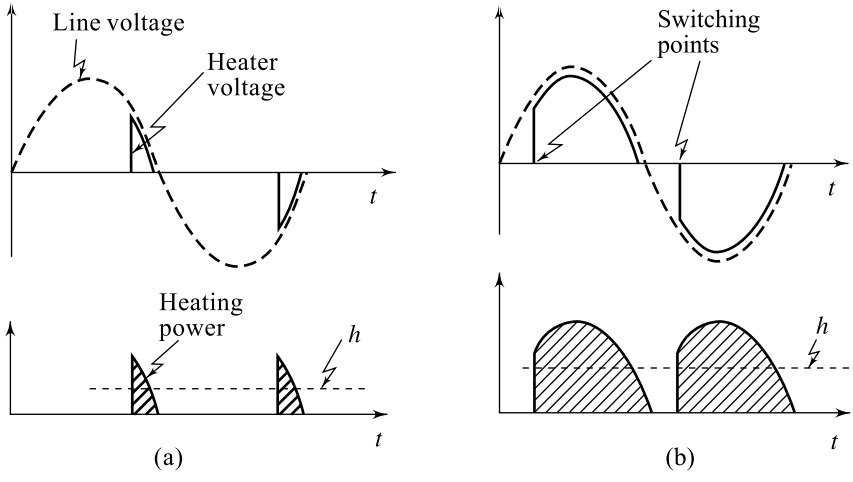

Fig. 3.61 SCR control of heating rate; (a) low heating rate (b) high heating rate

$$V\rho c\frac{d\theta}{dt} = h + Q\rho c\,\theta_i - Q\rho c\,\theta \tag{3.59}$$

where ρ = density of the liquid;
c = specific heat of the liquid; and
θ_i = perturbation in the temperature of the inflowing stream; this will be treated as a disturbance in our model.

Taking the Laplace transform of Eqn. (3.59) and reorganizing, we get

$$(s\tau + 1)\,\theta(s) = \frac{1}{Q\rho c}H(s) + \theta_i(s) \tag{3.60}$$

where $\tau = \dfrac{V}{Q}$ = process time-constant.

Although we generally prefer to measure the controlled variable as directly as possible, the location of the thermocouple (which has an output of a few millivolts) in the tank encounters problems of electrical noise due to high-power SCR switching, and vibrations caused by the tank stirrer. Thus, we locate it in the pipeline downstream of the tank causing a deadtime τ_D between θ and its measurement θ_o:

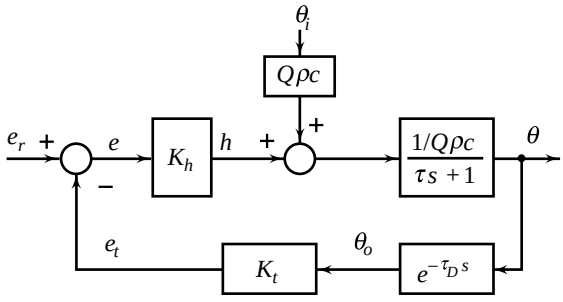

Fig. 3.62 A block diagram for the system of Fig. 3.60

$$\frac{\theta_o(s)}{\theta(s)} = e^{-s\tau_D} \tag{3.61}$$

Using Eqns (3.60) and (3.61), we can draw the block diagram of the system as shown in Fig. 3.62.

Review Example 3.2 In a steel or paper mill, the products are moved by rollers, as shown in Fig. 3.63a. In order to maintain a prescribed uniform tension, the roller speeds are kept constant and equal to each other. This can be achieved by using the control system shown in Fig. 3.63b. Each roller is driven by an armature-controlled dc motor.

The motor speed is measured by the dc tachogenerator coupled to the motor shaft. The tachogenerator output is K_t volts/(rad/sec). This voltage is compared with the reference voltage e_r which represents the desired motor speed. The difference in voltage is amplified by a pre-amplifier of gain K_A, and then power-amplified by a power amplifier.

In the thyristor-driven speed control system of Fig. 3.63b, a linear relationship between the input voltage e_c and output voltage e_a can be obtained when a proper firing control scheme is used [5]. The time-constants associated with the thyristor rectifier are negligibly small. Neglecting the dynamics of the rectifier, we get

$$e_a = K_r e_c \tag{3.62}$$

where K_r is the gain of the rectifier.

The motor is separately excited with a constant field current and has a counter emf of K_b volts/(rad/sec). It produces a torque of K_T newton-m/amp of armature current. It drives a load of moment of inertia J newton-m/(rad/sec^2) and viscous friction with coefficient B newton-m/(rad/sec), against the load-torque disturbance T_w newton-m.

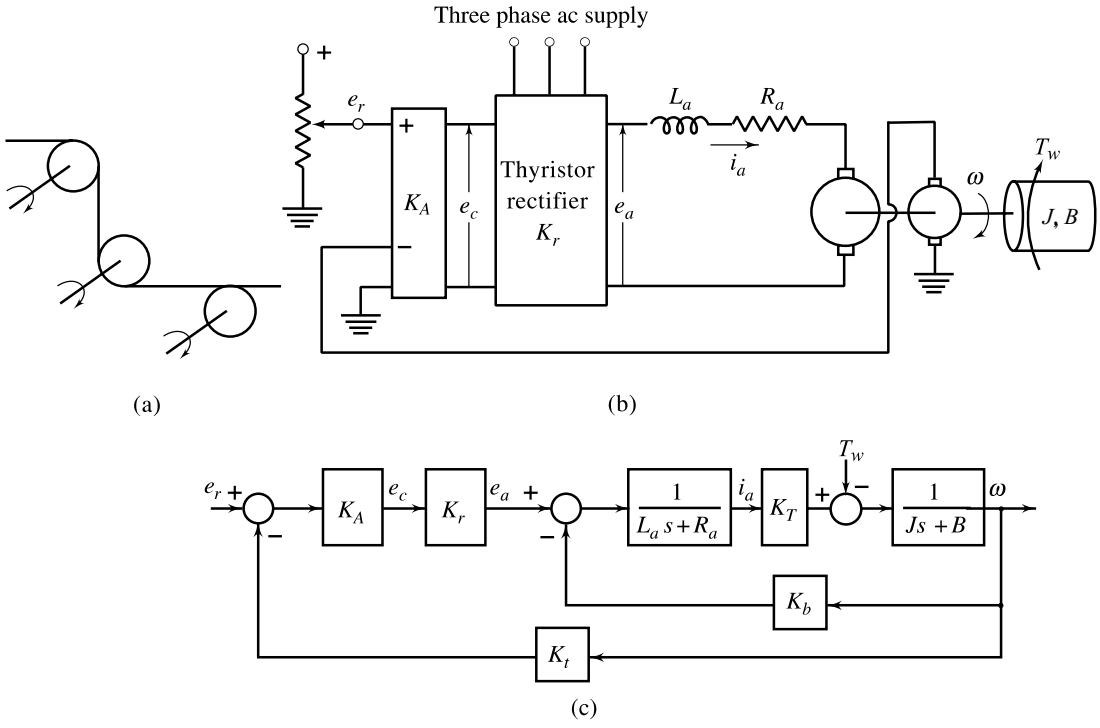

Fig. 3.63 Speed control of rollers

The functional block diagram of the speed control system is shown in Fig. 3.63c.

The thyristorized drives are usually provided with current-limiting features to prevent damage to the thyristors. A current limit can be implemented by constructing a current-control loop as shown in Fig. 3.64. A resistance R is inserted in the armature circuit to generate a voltage proportional to the armature current. An isolating amplifier is used to take care of the loading effect.

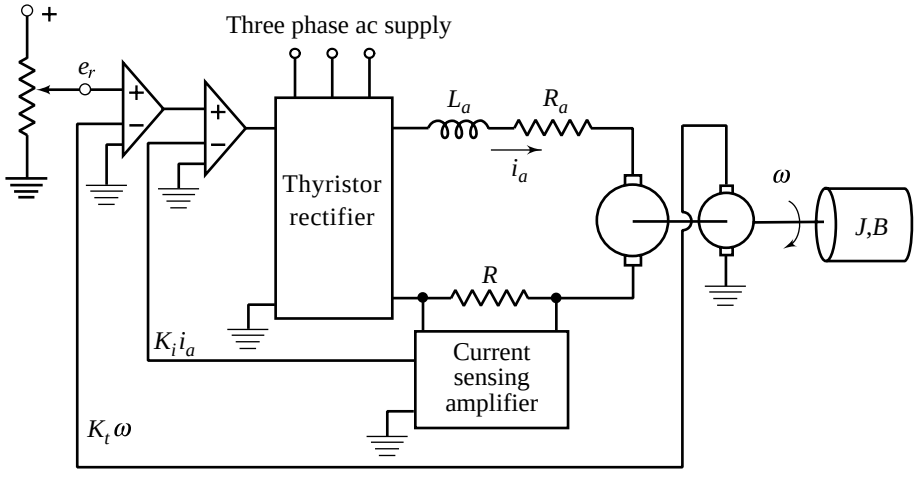

Fig. 3.64 Speed control system with inner current-control loop

Review Questions

3.1 X_{in} is the input-node variable and X_{out} is the output node variable of a signal flow graph with N forward paths. Describe the Mason's gain rule for the determination of the overall gain X_{out}/X_{in} of the signal flow graph.

3.2 Unity-feedback block diagram model can be obtained only for control systems with sensor gain of unity. Do you agree with this statement? Justify your answer.

3.3 (a) Derive an expression for the transfer function of an armature-controlled dc servomotor. State clearly the assumptions made.
(b) How is the torque constant of the motor related to the back emf constant?

3.4 (a) Derive an expression for the transfer function of a field-controlled dc servomotor. State clearly the assumptions made.
(b) List the advantages and disadvantages of the field control compared to the armature control of a dc motor.

3.5 (a) Describe the construction and working of a two-phase motor suitable for use in ac servo systems. Give the torque-speed characteristics of the motor and derive the transfer function model based on the linearized characteristics. Justify the use of linear model. Appropriate symbols for variables and parameters may be used in your derivation.
(b) Compare and contrast the usefulness of ac and dc servomotors in motion control systems.

3.6 Given a two-gear system with angular displacements θ_1 and θ_2, number of teeth N_1 and N_2, and torques T_{12} (exerted on gear 1 by gear 2) and T_{21} (transmitted to gear 2 by gear 1), develop the mathematical relations between these variables and parameters. Clearly state the assumptions made.

3.7 Explain using labelled diagrams, the construction and operation of the following transducers:
(a) AC tachogenerator (b) DC tachogenerator
Describe briefly using suitable block diagrams, an application of each in motion control systems.

3.8 Explain with the aid of a sketch, the construction and operation of a linear variable differential transformer (LVDT). Describe briefly using appropriate diagrams, an application of LVDT in motion control systems.

3.9 (a) Explain with the aid of appropriate diagrams, the construction and operation of
(i) synchro transmitter; and (ii) synchro control transformer
Give a schematic diagram showing how the synchro pair (transmitter and control transformer) would be embodied in an ac position control system.

3.10 (a) A feedback control system is controlling the position of a single-link robot manipulator on a manufacturing floor. It comprises of a sensor, a proportional controller, and an actuator.
(i) Suggest suitable devices and describe their characteristics.
(ii) Interconnect the devices to build a feedback control system and describe the processing of signals in the loop. Given units of signals involved in the loop.
(b) Modify this feedback control system to include techogenerator damping.

3.11 Draw an electromechanical schematic diagram of a dc position control servosystem incorporating tachogenerator damping. Describe the operation of the main components used, explaining clearly how the error signal is formed.

3.12 Armature control of a dc motor is used in a closed-loop speed control system. Draw a schematic layout for the system. Describe the operation of main components used, explaining clearly how the error signal is formed.

3.13 Using appropriate diagrams, give the constructional and operational features of a hydraulic linear actuator. Derive the transfer function model of the actuator. Use appropriate symbols for variables and parameters. Clearly state the assumptions made.

3.14 Draw a schematic diagram of position control system for controlling the linear displacement of a load mass. Use potentiometers for formation of error and hydraulic linear actuator for moving the mass. Give a brief description of the equipment used in the system.

3.15 Pneumatic devices are widely used in process control systems. In a thermal system, the following hardware has been used to control the temperature of the process stream leaving a CSTR (Continuously Stirred Tank Reactor):
Sensor (temperature to current); Controller (current to current); Transducer (current to pressure); and Control valve (pressure to flow rate).
Select appropriate control hardware and draw a schematic diagram describing the complete temperature control system. Explain the constructional and operational features of the selected hardware.

3.16 Pneumatic devices are widely used in process control systems. A system uses the following hardware to regulate the level of liquid in a tank:
Sensor (pressure (liquid head) to current); Controller (current to current); Transducer (current to pressure); and Control valve (pressure to flow rate).
Select appropriate control hardware and draw a schematic diagram describing the complete liquid-level control system. Explain the constructional and operational features of the selected hardware.

Problems

3.1 A linear feedback control system has the block diagram shown in Fig. P3.1. Using block diagram reduction rules, obtain the closed-loop transfer function $Y(s)/R(s)$.

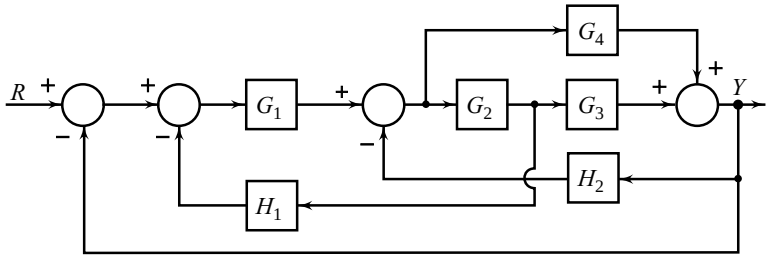

Fig. P3.1

3.2 Using block diagram reduction rules, convert the block diagram of Fig. P3.2 to a simple loop.

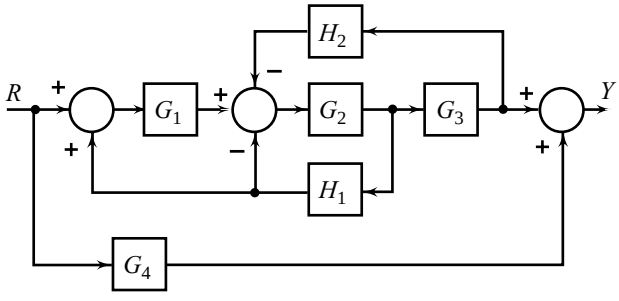

Fig. P3.2

3.3 Convert the block diagram of Fig. P3.3 to a signal flow graph, and therefrom obtain the input–output transfer function using Mason's gain rule.

3.4 The block diagram of a feedback control system is shown in Fig. P3.4. The output

$$Y(s) = M(s)R(s) + M_w(s)W(s)$$

Find the transfer functions $M(s)$ and $M_w(s)$.

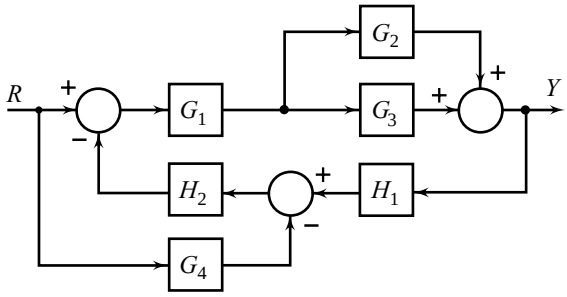

Fig. P3.3

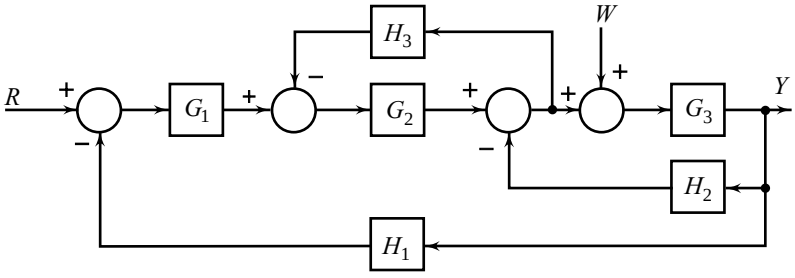

Fig. P3.4

3.5 (a) Consider the block diagram of a position control system shown in Fig. 3.34b. Obtain the closed-loop transfer functions $\theta_L(s)/\theta_R(s)$ of the system by block diagram manipulation. Also manipulate the block diagram to obtain $\theta_L(s)/nT_w(s)$.

(b) Consider the block diagram of a temperature control system shown in Fig. 3.57b. Obtain the transfer functions $\theta_2(s)/\theta_r(s)$, and $\theta_2(s)/\theta_i(s)$ by block diagram manipulation.

(c) Convert the block diagrams of Figs 3.34b and 3.57b to signal flow graphs and apply Mason's gain rule to obtain the transfer fucntions required in parts (a) and (b) above.

3.6 In the speed control system shown in Fig. P3.6, the generator field time-constant is negligible. It is driven at constant speed giving a generated voltage of K_g volts/field amp. The separately excited motor has a back emf of K_b volts/(rad/sec). It produces a torque of K_T N-m/amp. The motor and its load have a combined moment of inertia J kg-m^2 and negligible friction. The tachogenerator gives K_t volts/(rad/sec) and the amplifier gain is K_A amps/volt.

Draw a block diagram of the system and determine therefrom the transfer function $\omega(s)/E_r(s)$, where ω is the load speed and e_r is the reference signal which corresponds to the desired speed.

With the system initially at rest, $e_r = 100$ volts is suddenly applied. Determine how the load speed will change with time.

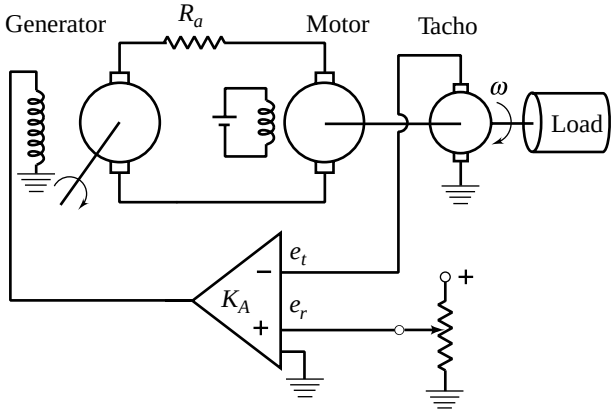

Fig. P3.6

Given: $K_A = 4$ amps/volt; $K_T = 1.5$ N-m/amp;
$K_g = 50$ volts/amp; $K_t = 0.2$ volts/(rad/sec); $R_a = 1\Omega$; $J = 6$ kg-m^2

MATLAB Exercise Use MATLAB's Simulink to obtain the step response under the following conditions.

(i) The system is linear and is driven by the generator whose gain is K_g, and field time-constant is negligible.

(ii) Taking the field time-constant to be half of the motor and load time-constant, determine its effect on the system's output)

3.7 Consider the positional servomechanism shown in Fig. P3.7. Assume that the input to the system is reference shaft position θ_R and the system output is the load shaft position θ_L. Draw a block diagram of the system indicating the transfer function of each block. Simplify the block diagram to obtain $\theta_L(s)/\theta_R(s)$. The parameters of the system are given below.

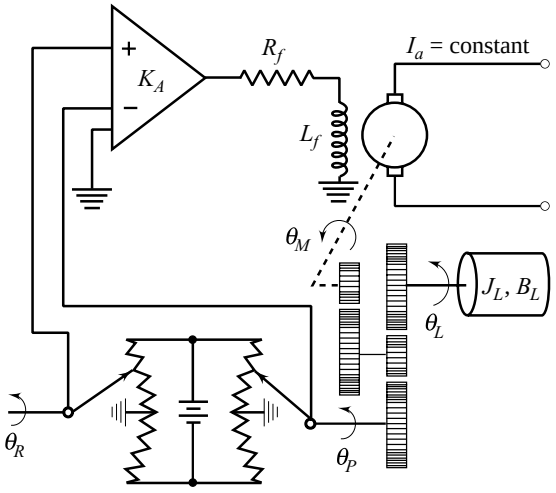

Fig. P3.7

Sensitivity of error detector	$K_P = 10$ volts/rad
Amplifier gain	$K_A = 50$ volts/volt
Motor field resistance	$R_f = 100$ ohms
Motor field inductance	$L_f = 20$ henrys
Motor torque constant	$K_T = 10$ Newton-m/amp
Moment of inertia of load	$J_L = 250$ kg-m^2
Coefficient of viscous friction of load	$B_L = 2500$ Newton-m/(rad/sec)
Motor to load gear ratio	$\dot{\theta}_L / \dot{\theta}_M = 1/50$
Load to potentiometer gear ratio	$\dot{\theta}_P / \dot{\theta}_L = 1$

Motor inertia and friction are negligible.

3.8 Consider the system shown in Fig. P3.8a. The characteristic of ac motor is shown in Fig. P3.8b. The moment of inertia of the motor is $J_M = 0.003$ N-m/(rad/sec^2). The motor drives a load through a gear train. N_1, N_2, N_3, and N_4 are the number of teeth with $N_1/N_2 = 1/2$ and $N_3/N_4 = 1/5$. The moment of inertia of the load is $J_L = 0.02$ N-m/(rad/sec^2), and coefficient of viscous friction of the load is $B_L = 0.001$ N-m/(rad/sec). Find the transfer function $\theta_L(s)/E_c(s)$.

3.9 Consider the system shown in Fig. P3.9 with $R_a = 10\ \Omega$, $L_a = 0.1$H, $K_b = 1$ volt/(rad/sec), $\dot{\theta}_L / \dot{\theta}_M = 1/2$, $K_t = 0.8$ volt/(rad/sec), $K_P = 1.5$ volt/rad.
Moment of inertia of load, $J_L = 2$ N-m/(rad/sec^2).
Moment of inertia of motor shaft, $J_M = 0.1$ N-m/(rad/sec^2).
Coefficient of viscous friction of load, $B_L = 0.02$ N-m/(rad/sec).
Coefficient of viscous friction on motor shaft, $B_M = 0.01$ N-m/(rad/sec)

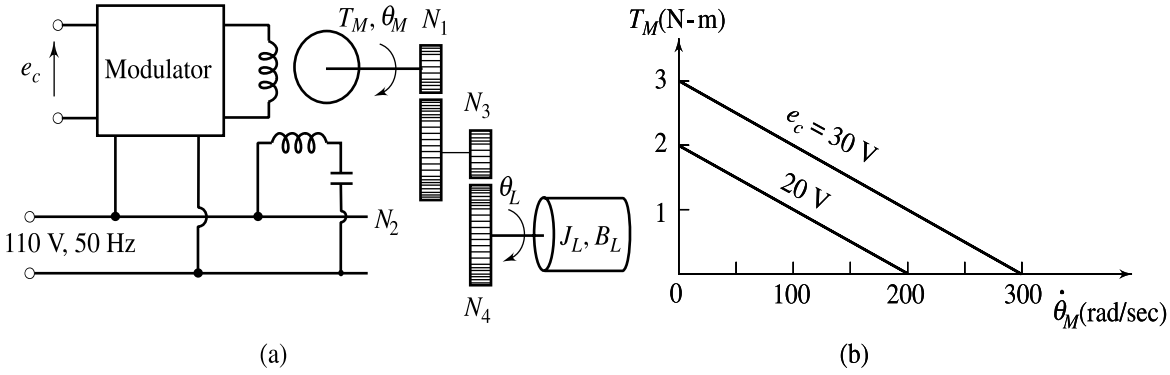

Fig. P3.8

(i) Find the transfer function $\theta_M(s)/E_a(s)$

(ii) A multi-loop (consisting of a speed-feedback loop and a position-feedback loop) feedback control system built around the system of Fig. P3.9 with suitable additional hardware drives the load to the commanded position θ_R inspite of load torque disturbances.
Make a sketch of the feedback control system showing how the hardware is connected.

(iii) What will be the effect of opening the position feedback loop on the performance of the control system?

(iv) What will be the effect of opening the speed feedback loop on the performance of the control system?

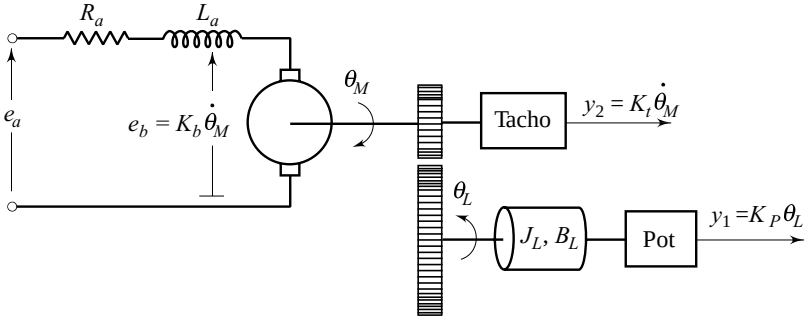

Fig. P3.9

3.10 The schematic diagram of a servo system is shown in Fig. P3.10. The two-phase servomotor develops a torque in accordance with the equation

$$T_M = K_1 e_c - K_2 \dot{\theta}_M$$

where

$$K_1 = 1 \times 10^{-5} \text{ N-m/volt}; \; K_2 = 0.25 \times 10^{-5} \text{ N-m/(rad/sec)}$$

The other parameters of the system are:

Synchro sensitivity	$K_s = 1$ volt/rad
Amplifier gain	$K_A = 20$ volt/volt
Tachogenerator constant	$K_t = 0.2$ volt/(rad/sec)
Load inertia	$J_L = 1.5 \times 10^{-5}$ kg-m^2

Viscous friction $B_L = 1 \times 10^{-5}$ N-m/(rad/sec)

$\dot{\theta}_M / \dot{\theta}_S = 1;\ \dot{\theta}_M / \dot{\theta}_T = 1$

Motor inertia and friction are negligible.

Draw the block diagram of the system and therefrom obtain the transfer function $\theta_M(s)/\theta_R(s)$.

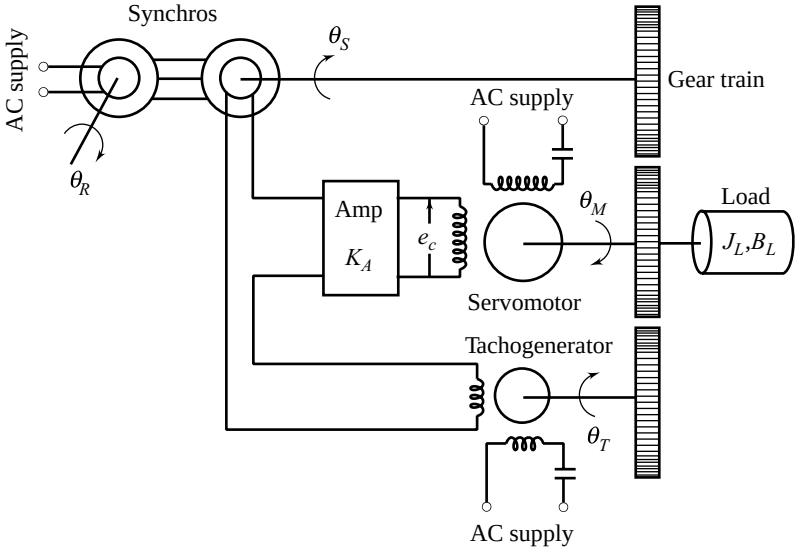

Fig. P3.10

3.11 Figure P3.11 shows a closed-loop drive system. The desired speed is ω_r and the corresponding reference voltage is e_r. The parameters describing the system are given below:

$R_a = 6\ \Omega$,	$L_a = 46$ mH
$J = 0.093$ kg-m^2,	$B = 0.008$ N-m/(rad/sec)
Motor torque constant	$K_T = 0.55$ N-m/amp
Thyristor rectifier gain constant	$K_r = 25$
Amplifier gain	$K_A = 20$
Tachogenerator sensitivity	$K_t = 0.057$ volt/(rad/sec)

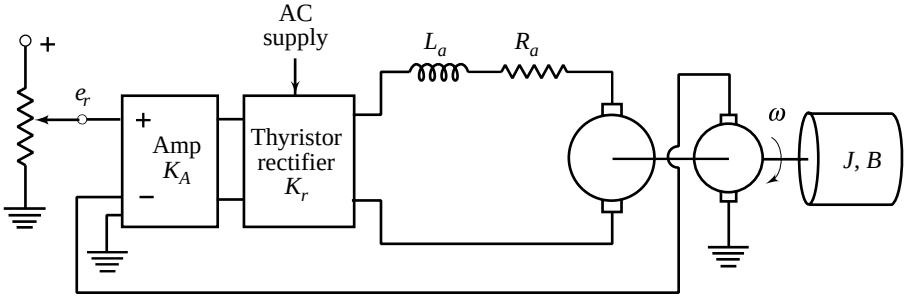

Fig. P3.11

(a) Draw a block diagram of the system that includes transfer functions of all the sub-systems, and therefrom obtain $\omega(s)/E_r(s)$.

(b) The thyristorized drives are usually provided with a current-limiting feature to prevent damage to the thyristors. Modify the drive system of Fig. P3.11 to implement the current limit. Draw a block diagram of the proposed system.

3.12 A dc position control servomechanism comprises of a field-controlled dc servomotor with constant armature current, potentiometer error detector with sensitivity K_P volts/rad, and a dc amplifier of gain K_A amps/volt. The motor produces a torque of K_T N-m/amp. Separate motor and load inertias J_M (kg-m^2) and J_L (kg-m^2) are identified, and the connecting structure is modelled by a shaft with spring constant K (N-m/rad) and damping coefficient B (N-m per (rad/sec)). A load disturbance T_w (N-m) acts on J_L opposite the developed motor torque T_M (N-m). T_M accelerates J_M and supplies the torque transmitted by the shaft. This shaft torque, in turn, accelerates J_L and supplies T_w.

Motor field time-constant is assumed to be negligible.

(a) Make a sketch of the system showing how the hardware is connected.

(b) Determine the transfer functions $\theta_L(s)/\theta_R(s)$ and $\theta_L(s)/T_w(s)$, where θ_L (rad) and θ_R (rad) are, respectively, the actual and commanded load positions.

3.13 The electrohydraulic position control system shown in Fig. P3.13 positions a mass M with negligible friction. Assume that rate of oil flow in the power cylinder is $q = K_1x - K_2\Delta p$ where x is the displacement of the spool and Δp is the differential pressure across the power piston. Draw a block diagram of the system and obtain therefrom the transfer function $Y(s)/R(s)$.

The system constants are given below.

Mass $M = 1000$ kg

Constants of the hydraulic actuator:

$K_1 = 200$ cm^2/sec per cm of spool displacement

$K_2 = 0.5$ cm^2/sec per gm-wt/cm^2

Potentiometer sensitivity	$K_P =$ 1 volt/cm
Power amplifier gain	$K_A =$ 500 mA/volt
Linear transducer constant	$K =$ 0.1 cm/mA
Piston area	$A =$ 100 cm^2

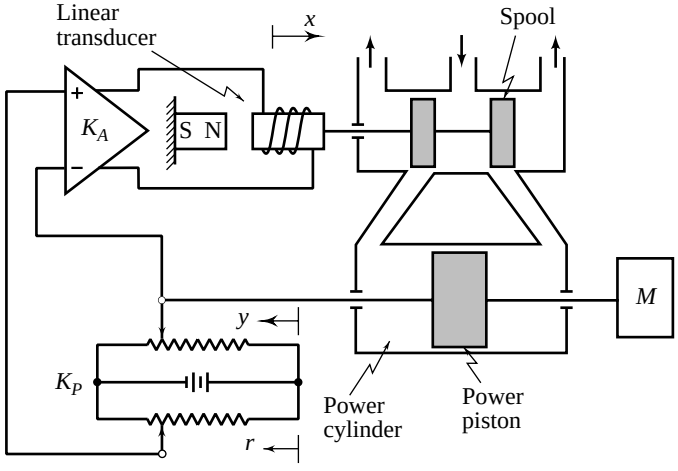

Fig. P3.13

3.14 The schematic diagram of a steel-rolling process is shown in Fig. P3.14. The steel plate is fed through rollers at a constant speed of v cm/sec. The distance between the rollers and the point where the thickness is measured is d cm. The thickness gauge provides a feedback voltage $e_o(t)$ proportional to the actual thickness $y(t)$ of the plate ($e_o(t) = K_s\, y(t)$; K_s is a constant). A voltage e_r corresponding to the desired thickness is the reference input to the system. The error $(e_r - e_o)$ is amplified by an amplifier of gain K_A amps/volt. The servo valve regulates the spool displacement and hence controls port opening x; $x = K_v i$, where K_v is the valve gain. The rate of oil flow in the power cylinder is $q = K_1 x - K_2 \Delta p$ where Δp is the differential pressure across the piston of area A, and K_1 and K_2 are constants.

The load on the piston is that of the roller mass M and viscous friction with coefficient B. Normal force F_w on the roller is a load disturbance.

Assuming all the variables to be deviations from an equilibrium position, draw a functional block diagram that describes perturbation dynamics of the system. Derive the transfer function $Y(s)/E_r(s)$.

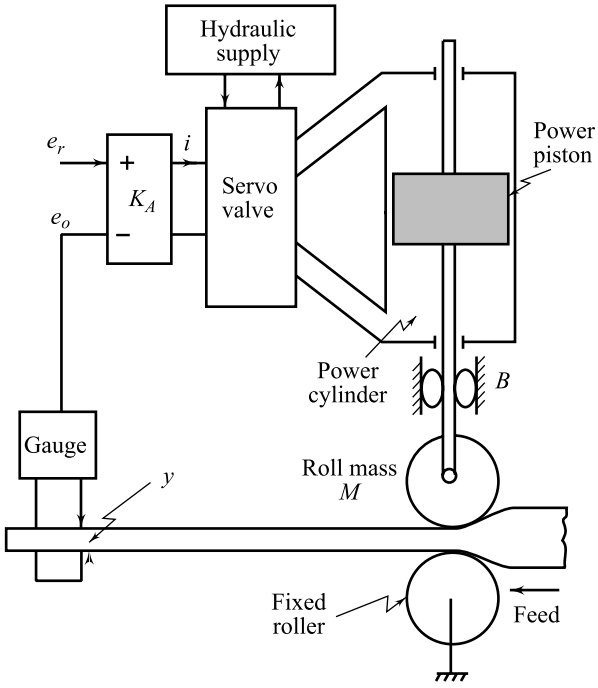

Fig. P3.14

3.15 Consider the two-tank system shown in Fig. P3.15. The height h_2 in the second tank is to be controlled by adjusting the flow rate q_1 into the first tank. The system disturbance is the flow rate q_w drawn off from the first tank (to be used elsewhere in the processing operation) by a variable displacement pump.

The command signal h_r for the desired height in tank 2 is set on a pot whose output is $e_r = K_s h_r$. The sensor output is $e_o = K_s h_2$. The differential amplifier has a gain K_a, the electropneumatic transducer has a gain K_e,

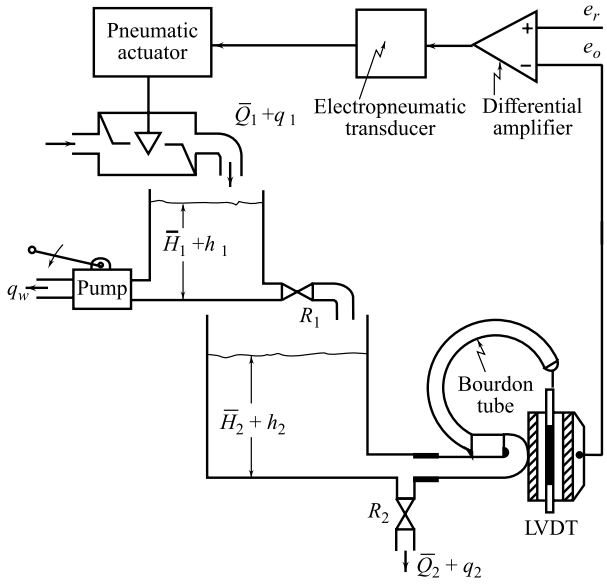

Fig. P3.15

and the pneumatic control valve (pneumatic actuator + flow control valve) has a gain K_v. At the initial equilibrium point, the inflow rate exactly matches the outflow rates, and the heights in the two tanks are $\bar{H}_1$ and $\bar{H}_2$ with $h_2 = h_r = 0$. A_1 is the surface area of tank 1, and R_1 is the resistance to flow offered by the valve in the outflow path (R = incremental change in pressure across the valve/incremental change in flow through the valve). A_2 and R_2 are the corresponding values for tank 2.

Draw a functional block diagram of the system and therefrom derive the transfer function between h_2 and h_r.

3.16 A system to control the temperature of an oven chamber is shown in Fig. P3.16. The temperature θ is sensed by a thermocouple whose output is $K_t\,\theta_2$. The desired temperature is θ_r and the corresponding reference voltage is e_r. The differential amplifier generates a signal e_A which controls the electrical resistance heater through an SCR amplifier and gives rise to heat flow at the rate $h = K_h\,e_A$ to the oven chamber. Heat also flows out of the oven due to imperfect insulation of its walls. The temperature of the ambient air is θ_a. Thermal capacitance of the medium inside the chamber is C_t and thermal resistance of the wall material is R_t. Thermal capacitances of the heater and wall are negligible.

Assuming all the variables are deviations from the equilibrium, obtain a block diagram model of the system that includes the transfer functions of all the sub-systems. Derive the transfer function $\theta(s)/E_r(s)$.

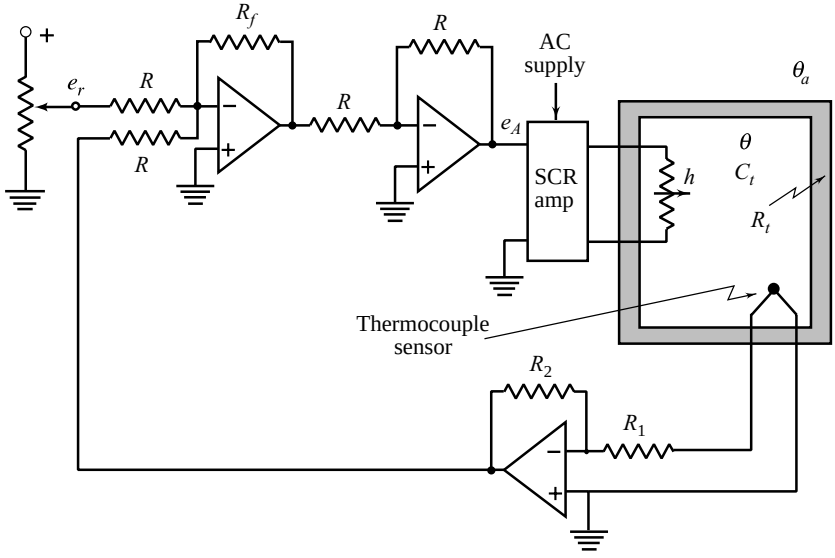

Fig. P3.16

3.17 In a heating system, air flows at constant volumetric flow rate Q into and out of a chamber of volume V. The density of the inflowing air is ρ, specific heat c, and temperature θ_i.

A system to control the outflow temperature is shown in Fig. P3.17. The temperature θ is sensed by a thermistor with a Wheatstone bridge whose output $e_o = K_s\theta$. The desired temperature is θ_r and the corresponding $e_r = K_s\,\theta_r$. The differential amplifier generates a signal e_A which controls electrical resistance heater through an SCR amplifier and gives rise to heat flow at the rate $h = K_h\,e_A$. The heater has temperature θ_1, thermal capacitance C_1, and thermal resistance R_1. The walls of the chamber are perfectly insulated and have negligible thermal capacitance.

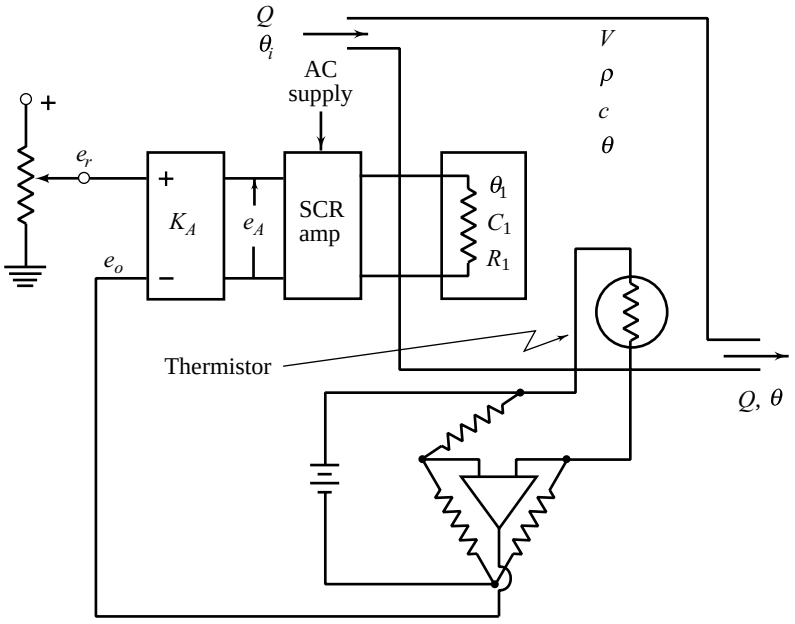

Fig. P3.17

Assume that the variables $\{\theta_r, \theta, \theta_1, \theta_i\}$ are deviations from the equilibrium position. Considering θ_i as the disturbance, draw a functional block diagram of the system that includes the transfer functions of all the sub-systems. Derive the transfer functions $\theta(s)/\theta_r(s)$, and $\theta(s)/\theta_i(s)$.

3.18 **MATLAB/Simulink Exercise** (i) Consider the liquid-level control system shown in Figs 3.58 and 3.59. Create this system in the SIMULINK window, and study its response to step values of command and disturbance signals. (ii) Actuators(valves) and sensors(measurement devices) often have additional dynamic lags that can be simulated by transfer functions. Study the effect of neglecting these dynamic lags in the model of Fig. 3.59. (iii) Manipulated vaiables are often constrained between minimum (0 flow, for example) and maximum (fully open valve) values. A **Saturation** icon from the Simulink library can be used to simulate this behaviour. For the system of Fig. 3.58, study the effect of valve saturation.

3.19 **MATLAB/Simulink Exercise** (i) Consider the temperature control system described in Figs 3.56 and 3.57. Create this system in the SIMULINK window, and study its response to step values of command and disturbance signals. (ii) Often you will want to simulate the behaviour of systems that have deadtime. The **Transport Delay** icon can be selected from the Simulink library. Simulate the system of Fig. 3.56 when it includes transport delay, and study the effect of deadtime on the system output.

4 Basic Principles of Feedback and Characteristics of Proportional-Integral-Derivative Modes of Control

4.1 INTRODUCTION

Although a detailed exploration of the possibilities and problems of feedback control will mostly occupy the rest of this text, some essential characteristics can be illustrated quite easily to give a helpful preview of the forthcoming developments.

Recall the basic feedback system block diagram defined in Chapter 3, and shown in an abridged form as Fig. 4.1. When we speak of a controller $D(s)$, our concern is mainly with the *information handling devices*; the sources of information are the reference input $r(t)$ which is derived from the command $y_r(t)$, and the feedback signal $b(t)$ which is produced by the feedback path elements $H(s)$ from the controlled output $y(t)$. The *power handling devices*—actuators and the controlled process itself—are represented by $G(s)$ in the block diagram of Fig. 4.1. $N(s)$ is the plant transfer function from the disturbance input $w(t)$ to the output $y(t)$.

The controller $D(s)$ is designed to act on the actuating error signal $\hat{e}(t) = r(t) - b(t)$ to produce the control signal $u(t)$. The control logic that is physically implemented for this purpose is the *control law* or *control action*.

A non-zero system error $e(t) = y_r(t) - y(t)$ results from either a change in command or a disturbance. The general function of the controller is to keep the controlled variable near its desired value. Since we never know the numerical values of the parameters of the controlled process with certainty, and some controller designs can be more sensitive to such

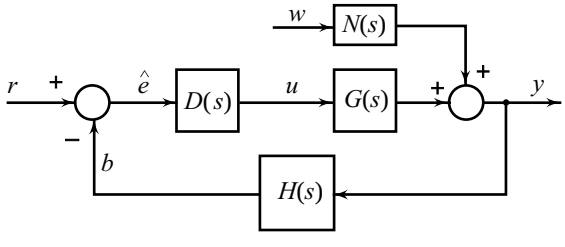

Fig. 4.1 A nonunity feedback system

parameter variations than others, a parameter sensitivity specification might also be included. In this chapter, we will demonstrate that by using feedback control configuration of the form shown in Fig. 4.1, we can meet these control requirements.

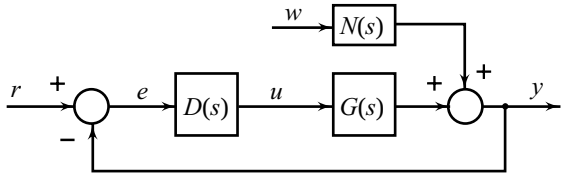

Fig. 4.2 A unity feedback system

A special case of feedback systems which is of particular interest arises when $H(s) = 1$ (Fig. 4.2) and is often referred to as a *unity-feedback system*. The reference input $r(t)$, in this case, is equal to the commanded value of the controlled output. It may be noted that a system's block diagram may not appear to be of unity-feedback form when initially derived. It is often possible and convenient to manipulate the block diagram into a unity-feedback model where the system error appears explicitly as the actuating signal.

An important aspect of feedback control covered in this chapter is the characteristics of PID control logic, which is widely used in industry. We have already introduced this control logic in Section 2.13; the control structure is given by the block diagram of Fig. 2.37, and the Eqns (2.136)–(2.137) give the functional relationships.

For a controller with proportional control mode, the relationship between the control variable $u(t)$ and the error signal $e(t)$ is

$$u(t) = K_c\, e(t) \tag{4.1a}$$

or

$$U(s) = K_c\, E(s) \tag{4.1b}$$

where K_c is the *controller gain*.

Whatever the actual mechanism may be and whatever the form of operating power, the proportional controller is essentially an amplifier with an adjustable gain. A block diagram of such a controller is shown in Fig. 4.3a.

In the integral control mode, also called the *reset control*, the change in the control signal is proportional to the integral of the error:

$$u(t) = K_I \int_0^t e(t)dt \tag{4.2a}$$

or

$$U(s) = \frac{K_I}{s}\, E(s) \tag{4.2b}$$

where K_I is the *integral gain*.

Figure 4.3b shows the block diagram of such a controller.

Integral control can be used by itself or in combination with other control modes; indeed *proportional plus integral* (PI) control is the most common mode. The control action of a PI controller is defined by the following equations:

$$U(s) = K_c\, E(s) + \frac{K_I}{s}\, E(s) = K_c \left(1 + \frac{1}{T_I s}\right) E(s) \tag{4.3a}$$

$$u(t) = K_c \left[e(t) + \frac{1}{T_I} \int_0^t e(t)dt \right] \tag{4.3b}$$

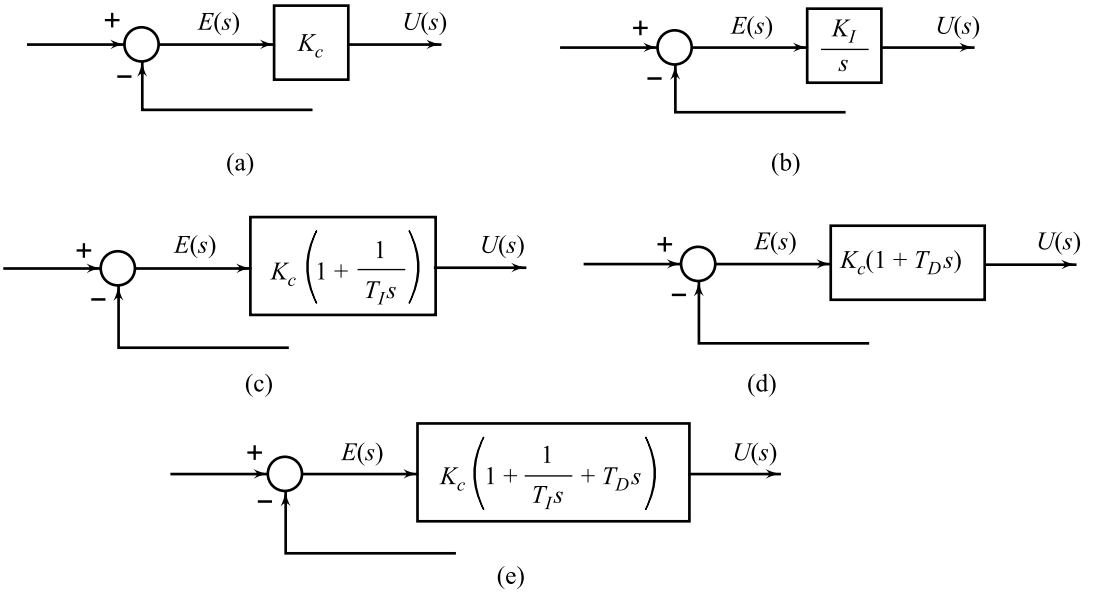

Fig. 4.3 (a) Proportional control (b) Integral control (c) PI control (d) PD control (e) PID control

where T_I is the *integral* or *reset time*.

Figure 4.3c shows the block diagram of a PI controller.

The derivative control mode, also called the *rate control*, is described by the following equations:

$$u(t) = K_D \frac{d}{dt} e(t) \tag{4.4a}$$

or

$$U(s) = K_D s E(s) \tag{4.4b}$$

where K_D is the *derivative gain*.

Derivative control mode is normally not used alone because the control produces no corrective effort for any constant error, and would therefore allow uncontrolled steady-state errors. A combination of proportional and derivative controls is a practical mode of control for industrial processes. The control action of a *proportional plus derivative* (PD) controller is defined by the following equations:

$$U(s) = K_c E(s) + K_D s E(s) = K_c (1 + T_D s) E(s) \tag{4.5a}$$

$$u(t) = K_c \left[e(t) + T_D \frac{de(t)}{dt} \right] \tag{4.5b}$$

where T_D is the *derivative* or *rate time*.

Figure 4.3d shows the block diagram of a PD controller.

A combination of the three basic modes—proportional, integral and derivative—results in a *proportional plus integral plus derivative* (PID) controller described by the following equations:

$$U(s) = K_c \left(1 + \frac{1}{T_I s} + T_D s \right) E(s) \tag{4.6a}$$

$$u(t) = K_c\left[e(t) + \frac{1}{T_I}\int_0^t e(t)dt + T_D\frac{de(t)}{dt}\right] \tag{4.6b}$$

Figure 4.3e shows the block diagram of such a controller.

In the block diagrams of Fig. 4.3, the controller is in the forward path and therefore the control actions are based on the error signal. This, however, is not a restriction. The control actions may be taken on controlled output variable; many a times to advantage , as we shall see in this chapter. The resulting *multiloop* (loop within a loop) *control configuration* is known in the literature as *minor-loop feedback control*.

4.2 THE CONTROL OBJECTIVES

In this section, we describe a control problem in general terms. Given a plant, which cannot be altered by the designer, with the following variables associated with it (Fig. 4.4):

1. A controlled variable $y(t)$, which is the variable we wish to control.
2. A command variable $y_r(t)$, which represents the prescribed value of the controlled variable.
3. An observed variable $b(t)$, which is measured by means of a sensor and which is used to obtain information about the plant during operation; the observed variable is usually contaminated with observation noise $w_n(t)$.
4. A disturbance variable $w(t)$, which influences the plant but which cannot be manipulated.
5. A control variable $u(t)$, which influences the plant and which can be manipulated.

The *control problem* is roughly described below.

For a given command variable, find an appropriate input $u(t)$ so that the controlled variable follows the command variable:

$$y(t) \cong y_r(t);\ t \geq t_0$$

where t_0 is the time at which the control starts.

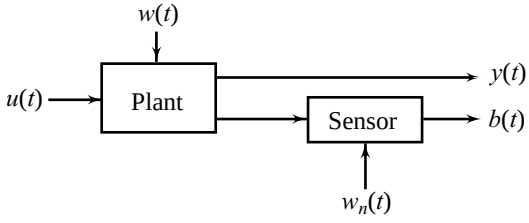

Fig. 4.4 The plant of a control system

An important class of control problems consists of those problems where the command variable is constant over long periods of time; the control objective is to force the controlled variable to reach the commanded value quickly and to maintain the controlled variable at that value thereafter. The duration of the transient period of control, which starts at the beginning of the control process and terminates when the controlled variable approximately reaches its prescribed value, will be referred to as the *settling time*. The lower the settling time, the higher the *speed of response* of the process. The *steady-state accuracy* (negligible error between the controlled output and command input during steady-state period of control) is of critical importance in control systems.

In designing control systems, the following aspects must be taken into account.

1. Stability Roughly speaking, stability in a system implies that small changes in reference inputs, disturbance inputs, and/or initial conditions do not result in large changes in the system output. Stability is a very important property of control systems. Almost every working system is designed to be stable; we seek to improve the speed of response, steady-state accuracy, and other aspects of system performance within the constraints imposed by stability considerations. Analytical study of stability will be taken up in Chapter 5.

Feedback control systems are prone to instability. For a stable plant, the closed-loop system may not be always stable. Feedback control system design may therefore demand a trade off between the accuracy in realizing control objectives and the stability.

2. Input Amplitude Constraints For a control system designed according to linear theory and methods, it is essential that the devices used in the system operate in linear fashion under various operating conditions. If under certain circumstances, the devices are driven into the region of nonlinear characteristics, linear design theory may describe only approximately, or quite often may give a completely erroneous prediction of the system performance. Excessively large magnitudes of signals at various levels in a control system can drive the devices into the nonlinear region of operation. Some examples are: torque-speed curves of motors, synchro error detectors, process control valves, hydraulic servovalves, amplifiers, gears, dampers, etc. The requirement of linear operation of devices under various operating conditions imposes a constraint on the range of values over which the plant input $u(t)$ is allowed to vary. As will be seen, this constraint is of major importance and prevents us from obtaining perfect command-following systems.

3. Disturbance Rejection External disturbances $w(t)$ influence the plant in an unpredictable way. They are typically the uncontrolled variations in the load on a system. In systems controlling mechanical motions, load disturbances may represent forces, e.g., wind gusts on a stabilized antenna, waves on a ship, variations in payload of a robot manipulator, etc. In voltage regulating systems, variations in electrical load is a major source of disturbances. In thermal systems, the load disturbances may be caused by variations in surrounding temperature. In fluid systems, the load disturbances may result from variations in feed flow or variations in demanded flow.

Load disturbances typically vary slowly. As we shall see later in this chapter, the errors due to load disturbances tend to be corrected by proper design of feedback control.

4. Noise Filtering Excitation of the plant by high-frequency measurement-error signals (observation noise) $w_n(t)$, entering through the sensors of the controlled variable, influences the plant in an unpredictable way. In systems controlling mechanical motions, mechanical vibrations may lead to high-frequency components in the output signals of position and speed sensors. Continuous stirring of fluid in tank reactors gives rise to noise in output signals of thermocouple or other temperature sensors.

Feedback control depends virtually on accurate measurement of controlled variables, because the feedback action has little correcting effect for the wrong information given by the sensors. The character of the measurement errors often depends on filtering in the instruments. Effects of measurement errors on control system performance can therefore be reduced by examining the instrument and modifying the filtering so that it satisfies the requirements of the particular control problem.

5. Sensitivity and Robustness Robustness is an important concern in control system design. We will briefly discuss two aspects of the robustness problem.

The first aspect arises because every control system is designed on the basis of a necessarily approximate model of the plant. Since the success of the analytical approach of design is heavily dependent on the simplicity of the mathematical model, many idealizing assumptions are usually made which lead to uncertainties not only in the parameters of the model but also in the model structure. Using a linear model for an intrinsically nonlinear process is an example of deviation in model structure; omitting certain time lags in order to obtain a reduced-order model is another example. The question arises: will the physical system have a performance that is sufficiently close to the performance predicted by the idealized model? For example, if the linear model is stable, will the physical system, which in fact is a small perturbation (possibly nonlinear) from the linear model, still be stable?

The second aspect of the robustness appears in the following manner: the design is based on the (idealized) model which characterizes a number of nominal properties of the plant. Once the controller is implemented and the controlled plant is operating in the field, the properties of the physical system differ from the nominal properties because of environment effects, wear, aging, and other natural factors. So the question is: what is the effect of all such time dependent deviations from nominal values on the performance of the

physical system in the field? Such questions can be studied by calculating the effect on the system performance due to changes in design parameters and exogenous disturbances. It is a fact that some designs, which perform nominally perfectly, are totally inadequate in the field because they are too sensitive to small perturbations in some of their parameters.

In the course of this text, we will discuss from time to time these questions of *robustness*.

The effect of differentially small deviations in the parameters of a model of known structure can be studied using *sensitivity* analysis. The motivation for sensitivity analysis is given by the practical experience that parameters often drift during the operation of the system in the field, but they typically remain in the vicinity of their nominal values. It is interesting to know whether such parameter variations cause severe changes of the system behaviour or have merely a minor influence on the important system properties.

As we shall see later in this chapter, the errors due to parameter variations tend to be corrected by the proper design of feedback control.

The next section will demonstrate that feedback control can

(i) force the controlled variable to accurately follow its prescribed value in steady-state;
(ii) shape the dynamics of the controlled variable;
(iii) greatly reduce the effect on the controlled variable of all external disturbances except those associated with the sensor; and
(iv) make the system tolerant of variations in hardware parameters other than those of the sensor.

The use of feedback is motivated by the presence of external disturbances and model uncertainties. More strictly, the use of feedback can be regarded as unreasonable if there is no uncertainty in the system because, for the unperturbed system, open-loop control may produce the same or probably better result.

Example 4.1 In the following, we review the control objectives of heat-exchanger control system discussed in Chapter 1 (Fig. 1.15). A sketch of the exchanger is given in Fig. 4.5a.

The objective is to maintain the outlet temperature of the process fluid, $\theta(t)$ °C, at its desired value or set point, θ_r°C, in the presence of disturbances in the process fluid flow, $q_m(t)$ kg/sec (= $Q\rho$; Q m^3/sec is the volumetric fluid flow and ρ kg/m^3 is the fluid density), flowing inside the tubes of the heat exchanger, and inlet temperature $\theta_i(t)$ °C. The steam flow, $q_{ms}(t)$ kg/sec, condensing on the outside of the tubes, is the variable that can be adjusted to control the outlet temperature, as it determines the amount of energy supplied to the process fluid. In addition to counteracting the effects of disturbances, the control system will be called upon to follow the commands for change in the outlet temperature of the process fluid.

The first step in the design is the selection of the temperature sensor and steam-valve actuator. For temperature measurement, we select an intelligent sensor which has, in addition to the basic device such as a thermocouple, a signal processing circuit which takes the output from the thermocouple and converts it to a current signal (in the range of 4 to 20 mA) that is proportional to the temperature. The signal processing circuit includes an amplifier and a filter. For steam valve adjustments, we select a pneumatic actuator which can provide large output power. Since the valve actuator must be operated by air pressure and the sensor generates electric current signals, a current to pressure transducer is also required in the feedback loop.

The feedback control scheme works as follows: the measured controlled variable is compared with the set-point; K_r in Fig. 4.5a represents the conversion of set-point scale. The controller generates a control signal (in the range of 4 to 20 mA), $u(t)$, on the basis of the difference between the measurement and set-point. The control signal is then connected to the pneumatic actuator of the steam valve through an electropneumatic device—a current to pressure transducer. The function of the valve actuator is to position the valve in proportion to the control signal. The steam flow is then a function of the valve position.

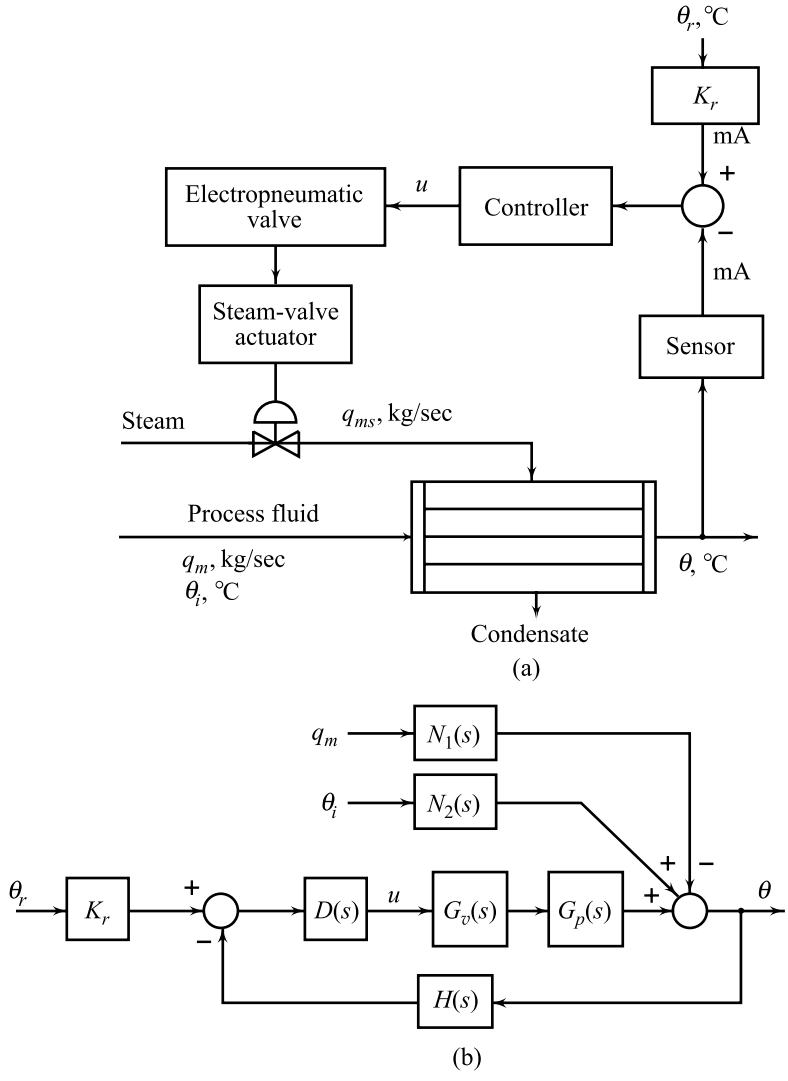

Fig. 4.5 Heat exchanger control loop

Once the hardware is chosen, the remainder of the design is concerned with trying to make the best use of the process. If the design is to be carried out analytically, a transfer function description of the feedback system must be found. Figure 4.5b shows the block diagram of the entire feedback loop. We now find the transfer function model of each block. Let us start with the heat exchanger.

As shown in Fig. 4.5b, the heat exchanger consists of three blocks, one for each of its three inputs. $G_p(s)$ is the process transfer function relating the outlet temperature to the steam flow, $N_1(s)$ is the process transfer function relating the outlet temperature to disturbance in process fluid flow, and $N_2(s)$ is the process transfer function to disturbance in inlet temperature.

The following experimentally obtained parameters will be used in developing a model of the feedback system.

The exchanger response to the steam flow has a gain of 50 °C/(kg/sec), and a time-constant of 30 sec. The exchanger response to the process fluid flow has a gain of 3 °C/(kg/sec), and to inlet temperature the gain is 1°C/°C. Therefore

$$G_p(s) = \frac{50}{30s+1};\ N_1(s) = \frac{3}{30s+1};\ N_2(s) = \frac{1}{30s+1}$$

The time-constant of the process depends on the residence time (tube volume/volumetric flow rate) of the fluid in the tubes. As a consequence, the time-constant may vary because of flow rate fluctuations and fouling. Therefore, we should ascertain how sensitive the performance of the final system design will be to changes in the time-constant of the process.

The control valve has a maximum capacity of 1.6 kg/sec of steam, linear characteristics, and a time-constant of 3 sec. The nominal pressure range of the valve is 3 to 15 psig.

$$\text{Valve gain} = \frac{1.6(\text{kg/sec})}{(15-3)\text{psi}} = \frac{1.6}{12}(\text{kg/sec})/\text{psi}$$

The electropneumatic valve has a constant gain

$$\frac{\Delta P}{\Delta I} = \frac{(15-3)\text{psi}}{(20-4)\text{mA}} = \frac{12}{16}\text{psi/mA}$$

Including the constant gain of the current-to-pressure transducer in the control-valve transfer function, $G_v(s)$, we obtain

$$G_v(s) = \frac{0.1}{3s+1}$$

The sensor has a calibrated range of 50 to 150°C and a time-constant of 10 sec.

$$\text{Sensor gain} = \frac{16\,\text{mA}}{(150-50)°\text{C}} = 0.16\ \text{mA/°C}$$

The transfer function of the sensor is given by

$$H(s) = \frac{0.16}{10s+1}$$

The set-point scale factor

$$K_r = 0.16\ \text{mA/°C}$$

The block diagram of the temperature control loop, as initially proposed, is shown in Fig. 4.6. θ_r is the change in the set-point value from the initial setting $\bar{\theta}_r$, θ_i is the deviation in the process fluid temperature from the nominal value $\bar{\theta}_i$, q_m is the deviation in the process fluid flow from the nominal value $\bar{Q}_m$, θ is the deviation in the outlet temperature from the nominal value $\bar{\theta}$, and q_{ms} is the deviation in the steam flow rate from the nominal value $\bar{Q}_{ms}$ (more on control objectives for a heat exchanger control loop, and their realization using PID control, will appear later in this chapter).

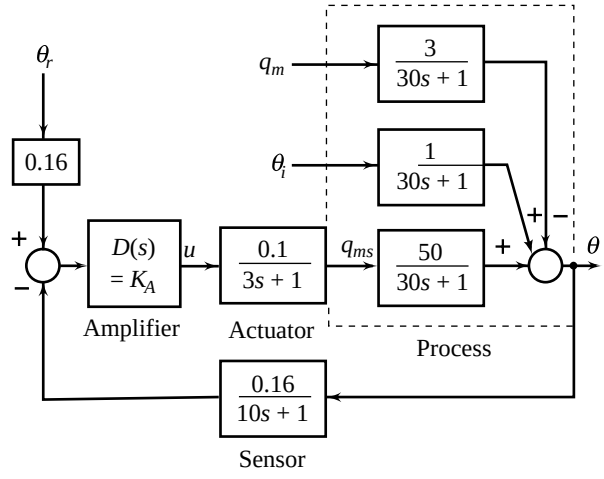

Fig. 4.6 A model of a heat exchanger control loop

Example 4.2 Consider the problem of design of an attitude control system for a rigid satellite. Satellites usually require attitude control so that antennas, sensors, and solar panels are properly oriented. For example, antennas are usually pointed toward a particular location on earth, while solar panels need to be oriented toward the sun for maximum power generation.

The satellite will be subjected to a variety of disturbance torques from such sources as aerodynamic drag, solar pressure, gravity gradient torques, and the rotation of various satellite components, e.g., pumps, motors and antennas. It will be assumed that the vehicle has initially been aligned to the desired attitude. Due to the above mentioned disturbance torques, it will be necessary to provide a feedback control system in order to maintain the satellite very close to the desired attitude. In addition to counteracting the effects of the disturbance torques acting on the vehicle, the control system will be called upon to change the attitude, subject to commands received from ground stations.

In this example, we shall highlight the important physical aspects of the system, taking a number of liberties with the practical aspects so as to avoid undue complication which should tend to obscure our main objectives.

So long as the angular velocity and the error angles of the vehicle are small, angular motions about the three axes are essentially *uncoupled* and may be controlled independently. Thus, we may design each of the three attitude-control loops independently, which is an important simplification. Figure 4.7 depicts single-axis attitude control schematic, where motion is only allowed about the axis perpendicular to the page. The angle θ that describes the satellite orientation must be measured with respect to an 'inertial' reference, that is, a reference that has no angular acceleration. The control signal comes from the gas jets that produce a torque $T(t)(= F \times d)$ about the mass centre.

A block diagram of the control system, as initially proposed, is given in Fig. 4.8. The command signal θ_r rad, transmitted from earth, is converted to electrical form ($e_r = K_P \theta_r(t)$ volts) in the satellite. A sensor on the satellite measures the deviation θ rad; its output is a voltage equal to $K_P \theta(t)$. A difference amplifier provides the voltage $u(t)$ proportional to $\hat{e}(t)$: the difference of the voltages corresponding to the command signal and measured signal. The amplifier must provide sufficient power to actuate the gas jets. The gas jets exert a torque $T(t) = K_T u(t)$ about the mass centre. We have neglected the dynamics of the gas jets, assuming that the opening time is short compared to the important time-constants of the system.

The vehicle dynamics are governed by the differential equation (assuming frictionless environment)

$$J\ddot{\theta} = T(t) + T_w(t)$$

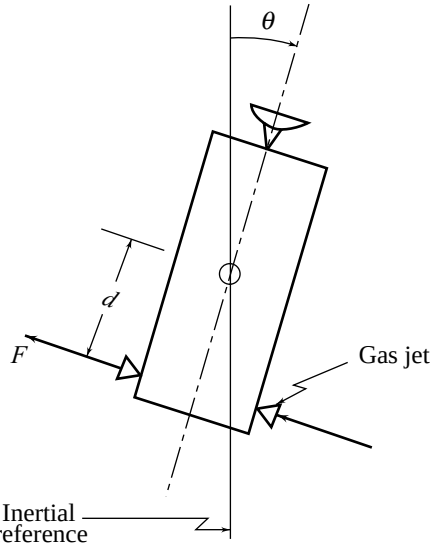

Fig. 4.7 Satellite control schematic

where J is the moment of inertia about the axis of rotation, and the total torque is the sum of control torque and the disturbance torque. Although the moment of inertia will vary over the life of the satellite because of the consumption of fuel, it presumably changes very slowly compared with the response of the vehicle. Thus, we are justified in treating it as a constant but should ascertain how sensitive the performance of the final system design is to anticipated changes in J (more on control objectives for satellite attitude control system, and their realization using PID control, will appear later in this chapter).

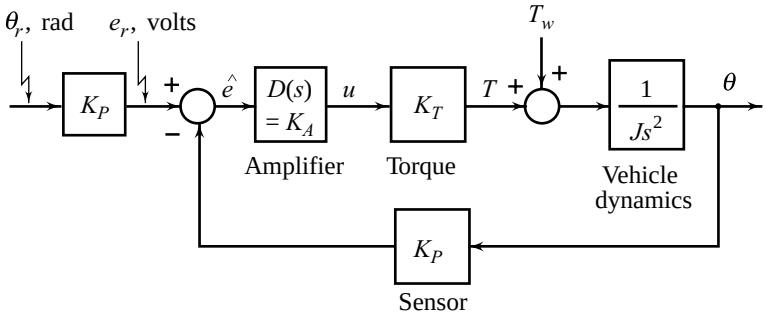

Fig. 4.8 A model of a satellite attitude control system

4.3 FEEDBACK CONTROL SYSTEM CHARACTERISTICS

Feedback systems play an important role in control engineering practice because the use of feedback can accomplish certain desirable results that would not be readily possible with an open-loop system. Some of the potential benefits (and liabilities) of feedback will be discussed in this section. Generally, the material presented here is applicable to any system whose mathematical model takes the form of a fixed linear feedback configuration. These occur not only in automatic control systems and electronic circuits, where the feedback is introduced by design, but also in much diverse fields as physiology, economics, ecology, etc., where feedback is inherent in the natural laws governing the process. However, consistent with the major thrust of this book, our terminology, convention, and illustrations will be taken in the context of control engineering.

4.3.1 System Sensitivity

A process represented by the transfer function $G(s)$, whatever its nature, is subject to modelling errors, changing environment, aging, and other natural factors that affect the control system performance. Consider the open-loop control system of Fig. 4.9. Assume that the controller $D_o(s)$ has been designed using a given transfer function model of the process, and it meets the specifications on the system output $y(t)$. Obviously, the output will approach the desired value only if the dynamic behaviour of the real process approaches that of its model. The modelling approximations and the process-behaviour changes with time during operation result in an inaccurate output. There is no provision within the system for supervision of the output and no mechanism is provided to correct the output. Consider now the closed-loop control system of Fig. 4.10. This system senses the change in the output through the feedback signal and attempts to correct the output. The feedback signal gives this system the capability to act as a self-correcting mechanism.

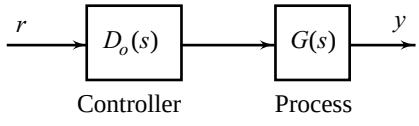

Fig. 4.9 An open-loop control system

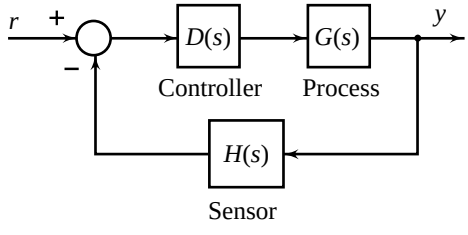

Fig. 4.10 A closed-loop control system

For simplicity, we assume that the structure and order of the process model are chosen exactly and they do not change with time. Then the differences between the process model and the real process behaviour are manifested as *parameter errors*. Let $\theta_1, \theta_2, \ldots$, be the parameters of the process model $G(s)$ which are subject to change.

In the following, we consider deviation in only one parameter, θ (extension of analysis to the case of deviations in more than one parameter is straightforward). If θ_n is the nominal value of the parameter, then the process model corresponding to the nominal working point may be expressed as $G(\theta_n, s)$. $G(\theta, s)$ represents a set of perturbed process models when the parameter θ changes over a specified range. We assume that $H(s)$ is not subject to parameter variations.

Sensitivity is the dependence of the system performance upon the value of the parameter θ. This property is usually investigated in terms of some specific performance measure, e.g., speed of response; or in terms of some characteristic performance function such as the frequency response of the closed-loop system. We take closed-loop transfer function $M(s)$ as the performance function characterizing the system behaviour, which depends on parameter θ in addition to other parameters. Consider perturbation only in the parameter θ. For the nominal value θ_n of this parameter, we get the nominal value of the performance function as $M(\theta_n, s)$.

Parameter changes $\Delta\theta$ induce changes ΔM in the performance function. Hence, instead of $M(\theta_n, s)$, we get the new value $M(\theta_n, s) + \Delta M = M(\theta_n + \Delta\theta, s) = M(\theta, s)$.

The Taylor's series expansion of $M(\theta,s)$ about the nominal point θ_n yields (assuming that the function is differentiable)

$$M(\theta_n + \Delta\theta, s) = M(\theta_n, s) + \left(\left. \frac{\partial M(\theta,s)}{\partial \theta} \right|_{\theta=\theta_n} \right) \Delta\theta + \cdots$$

If we restrict our attention to terms of atmost first order, we get

$$\Delta M(\theta_n, s) = \left(\left. \frac{\partial M(\theta,s)}{\partial \theta} \right|_{\theta=\theta_n} \right) \Delta\theta$$

Expressing deviations in terms of relative changes, we obtain

$$\frac{\Delta M(\theta_n,s)}{M(\theta_n,s)} = \frac{\Delta\theta}{\theta_n} \left[\left(\left. \frac{\partial M(\theta,s)}{\partial \theta} \right|_{\theta=\theta_n} \right) \frac{\theta_n}{M(\theta_n,s)} \right] \tag{4.7}$$

System sensitivity to parameter θ is defined as the ratio of the percentage change in the system performance measure M from its nominal value to the percentage change in the parameter. S_θ^M denotes the sensitivity of M with respect to θ, and is given by

$$S_\theta^M \triangleq \lim_{\Delta\theta \to 0} \frac{\Delta M(\theta_n,s)/M(\theta_n,s)}{\Delta\theta/\theta_n} = \left[\left. \frac{\partial M(\theta,s)}{\partial \theta} \right|_{\theta=\theta_n} \right] \frac{\theta_n}{M(\theta_n,s)} \tag{4.8}$$

If $S_\theta^M = 0$, then the measure M is insensitive to the parameter θ at the nominal point θ_n. If $S_\theta^M \neq 0$, then M is sensitive and the value of S_θ^M is a measure of the degree of dependence of M on θ.

A plausible interpretation of the sensitivity function is shown in Fig. 4.11. Here we treat the relative change in the parameter θ, $\Delta\theta/\theta_n$, as an input to the process modelled by the sensitivity function, with the output being the relative change in the system performance measure.

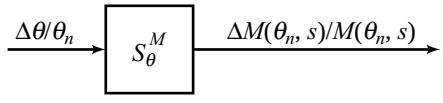

Fig.4.11 Interpretation of sensitivity function as a gain function

Note that sensitivity function deals with infinitesimally small parameter perturbations near a given nominal parameter value and does not refer to the amount of perturbation. Experience on use of such functions, however, shows that sensitivity function is a reasonable characteristic of the effects of small rather than infinitesimally small perturbations. As we shall see shortly, the errors due to parameter variations tend to be corrected by the proper design of feedback control.

The sensitivity analysis of feedback systems represented by block diagram of Fig. 4.10 is frequently carried out using the sensitivity function S_G^M: the sensitivity of closed-loop transfer function $M(\theta_n, s)$ to variations in $G(\theta_n, s)$. We may define this function as

$$S_G^M \triangleq \frac{\Delta M(\theta_n, s)/M(\theta_n, s)}{\Delta G(\theta_n, s)/G(\theta_n, s)} \tag{4.9}$$

i.e., the ratio of the percentage change in the performance measure from its nominal value to percentage change in uncertain plant model from its nominal value.

Referring to Eqn. (4.7), we may express relative changes in $G(\theta_n, s)$ as

$$\frac{\Delta G(\theta_n, s)}{G(\theta_n, s)} = \frac{\Delta\theta}{\theta_n}\left[\left(\frac{\partial G(\theta, s)}{\partial\theta}\bigg|_{\theta=\theta_n}\right)\frac{\theta_n}{G(\theta_n, s)}\right] \tag{4.10a}$$

Relative changes in (refer Fig. 4.10)

$$M(\theta_n, s) = \frac{D(s)G(\theta_n, s)}{1 + D(s)G(\theta_n, s)H(s)} \tag{4.10b}$$

are given by

$$\frac{\Delta M(\theta_n, s)}{M(\theta_n, s)} = \frac{\Delta\theta}{\theta_n}\left[\left(\frac{\partial}{\partial\theta}\left\{\frac{D(s)G(\theta, s)}{1 + D(s)G(\theta, s)H(s)}\right\}\bigg|_{\theta=\theta_n}\right)\frac{\theta_n}{M(\theta_n, s)}\right]$$

$$= \frac{\Delta\theta}{\theta_n}\left[\frac{D(s)}{\left[1 + D(s)G(\theta_n, s)H(s)\right]^2}\left(\frac{\partial G(\theta, s)}{\partial\theta}\bigg|_{\theta=\theta_n}\right)\frac{\theta_n}{M(\theta_n, s)}\right]$$

$$= \frac{\Delta\theta}{\theta_n}\left[\left\{\frac{D(s)G(\theta_n, s)}{1 + D(s)G(\theta_n, s)H(s)}\right\}\left\{\frac{1}{1 + D(s)G(\theta_n, s)H(s)}\right\}\left\{\frac{1}{G(\theta_n, s)}\right\}\left(\frac{\partial G(\theta, s)}{\partial\theta}\bigg|_{\theta=\theta_n}\right)\frac{\theta_n}{M(\theta_n, s)}\right]$$

From Eqns (4.10), it follows that

$$\frac{\Delta M(\theta_n, s)}{M(\theta_n, s)} = S(\theta_n, s)\frac{\Delta G(\theta_n, s)}{G(\theta_n, s)} \tag{4.11a}$$

with the *sensitivity function* of the feedback control given as

$$S_G^M = S(\theta_n, s) = \frac{1}{1 + D(s)G(\theta_n, s)H(s)} \tag{4.11b}$$

The sensitivity function given by Eqns (4.11) shows how relative changes in the input/output behaviour of the closed-loop depend on the changes in the process transfer function. In general, the sensitivity function is a function of the Laplace transform variable s, which makes sensitivity very difficult to interpret. However, if we replace s in Eqn. (4.11b) by $j\omega$, we get the sensitivity as a frequency response. Then, we can assign meaning to the sensitivity for frequencies within the bandwidth[1] of the system. Since the system will not transmit frequencies outside its bandwidth (an approximation), the sensitivity for frequencies much greater than the system bandwidth is of little interest.

Evaluating the sensitivity in Eqn. (4.11b) as a function of frequency, yields

$$S_G^M = S(\theta_n, j\omega) = \frac{1}{1 + D(j\omega)G(\theta_n, j\omega)H(j\omega)} \tag{4.12}$$

The term DGH evaluated at a specific frequency is called the *loop gain* at that frequency (refer Eqn. (3.1d)). At frequencies within the system bandwidth, we would like the loop gain to be as large as possible to reduce the sensitivity of the closed-loop behaviour to the process parameters. Generally, one of the purposes of the controller $D(s)$ is to allow the loop gain to be increased without destabilizing the system.

Assume now that we are dealing with an open-loop system such as the one depicted in Fig. 4.9. It is clear that for this system we can apply the result given by Eqns (4.11) with $H(s) = 0$. Thus

$$S_G^M = 1, \text{ where } M(\theta_n, s) = D_o(s)G(\theta_n, s) \tag{4.13}$$

It can readily be seen that feedback reduces the system sensitivity to changes in process parameters.

Next we derive the sensitivity of the closed-loop transfer function to parameter changes in the sensor $H(s)$. Assume that the parameter θ_n is a part of $H(s)$, and the process transfer function $G(s)$ is not subject to parameter variations. For this case, the closed-loop transfer function becomes

$$M(\theta_n, s) = \frac{Y(s)}{R(s)} = \frac{D(s)G(s)}{1 + D(s)G(s)H(\theta_n, s)} \tag{4.14}$$

For an infinitesimal change $\Delta\theta$ in the nominal parameter, θ_n, we obtain

$$\left.\frac{\partial M(\theta, s)}{\partial \theta}\right|_{\theta=\theta_n} = -\left[\frac{D(s)G(s)}{1 + D(s)G(s)H(\theta_n, s)}\right]^2 \left.\frac{\partial H(\theta, s)}{\partial \theta}\right|_{\theta=\theta_n} \tag{4.15}$$

From Eqns (4.14) and (4.15), it follows that

$$\frac{\Delta M(\theta_n, s)}{M(\theta_n, s)} = S_H^M \frac{\Delta H(\theta_n, s)}{H(\theta_n, s)} \tag{4.16a}$$

where

$$S_H^M = \frac{-D(s)G(s)H(\theta_n, s)}{1 + D(s)G(s)H(\theta_n, s)} \tag{4.16b}$$

This equation shows that for large values of loop gain DGH, sensitivity of the feedback system with respect to H approaches unity. Thus, we see that the changes in H directly affect the system output. To solve this problem, we generally can use high-quality components for the sensor.

The use of feedback in reducing sensitivity to parameter variations is an important advantage of the feedback control systems. To have a highly accurate open-loop system, the components of the process plant

[1]It gives the significant frequency range of the closed-loop system (refer Fig. 2.22). Chapter 9 on frequency response analysis will describe this important parameter of control system performance.

must be carefully selected so that the parameters of the physical system are close to that of $G(s)$—the model used in design, under all operating conditions. On the other hand, a closed-loop system allows $G(s)$ to be less accurately specified, since the effects of parameter variations are mitigated by the use of feedback. However, a closed-loop system requires careful selection of the components of the feedback sensor. Since the plant is made up of power elements and the sensor is made up of measuring elements which operate at low power levels, the selection of accurate $H(s)$ is far less costly than that of $G(s)$ to meet the exact specifications.

Many plants, by their very nature, have parameters that vary extensively during operation. An example is an aircraft whose parameters vary over very wide ranges with speed, altitude, and so on. Hence, aircraft autopilot design must satisfy a rigorous specification on sensitivity to plant parameter variations. Feedback control is the only solution.

The price for improvement in sensitivity by use of feedback is paid in terms of *loss of system gain*. The gain of the closed-loop system shown in Fig. 4.10 is $D(s)G(s)/[1 + D(s)G(s)H(s)]$ while with $H(s) = 0$, the gain becomes $D(s)G(s)$. Hence, by use of feedback, the system gain is reduced by the same factor as by which the sensitivity of the system to parameter variations is reduced. Sufficient open-loop gain can, however, be built into a system so that we can afford to lose some gain to achieve improvement in sensitivity. We should not place a gain outside the feedback loop; the overall system will be quite sensitive to elements outside the loop.

Example 4.3 Several important speed control systems are used in steel mills for rolling steel sheets and moving the steel through the mill (Fig. 4.12). We consider here a speed control system employing an armature-controlled dc motor with negligible armature inductance, as the actuator. Figure 4.13a gives the schematic of the speed control system and Fig. 4.13b gives the operational block diagram:

$e_a(t)$ = armature applied voltage
R_a = armature resistance
K_b = motor back-emf constant
K_T = motor torque constant
J = moment of inertia of motor and load
B = viscous-friction coefficient of motor and load
$T_w(t)$ = disturbance torque representing loading effect on the rolls when the steel bar engages in the rolls
$\omega(t)$ = motor velocity

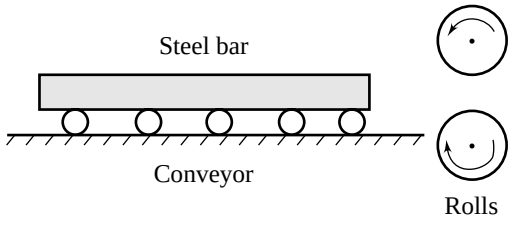

Fig. 4.12

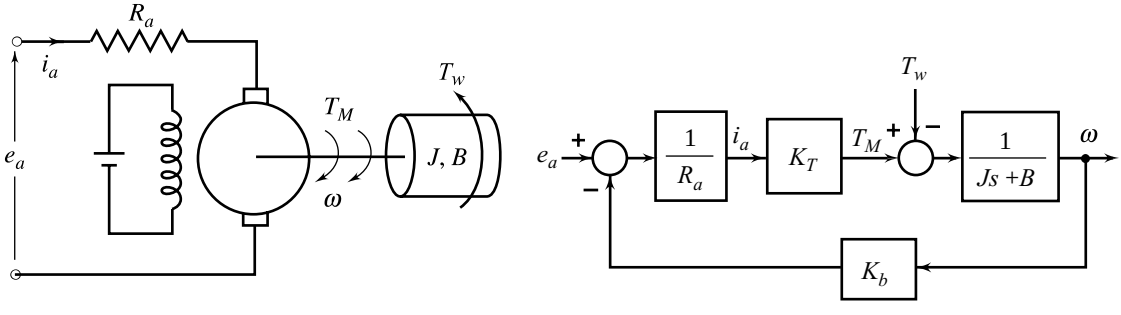

(a) (b)

Fig. 4.13 Open-loop speed control system

The transfer function of the open-loop speed control system obtained from Fig. 4.13b, is

$$M_o(s) = \frac{\omega(s)}{E_a(s)} = \frac{K}{\tau s + 1} \tag{4.17}$$

where $$K = \frac{K_T}{BR_a + K_T K_b}; \tau = \frac{J R_a}{BR_a + K_T K_b}$$

The sensitivity of the open-loop mode of operation to variation in the constant K is (refer Eqn. (4.8))

$$S_K^{M_o} = \frac{\partial M_o}{\partial K}\left(\frac{K}{M_o}\right) = 1 \tag{4.18}$$

A closed-loop speed control system is easily obtained by utilizing a tachogenerator to generate a voltage proportional to speed, as shown in Fig. 4.14. This voltage is subtracted from the reference voltage representing the desired speed, and amplified. The closed-loop transfer function is

$$\frac{\omega(s)}{\omega_r(s)} = M(s) = \frac{KK_A K_t}{\tau s + 1 + KK_A K_t} \tag{4.19}$$

where K_t = tachogenerator constant; and K_A = amplifier gain.

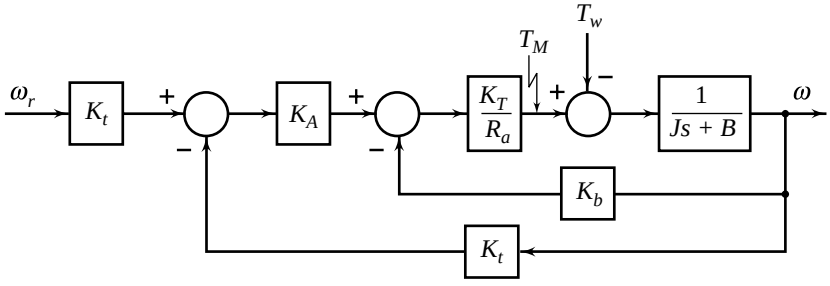

Fig. 4.14 Closed-loop speed control system

The sensitivity of the closed-loop system to variation in K is

$$S_K^M = \frac{\partial M}{\partial K}\left(\frac{K}{M}\right) = \frac{\tau s + 1}{\tau s + 1 + KK_A K_t} \tag{4.20}$$

For a typical application, we might have $1/\tau = 0.1$, and $(1 + KK_A K_t)/\tau = 10$. Therefore, from Eqn. (4.20) we obtain

$$S_K^M = \frac{s + 0.1}{s + 10}$$

We find that the sensitivity is a function of s and must be evaluated for various values of frequency. This type of frequency analysis is straightforward (refer Review Example 4.2). However, it is clearly seen that at a specific frequency, for example, $s = j\omega = j1$, the magnitude of the sensitivity of the closed-loop system is

$$\left|S_K^M\right| \cong 0.1$$

Thus, compared to that of the open-loop case, the sensitivity of the closed-loop speed control system at $\omega = 1$ is reduced by a factor of ten.

It should be noted that in order to reduce sensitivity of the closed-loop system to parameter variations, the amplifier gain K_A must be reasonably large (refer Eqn. (4.20)). The armature voltage signal and its associated torque signal will be larger for the closed-loop than for the open-loop operation. Therefore a large motor will be required in order to avoid saturation of the motor.

4.3.2 Disturbance Rejection

The second most important effect of feedback in a control system is the control and partial elimination of the effects of disturbance signals. A feedback control system with a disturbance input is shown in Fig. 4.1. By superposition, the system output is

$$Y(s) = \frac{D(s)G(s)}{1 + D(s)G(s)H(s)} R(s) + \frac{N(s)}{1 + D(s)G(s)H(s)} W(s) \tag{4.21}$$

With $R(s) = 0$, the system output becomes

$$Y(s) = \frac{N(s)}{1 + D(s)G(s)H(s)} W(s) \tag{4.22}$$

For the open-loop system,

$$Y(s) = N(s)W(s) \tag{4.23}$$

It can readily be seen that feedback reduces the effect of disturbances on the controlled output.

We use a frequency-response approach to investigate disturbance-rejection property of feedback control systems. Replacing s in Eqn. (4.22) by $j\omega$, we get

$$\frac{Y(j\omega)}{W(j\omega)} = \frac{N(j\omega)}{1 + D(j\omega)G(j\omega)H(j\omega)}$$
$$= S(j\omega)N(j\omega)$$

where

$$S(j\omega) = \frac{1}{1 + D(j\omega)G(j\omega)H(j\omega)}$$

is the sensitivity function of the control system defined in Eqn. (4.11b). Recall from the preceding subsection that the loop gain $D(j\omega)G(j\omega)H(j\omega)$ must be made large to reduce sensitivity to variations in plant parameters. This condition also meets the requirement of reducing the effects of disturbance input on the controlled output of the system.

For the case that loop gain is large ($DGH >> 1$), the disturbance transfer function

$$\frac{Y(j\omega)}{W(j\omega)} \cong \frac{N(j\omega)}{D(j\omega)G(j\omega)H(j\omega)}$$

An obvious way to accomplish disturbance rejection is to make $N(j\omega)$ small. Since $N(j\omega)$ is a function of the plant parameters, it cannot be modified. Alternatively, we may increase the loop gain by increasing the gain of $D(j\omega)$. Note that increasing the plant gain (if possible) will also increase the loop gain, but increasing the plant gain may also increase the gain of $N(j\omega)$. Hence, in this case, disturbance rejection may not be improved. Thus, to reject disturbances, the loop gain must be increased in such a manner that the gain from the disturbance input to the system output is not increased.

Figure 4.15 gives a block diagram of the situation wherein measurement noise $W_n(s)$ enters the system through the feedback link. The closed-loop transfer function for this disturbance is

$$\frac{Y(s)}{W_n(s)} = -\frac{D(s)G(s)}{1 + D(s)G(s)H(s)}$$

Thus, large loop gain will lead to large output error due to measurement noise. This is in conflict with the disturbance-rejection property with respect to the configuration of Fig. 4.1. To solve this problem, we generally can examine the measuring instrument and modify the filtering so that it satisfies the requirements of a particular control system.

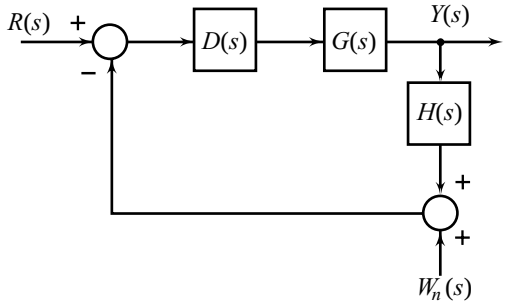

Fig. 4.15 Closed-loop system with measurement noise

Example 4.4 As a specific example of a system with an unwanted disturbance, let us reconsider the speed control system for a steel rolling mill (Figs 4.12–4.14). Rolls passing steel through are subject to large load changes or disturbances. As a steel bar approaches the rolls, the rolls turn unloaded. However, when the bar engages in the rolls, the load on the rolls increases immediately to a large value. This loading effect can be approximated by a step change of disturbance torque $T_w(s)$.

Let us study the effect of load torque $T_w(s) = A/s$ in the open-loop speed control system of Fig. 4.13b and the closed-loop speed control system of Fig. 4.14.

In the open-loop case, the change in speed due to load disturbance (obtained by manipulation of the block diagram of Fig. 4.13b) is,

$$\omega(s) = \left(\frac{-1}{Js + B + K_T K_b / R_a}\right) T_w(s)$$

The steady-state error in speed due to $T_w(s) = A/s$ is found by using the final value theorem:

$$\lim_{t\to\infty} \omega(t) = \lim_{s\to 0} s\omega(s) = \lim_{s\to 0} s\left[\frac{-1}{Js + B + K_T K_b / R_a}\right]\frac{A}{s}$$

$$= \frac{-A}{B + K_T K_b / R_a}$$

Manipulation of the block diagram of Fig. 4.14 gives the following relation between output speed and load disturbance (alternatively, draw a signal flow graph and use Mason's gain rule) for the closed-loop speed control system:

$$\omega(s) = \frac{-1}{Js + B + (K_T / R_a)[K_b + K_A K_t]} T_w(s)$$

Again the steady-state output is obtained by utilizing the final value theorem, and we have

$$\lim_{t\to\infty} \omega(t) = \lim_{s\to 0} s\omega(s) = \frac{-A}{B + (K_T / R_a)[K_b + K_A K_t]}$$

The ratio of the closed-loop to open-loop steady-state speed output due to an undesirable disturbance is

$$\frac{\omega_{ss}(CL)}{\omega_{ss}(OL)} = \frac{BR_a + K_T K_b}{BR_a + K_T(K_b + K_A K_t)}$$

and is usually less than 0.02.

4.3.3 Shaping the Dynamic Response

Consider the feedback control system of Fig. 4.1. The output with $W(s) = 0$ is given by

$$Y(s) = \frac{D(s)G(s)}{1 + D(s)G(s)H(s)} R(s) \tag{4.24a}$$

$$= M(s)R(s) \tag{4.24b}$$

By finding the poles and zeros of $M(s)$, we can characterize the behaviour of the closed-loop system's response to a reference input.

Assume that $D(s)$, $G(s)$ and $H(s)$ are rational functions of s; they can each be expressed as ratios of their numerator and denominator polynomials of the form

$$\frac{D_1(s)}{D_2(s)} \triangleq D(s) \tag{4.25a}$$

$$\frac{G_1(s)}{G_2(s)} \triangleq G(s) \tag{4.25b}$$

and

$$\frac{H_1(s)}{H_2(s)} \triangleq H(s) \tag{4.25c}$$

Substituting $D(s)$, $G(s)$ and $H(s)$ from Eqns (4.25) into Eqns (4.24), we obtain

$$M(s) = \frac{D_1(s)\, G_1(s)/D_2(s)\, G_2(s)}{1 + D_1(s)\, G_1(s) H_1(s)/D_2(s)\, G_2(s) H_2(s)}$$

which reduces to

$$M(s) = \frac{D_1(s)G_1(s)H_2(s)}{D_2(s)G_2(s)H_2(s) + D_1(s)G_1(s)H_1(s)} \tag{4.26}$$

Having obtained the closed-loop transfer function in rational form, we are ready to make two rather important observations.

First, the finite *zeros* of $M(s)$ are given by the zeros of the plant transfer function $G(s)$, the poles of the feedback block $H(s)$, and the zeros of the controller transfer function $D(s)$. Second, the *poles* of $M(s)$ are the roots of the equation

$$D_2(s)G_2(s)H_2(s) + D_1(s)G_1(s)H_1(s) = 0 \tag{4.27}$$

which, because its left-hand side is the denominator polynomial of the transfer function, is the *characteristic equation* of the closed-loop system.

We will see in the next chapter that the poles of $M(s)$ determine the modes of closed-loop system's response; poles in the left-half of the complex plane give rise to decaying modes (a requirement for system stability) and the poles in the right-half of the complex plane give rise to growing modes (making the system unstable). The zeros of $M(s)$ control the magnitude of each mode and, hence, the contribution of each mode in the total response. Thus, we can shape the dynamic response of the closed-loop system by controlling the locations of poles and zeros of $M(s)$ through the controller $D(s)$.

We see from Eqn. (4.26) that the poles of a feedback system do not have a direct relationship to the open-loop poles and zeros; this tends to complicate the analysis. However, it does mean that the designer has the capability of making the closed-loop system behave quite differently from the open-loop system. In order to make effective use of this ability, it is necessary to have methods for analyzing the effects of changes in parameters of the controller $D(s)$ without having to solve Eqn. (4.26) for $M(s)$ or Eqn. (4.27) for the closed-loop poles each time a parameter is changed. Much of our subsequent work will be directed toward developing analytical tools that will allow us to take advantage of this unusual property of feedback systems.

Consider now the total response of the closed-loop system of Fig. 4.1 to both the reference and the disturbance inputs (refer Eqn. (4.21)):

$$Y(s) = \frac{D(s)G(s)}{1 + D(s)G(s)H(s)} R(s) + \frac{N(s)}{1 + D(s)G(s)H(s)} W(s)$$

$$= M(s)R(s) + M_w(s)W(s)$$

The denominators of $M(s)$ and $M_w(s)$ are identical, implying that both the transfer functions have precisely the same poles. This situation is a consequence of the fact that the characteristic equation is a property of the closed-loop configuration and not of the particular variables that happen to be designated as the input and output.

The zeros of $M(s)$ and $M_w(s)$ are different. In fact, it would be rather unfortunate if this difference did not exist because we certainly do not want the output to respond to disturbance inputs in the same way that it responds to reference inputs—generally we would prefer $M(s)$ to be unity, so that the output follows the reference input exactly, and $M_w(s)$ to be zero, so that the output would be unaffected by disturbances.

Upon examination of Fig. 4.9, one notes that the open-loop control system can easily shape the dynamics of the controlled output: the output y follows the input r exactly if

$$D_o(s) = \frac{1}{G(s)}$$

If $D_o(s)$ is realizable (i.e., a physical system with transfer function $D_o(s)$ can be constructed), it can cancel the process dynamics completely since it has the reciprocal transfer function behaviour. Therefore, one may logically ask, what is the advantage of the closed-loop system in this case? Again, we return to the concepts of the sensitivity of the system to parameter changes and effects of disturbances as our answer to this question. In the open-loop control configuration of Fig. 4.9, one may implement $D_o(s)$ so that it is equal to the inverse of the nominal transfer function $G(s)$, but $G(s)$ is usually an approximate model of the process. Moreover, during the operation of the system it is inevitable that the parameters of $G(s)$ will change due to environmental changes and $D_o(s)G(s)$ will no longer be equal to unity. Also, because of the disturbances acting on the process $G(s)$ but not on the controller $D_o(s)$, the output $y(t)$ will deviate from the input $r(t)$. In contrast, a closed-loop system continually monitors the output $y(t)$, and provides an actuating signal in order to reduce the effects of parameter variations and disturbances. Thus, we find that the properties of insensitivity to model uncertainties, parameter variations, and disturbance rejection encourage the introduction of feedback.

Example 4.5 Figure 4.6 gives the block diagram description of a heat-exchanger control system (refer Example 4.1). Assume that the actuator and the sensor devices have zero dynamic lags, i.e., the transfer function of the actuator is 0.1, and that of the sensor is 0.16. Under this assumption,

$$\frac{\theta(s)}{\theta_i(s)} = \frac{D(s)G(s)}{1 + D(s)G(s)}$$

where $$G(s) = \frac{0.8}{30s + 1}.$$

If the controller $D(s)$ is an amplifier of gain K_A with negligible dynamic lag, we get

$$\frac{\theta(s)}{\theta_r(s)} = \frac{0.8K_A}{30s + 1 + 0.8K_A}$$

For positive values of K_A, the effect of the feedback is to shift the pole negatively from the open-loop location $s = -1/30$ to the location $s = -(1+ 0.8K_A)/30$; the time-constant reduces from 30 to $30/(1 + 0.8K_A)$. This implies that as K_A (and hence the loop gain) increases, the system dynamics continuously becomes faster, i.e., the transient response decays more quickly. Thus, the *relative stability* (which is a quantitative measure of how fast the transients die out in the system) improves with an increase in loop gain.

Consider now the situation which is more closer to the real world: the actuator and the sensor devices in heat-exchanger control system have dynamic lags as shown in Fig. 4.6. Excessive loop gain may result in the instability of the feedback system. The instability phenomenon may be qualitatively described as follows (quantitative discussion will appear in the next chapter).

Consider the feedback system of Fig. 4.6 with a fixed desired value θ_r, and in equilibrium with the controlled variable θ at the desired value. If a process disturbance occurs, the ensuing deviation of the controlled variable will cause a correction to be applied but it will be delayed by the cumulative lags of the sensor, actuator, and process. Eventually, however, the trend of the controlled variable caused by the disturbance will be reversed by the opposition of the process manipulated input q_{ms}, returning the controlled variable toward the desired value. Now if the loop gain is high, a *strong* correction is applied and the controlled variable overshoots the desired value, causing a reversal in the algebraic sign of the system error (difference between desired value and controlled variable). Unfortunately, because of system lags, a reversal of the correction does not occur immediately, and the process manipulated input (acting on 'old' information) is now actually driving the controlled variable in the same direction as it was already going, rather than opposing its excursions, leading to a larger deviation. If the loop gain is not too large and/or system lag is not too large, it may be possible to bring the controlled variable back to its desired value. The combination of excessive loop gain with excessive lags always results in feedback system instability.

4.3.4 Steady-State Accuracy

A feedback control system is valuable because the sensitivity of the system to parameter variations, and effect of disturbances can be reduced significantly. In addition, as we have seen, it provides us with the ability to adjust the transient response. However, as a further requirement, one must examine and compare the final steady-state error for an open-loop and a closed-loop system.

The error of the closed-loop system shown in Fig. 4.2 with $W(s) = 0$ is given by

$$E(s) = \frac{1}{1 + D(s)G(s)} R(s)$$

For a unit step input, $R(s) = \frac{1}{s}$, the steady-state error is given by

$$e_{ss} = \lim_{t \to \infty} [r(t) - y(t)] = \lim_{s \to 0} sE(s)$$

$$= \lim_{s \to 0} s \left[\frac{1}{1 + D(s)G(s)} \right] \frac{1}{s}$$

$$= \frac{1}{1 + D(0)G(0)} \tag{4.28}$$

The value of $D(s)G(s)$ when $s = 0$ is often called the *dc loop gain*. Therefore, a closed-loop system with a reasonably large dc loop gain will have a small steady-state error.

Consider now the open-loop control system shown in Fig. 4.9. The error

$$E(s) = R(s) - Y(s) = [1 - D_o(s)G(s)]\, R(s)$$

For a unit-step input, the steady-state error is given by

$$e_{ss} = \lim_{s \to 0} sE(s) = 1 - D_o(0)G(0) \tag{4.29}$$

Upon examination of Eqn. (4.29), one notes that the open-loop control system can possess a zero steady-state error by simply adjusting the dc loop gain so that $D_o(0)G(0) = 1$. However, during the operation of the system,it is inevitable that the parameters of $G(s)$ will change and dc loop gain of the system will no longer be equal to unity. The steady-state error will continue to be other than zero until the system is recalibrated. By contrast, the feedback system of Fig. 4.2 continually monitors the steady-state error and provides an actuating signal in order to reduce the steady-state error.

4.3.5 The Case for High-Gain Feedback

Summarizing the benefits of negative feedback in systems with high loop gain, we can state that such systems result in:

(i) good steady-state tracking accuracy;
(ii) good disturbance signal rejection;
(iii) low sensitivity to process parameter variations; and
(iv) good relative stability, i.e., rate of decay of transients.

There are, however, factors limiting the gain:

(i) High gain may result in instability problems.
(ii) Input amplitudes limit the gain; excessively large amplitudes of control signals will drive the process to the saturation region of its operation, and the control system design based on linear model of the plant will no longer give satisfactory performance.
(iii) Measurement noise limits the gain; with high gain feedback, measurement noise appears unattenuated in the controlled output.

Therefore, in design we are faced with trade offs.

4.3.6 Positive Feedback

Positive feedback is an operation which augments an imbalance, thereby precluding stability. If a temperature controller with positive feedback were used to heat a room, it would increase the heat when the temperature was above the set-point, and turn it off when it was below. Obviously, this property is not conducive to regulation. Sometimes positive feedback is used in minor loops of feedback control configurations; the stability and regulation of the controlled variable is provided by the primary feedback loop. Figure 4.16a shows a feedback system with the minor loop having positive feedback. The equivalent single-loop block diagram is shown in Fig. 4.16b. If $G_m(s)$ is selected to be nearly unity, the loop gain becomes very high and the closed-loop transfer function approximates to

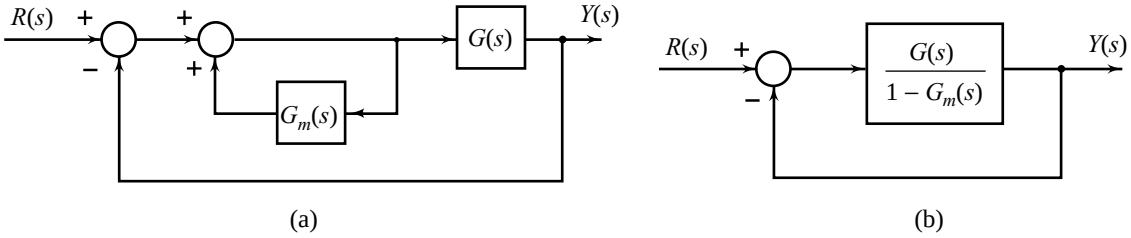

Fig. 4.16 A system with positive feedback in minor loop

$$\frac{Y(s)}{R(s)} = \frac{G(s)}{1 - G_m(s) + G(s)} \cong 1$$

Thus, due to the high loop gain provided by the minor positive feedback loop, the closed-loop transfer function becomes insensitive to $G(s)$.

4.4 PROPORTIONAL MODE OF FEEDBACK CONTROL

We use a temperature control system to develop an understanding of proportional control characteristics.

The system shown in Fig. 4.17 is designed to maintain the chamber temperature θ at desired value θ_r in the face of disturbances in outdoor temperature. We will assume an initial equilibrium operating point (all variables steady) at which steam inflow $\bar{Q}_m$ kg/sec exactly matches the heat loss to the surroundings with

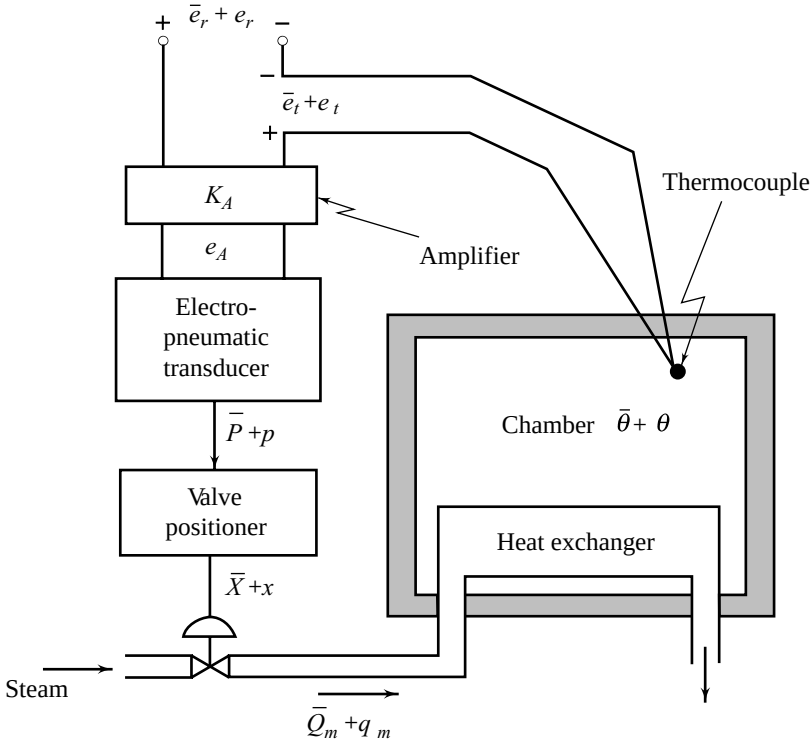

Fig. 4.17 Heating system with proportional control

chamber temperature $\bar{\theta}$ = set-point value $\bar{\theta}_r$. The necessary steam flow rate $\bar{Q}_m$ can be achieved because the electropneumatic transducer has a zero adjustment which allows pressure $\bar{P}$ to be set at the middle (9 psig) of its 3 to 15 psig range when $e_A = 0$, and the valve positioner has a zero adjustment which allows the valve opening to be put anywhere desired, with the pressure $\bar{P}$ at 9 psig. With these initial 'trimming' adjustments made, all the variables named in Fig. 4.18 are considered as small perturbations away from the initial steady state.

The thermocouple output is $e_t = K_t\theta$. This simple model is justifiable if the dynamics of the sensor are negligible relative to the process time-constant τ_p. The electronic amplifier is obviously fast enough to be treated as zero-order system. The dynamics of the electropneumatic transducer and valve positioner have been neglected in the block diagram of Fig. 4.18, assuming their response to be very fast relative to τ_p. Also the relation between q_m and x is assumed statically linear and dynamically instantaneous.

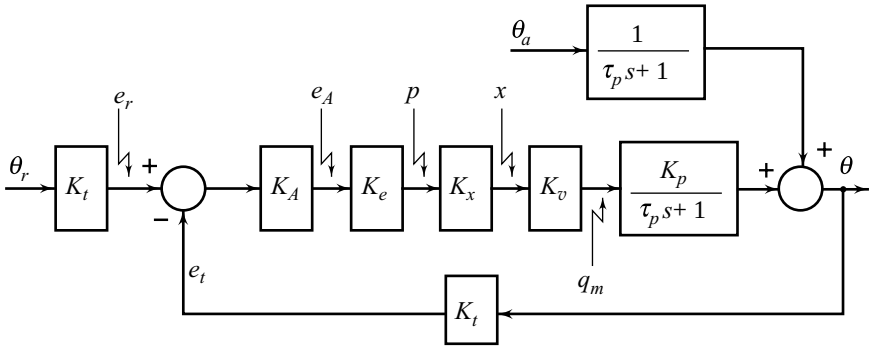

Fig. 4.18 A block diagram for the system of Fig. 4.17

Having justified the block diagram of Fig. 4.18, we now use it directly to obtain the transfer function of the closed-loop system, relating θ to θ_r and θ_a:

$$[(K_t\theta_r(s) - K_t\theta(s))K_AK_eK_xK_v]\frac{K_p}{\tau_p s+1} + \left(\frac{1}{\tau_p s+1}\right)\theta_a(s) = \theta(s)$$

or
$$(\tau_p s + 1)\theta(s) + K_tK_AK_eK_xK_vK_p\theta(s) = K_tK_AK_eK_xK_vK_p\theta_r(s) + \theta_a(s)$$

or
$$(\tau s + 1)\theta(s) = \frac{K}{1+K}\theta_r(s) + \frac{1}{1+K}\theta_a(s) \qquad (4.30)$$

where $\tau \triangleq$ closed-loop system time-constant $= \dfrac{\tau_p}{1+K}$;

$K \triangleq$ system loop gain $= K_tK_AK_eK_xK_vK_p$

For the linear model of Eqn. (4.30), superposition holds and we can investigate the effects of command θ_r and disturbance θ_a separately. For θ_r, a step input of size unity (perturbation θ_a is held at zero), we get

$$\theta(t) = \frac{K}{1+K}(1 - e^{-t/\tau}) \qquad (4.31)$$

Figure 4.19 shows the first-order system response with speed determined by τ and the steady-state error given by

$$e_{ss} = 1 - \theta_{ss} = \frac{100}{K+1}\%$$

Since $\tau = \tau_p/(K + 1)$, we see that both the speed of response and the steady-state error are improved if we increase loop gain K. For step disturbance input $\theta_a(s) = 1/s$ ($\theta_r = 0$), we get

$$\theta(t) = \frac{1}{(K+1)}(1 - e^{-t/\tau}) \qquad (4.32)$$

and again increasing K improves both the speed of response and the steady-state error.

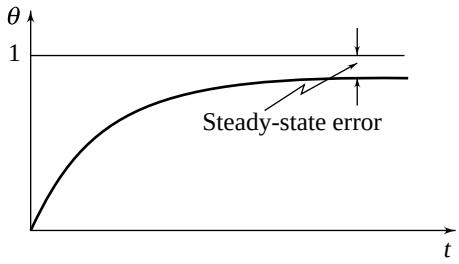

Fig. 4.19 System response to step command

The steady-state errors discovered in the present example are in fact characteristic of the proportional control in general. The basic reason for this behaviour can be explained as follows. For the initial equilibrium point assumed, we are able to get zero steady-state error because the zero adjustments on various devices allow us to open the valve exactly the right amount to supply the steam with $e = \theta_r - \theta = 0$. When we then ask θ_r to change by a unit step, a different valve opening is required to reach equilibrium at the new θ_r because the required rate of steam flow will be larger than that for the initial equilibrium state. When flow rate q_m is proportional to e, a new q_m can only be achieved if e is different from zero; thus there must be a steady-state error. Similar reasoning holds for step changes in disturbances. Thus for any initial equilibrium condition, we can 'trim' the system for zero error but subsequent steady commands and/or disturbances must cause steady-state errors.

The steady-state error due to step commands can theoretically be eliminated from proportional control systems by intentionally 'misadjusting' θ_r. For example, for a step input θ_r of size $(1 + K)/K$ with $\theta_a = 0$, we get from Eqn. (4.30):

$$\theta(t) = 1 - e^{-t/\tau};\ \theta_{ss} = \text{steady-state value of } \theta(t) = 1$$

Thus, if we want θ to change by a unit step, we ask for a step input of size $(1 + K)/K$.

This trick does in fact work, but depends upon our knowledge about K. If K is not accurately known or varies, then the trick is not 100% effective. Also, the trick does not help in reducing steady-state errors caused by disturbances. In the next section we will see that the *integral mode* of feedback control removes steady-state errors due to both commands and disturbances and does not depend on the knowledge of specific numerical values for system parameters.

Equations (4.30)–(4.32) indicate that the following aspects of systems behaviour are improved by increasing loop gain:

(i) steady-state tracking accuracy;
(ii) disturbance signal rejection; and
(iii) relative stability, i.e., rate of decay of the transients.

In addition, it can easily be established that increase in loop gain decreases the sensitivity of the system to parameter variations. Thus all aspects of system behaviour are improved by high-gain proportional control. This is, however, true up to a point but cannot be carried to extremes because the system will go unstable. Note that the model of Fig. 4.18 gives no warning of instability[2]. This defect in our model is caused by our neglect of dynamics in some of the system components. We originally neglected these dynamics relative to τ_p, but in the closed-loop system, response speed is determined by τ and not τ_p. Equation (4.30) shows that τ decreases as K is increased and therefore at some point the initially neglected dynamics are no longer

[2]The characteristic equation of the system is (refer Eqn. (4.30))

$$\tau_p s + 1 + K = 0$$

The characteristic root (closed-loop pole) is always in the left half of complex plane.

negligible. Thus, the model of Fig. 4.18 correctly predicts system behaviour, as long as loop gain is not made 'too large'; it is not valid for stability predictions. If we want to make valid stability predictions, we must include enough dynamics in our system model. The next chapter will show that instability will occur for large values of loop gain when the closed-loop system is of order 3 or more.

In addition to neglecting some 'fast' dynamics, the model of Fig. 4.18 further differs from reality because of its perfect linearity, which assumes no limit on the magnitude of corrective control action that can be applied by the system. Actually the amplifier, the electropneumatic transducer, and valve positioner all exhibit saturation, limiting their output when input becomes too large. All aspects of closed-loop system behaviour suffer from saturation.

4.5 INTEGRAL MODE OF FEEDBACK CONTROL

Consider the closed-loop system of Fig. 4.20a. Assume that the initial 'trimming' (zero adjustments) of the control system has been done to obtain $y = r$, with $e = u = 0$. In response to a change in the set-point, the controller must change the flow of energy and/or material to the process in order to achieve equilibrium at the new operating conditions. If the controller is based on proportional logic, then in the new steady-state, a non-zero error e_{ss} must exist to get a non-zero value of control signal u_{ss} (Fig. 4.20b). The new set-point is, say, 10. It will result in a response y_{ss} of less value, say 9.9. The steady-state error is 0.1 and the steady value of the control signal is $0.1K_c$ where K_c is controller gain. The operator must then 'reset' the set-point to bring the output to the desired value of 10.

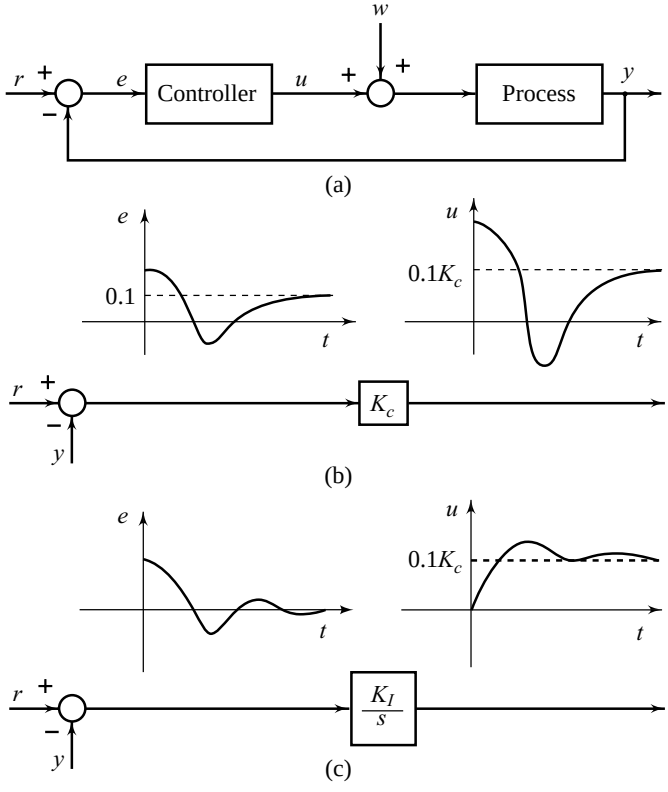

Fig. 4.20 Comparison of proportional and integral control

We need a controller that automatically brings the output to 10 with a set-point of 10, i.e., it gives a steady control signal of value $0.1K_c$ with system error $e_{ss} = 0$. An integrator is capable of exactly this type of behaviour (Fig. 4.20c). Integral control is thus a means of removing steady-state errors without the need for manual reset and, in fact, it is sometimes called *automatic reset*. We shall see that integral control can be used by itself or in combination with other control modes; indeed, PI control is the most common mode (refer Eqns (4.3)):

$$u(t) = K_c \left[e(t) + \frac{1}{T_I} \int_0^t e(t)dt \right] \tag{4.33a}$$

or

$$U(s) = K_c \left(1 + \frac{1}{T_I s} \right) E(s) \tag{4.33b}$$

where T_I is the integral or reset time.

Although integral control is very useful for removing or reducing steady-state errors, it has the undesirable side-effects of degrading stability. Conversion of the proportional control system of Fig. 4.18 to integral control will bring out some general results about integral mode. Suppose we replace the amplifier block K_A by K_I /s. The closed-loop system is then described by the equation

$$\left[(K_t\theta_r(s) - K_t\theta(s)) \frac{K_I}{s} K_e K_x K_v \right] \frac{K_p}{\tau_p s + 1} + \frac{1}{\tau_p s + 1} \theta_a(s) = \theta(s)$$

or

$$(\tau_p s + 1)\theta(s) + \frac{K_t K_I K_e K_x K_v K_p}{s} \theta(s) = \frac{K_t K_I K_e K_x K_v K_p}{s} \theta_r(s) + \theta_a(s)$$

or

$$(\tau_p s^2 + s + K)\theta(s) = K\theta_r(s) + s\theta_a(s) \tag{4.34}$$

where $K \triangleq$ loop gain $= K_t K_I K_e K_x K_v K_p$

For θ_r, step input of size unity (perturbation θ_a held at zero), we get

$$\theta(s) = \left(\frac{K}{\tau_p s^2 + s + K} \right) \frac{1}{s}$$

By final-value theorem, the steady-value of the output is unity, and therefore steady-state error is zero. For step disturbance input $\theta_a(s) = 1/s$ ($\theta_r = 0$), we get

$$\theta(s) = \left(\frac{s}{\tau_p s^2 + s + K} \right) \frac{1}{s} \; ; \; \theta_{ss} = \text{steady-state value of output} = 0$$

Thus, step changes of θ_r and θ_a give zero steady-state errors regardless of the value of loop gain K. The steady-state performance of the system with constant inputs is thus insensitive to parameter variations.

We need to consider what integral control does to the dynamic response. For this we need to look at the characteristic equation corresponding to Eqn. (4.34), which is

$$\tau_p s^2 + s + K = 0.$$

The roots of this equation, which are readily computed, vary as gain K is varied. In fact, it is informative to compute these roots and plot them as a function of K. By quadratic formula of algebra, the roots are

$$s = \frac{-1 \pm \sqrt{1 - 4K\tau_p}}{2\tau_p}$$

and are plotted in Fig. 4.21b for changing values of the gain K. When the gain is zero, the roots are at $-1/\tau_p$ and at 0. As the gain is raised, the roots move closer until there is a double root at $-1/2\tau_p$, and then for higher gains, the roots become complex conjugate.

Recall the case of proportional control; from Eqn. (4.30), we obtain the following characteristic equation:

$$\frac{\tau_p}{1+K}\, s + 1 = 0$$

The root of this equation, $s = -\dfrac{1+K}{\tau_p}$, moves increasingly to the left in the complex plane for increasing values of K (Fig. 4.21a) which implies a decreasing time-constant for the closed-loop system; the larger the loop gain, faster is the rate of decay of transients. With integral control, the rate of decay of transients is dictated by the real root closer to the imaginary axis or real part of the pair of complex conjugate roots. There is obviously a limit on the speed of response; also the response will be oscillatory for large values of K rather than exponential as with proportional control. Due to our too-simple dynamic modelling, instability for large values of loop gain is not predicted.

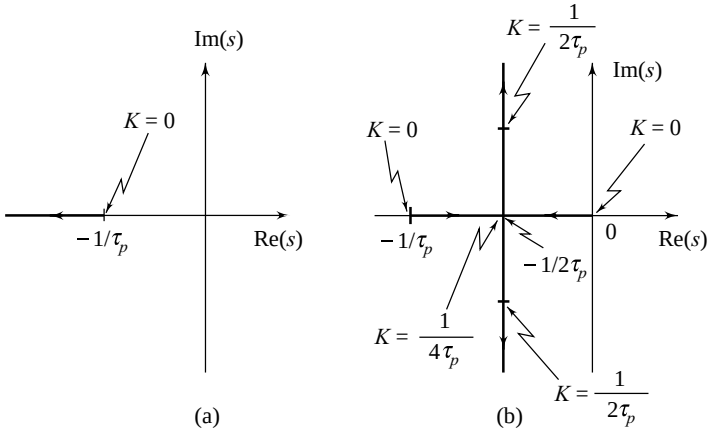

Fig. 4.21 Destabilizing effect of integral control

Example 4.6 Figure 4.22 shows an electro-mechanical servo wherein motor torque T_M controls position θ of inertia J which is subject to torque disturbance T_w. The field time-constant $\tau_f = L_f/R_f$ is negligibly small; K_T is the motor torque constant and K_P is the potentiometer sensitivity.

Notice that integrating effect naturally appears in the system plant. Let us examine whether we need integral control for such a plant. The block diagram in Fig. 4.23 shows the integrating plant with proportional control. The following equation easily follows from this block diagram:

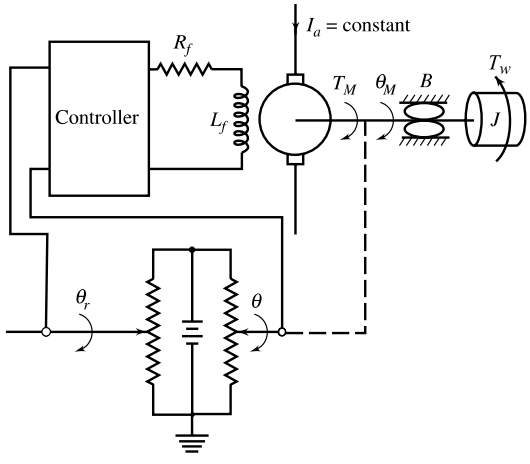

Fig. 4.22 An electromechanical servo

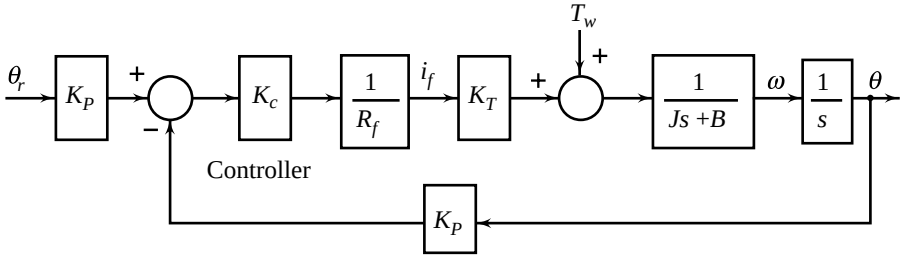

Fig. 4.23 A block diagram of the system in Fig. 4.22

$$[(\theta_r(s)K_P - \theta(s)K_P)K_c(K_T/R_f) + T_w(s)]\frac{1}{Js^2 + Bs} = \theta(s)$$

or
$$(Js^2 + Bs + K)\theta(s) = K\theta_r(s) + T_w(s) \tag{4.35}$$

where
$$K \triangleq \frac{K_P K_c K_T}{R_f} = \text{loop gain}$$

For a unit-step command input with $T_w = 0$, we have $\theta(s) = \left(\frac{K}{Js^2 + Bs + K}\right)\frac{1}{s}$

By final-value theorem, the steady-state value of the output is given by

$$\theta_{ss} = \lim_{s\to 0} s\left(\frac{K}{Js^2 + Bs + K}\right)\frac{1}{s} = 1$$

and therefore, the steady-state error, $e_{ss} = \theta_r - \theta_{ss}$, is zero.

For a unit step disturbance with $\theta_r = 0$, we have $\theta(s) = \left(\frac{1}{Js^2 + Bs + K}\right)\frac{1}{s}$

and the steady-state value of the output is $\theta_{ss} = \frac{1}{K}$.

The plant integrator, thus, gives zero steady-state error for a step command but not for a step disturbance. If we replace the controller gain K_c by $K_c\left(1 + \frac{1}{T_I s}\right)$, and examine the system for steady-state accuracy, we find that the steady-state errors to step commands as well as the step disturbances are zero. Therefore, the location of the integrator relative to disturbance injection points determines its effectiveness in removing steady-state errors. The integrator must be located before the disturbance enters the system if it is to be effective in removing steady-state error due to disturbance; however, location is not significant for steady-state errors caused by commands.

Let us study the effect of the integrator on the stability of the system of Fig. 4.23. With proportional control, the characteristic equation of the system is (refer Eqn. (4.35))

$$Js^2 + Bs + K = 0$$

which has roots in the left-half of the complex plane for all values of K; hence the system is stable for all values of loop gain.

Replacing K_c by $K_c\left(1+\frac{1}{T_I s}\right)$, we get the following characteristic equation:

$$Js^3 + Bs^2 + Ks + K/T_I = 0$$

It is a third-order characteristic equation and, as we shall see in the next chapter, large values of loop gain K lead to instability.

Although controllers with a single integrator are most common, double (and occasionally triple) integrators are useful for the more difficult steady-state error problems; however they require careful stability augmentation. Conventionally, the number of integrators in the forward path has been called the system *type number*; type 0 systems have no integrators, type 1 have one, and so forth. In addition to the number of integrators, their location (relative to disturbance injection points) determines their effectiveness in removing steady-state errors. Detailed treatment of steady-state error analysis will appear in Chapter 6.

4.6 DERIVATIVE MODE OF FEEDBACK CONTROL

Consider the closed-loop system shown in Fig. 4.24. The controller is given the information on system error $e(t)$ and has the task of changing control variable $u(t)$ so as to keep $e(t)$ close to zero. If the control logic is a proportional control action, then the value of u at time t_1 will be same as that at t_2. However, a stronger corrective effort seems appropriate at t_1 and a lesser one at t_2, since at t_1 the error is e_{12} and *increasing*, whereas at t_2 it is again e_{12} but *decreasing*. That is, the controller must sense not only the ordinate of the error curve but also its trend or slope. The slope is clearly de/dt; so to mechanize this desirable control logic, we need a controller sensitive to error derivative. Such a controller can, however, not be used alone since it acts as open circuit for *steady* errors of any size, as at t_3; thus a combination of proportional plus derivative (PD), for example, makes sense (refer Eqns (4.5)):

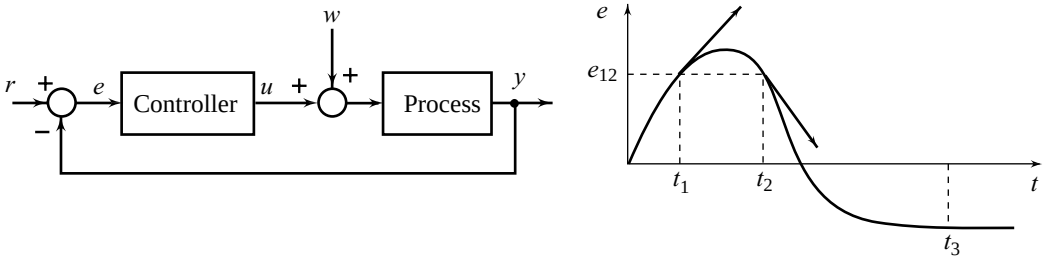

Fig. 4.24 Genesis of derivative control

$$u(t) = K_c\left[e(t) + T_D\frac{de(t)}{dt}\right] \tag{4.36a}$$

or

$$U(s) = K_c\,(1 + T_D s)E(s) \tag{4.36b}$$

where K_c is the controller gain and T_D is the derivative or rate time.

The noise-accentuating characteristics of derivative operations may often require use of approximate (low-pass filtered) derivative signals (refer Section 2.13). This prevents realization of ideal performance but significant system improvement is still often possible. Here we will explore idealized versions of derivative controls in order to make clear their basic characteristics. Later chapters will develop their practical implementation in a more comprehensive way.

Example 4.7 Figure 4.22 shows an electromechanical servo where motor torque T_M controls position θ of inertia J which is subject to torque disturbance T_w. The damper torque on J, due to viscous friction with coefficient B, behaves exactly like a derivative control mode in that it always opposes velocity $d\theta/dt$ with a strength proportional to $d\theta/dt$, making motion less oscillatory. We can therefore, by careful mechanical design, reduce the real friction B to nearly zero and obtain desired damping electronically by introducing derivative control as shown in Fig. 4.25a. The field time-constant $\tau_f = L_f/R_f$ has been assumed to be negligibly small; K_T is the motor torque constant and K_P is the potentiometer sensitivity. The closed-loop system is described by the following equation:

$$[(\theta_r(s)K_P - \theta(s)K_P)K_c(1 + T_D s)(K_T/R_f) + T_w(s)]\frac{1}{Js^2} = \theta(s)$$

or

$$\left(s^2 + \frac{KT_D}{J}s + \frac{K}{J}\right)\theta(s) = \frac{K}{J}(1 + T_D s)\theta_r(s) + \frac{1}{J}T_w(s) \tag{4.37}$$

where

$$K \triangleq \frac{K_P K_c K_T}{R_f} = \text{loop gain.}$$

The second-order characteristic equation is

$$s^2 + 2\zeta\omega_n s + \omega_n^2 = s^2 + \frac{KT_D}{J}s + \frac{K}{J} = 0$$

Therefore

$$\omega_n = \sqrt{\frac{K}{J}}\ ;\ \zeta = \frac{T_D}{2}\sqrt{\frac{K}{J}}$$

If T_D is positive, motor torque is felt by the load in exactly the same way as a mechanical viscous damping torque; the load cannot distinguish between them. The derivative control may therefore be interpreted as pseudo-friction effect.

We now change the system of Fig. 4.25a by using a proportional controller in the forward path and adding derivative mode at the controlled variable θ (Fig. 4.25b). Derivative modes of angular position are extremely common in all kinds of servomechanisms and are usually implemented using a tachogenerator to get a voltage proportional to shaft speed (Fig. 4.25c).

From the block diagram of Fig. 4.25b, we obtain

$$\left[[(\theta_r(s) - \theta(s))K_P K_1 - K_2 s\theta(s)]\frac{K_T}{R_f} + T_w(s)\right]\frac{1}{Js^2} = \theta(s)$$

or

$$\left(s^2 + \frac{K_2 K_T}{JR_f}s + \frac{K_P K_1 K_T}{JR_f}\right)\theta(s) = \frac{K_P K_1 K_T}{JR_f}\theta_r(s) + \frac{1}{J}T_w(s) \tag{4.38}$$

In comparing derivative control applied to system error with that applied to the controlled variable, we see that the effects on the characteristic equation are identical. Error-derivative control, however, has a more violent response to sudden command changes (such as steps) because of the presence of derivative term of θ_r (refer Eqn. (4.37)).

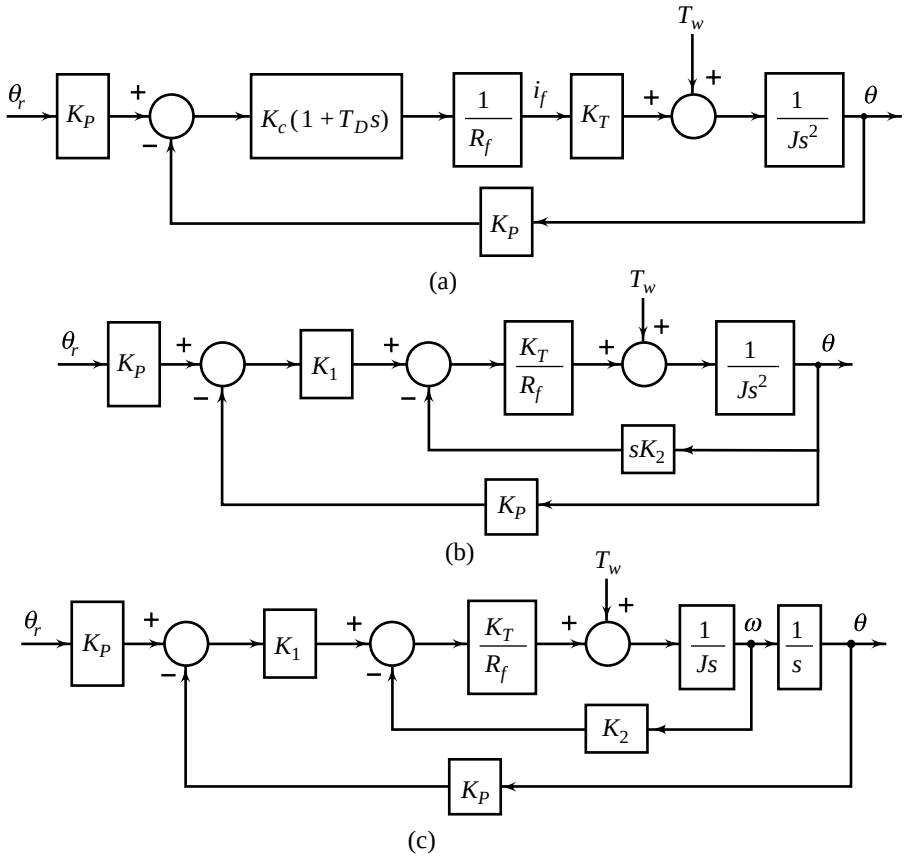

Fig. 4.25 PD control of the system in Fig. 4.22

Let us now study the effect of derivative control on steady-state errors. For a unit-step disturbance with $\theta_r = 0$, the steady-state value of the output, obtained from Eqn. (4.38), is given below.

$$\theta_{ss} = \lim_{s\to 0} s\left[\frac{1/J}{s^2 + (K_2 K_T/JR_f)s + K_P K_1 K_T/JR_f}\right]\frac{1}{s} = \frac{R_f}{K_P K_1 K_T}$$

This constant steady-state error for a step disturbance does not depend on K_2; so this feature of performance is unaffected by the derivative control mode. However, there is an indirect method for possibly gaining some improvement in steady-state accuracy using a PD controller: improvement of relative stability by proper choice of K_2 (derivative mode) allows the use of higher values of K_1 (proportional gain), thereby improving the steady-state accuracy. The benefit obtained this way will however be limited because saturation will prevent the use of large values of K_1.

A suitable combination of the three basic modes—proportional, integral, and derivative (PID)—can improve 'all' aspects (stability, speed of response, and steady-state errors) of system performance and is the most complex method available as an off-the-shelf, general-purpose controller. The 'staying power' of PID control over the years is testimony to the basic soundness of these fundamental control actions.

In the preceding sections, we have introduced the basic control modes. Each of these has its own advantages and drawbacks; thus it should not be surprising that many practical applications are best served by some combinations of the basic modes. In fact, we have already encountered some examples of this. We have considered the idealized versions of the modes so that their essential features could be brought out most clearly without confusing side issues. Practical versions (refer Section 2.13) of these controllers—*lag compensator, lead compensator* etc.—will appear in later chapters.

Review Examples

Review Example 4.1 Figure 4.8 shows the block diagram model of satellite attitude system with proportional control. The closed-loop system is described by the equation

$$[(K_P\theta_r(s) - K_P\theta(s))K_AK_T + T_w(s)]\frac{1}{Js^2} = \theta(s)$$

or
$$(Js^2 + K_PK_AK_T)\theta(s) = K_PK_AK_T\,\theta_r(s) + T_w(s) \tag{4.39}$$

Let us first set the disturbance torque equal to zero and investigate the effects of changes in command θ_r. The closed-loop reference transfer function, obtained from (4.39), is

$$M(s) = \frac{\theta(s)}{\theta_r(s)} = \frac{\omega_n^2}{s^2 + \omega_n^2};\ \omega_n \triangleq (K_PK_AK_T/J)^{1/2} \tag{4.40}$$

The response to a unit step change in θ_r is

$$\theta(t) = 1 - \cos\omega_n t$$

It is obvious that the control system of Fig. 4.8 does not provide a satisfactory response because the oscillations following a change in θ_r do not decay with time. One way of approaching a solution to this problem is to replace the amplifier block K_A by $K_c(1 + T_Ds)$.

This, as we know, is the transfer function of a PD controller with controller gain K_c and derivative time T_D. The closed-loop system with the PD controller is described by the equation

$$[(K_P\theta_r(s) - K_P\theta(s))K_c(1 + T_Ds)K_T + T_w(s)]\frac{1}{Js^2} = \theta(s)$$

or
$$(Js^2 + K_PK_cT_DK_Ts + K_PK_cK_T)\theta(s)$$
$$= K_PK_cK_T(1 + T_Ds)\theta_r(s) + T_w(s) \tag{4.41}$$

The closed-loop reference transfer function is found to be

$$M(s) = \frac{\theta(s)}{\theta_r(s)} = \frac{\omega_n^2(1 + T_Ds)}{s^2 + T_D\omega_n^2 s + \omega_n^2};\ \omega_n = (K_PK_cK_T/J)^{1/2} \tag{4.42}$$

A comparison of Eqn. (4.42) with Eqn. (4.40) reveals two major changes in the reference transfer function of the closed-loop system due to the inclusion of the derivative term. The most important change is that the denominator of Eqn. (4.42) contains a term proportional to s, which means that for $T_D > 0$, the oscillations will be damped out. An increase in value of T_D results in increased damping.

The other difference in the two cases is that $M(s)$ now has closed-loop zero at $s = -1/T_D$ whereas the previous version has no zeros in the finite s-plane. A large value of T_D will result in a violent response to sudden command changes (such as steps) because of the differentiating action of the PD controller.

Thus, although the basic ingredients of the derivative control are favourable for increased damping and reduction of overshoots, the designer still has to design the PD controller properly, otherwise a negative effect could very well result. We will deal with the design problem in later chapters of the book.

Thus far our attention has been directed towards the control system's ability to make the satellite follow the reference pointing angle θ_r. An equally important task for the system is that of reducing the effects of disturbance torque upon the vehicle's orientation. From Eqn. (4.41), we get the following disturbance transfer function:

$$\frac{\theta(s)}{T_w(s)} = \frac{1/J}{s^2 + T_D\omega_n^2 s + \omega_n^2}\ ;\ \omega_n \triangleq (K_P K_c K_T/J)^{1/2}$$

Let us examine the steady-state response to a constant disturbance torque.
Letting $T_w(s) = A/s$, it follows that

$$\theta(s) = \frac{A/J}{s(s^2 + T_D\omega_n^2 s + \omega_n^2)}$$

Provided that $T_D > 0$, the final-value theorem may be applied to $\theta(s)$ in order to find the steady-state component of the pointing angle; the result is

$$\theta_{ss} = \frac{A}{J\omega_n^2} = \frac{A}{K_P K_c K_T}$$

The magnitude of the steady-state offset angle is proportional to the magnitude of the disturbance torque and inversely proportional to the loop gain.

Thus, if the satellite specifications require that it be capable of having no pointing error while subjected to a constant or very low frequency disturbance torque, it is not possible to meet this objective with a PD controller because the loop gain must certainly remain finite. The obvious conclusion is that the structure of the control system must be modified.

One way of approaching a solution to this problem is to replace the PD controller $K_c(1 + T_D s)$ by a PID controller $K_c\left(1 + T_D s + \frac{1}{T_I s}\right)$, where T_I is the integral time. With the PID controller, the closed-loop system of Fig. 4.8 is described by the equation

$$\left[(K_P\theta_r(s) - K_P\theta(s))K_c\left(1 + T_D s + \frac{1}{T_I s}\right)K_T + T_w(s)\right]\frac{1}{Js^2} = \theta(s)$$

or

$$(Js^3 + K_P K_c K_T T_D s^2 + K_P K_c K_T s + K_P K_c K_T/T_I)\theta(s)$$
$$= K_P K_c K_T(T_D s^2 + s + 1/T_I)\theta_r(s) + sT_w(s)$$

or

$$\left(s^3 + T_D\omega_n^2 s^2 + \omega_n^2 s + \frac{1}{T_I}\omega_n^2\right)\theta(s)$$

$$= \omega_n^2(T_D s^2 + s + 1/T_I)\theta_r(s) + \frac{1}{J}sT_w(s);\ \omega_n \triangleq (K_P K_c K_T/J)^{1/2}$$

The disturbance transfer function is

$$\frac{\theta(s)}{T_w(s)} = \frac{s/J}{s^3 + T_D\omega_n^2 s^2 + \omega_n^2 s + \frac{1}{T_I}\omega_n^2}$$

For $T_w(s) = A/s$,

$$\theta_{ss} = \lim_{s\to 0} s\left[\frac{s/J}{s^3 + T_D\omega_n^2 s^2 + \omega_n^2 s + \frac{1}{T_I}\omega_n^2}\right]\frac{A}{s} = 0$$

provided that the transients decay.

Before we can attain the improved steady-state response, we must be assured that the transients will indeed decay, which is to say that the roots of the characteristic equation must lie in the left half of the complex plane. Inspection of the characteristic equation

$$s^3 + T_D\,\omega_n^2\, s^2 + \omega_n^2\, s + \frac{1}{T_I}\omega_n^2 = 0;\ \omega_n = (K_P\, K_c\, K_T/J)^{1/2}$$

reveals that it is possible to meet this requirement by adjusting the parameters K_c, T_D, and T_I.

The task of ascertaining a combination of K_c, T_D, and T_I which, in addition to meeting the stability requirement, results in an acceptable transient response, is not likely to be a simple one. We will deal with this problem in later chapters of this book.

Review Example 4.2 Consider the unity feedback system shown in Fig. 4.26, with the compensator $D(s)$. The system output is y, and the inputs are: r = reference (or command) input; w = disturbance input, and w_n = measurement noise.

Assume that the process model uncertainties are given by the parameters $\boldsymbol{\theta} = [\theta_1, \theta_2, \ldots, \theta_N]^T$, that vary over ranges. Corresponding to nominal parameter vector $\boldsymbol{\theta}_n = [\theta_{n1}, \theta_{n2}, \ldots, \theta_{nN}]^T$, the process transfer function is $G(\boldsymbol{\theta}_n, s)$. The closed-loop input-output behaviour at the nominal working point is given by

$$M(\boldsymbol{\theta}_n, s) = \frac{Y(s)}{R(s)} = \frac{D(s)G(\boldsymbol{\theta}_n, s)}{1 + D(s)G(\boldsymbol{\theta}_n, s)} \tag{4.43}$$

The sensitivity of closed-loop system $M(\boldsymbol{\theta}_n, s)$ to variations in $G(\boldsymbol{\theta}_n, s)$ is given by (refer Eqn. (4.11b))

$$S_G^M = S(\boldsymbol{\theta}_n, s) = \frac{1}{1 + D(s)G(\boldsymbol{\theta}_n, s)} \tag{4.44}$$

Note that

$$S(\boldsymbol{\theta}_n, s) + M(\boldsymbol{\theta}_n, s) = 1 \tag{4.45}$$

As a consequence of this relation, the choice of a particular sensitivity function $S(\boldsymbol{\theta}_n, s)$ directly implies a corresponding unique choice for the function $M(\boldsymbol{\theta}_n, s)$, and *vice versa*. This observation underlines an important factor in design; namely the trade offs that must be made when selecting these two mutually dependent transfer functions. We call the function $M(\boldsymbol{\theta}_n, s)$, a *complimentary sensitivity function*.

For the notational convenience, let us represent sensitivity function $S(\boldsymbol{\theta}_n, s)$ as $S(s)$, plant transfer function $G(\boldsymbol{\theta}_n, s)$ as $G(s)$ and closed-loop transfer function $M(\boldsymbol{\theta}_n, s)$ as $M(s)$. From the block diagram of Fig. 4.26 we may write

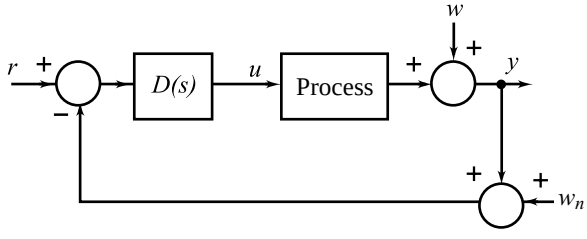

Fig. 4.26 Block diagram of a feedback system including disturbance and measurement noise inputs

$$Y(s) = W(s) + D(s)G(s)[R(s) - Y(s) - W_n(s)]$$

or $$[1 + D(s)G(s)]Y(s) = W(s) + D(s)G(s)R(s) - D(s)G(s)W_n(s)$$

Therefore, the total output of the closed-loop system is

$$Y(s) = \frac{D(s)\,G(s)}{1 + D(s)\,G(s)}\,R(s) + \frac{1}{1 + D(s)\,G(s)}\,W(s) - \frac{D(s)\,G(s)}{1 + D(s)\,G(s)}\,W_n(s) \qquad (4.46)$$

If we define the tracking error as $e = r - y$, we get

$$E(s) = \frac{1}{1 + D(s)\,G(s)}\,R(s) - \frac{1}{1 + D(s)\,G(s)}\,W(s) + \frac{D(s)\,G(s)}{1 + D(s)\,G(s)}\,W_n(s) \qquad (4.47)$$

Finally, the controller output (i.e., the plant input) is given by

$$U(s) = \frac{D(s)}{1 + D(s)\,G(s)}\,R(s) - \frac{D(s)}{1 + D(s)\,G(s)}\,W(s) - \frac{D(s)}{1 + D(s)\,G(s)}\,W_n(s) \qquad (4.48)$$

In the analysis to follow, it will always be assumed that the feedback system is stable; therefore S and M are stable, proper transfer functions. Equations (4.46)–(4.48) may be expressed in terms of sensitivity functions as follows.

$$Y(s) = M(s)R(s) + S(s)W(s) - M(s)W_n(s) \qquad (4.49)$$

$$E(s) = S(s)R(s) - S(s)W(s) + M(s)W_n(s) \qquad (4.50)$$

$$U(s) = D(s)S(s)R(s) - D(s)S(s)W(s) - D(s)S(s)W_n(s) \qquad (4.51)$$

We are now ready to draw the following conclusions from these relations:

1. ***Disturbance rejection:*** $S(s)$ must be kept small to minimize the effect of disturbances. From the definition of S, this can be met if the loop gain is large.
2. ***Tracking:*** $S(s)$ must be kept small to keep the tracking errors small.
3. ***Noise suppression:*** $M(s)$ must be kept small to reduce the effects of measurement noise on the output and error. From the definition of M, this is met if loop gain is small.
4. ***Actuator limits:*** $D(s)S(s)$ must be bounded to ensure that the actuating signal driving the plant does not exceed plant tolerances. Another reason for taking this into consideration is to reduce the control energy so that we can use smaller actuators (such as motors). Note that

$$D(s)S(s) = \frac{D(s)}{1 + D(s)\,G(s)} = \frac{M(s)}{G(s)} \qquad (4.52)$$

Hence, by keeping M small, we can reduce control energy.

Tracking and disturbance rejection require small sensitivity. Noise suppression and reduction in control energy require small complimentary sensitivity. As these two transfer functions add up to unity, we cannot reduce both the transfer functions to zero simultaneously. We can, however, avoid the conflict by noting that in practice, command inputs and disturbances are low-frequency signals (i.e., they vary slowly with time) whereas measurement noise is a high-frequency signal. Therefore we can meet both the objectives by keeping S small in the low-frequency range and M small for high frequencies. Figure 4.27 depicts typical plots of both the sensitivity function and the complimentary sensitivity function that are consistent with our goals.

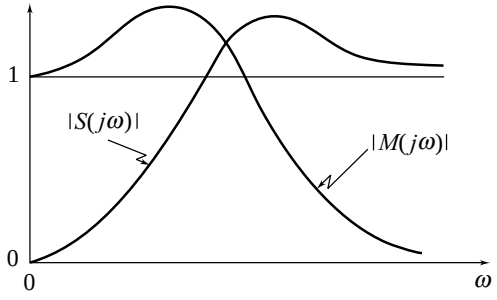

Fig. 4.27 Typical magnitude plots of $S(j\omega)$ and $M(j\omega)$

The intermediate frequencies typically control the dynamic characteristics of the feedback system.

A numerical example will be helpful to illustrate the concepts involved. Assume that the system of Fig. 4.26 has a proportional controller $D(s) = K_c$, and process transfer function

$$G(s) = \frac{0.05K}{s + 0.1}$$

where K has a nominal value of 5.0. The process parameter K is subject to small changes about the nominal value. The closed-loop transfer function of the system is

$$M(s) = \frac{K_c G(s)}{1 + K_c G(s)} = \frac{0.05 K_c K}{s + 0.1 + 0.05 K_c K}$$

The sensitivity of $M(s)$ with respect to K is

$$S_K^M = \frac{s + 0.1}{s + 0.1 + 0.05 K_c K}$$

The sensitivity S_K^M is a function of the complex variables s. For $K = 5.0$, the sensitivity is

$$S_K^M = \frac{s + 0.1}{s + 0.1 + 0.25 K_c}$$

The sensitivity about the nominal value of K, as a function of frequency, is

$$S_K^M(j\omega) = \frac{0.1 + j\omega}{0.1 + 0.25 K_c + j\omega}$$

Figure 4.28 shows these sensitivity functions plotted as a function of frequency for values of the controller gain K_c of 0.4 and 1.0. These values were chosen somewhat arbitrarily.

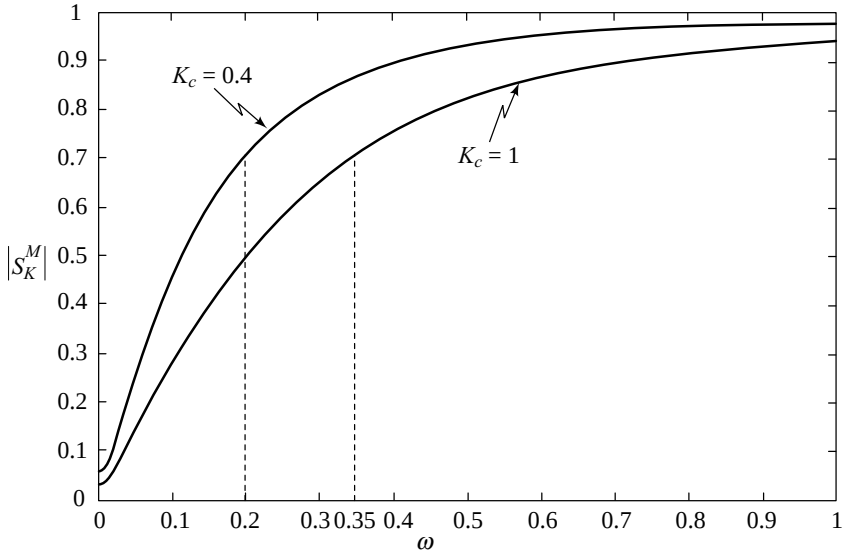

Fig. 4.28 Sensitivity vs frequency graph

Note that the sensitivity of the system transfer function to the gain K is smaller at low frequencies, and the transfer function $M(s)$ primarily passes low frequencies. The bandwidth (refer Fig. 2.22)of the system can be obtained from the transfer function

$$M(j\omega) = \frac{0.25K_c}{0.1+0.25K_c + j\omega}$$

The system gain is reduced to $0.707M(j0)$ at the frequency $\omega = (0.1 + 0.25K_c)$, and thus the bandwidth is $\omega_b = (0.1+ 0.25K_c)$. For $K_c = 0.4$, the bandwidth is $\omega_b = 0.2$ rad/sec; and for $K_c = 1$, $\omega_b = 0.35$ rad/sec. Figure 4.29 shows the plots of $M(j\omega)$ as a function of frequency, with the bandwidths indicated therein.

We can draw the following conclusions form our analysis:

1. The sensitivity of the system to K decreases with increasing loop gain.
2. The system is very sensitive to K outside the system bandwidth, which in general, is not significant.

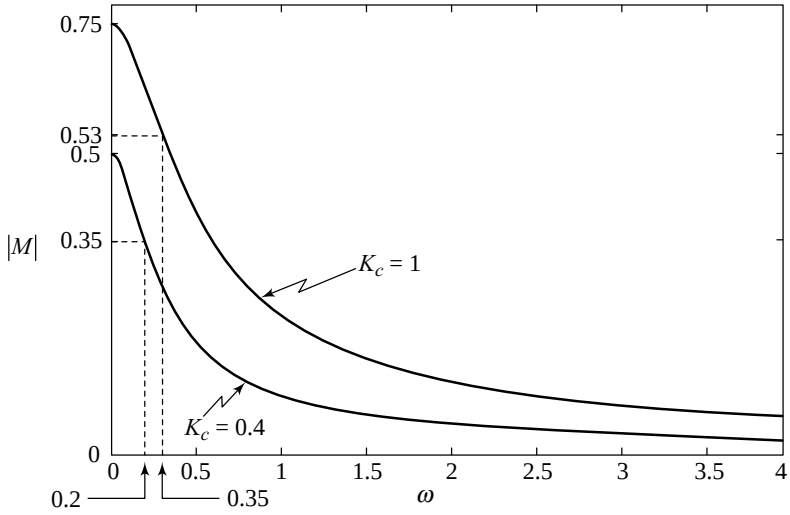

Fig. 4.29 Bandwidth of the system

Putting together the effects of feedback, we arrive at a general desired shape for the loop gain $D(s)G(s)$. This is shown in Fig. 4.30. The general feature of loop gain is that it has high value at low frequencies (for good disturbance rejection) and low value at high frequencies (for noise suppression). The intermediate frequencies typically control the dynamic characteristics of the feedback system.

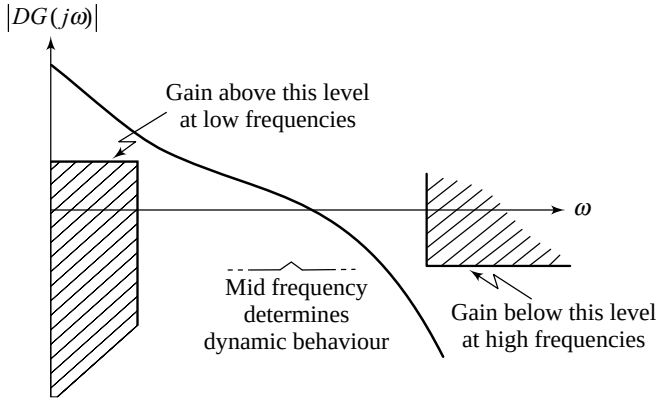

Fig. 4.30 Desirable shape for the loop gain of a feedback system

Review Questions

4.1 Open-loop control action on a stable plant does not run the risk of instability, but negative feedback control action may result in instability problems. Inspite of this fact, most of the industrial control schemes are based on negative feedback concept.Why?

4.2 In designing control systems, the following aspects must be taken into account.

(a) Stability
(b) Input amplitude constraints
(c) Disturbance rejection
(d) Noise filtering
(e) Sensitivity and robustness

Explain the significance of each.

4.3 The use of feedback in control systems is motivated by the presence of external disturbance uncertainties and model uncertainties. The use of feedback can be regarded as unreasonable if there is no uncertainty in the system. Show that feedback control can

(a) greatly reduce the effect on the controlled variable of all external disturbances except those associated with the sensor (measurement system); and
(b) make the system tolerant of variations in hardware parameters other than those of the sensor.

How can we reduce the effects of measurement errors on control system performance?

4.4 Show that high loop gain in feedback systems results in

(i) good steady-state tracking accuracy;
(ii) good disturbance signal rejection;
(iii) low sensitivity to process parameter variations; and
(iv) good relative stability, i.e., rate of decay of transients.

What are the factors limiting the gain?

4.5 The configuration shown in Fig. 4.1 is that of a basic feedback control system, but it is not the only configuration used. In many systems, it is possible and profitable to improve the performance attained with feedback control by using other control configurations. Discuss the use of minor-loop feedback control structure for performance improvement.

4.6 (a) Show with the help of examples that introduction of derivative mode of control in a feedback system with proportional control, makes the system response less oscillatory. What is its effect on steady-state accuracy?
(b) Derivative control may be applied to the system error or the controlled variable. Which scheme do you prefer? Why?
(c) When do we introduce integral mode in a feedback system with proportional-derivative control?

Problems

4.1 The block diagram of a position control system is shown in Fig. P4.1. Determine the sensitivity of the closed-loop transfer function $M(s)$ with respect to G and H, the forward path, and feedback path transfer functions respectively, for $s = j\omega = j1$.

MATLAB Exercise Using MATLAB, plot the sensitivity vs frequency graphs.

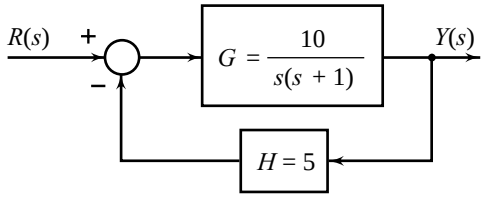

Fig. P4.1

4.2 A servo system is represented by the signal flow graph shown in Fig. P4.2. The nominal values of the parameters are $K_1 = 1$, $K_2 = 5$ and $K_3 = 5$. Determine the overall transmission $Y(s)/R(s)$, and its sensitivity to changes in K_1 under steady dc conditions, i.e., $s = 0$.

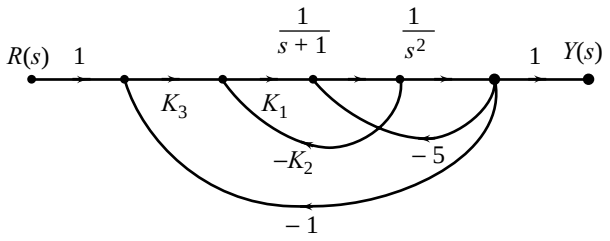

Fig. P4.2

4.3 A unity feedback system has forward path transfer function $G(s) = 20/(s + 1)$. Determine the response of open- and closed-loop systems for unit-step input.

Suppose now that parameter variations occurring during operating conditions cause $G(s)$ to modify to $G'(s) = 20/(s + 0.4)$. What will be the effect on unit-step response of open- and closed-loop systems? Comment upon the sensitivity of the two systems to parameter variations.

MATLAB Exercise After completing the hand calculations, verify your results using MATLAB.

4.4 Consider the two control systems shown in Fig. P4.4. In the open-loop control system, gain K_c is calibrated so that $K_c = 1/10$. In the closed-loop control system, gain K_p of the controller is set so that $K_p = 10$. Find the steady-state error to unit-step input in both the cases.

Suppose now that parameter variations occurring during operating conditions cause $G(s)$ to modify to $G'(s) = 11/(\tau s + 1)$. What will be the effect on the steady-state error of open- and closed-loop systems? Comment upon the sensitivity of the two systems to parameter variations.

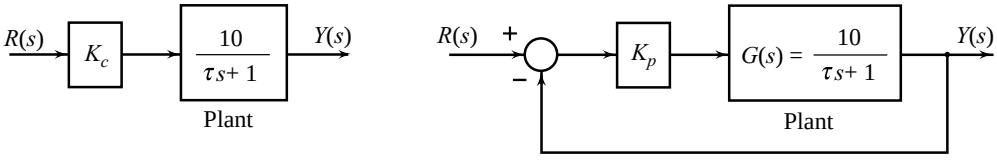

Fig. P4.4

4.5 Consider the system shown in Fig. P4.5, where $w(t)$ is a unit-step disturbance. Calculate K such that the steady-state error in $y(t)$ due to $w(t)$ is less than one percent of $w(t)$.

MATLAB Exercise Using MATLAB, plot the time response to step disturbance. Also obtain the plot in Simulink window.

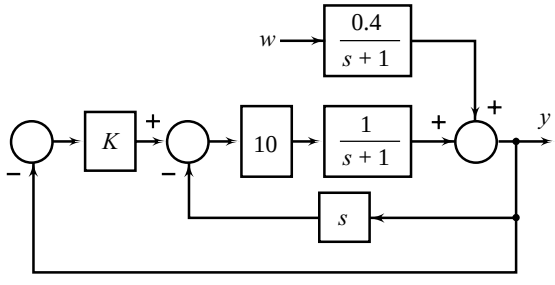

Fig. P4.5

4.6 The two control configurations shown in Fig. P4.6 have identical plants; however, external disturbances enter the two systems at different points along the forward path. Find the steady-state error in the two cases in response to step disturbance of unit magnitude. If in any of the two cases the steady-state error is non-zero, suggest a suitable control scheme to eliminate this error.

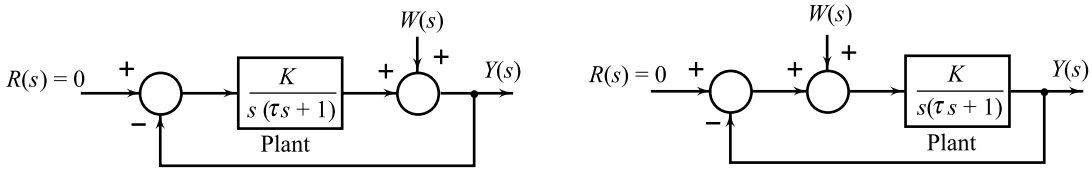

Fig. P4.6

4.7 A temperature control system has the block diagram given in Fig. P4.7. The input signal is a voltage and represents the desired temperature θ_r. Find the steady-state error of the system when θ_r is a unit step function and (i) $D(s) = 1$, (ii) $D(s) = 1 + \frac{0.1}{s}$, (iii) $D(s) = 1 + 0.3s$. What is the effect of the integral term in the PI controller, and derivative term in the PD controller on the steady-state error ?

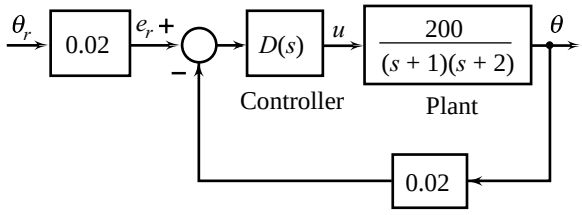

Fig. P4.7

4.8 Consider the closed-loop system of Fig. P4.8. Compute the characteristic equation and therefrom determine the stability of the system when

(i) $D(s) = 1$, (ii) $D(s) = 1 + 2s$, and

(iii) $D(s) = 1 + \frac{2}{s}$.

What is the effect of derivative term in the PD controller, and integral term in the PI controller on system stability?

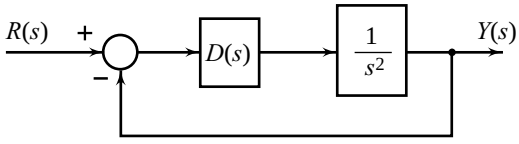

Fig. P4.8

4.9 For the speed control system shown in Fig. P4.9, assume that

(i) generator field time-constant is negligible and its generated voltage is K_g volts/amp;

(ii) friction of the motor and mechanical load is negligible.

(a) Find the time variation of output speed (ω_o) for a sudden command input (ω_r) of 10 rad/sec. Find also the steady-state output speed.

(b) If the feedback loop is opened and gain K_A adjusted to give the same steady-state speed as in the case of closed loop, determine how the output speed varies with time, and compare the speed of response in the two cases.

(c) Compare the sensitivity of $\omega_o(s)/\omega_r(s)$ to changes in amplifier gain K_A and generator speed ω_g with and without feedback.

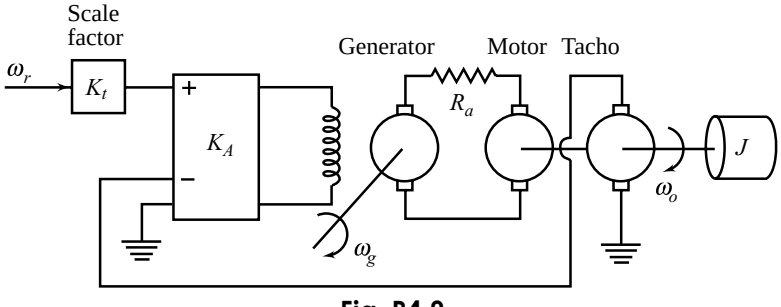

Fig. P4.9

The system parameters are given below:

Moment of inertia of motor and load	$J = 5$ kg-m^2
Motor back emf constant	$K_b = 5$ volts per rad/sec
Total armature resistance of motor and generator	$R_a = 1$ ohm
Generator gain constant	$K_g = 50$ volts/amp
Amplifier gain	$K_A = 5$ amps/volt
Tachogenerator constant	$K_t = 0.5$ volts per rad/sec

4.10 Figure P4.10 shows a control scheme for controlling the azimuth angle of a rotating antenna. The plant consists of an armature-controlled dc motor with dc generator used as an amplifier. The parameters of the plant are given below:

Motor torque constant	$K_T = 1$ N-m/amp
Motor back emf constant	$K_b = 1$ volt/(rad/sec)
Generator gain constant	$K_g = 100$ volt/amp
Potentiometer sensitivity	$K_P = 1$ volt/rad
Amplifier gain	$K_A = 50$ volt/volt
Moment of inertia of load	$J_L = 4$ N-m/(rad/sec^2)

$$\dot{\theta}_L / \dot{\theta}_M = \dot{\theta}_L / \dot{\theta}_C = 1/2;\ R_f = 20\ \Omega,\ L_f = 5\text{H},\ R_a = 1\Omega$$

Load friction, motor inertia and friction are negligible.

The antenna is subject to wind gust torque T_w. Experiments on the antenna show that wind exerts a maximum disturbance of 100 N-m at the antenna.

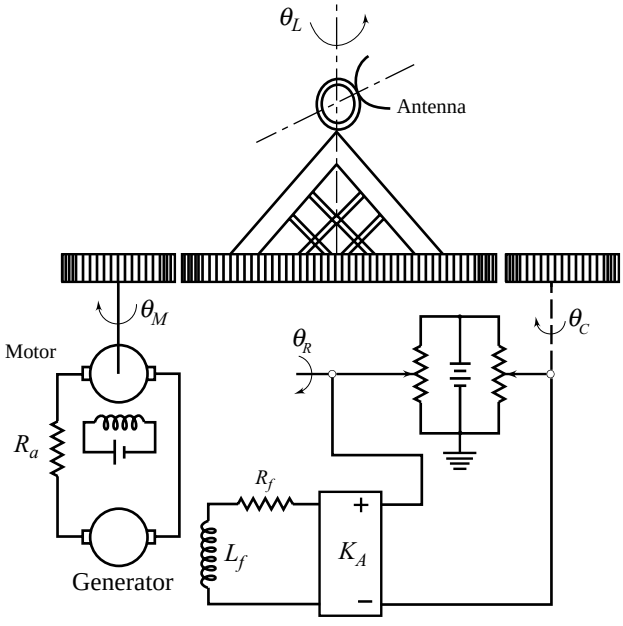

Fig. P4.10

(a) Draw a block diagram of the system showing the variables θ_R, θ_C, θ_M, θ_L, and T_w. Give the transfer function of each block.

(b) Determine the sensitivity of $\theta_L(s)/\theta_R(s)$ to changes in generator gain K_g for $s = j\omega = j0.1$.

(c) Determine the steady-state error in θ_L when the antenna is subjected to a constant wind gust torque of 100 N-m, with the reference position $\theta_R = 0$.

(d) The antenna is required to have steady-state error of less than 0.2°. Propose a control scheme to meet this objective.

MATLAB Exercise Use MATLAB's Simulink to obtain the time response when the antenna is subjected to a constant wind gust torque of 100 N-m, with the reference position $\theta_R = 0$.

4.11 In the system shown in Fig. P4.11, $h(t)$ represents deviation of liquid head from the steady-state value $\bar{H}$ and $q(t)$ represents the deviation of liquid outflow rate from the steady-state value $\bar{Q}$. The pump controls the liquid head/outflow rate by supplying liquid at a rate $\bar{Q}_i + q_i(t)$; $q_i(t) = -K[h(t) - h_r(t)]$, where K is a constant and $h_r(t)$ is the desired change in the initial set-point value.

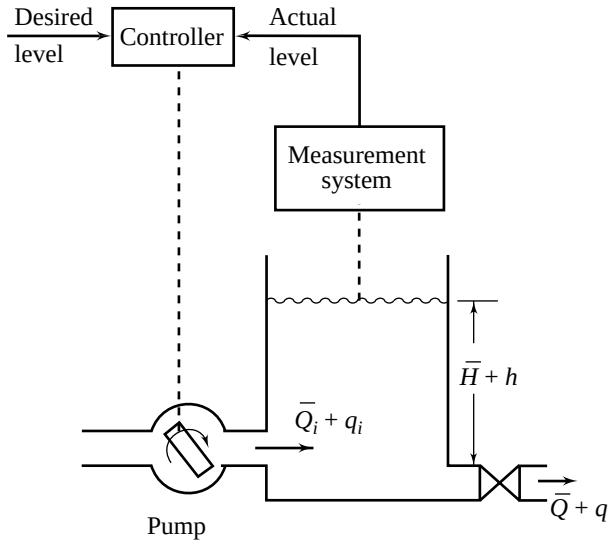

Fig. P4.11

(a) Prove that the following equation represents perturbation dynamics:

$$RC\frac{dh(t)}{dt} + h(t) = R\,q_i(t)$$

where R is a constant so that $q(t) = h(t)/R$, and C = cross-sectional area of the tank.

(b) Draw a block diagram of the closed-loop system showing the variables h_r, q_i, h and q.

(c) Determine the sensitivity of the closed-loop transfer function $H(s)/H_r(s)$ to changes in the parameter R under steady dc conditions, i.e., $s = 0$.

(d) Determine the steady-state error for a unit-step command $h_r(t)$. Explain what modification could be made in the system to eliminate the steady-state error to step input. What is the effect of the proposed modification on system sensitivity to changes in R under steady dc conditions?

4.12 The temperature control system of Fig. P4.12 is set up to produce a steady stream of hot liquid at a controlled temperature. The liquid enters at a constant flow rate Q and variable temperature $\bar{\theta}_i + \theta_i$, and leaves at constant flow rate Q with temperature $\bar{\theta} + \theta$. The temperature of the outflowing liquid is measured by means of a thermocouple which produces an output voltage proportional to the temperature of the outflowing liquid ($e_t = K_t\theta$). This voltage is subtracted from the reference voltage to generate an error signal which in turn regulates the heating rate produced by electrical resistance heater controlled by an SCR amplifier.

The perturbation dynamics of the temperature control system is described by the equation

$$K(e_r - e_t) = C\frac{d\theta}{dt} + \frac{\theta - \theta_i}{R_1}$$

where

C = thermal capacitance of the liquid in the tank; (Joules/ °C)
R_1 = thermal resistance of the carrier fluid; (°C/(Joules/sec))
K = gain of the SCR amplifier-heater circuit; ((Joules/sec)/volt).

(a) Draw a block diagram of the closed-loop system showing reference voltage, e_r, disturbance in temperature, θ_i, and the controlled temperature, θ.

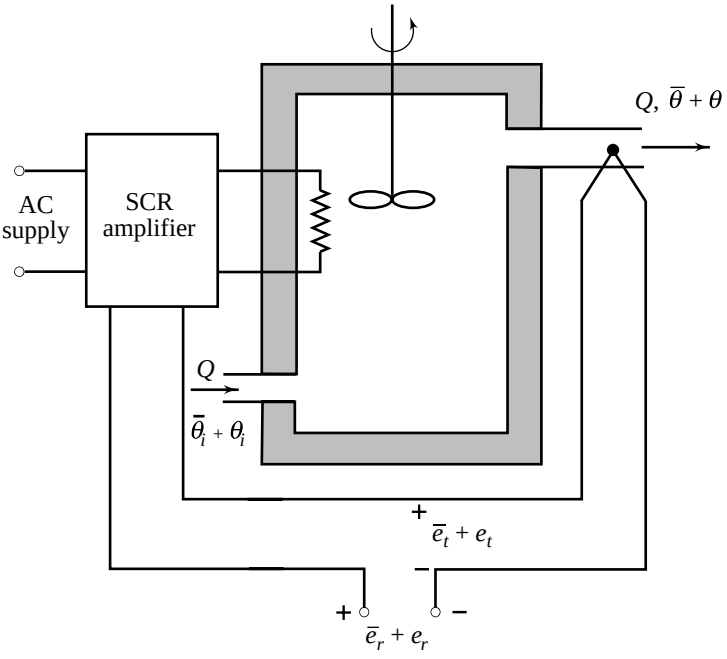

Fig. P4.12

(b) Compare the open-loop ($K_t = 0$) and the closed-loop systems for (i) sensitivity to changes in parameter K, (ii) the ability to reduce the effects of step disturbance θ_i, and (iii) the system time-constants in the two cases.

(c) Modify the block diagram of part (a) to include the effect of the disturbance signal θ_a caused by changes in the ambient temperature. Find the steady change in the temperature of the outflowing liquid for open- and closed-loop cases due to a unit-step disturbance θ_a. The surface area of the tank is A m^2, and the heat transfer coefficient of the tank-air interface is U Joules/(m^2)(°C) (sec).

4.13 Figure P4.13 shows a field-controlled dc motor with a dc amplifier. The parameters of the system are given below:

Amplifier gain	$K_A = 50$ volt/volt
Motor field resistance	$R_f = 99\ \Omega$
Motor field inductance	$L_f = 20$ H
Motor torque constant	$K_T = 10$ N-m/amp
Moment of inertia of load,	$J = 0.5$ N-m/(rad/sec^2)

Coefficient of viscous friction of load, $B = 0.5$ N-m/(rad/sec)

Motor inertia and friction are negligible.

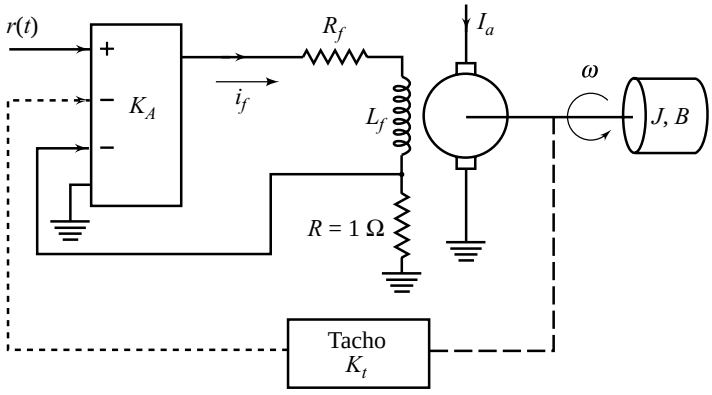

Fig. P4.13

(a) The time-constant of devices with high inductance, such as the field-controlled dc motor, is too long for design requirements. Current feedback may be used to decrease the time-constant. For the system of Fig. P4.13, determine the time-constant of the field circuit with and without current feedback.

(b) Now add a speed-feedback loop (shown dotted in Fig. P4.13) around the current-feedback loop and obtain the closed-loop transfer function of the system.

(c) Modify the system of part (b) to convert it into a position control system. Use both the current-feedback and the speed-feedback loops in the modified scheme.

4.14 Figure P4.14 shows a position control system.

(a) Compute the values of K_c and T_D so that the characteristic equation of the closed-loop system will have roots at $-1 \pm j1.732$.

(b) We know that it is advantageous to avoid derivative action on the error signal if it is possible to obtain equivalent effect with an alternative control configuration. Suggest an alternative control scheme that results in the same characteristic roots of closed-loop system as in part (a) and avoids derivative action on the error signal.

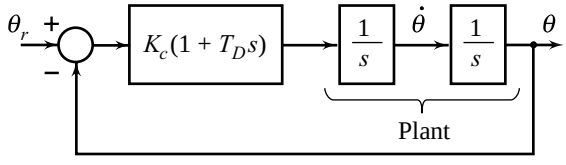

Fig. P4.14

4.15 Figure P4.15a shows the block diagram of a dc servomechanism. Determine the sensitivity of the closed-loop transfer function $M(s)$ to the variations in K at $\omega = 5$ rad/sec. The nominal value of $K = 1$. Change the control configuration of the system to two-loop configuration with feedback of θ and $\dot{\theta}$ (see Fig. P4.15b); the closed-loop transfer function of the two-loop configuration must be equal to that of the system shown in Fig. P4.15a. Obtain sensitivity of $M(s)$ to variations in K at $\omega = 5$ for the new configuration. Comment on the result.

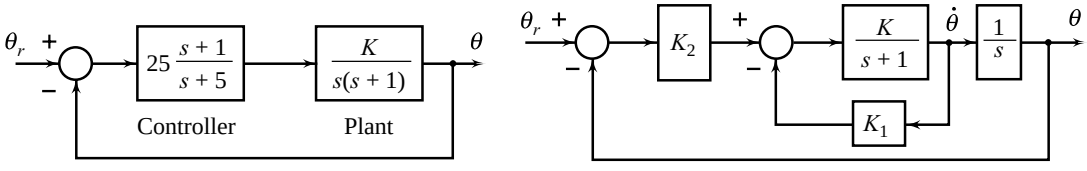

Fig. P4.15

MATLAB Exercise Using MATLAB, plot the sensitivity vs frequency graphs.

4.16 **MATLAB/Simulink Exercise** Consider a heating control system with the plant model

$$Y(s) = \frac{0.3}{2s+1}U(s)$$

The input signal $U(s)$ is the power in kW from the heater and the output signal $Y(s)$ is the resulting temperature. The time-constant of the process is 2 hrs. The sensor has a very short time-constant in comparison to the process time-constant; so we can model the system as a unity feedback system (Fig. P4.16). The step reference signal $R(s) = 1/s$, and the constant load disturbance effect is modelled as $W(s) = 0.5/s$.

Using MATLAB/Simulink, plot the time response to reference and disturbance inputs for different values of K_c. Also plot the signal $u(t)$ for these values of K_c. Comment upon the effects of increasing the values of K_c on transient response and steady-state error, and also on the required control signal.

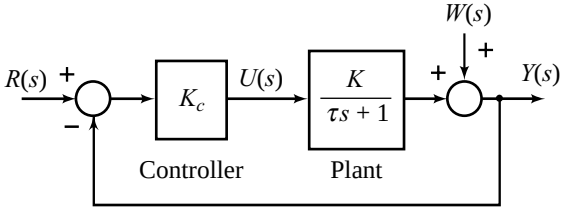

Fig. P4.16

4.17 **MATLAB/Simulink Exercise** Reconsider the heating control system that was simulated in Problem 4.16 for proportional control. We replace the proportional controller K_c by integral controller K_I/s. Plot the closed-loop system response to command and disturbance signals for $K_I = 0.25$, 0.417, and 1.8. Comment upon the effects of increasing K_I on transient response and steady-state error. Through simulations, examine the effect on transient performance when the integral controller is replaced by a PI controller $K_c + K_I/s$, with fixed proportional gain $K_c = 4$.

4.18 **MATLAB/Simulink Exercise** Consider a position control system shown in Fig. P4.18. The reference signal is a unit step ($R(s)=1/s$) and we model the constant load disturbance by $W(s) = 0.5/s$. A PD controller with a fixed proportional gain $K_c = 0.2$ is used. Plot output response to command and disturbance for $K_D = 0.2$, and 1.22. Comment on the effect of K_D on transient and steady-state performance.

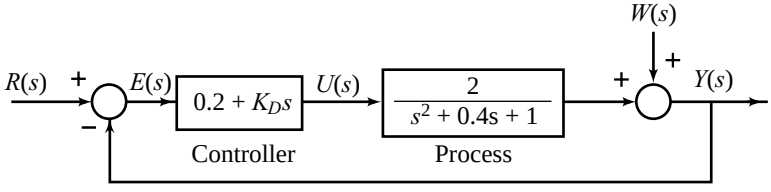

Fig. P4.18

4.19 **MATLAB/Simulink Exercise** Consider two control structures of a position control system, shown in Figs P4.19. Plot the response of the two structures to a reference input of $\theta_r = 0.1$ occurring at $t = 0.5$ seconds and comment on the results.

Observe the control signal trace in these structures. You will find high control-signal magnitudes which are not very desirable. Going for a PID control structure is one solution to this problem. Find appropriate values of PID parameters through simulations.

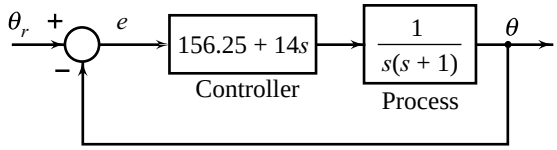

(a)

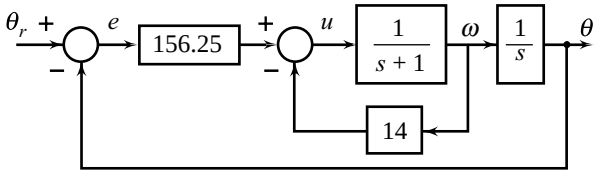

(b)

Fig. P4.19

4.20 **MATLAB Exercise** A unity-feedback system has open-loop transfer function

$$G(s) = \frac{10}{s(1 + 0.1s)(1 + 0.05s)}$$

Find the sensitivity of the closed-loop transfer function with respect ot G. Plot the sensitivity vs frequency graph and therefrom determine the peak sensitivity and the frequency at which it occurs.

5 Concepts of Stability and the Routh Stability Criterion

5.1 INTRODUCTION

Roughly speaking, stability in a system implies that small changes to the system stimulus do not result in large effects on system response. Stability is a very important characteristic of the transient performance of a system. Almost every working system is designed to be stable. Within the boundaries of parameter variations permitted by stability considerations, we can then seek to improve the system performance.

In testing the stability of a dynamic system we must carefully define the terms 'response', 'stimulus', 'small change', and 'large effect'. For example, it is possible for a system to have a well-behaved output while an internal variable (state variable) is growing without bound. If we consider only the output as the 'response', we might call such a system stable. However, if we consider the state variables to be the response, we might just as reasonably call this system unstable. The stimulus might be a signal persisting for all time, or it might be only a set of initial conditions. Finally, we might require that the response not grow if the stimulus is removed, or we might require that the response go to zero if the stimulus is removed. For systems that are nonlinear or time-varying, the number of definitions of stability is large, and some of the definitions can be quite complicated in order to account for the varieties of the responses the systems can display. We will describe a few elementary results, particularly those useful in the study of linear time-invariant systems.

Consider an n-dimensional linear time-invariant system described by a state variable model of the form (refer Eqns (2.4))

$$\dot{\mathbf{x}}(t) = \mathbf{A}\mathbf{x}(t) + \mathbf{b}r(t);\ \mathbf{x}(t=0) \triangleq \mathbf{x}^0$$
$$y(t) = \mathbf{c}\mathbf{x}(t) + du(t) \tag{5.1}$$

where $\mathbf{x}$ is the $n \times 1$ state vector, r is the scalar input, y is the scalar output, $\mathbf{A}$ is $n \times n$ real constant matrix, $\mathbf{b}$ and $\mathbf{c}$ are, respectively, $n \times 1$ and $1 \times n$ real constant vectors, and d is a constant scalar.

The system (5.1) has two sources of excitation:

(i) the initial state $\mathbf{x}^0$ representing initial internal energy storage; and
(ii) external input $r(t)$; $t \geq 0$.

In the stability study, we are generally concerned with the following questions:

1. If the system is relaxed ($\mathbf{x}^0 = \mathbf{0}$), will a bounded input $r(t)$; $t \geq 0$, produce a bounded output $y(t)$ for all t (regardless of what goes on inside the system)?
2. A relaxed system ($\mathbf{x}^0 = \mathbf{0}$) with input $r(t) = 0$; $t \geq 0$, will continue to be in the zero state for all time. This condition can be viewed as the *equilibrium state* of the system: the system is said to be in equilibrium state $\mathbf{x}^e = \mathbf{0}$ when both the initial internal energy storage and the external input are zero.

Taking changes in initial conditions as the stimulus and system state $\mathbf{x}(t)$ as the response, we pose the following question:

If the system with zero input ($r(t) = 0$; $t \geq 0$) is perturbed from its equilibrium state $\mathbf{x}^e = \mathbf{0}$ at $t = 0$, will the state $\mathbf{x}(t)$ return to $\mathbf{x}^e$, remain 'close' to $\mathbf{x}^e$, or diverge from $\mathbf{x}^e$?

The first notion of stability is concerned with the boundedness of the output of a relaxed system in response to bounded input, and is called *bounded-input, bounded-output* (BIBO) *stability*. Clearly, if a system is subjected to an unbounded input and produces an unbounded response, nothing can be said about its stability. However, if it is subjected to a bounded input and produces an unbounded response, it is, by definition, unstable. Actually the output of an unstable system may increase to a certain extent and then the system may break down or become nonlinear, after the output exceeds a certain magnitude, so that the linear mathematical model no longer applies.

The second notion of stability is concerned with the boundedness of the state of free (unforced) system in response to arbitrary initial state, and is called *zero-input stability*.

As we shall see in this chapter, the two notions of stability defined above are essentially equivalent in linear time-invariant systems. Simple and powerful tools are available to determine the stability of such systems.

In nonlinear systems, there is no definite correspondence between the two notions. For a free stable nonlinear system, there is no guarantee that the output will be bounded whenever input is bounded. Also, if the output is bounded for a particular input, it may not be bounded for other inputs. Most of the important results obtained thus far concern the stability of nonlinear systems in the sense of the second notion above, i.e., when the system has no input. It may be noted that even for this class of nonlinear systems, the concept of stability is not clear cut. System behaviour for small deviations about the equilibrium point may be different from that for large deviations. Also because of possible existence of multiple equilibrium states in nonlinear systems, the system may move away from one equilibrium state to the other as time progresses.

Another important point to be kept in mind is that when oscillations occur in free linear time-invariant systems, the amplitude of the oscillations is not fixed; it changes with the size of the initial conditions. Slight changes in system parameters will destroy the oscillations. In nonlinear systems, on the other hand, there can be oscillations that are independent of the size of initial conditions and these oscillations (*limit cycles*) are usually much less sensitive to parameter variations. Limit cycles of fixed amplitude and period can be sustained over a finite range of system parameters.

Chapter 14 highlights the problems associated with nonlinear control systems, and presents commonly used analysis tools. In this chapter, we concern ourselves exclusively with the stability of linear time-invariant systems.

5.2 BOUNDED-INPUT BOUNDED-OUTPUT STABILITY

A linear relaxed system (initial conditions zero) is said to have BIBO stability if every bounded input results in a bounded[1] output. A test for this property is readily found using convolution (refer Section 2.3). If the system has input $r(t)$, output $y(t)$, and impulse response $g(t)$, then

$$y(t) = \int_0^\infty g(\tau)\, r(t-\tau) d\tau \tag{5.2}$$

If $r(t)$ is bounded, there exists a constant M such that $|\, r(t)\,| \le M < \infty$, and the output is bounded by

$$|y(t)| = \left| \int_0^\infty g(\tau)\, r(t-\tau) d\tau \right| \tag{5.3}$$

Since the absolute value of an integral is not greater than the integral of the absolute value of the integrand, Eqn. (5.3) may be written as

$$|y(t)| \le \int_0^\infty |g(\tau)\, r(t-\tau)|\, d\tau \le \int_0^\infty |g(\tau)|\,|r(t-\tau)|\, d\tau \le M \int_0^\infty |g(\tau)|\, d\tau$$

Therefore, the output will be bounded if

$$\int_0^\infty |\, g(\tau)|\, d\tau < \infty \tag{5.4}$$

The condition given by (5.4) is *sufficient* to guarantee BIBO stability. This condition is also *necessary*, for if we consider the bounded input

$$r(t-\tau) = \begin{cases} +1 & \text{if } g(\tau) > 0 \\ 0 & \text{if } g(\tau) = 0 \\ -1 & \text{if } g(\tau) < 0 \end{cases}$$

then the output at any fixed value of t is given by

$$|y(t)| = \left| \int_0^\infty g(\tau)\, r(t-\tau) d\tau \right| = \int_0^\infty |g(\tau)|\, d\tau$$

Thus, unless the condition given by (5.4) is true, the system is not BIBO stable.

We, therefore, conclude that a system with impulse response $g(t)$ is BIBO stable if and only if the impulse response is absolutely integrable, i.e., $\int_0^\infty |g(\tau)|\, d\tau$ is finite (area under the absolute-value curve of the impulse response $g(t)$ evaluated from $t = 0$ to $t = \infty$ must be finite).

We shall now show that the requirement (5.4) on the impulse response for BIBO stability can be linked to the restrictions on the poles of the transfer function $G(s)$, given by

[1] A function $f(t)$ is said to be bounded if its magnitude does not go to infinity in the tme interval $[0, \infty)$, or equivalently there exists a real constant M such that $|f(t)| \le M < \infty$ for all t in $[0, \infty)$.

$$G(s) = \frac{Y(s)}{R(s)} = \frac{b_0 s^m + b_1 s^{m-1} + \cdots + b_{m-1} s + b_m}{a_0 s^n + a_1 s^{n-1} + \cdots + a_{n-1} s + a_n} \; ; m \le n \tag{5.5}$$

The nature of $g(t) = \mathscr{L}^{-1}[G(s)]$ is dependent on the roots of the characteristic equation

$$\Delta(s) = a_0 s^n + a_1 s^{n-1} + \cdots + a_{n-1} s + a_n = 0 \tag{5.6}$$

i.e., the poles of the transfer function $G(s)$. These poles may be both real and complex-conjugate, and may have multiplicity of various orders.

Consider a second-order system

$$\frac{Y(s)}{R(s)} = G(s) = \frac{1}{s^2 + a_1 s + a_2}$$

For impulse input, $R(s) = 1$. Therefore, response transform

$$Y(s) = \frac{1}{s^2 + a_1 s + a_2}$$

The impulse response of the system is given by

$$y(t) = g(t) = \mathscr{L}^{-1}\left[\frac{1}{s^2 + a_1 s + a_2}\right]$$

Assume that the poles of the response transform $Y(s)$ are real and distinct:

$$s^2 + a_1 s + a_2 = (s - \alpha_1)(s - \alpha_2)$$

Partial fraction expansion of $Y(s)$ is then of the form

$$Y(s) = \frac{A_1}{s - \alpha_1} + \frac{A_2}{s - \alpha_2}$$

where A_1 and A_2 are real constants.

This gives

$$y(t) = A_1 e^{\alpha_1 t} + A_2 e^{\alpha_2 t}$$

The time functions $e^{\alpha_1 t}$ and $e^{\alpha_2 t}$ are the response functions contributed by the system poles at $s = \alpha_1$ and $s = \alpha_2$, respectively. These time functions dictate the qualitative nature of the impulse response of the system. A time function $e^{\alpha t}$ is either a constant or a growing or decaying exponential depending on whether $\alpha = 0$, $\alpha > 0$, or $\alpha < 0$, respectively, as sketched in Fig. 5.1.

For complex-conjugate pole pair at $s = p = \sigma + j\omega$ and $s = p^* = \sigma - j\omega$ of $Y(s)$, the response $y(t)$ is obtained as follows:

$$Y(s) = \frac{A}{s - p} + \frac{A^*}{s - p^*}$$

where $A = |A| \angle \phi$, and A^* is complex-conjugate of A.

$$\begin{aligned} y(t) &= Ae^{pt} + A^* e^{p^* t} = Ae^{pt} + (Ae^{pt})^* = 2\,\mathrm{Re}[Ae^{pt}] \\ &= 2\,\mathrm{Re}[|A|\, e^{j\phi} e^{\sigma t} e^{j\omega t}] = 2\,|A| e^{\sigma t}\,\mathrm{Re}[e^{j(\omega t + \phi)}] \\ &= 2\,|A| e^{\sigma t} \cos(\omega t + \phi) \end{aligned} \tag{5.7}$$

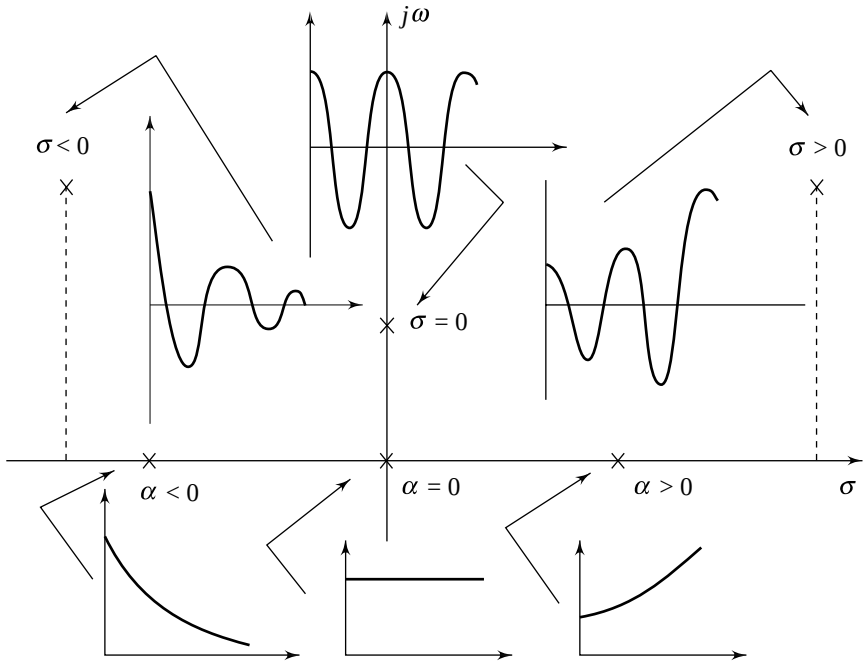

Fig. 5.1 Time functions associated with poles in the s-plane

Therefore, the complex-conjugate pair of poles of the response transform $Y(s)$ gives rise to a sinusoidal or oscillatory response whose envelope $2|A|e^{\sigma t}$ can be constant, growing or decaying depending on whether $\sigma = 0$, $\sigma > 0$, or $\sigma < 0$, respectively, as sketched in Fig. 5.1.

For an nth-order linear system, the response transform $Y(s)$ has an nth-order characteristic polynominal. Assume that $Y(s)$ has real pole at $s = \alpha$ of multiplicity m, and partial fraction expansion of $Y(s)$ is of the form

$$Y(s) = \frac{A_{1(m)}}{(s-\alpha)^m} + \frac{A_{1(m-1)}}{(s-\alpha)^{m-1}} + \cdots + \frac{A_{12}}{(s-\alpha)^2} + \frac{A_{11}}{(s-\alpha)} + \cdots$$

where $A_{1(m)}, \ldots, A_{12}, A_{11}$ are real constants.

Response function contributed by the real pole of multiplicity m can be evaluated as follows:

Consider the transform pair

$$\frac{1}{s-\alpha} \leftrightarrow e^{\alpha t}$$

Using Eqn. (2.33)

$$-\frac{d}{ds}\left(\frac{1}{s-\alpha}\right) \leftrightarrow te^{\alpha t} \text{ or } \frac{1}{(s-\alpha)^2} \leftrightarrow te^{\alpha t}$$

Performing differentiation once again,

$$\frac{1}{(s-\alpha)^3} \leftrightarrow \frac{1}{2!}t^2e^{\alpha t}$$

In general,

$$\frac{1}{(s-\alpha)^m} \leftrightarrow \frac{1}{(m-1)!} t^{m-1} e^{\alpha t}$$

It can easily be established using final-value theorem (Eqn. (2.45)) that the response function $[1/(m-1)!]$ $t^{m-1}e^{\alpha t}$ equals zero as $t \to \infty$ if $\alpha < 0$. However, the response function grows without bound for $\alpha \geq 0$.

Similar conclusions can be derived in case of response functions corresponding to complex-conjugate pair of poles $(\sigma \pm j\omega)$ of multiplicity m. The limit of each response function as $t \to \infty$ equals zero if $\sigma < 0$. The case of $\sigma \geq 0$ contributes growing response functions.

From the foregoing discussion it follows that the nature of response terms contributed by the system poles (i.e., the poles of the transfer function $G(s)$) gives the nature of the impulse response $g(t) = \mathscr{L}^{-1}[G(s)]$ of the system, and hence answers the question of BIBO stability through condition (5.4) which says that for a system with transfer function $G(s)$ to be BIBO stable, it is necessary and sufficient that $\int_0^\infty |g(\tau)|\, d\tau < \infty$.

Our observations lead us to the following general conclusions on BIBO stability.

1. If all the roots of the characteristic equation lie in the left half of the s-plane, then the impulse response is bounded and eventually decays to zero. Therefore $\int_0^\infty |g(\tau)|\, d\tau$ is finite and the system is BIBO stable.
2. If any root of the characteristic equation lies in the right half of the s-plane, $g(t)$ grows without bound and $\int_0^\infty |g(\tau)| d\tau$ is infinite. The system is therefore unstable.
3. If the characteristic equation has repeated roots on the $j\omega$-axis in the s-plane, $g(t)$ grows without bound and $\int_0^\infty |g(\tau)| d\tau$ is infinite. The system is therefore unstable.
4. If one or more non-repeated roots of the characteristic equation are on the $j\omega$-axis in the s-plane, then $g(t)$ is bounded but $\int_0^\infty |g(\tau)| d\tau$ is infinite. The system is therefore unstable.

An exception to the definition of BIBO stability is brought out by the following observations.

Consider a system with transfer function

$$G(s) = \frac{N(s)}{s(s - j\omega)\,(s + j\omega)}$$

The system has non-repeated poles on the $j\omega$-axis in the s-plane. The response functions contributed by the poles at $s = 0$, and $s = \pm j\omega$ are, respectively, A_1, and $A_2\cos(\omega t + \phi)$, where A_1 and A_2 are real constants. The terms A_1 and $A_2\cos(\omega t + \phi)$ are bounded, $\int_0^\infty |g(\tau)| d\tau$ is infinite and the system is unstable in the sense of our definition of BIBO stability.

Careful examination of the input–output relation

$$Y(s) = G(s)R(s) = \frac{N(s)}{s(s - j\omega)(s + j\omega)} R(s)$$

shows that $y(t)$ is bounded for all bounded $r(t)$ unless the input has a pole matching one of the system poles on the $j\omega$-axis. For example, for a unit step input $r(t) = \mu(t)$,

$$R(s) = \frac{1}{s}, \text{ and } Y(s) = \frac{N(s)}{s^2(s - j\omega)(s + j\omega)}$$

The response $y(t)$ is a linear combination of the terms A_3, $A_4 t$ and $A_5\cos(\omega t + \phi)$, and therefore $y(t) \to \infty$ as $t \to \infty$. Such a system which has bounded output for all bounded inputs except for the inputs having poles matching the system poles, may be treated as acceptable or non-acceptable. We will bring the situations where the system has non-repeated poles on the $j\omega$-axis under the class of *marginally stable systems.*

5.3 ZERO-INPUT STABILITY

This concept of stability is based on the dynamic evolution of the system state in response to the arbitrary initial state representing initial internal energy storage. State variable model[2] (refer Eqns (5.1))

$$\dot{\mathbf{x}}(t) = \mathbf{A}\mathbf{x}(t);\ \mathbf{x}(t = 0) \triangleq \mathbf{x}^0 \tag{5.8}$$

is most appropriate to study dynamic evolution of the state $\mathbf{x}(t)$ in response to the initial state $\mathbf{x}(0)$.

We may classify stability as follows:

1. *Unstable*: There is at least one finite initial state $\mathbf{x}(0)$ such that $\mathbf{x}(t)$ grows thereafter without bound as $t \to \infty$.
2. *Asymptotically stable:* For all possible initial states $\mathbf{x}(0)$, $\mathbf{x}(t)$ eventually decays to zero as $t \to \infty$.
3. *Marginally stable:* For all initial states $\mathbf{x}(0)$, $\mathbf{x}(t)$ remains thereafter within finite bounds for $t > 0$.

Taking Laplace transform on both the sides of Eqn. (5.8), yields (refer Eqn. (2.42a))

$$s\mathbf{X}(s) - \mathbf{x}(0) = \mathbf{A}\mathbf{X}(s)$$

where $$\mathbf{X}(s) \triangleq \mathscr{L}[\mathbf{x}(t)].$$

Solving for $\mathbf{X}(s)$, we get ($\mathbf{I}$ is a unit (identity) matrix)

$$\mathbf{X}(s) = (s\mathbf{I} - \mathbf{A})^{-1}\mathbf{x}(0) = \mathbf{\Phi}(s)\mathbf{x}(0)$$

where $$\mathbf{\Phi}(s) = (s\mathbf{I} - \mathbf{A})^{-1} = \frac{(s\mathbf{I} - \mathbf{A})^{+}}{|s\mathbf{I} - \mathbf{A}|} = \frac{adj(s\mathbf{I} - \mathbf{A})}{det(s\mathbf{I} - \mathbf{A})}$$

The state vector $\mathbf{x}(t)$ can be obtained by inverse transforming $\mathbf{X}(s)$:

$$\mathbf{x}(t) = \mathscr{L}^{-1}[\mathbf{\Phi}(s)\mathbf{x}(0)]$$

Note that for an $n \times n$ matrix $\mathbf{A}$, $|s\mathbf{I} - \mathbf{A}|$ is an nth-order polynomial in s. Also, each element of the adjoint matrix $(s\mathbf{I} - \mathbf{A})^{+}$ is a polynomial in s of order less than or equal to $(n - 1)$. Therefore, each element of $\mathbf{\Phi}(s)$

[2] This, in fact, is the model of a linear *autonomous system*. An autonomous system is one that is both free (zero input) and time-invariant . With no background on state variable methods, the reader can hopefully, appreciate the analysis that follows. For better appreciation, refer Chapter 12.

is a strictly proper rational function, and can be expanded in a partial fraction expansion. Using the time-response analysis given in the earlier section, it is easy to establish that

$$\lim_{t\to\infty} \mathbf{x}(t) \to 0$$

if all the roots of the characteristic polynomial $|s\mathbf{I} - \mathbf{A}|$ lie strictly in the left half of the complex plane. In Chapter 12 we will see that under mildly restrictive conditions (namely, the system must be both controllable and observable), the roots of the characteristic polynomial $|s\mathbf{I} - \mathbf{A}|$ are same as the poles of the corresponding transfer function, and asymptotic stability ensures BIBO stability and *vice versa*. This implies that stability analysis can be carried out using only the BIBO stability test (or only the asymptotic stability test).

We will use the following terminology and tests for stability analysis of linear time-invariant systems described by the transfer function $G(s) = N(s)/\Delta(s)$, with the characteristic equation $\Delta(s) = 0$.

1. If all the roots of the characteristic equation lie in the left half of the s-plane, the system is *stable*.
2. If any root of the characteristic equation lies in the right half of the s-plane, the system is *unstable.*
3. If condition 1 is satisfied except for the presence of one or more non-repeated roots on the $j\omega$-axis in the s-plane, the system is *marginally stable.*

It follows from the above discussion that stability of a linear time-invariant system can be determined by finding the roots of its characteristic polynomial. For first- and second-order polynomials, this is trivial. Algebraic methods are available for third-order polynomials, but are somewhat difficult to apply. For polynomials of order higher than three, numerical procedures are usually required. Computer Programs are available [151–154] that can be used to find the roots of a polynomial. A disadvantage of using numerical techniques is that all parameters in the system must be assigned numerical values. Finding the range of a certain parameter that results in a stable system becomes difficult when a numerical technique is used to determine the stability. From the point of view of control system design, information on range of system parameters for stability is important.

The Routh stability criterion, which is an analytical procedure of stability study, is well suited for finding the range of a parameter for stability.

5.4 THE ROUTH STABILITY CRITERION

The Routh stability criterion is an analytical procedure for determining if all the roots of a polynomial have negative real parts, and is used in the stability analysis of linear time-invariant systems. The characteristic equation for a linear time-invariant system is a polynomial equation, except for the case that the system contains dead-time elements. For this special class, the Routh stability criterion cannot be employed (the Nyquist stability criterion, which is covered later in chapter 9, can be employed). However, with dead-time approximations (refer Eqns (2.47)–(2.49)), the characteristic equation reduces to a polynomial equation and the Routh stability criterion becomes applicable.

Characteristic equation of linear time-invariant systems is of the form

$$\Delta(s) = a_0 s^n + a_1 s^{n-1} + \cdots + a_{n-1} s^1 + a_n s^0 = 0 \tag{5.9}$$

where the coefficients a_i are real numbers.

One can assume with no loss of generality that a_n, the coefficient of s^0, is not zero. Otherwise, the characteristic polynomial $\Delta(s)$ can be expressed as a power of s times a polynomial in which the coefficient of s^0 is non-zero. The power of s indicates roots at the origin of the s-plane, the number of which is evident; hence only the latter polynomial should be investigated using the Routh stability criterion. We assume in the following development that the coefficient of s^0 is not zero.

We will also assume with no loss of generality that $a_0 > 0$. In case $a_0 < 0$, it can be made positive by multiplying the characteristic equation by -1 throughout.

In order to ascertain the stability of a linear time-invariant system, it is necessary to determine if any of the roots of its characteristic equation lie in the right half of the s-plane. Assume that the roots of nth-order characteristic equation (5.9) are given by $s = r_1, r_2, \ldots, r_n$. These roots are functions of the coefficients a_0, $a_1, \ldots, a_{n-1}$, a_n.

A second-order polynomial

$$\begin{aligned} a_0 s^2 + a_1 s + a_2 &= a_0(s - r_1)(s - r_2) \\ &= a_0 s^2 - a_0(r_1 + r_2)\, s + a_0 r_1 r_2 \end{aligned} \tag{5.10}$$

A third-order polynomial

$$\begin{aligned} a_0 s^3 + a_1 s^2 + a_2 s + a_3 &= a_0(s - r_1)(s - r_2)(s - r_3) \\ &= a_0 s^3 - a_0(r_1 + r_2 + r_3)\, s^2 + a_0(r_1 r_2 + r_1 r_3 + r_2 r_3)\, s - a_0 r_1 r_2 r_3 \end{aligned} \tag{5.11}$$

Extending this expansion to the nth-order polynomial, we get

$$\begin{aligned} \Delta(s) &= a_0 s^n + a_1 s^{n-1} + \cdots + a_{n-1} s + a_n \\ &= a_0 s^n - a_0 (\text{sum of all the roots})\, s^{n-1} \\ &\quad + a_0 (\text{sum of the products of the roots taken 2 at a time})\, s^{n-2} \\ &\quad - a_0 (\text{sum of the products of the roots taken 3 at a time})\, s^{n-3} \\ &\quad + \cdots + a_0 (-1)^n (\text{product of all the } n \text{ roots}) \end{aligned} \tag{5.12}$$

Suppose that all the roots of a polynomial are real and in the left half plane. Then all r_i in Eqns (5.10) and (5.11) are real and negative. Therefore, all polynomial coefficients are positive. This characteristic also applies to the general case of Eqn. (5.12). The only case for which a coefficient can be negative is that there be atleast one root in the right half plane. Note also that if all the roots are in the left half plane, no coefficient can be zero.

If any roots of the polynomials above are complex, the roots must appear in complex-conjugate pairs, since the polynomial coefficients are assumed real. Then, as per the rules given for forming the polynomial coefficients, all imaginary parts of roots/products of roots will cancel. Therefore, if all roots occur in the left half plane, all coefficients of the general polynomial of Eqn. (5.12) will be positive. Presence of a negative coefficient implies that there is at least one root in the right half plane. A zero coefficient indicates presence of complex-conjugate roots on the $j\omega$-axis and/or one or more roots in the right half plane.

In summary, given a polynomial as in Eqn. (5.12):

(i) if any coefficient a_i is equal to zero, then *not all* the roots are in the left half plane; and
(ii) if any coefficient a_i is negative, then *at least one root* is in the right half plane.

We therefore conclude that the absence or negativeness of any of the coefficients of a characteristic polynomial indicates that the system is either unstable or at most, marginally stable. Thus, it is necessary for a stable system that all the coefficients of its characteristic polynomial be positive. If any coefficient is zero/negative, we immediately know that the system is not stable. The converse is, however, not true: when all the coefficients are positive, the system is not necessarily stable; there may still be roots in the right half plane and/or on the imaginary axis. In order for all the roots to have negative real parts, it is *necessary but not sufficient* that all of the coefficients of the characteristic equation be positive. For example, when the characteristic equation is

$$\Delta(s) = (s + 2)\left(s - \frac{1}{2} - j\frac{\sqrt{15}}{2}\right)\left(s - \frac{1}{2} + j\frac{\sqrt{15}}{2}\right) = s^3 + s^2 + 2s + 8 = 0,$$

the system is unstable, and yet the polynomial possesses all positive coefficients.

The first step in analysing the stability of a system is to examine its characteristic equation. If some of the coefficients are zero or negative, it can be concluded that the system is not stable. On the other hand, if all the coefficients of the characteristic equation are positive, the possibility of the stability of the system exists and one should proceed further to examine the sufficient conditions of stability.

A. Hurwitz, and E. J. Routh independently published the method of investigating the sufficient conditions of stability of a system. The Hurwitz criterion is in terms of determinants and the Routh criterion is in terms of array formulation, which is more convenient to handle. We present here the Routh stability criterion[3].

The Routh stability criterion is based on ordering the coefficients of the characteristic equation

$$\Delta(s) = a_0 s^n + a_1 s^{n-1} + a_2 s^{n-2} + \cdots + a_{n-1} s + a_n = 0;\ a_0 > 0 \tag{5.13}$$

into a schedule, called the *Routh array.*

A necessary and sufficient condition for stability is that all of the elements in the first column of the Routh array be positive. If this condition is not met, the system is unstable, and the number of sign changes in the elements of the first column of the Routh array corresponds to the number of roots of the characteristic equation in the right half of the s-plane.

To determine the Routh array, coefficients of the characteristic equation are arranged in two rows, beginning with the coefficients of s^n and s^{n-1}, respectively, and followed by even-numbered and odd-numbered coefficients as follows:

$$\begin{aligned} s^n &: a_0 \quad a_2 \quad a_4 \quad . \ . \ . \\ s^{n-1} &: a_1 \quad a_3 \quad a_5 \quad . \ . \ . \end{aligned}$$

The following rows are subsequently added to complete the Routh array:

$$\begin{aligned} \text{row } n &: s^n \quad a_0 \quad a_2 \quad a_4 \quad . \ . \ . \\ \text{row}(n-1) &: s^{n-1} \quad a_1 \quad a_3 \quad a_5 \quad . \ . \ . \\ \text{row}(n-2) &: s^{n-2} \quad b_1 \quad b_2 \quad b_3 \quad . \ . \ . \\ \text{row}(n-3) &: s^{n-3} \quad c_1 \quad c_2 \quad c_3 \quad . \ . \ . \\ &\vdots \\ \text{row } 2 &: s^2 \quad * \quad a_n \\ \text{row } 1 &: s^1 \quad * \\ \text{row } 0 &: s^0 \quad a_n \end{aligned} \tag{5.14}$$

where the elements from $(n-2)$th row on are computed as follows (the column with the powers of s is included as a convenient accounting method for rows).

$$\begin{aligned} b_1 &= \frac{-\det \begin{bmatrix} a_0 & a_2 \\ a_1 & a_3 \end{bmatrix}}{a_1} = (a_1 a_2 - a_0 a_3)/a_1 \\ b_2 &= \frac{-\det \begin{bmatrix} a_0 & a_4 \\ a_1 & a_5 \end{bmatrix}}{a_1} = (a_1 a_4 - a_0 a_5)/a_1 \\ &\vdots \end{aligned} \tag{5.15}$$

[3]Proof of the Routh stability criterion involves delicate algebra and is omitted here. This algebraic criterion is derived in textbooks, such as Schwarz and Friedland [40], on linear systems.

Note that the elements b_i of the s^{n-2}-row are formed from the elements of the two previous rows, s^n-row and s^{n-1}-row, using determinants with the two elements in the first column and other elements in the successive columns. This pattern is continued until the rest of the b_i's are all equal to zero.

Elements of s^{n-3}-row are formed from the elements of the two previous rows, s^{n-1}-row and s^{n-2}-row, as follows:

$$c_1 = \frac{-\det\begin{bmatrix} a_1 & a_3 \\ b_1 & b_2 \end{bmatrix}}{b_1} = (b_1a_3 - a_1b_2)/b_1$$

$$c_2 = \frac{-\det\begin{bmatrix} a_1 & a_5 \\ b_1 & b_3 \end{bmatrix}}{b_1} = (b_1a_5 - a_1b_3)/b_1 \qquad (5.16)$$

$$\vdots$$

This is continued until no more c_i elements are present. The rest of the rows are formed in this way down to the s^0-row. The complete array is triangular. Notice that the s^1-row and s^0-row contain one term each.

The elements of the first column of the Routh array must all be positive if all the roots of the characteristic equation are in the left half of s-plane. However, if the elements of the first column are not all positive, the number of roots in the right half of s-plane equals the number of sign changes in the first column. A pattern of +, –, + is counted as *two* sign changes, one going from + to – and the other from – to +.

It is to be noted here that in the process of generating the Routh array, the missing terms are regarded as zeros. Also, all the elements of any row can be multiplied or divided by a positive constant during the process to simplify the computational work; this modification does not change the signs of the elements of first column.

Example 5.1 Consider a fourth-order system with the characteristic equation

$$s^4 + 8s^3 + 18s^2 + 16s + 5 = 0$$

Since the equation has no missing terms and the coefficients are all positive, it satisfies the necessary condition for stability. However, the sufficient condition must still be checked. Routh array is made as follows:

s^4	1	18	5
s^3	8	16	0 (for the missing term)
s^2	$16 = \frac{(8)(18) - (1)(16)}{8}$	$5 = \frac{(8)(5) - (1)(0)}{8}$	
s^1	$\frac{27}{2} = \frac{(16)(16) - (8)(5)}{16}$	0	
s^0	5		

The elements of the first column are all positive, and hence the system is stable.

Example 5.2 Consider the characteristic equation

$$3s^4 + 10s^3 + 5s^2 + 5s + 2 = 0$$

which satisfies the necessary condition for stability since all the coefficients are positive and non-zero. The Routh array for this equation is

s^4	3	5	2
s^3	~~10~~	~~5~~	~~0~~ ← divide by 5
	2	1	0
s^2	$\frac{7}{2} = \frac{(2)(5)-(3)(1)}{2}$	$2 = \frac{(2)(2)-(3)(0)}{2}$	
s^1	$-\frac{1}{7} = \frac{(7/2)(1)-(2)(2)}{(7/2)}$		
s^0	2		

It may be noted that in order to simplify computational work, the s^3 -row in the formation of the Routh array has been modified by dividing it by 5 throughout. The modified s^3 -row is then used to complete the process of array formation.

Examining the first column of the Routh array, it is found that there are two changes in sign $\left(\text{from } \frac{7}{2} \text{ to } -\frac{1}{7} \text{ and from } -\frac{1}{7} \text{ to } 2\right)$. Therefore the system under consideration is unstable with two poles in the right half of s-plane.

The Routh stability criterion gives only the number of roots in the right half of s-plane. It gives no information as regards the values of the roots, and also does not distinguish between real and complex roots.

Example 5.3 Consider the polynomial

$$\Delta(s) = s^6 + 4\,s^5 + 3\,s^4 + 2\,s^3 + s^2 + 4\,s + 4$$

which satisfies the necessary condition for stability since all the $\{a_i\}$'s are positive and non-zero. The Routh array for this polynomial is

s^6	1	3	1	4	
s^5	~~4~~	~~2~~	~~4~~	~~0~~	← divide by 2
	2	1	2	0	
s^4	$\frac{5}{2}$	0	4		
s^3	1	$-\frac{6}{5}$	0		
s^2	3	4			
s^1	$-\frac{38}{15}$				
s^0	4				

It is seen that the polynomial has right-half plane roots, since the elements of the first column are not all positive. In fact, there are two roots in the right-half plane since there are two sign changes.

5.4.1 Special Cases

Formation of Routh array for the polynomials of Examples 5.1– 5.3 could easily be carried out using the standard procedure given in Eqns (5.15) – (5.16). However, the standard procedure fails if we encounter any of the following situations on our way to formation of the array.

I. A row of all zeros appears.
II. *Pivot element* (first element of a row, appearing in first column of the array) of a row is zero, but the entire row is not all zeros.

For these special situations, we have to use special techniques to complete the process of array formation.

Case I: A row of all zeros When we encounter a row with all zero elements (or with single element which is zero) on our way to formation of Routh array, the process of array formation terminates prematurely because all the terms in the row next to the all-zero row become infinite.

An all-zero row indicates the existence of an even polynomial as a factor of the given characteristic polynomial. An even polynomial is one in which the exponents of s are even integers or zero only. This even-polynomial factor is called the *auxiliary polynomial.* The coefficients of the auxiliary polynomial will always be the elements in the row directly above the row of zeros in the array. The highest power in the auxiliary polynomial is the exponent that denotes the row containing its coefficients.

The roots of an even polynomial occur in pairs that are equal in magnitude and opposite in sign. Hence, these roots can be purely imaginary (Fig. 5.2a), purely real (Fig. 5.2b) or complex (Fig. 5.2c). Since complex roots must occur in conjugate pairs, any complex roots of an even polynomial must occur in groups of four, which is apparent in Fig. 5.2c. Such roots have quadrantal symmetry, that is, the roots are symmetrical with respect to both the real and the imaginary axes.

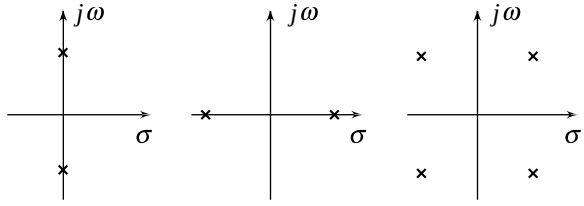

Fig. 5.2 The roots of an even polynomial

The *Case I* polynomial may be analyzed in either of the two ways:

(i) Once the auxiliary polynomial $A(s)$ is found, it is factored from the characteristic equation, leaving a second factor which may be analyzed by applying the Routh stability criterion. The auxiliary polynomial may be factored algebraically to give the roots.

(ii) Once the auxiliary polynomial $A(s)$ is found, it is differentiated with respect to s, and the row of zeros is replaced with the coefficients of $dA(s)/ds$. The construction of the array then continues in the usual manner, and the array is interpreted in the usual way. However, the roots of the auxiliary polynomial are also roots of the given characteristic equation, and these must be tested separately.

Example 5.4 Consider a fifth-order system with the characteristic equation

$$\Delta(s) = s^5 + s^4 + 4\,s^3 + 24\,s^2 + 3\,s + 63 = 0$$

for which the Routh array is constructed as

s^5	1	4	3	
s^4	1	24	63	
s^3	~~– 20~~	~~– 60~~	~~0~~	← divide by 20
	– 1	– 3	0	
s^2	~~21~~	~~63~~		← divide by 21
	1	3		
s^1	0	0		

Since a row of zeros appears prematurely, we form the auxiliary polynomial using the coefficients of the s^2-row.

$$A(s) = s^2 + 3$$

Solving the auxiliary equation

$$A(s) = s^2 + 3 = 0,$$

we get the roots at $s = \pm j\sqrt{3}$.

In order to examine the remaining roots, we divide $\Delta(s)$ by $A(s)$ to obtain

$$\frac{\Delta(s)}{A(s)} = s^3 + s^2 + s + 21$$

Establishing Routh array for this factor, we have

s^3	1	1
s^2	1	21
s^1	– 20	0
s^0	21	

The two changes in sign in the first column indicate the presence of two roots in the right-half plane, and the system is unstable.

Example 5.5 Consider a sixth-order system with the characteristic equation

$$\Delta(s) = s^6 + 2\,s^5 + 8\,s^4 + 12\,s^3 + 20\,s^2 + 16\,s + 16 = 0$$

for which the Routh array is constructed as

s^6	1	8	20	16	
s^5	~~2~~	~~12~~	~~16~~	~~Ø~~	← divide by 2
	1	6	8	0	
s^4	~~2~~	~~12~~	~~16~~		← divide by 2
	1	6	8		
s^3	0	0			

The auxiliary polynomial

$$A(s) = s^4 + 6\,s^2 + 8$$

The derivative of the polynomial with respect to s is

$$\frac{dA(s)}{ds} = 4\,s^3 + 12$$

The zeros in the s^3-row are now replaced by the coefficients 4 and 12. The Routh array then becomes

s^6	1	8	12	16	
s^5	~~2~~	~~12~~	~~16~~	0	← divide by 2
	1	6	8	0	
s^4	~~2~~	~~12~~	~~16~~		← divide by 2
	1	6	8		
s^3	0	0			$\frac{dA(s)}{ds} = 4s^3 + 12$
	~~4~~	~~12~~			← divide by 4
	1	3			
s^2	3	8			
s^1	$\frac{1}{3}$				
s^0	8				

Since there are no sign changes in the first column of the Routh array, the polynomial $\Delta(s)/A(s)$ does not have any root in the right half of s-plane. Solving the auxiliary equation

$$A(s) = s^4 + 6s^2 + 8 = 0$$

we get the roots at $s = \pm j\sqrt{2}$, and $s = \pm j2$, which are also the roots of $\Delta(s)$. Therefore the system under consideration is marginally stable. The oscillation frequencies are $\sqrt{2}$ rad/sec, and 2 rad/sec.

Case II: A zero pivot element, but the entire row is not all zero Consider now a situation wherein we encounter a row with zero pivot element while atleast one element of the row is non-zero. Because of the zero pivot element, the terms in the next row all become infinite and the array formation cannot continue.

To remedy this situation, we replace the zero pivot element by an arbitrary small number ε and then proceed with the construction of the array. The limit $\varepsilon \to 0$ is then taken to determine the changes in algebraic signs of the first column terms, yielding the information regarding the number of right-half plane roots.

Let us examine the rationale of the method. If the polynomial under test had slightly different coefficients, the troublesome zero pivot element would instead be some small non-zero number. As long as the polynomial has no roots on the imaginary axis, sufficiently small perturbations of its coefficients will not alter the number of right-half plane roots. Rather than to actually perturb the polynomial coefficients, the effect of such perturbations is indicated by replacing the zero term with ε. Therefore, for a polynomial with no imaginary-axis roots, $\varepsilon \to 0$ from positive or negative side would give identical results. ε is generally taken to be positive for convenience.

Example 5.6 Consider the polynomial

$$\Delta(s) = s^5 + 3s^4 + 2s^3 + 6s^2 + 6s + 9$$

for which the Routh array is

s^5	1	2	6	
s^4	3	6	9	← divide by 3
	1	2	3	
s^3	0	3		← replace 0 by ε
	ε	3		
s^2	$\dfrac{2\varepsilon - 3}{\varepsilon}$	3		
s^1	$3 - \dfrac{3\varepsilon^2}{2\varepsilon - 3}$			
s^0	3			

The first element in the s^2-row is $(2\varepsilon - 3)/\varepsilon$ which has a negative sign as $\varepsilon \to 0$ (in the Routh stability criterion, we are interested only in the signs of terms in the first column and not in their magnitudes). The first term of s^1-row is $[3 - 3\varepsilon^2/(2\varepsilon - 3)]$ which has a limiting value of +3 as $\varepsilon \to 0$. Examining the terms in the first column of the Routh array, it is found that there are two changes in sign, which implies that there are two poles in the right-half plane.

For the case where the characteristic equation has imaginary-axis roots, replacement of the zero pivot element by ε would cause the imaginary-axis roots to move into either left or right half of the s-plane, with the result that the roots of the characteristic polynomial in the right-half s-plane cannot be correctly determined. Therefore, to apply the ε-limiting method for a characteristic polynomial with the imaginary-axis roots, one must first extract these roots and then apply the test on the remainder polynomial with no imaginary-axis roots.

Example 5.7 Consider the polynomial

$$\Delta(s) = s^6 + s^5 + 3\,s^4 + 3\,s^3 + 3\,s^2 + 2\,s + 1$$

The Routh array is

s^6	1	3	3	1	
s^5	1	3	2		
s^4	0	1	1		← replace 0 by ε
s^3	$\dfrac{3\varepsilon - 1}{\varepsilon}$	$\dfrac{2\varepsilon - 1}{\varepsilon}$			
s^2	$\dfrac{-2\varepsilon^2 + 4\varepsilon - 1}{3\varepsilon - 1}$	1			
s^1	$\dfrac{4\varepsilon^2 - \varepsilon}{2\varepsilon^2 - 4\varepsilon + 1}$				
s^0	1				

As $\varepsilon \to 0$, the elements of s^1-row tend to zero. This indicates the possibility of existence of imaginary-axis roots in the s-plane. We therefore need to examine the auxiliary polynomial. If the imaginary-axis roots do not exist, the usual procedure of replacing the all-zero row by coefficients of the derivative of

the auxiliary polynomial is adopted. If the imaginary-axis roots are found to exist, the original polynomial is divided out by the auxiliary polynomial and the test is performed on the remainder polynomial.

For the example under consideration, the auxiliary polynomial is (let $\varepsilon \to 0$ in s^2-row):

$$A(s) = s^2 + 1 = 0$$

yielding two roots on the imaginary axis. Dividing the original polynomial $\Delta(s)$ by $A(s)$, we get

$$\frac{\Delta(s)}{A(s)} = s^4 + s^3 + 2\,s^2 + 2\,s + 1$$

The Routh array for this polynomial is

s^4	1	2	1	
s^3	1	2		
s^2	$\cancel{0}$	$\cancel{1}$		← replace 0 by ε
	ε	1		
s^1	$\frac{2\varepsilon - 1}{\varepsilon}$			
s^0	1			

As $\varepsilon \to 0$, there are two sign changes in the first column of the array. This indicates that there are two roots in the right half s-plane. The original polynomial $\Delta(s)$, therefore, has two roots in the right-half plane and two roots on the imaginary axis.

5.4.2 Relative Stability (Shifting the Origin)

The Routh stability criterion ascertains *absolute stability* of a system by determining if all the roots of the characteristic equation lie in the left half of s-plane. Once a system is found to be absolutely stable (all characteristic roots in left half of s-plane), it is desirable to determine its *relative stability,* which is concerned with the attributes of transient behaviour of the system. We shall see in the next chapter that parameters such as overshoot, settling time, etc., are used to capture important attributes of transient response of a stable system; these parameters are therefore quantitative measures of relative stability. Stability margins (gain margin, phase margin) are commonly used as frequency-domain measures of relative stability. Frequency-domain analysis will appear in Chapter 8.

In the following paragraphs, we show that the Routh stability criterion can be extended for a preliminary relative-stability analysis. We know that for a real root or a complex-conjugate pair of roots on the vertical line in the s-plane defined by $s = -\sigma$, $\sigma > 0$ (refer Fig. 5.3), the time-constant $\tau = 1/\sigma$. The transient response modes corresponding to smaller time-constants decay faster, and therefore the dynamic behaviour of a system is dominated by the roots with larger time-constants. The largest time-constant associated with a system can be obtained by determining the minimum distance of the characteristic roots from the imaginary axis.

We substitute

$$s = \hat{s} - \sigma \qquad (5.17)$$

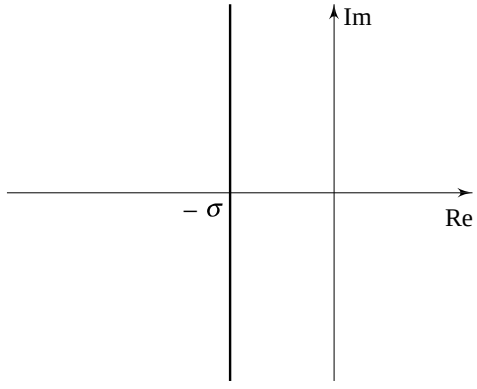

Fig. 5.3 Shifting of the origin in the s-plane

into the characteristic equation, write a polynomial in terms of $\hat{s}$, and apply Routh stability criterion to the new polynomial in $\hat{s}$. If there are no changes of sign in the first column of the array developed for the polynomial in $\hat{s}$, it implies that all the roots of the original characteristic equation are more negative than $-\sigma$. Shifting the vertical axis on a trial-and-error basis, we can find the minimum distance of the roots from the imaginary axis, and hence the largest time-constant associated with the system.

Example 5.8 Consider a third-order system with the characteristic equation

$$s^3 + 7s^2 + 25\,s + 39 = 0$$

which, by the Routh stability criterion, can be shown to have all its roots in the left half of the s-plane. Let us check if all the roots of this equation have real parts more negative than -1.

The substitution

$$s = \hat{s} - 1$$

results in the following polynomial in $\hat{s}$:

$$f(\hat{s}) = \hat{s}^3 + 4\hat{s}^2 + 14\hat{s} + 20$$

Forming the Routh array, we get

$\hat{s}^3$	1	14	
$\hat{s}^2$	~~4~~	~~20~~	← divide by 4
	1	5	
$\hat{s}^1$	9		
$\hat{s}^0$	5		

As the signs of all the elements of the first column of the Routh array are positive, all the roots of the original characteristic polynomial are more negative than –1.

5.5 STABILITY RANGE FOR A PARAMETER

Our discussion so far has centred on determining whether or not a given characteristic equation has roots in the right half of the s-plane, using the Routh stability criterion. Since even pocket calculators can find roots of polynomials these days, the real value of the Routh test is in design of control systems where ranges of certain parameters have to be obtained ensuring a stable operation. We illustrate the concepts involved using a couple of examples.

Example 5.9 Consider the closed-loop system shown in Fig. 5.4. Let us determine the range of K for which the system is stable.

The closed-loop transfer function of the system is

$$\frac{Y(s)}{R(s)} = \frac{K}{s\left(s^2 + s + 1\right)(s + 4) + K}$$

Therefore, the characteristic equation is

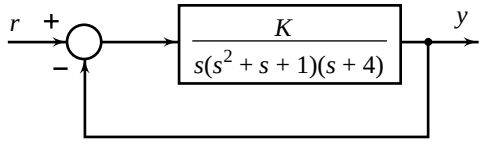

Fig. 5.4 A feedback system

$$s(s^2 + s + 1)(s + 4) + K = 0$$

or $$s^4 + 5\,s^3 + 5\,s^2 + 4\,s + K = 0$$

The Routh array for this equation is

s^4	1	5	K
s^3	5	4	
s^2	21/5	K	
s^1	$\left(\frac{84}{5} - 5K\right) \Big/ \left(\frac{21}{5}\right)$		
s^0	K		

Since for a stable system, the signs of elements of the first column of the Routh array should be all positive, the condition of system stability requires that

$$K > 0 \text{ and } \left(\frac{84}{5} - 5K\right) > 0$$

Therefore for stability, K should lie in the range

$$\frac{84}{25} > K > 0$$

If we let $K = \frac{84}{25}$, the s^1-row of the Routh array becomes an all-zero row, resulting in the auxiliary equation

$$\frac{21}{5}s^2 + \frac{84}{25} = 0$$

which has roots at $s = \pm j\sqrt{(4/5)} = \pm j\omega_0$. Therefore, $K = \frac{84}{25}$ will cause sustained oscillations of frequency $\omega_0 = \sqrt{(4/5)}$ rad/sec.

Example 5.10 Consider the closed-loop system shown in Fig. 5.5. A PI controller controls a second-order plant. Let us determine the range of K_c for which the closed-loop poles satisfy Re(s) < – 2.

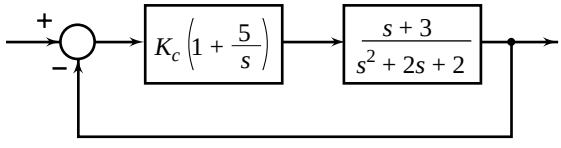

Fig. 5.5 A feedback system

The characteristic equation of the system is

$$s^2 + 2\,s + 2 + K_c\left(1 + \frac{5}{s}\right)(s + 3) = 0$$

or $$s^3 + (2 + K_c)s^2 + (2 + 8K_c)s + 15K_c = 0$$

Letting $s = \hat{s} - 2$, we have

$$(\hat{s} - 2)^3 + (2 + K_c)(\hat{s} - 2)^2 + (2 + 8K_c)(\hat{s} - 2) + 15K_c = 0$$

or $$\hat{s}^3 + (K_c - 4)\,\hat{s}^2 + (4K_c + 6)\,\hat{s} + (3K_c - 4) = 0$$

Applying the Routh's test yields the array

$\hat{s}^3$	1	$4K_c + 6$
$\hat{s}^2$	$K_c - 4$	$3K_c - 4$
$\hat{s}^1$	$\dfrac{4K_c^2 - 13K_c - 20}{K_c - 4}$	
$\hat{s}^0$	$3K_c - 4$	

If there are no sign changes in the first column of the array, then all roots satisfy Re ($\hat{s}$) < 0, that is, the roots of the original characteristic equation satisfy Re (s) < – 2. Thus, we require that K_c satisfy all the following conditions:

$$K_c > 4;\ K_c > 4.3892 \quad \text{or} \quad K_c < -1.1392;\ K_c > \frac{4}{3}$$

The requirement $K_c < -1.1392$ is disregarded since K_c cannot be negative. Therefore, we have Re(s) < – 2 for all closed-loop poles provided that $K_c > 4.3892$.

It is probably more insightful to think about the characteristic equation of a feedback system geometrically rather than algebraically. The root locus technique developed later in Chapter 7, is intrinsically geometric as opposed to the algebraic approach of the Routh criterion. It enables us to rapidly sketch the locus of all solutions to the characteristic equation of the closed-loop transfer function. This sketch offers great insight by showing how the locations of the poles of the closed-loop transfer function change as a specific parameter is varied.

Review Examples

Review Example 5.1 Consider the polynomial

$$\Delta(s) = s^5 + 2\,s^4 + 2\,s^3 + 4\ s^2 + 11\,s + 10$$

The Routh array is calculated as

s^5	1	2	11	
s^4	~~2~~	~~4~~	~~10~~	← divide by 2
	1	2	5	
s^3	~~0~~	~~6~~		← replace 0 by ε
	ε	6		
s^2	$-\dfrac{6}{\varepsilon}$	5		
s^1	6			
s^0	5			

In array formation, the limits were taken as $\varepsilon \to 0$ at convenient points in the calculations rather than waiting until the array was complete. This procedure simplifies the calculations and the final form of the array.

From the array we see that there are two sign changes in the first column; the polynomial $\Delta(s)$, by Routh stability criterion, has two roots in the right half s-plane.

Review Example 5.2 A feedback control system is shown in Fig. 5.6. The process transfer function is

$$G(s) = \frac{K(s+40)}{s(s+10)}$$

and the sensor transfer function is

$$H(s) = \frac{1}{s+20}$$

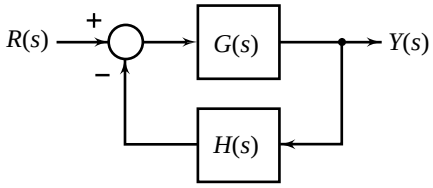

Fig. 5.6 A feedback control system

(a) Find the gain K that results in marginal stability. Determine the oscillation frequency.

(b) Reduce the gain to half the value found in (a) and study the relative stability of the system.

Solution

The characteristic equation of the system is

$$1 + G(s)H(s) = 0$$

This gives $s(s + 10)(s + 20) + K(s + 40) = 0$

or

$$s^3 + 30\,s^2 + (K + 200)\,s + 40\,K = 0$$

for which the Routh array is

s^3	1	$K + 200$	
s^2	~~30~~	~~40~~ K	← divide by 10
	3	$4K$	
s^1	$\frac{600 - K}{3}$		
s^0	$4K$		

(a) $K = 600$ results in an all-zero row in the array. The auxiliary equation, for this value of K, is

$$3\,s^2 + 2400 = 0$$

which has the roots $s = \pm j\sqrt{800}$.

Therefore, $K = 600$ results in marginal stability; the oscillation frequency is $\sqrt{800}$ rad/sec.

(b) The characteristic polynomial of the system for $K = 300$ is

$$\Delta(s) = s^3 + 30\,s^2 + 500\,s + 12000$$

The substitution $s = \hat{s} - 1$ results in the following polynomial in $\hat{s}$:

$$f(\hat{s}) = \hat{s}^3 + 27\,\hat{s}^2 + 443\,\hat{s} + 11529$$

Forming the Routh array, we get

$\hat{s}^3$	1	443	
$\hat{s}^2$	~~27~~	~~11529~~	← divide by 27
	1	427	
$\hat{s}^1$	16		
$\hat{s}^0$	427		

As the signs of all the elements of the first column of the Routh array are positive, all the roots of the original characteristic polynomial $\Delta(s)$ are more negative than -1.

The substitution $s = \bar{s} - 2$ in $\Delta(s)$, results in the following polynomial:

$$g(\bar{s}) = \bar{s}^3 + 24\bar{s}^2 + 392\bar{s} + 11112$$

Forming the Routh array, we get

$\bar{s}^3$	1	392	
$\bar{s}^2$	~~24~~	~~11112~~	← divide by 24
	1	463	
$\bar{s}^1$	− 71		
$\bar{s}^0$	463		

There are two sign changes in the first column of the Routh array; there are, therefore, two roots of the original characteristic polynomial that satisfy $\text{Re}(s) > -2$.

The largest time-constant of the closed-loop system is greater than 0.5 and less than 1.

Review Example 5.3 Consider the feedback system shown in Fig. 5.6. The process transfer function

$$G(s) = \frac{K}{s(s+1)}$$

and the feedback transfer function is a first-order Pade approximation (refer Eqn. (2.49)) for the transducer delay:

$$H(s) = \frac{1 - \frac{\tau_D}{2}s}{1 + \frac{\tau_D}{2}s} = \frac{1 - Ts}{1 + Ts}; \tau_D = 2T$$

The question to be studied is: what are the combinations of K and T for which the system is stable?

The characteristic polynomial of the system is

$$\Delta(s) = Ts^3 + (1 + T)s^2 + (1 - KT)s + K$$

The Routh array is

s^3	T	$1 - KT$
s^2	$1 + T$	K
s^1	$\frac{1 + T - 2KT - KT^2}{1 + T}$	
s^0	K	

The stability boundary is given by the condition

$$1 + T - KT(2 + T) = 0$$

or

$$KT = \frac{1+T}{2+T}$$

The relationship between the maximum allowable gain K_{max} and the delay T is sketched in Fig. 5.7.

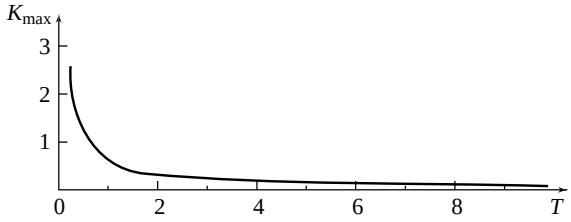

Fig. 5.7 Maximum allowable gain versus delay

Review Questions

5.1 Define the terms:

(a) bounded-input, bounded-output (BIBO) stability; and
(b) asymptotic stability

State the conditions under which asymptotic stability of a linear time-invariant system ensures BIBO stability and vice versa.

5.2 (a) Define the terms: absolute stability, and relative stability.
(b) Derive conditions for absoulte stability of a linear time-invariant system described by the transfer function

$$G(s) = \frac{b_0 s^m + b_1 s^{m-1} + \cdots + b_{m-1}\, s + b_m}{a_0 s^n + a_1\, s^{n-1} + \cdots + a_{n-1}\, s + a_n};\ m \le n$$

Comment upon the stability property of the system when $G(s)$ has non-repeated poles on the imaginary axis in the s-plane.

Problems

5.1 Use the Routh stability criterion to determine the number of roots in the left-half plane, the right-half plane, and on the imaginary axis for the given characteristic equation:

(a) $s^4 + 2s^3 + 8s^2 + 4s + 3 = 0$
(b) $s^6 + 3s^5 + 2s^4 + 9s^3 + 5s^2 + 12s + 20 = 0$
(c) $s^5 + s^4 + 2s^3 + 2s^2 + 3s + 5 = 0$
(d) $s^5 + 4s^4 + 8s^3 + 8s^2 + 7s + 4 = 0$
(e) $s^4 + 9s^3 + 4s^2 - 36s - 32 = 0$
(f) $s^7 + 5s^6 + 9s^5 + 9s^4 + 4s^3 + 20s^2 + 36s + 36 = 0$

5.2 Obtain the roots of the given characteristic polynomial on the basis of the Routh array:

(a) $s^4 + 2s^3 + 11s^2 + 18s + 18 = 0$
(b) $s^5 + 2s^4 + 24s^3 + 48s^2 - 25s - 50 = 0$
(c) $s^6 + 3s^5 + 5s^4 + 9s^3 + 8s^2 + 6s + 4 = 0$

5.3 Determine whether the largest time-constant of the roots of the characteristic equation given below is greater than, less than or equal to 1.0 sec.

$$s^3 + 4s^2 + 6s + 4 = 0$$

5.4 The characteristic equations for certain feedback control systems are given below. In each case, determine the range of values of K ($K > 0$) for which the system is stable.

(a) $s^4 + s^3 + s^2 + s + K = 0$ (b) $s^4 + Ks^3 + s^2 + s + 1 = 0$

(c) $s^4 + 3s^3 + 3s^2 + 2s + K = 0$ (d) $s^3 + 3Ks^2 + (K + 2)s + 4 = 0$

5.5 Determine the range of values of K ($K > 0$) such that the characteristic equation

$$s^3 + 3(K + 1)s^2 + (7K + 5)s + (4K + 7) = 0$$

has roots more negative than $s = -1$.

MATLAB Exercise After completing the hand calculations based on Routh criterion, verify your results using root locus plots in MATLAB window.

5.6 The block diagram of a feedback control system is shown in Fig. P5.6. Determine the values of K ($K > 0$) that result in a stable closed-loop system.

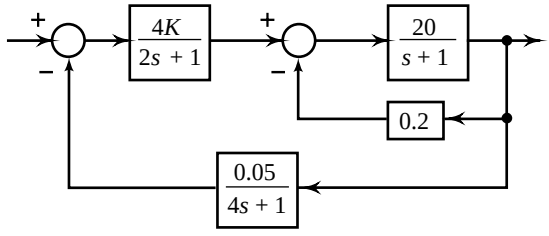

Fig. P5.6

MATLAB Exercise After completing the hand calculations based on Routh criterion, verify your results using root locus plots in MATLAB window.

5.7 A feedback system has open-loop transfer function

$$G(s)H(s) = \frac{Ke^{-\tau_D s}}{s(s^2 + 5s + 9)}$$

Determine the range of K ($K > 0$) for which the system is stable when

(i) dead-time $\tau_D = 0$,

(ii) dead-time $\tau_D = 1$, and $e^{-\tau_D s}$ is approximated by $(1 - \tau_D s)$, and

(iii) dead-time $\tau_D = 1$, and $e^{-\tau_D s}$ is approximated by a first-order Pade approximation:

$$e^{-\tau_D s} = \frac{1 - \frac{\tau_D}{2}s}{1 + \frac{\tau_D}{2}s}$$

5.8 Open-loop transfer functions of certain unity-feedback systems are given below. In each case, determine

(i) the range of values of K ($K > 0$) for which the system is stable,

(ii) the value of K that will result in the system being marginally stable, and

(iii) the location of the roots of the characteristic equation for the value of K found in (ii).

(a) $G(s) = \dfrac{K(s + 13)}{s(s + 3)(s + 7)}$ (b) $G(s) = \dfrac{K(s + 1)}{s(s - 1)(s + 6)}$

(c) $G(s) = \dfrac{K(s + 2)}{s(s + 5)(s^2 + 2s + 5)}$

5.9 The open-loop transfer functions of certain unity-feedback control systems are given below. In each case, discuss the stability of the closed-loop system as a function of $K > 0$. Determine the values of K which will cause sustained oscillations in the closed-loop system. What are the corresponding oscillation frequencies?

(a) $G(s) = \dfrac{K}{(s+2)(s+4)(s^2+6s+25)}$ (b) $G(s) = \dfrac{K(s+1)}{s(s-1)(s^2+4s+16)}$

MATLAB Exercise After completing the hand calculations based on Routh criterion, verify your results using root locus plots in MATLAB window.

5.10 Determine the values of $K > 0$ and $a > 0$, so that the system shown in Fig. P5.10 oscillates at a frequency 2 rad/sec.

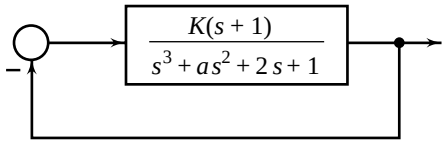

Fig. P5.10

MATLAB Exercise After completing the hand calculations based on Routh criterion, verify your results using root locus plots in MATLAB window.

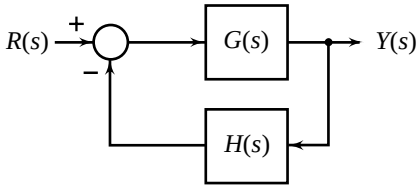

Fig. P5.11

5.11 A feedback control system is shown in Fig. P5.11. The process transfer function is

$$G(s) = \frac{K}{s(0{\cdot}2s+1)}$$

and the sensor transfer function is $H(s) = 1/(0.1s + 1)$.

(a) Determine the limiting value of gain $K > 0$ for a stable system.
(b) For the gain that results in marginal stability, determine the oscillation frequency.
(c) Reduce the gain to half the value found in (b) and study the relative stability of the system by shifting the axis and using the Routh stability criterion.

5.12 A unity-feedback control system has the open-loop transfer function

$$G(s) = \frac{K_c(1+T_D s)}{s^2(\tau s+1)}$$

Determine the stability limits on the controller parameters $K_c > 0$ and T_D for the following cases:

(a) proportional-only control ($T_D = 0$); and
(b) proportional-derivative control ($T_D > 0$).

5.13 Shown in Fig. P5.13 is a closed-loop control system.

(a) Find the range of gain K ($K > 0$), for which the system is stable.
(b) Suppose that the gain K is set to a value of 20. In addition, suppose that the sensor has a general time-constant of τ, rather than 0.1 sec given value. The transfer function of the sensor is then $1/(\tau s + 1)$. Find the allowable range for time-constant $\tau > 0$ such that the system is stable.

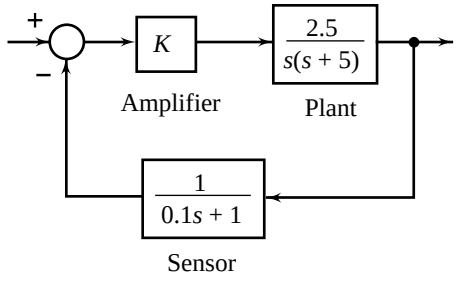

Fig. P5.13

(c) Suppose that in (b), the gain K is also variable. Find the range of gain K as a function of the sensor time-constant τ such that the system is stable.

The parameters K and τ may be represented in a plane with τ as the horizontal axis and K as the vertical axis. Determine the regions in the K-*vs*-τ plane in which the closed-loop system is stable, and unstable. Indicate the boundary on which the system is marginally stable.

5.14 Figure P5.14 shows a closed-loop system with a proportional-integral controller. Find the range of gain $K_c > 0$ as a function of integral time $T_I > 0$ such that the system is stable. Comment on the effect of decreasing T_I on the limit on gain K_c for stability.

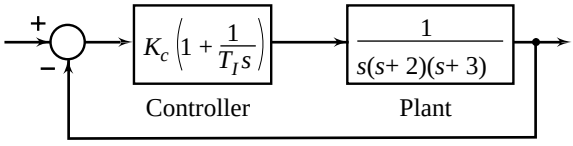

Fig. P5.14

5.15 The block diagram of a motor-control system with tachogenerator feedback is shown in Fig. P5.15. Find the range of $K > 0$ as a function of $K_t > 0$ such that the system is stable. Comment on the effect of increasing K_t on the limit on gain K for stability.

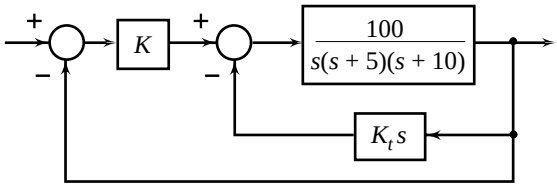

Fig. P5.15

Performance Specifications on System Time Response

6

6.1 INTRODUCTION

Recall the basic feedback system block diagram defined in Chapter 3; shown as Fig. 6.1 in a form convenient for analysis. The control system objectives are that output y follow input r, and disturbance w is ignored. Performance criteria must have to do with how well these two objectives are attained.

Clearly, the performance depends both on the system characteristics and on the nature of r and w. Precise mathematical functions for r and w will not generally be known in practice. For example, in a residential heating system (Example 1.2), we may be quite clear that r will be constant (say, 20°C) but we cannot predict the variation of the main disturbance—outdoor temperature. In a contouring machine control (Fig. 3.53), we don't know at the design stage, all the different shapes of parts that the machine will need to produce during its lifetime. In a radar tracking system (Example 1.3), the position and speed of the target to be tracked may vary in a random fashion. The uncertain nature of many practical commands and disturbances makes the development of performance criteria, based on the actual r and w experienced by the real system, difficult. It is common to base performance evaluation on system response to simple 'standard' test signals such as impulse, step, ramp, parabola, and sine wave (refer Section 2.5). This approach has been successful for a number of reasons.

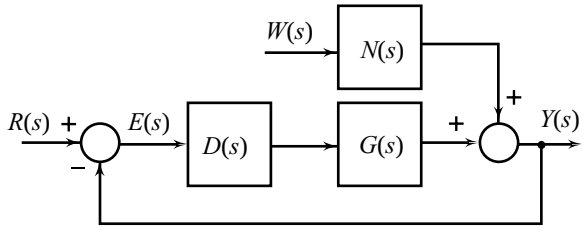

Fig. 6.1 Block diagram representation of a feedback system

1. The characteristics of actual signals which severely strain a control system are a sudden shock (impulse), a sudden change (step), constant velocity (ramp), and constant acceleration (parabola). Experience with the actual performance of various classes of control systems has established a good correlation between the response of systems to standard inputs and the capability of the systems to accomplish their required tasks.

2. Design is much concerned with the comparison of competitive systems. This comparison can often be made nearly as well in terms of standard inputs as for real inputs.
3. The simplicity of the form of standard inputs facilitates mathematical analysis and experimental verification.
4. For linear time-invariant systems, frequency-response curves (Chapter 9) are a complete description of the system's dynamic behaviour and allow one to compute the response to any input, not just sine waves.

The standard performance criteria in common use may be classified as falling into the *time domain* or the *frequency domain*. Time-domain specifications have to do with the response to steps, ramps, parabolas, and the like; while frequency-domain specifications are concerned with certain characteristics of the system's frequency response. Both types of specifications are often applied for the same system to ensure that certain behaviour characteristics will be obtained. It may be noted that all performance specifications are meaningless unless the system is absolutely stable.

The majority of analysis and design tools for feedback systems presuppose that a sufficiently accurate model of the process to be controlled has been set up. Using this model, the design is carried out to meet the time-domain and/or frequency-domain performance specifications. The analysis tools that verify the design also use the same model. This design is bound to be a disappointing one when the control system is put to real-life use. This is because in a reasonably complex system, there are always discrepancies between the model and the real process. Design methods that enable us to explicitly consider these discrepancies, i.e., designing a controller without having a precise mathematical model at hand, have yet to mature [74 –79]. We need a design that is not only valid for the approximate model but does hold with certainty for a class of plant models and hence for the real process. Good robustness against modelling errors and against variations in parameters of the model due to environmental and other effects, is an important design requirement.

We will not include the robustness/insensitivity requirements in our performance specifications for design. Our design is based on the assumption that the model is fixed once the model structure and parameters are given. The design is then analysed to study its robustness properties. Qualitative guidelines will be given to improve robustness.

6.2 THE PERFORMANCE SPECIFICATIONS

The study of a control system essentially involves the evaluation of transient and steady-state responses of the system, and robustness of this performance against model uncertainties and disturbances. The nature of transient response of a linear control system is revealed by any of the standard test signals—impulse, step, ramp, parabola—as this nature is dependent upon system poles only and not on the type of the input. It is therefore sufficient to analyse the transient response to one of the standard test signals; a step is generally used for this purpose. Steady-state response depends on both the system and the type of input. From the steady-state viewpoint, the 'easiest' input is generally a step since it requires only maintaining the output at a constant value once the transient is over. A more difficult problem is the tracking of a ramp input. Tracking of a parabola is even more difficult since a parabolic function is one degree faster than the ramp function. In practice, we seldom find it necessary to use a signal faster than a parabolic function; characteristics of actual signals, which the control systems encounter, are adequately represented by step, ramp, and parabolic functions.

The superposition principle allows us to consider response to commands apart from response to disturbances. If both occur simultaneously, the total response is just the superposition of the two individual responses.

Robustness describes the ability of the system to satisfactorily perform in the face of inconsistencies of the model used for design and the real plant.

6.2.1 Transient Response

The transient response of a practical control system often exhibits damped oscillations before reaching steady state. In specifying the transient-response characteristics of a control system to a unit-step input, it is common to specify the following:

(i) rise time, t_r;
(ii) peak time, t_p;
(iii) peak overshoot, M_p; and
(iv) settling time, t_s.

These specifications are defined below and are shown graphically in Fig. 6.2.

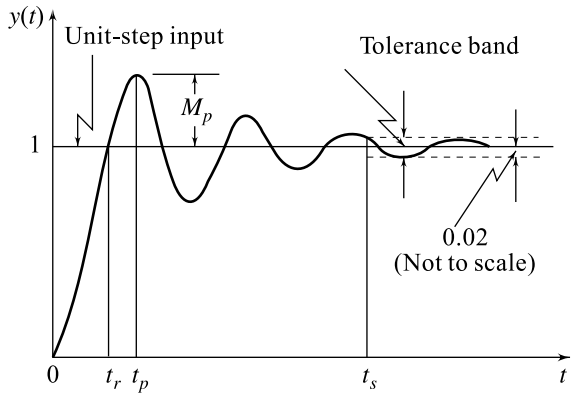

Fig. 6.2 Typical unit-step response of a control system

Rise Time, t_r For underdamped systems, the rise time is normally defined as the time required for the step response to rise from 0 to 100% of its final value. For overdamped systems, the 10 to 90% rise time is commonly used.

Peak Time, t_p It is the time required for the response to reach the first peak of the overshoot.

Peak Overshoot, M_p It is the peak value of the response curve measured from unity. If the final steady-state value of the response differs from unity, then it is common to use *per cent peak overshoot*. It is defined by

$$\text{Per cent peak overshoot} = \frac{y(t_p) - y(\infty)}{y(\infty)} \times 100\% \tag{6.1}$$

Settling Time, t_s The time required for the response to damp out all transients is commonly called the setting time. Theoretically, the time taken to damp out all transients may be infinity. In practice, however, the transient is assumed to be over when the error is reduced below some acceptable value. Typically, the acceptable level is set at two or five per cent of the final value. Figure 6.2 shows a *tolerance band* of $\pm$ 2%.

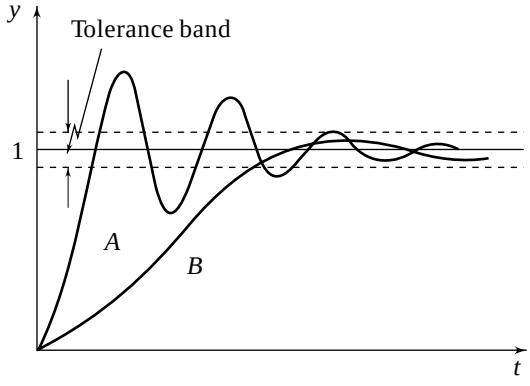

Fig. 6.3 Significance of settling time

Rise time and peak time are intended as speed of response criteria. Clearly, the smaller these values, the faster the system response. Peak overshoot is used mainly for relative stability. Values in excess of about 40% may indicate that the system is dangerously close to absolute instability. Settling time combines stability and speed of response aspects and is widely used. Note in Fig. 6.3 that system *A* (which has a much shorter rise time than system *B*) is, in a sense, not really faster than *B* since it does not settle in the neighbourhood of the desired value until a later time because of the undesirable feature of overshooting (or undershooting) the final value and then having to come back in the opposite direction.

6.2.2 Steady-State Response

Steady-state error, e_{ss}, is an index of steady-state response of a system to a specified input. It indicates the error between the actual output and the desired output as time t tends to infinity. With reference to the block diagram of Fig. 6.1, the steady-state error is defined as

$$e_{ss} = \lim_{t \to \infty} [r(t) - y(t)] \tag{6.2}$$

In specifying the steady-state response characteristics of a system, it is common to specify the steady-state error of the system to one or more of the standard test signals—step, ramp, parabola. We will discover later a certain pattern of behaviour as the input is made more difficult from the steady-state viewpoint. Figure 6.4 is a typical illustration of the effect of input severity on steady-state error. The steady-state error to step inputs is zero, as in Fig. 6.4a. The very same system subjected to a ramp input has constant e_{ss}, as shown in Fig. 6.4b. The parabolic input of Fig. 6.4c causes an error that increases linearly with respect to time.

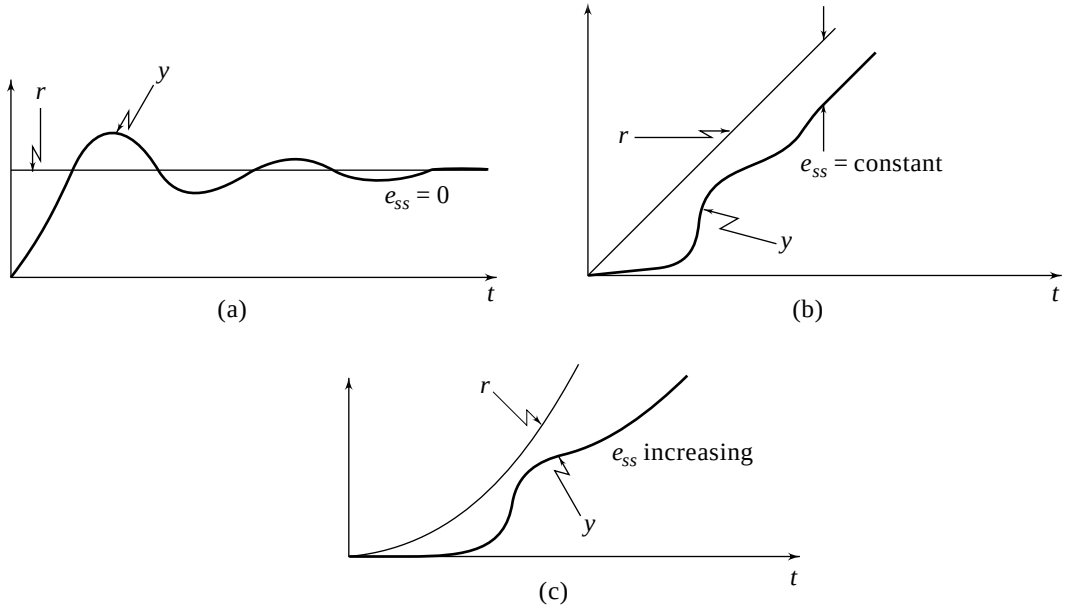

Fig. 6.4 Effect of input severity on steady-state error

When the system input is a disturbance w ($r \equiv 0$), some of the performance criteria given above can still be used, although others cannot. It is still possible to define a peak time t_p (Fig. 6.5). However, t_r, t_s, and M_p are all referenced to the desired step size, which is now zero; thus these indices cannot be used.

Decay ratio, the ratio of the second overshoot divided by the first, is a transient performance criterion often used in process control systems, the most common design value being 1/4. We could also use the number of cycles to damp the amplitude to, say, 10%

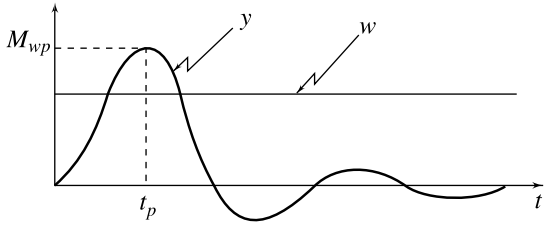

Fig. 6.5 Time-domain specifications for disturbance input

of M_{wp}—the peak value of the response to disturbance input. The smaller the number of cycles, the better is the speed of response and relative stability.

When the system input is a disturbance w, the definition of steady-state error still applies and we would expect the trend of worsening error as w is changed from step to ramp to parabola, similar to the behaviour of Fig. 6.4.

6.2.3 Robustness

So far the design objectives have been formulated as requirements on the closed-loop response $y(t)$ to command and disturbance inputs. These specifications on stability, speed of response, and steady-state accuracy are considered in design under the assumption that a nearly precise model of the plant is available.

The basic assumption of availability of precise model of the plant, is almost never true. There are almost always inconsistencies of the model and the real plant—called *model uncertainties*. Following are three main reasons for model uncertainties:

(a) Model uncertainties occur because of an incomplete knowledge of the system. As a typical example, the structure of the model equations can be determined by means of basic laws of physics and engineering, but the numerical values of the parameters are only known within tolerances. If the model parameters are determined experimentally, the uncertainties depend on the amount of disturbances that excited the plant during the experiment.

All models in our examples contain parameters: mass, inertia, damping coefficient, spring constant; electrical resistance, inductance, capacitance; thermal resistance, capacitance; hydraulic resistance, capacitance; etc. The parameter values are known only to certain tolerances; hence the discrepancy between the model and the physical system. Parameters may also vary with temperature or other environmental conditions; aging of components, etc.

(b) Achievable performance of a control system depends, in part, on the quality of a model: the more stringent the requirements, the better the model must be. On the other hand, increased complexity of the model often goes hand in hand with increased complexity of design of a control system. Therefore, we use a model of no greater complexity than is needed by the performance to be achieved. This implies that the design of the control system needs to take into account the inaccuracy of the model. The use of a linearized model of a nonlinear system falls in this category, as does the use of a single linear model for all expected operating points, as opposed to a different model for each case. Different components of systems (actuators, sensors, amplifiers, gears, belts, etc.) are sometimes modelled by constant gains, even though they have dynamics or nonlinearities. Dynamic structures (e.g., aircrafts, satellites, missiles) have complicated dynamics at high frequencies, and these may initially be ignored. There is often a *truth model*, the most accurate model we have, and a simplified *design model*, used as a basis for the design. The design model may therefore have inadequate structure; though the structure of truth model (often known) may be adequate.

(c) A model is based upon consideration of some physical phenomena thought to represent the salient features of the plant. In practice, a model used for control system design does not include all physical effects; secondary physical effects are excluded because of complexity and engineering study costs. Examples are parasitic capacitances, structural vibration modes in a robot whose links have some compliance, and vibration dynamics due to oil compressibility in a hydraulic system. Since we have no truth model, we cannot precisely assess the effect of these uncertainties. Engineering judgement and experience are invoked to produce rough estimates of the bounds of the magnitude of deviations of the input-output behaviour.

In any case, the model at hand yields merely an approximation of the original system performance. We call this model the *nominal model* of the plant. *Model uncertainties* are the general notion for deviations of

the model dynamics from the original system behaviour. Different specific notions are commonly used in literature to describe the special forms of uncertainties. Model uncertainties can be caused by *inaccuracies* or *perturbations* of the parameter values and/or the *model structure*. With respect to the knowledge available about the causes of the uncertainties, *structured* and *unstructured* uncertainties are distinguished. Uncertainties of particular parameters, or the modelling errors that occur because of imperfect structure of the model, e.g., by the use of a linear model for an intrinsically nonlinear process or by omitting high-frequency dynamics or time lags; are examples of structured uncertainties. In the case of structured uncertainties, particular points within the plant are made responsible for the uncertainties. On the contrary, in the case of unstructured uncertainties, it is only known that there are some discrepancies between the model and the real plant and, probably, how large the resulting deviations of the input-output behaviour may be. Particular points within the plant responsible for the uncertainties are not known.

It is usually possible to quantify and bound the discrepancy between the plant and the model. For example, a particular parameter may be thought to lie between two limits, with a specific midrange value used in the design model. Very often, these bounds are really educated guesses as engineering, like any other profession, has its share of art. The design model then becomes a member of a *class* of models, one member of which is believed to represent the plant.

Since we do not know which member of the class represents the plant, the safe and reasonable course is to require that the control system stabilize *all* members of the class. Since that is more difficult to do than simply stabilizing a single model, we may have to give up something from the single-model performance to satisfy the additional requirement.

The deterministic way of modelling uncertain systems leads to a family $\mathcal{G}$ of plants, where each member of the family may represent the original system, but it remains unknown which member does. This can be reflected by the equation

$$\hat{G}(s) = G(s) + \Delta(s)G(s)$$

where $G(s)$ represents the nominal model of the plant, and the family $\mathcal{G}$ consists of a set of perturbed plants $\hat{G}(s)$; $\Delta(s)G(s)$ represents the error model (refer Fig. 6.6).

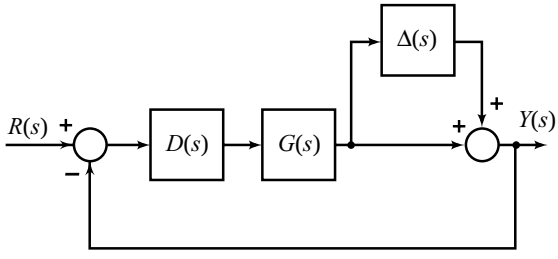

Fig. 6.6 Block diagram model of a plant with unmodelled dynamics

Robustness describes the ability of the system to satisfactorily perform for all the models $\hat{G}(s)$ in the family $\mathcal{G}$. A *robust controller* is a feedback controller that satisfies the design requirements on stability, speed of response, and steady-state accuracy in connection with all the models of a given family $\mathcal{G}$.

Robustness against unmodelled dynamical elements and disturbances is a 'structural' property of the feedback systems. Feedback makes it possible to improve robustness against variations of the performance of some system part or to attenuate the effects of unmeasurable external disturbances. These are the main reasons for deliberately introducing feedback into already existing processes. The introduction of feedback is mainly motivated by the incompleteness of the knowledge of the system to be controlled and the effects of external disturbances. More strictly, the use of feedback can be regarded as unreasonable if there is no uncertainty in the system, because for the unperturbed system, open-loop control may produce the same or a probably better output.

In *linear control theory*, the robustness requirement plays a minor role in the design procedure; the design engineer focuses his attention primarily on the dynamics specifications while observing some general

guidelines concerning the robustness improvement through feedback control. These qualitative robustness considerations work very well when small model uncertainties are encountered.

On the other hand, in *robust control theory*, the robustness requirement is the primary aim of design. Quantitatively specified relations between the amount of uncertainties and the properties to be attained dominate the design process. The quantitative robustness considerations become significant when model uncertainties are large [74–79].

Our focus in this book is on linear control design (based on root locus plots, Bode plots and Nichols chart) using nominal plant models for realization of specifications on stability, speed of response and steady-state accuracy. Qualitative robustness considerations will be used to evaluate the performance of the resulting controllers for real plants. In Appendix A, we will demonstrate the power of MATLAB/Simulink for evaluation of robustness properties of feedback controllers.

6.3 TRANSIENT RESPONSE SPECIFICATIONS IN TERMS OF POLE LOCATIONS

The design algorithms presented later require the transient specifications to be translated into a set of desired poles of the closed-loop system. This equivalently means that we have to identify a model whose response to a step input resembles the specified response. We first attempt a second-order continuous-time model.

The desired closed-loop transfer function of the system is assumed to be of the form (refer Section 2.8)

$$\frac{Y(s)}{R(s)} = \frac{\omega_n^2}{s^2 + 2\zeta\omega_n s + \omega_n^2} \tag{6.3}$$

where ζ and ω_n are, respectively, the *damping ratio* and the *undamped natural frequency* of the system; $\zeta = 0$ for an *undamped* system, $0 < \zeta < 1$ for an *underdamped* system, $\zeta = 1$ for a *critically damped* system, and $\zeta > 1$ for an *overdamped* system.

The characteristic equation of the closed-loop system is

$$\Delta(s) = s^2 + 2\zeta\omega_n s + \omega^2{}_n = 0 \tag{6.4a}$$

The characteristic roots

$$s_{1,2} = -\zeta\omega_n \pm j\omega_n\sqrt{1-\zeta^2} \tag{6.4b}$$

are the closed-loop poles of the system.

Figure 6.7 shows the locus of the poles of the standard second-order system (6.3), with ω_n held constant and ζ varying. For $\zeta = 0$, the poles are on the imaginary axis. As ζ increases, the poles move away from the imaginary axis along a circular path of radius ω_n meeting at the point $s = -\omega_n$, and then separating and travelling along the real axis, one towards zero and the other towards infinity. For $0 < \zeta < 1$, the poles are complex conjugate pair making an angle

$$\theta = \cos^{-1}\zeta \tag{6.5}$$

with the negative real axis; θ may be referred to as *damping angle.* For $\zeta = 1$, both the poles are on the negative real axis, repeated, and for $\zeta > 1$, the two poles are on the negative real axis, distinct.

We now study the transient response of the second-order system to unit-step input. The unit-step response has the Laplace transform (refer Eqn. (6.3))

$$Y(s) = \frac{\omega_n^2}{s(s^2 + 2\zeta\omega_n s + \omega_n^2)} \tag{6.6}$$

For $0 < \zeta < 1$, the inverse Laplace transformation gives (refer Eqn. (2.79))

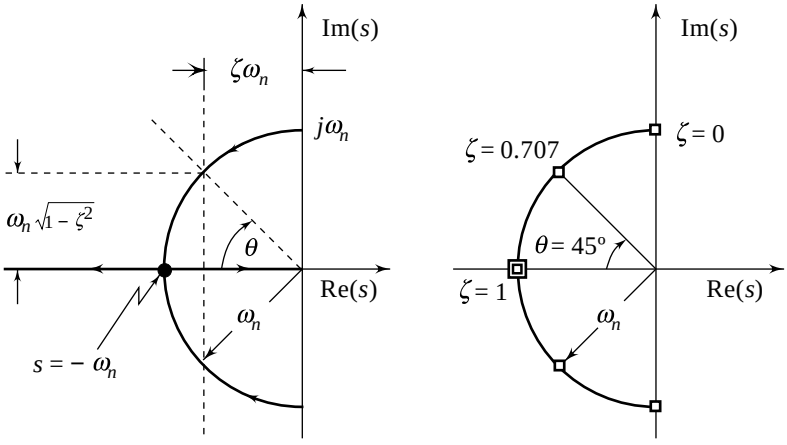

(a) (b)

Fig. 6.7 Pole locations for the standard second-order system

$$y(t) = 1 - \frac{e^{-\zeta\omega_n t}}{\sqrt{1-\zeta^2}} \sin\left(\omega_n\sqrt{1-\zeta^2}\, t + \theta\right) \tag{6.7}$$

where $\theta = \cos^{-1}\zeta$

The characteristic features of this response are shown in Fig. 6.8. The response exhibits decaying oscillations of frequency $\omega_d = \omega_n\sqrt{1-\zeta^2}$; ω_d is called the *damped natural frequency*. The curves

$$\left[1 \pm \frac{e^{-\zeta\omega_n t}}{\sqrt{1-\zeta^2}}\right]$$

are the envelope curves for the step response. The response curve $y(t)$ always remains within this pair of envelope curves. The time-constant of these envelope curves is $1/\zeta\omega_n$. The speed of decay of the transient response depends on the value of the *time-constant*

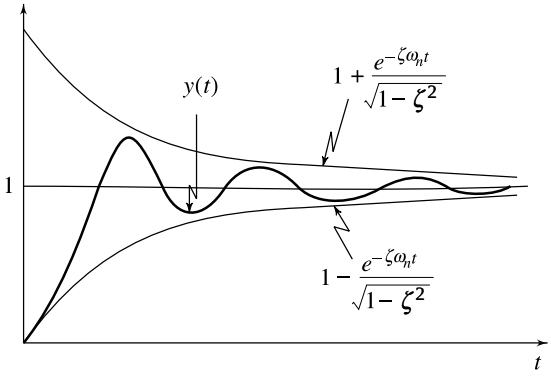

Fig. 6.8 Typical unit-step response of underdamped standard second-order system

$$\tau = \frac{1}{\zeta\omega_n} \tag{6.8}$$

Therefore, the larger the product $\zeta\omega_n$, the greater is the decay of the transient.

The time response curves for various values of ζ plotted against normalized time $\omega_n t$ are shown in Fig. 6.9. For $\zeta = 0$, the system response exhibits continuous oscillations (refer Eqn. (2.76)). As ζ is increased, the response becomes progressively less oscillatory till it becomes critically damped (just non-oscillatory) for $\zeta = 1$ (refer Eqn. (2.81)), and overdamped for $\zeta > 1$ (refer Eqn. (2.82)).

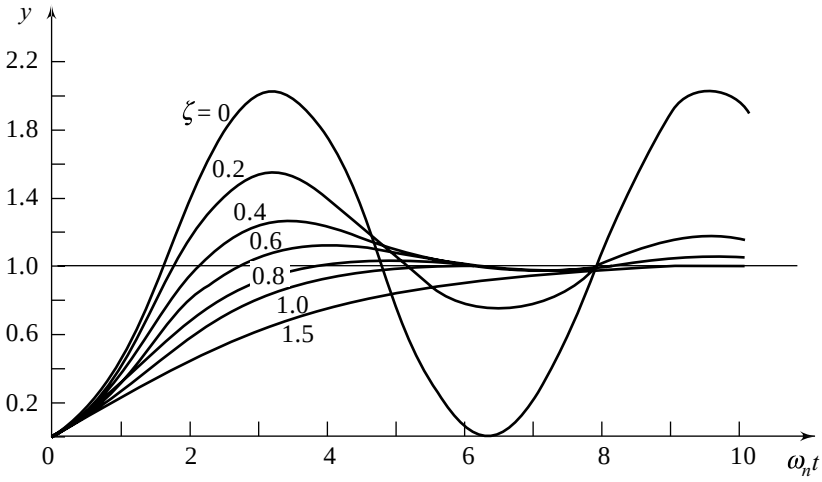

Fig. 6.9 Unit-step response curves of standard second-order system

Larger values of ζ give smaller values of peak overshoot but a slower rise of response. No overshoot at all is sometimes desirable; but usually this needlessly penalizes speed of response. Many systems are designed for 5 to 25% peak overshoot. For designs with peak overshoot less than five per cent, the price is paid in terms of speed of response, and the designs with peak overshoot more than 25% run the risk of being close to absolute instability.

Let us obtain the expressions for rise time, peak time, peak overshoot, settling time, and steady-state error, for a second-order system whose dynamics for the underdamped case are described by Eqn. (6.7).

6.3.1 Measures of Performance of the Standard Second-Order System

Rise Time, t_r Of the various definitions for rise time, the 0 – 100% rise time is meaningful for the underdamped response and easy to find. Referring to Eqn. (6.7), we observe that $y(t)$ crosses the final value of unity where the sine function is zero. The first crossing will occur when the argument is equal to π. Therefore, the rise time is

$$t_r = \frac{\pi - \theta}{\omega_n \sqrt{1 - \zeta^2}}; \quad \theta = \cos^{-1}\zeta \tag{6.9}$$

It can be seen that the value of θ lies between $\pi/2$ and 0 for $0 < \zeta < 1$. For moderate overshoots of 5–25%, the damping ratio ζ is in the range 0.4–0.7 (this we will prove shortly) and the normalized rise time $\omega_n t_r$ is approximately the same over this range, as is seen from Fig. 6.10. Thus, for a small value of t_r, ω_n must be large.

In frequency domain, the speed of response of a system is characterized by its *bandwidth* (refer Fig. 2.22). Precise significance of bandwidth in control design, and its relationship to speed of response will be given in Chapter 9. Here we

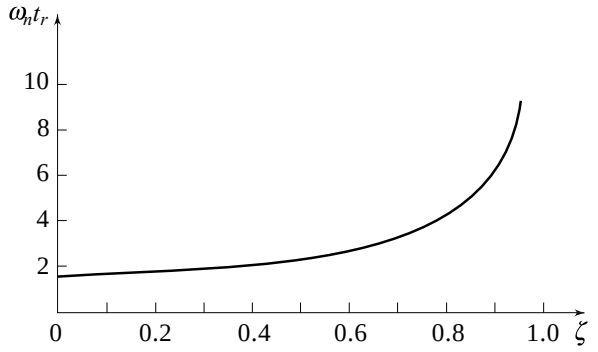

Fig. 6.10 Normalized rise time versus damping ratio

rely on the intuitive notion of bandwidth by reasoning as follows: every input can be regarded as comprising components at various frequencies; a rapidly changing input means that it has a large high-frequency content, while a smooth, slow varying input has a relatively smaller high-frequency content. Thus, if the control system is to faithfully reproduce an input that is changing rapidly, it must be capable of faithfully reproducing inputs at high frequencies, i.e., have a large bandwidth. A step change (i.e., a discontinuity) in the input has a large amount of high-frequency content: to reproduce it faithfully (with a short rise time) requires a high bandwidth.

In a control system, the input signal may contain spurious noise signals in addition to the true signal input, or there may be sources of noise within the closed-loop system. This noise is generally in a band of frequencies above the dominant frequency band of the true signal. Thus, in order to reproduce the true signal and attenuate the noise, feedback control systems are designed to have a moderate bandwidth. This imposes a limit on reducing rise time and increasing ω_n. Large ω_n has a large bandwidth and will therefore allow the high-frequency noise signals to affect the performance.

Peak time, t_p Equating the derivative of $y(t)$ in Eqn. (6.7) to zero to determine the extrema of the response, easily yields the equation

$$\frac{\zeta \omega_n}{\sqrt{1-\zeta^2}} e^{-\zeta \omega_n t} \sin\left(\omega_n \sqrt{1-\zeta^2}\, t + \theta\right)$$

$$- \frac{e^{-\zeta \omega_n t}}{\sqrt{1-\zeta^2}} \omega_n \sqrt{1-\zeta^2} \cos\left(\omega_n \sqrt{1-\zeta^2}\, t + \theta\right) = 0$$

or

$$\frac{\omega_n e^{-\zeta \omega_n t}}{\sqrt{1-\zeta^2}} \left[\zeta \sin\left(\omega_n \sqrt{1-\zeta^2}\, t + \theta\right) - \sqrt{1-\zeta^2} \cos\left(\omega_n \sqrt{1-\zeta^2}\, t + \theta\right)\right] = 0 \qquad (6.10)$$

From Fig. 6.7a, we observe that $\zeta = \cos\theta$, and $\sqrt{1-\zeta^2} = \sin\theta$. Therefore, the quantity inside the brackets in Eqn. (6.10) can be expressed as

$$\sin\left(\omega_n \sqrt{1-\zeta^2}\, t + \theta\right)\cos\theta - \cos\left(\omega_n \sqrt{1-\zeta^2}\, t + \theta\right) \sin\theta = 0$$

which gives $\sin\left(\omega_n \sqrt{1-\zeta^2}\, t\right) = 0$

This implies that at the extrema of the response,

$$\omega_n \sqrt{1-\zeta^2}\, t = m\pi;\ m = 0, 1, 2, \ldots \qquad (6.11)$$

Since the peak time corresponds to first overshoot,

$$t_p = \frac{\pi}{\omega_n \sqrt{1-\zeta^2}} \qquad (6.12)$$

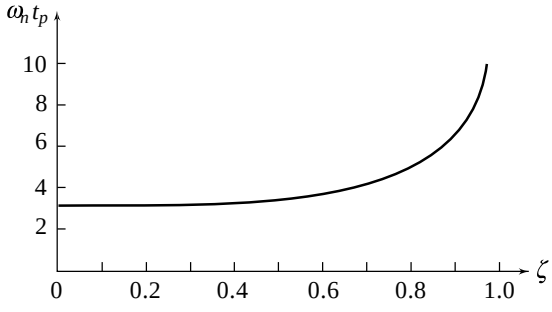

Fig. 6.11 Normalized peak time versus damping ratio

The first undershoot will occur at $t = 2\pi \Big/ \left[\omega_n \sqrt{1-\zeta^2}\right]$, the second overshoot at $t = 3\pi \Big/ \left[\omega_n \sqrt{1-\zeta^2}\right]$, and so on. A plot of normalized peak time $\omega_n t_p$ vs ζ is given in Fig. 6.11.

Peak overshoot, M_p From Eqns (6.7) and (6.12), we obtain

$$M_p = y(t_p) - 1 = -\frac{e^{-\zeta\omega_n t_p}}{\sqrt{1-\zeta^2}} \sin\left(\omega_n\sqrt{1-\zeta^2}\, t_p + \theta\right)$$

which gives
$$M_p = e^{-\pi\zeta/\sqrt{1-\zeta^2}} \tag{6.13}$$

Therefore, the per cent peak overshoot

$$= 100\ e^{-\pi\zeta/\sqrt{1-\zeta^2}}\ \% \tag{6.14}$$

Solving for ζ from Eqn. (6.13), we get

$$\zeta^2 = \frac{\left[\ln\left(M_p\right)\right]^2}{\left[\ln\left(M_p\right)\right]^2 + \pi^2} \tag{6.15}$$

As seen from Fig. 6.12, the peak overshoot is a monotonically decreasing function of damping ζ and is independent of ω_n. It is therefore an excellent measure of system damping.

Settling time t_s In the following discussion, the product of undamped natural frequency and settling time will be called the *normalized settling time*, and the product of undamped natural frequency and time is called *normalized time*. For a five per cent tolerance band, the normalized settling time *versus* damping ratio curve is shown in Fig. 6.13a. This curve can be understood by examining Fig. 6.13b which has an exaggerated scale to facilitate the discussion. If the damping ratio is 1, the response enters the tolerance band when the normalized time is 4.7 and stays within the band thereafter. This result has been obtained from Eqn. (2.81):

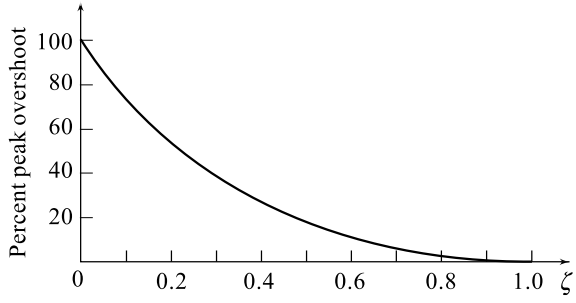

Fig. 6.12 Per cent peak overshoot versus damping ratio

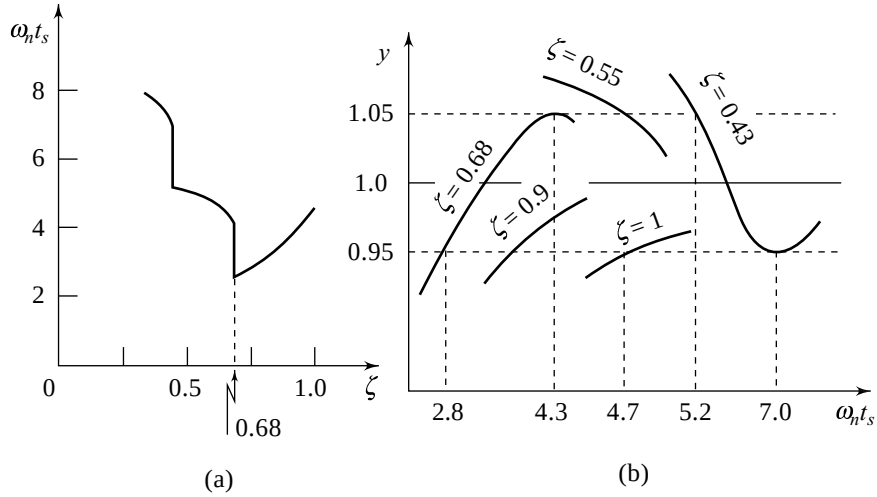

(a) (b)

Fig. 6.13 Normalized settling time versus damping ratio

For a critically damped system, the response

$$y(t) = 1 - e^{-\omega_n t} - \omega_n t\, e^{-\omega_n t}$$

The equation $1 - e^{-\eta} - \eta\, e^{-\eta} = 0.95$

gives $\eta = \omega_n t = 4.7$

As the damping ratio is reduced, $\omega_n t_s$ reduces. A damping ratio of 0.68 has the smallest $\omega_n t_s$ since the response curve crosses the lower limit of the band at $\omega_n t_1 = 2.8$ and overshoots five per cent reaching the upper limit at $\omega_n t_2 = 4.3$; a small decrease in ζ from the value 0.68 will result in a jump in $\omega_n t_s$ from 2.8 to 4.3. These results have been obtained from the following equations.

$$t_2 = \frac{\pi}{\omega_n \sqrt{1-\zeta^2}}$$

$$y(t) = 1 - \frac{e^{-\zeta\omega_n t}}{\sqrt{1-\zeta^2}} \sin\left(\omega_n \sqrt{1-\zeta^2}\, t + \cos^{-1}\zeta\right)$$

When $\zeta = 0.68$, $\omega_n t_2 = 4.3$ and $y(t_2) = 1.05$. Also, when $\zeta = 0.68$, the equation $y(t_1) = 0.95$ gives $\omega_n t_1 = 2.8$. The normalized settling time increases from the value 4.3 as ζ is reduced. At a damping ratio of 0.43, the response curve crosses the upper limit of the band at $\omega_n t = 5.2$ and undershoots five per cent reaching the lower limit at $\omega_n t = 7$. Therefore, there is a jump in normalized settling time at $\zeta = 0.43$. Extending this logic, we can get the $\omega_n t_s$ vs ζ curve.

We observe that normalized settling time is minimum for $\zeta = 0.68$. This fact justifies why control systems are normally designed to be underdamped.

Analytical expression for the $\omega_n t_s$ vs ζ curve of Fig. 6.13a is difficult to obtain. We can use an approximation for the range $0 < \zeta < 0.68$ by using the envelope of the damped sinusoid shown in Fig. 6.8. Setting the time at which the lower envelope of $y(t)$ equals the value of 0.95 as the settling time t_s, we get

$$1 - \frac{e^{-\zeta\omega_n t_s}}{\sqrt{1-\zeta^2}} = 0.95$$

Solving for t_s, we obtain

$$t_s = -\frac{1}{\zeta\omega_n} \ln\left(0.05\sqrt{1-\zeta^2}\right) \tag{6.16}$$

The value of $\ln\left(0.05\sqrt{1-\zeta^2}\right)$ varies between -3.0 and -3.3 as ζ varies from 0 to 0.68. A common design practice is to approximate settling time to three time-constants of the envelope of the damped sinusoidal oscillations (refer Eqn. (6.8)):

$$t_s \text{ (5\% tolerance)} \cong \frac{3}{\zeta\omega_n};\ 0 < \zeta < 0.68 \tag{6.17}$$

On similar lines, it can be established that for a two per cent tolerance band, normalized settling time is minimum at $\zeta = 0.8$. For $0 < \zeta < 0.8$, the settling time

$$t_s = -\frac{1}{\zeta\omega_n} \ln\left(0.02\sqrt{1-\zeta^2}\right) \tag{6.18}$$

The value of $\ln\left(0.02\sqrt{1-\zeta^2}\right)$ varies between -3.91 and -4.42 as ζ varies from 0 to 0.8. A common design practice is to approximate settling time to four time-constants of the envelope of the damped sinusoidal oscillation (refer Eqn. (6.8)):

$$t_s\,(2\%\text{ tolerance}) \cong \frac{4}{\zeta\omega_n};\ 0 < \zeta < 0.8 \tag{6.19}$$

Unless otherwise specified, we will use two per cent tolerance band for settling-time calculations.

Steady-state Error, e_{ss} From Eqn. (6.7), we obtain

$$e_{ss}\big|_{\text{unit step}} = \lim_{t\to\infty}\left[1 - y(t)\right] = 0$$

Thus, the standard second-order system has zero steady-state error to step inputs.

We now study the response of the standard second-order system to unit-ramp input $R(s) = 1/s^2$. The unit-ramp response has the Laplace transform (refer Eqn. (6.3))

$$Y(s) = \frac{\omega_n^2}{s^2(s^2 + 2\zeta\omega_n s + \omega_n^2)} \tag{6.20}$$

For $0 < \zeta < 1$, the inverse Laplace transformation gives (refer Eqn. (2.157))

$$y(t) = t - \frac{2\zeta}{\omega_n} + \frac{e^{-\zeta\omega_n t}}{\omega_n\sqrt{1-\zeta^2}}\sin(\omega_d t + 2\theta) \tag{6.21}$$

where $\theta = \cos^{-1}\zeta$

The response $y(t)$ for a typical value of ζ is plotted in Fig. 6.14. The steady-state error for unit-ramp input is given by

$$e_{ss}\big|_{\text{unit ramp}} = \lim_{t\to\infty}\left[t - y(t)\right] = \frac{2\zeta}{\omega_n} \tag{6.22}$$

From Fig. 6.14 it is observed that the nature of transient response to ramp input is similar to that of step input (damped oscillatory) and yields no new information about the transient behaviour of the system. As pointed out earlier, it is sufficient to investigate the transient response of a system to a step input only. Ramp-input response, of course, gives new information about the steady-state behaviour, which may be evaluated directly by the final-value theorem (Eqn. (2.45)).

The error response has the Laplace transform

$$E(s) = R(s) - Y(s)$$

Using Eqn.(6.3), we have

$$E(s) = \frac{s(s + 2\zeta\omega_n)}{s^2 + 2\zeta\omega_n s + \omega_n^2} R(s) \tag{6.23}$$

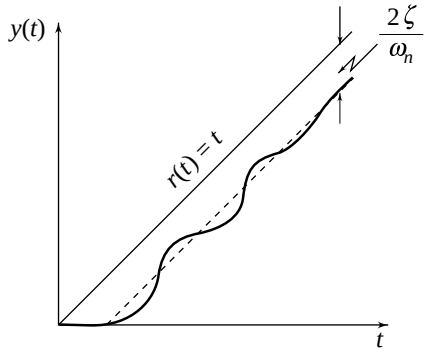

Fig. 6.14 Typical unit-ramp response of an underdamped standard second-order system

For a unit-ramp input, $R(s) = 1/s^2$ and

$$E(s) = \frac{s + 2\zeta\omega_n}{s(s^2 + 2\zeta\omega_n s + \omega_n^2)}$$

$$e_{ss}\big|_{\text{unit ramp}} = \lim_{s\to 0} s\,E(s) = \frac{2\zeta}{\omega_n} \tag{6.24}$$

To investigate the steady-state behaviour of the standard second-order system to unit-parabolic input, we substitute $R(s) = 1/s^3$ in Eqn. (6.23):

$$E(s) = \frac{s + 2\zeta\omega_n}{s^2(s^2 + 2\zeta\omega_n s + \omega_n^2)}$$

Since $E(s)$ has repeated pole at $s = 0$, the error response $e(t)$ will be unbounded, and therefore

$$\lim_{t\to\infty} e(t) = \infty = e_{ss}\big|_{\text{unit parabola}} \tag{6.25}$$

Therefore, in control systems represented by the standard second-order model, the steady-state error will be finite only if the actual signals which the control systems encounter are not faster than a ramp function.

From Eqns (6.9), (6.12), (6.13), (6.19) and (6.24), we observe that rise time, peak time, peak overshoot, settling time and steady-state error measures of the performance of a standard second-order system are mutually dependent, and therefore must be specified in a consistent manner.

6.3.2 What is the Best Damping Ratio to Use?

A very important question to answer before leaving this section is the best value of damping ratio ζ to choose for a control system.

Selection of damping ratio for industrial control applications requires a trade-off between relative stability and speed of response. A smaller damping ratio decreases normalized rise time (refer Fig. 6.10), but it increases the peak overshoot (refer Fig. 6.12). The final choice of the damping ratio is subjective. Many systems are designed for damping ratio in the range of 0.4 – 0.7 (this corresponds to peak overshoot in the range of 5 – 25%). If allowed by rise-time considerations, ζ close to 0.7 is the most obvious choice because it results in minimum normalized settling time (refer Fig. 6.13a).

If the requirement is to design an extremely accurate control system whose steady-state errors to position and velocity inputs are extremely small (e.g., to be used for navigation purposes), the transient response is not the primary performance criterion to optimize; minimum steady-state error is the major objective. With reference to Eqn. (6.24) we observe that the damping ratio ζ should be as small as possible because the steady-state error is proportional to ζ. Values close to 0.1 are not unreasonable for such applications; the disadvantage of relatively long settling time must be tolerated.

There are situations (e.g., in some robot-manipulator applications) where the overshoot cannot be tolerated. A good compromise between rise time and overshoot is $\zeta = 1$.

Example 6.1 Figure 6.15 shows block diagram of a control system whose objective is to control the position of mechanical load. The two potentiometers having sensitivity K_P convert the input and output positions into proportional electrical signals, which are in turn compared, and the error signal amplified by a factor K_A, is applied to the armature circuit of a dc motor whose field winding is excited with a constant voltage. The motor is coupled to the load through a gear train of ratio n. The block diagram also shows a minor feedback loop which corresponds to a tachogenerator connected in the system to improve damping. In this example, we consider proportional control only (tachogenerator disconnected); K_A is

the only design parameter. The other control schemes (PD, PI, minor-loop feedback) for this system will be considered later in this chapter.

When switch 'S' is open (tachogenerator disconnected), the block diagram of Fig. 6.15 reduces to that given in Fig. 6.16. The open-loop transfer function

$$D(s)G(s) = \frac{4500K_A}{s(s+361.2)} \tag{6.26}$$

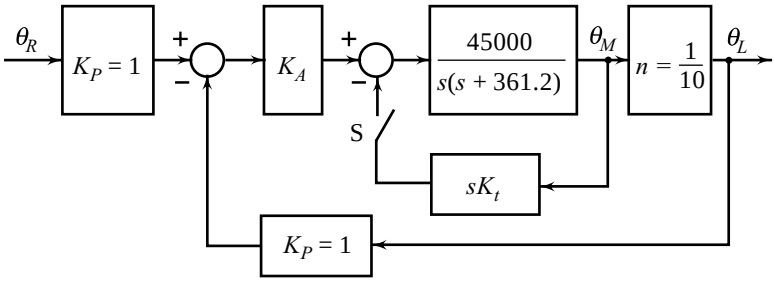

Fig. 6.15 Block diagram of a position control system

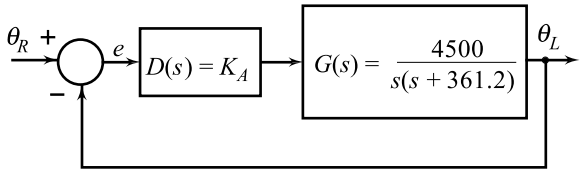

Fig. 6.16 Simplified block diagram of the system in Fig. 6.15 with $K_t = 0$

The characteristic equation of the unity-feedback system is

$$s^2 + 361.2s + 4500K_A = s^2 + 2\zeta\omega_n s + \omega_n^2 = 0 \tag{6.27a}$$

Natural frequency

$$\omega_n = \sqrt{4500K_A} \tag{6.27b}$$

Damping ratio

$$\zeta = \frac{361.2}{2\sqrt{4500K_A}} = \frac{2.692}{\sqrt{K_A}} \tag{6.27c}$$

The closed-loop poles are

$$s_{1,2} = -180.6 \pm \sqrt{32,616.36 - 4500K_A} \tag{6.28}$$

From the block diagram of Fig. 6.16, we obtain

$$\frac{E(s)}{\theta_R(s)} = \frac{1}{1 + D(s)G(s)} = \frac{1}{1 + \dfrac{4500K_A}{s(s+361.2)}} = \frac{s(s+361.2)}{s(s+361.2) + 4500K_A}$$

The steady-state error of the system due to a ramp input $\theta_R(s) = 1/s^2$ is given by

$$e_{ss}\big|_{\text{unit ramp}} = \lim_{s\to 0} s\,E(s) = \frac{361.2}{4500K_A} = \frac{0.0803}{K_A} \tag{6.29}$$

(i) *System with critical damping*

For $K_A = 7.247$, the damping ratio $\zeta = 1$, the natural frequency $\omega_n = 180.6$, and both the closed-loop poles are located at -180.6.

The steady-state error (Eqn. (6.29))

$$e_{ss}\big|_{\text{unit ramp}} = 0.011 \text{ rad}$$

(ii) *System with moderate damping*

For $K_A = 14.5$, the damping ratio $\zeta = 0.707$, the natural frequency $\omega_n = 255.44$ rad/sec, and the closed-loop poles are located at $-180.6 \pm j\,180.6$. The damped natural frequency is $\omega_d = \omega_n\sqrt{1-\zeta^2} = 180.6$ rad/sec.

Rise time $$t_r = \frac{\pi - \cos^{-1}\zeta}{\omega_d} = \frac{\pi - 45\left(\frac{\pi}{180}\right)}{180.6} = 0.013 \text{ sec}$$

Peak time $$t_p = \frac{\pi}{\omega_d} = 0.0174 \text{ sec}$$

Peak overshoot $$M_p = e^{-\pi\zeta/\sqrt{1-\zeta^2}} \times 100 = 4.3\%$$

Settling time t_s (two per cent tolerance) $= \dfrac{4}{\zeta\omega_n} = 0.0221$ sec

(Note that approximate expressions (6.17) and (6.19) cannot be used for calculation of settling time for systems with critical damping. However, using Fig. 6.13a we can easily establish the fact that settling time for the system with $K_A = 14.5$ is lower than for the system with $K_A = 7.247$)

The steady-state error

$$e_{ss}\big|_{\text{unit ramp}} = 0.0055 \text{ rad}$$

Therefore, the increase in amplifier gain K_A from the value 7.247 to 14.5 has resulted in a decrease in damping from $\zeta = 1$ to $\zeta = 0.707$, decrease in settling time, and decrease in steady-state error from 0.011 to 0.0055 rad. The price has been paid in terms of overshoot. Since 4.3 % peak overshoot is acceptable in many industrial control applications, moderate value of ζ results in better system performance compared to the critical value $\zeta = 1$.

(iii) *System with low damping*

For larger values of K_A, the damping ratio ζ reduces, natural frequency ω_n increases, and the real part of the poles is constant at -180.6, i.e., $\zeta\omega_n = 180.6$. As given by the approximate expression (6.19), the settling time does not change for $K_A > 14.5$. However, increase in K_A will result in reduced steady-state error to ramp input. Also, it will result in reduced rise time and hence better speed of response. The price is paid in terms of increased peak overshoot and hence poor relative stability. This means K_A can be increased at the most to a value for which the step-response overshoot is acceptable.

If 25% peak overshoot is considered acceptable, we have from Eqn. (6.15), $\zeta = 0.4$. $K_A = 45.3$ gives this value of damping. The other performance measures are:

$$\omega_n = 451.5 \text{ rad/sec}, \ \omega_d = 413.8 \text{ rad/sec}$$

$$t_r = 0.0048 \text{ sec}, \ t_p = 0.0076 \text{ sec},$$

$$e_{ss}\big|_{\text{unit ramp}} = 0.0018 \text{ rad.}$$

6.4 EFFECTS OF AN ADDITIONAL ZERO AND AN ADDITIONAL POLE

The expressions for features of the step response of a system—rise time, peak time, peak overshoot, settling time—derived in the last section, are valid only for the standard second-order system with closed-loop transfer function

$$M(s)= \frac{Y(s)}{R(s)} = \frac{\omega_n^2}{s^2 + 2\zeta\omega_n s + \omega_n^2} \tag{6.30}$$

The transfer function $M(s)$ has two poles and no zeros. For many practical systems, the closed-loop transfer function has more than two poles and/or finite zeros. In this section, we study the effects of adding poles and zeros to the standard second-order model.

Let a zero be added to $M(s)$ of Eqn. (6.30). Then we have

$$M_1(s) = \frac{Y_1(s)}{R(s)} = \frac{(s+\alpha)\,(\omega_n^2/\alpha)}{s^2 + 2\zeta\omega_n s + \omega_n^2} \tag{6.31}$$

The transfer function $M_1(s)$ has been normalized to have the gain at $s = 0$ equal to unity. This makes the final value of the unit-step response also 1, and thus the transfer function has been adjusted so that the system will track a step with zero steady-state error. The unit-step response of the one-zero, two-pole system may be determined from

$$Y_1(s) = \frac{(s+\alpha)\,(\omega_n^2/\alpha)}{s(s^2 + 2\zeta\omega_n s + \omega_n^2)} \tag{6.32}$$

$$= \frac{\omega_n^2}{s(s^2 + 2\zeta\omega_n s + \omega_n^2)} + \frac{s}{\alpha}\frac{\omega_n^2}{s(s^2 + 2\zeta\omega_n s + \omega_n^2)}$$

$$= Y(s) + \frac{s}{\alpha}Y(s) \tag{6.33a}$$

where $Y(s)$ is the Laplace transform of the unit-step response of standard second-order system (6.30).

From Eqn. (6.33a), we obtain

$$y_1(t) = y(t) + \frac{1}{\alpha}\frac{dy(t)}{dt} \tag{6.33b}$$

The effect of the added derivative term may be seen by examining Fig. 6.17a, where a case for a typical value of ζ is considered. We see from the figure that the effect of the zero is to contribute a pronounced early peak to the system's response whereby the peak overshoot may increase appreciably. From Fig. 6.17b, it is seen that the smaller the value of α, i.e., the closer the zero to the origin, the more pronounced is the peaking phenomenon. On account of this fact, *the zeros on the real axis near the origin are generally avoided in design.* However, in a sluggish system, the artful introduction of zero at the proper position can improve the transient response.

We further observe from Eqn. (6.33b) that as α increases, i.e., the zero moves farther into the left half of the s-plane; its effect becomes less pronounced. For sufficiently large values of α, the effect of zero on transient response may become negligible.

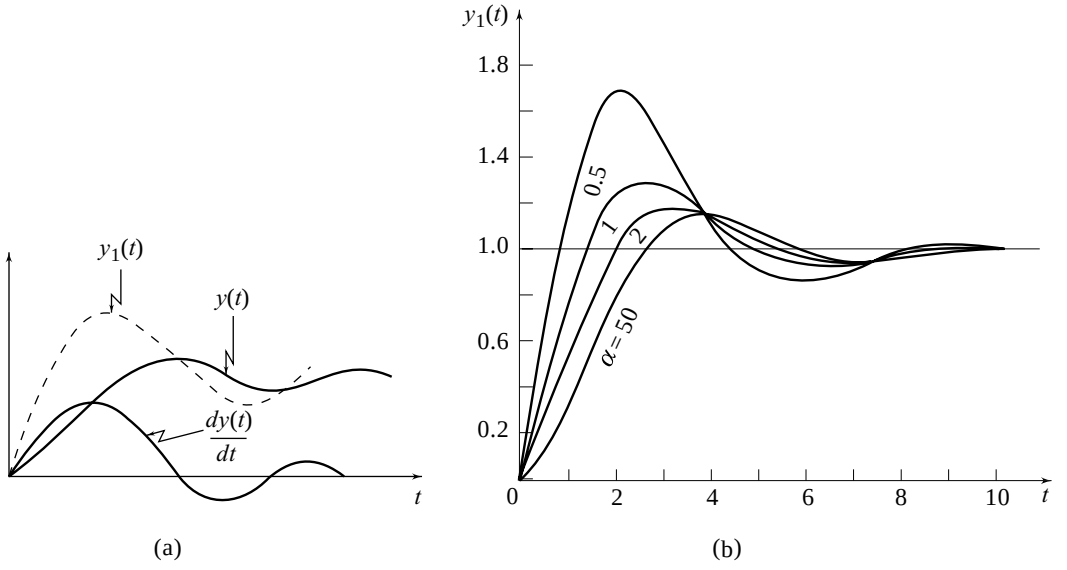

Fig. 6.17 (a) Unit-step response of a standard second-order system with an additional zero
(b) Response for several zero locations with $\zeta = 0.5, \omega_n = 1$

The transient analysis given by Eqn. (6.33b) is very informative in case the zero is in the right-half plane. In this case, α is negative and the derivative term is subtracted rather than added. A typical case is sketched in Fig. 6.18; the response has become sluggish.

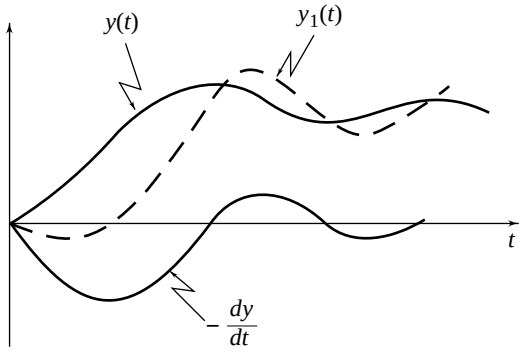

Fig. 6.18 Unit-step response of a standard second-order system with a zero in the right-half plane

For a quantitative transient analysis of the standard second-order system with a finite zero, we obtain $y_1(t)$ from $Y_1(s)$ of Eqn. (6.32). Partial-fraction expansion of $Y_1(s)$ gives

$$Y_1(s) = \frac{1}{s} + \frac{A}{s + \zeta\omega_n - j\omega_n\sqrt{1-\zeta^2}} + \frac{A^*}{s + \zeta\omega_n + j\omega_n\sqrt{1-\zeta^2}}$$

where A^* is complex-conjugate of A.

The pole-zero pattern of $Y_1(s)$ is shown in Fig. 6.19. From the geometry of this figure, we obtain

$$A = \frac{\omega_n^2}{\alpha} \left. \frac{s+\alpha}{s\left(s + \zeta\omega_n + j\omega_n\sqrt{1-\zeta^2}\right)} \right|_{s=-\zeta\omega_n + j\omega_n\sqrt{1-\zeta^2}}$$

$$= \frac{\omega_n^2}{\alpha} \frac{K e^{j\phi}}{\left[\omega_n e^{j(\pi-\theta)}\right]\left[2\omega_n\sqrt{1-\zeta^2}\, e^{j\pi/2}\right]} = \frac{K}{2\alpha\sqrt{1-\zeta^2}} e^{j\left(\phi+\theta+\frac{\pi}{2}\right)}$$

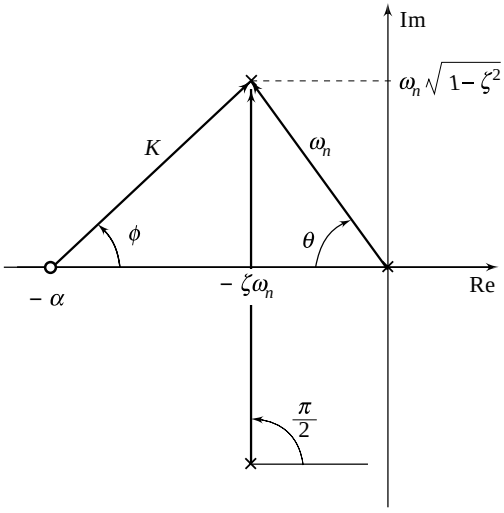

Fig. 6.19 Pole-zero pattern of $Y_1(s)$ in Eqn. (6.32)

The response $y_1(t)$ is obtained as follows (refer Eqn. (5.7)):

$$y_1(t) = 1 + 2\,\frac{K}{2\alpha\sqrt{1-\zeta^2}}\,e^{-\zeta\omega_n t}\cos\left(\omega_n\sqrt{1-\zeta^2}\,t + \phi + \theta + \frac{\pi}{2}\right)$$

$$= 1 + \frac{K}{\alpha\sqrt{1-\zeta^2}}\,e^{-\zeta\omega_n t}\cos\left(\omega_n\sqrt{1-\zeta^2}\,t + \phi + \theta + \frac{\pi}{2}\right) \qquad (6.34)$$

Figure 6.20 shows the effect of the zero on peak overshoot of the step response $y_1(t)$ when $\zeta = 0.5$ and $\omega_n = 1$. The parameter η in the figure represents normalized zero location: $\alpha = \eta\zeta\omega_n$. When η is large, the zero is far removed from the poles and will have little effect on the response. If $\eta = 1$, the zero is at the value of the real part of the poles and has a substantial influence on the response. $\eta < 1$ results in the highly pronounced peaking phenomenon.

Now let us consider the effect of an additional pole on the response of a standard second-order system (6.30). To this end we consider a transfer function of the form

$$M_2(s) = \frac{Y_2(s)}{R(s)} = \frac{\omega_n^2\,\alpha}{(s+\alpha)(s^2 + 2\zeta\omega_n\,s + \omega_n^2)} \qquad (6.35)$$

The transfer function $M_2(s)$ has been normalized to have the gain at $s = 0$ equal to unity. The unit-step response of this no-zero, three-pole system may be determined from

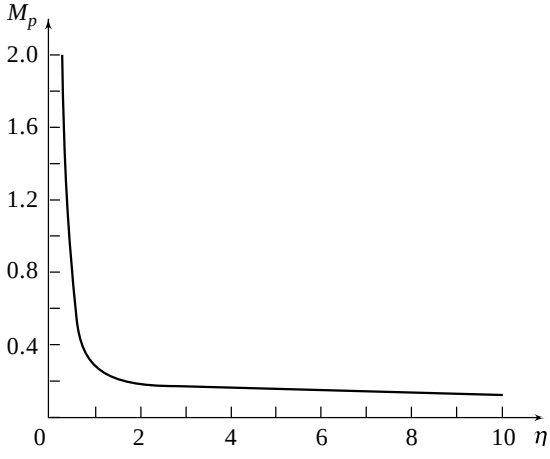

Fig. 6.20 Plot of peak overshoot for several locations of an additional zero ($\zeta = 0.5$, $\omega_n = 1$)

$$Y_2(s) = \frac{\omega_n^2\,\alpha}{s(s+\alpha)(s^2+2\zeta\omega_n s+\omega_n^2)}$$

$$= \frac{1}{s} + \frac{A_1}{s+\alpha} + \frac{A_2}{s+\zeta\omega_n - j\omega_n\sqrt{1-\zeta^2}} + \frac{A_2^*}{s+\zeta\omega_n + j\omega_n\sqrt{1-\zeta^2}}$$

From the geometry of Fig. 6.21a, we obtain

$$A_1 = \frac{\omega_n^2\,\alpha}{\alpha e^{j\pi}\; Ke^{j(\pi+\phi)}\; Ke^{j(\pi-\phi)}} = \frac{\omega_n^2}{K^2\,e^{j\pi}} = \frac{-\omega_n^2}{K^2} \tag{6.36a}$$

From the geometry of Fig. 6.21b, we obtain

$$A_2 = \frac{\omega_n^2\,\alpha}{\omega_n\,e^{j(\pi-\theta)}\left(2\omega_n\sqrt{1-\zeta^2}\;e^{j\pi/2}\right)Ke^{j\phi}}$$

$$= \frac{\alpha}{2K\sqrt{1-\zeta^2}\;e^{j\left(\pi-\theta+\frac{\pi}{2}+\phi\right)}} = \frac{\alpha\,e^{j\left(\frac{\pi}{2}+\theta-\phi\right)}}{2K\sqrt{1-\zeta^2}} \tag{6.36b}$$

The response

$$y_2(t) = 1 - \frac{\omega_n^2}{K^2}e^{-\alpha t} + \frac{\alpha}{K\sqrt{1-\zeta^2}}e^{-\zeta\omega_n t}\cos\left(\omega_n\sqrt{1-\zeta^2}\;t+\theta+\frac{\pi}{2}-\phi\right) \tag{6.37}$$

From Fig. 6.21 and Eqns (6.36), it can be seen that

$$\lim_{\alpha\to 0}|A_1| = 1;\ \lim_{\alpha\to 0}|A_2| = 0$$

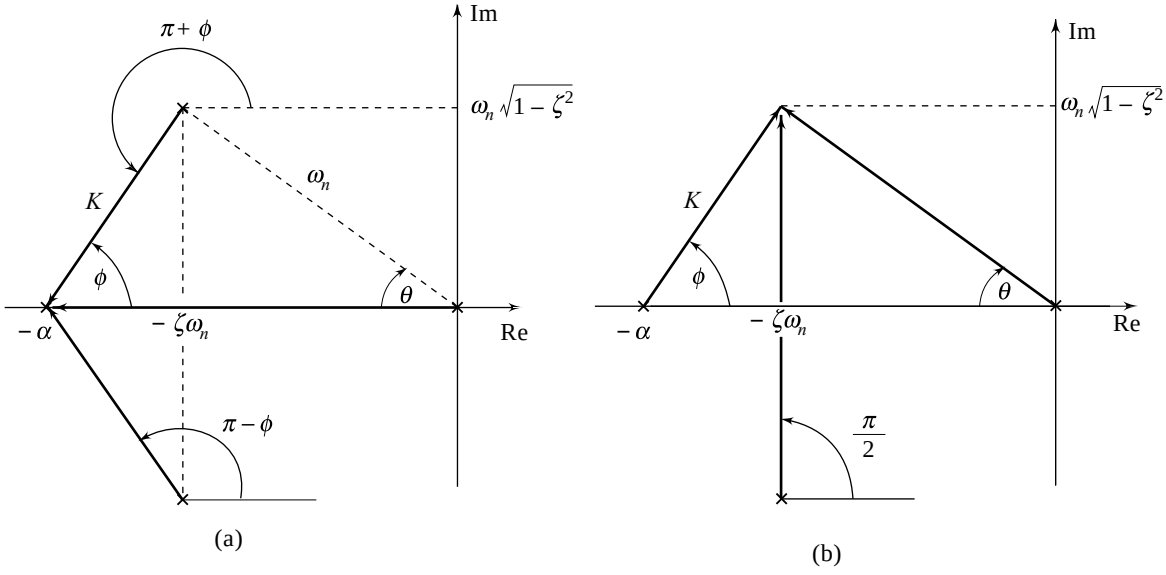

Fig. 6.21 Pole-zero pattern of $Y_2(s)$ in Eqn. (6.35)

from which we deduce that as $\alpha \to 0$, the effect of the two complex poles at $-\zeta\omega_n \pm j\omega_n\sqrt{1-\zeta^2}$ diminishes and the transient response becomes dominated by the pole at $-\alpha$, i.e., the term $e^{-\alpha t}$ of Eqn. (6.37). This means that a pole on the negative real axis near the origin will dominate the response of the system. This domination is enhanced by the fact that if $\alpha << \zeta\omega_n$, the effect of the term $e^{-\alpha t}$ will last much longer than that of the term $e^{-\zeta\omega_n t}$.

Now let us see what happens as α becomes large. From Fig. 6.21 and Eqns (6.36), it can be seen that

$$\lim_{\alpha\to\infty} |A_1| = 0; \quad \lim_{\alpha\to\infty} |A_2| = \frac{1}{2\sqrt{1-\zeta^2}}$$

from which we see that as α increases, an opposite effect is observed. The complex poles at $-\zeta\omega_n \pm j\omega_n\sqrt{1-\zeta^2}$ now dominate the response, while the contribution of the pole at $-\alpha$ diminishes in significance. Further, if $\zeta\omega_n << \alpha$, the effect of the term $e^{-\alpha t}$ will be over much more quickly than the term whose magnitude decreases as $e^{-\zeta\omega_n t}$. All the preceding effects may be seen quite clearly in Fig. 6.22. Fig. 6.23 shows the effect of the third pole at $s = -\alpha = -\eta\zeta\omega_n$ on rise time of the step response. When η is large, the real pole is far removed from the complex poles and will have little effect on the response. If $\eta = 1$, the real pole is at the value of the real part of the complex pole pair and has a substantial effect on the response. $\eta < 1$ makes the system very sluggish.

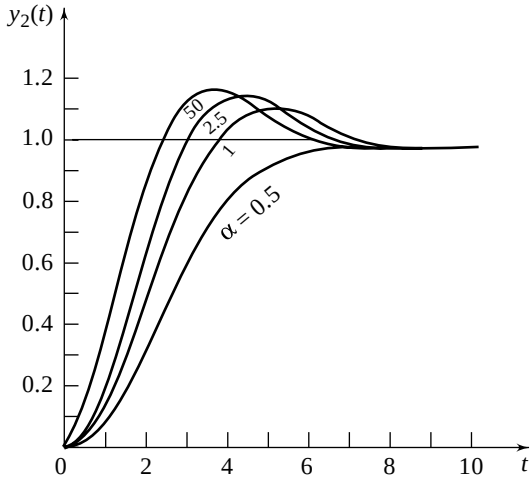

Fig. 6.22 Unit-step response of a standard second-order system ($\zeta = 0.5$, $\omega_n = 1$) for several locations of an additional pole

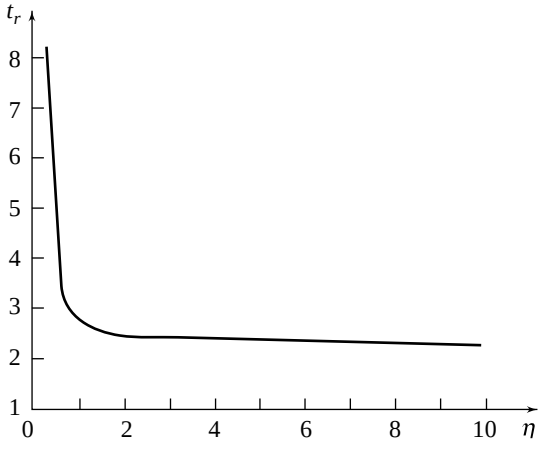

Fig. 6.23 Plot of rise time for several locations of an additional pole ($\zeta = 0.5$, $\omega_n = 1$)

6.5 DESIRED CLOSED-LOOP POLE LOCATIONS AND THE DOMINANCE CONDITION

From the discussion given in the preceding sections, it becomes apparent that for second-order feedback control systems with no finite zeros, the transient performance specifications can be translated into the desired locations for the two closed-loop poles. Acceptable values of damping ratio ζ and undamped natural frequency ω_n are first obtained from the consistent set of specifications on rise time, peak time, peak overshoot, and settling time using the second-order correlations given below (refer Eqns (6.9), (6.12), (6.13) and (6.19)):

Rise time: $$t_r = \frac{\pi - \cos^{-1}\zeta}{\omega_n\sqrt{1-\zeta^2}} \tag{6.38a}$$

Peak time: $$t_p = \frac{\pi}{\omega_n\sqrt{1-\zeta^2}} \tag{6.38b}$$

Peak overshoot: $$M_p = e^{-\pi\zeta/\sqrt{1-\zeta^2}} \tag{6.38c}$$

Settling time: $$t_s = \frac{4}{\zeta\omega_n} \tag{6.38d}$$

The desired locations of the closed-loop poles are then obtained as

$$s_{1,2} = -\zeta\omega_n \pm j\omega_n\sqrt{1-\zeta^2} \tag{6.39}$$

We know that a large ω_n is desirable because it results in high speed of response. However, measurement noise considerations impose a limit on ω_n; a system with large ω_n has a large bandwidth and will therefore allow the high-frequency noise signals to affect the performance. We also know that damping ratio in the range of 0.4 to 0.7 is desirable from relative stability and speed of response considerations. Therefore, the desired closed-loop poles should most likely be located in the shaded regions in Fig. 6.24. We have intentionally not assigned numerical values to ω_{n1} and ω_{n2}, since these are relative to a given system. A large value of ω_{n1} is desirable from the speed of response considerations; ω_{n2} represents the limit imposed by noise considerations. The design problem is to force the closed-loop poles of the controlled system to the desired locations.

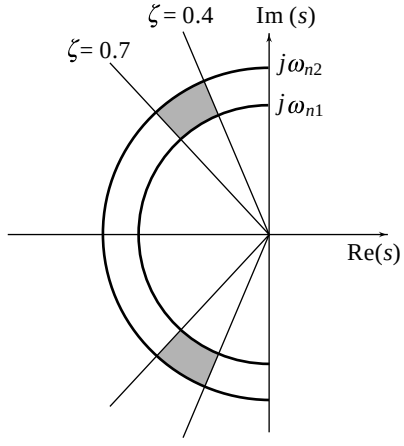

Fig. 6.24 Region of dominant poles in the s-plane

The second-order correlations (6.38)–(6.39) derived for the standard second-order system, can be used for a second-order system with a finite zero by appropriately accommodating the effect of the zero on the transient response. The effect of a zero in the left half *s*-plane is to contribute a pronounced early peak to the system's response whereby the peak overshoot may increase appreciably. The closer the zero is to the origin, the more pronounced is the peaking phenomenon. If the zero moves farther into the left half *s*-plane, its effect becomes less pronounced. *If the magnitude of the zero is more than five times the magnitude of the real part of the complex-conjugate poles of the second-order system, then the zero may be regarded as insignificant insofar as the transient response is concerned* (Fig. 6.25). However, if

it is not possible to avoid a zero in the region of significant effect on the transient response, we may design the system for a higher value of ζ than the one that is acceptable, to account for the effect of increase in overshoot due to the presence of zero. A simulation study is carried out to see whether the design is acceptable. If not, one has to re-enter the design cycle with a different and more appropriate choice of ζ.

When a system is higher than second-order, strictly we can no longer characterize its dynamics by damping ratio ζ and undamped natural frequency ω_n, which are defined for standard second-order systems. However, by a proper design, it may be possible to force the closed-loop poles of a higher-order system to the two regions shown in Fig. 6.26; a complex-conjugate pole pair in region I and all other poles in region II. It has been recognized in practice that *if the magnitudes of the real parts of all the poles in region* II *are more than five times that of poles in region* I*, then the poles of region* II *may be regarded as insignificant insofar as the transient response is concerned.* The pair of complex-conjugate poles in region I has a dominant effect on transient response; we will refer to these poles as *dominant poles* of the higher-order system. The parameters (ζ, ω_n), associated with the dominant poles, characterize the dynamics of the higher-order system.

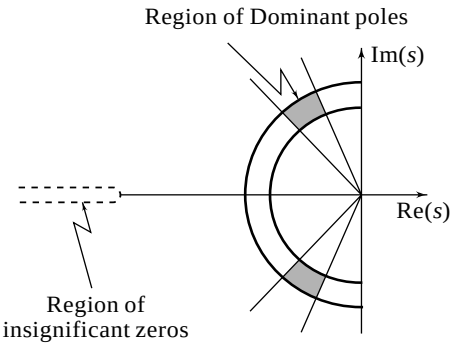

Fig. 6.25 Regions of dominant poles and insignificant zeros in the s-plane

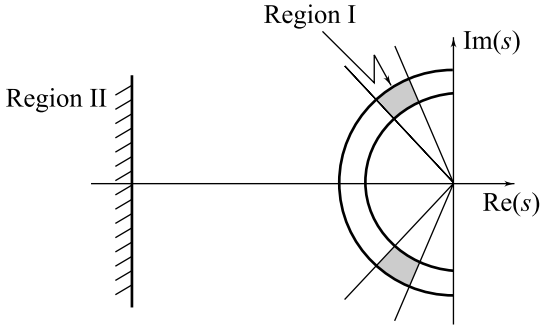

Fig. 6.26 Regions of dominant and insignificant poles in the s-plane

The design procedure for the higher-order systems is as follows. The specifications of relative stability and speed of response are translated into a pair of dominant closed-loop poles using the correlations (6.38)–(6.39). The design requirement is to force two of the closed-loop poles at the specified dominant positions and all other poles in the insignificant region. If the dominance condition is not satisfied, nothing can be said about the usefulness of design. A simulation study is carried out to see whether the design is acceptable. If not, one has to re-enter the design cycle to get a different distribution of closed-loop poles.

When a system is higher than second-order and has finite zeros, the dominance condition is satisfied only when the contributions to the transient response of the zeros and all the poles other than the pair corresponding to specified ζ and ω_n, are insignificant. An artful placement of a zero can cancel the dynamics contributed by a pole; this technique of *pole-zero cancellation* may be utilized to meet the dominance condition. To illustrate this concept, we consider the following two transfer functions, which have the same poles but differ in the locations of their zeros. They are normalized to have the same gain at $s = 0$.

$$G_1(s) = \frac{2}{(s+1)(s+2)} = \frac{2}{(s+1)} - \frac{2}{(s+2)}$$

$$G_2(s) = \frac{2(s+1.1)}{1.1(s+1)(s+2)} = \frac{2}{1.1}\left\{\frac{0.1}{s+1} + \frac{0.9}{s+2}\right\} = \frac{0.18}{s+1} + \frac{1.64}{s+2}$$

Notice that the coefficient of the $(s + 1)$ term has been modified from 2 in $G_1(s)$ to 0.18 in $G_2(s)$. This dramatic reduction is brought out by the zero at $s = -1.1$ in $G_2(s)$, which almost cancels the pole at $s = -1$. Of course, if we place the zero exactly at $s = -1$, this term will vanish completely.

The following remarks generalize the implications of this example for the significance of zeros in the system pole-zero pattern.

1. The residue A_i at pole $s = -\alpha_i$ corresponds to the transient term $A_i e^{-\alpha_i t}$; the significance of the residue is that its magnitude is the initial size of the transient corresponding to the pole.
2. If a zero is close to a pole, the residue at the pole tends to be small, and the corresponding transient becomes small.
3. If the zero coincides the pole, it cancels it and the corresponding transient term is zero.

Thus, the significance of zeros is that they affect the residues at the poles, and hence the sizes of the corresponding transients. Any pole outside the insignificant region (region II in Fig. 6.26) is acceptable if the nearby zero makes the corresponding transient small. Therefore, for the dominance condition to be satisfied, all the closed-loop poles other than the two corresponding to specified ζ and ω_n, should either lie in the insignificant region or have zeros nearby.

6.6 STEADY-STATE ERROR CONSTANTS AND SYSTEM-TYPE NUMBER

Steady-state error is a measure of system accuracy when a specific type of input is applied to a control system. The designer always strives to design the system to minimize the error for a certain anticipated class of inputs. This section considers the techniques that are available for determining the system accuracy.

Theoretically, it is desirable for a control system to have the capability of responding with zero error to all the polynomial inputs

$$r(t) = (t^k/k!)\,\mu(t) \tag{6.40}$$

of degree k. If $k = 0$, the input is a step of unit magnitude; if $k = 1$, the input is a ramp with unit slope; if $k = 2$, the input is a parabola with unit second derivative; $k = 3$ corresponds to an input one degree faster than parabola, and so on. From the common problems of mechanical motion control, the *step, ramp,* and *parabolic* inputs are called, respectively, *position, velocity* and *acceleration* inputs.

The specification of the zero-error response to all the polynomial inputs is very impractical and unrealistic. Fortunately, the requirements of practical systems are much less stringent. For example, consider the position control system for a robot manipulator. For a typical application, it would be desirable for this system to respond well to inputs of position and velocity, but not necessarily to those of acceleration. In addition, it would be desirable for this system to respond with zero error for positional-type inputs. However, a finite error could probably be tolerated for inputs of velocity.

For quantitative analysis, we consider the unity-feedback system shown in Fig. 6.27. The input is $R(s)$, the output $Y(s)$, and the difference between the input and the output is the error $E(s)$. For a stable system, the *transient component* of the error response $e(t)$ will eventually die away, leaving only the *steady-state component* $e_s(t)$ whose form is dictated directly by the forcing input.

The steady-state error

$$e_{ss} = \lim_{t \to \infty} e_s(t) = \lim_{t \to \infty} e(t) = \lim_{t \to \infty} [r(t) - y(t)] \tag{6.41a}$$

By the final-value theorem (Eqn. (2.45)),

$$e_{ss} = \lim_{s \to 0} sE(s) \tag{6.41b}$$

provided that $sE(s)$ has no poles on the $j\omega$-axis and in the right half plane.
For the system shown in Fig. 6.27,

$$E(s) = R(s) - Y(s) = \left[1 - \frac{Y(s)}{R(s)}\right] R(s) = \frac{1}{1 + D(s)\,G(s)}\, R(s) \tag{6.42}$$

Substituting Eqn. (6.42) into Eqn. (6.41b), we obtain

$$e_{ss} = \lim_{s \to 0} \frac{s\,R(s)}{1 + D(s)\,G(s)} \tag{6.43}$$

Thus, the steady-state of a system with unity feedback depends on the input signal $R(s)$ and the open-loop transfer function $D(s)G(s)$. By the nature of the limit in Eqn. (6.43), we see that the result of the limit can be zero, can be a constant different from zero, or the limit may not exist in which case the final-value theorem does not apply; but it is easy to see from the basic definition (6.41a) that $e_{ss} = \infty$ in this case anyway because $E(s)$ will have a pole at $s = 0$ that is of order higher than one. Systems having a finite non-zero steady-state error when the reference input is a zero-order polynomial input (a step) are labelled "type-0". Similarly, a system that has finite non-zero steady-state error to a first-order polynomial input (a ramp) is called a "type-1" system; a system with finite non-zero steady-state error to a second-order polynomial input (a parabola) is called a "type-2" system, and so on.

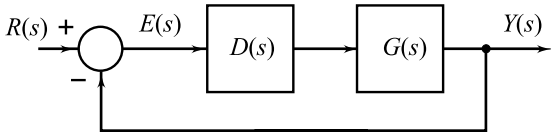

Fig. 6.27 A unity-feedback system

The control engineer is usually interested in step (position), ramp (velocity), and parabola (acceleration) inputs. For a step input $r(t) = \mu(t)$, the steady-state error may be obtained by substituting $R(s) = 1/s$ into Eqn. (6.43):

$$e_{ss} = \lim_{s \to 0} \frac{1}{1 + D(s)\,G(s)} = \frac{1}{1 + \lim\limits_{s \to 0} D(s)\,G(s)}$$

The quantity $\lim\limits_{s \to 0} D(s)G(s)$ is defined as the *position error constant* and is denoted by K_p:

$$K_p = \lim_{s \to 0} D(s)G(s) \tag{6.44a}$$

Therefore, steady-state error in terms of K_p is given by

$$e_{ss} = \frac{1}{1 + K_p} \tag{6.44b}$$

The steady-state error to a velocity input $r(t) = t\mu(t)$ can be obtained by substituting $R(s) = 1/s^2$ into Eqn. (6.43):

$$e_{ss} = \lim_{s \to 0} \frac{1}{s\left(1 + D(s)\,G(s)\right)} = \frac{1}{\lim\limits_{s \to 0} s\,D(s)\,G(s)}$$

The quantity $\lim\limits_{s \to 0} sD(s)G(s)$ is defined as the *velocity error constant* and is denoted by K_v:

$$K_v = \lim_{s \to 0} sD(s)G(s) \tag{6.45a}$$

Therefore, the steady-state error in terms of K_v is given by

$$e_{ss} = 1/K_v \tag{6.45b}$$

An expression for steady-state error due to acceleration input $r(t) = \frac{1}{2} t^2 \mu(t)$ can be obtained by substituting $R(s) = 1/s^3$ into Eqn. (6.43):

$$e_{ss} = \lim_{s \to 0} \frac{1}{s^2 \left(1 + D(s)\, G(s)\right)} = \lim_{s \to 0} \frac{1}{s^2\, D(s)\, G(s)}$$

The quantity $\lim_{s \to 0} s^2 D(s)G(s)$ is defined as the *acceleration error constant* and is denoted by K_a:

$$K_a = \lim_{s \to 0} s^2 D(s)G(s) \tag{6.46a}$$

Therefore, the steady-state error in terms of K_a is

$$e_{ss} = 1/K_a \tag{6.46b}$$

As said earlier, feedback systems can be classified on the basis of their steady-state response to polynomial inputs. We can always express the open-loop transfer function $D(s)G(s)$ as

$$D(s)G(s) = \frac{K \prod_i \left(s + z_i\right)}{s^N \prod_j \left(s + p_j\right)};\ z_i \neq 0,\ p_j \neq 0 \tag{6.47}$$

The term $1/s^N$ corresponds to N number of pure integrations in $D(s)G(s)$. As $s \to 0$, this term dominates in determining the steady-state error. Feedback systems are therefore classified in accordance with the number of pure integrators in the open-loop transfer function $D(s)G(s)$, as described below:

Type-0 System If $N = 0$, the steady-state error to various standard inputs obtained from Eqns. (6.44)–(6.46) are

$$e_{ss} = \begin{cases} \dfrac{1}{1 + K_p} & \text{in response to unit-step input; } K_p = \left.\dfrac{K \prod_i \left(s + z_i\right)}{\prod_j \left(s + p_j\right)}\right|_{s=0} \\ \infty & \text{in response to unit-ramp input} \\ \infty & \text{in response to unit-parabolic input} \end{cases} \tag{6.48}$$

Thus, a system with $N = 0$ (i.e., with no integrator in $D(s)G(s)$) has a finite non-zero position error, infinite velocity and acceleration errors at steady state.

Type-1 System If $N = 1$, the steady-state errors to various standard inputs are

$$e_{ss} = \begin{cases} 0 & \text{in response to unit-step input} \\ \dfrac{1}{K_v} & \text{in response to unit-ramp input; } K_v = \left.\dfrac{K \prod_i \left(s + z_i\right)}{\prod_j \left(s + p_j\right)}\right|_{s=0} \\ \infty & \text{in response to unit-parabolic input} \end{cases} \tag{6.49}$$

Thus, a system with $N = 1$ (i.e., with one integrator in $D(s)G(s)$) has zero position error, a finite non-zero velocity error, and infinite acceleration error at steady state.

Type-2 System If $N = 2$, the steady-state errors to various standard inputs are

$$e_{ss} = \begin{cases} 0 & \text{in response to unit-step input} \\ 0 & \text{in response to unit-ramp input} \\ \dfrac{1}{K_a} & \text{in response to unit parabolic input; } K_a = \left.\dfrac{K \prod\limits_i (s + z_i)}{\prod\limits_j (s + p_j)}\right|_{s=0} \end{cases} \tag{6.50}$$

Thus, a system with $N = 2$ (i.e., with two integrators in $D(s)G(s)$) has zero position and velocity errors and a finite non-zero acceleration error at steady state.

Steady-state errors for various inputs and systems are summarized in Table 6.1.

Table 6.1 Steady-state errors for various inputs and systems

Type of input	*Steady-state error*		
	Type-0 system	*Type-1 system*	*Type-2 system*
Unit-step	$\dfrac{1}{1 + K_p}$	0	0
Unit-ramp	∞	$\dfrac{1}{K_v}$	0
Unit-parabolic	∞	∞	$\dfrac{1}{K_a}$
	$K_p = \lim\limits_{s \to 0} D(s)G(s)$	$K_v = \lim\limits_{s \to 0} sD(s)G(s)$	$K_a = \lim\limits_{s \to 0} s^2 D(s)G(s)$

The development above indicates that, in general, increased system gain K and/or addition of an integration in $D(s)G(s)$ tend to decrease steady-state errors. However, as we have seen earlier in Chapters 4 and 5, both large system gain and the integrator in $D(s)G(s)$ have destabilizing effects on the system. Thus, a control system design is usually a trade-off between steady-state accuracy and acceptable relative stability.

For non-unity feedback system (Fig. 6.28), the difference between the input signal $R(s)$ and the feedback signal $B(s)$ is the actuating error signal $\hat{E}(s)$ which is given by

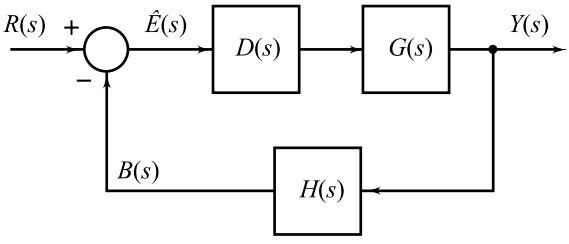

Fig. 6.28 A non-unity feedback system

$$\hat{E}(s) = \frac{1}{1 + D(s)\,G(s)\,H(s)}\,R(s) \tag{6.51}$$

Therefore, the steady-state actuating error is

$$\hat{e}_{ss} = \lim_{s \to 0} \frac{s\,R(s)}{1 + D(s)\,G(s)\,H(s)} \tag{6.52}$$

The error constants for non-unity feedback systems may be obtained from Table 6.1 by replacing $D(s)G(s)$ by $D(s)G(s)H(s)$.

6.7 INTRODUCTION TO DESIGN AND COMPENSATION

Recall the basic feedback system block diagram defined in Chapter 3 and shown in abridged form as Fig. 6.1. When we speak of a controller $D(s)$, our concern is mainly with the *information handling devices*; the sources of information are the reference input $r(t)$, which is derived from the command $y_r(t)$, and the feedback signal produced from the controlled output $y(t)$. The *power handling devices*—actuators and the controlled process itself—are represented by $G(s)$ in the block diagram of Fig. 6.1. $N(s)$ is the plant transfer function from the disturbance input $w(t)$ to the output $y(t)$.

The design procedures developed in this book are based on shaping the three aspects of a system's response discussed at length in Chapters 5 and 6, namely, stability, speed of response, and steady-state accuracy. For a stable closed-loop system, all the closed-loop poles must strictly lie in the left half of the s-plane. Since stability is the prime objective of design, we always ensure that our controller $D(s)$ stabilizes the system by relocating the poles such that they all lie in the left-half of the s-plane. Once we have ensured closed-loop stability, we then refine the controller to achieve the desired performance.

The performance is often specified in terms of figures of merit, such as peak overshoot, settling time, steady-state error constant, ⋯, which we have already met; and bandwidth, phase margin, gain margin, ⋯, which we meet later in this book. One of the ideas which has been emerging from the previous chapters is that of turning the specifications into a target closed-loop characteristic polynomial and then selecting the controller $D(s)$ to match this polynomial. An appropriate choice of a target closed-loop polynomial is to use a second-order pole pair in the quadratic factor $(s^2 + 2\zeta\omega_n s + \omega_n^2)$ and all other real/complex poles faster than this quadratic pair, so that the response of the higher-order system is dominated by the second-order response characteristic. Overshoot, settling time or other performance indices can be used in this step.

At several places in the preceding chapters, we have used gain setting to improve the performance of a feedback system. Merely by gain setting, it may be possible to meet the given specifications of simple control systems. However, in most practical cases, the gain adjustment does not provide the desired result. As is usually the case, increasing the gain reduces the steady-state error but results in oscillatory transient response or even instability. Under such circumstances, it is possible to introduce appropriate corrective action, integral or derivative, to force the plant to meet the given specifications. The job of integral or derivative actions is to *compensate* for the deficiency in the performance. The sub-system $D(s)$ in the feedback loop (Fig. 6.1) is thus a *compensator*. The transfer function $D(s)$ will, in the sequel, be referred to as a controller transfer function or a compensator transfer function; *both the terms (controller/compensator) will point to D(s) in the feedback loop*.

The selection of a compensator $D(s)$ is basically a search problem in n-dimensional parametric space where n is the number of design parameters of $D(s)$. Points in the search space correspond to different selections of compensators. By choosing different points of the parametric space, we can generate feedback systems with different performances. A compensator that meets the given performance specifications can be determined by moving in this search space on trial-and-error basis. Classical control theory provides systematic methods for solving this trial-and-error search problem. The two most successful practical methods, the *root-locus method* and the *frequency-response method*, will be presented in Chapter 7 and in Chapter 10, respectively.

6.7.1 Design of compensators

Our real interest is how the closed-loop system behaves in the time domain, but we find that the easiest way to predict this behaviour is to examine the loop transfer function in the s-domain. We use this strategy in root-locus method (Chapter 7). In Chapter 10, we look at the loop transfer function in another way, but our

ultimate goal will be the same: to use the loop transfer function to study the closed-loop system behaviour in time domain. We look at the loop transfer function in s-domain with $s = j\omega$, *i.e.,* we determine the frequency response of the open-loop system.

Our application examples for design using root locus method and frequency response method, will primarily be SISO systems from motion control and process control areas. Complex processes are often MIMO systems. Our design study for such systems is limited to situations where it is possible to consider the multivariable systems as consisting of an appropriate number of separate SISO systems (refer Section 1.4 and Eqns (2.65)). When this assumption is not satisfied, the methods given in this book are not applicable and one has to consider the MIMO model that includes all interaction effects. Optimal control provides one solution to the problem of design of such systems (refer Gopal [155]).

There is no guarantee that a compensator in the feedback control structure of Fig. 6.1 will meet all system specifications. When the failure occurs after repeated trial-and-error design, changes other than alternative parametric design of $D(s)$ must be tried. These include the use of components with improved dynamics and /or totally new system concepts (change from electric drive to hydraulic drive, for example). The changes in control structure of Fig. 6.1 may also yield acceptable performance. For example, one may include feedforward control (in addition to feedback) for improving the performance (refer Section 1.3). Another way could be supplying the controller with more complete information about the dynamical status of the process. This equivalently means changing the structure from 'output feedback' to 'state feedback'.

In the following, we discuss basic features of the well-known compensation[1] schemes. The next four chapters are primarily concerned with the compensator design problem.

6.7.2 Derivative Error Compensation

A system is said to possess derivative error compensation when the generation of its output depends in some way on the rate of change of actuating signal. In the feedback control system of Fig. 6.29, this type of compensation has been introduced by using a PD controller. The plant transfer function is

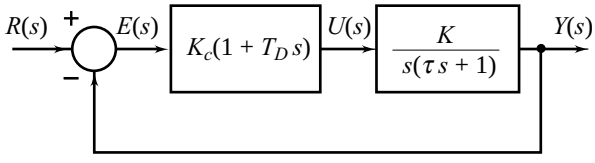

Fig. 6.29 Derivative error compensation scheme

$$G(s) = \frac{K}{s(\tau s + 1)} \tag{6.53}$$

The controller transfer function is

$$\begin{aligned} D(s) &= K_c(1 + T_D s) \\ &= K_c + K_c T_D s = K_c + K_D s \end{aligned} \tag{6.54}$$

The control signal is

$$u(t) = K_c e(t) + K_D \frac{de(t)}{dt} \tag{6.55}$$

[1]The term 'compensation' is usually used to indicate the process of increasing accuracy and speeding up the response. The gain adjustment which is a simple proportional control, is therefore viewed as a compensation scheme. We use the term 'design' to incompass the entire process of basic system selection and modifications; compensation is an important aspect of overall system design.

The open-loop transfer function of the overall system is

$$D(s)G(s) = \frac{K\left(K_c + K_D s\right)}{s\left(\tau s + 1\right)} \tag{6.56}$$

which shows that the PD control is equivalent to adding a simple zero at $s = -K_c/K_D$ to the open-loop transfer function.

The proper selection of performance specifications is the most important step in control system design. The desired behaviour is specified in terms of transient response measures and steady-state error. The steady-state error is usually specified in terms of error constants for specific inputs while the transient response is specified by measures of relative stability and speed of response; the relative stability is measured in terms of damping ζ or peak overshoot M_p, while the speed of response is measured in terms of rise time, settling time or natural frequency.

For the system under consideration, velocity error constant

$$K_v = \lim_{s \to 0} sD(s)G(s) = KK_c \tag{6.57a}$$

Therefore, the steady-state error to velocity input

$$e_{ss} = \frac{1}{K_v} = \frac{1}{K\,K_c} \tag{6.57b}$$

The characteristic equation of the system is

$$\tau s^2 + (1 + KK_D)s + KK_c = 0$$

or

$$s^2 + \left(\frac{1 + KK_D}{\tau}\right)s + \frac{KK_c}{\tau} = 0 \tag{6.58}$$

The natural frequency and damping of the compensated system are given by

$$\omega_n = \sqrt{\frac{KK_c}{\tau}} \tag{6.59a}$$

$$\zeta = \frac{1}{2}\left[\frac{1 + KK_D}{\sqrt{KK_c\tau}}\right] \tag{6.59b}$$

It is obvious from the above equations that only two of the three specifications, i.e., K_v, ζ and ω_n, can be met exactly by a suitable choice of K_c and K_D. For a specified K_v, the proportional gain K_c of the PD controller gets fixed (refer Eqn. (6.57a)). The closed-loop damping can now be raised to the desired level by a suitable choice of K_D (refer Eqn. (6.59b)) which is the gain of derivative term of the PD controller. These values of K_c and K_D may not satisfy the requirement on speed of response, specified in terms of ω_n (refer Eqn. (6.59a)) or settling time $t_s = 4/(\zeta\omega_n)$. Practically, most control systems require a trial-and-error parameter adjustment to achieve at least an acceptable performance if it is not possible to satisfy exactly all the performance specifications. Two commonly used trial-and-error procedures—the root-locus method and the frequency-response method—will be presented in Chapters 7–10.

We should point out here that since Eqn. (6.56) no longer represents a standard second-order system, the transient response is also affected by the zero of the transfer function at $s = -K_c/K_D$. In general, if the value of K_D is very large, the zero will be very close to the origin in the s-plane, the overshoot could be increased substantially, and the damping ratio ζ is then no longer an accurate estimate on the maximum overshoot of

the output. Simulation of the compensated system is necessary to check the design. If the transient response is not acceptable, we have to re-enter the design cycle to make necessary changes in design.

Example 6.2 Reconsider the design problem of Example 6.1. The position control system of Fig. 6.16 has open-loop transfer function

$$D(s)G(s) = \frac{4500\,K_A}{s(s+361.2)}$$

Let us consider an application wherein static accuracy requirement is very high; steady-state error to unit-ramp input is required to be less than 0.025 deg (0.000436 rad).

Required $$K_v = \frac{1}{0.000436} = 2293.6$$

This requirement is satisfied if

$$K_A = \frac{2293.6 \times 361.2}{4500} = 184.1$$

For this value of K_A, the characteristic equation of the system becomes

$$s^2 + 361.2\,s + 828450 = 0$$

Therefore

$$\omega_n = \sqrt{828450} = 910.2;\ \zeta = \frac{361.2}{2 \times 910.2} = 0.198;\ M_p = e^{-\pi\zeta/\sqrt{1-\zeta^2}} \times 100 = 53\%$$

Relative stability is obviously very poor. To improve damping and peak overshoot while maintaining K_v at 2293.6, we propose the replacement of amplifier with gain K_A by a PD controller (refer Fig. 6.16)

$$D(s) = K_c + K_D s$$

With the PD controller, the open-loop transfer function becomes

$$D(s)G(s) = \frac{4500\,(K_c + K_D s)}{s(s+361.2)} \tag{6.60}$$

The closed-loop transfer function

$$\frac{\theta_L(s)}{\theta_R(s)} = \frac{4500\,(K_c + K_D s)}{s^2 + (361.2 + 4500\,K_D)\,s + 4500\,K_c} \tag{6.61}$$

Velocity error constant

$$K_v = \frac{4500\,K_c}{361.2} = 2293.6$$

when $$K_c = 184.1$$

For this value of K_c, the characteristic equation of the system becomes

$$s^2 + (361.2 + 4500\,K_D)s + 828450 = 0$$

Therefore

$$\omega_n = \sqrt{828450} = 910.2$$

$$\zeta = \frac{361.2 + 4500\,K_D}{2 \times 910.2} = 0.198 + 2.472\,K_D$$

This clearly shows the positive effect of K_D on damping. For critical damping,

$$K_D = \frac{1 - 0.198}{2.472} = 0.324$$

We should point out here that Eqn. (6.61) no longer represents a standard second-order system; the transient response is also affected by the zero of the transfer function at $s = -K_c/K_D$. In general, if K_D is large, zero will be close to the origin in the s-plane, the overshoot will be increased substantially and damping ratio ζ no longer gives an accurate estimate on the peak overshoot of the output. In the present case, the increase in the overshoot is acceptable as seen from the unit-step response curves in Fig. 6.30. Without the PD controller, the response has a peak overshoot of 53%. With the PD controller, the peak overshoot is about four per cent. Although K_D was chosen for critical damping, the overshoot is due to the zero at $s = -K_c/K_D = -568.2$ (the two closed-loop poles are located at $s = -\omega_n = -910.2$ when $\zeta = 1$).

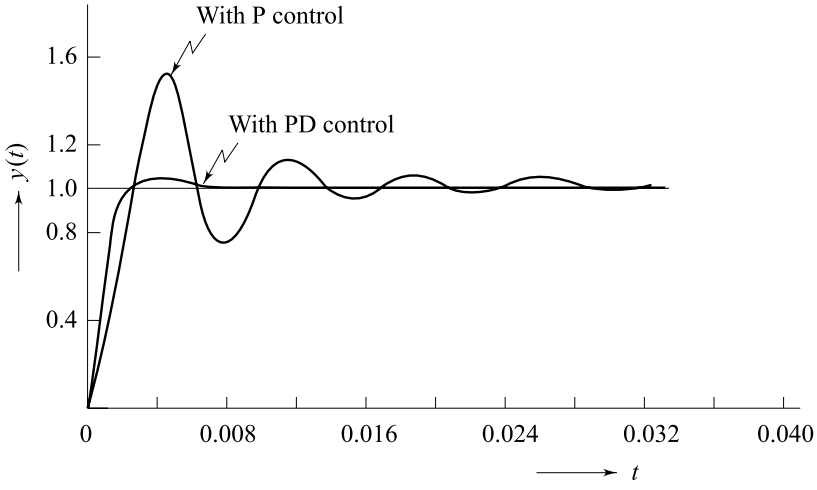

Fig. 6.30 Unit-step responses for system of Example 6.2

6.7.3 Derivative Output Compensation

The philosophy of using the derivative of the actuating error signal to improve the damping of a system can also be extended to the output signal. Fig. 6.31 shows the block diagram of a second-order system with a secondary path feeding back the derivative of the output.

Eliminating the minor feedback loop, we obtain the following forward-path transfer function.

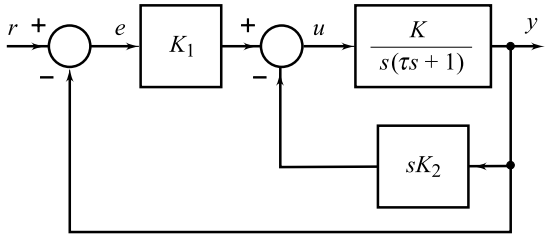

Fig. 6.31 Derivative output compensation scheme

$$G(s) = \frac{K K_1}{s(\tau s + 1 + K K_2)} \tag{6.62}$$

The velocity error constant

$$K_v = \lim_{s \to 0} sG(s) = \frac{K K_1}{1 + K K_2} \tag{6.63}$$

The closed-loop transfer function is given by

$$\frac{Y(s)}{R(s)} = \frac{K K_1}{\tau s^2 + (1 + K K_2)s + K K_1} \tag{6.64}$$

and the characteristic equation is

$$s^2 + \frac{(1 + K K_2)}{\tau} s + \frac{K K_1}{\tau} = 0 \tag{6.65}$$

The natural frequency and damping of the compensated system are given by

$$\omega_n = \sqrt{\frac{K K_1}{\tau}} \tag{6.66a}$$

$$\zeta = \frac{1}{2}\left[\frac{1 + K K_2}{\sqrt{K K_1 \tau}}\right] \tag{6.66b}$$

For a specified K_v and ζ, we can write from Eqns (6.63) and (6.66b),

$$\zeta K_v = \frac{1}{2}\left[\sqrt{\frac{K K_1}{\tau}}\right] \tag{6.67}$$

from which K_1 can be determined. Using this value of K_1, K_2 is obtained from Eqn. (6.63). Thus, we notice that by a suitable choice of K_1 and K_2, we can simultaneously meet the specifications on K_v and ζ. We will have to resort to trial-and-error methods of compensator design if the resulting speed of response is not acceptable.

Example 6.3 Consider the position control system of Fig. 6.15. When switch 'S' is open (tachogenerator disconnected), the forward-path transfer function of the system becomes

$$G(s) = \frac{4500 K_A}{s(s + 361.2)}$$

Assume that the steady-state error to unit-ramp input is required to be less than 0.025 deg (0.000436 rad).

Required $$K_v = \frac{1}{0.000436} = 2293.6$$

This requirement is satisfied if

$$K_A = \frac{2293.6 \times 361.2}{4500} = 184.1$$

For this value of K_A, the characteristic equation of the system becomes

$$s^2 + 361.2s + 828450 = 0$$

This gives

$$\omega_n = 910.2,\ \zeta = 0.198$$

Relative stability is obviously very poor.

Closing the switch 'S' will result in a minor feedback loop which represents the feeding back of the derivative of the output signal using a tachogenerator. Eliminating the minor feedback loop, we obtain the following forward-path transfer function:

$$G(s) = \frac{4500\ K_A}{s\left(s + 361.2 + 45000\ K_t\right)} \tag{6.68}$$

The closed-loop transfer function

$$\frac{\theta_L(s)}{\theta_R(s)} = \frac{4500\ K_A}{s^2 + \left(361.2 + 45000\ K_t\right)s + 4500\,K_A} \tag{6.69}$$

Velocity error constant

$$K_v = \frac{4500\ K_A}{361.2 + 45000\ K_t} \tag{6.70}$$

The characteristic equation of the system is

$$s^2 + (361.2 + 45000K_t)s + 4500K_A = 0 \tag{6.71a}$$

from which we obtain

$$\omega_n = \sqrt{4500\ K_A} \tag{6.71b}$$

$$\zeta = \frac{361.2 + 45000\ K_t}{2\sqrt{4500\ K_A}} \tag{6.71c}$$

From these equations, it is apparent that the tachogenerator feedback increases the damping of the system; it, however, reduces the system K_v.

With $K_A = 184.1$, we get critical damping when $K_t = 0.0324$. For these values of K_A and K_t, we obtain from Eqn. (6.70):

$$K_v = 455.4$$

Therefore

$$e_{ss}|_{\text{unit ramp}} = 0.0022 \text{ rad} = 0.126 \text{ deg.}$$

With the amplifier gain K_A set at the value 184.1, the tachogenerator feedback ($K_t = 0.0324$) increases the damping ratio from 0.198 to 1; it also increases the steady-state error to unit-ramp input from 0.025 deg to 0.126 deg.

Equations (6.70) and (6.71c) show that specified values of K_v and ζ can be realized by appropriate choice of K_A and K_t. For example, $K_v = 2293.6$ (steady-state error to unit-ramp input = 0.025 deg) and $\zeta = 1$ are realized by

$$K_A = 4676.4 \text{ and } K_t = 0.196$$

This choice of K_A gives $\omega_n = 4587.35$ rad/sec. Hardware considerations (e.g., amplifier saturation) and bandwidth considerations (large ω_n corresponds to large bandwidth) impose a limit on K_A which in turn imposes a limit on achievable accuracy/relative stability.

6.7.4 Integral Error Compensation

In an integral error compensation scheme, the output response depends in some manner upon the integral of the actuating signal. In the feedback control system of Fig. 6.32, this type of compensation has been introduced by using a PI controller. The plant transfer function is

$$G(s) = \frac{K}{s(\tau s + 1)} \tag{6.72a}$$

The controller transfer function is

$$D(s) = K_c\left(1 + \frac{1}{T_I s}\right)$$

$$= K_c + \frac{K_c}{T_I s} = K_c + \frac{K_I}{s} \tag{6.72b}$$

The control signal is

$$u(t) = K_c e(t) + K_I \int_0^t e(\tau)\, d\tau$$

The open-loop transfer function of the overall system is

$$D(s)G(s) = \frac{K(K_c s + K_I)}{s^2(\tau s + 1)} \tag{6.73}$$

Clearly, the PI control adds a zero at $s = -K_I/K_c$, and a pole at $s = 0$ to the open-loop transfer function. One obvious effect of the integral control is that it increases the order of the system by one; it may therefore be less stable than the original second-order system or even become unstable if the parameters K_c and K_I are not properly chosen.

Integral control increases the *type* of the system by one. The PI controller in Fig. 6.32 converts a type-1 system to type-2. Therefore, the steady-state error of the compensated system is always zero for velocity input. The problem is to choose a proper combination of K_c and K_I so that the transient response is satisfactory.

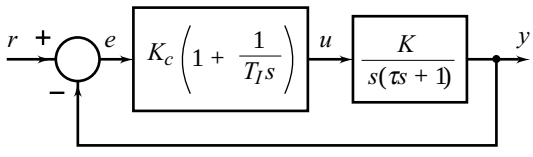

Fig. 6.32 Integral error compensation scheme

The characteristic equation of the closed-loop system is

$$\tau s^3 + s^2 + KK_c s + KK_I = 0 \tag{6.74}$$

Applying Routh's test to this equation yields the result that the system is stable for $0 < K_I < K_c/\tau$. This means that the system zero at $s = -K_I/K_c$ cannot be placed too far to the left in the left half of s-plane, or the system would be unstable.

A viable method of designing a PI controller is to determine the ranges of parameters K_c and K_I that result in a pair of complex-conjugate closed-loop poles and a real closed-loop pole. The zero at $s = -K_I/K_c$ is then selected so that it is relatively close to the real closed-loop pole. We know that if the zero is close to a pole, the residue at the pole tends to be small so that the corresponding transient is small. The dynamics of the system is then dominated by only the complex-conjugate pair of closed-loop poles. By trial-and-error parameter adjustments, it is possible to almost cancel a closed-loop pole with a zero, and simultaneously achieve the desired transient performance. Trial-and-error procedures of parameter adjustment are given in Chapters 7–10.

Example 6.4 Reconsider the design problem of Example 6.1. Assume that we require zero steady-state error to ramp inputs. To realize this objective, we replace the amplifier with gain K_A (refer Fig. 6.16) by a PI controller

$$D(s) = K_c + \frac{K_I}{s}$$

With the PI controller, the open-loop transfer function becomes

$$D(s)G(s) = \frac{4500\left(K_c s + K_I\right)}{s^2\left(s + 361.2\right)} \tag{6.75}$$

The closed-loop transfer function

$$\frac{\theta_L(s)}{\theta_R(s)} = \frac{4500\left(K_c s + K_I\right)}{s^3 + 361.2\,s^2 + 4500\,K_c s + 4500\,K_I} \tag{6.76}$$

From Eqn. (6.75), we see that with the PI controller, the system has become a type-2 system; therefore the steady-state error to ramp inputs is zero. To study the effect of PI controller on transient response, we consider the characteristic equation

$$s^3 + 361.2\,s^2 + 4500K_c s + 4500K_I = 0 \tag{6.77}$$

Applying Routh's test to this equation yields the result that the system is stable for $0 < K_I < 361.2\,K_c$. This means that the system zero at $s = -K_I/K_c$ cannot be placed too far to the left in the left half of s-plane.

Design to determine suitable values of K_c and K_I can be carried out using the root-locus and frequency-response methods discussed in the following chapters. Here we analyse the performance of the system for a typical design:

$$K_c = 14.728;\ K_I = 147.28$$

For these values of K_c and K_I, the characteristic equation becomes

$$s^3 + 361.2\,s^2 + 66276\,s + 662760 = 0$$

or $(s + 10.59)\,(s + 175.30 + j178.41)\,(s + 175.30 - j178.41) = 0$

The pole at $s = -10.59$ is insignificant as far as the transient response is concerned, because the zero at $s = -K_I/K_c = -10$ is close to this pole. The transient response is therefore dominated by the quadratic factor

$$(s + 175.30 + j\,178.41)\,(s + 175.30 - j\,178.41) = 0$$

or $$s^2 + 350.6\,s + 62560.22 = 0$$

The unit-step response of the third-order system, therefore, resembles a second-order system with

$$\omega_n = \sqrt{62560.22} = 250.12 \text{ rad/sec; and } \zeta = \frac{350.6}{2 \times 250.12} = 0.7$$

The unit-step response of the PI-compensated system with $K_c = 14.728$ and $K_I = 147.28$ is shown in Fig. 6.33. Notice that although the damping is adequate, the integral control causes the step response to have long rise and settling times.

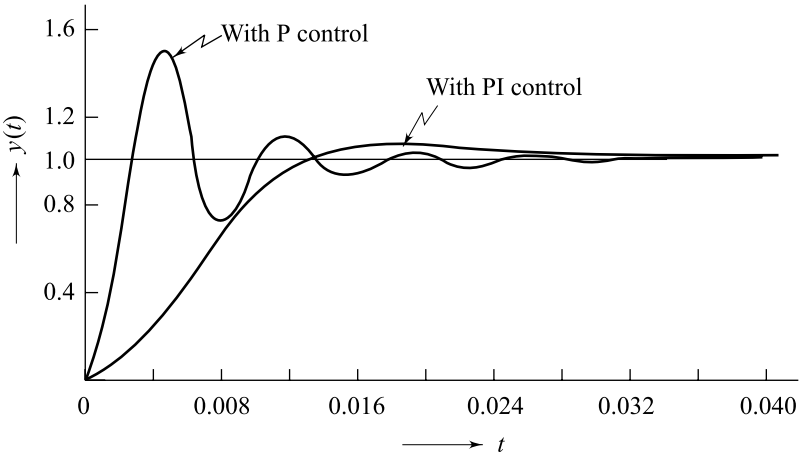

Fig. 6.33 Unit-step responses for the system of Example 6.4

6.8 TUNABLE PID CONTROLLERS

As we shall see in later chapters, sophisticated methods are available to develop a controller that will meet steady-state response and transient response specifications, for both tracking input references and rejecting disturbances. These methods require that the designer has either a dynamic model of the process in the form of transfer function/state-space equations or a frequency response over a wide range of frequencies.

In the process control field, it is not uncommon for a controller to be installed on a process with a little analytical study being done beforehand. Such a practice may not be as irrational as it first seems. Industrial processes are relatively slow and complex, which in many cases can be expensive and time-consuming to model. Also many years of experience has shown that a PID controller is versatile enough to control a wide variety of processes. Thus, an approach that selects a certain class (P, PI, PID) of controller based on past experience with certain classes of processes (pressure, flow, liquid-level, temperature, composition, etc.), and then sets controller parameters by experiment once the controller is installed, is not unreasonable. This experimental 'design' of controller settings has come to be known as *controller tuning*. Tuning is thus the procedure of adjusting the parameters of a feedback controller to obtain specific closed-loop response.

Engineers early on explored ways to avoid detailed analytical study of the processes, and developed some tuning rules based on experience with various classes of processes. The tuning rules are only a help in an initial search; the fine tuning is done by the operating engineer online. In the following, a brief description of the tuning rules is given. For more detailed study, refer Gopal [155].

J.G. Ziegler and N.B. Nichols proposed a design for the widely used PID controller by specifying satisfactory values for the controller settings based on estimates of the plant parameters that an operating engineer could make from experiments on the process itself. They recognized that the step responses of a large number of processes exhibit a *process reaction curve* like that shown in Fig. 6.34, which can be generated from experimental step response data. The *S*-shape of the curve can be approximated by the step response of

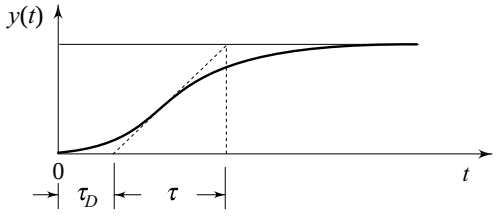

Fig. 6.34 Process reaction curve

$$\frac{Y(s)}{U(s)} = \frac{Ke^{-s\tau_D}}{\tau s + 1} \tag{6.78}$$

which is a first-order system with a deadtime of τ_D seconds. The constants in Eqn. (6.78) can be determined from the unit-step response of the process. If a tangent is drawn at the inflection point of the reaction curve, then the slope of the line is K/τ, and the intersection of the tangent line with the time axis identifies the deadtime τ_D.

Ziegler and Nichols proposed that the parameters K, τ and τ_D characterizing a process be used in tuning the PID controller for the QDR (Quarter-Decay Ratio) response. This means that the transient in closed-loop step response decays to a quarter of its value after one period of oscillation, as shown in Fig. 6.35. The controller parameters suggested by Ziegler and Nichols for the proportional (P), integral (I), and derivative(D), terms defined by (refer Fig. (4.3))

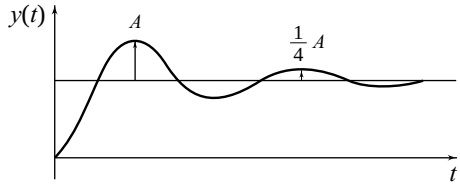

Fig. 6.35 QDR response

$$D(s) = K_c\left(1 + \frac{1}{T_I s} + T_D s\right)$$

are given in Table 6.2.

Table 6.2 QDR tuning formulas based on process reaction curve

Controller	*Gain*	*Integral time*	*Derivative time*
P	$K_c = \tau / K\tau_D$	–	–
PI	$K_c = 0.9\tau / K\tau_D$	$T_I = 3.33\ \tau_D$	–
PID	$K_c = 1.5\tau / K\tau_D$	$T_I = 2.5\ \tau_D$	$T_D = 0.4\ \tau_D$

In an alternative method suggested by Ziegler and Nichols, the criteria for adjusting the controller parameters are based on evaluating the amplitude and frequency of the oscillations of the system at the limit of stability, rather than on taking a step response. To use the method, the proportional gain is increased until the system becomes marginally stable and continuous oscillations just begin. The corresponding gain is defined as K_u (called the *ultimate gain*) and the period of oscillation is T_u (called the *ultimate period*). These are determined as shown in Fig. 6.36. Then the tuning parameters are selected as given in Table 6.3.

Experience has shown that the controller settlings according to Ziegler-Nichols rules provide acceptable closed-loop response for many systems. The process operator will often do final tuning of the controller iteratively on the actual process to yield satisfactory control.

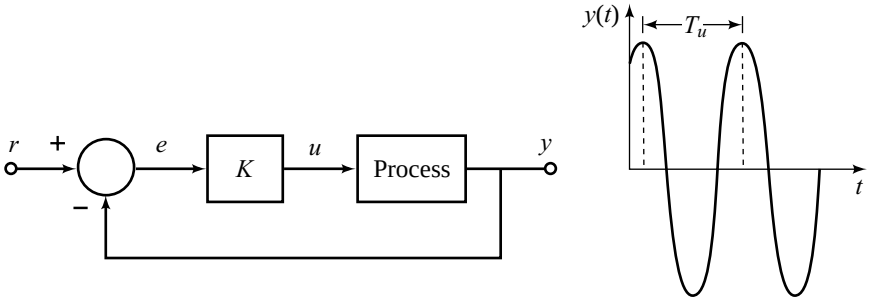

Fig. 6.36 Determination of the ultimate gain and period

Table 6.3 QDR tuning formulas based on ultimate gain and period

Controller	*Gain*	*Integral time*	*Derivative time*
P	$K_c = 0.5\ K_u$	–	–
PI	$K_c = 0.45\ K_u$	$T_I = T_u/1.2$	–
PID	$K_c = 0.75\ K_u$	$T_I = T_u/1.6$	$T_D = T_u/10$

Note that the closed-loop tuning method based on ultimate gain and period, is expected to give better trial values for fine tuning, compared to the open-loop method for characterizing the dynamic response of the process in the loop by the process reaction curve. However, it is not always possible to determine ultimate gain and period of a loop; some loops would not exhibit sustained oscillations with a proportional controller. Further, using more than one method is helpful in trial-and-error approach.

Review Examples

Review Example 6.1 The open-loop transfer function of a unity-feedback system is given by

$$G(s) = \frac{K}{s(\tau s + 1)};\ K > 0,\ \tau > 0$$

By what factor should the gain K be reduced so that the peak overshoot of unit-step response of the system is reduced from 75 to 25%?

Solution The characteristic equation of the system is

$$s^2 + \frac{1}{\tau}s + \frac{K}{\tau} = 0$$

Assume that corresponding to 75% overshoot, the gain is K_1 and damping ratio is ζ_1; and for 25% overshoot, the gain is K_2 and damping ratio is ζ_2. From the characteristic equation, we obtain

$$2\zeta_1 = \frac{1/\tau}{\sqrt{K_1/\tau}} = \frac{1}{\sqrt{K_1\tau}};\ 2\zeta_2 = \frac{1}{\sqrt{K_2\tau}}$$

Therefore
$$\left(\frac{\zeta_2}{\zeta_1}\right)^2 = \frac{K_1}{K_2} \tag{6.79}$$

Since $e^{-\pi\zeta/\sqrt{1-\zeta^2}} = M_p$

we have
$$\frac{\pi\zeta_1}{\sqrt{1-\zeta_1^2}} = -\ln(0.75) = 0.29 = \frac{\pi}{\sqrt{\frac{1}{\zeta_1^2} - 1}} \tag{6.80}$$

and
$$\frac{\pi\zeta_2}{\sqrt{1-\zeta_2^2}} = -\ln(0.25) = 1.4 = \frac{\pi}{\sqrt{\frac{1}{\zeta_2^2} - 1}} \tag{6.81}$$

Dividing, squaring and rearranging we get $\frac{\zeta_2^2}{\zeta_1^2} = 20 = \frac{K_1}{K_2}$.

Therefore the gain K should be reduced by a factor of 20 so that the peak overshoot of unit-step response of the system is reduced from 75 to 25%.

Review Example 6.2 A unity-feedback system is characterized by the open-loop transfer function

$$G(s) = \frac{1}{s(0.5s+1)(0.2s+1)}$$

(a) Determine the steady-state errors to unit-step, unit-ramp, and unit-parabolic inputs.
(b) Determine rise time, peak time, peak overshoot, and settling time of the unit-step response of the system.

Solution (a) The given system is a type-1 system. The error constants are obtained as follows:

$$K_p = \lim_{s\to 0} G(s) = \infty;\ K_v = \lim_{s\to 0} sG(s) = 1;\ K_a = \lim_{s\to 0} s^2G(s) = 0$$

Therefore

$$e_{ss}|_{\text{unit step}} = \frac{1}{1+K_p} = 0;\ e_{ss}|_{\text{unit ramp}} = \frac{1}{K_v} = 1;\ e_{ss}|_{\text{unit parabola}} = \frac{1}{K_a} = \infty$$

(b) Since the system is of third order, we can no longer use the correlations (6.38) for rise time, peak time, peak overshoot, and settling time. These correlations were derived for a standard second-order system. For the transient analysis of the given system, we may determine the unit-step response (Eqn. (6.37)) and therefrom compute rise time, peak time, peak overshoot, and settling time.
However, if the system dynamics can be accurately represented by a pair of dominant poles, then the correlations (6.38) may be used. The characteristic equation of the given system is

$$s(0.5\,s+1)(0.2\,s+1)+1=0$$

or $$s^3 + 7s^2 + 10\,s + 10 = 0$$

Factorizing the characteristic equation, we obtain

$$(s+5.5157)(s^2+1.4844\,s+1.8131)=0$$

The magnitude of the real root is more than 7 times the magnitude of the real part of the complex roots. Therefore, the complex-conjugate root pair gives the dominant closed-loop poles with

$$\omega_n = \sqrt{1.8131} = 1.3465 \text{ rad/sec};\ \zeta = \frac{1.4844}{2\times 1.3465} = 0.55;\ \omega_d = \omega_n\sqrt{1-\zeta^2} = 1.1245$$

$$t_r = \frac{\pi - \cos^{-1}\zeta}{\omega_d} = \frac{\pi - 56.63\times\frac{\pi}{180}}{1.1245} = 1.91 \text{ sec};\ t_p = \frac{\pi}{\omega_d} = 2.79 \text{ sec};\ M_p = e^{-\pi\zeta/\sqrt{1-\zeta^2}} = 0.1265;$$

$$t_s = \frac{4}{\zeta\omega_n} = 5.4 \text{ sec}$$

Review Example 6.3 A servomechanism controls the angular position θ_L of a mass through a command signal θ_R. The moment of inertia of the moving parts referred to the load shaft is 200 kg-m^2 and the motor torque at the load is 6.88×10^4 Newton-m per rad of error. The damping torque coefficient referred to the load shaft is 5×10^3 N-m per rad/sec.

(a) Determine the frequency of transient oscillation, the peak overshoot, the time to peak, and the steady-state error resulting from the application of a step input of 1 rad.
(b) Determine the steady-state error when the command signal is a constant angular velocity of 1 rev/min.
(c) Determine the steady-state error which exists when a steady torque of 1200 N-m is applied at the load shaft.

Solution Since the torque applied to the load must equal the reaction torque, we have

$$(200\ \ddot{\theta}_L + 5\times 10^3\ \dot{\theta}_L) = 6.88\times 10^4(\theta_R - \theta_L) - T_w \tag{6.82}$$

Figure 6.37 gives a block-diagram representation of this differential equation.

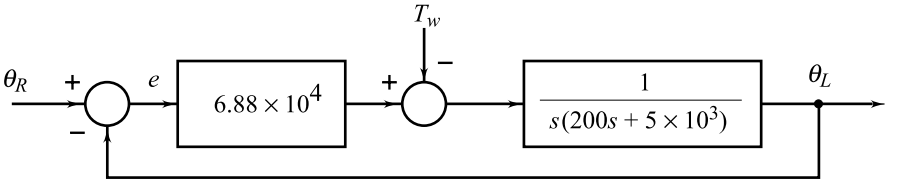

Fig. 6.37 Block diagram representation of Eqn. (6.82)

From the block diagram, we obtain

$$\frac{\theta_L(s)}{\theta_R(s)} = \frac{6.88\times 10^4}{200s^2 + 5\times 10^3 s + 6.88\times 10^4}$$

$$= \frac{344}{s^2 + 25s + 344}$$

$$\frac{\theta_L(s)}{T_w(s)} = \frac{-1}{200s^2 + 5\times 10^3 s + 6.88\times 10^4} \tag{6.83}$$

(a) The characteristic equation of the system is

$$s^2 + 25\,s + 344 = 0$$

Comparing with the standard characteristic equation

$$s^2 + 2\zeta\omega_n s + \omega^2{}_n = 0$$

we obtain $\omega_n = \sqrt{344} = 18.547;\ \zeta = \dfrac{25}{2\times 18.547} = 0.674$

Frequency of transient oscillation, $\omega_d = \omega_n\sqrt{1-\zeta^2} = 13.7$ rad/sec

Peak overshoot, $M_p = e^{-\pi\zeta/\sqrt{1-\zeta^2}} \times 100 = 5.69\%$

Time to peak, $t_p = \pi/\omega_d = 0.229$ sec

Steady-state error, $e_{ss}|_{\text{step input}} = 0$

(b) Input = 1 rpm = $2\pi/60$ rad/sec; $\theta_R(t) = \dfrac{2\pi}{60}\,t$

$$e_{ss}|_{\text{unit ramp}} = \frac{2\zeta}{\omega_n} = 0.07268$$

For a ramp input of slope $2\pi/60$, steady-state error = $0.07268 \times \frac{2\pi}{60} = 0.0076$ rad = 0.436 deg.

(c) Steady-state output in response to load torque of 1200 N-m is given by (refer Eqn. (6.83))

$$\theta_{Lss} = \lim_{s \to 0} s\theta_L(s)$$

$$= \lim_{s \to 0} s\left[\frac{-1}{200s^2 + 5\times 10^3 s + 6.88\times 10^4}\right]\frac{1200}{s}$$

$$= \frac{-1200}{6.88 \times 10^4} \text{ rad} = -1 \text{ deg}$$

Therefore, the steady-state error for a disturbance torque of 1200 N-m is 1 deg.

Review Example 6.4 Consider the unity-feedback system shown in Fig. 6.38. Assume that the controller is a proportional gain. With $D(s) = K$, the open-loop transfer function

$$D(s)G(s) = \frac{K}{(s+1)(0.5s+1)}$$

It is a type-0 system. The position error constant $K_p = K$, and

$$e_{ss}|_{\text{unit step}} = \frac{1}{1+K}$$

Improvement in steady-state accuracy with higher gain is evident. Relative stability considerations, however, impose a limit on the gain K. Large values of gain give rise to large overshoots.

The closed-loop transfer function of the system is

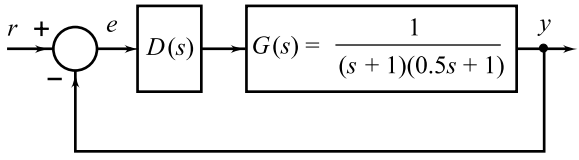

Fig. 6.38 A unity-feedback system

$$\frac{Y(s)}{R(s)} = \frac{2K}{s^2 + 3s + 2 + 2K}$$

The characteristic equation is

$$s^2 + 3s + 2 + 2K = s^2 + 2\zeta\omega_n s + \omega^2{}_n = 0$$

$\zeta = 0.5$ corresponds to peak overshoot $M_p = 16.3\%$. The limiting value of K for $M_p \le 16.3\%$ is obtained from the following equations:

$$\omega_n = \sqrt{2 + 2K}\ ;\ 2 \times 0.5 \times \omega_n = 3$$

Solving for K, we get $K = 3.5$

The steady-state error for this value of K is

$$e_{ss}|_{\text{unit step}} = \frac{1}{1+3.5} = 0.2222 = 22.22\%$$

An error of 22.22% is too large. We can reduce the error by increasing K, but this will result in an overshoot more than 16.3%. The objective of reducing the steady-state error without increasing overshoot can be realized using a PD controller:

$$D(s) = K_c + K_D s$$

With the PD controller, the open-loop transfer function becomes

$$D(s)G(s) = \frac{K_c + K_D s}{(s+1)(0.5s+1)}$$

The closed-loop transfer function

$$\frac{Y(s)}{R(s)} = \frac{2(K_c + K_D s)}{s^2 + (3 + 2K_D)s + 2 + 2K_c}$$

For $K_D = 0$, the characteristic equation is

$$s^2 + 3s + 2 + 2K_c = 0 = s^2 + 2\zeta\omega_n s + \omega^2_n$$

To achieve $\zeta = 0.5$, we require $K_c = 3.5$. The steady-state error for unit-step input is $1/(1 + K_c) = 0.2222$ or 22.22%.

If the specifications permit an error of 10%, $K_c = 9$ is required. Then for $K_D = 0$, the damping ratio ζ is 0.335 which is inadequate. With derivative control, the damping can be increased to 0.5 without affecting the value of e_{ss} as is seen below.

$$\omega_n = \sqrt{2 + 2K_c}\ ;\ 2\zeta\omega_n = 3 + 2K_D$$

With $K_c = 9$, $\zeta = 0.5$ is obtained when K_D statisfies the following relations:

$$\omega_n = \sqrt{2 + 18} = 4.47;\ 3 + 2K_D = 2 \times 0.5 \times \omega_n$$

This gives $K_D = 0.736$

The zero of the closed-loop transfer function is at $s = -K_c/K_D = -9/0.736 = -12.23$. The magnitude of the zero is about 5.5 times the magnitude of the real part of the poles ($\zeta\omega_n = 2.235$). So the unit-step response of the system with the PD controller should closely resemble the response of a standard second-order system with $\zeta = 0.5$ and $\omega_n = 4.47$.

If static accuracy demand is very high, PI control would probably be necessary. With $D(s) = K_c + K_I/s$, the open-loop transfer function becomes

$$D(s)G(s) = \frac{sK_c + K_I}{s(s+1)(0.5s+1)}$$

The system has become a type-1 system and the steady-state error to step inputs is zero.

The velocity error constant $K_v = K_I$, and

$$e_{ss}\big|_{\text{unit ramp}} = \frac{1}{K_I}$$

Thus, the steady-state error to ramp inputs reduces as the integral gain factor K_I is increased (note that the steady-state error to ramp inputs is infinity for the system with only proportional control or PD control). As one would expect, this improvement in static accuracy is limited by considerations of relative stability. The closed-loop transfer function

$$\frac{Y(s)}{R(s)} = \frac{s K_c + K_I}{0.5s^3 + 15s^2 + (1 + K_c)s + K_I}$$

shows a third-order characteristic equation. Design to determine suitable values of K_c and K_I can be carried out using the root-locus and frequency-response methods discussed in the following chapters. This will show that careful design is necessary to avoid oscillatory or slow system dynamic behaviour.

Review Example 6.5 The system shown in Fig. 6.39 is a unity-feedback control system with a minor rate-feedback loop.

(a) In the absence of rate feedback ($\alpha = 0$), determine the peak overshoot of the system to unit-step input, and the steady-state error resulting from a unit-ramp input.

(b) Determine the rate-feedback constant α which will decrease the peak overshoot of the system to unit-step input to 1.5%. What is steady-state error to unit-ramp input with this setting of the rate-feedback constant?

(c) Illustrate how in the system with rate feedback, the steady-state error to unit-ramp input can be reduced to the same level as in part (a), while the peak overshoot to unit-step input is maintained at 1.5%.

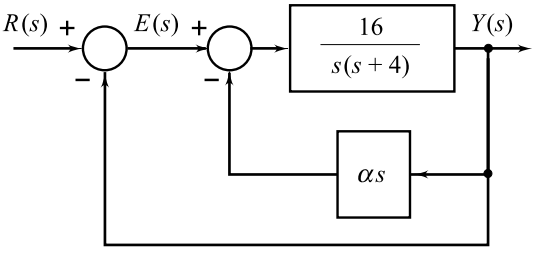

Fig. 6.39 A unity-feedback system with a minor rate-feedback loop

Solution (a) With $\alpha = 0$, the forward-path transfer function

$$G(s) = \frac{16}{s(s+4)}$$

Velocity error constant $$K_v = \lim_{s \to 0} sG(s) = 4$$

$$e_{ss}\big|_{\text{unit ramp}} = \frac{1}{K_v} = 0.25$$

The characteristic equation of the system is

$$s^2 + 4s + 16 = 0$$

Comparison with the standard characteristic equation

$$s^2 + 2\zeta\omega_n s + \omega_n^2 = 0$$

gives $\omega_n = 4$, and $\zeta = 0.5$

Therefore $$M_p = e^{-\pi\zeta/\sqrt{1-\zeta^2}} \times 100 = 16.3\%$$

(b) With rate feedback, the forward-path transfer function is obtained by eliminating the inner loop:

$$G(s) = \frac{\dfrac{16}{s(s+4)}}{1 + \dfrac{16\alpha s}{s(s+4)}} = \frac{16}{s(s + 4 + 16\alpha)} \tag{6.84}$$

$$K_v = \frac{16}{4+16\alpha} = \frac{4}{1+4\alpha}$$

The characteristic equation now takes the form

$$s^2 + (4 + 16\alpha)s + 16 = 0 \tag{6.85}$$

Corresponding to 1.5% overshoot, the damping ratio ζ is given by

$$\zeta^2 = \frac{\left[\ln(0.015)\right]^2}{\left[\ln(0.015)\right]^2 + \pi^2}$$

Solving, we get $\zeta = 0.8$.

The value of α that results in $\zeta = 0.8$ is given by the following equation (refer Eqn. (6.85)):

$$2 \times 0.8 \times 4 = 4 + 16\alpha$$

Solving, we get $\alpha = 0.15$.

For this value of α, $e_{ss}|_{\text{unit ramp}} = \frac{1}{K_v} = \frac{1+4\alpha}{4} = 0.4$

(c) The system of Fig. 6.39 may be extended by including an amplifier K_A as shown in Fig. 6.40. The forward-path transfer function now becomes

$$G(s) = \frac{16\,K_A}{s(s+4+16\alpha)} \tag{6.86}$$

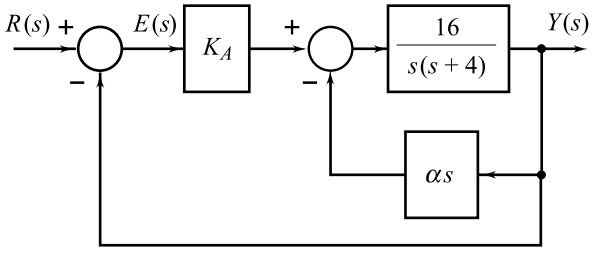

Fig. 6.40 Amplifier added to the system shown in Fig. 6.39

$$K_v = \frac{16\,K_A}{4+16\alpha} = \frac{4\,K_A}{1+4\alpha}$$

The required $K_v = 4$. Therefore

$$\frac{4\,K_A}{1+4\alpha} = 4 \tag{6.87}$$

The characteristic equation of the extended system is

$$s^2 + (4 + 16\alpha)\,s + 16K_A = 0 \tag{6.88}$$

The requirement of $\zeta = 0.8$ gives rise to the following equation:

$$2 \times 0.8 \times \sqrt{16\, K_A} = 4 + 16\alpha \tag{6.89}$$

From Eqns (6.87) and (6.89), we obtain

$$K_A = 2.56;\ \alpha = 0.39$$

Review Questions

6.1 Describe a set of performance specifications characterizing desired time response, that are frequently used in the design of linear control systems using root-locus plots.

6.2 Given the following measures of step response of a feedback system with transfer function

$$\frac{Y(s)}{R(s)} = M(s) = \frac{\omega_n^2}{s^2 + 2\zeta\omega_n s + \omega_n^2}:$$

(i) rise time, t_r; (ii) peak time, t_p;
(iii) peak overshoot; M_p; (iv) settling time, t_s.

Through graphical plots, explain the correlations of these measures with ζ and ω_n. Show that rise time, peak time, and settling time measures of performance are mutually dependent, and therefore must be specified in a consistent manner.

6.3 A feedback system is higher than second-order and has finite zeros.

(i) Determine the region in the s-plane which is feasible for the system's dominant poles corresponding to a percentage overshoot $5\% \le M_p \le 10\%$, and a settling time $3 \le t_s \le 5$ seconds.
(ii) Define the regions of dominant and insignificant poles, and insignificant zeros in the s-plane.
(iii) Show that pole-zero cancellation may be utilized to meet the dominance condition when non-dominant poles, and zeros do not lie in insignificant regions.

6.4 (a) What is system-type number? Explain the practical significance of this number.
(b) Define the error constants K_p, K_v, and K_a.
(c) Consider a unity feedback system with forward-path transfer function $D(s)G(s)$, where $G(s)$ is the transfer function of the plant and $D(s)$ corresponds to controller. Show that, in general, increased system gain and/or addition of an integrator in $D(s)G(s)$ tend to decrease steady-state errors; however, both large system gain and the integrator in $D(s)G(s)$ have destabilizing effects on the system.

6.5 A unity feedback system has a plant

$$G(s) = \frac{K}{s(\tau s + 1)}$$

with a cascade controller

$$D(s) = K_c(1 + T_D s)$$

Describe the effects of K_c and T_D on steady-state error, settling time, and peak overshoot of the system response.

6.6 A unity feedback system has a plant

$$G(s) = \frac{K}{s(\tau s + 1)}$$

with a cascade controller

$$D(s) = K_c\left(1 + \frac{1}{T_I s}\right)$$

Describe the effects of K_c and T_I on steady-state error, settling time, and peak overshoot of the system response.

6.7 A unity feedback servosystem has the plant

$$G(s) = \frac{K}{s(\tau s + 1)}$$

Show how a cascade PD controller could be used to achieve acceptable performance. Compare the cascade PD compensation with that of minor-loop feedback compensation using a tachogenerator.

6.8 Sketch a typical process reaction curve for an industrial process and explain how it can be used to obtain a first-order plus dead-time model of the process.

6.9 (a) What is QDR response?

(b) Describe two tuning methods, one based on ultimate gain and period and the other based on process reaction curve. How do we make a selection for a process control application?

Problems

6.1 (a) A feedback system has transfer function

$$\frac{Y(s)}{R(s)} = M(s) = \frac{\omega_n^2}{s^2 + 2\zeta\omega_n s + \omega_n^2};\ \zeta < 1$$

Derive expressions for peak overshoot M_p and peak time t_p of the time response of the given system to unit-step input.

(b) The feedback configuration of Fig. P6.1 is used to position a device in response to an input. The motor selected for this application has a gain constant $K_m = 0.5$ and a time-constant $\tau_m = 0.1$. For an amplifier gain $K_A = 20$, determine the following:

(i) Undamped natural frequency, damping ratio, and damped natural frequency.

(ii) Rise time, peak time, peak overshoot, and settling time.

(iii) Position, velocity and acceleration error constants K_p, K_v, and K_a.

(iv) Steady-state error resulting from the application of (a) unit-step input, (b) unit-ramp input, and (c) unit-parabolic input.

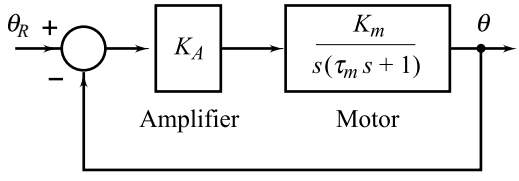

Fig. P6.1

6.2 Assume that control of one of the axes of a robot can be represented by the block diagram of Fig. P6.2.

(a) Determine the amplifier gain K_A so that the robot reaches steady-state in this axis in minimum time with no overshoot.

(b) Determine the steady-state error for an input command signal of $\theta_R = (5 + t)\mu(t)$, with the value of K_A obtained in part (a).

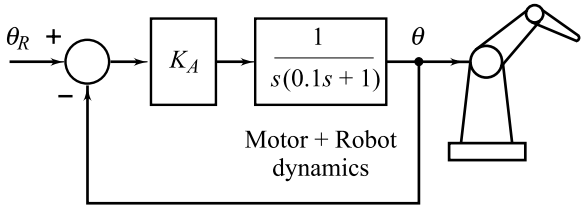

Fig. P6.2

6.3 A ground-based tracking radar is used to track aircraft targets. Assume that azimuth axis position control loop of the tracking radar can be represented by the block diagram of Fig. P6.3a.

(a) Determine the steady-state errors of the tracker for the following inputs caused by the aircraft motion.
(i) $\theta_R = 10t$
(ii) $\theta_R = 10t + 0.1t^2$

(b) Compare the steady-state performance of system of Fig. P6.3b with that of Fig. P6.3a.

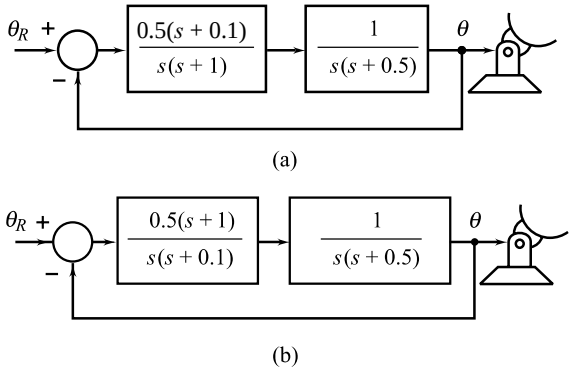

Fig. P6.3

6.4 The system of Fig. P6.4 has a constant reference input $r = 10$ and a constant disturbance input $w = 4$. Find the steady-state error.

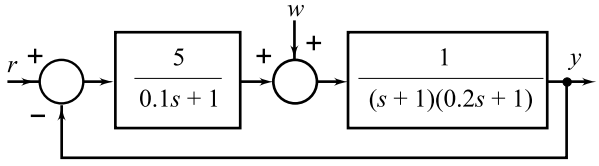

Fig. P6.4

6.5 Consider the heat-exchanger temperature control loop shown in Fig. P6.5.

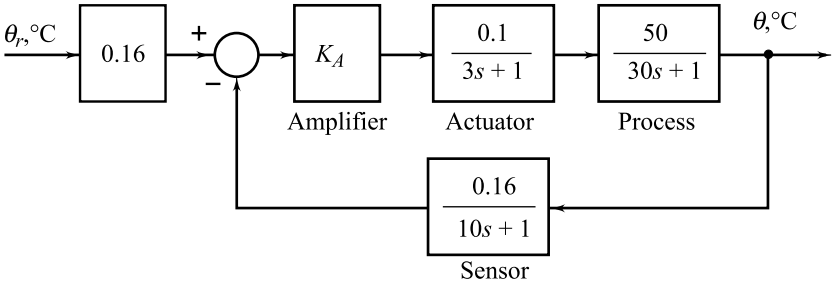

Fig. P6.5

(a) Find the range of values of $K_A > 0$ for which the system is stable.

(b) The acceptable value of steady-state error is 1°C for the step input of 10°C. Find the value of K_A that meets this specification on static accuracy.

6.6 Consider the control system in Fig. P6.6 in which a proportional compensator is employed. A specification on the control system is that the steady-state error must be less than two per cent for constant inputs.

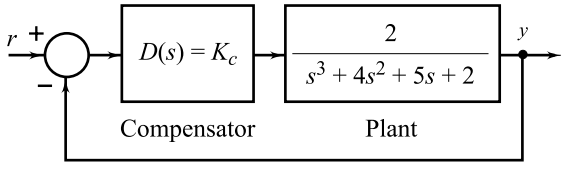

Fig. P6.6

(a) Find K_c that satisfies this specification.

(b) If the steady-state criterion cannot be met with a proportional compensator, use a dynamic compensator $D(s) = 3 + \dfrac{K_I}{s}$. Find the range of K_I that satisfies the requirement on steady-state error.

6.7 A control system with a PD controller is shown in Fig. P6.7.

(a) Find the values of K_c and K_D so that the velocity error constant K_v is 1000, and the damping ratio is 0.5.

(b) Is damping ratio ζ a reasonably accurate estimate of peak overshoot of the unit-step response? If not, why?

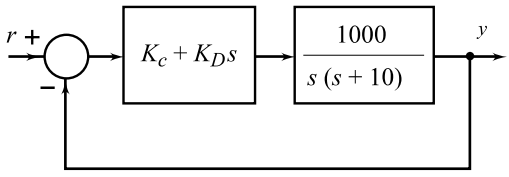

Fig. P6.7

MATLAB Exercise Find the peak overshoot using MATLAB, and compare it with one estimated from ζ value.

6.8 A control system with a type-0 process and a PI controller is shown in Fig. P6.8.

(a) Find the value of K_I so that the velocity error constant K_v is 10.

(b) With the value of K_I found in part (a), determine the value of K_c so that the real part of the conjugate pair of complex roots of the characteristic equation of the closed-loop system is -1.

(c) Find the conjugate pair of complex roots and therefrom obtain the value of ζ.

(d) Is ζ a reasonably accurate estimate on peak overshoot of the unit-step response? Give reasons.

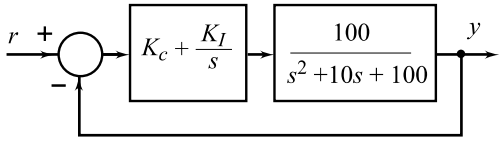

Fig. P6.8

6.9 A three-term controller with transfer function

$$D(s) = 20\left[1 + \frac{1}{T_I s} + T_D s\right]$$

is used to control a process with transfer function

$$G(s) = \frac{4}{s^2 + 8s + 80}$$

The closed-loop system is a unity-feedback structure with $D(s)$ and $G(s)$ in cascade.

(a) If integral action is not employed, find the derivative time T_D required to make the closed-loop damping ratio unity.

(b) A simulation study on your design in part (a) shows overshoot in unit-step response. Give reasons.

(c) If the value of derivative time is maintained as in part (a), determine the minimum value of reset time T_I that can be used without instability arising.

6.10 (a) For the motor position servo shown in Fig. P6.10a without the rate feedback ($K_t = 0$), show that $K = 10$ will give a steady-state unit-ramp following error of 0.1. What is the corresponding damping ratio?

(b) With $K = 10$, what value of K_t will give a system damping ratio of 0.5? How does the steady-state error compare with that in part (a)?

(c) The system of Fig. P6.10a with $K = 10$ has been extended by including the amplifier K_A as shown in Fig. P6.10b. Determine whether it is now possible to achieve both the steady-state error of 0.1 and damping ratio of 0.5. If so, find the values of K_t and K_A required.

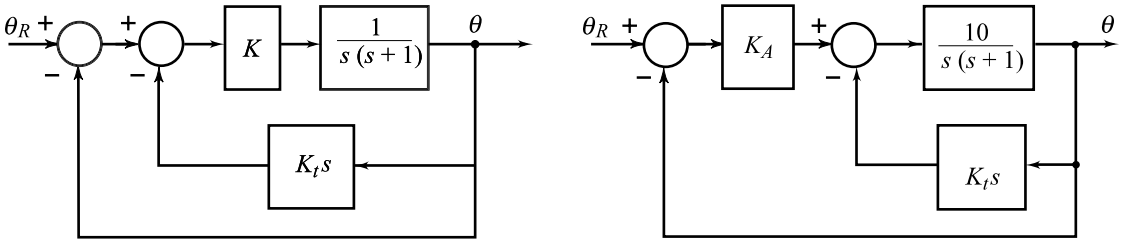

(a) (b)

Fig. P6.10

6.11 The block diagram of a control system is shown in Fig. P6.11.

(a) Find the values of K_1 and K_2 so that peak overshoot is 10% and settling time is 0.05 sec.

(b) For the values of K_1 and K_2 obtained in part (a), find the step, ramp and parabolic error constants.

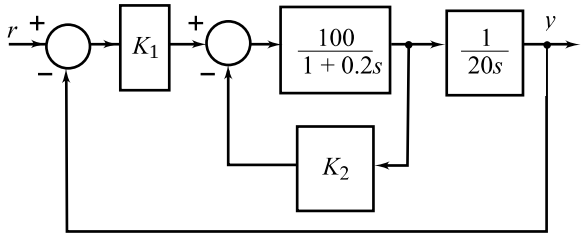

Fig. P6.11

MATLAB Exercise Using MATLAB, plot the time response to step command. Also obtain the plot in simulink window.

6.12 The block diagram of a motor position servo with a load disturbance torque T_w is shown in Fig. P6.12. Find K and K_t to obtain a system damping ratio 0.5 and 5% steady-state error for step input T_w.

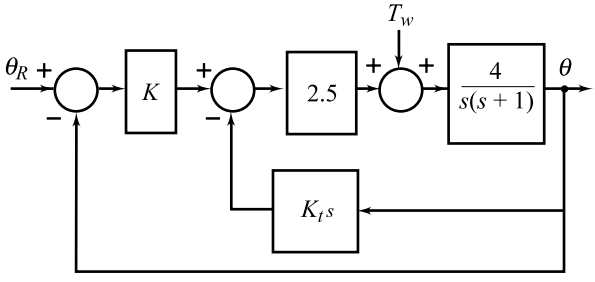

Fig. P6.12

MATLAB Exercise Using MATLAB, plot the time responses to step command and step disturbance, respectively. Also obtain these plots in Simulink window.

6.13 Figure P6.13a shows a mechanical vibrating system. When 9 Newton of force is applied to the system, the mass oscillates as shown in Fig. P6.13b. Determine the parameters M, B, and K of the system from the response.

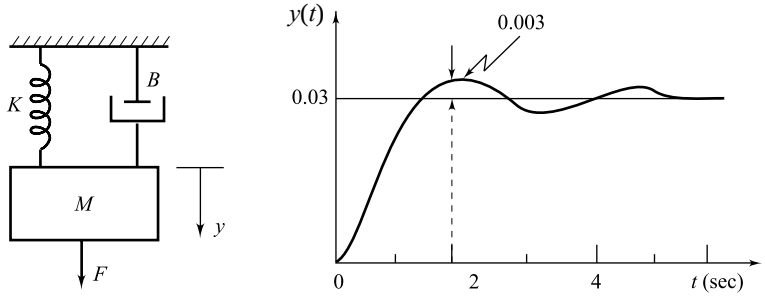

Fig. P6.13

6.14 A servomechanism controls the angular position θ of a mass through a command signal θ_R. The moment of inertia of the moving parts referred to the load shaft is J kg-m^2 and the motor torque at the load is K_T N-m per rad of error. The damping torque coefficient referred to the load shaft is B N-m per rad/sec.

The following tests were conducted on the position control system.

(i) Unit-step response was recorded and peak overshoot measured therefrom has a value of 25%.

(ii) A constant velocity input of 1 rad/sec produced a steady-state error of 0.04 rad.

(iii) With the command θ_R held fixed, a torque of 10 N-m applied at the load shaft produced a steady-state error of 0.01 rad.

From the above data, determine the parameters J, B and K_T of the system.

6.15 The speed of a flywheel, driven by an electric motor, is to be controlled from the setting of an input potentiometer using a closed-loop control system. The moment of inertia of the flywheel and the motor is 100 kg-m^2, and the motor torque at the flywheel is 45 N-m for a speed error of 1 rad/sec. Frictional torque is 5 N-m when the flywheel velocity is 1 rad/sec. With the system at rest, the input pot setting is suddenly increased from zero to 50 rev/min. Determine an expression for the subsequent flywheel angular velocity as a function of time, and calculate steady-state velocity error of the flywheel. Explain what modification could be made to the system to eliminate the steady-state error.

MATLAB Exercise Plot the angular velocity as a function of time using MATLAB.

6.16 A flywheel driven by an electric motor is automatically controlled to follow the movement of a handwheel. The moment of inertia of the flywheel and the motor is 150 kg-m^2 and the motor torque applied to the flywheel is 2400 N-m per radian of misalignment between the flywheel and the handwheel. The viscous friction is equivalent to a torque of 600 N-m per rad/sec.

If the handwheel is suddenly turned through 60° when the system is at rest, determine an expression for the subsequent angular position of the flywheel as a function of time, and calculate the peak overshoot of the response. Explain what modification could be made to the system to eliminate the overshoot.

MATLAB Exercise Plot the angular position as a function of time using MATLAB.

6.17 The schematic of a servo system is shown in Fig. P6.17. The two-phase servomotor develops a torque in accordance with the equation

$$T_M = K_1 e_c - K_2\ \dot{\theta}_M$$

where $K_1 = 2 \times 10^{-3}$ N-m/volt, and $K_2 = 0.5 \times 10^{-3}$ N-m per rad/sec.
The other parameters of the system are: load inertia, $J_L = 2.5$ kg-m^2; coefficient of load friction, B_L = 250 N-m per rad/sec; motor to load gear ratio, $\left(\dot{\theta}_L / \dot{\theta}_M\right)$ = 1/50; motor to synchro gear ratio, $\left(\dot{\theta}_S / \dot{\theta}_M\right)$ = 1/1, and sensitivity of synchro error detector, K_s = 100 volts/rad. The motor inertia and friction are negligible.

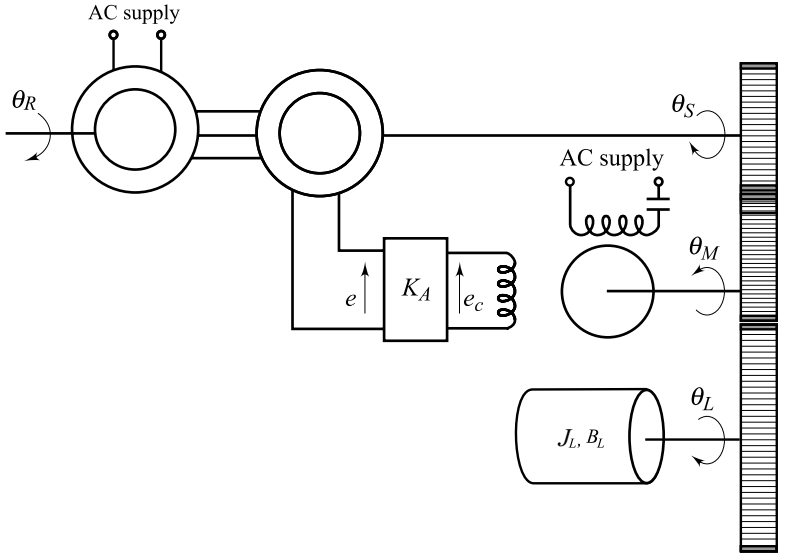

Fig. P6.17

(a) Draw a block diagram of the system indicating the transfer function of each block.
(b) If the input shaft is driven at a constant speed of π rad/sec, determine the value of the amplifier gain K_A such that the steady-state deviation between input and output positions is less than five degrees. For this value of amplifier gain, determine the peak overshoot and settling time of the system.
(c) The amplifier is now replaced by another which gives an output voltage of

$$e_c(t) = K_A e(t) + K_A \int e(t)dt$$

where the value of K_A is same as that obtained in part (b). Compare the steady-state behaviour of the system with that of part (b).
(d) A simulation study on the system of part (c) shows that the transient behaviour of the third-order system resembles that of the standard second-order system with characteristic equation

$$s^2 + 99.4508\ s + 3514.6322 = 0$$

Give reasons. Also determine the peak overshoot and settling time of the system.

6.18 In a dc position control servomechanism, the load is driven by a motor, supplied with constant armature current. The motor field current is supplied from a dc amplifier, the input to which is the difference between the voltages obtained from input and output potentiometers. A tachogenerator is coupled to the motor shaft and a fraction K of tachogenerator output is fed back to produce a stabilizing effect. The following particulars refer to the system: moment of inertia of motor, $J_M = 2 \times 10^{-3}$ kg-m^2;

moment of inertia of load, J_L = 5 kg-m^2; motor to load gear ratio, $(\dot{\theta}_L/\dot{\theta}_M)$ = 1/50; load to potentiometer gear ratio, $\dot{\theta}_P/\dot{\theta}_L$ = 1/1; motor torque constant, K_T = 2 N-m/amp; tachogenerator constant, K_t = 0.2 volt per rad/sec; sensitivity of error detector, K_P = 0.6 volt/rad, and amplifier gain = K_A amps/volt.

(a) Make a sketch of the system showing how the hardware is connected.
(b) Draw a block diagram of the system indicating the transfer function of each block.
(c) Determine the amplifier gain required and a fraction of the tachogenerator voltage fed back to give an undamped natural frequency of 4 rad/sec and damping ratio of 0.8.

6.19 The schematic diagram of a servomechanism is given in Fig. P6.19. The system constants are given below. Sensitivity of error detector, K_P = 1 volt/rad; gain of dc amplifier = K_A volts/volt; resistance of armature of motor, R_a = 5 ohms; equivalent inertia at the motor shaft, $J = 4 \times 10^{-3}$ kg-m^2; equivalent friction at the motor shaft, $B = 2 \times 10^{-3}$ N-m per rad/sec; torque constant of motor, K_T = 1 N-m/amp; and gear ratio $\left(\dot{\theta}_L/\dot{\theta}_M\right)$, n = 1/10.

(a) Draw a block diagram of the system indicating the transfer function of each block.
(b) Find amplifier gain K_A so that the steady-state error to unit-ramp input is less than 0.01 rad. For this value of amplifier gain, determine the damping ratio, and peak overshoot to unit-step input.
(c) To improve the system damping, the amplifier is modified by introducing an additional derivative term such that its output is given by

$$e_a(t) = K_A e(t) + K_D \frac{de(t)}{dt}$$

where the value of K_A is same as that obtained in part (b). Does this modification affect the steady-state error as in part (b)?
Determine the value of K_D such that the damping ratio is improved to 0.6. Also calculate peak overshoot corresponding to this damping ratio using correlation for standard second-order systems.
(d) A simulation study of your design in part (c) shows a different value of peak overshoot. Give reasons.

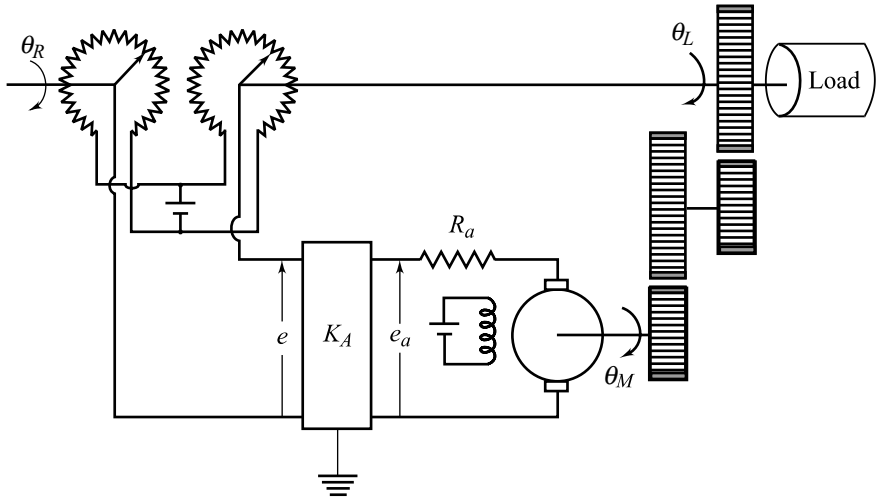

Fig. P6.19

MATLAB Exercise Use MATLAB's Simulink to obtain the step response under the following conditions.

(i) The system is linear and is driven by amplifier whose gain K_A is given by the solution to part (b).

(ii) The amplifier saturates at ± 5 volts. Describe the effect of the saturation on the system's output (Drag **Saturation** icon from Simulink library).

(iii) The amplifier with gain K_A drives the gear train that has backlash (As the motor reverses direction, the output shaft remains stationary while the motor begins to reverse. When the gears finally connect, the output shaft itself begins to turn in the reverse direction; refer Chapter 14). The deadband width of the backlash is 0.15. Describe the effect of backlash on the system's output (Drag **Backlash** icon from Simulink library).

(iv) Deadzone (refer Chapter 14) is present when the motor cannot respond to small voltages. The response begins when the input voltage to the motor exceeds a threshold. The deadzone width is ±2. Describe the effect of deadzone on the system output (Drag **Deadzone** icon from Simulink library).

6.20 Hydraulic actuators are used to drive cutting tools in machining applications (Fig. P6.20a). The reference input e_r is a voltage representing the desired position y_r of the cutting tool as function of time. It can be generated by a cam drive, a punched paper tape, or a computer program. A model of a feedback control system is shown in Fig. P6.20b. The load disturbance due to reactive force F_w of the cutting tool is also shown.

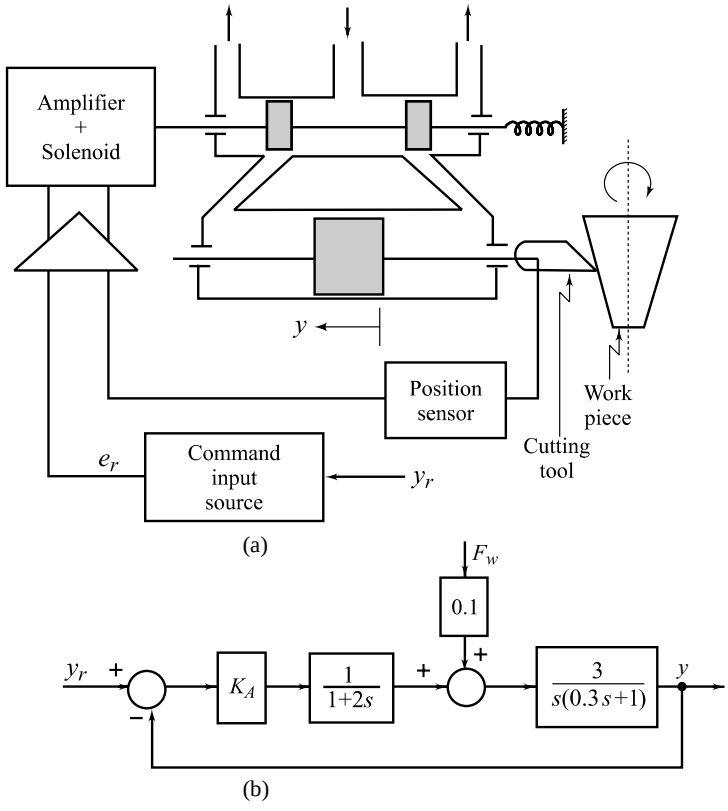

Fig. P6.20

(a) When $F_w = 0$, determine the steady-state tracking error for a constant velocity input of 0.03 mm/sec, as a function of K_A.
(b) Determine the steady-state error in $y(t)$ introduced by a unit-step disturbance, as a function of K_A.
(c) Find the minimum values of error in part (a) and that in part (b) which can be obtained by the control configuration of Fig. P6.20b.
(d) Design a PD controller to meet the following specifications: $t_s \le 0.4$ sec; peak overshoot $\le 20\%$.

6.21 A tank-level control system is shown in Fig. P6.21a. If the level is not correct, an error voltage e is developed and a signal $K_c e + K_D \dot{e}$ is applied to a servomotor. This in turn adjusts a valve through appropriate gearing and thereby restores balance by adjusting the inlet flow rate. A model of the feedback control system is shown in Fig. P6.21b.
(a) What is the system type number?
(b) Find the ranges of values of K_c and K_D for which the steady-state error to unit-ramp disturbance is less than 0.1.

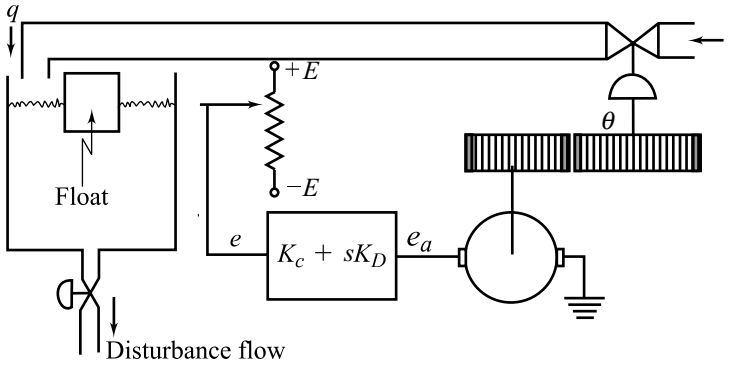

(a)

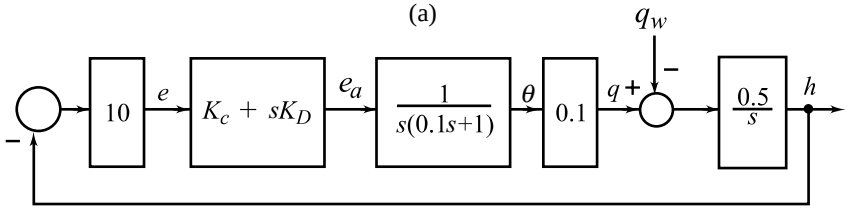

(b)

Fig. P6.21

6.22 Figure P6.22 shows a thermal system in which hot air is circulated to keep the temperature of a chamber constant. The transfer function of the plant can be adequately represented by

$$\frac{\theta(s)}{U(s)} = \frac{1}{s+1}$$

Determine the values of K_1 and K_2 which meet the following specifications on the feedback system:

$$M_p \le 20\%, \; t_s \le 2 \text{ sec}$$

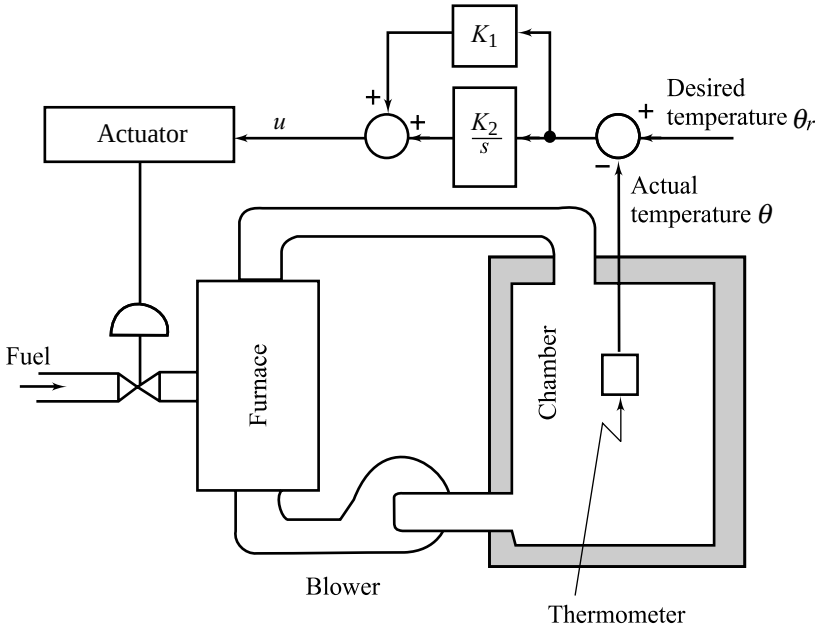

Fig. P6.22

6.23 From a test conducted on a temperature control loop, it is determined that the controller gain required to cause sustained oscillations is 1.2 and the period of oscillations is 4.5 min. Determine the QDR tuning parameters for

(i) a PI controller

(ii) a PID controller

6.24 The following table gives the measured open-loop response of a process using unit-step input. Approximate this response curve by a first-order plus dead-time model.

Time(min) t	0	0.5	1.0	1.5	2.0	2.5	3.0	3.5
Response y	0	0.009	0.056	0.15	0.28	0.428	0.572	0.7
t	4.0	4.5	5.0	5.5	6.0	7.0		
y	0.802	0.8876	0.924	0.953	0.967	0.973		

(a) Tune a proportional-only controller for QDR response.

(b) Tune a PI controller for QDR response.

The Root Locus Technique and Compensator Design using Root Locus Plots

7

7.1 INTRODUCTION

This is the first chapter devoted exclusively to control system design. The design procedures developed in this chapter are based on shaping the three aspects of a system's response, discussed at length in Chapters 5 and 6; namely, stability, speed, and steady-state accuracy of the closed-loop response. For a stable closed-loop system, all the closed-loop poles must strictly lie in the left half of the s-plane. Since stability is the prime objective of design, we always ensure that our controller $D(s)$ stabilizes the system by relocating the poles such that they all lie in the left-half of the s-plane. Once we have ensured closed-loop stability, we then refine the controller to achieve the desired performance.

The performance is often specified in terms of figures of merit, such as peak overshoot, settling time, steady-state error constant, ⋯, which have already been discussed; and bandwidth, phase margin, gain margin, ⋯, which we deal with later in this book. One of the ideas which has been emerging from the previous chapters is that of turning the specifications into a target closed-loop characteristic polynomial and then selecting the controller $D(s)$ to match this polynomial. An appropriate choice of a target closed-loop polynomial is to use a second-order pole pair in the quadratic factor $(s^2 + 2\zeta\omega_n s + \omega_n^2)$ and all other real/complex poles faster than this quadratic pair so that the response of the higher-order system is dominated by the second-order response characteristic.

In this chapter, we introduce design techniques based on root locus analysis that use the figures of merit developed in Chapter 6. The advantage of root locus design is that it is very intuitive. The root locus plot provides the designer with a picture of all potential closed-loop pole locations. This picture, when combined with the figures of merit, makes it an easy matter to find a good compensator. The root locus technique was introduced by Walter R. Evans in 1948, and has been developed and utilized extensively in control engineering practice.

The root locus design approach primarily relocates the closed-loop poles to meet the performance specifications on overshoot, settling time, etc. In an alternative approach based on frequency response (Bode plots), the performance is specified in terms of band width, gain margin, phase margin, etc. Meeting these specifications not only ensures acceptable transient response but also yields better robustness properties.

The Bode plot design technique, presented later in Chapter 10, is generally superior to the root locus design method. However, the two approaches are related and the intuition developed in this chapter will stand us in good stead when we discuss Bode plot design in Chapter 10.

This chapter first introduces the basic concept of the root locus method and presents useful rules for graphically constructing the root loci. The use of the rechnique for compensator design problems is then considered.

7.2 THE ROOT LOCUS CONCEPT

We introduce the root locus concept through an example. Consider the second-order system shown in Fig. 7.1, which represents a typical position control system. The plant consists of servomotor and load, driven by a power amplifier with gain K. The open-loop transfer function of the system is

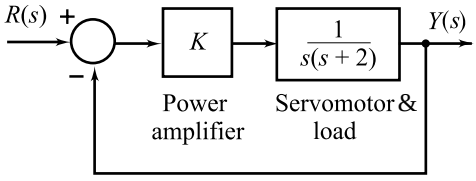

Fig. 7.1 A position control system

$$G(s) = \frac{K}{s(s+2)} \tag{7.1}$$

The open-loop poles, marked × in Fig. 7.2, are at $s = 0$ and $s = -2$. The closed-loop transfer function of the system is

$$M(s) = \frac{G(s)}{1+G(s)} = \frac{K}{s^2+2s+K} \tag{7.2}$$

The characteristic equation is

$$\Delta(s) = s^2 + 2s + K = 0 \tag{7.3}$$

The second-order system under consideration is always stable for positive values of K. The relative stability of the system depends on the location of the characteristic roots (closed-loop poles)

$$s_{1,2} = -1 \pm \sqrt{1-K} \tag{7.4}$$

and hence on the choice of the parameter K. As K is varied from zero to infinity, the characteristic roots move in the s-plane as shown in Fig. 7.2. At $K = 0$, the root s_1 is equal to the open-loop pole at $s = 0$, and the root s_2 is equal to the open-loop pole at $s = -2$. As K increases, the roots move toward each other. The two roots meet at $s = -1$ for $K = 1$. As K is increased further, the roots break away from the real axis, become complex conjugate, and since the real part of both the roots remains fixed at $s = -1$, the roots move along the line $\sigma = -1$.

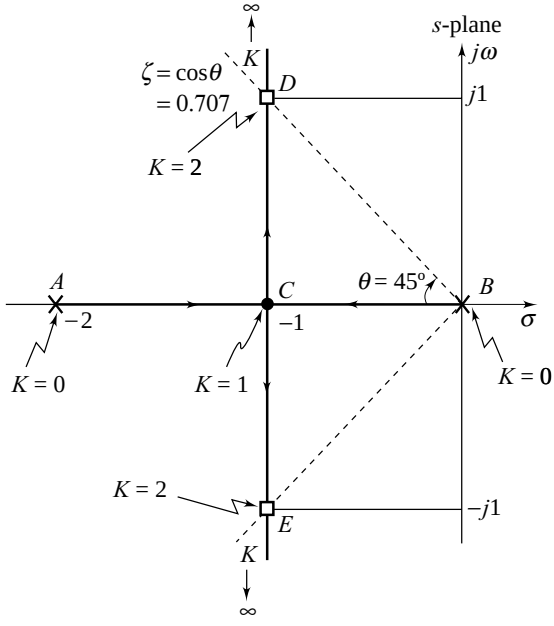

Fig. 7.2 Root locus plot for Eqn. (7.3)

A root locus of a system is a plot of the roots of the system characteristic equation (poles of the closed-loop transfer function) as some parameter of the system is varied.

The two branches[1] *A-C-E* and *B-C-D* of the plot of Fig. 7.2 are thus two *root loci* of the system of Fig. 7.1. Each root locus starts at an open-loop pole with $K = 0$ and terminates at infinity as $K \to \infty$. Each root locus gives one characteristic root (closed-loop pole) for a specific value of K.

The root locus plot gives us a great deal of information concerning the transient behaviour of the system as the gain K is varied. We can see from the plot that for $0 < K < 1$, the roots are real and distinct and the system is overdamped. For $K = 1$, the roots are real and repeated and the system is critically damped. For $K > 1$, the roots are complex conjugate and the system is underdamped with the value of ζ decreasing as K increases. From the viewpoint of design, we see that by the choice of gain K, we can cause a characteristic root at any point on the root locus. For example, suppose that a system specification requires damping ζ equal to 0.707. The dashed lines in Fig. 7.2 correspond to $\zeta = 0.707$. The points when the root loci cross the dashed lines have been marked □. These points correspond to characteristic roots for $K = 2$. We could easily compute K in this case because we know that if $\zeta = 0.707$, the magnitude of the imaginary part of the root

$$\left|\sqrt{1-K}\right| = 1$$

which is true if $K = 2$.

Consider now the second-order system shown in Fig. 7.3 which represents a typical position control system with velocity feedback. It is a multi-loop system with closed-loop transfer function

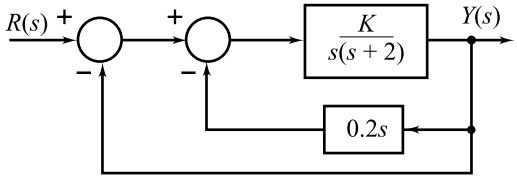

Fig. 7.3 A position control system with velocity feedback

$$M(s) = \frac{K}{s^2 + (0.2K + 2)s + K} \tag{7.5}$$

The characteristic equation is

$$\Delta(s) = s^2 + (0.2K + 2)s + K = 0 \tag{7.6}$$

which can be rearranged as

$$s^2 + 2s + K(0.2s + 1) = 0$$

or

$$1 + \frac{0.2K(s+5)}{s(s+2)} = 0 \tag{7.7}$$

Note that Eqn. (7.7) is also the characteristic equation of a unity feedback system with (open-loop) transfer function

$$F(s) = \frac{K'(s+5)}{s(s+2)}\,;\; K' = 0.2K \tag{7.8}$$

which has two poles at $s = 0$ and $s = -2$, and a zero at $s = -5$. In Fig. 7.4, the open-loop poles (poles of $F(s)$) are indicated by × and the open-loop zero (zero of $F(s)$) is indicated by ○.

Let us examine the nature of characteristic roots

$$s_{1,2} = -(0.1K + 1) \pm \sqrt{(0.1K + 1)^2 - K} \tag{7.9}$$

As K is varied from zero to infinity, the characteristic roots move in the s-plane as shown in Fig. 7.4. At $K = 0$, the root s_1 is equal to the open-loop pole at $s = 0$ and the root s_2 is equal to the open-loop pole at $s = -2$.

[1]Treating the two branches *A-C-D* and *B-C-E* as two root loci will give identical results.

As K increases, the roots move towards each other. The two roots meet at $s = -1.127$ for $K = 1.27$. As K is increased further, the roots break away from the real axis and become complex conjugate. It turns out that the complex roots move along a circle[2] of radius $\sqrt{15}$ with centre at $s = -5$.

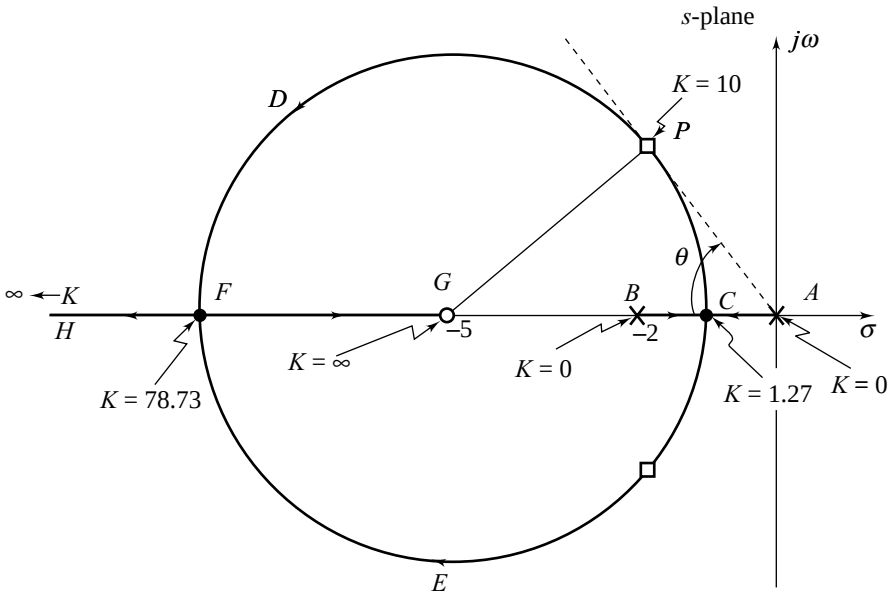

Fig. 7.4 Root locus plot for Eqn. (7.6)

The two complex-conjugate roots meet at $s = -8.873$ for $K = 78.73$. As K is increased further, the roots break away and depart in opposite directions along the real axis.

From Eqn. (7.9), we obtain

$$s_{1,2} = -(0.1K + 1) \pm (0.01K^2 - 0.8K + 1)^{1/2}$$

$$= -(0.1K + 1) \pm 0.1K\left(1 - \frac{80}{K} + \frac{100}{K^2}\right)^{1/2}$$

For large K,

$$s_{1,2} \cong -(0.1K + 1) \pm 0.1K\left(1 - \frac{80}{K}\right)^{1/2}$$

$$\cong -(0.1K + 1) \pm 0.1K\left(\left(1 - \frac{40}{K}\right)\left(1 - \frac{40}{K}\right)\right)^{1/2}$$

$$\cong -0.1K - 1 \pm 0.1K \mp 4$$

Therefore as $K \to \infty$, $s_1 \to -5$ and $s_2 \to -\infty$.

Figure 7.4 shows the two root loci: *A-C-D-F-G* and *B-C-E-F-H*.

[2]This can easily be proved as we shall see later in Example 7.1.

As with the earlier example of Fig. 7.2, valuable information can be obtained from the root locus plot of Fig. 7.4. As K increases, the root loci move away from imaginary axis and the system becomes more stable. The least damped complex-conjugate poles are obtained by drawing straight line AP tangential to the circular locus as shown in Fig. 7.4.

By geometry,

$$\zeta_{\min} = \cos\theta = \frac{AP}{AG} = \frac{\sqrt{(AG)^2 - (GP)^2}}{AG}$$

$$= \frac{\sqrt{25-15}}{5} = \frac{\sqrt{10}}{5} = 0.632$$

The least damped complex-conjugate closed-loop poles, marked □ in Fig. 7.4, are

$$s_1 = -(0.1K+1) + \sqrt{(0.1K+1)^2 - K} = -\sqrt{10}\cos\theta + j\sqrt{10}\sin\theta$$

$$= -2 + j2.45 \tag{7.10}$$

$$s_2 = -(0.1K+1) - \sqrt{(0.1K+1)^2 - K} = -\sqrt{10}\cos\theta - j\sqrt{10}\sin\theta$$

$$= -2 - j2.45 \tag{7.11}$$

From Eqns (7.10)–(7.11), we find that corresponding to $\zeta = 0.632$,

$$0.1K + 1 = 2$$

which is true if $K = 10$. Therefore, $K = 10$ results in the least damping.

The two root locus plots we have presented, illustrate a number of properties which will be derived and discussed in the next section. First, a root locus plot is always symmetrical with respect to the real axis. This is so because the roots must always be complex conjugate. Second, a root locus plot is made of as many branches as there are poles in the open-loop transfer function, and each branch starts from one of the open-loop poles. The branches either go off to infinity or end on an open-loop zero.

The two cases we have discussed involved only a modest amount of analysis. The effort rapidly grows with the order of the system. The sketching rules given in the next section serve the purpose of avoiding direct solution for the roots. As one can imagine, repeated formation of the characteristic polynomial and factoring by hand calculator is a tedious job. Programs are now available [151–154] to generate the root locus plots; some of them based on repeated factoring and some that mechanize the sketching rules. Whatever the package available to us does, it will be useful to know its basis and its limitations. The hand-sketching process trains our intuition and helps us to avoid buying computer-generated trash results.

A graphical procedure for sketching root locus plots was developed by W.R. Evans in 1948. In the following, we present the locus equations which form the basis of the Evans method; guidelines for sketching root loci will be given in the next section.

7.2.1 The Locus Equations

Most control systems can be expressed in the form of Fig. 7.5, where the closed-loop transfer function is

$$M(s) = \frac{Y(s)}{R(s)} = \frac{G(s)}{1 + G(s)H(s)} \tag{7.12}$$

The characteristic equation of the system is

$$1 + G(s)H(s) = 0 \tag{7.13}$$

The open-loop transfer function (refer Eqn. (3.1c)) $G(s)H(s)$ is generally known in the factored form as it is obtained by modelling the transfer function of individual components comprising the system. Therefore $G(s)H(s)$ can generally be expressed in either of the factored forms given below:

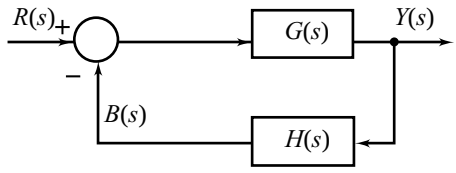

Fig. 7.5 A feedback system

Pole-zero form

$$G(s)H(s) = \frac{K\prod_{i=1}^{m}(s + z_i)}{\prod_{j=1}^{n}(s + p_j)}\ ;\ m \le n,\ K \ge 0 \tag{7.14}$$

Time-constant form

$$G(s)H(s) = \frac{K'\prod_{i=1}^{m}(\tau_{zi}s + 1)}{\prod_{j=1}^{n}(\tau_{pj}s + 1)}\ ;\ m \le n,\ K \ge 0 \tag{7.15}$$

These forms are interrelated by the following expressions.

$$-z_i = -\frac{1}{\tau_{zi}}\ ;\ i = 1, 2, \ldots, m;\ -p_j = -\frac{1}{\tau_{pj}}\ ;\ j = 1, 2, \ldots, n \tag{7.16}$$

$$K = \frac{K'\prod_{j=1}^{n} p_j}{\prod_{i=1}^{m} z_i}$$

K' is the open-loop gain in time-constant form, K is the open-loop gain in pole-zero form, $-z_i$ are m open-loop zeros, and $-p_j$ are n open-loop poles. In all physically realizable systems, $n \ge m$.

The pole-zero form of Eqn. (7.14) is more convenient for drawing root locus and will be used throughout this chapter. The open-loop gain K is considered variable for drawing the root locus of the system.

Substituting Eqn. (7.14) into Eqn. (7.13), we obtain the characteristic equation

$$1 + \frac{K\prod_{i=1}^{m}(s + z_i)}{\prod_{j=1}^{n}(s + p_j)} = 0 \tag{7.17}$$

or

$$\prod_{j=1}^{n}(s + p_j) + K\prod_{i=1}^{m}(s + z_i) = 0 \tag{7.18}$$

The characteristic equation given in (7.18) is in conventional polynomial form. The characteristic equation given in (7.17) is not in conventional form; however, the values of s for which it is satisfied will be same as those for which Eqn. (7.18) is satisfied provided that the numerator and denominator polynomials in Eqn. (7.17) have no common factors.

If the variable parameter is other than open-loop gain, the characteristic equation can be rearranged to obtain the form (7.17) with the parameter of interest appearing as the multiplying factor. The characteristic equation of a multi-loop control configuration can also be brought to the form (7.17) by block diagram manipulation rules or by Mason's gain formula. In our study of the root locus technique, we therefore consider a general characteristic equation:

$$1 + F(s) = 0 \tag{7.19a}$$

with

$$F(s) = \frac{K\prod_{i=1}^{m}(s + z_i)}{\prod_{j=1}^{n}(s + p_j)}; \; m \le n \tag{7.19b}$$

where $K \ge 0$ is the *root locus gain*.

From Eqns (7.19) it is seen that the roots of the characteristic equation occur only for those values of s where

$$F(s) = \frac{K\prod_{i=1}^{m}(s + z_i)}{\prod_{j=1}^{n}(s + p_j)} = -1 \tag{7.20}$$

7.2.2 Magnitude and Angle Conditions

Since s is a complex variable, Eqn. (7.20) is converted into two Evans conditions given below:

Magnitude criterion

$$|F(s)| = \frac{K\prod_{i=1}^{m}|s + z_i|}{\prod_{j=1}^{n}|s + p_j|} = 1 \tag{7.21a}$$

Angle criterion

$$\angle F(s) = \sum_{i=1}^{m}\angle s + z_i - \sum_{j=1}^{n}\angle s + p_j = \pm 180°\,(2q + 1);$$
$$q = 0, 1, 2, \ldots \tag{7.21b}$$

Equations (7.21) imply that the roots of $1 + F(s) = 0$ are those values of s at which the magnitude of $F(s)$ equals 1 and the angle of $F(s)$ equals an odd multiple of 180°. Figure 7.6 illustrates graphical evaluation of $|s_0 + p_j|$, $|s_0 + z_i|$, $\angle s_0 + p_j$ and $\angle s_0 + z_i$ at a point s_0 in the s-plane.

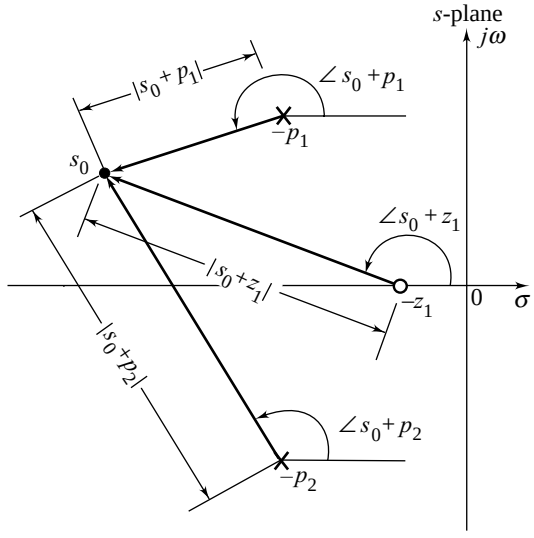

Fig. 7.6 Evaluation of $|F(s)|$ and $\angle F(s)$

It should be appreciated that not all values of s that satisfy Eqn. (7.21a) also satisfy Eqn. (7.21b), while for every s that satisfies Eqn. (7.21b), there exists a K satisfying Eqn. (7.21a). The root locus, thus, is a plot of the points in the complex plane where the angle criterion (7.21b) is satisfied. The value of gain corresponding to a root, i.e., a point on the root locus, can be obtained from the magnitude criterion (7.21a).

Example 7.1 Consider the second-order characteristic equation

$$1 + F(s) = 0$$

with

$$F(s) = \frac{K(s+b)}{(s+a_1)(s+a_2)}; K \geq 0$$

having pole-zero configuration shown in Fig. 7.7a.

We will search for all the points in the s-plane for which the angle criterion (7.21b) is satisfied. A plot of these points is the root locus of the given characteristic equation.

We begin our search process with the real axis of the s-plane. Let us examine any point s_0 in between the two poles (refer Fig. 7.7a). As this point is joined by phasors to the poles at $s = -a_1$ and $s = -a_2$, and the zero at $s = -b$, it is easily seen that

(i) the pole at $s = -a_1$ contributes an angle of 180°,
(ii) the pole at $s = -a_2$ contributes an angle of 0°, and
(iii) the zero at $s = -b$ contributes an angle of 0°.

Therefore, the angle criterion (7.21b) is satisfied and the point s_0 is on the root locus. Scanning all the points on the real axis, yields the real-axis root locus segments shown in Fig. 7.7b by dark lines.

To examine s-plane points not on the real axis, we consider a representative point $s = \sigma + j\omega$. At this point

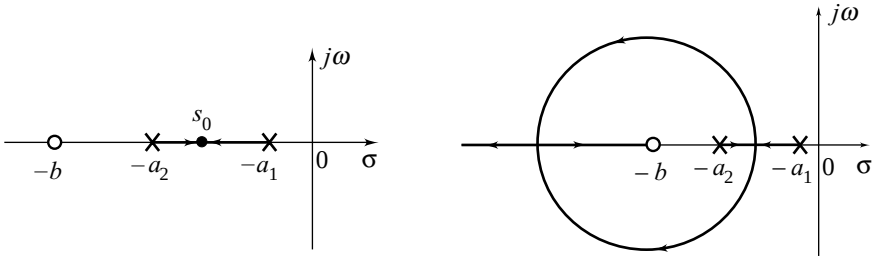

(a) (b)

Fig. 7.7 Search for points on root loci

$$F(s) = \frac{K(\sigma + j\omega + b)}{(\sigma + j\omega + a_1)(\sigma + j\omega + a_2)}$$

$$= \frac{K(\sigma + b + j\omega)}{(\sigma + a_1)(\sigma + a_2) + j\omega(\sigma + a_1 + \sigma + a_2) - \omega^2}$$

$$= \frac{K(\sigma + b + j\omega)}{(\sigma + a_1)(\sigma + a_2) - \omega^2 + j\omega(2\sigma + a_1 + a_2)}$$

$$\angle F(s) = \tan^{-1}\frac{\omega}{\sigma+b} - \tan^{-1}\frac{\omega(2\sigma+a_1+a_2)}{(\sigma+a_1)(\sigma+a_2)-\omega^2}$$

$$= \tan^{-1}\left\{\frac{\dfrac{\omega}{\sigma+b} - \dfrac{\omega(2\sigma+a_1+a_2)}{(\sigma+a_1)(\sigma+a_2)-\omega^2}}{1+\dfrac{\omega}{\sigma+b}\left[\dfrac{\omega(2\sigma+a_1+a_2)}{(\sigma+a_1)(\sigma+a_2)-\omega^2}\right]}\right\}$$

$\angle F(s)$ is a multiple of 180° if

$$\frac{\dfrac{\omega}{\sigma+b} - \dfrac{\omega(2\sigma+a_1+a_2)}{(\sigma+a_1)(\sigma+a_2)-\omega^2}}{1+\dfrac{\omega}{\sigma+b}\left[\dfrac{\omega(2\sigma+a_1+a_2)}{(\sigma+a_1)(\sigma+a_2)-\omega^2}\right]} = 0$$

Manipulation of this equation gives

$$(\sigma+b)^2 + \omega^2 = (b-a_1)(b-a_2)$$

This is the equation of a circle with centre at $(-b, 0)$ and radius $= \sqrt{(b-a_1)(b-a_2)}$. It can easily be verified that at every point on this circle in the s-plane, $\angle F(s)$ is ± 180°. Every point on the circle, therefore, satisfies the angle criterion (7.21b).

Let us assume the following numerical values for open-loop poles and zeros.

$$a_1 = 1,\ a_2 = 2,\ b = 5$$

The root locus plot for this case is shown in Fig. 7.8. The two root loci are *A-C-D-F-G* and *B-C-E-F-H*; the locus *A-C-D-F-G* starts at open-loop pole $s = -2$ with $K = 0$ and terminates at open-loop zero $s = -5$ with $K = \infty$; and the locus *B-C-E-F-H* starts at open-loop pole $s = -1$ with $K = 0$ and goes off to infinity along the negative real axis as $K \to \infty$.

The value of K corresponding to least damping may be obtained by applying the magnitude criterion (7.21a) at the point P where OP is a straight line tangential to the circular locus.

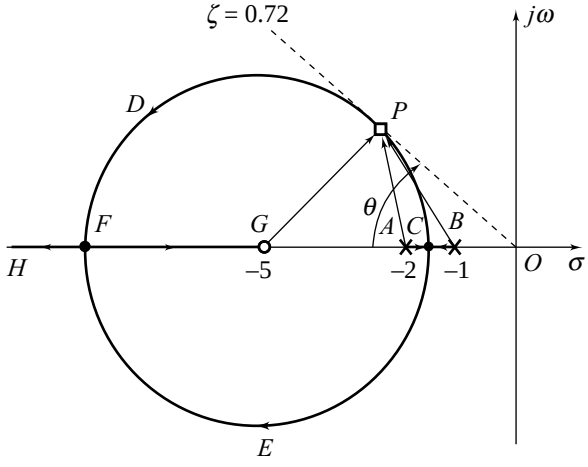

Fig. 7.8 A root locus plot (Example 7.1)

$$K = \frac{\text{length of the vector } AP \times \text{length of the vector } BP}{\text{length of the vector } GP}$$

$$= \frac{2.6 \times 2.9}{3.45} \cong 2.2;\ \zeta_{\min} = \cos\theta = 0.72$$

The closed-loop poles corresponding to this value of damping are (read from Fig. 7.8): $s_{1,2} = -2.6 \pm j2.5$.

Example 7.2 Consider the second-order characteristics equation

$$1 + F(s) = 0$$

with

$$F(s) = \frac{K(s+b)}{(s+\alpha+j\beta)(s+\alpha-j\beta)}\,;\; K \geq 0$$

having pole-zero configuration shown in Fig. 7.9.

Let us examine any point s_0 on the negative real axis to the left of the zero at $s = -b$. As this point is joined by phasors to the two poles at $s = -\alpha \pm j\beta$ and the zero at $s = -b$, it is easily seen that (i) the zero contributes an angle of 180°, and (ii) the net angle contribution of complex-conjugate pole pair is zero. Therefore, angle criterion (7.21b) is satisfied for all the points on the negative real axis to the left of the zero at $s = -b$. It can easily be verified that the angle criterion is not satisfied for all the points on the real axis to the right of the zero at $s = -b$.

To examine s-plane points not on the real axis, we consider a representative point $s = \sigma + j\omega$. At this point,

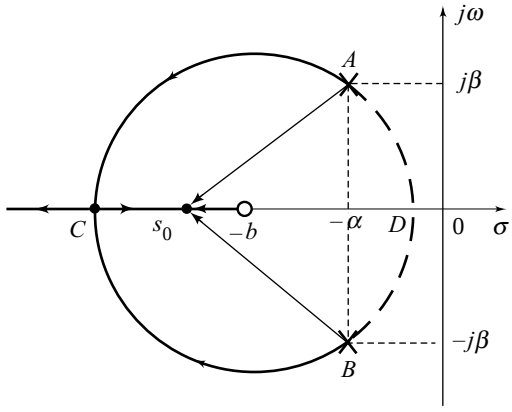

Fig. 7.9 Search for points on root loci

$$F(s) = \frac{K(\sigma + j\omega + b)}{(\sigma + j\omega + \alpha + j\beta)(\sigma + j\omega + \alpha - j\beta)}$$

$$= \frac{K(\sigma + b + j\omega)}{\left(\sigma^2 + \alpha^2 + 2\sigma\alpha - \omega^2 + \beta^2\right) + j2\omega(\sigma + \alpha)}$$

$$\angle F(s) = \tan^{-1}\frac{\omega}{\sigma + b} - \tan^{-1}\frac{2\omega(\sigma+\alpha)}{\left(\sigma^2 + \alpha^2 + 2\sigma\alpha - \omega^2 + \beta^2\right)}$$

$$= \tan^{-1}\left\{\frac{\dfrac{\omega}{\sigma+b} - \dfrac{2\omega(\sigma+\alpha)}{\sigma^2+\alpha^2+2\sigma\alpha-\omega^2+\beta^2}}{1 + \dfrac{\omega}{\sigma+b}\left[\dfrac{2\omega(\sigma+\alpha)}{\sigma^2+\alpha^2+2\sigma\alpha-\omega^2+\beta^2}\right]}\right\}$$

$\angle F(s)$ is a multiple of 180° if

$$\frac{\dfrac{\omega}{\sigma+b} - \dfrac{2\omega(\sigma+\alpha)}{\sigma^2+\alpha^2+2\sigma\alpha-\omega^2+\beta^2}}{1 + \dfrac{\omega}{\sigma+b}\left[\dfrac{2\omega(\sigma+\alpha)}{\sigma^2+\alpha^2+2\sigma\alpha-\omega^2+\beta^2}\right]} = 0$$

Manipulation of this equation gives

$$(\sigma + b)^2 + \omega^2 = (\alpha - b)^2 + \beta^2$$

This is the equation of a circle with centre at $(-b, 0)$ and radius $= \sqrt{(\alpha - b)^2 + \beta^2}$. It can easily be verified that at every point of the *A-C-B* section of the circle, $\angle F(s)$ is $\pm 180°$; and at every point of the *A-D-B* section of the circle, $\angle F(s) = 0°$. Every point of the *A-C-B* section, therefore, satisfies the angle criterion (7.21b).

Let us assume the following numerical values for the open-loop poles and zeros:

$$\alpha = 1, \beta = \sqrt{2}, b = 2$$

The root locus plot for this case is shown in Fig. 7.10. The two root loci are *A-C-E* and *B-C-F*; the locus *A-C-E* starts at open-loop pole at $s = -1 + j\sqrt{2}$ with $K = 0$ and terminates at open-loop zero at $s = -2$ with $K = \infty$, and the locus *B-C-F* starts at open-loop pole at $s = -1 - j\sqrt{2}$ with $K = 0$ and goes off to infinity along the negative real axis as $K \to \infty$.

The value of K corresponding to a damping ratio of 0.7 may be obtained by applying the magnitude criterion (7.21a) at the point *P* in Fig. 7.10.

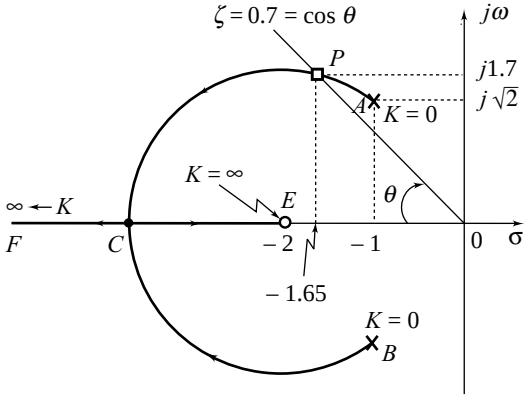

Fig. 7.10 A root locus plot (Example 7.2)

$$K = \frac{\text{length of the vector } AP \times \text{length of the vector } BP}{\text{length of the vector } EP}$$

$$= \frac{0.7 \times 3.2}{1.73} \cong 1.3$$

The closed-loop poles corresponding to this value of K are (read from Fig. 7.10): $s_{1,2} = -1.65 \pm j1.7$.

In systems of Examples 7.1 and 7.2, the root loci in the complex plane are a part of a circle. Circular root loci may occur in systems that involve two poles and one zero, two poles and two zeros, or one pole and two zeros. Even in such systems, whether or not circular root loci occur depends on the locations of poles and zeros involved.

It is important to note that easily interpretable equations for the root locus can be derived for simple systems only. For complicated systems having many poles and zeros, any attempt to derive equations for the root loci is discouraged. Such derived equations are very complicated and their configuration in the complex plane is difficult to visualize. The next section provides a solution to this problem.

7.3 GUIDELINES FOR SKETCHING ROOT LOCI

The purpose of the root locus is to show in graphical form the general trend of the roots of the characteristic equation

$$1 + F(s) = 0 \tag{7.22a}$$

where

$$F(s) = \frac{K \prod_{i=1}^{m} (s + z_i)}{\prod_{j=1}^{n} (s + p_j)}; \; m \le n \tag{7.22b}$$

as the parameter K is varied from zero to infinity. Every point $s = \sigma + j\omega$ in the complex plane that satisfies the *angle criterion* (refer Eqn. (7.21b))

$$\angle F(s) = \sum_{i=1}^{m} \angle s + z_i - \sum_{j=1}^{n} \angle s + p_j = \pm 180° (2q + 1);\ q = 0, 1, 2, \ldots \tag{7.23a}$$

is on the root locus. The value of the parameter K (*root locus gain*) corresponding to a point on the root locus can be obtained from the *magnitude criterion* (refer Eqn. (7.21a))

$$|F(s)| = \frac{K \prod_{i=1}^{m} |s + z_i|}{\prod_{j=1}^{n} |s + p_j|} \tag{7.23b}$$

We can, in principle, sketch a root locus for a given $F(s)$ by measuring $\angle F(s)$ at all the points of the complex plane and marking down those places where we find $\angle F(s)$ equal to an odd multiple of 180°. This trial-and-error procedure of sketching the root locus is illustrated in Fig. 7.6. The poles and zeros of $F(s)$ are located on the s-plane on a graph sheet and a trial point s_0 is selected. The lines joining each of the poles $(-p_j)$ and zeros $(-z_i)$ to s_0 represent the phasors $(s_0 + p_j)$ and $(s_0 + z_i)$ respectively, as shown in Fig. 7.6. The angles of these phasors can be measured by placing a protector at the pole and zero locations, and the angle values are substituted in the angle criterion given by Eqn. (7.23a). The trial point s_0 is suitably shifted till the angle criterion is satisfied to a desired degree of accuracy. A number of points on the s-plane are determined in this manner and a smooth curve drawn through these points gives the root locus with variable K.

The value of K for a particular root location s_0 can be obtained from the magnitude criterion given by Eqn. (7.23b) by substituting the phasor magnitudes read to scale. It is to be noted that the same scale must be employed for both the real and imaginary axes of the complex plane.

From the magnitude criterion of Eqn. (7.23b),

$$K = \frac{\prod_{j=1}^{n} |s_0 + p_j|}{\prod_{i=1}^{m} |s_0 + z_i|} \tag{7.24a}$$

With reference to Fig. 7.6, we can write

$$K = \frac{\left[\begin{array}{l}\text{Product of phasor lengths (read to scale)}\\ \text{from } s_0 \text{ to pole of } F(s)\end{array}\right]}{\left[\begin{array}{l}\text{Product of phasor lengths (read to scale)}\\ \text{from } s_0 \text{ to zeros of } F(s)\end{array}\right]} \tag{7.24b}$$

If we were to use the trial-and-error method just described, the search for all the root locus points in the s-plane that satisfy the angle criterion (7.23a) would in general be a very tedious task. In order to help reduce the tedium of the trial-and-error procedure, certain rules have been developed for making a quick approximate sketch of the root locus. This approximate sketch provides a guide for the selection of trial points such that a reasonably accurate root locus can be obtained by a few trials. Further, the approximate root locus sketch is very useful in vizualizing the effects of variation of system parameter K, the effects of shifting pole-zero locations and of bringing in a new set of poles and zeros.

With the availability of digital computers and efficient root-finding techniques, the trial-and-error method has become obsolete. Nevertheless, the analyst should still have an understanding of the properties of the root loci in order to interpret the computer results correctly and apply the root locus techniques for the design of linear control systems. Presentation of guidelines for hand-sketching an approximate root locus plot is, therefore, in order.

7.3.1 Rules for Constructing Root Loci

To help in the rough drafting of the general form of a root locus, construction rules have been devised. We shall discuss several of them, first stating the rule, then giving a justification for its validity, and finally citing an example if appropriate. We assume that $F(s)$ for which the root locus is desired, is of the form given by Eqn. (7.22b), i.e., with m zeros at $s = -z_i$, and n poles at $s = -p_j$; $m \le n$. The m zeros and n poles of $F(s)$ will be referred to as open-loop zeros and open-loop poles, respectively[3].

Rule 1 Number of Root Loci *The root locus plot consists of n root loci as K varies from 0 to ∞. The loci are symmetric with respect to the real axis.*

The characteristic equation (7.22a) can be written as

$$\prod_{j=1}^{n}(s + p_j) + K \prod_{i=1}^{m}(s + z_i) = 0$$

This equation has degree n. Thus for each real K, there are n roots. As the roots of this equation are continuous functions of its coefficients, the n roots form n continuous loci as K varies from 0 to ∞.

Since the complex roots of the characteristic equation always occur in conjugate pairs, the n root loci, must be symmetrical about the real axis.

Rule 2 Starting and Terminal Points of Root Loci *As K increases from zero to infinity, each root locus originates from an open-loop pole with K = 0 and terminates either on an open-loop zero or on infinity with K = ∞. The number of loci terminating on infinity equals the number of open-loop poles minus zeros.*

The characteristic equation (7.22a) can be written as

$$\prod_{j=1}^{n}(s + p_j) + K \prod_{i=1}^{m}(s + z_j) = 0 \tag{7.25}$$

When $K = 0$, this equation has roots at $-p_j$ ($j = 1, 2, \ldots, n$), which are the open-loop poles. The root loci, therefore, start at the open-loop poles.

The characteristic equation (7.25) can be rearranged as

$$\frac{1}{K}\prod_{j=1}^{n}(s + p_j) + \prod_{i=1}^{m}(s + z_i) = 0$$

When $K = \infty$, this equation has roots at $-z_i (i = 1, 2, \ldots, m)$, which are the open-loop zeros. Therefore, m root loci terminate on the open-loop zeros.

In case $m < n$, the open-loop transfer function has $(n - m)$ zeros at infinity. Examining the magnitude criterion (7.23b) in the form

[3]The equation $1 + F(s) = 0$ can be interpreted as the characteristic equation of a unity-feedback system with open-loop transfer function equal to $F(s)$.

$$\frac{\prod_{i=1}^{m} |s + z_i|}{\prod_{j=1}^{n} |s + p_j|} = \frac{1}{K}$$

we find that this is satisfied by $s \to \infty\, e^{j\phi}$ as $K \to \infty$. Therefore, $(n - m)$ root loci terminate on infinity.

Rule 3 Asymptotes to Root Loci *The $(n - m)$ root loci which tend to infinity do so along straight line asymptotes radiating out from a single point $s = -\sigma_A$ on the real axis (called the centroid), where*

$$-\sigma_A = \frac{\sum (\text{real parts of open-loop poles}) - \sum (\text{real parts of open-loop zeros})}{n - m} \tag{7.26a}$$

These $(n - m)$ asymptotes have angles

$$\phi_A = \frac{(2q + 1)180°}{n - m};\ q = 0, 1, \ldots, (n - m - 1) \tag{7.26b}$$

We justify the rule by using the pole-zero pattern shown in Fig. 7.11a. For a point s_0 far away from the origin, the poles and zeros can be considered to cluster at the same point, say $-\sigma_A$, as shown in Fig. 7.11b.

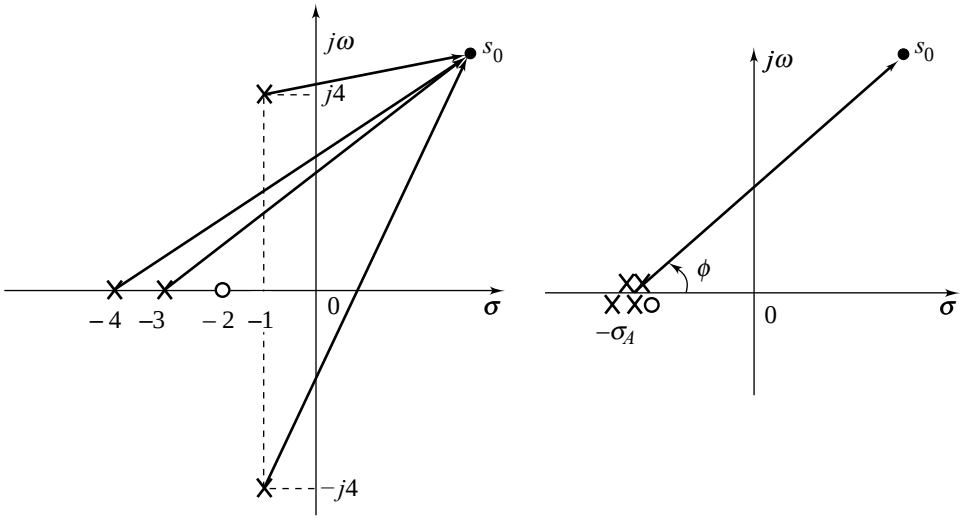

Fig. 7.11 Asymptotes to root loci

Consequently, the characteristic equation in (7.22a) can be approximated by

$$1 + \frac{K \prod_{i=1}^{m} (s + z_i)}{\prod_{j=1}^{n} (s + p_j)} \cong 1 + \frac{K}{(s + \sigma_A)^{n-m}} = 0 \tag{7.27}$$

In other words, all m finite zeros are cancelled by poles, and only $(n-m)$ poles are left at $-\sigma_A$. Now we compute the relationship among z_i, p_j, and $-\sigma_A$. From Eqn. (7.27), we obtain

$$\frac{\prod_{j=1}^{n}(s+p_j)}{\prod_{i=1}^{m}(s+z_i)} \cong (s+\sigma_A)^{n-m}$$

or

$$\frac{s^n+\left(\sum_{j=1}^{n}p_j\right)s^{n-1}+\cdots+\prod_{j=1}^{n}p_j}{s^m+\left(\sum_{i=1}^{m}z_i\right)s^{m-1}+\cdots+\prod_{i=1}^{m}z_i} \cong (s+\sigma_A)^{n-m}$$

which implies, by direct division and expansion,

$$s^{n-m}+\left(\sum_{j=1}^{n}p_j-\sum_{i=1}^{m}z_j\right)s^{n-m-1}+\cdots$$
$$\cong s^{n-m}+(n-m)\sigma_A\, s^{n-m-1}+\cdots$$

Equating the coefficients of s^{n-m-1} yields

$$(n-m)\sigma_A=\sum_{j=1}^{n}p_j-\sum_{i=1}^{m}z_i$$

or

$$-\sigma_A=\frac{\sum_{j=1}^{n}(-p_j)-\sum_{i=1}^{m}(-z_i)}{n-m}$$

This establishes Eqn. (7.26a).

For the point s_0 in Fig. 7.11b to be on the root locus,

$$-(n-m)\phi=-(2q+1)\,180°;\ q=0,\,1,\,\ldots$$

or

$$\phi=\frac{(2q+1)180°}{n-m};\ q=0,\,1,\,\ldots$$

The $(n-m)$ angles given by this equation divide 360° equally and are symmetric with respect to real axis. The $(n-m)$ root loci, therefore, tend to infinity along $(n-m)$ asymptotes radiating out from $s=-\sigma_A$ given by Eqn. (7.26a) at angles ϕ_A given by Eqn. (7.26b).

The pole-zero map of Fig. 7.11a corresponds to

$$F(s)=\frac{K(s+2)}{(s+1+j4)(s+1-j4)(s+3)(s+4)} \qquad (7.28a)$$

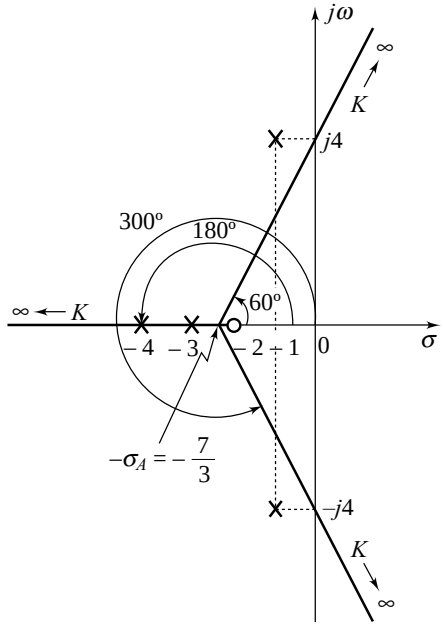

Fig. 7.12 Asymptotes for the characteristic equation (7.28)

The root locus plot of

$$1 + F(s) = 0 \tag{7.28b}$$

will consist of four root loci, each starting from an open-loop pole with $K = 0$. One root locus will terminate on open-loop zero with $K = \infty$. The other three loci will terminate on infinity as $K \to \infty$ along the asymptotes radiating out from $s = -\sigma_A$

where $$-\sigma_A = \frac{-1-1-3-4-(-2)}{4-1} = -7/3$$

at angles 60°, 180°, and 300° respectively. Figure 7.12 shows the asymptotes. Note that asymptotes are developed for large s; thus the root loci will *approach* them for large s or large K.

Rule 4 On-Locus Segments of the Real Axis *A point on the real axis lies on the locus if the number of open-loop poles plus zeros on the real axis to the right of this point is odd.*

For the fourth-order example under consideration (refer Eqns (7.28)), open-loop pole-zero configuration is shown in Fig. 7.13a. Let us examine any point s_0 on the real axis. As this point is joined by phasors to all the open-loop poles and zeros, it is easily seen that (i) the poles and zeros on the real axis to the right of this point contribute an angle of 180° each, (ii) the poles and zeros on the real axis to the left of this point contribute an angle of 0° each, and (iii) the net angle contribution of a complex conjugate pole or zero pair is always zero.

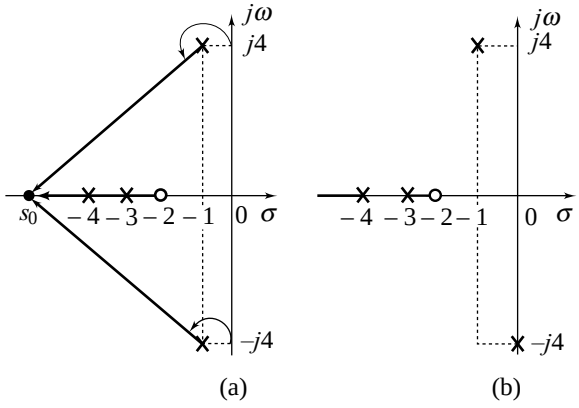

Fig. 7.13 On-locus segments of the real axis

Therefore,

$$\angle F(s) = (m_r - n_r)180° = \pm (2q + 1)180°,\ q = 0, 1, 2, \ldots$$

where

m_r = number of open-loop zeros on the real axis to the right of s_0; and
n_r = number of open-loop poles on the real axis to the right of s_0.

We therefore see that for a point on the real axis, the angle criterion is met only if $(n_r - m_r)$ or $(n_r + m_r)$ is odd and hence the rule. If this rule is satisfied at any point on the real axis, it continues to be satisfied as the point is moved on either side unless the point crosses a real axis pole or zero. By use of this additional fact, the real axis can be divided into segments *on-locus* and *not-on-locus*; the dividing points being the real open-loop poles and zeros. The on-locus segments of the real axis alternate as shown in Fig. 7.13b.

Rule 5 On-Locus Points of the Imaginary Axis *The intersections (if any) of root loci with the imaginary axis can be determined by use of the Routh criterion.*

Segments of root loci can exist in the right half of s-plane. This signifies instability. The points at which the root loci cross the imaginary axis define the stability limits. Basic application of the Routh array (Chapter 5) determines the gains at the stability limit. By substituting this value of gain in the auxiliary equation, the value of $s = j\omega_0$ at the stability limit is evaluated.

For the fourth-order example under consideration (refer Eqns (7.28)), the characteristic equation is

$$1 + \frac{K(s+2)}{(s+1+j4)(s+1-j4)(s+3)(s+4)} = 0.$$

which is equivalent to

$$s^4 + 9s^3 + 43s^2 + (143 + K)s + 204 + 2K = 0 \tag{7.29}$$

The Routh array for the characteristic polynomial is

s^4	1	43	$204 + 2K$
s^3	9	$143 + K$	
s^2	$\frac{244 - K}{9}$	$204 + 2K$	
s^1	$\frac{18368 - 61K - K^2}{244 - K}$		
s^0	$204 + K$		

For Eqn. (7.29) to have no roots on $j\omega$-axis or in the right-half s-plane, the elements in the first column of Routh array must all be of the same sign. Therefore, the following inequalities must be satisfied:

$$244 - K > 0$$
$$18368 - 61K - K^2 > 0$$
$$204 + K > 0$$

These inequalities are satisfied if K is less than 108.4, which means that the critical value of K which corresponds to the roots on the $j\omega$-axis is 108.4.

The value of $K = 108.4$ makes all the coefficients of s^1-row of the Routh array zero. For this value of K, the auxiliary equation formed from the coefficient of the s^2-row, is given by

$$\left(\frac{244 - K}{9}\right) s^2 + (204 + 2K) = 0$$

For $K = 108.4$, the roots of the above equation lie on the $j\omega$-axis and are given by

$$s = \pm j5.28$$

Thus the root loci intersect the $j\omega$-axis at $s = \pm j5.28$ and the value of K corresponding to these roots is 108.4.

Rule 6 Angle of Departure from Complex Poles *The angle of departure, ϕ_p, of a locus from a complex open-loop pole is given by*

$$\phi_p = 180° + \phi \tag{7.30}$$

where ϕ is the net angle contribution at this pole of all other open-loop poles and zeros.

For the fourth-order example under consideration (refer Eqns (7.28)), the characteristic equation is

$$1 + F(s) = 1 + \frac{K(s+2)}{(s+1+j4)(s+1-j4)(s+3)(s+4)} = 0$$

The pole-zero map of $F(s)$ is shown in Fig. 7.14. Let s_0 be an arbitrary point on the root locus starting from the pole at $s = -1 + j4$. Let the phase from this pole to s_0 be denoted by ϕ_p. The net angle contribution of all other open-loop poles and zeros at the point s_0 is

$$\phi = \theta_2 - (\theta_1 + \theta_3 + \theta_4)$$

Therefore the total phase of $F(s)$ at s_0 is $\phi - \phi_p$. In order for s_0 to be on the root locus, the total phase must be $\pm 180°$. Thus we have $\phi_p = 180° + \phi$. This is the angle of departure from the complex open-loop pole.

If the point s_0 is very close to the pole at $-1 + j4$, then the vectors drawn from the zero and all other open-loop poles to s_0 can be approximated by the vectors drawn to the pole at $-1 + j4$, i.e., we consider the point s_0 to be at $-1 + j4$ for measurement of angles θ_1, θ_2, θ_3, and θ_4. Under this approximation, $\theta_1 = 90°$, $\theta_2 = 76°$, $\theta_3 = 63°$, and $\theta_4 = 53°$. Therefore

$$\phi = \theta_2 - (\theta_1 + \theta_3 + \theta_4) = -130°;\ \phi_p = 180° + \phi = 50°$$

We can now sketch a rough root locus plot for the fourth-order example under consideration. The plot is shown in Fig. 7.15. The information given in Figs 7.12–7.14 has been used to construct this plot.

There are four open-loop poles; so there are four loci. One locus departs from the real pole at -3 and terminates on the zero at -2 along the real axis. The second locus departs from another real pole at -4 and moves along the asymptote on the negative real axis. The third locus departs from the complex pole at $-1 + j4$ with a departure angle of $\phi_p = 50°$, and moves toward the asymptote radiating out from $-\sigma_A = -7/3$ at an angle $+60°$; it crosses the imaginary axis at $j\omega_0 = j5.28$. Using the symmetry property, the fourth locus is obtained immediately by reflection about the real axis.

Rule 7 Angle of Arrival at Complex Zeros The angle of arrival, ϕ_z, of a locus at a complex zero is given by

$$\phi_z = 180° - \phi \qquad (7.31)$$

where ϕ is the net angle contribution at this zero of all other open-loop poles and zeros.

Consider the characteristic equation

$$1 + F(s) = 1 + \frac{K(s^2+1)}{s(s+2)} = 0 \qquad (7.32)$$

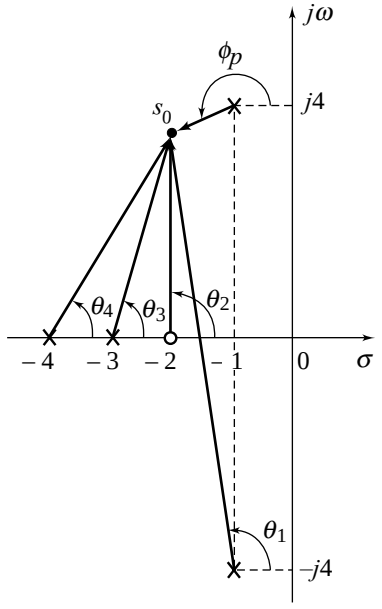

Fig. 7.14 Angle of departure from complex poles

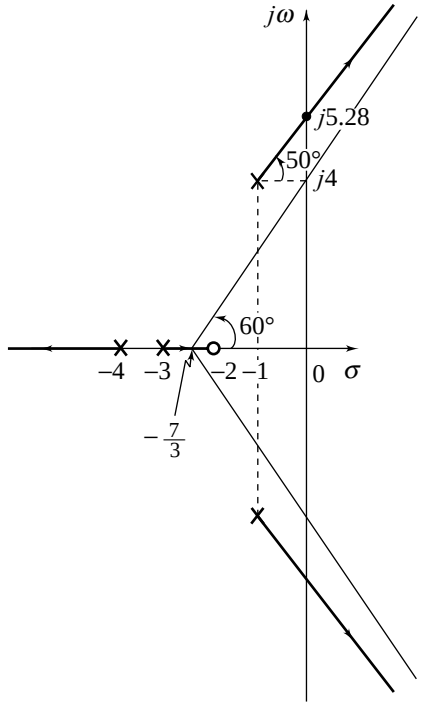

Fig. 7.15 Root locus plot for the characteristic equation (7.28)

The pole-zero map of $F(s)$ is shown in Fig. 7.16. The open-loop poles are located at $s = 0$ and $s = -2$ and the open-loop zeros are located at $s = \pm j1$. Let s_0 be an arbitrary point on the root locus terminating on the zero at $s = j1$. Let the phase from this zero to s_0 be denoted by ϕ_z (refer Fig. 7.16a).

If the point s_0 is very close to the zero at $j1$, then the vectors drawn from the other zero at $-j1$ and open-loop poles at 0 and -2 to s_0 can be approximated by vectors drawn to the zero at $j1$. Under this approximation, the net angle contribution at s_0 of the zero at $-j1$ and open-loop poles at 0 and -2 is given by (refer Fig. 7.16b)

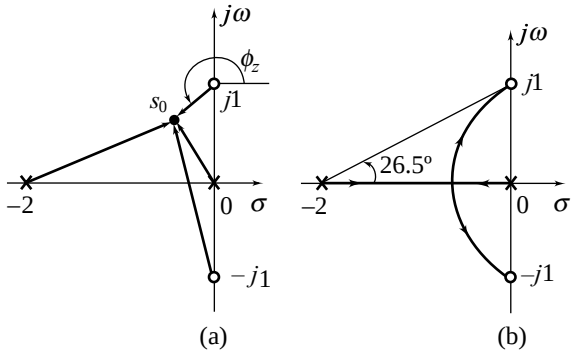

Fig. 7.16 Angle of arrival at complex zeros

$$\phi = 90° - 90° - 26.5° = -26.5°$$

In order for s_0 to be on the root locus, the total phase must be $\pm 180°$. Thus we have $\phi_z = 180° - \phi = 206.5°$.

The complete root locus plot for roots of Eqn. (7.32) is shown in Fig. 7.16b; it can easily be proved (refer Example 7.2) that the complex root branches lie on a circle with centre at (1/2, 0) and radius equal to $\sqrt{5}/2$.

Rule 8 Locations of Multiple Roots *Points at which multiple roots of the characteristic equation occur (breakaway points of root loci) are the solutions of*

$$\frac{dK}{ds} = 0 \tag{7.33a}$$

where

$$K = -\frac{\prod_{j=1}^{n}(s + p_j)}{\prod_{i=1}^{m}(s + z_i)} \tag{7.33b}$$

Assume that the characteristic Eqn. (7.22a) has a multiple root at $s = s_0$ of multiplicity r.

Then
$$1 + F(s) = (s - s_0)^r M(s) \tag{7.34}$$

where $M(s)$ does not contain the factor $(s - s_0)$.

Differentiating Eqn. (7.34) with respect to s, we have

$$\frac{dF(s)}{ds} = (s - s_0)^{r-1}\,[rM(s) + (s - s_0)M'(s)] \tag{7.35}$$

where $M'(s)$ represents the derivative of $M(s)$.

At $s = s_0$, the right hand side of this equation is zero because it has a factor $(s - s_0)^{r-1}$ and $r \geq 2$. Therefore, at $s = s_0$,

$$\frac{dF(s)}{ds} = 0$$

In pole-zero form, the characteristic equation may be written as

$$1 + F(s) = 1 + \frac{K\prod_{i=1}^{m}(s + z_i)}{\prod_{j=1}^{n}(s + p_j)} = 1 + \frac{KB(s)}{A(s)} = 0 \tag{7.36a}$$

Taking the derivative of this equation with respect to s, we get

$$\frac{dF(s)}{ds} = K\frac{A(s)B'(s) - A'(s)B(s)}{[A(s)]^2} = 0$$

Therefore, the breakaway points are given by the roots of

$$A(s)B'(s) - A'(s)B(s) = 0 \tag{7.36b}$$

This equation can equivalently be represented as

$$\frac{dK}{ds} = 0 \tag{7.36c}$$

where

$$K = -\frac{A(s)}{B(s)} = -\frac{\prod_{j=1}^{n}(s + p_j)}{\prod_{i=1}^{m}(s + z_i)}$$

Consider the characteristic equation

$$1 + \frac{K(s+2)(s+3)}{s(s+1)} = 1 + \frac{KB(s)}{A(s)} = 0 \tag{7.37}$$

Figure 7.17 shows open-loop poles and zeros on the complex plane. Root loci segments exist on the negative real axis between 0 and – 1 and between – 2 and – 3. At $K = 0$, the roots are at $s = 0$ and $s = -1$. As K increases, the two real roots move away from poles $s = 0$ and $s = -1$ toward each other inside the real-axis segment [– 1, 0]. As K continues to increase, the two real roots will eventually coalesce into a repeated real root and then break away from the real axis into two complex conjugate roots. Such a point is called a *breakaway point*.

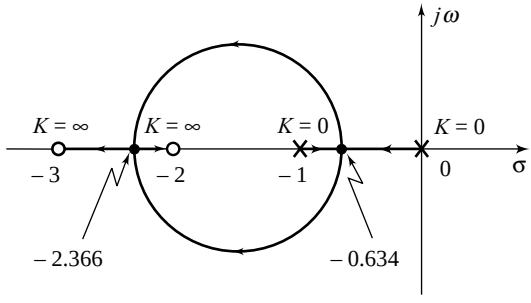

Fig. 7.17 Root locus plot for characteristic Eqn. (7.37)

Similarly, as K approaches infinity, one root will approach zero at $s = -2$ along the negative real axis and another will approach zero at $s = -3$ along the negative real axis. As the root loci are continuous, the two complex-conjugate roots will approach the real axis somewhere inside the segment [– 3, – 2] and then depart in opposite directions along the real axis. Such a point is also called a *breakaway point*.

From Eqns (7.36)–(7.37), we have

$$B(s) = (s + 2)(s + 3) = s^2 + 5s + 6;\ B'(s) = 2s + 5$$

$$A(s) = s(s + 1) = s^2 + s;\ A'(s) = 2s + 1$$

and

$$A(s)B'(s) - A'(s)B(s) = (s^2 + s)(2s + 5) - (2s + 1)(s^2 + 5s + 6)$$

$$= -3s^2 - 12s - 6 = 0$$

Its roots are – 0.634 and – 2.366. Thus the root locus plot has two break-away points: $s = -0.634$ and $s = -2.366$.

The complete root locus plot for roots of Eqn. (7.37) is shown in Fig. 7.17; it can easily be proved (refer Example 7.1) that the complex root branches lie on a circle with centre at (– 1.5, 0) that passes through the breakaway points.

It is important to note that the condition for the breakaway point given by Eqns (7.33) is *necessary* but not *sufficient*. In other words, all breakaway points on the root locus must satisfy Eqns (7.33) but not all solutions of Eqns (7.33) are breakaway points. To be a breakaway point, the solution of Eqns (7.33) must satisfy the characteristic equation (7.22) for some real K. This and many other important aspects of breakaway points will be illustrated through examples in the next section.

7.3.2 Summary of the Rules

Except for extremely complex cases, the rules described above should be adequate for making a reasonably accurate sketch of the root locus plot. For quick reference, these rules are summarized in Table 7.1.

Table 7.1 Rules for construction of Root Locus Plot of

$$1 + F(s) = 0;\ F(s) = \frac{K\prod_{i=1}^{m}(s + z_i)}{\prod_{j=1}^{n}(s + p_j)};\ K \geq 0,\ n \geq m$$

z_i: m open-loop zeros; p_j: n open-loop poles

Rules
(i) The root locus plot consists of n root loci as K varies from 0 to ∞. The loci are symmetric with respect to the real axis.
(ii) As K increases from zero to infinity, each root locus originates from an open-loop pole with $K = 0$ and terminates either on an open-loop zero or on infinity with $K = \infty$. The number of loci terminating on infinity equals the number of open-loop poles minus zeros.
(iii) The $(n - m)$ root loci which tend to infinity, do so along straight-line asymptotes radiating out from a single point $s = -\sigma_A$ on the real axis (called the centroid), where $$-\sigma_A = \frac{\sum(\text{real parts of open-loop poles}) - \sum(\text{real parts of open-loop zeros})}{n - m}$$ These $(n - m)$ asymptotes have angles $$\phi_A = \frac{(2q+1)180^\circ}{n - m};\ q = 0, 1, \ldots, (n - m - 1)$$
(iv) A point on the real axis lies on the locus if the number of open-loop poles plus zeros on the real axis to the right of this point is odd. By use of this fact, the real axis can be divided into segments *on-locus* and *not-on-locus*; the dividing points being the real open-loop poles and zeros.
(v) The intersections (if any) of root loci with the imaginary axis can be determined by use of the Routh criterion.
(vi) The angle of departure, ϕ_p, of a root locus from a complex open-loop pole is given by $$\phi_p = 180^\circ + \phi$$ where ϕ is the net angle contribution at this pole of all other open-loop poles and zeros.
(vii) The angle of arrival, ϕ_z, of a locus at a complex zero is given by $$\phi_z = 180^\circ - \phi$$ where ϕ is the net angle contribution at this zero of all other open-loop poles and zeros.

(*Contd.*)

Table 7.1 *(Contd).*

Rules
(viii) Points at which multiple roots of the characteristic equation occur (breakaway points of root loci) are the solutions of $\frac{dK}{ds} = 0$ where $K = -\frac{\prod_{j=1}^{n}(s + p_j)}{\prod_{i=1}^{m}(s + z_i)}$
(ix) The gain K at any point s_0 on a root locus is given by $K = \frac{\prod_{j=1}^{n}\lvert s_0 + p_j\rvert}{\prod_{i=1}^{m}\lvert s_0 + z_i\rvert} = \frac{\text{[Product of phasor lengths (read to scale) from } s_0 \text{ to poles of } F(s)\text{]}}{\text{[Product of phasor lengths (read to scale) from } s_0 \text{ to zeros of } F(s)\text{]}}$

7.4 SELECTED ILLUSTRATIVE ROOT LOCI

The root locus concept was introduced in Section 7.2 and locus equations were derived in Examples 7.1 and 7.2 for two simple characteristic equations. Since for complex cases, it is not possible to derive easily interpretable locus equations, point-by-point plotting of the root loci becomes necessary. In Section 7.3, we presented some construction rules which help in making a quick rough sketch of the root locus plot.

In order to gain experience with the root-locus method, it is helpful to sketch a number of locus plots and visualize the various alternative shapes a locus of a given complexity can take. In this section, we will go through the construction rules for several cases selected to illustrate important features of root loci.

Example 7.3 Consider a feedback system with the characteristic equation

$$1 + \frac{K}{s(s+1)(s+2)} = 0; K \geq 0 \tag{7.38}$$

The open-loop poles are located at $s = 0, -1$ and -2, while there are no finite open-loop zeros. The pole-zero configuration is shown in Fig. 7.18.

Rule (i) (refer Table 7.1) tells us that the root locus plot consists of three root loci as K is varied from 0 to ∞.

Rule (ii) tells us that the three root loci originate from the three open-loop poles with $K = 0$ and terminate on infinity with $K = \infty$.

Rule (iii) tells us that the three root loci tend to infinity along asymptotes radiating out from

$$s = -\sigma_A = \frac{\sum \text{real parts of poles} - \sum \text{real parts of zeros}}{\text{number of poles} - \text{number of zeros}} = \frac{-2-1}{3} = -1$$

with angles $$\phi_A = \frac{(2q+1)180^\circ}{\text{number of poles} - \text{number of zeros}}; q = 0, 1, \ldots$$

$$= \frac{(2q+1)180°}{3}; q = 0, 1, 2$$

$$= 60°, 180°, 300°$$

The asymptotes are shown by dotted lines in Fig. 7.18.

Rule (iv) tells us that the segments of the real axis between 0 and -1, and between -2 and $-\infty$ lie on the root locus. On-locus segments of the real axis are shown by thick lines in Fig. 7.18.

From Fig. 7.18, it is seen that out of the three loci, one is a real-root locus which originates from $s = -2$ and terminates on $-\infty$. The other two loci originate from $s = 0$ and $s = -1$, and move on the real axis approaching each other as K is increased. These two loci must therefore meet on the real axis. The characteristic equation has a double root at such a point. As the gain K is further increased, the root loci breakaway from the real axis to give a complex conjugate pair of roots.

Rule (v) tells us to check by use of the Routh criterion if the two root loci breaking away from the real axis will intersect the imaginary axis. The system characteristics equation is

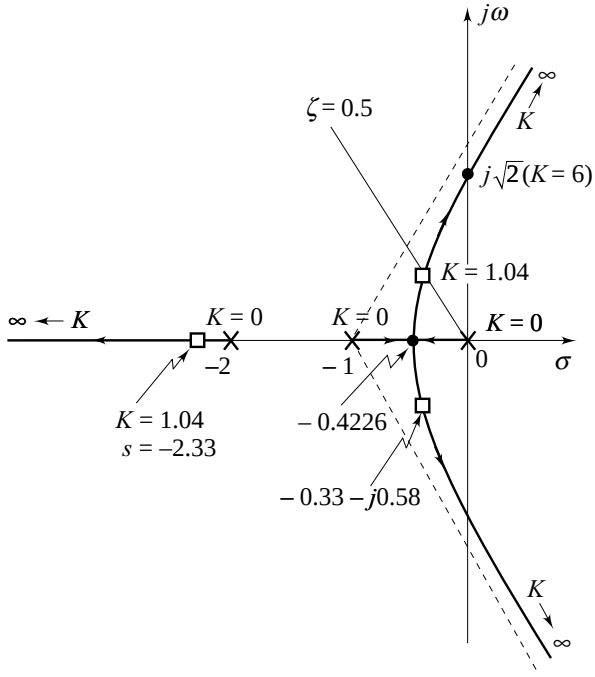

Fig. 7.18 Root locus plot for the characteristic equation (7.38)

$$s(s+1)(s+2) + K = 0$$

or
$$s^3 + 3s^2 + 2s + K = 0$$

The Routh array becomes

s^3	1	2
s^2	3	K
s^1	$(6 - K)/3$	
s^0	K	

For all the roots of the characteristic equation to lie to the left of the imaginary axis, the following conditions must be satisfied:

$$K > 0; (6 - K)/3 > 0$$

Therefore the critical value of K which corresponds to the location of roots on the $j\omega$-axis is 6. This value of K makes all the coefficients of s^1-row of Routh array zero. The auxiliary equation formed from the coefficients of the s^2-row is given by

$$3s^2 + K = 3s^2 + 6 = 0$$

The roots of this equation lie on the $j\omega$-axis and are given by

$$s = \pm j\sqrt{2}$$

Thus the complex-root branches intersect the $j\omega$-axis at $s = \pm j\sqrt{2}$, and the value of K corresponding to these roots is 6.

The characteristic equation under consideration does not require application of rules (vi) and (vii).

Rule (viii) is used below to determine the breakaway points.

From the characteristic equation of the system,

$$K = -s(s+1)(s+2) = -(s^3 + 3s^2 + 2s)$$

Differentiating this equation, we get

$$\frac{dK}{ds} = -(3s^2 + 6s + 2)$$

The roots of the equation $dK/ds = 0$, are $s_{1,2} = -0.4226, -1.5774$

From Fig. 7.18, we see that the breakaway point must lie between 0 and – 1. Therefore $s = -0.4226$ corresponds to the breakaway point. The other solution of the equation $dK/ds = 0$ is $s = -1.5774$. This solution is not on the root locus (it does not satisfy Eqn. (7.38) for any $K \geq 0$) and therefore does not represent a breakaway point. The derivative condition $dK/ds = 0$ is therefore necessary but not sufficient to indicate a breakaway, or multiple-root situation.

If two loci breakaway from a breakaway point, then their tangents will be 180° apart. In general, as we shall see in other illustrative examples, if r loci breakaway from a breakaway point, then their tangents will be $360°/r$ apart, i.e., the tangents will equally divide 360°.

With the information obtained through the use of these rules, the root locus is sketched in Fig. 7.18 from where it is seen that for $K > 6$, the system has two closed-loop poles in the right half of the s-plane and is thus unstable.

It is important to note that the root locus plot given in Fig. 7.18 is only a rough sketch; it gives qualitative information about the behaviour of the closed-loop system when the parameter K is varied. For quantitative analysis, the loci or specific segments of the loci need be constructed with sufficient accuracy.

Suppose it is required to determine dominant closed-loop poles with damping ratio $\zeta = 0.5$. A closed-loop pole with $\zeta = 0.5$ lies on a line passing through the origin and making an angle $\cos^{-1}\zeta = \cos^{-1} 0.5 = 60°$ with the negative real axis. The point of intersection of the ζ-line with the rough sketch of the root locus plot gives the first guess. In the region where the rough root locus sketch intersects the ζ-line, a trial-and-error procedure is adapted along the ζ-line by applying the angle criterion to determine the point of intersection accurately. From Fig. 7.18, we see that the point $-0.33 + j0.58$, which lies on the ζ-line, satisfies the angle criterion. Therefore the dominant closed-loop poles of the system are $s_{1,2} = -0.33 \pm j0.58$.

The value of K that yields these poles is found from the magnitude criterion as follows:

$$\begin{aligned} K &= \{|s|\,|s+1|\,|s+2|\}_{s=-0.33+j0.58} \\ &= \text{Product of the distances from the open-loop poles to the point } -0.33 + j0.58 \\ &= 0.667 \times 0.886 \times 1.768 = 1.04 \end{aligned}$$

The third closed-loop pole will lie on the third locus which is along the negative real axis. We need to guess a test point, compute a trial gain, and correct the guess until we found the point where $K = 1.04$. Using this trial-and-error procedure, we find from Fig. 7.18 that the point $s = -2.33$ corresponds to $K = 1.04$. Therefore, the third closed-loop pole is at $s = -2.33$.

The closed-loop transfer function of the system under consideration is

$$M(s) = \frac{1.04}{(s + 0.33 - j0.58)(s + 0.33 + j0.58)(s + 2.33)}$$

Example 7.4 Consider a feedback system with the characteristic equation

$$1 + \frac{K}{s(s+3)(s^2 + 2s + 2)} = 0;\ K \geq 0 \tag{7.39}$$

The open-loop poles are located at $s = 0, -3, -1 + j1$ and $-1 - j1$, while there are no finite open-loop zeros. The pole-zero configuration is shown in Fig. 7.19.

Rule (i) tells us that the root locus plot consists of four root loci as K is varied from 0 to ∞.

Rule (ii) tells us that the four root loci originate from the four open-loop poles with $K = 0$ and terminate on infinity with $K = \infty$.

Rule (iii) tells us that the four root loci tend to infinity along asymptotes radiating out from

$$s = -\sigma_A = \frac{-3 - 1 - 1}{4} = -1.25$$

with angles

$$\phi_A = \frac{(2q+1)180°}{4}; \; q = 0, 1, 2, 3$$

$$= 45°, 135°, 225°, 315°$$

The asymptotes are shown by dotted lines in Fig. 7.19.

Rule (iv) tells us that root loci exist on the real axis for $-3 \le s \le 0$; shown by thick lines on the real axis in Fig. 7.19.

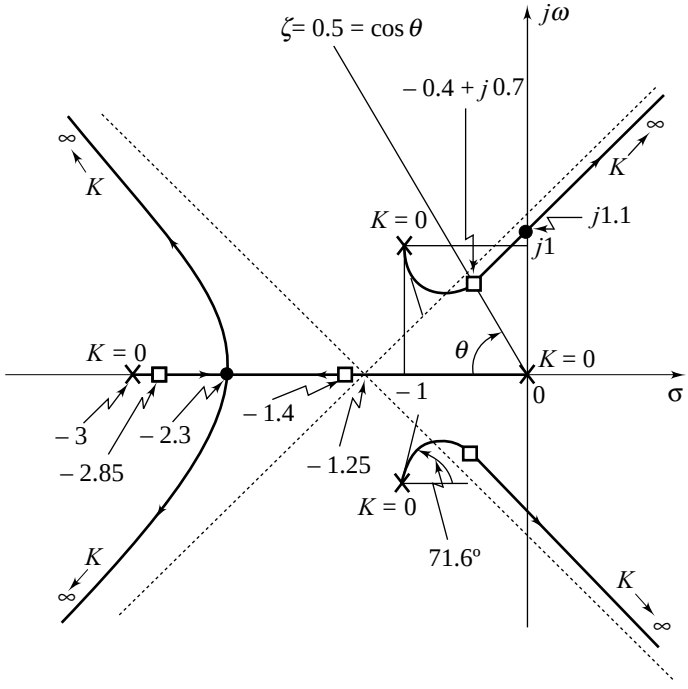

Fig. 7.19 Root locus plot for the characteristic equation (7.39)

Rule (v) tells us to check by use of the Routh criterion if the root loci will intersect the imaginary axis. The system characteristic equation is

$$s(s + 3)(s^2 + 2s + 2) + K = 0$$

or

$$s^4 + 5s^3 + 8s^2 + 6s + K = 0$$

The Routh array becomes

s^4	1	8	K
s^3	5	6	
s^2	34/5	K	
s^1	$\frac{\{(204/5) - 5K\}}{34/5}$		
s^0	K		

Examination of the elements in the first column of the Routh array reveals that the root loci will intersect the imaginary axis at a value of K given by

$$(204/5) - 5K = 0$$

from which $K = 8.16$.

The auxiliary equation, formed from the coefficients of the s^2-row when $K = 8.16$, is

$$(34/5)s^2 + 8.16 = 0$$

from which $s = \pm j1.1$.

Therefore, purely imaginary closed-loop poles of the system are located at $s = \pm j1.1$ as shown in Fig. 7.19; the value of K corresponding to these poles is 8.16.

Rule (vi) tells us that a root locus leaves the pole at $s = -1 + j1$ at angle ϕ_p, given by (refer Fig. 7.19)

$$\phi_p = 180° + [-135° - 90° - 26.6°] = -71.6°$$

The characteristic equation under consideration does not require application of rule (vii).

Rule (viii) is used below to determine the breakaway points.

From the characteristic equation of the system,

$$K = -s(s + 3)(s^2 + 2s + 2) = -(s^4 + 5s^3 + 8s^2 + 6s)$$

Differentiating this equation, we get

$$\frac{dK}{ds} = -4(s^3 + 3.75s^2 + 4s + 1.5)$$

The solutions to the cubic

$$s^3 + 3.75s^2 + 4s + 1.5 = 0 \tag{7.40}$$

are the possible breakaway points.

From Fig. 7.19, we see that a breakaway point must lie between 0 and -3 on the real axis. By trial-and-error procedure, we find that $s = -2.3$ satisfies Eqn. (7.40) to a reasonable accuracy. The CAD software (MATLAB, for example) may be used to obtain the plot whenever the problem becomes a little complex. Experience of hand-sketching will be helpful in interpreting the CAD results. The other two solutions of Eqn. (7.40) are $s_{1,2} = -0.725 \pm j0.365$.

It can easily be checked that $-0.725 \pm j0.365$ are not the root locus points as the angle criterion is not met at these points.

The root locus plot, therefore, has only one breakaway point at $s = -2.3$. Tangents to the two loci breaking away from this point will be 180° part.

With the information obtained through the use of these rules, the root locus plot is sketched in Fig. 7.19 from where it is seen that for $K > 8.16$, the system has two closed-loop poles in the right half of s-plane and is thus unstable.

Dominant roots of the characteristic equation with damping $\zeta = 0.5$ are determined as follows. A ζ-line is drawn in the second quadrant at an angle of $\theta = \cos^{-1}0.5 = 60°$ with the negative real axis. By trial-and-error procedure, it is found that the point $s = -0.4 + j0.7$ which lies on the ζ-line, satisfies the angle criterion. Therefore the dominant roots of the characteristic equation are $s_{1,2} = -0.4 \pm j0.7$. The value of gain K at the dominant root is

$$K = \text{Product of distances from open-loop poles to the point } -0.4 + j0.7$$
$$= 0.84 \times 1.86 \times 2.74 \times 0.68 = 2.91$$

The other two roots of the characteristic equation are obtained from the loci originating from the poles at $s = 0$ and $s = -3$. From Fig. 7.19, it is seen that at the double-root location $s = -2.3$, the value of K is 4.33:

$$K = \{|s||s+3|\,|s+1+j1|\,|s+1-j1|\}_{s=-2.3}$$
$$= 2.3 \times 0.7 \times 1.64 \times 1.64 = 4.33$$

Therefore, the points corresponding to $K = 2.91$ must lie on the real-root segments of these loci. Using the trial-and-error procedure, it is found that the points $s = -1.4$ and $s = -2.85$ have gain $K = 2.91$. Thus the closed-loop transfer function of the system under consideration is

$$M(s) = \frac{2.91}{(s+0.4+j0.7)(s+0.4-j0.7)(s+1.4)(s+2.85)}$$

Example 7.5 In this example, we illustrate multiple roots of multiplicity more than two. Consider the root locus of $1 + F(s)$,

where $$F(s) = \frac{K(s+1)}{s^2(s+9)};\ K \geq 0$$

The pole-zero configuration is shown in Fig. 7.20.

Rule (i) tells us that the root locus plot consists of three root loci as K is varied from 0 to ∞.

Rule (ii) tells us that the three root loci originate from open-loop poles with $K = 0$; one of these terminates on the zero at $s = -1$ with $K = \infty$, and the other two terminate on infinity with $K = \infty$.

Rule (iii) tells us that the two root loci tend to infinity along asymptotes radiating out from

$$s = -\sigma_A = \frac{-9-0-(-1)}{3-1} = -4$$

with angles

$$\phi_A = \frac{(2q+1)180°}{3-1};\ q = 0, 1 = 90°, 270°$$

The asymptotes are shown by dotted lines in Fig. 7.20.

Rule (iv) tells us that root loci exist on the real axis for $-9 \leq s \leq -1$; shown by thick lines on the real axis in Fig. 7.20.

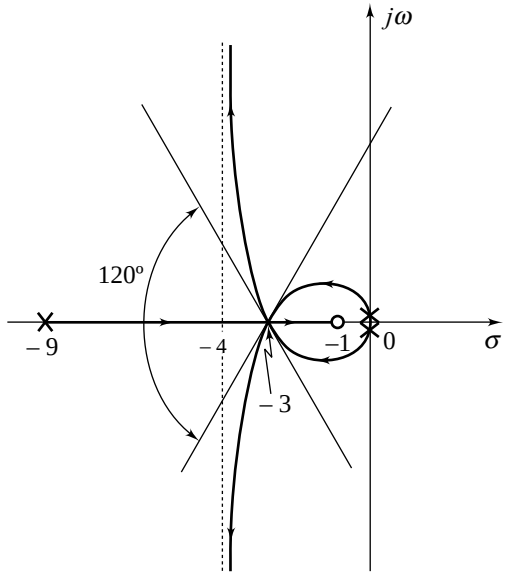

Fig. 7.20 Root locus plot (Example 7.5)

Rule (v) tells us to check by use of the Routh criterion if the root loci will intersect the imaginary axis. It is found that the root loci do not cross the imaginary axis.

The characteristic equation under consideration does not require application of rules (vi) and (vii).

Rule (viii) is used below to determine the breakaway points.

From the characteristic equation of the system,

$$K = -\frac{s^2(s+9)}{s+1} = -\frac{s^3+9s^2}{s+1}$$

Differentiating this equation, we get

$$\frac{dK}{ds} = \frac{\left(s^3+9s^2\right)-(s+1)\left(3s^2+18s\right)}{(s+1)^2}$$

$$= \frac{-2s(s+3)^2}{(s+1)^2}$$

Possible points of multiple roots are at $s = 0, -3, -3$, which are on the locus as seen in Fig. 7.20.

One feature of the breakaway point at $s = -3$ needs special attention. At $s = -3$, we have double root in the derivative dK/ds; which means that not only $dK/ds = 0$ at this point but d^2K/ds^2 is also zero. This equivalently means that (refer Eqns (7.36)) $d^2F(s)/ds^2 = 0$ at $s = -3$ which is possible only if $1 + F(s)$ has a root of multiplicity three at $s = -3$ (refer Eqn. (7.34)). Therefore the characteristic equation has three roots at $s = -3$; the three loci originating from the open-loop poles will approach this point and then break away. Tangents to the three loci breaking away from $s = -3$ will be $360°/3 = 120°$ apart.

Tangents to the two loci originating from $s = 0$ will be 180° apart.

With the information obtained through the use of these rules, the root locus is sketched in Fig. 7.20. (The specific examples discussed in this section, serve the objective of explaining various features of root locus plots. If a problem becomes too complex for hand-sketching, the help of CAD tools (MATLAB, for example) may be taken).

Example 7.6 In this example, we illustrate multiple roots off the real axis. Consider the root locus of $1 + F(s)$,

where $$F(s) = \frac{K}{s(s+2)\left(s^2+2s+5\right)}; \; K \geq 0$$

The pole-zero configuration is shown in Fig. 7.21.

Rule (i) tells us that the root locus plot consists of four root loci as K is varied from 0 to ∞.

Rule (ii) tells us that the four loci originate from open-loop poles with $K = 0$ and terminate on infinity with $K = \infty$.

Rule (iii) tells us that the four loci tend to infinity along asymptotes radiating out from

$$s = -\sigma_A = \frac{-1-1-2}{4} = -1$$

with angles $$\phi_A = \frac{(2q+1)180°}{4}; \; q = 0, 1, 2, 3$$

$$= 45°, 135°, 225°, 315°$$

The asymptotes are shown by dotted lines in Fig. 7.21.

Rule (iv) tells us that root loci exist on the real axis for $-2 \le s \le 0$; shown by thick line on the real axis in Fig. 7.21.

Rule (v) tells us to check, by using the Routh criterion, if the root loci will intersect the imaginary axis.

The characteristic equation is

$$s(s+2)(s^2+2s+5)+K=0$$

or $$s^4+4s^3+9s^2+10s+K=0$$

The Routh array becomes

s^4	1	9	K
s^3	4	10	
s^2	26/4	K	
s^1	$\dfrac{\{(260/4)-4K\}}{26/4}$		
s^0	K		

Examination of the elements in the first column of the Routh array reveals that the root loci will intersect the imaginary axis at a value of K given by

$$(260/4)-4K=0$$

from which $K = 16.25$.

The auxiliary equation formed from the elements of s^2-row when $K = 16.25$, is

$$(26/4)s^2+16.25=0$$

from which $$s=\pm j1.58.$$

Therefore the root loci cross the imaginary axis at $s = \pm j1.58$; the value of K corresponding to these roots is 16.25.

Rule (vi) tells us that a root locus leaves the pole at $s = -1 + j2$ at angle ϕ_p, given by (refer Fig. 7.21)

$$\phi_p = 180° + [-116.6° - 90° - 63.4°] = -90°$$

In fact, we can observe at once that along the line $s = -1 + j\omega$, the angles contributed by the poles at $s = 0$ and $s = -2$ always add to 180°, and the angles contributed by the poles at $s = -1 + j2$ and $s = -1 - j2$ are respectively, $-90°$ and 90°; so the entire line from one complex pole to the other is on the locus *in this special case*.

The characteristic equation under consideration does not require application of rule (vii).

Rule (viii) is used below to determine the breakaway points.

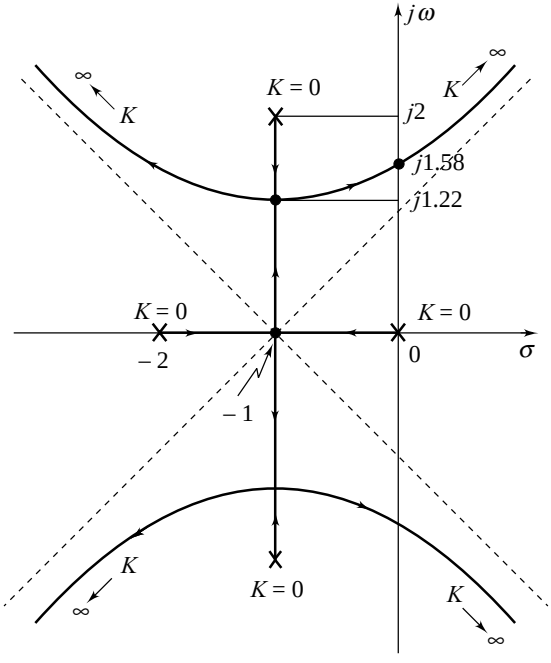

Fig. 7.21 Root locus plot (Example 7.6)

From the characteristic equation of the system,

$$K = -s(s+2)(s^2+2s+5) = -(s^4+4s^3+9s^2+10s)$$

Differentiating this equation, we get

$$\frac{dK}{ds} = -4(s^3+3s^2+4.5s+2.5)$$

We could find solutions to the cubic

$$s^3+3s^2+4.5s+2.5=0,$$

but from the application of rule (vi) we know that the entire line $s=-1+j\omega$ is on the locus; so there must be a breakaway at $s=-1$. Therefore $(s+1)$ is one of the factors of the cubic. We can now easily show that

$$(s^3+3s^2+4.5s+2.5) = (s+1)(s+1+j1.22)(s+1-j1.22)$$

Since the solutions $-1 \pm j1.22$ are on the line between the complex poles, they are true points of multiple roots on the locus.

The complete root locus plot is sketched in Fig. 7.21. Notice that here we have complex multiple roots of multiplicity 2. Segments of the root loci come together at $-1 \pm j1.22$ and break away; tangents to the loci breaking away will be 180° apart.

7.5 RESHAPING THE ROOT LOCUS

A simple control-system configuration of Fig. 7.22 is created by providing feedback around the plant $G_p(s)$ and adding an error signal amplifier with gain K_c. The amplifier gain is adjusted to provide acceptable performance, if possible. The system of Fig. 7.22 is often referred to as having *proportional compensation.*

If the plant dynamics are of such a nature that a satisfactory design *cannot* be obtained by a gain adjustment alone, some dynamic compensation for the plant dynamics is required. A simple control-system configuration that includes dynamic compensation is shown in Fig. 7.23; the compensator $D_c(s)$ is placed in cascade with the forward-path transfer function $G_p(s)$. The system of Fig. 7.23 is often referred to as having *cascade compensation.*[4]

The dynamic compensator will generally also have a gain K that has to be adjusted to improve steady-state accuracy, i.e., the transfer function $D_c(s)$ is typically of the form

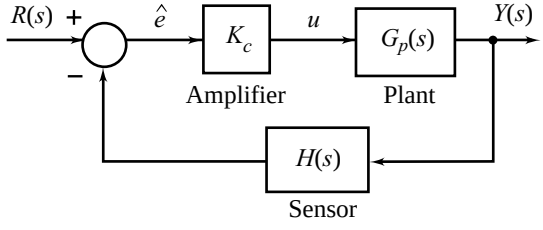

Fig. 7.22 A simple control system configuration

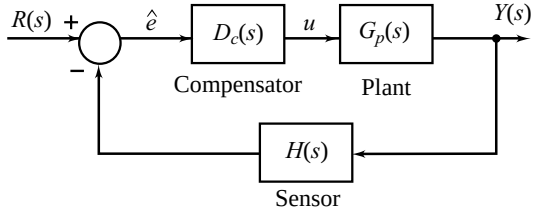

Fig. 7.23 A control system with dynamic compensation

[4]The term 'cascade compensation' used in Chapters 7–10 refers to the use of compensator (controller) in cascade (series) with the forward-path transfer function. It may be pointed out here that in process control field, the term 'cascade control' is frequently used for feedback configurations having 'loop within a loop'.

$$D_c(s) = \frac{K\prod_{i=1}^{m}(s+z_i)}{\prod_{j=1}^{n}(s+p_j)} \quad (7.41a)$$

$$= KD(s) \quad (7.41b)$$

For the purpose of simplifying the design procedure, we normally associate the adjustable gain parameter K with the plant transfer function and then design the dynamic compensator $D(s)$ given by Eqns (7.41) based on the new plant transfer function $KG_p(s)$. At the implementation stage, the gain K is associated with the compensator and the transfer function $D_c(s)$ is realized.

The configuration of Fig. 7.24a will accordingly be referred to as the *uncompensated system* and that of Fig. 7.24b as *compensated system.*

We introduce root-locus design through selected design problems.

7.5.1 Design Problem 1

Consider the system of Fig. 7.25 which has an open-loop transfer function

$$G(s) = \frac{K_A}{s(s+1)\left(\frac{1}{5}s+1\right)} \quad (7.42)$$

From Eqn. (7.42), we have

$$G(s) = \frac{5K_A}{s(s+1)(s+5)} = \frac{K}{s(s+1)(s+5)} \quad (7.43)$$

The root locus plot of the uncompensated system appears in Fig. 7.26.

Assume that the relative stability specification calls for a damping ratio $\zeta = 0.45$ (peak overshoot $\cong$ 20%). The ζ-line intersects the root locus at $s = -0.404 + j0.802$. For the dominant root pair, the undamped natural frequency ω_n is 0.898 rad/sec. The settling time ($= 4/\zeta\omega_n$) for the response is about 9.9 sec. The uncompensated system, therefore, has sluggish transient response.

In order to improve the speed of response, the root locus must be reshaped so that it is moved farther to the left, away from the imaginary axis. To accomplish this goal, let us consider the proposition of adding a

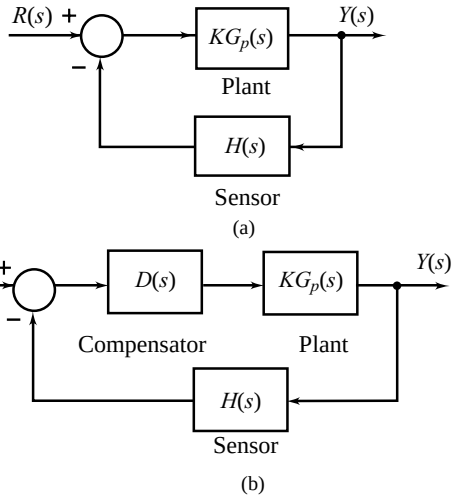

Fig. 7.24 (a) Uncompensated system (b) Compensated system

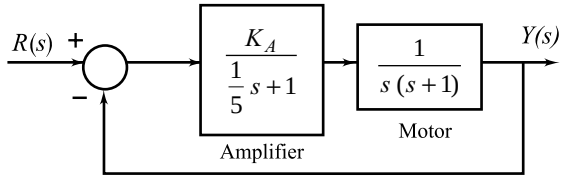

Fig. 7.25 A position control system

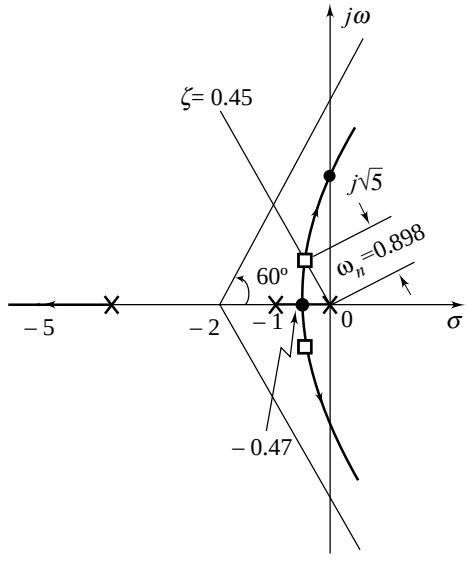

Fig. 7.26 Root locus plot of $1 + \frac{K}{s(s+1)(s+5)}$

compensating zero. Fig. 7.27 shows the root locus plot of the system with the compensating zero placed at $s = -1.5$. Notice that the effect of the zero is to move the locus to the left, toward the more stable part of the plane. The ζ (= 0.45) line intersects the root locus at $-2.2 + j4.3$. For the dominant root pair, the undamped natural frequency ω_n is 4.85 rad/sec. The settling time for the response is therefore about 1.7 sec. Thus, the addition of a compensating zero helps to improve the speed of response for $\zeta = 0.45$.

A further observation about the effect of adding a compensating zero is made from Figs 7.26 and 7.27. Without the compensating zero, the real root in addition to the dominant complex-root pair is always located to the left of the open-loop pole at $s = -5$. On the other hand, in the presence of compensating zero, this root moves over to the right of $s = -5$ and the dominance condition is therefore weakened. Since the real root (which is the closed-loop pole) will be located close to the compensating zero, the amplitude of the response term due to this root will be small. Also, the time-constant of the real root will be comparable to that of complex dominant root-pair; therefore, its effect on settling time may be tolerable.

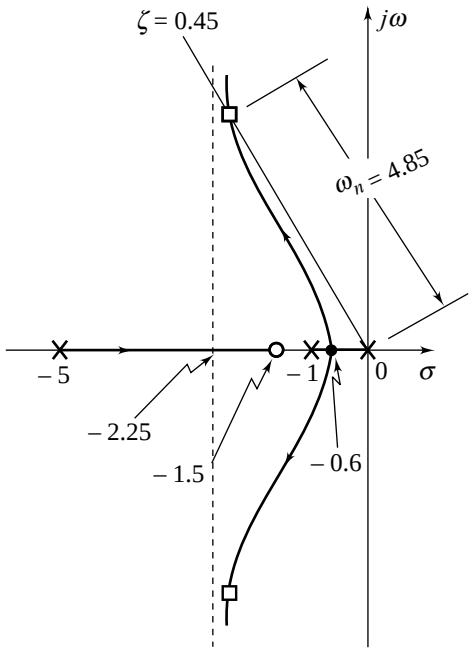

Fig. 7.27 Root locus plot of $1 + \dfrac{K(s+1.5)}{s(s+1)(s+5)}$

An acceptable transient response can generally be obtained by trial-and-error adjustments of the compensating zero on the real axis. It can easily be verified that if we place the compensating zero too far to the left (say, near the open-loop pole at $s = -5$), the dominance condition is improved but complex branches of the root locus are pressed toward the right and the dynamic response becomes poor. If, on the other hand, the zero is placed close to the origin (say, to the right of the open-loop pole at $s = -1$), the complex branches are advantageously far into the left, but a real root close to the origin appears. This root will also be close to the compensating zero; therefore amplitude of the response term due to this root may be small. However, since the real root will have a large time-constant compared to that of dominant complex root pair, its effect on settling time may be appreciable.

No general rule can be laid down for selecting the location of compensating zero that satisfactorily meets all the design requirements. Trial-and-error procedure is the best tool in hand. However, the following *guidelines* can be of considerable help.

Place the compensating zero on the real axis in the region below the desired closed-loop pole location such that it lies close to the left of any open-loop pole in this region. This technique ensures that the closed-loop pole on the real axis caused by the introduction of the compensating zero will be located close to it with a time-constant comparable to that of desired dominant closed-loop pole-pair, and would therefore make a negligible contribution to system dynamics. In case the uncompensated system does not have any open-loop pole in the region below the desired closed-loop poles, the dominance condition must be checked by locating the real-axis closed-loop pole created by the compensating zero.

The addition of a zero in the open-loop transfer function can be achieved by placing a compensator

$$D(s) = s + z = s + 1/\tau \tag{7.44a}$$

in cascade with the forward-path transfer function. This results in (refer Fig.7.23)

$$D_c(s) = K(s + 1/\tau) \tag{7.44b}$$

It is seen that $D_c(s)$ given by Eqn. (7.44b) is a *proportional plus derivative (PD) controller:*

$$D_c(s) = \frac{K}{\tau}(1 + \tau s) = K_c(1 + T_D S)$$

$$= \frac{K}{\tau} + Ks = K_P + K_D s$$

An op amp circuit realization of this controller is of the form shown in Fig.7.28 (refer Fig. P2.17 for circuit details).

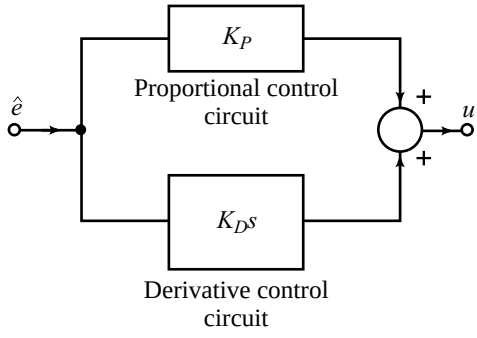

Fig.7.28 A physical realization of PD controller

The problem with PD compensation is that the inevitable high-frequency noise present at the input to the $D_c(s)$ will be greatly amplified. The usual method for overcoming this problem is to add a pole to the compensator transfer function which limits the high-frequency gain. The pole must of course be added such that it has relatively negligible effect on the root locus in the region where the two dominant closed-loop poles are to occur.

Figure 7.29 shows the root locus plot in the presence of both a compensating zero and a pole. The root locus near the dominant closed-loop poles gets somewhat modified by the presence of the compensating pole. The effect on the transient response of the system is not very pronounced. The ζ (= 0.45) line intersects the root locus at $s = -1.531 + j3.039$. For the dominant root-pair, the undamped natural frequency ω_n is 3.4 rad sec. The settling time for the response is about 2.6 sec.

As can be easily seen from Figs 7.27 and 7.29, the effect of the compensator pole is to press the locus toward the right. However, if the pole is added far away from the $j\omega$-axis, it has relatively negligible effect on the root locus in the region where the two dominant closed-loop poles are to occur.

The choice of the compensator pole location is a compromise between the conflicting effects of noise suppression and compensator effectiveness. In general, if the pole is too close to the zero, then the root locus moves back too far toward its uncompensated shape, and the zero is not successful in doing its job. On the

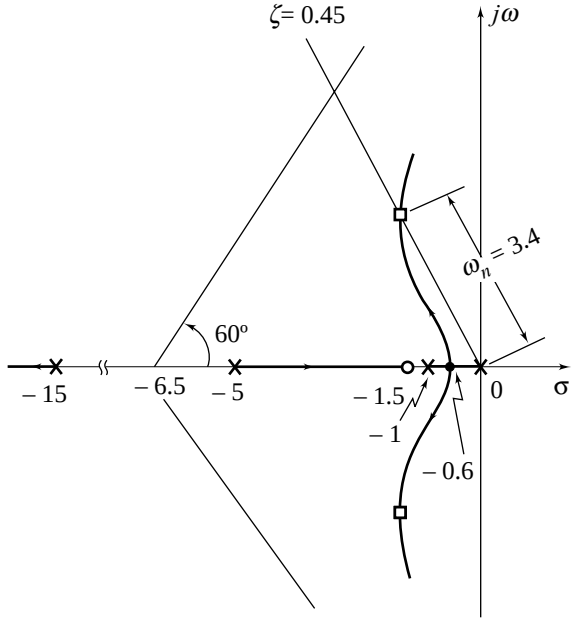

Fig. 7.29 Root locus plot of $1 + \dfrac{K(s+1.5)}{s(s+1)(s+5)(s+15)}$

other hand, if the pole is too far to the left, the magnification of noise at the output of $D(s)$ is too great and the motor or other actuator of the process will be overheated by noise energy. In many cases, a pole located at a distance from 3 to 10 times the value of the zero location resolves the conflict.

We see from the above discussion that the compensating pole must be located to the left of the compensating zero; both the pole and the zero confined to the left half of the s-plane. The transfer function of such a first-order compensator then becomes

$$D(s) = \frac{s+z}{s+p} = \frac{s+1/\tau}{s+1/\alpha\tau}\,;\ \alpha = \frac{z}{p} < 1,\ \tau > 0 \tag{7.45a}$$

Note that $\alpha < 1$ ensures that the pole is located to the left of the zero. The contribution of $D(s)$ to the angle criterion of the root locus is always positive. This type of compensator is called *lead compensator*. The name 'lead compensator' has a clearer meaning with respect to frequency-domain design, which is covered later in Chapter 10.

The compensator (7.45a) results in (refer Fig.7.23)

$$D_c(s) = K\left(\frac{s+1/\tau}{s+1/\alpha\tau}\right);\ \alpha < 1,\ \tau > 0 \tag{7.45b}$$

It is seen that $D_c(s)$ given by Eqn.(7.45b) is a form of *proportional plus derivative controller wherein the derivative action is bandwidth limited*.

$$D_c(s) = K\alpha + \frac{K\alpha\tau(1-\alpha)s}{\alpha\tau s+1}$$

$$= K_P + \frac{K_D s}{\tau_D s+1}$$

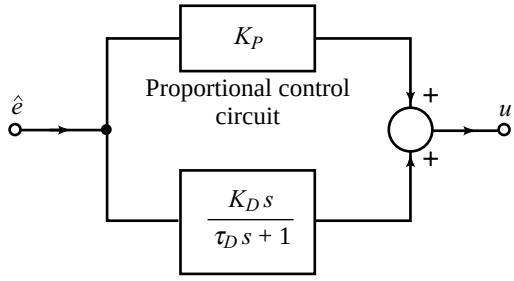

Fig. 7.30 A physical realization of lead compensator

An op amp realization of this controller is of the form shown in Fig.7.30 (refer Fig. P2.20 for circuit details).

The following is the summary of the results obtained for uncompensated and compensated systems.

The system of Fig. 7.25 has an open-loop transfer function

$$G(s) = \frac{K}{s(s+1)(s+5)}$$

The root locus plot of this uncompensated system is shown in Fig. 7.26. A damping ratio $\zeta = 0.45$ yields the following pertinent data.

Dominant roots: $s_{1,2} = -0.404 \pm j0.802$

Root locus gain at s_1: $K = |s_1|\,|s_1 + 1|\,|s_1 + 5| = 4.188$

Velocity error constant: $K_v = \lim_{s\to 0} sG(s) = \frac{K}{5} = 0.838$

Undamped natural frequency: $\omega_n = 0.898$ rad/sec

Settling time $(= 4/\zeta\omega_n)$: $t_s = 9.9$ sec

Figure 7.29 is the root locus of lead-compensated system with open-loop transfer function

$$D(s)G(s) = \frac{K(s+1.5)}{s(s+1)(s+5)(s+15)}$$

A damping ratio $\zeta = 0.45$ yields the following pertinent data.

Dominant roots: $s_{1,2} = -1.531 \pm j3.039$

Root locus gain at s_1: $K = \dfrac{|s_1||s_1+1||s_1+5||s_1+15|}{|s_1+1.5|} = 220$

Velocity error constant: $K_v = \lim\limits_{s\to 0} sD(s)G(s) = \dfrac{K(1.5)}{5\times 15} = 4.4$

Undamped natural frequency: $\omega_n = 3.4$ rad/sec

Settling time: $t_s = 2.6$ sec

The positive angle contributed by the lead compensator shifts the root locus towards the left in the s-plane; this results in improvement in the dynamic response of the system. The lead compensator also helps to increase system error constant, though to a limited extent.

7.5.2 Design Problem 2

Consider the system of Fig. 7.25 which has an open-loop transfer function

$$G(s) = \frac{5K_A}{s(s+1)(s+5)} = \frac{K}{s(s+1)(s+5)} \tag{7.46}$$

The root locus plot of the uncompensated system appears in Fig. 7.26. Suppose that the relative stability specification calls for a damping ratio $\zeta = 0.45$. The ζ-line intersects the root locus at $s = -0.404 + j0.802$ for a value of $K = 4.188$. Therefore, the undamped natural frequency ω_n of the closed-loop system is 0.898 rad/sec, and the settling time ($= 4/\zeta\omega_n$) for the response is 9.9 sec. We assume that the dynamic response of the uncompensated system with $K = 4.188$ is satisfactory.

For the uncompensated system with $K = 4.188$, the velocity error constant is

$$K_v = \lim_{s\to 0} sG(s) = \lim_{s\to 0} s\left\{\frac{K}{s(s+1)(s+5)}\right\} = \frac{K}{5} = 0.898$$

and thus with a unit-ramp input (1 rad/sec), the steady-state error

$$e_{ss} = \frac{1}{K_v} = 1.114 \text{ rad}$$

which is too large. It is therefore required to raise the system K_v. To accomplish this, consider the proposition of adding a *proportional plus integral (PI) controller* in cascade with the plant transfer function in the forward path. A PI controller has transfer function of the form

$$D_c(s) = K_c\left(1 + \frac{1}{T_I s}\right) = K_c\left(\frac{s+1/T_I}{s}\right) = K_c\frac{(s+z)}{s} \tag{7.47}$$

The PI controller, thus, adds a pole at $s = 0$ and a zero at $s = -z$ to the open-loop transfer function. System type increases by one because of the added open-loop pole at the origin. Hence, for stable design, the corresponding error constant is infinity and steady-state error is zero.

An op amp circuit realization of the PI controller given by Eqn. (7.47) is of the form shown in Fig. 7.31 (refer Fig. P2.18 for circuit details).

Let us now investigate the effects of the pole-zero pair of the PI controller on transient response of the system. It can easily be verified that the pole alone would move the root locus to the right, thereby making the system unstable. The zero must be near the pole in order to minimize the effect on the transient response. Fig. 7.32 shows the root locus plot of the system with the compensating zero placed at $s = -0.01$; the compensating pole being at the origin. Notice that the angle contribution of the compensating pole-zero pair at the desired closed-loop pole $-0.404 \pm j0.802$ is negligibly small, and therefore the root locus in the vicinity of this point is not appreciably disturbed.

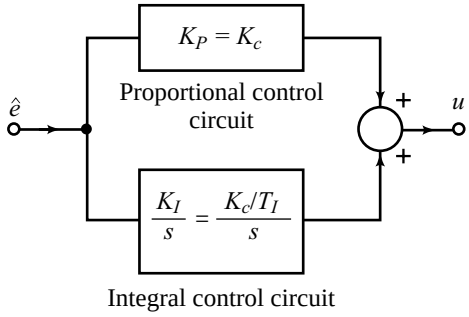

Fig. 7.31 A physical realization of PI controller

A further observation about the effect of adding pole-zero pair is made from Figs 7.26 and 7.32. Without the compensating pole-zero pair, the root locus has a real root in addition to the desired dominant complex root-pair $-0.404 \pm j0.802$. The real root is always located to the left of the open-loop pole at $s = -5$, and therefore its effect on transient response of the system will be negligible. On the other hand, in the presence of compensating pole-zero pair, there are two real roots in addition to the desired complex root-pair; one to the left of open-loop pole at $s = -5$ and the other on the real-axis segment between -0.02 and -0.01. The additional real root contributed by the compensating pole-zero pair is too close to the origin and therefore will have a very large time-constant, affecting the settling time appreciably. There is, however, a zero very close to this real root, and therefore the magnitude of the response term contributed by this root will be negligibly small. The closed-loop pole-zero *dipole* introduced by PI controller will not contribute significantly to the response of the closed-loop system.

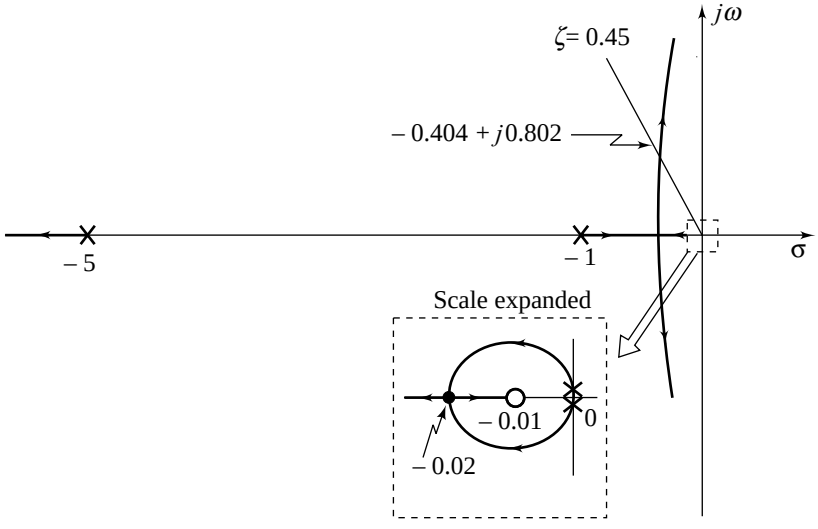

Fig. 7.32 Root locus plot of $1 + \frac{K(s+0.01)}{s^2(s+1)(s+5)}$

It is desirable to place the compensating pole-zero combination as far to the left as possible without causing major shifts in the dominant root locations and giving required improvement in the steady-state response. The compensating pole-zero pair near the origin (the pole not necessarily at the origin) will give rise to a closed-loop pole-zero dipole shifted relatively to the left compared to the case of PI controller; therefore, the time-constant of the additional root will be relatively less, resulting in a smaller effect on the settling time of the system. In system response, a long tail of small amplitude introduced by closed-loop dipole will decay relatively faster (refer Example 7.10 for more details).

It can easily be verified that if the compensating pole-zero pair is placed too far to the left (say, on the real-axis segment to the left of desired dominant complex closed-loop poles), no significant improvement in the steady-state response is possible.

Figure 7.33 shows the root locus plot in the presence of compensating pole at $s = -0.005$ and the compensating zero at $s = -0.05$. The angle contributed by the compensator pole-zero pair at $s = -0.404 + j0.802$, the desired dominant root, is about 2.6° and is therefore acceptable. For the damping ratio $\zeta = 0.45$, the new locus is close to the locus of uncompensated system. The new dominant roots are $s_{1,2} = -0.384 \pm j0.763$; thus the roots are essentially unchanged.

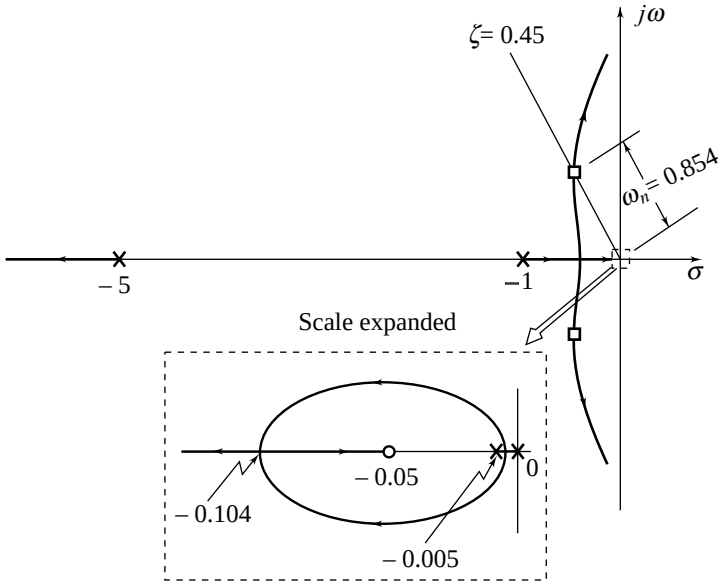

Fig. 7.33 Root locus plot of $1 + \dfrac{K(s+0.05)}{s(s+0.005)(s+1)(s+5)}$

For the compensated system adjusted to a damping ratio of 0.45, the following results are obtained.

Dominant roots: $s_{1,2} = -0.384 \pm j0.763$

Root locus gain at s_1: $$K = \frac{|s_1||s_1+1||s_1+5||s_1+0.005|}{|s_1+0.05|} = 4.01$$

Velocity error constant: $$K_v = \lim_{s\to 0} s\left\{\frac{K(s+0.05)}{s(s+1)(s+5)(s+0.005)}\right\}$$

$$= \frac{K(0.05)}{5 \times 0.005} = 8.02$$

Undamped natural frequency: $\omega_n = 0.854$ rad/sec.

A comparison of the uncompensated system and the compensated system shows that the undamped natural frequency has decreased slightly from 0.898 to 0.854 rad/sec, but there is considerable increase in velocity error constant: from 0.838 to 8.02. This increase in K_v is in fact, approximately equal to $|z|/|p|$ where $s = -z$ is the location of the compensating zero and $s = -p$ is the location of the compensating pole.

We see from the above discussion that the compensating zero must be located to the left of the compensating pole; both the zero and the pole confined to the left half of the s-plane. The transfer function of such a first-order compensator then becomes

$$D(s) = \frac{s+z}{s+p} = \frac{s+1/\tau}{s+1/\beta\tau}; \beta = \frac{z}{p} > 1, \tau > 0 \qquad (7.48a)$$

Note that $\beta > 1$ ensures that the pole is located to the right of the zero, i.e., nearer the origin than the zero. The contribution of $D(s)$ to the angle criterion of the root locus is always negative. This type of compensator is called *lag compensator*. The name 'lag compensator' has a clearer meaning with respect to frequency-domain design, which is covered later in Chapter 10.

The compensator (7.48a) results in (refer Fig.7.23)

$$D_c(s) = K\left(\frac{s+1/\tau}{s+1/\beta\tau}\right); \beta > 1, \tau > 0 \qquad (7.48b)$$

It is seen that $D_c(s)$ given by Eqn.(7.48b) is a form of *proportional plus integral controller wherein the integral action is low-frequency gain limited* :

$$D_c(s) = K + \frac{K(\beta-1)}{\beta\tau s+1}$$

$$= K_P + \frac{K_I}{\tau_I s+1}$$

An op amp realization of the controller is of the form shown in Fig.7.34 (refer Fig. P2.21 for circuit details).

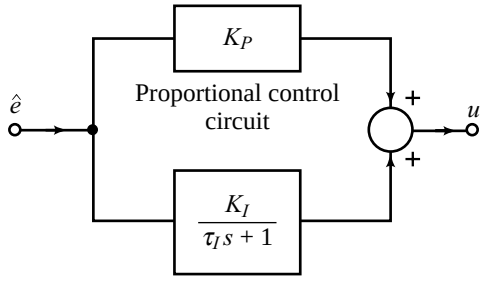

Fig. 7.34 A physical realization of lag compensator

7.5.3 Concluding Comments

The purpose of reshaping the root locus generally falls into one of the following categories.

1. A given system is stable and its transient response is satisfactory, but its steady-state error is too large. Thus, the corresponding error constant must be increased while nearly preserving the transient response. This can be achieved by a cascade PI/lag compensator.
2. A given system is stable, but its transient response is unsatisfactory. Thus the root locus must be reshaped so that it is moved farther to the left, away from the imaginary axis. This can be achieved by a cascade PD/lead compensator.

3. A PD/lead-compensated system has satisfactory transient response but its steady-state error is too large. The steady-state error can be decreased by cascading a PI/lag compensator to the PD/lead-compensated system. This is equivalent to using a second-order compensator.

Consider first the cascade of PI and PD compensators :

$$D_c(s) = \left(K_1 + \frac{K_i}{s}\right)(K_2 + K_d s)$$

$$= K_1K_2 + K_iK_d + \frac{K_1K_i}{s} + K_2K_d s$$

$$= K_P + \frac{K_I}{s} + K_D s$$

Thus c*ascading a PI compensator with a PD compensator is completely equivalent to a PID compensator*; an op amp realization of this compensator is of the form shown in Fig.7.35 (refer Fig. P2.19 for circuit details). Consider now the cascade of lag and lead compensators :

$$D_c(s) = K\left(\frac{s+1/\tau_2}{s+1/\beta\tau_2}\right)\left(\frac{s+1/\tau_1}{s+1/\alpha\tau_1}\right); \beta > 1, \alpha < 1, \tau_2 > 0, \tau_1 > 0$$

This is a second-order compensator, called the *lag-lead* compensator.

Expressed explicitly in the form of proportional, integral, and derivative control actions, $D_c(s)$ looks like

$$D_c(s) = \left(K_{P1} + \frac{K_I}{\tau_I s + 1}\right)\left(K_{P2} + \frac{K_D s}{\tau_D s + 1}\right)$$

An op amp realization of this $D_c(s)$ is obtained by *cascading* a (low frequency) *gain-limited PI compensator with a bandwidth-limited PD compensator* (refer Fig. P2.22 for circuit details).

In the next three sections, we will focus on the design procedures for lag, lead, and lag-lead compensators. The design of PI, PD and PID compensators follows from these procedures in a straight forward way. Placing the pole of the compensator at the origin gives us a PI compensator (A PI compensator is recommended for a system if compensator pole at the origin does not degrade closed-loop stability appreciably). Placing the pole of a lead compensator at – ∞ (equivalently, designing a lead compensator by appropriately placing a zero only) gives us a PD compensator (A PD compensator is recommended if the feedback loop is free from high-frequency noise problems. This is unlikely in real-life applications). An example of PID compensation will be given later in Section 7.9.

The systems, which are type-2 or higher, are usually absolutely unstable. For these types of systems, clearly PD/lead compensators are required, as only a PD/lead compensator increases the margin of stability. In type-1 and type-0 systems, stable operation is always possible if the gain is sufficiently reduced. In such cases, any of the three compensators, namely, PI/lag, PD/lead, or PID/lag-lead, may be used to obtain the desired performance. The particular choice is based upon transient and steady-state response characteristics of uncompensated system.

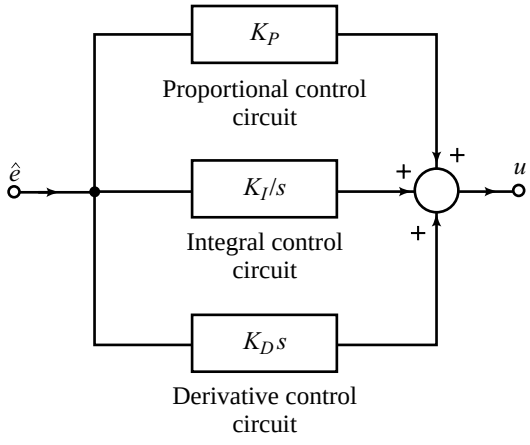

Fig. 7.35 A physical realization of PID controller

7.6 CASCADE LEAD COMPENSATION

As has been pointed out in the previous section, lead compensation generally is used to improve the transient response of a system. In this section, we consider how the root locus may be used to design a compensator so as to realize a desired improvement in transient response.

Consider a unity-feedback system with a forward-path transfer function $G(s)$. The transfer function $G(s)$ is assumed to be unalterable except for the adjustment of gain. Let the system dynamic response specifications be translated into the desired location s_d for the dominant complex closed-loop poles as shown in Fig. 7.36.

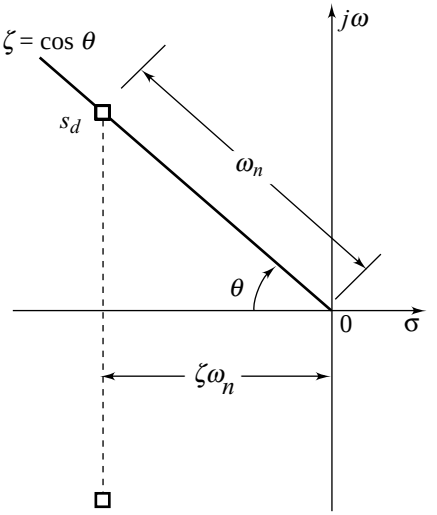

Fig. 7.36 Desired dominant closed-loop poles

If the angle criterion at s_d is not met, i.e., $\angle G(s_d) \neq \pm 180°$, the uncompensated root locus with variable open-loop gain will not pass through the desired root location, indicating the need for compensation. Let us introduce a first-order lead compensator with zero and pole in the left half of the complex plane:

$$D(s) = \frac{s+z}{s+p} = \frac{s+1/\tau}{s+1/\alpha\tau}\,;\ \alpha = \frac{z}{p} < 1,\ \tau > 0 \qquad (7.49)$$

in cascade with the forward-path transfer function $G(s)$ as shown in Fig. 7.37.

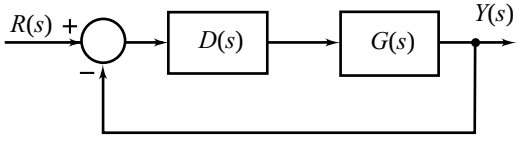

Fig. 7.37 A feedback system with cascade compensator

The compensator $D(s)$ has to be so designed that the compensated root locus passes through s_d. In terms of the angle criterion, this requires that

$$\angle D(s_d)G(s_d) = \angle D(s_d) + \angle G(s_d) = \pm 180°$$

or
$$\angle D(s_d) = \phi = \pm 180° - \angle G(s_d) \qquad (7.50)$$

Thus, for the root locus of the compensated system to pass through the desired root location, the lead compensator pole-zero must contribute an angle ϕ given by Eqn. (7.50) and shown in Fig. 7.38. For a given angle ϕ for lead compensation, there is no unique location for the pole-zero pair. Out of many possible solutions, we select the one that satisfies the following additional requirements:

(i) The least-damped complex poles of the resulting closed-loop transfer function correspond to the desired dominant poles, and all other closed-loop

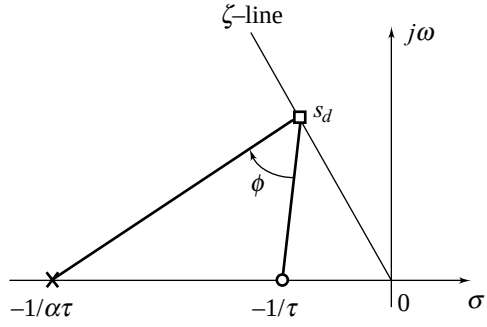

Fig. 7.38 Angle contribution of lead compensator

poles are either located very close to the open-loop zeros or are relatively far away from the $j\omega$-axis. This ensures that the poles other than the dominant poles make a negligible contribution to the system dynamics.

(ii) Changing the locations of the compensator pole and zero can produce a range of values for the gain while maintaining the desired root s_d. The pole-zero pair location that produces maximum gain (and hence results in minimum steady-state error) is preferred.

(iii) Realization of requirements (i) and (ii) may demand a large value of the ratio p/z. If we choose this ratio to be too large, high frequency noise problems can, and probably will, become significant. A rule of thumb that is sometimes used is to limit this ratio to 10 (pole is located at a distance 10 times the value of the zero location), but this depends on the physical system under consideration and particularly on the noise present.

In the light of the above discussion, the steps for lead compensator design are summarized below.

1. Translate the transient response specifications into a pair of complex dominant roots.
2. Sketch the pole-zero plot of the uncompensated system and determine using angle criterion whether the desired root locations can be realized by gain adjustment alone. If not, calculate the angle deficiency ϕ. This angle must be contributed by the lead compensator if the root locus is to pass through the desired root locations.
3. Place the compensating zero on the real axis in the region below the desired dominant root s_d. If the uncompensated system has an open-loop pole on the real axis in the region below s_d, the compensating zero should lie to the left of this pole.
4. Determine the compensator pole location so that the total angle contributed by compensator pole-zero pair at s_d is ϕ.
5. Evaluate the gain at s_d and then calculate the error constant.
6. Repeat the steps if transient performance is unsatisfactory because of a weak dominance condition and/or if the error constant is not satisfactory.

Example 7.7 Let us first consider the example of a unity-feedback type-2 system with open-loop transfer function

$$G(s) = \frac{K}{s^2}$$

It can be seen from its root locus plot that the closed-loop poles always lie on the $j\omega$-axis. As explained earlier, lead compensator is the only choice for this system.

It is desired to compensate the system so as to meet the following transient response specifications:
Settling time, $t_s \leq 4$ sec
Peak overshoot for step input $\leq 20\%$
These specifications imply that

$$\zeta \geq 0.45, \text{ and } \quad \zeta\omega_n \geq 1$$

We choose a desired dominant root location as

$$s_d = -\zeta\omega_n + j\omega_n\sqrt{1-\zeta^2} = -1 + j2$$

Figure 7.39a shows the pole-zero map of $G(s)$, and the desired dominant root location s_d. From this figure, we find that

$$\angle G(s_d) = -2 \times 116^\circ = -232^\circ$$

Therefore the angle contribution at s_d required of the lead compensator pole-zero pair is

$$\phi = -180° - (-232°) = 52°$$

Place the zero of the compensator on the real-axis segment directly below s_d, at $s = -z = -1$. Join the compensator zero to s_d and locate the compensator pole by making an angle of $\phi = 52°$, as shown in Fig. 7.39a. The location of the pole is found to be at $s = -p = -3.6$.

With the addition of the cascade lead compensator

$$D(s) = \frac{s+1}{s+3.6},$$

the open-loop transfer function of the system becomes

$$D(s)G(s) = \frac{K(s+1)}{s^2(s+3.6)}$$

The gain K is evaluated by measuring the vector lengths from the poles and zeros to the root location s_d:

$$K = \frac{(2.23)^2(3.25)}{2} = 8.1$$

Therefore the open-loop transfer function of the compensated system is

$$D(s)G(s) = \frac{8.1(s+1)}{s^2(s+3.6)} \tag{7.51}$$

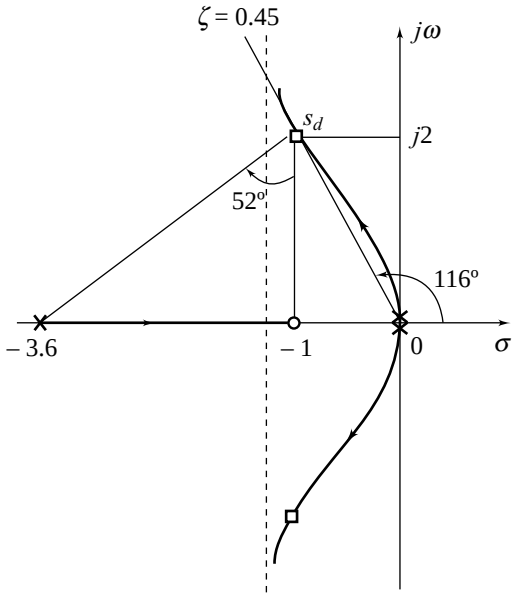

Fig. 7.39(a) Cascade lead compensation (Example 7.7)

The root locus plot of the compensated system is shown in Fig. 7.39a. The third closed-loop pole introduced because of the lead compensator lies on the real-axis root locus between $s = -3.6$ and $s = -1$. Due to this closed-loop pole, there will be an exponential term in the transient response in addition to the oscillatory term due to the complex pair of closed-loop poles. The specifications for the transient response were originally expressed in terms of the overshoot and the settling time of the system. These specifications were translated on the basis of an approximation of the system by a second-order system, to an equivalent ζ and ω_n, and therefrom to the desired closed-loop pole locations. However, the original specifications will be satisfied only if the poles selected are dominant. Often the designer will simulate the final design and obtain the actual transient response of the system. If the peak overshoot and settling time indices of the transient response do not compare well with the specified values, the system is redesigned.

Computer simulation (Appendix A) of the unity-feedback system with open-loop transfer function (7.51) resulted in a peak overshoot of 46.7% and a settling time of 3.78 sec for a step input (Fig. 7.39b). The difference in the overshoot from the specified value is due to the third closed-loop pole, which is not negligible. A second attempt to obtain a compensated system with an overshoot of 20% would utilize a compensator with zero at say $s = -2$. This approach would move the third closed-loop pole farther to the left in the s-plane, reduce the effect of the third closed-loop pole on the transient response, and reduce the overshoot.

Finally, the error constants of the system are evaluated. We find that the system under consideration is type-2, and therefore will result in zero steady-state error for step and ramp input signals. The acceleration error constant is

$$K_a = \lim_{s \to 0} s^2 D(s)G(s) = \frac{8.1}{3.6} = 2.25$$

The steady-state performance of the system is quite satisfactory. With the compensator zero shifted farther to the left in a redesign attempt, the error constant K_a will increase marginally.

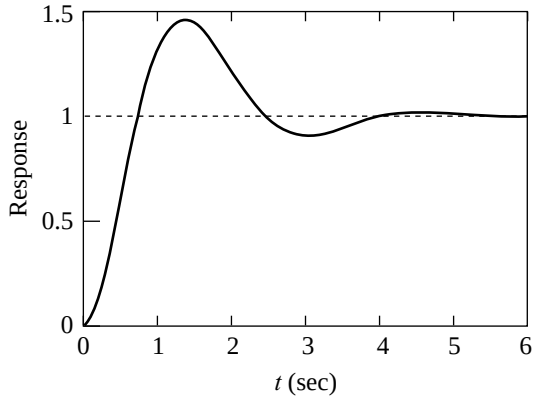

Fig. 7.39(b) Simulation results (Example 7.7)

Example 7.8 Now let us consider a unity-feedback type-1 system with open-loop transfer function

$$G(s) = \frac{K}{s(s+2)}$$

It is desired to design a cascade lead compensator such that the dominant closed-loop poles provide a damping ratio $\zeta = 0.5$ and have an undamped natural frequency $\omega_n = 4$ rad/sec.

Our specifications provide the location of the desired dominant closed-loop poles. An s-plane diagram showing the desired pole location s_d and the open-loop poles of the uncompensated transfer function is given in Fig. 7.40. The desired closed-loop pole is at

$$s_d = -\zeta\omega_n + j\omega_n\sqrt{1-\zeta^2} = -2 + j3.46$$

The angle of $G(s)$ at the desired closed-loop pole, obtained from Fig. 7.40, is

$$\angle G(s_d) = -210°$$

Thus, if we need to force the root locus to go through the desired closed-loop pole, the lead compensator must contribute $\phi = 30°$ at this point.

Let us locate the compensator zero at $s = -2.9$, i.e., in the region below the desired dominant closed-loop pole location and just to the left of the open-loop pole at $s = -2$. Join the compensator zero to s_d and locate the compensator pole by making an angle $\phi = 30°$ as shown in Fig. 7.40. The location of the pole is found to be at $s = -5.4$.

The open-loop transfer function of the compensated system becomes

$$D(s)G(s) = \left(\frac{s+2.9}{s+5.4}\right)\left[\frac{K}{s(s+2)}\right]$$

The gain K at s_d, evaluated using magnitude criterion, is 18.7. It follows that

$$D(s)G(s) = \frac{18.7(s+2.9)}{s(s+2)(s+5.4)}$$

The root locus plot of the compensated system is shown in Fig. 7.40. The third closed-loop pole is at $s = -3.4$, which is close to the added zero at $s = -2.9$. Therefore the effect of this pole on the transient

response is expected to be small. This should be verified by simulation study on the closed-loop transfer function

$$\frac{Y(s)}{R(s)} = M(s) = \frac{18.7(s+2.9)}{(s+2+j3.46)(s+2-j3.46)(s+3.4)}$$

Simulation study (Appendix A) shows that the response has a peak overshoot of 20.8% and a settling time of 2.05 sec for a step input.

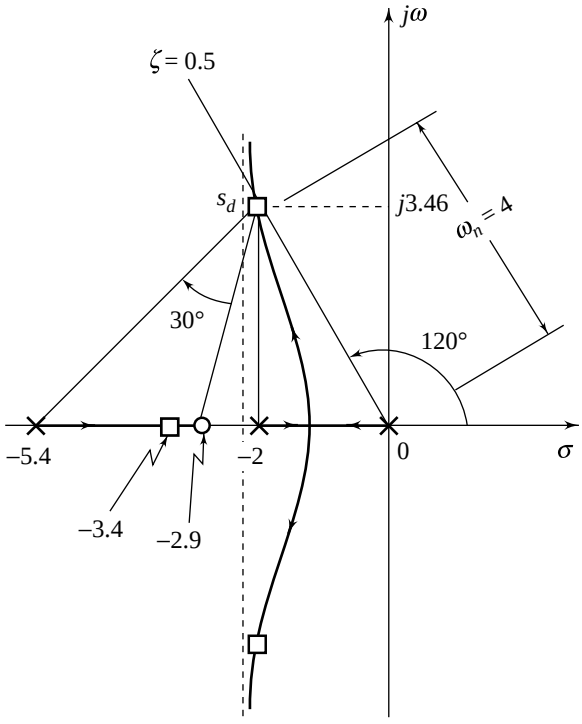

Fig. 7.40 Root locus plot (Example 7.8)

The velocity error constant of the compensated system is

$$K_v = \lim_{s\to 0} sD(s)G(s) = \frac{18.7 \times 2.9}{2 \times 5.4} = 5.02 \text{ sec}^{-1}$$

Although a certain change in the value of K_v can be made by altering the pole-zero location of the lead compensator, if a large increase in the value of K_v is desired, then we must alter the lead compensator to a lag-lead compensator.

Example 7.9 A unity-feedback system with open-loop transfer function

$$G(s) = \frac{K}{s^2(s+1.5)}$$

is to be compensated to meet the following specifications:

Settling time, $t_s < 5$ sec

Peak overshoot for step input $\cong$ 25%.

For a second-order system, damping ratio ζ =0.45 gives 20% overshoot, and with undamped natural frequency ω_n = 2.2 rad/sec, the settling time $t_s = 4/\zeta\omega_n = 4$ sec.

These specifications provide the location of desired dominant roots:

$$s_{1,2} = -\zeta\omega_n \pm j\omega_n\sqrt{1-\zeta^2} = -1 \pm j2$$

At $s_d = -1 + j2$ (refer Fig. 7.41), $\angle G(s_d) = -2 \times 116° - 75° = -307°$

Therefore the angle contribution required from a lead compensator is $\phi = -180° - (-307°) = 127°$.

The large value of ϕ here is an indication that a double lead compensator[5] is appropriate. Each section of the compensator has then to contribute an angle of 63.5° at s_d.

In the region below the desired root, there is an open-loop pole at $s = -1.5$. We may place zero of the compensator at $s = -z = -1.5$, cancelling the plant pole. Join the compensator zero to s_d and locate the compensator pole by making an angle of $\phi = 63.5°$, as shown in Fig. 7.41. The location of the pole is found to be at $s = -10$.

With the cascade double lead compensator $D(s) = \dfrac{(s+1.5)^2}{(s+10)^2}$, the open-loop transfer function of the compensated system becomes

$$D(s)G(s) = \frac{K(s+1.5)^2}{s^2(s+1.5)(s+10)^2} = \frac{K(s+1.5)}{s^2(s+10)^2}$$

The gain K at s_d, evaluated using magnitude criterion, is 247. It follows that

$$D(s)G(s) = \frac{247(s+1.5)}{s^2(s+10)^2}$$

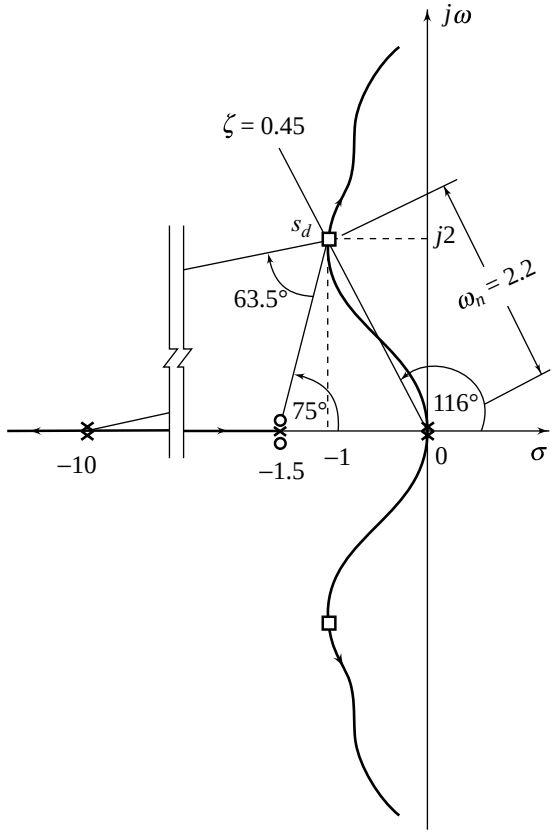

Fig. 7.41 Root locus plot (Example 7.9)

A rough root locus plot of the compensated system is shown in Fig. 7.41. By locating all the closed-loop poles and carrying out a simulation study on the closed-loop system, we can determine whether the dominance of the complex pole-pair is ensured, i.e., whether the actual transient response compared well with the specified one. Simulation study shows that the response has a peak overshoot of 53.1% and a settling time of 3.96 sec for a step input.

[5] An important consideration governing this choice is the inherent noise in control systems. Refer Example 10.3.

7.7 CASCADE LAG COMPENSATION

As pointed out earlier in Section 7.5, a lag compensator improves the steady-state behaviour of a system, while nearly preserving its transient response. In this section, we consider how the root locus may be used to design a compensator so as to realize a desired improvement in steady-state response.

Consider a unity-feedback system with a forward-path transfer function

$$G(s) = \frac{K \prod_{i=1}^{m}(s + z_i)}{s^r \prod_{j=r+1}^{n}(s + p_j)} \tag{7.52}$$

We assume that at a certain value of K, this system has satisfactory transient response, i.e., its root locus plot passes through (or is close to) the desired closed-loop pole location s_d indicated in Fig. 7.42. It is required to improve the system error constant K_p, K_v or K_a (depending on whether the system is type-0, -1 or -2, respectively) to a specified value without impairing its transient response. This requires that after compensation, the root locus should continue to pass through s_d, while the error constant at s_d is raised to the specified value. To accomplish this, consider adding a lag compensator pole-zero pair close to origin, with zero to the left of the pole. If pole and zero of this pair are located close to each other, it will contribute a negligible angle λ at s_d such that s_d continues to lie on the root locus of the compensated system. Figure 7.42 shows the location of such a lag compensator pole-zero pair.

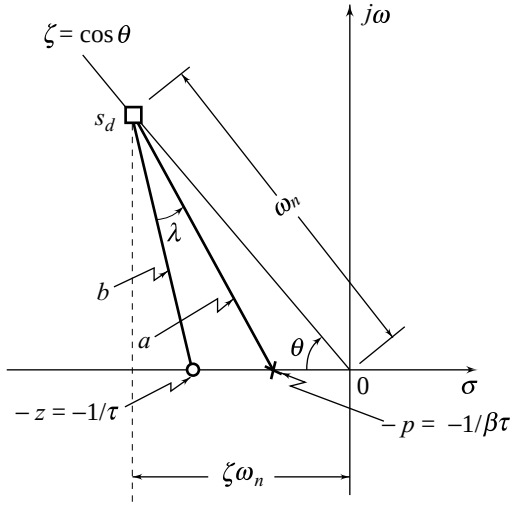

Fig. 7.42 Locating the lag compensator pole-zero pair

The gain of the uncompensated system at s_d is given by

$$K^{uc}(s_d) = \frac{|s_d|^r \prod_{j=r+1}^{n} |s_d + p_j|}{\prod_{i=1}^{m} |s_d + z_i|} \tag{7.53}$$

For the system with a cascade lag compensator

$$D(s) = \frac{s+z}{s+p} = \frac{s+1/\tau}{s+1/\beta\tau}; \beta = \frac{z}{p} > 1, \tau > 0 \tag{7.54}$$

the system gain at s_d is (refer Fig. 7.42)

$$K^{c}(s_d) = \frac{|s_d|^r \prod_{j=r+1}^{n} |s_d + p_j|}{\prod_{i=1}^{m} |s_d + z_i|} \left(\frac{a}{b}\right) \tag{7.55}$$

where $a = |s_d + 1/\beta\tau|$, and $b = |s_d + 1/\tau|$.

Since the compensator pole and zero are located close to each other, they are nearly equidistant from s_d, i.e., $a \cong b$. It therefore follows from Eqns (7.53) and (7.55) that

$$K^c(s_d) \cong K^{uc}(s_d)$$

The error constant K_e (which is equal to K_p, K_v, or K_a depending on the type of the system) of the uncompensated system is given by

$$K_e^{uc} = K^{uc}(s_d) \frac{\prod_{i=1}^{m} z_i}{\prod_{j=r+1}^{n} p_j}$$

The error constant of the compensated system is given by (refer Fig. 7.42)

$$K_e^c = K^c(s_d) \frac{\prod_{i=1}^{m} z_i}{\prod_{j=r+1}^{n} p_j} \left(\frac{z}{p}\right) \cong K_e^{uc} \left(\frac{z}{p}\right)$$

Since the error constant K_e^c must equal the desired value K_e^d, we have

$$K_e^d \cong K_e^{uc} \left(\frac{z}{p}\right)$$

or

$$\beta = \left(\frac{z}{p}\right) \cong \frac{K_e^d}{K_e^{uc}} \tag{7.56}$$

Thus the β-parameter of the lag compensator (refer Eqn. (7.54)) is nearly equal to the ratio of the desired error constant to the error constant of the uncompensated system.

Since the lag compensator does contribute a small negative angle λ at s_d, the compensated root locus will not pass through s_d. The effect of the small lag angle λ is to press the root locus slightly to the right. The intersection of the compensated root locus with the specified ζ-line will be at s_d' having slightly lower value of ω_n compared to the one corresponding to s_d. Also the actual error constant will somewhat fall short of the specified value if β obtained from Eqn. (7.56) is used.

The effects of lag angle λ can be anticipated and counteracted by taking design parameter ω_n to be somewhat larger than the specified value. Also in the design process, we may choose a β somewhat larger than that given by Eqn. (7.56).

In the light of the above discussion, the steps for lag compensator design are summarized below.

1. Draw the root locus plot for the uncompensated system.
2. Translate the transient response specifications into a pair of complex dominant roots and locate these roots on the uncompensated root locus plot. It is assumed that acceptable transient performance can be obtained by gain adjustment; the desired dominant root will therefore lie on (or close to) the uncompensated root locus.
3. Calculate the gain of the uncompensated system at the dominant root s_d and evaluate the corresponding error constant.
4. Determine the factor by which the error constant of the uncompensated system should be increased to meet the specified value. Choose the β-parameter of lag compensator to be somewhat greater than this factor.

5. Select zero ($s = -z$) of the compensator sufficiently close to the origin. As a guide rule, we may construct a line making an angle of 10° (or less) with the desired ζ-line from s_d; the intersection of this line with the real axis gives location of the compensator zero.
6. The compensator pole can then be located at $s = -p = -z/\beta$. It is important to note that the compensator pole-zero pair should contribute an angle λ less than 5° at s_d so that the root locus plot in the region of s_d is not appreciably changed and hence satisfactory transient behaviour of the system is preserved.

Example 7.10 Reconsider the uncompensated system of Example 7.8, where the uncompensated open-loop transfer function is

$$G(s) = \frac{K}{s(s+2)}$$

The system is to be compensated to meet the following specifications.

Damping ratio, $\zeta = 0.707$

Settling time, $t_s \le 5$ sec

Velocity error constant, $K_v \ge 4$

The uncompensated root locus is a vertical line at $s = -1$ and results in a root on the $\zeta = 0.707$ line at $s_d = -1 + j1$, as shown in Fig. 7.43a. Settling time corresponding to this root is $4/\zeta\omega_n = 4$ sec. The gain at s_d is $K = 2$. Therefore, the uncompensated system with the gain adjusted to a value of 2 meets the transient response specifications. Slight reduction in ω_n due to the small lag angle of the compensator required to improve steady-state performance, is also permissible.

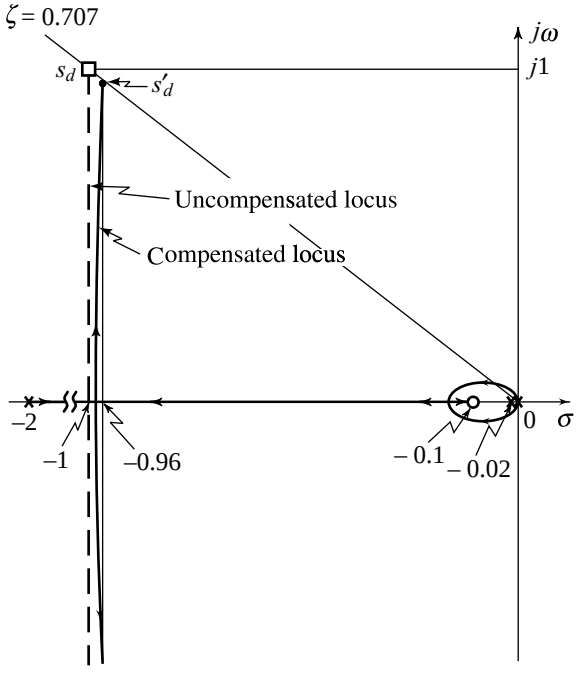

Fig. 7.43(a) Root locus plot (Example 7.10)

The velocity error constant of the uncompensated system is

$$K_v^{uc} = \lim_{s \to 0} sG(s) = K/2 = 1$$

The desired velocity error constant is

$$K_v^d \ge 4$$

Thus, the velocity error constant must be increased by at least a factor of 4. Lag compensator with $\beta = 5$ is expected to meet this requirement. We might set compensator zero at $s = -z = -0.1$. Note that $|z|$ is much smaller compared to $|s_d| = \sqrt{2}$. The compensator pole is located at $s = -p = -z/\beta = -0.02$. The difference of the angles from compensator zero and pole at the desired root s_d is about 3°; therefore $s_d = -1 + j1$ will lie close to compensated root locus.

The open-loop transfer function of the compensated system becomes

$$D(s)G(s) = \left(\frac{s+0.1}{s+0.02}\right)\left[\frac{K}{s(s+2)}\right]$$

The root locus plot of the compensated system is shown in Fig. 7.43a. It intersects the $\zeta = 0.707$ line at $s_d' = -0.96 + j0.96$. The gain K at s_d', evaluated by magnitude criterion, remains approximately equal to 2. It follows that

$$D(s)G(s) = \frac{2(s+0.1)}{s(s+0.02)(s+2)}$$

From Fig. 7.43a, we find that corresponding to $K = 2$, the third closed-loop pole is at $s = -0.11$. Note that the real pole has a time-constant of $\tau = 1/0.11 = 9.1$ sec, which would appear to make the system so slow as to be unusable. However, there is a zero close to this additional pole. The net effect is that the settling time will increase because of the third pole, but the amplitude of the response term contributed by this pole will be very small. In system response, a long tail of small amplitude will appear which may not degrade the performance of the system appreciably. This should be verified by simulation study on the closed-loop transfer function,

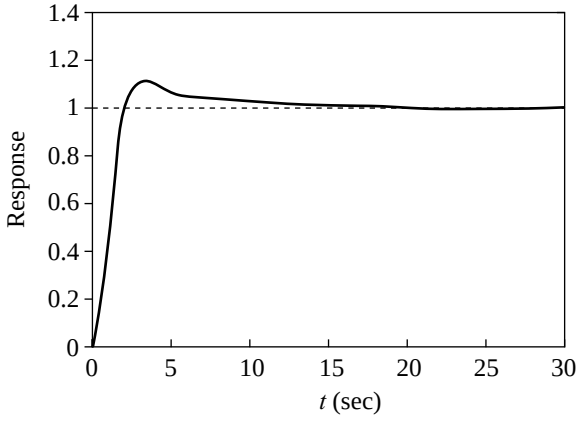

Fig. 7.43(b) Simulation results (Example 7.10)

$$\frac{Y(s)}{R(s)} = M(s) = \frac{2(s+0.1)}{(s+0.11)(s+0.96+j0.96)(s+0.96-j0.96)}$$

Simulation study (Appendix A) shows that the response have peak overshoot of 12% and a settling time of 15 sec (Fig. 7.43b).

7.8 CASCADE LAG-LEAD COMPENSATION

In the preceding sections, we have seen that the lead compensator is suitable for systems having unsatisfactory transient response. However, it provides only a limited improvement in steady-state response. If the steady-state behaviour is highly unsatisfactory, the lead compensator may not be the answer. On the other hand, for systems with satisfactory transient response but unsatisfactory steady-state response, the lag compensator is found to be a good choice.

When both transient and steady-state responses are unsatisfactory, we must draw upon the combined powers of lag and lead compensators in order to meet the specifications. The transfer function for the lag-lead compensator is of the form

$$D(s) = \left(\frac{s+z_2}{s+p_2}\right)\left(\frac{s+z_1}{s+p_1}\right) \tag{7.57a}$$

$$= \underbrace{\left(\frac{s+1/\tau_2}{s+1/\beta\tau_2}\right)}_{\text{Lag Section}}\underbrace{\left(\frac{s+1/\tau_1}{s+1/\alpha\tau_1}\right)}_{\text{Lead Section}}; \beta = \frac{z_2}{p_2} > 1, \alpha = \frac{z_1}{p_1} < 1, \tau_2 > 0, \tau_1 > 0 \tag{7.57b}$$

In designing a lag-lead compensator, we frequently choose $\beta = 1/\alpha$ (this is not necessary; we can, of course, choose $\beta \neq 1/\alpha$). The reason for this choice is that with the reduction in number of design parameters, the design problem becomes simpler. With $\beta = 1/\alpha$, the transfer function (7.57) of the lag-lead compensator reduces to

$$D(s) = \underbrace{\left(\frac{s+1/\tau_2}{s+\alpha/\tau_2}\right)}_{\text{Lag Section}}\underbrace{\left(\frac{s+1/\tau_1}{s+1/\alpha\tau_1}\right)}_{\text{Lead Section}}; \tau_2, \tau_1 > 0 \tag{7.58}$$

We first design the lead section to realize the required ζ and ω_n for the dominant closed-loop poles. The error constant is then determined for the lead-compensated system, say it is K_e^{lc}. If K_e^{lc} is sufficiently high to give the desired steady-state response, we need not go further. Lead compensation is all that is required. If, however, K_e^{lc} is not large enough, we consider adding the lag section with $\beta = 1/\alpha$. This results in an error constant

$$K_e^{llc} \cong \frac{1}{\alpha} K_e^{lc} \tag{7.59}$$

If K_e^{llc}, as given in Eqn. (7.59), is not large enough to meet steady-state specifications, we choose $\beta > 1/\alpha$ and redesign the lag section.

Example 7.11 Consider a plant with transfer function

$$G(s) = \frac{4}{s(s+0.5)}$$

We design a feedback system to meet the following specifications:

1. Damping ratio of dominant closed-loop poles, $\zeta = 0.5$.
2. Undamped natural frequency of dominant closed-loop poles, $\omega_n = 5$ rad/sec.
3. Velocity error constant = 80 sec.$^{-1}$

We choose the unity-feedback control configuration shown in Fig. 7.44. Root locus plot of the system with $A > 0$ and $D(s) = 1$ is shown by dashed line in Fig. 7.45. The $\zeta = 0.5$ line intersects the root locus at the point $s = -0.25 + j0.433$. The undamped natural frequency corresponding to this root is 0.5 rad/sec. Therefore the configuration in Fig. 7.44 with $D(s) = 1$ cannot meet the specifications.

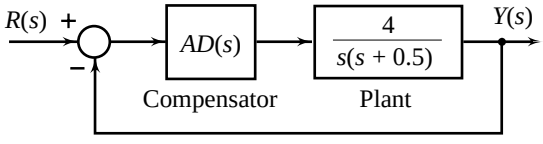

Fig. 7.44 Control configuration (Example 7.11)

We introduce a cascade lead compensator. From the performance specifications we find that the dominant closed-loop poles must be at $s = -2.5 \pm j4.33$. Consider the desired location

$$s_d = -2.5 + j4.33$$

Since (refer Fig. 7.45) $\angle G(s_d) = -120° - 115° = -235°$, the lead compensator must contribute 55° so that the root locus passes through the desired root s_d. To design the lead compensator, we first determine the location of the compensator zero. There are many possible choices, but we shall here choose the

zero at $s = -z = -0.5$ so that it cancels the open-loop pole at $s = -0.5$. Once the compensator zero is chosen, the compensator pole can be located such that the angle contribution of the pole-zero pair is 55°. By simple graphical analysis (refer Fig. 7.45), we find that the pole must be located at $s = -p = -5$. Thus, with the lead compensator

$$D_1(s) = \frac{s + 1/\tau_1}{s + 1/\alpha\tau_1} = \frac{s + 0.5}{s + 5}, \ \alpha = 0.1,$$

the open-loop transfer function of the system becomes

$$D_1(s)G(s) = \frac{K(s + 0.5)}{s(s + 0.5)(s + 5)} = \frac{K}{s(s + 5)}; \ K = 4A$$

The value of K obtained by magnitude criterion, is

$$K = |s_d| \, |s_d + 5| \cong 25$$

Root locus plot of the lead-compensated system is shown in Fig. 7.45. Let us evaluate the steady-state performance of this system.

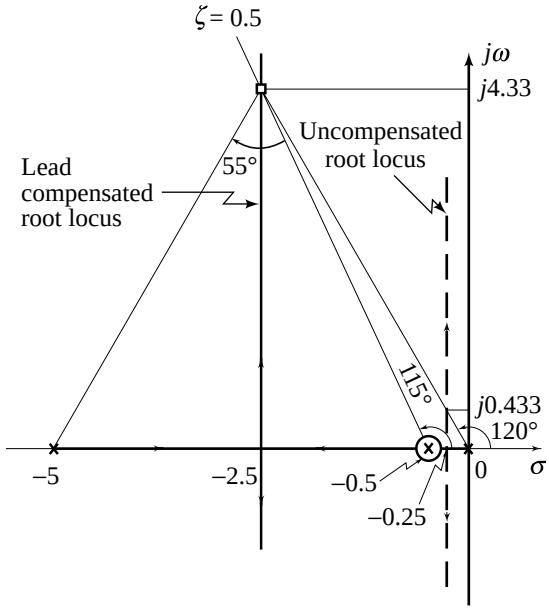

Fig. 7.45 Root locus plot (Example 7.11)

$$K_v = \lim_{s \to 0} sD_1(s)G(s) = \frac{K}{5} = 5$$

The desired K_v is 80. A large increase in K_v cannot be obtained by adjustment of pole-zero pair of the lead compensator. We, therefore, must alter the lead compensation to a lag-lead compensation.

Let us design a lag compensator

$$D_2(s) = \frac{s + 1/\tau_2}{s + 1/\beta\tau_2}; \ \beta > 1$$

for the lead-compensated system. If we choose $\beta = 1/\alpha = 10$, the velocity error constant will increase by a factor of about 10, i.e., the velocity error constant of the lag-lead compensated system will become about 50. The choice $\beta = 1/\alpha$, therefore, does not meet our requirements on steady-state accuracy.

The velocity error constant of the lead-compensated system is $K_v^{lc} = 5$.

The desired velocity error constant is $K_v^d = 80$.

Thus, the velocity error constant must be increased by a factor of 16. The lag compensator with $\beta = 16$ will meet this requirement. We now choose the pole-zero pair of the lag compensator. We want that

$$|D_2(s_d)| = \left| \frac{s_d + z_2}{s_d + p_2} \right| \cong 1$$

$$-5° < \angle D_2(s_d) = \angle s_d + z_2 - \angle s_d + p_2 < 0°$$

$z_2 = 0.2$, and $p_2 = z_2/\beta = 0.2/16 = 0.0125$ meet these requirements.

The open-loop transfer function of the lag-lead compensated system becomes

$$D_2(s)D_1(s)G(s) = \frac{25(s + 0.2)}{s(s + 0.0125)(s + 5)}$$

$$= \frac{25}{4}\frac{(s+0.2)(s+0.5)}{(s+0.0125)(s+5)}\left[\frac{4}{s(s+0.5)}\right]$$

Therefore (refer Fig. 7.44)

$$AD(s) = \frac{25}{4}\frac{(s+0.2)(s+0.5)}{(s+0.0125)(s+5)}$$

Root locus analysis of the lag-lead compensated feedback system is left as an exercise for the reader.

7.9 CASCADE PID COMPENSATION

The design of a controller is basically a search problem is n-dimensional parametric space where n is the number of design parameters of the controller. Points in the search space correspond to different selections of controllers. By choosing different points of the parametric space, we can generate feedback systems with different performances. A controller that meets the given performance specifications can be determined by moving in this search space on trial-and-error basis.

The design of PI/PD/PID compensator is a simpler problem with 2 to 3 trial parameters. The filtering and other signal conditioning may be independently designed. The lag/lead/lag-lead compensator design involves 3 to 5 parameters.

In the case of design wherein the primary requirement is to improve transient performance, a PD compensator may be attempted. This corresponds to a search problem in 2-dimensional parametric space. This compensation will, however, be useful if the feedback loop is free from high-frequency noise problem. This is unlikely in real-life applications. Therefore, the total design problem includes the design of a filter in addition to the design of a PD compensator. An alternative to this strategy is the design of a lead compensator. This corresponds to a search problem in 3-dimensional parametric space. Lead compensator may meet the filtering requirement in addition to satisfying the specifications on transient performance.

Consider now the problem of design wherein the primary requirement is to improve steady-state performance. A PI compensator may be attempted. This corresponds to a search problem in 2-dimensional parametric space. The compensator will, however, be useful if its pole at the origin does not degrade closed-loop stability appreciably. The lag compensator, which is a search problem in 3-dimensional parametric space, is an alternative strategy; it may yield an acceptable improvement in the steady-state performance without appreciably degrading the closed-loop stability.

The design of PI, PD and PID compensators follows in a straight-forward way from the procedures of the design of lag, lead and lag-lead compensators detailed in earlier sections. An illustrative example follows.

Example 7.12 A unity feedback system has forward path transfer function

$$G(s) = \frac{K(s+8)}{(s+3)(s+6)(s+10)}$$

Our goal is to design a cascade PID compensator that improves the transient as well as steady-state performance of the closed-loop system.

Let us fix specifications for design. Say, we want to achieve a transient response that has no more that 20% overshoot with peak time $t_p = 0.2$ sec. The steady-state error to step input is required to be zero. The root locus plot of the uncompensated system is shown in Fig. 7.46. The $Mp = 20\%$ ($\zeta = 0.456$) line intersects the root locus at the point $s = -5.4 + j\,10.5$. (It is observed that the effect of the third closed-

loop pole will be nearly cancelled by a zero.) The damped natural frequency corresponding to this root is 10.5 rad/sec:

$$t_p = \frac{\pi}{10.5} = 0.3 \text{ sec}$$

The value of K obtained by magnitude criterion is 119.66.

The position error constant

$$K_p = \lim_{s\to 0} G(s) = \frac{119.66 \times 8}{3 \times 6 \times 10} = 5.32$$

Steady-state error to unit-step input,

$$e_{ss} = \frac{1}{1 + K_p} = 0.158$$

Therefore, the uncompensated system (gain adjustment only) cannot meet the specifications.

We introduce a cascade PD compensator. From the performance specifications we find that the dominant closed-loop poles must be at $s_d = -8.16 \pm j\,15.92$ (The imaginary part of the compensated dominant poles is $\omega_d = \pi/t_p = \pi/0.2 = 15.92$; and the real part is $-\zeta\omega_n = -\zeta\omega_d/\sqrt{1-\zeta^2} = -8.16$).

We search for compensator's zero location so that the root locus of the compensated system passes through the desired dominant pole location.

The sum of the angles from uncompensated system's poles and zeros to the desired compensted dominant pole is $-198.5°$. Thus the contribution required from the compensator zero is $198.5 - 180 = 18.5°$ Assuming that compensator zero is located at $s = -z_c$, as shown in Fig. 7.47, we obtain

$$\frac{15.92}{z_c - 8.16} = \tan(18.5°)$$

This gives

$$z_c = 55.75$$

Thus the PD compensator is

$$D_1(s) = s + 55.75$$

With this compensator, the open-loop transfer function of the system becomes

$$D_1(s)G(s) = \frac{K(s+8)(s+55.75)}{(s+3)(s+6)(s+10)}$$

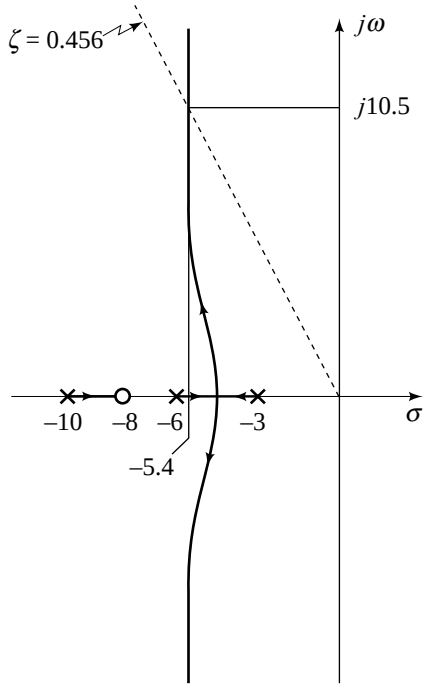

Fig. 7.46 Root locus plot of uncompensated system (Example 7.12)

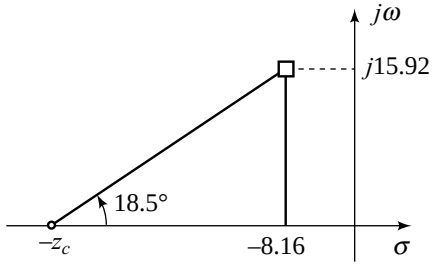

Fig. 7.47

Root locus plot of the PD-compensated system is shown in Fig. 7.48. The root locus passes through the design point s_d. It is observed that the effect of the third closed-loop pole will be nearly cancelled by a zero.

The value of K obtained by the magnitude criterion is 5.24. Let us evaluate the steady-state performance of this system.

$$K_p = \lim_{s\to 0} D_1(s)G(s) = \frac{5.24\times 8\times 55.75}{3\times 6\times 10}$$

$$e_{ss} = \frac{1}{1+K_p} = 0.072$$

The PD-compensated system, thus, gives reduction in peak time with improvement in steady-state error over uncompensated system. The desired steady-state error is zero. We therefore alter the PD compensation to a PID compensation.

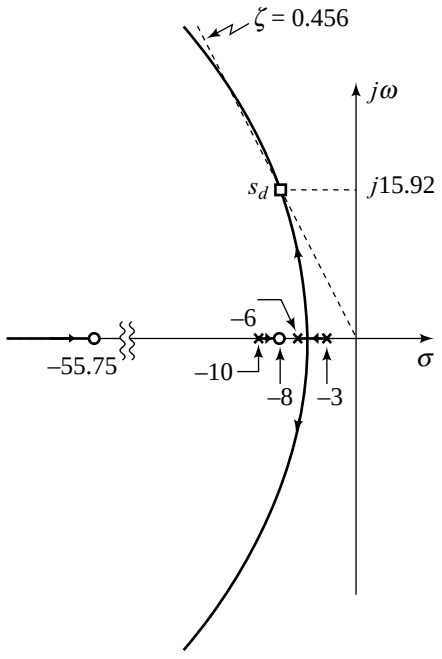

Fig. 7.48 Root locus plot of PD-compensated system (Example 7.12)

Let us design a PI compensator for the PD-compensated system. Any PI compensator will work as long as its zero is placed close to the origin to ensure that the compensator pole-zero pair will not appreciably change the transient response of the PD-compensated system (The placement of the zero of the PI compensator is not entirely arbitrary. If K_v were specified, the location of the zero would have influenced the steady-state error to ramp inputs). Choosing

$$D_2(s) = \frac{s+0.5}{s}$$

the open-loop transfer function of the PID-compensated system becomes

$$D_2(s)D_1(s)G(s) = \frac{K(s+0.5)(s+8)(s+55.75)}{s(s+3)(s+6)(s+10)}$$

The value of K obtained by magnitude criterion is 4.4. Complete root locus analysis of the PID compensated system is left as an exercise for the reader.

The PD compensator improved the transient response by decreasing the time required to reach the first peak, as well as yielding some improvement in the steady-state error. The complete PID compensator further improved the steady-state error without appreciably changing the transient response designed with PD compensator.

7.10 MINOR-LOOP FEEDBACK COMPENSATION

The feedback control schemes discussed in the preceding sections have all utilized a compensator $D(s)$ placed in the forward path in cascade with the plant transfer function $G(s)$. The compensator $D(s)$ typically involves PI terms (lag compensator), PD terms (lead compensator), or PID terms (lag-lead compensator).

Derivative action of a compensator need not be implemented with the derivative term in the forward path, especially when there are step changes in the reference input that could produce plant input saturation. In such cases, a practical implementation of compensation is realized by means of a minor loop around the plant implementing derivative term, with a proportional (P) or a lag (PI) compensator in the forward path (Revisiting Section 4.6 will be helpful).

Example 7.13 The feedback system shown in Fig. 7.49 provides the opportunity for varying three parameters: A, K, and K_t. The larger the number of variables inserted into a system, the better the opportunity for achieving a specified performance. However, the design problem becomes much more complex. The characteristic equation of the given system is (refer Fig. 7.49)

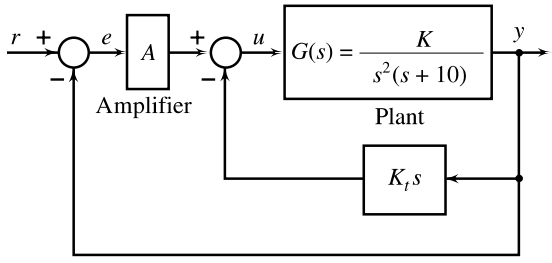

Fig. 7.49 Rate feedback compensation

$$1 + \frac{AG(s)}{1 + sK_tG(s)} = 1 + \frac{AK}{s^2(s+10) + KK_ts} = 0 \tag{7.60}$$

Rearranging, we get

$$s^3 + 10\,s^2 + KK_t\,s + AK = 0$$

There are three variable parameters: A, K, and K_t. By appropriate partitioning of the characteristic equation, we can use single-parameter root loci for the design of three parameters (A, K, K_t) of the given system.

Consider the following partitioning:

$$1 + \frac{KK_t(s + A/K_t)}{s^2(s+10)} = 0 \tag{7.61}$$

This equation shows that the net effect of rate feedback is to add a zero at $s = -A/K_t$. Now the design procedure calls for a search for suitable location for this additional zero to satisfy the specifications.

Assume that the system is to be compensated to meet the following specifications:

Per cent peak overshoot	$\leq 10\%$
Settling time	≤ 4 sec

The damping ζ and natural frequency ω_n of the dominant roots, obtained from the relations

$$e^{-\pi\zeta/\sqrt{1-\zeta^2}} \cong 0.1; \quad \text{and} \quad \frac{4}{\zeta\omega_n} = 4$$

are

$$\zeta = 0.6,\ \omega_n = 1.67 \text{ rad/sec.}$$

The desired dominant roots are then given as $s_d = -1 \pm j1.34$.

From Fig. 7.50, we see that the angle contribution of the open-loop poles at s_d is $-2(127°) - 8° = -262°$. Therefore, for the point s_d to be on the root locus, the compensating zero should contribute an angle of $\phi = -180° - (-262°) = 82°$. The location of the compensating zero is thus found to be at $s = -1.2$. The open-loop transfer function of the compensated system becomes

$$F(s) = \frac{KK_t(s+1.2)}{s^2(s+10)} \tag{7.62}$$

The root locus plot of the compensated system is shown in Fig. 7.50. It is now observed that for all values of KK_t, the system is stable. The value of KK_t at s_d is found to be 17.4. The third closed-loop pole

is at $s = -8$ which is far away from the imaginary axis compared to dominant closed-loop poles. Hence, its effect on the transient behaviour is negligible.

From Fig. 7.50, we observe that the root locus intersects the $\zeta = 0.6$ line at two points, P and Q. Thus, two values of KK_t will give the damping ratio ζ of the closed-loop poles equal to 0.6. $KK_t = 17.4$ at point P results in a pair of dominant complex-conjugate closed-loop poles which satisfy the transient response specifications. The third closed-loop pole is at $s = -8$ which has insignificant contribution to system dynamics. At point Q, the dominance condition will be weakened; the third closed-loop pole on the real axis will force a slow overdamped response. It is important to point out that the zero at $s = -1.2$ is not the zero of the system of Fig. 7.49. It is the open-loop zero of $F(s)$ (refer Eqn. 7.62) which was introduced in the process of partitioning the characteristic equation such that the adjustable variable KK_t appears as a multiplying factor.

Let us now investigate the steady-state behaviour of the compensated system. From Eqn. (7.60), the velocity error constant K_v is given by

$$K_v = \lim_{s \to 0} s \left[\frac{AK}{s^2(s+10) + KK_t s} \right] = \frac{AK}{KK_t} = A/K_t = 1.2$$

If this value of K_v is acceptable, then the design is complete. Otherwise, the design procedure given above cannot satisfy the steady-state and transient specifications simultaneously. A trade-off between the steady-state and transient behaviour becomes necessary.

We have three parameters and two equations:

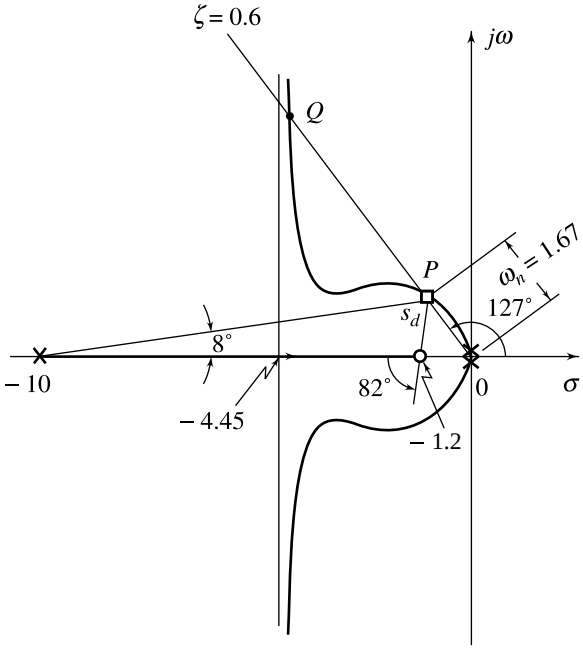

Fig. 7.50 Root locus plot for the characteristic equation (7.61)

$$A/K_t = 1.2; \quad KK_t = 17.4$$

If we select $K_t = 0.4$, then the other two parameters become: $A = 0.48$ and $K = 43.5$. K can be decreased with no change in performance by increasing A and K_t; e.g., $K_t = 0.8$ gives $A = 0.96$ and $K = 21.75$.

7.11 THE ROOT LOCUS OF SYSTEMS WITH DEAD-TIME

Let us consider the problem of constructing the root locus for systems where a dead-time τ_D is involved in the loop function. Fig. 7.51 shows in block diagram form two systems involving delay in the forward path and the feedback path. In either case, the characteristic equation is given by

$$1 + KG(s)H(s)e^{-\tau_D s} = 0;\ K \geq 0 \tag{7.63}$$

Equation (7.63) is not a polynomial and thus does not fall in the same class as our other examples so far. How would one plot the root locus corresponding to this equation? There are two basic approaches: direct application, and approximation of the phase criterion.

The direct application approach demands the use of angle and magnitude criteria directly on the given characteristic equation without any approximation. These criteria are not changed if the process is non-rational.

Angle criterion

$$\angle G(s)H(s)e^{-\tau_D s} = \pm\, 180°(2q + 1);\ q = 0,1,... \tag{7.64a}$$

Magnitude criterion

$$|KG(s)H(s)e^{-\tau_D s}| = 1 \tag{7.64b}$$

One can formulate a root-locus problem as searching for locations where the angle criterion (7.64a) is satisfied. The value of the root locus gain K at any point on the root locus can then be determined by using the magnitude criterion (7.64b). It may however be noted that the rules given in Table 7.1 are not applicable for such a problem.

In the second approach, we reduce the given problem close to the one we have previously solved by approximating the non-rational function $e^{-\tau_D s}$ with a rational function. Since we are concerned with control systems (systems with low frequencies), we want an approximation that will be good for $s = 0$ and nearby. The most common means used to find such an approximation is attributed to Pade, and is based on matching the series expansion of $e^{-\tau_D s}$ with that of a rational function; a ratio of numerator polynomial of degree p and denominator polynomial of degree q. For our purposes, we will consider only the case $p = q = 1$ (refer Eqn. (2.49)):

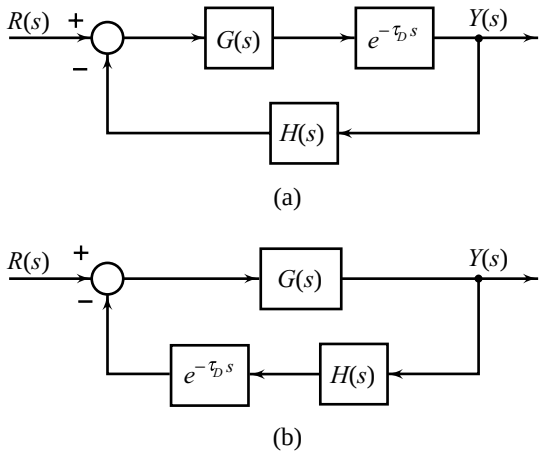

Fig. 7.51 Closed-loop systems with time delays involved

$$e^{-\tau_D s} \cong \frac{1 - \frac{\tau_D}{2}s}{1 + \frac{\tau_D}{2}s} = \frac{-[s - (2/\tau_D)]}{s + (2/\tau_D)} \tag{7.65}$$

With this approximation, the characteristic Eqn. (7.63) becomes

$$1 - KG(s)H(s)\,[s - (2/\tau_D)]\,/\,[s + (2/\tau_D)] = 0 \tag{7.66}$$

Examining Eqn. (7.66), we note that the equation is of the form

$$1 - F(s) = 0 \tag{7.67}$$

where $$F(s) = \frac{K\prod_{i=1}^{m}(s + z_i)}{\prod_{j=1}^{n}(s + p_j)}$$

This equation again is not of the standard form (7.22) used earlier to derive construction rules of Table 7.1. Therefore, the construction rules of Table 7.1 cannot be used directly even in the approach based on approximation of non-rational function $e^{-\tau_D s}$. However, only a minor modification in the rules of Table 7.1 is required to deal with characteristic equations of the form (7.67). Our discussion will be limited to second approach; the approach based on approximation given by Eqn. (7.65).

In a manner similar to the development of the root-locus method in Section 7.2, we require that the root locus of the characteristic equation (7.67) satisfy the equations:

Angle criterion

$$\angle F(s) = \sum_{i=1}^{m}(s + z_i) - \sum_{j=1}^{n}(s + p_j) = \pm q(360°);\ q = 0, 1, 2, \ldots \tag{7.68a}$$

Magnitude criterion

$$|F(s)| = \frac{K\prod_{i=1}^{m}|s + z_i|}{\prod_{j=1}^{n}|s + p_j|} = 1 \tag{7.68b}$$

The locus of roots follows a zero-degree locus (Eqn. (7.68a)) in contrast with the 180° locus considered previously. However, the root locus rules of Table 7.1 may be altered to account for the zero-degree phase angle requirement, and then the root locus may be obtained as in the preceding sections.

Rule (i) : No change

Rule (ii) : No change

Rule (iii) : No change in centroid calculation. Angles of asymptotes are now given by the relation

$$\phi_A = \frac{q(360°)}{n - m};\ q = 0,1, \ldots, (n - m - 1) \tag{7.69}$$

Rule (iv) : A point on the real axis lies on the locus if the number of open-loop poles plus zeros on the real axis to the right of this point is even.

Rule (v) : No change

Rule (vi) : The angle of departure, ϕ_p, of a locus from a complex open-loop pole is given by

$$\phi_p = \phi \tag{7.70}$$

where ϕ is the net angle contribution at this pole of all other open-loop poles and zeros.

Rule (vii) : The angle of arrival, ϕ_z, of a locus at a complex zero is given by

$$\phi_z = -\phi \tag{7.71}$$

where ϕ is the net angle contribution at this zero of all other open-loop poles and zeros.

Rule (viii) : No change

Rule (ix) : No change

Example 7.14 Suppose that the plant in Fig. 7.51 is $G(s) = K/s$, the sensor $H(s) = 1$ and the dead-time $\tau_D = 1$ sec.

The characteristic equation of the system becomes

$$1 + \frac{Ke^{-s}}{s} = 0;\ K \geq 0$$

With the approximation $e^{-s} \cong \frac{1 - s/2}{1 + s/2}$, the characteristic equation becomes

$$1 - \frac{K(s-2)}{s(s+2)} = 0 \qquad (7.72)$$

Examining the real-axis segments of the root loci shown in Fig. 7.52, it is obvious that there will be two breakaway points. These points are the solutions of the equation $\frac{dK}{ds} = 0$; where $K = \frac{s(s+2)}{(s-2)}$.

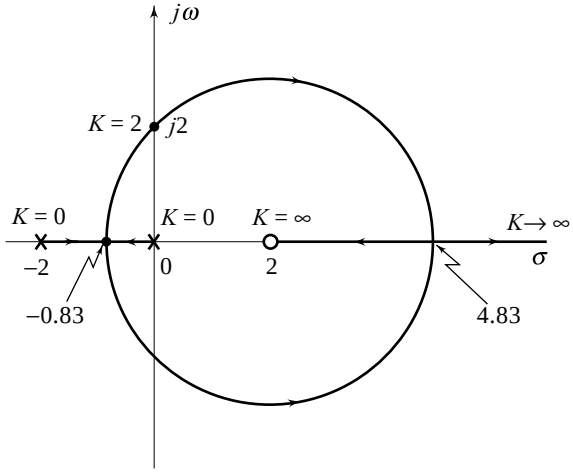

Fig. 7.52 Root locus plot for the characteristic equation (7.72)

The solutions are $s = -0.83,\ 4.83$.

The characteristic equation (7.72) can equivalently be expressed as

$$s^2 + (2 - K)\, s + 2K = 0$$

Obviously, $K = 2$ results in oscillations of frequency $\omega_0 = 2$. Therefore, the root loci intersect the imaginary axis at $s = \pm j2$; the value of K corresponding to these points is 2.

The complete root locus plot is sketched in Fig. 7.52. It can, in fact, be shown that the complex root branches of the root loci form a circle (refer Example 7.1).

Review Examples

Review Example 7.1 Several open-loop pole-zero configurations and their corresponding approximate root loci are given in Table 7.2. Computing (where applicable) (i) the large-gain asymptotes, (ii) the angles of departure from complex poles, (iii) the angles of arrival at complex zeros, (iv) the breakaway points, and (v) the frequency at which the root loci cross the imaginary axis, is left as an exercise for the reader. This exercise will help attain good practice on hand-sketching rules for constructing root-locus plots.

Table 7.2 Open-loop pole-zero configurations and the corresponding root loci (equal axes scales)

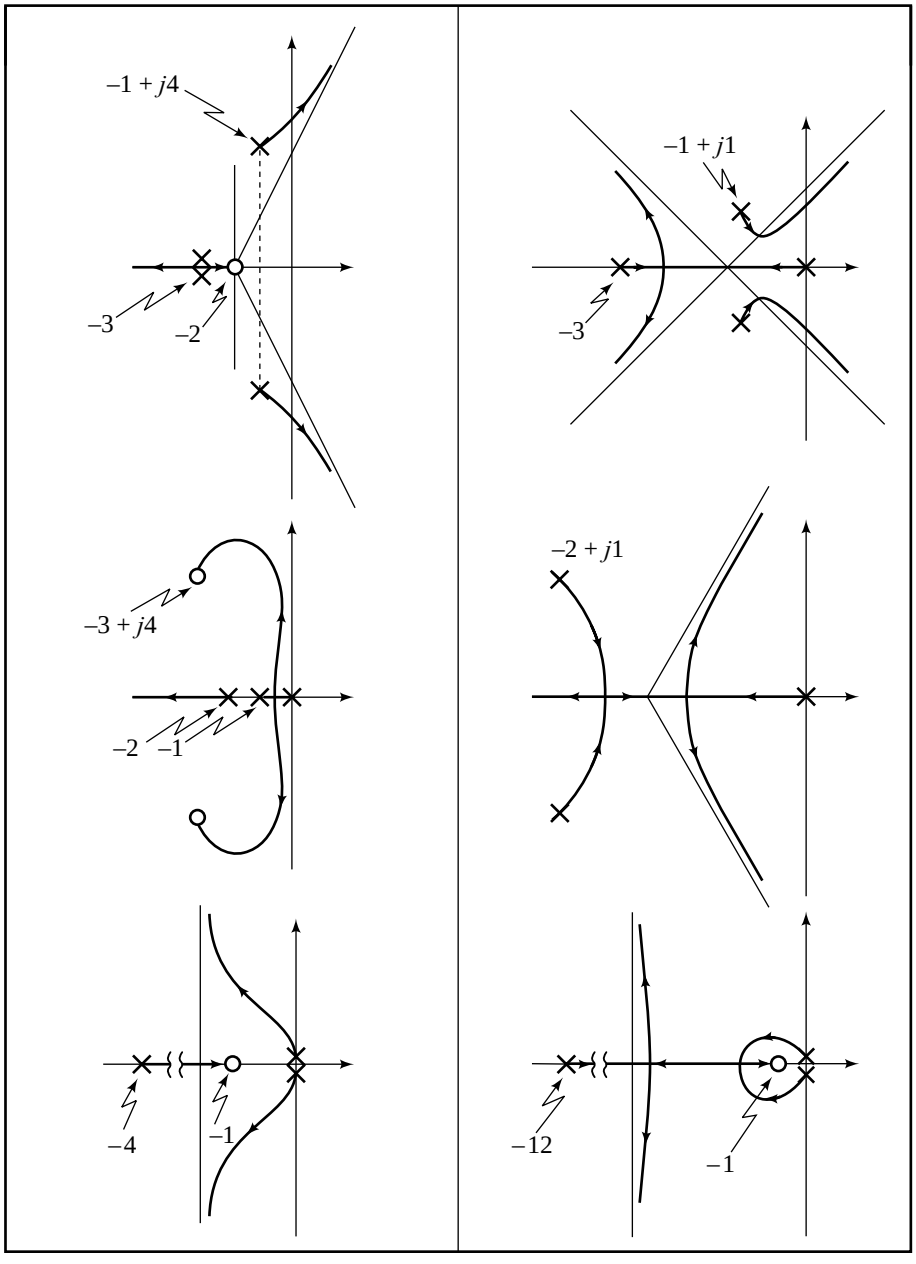

Review Example 7.2 Several open-loop pole-zero configurations and their corresponding approximate root loci were given in Table 7.2. Some additional examples are tabulated in Table 7.3. These examples have been selected to show multiple roots of various orders in root-locus plots. Estimating the locations of multiple roots (if any) and the order of multiplicity of the roots, is left as an exercise for the reader.

Table 7.3 Open-loop pole-zero configurations and the corresponding root loci (equal axes scales)

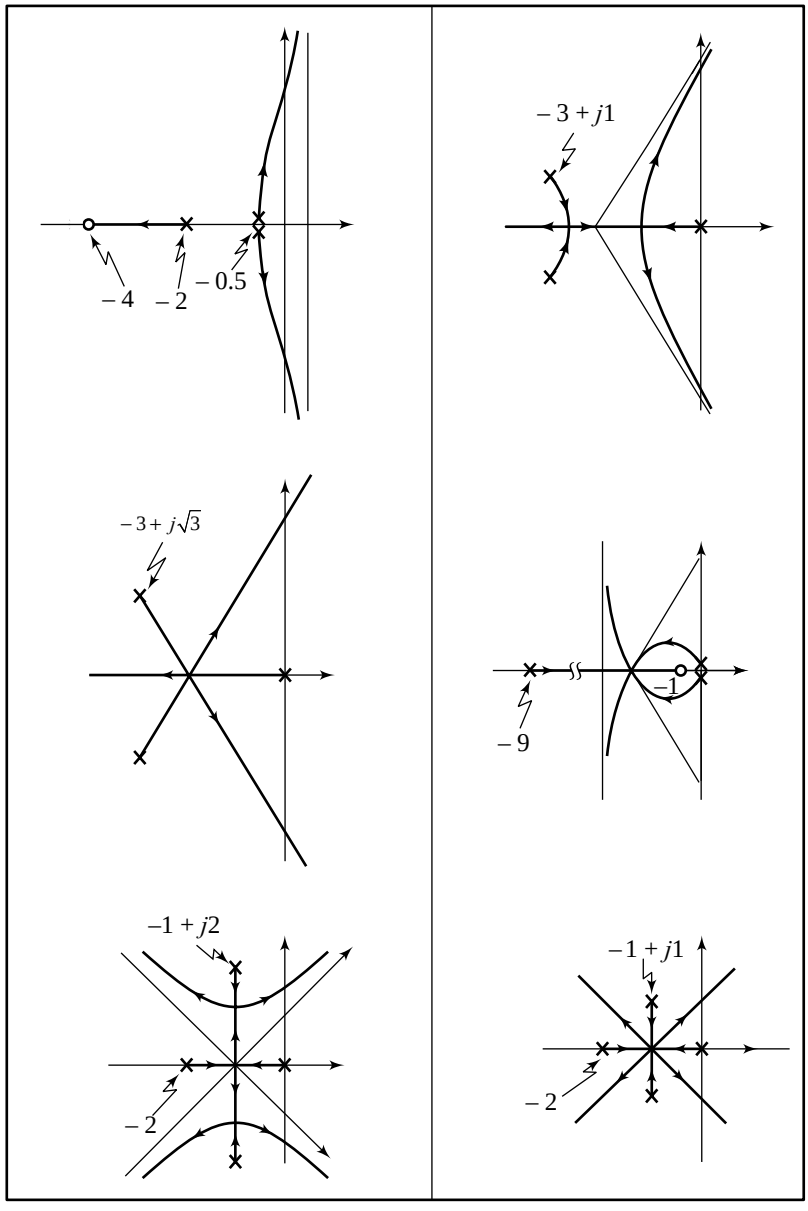

Review Example 7.3 The block diagram of Fig. 7.53 represents a position control system. The open-loop transfer function of the uncompensated system is

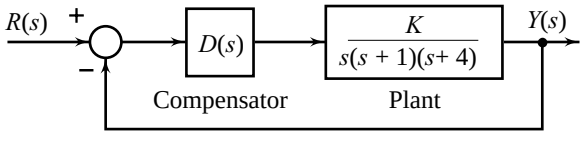

Fig. 7.53 A position control system

$$G(s) = \frac{K}{s(s+1)(s+4)}$$

The specifications of the system are as follows:

Damping ratio, $\zeta = 0.5$

Undamped natural frequency, $\omega_n = 2$ rad/sec

Velocity error constant, $K_v \geq 5$ sec^{-1}

The desired dominant closed-loop poles are required to be located at

$$s_{1,2} = -\zeta\omega_n \pm j\omega_n\sqrt{1-\zeta^2} = -1 \pm j1.73$$

Figure 7.54 shows the pole-zero plot of the plant $G(s) = \dfrac{K}{s(s+1)(s+4)}$, and a desired closed-loop pole at $s_d = -1 + j1.73$. From this figure, we find that

$$\angle G(s_d) = -120° - 90° - 30° = -240°$$

The point s_d, therefore, does not lie on the uncompensated root locus and transient response specifications cannot be met by gain adjustment alone. We propose to add a cascade lead compensator to meet the transient response specifications. In order for the root locus to go through s_d, the angle contribution from the lead compensator pole-zero pair must be

$$\phi = -180° - \angle G(s_d) = -180° - (-240°) = 60°$$

Further, it is observed that the open-loop pole at $s = -1$ lies directly below the desired closed-loop pole location. It appears that the best transient response due to the complex closed-loop pole will occur when the zero of the compensator cancels the open-loop pole at $s = -1$; there will be no real closed-loop pole near the imaginary axis in this case. This ideal situation, however, cannot be realized practically because of imperfect cancellation. A real closed-loop pole near the imaginary axis will occur but a zero will be very close to it; the dominance condition will therefore be ensured.

Join the compensator zero to s_d and locate the compensator pole making an angle of $\phi = 60°$ as shown in Fig. 7.54. The location of the pole is found to be at $s = -4$.

With the addition of the cascade lead compensator

$$D_1(s) = \frac{s+1}{s+4} = \frac{s+1/\tau_1}{s+1/\alpha\tau_1}; \ \tau_1 = 1, \ \alpha = \frac{1}{4}$$

the open-loop transfer function of the system becomes

$$D_1(s)G(s) = \frac{K(s+1)}{s(s+1)(s+4)^2} = \frac{K}{s(s+4)^2}$$

The value of K at s_d is found to be 24. Therefore,

$$D_1(s)G(s) = \frac{24}{s(s+4)^2}$$

The velocity error constant of the lead compensated system is

$$K_v^{lc} = \lim_{s\to 0} s\, D_1(s)G(s) = 1.5$$

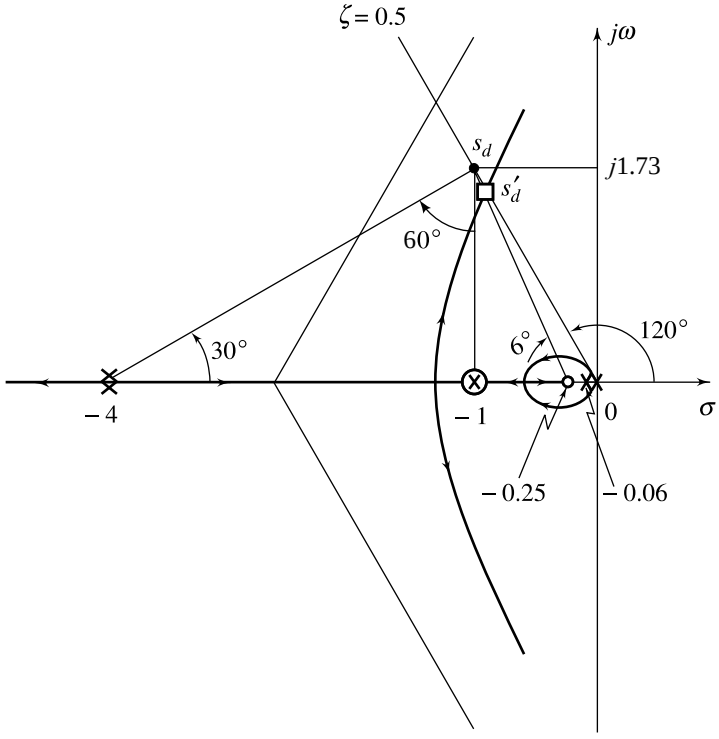

Fig. 7.54 Root locus plot (Review Example 7.3)

This does not meet the specified $K_v \geq 5$. A lag section

$$D_2(s) = \frac{s + 1/\tau_2}{s + \alpha/\tau_2} = \frac{s + 1/\tau_2}{s + 1/4\tau_2}$$

will increase K_v by about four times, which then satisfies the specifications on steady-state performance.

The line drawn from s_d making an angle of 6° with the desired ζ-line intersects real axis at – 0.25, which gives the location of the zero of the lag section. The pole of the lag section is then found to be at $-0.25/4 \cong -0.06$.

The open-loop transfer function of the lag-lead compensated system then becomes

$$D_2(s)D_1(s)G(s) = \frac{K^c(s + 0.25)}{s(s + 0.06)(s + 4)^2}$$

The root locus plot for the lag-lead compensated system is shown in Fig. 7.54. From this figure, the gain at s'_d (which is slightly shifted from s_d due to introduction of the lag section) is given by $K^c = 23.5$.

Therefore, the open-loop transfer function of the lag-lead compensated system is

$$D_2(s)D_1(s)G(s) = \frac{23.5(s + 0.25)}{s(s + 0.06)(s + 4)^2}$$

Review Example 7.4 Consider a plant with transfer function

$$G(s) = \frac{2}{s(s+1)(s+5)}$$

Design a feedback system to meet the specifications:

1. Velocity error as small as possible
2. $\zeta = 0.707$
3. Settling time < 4.5 seconds

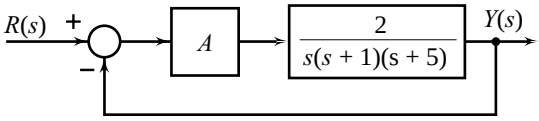

Fig. 7.55 A control configuration (Review Example 7.4)

Solution

As a first try, we choose a unity-feedback system shown in Fig. 7.55. The root locus plot of this system for $A > 0$ is shown in Fig. 7.56. In order for the feedback system to have settling time less than 4.5 seconds, all the closed-loop poles must lie on the left hand side of the vertical line passing through the point $-4/t_s = -4/4.5 = -0.9$. From the root loci in Fig. 7.56 we see that this is not possible for any $A>0$. Therefore, the configuration in Fig. 7.55 cannot meet the specifications.

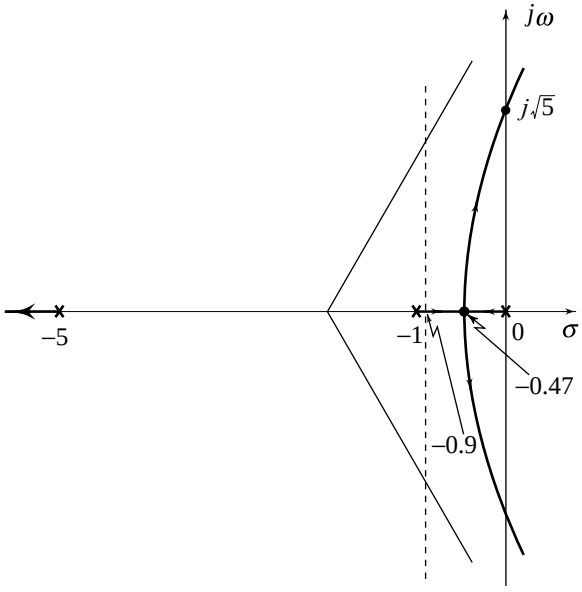

Fig. 7.56 Root locus plot for the system of Fig. 7.55

As a next try, we introduce an additional tachogenerator feedback as shown in Fig. 7.57. The characteristic equation of the system becomes

$$1 + \frac{AG(s)}{1 + sK_t G(s)} = 0 \qquad (7.73)$$

where $$G(s) = \frac{2}{s(s+1)(s+5)}.$$

Rearranging, we get

$$s^3 + 6\,s^2 + (5 + 2\,K_t)\,s + 2\,A = 0$$

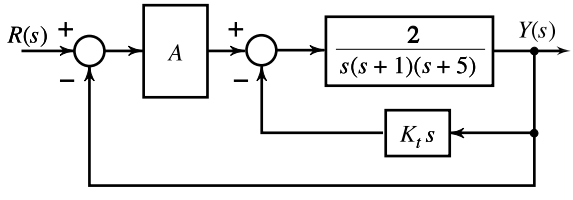

Fig. 7.57 Tachogenerator feedback control configuration (Review Example 7.4)

There are two variable parameters: A and K_t. We can use single-parameter root loci for the design by choosing a value for A. First we choose $A = 5$ and carry out the design. We will change the value of A appropriately if we find that the design is not acceptable with $A = 5$.

Partitioning of the characteristic equation with $A = 5$ gives

$$1 + \frac{2K_t s}{s^3 + 6s^2 + 5s + 10} = 0$$

or

$$1 + \frac{Ks}{(s + 5.42)(s + 0.29 + j1.33)(s + 0.29 - j1.33)} = 0$$

The root loci of this equation are plotted in Fig. 7.58. The $\zeta = 0.707$ line intersects the root locus at two points. Both the points lie on the left-hand side of the vertical line passing through -0.9. From Fig. 7.58, we see that the point $-1.2 + j1.2$ that corresponds to $K = 6.3$ (or $K_t = 3.15$), meets the dominance requirement better compared to the other point. We therefore select $K_t = 3.15$

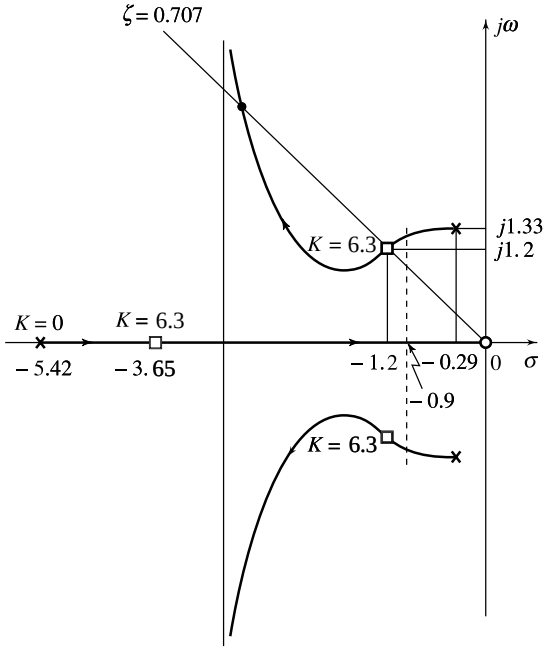

Fig. 7.58 Root locus plot for the system of Fig. 7.57

Let us now investigate the steady-state behaviour of the compensated system. From Eqn. (7.73), the velocity error constant K_v is given by

$$K_v = \lim_{s \to 0} s \left[\frac{AG(s)}{1 + sK_t G(s)} \right]$$

$$= \lim_{s \to 0} s \left[\frac{10}{s(s + 1)(s + 5) + 6.3s} \right] = \frac{10}{11.3}$$

A marginal increase in K_v above this value can be achieved by readjustment of the parameter A.

Review Questions

7.1 Discuss the compensation characteristics of cascade lag and lead compensators using root locus plots. Show that

(i) lead compensation is suitable for systems having unsatisfactory transient response, and it provides a limited improvement in steady-state performance; and

(ii) lag compensation is suitable for systems with satisfactory transient response but unsatisfactory steady-state response.

7.2 In many control systems, it is desirable to use a feedback compensator forming a minor loop around the plant, in addition to a cascade gain compensator which is used to adjust the overall performance. Discuss compensation characteristics of the minor-loop feedback scheme.

7.3 Sketch op amp circuits capable of realizing (i) PD, (ii) PI and (iii) PID control actions.

7.4 Sketch op amp circuits capable of realizing

(i) lead compensator. (ii) lag compensator, and (iii) lag-lead compensator.

Problems

7.1 For each of the open-loop transfer functions $F(s)$ given below, sketch the general shape of the root locus plot of the characteristic equation $1+F(s) = 0$, as the gain K is varied from 0 to ∞. Where applicable, the plot should include (i) the large-gain asymptotes, (ii) the angles of departure from complex poles of $F(s)$, (iii) the angles of arrival at complex zeros of $F(s)$, (iv) breakaway points, and (v) the frequency at which the root loci cross the $j\omega$-axis.

(a) $F(s) = \dfrac{K(s+2)}{(s+3)^2(s+1+j4)(s+1-j4)}$ (b) $F(s) = \dfrac{K}{s(s+3)(s^2+2s+2)}$

(c) $F(s) = \dfrac{K(s^2+6s+25)}{s(s+1)(s+2)}$ (d) $F(s) = \dfrac{K}{s(s^2+4s+5)}$

(e) $F(s) = \dfrac{K(s+1)}{s^2(s+4)}$ (f) $F(s) = \dfrac{K(s+1)}{s^2(s+12)}$

(g) $F(s) = \dfrac{K(s+4)}{(s+0.5)^2(s+2)}$

7.2 For each of the characteristic equations given below, estimate locations of multiple roots (if any), and the order of multiplicity of roots. Roughly sketch the root locus plot in each case showing clearly the directions of root loci approaching the points of multiple roots, and the directions at which the loci break away from these points.

(i) $1 + \dfrac{K}{s(s^2+6s+10)} = 0; K \geq 0$ (ii) $1 + \dfrac{K}{s(s^2+6s+12)} = 0; K \geq 0$

(iii) $1 + \dfrac{K(s+1)}{s^2(s+9)} = 0;\ K \geq 0$ (iv) $1 + \dfrac{K}{s(s+2)(s^2+2s+5)} = 0;\ K \geq 0$

(v) $1 + \dfrac{K}{s(s+2)(s^2+2s+2)} = 0;\ K \geq 0$

7.3 A unity-feedback control system has an open-loop transfer function

$$G(s) = \frac{K}{s(s+1)(s+2)};\ K \geq 0$$

Make a rough sketch of the root locus plot of the system, explicitly identifying the centroid, the asymptotes, the breakaway points and $\pm j\omega$-axis cross-over points. By a trial-and-error application of the angle criterion, locate a point on the locus that gives dominant closed-loop poles with $\zeta = 0.5$. Determine the value of K at this point. Corresponding to this value of K, determine the closed-loop transfer function of the system.

MATLAB Exercise Verify your rough sketch with a MATLAB plot. Turn in your hand sketch and the MATLAB plot on the same scale. Also use MATLAB to obtain the closed-loop step response and validate or refute your second-order approximation.

7.4 A unity-feedback control system has an open-loop transfer function

$$G(s) = \frac{K}{s(s+4)(s^2+8s+32)};\ K \geq 0$$

Make a rough sketch of the root locus plot of the system, explicitly identifying the centroid, the asymptotes, the breakaway points, the departure angles from poles of $G(s)$, and the $\pm j\omega$-axis cross-over points. By a trial-and-error application of the angle criterion, locate a point on the locus that gives dominant closed-loop poles with $\zeta = 0.707$. Determine the value of K at this point. Corresponding to this value of K, roughly locate the other two closed-loop poles and comment upon the dominance condition.

MATLAB Exercise Verify your rough sketch with a MATLAB plot. Turn in your hand sketch and the MATLAB plot on the same scale. Also check the accuracy of the second-order approximation using MATLAB to simulate the system.

7.5 A unity-feedback control system has an open-loop transfer function

$$G(s) = \frac{K}{s(s^2+8s+32)};\ K \geq 0$$

Make a rough sketch of the root locus plot of the system, explicitly identifying the centroid, the asymptotes, the departure angles from complex poles of $G(s)$, and the $\pm j\omega$-axis cross-over points. By a trial-and-error application of the angle criterion, locate a point on the locus that gives dominant closed-loop poles with $\zeta = 0.5$. Determine the value of K at this point. Corresponding to this value of K, roughly locate the third closed-loop pole and comment upon the dominance condition.

MATLAB Exercise Verify your rough sketch with a MATLAB plot. Turn in your hand sketch and the MATLAB plot on the same scale. Also check the accuracy of the second-order approximation using MATLAB to simulate the system.

7.6 Draw the root locus plot for a control system with unity feedback having the forward-path transfer function

$$G(s) = \frac{K}{s(s+1)(s+5)}\,;\ K \geq 0$$

Give all relevant characteristics of the curves that are useful in establishing the locus.
Find the least value of K to give an oscillatory response and the greatest value of K that can be used before continuous oscillations occur. Find the frequency of the continuous oscillations when K is just large enough to give this condition.

MATLAB Exercise Attempt this problem using MATLAB dialogues.

7.7 Prove that a combination of two poles $s = -a_1$ and $s = -a_2$ and one zero $s = -b$ to the left of both of them on the real axis, results in a root locus whose complex root branches form a circle centred at the zero with radius given by $\sqrt{(b-a_1)(b-a_2)}$; the root locus gain varying from 0 to ∞.

7.8 Consider a unity-feedback system with a forward path transfer function

$$G(s) = \frac{K(s+3)}{s(s+2)}\,;\ K \geq 0$$

Show that part of the root locus is a circle.
Construct the root locus and determine the damping ratio for maximum oscillatory response. What is the value of K at this point of the locus?

7.9 Prove that the combination of two complex-conjugate poles $s_{1,2} = -\alpha \pm j\beta$ and a real zero $s = -b$ results in a root locus whose complex root branches lie on a circle centred at the zero with radius = $\sqrt{(\alpha-b)^2+\beta^2}$; the root locus gain varies from 0 to ∞.

7.10 Consider a unity-feedback system with open-loop transfer function

$$G(s) = \frac{K(s^2+1)}{s(s+2)}\,;\ K \geq 0$$

Sketch the root locus plot. Show that the complex root branches lie on a circle.

7.11 Consider a unity-feedback system with a forward path transfer function

$$G(s) = \frac{K(s+4)}{(s+2)(s-1)}\,;\ K \geq 0$$

Draw a root locus plot and find the value of K that results in $\zeta = 0.707$ and $t_s < 4$ sec. Determine the peak overshoot, the settling time, and the position error for this value of K.

MATLAB Exercise Attempt this problem using MATLAB dialogues.

7.12 Sketch the root locus plot for the system shown in Fig. P7.12 as K varies from 0 to ∞. Show that the complex root branches of the plot form a circle.
Find the value of K that results in (i) damping ratio ζ =1, and (ii) minimum steady-state error to ramp inputs.

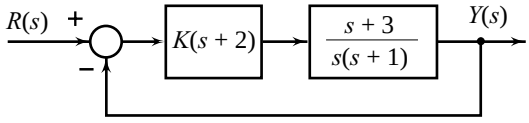

Fig. P7.12

7.13 Consider the control loop shown in Fig. P7.13. Sketch the root locus plot as K varies from 0 to ∞. Find the value of K that yields an oscillatory response of the control loop with a damping ratio of 0.707.

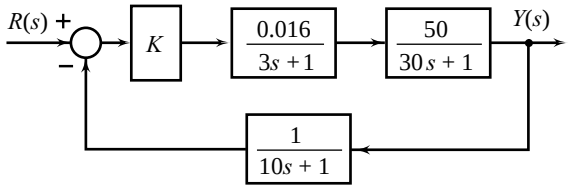

Fig. P7.13

MATLAB Exercise Attempt this problem using MATLAB dialogues.

7.14 Figure P7.14 represents a position servo with an appreciable sensor time-constant.
(a) Plot root loci and find $K > 0$ for a damping ratio of 0.5 for unity feedback (i.e., assuming an ideal feedback sensor).
(b) If the actual sensor has in fact an appreciable time-constant, what will be the actual damping ratio if the value of K found in part (a) is used? An approximate answer will suffice.

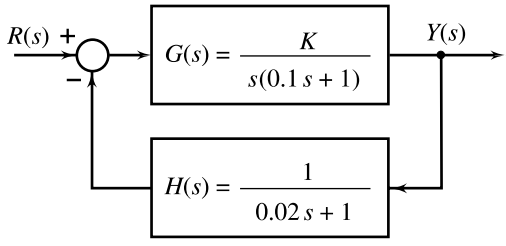

Fig. P7.14

7.15 Consider the system shown in Fig. P7.15. Sketch the root locus plot of the system as gain K varies from 0 to ∞. Determine the value of K such that the damping ratio ζ of the dominant closed-loop poles is 0.5. For the selected value of K, find all the closed-loop poles.

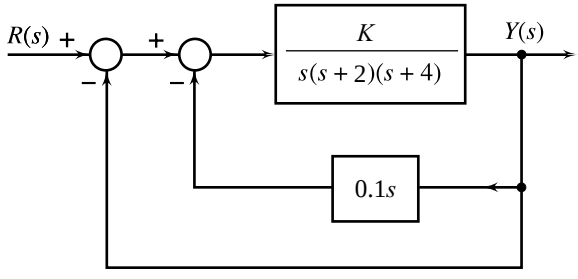

Fig. P7.15

MATLAB Exercise Attempt this problem using MATLAB dialogues.

7.16 Consider the servo system shown in Fig. P7.16. Sketch the root locus plot of the system as the velocity feedback constant K_t varies from 0 to ∞. Determine the value of K_t such that the closed-loop poles have a damping ratio of 0.7.

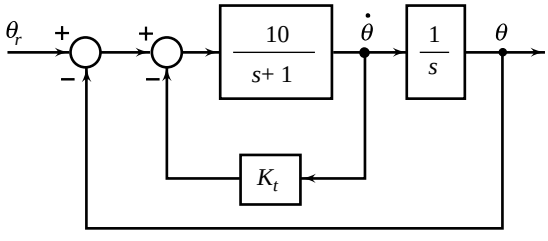

Fig. P7.16

MATLAB Exercise Attempt this problem using MATLAB dialogues.

7.17 Consider the system shown in Fig. P7.17. Draw the root locus plot of the system as K_t is varied from 0 to ∞. Determine the value of K_t such that damping ratio of the dominant closed-loop poles is 0.4.
If more than one solution to the above problem is possible, then select a solution that meets the dominance condition better.

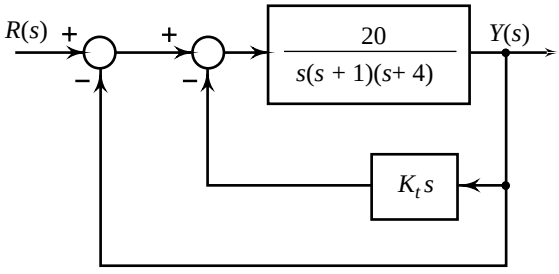

Fig. P7.17

7.18 Consider the system shown in Fig. P7.18. Draw the root locus plot of the system as α is varied from 0 to ∞. Determine the value of α such that damping ratio ζ of the dominant closed-loop poles is 0.5. For the selected value of α, find all the closed-loop poles.

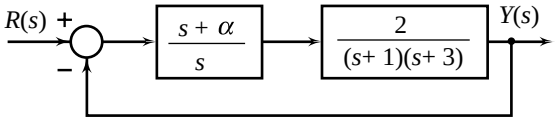

Fig. P7.18

MATLAB Exercise After solving the problem using hand sketches, attempt it using MATLAB. Determine settling time and peak overshoot of the compensated and uncompensated systems.

7.19 Consider the system shown in Fig. P7.19. Draw the root locus plot of the system as α is varied from 0 to ∞. Determine the value of α such that damping ratio ζ of the dominant closed-loop poles is 0.5. For the selected value of α, find all the closed-loop poles.

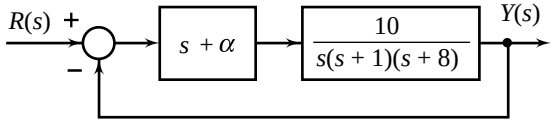

Fig. P7.19

MATLAB Exercise After solving the problem using hand sketches, attempt it using MATLAB. Determine settling time and peak overshoot of the compensated and uncompensated systems.

7.20 Consider the feedback system of Fig. P7.20. Note that the plant is open-loop unstable.

(a) Plot the root loci to determine whether the system can be stabilized by proportional control, i.e., $D(s) = K$.

(b) If not, could the unstable pole of $G(s)$ be cancelled by a zero of $D(s)$ to stabilize the system, and if not, why not?

(c) Choose a compensator $D(s) = \dfrac{K(s+1)}{s+8}$ and sketch root loci. How does this phase-lead compensator affect the transient as well as steady-state behaviour?

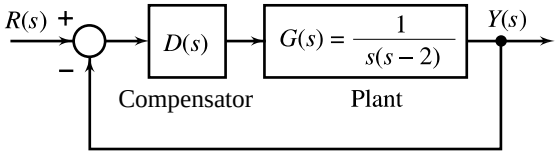

Fig. P7.20

MATLAB Exercise The pole of the physical plant may be different from the one given by its model. Cancellation of the pole of the model by compensator zero may not yield stable closed-loop when the compensator is cascaded to the physical plant. Show this by generating root locus plots in MATLAB window with compensator zero at $s = 2$, and the plant pole varying between $s = 1.5$ and $s = 2.5$.

7.21 A unity-feedback system has an open-loop transfer function

$$G(s) = \frac{K}{s(s+1)(s+5)}$$

Draw the root locus plot and determine the value of K that yields a damping ratio of 0.3 for the dominant closed-loop poles. A phase-lag compensator having a transfer function

$$D(s) = \frac{10s+1}{100s+1}$$

is now introduced in tandem. Find the new value of K that gives the same damping ratio for the dominant closed-loop poles. Compare the velocity error constant and settling time of the original and the compensated systems.

MATLAB Exercise You have approximated the closed-loop system by a second-order system, assuming the dominance condition is satisfied. Generate root locus plots of the original and compensated systems in MATLAB window and determine all the closed-loop poles for the two systems. Also generate step responses in the MATLAB window and find settling time and steady-state error in the two cases. Comment whether dominance condition was satisfied.

7.22 A unity-feedback system has forward path transfer function

$$G(s) = \frac{K}{s(s+1)}$$

It is required that the closed-loop poles be located at $s_{1,2} = -1.6 \pm j4$ using a lead compensator with transfer function $D(s) = \dfrac{s+2.5}{s+\alpha}$.

Determine the values of α and K to locate the closed-loop poles as required. What is the location of the third closed-loop pole?

MATLAB Exercise Attempt this problem using MATLAB dialogues.

7.23 Consider the type-1 system of Fig. P7.23. We would like to design the compensator $D(s)$ to meet the following specifications:

(i) Damping ratio $\zeta = 0.707$ (ii) Settling time ≤ 2 sec

(a) Show that the proportional control is not adequate.

(b) Show that proportional plus derivative control will work.

(c) For $D(s) = K_P + K_D s$, find gains K_P and K_D to meet the design specifications.

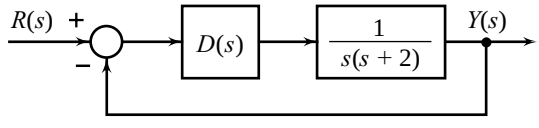

Fig. P7.23

MATLAB Exercise After solving the problem using hand sketches, attempt it using MATLAB. Determine settling time and peak overshoot of the compensated and uncompensated systems.

7.24 A unity-feedback servo system has open-loop transfer function

$$G(s) = \frac{100(1+10s)}{s(1+0.2s+0.25s^2)}$$

A second-order cascade compensator

$$D(s) = \frac{s^2+0.8s+4}{(s+0.384)(s+10.42)}$$

cancels the complex poles of $G(s)$. Using root-locus analysis, compare the transient performance of compensated and uncompensated systems. What is the effect of $D(s)$ on steady-state performance?

7.25 Determine the values of K, z, and p of the system shown in Fig. P7.25, so that (i) the dominant closed-loop poles have damping ratio $\zeta = 0.45$ and (ii) velocity error constant $K_v = 20$.

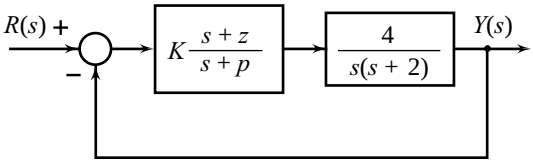

Fig. P7.25

MATLAB Exercise Verify your solution using MATLAB, and if required refine your design. Due to uncertainties in the load, the time-constant of the plant may vary by 10%. Check the robustness of your design by determining transient and steady-state performance for various values of this time-constant.

7.26 The controlled plant of a unity-feedback system is

$$G(s) = \frac{K}{s(s+1)(s+5)}$$

It is desired to compensate the system so as to meet the following transient response specifications.
Settling time, $t_s \leq 3$ sec
Peak overshoot for step input ≤ 20 %

Design a suitable cascade compensator (choose the compensator zero so as to cancel the plant pole at $s = -1$). What is the velocity error constant of the compensated system?

MATLAB Exercise Attempt this problem using MATLAB dialogues.

7.27 The controlled plant of a unity-feedback system is

$$G(s) = \frac{K}{s(s+1)}$$

It is desired to compensate the system so as to meet the following transient response specifications:
Damping ratio, $\zeta = 0.707$
Settling time, $t_s = 1.4$ sec

Design a suitable first-order or second-order (two first-order sections in cascade) lead compensator for the system.

7.28 The controlled plant of a unity-feedback system is

$$G(s) = \frac{1.06}{s(s+1)(s+2)}$$

Sketch a root locus plot of the system, and determine the dominant closed-loop poles and the velocity error constant.

It is desired to increase the velocity error constant to about 5 sec^{-1} without appreciably changing the location of the dominant closed-loop poles. Design a first-order cascade compensator $D(s) = \dfrac{K(s+z)}{s+p}$ to meet this specification.

MATLAB Exercise Attempt this problem using MATLAB dialogues.

7.29 Consider the type-0 system of Fig. P7.30. We would like to design the compensator $D(s)$ to meet the following specifications:

(i) Damping ratio, $\zeta = 0.6$
(ii) Time constant $\tau = 1/\zeta\omega_n = 1/0.75$
(iii) Zero steady-state error for a step input.

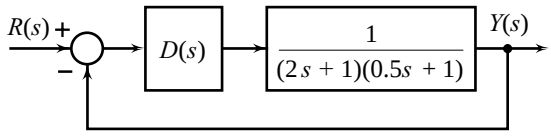

Fig. P7.30

(a) Show that the proportional control is not adequate.
(b) Show that proportional plus integral control will work.
(c) For $D(s) = K_P + \dfrac{K_I}{s}$, find gains K_P and K_I to meet the design specifications.

MATLAB Exercise After solving the problem using hand sketches, attempt it using MATLAB. Determine settling time and peak overshoot of the compensated and uncompensated systems.

7.30 The controlled plant of a unity-feedback system is

$$G(s) = \frac{K}{s(s+10)(s+20)}$$

Determine the value of K so that the damping ratio of the dominant closed-loop poles is 0.6. For this value of K, determine the velocity error constant K_v.

It is desired to increase K_v by a factor of 10. It is also desired to keep the damping ratio of the dominant closed-loop poles at 0.6. A small change in the undamped natural frequency of the dominant closed-loop poles is permissible.

(a) Design a suitable cascade lead, lag, or lag-lead compensator to realize the given objectives.
(b) Design a suitable cascade PD, PI, or PID compensator to realize the given objectives.

MATLAB Exercise Attempt this problem using MATLAB dialogues.

7.31 The controlled plant of a unity-feedback system is

$$G(s) = \frac{K}{s(s+10)^2}$$

It is specified that velocity error constant of the system be equal to 20, while the damping ratio of the dominant roots be 0.707.

(a) Design a suitable cascade lead, lag, or lag-lead compensator to realize the given objectives.
(b) Design a suitable cascade PD, PI, or PID compensator to realize the given objectives

MATLAB Exercise Attempt this problem using MATLAB dialogues.

7.32 Controlled plant of a unity-feedback system is

$$G(s) = \frac{K}{s(s+1)(s+5)}$$

It is desired to compensate the system so as to meet the following specifications:
Damping ratio of dominant roots = 0.45
Undamped natural frequency of dominant roots = 3.5 rad/sec
Velocity error constant = 30 sec^{-1}

Design a cascade lag-lead compensator to meet these objectives (choose the zero of the lead section of the compensator to cancel the plant pole at $s = -1$).

MATLAB Exercise Verify and refine your design using MATLAB. Determine settling time and peak overshoot of the compensated system.

7.33 Controlled plant of a unity-feedback system is

$$G(s) = \frac{1}{s^2+1}$$

(a) Design a PD controller such that the dominant closed-loop poles are located at $-1 \pm j\sqrt{3}$. What is the position error constant of the compensated system?
(b) It is desired to reduce the steady-state error to step inputs to zero. Design a PID controller that meets the requirements on both the transient and the steady-state performance.

7.34 A unity-feedback system is characterized by the open-loop transfer function

$$G(s) = \frac{K}{s(s+3)(s+9)}$$

(a) Determine the value of K if 20% overshoot to a step input is desired.
(b) For the above value of K, determine the settling time and velocity error constant K_v.
(c) Design a suitable cascade lead, lag or lag-lead compensator that will give approximately 15% overshoot to a unit-step input, while the settling time is decreased by a factor of 2.5 with $K_v \geq 20$.
(d) Design a suitable PD, PI, or PID compensator to realize the objectives given in (c).

MATLAB Exercise You have employed second-order correlations to solve this problem using hand sketches. Verify your solution using MATLAB, and if required refine your design.

7.35 For a plant with transfer function $G(s) = \dfrac{K}{s(s+2)}$, a feedback system is to be designed to satisfy the following specifications:

(i) Steady-state error for a ramp input $\leq$ 35 % of input slope
(ii) Damping ratio of dominant roots ≥ 0.707
(iii) Settling time of the system ≤ 3 sec

The structure of the control system is shown in Fig. P7.35. Select the parameters K and K_t to meet the given specifications.

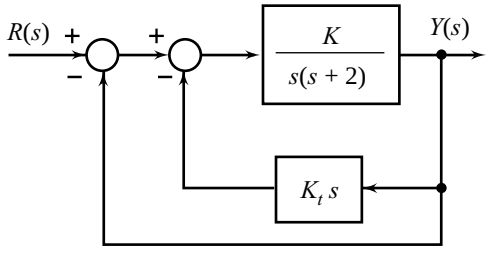

Fig. P7.35

MATLAB Exercise The parameter K_t is subject to variations by 10%. Check by simulation the robustness of the closed-loop system to these variations by determining settling time and K_v for various values of K_t.

7.36 For a plant with transfer function $G(s) = \dfrac{K}{s(s+1)(s+5)}$, a feedback system is to be designed to satisfy the following specifications:

(i) Dominant closed-loop poles at $-1 \pm j2$.
(ii) Ramp error constant, $K_v \geq 1.5$.

The structure of the control system is shown in Fig. P7.36.

(a) Select the parameters A, K, and K_t to meet the given specifications.
(b) Find the closed-loop transfer function of the system.

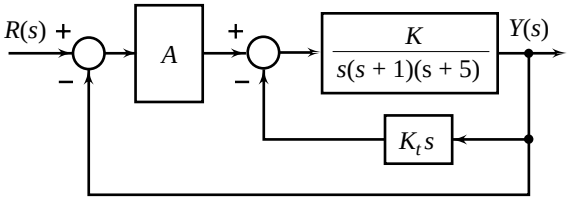

Fig. P7.36

7.37 A unity-feedback control system has an open-loop transfer function

$$G(s) = \frac{Ke^{-s}}{s+1}$$

Sketch a root locus plot of the system as K is varied from 0 to ∞, using the approximation

$$e^{-s} = \left(1 - \frac{1}{2}s\right) \Big/ \left(1 + \frac{1}{2}s\right) .$$

Show that the complex root branches form a circle.

Nyquist/Bode Frequency Response Plots and System Stability

8

8.1 INTRODUCTION

In the preceding chapters, we have presented techniques for the analysis and design of feedback control systems based on pole-zero (root locus) formalism. An overview of the control-system design procedure is as follows.

Step 1: Construct transfer function models for the controlled process, the actuator, and the sensor. Validate the models with experimental data where possible.

Step 2: Investigate the stability properties of a feedback structure of the form shown in Fig. 8.1.
The stability as we know, is dictated by the poles of the closed-loop transfer function

$$\frac{Y(s)}{R(s)} = \frac{G(s)}{1 + G(s)H(s)}$$

Given the open-loop transfer function $G(s)H(s)$, the stability of the closed-loop transfer function can be determined using Routh stability criterion, without actually computing the closed-loop poles. The root locus plots are more informative.

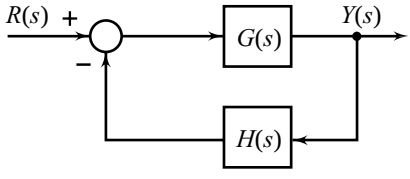

Fig. 8.1 A feedback control system

Step 3: Translate the performance requirements on time response into pole-zero specifications.
A typical result of this step is a requirement that the system has a step response with specified limits on rise time, peak overshoot, and settling time. This requirement is translated into a pair of dominant poles in the specified region of the s-plane. The maximum allowable steady-state error in tracking standard test signals is also specified.

Step 4: Shape the root locus plot by simple cascade compensators and/or minor-loop feedback compensators. Try to meet the specifications on dominant closed-loop poles and steady-state accuracy.
Compare the trial-and-error compensators with respect to parametric sensitivity, and the effects of sensor noise and external disturbances. If a design seems satisfactory, go to step 6; otherwise try step 5.

Step 5: Re-evaluate the specifications, the physical configuration of the process, and the actuator and sensor selections in the light of the current design and go to step 1.

Step 6: Build a computer model and compute (simulate) the performance of the design (Appendix A). The computer model of the system must include important nonlinearities, and other modelling uncertainties. Such a simulation of the design will confirm robustness, and allow one to predict the true performance to be expected from the system. If the performance is not satisfactory, go to step 1.

Step 7: Build a prototype.
As a final test before production, a prototype can be built and tested. After these tests, one might want to reconsider the sensor, actuator, and process, and conceivably return to step 1—unless time, money, or ideas have run out.

The root locus design technique, developed by Walter R. Evans in 1948, is highly attractive because it offers the designer the advantage of dealing directly with the poles and zeros of a closed-loop system, enabling him/her to exert direct influence on the dynamic behaviour of the system. By the judicious location of poles and zeros of compensation devices, the designer can see almost at a glance the manner in which the transient response of the closed-loop system is affected. Construction of the root locus plots to acceptable engineering accuracy is straightforward. The success of the method is, however, dependent upon the availability of reasonably accurate pole-zero models of the process, the actuator, and the sensor. Robustness against modelling uncertainties may not be satisfactory.

We now turn our attention to a design technique that uses only the information of $G(s)$ and $H(s)$ along the positive imaginary axis, that is, $G(j\omega)$ and $H(j\omega)$ for all $\omega \geq 0$; and is called the *frequency domain technique*. Chronologically, the frequency-domain technique was the first method developed to design control systems. Harry Nyquist in 1932 published his study of stability theory, which is the foundation of the frequency-domain approach to control system analysis and design. The Nyquist criterion is a graphical procedure for illustrating system stability, or lack thereof. The required Nyquist plot can usually be sketched quickly without extensive mathematical calculations. System stability and the margins by which that stability is obtained (relative stability) are readily apparent from the sketch.

The general objective in all the frequency-domain design procedures is to shape the Nyquist plot to achieve acceptable closed-loop response characteristics. Direct use of the Nyquist plot for design is not particularly convenient, since changes in parameters other than gain require extensive plot revisions. The work of Hendrik W. Bode during the 1930s led to a more efficient design procedure: the general characteristics of the Nyquist plot can be visualized with reasonable accuracy in most cases of interest from the Bode plot and the Bode plot is easily constructed and modified. The frequency-domain design procedures are reduced to orderly graphical trial-and-error processes carried out using the Bode plot. Thus, although the Nyquist plot characteristics form the basis for all of our designs, the mechanics of the design procedures are readily established on the Bode plot without requiring the construction of Nyquist plot.

A preview of the frequency-domain design procedure is as follows.

Step 1: Construct transfer function models for the controlled process, the actuator, and the sensor. Validate the models $G(s)$ and $H(s)$ (refer Fig. 8.1) with experimental data where possible. Compute $G(j\omega)$ and $H(j\omega)$; $\omega \geq 0$.

Note that the frequency-domain methods use only $G(j\omega)$ and $H(j\omega)$ which, for stable devices, can be obtained by direct measurement. Once $G(j\omega)$ and $H(j\omega)$ are measured, we may proceed directly to the design without computing the transfer functions $G(s)$ and $H(s)$.

Step 2: Investigate stability properties of a feedback structure of the form shown in Fig. 8.1. Given the data $G(j\omega)$ and $H(j\omega)$; $\omega \geq 0$, computed from $G(s)$ and $H(s)$ with s replaced by $j\omega$, or obtained by experimental measurement, the stability of the closed-loop system can be determined by the Nyquist stability criterion using Nyquist plots/Bode plots.

Step 3: Translate the performance requirements into frequency-domain specifications. There is a definite correlation between the time-domain and frequency-domain modes of behaviour. A common procedure is to interpret desired time-domain behaviour (step response with specified limits on rise time, peak overshoot, and settling time) in terms of frequency-domain characteristics. Design is carried out in the frequency domain and is translated back into the time domain. There is a constant interplay of characteristics between the two domains.

Thus the correlation between the time-domain and frequency-domain modes of behaviour plays a major role in the design procedure. Unfortunately, this correlation is not a simple one mathematically. Accordingly, in dealing with the problem of stabilizing and compensating control systems by using the frequency-domain techniques, control over the time-domain behaviour is most conveniently secured in terms of appropriate figures of merit such as gain margin, phase margin, bandwidth, etc., which although defined in frequency domain, are used as indicators of the performance in time domain. These figures of merit provide only an approximate correlation between the time-domain and frequency-domain characteristics. This is probably the major limitation of the frequency-domain approach; it sacrifices direct control on the time-domain performance. The major gain is the robustness against modelling uncertainties and external disturbances.

Step 4: Shape the Bode plot by simple cascade compensators and/or minor-loop feedback compensators. Try to meet the specifications on transient response (given in terms of frequency-domain measures) and steady-state accuracy.

Compare the trial-and-error compensators with respect to parameteric sensitivity, and the effects of sensor noise and external disturbances. If a design seems satisfactory, go to step 6; otherwise try step 5.

Step 5: Re-evaluate the specifications, the physical configuration of the process, and the actuator and sensor selections in the light of the current design and go to step 1.

Step 6: Build a computer model and compute (simulate) the performance of the design. The computer model must include important nonlinearities, and other modelling uncertainties (Appendix A).

Since the preliminary design is based on the approximate correlations between time-domain and frequency-domain modes of behaviour, the time-domain specifications must be checked before final parameter choices are made. A simulation study is generally the most appropriate method for this purpose.

Step 7: Build a prototype.

It may be noted that each design method, root locus or Bode plot, has its own particular use and advantage in a particular situation. As the reader becomes fully acquainted with these methods, he/she will become aware of the potentialities of each and will know when each should be used. We normally attempt the design using both the time-domain and frequency-domain approaches; this way one can gain an additional perspective to the complex analysis and design problems of feedback control systems.

The following strengths of the frequency-domain approach will become clear as we take up the subject.

1. The method does not need precise mathematical description of systems. The root locus method needs reasonably accurate mathematical description. The frequency-domain approach leads to robust design.
2. The method is independent of the complexity of systems and is applicable to systems containing time-delay elements. The root locus method, as we know, needs an approximate description of time-delay elements.
3. The method gives a simple and orderly approach for trial-and-error design.
4. It provides a very good indication of the system bandwidth which often appears explicitly in the specifications, and can only be approximated with the root-locus method of design.

The major limitation is that the direct control on the time-domain performance is lost.

The present chapter is concerned with the stability analysis in frequency domain. A frequency-domain stability criterion was developed by H. Nyquist in 1932 and remains a fundamental approach to the investigation of stability of linear control systems. In addition to answering the question of absolute stability, this criterion also gives some useful results on relative stability. The relative stability measures given by the Nyquist stability criterion are, in fact, central to the great importance of frequency-domain design methods.

We first develop the Nyquist stability criterion. Two common types of frequency-domain plots (Nyquist plots, Bode plots) are then introduced, and using these plots, absolute and relative stability are investigated on the basis of the Nyquist stability criterion. The use of the Nyquist criterion in frequency-domain design procedures will appear in the next two chapters.

8.2 DEVELOPMENT OF THE NYQUIST STABILITY CRITERION

In order to investigate the stability of a control system, we consider the closed-loop transfer function

$$\frac{Y(s)}{R(s)} = \frac{G(s)}{1 + G(s)H(s)} \tag{8.1}$$

keeping in mind that the transfer functions of both the single-loop and the multiple-loop control systems can be expressed in this form. The characteristic equation of the closed-loop system is obtained by setting the denominator of $Y(s)/R(s)$ to zero, which is same as setting the numerator of $1 + G(s)H(s)$ to zero. Thus, the roots of the characteristic equation must satisfy

$$1 + G(s)H(s) = 0 \tag{8.2}$$

We assume at this point that $G(s)H(s)$ can be expressed by a ratio of finite algebraic polynomials in s. This assumption has been made for convenience; the Nyquist criterion applies to more general situations, as shown subsequently. Let

$$G(s)H(s) = \frac{K(s + z_1')(s + z_2') \cdots (s + z_m')}{(s + p_1)(s + p_2) \cdots (s + p_n)}; \; m \le n \tag{8.3}$$

$G(s)H(s)$ is the product of plant, compensator, and sensor transfer functions; its pole and zero locations are assumed to be known since these transfer functions are generally available in factored form. Substituting for $G(s)H(s)$ from Eqn. (8.3) into Eqn. (8.2), we obtain

$$\begin{aligned} 1 + G(s)H(s) &= 1 + \frac{K(s + z_1')(s + z_2') \cdots (s + z_m')}{(s + p_1)(s + p_2) \cdots (s + p_n)} \\ &= \frac{(s + p_1)(s + p_2) \cdots (s + p_n) + K(s + z_1')(s + z_2') \cdots (s + z_m')}{(s + p_1)(s + p_2) \cdots (s + p_n)} \\ &= \frac{(s + z_1)(s + z_2) \cdots (s + z_n)}{(s + p_1)(s + p_2) \cdots (s + p_n)} \end{aligned} \tag{8.4}$$

It is apparent from Eqn. (8.4) that the poles of $1 + G(s)H(s)$ are identical to those of $G(s)H(s)$, i.e., the open-loop poles of the system; and the zeros of $1 + G(s)H(s)$ are identical to the roots of the characteristic equation, i.e., the closed-loop poles of the system. For the closed-loop system to be stable, the zeros of $1 + G(s)H(s)$ must lie in the left half of the s-plane. It is important to note that even if some of the open-loop poles lie in the right half s-plane, all the zeros of $1 + G(s)H(s)$, i.e., the closed-loop poles may lie in the left half s-plane, meaning thereby that an open-loop unstable system may lead to closed-loop stable operation.

Recall that we have introduced two methods of checking whether or not all zeros of $1 + G(s)H(s)$ have negative real parts. The zeros of $1 + G(s)H(s)$ are roots of the polynomial

$$(s + p_1)(s + p_2) \cdots (s + p_n) + K(s + z_1')(s + z_2') \cdots (z + z_m')$$

and we may apply the Routh test. Another method is to plot the root loci of

$$\frac{K(s + z_1')(s + z_2') \cdots (s + z_m')}{(s + p_1)(s + p_2) \cdots (s + p_n)} = -1$$

as a function of K. In this section, we shall introduce yet another method of checking whether or not all zeros of $1 + G(s)H(s)$ lie inside the open left half s-plane. The method, called the *Nyquist stability criterion*, is based on the *principle of argument* in the theory of complex variables [32]. The basic concept used in the Nyquist criterion is explained below (more details in Review Example 8.1).

Consider a rational function

$$1 + G(s)H(s) = Q(s) = \frac{s + z_1}{s + p_1}$$

The pole-zero map of $Q(s)$ is shown in Fig. 8.2a. This figure also shows a closed contour Γ_1. A point or an area is said to be *enclosed* by a closed path if it is found to lie to the right of the path when the path is traversed in the clockwise direction. The pole $-p_1$ and the zero $-z_1$ are therefore enclosed by the contour Γ_1 in Fig. 8.2a.

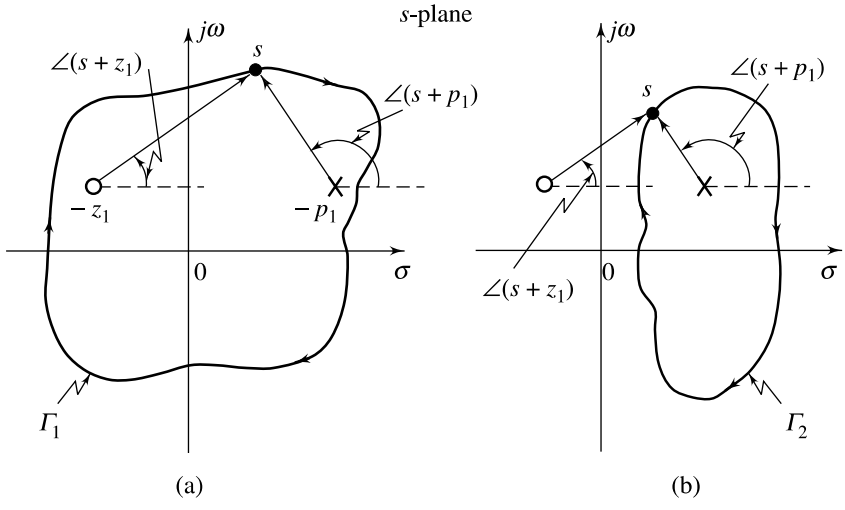

Fig. 8.2 (a) A contour which encloses both the pole and the zero
(b) A contour which encloses only the pole

Now we see that as the point s follows the prescribed path (i.e., clockwise direction) on the s-plane contour Γ_1, both $\angle(s + z_1)$ and $\angle(s + p_1)$ decrease continuously. For one clockwise traversal of Γ_1, we have

$$\delta_{\Gamma_1}\angle(s + z_1) = -2\pi$$
$$\delta_{\Gamma_1}\angle(s + p_1) = -2\pi$$

where $\delta_{\Gamma_1}\angle$ indicates the change in angle as Γ_1 is traversed.

$$\delta_{\Gamma_1}\angle Q(s) = \delta_{\Gamma_1}\angle(s+z_1) - \delta_{\Gamma_1}\angle(s+p_1)$$
$$= -2\pi - (-2\pi) = 0$$

Thus the change in $\angle Q(s)$ as s traverses Γ_1 (which is a completely general contour in the s-plane except that it encloses both $-z_1$ and $-p_1$) once in clockwise direction, is zero. Using these arguments on the contour Γ_2 in the s-plane which encloses only $-p_1$ and not $-z_1$ (Fig. 8.2b), we find that (for the zero $s = -z_1$ not enclosed by the contour Γ_2, $\delta_{\Gamma_2}\angle(s+z_1) = 0$ for one clockwise traversal of Γ_2)

$$\delta_{\Gamma_2}\angle Q(s) = 0 - (-2\pi) = 2\pi$$

We thus see that a change in $\angle Q(s)$ that one gets in traversing a contour in the s-plane, is strictly a function of how many poles and zeros of $Q(s)$ are enclosed by the s-plane contour. Let us consider a general $Q(s) = 1 + G(s)H(s)$, given by Eqn. (8.4), for which a typical pole-zero plot might be made as shown in Fig. 8.3. The figure also shows an s-plane contour Γ_s which encloses Z zeros and P poles of $Q(s)$. Note that Γ_s does not go through any of the poles or zeros of $Q(s)$. If we make one clockwise traversal of the contour Γ_s, it may be seen that

$$\delta_{\Gamma_s}\angle Q(s) = Z(-2\pi) - P(-2\pi)$$
$$= (P - Z)\,2\pi \qquad (8.5)$$

Another way of looking at the result of Eqn. (8.5) is to consider $Q(s)$ given by Eqn. (8.4) evaluated on the s-plane contour Γ_s of Fig. 8.3 and plotted in the $Q(s)$-plane. For every point $s = \sigma + j\omega$ on the s-plane contour Γ_s, we obtain $Q(s) = \mathrm{Re}Q + j\mathrm{Im}Q$. Alternatively, it can be stated that the function $Q(s)$ *maps* the point $\sigma + j\omega$ in the s-plane into the point $\mathrm{Re}Q + j\mathrm{Im}Q$ in the $Q(s)$-plane. It follows that for the closed contour Γ_s in the s-plane, there corresponds a closed contour Γ_Q in the $Q(s)$-plane. A typical Γ_Q is shown in Fig. 8.4. The arrowheads on this contour indicate the direction that $Q(s)$ takes as s moves on Γ_s in the clockwise direction. Now as we traverse Γ_Q once in the direction indicated by arrowheads, contour Γ_s in the s-plane is traversed once in the clockwise direction. For the example of Fig. 8.4, traversing Γ_Q once in the clockwise direction gives a change in $\angle Q(s)$ of -4π, since the origin is encircled twice in the negative direction. Thus Eqn. (8.5) gives

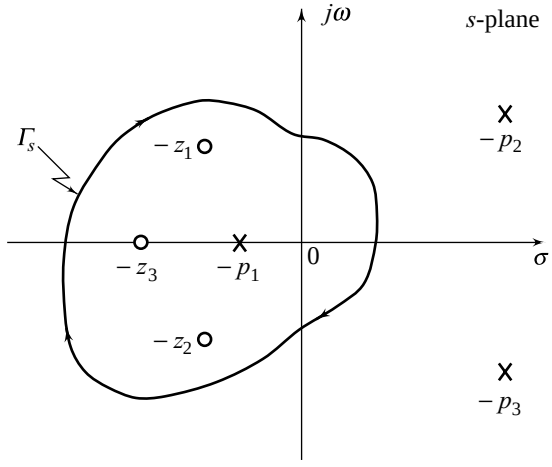

Fig. 8.3 A general pole-zero plot with contour Γ_s which encloses Z zeros and P poles

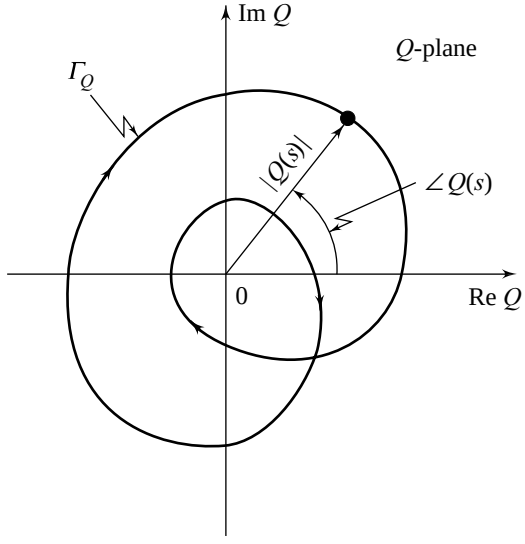

Fig. 8.4 Q(s) evaluated on the contour Γ_s in Fig. 8.3

$$\delta_{\Gamma_s} \angle Q(s) = 2\pi(P - Z) = -4\pi$$

or $$Z - P = 2$$

In general,

$$Z - P = N \tag{8.6}$$

where N is the number of clockwise encirclements of the origin that Γ_Q makes in the $Q(s)$-plane. It may be noted that we are not interested in the exact shape of the $Q(s)$-plane contour. The important fact that concerns us is the encirclements of the origin by the $Q(s)$-plane contour.

The relation (8.6) between the enclosure of poles and zeros of $Q(s)$ by the s-plane contour and the encirclements of the origin by the $Q(s)$-plane contour is commonly known as the *principle of argument* which may be stated as follows.

Let $Q(s)$ be a ratio of polynomials in s. Let P be the number of poles and Z be the number of zeros of $Q(s)$ which are enclosed by a simple closed contour in the s-plane, multiplicity accounted for. Let the closed contour be such that it does not pass through any poles or zeros of $Q(s)$. The s-plane contour then maps into the $Q(s)$-plane contour as a closed curve.

The number N of clockwise encirclements of the origin of the $Q(s)$-plane, as a representative point s traces out the entire contour in the s-plane in the clockwise direction, is equal to $Z - P$.

Since $$Q(s) = 1 + G(s)H(s),$$

we can obtain $Q(s)$-plane contour from the $G(s)H(s)$-plane contour simply by adding +1 to each point of $G(s)H(s)$-plane contour. Figure 8.5 shows a typical $G(s)H(s)$-plane contour Γ_{GH}. The effect of adding +1 to each point of Γ_{GH} to obtain $Q(s)$-plane contour Γ_Q is accomplished simply by adding +1 to the scale of the real axis, as shown by the numbers in parentheses in Fig. 8.5. It is seen that $-1+j0$ point of the $G(s)H(s)$ map Γ_{GH} corresponds to the origin of the $Q(s)$ map Γ_Q. For convenience, we designate the $-1+j0$ point of the $G(s)H(s)$-plane as the *critical point*. Thus the encirclements of the origin by the contour Γ_Q is equivalent to the encirclements of the critical point $-1+j0$ by the contour Γ_{GH}. In the light of these observations, we can express Eqn. (8.6) as follows:

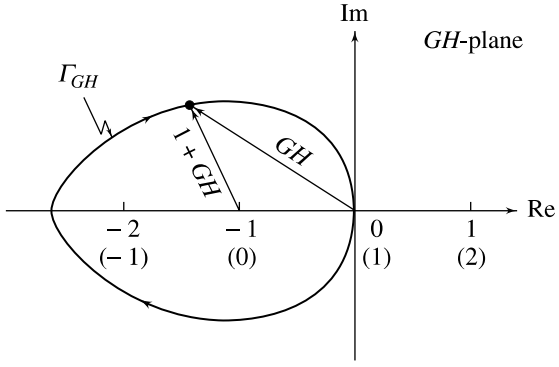

Fig. 8.5 Evaluating $1+G(s)H(s)$ from the $G(s)H(s)$ map

$$Z - P = N \tag{8.7}$$

where

Z = number of zeros of $1+G(s)H(s)$ enclosed by the s-plane contour Γ_s;

P = number of poles of $G(s)H(s)$ enclosed by the s-plane contour Γ_s; and

N = number of clockwise encirclements of the critical point $-1+j0$ made by the $G(s)H(s)$-plane contour Γ_{GH}.

In general N can be positive ($Z > P$), zero ($Z = P$), or negative ($Z < P$). $N > 0$ corresponds to N *net* encirclements of the critical point $-1+j0$ in clockwise direction by the Γ_{GH} contour. $N = 0$ indicates zero *net* encirclements of the critical point by the Γ_{GH} contour. $N < 0$ corresponds to N *net* encirclements of the critical point in counterclockwise direction by the Γ_{GH} contour.

A convenient way of determining N with respect to the critical point $-1+j0$ of the $G(s)H(s)$-plane is to draw a radial line from this point. The number of *net* intersections of the radial line with the Γ_{GH} contour gives the magnitude of N. Figure 8.6 gives several examples of the method of determining N.

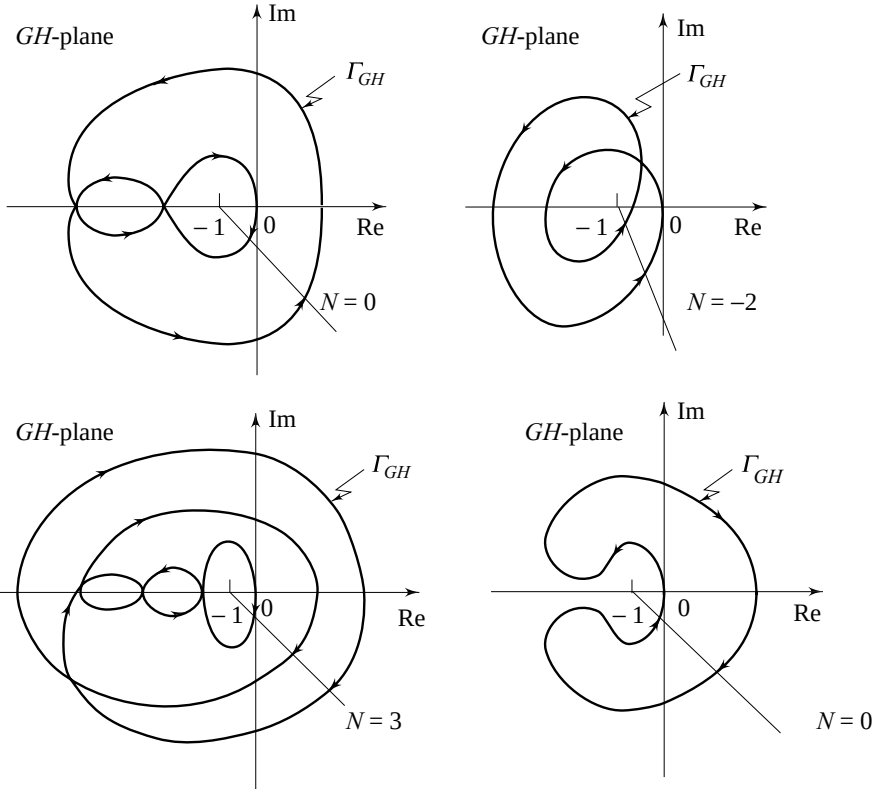

Fig. 8.6 Examples of determination of N

8.2.1 The Nyquist Contour

At this point the reader may place himself/herself in the position of Nyquist many years ago, confronted with the problem of stability of the closed-loop system that has the transfer function of Eqn. (8.1), which is equivalent to determining whether or not the function $1+G(s)H(s)$ has zeros in the right half s-plane. Apparently, Nyquist discovered that the principle of argument of the complex-variable theory could be applied to solve the stability problem if the s-plane contour Γ_s is taken to be one that encloses the entire right half of the s-plane. Of course, as an alternative, Γ_s can be chosen to enclose the entire left half of the s-plane, as the solution is a relative one.

Figure 8.7 illustrates a Γ_s contour that encloses the entire right half of the s-plane. Such a contour is called the *Nyquist contour*. It is directed clockwise and comprises of an infinite line segment C_1 along the $j\omega$-axis and arc C_2 of infinite radius.

Along C_1, $s = j\omega$ with s varying from $-j\infty$ to $+j\infty$.

Along C_2, $s = R\,e^{j\theta}$ with $R \to \infty$ and θ varying from $+90°$ through $0°$ to $-90°$.

As the s-plane contour Γ_s must avoid all poles of $1+G(s)H(s)$, modifications in the Nyquist contour defined in Fig. 8.7 are required when $G(s)H(s)$, and therefore $1+G(s)H(s)$, has one or more poles on the

imaginary axis (the zeros of $1 + G(s)H(s)$ are unknown to us; we will shortly see the implications of s-plane contour passing through the zeros of $1 + G(s)\,H(s)$). The basic trick, of course, is to take a small detour around the imaginary axis poles. Figure 8.8 illustrates a modified Nyquist contour when $G(s)H(s)$ has a pole at $s = 0$. Along the semicircular indent around the pole at the origin, $s = \rho e^{j\phi}$ with $\rho \to 0$ and ϕ varying from $-90°$ through 0° to + 90°. The indented Nyquist contour in Fig. 8.8 does not enclose the pole at the origin. Of course, as an alternative, the Nyquist contour may be indented to enclose the pole at the origin.

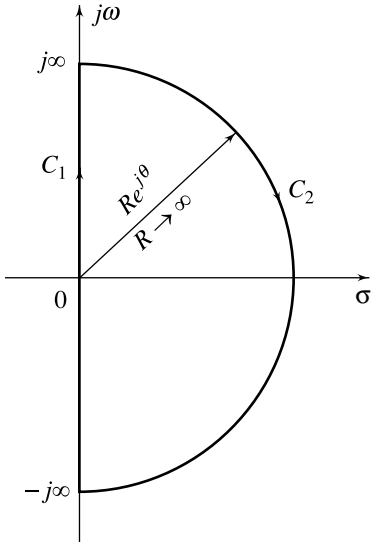

Fig. 8.7 The Nyquist contour

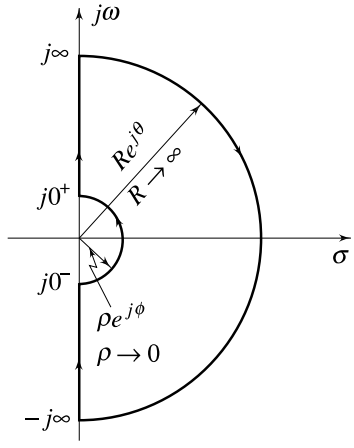

Fig. 8.8 Indented Nyquist contour

8.2.2 The Nyquist Plot

The Nyquist stability criterion is a direct application of the principle of argument when the s-plane contour Γ_s is the Nyquist contour. In principle, once the Nyquist contour is specified, the stability of a closed-loop system can be determined by plotting the $G(s)H(s)$ locus when s takes on values along the Nyquist contour, and investigating the behaviour of the $G(s)H(s)$ plot with respect to the critical point $-1+j0$. The $G(s)H(s)$ plot that corresponds to the Nyquist contour is called the *Nyquist plot* of $G(s)H(s)$.

With the additional dimension added to the stability problem, we define N, P, and Z as follows.

N = number of clockwise encirclements of the critical point $-1+j0$ made by the $G(s)H(s)$ locus of the Nyquist plot.

P = number of poles of $G(s)H(s)$, and therefore of $1+ G(s)H(s)$, enclosed by the Nyquist contour.

Then (refer Eqn. (8.7))

Z = number of zeros of $1+ G(s)H(s)$ enclosed by the Nyquist contour

$$= N + P \tag{8.8a}$$

Closed-loop stability requires that

$$Z = 0 \tag{8.8b}$$

This condition is met if

$$N = -P \tag{8.8c}$$

In the special case[1] (this is generally the case in most single-loop practical systems) of $P = 0$ (i.e., the open-loop transfer function $G(s)H(s)$ has no poles in right half s-plane), the closed-loop system is stable if

$$N = 0 \tag{8.8d}$$

8.2.3 The Nyquist Criterion

We can now state the Nyquist stability criterion as follows:

If the Nyquist plot of the open-loop transfer function G(s)H(s) corresponding to the Nyquist contour in the s-plane encircles the critical point $-1+j0$ in the counterclockwise direction as many times as the number of right half s-plane poles of G(s)H(s), the closed-loop system is stable.

In the commonly occurring case of G(s)H(s) with no poles in right half s-plane, the closed-loop system is stable if the Nyquist plot of G(s)H(s) does not encircle the $-1+j0$ point.

When the Nyquist plot of $G(s)H(s)$ passes through $-1+j0$ point, the number of encirclements N is indeterminate. This corresponds to the condition where $1+G(s)H(s)$ has zeros on the imaginary axis. A necessary condition for applying the Nyquist criterion is that the Nyquist contour must not pass through any poles or zeros of $1+G(s)H(s)$. When this condition is violated, the value for N becomes indeterminate and the Nyquist stability criterion cannot be applied.

8.3 SELECTED ILLUSTRATIVE NYQUIST PLOTS

The following examples serve to illustrate the application of the Nyquist criterion to the stability study of control systems.

Example 8.1 Consider a single-loop feedback control system with the open-loop transfer function given by

$$G(s)H(s) = \frac{K}{(\tau_1 s + 1)(\tau_2 s + 1)};\ \tau_1,\ \tau_2 > 0,\ K > 0 \tag{8.9}$$

$G(s)H(s)$ has no poles in the right-half s-plane; therefore, stability is assured if the Nyquist plot of $G(s)H(s)$ does not encircle the $-1+j0$ point.

The Nyquist plot of $G(s)H(s)$, as we know, is the mapping of the Nyquist contour in the s-plane onto $G(s)H(s)$-plane. In Fig. 8.9a, the Nyquist contour has been divided into three sections: C_1, C_2, and C_3. Section C_1 is defined by $s = j\omega$, $0 \le \omega < \infty$; section C_2 is defined by $s = j\omega$, $-\infty < \omega \le 0$; and section C_3 is defined by $s = Re^{j\theta}$, $R \to \infty$, and θ varies from $+90°$ through $0°$ to $-90°$.

Mapping of Section C_1 onto G(s)H(s)-plane

Substituting $s = j\omega$ into $G(s)H(s)$, we obtain

$$G(j\omega)H(j\omega) = \frac{K}{(j\omega\tau_1 + 1)(j\omega\tau_2 + 1)} \tag{8.10}$$

A plot of $G(j\omega)H(j\omega)$ on polar coordinates as ω is varied from 0 to ∞ is the map of section C_1 on the $G(s)H(s)$-plane. This plot is called the *polar plot* of sinusoidal transfer function $G(j\omega)H(j\omega)$.

[1]Example of a physical system whose transfer function model has a pole in right-half s-plane is given in Figs 12.14.

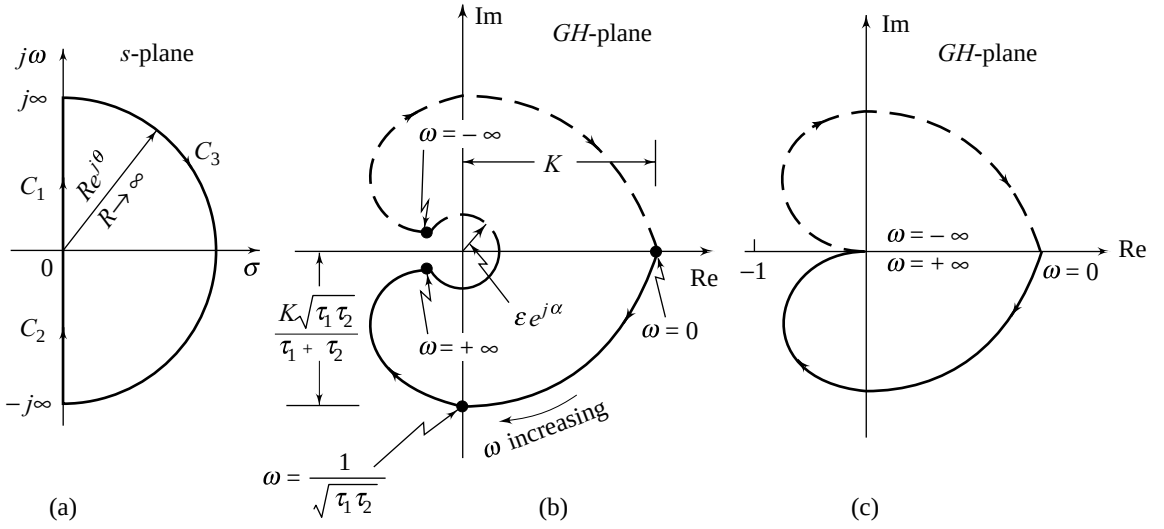

Fig. 8.9 (a) Nyquist contour; (b) Nyquist plot of $G(s)H(s)$ of Eqn. (8.9); (c) Simplified Nyquist plot

For application of the Nyquist stability criterion, an exact polar plot of $G(j\omega)H(j\omega)$ is not essential. Often a rough sketch is adequate for stability analysis. The general shape of the polar plot of $G(j\omega)H(j\omega)$ may be determined from the following information.

1. The behaviour of the magnitude and phase of $G(j\omega)H(j\omega)$ at $\omega = 0$ and $\omega = \infty$.
2. The points of intersection of the polar plot with the real and imaginary axes, and the values of ω at these intersections.
3. A few on-locus points in second and third quadrants in the vicinity of the critical point $-1+j0$.

For $G(j\omega)H(j\omega)$ given by Eqn. (8.10), the magnitude and phase at $\omega = 0$ and $\omega = \infty$ are calculated as follows:

$$\left|G(j\omega)H(j\omega)\right|_{\omega=0} = K;\ \angle G(j\omega)H(j\omega)\Big|_{\omega=0} = 0°$$

$$\left|G(j\omega)H(j\omega)\right|_{\omega\to\infty} = \left|\frac{K}{j^2\omega^2\tau_1\tau_2}\right|_{\omega\to\infty} = 0$$

$$\angle G(j\omega)H(j\omega)\Big|_{\omega\to\infty} = \angle\left(\frac{K}{j^2\omega^2\tau_1\tau_2}\right) = -180°$$

The intersections of the polar plot with the axes of $G(s)H(s)$-plane can easily be ascertained by identifying the real and imaginary parts of $G(j\omega)H(j\omega)$.

$$G(j\omega)H(j\omega) = \frac{K}{(1+j\omega\tau_1)(1+j\omega\tau_2)}\left[\frac{(1-j\omega\tau_1)(1-j\omega\tau_2)}{(1-j\omega\tau_1)(1-j\omega\tau_2)}\right]$$

$$= \frac{K\left[(1-\omega^2\tau_1\tau_2) - j\omega(\tau_1+\tau_2)\right]}{(1+\omega^2\tau_1^2)(1+\omega^2\tau_2^2)}$$

$$= \frac{K(1-\omega^2\tau_1\tau_2)}{\omega^4\tau_1^2\tau_2^2+\omega^2(\tau_1^2+\tau_2^2)+1} - j\frac{K\omega(\tau_1+\tau_2)}{\omega^4\tau_1^2\tau_2^2+\omega^2(\tau_1^2+\tau_2^2)+1}$$

$$= \text{Re}[G(j\omega)H(j\omega)] + j\text{Im}[G(j\omega)H(j\omega)]$$

When we let $\text{Im}[G(j\omega)H(j\omega)]$ to zero, we get $\omega = 0$, meaning that the polar plot intersects the real axis only at $\omega = 0$. Similarly, the intersection of $G(j\omega)H(j\omega)$-plot with the imaginary axis is found by setting $\text{Re}[G(j\omega)H(j\omega)]$ to zero, which gives

$$\omega = \frac{1}{\sqrt{\tau_1\tau_2}}$$

$$\left|G(j\omega)H(j\omega)\right|_{\omega=\frac{1}{\sqrt{\tau_1\tau_2}}} = \left.\frac{K\omega(\tau_1+\tau_2)}{\omega^4\tau_1^2\tau_2^2+\omega^2(\tau_1^2+\tau_2^2)+1}\right|_{\omega=\frac{1}{\sqrt{\tau_1\tau_2}}}$$

$$= \frac{K\sqrt{\tau_1\tau_2}}{\tau_1+\tau_2}$$

Based on this information, a rough sketch of the polar plot can easily be made, as shown in Fig. 8.9b (the portion of the locus from $\omega = 0$ to $\omega = +\infty$).

Mapping of Section C_2 onto G(s)H(s)-plane

Given $G(j\omega)H(j\omega)$, $0 \le \omega < \infty$, $G(j\omega)H(j\omega)$ for $-\infty < \omega \le 0$ is constructed by realizing

$$G(-j\omega)H(-j\omega) = [G(j\omega)H(j\omega)]^*$$

where * denotes conjugate. Thus, given the $G(j\omega)H(j\omega)$-locus for $0 \le \omega < \infty$, we get the $G(j\omega)H(j\omega)$-locus for the negative $j\omega$-axis by simply taking the mirror image about the real axis of the locus for positive ω. The dashed portion of the locus in Fig. 8.9b from $\omega = -\infty$ to $\omega = 0$ is thus the map of section C_2 of Nyquist contour.

Mapping of Section C_3 onto G(s)H(s)-plane

Along section C_3, $s = Re^{j\theta}$; $R \to \infty$ and θ varies from + 90° through 0° to − 90°. Substituting into $G(s)H(s)$, we obtain

$$G(s)H(s)\Big|_{s=Re^{j\theta}} = \frac{K}{(\tau_1 Re^{j\theta}+1)(\tau_2 Re^{j\theta}+1)}$$

$$= \frac{K}{\tau_1\tau_2 R^2 e^{j2\theta}} = \frac{K}{\tau_1\tau_2 R^2}e^{-j2\theta}$$

The infinitesimal semicircular locus around the origin (refer Fig. 8.9b), represented by

$$G(s)H(s) = \varepsilon e^{j\alpha}$$

with $\varepsilon \to 0$ and α varying from −180° through 0° to + 180°, is thus the map of section C_3 of Nyquist contour.

For application of the Nyquist stability criterion, exact shape of the Nyquist plot around the origin of $G(s)H(s)$-plane is of no interest to us. We can therefore take $\varepsilon = 0$; the resulting Nyquist plot is shown in Fig. 8.9c. This plot does not encircle the critical point $-1+j0$ for any positive values of K, τ_1, and τ_2. Therefore, the system is stable for all positive values of K, τ_1, and τ_2.

Example 8.2 Consider now a feedback system whose open-loop transfer function is given by

$$G(s)H(s) = \frac{K}{s(\tau s + 1)}; \; K > 0, \; \tau > 0 \tag{8.11}$$

We note here that for this type-1 system, there is one pole on the imaginary axis, precisely at the origin. The Nyquist contour is shown in Fig. 8.10a, where a semicircular detour about the origin is indicated. The Nyquist contour has been divided into four sections: C_1, C_2, C_3 and C_4. Section C_1 is defined by $s = j\omega$, $0 < \omega < \infty$; section C_2 is defined by $s = j\omega$, $-\infty < \omega < 0$; section C_3 is defined by $s = Re^{j\theta}$, $R \to \infty$, and θ varies from + 90° through 0° to – 90°; and section C_4 is defined by $s = \rho e^{j\phi}$, $\rho \to 0$, and ϕ varies from – 90° through 0° to + 90°.

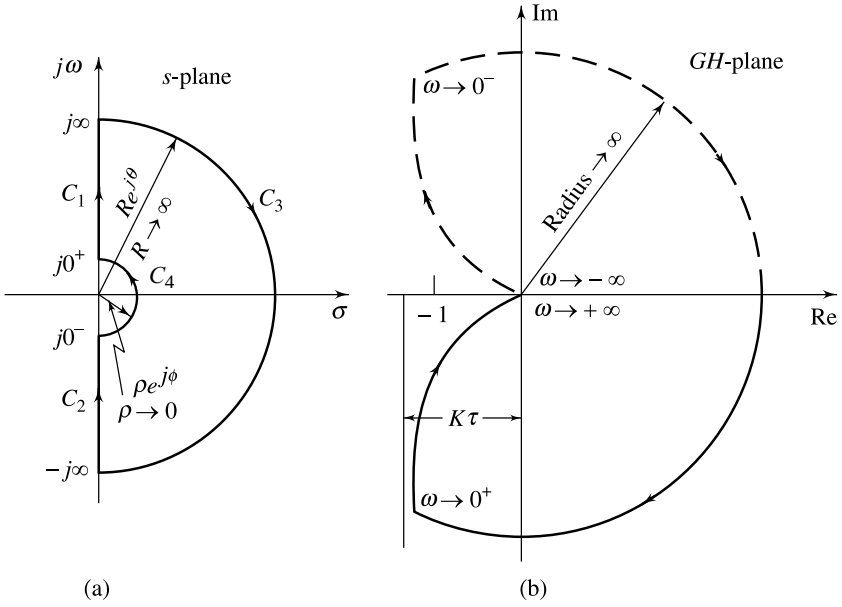

Fig. 8.10 (a) Nyquist contour; (b) Nyquist plot of $G(s)H(s)$ of Eqn. (8.11)

Mapping of section C_1 onto the $G(s)H(s)$-plane is given by the polar plot of sinusoidal transfer function

$$G(j\omega)H(j\omega) = \frac{K}{j\omega(j\omega\tau + 1)} \tag{8.12}$$

This sinusoidal transfer function can be expressed as

$$G(j\omega)H(j\omega) = -\frac{K\tau}{1 + \omega^2\tau^2} - j\frac{K}{\omega(1 + \omega^2\tau^2)}$$

The low-frequency portion of the polar plot becomes

$$\lim_{\omega \to 0} G(j\omega)H(j\omega) = -K\tau - j\infty$$

and the high-frequency portion is (refer Eqn. (8.12))

$$\lim_{\omega \to \infty} G(j\omega)H(j\omega) = \frac{K}{\omega^2\tau} \angle \left(\frac{K}{j^2\omega^2\tau} \right) \Bigg|_{\omega \to \infty} = 0 \angle -180°$$

The general shape of the polar plot is shown in Fig. 8.10b. The $G(j\omega)H(j\omega)$-plot is asymptotic to the vertical line passing through the point $-K\tau + j0$.

Mapping of section C_2 onto $G(s)H(s)$-plane is obtained simply by taking the mirror image about the real axis of the polar plot of $G(j\omega)H(j\omega)$.

Mapping of section C_3 onto the $G(s)H(s)$-plane is obtained as follows.

$$G(s)H(s)\Big|_{s=Re^{j\theta}} = \frac{K}{Re^{j\theta}(\tau\, Re^{j\theta}+1)} = \frac{K}{\tau R^2}e^{-j2\theta}$$

The $G(s)H(s)$-locus thus turns at the origin with zero radius from $-180°$ through $0°$ to $+180°$.

Mapping of section C_4 onto the $G(s)H(s)$-plane is obtained as follows. Along C_4, $s = \rho e^{j\phi}$; $\rho \to 0$, and ϕ varies from $-90°$ through $0°$ to $+90°$.

Substituting into $G(s)H(s)$, we obtain

$$G(s)\,H(s)\Big|_{s=\rho e^{j\phi}} = \frac{K}{\rho e^{j\phi}(\tau\rho e^{j\phi}+1)} = \frac{K}{\rho}e^{-j\phi}$$

The value K/ρ approaches infinity as $\rho \to 0$, and $-\phi$ varies from $+90°$ through $0°$ to $-90°$ as s moves along section C_4 of the Nyquist contour. Thus the infinitesimal semicircular indent around the origin in the s-plane maps into a semicircular arc of infinite radius on the $G(s)H(s)$-plane as shown in Fig. 8.10b.

The complete Nyquist plot for $G(s)H(s)$ given by Eqn. (8.11) is shown in Fig. 8.10b. In order to investigate the stability of this second-order system, we first note that the number of poles of $G(s)H(s)$ in the right-half s-plane is zero. Therefore, for this system to be stable, we require that the Nyquist plot of $G(s)H(s)$ does not encircle the critical point $-1+j0$. Examining Fig. 8.10b, we find that irrespective of the value of the gain K and the time-constant τ, the Nyquist plot does not encircle the critical point, and the system is always stable.

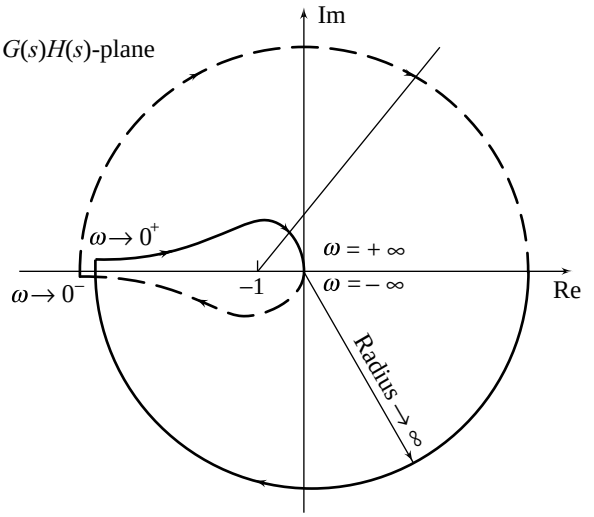

Fig. 8.11 Nyquist plot[2] for $G(s)H(s)$ of Eqn. (8.13)

Example 8.3 We now consider a type-2 system with open-loop transfer function

$$G(s)H(s) = \frac{K}{s^2(\tau s+1)};\ K>0,\ \tau>0 \qquad (8.13)$$

The Nyquist contour is shown in Fig. 8.10a. The Nyquist plot is shown in Fig. 8.11. Clearly the portion of the $G(s)H(s)$-locus from $\omega = 0^+$ to $\omega = +\infty$ is simply the polar plot of

$$G(j\omega)H(j\omega) = \frac{K}{j^2\omega^2(j\omega\tau+1)} \qquad (8.14)$$

[2] For $K = 1$, $\tau = 1$;

ω	0.01	0.05	0.1	0.5	1
$\lvert GH\rvert$	4×10^6	600	98.51	3.57	0.7
$\angle GH$	179.97	177.68	174.2	153.4	135

Note that

$$G(j\omega)H(j\omega)\Big|_{\omega\to 0^+} = \left(\frac{K}{\omega^2}\Big|_{\omega\to 0^+}\right)\angle -180^\circ = \infty \angle \pm 180^\circ$$

$$G(j\omega)H(j\omega)\Big|_{\omega\to +\infty} = \left(\frac{K}{\omega^3\tau}\Big|_{\omega\to +\infty}\right)\angle -270^\circ = 0 \angle -270^\circ \text{ or } +90^\circ$$

It can easily be examined that the locus of $G(j\omega)H(j\omega)$ does not intersect the real or imaginary axis; it lies in the second quadrant for all values of ω.

The $G(s)H(s)$-locus turns at the origin with zero radius from -270° through 0° to $+270^\circ$. This corresponds to the locus from $\omega = +\infty$ to $\omega = -\infty$. The portion of the $G(s)H(s)$-locus from $\omega = -\infty$ to $\omega = 0^-$ is the mirror image about the real axis of the locus for positive ω. From $\omega = 0^-$ to $\omega = 0^+$, $s = \rho e^{j\phi}$, $\rho \to 0$ and ϕ varies from -90° through 0°, to $+90^\circ$. This gives

$$G(s)H(s)\Big|_{s=\rho e^{j\phi}} = \frac{K}{\rho^2 e^{j2\phi}(\tau\rho e^{j\phi}+1)} = \frac{K}{\rho^2}e^{-j2\phi}$$

The portion of the $G(s)H(s)$ locus from $\omega = 0^-$ to $\omega = 0^+$ is a circular arc of infinite radius ranging from $+180^\circ$ at $\omega = 0^-$ through 0° to -180° at $\omega = 0^+$ ($+180^\circ \to +90^\circ \to 0^\circ \to -90^\circ \to -180^\circ$).

From Fig. 8.11, we observe that the Nyquist plot encircles the critical point $-1+j0$ twice in the clockwise direction, i.e., $N = 2$. Since P = number of poles of $G(s)H(s)$ in right-half s-plane = 0, we have from Eqn. (8.8a), $Z = 2$; i.e, there are two roots of the closed-loop system in the right-half s-plane and the system, irrespective of the gain K and time-constant τ, is unstable.

Example 8.4 Consider now an open-loop system with the transfer function

$$G(s)H(s) = \frac{s+1}{s^2(s-2)} \tag{8.15}$$

Let us determine whether the system is stable when the feedback path is closed.

From the transfer function of the open-loop system it is observed that there is one open-loop pole in the right half s-plane. Therefore $P = 1$.

The Nyquist contour is shown in Fig. 8.10a. The Nyquist plot is shown in Fig. 8.12. Clearly, the portion of the $G(s)H(s)$-locus from $\omega = 0^+$ to $\omega = +\infty$ is simply the polar plot of

$$G(j\omega)H(j\omega) = \frac{j\omega+1}{j^2\omega^2(j\omega-2)} \tag{8.16}$$

The following points were used to construct the polar plot:

$$G(j\omega)H(j\omega)\Big|_{\omega\to 0^+} \to \infty\angle 0^\circ$$

$$G(j\omega)H(j\omega)\Big|_{\omega=0.1} = 50\angle 9^\circ$$

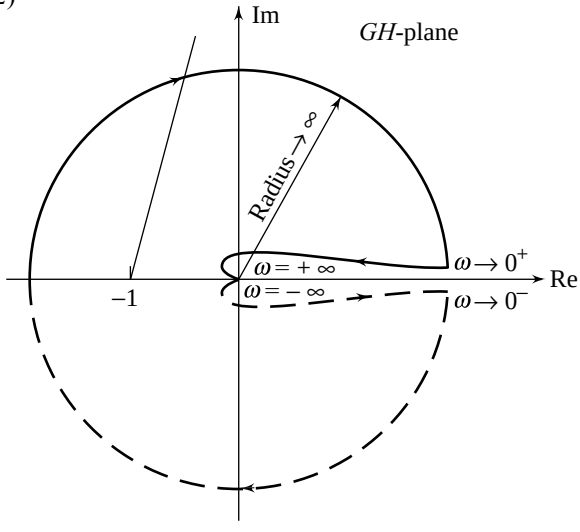

Fig. 8.12 Nyquist plot for $G(s)H(s)$ of Eqn. (8.15)

$$G(j\omega)H(j\omega)\big|_{\omega=1} = 0.6\angle 71°;\ G(j\omega)H(j\omega)\big|_{\omega=10} = 0.01\angle 162°$$

$$G(j\omega)H(j\omega)\big|_{\omega\to+\infty} \to 0\angle -180°$$

The plot of $G(j\omega)H(j\omega)$ for $\omega < 0$ is the reflection, with respect to the real axis, of the plot for $\omega > 0$. Every point on the large semicircle in Fig. 8.10a, is mapped by $G(s)H(s)$ into the origin of the $G(s)H(s)$-plane. A point $s = \rho e^{j\phi}$; $\rho \to 0$, ϕ varying from $-90°$ through $0°$ to $+90°$ is mapped by $G(s)H(s)$ into

$$G(s)H(s)\big|_{s=\rho e^{j\phi}} = \frac{s+1}{s^2(s-2)}\bigg|_{s=\rho e^{j\phi}} = -\frac{1}{2\rho^2 e^{j2\phi}} = \frac{1}{2\rho^2}\angle(180° - 2\phi)$$

The small semicircle in Fig. 8.10a is mapped by $G(s)\,H(s)$ into a circular arc of infinite radius ranging from $360°$ at $\omega = 0^-$ through $180°$ to $0°$ at $\omega = 0^+$ ($360° \to 270° \to 180° \to 90° \to 0°$).

Figure 8.12 indicates that the critical point $-1+j0$ is encircled by the Nyquist plot once in the clockwise direction. Therefore $N = 1$, and (refer Eqn. (8.8a))

Z = number of zeros of $1+G(s)H(s)$ enclosed by the Nyquist contour

$= N + P = 2$

Hence the feedback system is unstable with two poles in the right half s-plane.

Example 8.5 Consider a feedback system with the following open-loop transfer function:

$$G(s)H(s) = \frac{K}{s(s+3)(s+5)} \tag{8.17}$$

Let us investigate the stability of this system for various values of K.

First set $K = 1$ and sketch the Nyquist plot for the system using the contour shown in Fig. 8.10a. For all points on the imaginary axis,

$$G(j\omega)H(j\omega) = \frac{K}{s(s+3)(s+5)}\bigg|_{\substack{K=1\\ s=j\omega}} = \frac{-8\omega^2 - j(15\omega - \omega^3)}{64\omega^4 + \omega^2(15-\omega^2)^2} \tag{8.18}$$

At $\omega = 0$, $G(j\omega)H(j\omega) = -0.0356 - j\infty$.

Next, find the point where the Nyquist plot intersects the negative real axis. Setting the imaginary part of Eqn. (8.18) equal to zero, we find $\omega = \sqrt{15}$. Substituting this value of ω back into Eqn. (8.18), yields the real part of -0.0083.

Finally, at $\omega = \infty$, $G(j\omega)H(j\omega) = G(s)H(s)\big|_{s\to j\infty} = \dfrac{1}{(j\omega)^3} = 0\angle -270°$.

The Nyquist plot for $G(s)H(s)$ of Eqn. (8.17) with $K = 1$ is shown in Fig. 8.13. Application of the Nyquist criterion shows that with $K = 1$, the closed-loop system is stable.

If we were to increase the gain by a factor $1/0.0083 = 120.48$, all points on the $G(j\omega)H(j\omega)$-locus would increase in magnitude by this factor along radial lines centred at the origin. The length of the vector $G(j\sqrt{15})H(j\sqrt{15})$ would be $0.0083\ (1/0.0083) = 1$, and therefore the curve $G(j\omega)H(j\omega)$ would go through the critical point; the closed-loop system would be at the limit of instability. Hence, for stability, K must be less than 120.48, i.e., the stability range is $0 < K < 120.48$.

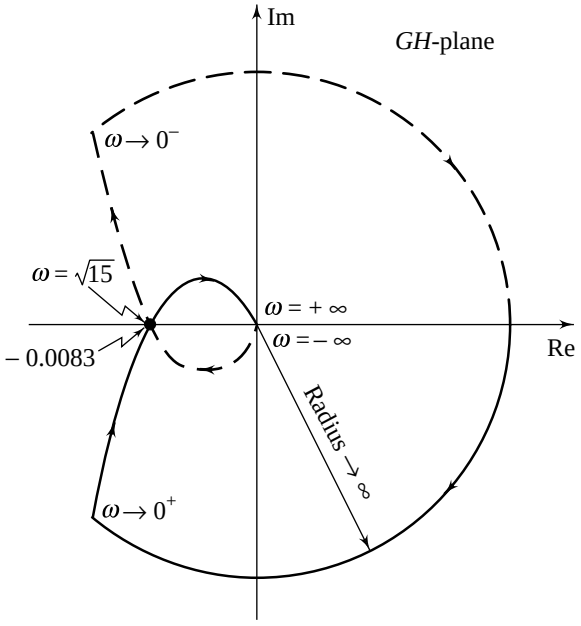

Fig. 8.13 Nyquist plot for $G(s)H(s)$ of Eqn. (8.17)

Example 8.6 Let us consider the control system shown in Fig. 8.14 and determine its stability. The characteristic equation of the system is

$$s(s-1) + K_A(1 + K_t s) = 0$$

We rearrange it in the form convenient for Nyquist plotting:

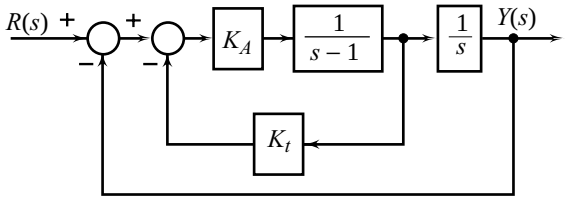

Fig. 8.14 A feedback control system

$$1 + \frac{K_A(1 + K_t s)}{s(s-1)} = 0$$

or

$$1 + G(s) = 0$$

$$G(s) = \frac{K_A(1 + K_t s)}{s(s-1)} \tag{8.19}$$

The open-loop transfer function has one pole in the right half s-plane, and therefore $P = 1$. In order for the closed-loop system to be stable, we require $N = -1$ (i.e., the Nyquist plot must encircle the critical point once in the counterclockwise direction).

Several important values of $G(j\omega)$-locus are given below:

$$G(j\omega)\Big|_{\omega \to 0^+} = \infty \angle +90°;\ G(j\omega)\Big|_{\omega \to +\infty} = 0\angle -90°$$

$$G(j\omega) = \frac{K_A(1 + K_t j\omega)}{-\omega^2 - j\omega}$$

$$= \frac{-K_A(\omega^2 + \omega^2 K_t) + j(\omega - K_t\omega^3)K_A}{\omega^2 + \omega^4} \quad (8.20)$$

$$G(j\omega)\Big|_{\omega^2 = 1/K_t} = -K_A K_t$$

At the semicircular detour at the origin in the s-plane (refer Fig. 8.10a), we let $s = \rho e^{j\phi}$; $\rho \to 0$ and ϕ varies from – 90° through 0° to + 90°.

$$G(s)\Big|_{s=\rho e^{j\phi}} = \frac{K_A}{-\rho e^{j\phi}} = \frac{K_A}{\rho}\angle(-180° - \phi)$$

Therefore the semicircular detour in the Nyquist contour is mapped into a semicircle of infinite radius in the left half of $G(s)$-plane, as shown in Fig. 8.15. When $-K_A K_t < -1$ or $K_A K_t > 1$, the Nyquist plot encircles the $-1 + j0$ point once in counterclockwise direction. Thus the system is stable when $K_A K_t > 1$.

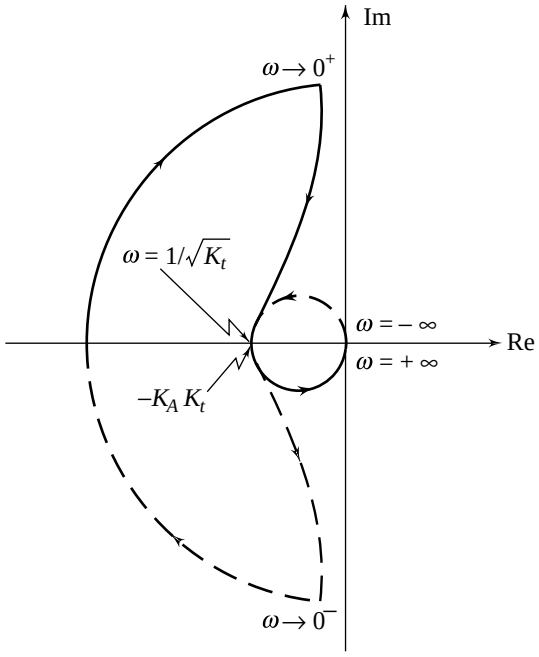

Fig. 8.15 Nyquist plot[3] for G(s) of Eqn. (8.19)

8.4 STABILITY MARGINS

In the preceding sections, the Nyquist plot was used to detemine if a system was stable or unstable. Of course, in general, a usable system must be stable. However, there are concerns beyond simple stability, for two reasons. First, a stable system must also have, among other characteristics, an acceptable transient response. Also, the model that is used in the analysis and design of a control system is never exact. Hence, the model may indicate that a system is stable, whereas in fact the physical system is unstable. Generally we require not only that a system be stable but also that it be stable by some margin of safety.

Measures of degree of stability of a closed-loop system that has open-loop transfer function with no poles in right half s-plane, can be conveniently created through Nyquist plot. The stability information for such a system becomes obvious by the inspection of the Nyquist plot of its open-loop transfer function $G(s)H(s)$, since the stability criterion is merely the non-encirclement of the critical point $-1 + j0$. It can be intuitively imagined that as the Nyquist plot gets closer to the critical point, the system tends towards instability.

Consider two different systems whose dominant closed-loop poles are shown on the s-plane in Figs 8.16a and 8.16b. Obviously, system A is 'more stable' than system B, since its dominant closed-loop poles are located comparatively away to the left from the $j\omega$-axis. The Nyquist plots of open-loop transfer functions of systems A and B are shown in Figs 8.16c and 8.16d, respectively. Comparison of the closed-loop pole locations of these systems with their corresponding Nyquist plots reveals that as a Nyquist plot moves closer

[3] for $K_A = 1$, $K_t = 3$;

ω	0.02	0.05	0.09	1
$\lvert G\rvert$	146.3	74	37.16	2.23
$\angle G$	91.57	93.1	96.14	153.56

to the critical point $-1+j0$, the system closed-loop poles move closer to the $j\omega$-axis and hence the system becomes relatively less stable and *vice versa*.

Thus, the distance between the Nyquist plot of open-loop transfer function $G(s)H(s)$ and the critical point $-1+j0$ can be used as a measure of degree of stability of the closed-loop system. Generally, the larger the distance, the more stable the system. The distance can be found by drawing a circle touching the Nyquist plot as shown in Figs 8.16c and 8.16d. Such a distance, however, is not convenient for analysis and design. The measures gain margin and phase margin, are commonly used to quantify the closeness of a Nyquist plot to the critical point.

8.4.1 Gain Margin

Figure 8.17 shows a 'typical' Nyquist plot of $G(j\omega)H(j\omega)$; $\omega \geq 0$. $G(s)H(s)$ is known to have no poles in the right half s-plane. A closed-loop system with the $G(s)H(s)$ as open-loop transfer function, is stable.

The point at which the Nyquist plot crosses the negative real axis is marked A, and the frequency at that point is designated ω_ϕ. The point A is thus the tip of the vector $G(j\omega_\phi)H(j\omega_\phi)$ with magnitude $|G(j\omega_\phi)H(j\omega_\phi)|$ and angle 180°. It is seen from Fig. 8.17 that $|G(j\omega_\phi)H(j\omega_\phi)| < 1$, and therefore the tip of the vector $G(j\omega_\phi)H(j\omega_\phi)$ does not reach the critical point $-1+j0$.

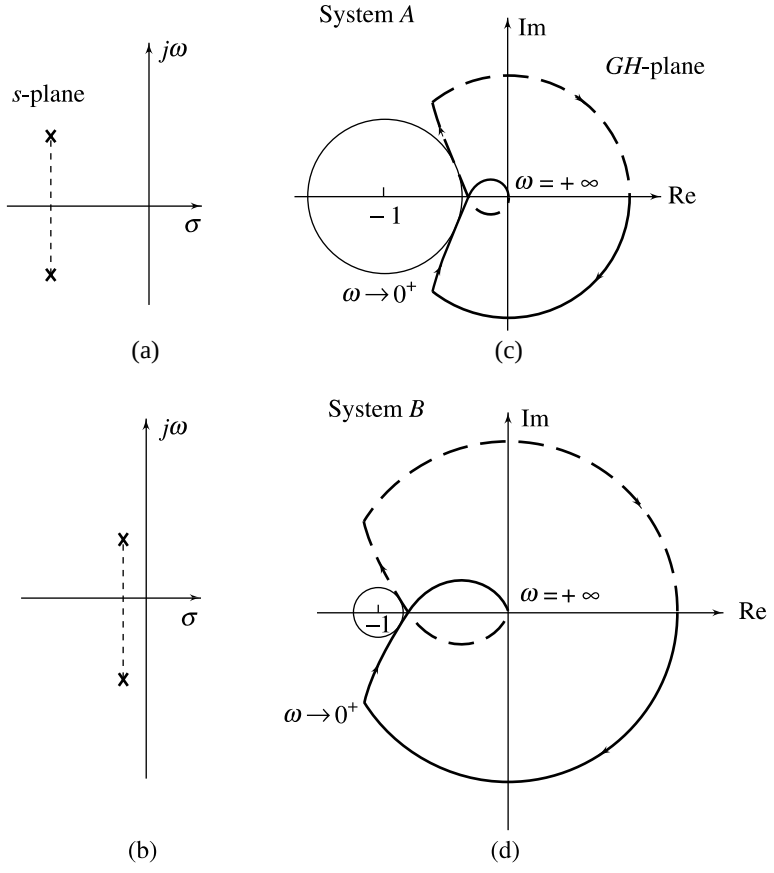

Fig. 8.16 Correlation between the closed-loop s-plane root locations and open-loop frequency-response curves

If we were to increase the gain of $G(j\omega)H(j\omega)$ by a factor $1/|OA|$ without altering its phase, all points on the Nyquist plot of $G(j\omega)H(j\omega)$ would increase in magnitude by this factor along radial lines centred at the origin. The length of the vector $G(j\omega_\phi)H(j\omega_\phi)$ would be $|OA|(1/|OA|) = 1$, and therefore the curve $G(j\omega)H(j\omega)$ would go through the critical point; the closed-loop system would be at the limit of stability. We call the multiplying factor $1/|OA|$ the *gain margin* because it is the factor by which the gain can be increased to drive the system to the verge of instability.

From the graphical description of Fig. 8.17, we now make the following definitions.

Phase crossover point It is a point on the $G(s)H(s)$-plane at which the Nyquist $G(j\omega)H(j\omega)$-plot intersects the negative real axis.

Phase crossover frequency ω_ϕ It is the frequency at the phase crossover point, or where

$$\angle G(j\omega_\phi)H(j\omega_\phi) = -180° \tag{8.21}$$

Gain margin The gain margin GM of the closed-loop system that has $G(s)H(s)$ as its open-loop transfer function is defined as the number

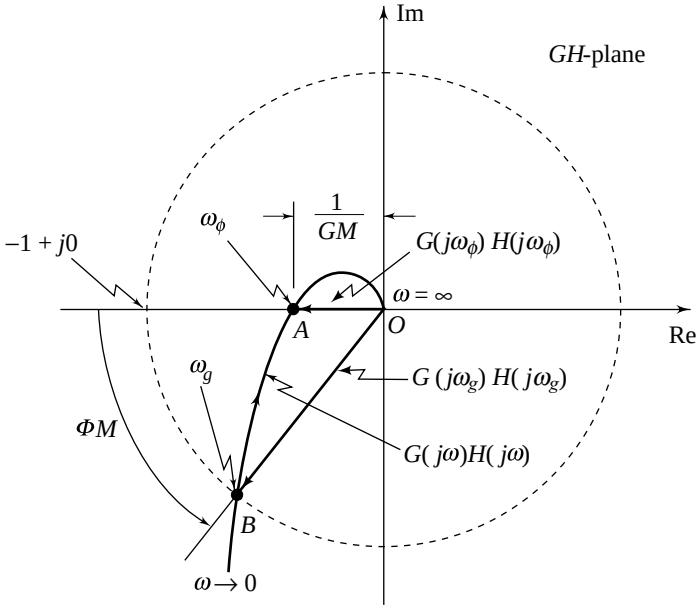

Fig. 8.17 Typical Nyquist plot of $G(j\omega)H(j\omega)$

$$GM = \frac{1}{|G(j\omega_\phi)H(j\omega_\phi)|} \tag{8.22}$$

For example, if $|G(j\omega_\phi)H(j\omega_\phi)| = 0.5$, then the $GM = 2$; the loop gain magnitude could be increased by a factor of 2 before the closed-loop system would go unstable. For stable systems, GM is always a number greater than one.

8.4.2 Phase Margin

A unit circle centred at the origin has been drawn in Fig. 8.17 in order to identify point B at which Nyquist $G(j\omega)H(j\omega)$-plot has unity magnitude; the frequency at point B has been designated ω_g. The point B is thus

the tip of the vector $G(j\omega_g)H(j\omega_g)$ with magnitude $|G(j\omega_g)H(j\omega_g)| = 1$ and angle $\angle G(j\omega_g)H(j\omega_g)$. It is seen from Fig. 8.17 that the tip of the vector $G(j\omega_g)H(j\omega_g)$ does not reach the critical point $-1+j0$.

If we were to decrease the phase of $G(j\omega)H(j\omega)$ without altering its gain, all points on the Nyquist $G(j\omega)H(j\omega)$-plot would rotate clockwise about the origin an angular amount equal to the increase in phase lag. In the light of Fig. 8.17, we see that the tip of the vector $G(j\omega_g)H(j\omega_g)$ would be placed at the critical point if the increase in phase lag of $G(j\omega)H(j\omega)$ were made equal to the angle ΦM. We call the angle ΦM, *measured positively in the counterclockwise direction from the negative real axis to the vector* $G(j\omega_g)H(j\omega_g)$, *the phase margin* because it is the angle by which the phase of $G(j\omega)H(j\omega)$ can be decreased to drive the system to the verge of instability.

From the graphical description of Fig. 8.17, we now make the following definitions.

Gain crossover point It is a point on the $G(s)H(s)$-plane at which the Nyquist $G(j\omega)H(j\omega)$-plot has unity magnitude.

Gain crossover frequency ω_g It is the frequency at the gain crossover point, or where

$$|G(j\omega_g)H(j\omega_g)| = 1 \tag{8.23}$$

Phase margin The phase margin ΦM of the closed-loop system that has $G(s)H(s)$ as its open-loop transfer function, is defined as

$$\Phi M = 180° + \angle G(j\omega_g)H(j\omega_g) \tag{8.24}$$

For example, if $\angle G(j\omega_g)H(j\omega_g) = -135°$, then $\Phi M = 45°$; an additional phase lag of 45° could be associated with $G(j\omega)H(j\omega)$ before the closed-loop system would go unstable. For stable systems, ΦM is always positive.

Consider now an unstable closed-loop system with Nyquist $G(j\omega)H(j\omega)$-plot of Fig. 8.18 ($G(s)H(s)$ is known to have no poles in the right half s-plane). Applying the definition of gain margin to this plot we find that $G(j\omega_\phi)H(j\omega_\phi)$ is a number greater than one and therefore GM is a number less than one. Applying the definition of phase margin, we observe that the vector $G(j\omega_g)H(j\omega_g)$ lies in the second quadrant. The angle measured from negative real axis to this vector is negative (counterclockwise measurement is taken as positive by definition) and therefore the phase margin ΦM is negative.

In general, the gain margin and the phase margin are mutually independent. For example, it is possible for $G(j\omega)H(j\omega)$ to reflect an excellent gain margin but a poor phase margin. Such is the case depicted in Fig. 8.19, where the $GM = \infty$ but the $\Phi M < 15°$. In such a case, the phase crossover frequency ω_ϕ is undefined. Conversely, $G(j\omega)H(j\omega)$ can reflect a poor gain margin but an excellent phase margin, as is the case depicted in Fig. 8.20, where the $\Phi M = \infty$ but the GM is only slightly greater than 1. In such a case, the gain crossover frequency ω_g is undefined.

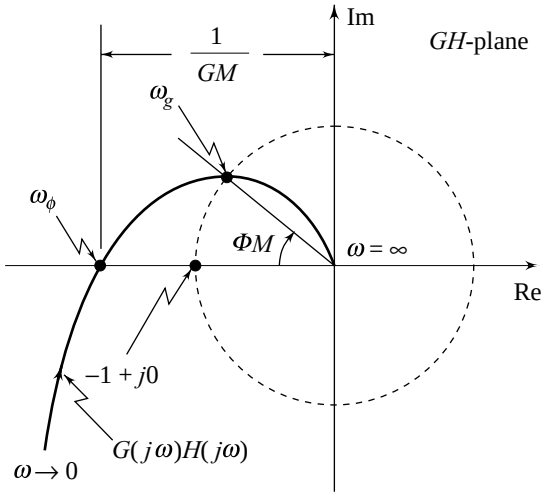

Fig. 8.18 Nyquist plot of an unstable closed-loop system

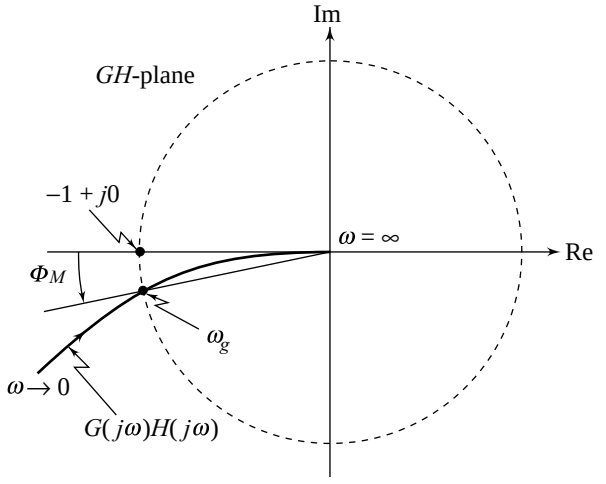

Fig. 8.19 Infinite GM, poor ΦM

In the light of these observations, gain and phase margins should be used in conjunction with one another when determining the degree of stability of a closed-loop system. Together, they represent a measure of the distance of $G(j\omega)H(j\omega)$ from the critical point $-1+j0$.

8.4.3 Some Constraints and Cautions

Gain margin and phase margin are valid measures of relative stability of a closed-loop system only if its open-loop transfer function $G(s)H(s)$ has no poles in the right half s-plane. If the open-loop transfer function has poles in the right half s-plane, it is safer to examine the complete Nyquist plot and/or root locus for interpreting relative stability of the closed-loop system.

It should be observed that the sketches of Figs 8.17–8.20 each cross the negative real axis or the unit circle atmost once. For systems with numerous zeros and poles, the Nyquist plot may cross the negative real axis several times, or it may cross the unit circle more than once. For such curves, several values of gain margin and phase margin are defined, as shown in Figs 8.21 (a) and (b). Caution is suggested when interpreting the stability of such systems. It is safer not to depend on the gain margin and phase margin for relative stability analysis.

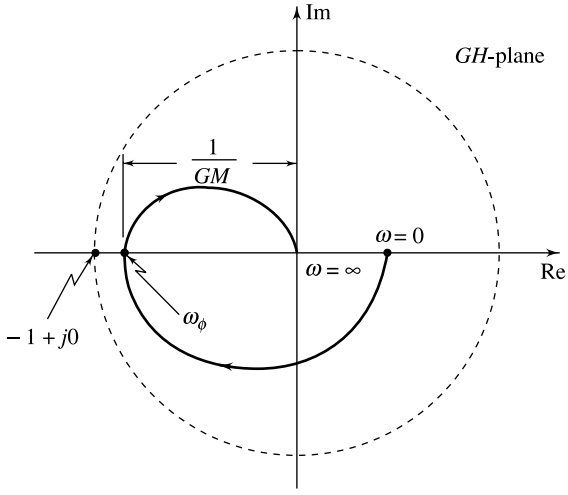

Fig. 8.20 Poor GM, infinite ΦM

It should also be observed that the sketches of Figs 8.12–8.20 correspond to systems where increasing gain leads to instability. There are certain practical situations wherein increase in gain can make the system stable. Consider, for example, unity-feedback system with open-loop transfer function

$$G(s) = \frac{K(s+10)^2}{s^3}$$

This is a system for which increasing gain causes a transition from instability to stability (The Routh criterion shows that the closed-loop system is unstable for $K < 5$ and stable for $K > 5$). The Nyquist plot in Fig. 8.21c has been drawn for the stable value $K = 7$. From this figure we observe that the phase margin is positive and the gain margin is less than one. According to the rules for stability discussed earlier, these two margins yield conflicting signals on system stability. Caution is suggested when interpreting the stability of such systems. It is safer not to depend on the gain margin and phase margin for relative stability analysis.

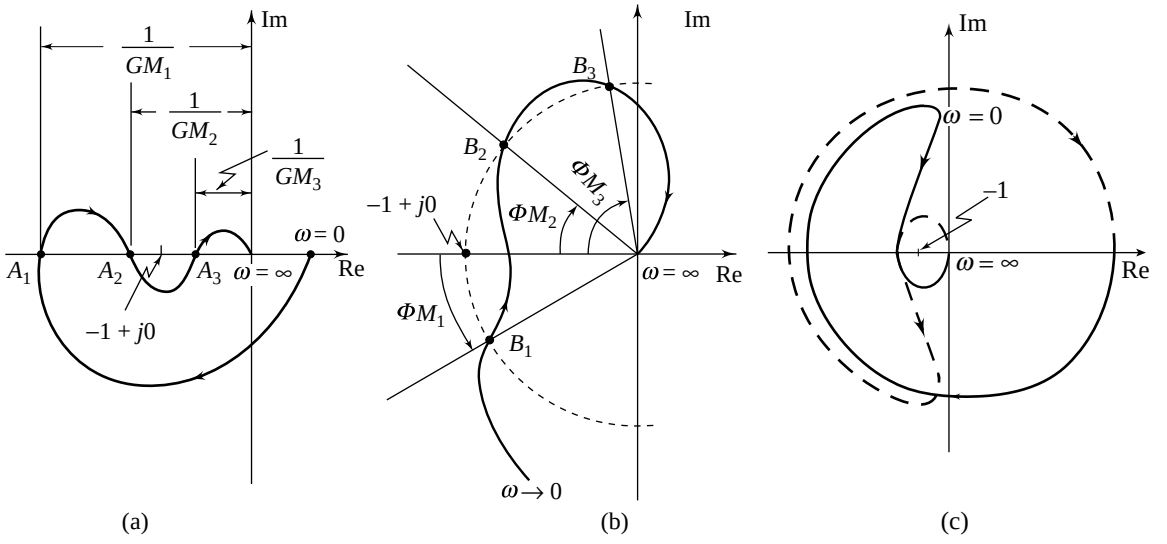

Fig. 8.21 Nyquist plots requiring careful interpretation of GM and ΦM

Example 8.7 A unity-feedback system has open-loop transfer function

$$G(s) = \frac{6}{(s^2 + 2s + 2)(s + 2)} \tag{8.25}$$

Since the open-loop poles are only in the left half s-plane, the Nyquist criterion tells us that we want no encirclement of $-1+j0$ point for stability. In such cases, closed-loop stability can be evaluated from Nyquist $G(j\omega)$-plot.

$$G(j\omega)|_{\omega=0} = 1.5\angle 0°;\ G(j\omega)|_{\omega\to\infty} = 0\angle 90°$$

$$G(j\omega) = \left.\frac{6}{(s^2 + 2s + 2)(s + 2)}\right|_{s=j\omega}$$

$$= \frac{6[4(1-\omega^2) - j\omega(6-\omega^2)]}{16(1-\omega^2)^2 + \omega^2(6-\omega^2)^2} \tag{8.26}$$

Setting the imaginary part to zero, we find the phase crossover frequency $\omega_\phi = \sqrt{6}$ rad/sec. At this frequency, the real part of $G(j\omega)$ in Eqn. (8.26) is calculated to be -0.3 (refer Fig. 8.22). Thus the gain can be increased by (1/0.3) before the real part becomes -1. The gain margin is $GM = 3.33$.

To find the phase margin, first find the gain crossover frequency ω_g: the frequency for which the magnitude of $G(j\omega)$ in Eqn. (8.26) is unity. As the problem stands, this calculation requires computational tools. Later in this chapter, we will simplify the calculation process by using Bode plots.

The gain crossover frequency $\omega_g = 1.253$ rad/sec. At this frequency, the phase angle of $G(j\omega)$ is $-112.33°$. The difference between this angle and 180° is 67.67°, which is the phase margin ΦM.

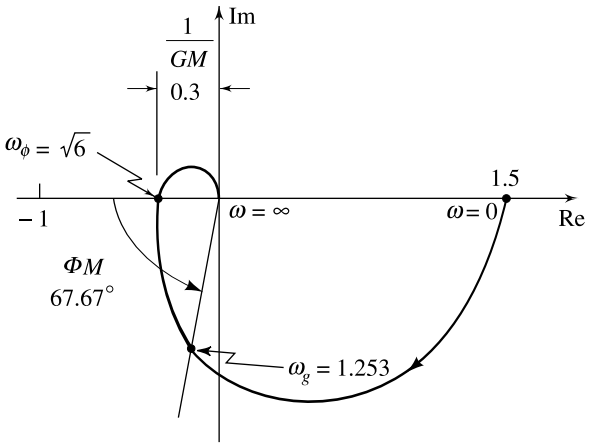

Fig. 8.22 Nyquist plot for $G(j\omega)$ of Eqn. (8.26)

8.5 THE BODE PLOTS

A sinusoidal transfer function may be represented by two separate plots; one giving the magnitude *versus* frequency, and the other the phase angle *versus* frequency. A *Bode plot* (named after Hendrick W. Bode) consists of two graphs: one is a plot of the logarithm of the magnitude of the sinusoidal transfer function, and the other is a plot of the phase angle in degrees; both are plotted against the frequency in logarithmic scale.

In a Bode plot, the logarithmic magnitude of sinusoidal transfer function $G(j\omega)$ is represented[4] as $20 \log |G(j\omega)|$, where the base of the logarithm is 10. The unit used in this representation of the magnitude is *decibel* (one-tenth of a 'Bel': a unit named after Alexander Graham Bell), usually abbreviated as dB.

The main advantage of using the logarithmic plot is that the multiplication of magnitudes can be converted into addition. Consider a typical rational transfer function $G(s)$ factored in the time-constant form:

$$G(s) = \frac{K(1+s\tau_a)(1+s\tau_b)\cdots}{s^N(1+s\tau_1)(1+s\tau_2)\cdots[1+(2\zeta/\omega_n)s+s^2/\omega_n^2]\cdots} \tag{8.27}$$

This transfer function has zeros at $s = -1/\tau_a, -1/\tau_b, \ldots$, N poles at the origin, real poles at $s = -1/\tau_1$, $-1/\tau_2, \ldots$, and complex poles at $-\zeta\omega_n \pm j\omega_n\sqrt{1-\zeta^2}$. We note that the constant multiplier $K = \lim_{s\to 0} s^N G(s)$, where N is the type number for the system with open-loop transfer function $G(s)$ given by Eqn. (8.27). Thus for a type-0 system, $K_p = K$. For a type-1 system, $K_v = K$, and for a type-2 system, $K_a = K$. Any rational $G(s)$ can be factored in the form of Eqn. (8.27). If $G(s)$ has complex zeros, then even though it is not shown in Eqn. (8.27), a quadratic term of the form $[1 + (2\zeta/\omega_n)s + s^2/\omega^2_n]$ will also appear in the numerator.

The magnitude of $G(j\omega)$ in dB is obtained by multiplying the logarithm to the base 10 of $|G(j\omega)|$ by 20.

[4] There is little reason for this choice; the choice dates from Alexander Graham Bell's study of the response of the human ear. In electromagnetics and some other applications, the natural logarithm is used; the unit then is *neper*.

$$
\begin{aligned}
|G(j\omega)|_{\text{dB}} &= 20 \log |G(j\omega)| \\
&= 20 \log K + 20 \log |1 + j\omega\tau_a| + 20 \log |1 + j\omega\tau_b| + \cdots \\
&\quad - 20N \log |j\omega| - 20 \log |1 + j\omega\tau_1| - 20 \log |1 + j\omega\tau_2| - \cdots \\
&\quad - 20 \log |1 + j2\zeta\omega/\omega_n - \omega^2/\omega_n{}^2| - \cdots \qquad (8.28a)
\end{aligned}
$$

The phase of $G(j\omega)$ is

$$
\begin{aligned}
\angle G(j\omega) &= \tan^{-1}\omega\tau_a + \tan^{-1}\omega\tau_b + \cdots - N(90°) - \tan^{-1}\omega\tau_1 - \tan^{-1}\omega\tau_2 - \cdots \\
&\quad - \tan^{-1} 2\zeta\omega\omega_n/(\omega_n{}^2 - \omega^2) - \cdots \qquad (8.28b)
\end{aligned}
$$

Equations (8.28) express the magnitude and the phase of $G(j\omega)$ as linear combinations of relatively simple terms. The curves for each term can be added together graphically to get the curves for the complete transfer function.

The logarithmic scale used for frequency in Bode plots, has some interesting properties. The frequency in a typical control system application varies over many powers of ten so that most information would be compressed near the origin if a linear scale were used. The logarithmic scale is nonlinear, that is, the distance between 1 and 2 is greater than the distance between 2 and 3 and so on. As a result, use of this scale enables us to cover a greater range of frequencies; both low and high frequency behaviour of a system can be adequately displayed in one plot. The other interesting property of the use of log scale for frequency, as we shall see shortly, is that the straight-line approximation of the Bode plots becomes possible. This property allows the plotting by hand that is quick and yet sufficiently accurate for control-system design. Most control-system designers will have access to computer programs that will diminish the need for hand plotting; however, it is still important to develop good intuition so that erroneous computer results are quickly identified, and for this one needs the ability to check results by hand plotting.

The phase angle graph of the Bode plot, $\angle G(j\omega)$ *versus* $\log\omega$, has a linear scale for phase in degrees and a logarithmic scale for frequency ω. The magnitude graph[5] of the Bode plot, $|G(j\omega)|_{\text{dB}}$ versus $\log\omega$, has a linear scale for magnitude in dB and a logarithmic scale for frequency ω.

In general, a rational transfer function $G(s)$ can contain just four simple types of factors:

1. Real constant: $K > 0$
2. Poles or zeros at the origin of order N: $(s)^{\mp N}$
3. Poles or zeros at $s = -1/\tau$ of order q: $(1 + s\tau)^{\mp q}$
4. Complex poles or zeros of order r: $(1 + 2\zeta s/\omega_n + s^2/\omega_n{}^2)^{\mp r}$

Equations (8.28) indicate one of the unique characteristics of Bode plot—each of the four types of factors listed can be considered as a separate plot; the individual plots are then algebraically added to yield the total plot of the given transfer function. Bode plots of the four types of factors are, therefore, the basic building blocks for the construction of the Bode plot of the given transfer function.

8.5.1 Magnitude Plot: Straight-Line Approximation

We shall now discuss how the $|G(j\omega)|_{\text{dB}}$ *versus* $\log\omega$ graph can be sketched with very little effort using straight-line approximation. We first examine the basic building blocks, and then use these blocks to build the magnitude plot of the given transfer function.

[5]An alternative presentation of the magnitude graph uses logarithm scale for frequency ω and logarithmic scale for magnitude $|G(j\omega)|$, resulting in $\log |G(j\omega)|$ *versus* $\log\omega$ locus.

The dB *versus* log ω graph can be sketched on a linear rectangular coordinate graph paper. However, use of semilog graph paper is more convenient as it eliminates the need to take logarithm of many numbers. The logarithmic scale of the semilog graph paper is used for frequency and the linear scale is used for dB.

The units used to express frequency bands or frequency ratios are the *octave* and the *decade*. An octave is a frequency band from ω_1 to ω_2 where $\omega_2/\omega_1 = 2$. There is an increase of one decade from ω_1 to ω_2 when $\omega_2/\omega_1 = 10$. Semilog graph papers come in two, three, four or five cycles, indicating the range of coverage in decades (refer Fig. 8.23). It may be noted that we cannot locate the point $\omega = 0$ on the log scale since log $0 = -\infty$.

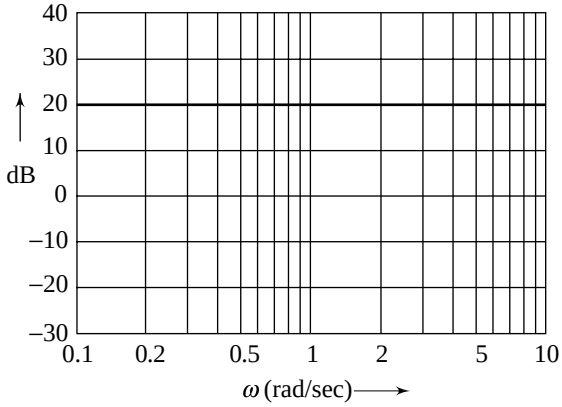

Fig. 8.23 Bode magnitude plot of *K*

Real constant K Since the constant K is frequency-invariant, the plot of

$$\text{dB} = 20 \log K \tag{8.29}$$

is a horizontal straight line. The magnitude plot for $K = 10$ is shown in Fig. 8.23 in semilog coordinates. The horizontal axis is log ω; labeled ω on logarithmic scale. The vertical axis is magnitude in decibels; labeled dB on linear scale.

Poles or zeros at the origin The factor $1/(j\omega)$ appearing in a transfer function $G(j\omega)$ has the magnitude

$$\text{dB} = 20 \log \left| \frac{1}{j\omega} \right| = -20 \log \omega \tag{8.30}$$

The dB versus log ω plot of Eqn. (8.30) is a straight line with a slope of -20 dB per unit change in log ω. A unit change in log ω means

$$\log(\omega_2/\omega_1) = 1 \text{ or } \omega_2 = 10\omega_1$$

This range of frequencies is called a *decade*. Thus the slope of Eqn. (8.30) is -20 dB/decade. The range of frequencies $\omega_2 = 2\omega_1$ is called an *octave*. Since $-20 \log 2 = -6$ dB, the slope of Eqn. (8.30) could also be expressed as -6 dB/octave. The plot of Eqn. (8.30) is shown in Fig. 8.24a; it intersects the 0-dB axis at $\omega = 1$.

For an Nth-order pole at the origin, the magnitude is

$$\text{dB} = 20 \log \left| \frac{1}{(j\omega)^N} \right| = -20N \log \omega \tag{8.31}$$

The magnitude plot is still a straight line that intersects the 0-dB axis at $\omega = 1$, but the slope is now $-20N$ dB/decade.

For the case that a transfer function has a zero at the origin, the magnitude of the term is given by

$$\text{dB} = 20 \log |j\omega| = 20 \log \omega \tag{8.32}$$

and the plot is the negative of that for a pole at the origin; it is a straight line with a slope of + 20 dB/decade that intersects the 0-dB axis at $\omega = 1$ (Fig. 8.24b). For the case of an Nth-order zero at the origin, it is seen that the plot is the negative of that for the Nth-order pole.

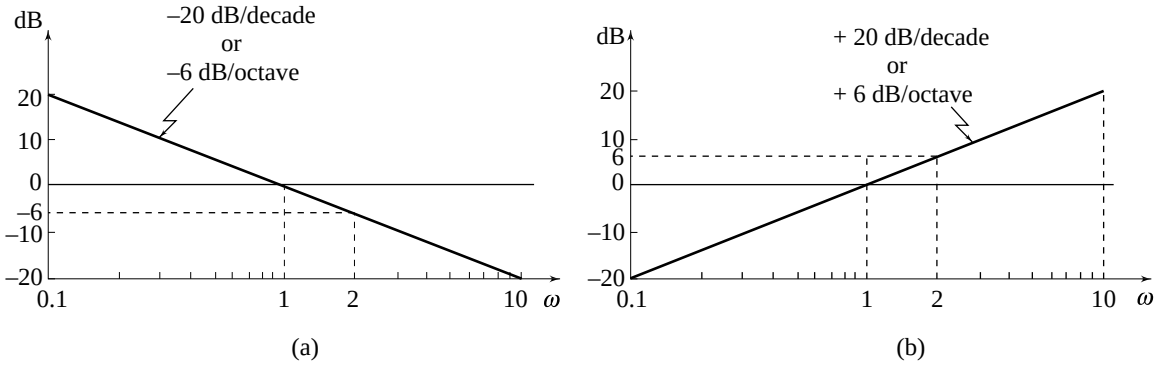

Fig. 8.24 Bode magnitude plot of (a) pole (b) zero at the origin

Example 8.8 Consider the transfer function

$$G(s) = \frac{K}{s^N}$$

There are two terms in $G(s)$: the constant K, and the repeated pole at the origin. We could add the Bode magnitude plots of the two terms to get the Bode magnitude plot of $G(s)$. However, treating K/s^N as a single term turns out to be more convenient, as is seen below.

$$\text{dB} = 20 \log \left| \frac{K}{(j\omega)^N} \right| = -20N \log \omega + 20 \log K \tag{8.33}$$

With $\log \omega$ as abscissa, the plot of Eqn. (8.33) is a straight line having a slope $-20N$ dB/decade and passing through $20 \log K$ dB when $\log \omega = 0$, i.e., when $\omega = 1$, as shown in Fig. 8.25. Further, the plot has a value of 0 dB at the frequency of

$$20N \log \omega = 20 \log K \quad \text{or} \quad \omega = (K)^{1/N}$$

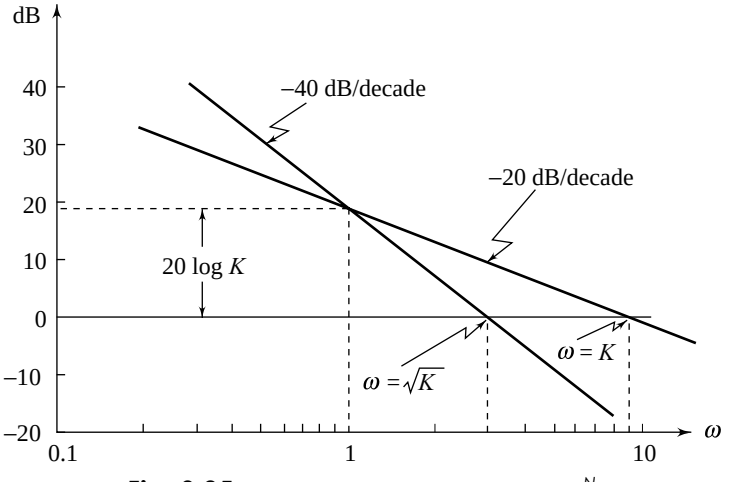

Fig. 8.25 Bode magnitude plot of K/s^N

Poles or zeros at s = –1/τ The factor $1/(1 + j\omega\tau)$ appearing in a transfer function $G(j\omega)$ has magnitude

$$\text{dB} = 20 \log \left| \frac{1}{1 + j\omega\tau} \right| = -20 \log \sqrt{1 + \omega^2\tau^2} \tag{8.34}$$

For low frequencies, such that $\omega << 1/\tau$, the magnitude may be approximated by

$$\text{dB} = -20 \log 1 = 0 \tag{8.35}$$

For high frequencies, such that $\omega >> 1/\tau$, the magnitude may be approximated by

$$\text{dB} = -20 \log(\omega\tau) = -20 \log \omega - 20 \log \tau \tag{8.36}$$

The plot of Eqn. (8.35) is a straight line coincident with the 0-dB axis. The plot of Eqn. (8.36) is also a straight line having a slope of –20 dB/decade intersecting the 0-dB axis at $\omega = 1/\tau$, as shown in Fig. 8.26. We call the straight line approximations the *asymptotes*. The low-frequency approximation is called the *low-frequency asymptote* and the high-frequency approximation is called the *high-frequency asymptote*. The frequency $\omega = 1/\tau$ at which the two asymptotes meet is called the *corner frequency* or *break frequency*.

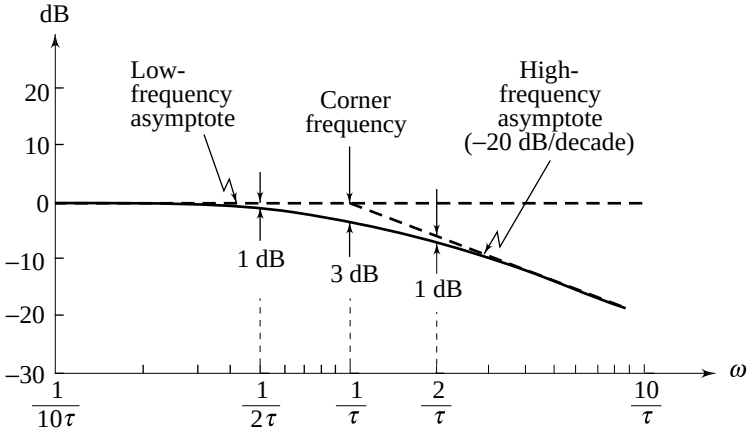

Fig. 8.26 Bode magnitude plot of $1/(1 + j\omega\tau)$

Though the asymptotic approximations hold good for $\omega << 1/\tau$ and $\omega >> 1/\tau$, with some loss of accuracy these could be extended for $\omega \leq 1/\tau$ and $\omega \geq 1/\tau$. Therefore, the dB *versus* log ω curve of $1/(1 + j\omega\tau)$ can be approximated by two asymptotes, one a straight line at 0 dB for the frequency range $0 < \omega \leq 1/\tau$ and the other, a straight line with a slope –20 dB/decade (or – 6 dB/octave) for the frequency range $1/\tau \leq \omega < \infty$. The corner frequency divides the plot into two regions, a low-frequency region and a high-frequency region.

The error in the magnitude plot caused by the use of asymptotes can easily be calculated. The maximum error occurs at the corner frequency $\omega = 1/\tau$ and is given by (refer Eqns (8.34) and (8.35))

$$-20 \log \sqrt{1 + 1} + 20 \log 1 = -3.01 \text{ dB}$$

The error at the frequency one octave below the corner frequency ($\omega = 1/(2\tau)$) is (refer Eqns (8.34) and (8.35))

$$-20 \log \sqrt{1 + \tfrac{1}{4}} + 20 \log 1 = -0.97 \text{ dB}$$

The error at the frequency one octave above the corner frequency ($\omega = 2/\tau$) is (refer Eqns (8.34) and (8.36))

$$-20 \log \sqrt{1+4} + 20 \log 2 = -0.97 \text{ dB}$$

The error at the frequency one decade below the corner frequency ($\omega = 1/(10\tau)$) is

$$-20 \log \sqrt{1+\tfrac{1}{100}} + 20 \log 1 = -0.04 \text{ dB}$$

The error at the frequency one decade above the corner frequency ($\omega = 10/\tau$) is

$$-20 \log \sqrt{1+100} + 20 \log 10 = -0.04 \text{ dB}$$

Similarly, the errors at other frequencies may be calculated.

In practice, a sufficiently accurate magnitude plot is obtained by correcting the asymptotic plot by -3 dB at the corner frequency and by -1 dB one octave below and one octave above the corner frequency, and then drawing a smooth curve through these points approaching the low and high frequency asymptotes, as shown in Fig. 8.26.

It is seen from Eqn. (8.28a) that the magnitude plot of the factor $1 + j\omega\tau$ is exactly of the same form as that of the factor $1/(1 + j\omega\tau)$, but with the opposite sign. The approximate plot consists of two straight line asymptotes, one a straight line at 0 dB for the frequency range $0 < \omega \le 1/\tau$, and the other a straight line with a slope of +20 dB/decade (or + 6 dB/octave) for the frequency range $1/\tau \le \omega < \infty$. The frequency $\omega = 1/\tau$ is the corner frequency. A sufficiently accurate plot is obtained by correcting the asymptotic plot by + 3 dB at the corner frequency and by + 1 dB one octave below and one octave above the corner frequency, and then drawing a smooth curve through these points approaching the low and high frequency asymptotes, as shown in Fig. 8.27.

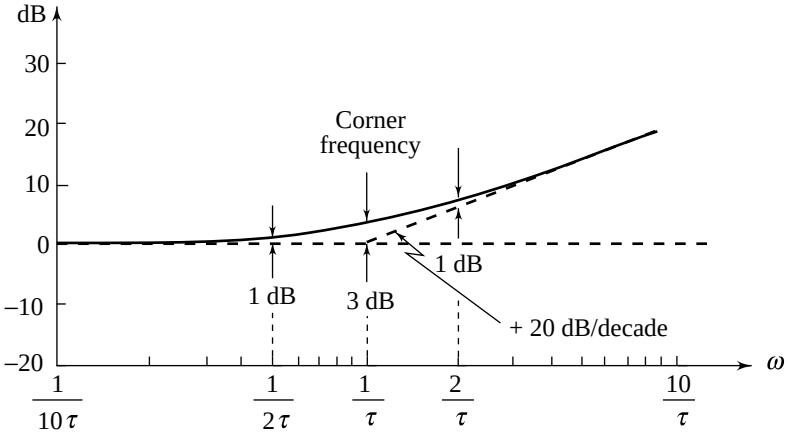

Fig. 8.27 Bode magnitude plot of $(1 + j\omega\tau)$

For the case when a given transfer function involves terms like $(1+j\omega\tau)^{\mp q}$, a similar asymptotic construction may be made. The corner frequency is still at $\omega = 1/\tau$ and the asymptotes are straight lines. The low-frequency asymptote is a straight line at 0 dB and the high-frequency asymptote has a slope of $\mp 20q$ dB/decade (or $\mp$ $6q$ dB/octave). The error involved in asymptotic approximation is q times that for $(1 + j\omega\tau)^{\mp 1}$; $\mp$ $3q$ dB at the corner frequency and $\mp$ q dB one octave below and one octave above the corner frequency.

Example 8.9 Let us draw the Bode magnitude plot for the transfer function

$$G(s) = \frac{200(s+1)}{(s+10)^2}$$

The rearrangement of the transfer function in the time-constant form gives

$$G(s) = \frac{2(1+s)}{(1+s/10)^2}$$

Therefore, the sinusoidal transfer function in the time-constant form is given by

$$G(j\omega) = \frac{2(1+j\omega)}{(1+j\omega/10)^2}$$

Our approach is to first construct an asymptotic plot and then apply corrections to it to get an accurate plot. The corner frequencies of the asymptotic plot in order of their occurrence as frequency increases, are

(i) $\omega_{c1} = 1$, due to zero at $s = -1$;

(ii) $\omega_{c2} = 10$, due to double pole at $s = -10$

At frequencies less than ω_{c1}, the first corner frequency, only the factor $K = 2$ is effective.

Pertinent characteristics of each factor of the transfer function are given in Table 8.1. By sketching the asymptotes for each factor and then algebraically adding them, we obtain the asymptotic plot for the transfer function $G(j\omega)$. We can, however, draw the composite asymptotic plot directly, as is outlined below.

Step 1: We start with the factor $K = 2$. Its magnitude plot is the asymptote 1; a horizontal straight line at the magnitude of 6 dB.

Step 2: Let us now add to the asymptote 1, the plot of the factor $(1 + j\omega)$ corresponding to the lowest corner frequency $\omega_{c1} = 1$. Since this factor contributes zero dB for $\omega \le \omega_{c1} = 1$, the resultant plot up to $\omega = 1$ is the same as that of the asymptote 1. For $\omega > \omega_{c1} = 1$, this factor contributes +20 dB/decade such that the resultant plot of the two factors is the asymptote 2 of slope + 20 dB/decade passing through (6 dB, 1 rad/sec) point. At $\omega = \omega_{c2} = 10$, the resultant plot has a magnitude of 26 dB as shown in Fig. 8.28.

Table 8.1 Asymptotic approximation table for Bode magnitude plot of $2(1 + j\omega)/(1 + j\omega/10)^2$

Factor	*Corner frequency*	*Asymptotic magnitude characteristic*
2	None	Constant magnitude of + 6 dB
$1 + j\omega$	$\omega_{c1} = 1$	Straight line of 0 dB for $\omega \le \omega_{c1}$; straight line of +20 dB/decade for $\omega \ge \omega_{c1}$
$1/(1 + j\omega/10)^2$	$\omega_{c2} = 10$	Straight line of 0 dB for $\omega \le \omega_{c2}$; straight line of – 40 dB/decade for $\omega \ge \omega_{c2}$

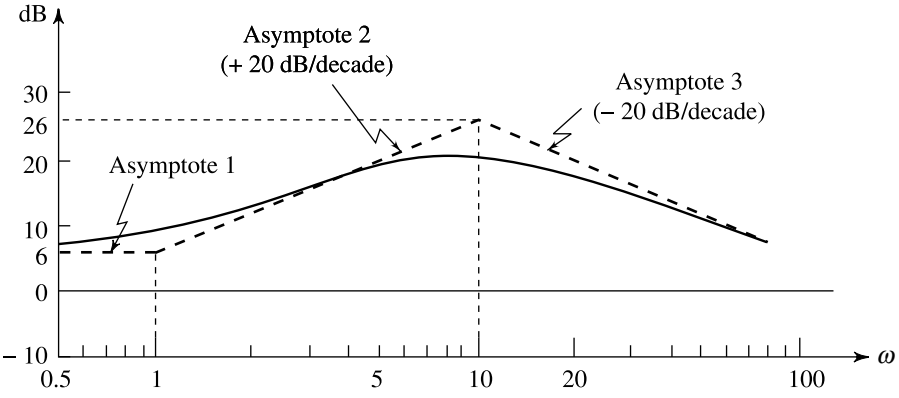

Fig. 8.28 Bode magnitude plot for Example 8.9

Step 3: We now add to the resultant plot of step 2, the plot of the factor $1/(1 + j\omega/10)^2$ corresponding to the corner frequency $\omega_{c2} = 10$. Since this factor contributes 0 dB for $\omega \le \omega_{c2} = 10$, the resultant plot up to $\omega = 10$ is the same as that of step 2. For $\omega > \omega_{c2} = 10$, this factor contributes – 40 dB/decade such that the resultant plot of the three factors is the asymptote 3 of slope (+ 20) + (– 40) = – 20 dB/decade passing through (26 dB, 10 rad/sec) point. Figure 8.28 shows the asymptotic magnitude plot of given $G(j\omega)$.

To the asymptotic plot thus obtained, corrections are to be applied. The corrections at each corner frequency and at an octave above and below the corner frequency are usually sufficient. The corner frequency $\omega_{c1} = 1$ corresponds to the first-order factor $(1 + j\omega)$: the corrections are + 3dB at $\omega = 1$, +1dB at $\omega = 0.5$ and + 1dB at $\omega = 2$. The corner frequency $\omega_{c2} = 10$ corresponds to second-order factor $1/(1 + j\omega/10)^2$: the corrections are – 6dB at $\omega = 10$, – 2 dB at $\omega = 5$ and – 2 dB at $\omega = 20$. Table 8.2 lists the net corrections.

Table 8.2 Corrections to the asymptotic magnitude plot of $2(1 + j\omega)/(1 + j\omega/10)^2$

Frequency, ω	0.5	1	2	5	10	20
Net correction	+1 dB	+3 dB	+1 dB	–2 dB	–6 dB	–2 dB

The corrected asymptotic magnitude plot of the given transfer function is shown in Fig. 8.28.

Example 8.10 Consider the transfer function $G(j\omega) = \dfrac{10(1 + j\omega/2)}{(j\omega)^2(1 + j\omega)}$

The corner frequencies of the asymptotic Bode magnitude plot of $G(j\omega)$ in order of their occurrence as frequency increases, are

(i) $\omega_{c1} = 1$, due to simple pole,
(ii) $\omega_{c2} = 2$, due to simple zero.

At frequencies less than ω_{c1}, only the factor $10/(j\omega)^2$ is effective.

Asymptotic magnitude plot of $G(j\omega)$ is shown in Fig. 8.29. The plot is obtained following the steps given below:

Step 1: We start with the factor $10/(j\omega)^2$ corresponding to double pole at the origin. Its magnitude plot is the asymptote 1, having a slope of -40 dB/decade and passing through the point 20 log 10 = 20 dB at $\omega = 1$. Asymptote 1 intersects the 0-dB line at $\omega = \sqrt{10}$.

Step 2: Let us now add to the asymptote 1, the plot of the factor $1/(1 + j\omega)$ corresponding to the lowest corner frequency $\omega_{c1} = 1$. Since this factor contributes zero dB for $\omega \leq 1$, the resultant plot up to $\omega = 1$ is the same as that of asymptote 1. For $\omega > 1$ this factor contributes -20 dB/decade such that the resultant plot of the two factors is the asymptote 2 of slope $(-40) + (-20) = -60$ dB/decade passing through (20 dB, 1 rad/sec) point. At $\omega = \omega_{c2} = 2$, the resultant plot has a magnitude of 2 dB as shown in Fig. 8.29.

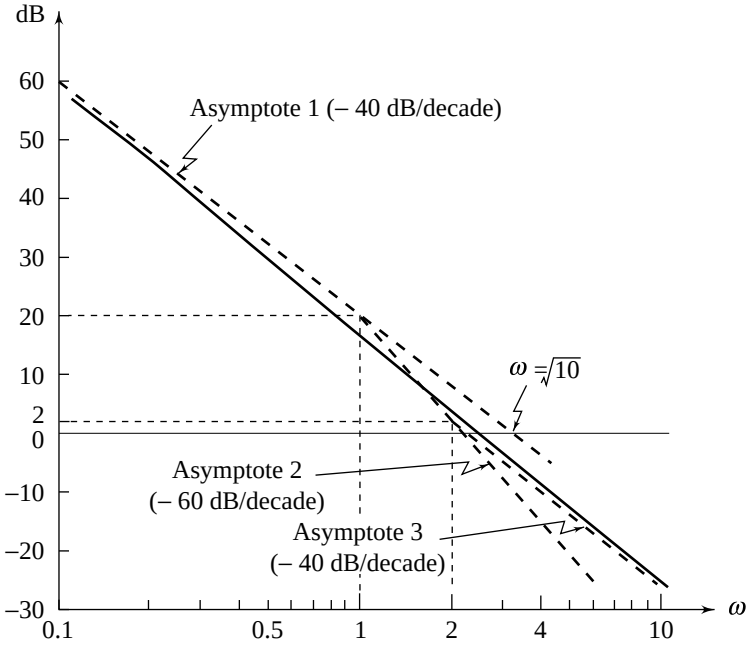

Fig. 8.29 Bode magnitude plot for Example 8.10

Step 3: We now add to the resultant plot of step 2, the plot of the factor $(1 + j\omega/2)$ corresponding to the corner frequency $\omega_{c2} = 2$. This gives rise to a straight line of slope + 20 dB/decade for $\omega > 2$, which when added to asymptote 2 results in asymptote 3 of slope $(-60) + (+20) = -40$ dB/decade passing through (2 dB, 2 rad/sec) point. Figure 8.29 shows the asymptotic magnitude plot of given $G(j\omega)$.

To the asymptotic plot thus obtained, corrections are to be applied. The corrections due to asymptotic approximation of magnitude plot of the pole factor are: -3 dB at $\omega = 1$, -1 dB at $\omega = 0.5$ and -1 dB at $\omega = 2$. To these corrections, we algebraically add the corrections due to the asymptotic approximation of magnitude plot of the zero factor: + 3 dB at $\omega = 2$, + 1 dB at $\omega = 1$, and +1 dB at $\omega = 4$. Table 8.3 lists the net corrections.

Table 8.3 Corrections to the asymptotic magnitude plot of $10(1+j\omega/2)/(j\omega)^2(1+j\omega)$

Frequency, ω	0.5	1	2	4
Net correction	–1 dB	–2 dB	+2 dB	+1 dB

The corrected asymptotic magnitude plot of the given transfer function is shown in Fig. 8.29.

Complex Poles or Zeros Transfer functions of control systems often possess quadratic factors of the form

$$\frac{1}{1+j(2\zeta/\omega_n)\omega-\omega^2/\omega_n^2};\ 0<\zeta\le 1 \tag{8.37a}$$

This term is slightly more complicated since besides being a function of ω as before, it is also a function of the variable ζ. As may be expected, the shape of the Bode plot depends strongly upon what value of damping ratio ζ is being considered.

In normalized form, the quadratic factor (8.37a) may be written as

$$\frac{1}{(1+j2\zeta u-u^2)} \tag{8.37b}$$

where $u=\omega/\omega_n$ is the normalized frequency. The magnitude of this factor is

$$\text{dB}=20\log\left|\frac{1}{1-u^2+j2\zeta u}\right|=-20\log\sqrt{(1-u^2)^2+(2\zeta u)^2} \tag{8.38}$$

For low frequencies, such that $u \ll 1$, the magnitude may be approximated by

$$\text{dB}=-20\log 1=0 \tag{8.39}$$

For high frequencies, such that $u \gg 1$, the magnitude may be approximated by

$$\text{dB}=-20\log(u^2)=-40\log u \tag{8.40}$$

Therefore an approximate magnitude plot of the quadratic factor (8.37b) consists of two straight line asymptotes, one horizontal line at 0 dB for $u \le 1$ and the other, a line with a slope -40 dB/decade for $u \ge 1$. The two asymptotes meet on 0-dB line at $u = 1$, i.e., $\omega = \omega_n$, which is the corner frequency of the plot. The asymptotic plot is shown in Fig. 8.30.

The error in the magnitude plot caused by the use of asymptotes can be calculated as follows.

For $0 < u \le 1$, the error is (refer Eqns (8.38) and (8.39))

$$-20\log\sqrt{(1-u^2)^2+(2\zeta u)^2}+20\log 1 \tag{8.41a}$$

and for $1 \le u < \infty$, the error is (refer Eqns (8.38) and (8.40))

$$-20\log\sqrt{(1-u^2)^2+(2\zeta u)^2}+40\log u \tag{8.41b}$$

The error at the corner frequency ($u = 1$ or $\omega = \omega_n$) is

$$-20\log 2\zeta \tag{8.42}$$

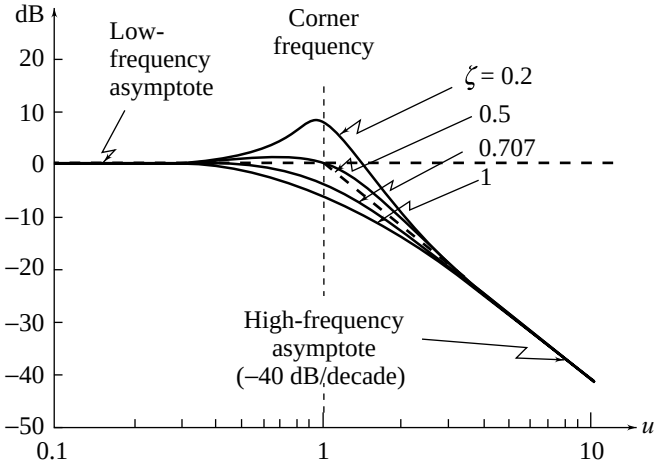

Fig. 8.30 Bode magnitude plot of $1/(1 + j2\zeta u - u^2)$

For $\zeta = 1$, the error at the corner frequency is $-20 \log 2 \cong -6$ dB. Note that for $\zeta = 1$, Eqn. (8.37) has two equal real poles:

$$\left.\frac{1}{(1 + j2\zeta u - u^2)}\right|_{\zeta=1} = \frac{1}{(1 + ju)^2} = \frac{1}{(1 + j\omega/\omega_n)^2}$$

From expression (8.42) we see that at the corner frequency, the error is negative for $\zeta > 0.5$ and positive for $\zeta < 0.5$. The corrected magnitude curves for various values of ζ are shown in Fig. 8.30. From this figure, it is seen that for small values of ζ, the magnitude curves have pronounced peak at a frequency slightly less than the corner frequency. In fact, smaller the value of ζ the higher the peak. We shall discuss this peak in some detail.

Consider Fig. 8.31, which shows what might be a typical plot of (refer Eqn. (8.38))

$$\text{dB} = -20 \log \sqrt{(1 - u^2)^2 + (2\zeta u)^2}$$

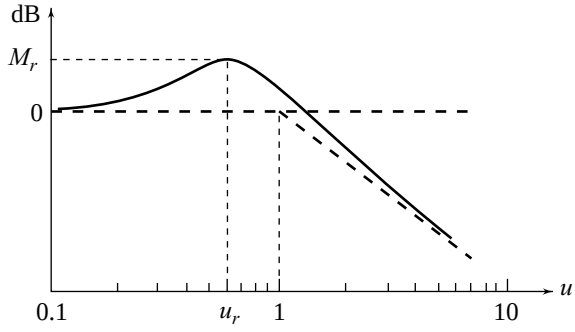

Fig. 8.31 A typical magnitude curve of $1/(1 + j2\zeta u - u^2)$

The peak value occurs at normalized frequency which is labeled u_r ($u_r = \omega_r/\omega_n$) and the height of the peak is M_r. This peak will occur at a u where $\sqrt{(1-u^2)^2 + (2\zeta u)^2}$ is at a minimum. The minimum can be found by simple differentiation.

$$\frac{d}{du}\left[\sqrt{(1-u^2)^2 + (2\zeta u)^2}\right]\Bigg|_{u=u_r} = \frac{\frac{1}{2}\left[-4(1-u_r^2)u_r + 8\zeta^2 u_r\right]}{[(1-u_r^2)^2 + (2\zeta u_r)^2]^{1/2}} = 0$$

which gives

$$4u_r^3 - 4u_r + 8\zeta^2 u_r = 0$$

or

$$u_r = \sqrt{1-2\zeta^2} \tag{8.43}$$

The corresponding peak value M_r is then

$$M_r = -20 \log \sqrt{(1-u_r^2)^2 + (2\zeta u_r)^2}$$

$$= -20 \log 2\zeta\sqrt{1-\zeta^2} \text{ dB} \tag{8.44}$$

Note that as ζ goes to zero, the peak value M_r goes off to infinity (refer Eqn. (8.44)) and frequency u_r approaches the corner frequency (refer Eqn. (8.43)). For $0 < \zeta < 1/\sqrt{2}$, u_r is less than the corner frequency. For $\zeta \geq 1/\sqrt{2}$, the errors given by expressions (8.41) are negative for all frequencies and therefore magnitude curves do not have a peak.

For given values of ζ and ω_n, an exact dB versus $\log\omega$ curve is obtained from the following expression (refer Eqn. (8.38)).

$$\text{dB} = -20 \log \sqrt{\left[1-\left(\frac{\omega}{\omega_n}\right)^2\right]^2 + \left(\frac{2\zeta\omega}{\omega_n}\right)^2} \tag{8.45}$$

Most control-system designers will have access to computer programs to do this job. The following procedure is useful for hand plotting.

Draw two straight line asymptotes: one a 0-dB line for $0 < \omega \leq \omega_n$ and the other a -40 dB/decade line for $\omega_n \leq \omega < \infty$. The two asymptotes meet at the corner frequency $\omega = \omega_n$. Correct the asymptotic plot by M_r dB at the frequency ω_r where (refer Eqns (8.44) and (8.43))

$$M_r = -20 \log 2\zeta\sqrt{1-\zeta^2} \text{ dB} \tag{8.46a}$$

$$\omega_r = \omega_n \sqrt{1-2\zeta^2} \text{ rad/sec} \tag{8.46b}$$

Of course, this correction is applied when $\zeta < 1/\sqrt{2}$. Correct the asymptotic plot by $-20 \log (2\zeta)$ dB at the corner frequency $\omega = \omega_n$ (refer expression (8.42)). Draw a smooth curve through these points approaching the low and high frequency asymptotes.

The accuracy of the plot can be improved by correcting the asymptotic plot at some other frequencies also; say one octave below and above the corner frequency. The errors are calculated from the following expressions (refer expressions (8.41)).

$$-20\log\sqrt{\left[1-\left(\frac{\omega}{\omega_n}\right)^2\right]^2+\left[2\zeta\left(\frac{\omega}{\omega_n}\right)\right]^2} \quad \text{for } 0<\omega\le\omega_n \tag{8.47a}$$

$$-20\log\sqrt{\left[1-\left(\frac{\omega}{\omega_n}\right)^2\right]^2+\left[2\zeta\left(\frac{\omega}{\omega_n}\right)\right]^2}+40\log\left(\frac{\omega}{\omega_n}\right) \quad \text{for } \omega_n\le\omega<\infty \tag{8.47b}$$

The magnitude plot of the factor $[(1+j(2\zeta/\omega_n)\omega-\omega^2/\omega^2{}_n]$ is exactly of the same form as that of the factor $1/[1+j(2\zeta/\omega_n)\omega-\omega^2/\omega_n{}^2]$, but with the opposite sign. Similar asymptotic construction may be made for the case when a given transfer function involves terms like $[1+j\,(2\zeta/\omega_n)\omega-\omega^2/\omega_n{}^2]^{\mp r}$.

Example 8.11 Let us draw the Bode magnitude plot of the transfer function

$$G(s)=\frac{200(s+2)}{s(s^2+10\,s+100)}$$

The rearrangement of the transfer function in time-constant form gives

$$G(s)=\frac{4(1+s/2)}{s[1+s/10+(s/10)^2]}$$

Therefore, the sinusoidal transfer function in time-constant form is given by

$$G(j\omega)=\frac{4(1+j\omega/2)}{j\omega(1+j\omega/10-\omega^2/100)} \tag{8.48}$$

The corner frequencies of the asymptotic plot of $G(j\omega)$, in order of their occurrence as frequency increases, are

(i) $\omega_{c1}=2$, due to zero at $s=-2$;

(ii) $\omega_{c2}=10$, due to pair of complex conjugate poles with $\zeta=0.5$ and $\omega_n=10$.

At frequencies less than ω_{c1}, only the factor $4/(j\omega)$ is effective.

Asymptotic magnitude plot of $G(j\omega)$ is drawn in Fig. 8.32. The plot is obtained following the steps given below.

Step 1: We start with the factor $4/(j\omega)$ corresponding to the pole at the origin. Its magnitude plot is the asymptote 1 having a slope of –20 dB/decade passing through the point 20 log 4 = 12 dB at $\omega = 1$. Asymptote 1 intersects the 0-dB line at $\omega=4$. At $\omega=\omega_{c1}=2$, the magnitude is 6 dB.

Step 2: We now add to the asymptote 1, the plot of the factor $(1+j\omega/2)$ corresponding to the lowest corner frequency $\omega_{c1}=2$. Since this factor contributes 0 dB for $\omega\le 2$, the resultant plot up to $\omega=2$ is the same as that of asymptote 1. For $\omega>2$, this factor contributes +20 dB/decade such that the resultant plot of the two factors is the asymptote 2 of slope (– 20) + (+ 20) = 0 dB/decade passing through (6 dB, 2 rad/sec) point. At $\omega=\omega_{c2}=10$, the resultant plot has a magnitude of 6 dB as shown in Fig. 8.32.

Step 3: We now add to the resultant plot of step 2, the plot of the factor $1/(1+j\omega/10-\omega^2/100)$ corresponding to the corner frequency $\omega_{c2}=\omega_n=10$. This gives rise to a straight line of slope – 40 dB/decade for $\omega>10$ which when added to asymptote 2 results in asymptote 3 with a slope 0 + (– 40) = – 40 dB/decade passing through the point (6 dB, 10 rad/sec).

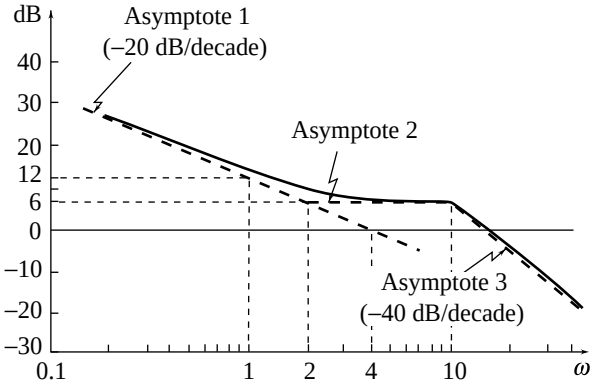

Fig. 8.32 Bode magnitude plot for Example 8.11

To the asymptotic plot thus obtained, corrections are to be applied. Table 8.4 lists the corrections.

Table 8.4 Corrections to the asymptotic plot of $4\,(1 + j\omega/2)/(j\omega)(1 + j\omega/10 - \omega^2/100)$

Frequency	*Correction*	*Remarks*
$\omega = 2$	+ 3 dB	
$\omega = 1$	+ 1 dB	
$\omega = 4$	+ 1 dB	
$\omega = 10$	0 dB	Error = $-20 \log 2\zeta = 0$
$\omega = 10/\sqrt{2}$	$-20 \log (\sqrt{3}/2)$ dB	$M_r = -20 \log 2\zeta\sqrt{1-\zeta^2}$

The corrected asymptotic plot of the given transfer function is shown in Fig. 8.32.

8.5.2 Phase Plot

The phase angle at any frequency can be obtained as the algebraic sum of the phase angles due to various factors in the transfer function, in a manner similar to that used for obtaining magnitude plots (refer Eqns (8.28)). To illustrate the procedure, we consider the transfer function

$$G(j\omega) = \frac{K(1 + j\omega\tau_1)}{j\omega(1 + j\omega\tau_2)(1 + (j2\zeta/\omega_n)\omega - \omega^2/\omega_n^2)} \tag{8.49}$$

The phase of $G(j\omega)$ is

$$\begin{aligned} \angle G(j\omega) &= \tan^{-1}\omega\tau_1 - 90° - \tan^{-1}\omega\tau_2 - \tan^{-1}2\zeta\omega\omega_n/(\omega_n^2 - \omega^2) \\ &= \phi_1 + \phi_2 + \phi_3 + \phi_4 \end{aligned} \tag{8.50}$$

The first term on the right-hand side of Eqn. (8.50) is due to the real zero, and is given by

$$\phi_1 = \tan^{-1}\omega\tau_1$$

The values of ϕ_1 for various values of ω are given in Table 8.5, and these values are plotted in Fig. 8.33. We can approximate the exact curve with the straight line construction shown in Fig. 8.33. The straight line approximation for the phase characteristic breaks from 0° at the frequency $\omega = 1/10\,\tau_1$, and breaks again to a

constant value of 90° at $\omega = 10/\tau_1$. The maximum error in the approximation is 5.7°, and occurs at the two corners $1/10\tau_1$ and $10/\tau_1$.

The second term on the right-hand side in Eqn. (8.50) is due to the pole at the origin and is identically equal to $-90°$. The third term in Eqn. (8.50) is due to the real pole and is similar to the first term but for reversal in sign. We shall now look at the fourth term, which is due to the complex-conjugate pair of poles, and is given by

$$\phi_4 = -\tan^{-1}\frac{2\zeta\omega_n\omega}{\omega_n^2 - \omega^2}$$

Table 8.5 Phase characteristics of $(1 + j\omega\tau_1)$

ω (rad/sec)	*Exact value*	*Straight line approximation*
$0.05/\tau_1$	2.9°	0°
$0.1/\tau_1$	5.7°	0°
$0.2/\tau_1$	11.3°	13.5°
$0.5/\tau_1$	26.6°	31.5°
$0.8/\tau_1$	38.7°	40.6°
$1/\tau_1$	45°	45°
$2/\tau_1$	63.4°	58.5°
$5/\tau_1$	78.7°	76.5°
$8/\tau_1$	82.9°	85.6°
$10/\tau_1$	84.3°	90°
$20/\tau_1$	87.1°	90°

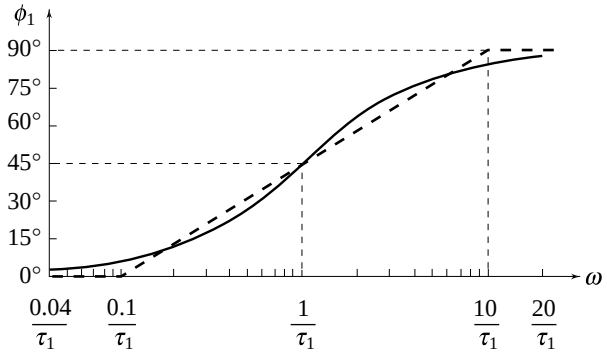

Fig. 8.33 Phase characteristics of $(1 + j\omega\tau_1)$

For $\omega << 0.1\omega_n$, we have $\phi_4 = 0$, and for $\omega >> 10\omega_n$, we get $\phi_4 = 180°$. At the intermediate frequency $\omega = \omega_n$, we have $\phi_4 = 90°$. The plots of the asymptotic approximation and the actual curve for various values of ζ are shown in Fig. 8.34. It is seen that for small values of ζ, the actual phase angle changes very rapidly for ω near the undamped natural frequency ω_n.

The overall phase angle is now obtained as the algebraic sum of the phase angle due to each factor. The addition, however, is not as simple as in the case of the magnitude plot due to the fact that the straight line approximation consists of three parts over four decades. The only exception arises when the various poles and zeros have 'large' separation, so that frequency range of phase angle plot of one factor does not overlap with the frequency range of phase angle plot of any other factor. In this case, the phase angle plots for the various factors can be superimposed on each other to obtain the overall phase.

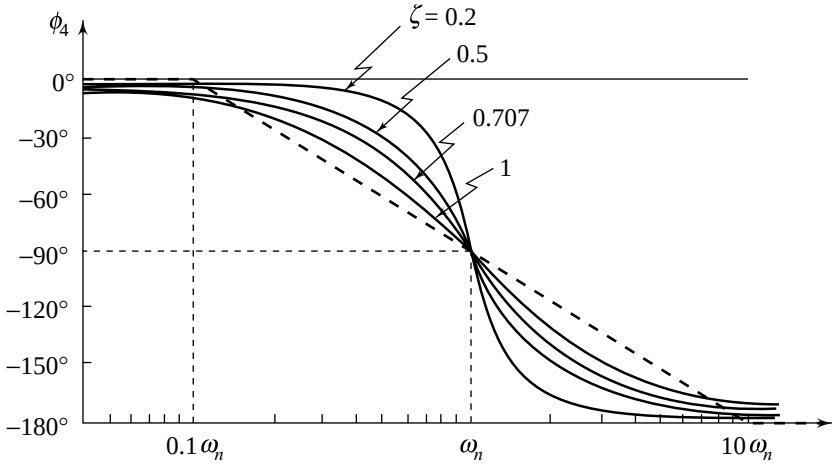

Fig. 8.34 Phase characteristics of $1/[1 + (j\,2\zeta/\omega_n)\omega - \omega^2/\omega_n{}^2\ ]$

For a general case, it is usually advisable to make a table of phase angle against frequency for each factor and then obtain the total phase as the algebraic sum of these. Better accuracy is obtained by using the exact values in the table instead of those obtained through the asymptotic approximation. The computational effort to achieve this accuracy is not heavy.

Example 8.12 Consider the transfer function given in Eqn. (8.48) for which the magnitude plot was obtained in Fig. 8.32. We shall now plot the phase curve.

The phase angle due to each factor for different values of ω is given in Table 8.6. The plot of the total phase is shown in Fig. 8.35.

Table 8.6 Phase angle due to different factors of the transfer function given by Eqn. (8.48)

ω (rad/sec)	*Poles at the origin*	*Zero at* $s = -2$	*Complex conjugate poles*	*Total phase angle,* ϕ
0.1	– 90°	2.86°	– 0.57°	– 87.71°
0.2	– 90°	5.71°	– 1.15°	– 85.44°
0.5	– 90°	14.04°	– 2.87°	– 78.33°
1	– 90°	26.57°	– 5.77°	– 69.20°
2	– 90°	45.00°	– 11.77°	– 56.77°
5	– 90°	68.20°	– 33.69°	– 55.49°
10	– 90°	78.69°	– 90.00°	– 101.32°
20	– 90°	84.29°	– 146.31°	– 152.02°
50	– 90°	87.71°	– 168.23°	– 170.52°
100	– 90°	88.85°	– 174.22°	– 175.68°

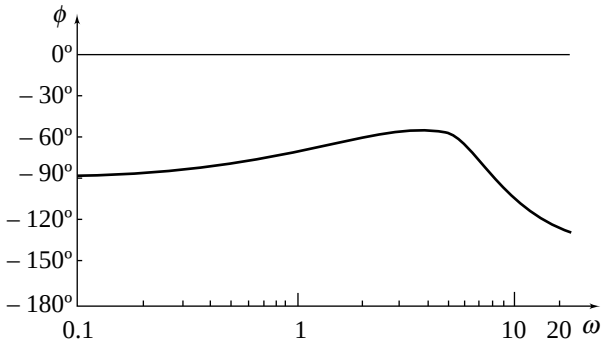

Fig. 8.35 Bode phase plot for Example 8.12

8.6 STABILITY MARGINS ON THE BODE PLOTS

The general objective of the frequency-domain design procedures is to shape the Nyquist plot such that the critical point $-1+j0$ is avoided with some reasonable stability margins, thereby providing acceptable closed-loop response characteristics. Direct use of the Nyquist plot for design is not particularly convenient, since changes in parameters other than gain require extensive plot revisions. Fortunately, general characteristics of Nyquist plots can be visualized with reasonable accuracy in most cases of interest from Bode plots, and Bode plots are easily constructed and modified.

Since the Bode plot corresponds to only the positive portion of the $j\omega$-axis from $\omega = 0$ to $\omega = \infty$ in the s-plane, its use in stability studies is limited to the determination of gain and phase crossover points and the corresponding phase and gain margins. In practice, the Bode plot is more convenient to apply when the system has open-loop transfer function with no poles in right half s-plane.

Since the straight line approximation of the Bode plot is relatively easier to construct, the data necessary for the other frequency-domain plots, such as the Nyquist plots, can be easily generated from the Bode plot.

Example 8.13 A unity-feedback system has open-loop transfer function

$$G(s) = \frac{K}{(s+2)(s+4)(s+5)}; K = 200 \tag{8.51a}$$

Let us determine the stability of this system implementing the Nyquist stability criterion using Bode plots.

We begin by sketching the Bode magnitude and phase plots. In the time-constant form, the transfer function $G(s)$ is expressed as

$$G(s) = \frac{5}{(1+s/2)(1+s/4)(1+s/5)} \tag{8.51b}$$

The sinusoidal transfer function

$$G(j\omega) = \frac{5}{(1+j\omega/2)(1+j\omega/4)(1+j\omega/5)}$$

Bode magnitude and phase plots for $G(j\omega)$ are shown in Fig. 8.36.

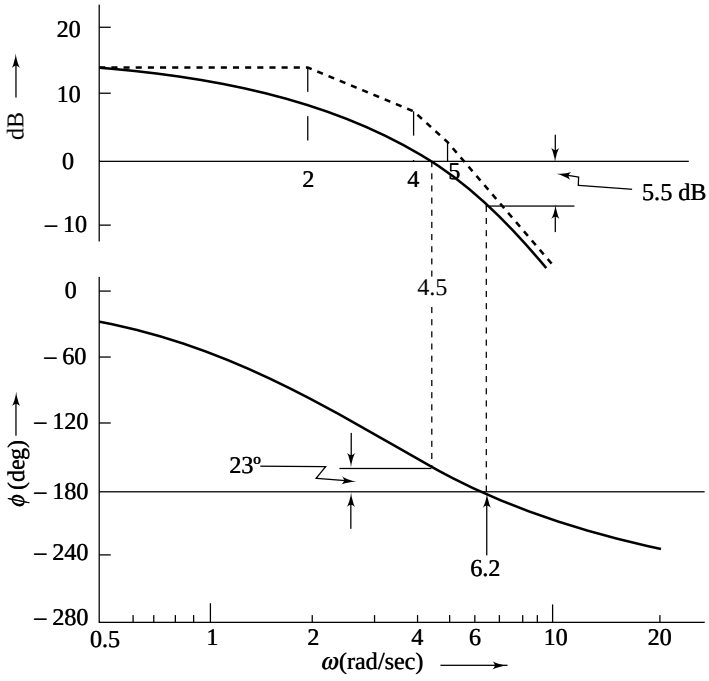

Fig. 8.36 Bode plot for Example 8.13

The Nyquist criterion for this example tells us that we want zero encirclements of the $-1+j0$ point for stability. Thus, we recognise that on Bode magnitude plot, the magnitude must be less than 0 dB (which corresponds to unity gain of $G(j\omega)$ on polar plane) at that frequency where the phase is $-180°$. Accordingly, we see that at a frequency of 6.2 rad/sec where the phase is $-180°$, the magnitude is -5.5 dB. Therefore, an increase in gain of +5.5 dB is possible before the system becomes unstable. Since the magnitude plot was drawn for a gain of 200 (refer Eqn. (8.51a)), + 5.5 dB (20 log 1.885 ≅ 5.5) represents the allowed increase in gain above 200. Hence the gain for instability is 200 × 1.885 = 377. The closed-loop system is stable for $0 < K < 377$.

Next we show how to evaluate the gain and phase margins using Bode plots. The gain margin is found by using the phase plot to find the phase crossover frequency ω_ϕ where the phase angle is $-180°$. At this frequency, look at the magnitude plot to determine the gain margin, GM, which is the gain required to raise the magnitude curve to 0 dB. From Fig. 8.36, we find that

$$\omega_\phi = 6.2 \text{ rad/sec}; \; GM = 5.5 \text{ dB}$$

The phase margin is found by using the magnitude curve to find the gain crossover frequency ω_g, where the gain is 0 dB. On the phase curve at that frequency, the phase margin, ΦM, is the difference between the phase value and $-180°$. From Fig. 8.36, we find that

$$\omega_g = 4.5 \text{ rad/sec}; \; \Phi M = -157° - (-180°) = 23°$$

Example 8.14 Consider now a unity-feedback system with open-loop transfer function

$$G(s) = \frac{K}{s(1+0.1s)(1+0.2s)}; \; K = 100$$

The Bode plot of $G(j\omega)$ is shown in Fig. 8.37. From this figure we find that

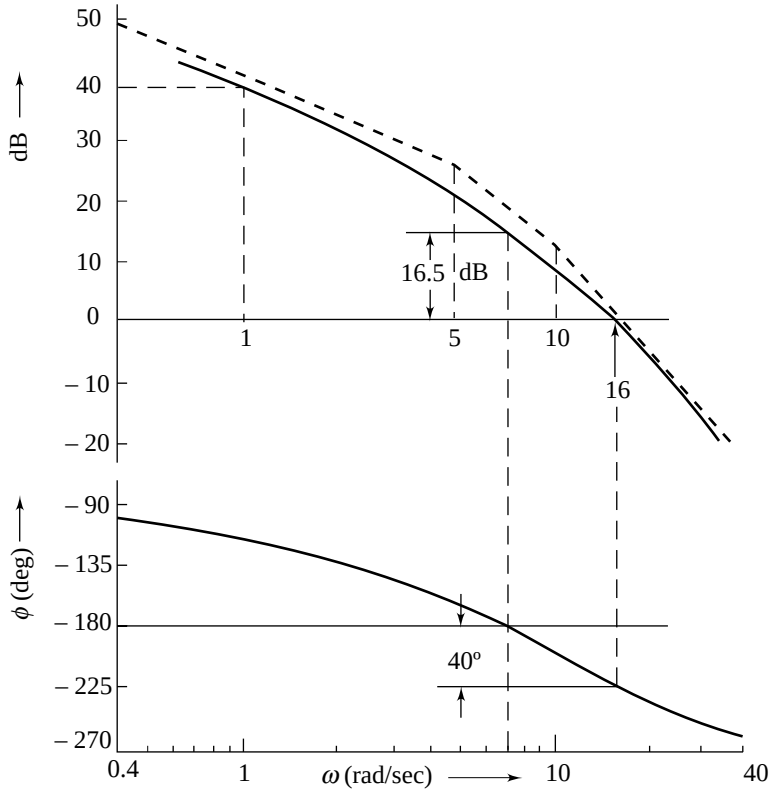

Fig. 8.37 Bode plot for Example 8.14

ω_ϕ = phase crossover frequency = 7 rad/sec

GM = gain margin = – 16.5 dB

ω_g = gain crossover frequency = 16 rad/sec

ΦM = phase margin = – 40°

The closed-loop system is thus unstable.

If we were to decrease the gain by 16.5 dB, all points on dB vs ω plot would decrease in magnitude by this amount without affecting the phase plot. The closed-loop system would be at the limit of instability. The gain K must be less than $100 \times x$ ($16.5 = 20 \log x$), i.e., the stability range is $0 < K < 668$.

8.7 STABILITY ANALYSIS OF SYSTEMS WITH DEAD-TIME

Figure 8.38 shows the block diagram of a system with dead-time elements in the loop. Open-loop transfer function of the system is

$$G(s)H(s) = G_1(s)e^{-s\tau_D} \tag{8.52}$$

where $G_1(s)$ is a rational function.

Root locus analysis of systems with dead-time elements is possible, but the method is quite complex. In Section 7.11, root locus analysis was carried out using the following approximation:

$$e^{-s\tau_D} \cong \frac{1 - s\tau_D/2}{1 + s\tau_D/2}$$

This approximation works fairly well as long as the dead-time τ_D is small in comparison to the system time-constants.

The frequency-domain graphical methods provide a simple yet exact approach to handle the dead-time problem since the factor $e^{-s\tau_D}$ is readily interpreted in terms of either the Nyquist or the Bode plot.

8.7.1 Nyquist Plots of Systems with Dead-Time

Assume that $G_1(s)$ in Fig. 8.38 is an integrator. Then the open-loop transfer function of the system becomes

$$G(s)H(s) = \frac{e^{-s\tau_D}}{s}$$

The sinusoidal transfer function is

$$G(j\omega)H(j\omega) = \frac{e^{-j\omega\tau_D}}{j\omega}$$

Clearly,

$$|G(j\omega)H(j\omega)| = 1/\omega;\ \angle G(j\omega)H(j\omega) = -\omega\tau_D - \pi/2$$

$$G(j\omega)H(j\omega) = \frac{1}{j\omega}(\cos\omega\tau_D - j\sin\omega\tau_D)$$

$$= -\frac{\sin\omega\tau_D}{\omega} - j\frac{\cos\omega\tau_D}{\omega}$$

$$\lim_{\omega\to 0}[G(j\omega)H(j\omega)] = -\tau_D - j\infty$$

Since the magnitude decreases monotonically, and the phase angle also decreases monotonically indefinitely, the polar plot of the given transfer function will spiral into the $\omega \to \infty$ point at the origin, as shown in Fig. 8.39. A curious reader may like to find some of the intersections with real and imaginary axes. For the first intersection with the real axis, set

$$\text{Im}\,[G(j\omega)H(j\omega)] = 0 \text{ to obtain } \omega\tau_D = \pi/2.$$

$$\text{Re}[G(j\omega)H(j\omega)]\Big|_{\omega=\frac{\pi}{2\tau_D}} = -\frac{1}{\omega}\Big|_{\omega=\frac{\pi}{2\tau_D}} = -2\tau_D/\pi$$

Once the Nyquist plot is constructed, the stability of the closed-loop system is determined in the usual manner. From Fig. 8.39, we observe that relative stability of the system reduces as τ_D increases. Sufficiently large values of τ_D may drive the system to instability.

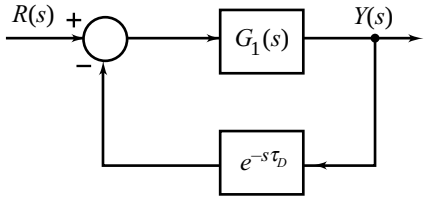

Fig. 8.38 A closed-loop system with dead-time elements in the loop

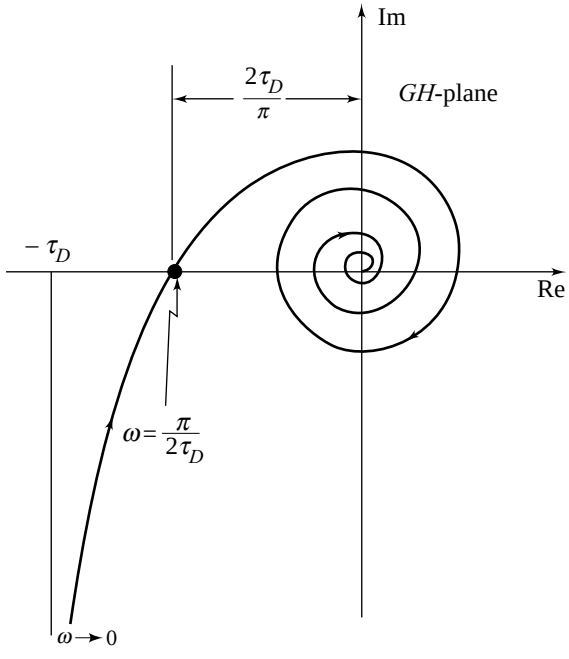

Fig. 8.39 Polar plot of $e^{-s\tau_D}/s$

The Critical Trajectory Thus far, we have used the point $-1+j0$ of the $G(s)H(s)$-plane as the critical point for stability analysis using Nyquist criterion. We can extend the critical-point idea into a trajectory if necessary.

The roots of the characteristic equation of the system shown in Fig. 8.38 satisfy (refer Eqn. (8.52))

$$1 + G_1(s)\, e^{-s\tau_D} = 0$$

or

$$G_1(s)\, e^{-s\tau_D} = -1 \tag{8.53}$$

The right-hand side of the last equation points to the fact that $-1+j0$ is the critical point for stability analysis of the closed-loop system. Equation (8.53) can be written as

$$G_1(s) = -e^{+s\tau_D} \tag{8.54}$$

The corresponding condition for the system without dead-time is

$$G_1(s) = -1 \tag{8.55}$$

Comparison of Eqns (8.54) and (8.55) reveals that the effect of dead-time is simply to shift the critical stability point $-1+j0$ to $-e^{s\tau_D}$, which describes a *critical trajectory*. When $\omega\tau_D = 0$, the trajectory starts at the point $-1+j0$, and as $\omega\tau_D$ increases, the critical point traces out a circle with unit radius centred at the origin of $G_1(s)$-plane, in the counterclockwise direction.

Example 8.15 Let us determine, with the help of Nyquist stability criterion, the maximum value of τ_D for stability of the closed-loop system of Fig. 8.38 with

$$G_1(s) = \frac{1}{s(s+1)(s+2)}$$

From Eqn. (8.54), we have with $s = j\omega$,

$$G_1(j\omega) = \frac{1}{j\omega(j\omega+1)(j\omega+2)} = -e^{+j\omega\tau_D}$$

Figure 8.40 shows the $G_1(j\omega)$ locus together with the critical trajectory of $-e^{+j\omega\tau_D}$. The frequency at which the $G_1(j\omega)$ locus intersects the critical trajectory is found by setting the magnitude of $G_1(j\omega)$ to unity, i.e.,

$$|G_1(j\omega)| = \left|\frac{1}{-3\omega^2 + j\omega(2-\omega^2)}\right| = 1$$

which gives $\omega = 0.446$ rad/sec.

Since

$$\angle G_1(j\omega)\big|_{\omega=0.446} = \angle -e^{j\omega\tau_D}\big|_{\omega=0.446}$$

we obtain (refer Fig. 8.40)

$$53.4\ (\pi/180) = 0.932 \text{ rad} = 0.446\ \tau_D \text{ rad}$$

which gives

$$\tau_D = 2.09 \text{ sec}$$

From Fig. 8.40, we observe that the critical point on the critical trajectory is encircled by the $G_1(j\omega)$ locus for $\omega\tau_D > 0.932$ ($\tau_D > 2.09$) and is not encircled for $\omega\tau_D < 0.932$ ($\tau_D < 2.09$); and hence we conclude that the system under discussion is stable if $\tau_D < 2.09$ sec.

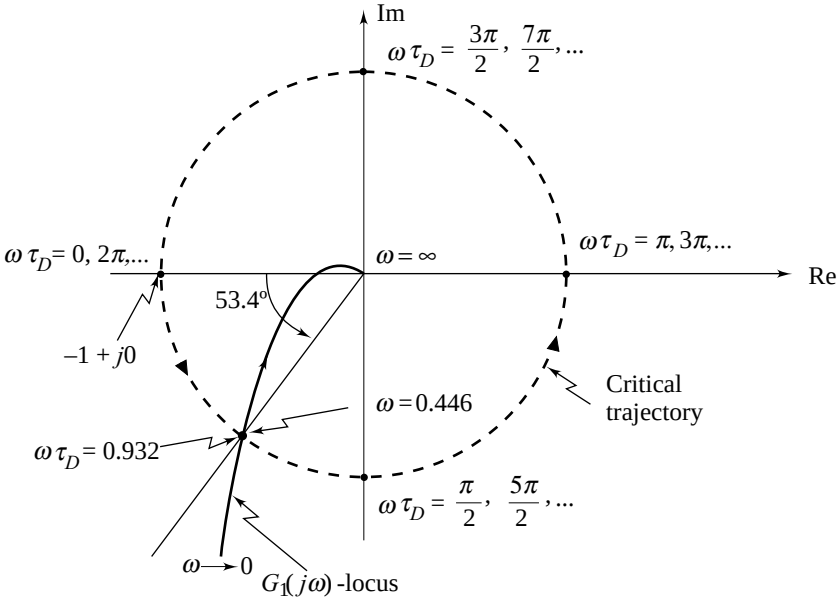

Fig. 8.40 Critical trajectory and $G_1(j\omega)$-locus for Example 8.15

8.7.2 Bode Plots of Systems with Dead-Time

The stability analysis of systems with dead-time can be conducted easily using the Bode plots. Since $20 \log |e^{-j\omega\tau_D}| = 0$, the magnitude plot of a system is unaffected by the presence of dead-time. The dead-time, of course, contributes a phase angle of $-(\omega\tau_D \times 180°)/\pi$, thereby causing the modification of the phase plot. An illustrative example follows.

Example 8.16 Consider the closed-loop system of Fig. 8.38 with

$$G_1(s) = \frac{K}{s(s+1)(s+2)} = \frac{K/2}{s(1+s)(1+s/2)}$$

Figure 8.41 shows the Bode plot of $G_1(j\omega)e^{-j\omega\tau_D}$ with $K = 1$ and $\tau_D = 0$. We find from this figure that

ω_g = gain crossover frequency = 0.446 rad/sec
ΦM = phase margin = 53.4°
ω_ϕ = phase crossover frequency = 1.4 rad/sec
GM = gain margin = 16 dB

The effect of dead-time is to add the phase shift of $-(\omega\tau_D \times 180)/\pi$ degrees to the phase curve while not affecting the magnitude curve. The adverse effect of dead-time on stability is apparent since the negative phase shift caused by the dead-time increases rapidly with the increase in ω. Let us set $\tau_D = 1$ sec and find the critical value of K for stability. Figure 8.41 also shows Bode plot of $G_1(j\omega)e^{-j\omega\tau_D}$ with $K = 1$ and $\tau_D = 1$. The magnitude curve is unchanged; the phase curve drops with the increase in ω, and the phase crossover frequency is now at 0.66 rad/sec. The gain margin is 4.5 dB. Note that 20 log 1.67 = 4.5 dB; therefore the critical value of K for stability when $\tau_D = 1$ is 1.67.

Let us now determine the critical value of dead-time, τ_D, for stability with $K = 1$. Since the phase margin with $\tau_D = 0$ and $K = 1$ is 53.4°, a phase lag of 53.4° can be introduced by dead-time before instability sets in. The critical value of dead-time is, therefore, given by the relation

$$\omega_g \tau_D \times 180/\pi = 53.4$$

which gives

$$\tau_D = 2.09 \text{ sec}$$

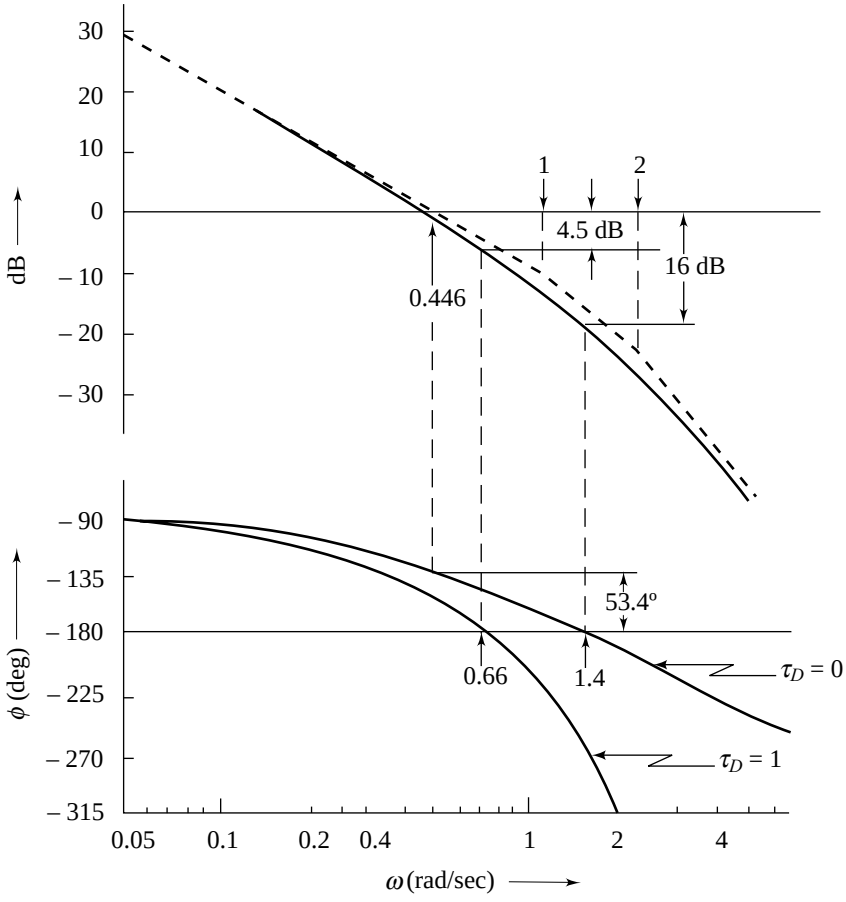

Fig. 8.41 Bode plots of Example 8.16

8.8 FREQUENCY RESPONSE MEASUREMENTS

In this section we will describe how a system responds to sinusoidal input—called the system's *frequency response*—and how the frequency response measurements can be used for design purposes.

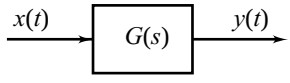

Fig. 8.42 A stable linear time-invariant system

To introduce the ideas, we consider a *stable* linear time-invariant system shown in Fig. 8.42. The input and output of the system are described by $x(t)$ and $y(t)$ respectively. The response of the system to sinusoidal input

$$x(t) = X \sin \omega t$$

will consist of two components: the transient component and the steady-state component (refer Section 2.9). The transient component will disappear as time goes by. The steady-state output that results after the transient dies out, is of the form

$$y(t) = A(\omega) \times \sin(\omega t + \phi(\omega))$$

which is a sine wave of the same frequency as the input; it differs from the sinusoidal input only in the amplitude and the phase angle. Both the amplitude and the phase angle change when we use a different frequency ω.

The output-input amplitude ratio $A(\omega)$, and the phase angle $\phi(\omega)$ between the output and input sinusoids, are given by the relations

$$A(\omega) = \frac{\text{Amplitude of the sinusoidal output}}{\text{Amplitude of sinusoidal input}} = |G(s = j\omega)|$$

$\phi(\omega)$ = Phase angle of the sinusoidal output – phase angle of the sinusoidal input

$$= \angle G(s = j\omega)$$

The variation of $A(\omega)$ and $\phi(\omega)$ with frequency ω is, by definition, the *frequency response* of the system.

If the system equations are known, complete with numerical values, we can derive its transfer function $G(s)$ and therefrom the *sinusoidal transfer function* $G(j\omega)$. Frequency response of the system can be computed from $G(j\omega)$.

If the equations and/or parameter values are not known, but the physical system or its components exist and are available for test, we can generate the frequency-response data by experimental measurements:

(i) A sinusoidal input of known amplitude and frequency is applied to the system.
(ii) The system output is allowed to 'settle' into a steady-state pattern.
(iii) The amplitude and relative phase of the sinusoidal output are measured and recorded.
(iv) This procedure is repeated for values of ω spanning the frequency range of interest.

Obviously, no steady-state response exists for an unstable system; so a frequency-response test will directly indicate instability.

Raw measurements of the output amplitude and phase of a stable plant undergoing a sinusoidal input are sufficient to analyse feedback system stability. No intermediate processing of the data is necessary because Nyquist plot/Bode plot can be sketched directly from experimental measurements.

Sometimes it is desirable to obtain an approximate model, in terms of a transfer function, directly from the frequency-response measurements. Determination of a transfer function $G(s)$ from measured data is an *identification problem*.

For a stable system, $|G(j\omega)|$ and $\angle G(j\omega)$ can be obtained by measurement. This is also possible if the system is marginally stable with a pole at $s = 0$. Experimental data are used to obtain the exact log-magnitude and phase angle curves of the Bode plot. Asymptotes are drawn on the exact log-magnitude curves by utilizing the fact that their slopes must be multiples of ± 20 dB/decade. From these asymptotes, the system type and approximate time-constants are determined.

Careful interpretation of the phase angle curve is necessary to identify whether the transfer function is a *minimum phase* or a *nonminimum phase* transfer function. Let us first define these terms.

Consider the following transfer functions:

$$G_1(j\omega) = \frac{1 - j\omega\tau}{(1 + j\omega\tau_1)(1 + j\omega\tau_2)}\ ;\ G_2(j\omega) = \frac{1 + j\omega\tau}{(1 + j\omega\tau_1)(1 + j\omega\tau_2)}$$

It can easily be deduced that the two transfer functions have the same magnitude characteristics:

$$|G_1(j\omega)| = |G_2(j\omega)|;\ \omega \geq 0$$

However, the phase characteristics are different for the two cases as illustrated in Fig. 8.43. The transfer function with a zero in the right half s-plane undergoes a net change in phase, when evaluated for frequency inputs between zero and infinity, which is greater than that for the transfer function with the zero in the left half s-plane; magnitude plots of two transfer functions being the same. Based on the phase shift characteristics, transfer functions are classified as minimum phase and nonminimum phase.

The range of phase shift of a *minimum phase transfer function* is the least possible corresponding to a given magnitude curve, whereas the range of phase shift of *nonminimum phase transfer function* is greater than the minimum possible for the given magnitude curve.

It can easily be established that a proper rational transfer function is a minimum phase transfer function if all of its zeros lie in the left half s-plane. It is a nonminimum phase transfer function if it has one or more zeros in the right half s-plane[6].

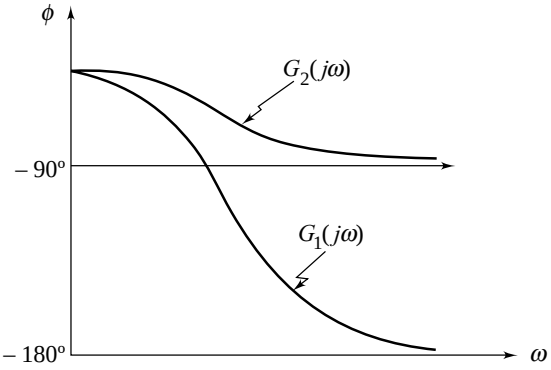

Fig. 8.43 Phase angle characteristics of minimum phase and nonminimum phase transfer functions

Using the basic definition, we can easily establish the minimum phase or nonminimum phase character of irrational transfer functions as well. A nonminimum phase irrational transfer function of practical importance is one with $e^{-\tau_D s}$ as its factor, e.g.,

$$G(j\omega) = \frac{(1 + j\omega\tau)\, e^{-j\omega\tau_D}}{(1 + j\omega\tau_1)(1 + j\omega\tau_2)}$$

With these observations, we can go back to the identification problem. If the Bode plot is obtained by frequency response measurements, then, except for a possible pole at $s = 0$, all the poles must lie in the left half s-plane. However, zeros in the right half s-plane and/or presence of dead-time elements cannot be ruled out. Therefore, care must be taken in interpreting the phase angle plot to detect the presence of right half plane zeros and/or dead-time elements. We illustrate the identification procedure through examples.

Example 8.17 Table 8.7 gives experimentally-obtained frequency-response data of a system. From this data, let us determine the approximate transfer function model of the system.

Bode plot shown in Fig. 8.44 is drawn using the data of Table 8.7. First we approximate the magnitude plot by the three straight dashed lines shown. They intersect at $\omega = 15$ and $\omega = 150$. We begin with the leftmost part of the magnitude plot. The low frequency asymptote is a horizontal line at 25 dB. It indicates that the transfer function represents a type-0 system with a gain K given by

$$20 \log K = 25 \text{ or } K = 17.8$$

[6] Nonminimum Phase response (also called *inverse response*) is exhibited by some processes, e.g., liquid level in a drum boiler. The dynamic behavior of such processes deviates drastically from what we have seen so far; initially the response is in the opposite (inverse) direction to what it eventually ends up. Such a behavior is the net result of two opposing effects. When a system possesses an inverse response, its transfer function has a zero in the right-half plane. Nonminimum phase systems are particularly difficult to control and require special attention.

Table 8.7 Experimental frequency response data

f(Hz)	*ω(rad/sec)*	*Gain(dB)*	*Phase(deg)*
60	377	– 7.75	– 155
50	314	– 4.3	– 150
40	251	– 0.2	– 145
35	219	0.75	– 140
25	157	5.16	– 135
20	126	7.97	– 120
16	100	10.5	– 110
10	63	15.0	– 100
7	44	16.9	– 85
2.5	16	20.4	– 45
1.3	8	21.6	– 30
0.22	1.38	24.0	– 5
0.16	1.0	24.1	0

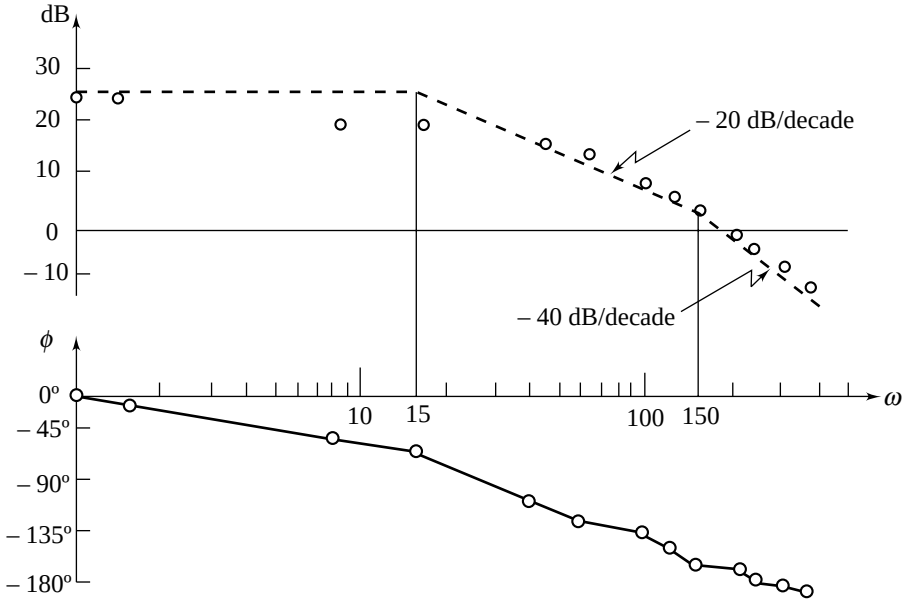

Fig. 8.44 Experimental data in Bode coordinate system

At $\omega = 15$, the slope becomes –20 dB/decade. Thus there is a pole with corner frequency 15. At $\omega = 150$, the slope becomes –40 dB/decade, a decrease of 20 dB/decade. Therefore, there is another pole with corner frequency 150.

The transfer function must be of the form: $G(s) = \dfrac{17.8}{(1 + s/15)(1 + s/150)}$.

The phase characteristics calculated from this transfer function are in fair agreement with experimentally obtained characteristics shown in Fig. 8.44. Dead-time element is therefore, not present.

Example 8.18 Let us find the transfer function of the experimentally obtained Bode plot shown in Fig. 8.45. First we approximate the magnitude plot by the three dashed lines shown. They intersect at

$\omega = 1$ and $\omega = 10$. In the low-frequency range, there is an asymptote with slope -20 dB/decade; it indicates the presence of a factor of the form $K/(j\omega)$ in the transfer function. At $\omega = 1$, the magnitude of the asymptote is 40 dB. Therefore

$$20 \log K = 40$$

This gives $K = 100$

At $\omega = 1$, the slope becomes -40 dB/decade, a decrease of 20 dB/decade; thus there is a pole with corner frequency $\omega = 1$. At $\omega = 10$, the slope becomes -20 dB/decade, an increase of 20 dB/decade; there is a zero with corner frequency $\omega = 10$. The transfer function must be of the form

$$G(s) = \frac{100\left(1 \pm \frac{s}{10}\right)}{s\,(1+s)}$$

We have assumed that the Bode plot of Fig. 8.45 is obtained by frequency response measurements; the pole in the right half s-plane is, therefore, not possible. However, a zero in the right half s-plane may exist, i.e., the system under experimental analysis may be a nonminimum-phase system.

Now we use the phase plot to determine the sign of the zero factor. If the sign of zero $(1 \pm 0.1s)$ is positive, the zero will introduce positive phase into $G(s)$ or, equivalently, the phase of $G(s)$ will increase as ω passes through the corner frequency at 10. This is not the case as seen from Fig. 8.45; thus we have $(1 - 0.1s)$, and the transfer function of the Bode plot is

$$G(s) = \frac{100\,(1 - 0.1s)}{s\,(1+s)}$$

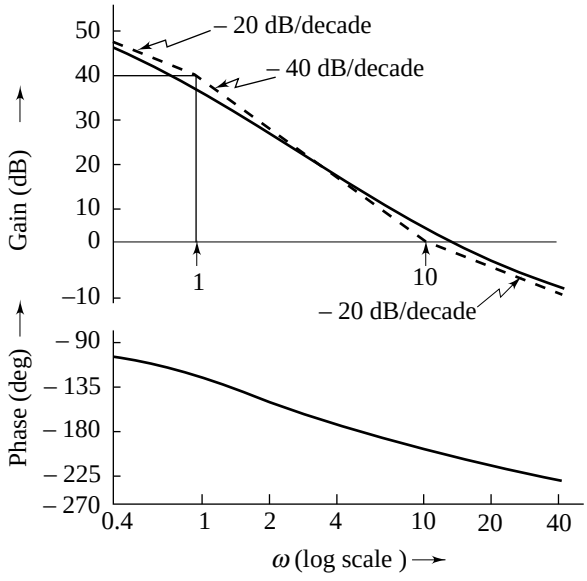

Fig. 8.45 Experimentally obtained Bode plot

The phase characteristics calculated from this transfer function are in fair agreement with experimentally obtained characteristics shown in Fig. 8.45.

Review Examples

Review Example 8.1 A heuristic derivation of a simple equation based on the *principle of argument* is as follows [64].
Consider the function

$$Q(s) = \frac{s - 0.5}{s(s-1)(s+4)} \tag{8.56}$$

Suppose $Q(s)$ is evaluated along the simple, circular contour Γ_s of radius 2.0 in the s-plane (shown in Fig. 8.46 a). We start the evaluation from the point $s = 2\angle 0°$ on the contour Γ_s. From Eqn. (8.56), we get

$$Q(s)|_{s=2\angle 0°} = \frac{|s-0.5|}{|s||s-1||s+4|}\angle[\angle(s-0.5) - \angle s - \angle(s-1) - \angle(s+4)]|_{s=2\angle 0°}$$

$$= \frac{1.5}{2\times 1\times 6}\angle 0° = 0.125\angle 0°$$

From Fig. 8.46a, we observe that the vectors $(s - 0.5)$, s, $(s - 1)$, and $(s + 4)$ have magnitudes 1.5, 2, 1, and 6, respectively, at $s = 2\angle 0°$. Each vector contributes an angle of 0° to $Q(s)$ at $s = 2\angle 0°$.

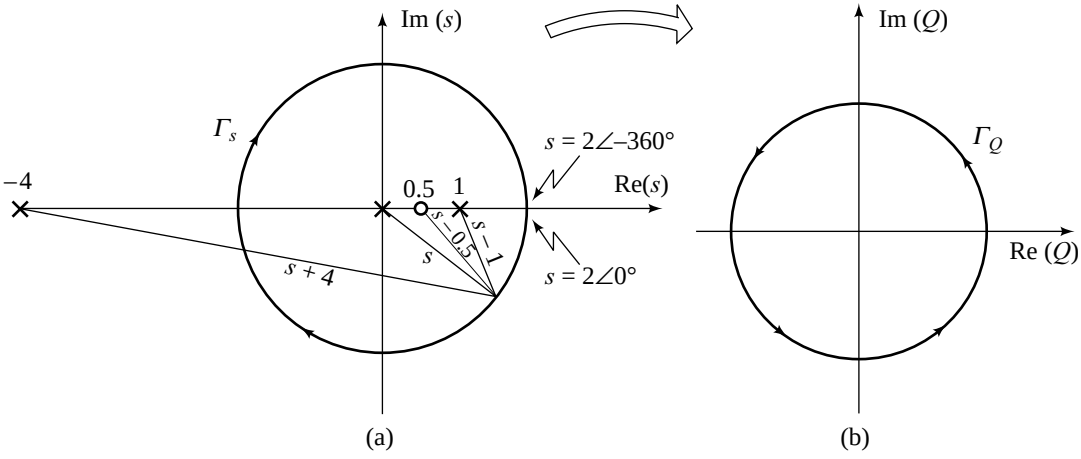

Fig. 8.46(a) Contour Γ_s in the s-plane, and (b) resulting contour Γ_Q in the Q(s)-plane

Contour Γ_s in the s-plane is a closed contour. Let us traverse the contour in the clockwise direction. A point or an area is said to be *enclosed* by a closed path if it is found to lie to the right of the path when the path is traversed in the clockwise direction. The closed path given by contour Γ_s in Fig. 8.46a encloses the circular region in the s-plane.

We started evaluation of $Q(s)$ from the point $s = 2\angle 0°$. Now we see that as the point s follows the prescribed path (i.e., clockwise direction) on the s-plane contour Γ_s, evaluation of $Q(s)$ at each point on Γ_s generates the closed contour Γ_Q in the $Q(s)$-plane, shown in Fig. 8.46b. The contour Γ_Q will be smooth because $Q(s)$ is a simple ratio of polynomials in the complex variable s that is well defined along Γ_s. It will become clear as the discussion proceeds that it is only the general shape of Γ_Q that is important.

Therefore, *exact* evaluation of $Q(s)$ along all the points of the contour Γ_s is not required. We evaluate $Q(s)$ at some key points along the contour Γ_s; the closed contour Γ_Q could then be approximated by simply plotting and connecting these values of $Q(s)$ (Γ_Q shown in Fig. 8.46b is not drawn to scale). Several features of Fig. 8.46 deserve comment.

1. As the evaluation of $Q(s)$ moves from $s = 2\angle 0°$ to $s = 2\angle -360°$ in the clockwise direction along the Γ_s contour, each of the vectors *inside* Γ_s rotates clockwise through 360°.
2. During this evaluation,
   (i) the vectors s and $(s - 1)$ in the denominator of $Q(s)$ will each contribute $-(-360°)$ of phase to $Q(s)$;
   (ii) the vector $(s - 0.5)$ in the numerator of $Q(s)$ will contribute $-360°$ of phase of $Q(s)$; and
   (iii) the vector $(s + 4)$ in the denominator of $Q(s)$ will contribute *no* net phase to $Q(s)$.
3. The net change in the phase of $Q(s)$ evaluated along Γ_s, traversing it once in the clockwise direction is 360°; or one *encirclement* of the origin of the $Q(s)$-plane in counterclockwise direction (refer Fig. 8.46 b).

We thus see that a change in phase of $Q(s)$ that one gets in traversing a contour Γ_s in the s-plane, is strictly a function of how many poles and zeros of $Q(s)$ are enclosed by the s-plane contour. Let us consider a general $Q(s)$ with m zeros and n poles. Assume that the s-plane contour Γ_s encloses Z zeros and P poles of $Q(s)$; and it does not go through any of the poles or zeros of $Q(s)$ (the poles of $Q(s)$ in s-plane are mapped to ∞ in $Q(s)$-plane, and the zeros are mapped to the origin). If we make one clockwise traversal of the contour Γ_s, it may be seen that:

$$\begin{aligned} \textit{net} \text{ change in phase of } Q(s) &= Z(-2\pi) - P(-2\pi) \\ &= (P - Z)2\pi \end{aligned}$$

A change in phase of $Q(s)$ by 2π leads to one counterclockwise encirclement of the origin in the $Q(s)$-plane by the Γ_Q contour. Therefore, net change in phase of $Q(s)$ by $(P - Z)\,2\pi$ as we traverse the contour Γ_s once in clockwise direction, will lead to $(P - Z)$ encirclements of the origin of the $Q(s)$-plane in counterclockwise direction by the Γ_Q contour.

In the case of simple function being considered here (Eqn. (8.56)), $P = 2$, $Z = 1$; and there is one encirclement of the origin by Γ_Q contour in counterclockwise direction.

Having made this qualitative analysis, it is possible to formulate a simple equation based on the contours Γ_s and Γ_Q, that can be applied to any function $Q(s)$ expressible as a ratio of polynomials in s with real coefficients. Let

N = number of *clockwise* encirclements of the origin of the $Q(s)$-plane by the contour Γ_Q;

P = number of poles of $Q(s)$ enclosed by the Γ_s contour in the s-plane, when traversed *clockwise*; and

Z = number of zeros of $Q(s)$ enclosed by the Γ_s contour in the s-plane, when traversed *clockwise*.

Then

$$N = Z - P \tag{8.57}$$

The relation (8.57) between the enclosure of poles and zeros of $Q(s)$ by the s-plane contour and the encirclement of the origin by the $Q(s)$-plane contour is commonly known as the *principle of argument*.

Equation (8.57) appears to be rather trivial. However, Nyquist managed to turn it into a very powerful tool for analyzing the stability of closed-loop control systems by carefully choosing the contour Γ_s and the function $Q(s)$.

Review Example 8.2 Consider a feedback system with an open-loop transfer function

$$G(s)H(s) = \frac{1 + 4s}{s^2(1 + s)(1 + 2s)}$$

which has a double pole at the origin. The indented Nyquist contour shown in Fig. 8.47a does not enclose these poles. The Nyquist plot shown in Fig. 8.47b is obtained as follows.

The portion of the $G(s)H(s)$-locus from $\omega = 0^+$ to $\omega = +\infty$ is simply the polar plot of

$$G(j\omega)H(j\omega) = \frac{1 + j4\omega}{(j\omega)^2 (1 + j\omega)(1 + j2\omega)}$$

The following points were used to construct the polar plot:

(i) $G(j\omega)H(j\omega)|_{\omega \to 0^+} \to \infty \angle -180°$

(ii) The $G(j\omega)H(j\omega)$-locus intersects the real axis at a point where

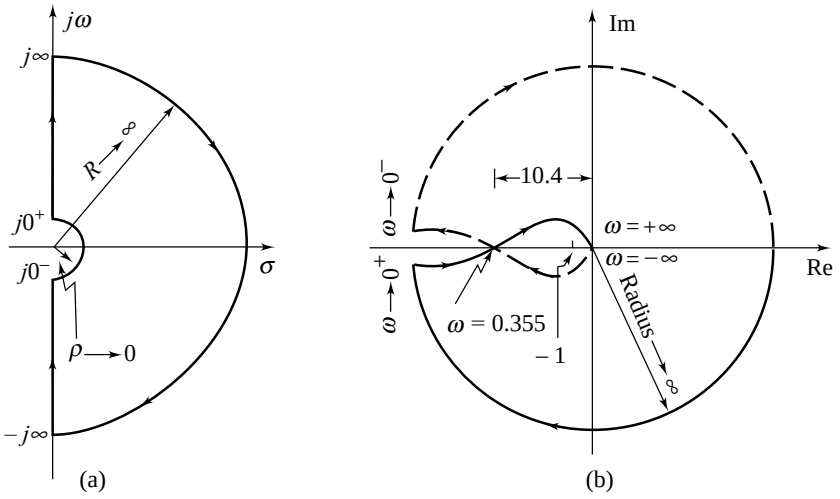

Fig. 8.47 Nyquist contour and the corresponding mapping[7] for $G(s)H(s) = (4s + 1)/[s^2(s + 1)(2s + 1)]$

$$\angle G(j\omega)H(j\omega) = -180°$$

or $$-180° - \tan^{-1}\omega - \tan^{-1}2\omega + \tan^{-1}4\omega = -180°$$

or $$\tan^{-1}4\omega - \tan^{-1}\omega = \tan^{-1}2\omega$$

Therefore $$\tan(\tan^{-1}4\omega - \tan^{-1}\omega) = \tan(\tan^{-1}2\omega)$$

or $$\frac{4\omega - \omega}{1 + 4\omega^2} = 2\omega$$

This gives $$\omega = \frac{1}{2\sqrt{2}} = 0.355 \text{ rad/sec}$$

$$|G(j\omega)H(j\omega)|_{\omega = 0.355} = 10.4$$

(iii) $G(j\omega)H(j\omega)\big|_{\omega \to +\infty} \to 0 \angle -270°$

7

ω	0.01	0.1	0.35	0.36
$\lvert GH\rvert$	4×10^6	104.09	11.4	10.3
$\angle GH$	− 179.97	− 175.2	− 179.35	179.64

The plot of $G(j\omega)H(j\omega)$ for $\omega < 0$ is the reflection with respect to the real axis, of the plot for $\omega > 0$. Every point on the large semicircle in Fig. 8.47a, is mapped by $G(s)H(s)$ into the origin of the $G(s)H(s)$-plane. A point $s = \rho e^{j\phi}$; $\rho \to 0$, ϕ varying from $-90°$, through $0°$ to $+90°$, is mapped by $G(s)H(s)$ into

$$G(s)H(s)\Big|_{s=\rho e^{j\phi}} = \frac{1+4s}{s^2(1+s)(1+2s)}\Big|_{s=\rho e^{j\phi}} = \frac{1}{\rho^2 e^{j2\phi}} = \frac{1}{\rho^2}\angle -2\phi$$

The small semicircle in Fig. 8.47a is mapped by $G(s)H(s)$ into a circular arc of infinite radius ranging from $180°$ at $\omega = 0^-$ through $0°$ to $-180°$ at $\omega = 0^+$ ($180° \to 90° \to 0° \to -90° \to -180°$).

Figure 8.47b indicates that the critical point $-1 + j0$ is encircled by the Nyquist plot twice in the clockwise direction. Therefore $N = 2$. From the given transfer function it is seen that no pole of $G(s)H(s)$ lies in the right half s-plane, i.e., $P = 0$. Therefore (refer Eqn. (8.8a))

Z = number of zeros of $1 + G(s)H(s)$ enclosed by the Nyquist contour
$= N + P = 2$

Hence the feedback system is unstable with two poles in the right half s-plane.

Review Example 8.3 The frequency response test data for the forward-path elements of a unity-feedback control system are given in Table 8.8. These data are sufficient to analyse feedback system stability, as is seen below.

Figure 8.48 shows the frequency response data of Table 8.8 on Bode magnitude and phase plots. From these plots we find that

phase crossover frequency $\omega_\phi = 48$ rad/sec,
gain crossover frequency $\omega_g = 3$ rad/sec,
gain margin $GM = 28$ dB, and
phase margin $\Phi M = 49°$.

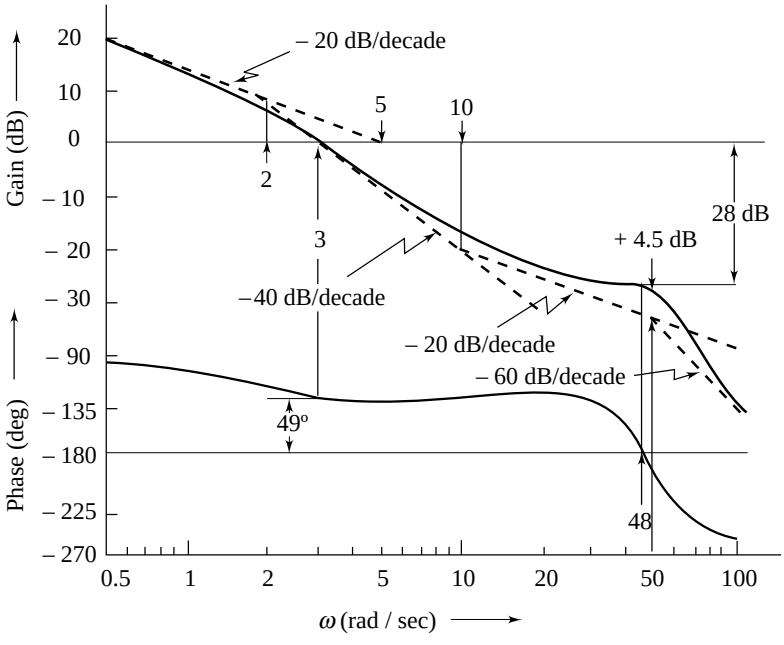

Fig. 8.48 Experimentally obtained magnitude and phase characteristics

Table 8.8 Experimental frequency response data

ω(rad/sec)	0.5	1	2	4	10	20	30
Gain (dB)	19.75	13	5	– 4	– 17	– 24	– 26
Phase (deg)	– 101	– 111	– 125	– 134	– 130	– 127	– 134
ω(rad/sec)	40	50	60	70	80	90	100
Gain (dB)	– 27	– 29	– 34	– 39	– 43	– 47	– 50
Phase (deg)	– 154	– 189	– 218	– 235	– 243	– 249	– 252

The feedback system is therefore stable.

It may be desirable to obtain a transfer function that approximates the experimental amplitude and phase characteristics. A series of straight-line asymptotes fitted to the experimentally obtained magnitude curve are shown in Fig. 8.48. The low frequency asymptote has a slope of –20 dB/decade and when extended, intersects the 0-dB axis at $\omega = 5$. Therefore, the asymptote is a plot of the factor $5/(j\omega)$. The corner frequencies are found to be located at $\omega = 2$, $\omega = 10$ and $\omega = 50$. At the first corner frequency, the slope of the curve changes by – 20 dB/decade and at the second corner frequency, it changes by + 20 dB/decade. Therefore, the transfer function has factors $1/(1 + j\omega/2)$ and $(1 + j\omega/10)$ corresponding to these corner frequencies. At $\omega = 50$, the curve changes by a slope of – 40 dB/decade. At this frequency, the error between actual and approximate plots is + 4.5 dB. The change of slope by – 40 dB/decade indicates the presence of either double pole on real axis or a pair of complex conjugate poles. The error of + 4.5 dB at the corner frequency and the peak occurring at a frequency less than the corner frequency indicate the presence of a quadratic factor with $\zeta < 0.5$. In fact, we can calculate the approximate value of ζ using expression (8.42):

$$-20 \log 2\zeta = 4.5$$

This gives $$\zeta = 0.3$$

Therefore, the transfer function has a quadratic factor

$$\frac{1}{1 + j2\zeta\,(\omega/50) + (j\omega/50)^2} \quad \text{where } \zeta = 0.3$$

Thus an approximate transfer function of the forward-path elements of the feedback system becomes

$$G(j\omega) = \frac{5\,(1 \pm j\omega/10)}{j\omega\,(1 + j\omega/2)\left[1 + j\,0.6\,(\omega/50) + (j\omega/50)^2\right]}$$

Now we use the phase plot to determine the sign of the zero factor. The phase characteristics calculated from the transfer function are in fair agreement with experimentally obtained characteristics shown in Fig. 8.48, when the sign of the zero factor is positive. Therefore, the transfer function of the Bode plot of Fig. 8.48 is

$$G(s) = \frac{5\,(1 + s/10)}{s\,(1 + s/2)\left[1 + 0.6s/50 + (s/50)^2\right]}$$

Review Questions

8.1 (a) Using the principle of argument, derive the Nyquist stability criterion.
(b) What is the interpretation of stability analysis when Nyquist plot crosses the $-1 + j0$ point?

8.2 (a) Give an account of meaning of the terms 'gain margin' and 'phase margin' with reference to Nyquist plots.

(b) How can a frequency response be represented by a Bode plot? Indicate what gain and phase margins are in this context.

(c) Why do we use logarithmic scale for frequency in Bode plots?

8.3 Give the properties of minimum-phase and nonminimum-phase transfer functions.
Describe a method of identification of transfer function model of a system using frequency-response measurements.

8.4 Give examples of Nyquist plots with

(i) poor ΦM, infinite GM (ii) poor GM, infinite ΦM

Problems

8.1 Sketch the general shapes of the polar plots for

(a) $G(j\omega) = \dfrac{1}{(1 + j\omega\tau_1)(1 + j\omega\tau_2)}$ (b) $G(j\omega) = \dfrac{1}{j\omega(1 + j\omega\tau)}$

(c) $G(j\omega) = \dfrac{1}{(j\omega)^2(1 + j\omega\tau)}$ (d) $G(j\omega) = \dfrac{1}{j\omega(1 + j\omega\tau_1)(1 + j\omega\tau_2)}$

(e) $G(j\omega) = \dfrac{1}{(j\omega)^2(1 + j\omega\tau_1)(1 + j\omega\tau_2)}$

based on magnitude and phase calculations at (i) $\omega = 0$, (ii) $\omega = \infty$, (iii) the point of intersection (if any) with the real axis, and (iv) the point of intersection (if any) with the imaginary axis.

8.2 Check the stability of unity-feedback systems whose Nyquist plots are shown in Fig. P8.2. $G(s)$ represents open-loop transfer function.

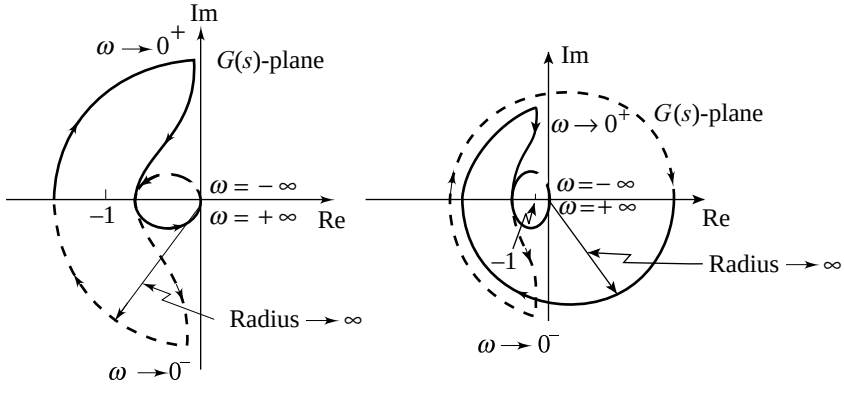

Number of poles of $G(s)$ in right half s-plane = 1

(a)

Number of poles of $G(s)$ in right half s-plane = 0

(b)

Fig. P8.2

8.3 Consider the unity-feedback system shown in Fig. P8.3a. The polar plot of $G(s)$ is of the form shown in Fig. P8.3b. Assuming that the Nyquist contour in s-plane encloses the entire right half s-plane, draw a complete Nyquist plot in the $G(s)$-plane. Then answer the following questions.

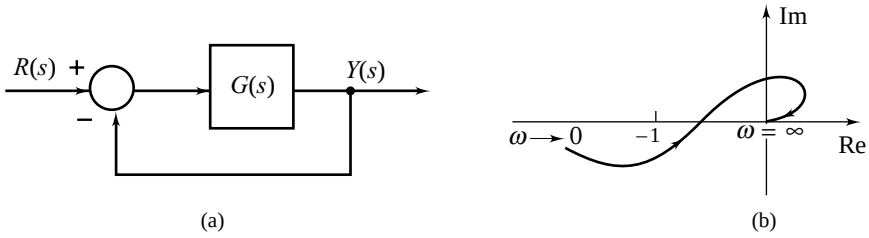

(a) (b)

Fig. P8.3

(i) If $G(s)$ has no poles and no zeros in the right half s-plane, is the closed-loop system stable?
(ii) If $G(s)$ has one pole and no zeros in the right half s-plane, is the closed-loop system stable?
(iii) If $G(s)$ has one zero and no poles in the right half s-plane, is the closed-loop system stable?

8.4 By use of the Nyquist criterion, determine whether the closed-loop systems having the following open-loop transfer functions are stable or not. If not, how many closed-loop poles lie in the right half s-plane?

(a) $G(s)H(s) = \dfrac{180}{(s+1)(s+2)(s+5)}$ (b) $G(s)H(s) = \dfrac{2}{s(s+1)(2s+1)}$

(c) $G(s)H(s) = \dfrac{s+2}{(s+1)(s-1)}$ (d) $G(s)H(s) = \dfrac{s+2}{s^2}$

(e) $G(s)H(s) = \dfrac{1}{s^2+100}$ (f) $G(s)H(s) = \dfrac{2(s+3)}{s(s-1)}$

MATLAB Exercise After completing the hand sketches, verify your results using MATLAB. Turn in your hand sketches and MATLAB-based plots on the same scale.

8.5 The stability of a closed-loop system with open-loop transfer function

$$G(s)H(s) = \frac{K(\tau_2 s+1)}{s^2(\tau_1 s+1)};\ K,\ \tau_1,\ \tau_2 > 0$$

depends on the relative magnitudes of τ_1 and τ_2. Draw Nyquist plots and therefrom determine stability of the system when (i) $\tau_1 < \tau_2$, and (ii) $\tau_1 > \tau_2$.

8.6 Use the Nyquist criterion to determine the range of values of $K > 0$ for the stability of the system in Fig. P8.6 with

(a) $G(s) = \dfrac{8}{(s+1)(s^2+2s+2)}$

(b) $G(s) = \dfrac{4(1+s)}{s^2(1+0.1s)}$

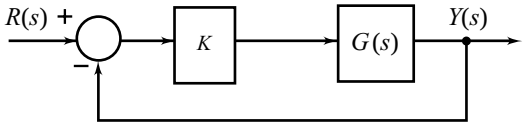

Fig. P8.6

(c) $G(s) = \dfrac{4(1+0.1s)}{s^2(1+s)}$

(d) $G(s) = \dfrac{e^{-0.8s}}{s+1}$

MATLAB Exercise (i)After completing the hand sketches, verify your results using MATLAB. Turn in your hand sketches and MATLAB-based plots on the same scale.(ii) Also verify your results using MATLAB-based root locus plots. Make suitable approximation for the deadtime in Problem 8.3d.

8.7 Sketch the Nyquist plot for a feedback system with open-loop transfer function

$$G(s)H(s) = \frac{K(s+3)(s+5)}{(s-2)(s-4)};\ K>0$$

Find the range of values of K for which the system is stable.

8.8 Sketch the Nyquist plot for a feedback system with open-loop transfer function

$$G(s)H(s) = \frac{K(1+0.5s)(s+1)}{(1+10s)(s-1)};\ K>0$$

Find the range of values of K for which the system is stable.

8.9 Consider the control system shown in Fig. P8.9. Using the Nyquist criterion, determine the range of gain $K > 0$ for stability of the system.

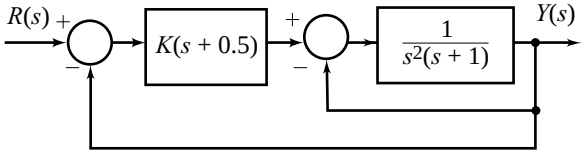

Fig. P8.9

MATLAB Exercise Make a rough sketch to decide on appropriate frequency range. Then generate a MATLAB-based plot over this frequency range. Also verify your result using MATLAB-based root locus plot.

8.10 Consider the feedback systems shown in Figs P8.10a and P8.10b. Sketch the Nyquist plot in each case and therefrom determine the maximum value of K for stability.

8.11 A unity-feedback system has open-loop transfer function

$$G(s) = \frac{e^{-s\tau_D}}{s(s+1)}$$

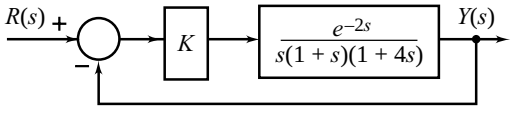

(a)

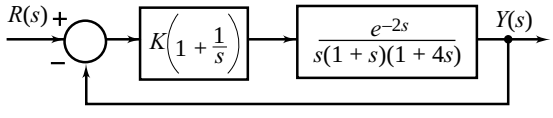

(b)

Fig. P8.10

Draw the Nyquist plot of $G_1(j\omega) = \dfrac{1}{j\omega\,(j\omega + 1)}$, together with the critical trajectory of $e^{-j\omega\tau_D}$. Using these curves, obtain the maximum value of deadtime τ_D in seconds for the closed-loop system to be stable.

8.12 Using the Nyquist plot, determine gain crossover frequency, phase crossover frequency, gain margin, and phase margin of feedback system with open-loop transfer function

$$G(s)H(s) = \frac{10}{s\,(1 + 0.2s)\,(1 + 0.02s)}$$

MATLAB Exercise Using MATLAB dialogues, sketch the Nyquist plot with selection of appropriate frequency range from the Bode plot of the system. From the Nyquist plot, determine the required performance indices. Also determine the indices using Bode plot.

8.13 Sketch the Nyquist plot for a feedback system with open-loop transfer function

$$G(s)H(s) = \frac{K\,(s + 10)^2}{s^3};\ K > 0$$

(a) Show that the feedback system is stable for $K > 5$.
(b) Determine the gain margin and phase margin when $K = 7$.

8.14 Sketch the Bode asymptotic plots showing the magnitude in dB as a function of log frequency for the transfer functions given below. Determine the gain crossover frequency in each case.

(a) $G(s) = \dfrac{25}{(s + 1)\,(0.1s + 1)\,(0.05s + 1)}$

(b) $G(s) = \dfrac{50\,(0.2s + 1)}{s\,(s + 1)\,(0.02s + 1)}$

(c) $G(s) = \dfrac{500\,(0.2s + 1)\,(0.1s + 1)}{s^2\,(s + 1)\,(0.02s + 1)}$

(d) $G(s) = \dfrac{50\,(0.05s + 1)}{s\,(0.1s + 1)\,(0.02s + 1)\left((s/200)^2 + (0.02s/200) + 1\right)}$

8.15 Using Bode plot, determine gain crossover frequency, phase crossover frequency, gain margin, and phase margin of a feedback system with open-loop transfer function

(a) $G(s) = \dfrac{10}{s\,(0.1s + 1)}$

(b) $G(s) = \dfrac{10}{s\,(0.1s + 1)^2}$

(c) $G(s) = \dfrac{20\,(0.2s + 1)}{s\,(0.5s + 1)}$

(d) $G(s) = \dfrac{20\,(0.2s + 1)\,e^{-0.1s}}{s\,(0.5s + 1)}$

(e) $G(s) = \dfrac{40}{(s + 2)\,(s + 4)\,(s + 5)}$

(f) $G(s) = \dfrac{10}{s^2\,(0.2s + 1)}$

MATLAB Exercise Generate Bode plots in MATLAB window and determine the performance indices.

8.16 Use Bode plots to determine the stability of the system shown in Fig. P8.16 for the two cases: (i) $K = 10$, and (ii) $K = 100$.

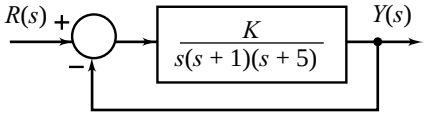

Fig. P8.16

MATLAB Exercise Determine the stability using both the Bode plots and the root locus plots, generated using MATLAB.

8.17 Use Bode plot to determine the range of K within which a unity-feedback system with open-loop transfer function $G(s)$ is stable. Given:

(a) $G(s) = \dfrac{K}{(s+2)(s+4)(s+5)}$ (b) $G(s) = \dfrac{K}{s(1+0.2s)(1+0.02s)}$

(c) $G(s) = \dfrac{Ke^{-s}}{s(s+1)(s+2)}$

MATLAB Exercise Determine the range using both the Bode plots and the root locus plots, generated using MATLAB. Note that the transfer function for Problem 8.9c has deadtime; it may be approximated by a rational function for generating root locus plot.

8.18 Open-loop transfer function of a closed-loop system is

$$G(s)H(s) = \frac{10e^{-s\tau_D}}{s(0.1s+1)(0.05s+1)}$$

(a) Find the gain margin and phase margin when $\tau_D = 0$.
(b) Find the gain margin and phase margin when $\tau_D = 0.04$ sec. Comment upon the effect of dead-time.
(c) Determine the maximum value of τ_D for the closed-loop system to be stable.

MATLAB Exercise Use MATLAB environment in dialogue mode to solve this problem.

8.19 The experimental frequency response data of certain systems presented on Bode plots and asymptotically approximated are shown in Fig. P8.19. Find the transfer function in each case (systems are known to have minimum-phase characteristics).

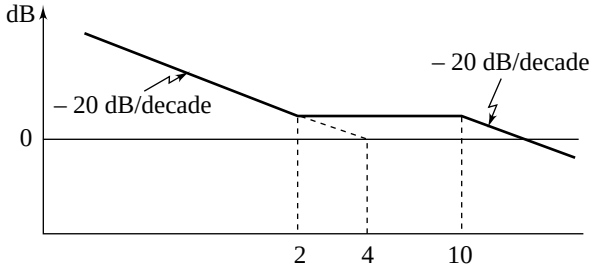

(a)

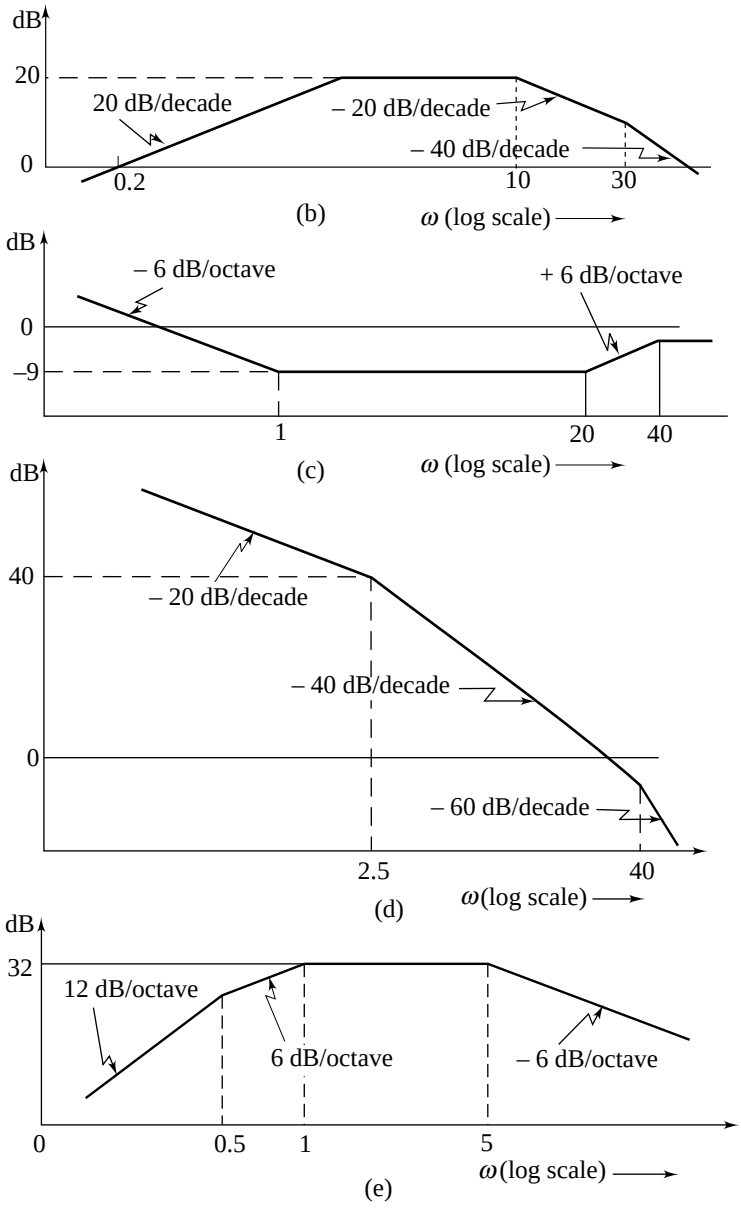

Fig. P8.19

8.20 Consider a minimum-phase system whose asymptotic amplitude frequency response is depicted in Fig. P8.20.

(a) Determine the transfer function $G(s)$ of the system.

(b) Determine the two gain crossover frequencies ω_{g1} and ω_{g2}.

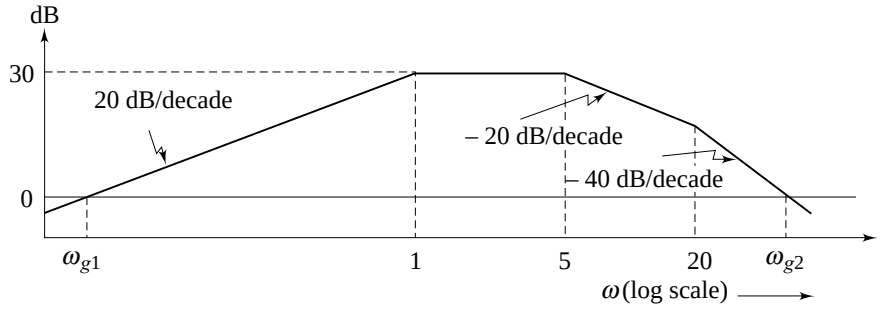

Fig. P8.20

8.21 The asymptotic amplitude frequency response of the open path of a feedback system is shown in Fig. P8.21. Determine the gain margin of the system. The system is known to have minimum-phase characteristics.

8.22 The following frequency response test data were obtained for a system known to have minimum-phase characteristics. Plot the data on semilog graph paper and determine the transfer function of the system using asymptotic approximation.

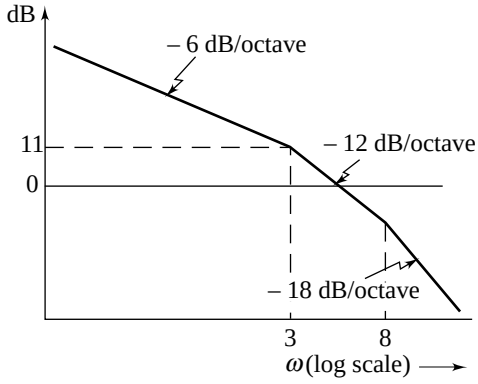

Fig. P8.21

Gain (dB)	34	28	24.6	14.2	8	1.5	– 3.5	– 7.2
Frequency (rad/sec)	0.1	0.2	0.3	0.7	1.0	1.5	2.0	2.5
Gain (dB)	– 12.5	– 14.7	– 16.0	– 17.5	– 17.5	– 17.5		
Frequency (rad/sec)	4.0	5.0	6.0	9.0	20	35		

8.23 Determine an approximate transfer function model of a system for which experimental frequency response data is given in the following table.

ω	*dB*	*Phase*
0.1	– 20	0
0.5	– 21	0
1.0	– 21	– 9°
2.0	– 22	– 54°
3.0	– 24	– 90°
5.0	– 28	– 135°
10.0	– 40	– 170°
30.0	– 60	– 178°
100.0	– 84	– 180°

Performance Specifications on System Frequency Response

9

9.1 INTRODUCTION

For the single-loop control system configuration shown in Fig. 9.1, the closed-loop transfer function is

$$\frac{Y(s)}{R(s)} = M(s) = \frac{G(s)}{1 + G(s)\,H(s)} \tag{9.1a}$$

For a stable closed-loop system, the function

$$M(j\omega) = \frac{Y(j\omega)}{R(j\omega)} = \frac{G(j\omega)}{1 + G(j\omega)\,H(j\omega)} \tag{9.1b}$$

completely characterizes the steady-state behaviour of the system to sinusoidal inputs. The variation of the magnitude $|M(j\omega)|$ and the phase angle $\angle M(j\omega)$ with frequency ω, is the frequency response of the closed-loop system.

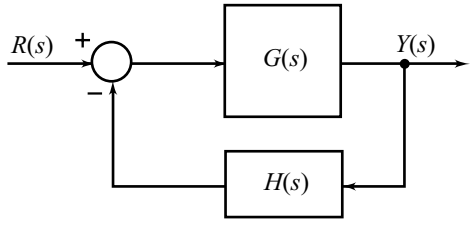

Fig. 9.1 A single-loop control system configuration

We know that a rapidly changing input has a large high frequency content, while a smooth slowly varying input has a relatively small high frequency content. Thus, if the control system is to faithfully follow a command that is changing rapidly, it must be capable of reproducing inputs at high frequencies, i.e., it must have a large bandwidth. On the other hand, if the command is slowly varying, the control system does not need a high bandwidth. A step change (i.e., a discontinuity) in the input has a large amount of high frequency content; to reproduce it faithfully (with a short rise time) requires a high bandwidth. Furthermore, all control systems are subject to noise during operation. Therefore, in addition to responding to the input signal, the system should be able to suppress noise and unwanted signals. The phase characteristics of the frequency response of a control system is also of importance, as it plays an important

role in the stability of closed-loop systems. Shaping the frequency-response characteristics is the objective of the frequency-domain design methods.

When one has the frequency-response curves (obtained experimentally, or analytically using Eqn. (9.1b)) for any stable system, evaluation of the steady-state response to a sinusoidal input is straightforward. What is not obvious, but is extremely important, is that the frequency-response curves are really a *complete* description of the system's dynamic behaviour and allow one to compute the response to *any* input, not just sine waves.

9.1.1 The Link between Time Functions and Frequency Functions

We are familiar with the time response of a dynamic system. However, difficulties arise in interpreting a frequency response plot of a dynamic system unless the link between time response and its equivalent frequency response plot is well understood [63]. The key point underlying the link between time and frequency is the idea that a time-varying signal may be resolved into a sum of sinusoidal functions of different frequencies (*Fourier analysis*). To illustrate the link, we examine how a square wave can be approximated by the sinusoidal functions of Fig. 9.2. We can see that in plot (a) we have used one sinusoid to approximate the square wave. As we include a combination of sinusoids of different magnitudes (plots (b) and (c)), we form a close approximation to the square wave. Hence we can consider a square wave as being composed of an infinite number of sinusoids.

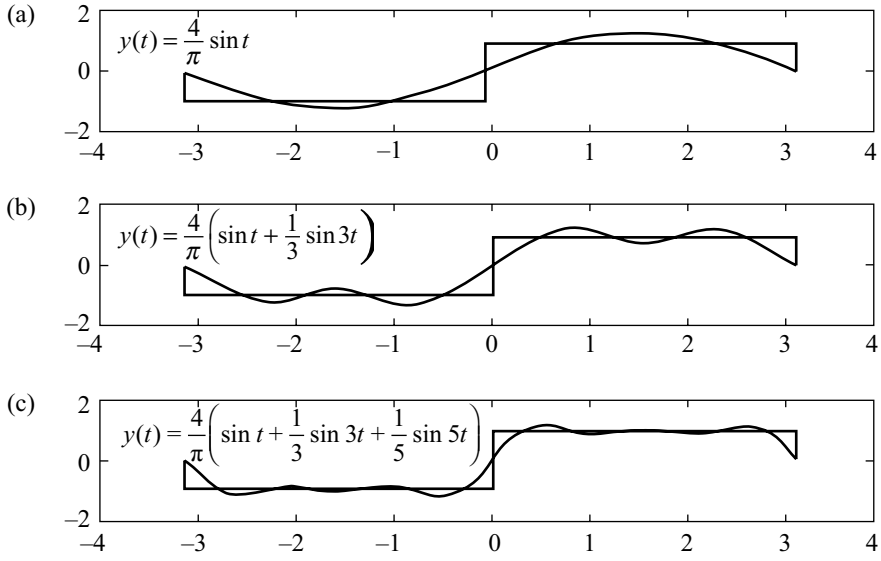

Fig. 9.2 Approximating a square wave

In general, a time function $y(t)$ can be expressed equivalently by a frequency function $Y(j\omega)$, given by the Fourier transform:

$$Y(j\omega) = \int_{-\infty}^{\infty} y(t)e^{-j\omega t}dt \tag{9.2}$$

By applying sinusoidal signals of different frequencies to a system and monitoring the change in amplitude and phase at the system output, we can obtain the frequency-domain information about a dynamic system. Magnitude and phase at different frequencies lead to the *frequency response* of the system. For a given control system, the frequency response of the controlled variable is $Y(j\omega)$. Inverse Fourier transformation of $Y(j\omega)$ then gives the controlled variable in time domain:

$$y(t) = \frac{1}{2\pi}\int_{-\infty}^{\infty} Y(j\omega)e^{j\omega t}d\omega \tag{9.3}$$

9.1.2 The Link between Time-domain and Frequency-domain Performance Measures

In Chapter 7, we have introduced design techniques based on root locus analysis that use the performance specifications developed in Chapter 6. The advantage of the root locus design is that it is very intuitive. The root locus plot provides the designer with a picture of all potential closed-loop pole locations. This picture, when combined with the performance specifications, makes it an easy matter to find a good compensator. The overriding principle is the use of *near* pole/zero cancellation to make the closed-loop transfer function as close as possible to the standard second-order transfer function. The assumption is that the response for near cancellation will be essentially the same as for perfect cancellation. We have not provided rigorous analysis to support this assumption, but the examples in Chapter 7 suggest that the assumption is generally true. With this assumption, the specifications on peak overshoot, settling time, etc., of the closed-loop time response are translated into the parameters ζ and ω_n of the standard second-order transfer function and a compensator that matches the closed-loop transfer function with the standard second-order transfer function is selected.

An alternative approach of design is based on frequency response analysis. The primary tools for this type of analysis are the Bode plot and the Nichols chart. Open-loop frequency response data on Bode plot, when examined in the light of Nyquist criterion, yield stability margins associated with the closed-loop system behaviour. The same data, when examined on a Nichols chart, easily gives (as we will see later in this chapter) a wealth of information on figures of merit of closed-loop frequency response, such as bandwidth, resonance peak and resonance frequency.

The correlation between transient response and frequency response through the Fourier integral forms an important basis of the design procedures that use frequency response analysis. The desired time-domain behaviour is interpreted in terms of frequency-response characteristics, the design is carried out in frequency domain, and the frequency response is then translated back into the time domain.

Through the design examples developed in the next chapter we will see that the design procedures based on frequency response analysis are essentially pole cancellation techniques. In many cases, the resulting closed-loop system closely approximates the standard second-order transfer function. Fortunately, direct and simple correlations exist between the transient response measures of performance and frequency-response measures of performance for the standard second-order system shown in Fig. 9.3 (the general correlation between transient response and frequency response through the Fourier integral is highly laborious to compute). The design based on these correlations proceeds very fast, though it is not exact. Sound engineering skill and judgment are necessary to estimate the accuracy of such a procedure. It is in fact essential to check the exact response after the design is completed.

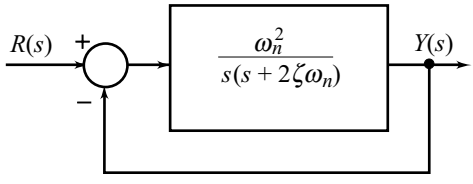

Fig. 9.3 Standard second-order feedback system

9.2 PERFORMANCE SPECIFICATIONS IN FREQUENCY DOMAIN

Recall the basic feedback system block diagram defined in Chapter 3; shown as Fig. 9.4 in a form convenient for analysis. The controlled process (and the actuators) as represented by $G(s)$, and $N(s)$ is the plant transfer function from the disturbance input to the output. The control system objectives are that output y follow input r, and ignore disturbance w.

The study of a control system essentially involves the evaluation of transient and steady state responses of the system, and robustness of this performance against model uncertainties and disturbances.

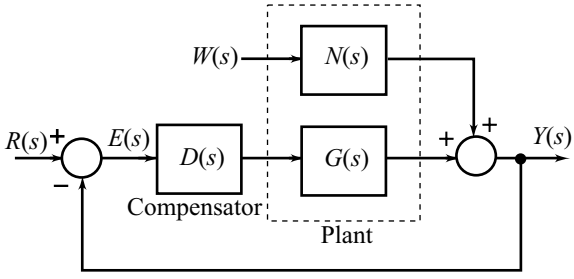

Fig. 9.4 A feedback system

9.2.1 Transient Response

The transient response of a practical control system (which often exhibits damped oscillations before reaching steady state) is revealed by rise time t_r, peak time t_p, peak overshoot M_p, and setting time t_s of the system response to a unit-step input (refer Section 6.2). Rise time and peak time are intended as speed of response criteria ; the smaller these values, the faster the system response. Peak overshoot is used mainly for relative stability. Values in excess of 40% may indicate the system is dangerously close to absolute instability. Settling time combines stability and speed of response aspects and is widely used. All these measures of transient behaviour of a control system are mutually dependent and therefore must be specified in a consistent manner.

In the design of linear control systems using frequency-domain methods, it is necessary to define a set of specifications so that the quality of the transient response can be described using frequency-response characteristics. It is common to specify the following for this purpose:

(i) resonance peak, M_r ;
(ii) resonance frequency, ω_r;
(iii) bandwidth, ω_b;
(iv) gain margin, GM;
(v) phase margin ΦM; and
(vi) gain crossover frequency, ω_g.

All these measures of transient behaviour of a control system, as will be seen in the next section, are mutually dependent and therefore must be specified in a consistent manner.

Resonance peak M_r, and resonance frequency ω_r Consider the feedback system shown in Fig. 9.4. A typical plot of $M(j\omega) = Y(j\omega)/R(j\omega)$, the closed-loop frequency response, is shown in Fig. 9.5. The magnitude $|M(j\omega)|$ approximates the ideal 1.0 for some range of 'low' frequencies but deviates for higher frequencies.

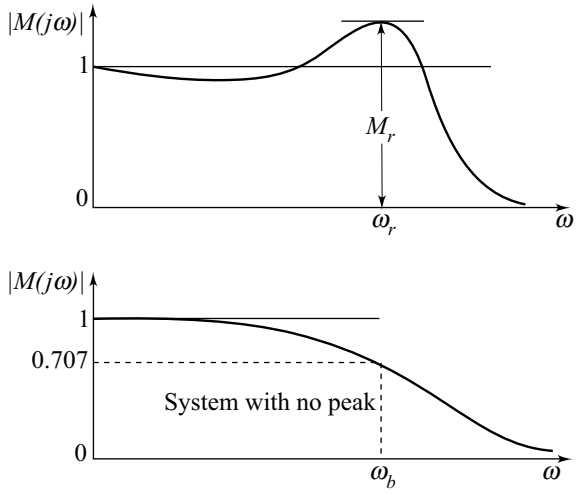

Fig. 9.5 Closed-loop frequency response criteria

We know that $|M(j\omega)|$ *versus* ω curve will have a pronounced peak if $M(s) = Y(s)/R(s)$ has complex poles with very small damping ratio. In fact, the smaller the value of damping ratio, higher the peak. The peak occurs at a frequency slightly less than the natural frequency of the complex poles (refer Figs 8.30 and 8.31). The maximum value M_r of $|M(j\omega)|$ is termed the *resonance peak*, and the frequency ω_r at which it occurs is the *resonance frequency* (refer Fig. 9.5).

Resonance peak M_r is a very good measure of relative stability of a closed-loop system; a large M_r corresponds to a large overshoot in transient response. Many systems are designed to exhibit resonance peak in the range 1.2 to 1.4.

The resonance frequency ω_r is a measure of speed of response; the higher the ω_r the faster the system.

Bandwidth ω_b For systems that exhibit no peak (refer Fig. 9.5), which is sometimes the case, the *bandwidth* ω_b is used for the speed of response specification. It can, of course, be specified even if there is a peak. (Bandwidth of the closed-loop frequency response is the frequency at which the magnitude M is $1/\sqrt{2} = 0.707$ times its value at zero frequency).

Gain Margin GM, and Phase Margin ΦM Alternative measures of relative stability are stability margins. We have seen in Chapter 8 that *both* a good *gain margin* and a good *phase margin* are needed for robust stability; neither is sufficient by itself. General numerical design goals for gain margin and phase margin cannot be given since systems that satisfy other specific performance criteria may exhibit a wide range of gain and phase margins. It is possible, however, to give useful lower bounds; gain margin should usually exceed 2.5 (20 log 2.5 dB) and phase margin should exceed 30°.

Gain Crossover Frequency ω_g Of particular importance for the speed of response analysis is the *gain crossover frequency* ω_g (refer Section 8.4). Raising the gain crossover frequency increases the speed of response.

With respect to disturbances, if we set $R \equiv 0$ and let W be a sine wave (refer Fig. 9.4), we can measure or calculate $Y(j\omega)/W(j\omega)$, which should of course ideally be zero for all frequencies. For low frequencies, the feedback action is effective in keeping Y near the ideal value of zero.

9.2.2 Steady-State Response

The steady-state behaviour of a practical control system is revealed by the steady-state error of the system to one or more of the standard test signals—step, ramp, parabola. The specification of the zero-error response to all the three test signals is very impractical and unrealistic. Fortunately, the requirements of practical system are much less stringent. A finite error is usually tolerated as the severity of the input increases (refer Section 6.6).

9.2.3 Robustness

So far the design objectives have been formulated as requirements on the frequency response of the closed-loop system. These specifications on stability, speed of response, and steady-state accuracy are considered in design under the assumption that a nearly precise model of the plant is available.

The basic assumption of the availability of precise model of the plant is almost never true. There are almost always inconsistencies of the model and the real plant—called *model uncertainties* (refer Section 6.2). It is usually possible to quantify and bound the discrepancy between the plant and the model. The design model then becomes a member of a class $\mathcal{G}$ of models, one member of which is believed to represent the plant.

Since we do not know which member of the class $\mathcal{G}$ represents the plant, the safe and the reasonable course is to require that the control system stabilize *all* members of the class $\mathcal{G}$. Since that is more difficult to

do than simply stabilizing a single (*nominal*) model, we may have to give up something from the single-model performance to satisfy the additional requirement.

Robustness describes the ability of the system to satisfactorily perform for all the models in class $\mathcal{G}$. A *robust controller* is a feedback controller that satisfies the design requirements on stability, speed of response, and steady-state accuracy in connection with all the models of a given family $\mathcal{G}$. The explicit consideration of the model uncertainties poses novel problems in the analysis and design of feedback systems. The problem of designing controllers for uncertain systems necessitates new concepts of modelling, analysis and design.

Since to fully understand the ramifications of modern *robust control theory* would take us on a lengthy and hard mathematical journey, we will content ourselves with the understanding of the intent of robust control, and its relation to the design techniques developed in this book. This is worthwhile exercise that will at least give us an appreciation of the implications of robust control.

From the viewpoint of single-input, single-output systems, the contributions of robust control theory are primarily an extension of Bode's work on sensitivity analysis plus a sounder theoretical basis for the loop-shaping techniques that had been in use for the past 60 years. Many of these results have been given more rigorous mathematical form in modern robust control theory.

Sensitivity optimization is currently receiving considerable attention. For the system of Fig. 9.4, the sensitivity function is (refer Eqn. (4.12))

$$|S(j\omega)| = \frac{1}{|1 + D(j\omega)G(j\omega)|}$$

Since a small sensitivity function $S(j\omega)$ ensures that the command tracking properties are weakly affected by parameter variations, the least requirement for command tracking is given by $|S(j\omega)| < 1$, i.e., we are looking for a controller such that the closed-loop system performance is less affected by plant uncertainties than a nominally equivalent open-loop control system for which $|S(j\omega)| = 1$ (refer Eqn. (4.13)). The aim is not only to reduce sensitivity, but to minimize a *weighted sensitivity* index such as

$$|W(j\omega)S(j\omega)| < 1 \;\forall\; \omega$$

where $W(j\omega)$ is the transfer function that can be tuned by the control system designer. Tuning of $W(j\omega)$ is guided by a thorough understanding of the process: what it is intended to do, how much system error is permissible, what the physical capabilities and limitations are, etc. For good disturbance attenuation, $|S(j\omega)|$ should be made small over the frequency range of disturbances. This can be ensured by choosing large $W(j\omega)$ in this frequency band; large gain in the band will achieve sensitivity minimization. The requirement of alleviation of the effects of sensor noise dictates that the gain of the system at high frequencies be kept low. The weighted sensitivity optimization must meet these constraints; therefore tuning of $W(j\omega)$ is guided by these considerations. Over the intermediate frequencies, the required stability margins tune the shape of $W(j\omega)$. Figure 9.6a shows graphical interpretation of inequality

$|S(j\omega)| < \dfrac{1}{|W(j\omega)|} \;\forall\; \omega$, which is equivalent to $|W(j\omega)| < |1 + D(j\omega)G(j\omega)| \;\forall\; \omega$

Figure 6.6 shows a block diagram of a plant with unmodelled dynamics. The closed-loop transfer function between input $R(s)$ and output $Y(s)$ is

$$\frac{Y(s)}{R(s)} = \frac{D(s)G(s)[1 + \Delta(s)]}{1 + D(s)G(s)[1 + \Delta(s)]}$$

where $\Delta(s)$ represents the unknown dynamics of the plant and $G(s)$ is its nominal plant model. We assume that number of poles of $D(s)G(s)$ in right-half s-plane is zero. The nominal closed-loop system is designed to be stable—the Nyquist plot of $D(j\omega)G(j\omega)$ in the complex plane does not encircle $-1 + j0$ point. The feedback system with perturbed plant is stable if the Nyquist plot of $D(j\omega)G(j\omega)$ $[1 + \Delta(j\omega)]$ does not encircle $-1 + j0$ point. A sufficient mathematical condition for robust closed-loop stability is

$$|D(j\omega)G(j\omega)\Delta(j\omega)| < |1 + D(j\omega)G(j\omega)| \forall\ \omega$$

This will ensure that $D(j\omega)G(j\omega)$ $[1 + \Delta(j\omega)]$ does not reach the $-1 + j0$ point because of unknown dynamics of the plant. Graphical interpretation of this inequality is given in Fig. 9.6b.

In fact, building of uncertainty models $W(j\omega)$ and $\Delta(j\omega)$ itself is subject to uncertainties; the industry, by and large, continue to rely on frequency-domain design methods with the gain margin and phase margin specifications for robustness. These specifications indirectly relate to the requirements dictated by $W(j\omega)$ and $\Delta(j\omega)$. Uncertainty models are not used implicitly in the conventional design process; however, the robustness properties may be checked by simulation for a given uncertainty information. Re-entering the design cycle may become necessary if the robustness requirements are not satisfied. In Appendix A we will demonstrate the power of MATLAB/Simulink for evaluation of robustness properties of feedback controllers.

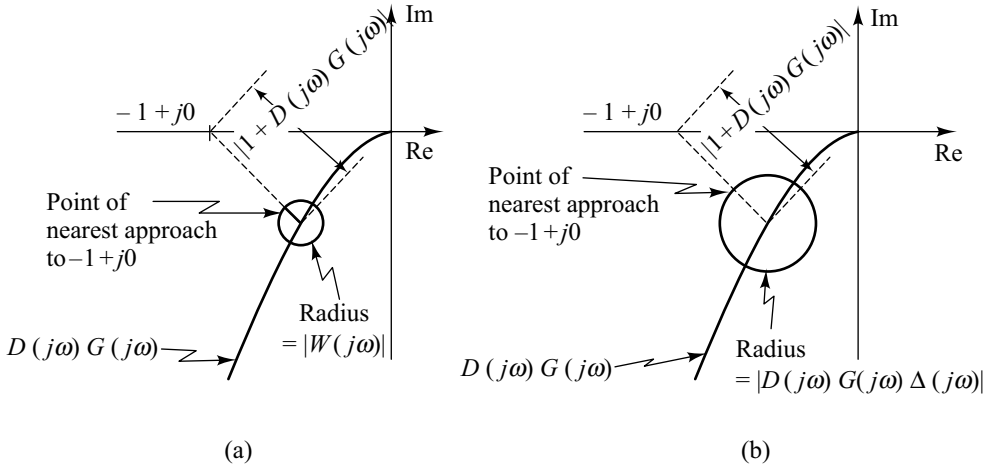

Fig. 9.6 Qualitative robustness considerations

9.3 FREQUENCY RESPONSE OF A STANDARD SECOND-ORDER SYSTEM

In Chapter 6, the transient performance of a control system was discussed by the examination of the standard second-order system of Fig. 9.3, with open-loop transfer function

$$G(s) = \frac{\omega_n^2}{s\left(s + 2\zeta\omega_n\right)} \tag{9.4}$$

and closed-loop transfer function

$$\frac{Y(s)}{R(s)} = M(s) = \frac{\omega_n^2}{s^2 + 2\zeta\omega_n s + \omega_n^2} \tag{9.5}$$

This was based on the fact that the performance of many control systems is dominated by a complex-conjugate pole pair. It is appropriate, therefore, to discuss the frequency response of this standard second-order system.

For the standard second-order system of Fig. 9.3, direct and simple correlations exist between frequency-domain specifications described in Section 9.2, and time-domain specifications described in Section 6.2. We will study these correlations in this section.

9.3.1 Damping Ratio and Phase Margin

In order to evaluate the phase margin, we first find the frequency for which

$$|G(j\omega)| = \frac{\omega_n^2}{\left|-\omega^2 + j2\zeta\omega_n\omega\right|} = 1 \tag{9.6}$$

The frequency, ω_g, that satisfies Eqn. (9.6) is given by

$$\omega_n^2 = \omega_g \sqrt{\omega_g^2 + \left(2\zeta\omega_n\right)^2}$$

or $$\omega_g^4 + 4\zeta^2\omega_n^2\omega_g^2 - \omega_n^4 = 0$$

The roots of this equation follow by applying the quadratic formula in terms of ω_g^2:

$$\omega_g^2 = \omega_n^2\left(-2\zeta^2 \pm \sqrt{4\zeta^4 + 1}\right)$$

For ω_g to be real-valued, the positive root must be used so that

$$\omega_g = \omega_n \sqrt{\sqrt{4\zeta^4 + 1} - 2\zeta^2} \tag{9.7}$$

The phase angle of $G(j\omega)$ at this frequency is

$$\angle G(j\omega_g) = -90° - \tan^{-1}\frac{\omega_g}{2\zeta\omega_n}$$

$$= -90° - \tan^{-1}\frac{\sqrt{\sqrt{4\zeta^4 + 1} - 2\zeta^2}}{2\zeta} \tag{9.8}$$

The difference between the angle of Eqn. (9.8) and $-180°$ is the phase margin ΦM. Thus

$$\Phi M = 90° - \tan^{-1}\frac{\sqrt{\sqrt{4\zeta^4 + 1} - 2\zeta^2}}{2\zeta}$$

$$= \tan^{-1}\frac{2\zeta}{\sqrt{\sqrt{4\zeta^4 + 1} - 2\zeta^2}} \tag{9.9}$$

Figure 9.7 shows phase margin, ΦM, in degrees, *versus* damping ratio ζ. The dashed line in the figure shows a straight line approximation to the function

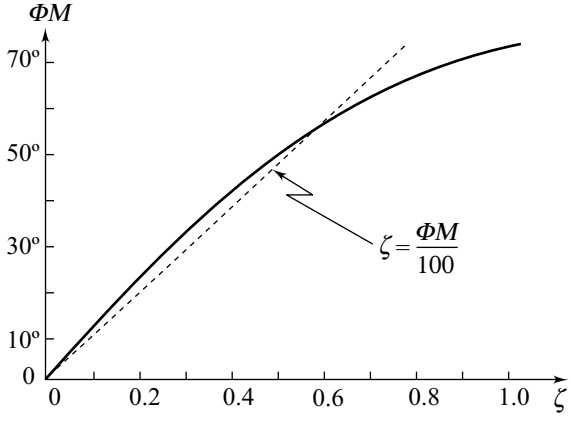

Fig. 9.7 Phase margin versus damping ratio

where $$\zeta = \frac{\Phi M}{100} \tag{9.10}$$

It is clear that the approximation only holds for phase margin below about 70°.

For the standard second-order system under consideration, we cannot define gain margin because $|G(j\omega)| \to 0$ as $\angle G(j\omega) \to -180°$.

9.3.2 Response Speed and Gain Crossover Frequency

Equation (9.7), reproduced below, relates the gain crossover frequency to the undamped natural frequency ω_n and damping ratio ζ.

$$\omega_g = \omega_n \sqrt{\sqrt{4\zeta^4 + 1} - 2\zeta^2} \tag{9.11}$$

Figure 9.8 shows a plot of ω_g/ω_n versus ζ.

We know that when a root-locus design holds the damping ratio constant, both the rise time and the settling time decrease as the undamped natural frequency increases. Therefore, when a frequency-domain design holds the phase margin constant while increasing the gain crossover frequency, the resulting rise time and settling time would diminish in the time domain.

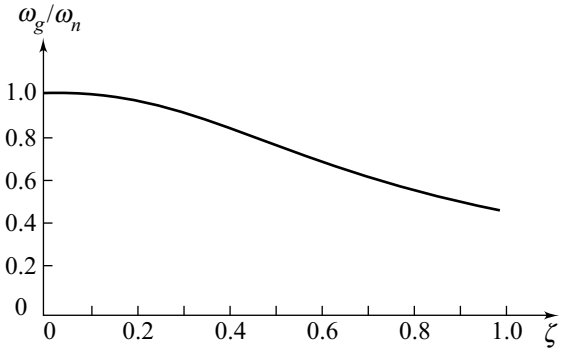

Fig. 9.8 ω_g/ω_n versus damping ratio

It should be remembered that the use of the second-order system of Fig. 9.3 as a standard for reference is based on the assumption of dominance. We are assuming that the contributions of all additional poles and zeros may be neglected. There will certainly be cases where this assumption is not valid. It is not practical to develop correlations for exceptions; so the transient response should be determined, usually by simulation, as a check.

9.3.3 Damping Ratio and Resonance Peak

To evaluate resonance peak and the frequency at which it occurs, we consider the closed-loop transfer function (9.5) with $s = j\omega$:

$$M(j\omega) = \frac{1}{\left(1 - \omega^2/\omega_n^2\right) + j2\zeta\left(\omega/\omega_n\right)} \tag{9.12}$$

For particular values of ζ and ω_n, a plot of $|M(j\omega)| \triangleq M$ *versus* ω can easily be obtained. Some representative curves are shown in Fig. 9.9.

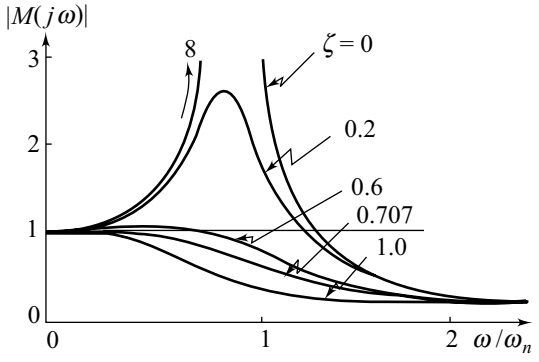

Fig. 9.9 M versus ω/ω_n

Next, consider the magnitude M^2 as derived from Eqn. (9.12):

$$M^2 = \frac{1}{\left(1 - \omega^2/\omega_n^2\right)^2 + 4\zeta^2\left(\omega^2/\omega_n^2\right)} \tag{9.13}$$

To find the peak value of M and the frequency at which it occurs, Eqn. (9.13) is differentiated with respect to frequency and set equal to zero:

$$\frac{dM^2}{d\omega} = -\frac{-4\left(1-\omega^2/\omega_n^2\right)\left(\omega/\omega_n^2\right)+8\zeta^2\left(\omega/\omega_n^2\right)}{\left[\left(1-\omega^2/\omega_n^2\right)^2+4\zeta^2\left(\omega^2/\omega_n^2\right)\right]^2} = 0 \qquad (9.14)$$

The frequency ω_r at which the value M exhibits a peak, as found from Eqn. (9.14), is

$$\omega_r = \omega_n\sqrt{1-2\zeta^2} \qquad (9.15)$$

This value of frequency is substituted into Eqn. (9.13) to yield resonance peak

$$M_r = \frac{1}{2\zeta\sqrt{1-\zeta^2}} \qquad (9.16)$$

From these equations, it is seen that as ζ approaches zero, resonance frequency ω_r approaches undamped natural frequency ω_n, and the resonance peak M_r goes off to infinity. For $0 < \zeta < 1/\sqrt{2}$, the resonance frequency has a value less than ω_n and the resonance peak has a value greater than one. For $\zeta = 1/\sqrt{2}$, the peak value of M is one at zero frequency. For $\zeta > 1/\sqrt{2}$, it is seen from Eqn. (9.14) that $dM^2/d\omega$ does not become zero for any real value of ω. For the range $\zeta \geq 1/\sqrt{2}$, the magnitude M decreases monotonically from $M = 1$ at $\omega = 0$ with increasing ω, as shown in Fig. 9.9. It, therefore, follows that for $\zeta \geq 1/\sqrt{2}$, there is no resonance peak as such and the greatest value of M equals one. This limiting value of ζ for peaking on the magnitude curve of closed-loop frequency response should not be confused with the overshoot on the step response, where there is overshoot for $0 < \zeta < 1$.

It is important to note that for the standard second-order system, resonance peak M_r is a function of damping ratio only. Figure 9.10 illustrates the relationship between M_r and ζ.

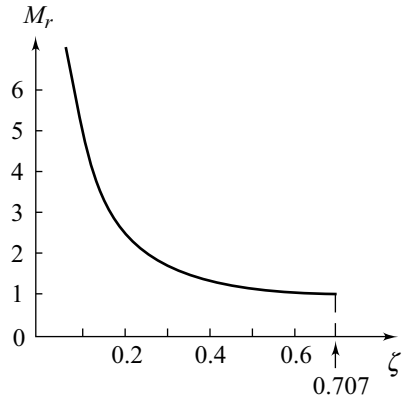

Fig. 9.10 M_r versus ζ

9.3.4 Response Speed and Resonance Frequency

Equation (9.15), reproduced below, relates the resonance frequency ω_r to the undamped natural frequency ω_n and damping ratio ζ.

$$\omega_r = \omega_n\sqrt{1-2\zeta^2}\ ;\ \zeta > 1/\sqrt{2} \qquad (9.17)$$

Figure 9.11 shows a plot of ω_r/ω_n versus ζ.

From Eqns (9.16) and (9.17), we see that when a frequency-domain design holds M_r constant while increasing the resonance frequency, the resulting rise time and settling time would diminish in time domain.

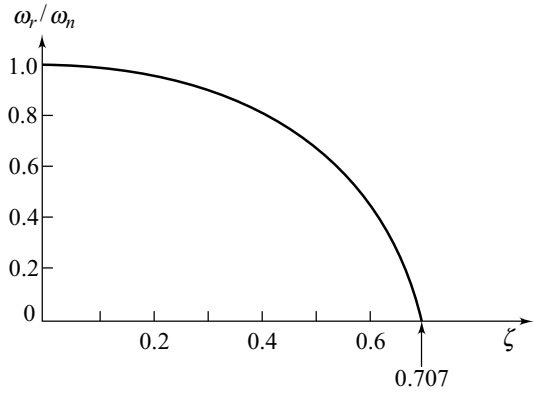

Fig. 9.11 ω_r/ω_n versus ζ

9.3.5 Response Speed and Bandwidth

Another relationship between the frequency response and time response is between the speed of time response (as measured by settling time, and rise time), and the *bandwidth* of the closed-loop frequency response, which is defined as the *frequency ω_b, at which the magnitude M is* $1/\sqrt{2} = 0.707$ *times its value at zero frequency* (see Fig. 9.12a). In Bode coordinate system, the bandwidth ω_b is the frequency at which the magnitude falls off by 3 dB from its low-frequency value (see Fig. 9.12b).

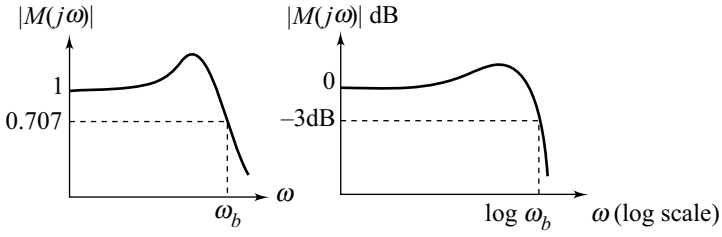

Fig. 9.12 Definition of bandwidth

The bandwidth of the standard second-order system can be found by finding that frequency for which $M = 1/\sqrt{2}$ in Eqn. (9.13):

$$\frac{1}{\left(1-\omega_b^2/\omega_n^2\right)^2 + 4\zeta^2\left(\omega_b^2/\omega_n^2\right)} = \frac{1}{2}$$

Thus $$(1 - \omega_b^2/\omega_n^2)^2 + 4\zeta^2(\omega_b^2/\omega_n^2) = 2$$

or $$(\omega_b^4/\omega_n^4) - 2(1 - 2\zeta^2)(\omega_b^2/\omega_n^2) - 1 = 0$$

Solving for ω_b^2/ω_n^2, we get

$$(\omega_b^2/\omega_n^2) = (1 - 2\zeta^2) \pm \sqrt{4\zeta^4 - 4\zeta^2 + 2}$$

In the last equation the plus sign should be chosen, since ω_b/ω_n must be a positive real quantity for any ζ. Therefore, the bandwidth of the standard second-order system is

$$\omega_b = \omega_n \sqrt{\left[\left(1-2\zeta^2\right) + \sqrt{4\zeta^4 - 4\zeta^2 + 2}\right]} \tag{9.18}$$

Figure 9.13 shows a plot of ω_b/ω_n *versus* ζ. For given ζ, ω_b is proportional to ω_n, and a measure of speed of response. Raising ω_b reduces settling time and rise time of the step response.

The reader is reminded here that the correlations between time-domain and frequency-domain performance specifications arrived at in this section apply only to the standard second-order system of Fig. 9.3. When other second-order or higher-order systems are involved, the correlations are different and more complex. It is not practical to develop correlations for all the cases.

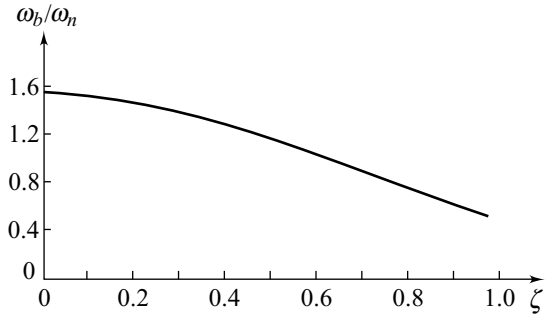

Fig. 9.13 ω_b/ω_n versus ζ

Application of correlations developed for standard second-order system to other second-order and higher-order systems is based on the assumption of dominance. There will certainly be cases where this assumption is not valid; therefore, the transient response must be determined, usually by simulation, as a check.

Example 9.1 The transient behaviour of the system of Fig. 9.14 can be estimated from Bode plots of $G(j\omega)$, as is seen below.

$$G(j\omega) = \frac{0.5e^{-j\omega}}{j\omega\,(1 + j\omega)\,(1 + 0.1j\omega)}$$

Bode plot for this transfer function are shown in Fig. 9.15. Note that the magnitude plot is not affected by the dead-time; however, the phase plot is affected. The dead-time yields a decreased phase margin since at any frequency, the phase angle is more negative. Using a second-order approximation, this decrease in phase margin implies a lower damping ratio and a more oscillatory response for the closed-loop system.

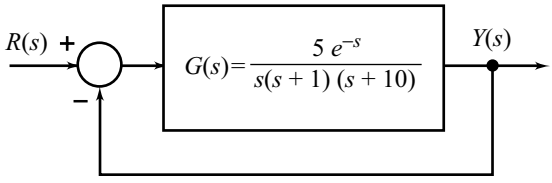

Fig. 9.14 A feedback system

The magnitude curve of Fig. 9.15 crosses the 0-dB axis at a frequency of 0.47 rad/sec; the corresponding phase angle is –145°. Therefore the gain crossover frequency $\omega_g = 0.47$ rad/sec, and the phase margin $\Phi M = -145° - (-180°) = 35°$.

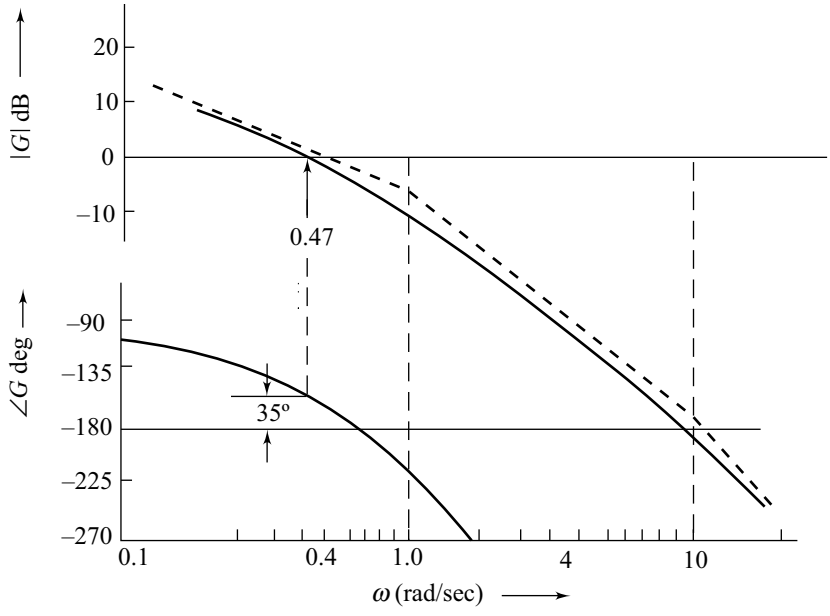

Fig. 9.15 Bode plot for G(s) of Fig. 9.14

The values of ζ and ω_n to be used for approximating the transient behaviour of the system of Fig. 9.14 can be determined from Eqns (9.9)–(9.11) or Figs 9.7–9.8. The values obtained from these second-order approximations are

$$\zeta = 0.33;\ \omega_n = 0.52 \text{ rad/sec}$$

An estimate of the transient behaviour of the system of Fig. 9.14 to step input is therefore obtained as:

$$M_p = \text{peak overshoot} = 100\, e^{-\pi\zeta/\sqrt{1-\zeta^2}} = 33\%$$

$$t_s = \text{settling time} = 4/\zeta\omega_n = 23.3 \text{ sec}$$

Computer simulation (Fig. 9.16) shows $M_p \cong 38\%$ and $t_s \cong 24$ sec.

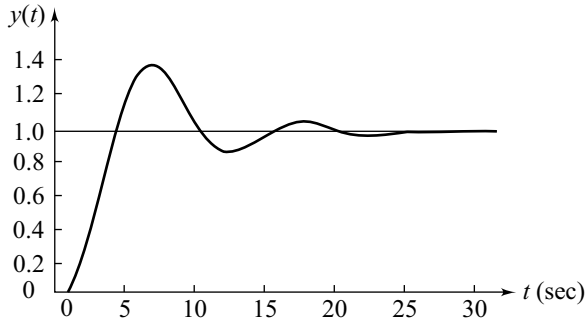

Fig. 9.16 Step response for system of Fig. 9.14

Example 9.2 From the correlation between damping ratio (equivalently, peak overshoot in step response) and phase margin developed for standard second-order systems, we observe that if we can vary the phase margin, we can vary the peak overshoot in the step response of the system. Looking at Fig. 9.17, we see that if we desire a phase margin represented by *CD*, we would have to lower the magnitude curve by *AB*. Thus, a simple gain adjustment can be used to design phase margin and hence percentage overshoot in step response. Such a design is acceptable if both the resulting gain crossover frequency (equivalently, speed of response) and gain margin are acceptable. Dynamic compensation (discussed in Chapter 10) will become necessary in cases wherein the design for specified phase margin by gain adjustment results in poor gain crossover frequency and/or gain margin.

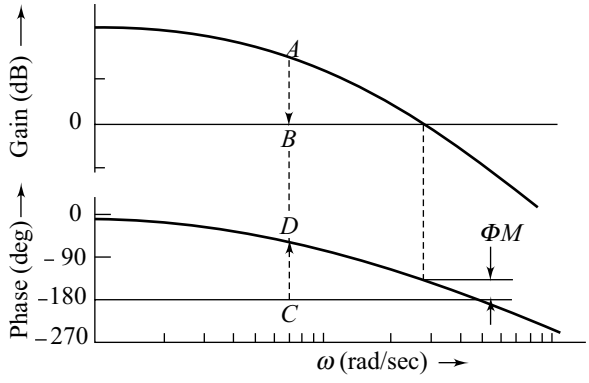

Fig. 9.17 Bode plot showing gain adjustment for desired phase margin

Gain adjustments can also be used to design gain margin. The resulting phase margin and gain crossover frequency are then examined to see whether the design is acceptable. Similarly, we could adjust the gain for specified gain crossover frequency and then examine the resulting gain margin and phase margin.

Consider a unity-feedback system with open-loop transfer function

$$G(s) = \frac{K}{s\,(1 + 0.1s)\,(1 + 0.05s)}$$

Figure 9.18 shows the Bode plot of $G(j\omega)$ with open-loop gain $K = 10$. From this figure, it is found that gain margin $GM = 10$ dB, phase margin $\Phi M = 33°$, and gain crossover frequency $\omega_g = 7.4$ rad/sec. The steady-state error for unit-ramp input for this type-1 system is $e_{ss} = 1/K = 1/10$.

Let us examine the effects of gain adjustments.

(i) Suppose that to reduce the steady-state error, a phase margin of 24° will be accepted. To obtain phase margin of 24°, we must first determine the frequency at which the phase angle of $G(j\omega)$ is $-156°$, and then adjust the value of K so that the gain at this frequency is 0 dB. From the Bode plot of Fig. 9.18, we find that for $\omega = 9$ rad/sec, we get this phase angle and a gain of -3 dB. Therefore, if the gain crossover frequency is changed to 9 rad/sec, a phase margin of 24° will be obtained. To change the gain crossover frequency to 9 rad/sec, the magnitude curve should be raised by 3 dB, i.e., the gain 10 must be raised by a factor of α given by $20 \log \alpha = 3$. Hence $\alpha = 1.4$ and the new gain is $K = 10 \times 1.4 = 14$.

From Fig. 9.18, we observe that increasing K reduces the phase margin and gain margin, and increases the gain crossover frequency. The system thus becomes relatively less stable (peak overshoot in transient response increases). The increase in gain crossover frequency will generally result in better speed of response (reduced rise time/settling time).

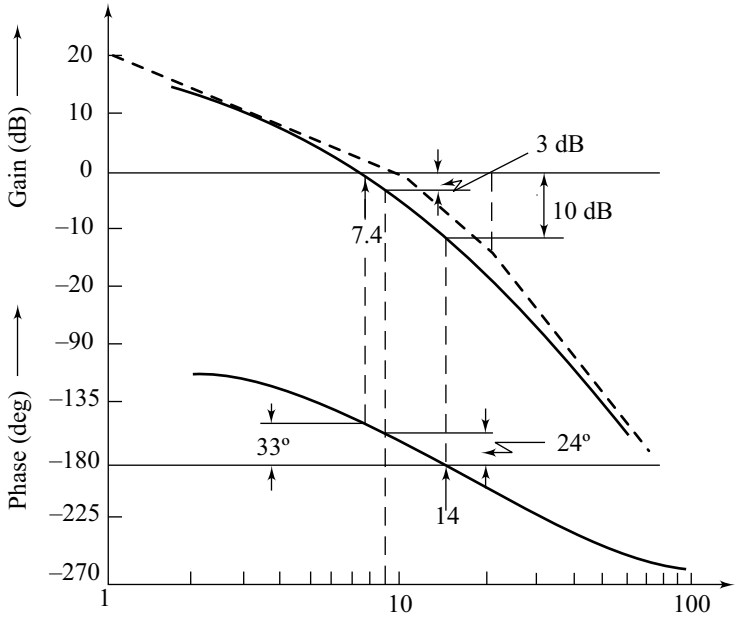

Fig. 9.18 Bode plot of $G(j\omega) = 10/j\omega(j0.1\omega + 1)\,(j0.05\,\omega + 1)$

(ii) Suppose it is desired to find the open-loop gain for a gain margin of 20 dB. To determine the gain margin of 20 dB, first we determine the phase crossover frequency and the gain at this frequency. From the Bode plot of Fig. 9.18 we find that phase crossover frequency $\omega_\phi = 14$ rad/sec and the gain

at ω_ϕ is –10 dB. Hence for the desired gain margin, we must decrease the gain by 10 dB. It means that magnitude curve must be lowered by 10 dB, i.e., the gain K must be reduced by a factor of β, given by $20 \log(1/\beta) = -10$. Hence $\beta = 3.16$ and the new gain is $K = 10/3.16 = 3.16$.

From Fig. 9.18 we observe that reducing K increases the phase margin and gain margin, and reduces the gain crossover frequency.

9.4 CONSTANT-M CIRCLES

A control system is a closed-loop system. By Nyquist stability criterion, we predict its stability using plots of the open-loop transfer function. Closed-loop performance measures such as gain crossover frequency, phase margin, and gain margin are also determined using plots of open-loop transfer functions.

Other useful measures of performance of a feedback system are resonance peak, resonance frequency, and bandwidth of the closed-loop frequency response. Fortunately, these closed-loop performance indices can also be determined using plots of the open-loop transfer function, as is seen below.

Consider a single-loop unity-feedback system shown in Fig. 9.19. The closed-loop transfer function is

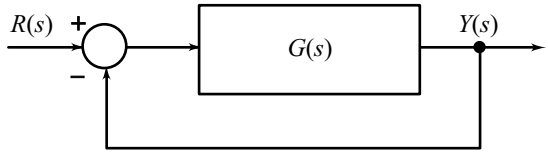

Fig. 9.19 A unity-feedback system

$$M(s) = \frac{G(s)}{1 + G(s)}$$

The frequency response of the closed-loop transfer function is given by

$$M(j\omega) = \frac{G(j\omega)}{1 + G(j\omega)} \tag{9.19}$$

Figure 9.20 shows a typical plot of $G(j\omega)$ in polar coordinates. Consider the point A on this plot associated with frequency ω_1. $G(j\omega_1)$ is a vector from the origin to the point A; and $1 + G(j\omega_1)$ is a vector from $-1 + j0$ point to the point A. One point on the closed-loop frequency response can be calculated by measuring lengths and angles of these vectors:

$$|M(j\omega_1)| = \frac{|G(j\omega_1)|}{|1 + G(j\omega_1)|}$$

$$\angle M(j\omega_1) = \angle G(j\omega_1) - \angle(1 + G(j\omega_1))$$

Obviously, this calculation can be repeated at many points on the $G(j\omega)$-curve, and the entire closed-loop frequency response can be calculated in this manner.

It is easier to prepare nomographs so that the results can be read off without additional calculations. Consider the graphical configuration of Fig. 9.20 as a problem in geometry and trigonometry, without regard to frequency response. The lines for $G(j\omega_1)$ and $1 + G(j\omega_1)$ are simply vectors which have

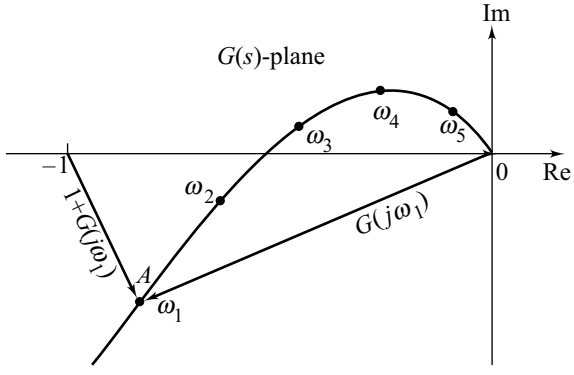

Fig. 9.20 Polar relationship between open-loop and closed-loop frequency responses

lengths and angles associated with them when drawn from the origin and the $-1+j0$ point, respectively, to a common point A in the complex plane.

$$G(j\omega_1) = \text{Re } G(j\omega_1) + j\text{Im } G(j\omega_1) = u + jv$$
$$1 + G(j\omega_1) = (1+u) + jv$$

By definition,

$$\frac{|G(j\omega_1)|}{|1+G(j\omega_1)|} = \frac{|u+jv|}{|(1+u)+jv|} = M, \text{ a number} \tag{9.20}$$

Are there any other points in the plane such that the same value of M would be associated with vectors drawn to them? The answer to this question is *yes*. In fact, the locus of constant-M points on the polar plane is a circle. This can be proved as follows.

From Eqn. (9.20), we have

$$M^2 = \frac{u^2+v^2}{(1+u)^2+v^2}$$

or
$$M^2(1+u^2+2u+v^2) = u^2+v^2$$

Rearranging, we get

$$(1-M^2)u^2 + (1-M^2)v^2 - 2M^2 u = M^2 \tag{9.21}$$

This equation is conditioned by dividing through by $(1-M^2)$ and adding the term $[M^2/(1-M^2)]^2$ on both sides. We have

$$u^2+v^2-\frac{2M^2}{1-M^2}u + \left(\frac{M^2}{1-M^2}\right)^2 = \frac{M^2}{1-M^2} + \left(\frac{M^2}{1-M^2}\right)^2$$

which is finally simplified to

$$\left(u-\frac{M^2}{1-M^2}\right)^2 + v^2 = \left(\frac{M^2}{1-M^2}\right)^2 \tag{9.22}$$

For a given M, Eqn. (9.22) represents a circle with the centre at $(M^2/(1-M^2), 0)$. The radius of the circle is $r = M/(1-M^2)$.

Note that Eqn. (9.22) is invalid for $M = 1$. For $M = 1$, Eqn. (9.21) gives

$$u = -\frac{1}{2} \tag{9.23}$$

which is the equation of a straight line parallel to the imaginary axis and passing through the point $\left(-\frac{1}{2}, 0\right)$ in the $G(s)$-plane.

When M takes on different values, Eqn. (9.22) describes in the $G(s)$-plane a family of circles that are called *constant-M circles*. A representative family of constant-M circles is shown in Fig. 9.21. The following conclusions are easily drawn regarding these circles.

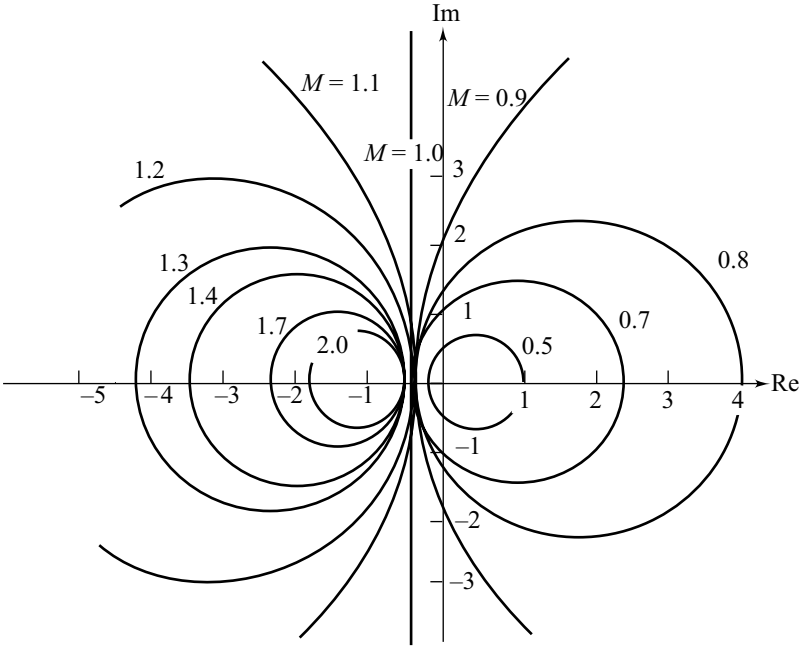

Fig. 9.21 Constant-*M* circles

Case I: M > 1

As *M* increases, the radii of constant-*M* circles reduce monotonically, and the centres located on negative real axis progressively shift towards (–1+ *j*0) point. *M* = ∞ circle has a radius zero and is centred at (–1+ *j*0).

Case II: M = 1

It follows that *M* = 1 circle is of infinite radius with centre at infinity on the real axis, i.e., it is a straight line parallel to the imaginary axis of the *G*(*s*)-plane. It intersects the real axis at –1/2.

Case III: M < 1

As *M* decreases, the radii of constant-*M* circles reduce monotonically, and centres located on positive real axis shift towards the origin. *M* = 0 circle has a radius zero and is centred at the origin.

The constant-*M* circles are useful when overlaid on the polar plot of $G(j\omega)$ as shown in Fig. 9.22. The intersection of $G(j\omega)$ plot with M_1 circle at frequencies ω_1 and ω_4 indicates that

$$\frac{G(j\omega_1)}{1+G(j\omega_1)} = M(j\omega_1) = M_1$$

$$\frac{G(j\omega_4)}{1+G(j\omega_4)} = M(j\omega_4) = M_1$$

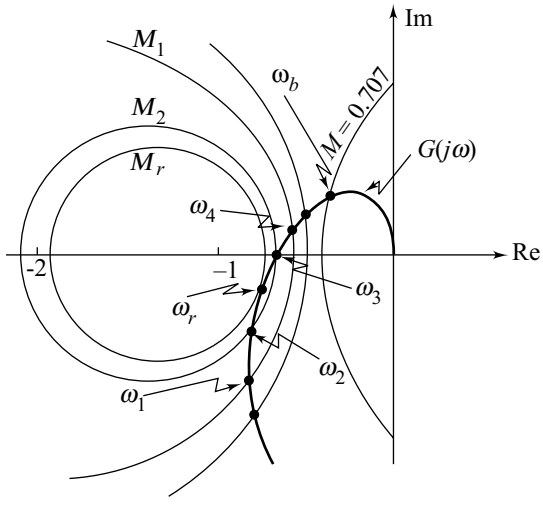

Fig. 9.22 Constant-*M* circles and $G(j\omega)$-plot

Similarly, the intersection of $G(j\omega)$ plot with M_2 circle at frequencies ω_2 and ω_3 indicates that

$$M(j\omega_2) = M(j\omega_3) = M_2$$

Note that the circle tangent to the $G(j\omega)$ plot provides us with the peak magnitude M_r of the closed-loop frequency response and the corresponding frequency ω_r. Using Fig. 9.22, we can also read the bandwidth; it is the frequency ω_b associated with the point of intersection of $G(j\omega)$ plot with the $M = 0.707$ circle. A typical magnitude curve of closed-loop frequency response is shown in Fig. 9.23.

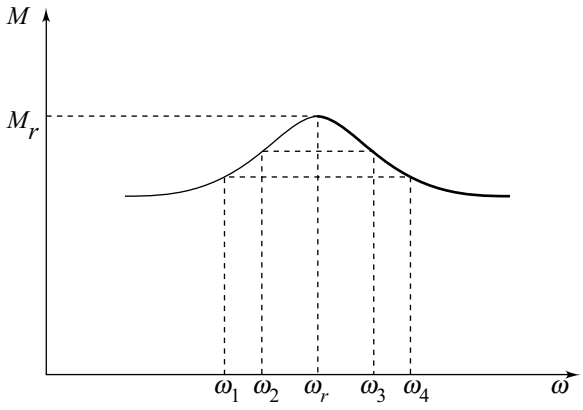

Fig. 9.23 Closed-loop frequency response

It is also possible to plot loci of constant phases of $M(j\omega)$ on the $G(s)$-plane. The plot consists of a family of circles called *constant-N circles*; $N = \tan\alpha$, $\alpha = \angle M(j\omega)$. When overlaid on the $G(j\omega)$ plot, the constant-N circles give the phase curve of closed-loop frequency response in a manner similar to that used for obtaining magnitude curve.

It may be noted that instead of using constant-M and constant-N circles, we can compute closed-loop frequency response directly from Eqn. (9.19) by use of a computer program. However, as we shall see shortly, the graphical method allows the design of a system with specified values of M_r, ω_r and/or ω_b. These performance measures are associated with only the magnitude curve of closed-loop frequency response and can be read off directly from a plot of $G(j\omega)$ superimposed on constant-M circles. Constant-N circles are not used in this text and, therefore, will not be discussed.

As is evident from the above discussion, the constant-M circles can be used only for systems with unity feedback. For nonunity feedback systems, we will translate the performance requirements into specifications on gain margin, phase margin, and gain crossover frequency, and then carry out the design using Bode plots. To check the design for requirements on resonance peak and resonance frequency/bandwidth, the magnitude curve of the closed-loop frequency response may be generated using a computer program.

Example 9.3 A unity-feedback control system has an open-loop frequency response $G(j\omega)$ with properties as follows:

ω (rad/sec)	2	3	4	5	6
$\lvert G(j\omega)\rvert$	2.7	1.7	0.97	0.63	0.4
$\angle G(j\omega)$ (degrees)	– 115	– 126	– 138	– 150	– 163

The open-loop frequency response, plotted in polar coordinates, is shown in Fig. 9.24. The $G(j\omega)$-plot is tangential to the $M = 1.4$ circle at a frequency $\omega = 4$ rad/sec. Therefore, the resonance peak $M_r = 1.4$, and the resonance frequency $\omega_r = 4$ rad/sec.

The values of ζ and ω_n to be used for approximating the transient behaviour of the system can be determined from Eqns (9.16)–(9.17) or Figs 9.10–9.11. Rearranging Eqn. (9.16), we obtain

$$\zeta^4 - \zeta^2 + (1/4\, M_r^2) = 0 \qquad (9.24)$$

Since $M_r = 1.4$, we have $\zeta = 0.39$ and 0.92. A damping ratio larger than 0.707 yields no peak above zero frequency. Thus, use select $\zeta = 0.39$. Using Eqn. (9.17) with $\omega_r = 4$ and $\zeta = 0.39$, we get $\omega_n = 4.8$ rad/sec.

The bandwidth of a system is defined as the frequency at which the magnitude of the closed-loop frequency response is 0.707 of its magnitude at $\omega = 0$. From Fig. 9.24, we see that $M = 0.707$ circle intersects the $G(j\omega)$-plot at $\omega = 6$ rad/sec. This frequency can be taken as the bandwidth if it is assumed that the closed-loop gain is unity at $\omega = 0$.

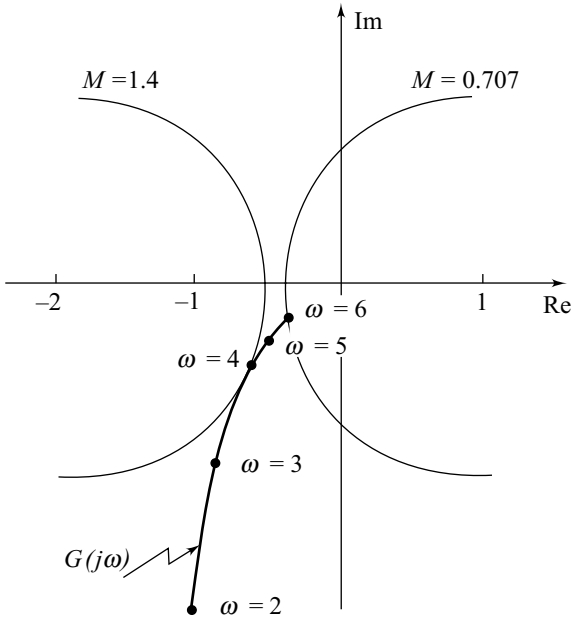

Fig. 9.24 Constant-*M* circles and $G(j\omega)$-plot for Example 9.3

9.5 THE NICHOLS CHART

In the previous section, we have seen that closed-loop frequency response of a unity-feedback system (refer Fig. 9.19) can easily be determined from polar plot of open-loop transfer function $G(j\omega)$ superimposed on constant-M circles. Use of constant-M circles on polar plane is straightforward but seldom used because Nyquist analysis is normally carried out on the Bode plots and it is more efficient to use a nomograph compatible with Bode data. The *Nichols Chart*, introduced by N.B. Nichols in the 1940s, is such a nomograph.

The Nichols chart consists of curves that are maps of the constant-M and constant-N circles on a new coordinate system. The Nichols coordinate system plots $|G(j\omega)|$ in dB as ordinate *versus* $\angle G(j\omega)$ in degrees as abscissa, with origin at $|G(j\omega)| = 0$ dB and $\angle G(j\omega) = -180°$. This origin is the map of the critical point $-1 + j0$ of the polar coordinate (Nyquist) plot. Figure 9.26 illustrates the coordinate system (not the nomograph) with a plot of Bode data from Fig. 9.25. Note that the phase and gain margins are readily identified.

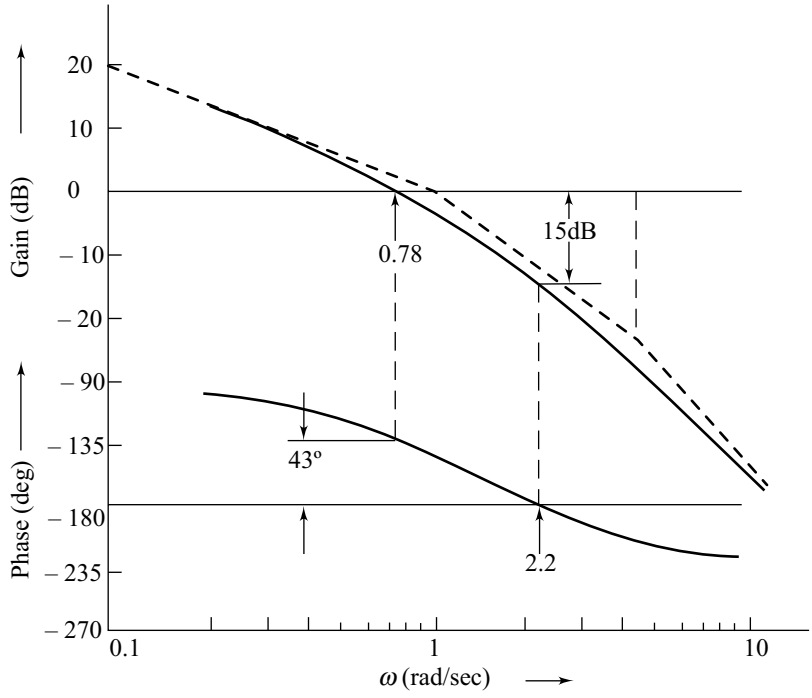

Fig. 9.25 Frequency-response plot in a Bode coordinate system

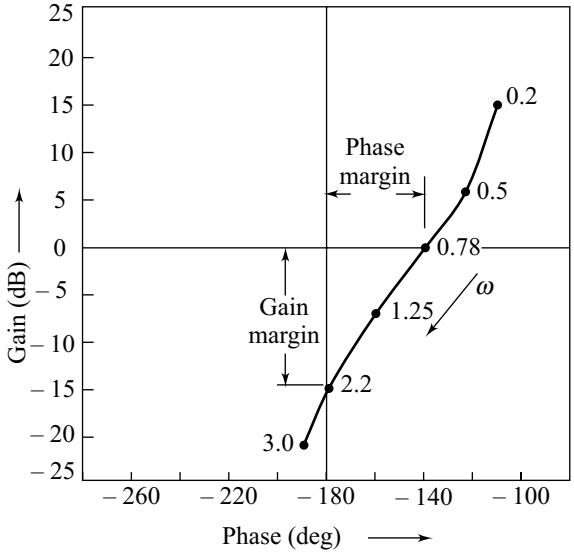

Fig. 9.26 Frequency-response plot in a Nichols coordinate system

The constant-M and constant-N circles in polar coordinates do not remain circles when mapped onto dB *versus* phase plane. A typical constant-M circle is shown in Fig. 9.27. The magnitude ρ and angle λ of a vector drawn to any point on this circle are shown. The equation of the M circle is (refer Eqn. (9.22))

$$\left(u - \frac{M^2}{1-M^2}\right)^2 + v^2 = \left(\frac{M^2}{1-M^2}\right)^2$$

where $u = \rho \cos \lambda$, and $v = \rho \sin \lambda$. Combining these equations produces

$$\left(\rho \cos\lambda - \frac{M^2}{1-M^2}\right)^2 + \rho^2 \sin^2 \lambda = \left(\frac{M^2}{1-M^2}\right)^2$$

or $$\rho^2 - 2 \cos \lambda \left(\frac{M^2}{1-M^2}\right) \rho - \frac{M^2}{1-M^2} = 0 \qquad (9.25)$$

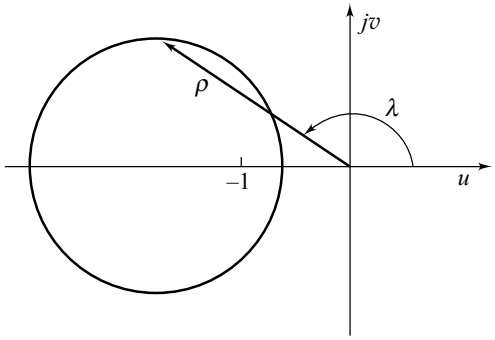

Fig. 9.27 A constant-M circle

For any value of M, a series of values of λ can be inserted in Eqn. (9.25) to solve for ρ. This magnitude must be changed to dB. The data thus generated when plotted in Nichols coordinate system, gives a constant-M locus. When M takes on different values, Eqn. (9.25) describes in the Nichols system a family of loci. A representative family of constant-M loci is shown in Fig. 9.28. The constant-N circles can be transferred on Nichols chart in a similar manner, if needed.

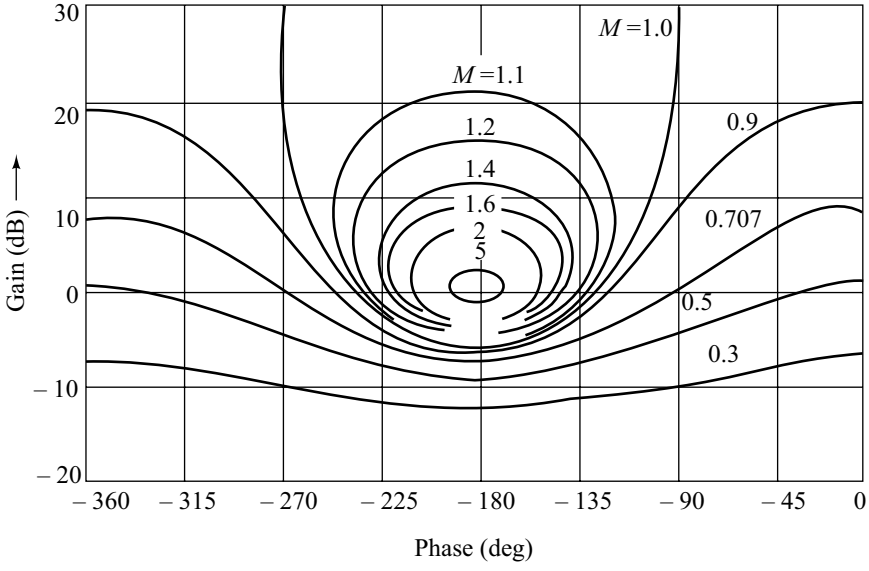

Fig. 9.28 Constant-M loci in Nichols coordinate system

Note that the $M = 1$ curve is asymptotic to $-90°$ and $-270°$ lines of Nichols coordinate system. The curves for $M > 1$ are closed curves inside the limits of $-90°$ and $-270°$ lines. The curves for $M < 1$ cross these limits. The curves are symmetrical about $-180°$ line.

The Nichols charts were commercially available until the middle 1970s. These charts cannot be purchased any more. They can, however, be easily generated with the help of a computer. An expanded section of the Nichols chart with selected constant-M loci is shown in Fig. 9.29; the values of M are given in dB.

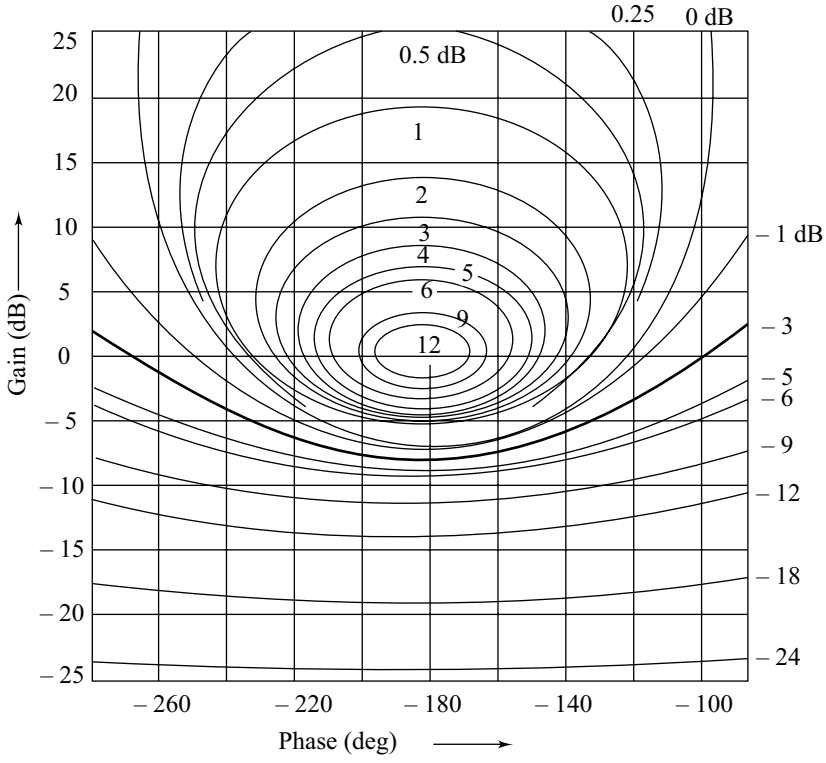

Fig. 9.29 An expanded section of the Nichols chart

Superimposing the dB versus phase angle curve of $G(j\omega)$ shown in Fig. 9.26, on the Nichols chart we obtain the plot of Fig. 9.30. The intersection of $G(j\omega)$-curve with $M = 1$ dB locus at frequencies ω_1 and ω_2 indicates that

$$\frac{|G(j\omega_1)|}{|1+G(j\omega_1)|} = |M(j\omega_1)| = 1 \text{ dB}$$

$$\frac{|G(j\omega_2)|}{|1+G(j\omega_2)|} = |M(j\omega_2)| = 1 \text{ dB}$$

Similarly, the intersections of $G(j\omega)$-curve with other constant-M loci determine the magnitude (in dB) of the closed-loop frequency response for various frequencies. The data so generated when plotted with magnitude in dB as ordinate and frequency ω (log scale) as abscissa, gives the Bode magnitude plot of the closed-loop frequency response.

Note that the constant-M locus tangent to the $G(j\omega)$-curve provides us with the peak magnitude M_r (in dB) of the closed-loop frequency response and the corresponding frequency ω_r. We can also directly read off the bandwidth from the Nichols chart; it is the frequency associated with the point of intersection of $G(j\omega)$-curve with $M = -3$ dB locus.

The Nichols chart of Fig. 9.30 has 2 dB and 3 dB closed-loop gain curves; the M_r value lies between 2 dB and 3 dB. One must do a little interpolation to determine M_r. From Fig. 9.30 we see that an approximate value of M_r is 2.5 dB and it occurs at a frequency $\omega_r = 0.8$ (the frequency ω_r corresponding to the point A has been determined from Fig. 9.25).

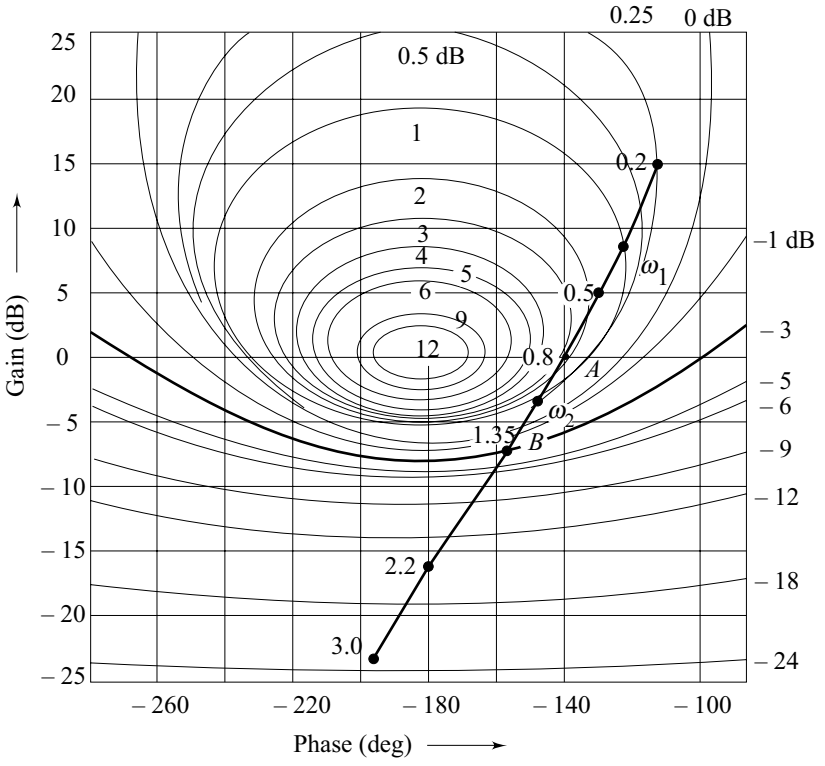

Fig. 9.30 The curve of Fig. 9.26 superimposed on the Nichols chart

Point B represents the intersection of $G(j\omega)$-curve with $M = -3$ dB contour. The frequency corresponding to this point (read from Fig. 9.25) is the bandwidth $\omega_b = 1.35$ rad/sec.

Example 9.4 The concept of constant-M circles will now be applied to the design of control systems. In obtaining acceptable performance, the adjustment of gain is usually the first consideration. The adjustment may be based on a desirable value for the resonance peak. In what follows, we shall demonstrate how the Nichols chart can be used to determine the gain K so that the system will have a desired value of M_r. Such a design is usually acceptable if the resulting bandwidth ω_b is satisfactory. Let us reconsider the system discussed in Example 9.2. The system has an open-loop transfer function

$$G(j\omega) = \frac{K}{j\omega\,(j0.1\omega + 1)\,(j0.05\omega + 1)}\,;\; K = 10$$

Figure 9.18 shows the Bode plot of $G(j\omega)$. Transferring the Bode data to a Nichols chart, we get the dB versus phase angle plot of $G(j\omega)$. This is shown in Fig. 9.31. From the figure, it is seen that

$$M_r = 5.3 \text{ dB, and } \omega_r = 8.14 \text{ rad/sec}$$

The dB versus phase angle plot of $G(j\omega)$ intersects the -3 dB M-locus at the point A. The frequency parameter at this point can be easily determined by transferring the open-loop dB data at A to the Bode plot of Fig. 9.18. We find the frequency to be 12.6 rad/sec. Therefore, bandwidth $\omega_b = 12.6$ rad/sec.

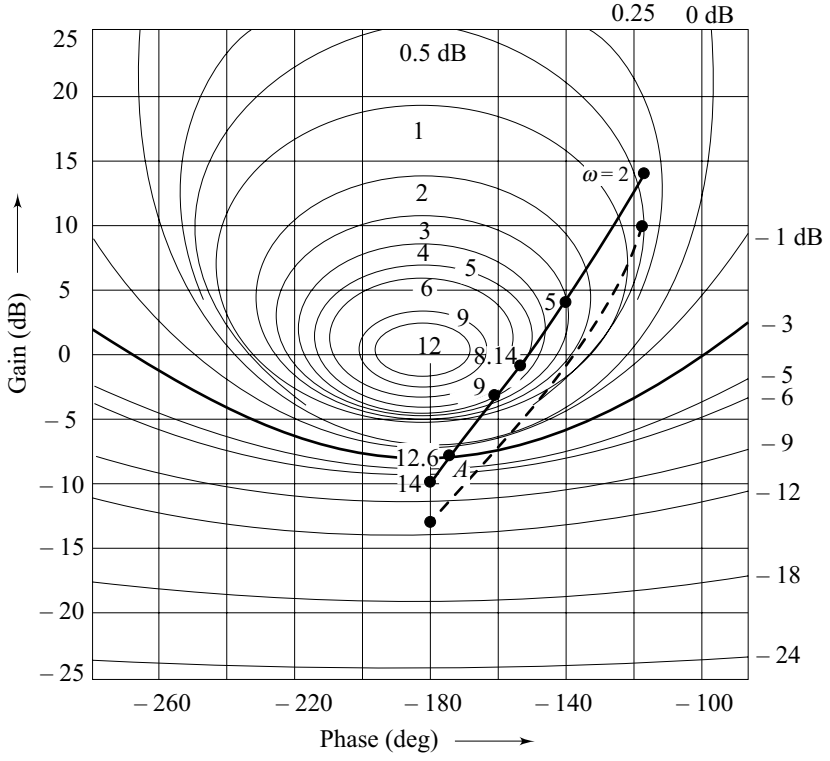

Fig. 9.31 The Nichols chart for Example 9.4

Let us examine the effects of gain adjustments. Suppose it is desired to find the open-loop gain for resonance peak of 2 dB. From Fig. 9.31, it is found that the dB versus phase angle plot of $G(j\omega)$ must be moved downwards by 3.5 dB in order that it be tangent to the 2 dB M-locus. It means that the gain $K = 10$ must be reduced by a factor of β, given by $20 \log (1/\beta) = -3.5$. Hence $\beta = 1.5$ and the new gain is $K = 10/1.5 = 6.33$.

From Fig. 9.31, we observe that reducing K reduces the resonance peak M_r; it also reduces the bandwidth ω_b. The system thus becomes relatively more stable (peak overshoot in transient response reduces). The reduced bandwidth will generally result in increased rise time/settling time of the transient response.

Review Examples

Review Example 9.1 Consider the unity-feedback system shown in Fig. 9.32. Let the compensator $D(s)$ be simply a constant K. Find a gain K such that

(i) phase margin ≥ 60°, and

(ii) bandwidth is as large as possible.

Solution The system under consideration is a standard second-order system. Correlations derived

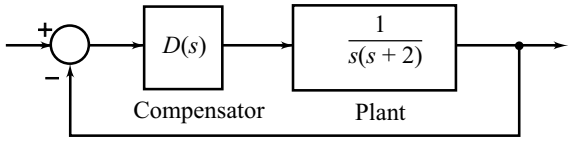

Fig. 9.32 Unity-feedback system

in Section 9.3 are applicable without any approximation. Using Eqns (9.11) and (9.18), we obtain the ratio of gain crossover frequency ω_g and bandwidth ω_b as a function of ζ. Table 9.1 shows this ratio for a range of values of ζ. It is quite interesting to note that the ratio is rather constant. Raising the gain crossover frequency increases the bandwidth of the system.

Table 9.1 Bandwidth-gain crossover frequency correlation

ζ	0.3	0.4	0.6	0.707	0.8
ω_g/ω_b	0.63	0.62	0.63	0.64	0.68

The Bode plot of

$$G(j\omega) = \frac{1}{j\omega\,(j\omega + 2)} = \frac{0.5}{j\omega\,(j0.5\omega + 1)}$$

is shown in Fig. 9.33. The magnitude plot crosses the 0-dB line roughly at 0.46; thus the gain crossover frequency is 0.46 rad/sec. The phase margin is then measured from the plot as 77°. The specification on phase margin is, thus, met without the need for a compensator $D(s)$.

Now we shall adjust K to make gain crossover frequency as large as possible. If we increase K from 1, the magnitude plot will move upward and the gain crossover frequency will increase. This will cause the phase margin to decrease, as can be seen from Fig. 9.33. In other words, as the gain crossover frequency increases, the phase margin will decrease. The largest permissible gain crossover frequency corresponds to a phase margin of 60°. It is seen from Fig. 9.33 that if magnitude plot is shifted up by 9 dB, then 1.15 rad/sec becomes the new gain crossover frequency and the phase margin is 60°. Therefore, the required gain K is given by 20 log K = 9, which implies K = 2.8.

We may determine the bandwidth of the gain-compensated closed-loop system using the Nichols chart. Transferring the Bode data from Fig. 9.33 corresponding to K = 2.8 to the Nichols coordinate system, we obtain Fig. 9.34. The – 3dB M-locus has been constructed using Table 9.2, obtained from the Nichols chart of Fig. 9.29. The dB versus phase angle curve of $KG(j\omega)$ intersects the –3dB M-locus at point A. The frequency parameter at this point can be easily determined by transferring the open-loop dB data at A to the Bode plot of Fig. 9.33. We find this frequency to be 2; therefore the bandwidth ω_b = 2 rad/sec.

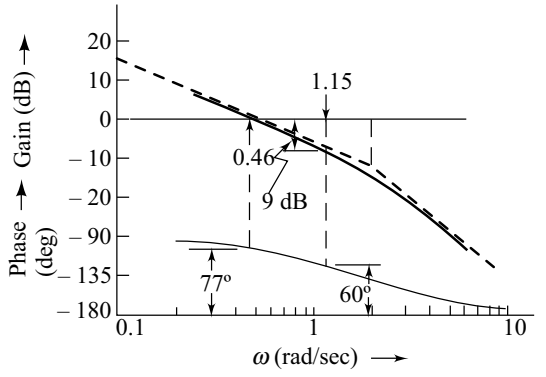

Fig. 9.33 Bode Plot of $G(j\omega) = 0.5/j\omega(j0.5\omega + 1)$

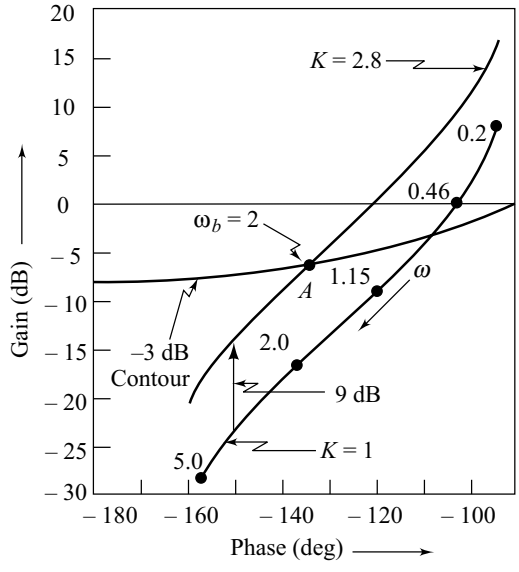

Fig. 9.34 Determination of bandwidth

Table 9.2 Data for construction of – 3dB M-locus of the Nichols chart

Degrees	– 90	– 100	– 120	– 140	– 160	– 180	– 200	– 220
dB	0	– 1.5	– 4.18	– 6.13	– 7.28	– 7.66	– 7.28	– 6.13

Note that the above design problem could also be solved analytically using correlations developed in Section 9.3; we opted for the graphical tools to illustrate a design procedure applicable to second-order as well as higher-order systems.

Review Example 9.2 Let us consider a unity-feedback system with open-loop transfer function

$$G(s) = \frac{0.64}{s\left(s^2 + s + 1\right)}$$

The $G(j\omega)$ plot in polar coordinate system is shown in Fig. 9.35. From this figure, we find that

$$\Phi M = 30°,\ M_r = 2.8$$

On the basis of phase margin, we estimate the system damping ratio as $\zeta \cong 0.30$ (refer Eqn. (9.10)), and on the basis of resonance peak we find that $\zeta \cong 0.175$ (refer Eqn. (9.16)). The apparent conflict discovered in this example clearly indicates that a designer must use the frequency-domain to time-domain correlations with caution. The correlations arrived at in Section 9.3 apply to standard second-order systems. Use of these correlations for higher-order systems where dominance condition is not satisfied, can lead to unclear and uncertain estimates. One is usually safe if the lesser of the two values of ζ resulting from ΦM and M_r relations is utilized for analysis and design purposes.

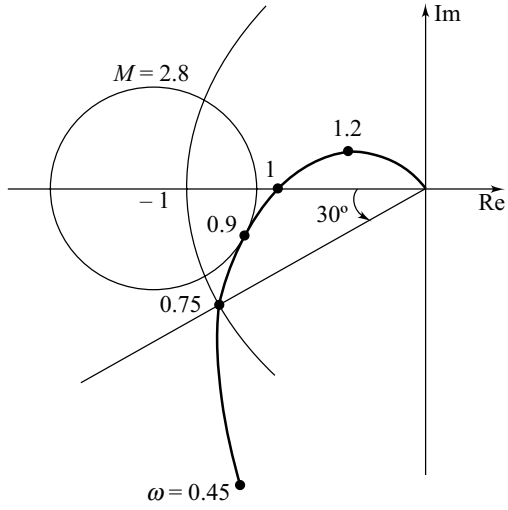

Fig. 9.35 Nyquist plot for $G(j\omega) = 0.64/j\omega\,[(j\omega)^2 + j\omega + 1)]$

Review Questions

9.1 (a) Describe a set of performance specifications characterizing desired frequency response, that are frequently used in the design of linear control systems using Bode plots.

(b) Frequency response of a feedback control system should be similar to that of an ideal low pass filter. Justify this statement.

9.2 Given the following measures of frequency response of a unity feedback system with open-loop transfer function $G(s) = \dfrac{\omega_n^2}{s\left(s + 2\zeta\omega_n\right)}$:

(i) phase margin, ΦM; (ii) gain crossover frequency, ω_g; (iii) resonance peak, M_r; (iv) resonance frequency, ω_r; (v) bandwidth, ω_b.

Through graphical plots, explain the correlation of these functions with ζ and ω_n.

9.3 (a) Define the terms resonance peak M_r, and the bandwidth ω_b of a closed-loop control system.
(b) What is the Nichols chart? How can we identify resonance peak and bandwidth from the Nichols chart?
(c) Nichols chart can be used only for systems with unity feedback. Suggest a suitable design procedure for non-unity feedback systems.

9.4 (a) What does it mean when a control system is described as being robust?
(b) Show that both a good *GM* and a good ΦM are needed for robust stability.

Problems

9.1 Consider a unity-feedback system with open-loop transfer function

$$G(s) = \frac{\omega_n^2}{s\left(s + 2\zeta\omega_n\right)}$$

Show that the phase margin (relative stability measure in frequency domain) is given by

$$\Phi M = \tan^{-1} \frac{2\zeta}{\sqrt{\sqrt{4\zeta^4 + 1} - 2\zeta^2}}$$

9.2 For the standard second-order system

$$\frac{Y(s)}{R(s)} = \frac{\omega_n^2}{s^2 + 2\zeta\omega_n s + \omega_n^2},$$

show that the bandwidth is given by

$$\omega_b = \omega_n \sqrt{\left[\left(1 - 2\zeta^2\right) + \sqrt{4\zeta^4 - 4\zeta^2 + 2}\right]}$$

9.3 Show that when $0 < \zeta < 0.707$, the frequency response of a system defined by a transfer function

$$M(s) = \frac{\omega_n^2}{s^2 + 2\zeta\omega_n s + \omega_n^2}$$

has a peak amplitude given by

$$M_r = \frac{1}{2\zeta\sqrt{1 - \zeta^2}}$$

which occurs at the resonance frequency

$$\omega_r = \omega_n \sqrt{1 - \zeta^2}$$

9.4 Consider the feedback system shown in Fig. P9.4.
(a) Find the values of K and a to satisfy the following frequency-domain specifications:

$$M_r = 1.04;\ \omega_r = 11.55 \text{ rad/sec}$$

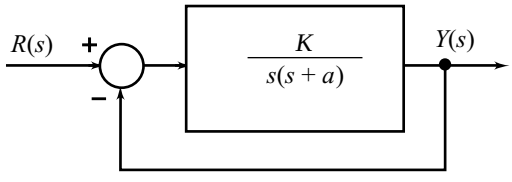

Fig. P9.4

(b) For the values of K and a determined in part (a), calculate the settling time and bandwidth of the system.

MATLAB Exercise Use MATLAB to obtain resonance peak, resonance frequency, settling time, and bandwidth for the values of K and a obtained in part(a).

9.5 Unit-step response data of a second-order system is given below. Obtain the corresponding frequency response indices (M_r, ω_r, ω_b) for the system.

t(sec)	0	0.05	0.10	0.15	0.20	0.25	0.30	0.35	0.40	0.45	0.50
$y(t)$	0	0.25	0.8	1.08	1.12	1.02	0.98	0.98	1.0	1.0	1.0

9.6 Phase margin for a second-order system is given by

$$\Phi M = \tan^{-1} \frac{2\zeta}{\sqrt{\sqrt{4\zeta^4 + 1} - 2\zeta^2}}$$

Write the approximate expression for ΦM for low values of ζ. Using the approximate expression, find the value of gain K such that the system shown in Fig. P9.6. has a phase margin of ϕ_m degrees.

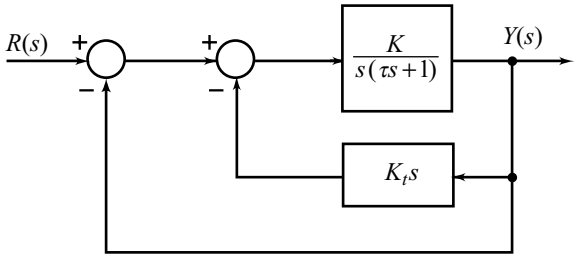

Fig. P9.6

9.7 The open-loop transfer function of a unity-feedback system is given by

$$G(s) = \frac{K}{s(\tau_1 s + 1)(\tau_2 s + 1)}$$

Derive an expression for gain K in terms of τ_1 and τ_2 and specified gain margin G_m.

9.8 Feedback system of Fig. P9.8 has open-loop transfer function

$$G(s)H(s) = \frac{199}{s(s + 1.71)(s + 100)}$$

(a) Using Bode plots, determine the gain crossover frequency and phase margin.

(b) Using second-order correlations between time-domain and frequency-domain measures, estimate the peak overshoot and settling time of the transient response to step input.

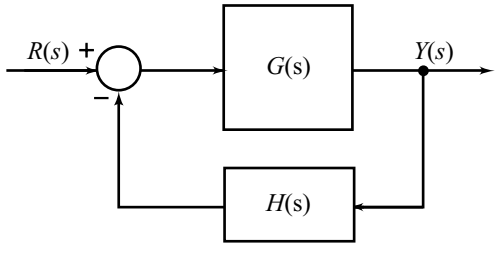

Fig. P9.8

MATLAB Exercise Use MATLAB to obtain gain crossover frequency, phase margin, peak overshoot and settling time.

9.9 The Bode magnitude plot of a system (known to have minimum-phase characteristics) is shown in Fig. P9.9. Deduce approximate Bode phase plot of the system.

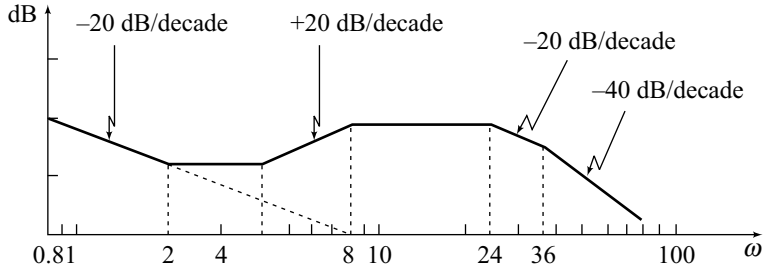

Fig. P9.9

Determine phase margin and gain margin of the system when operating in the closed-loop mode with unity feedback. From the frequency-domain performance measures, estimate the peak overshoot in transient response of the feedback system to step input.

9.10 Suppose that for the system of Fig. P9.8,

$$G(s)H(s) = \frac{4}{s(s+1)(s+2)}$$

(a) Using Bode plots of $G(j\omega)H(j\omega)$, determine the phase margin of the system.
(b) How should the gain be adjusted so that phase margin is 50°?
(c) Using second-order correlation between phase margin and damping ratio, estimate the peak overshoot in transient response of the system to step input.

MATLAB Exercise Attempt this problem using MATLAB dialogues. For the value of gain that gives 50° phase margin, determine peak overshoot in the MATLAB window.

9.11 Figure P9.11 shows block diagram of a control system. Determine the gain K such that the phase margin is 50°. What is the gain margin in this case?

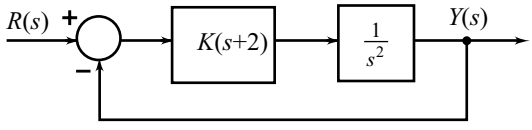

Fig. P9.11

MATLAB Exercise Attempt this problem using MATLAB dialogues.

9.12 A unity-feedback system has the following open-loop frequency response.

ω (rad/sec)	2	3	4	5	6	8	10
$\lvert G(j\omega)\rvert$	7.5	4.8	3.15	2.25	1.70	1.00	0.64
$\angle G(j\omega)$	– 118°	– 130°	– 140°	–150°	–157°	– 170°	– 180°

(a) Using Bode plots, evaluate the gain margin and phase margin of the system.
(b) Determine the change in gain required so that the gain margin of the system is 20 dB.
(c) Determine the change in gain required so that the phase margin of the system is 60°.

9.13 For the position control system shown in Fig. P9.13, find the value of the preamplifier gain K to yield a 9.48% overshoot in the transient response for a step input. For the gain-compensated system, determine t_p: the time to peak overshoot. Use only frequency-domain techniques based on Bode plots.

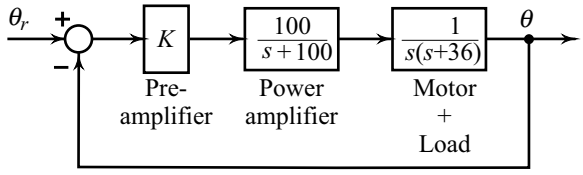

Fig. P9.13

9.14 The open-loop transfer function of a unity-feedback system is given by

$$G(s) = \frac{5}{s(s+1)(s^2+2s+5)}$$

(a) Using Bode plots, evaluate the gain margin, the phase margin, and the gain crossover frequency.
(b) How should the gain be adjusted in the system so that the gain margin becomes 10 dB?
(c) How should the gain be adjusted so that the gain crossover frequency becomes 1.27 rad/sec?
(d) How should the gain be adjusted so that the phase margin becomes 45°?

MATLAB Exercise Attempt this problem using MATLAB dialogues.

9.15 The open-loop transfer function of a unity-feedback system is

$$G(s) = \frac{K}{s(s+2)(s+10)}$$

Determine the value of K so that the system is stable with (i) a phase margin ≥ 45°, and (ii) gain crossover frequency as large as possible.

MATLAB Exercise Attempt this problem using MATLAB dialogues.

9.16 (a) The open-loop system with transfer function

$$G(s) = \frac{5e^{-s}}{s(s+1)(s+10)}$$

is used in unity-feedback configuration. Estimate the peak overshoot in transient response to step input. Use frequency-domain techniques based on Bode plots.
(b) Repeat part (a) for the system without dead-time.

9.17 The open-loop system with transfer function

$$G(s) = \frac{31.5e^{-s\tau_D}}{(s+1)(30s+1)\left[(s^2/9)+(s/3)+1\right]}$$

is used in unity-feedback configuration.
(a) Find phase margin when $\tau_D = 0$.
(b) Find phase margin when $\tau_D = 1$. Adjust the gain to obtain phase margin of 30°.
(c) Compare steady-state errors of the two cases with the same phase margin.

9.18 A unity-feedback system has open-loop transfer function

$$G(s) = \frac{50}{s(s+3)(s+6)}$$

(a) Using constant-M circles and polar plot of $G(j\omega)$, determine resonance peak M_r and bandwidth ω_b of the closed-loop frequency response.
(b) Using second-order correlations between time-domain and frequency-domain measures, estimate the peak overshoot and settling time of the transient response to step input.

9.19 A unity-feedback control system has the following open-loop frequency response.

ω (rad/sec)	2	3	4	5	6
$\lvert G(j\omega)\rvert$	2.7	1.7	0.97	0.63	0.4
$\angle G(j\omega)$	– 115°	– 126°	– 138°	– 150°	– 163°

(a) Plot the open-loop frequency response in polar coordinates.
(b) Find the resonance peak M_r and the resonance frequency ω_r of the closed-loop frequency response.
(c) From the frequency-domain performance measures, estimate the peak overshoot and settling time of the transient response of the feedback system to step input.

9.20 The open-loop transfer function of a unity-feedback system is

$$G(s) = \frac{11.7}{s(1+0.05s)(1+0.1s)}$$

(a) Draw Bode plot of $G(j\omega)$, and therefrom determine gain crossover frequency, phase crossover frequency, gain margin and phase margin.
(b) Transfer the Bode data to a Nichols chart and determine the resonance peak, resonance frequency and bandwidth.

MATLAB Exercise Attempt this problem using MATLAB dialogues.

9.21 The open-loop frequency response of a unity-feedback system is given below.

ω (rad/sec)	1	2	3	4	5
$\lvert G(j\omega)\rvert$(dB)	12.6	3.92	– 2.22	– 7	– 11
$\angle G(j\omega)$(degree)	– 127°	– 152°	– 168°	– 179°	– 188°

Transfer the frequency-response data to a Nichols chart and therefrom determine the gain margin, phase margin, resonance peak, resonance frequency and bandwidth.

9.22 A unity-feedback system has open-loop transfer function

$$G(s) = \frac{4}{s(s+1)(s+2)}$$

(a) Using Bode plots of $G(j\omega)$, determine the phase margin of the system.
(b) How should the gain be adjusted so that phase margin is 50°?
(c) Determine the bandwidth of the gain-compensated system.

The –3dB contour of the Nichols chart may be constructed using the following table.

Phase, degrees	0	– 30	– 60	– 90	– 120	– 150	– 180	– 210
Magnitude, dB	7.66	6.8	4.18	0	– 4.18	– 6.8	– 7.66	– 6.8

(d) Using second-order correlations between frequency-domain measures (phase margin, bandwidth) and time-domain measures (damping ratio, undamped natural frequency), estimate the peak overshoot and settling time of the transient response of gain-compensated system to step input.

9.23 A unity-feedback system has open-loop transfer function

$$G(s) = \frac{54}{(1+0.1s)(s^2+8s+25)}$$

(a) Using Nichols chart, determine M_r and ω_r.
(b) What value of ζ and ω_n should be used to approximate the transient behaviour of the system.

MATLAB Exercise Determine M_r and ω_r from the Nichols chart in the MATLAB window. Use second-order correlations to determine ζ and ω_n (peak overshoot and settling time). Compare these values of peak overshoot and settling time with the ones obtained from the step response of the given system generated using MATLAB.

9.24 For the system shown in Fig. P9.24, the transfer function $G(s)$ is

$$G(s) = \frac{100}{(1+0.1s)(s^2+8s+25)}$$

(a) Using Nichols chart, determine the factor K by which the gain of the system should be changed so that the resulting system will have an M_r of 1.4.
(b) Find the bandwidth of the gain-compensated system.

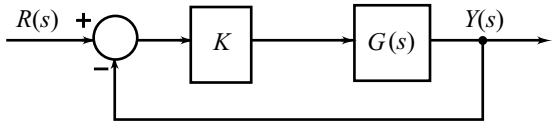

Fig. P9.24

MATLAB Exercise Attempt this problem using MATLAB dialogues.

9.25 The open-loop transfer function of a unity-feedback system is

$$G(s) = \frac{Ke^{-0.1s}}{s(1+0.1s)(1+s)}$$

By use of Bode plots and/or Nichols chart, determine the following.
(a) The value of K so that the gain margin of the system is 20 dB.
(b) The value of K so that the phase margin of the system is 60°.
(c) The value of K so that the resonance peak M_r of the system is 1 dB. What are the corresponding values of ω_r and ω_b?
(d) The value of K so that the bandwidth ω_b of the system is 1.5 rad/sec.

MATLAB Exercise Attempt this problem using MATLAB dialogues.

9.26 The following experimental results were obtained from an open-loop frequency response test of a unity-feedback control system.

ω	4	5	6	8	10
Gain	0.66	0.48	0.36	0.23	0.15
Phase angle	– 134°	– 143°	– 152°	– 167°	– 180°

Plot the locus of the loop transfer function in Nichols coordinates (dB versus angle) and measure the gain and phase margins.

By what factor should the gain be increased so that the resonance peak in closed-loop frequency response is 1.4, and what would then be the gain and phase margins?

9.27 The open-loop frequency response of a unity-feedback system is given below.

ω (rad/sec)	0.8	1.0	1.2	1.4	1.6
Re[$KG(j\omega)$]	– 3.5	– 2.9	– 2.3	– 2.0	– 1.2
Im[$KG(j\omega)$]	– 4.4	– 3.2	– 1.9	– 1.2	– 0.5

Determine the change in gain K required to make the resonance peak $M_r = 1.4$. For this value of gain, determine the phase margin of the system. Using second-order correlation between resonance peak and damping ratio, determine the value of ζ that approximates the transient behaviour of the gain-compensated system. Repeat the calculation for ζ using second-order correlation between phase margin and damping ratio, and comment on the result.

Compensator Design Using Bode Plots

10

10.1 INTRODUCTION

The design of feedback control systems in industry is probably accomplished using frequency-domain methods more often than other methods. The primary reason for the popularity of frequency-domain design is that the effects of disturbances, sensor noise and plant uncertainties are relatively easy to visualize and access in the frequency domain. Disturbance rejection can be specified in terms of low-frequency gain, and sensor-noise rejection can be specified in terms of high-frequency attenuation. The intermediate frequencies typically control the stability margins.

The robust control design methods developed over the last two decades seek to quantify uncertainties in the modelling of physical systems to ensure that the compensated system is always stable. It goes without saying that this has obviously always been the goal of control system designers. The recent advances are more mathematically rigorous than the work done during the 1940s and 1950s by Bode, Nichols, and others. From one point of view, the recent work on robust control serves to illustrate and corroborate the frequency-domain design techniques that have been developed over the last half century. There are strong connections between the classical design techniques presented in this chapter, and the modern robust control theory (refer Section 9.2). In fact building of uncertainty model itself is subject to uncertainties; the industry, by and large, continue to rely on gain margin and phase margin specifications for robustness.

Through the design examples developed in this chapter, we will see that Bode plot design is essentially a pole cancellation technique. In many cases, the resulting overall system closely approximates a standard second-order transfer function. The fact that Bode plot design approach can in many cases yield a closed-loop system that approximates standard second-order transfer function, accounts in large part for its power.

Our design strategy in this chapter is similar to the one we have used earlier in root locus design. Our real interest is how the closed-loop system behaves in the time domain but we predict this behaviour by examining the open-loop frequency response. We have seen in Chapter 8 that open-loop frequency response data on Bode plots, when examined in the light of Nyquist criterion, yield stability margins (gain margin and phase margin) of the closed-loop system. In Chapter 9, we have seen that open-loop frequency response data on Nichols chart, when examined in the light of *M*-contours, yield frequency-response (resonance peak,

resonance frequency, bandwidth) of the closed-loop systems. We have also examined the correlations between the frequency response measures—gain margin, phase margin, resonance peak, resonance frequency, bandwidth—with the time response measures—peak overshoot, settling time, etc.,through standard second-order system.

The design procedure calls for shaping the Bode plot/Nichols chart using a compensator, to match it to the specified closed-loop frequency response. The frequency-domain design thus involves "loop shaping" techniques. These techniques make it possible to build control systems with bandwidths sufficient to meet performance requirements, but no wider (Recall the dangers of building control systems with wide bandwidths using root-locus design).

From the 1940s to 1960, the Nichols chart was in wide use for loop shaping. Some very good designers of that era preferred it to the Bode plot as a design tool.

Some designers prefer to use the Bode magnitude and phase plots. The advantage here is that the frequency information is more readily available. Our preference is for Bode plots as design tools. We will use Nichols chart only for evaluation of the closed-loop frequency response from open-loop data.

The objective of the frequency-response design is to reshape, by means of a compensator, the frequency-response plot of the basic system and achieve the performance specifications in terms of M_r, ω_r, ω_b, gain margin, phase margin, etc. We can obtain the transient-response parameters from the frequency-response parameters using the correlations developed in the previous chapter. These correlations are, however, approximate and give only qualitative information about the transient response.

The root-locus design provides very good indicators of the transient response of a system. However, we do need a relatively accurate model of the system to obtain these benefits from the root locus plots. In fact, various design techniques supplement each other, rather than one method excluding others; the control engineer must therefore be familiar with all the design methods.

This chapter is concerned with the changes that can be made in the frequency-response characteristics of a given system by various types of compensators. Design procedures to obtain improvement in the system performance are described.

10.2 RESHAPING THE BODE PLOT

The performance of a closed-loop system may be described in terms of the following frequency-domain specifications:

1. Phase margin ΦM/resonance peak M_r—indicative of relative stability.
2. Gain crossover frequency ω_g/bandwidth ω_b/resonance frequency ω_r—indicative of speed of response.
3. Error constants $K_p/K_v/K_a$—indicative of steady-state error to step/ramp/parabolic input.

In case the transient-response specifications are given in time domain, we must first translate these into frequency domain to carry out frequency-domain compensation. This translation is carried out by using the explicit correlations between the two domains for the standard second-order system. These correlations are valid approximations for higher-order systems dominated by a pair of complex conjugate poles. The correlations, developed earlier in chapter 9, are reproduced below for convenience of use.

$$\Phi M = \tan^{-1} \frac{2\zeta}{\sqrt{\sqrt{4\zeta^4 + 1} - 2\zeta^2}} \cong 100\zeta \tag{10.1}$$

$$\omega_g = \omega_n \sqrt{\sqrt{4\zeta^4 + 1} - 2\zeta^2} \tag{10.2}$$

$$M_r = \frac{1}{2\zeta\sqrt{1-\zeta^2}} \tag{10.3}$$

$$\omega_r = \omega_n\sqrt{1-2\zeta^2} \tag{10.4}$$

$$\omega_b = \omega_n\sqrt{\left[(1-2\zeta^2)+\sqrt{4\zeta^4-4\zeta^2+2}\right]} \tag{10.5}$$

After completing the compensation design in the frequency domain, one must recheck the time response specifications by simulating (Appendix A) the compensated system. Based on the results of this check, it may sometimes be necessary to repeat the complete design process.

The design procedure usually starts with the gain adjustments to meet the performance specifications. If the desired specifications are not met by gain adjustments alone, compensating devices must be used. These devices alter the shape of the frequency-domain plot to meet the performance specifications.

The compensating device may be inserted into the system either in cascade with the forward portion of the loop as shown in Fig. 10.1 or as part of minor feedback loop as shown in Fig. 10.2. We have seen in Chapter 7 that cascade compensation is usually concerned with the addition of PD/lead, PI/lag, or PID/lag-lead device. The minor-loop feedback compensation is primarily concerned with the addition of rate feedback.

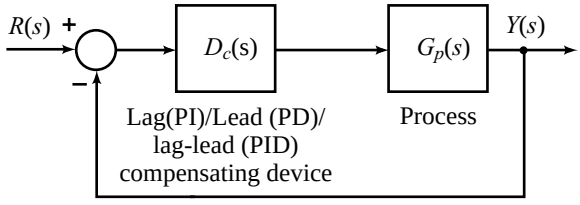

Fig. 10.1 Illustration of cascade compensation

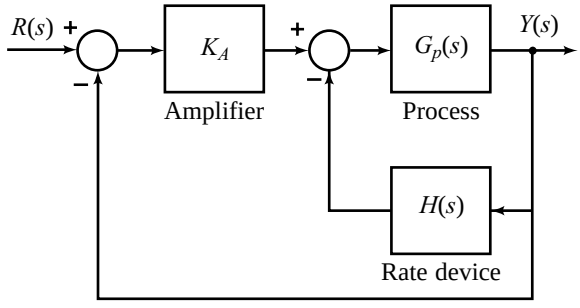

Fig. 10.2 Illustration of minor-loop feedback compensation

The decision to use a minor-loop feedback scheme (refer Section 7.10) is sometimes a matter of convenience, sometimes a matter of necessity, and for some problems it can be shown that minor-loop feedback scheme will do a better job. For example, the use of velocity feedback for damping is very effective and consequently quite popular. Servomotors with in-built tachogenerators are shelf items; so the use of velocity feedback can be very convenient. When designing compensation for process controls, it becomes necessary to take derivative action on controlled variable and not on error variable in order to avoid the derivative kick (violent response to sudden command changes (such as steps) because of differentiating action) on set-point changes. Finally, in systems subjected to frequent load disturbances, feedback compensation may be preferred as it provides greater stiffness against load disturbances. Besides all these factors, the available components, and designer's experience and preferences influence the choice between a cascade and a feedback compensation scheme.

A basic point of view that is helpful in developing techniques for analysis and design is to realize that either method, cascade or feedback compensation, ultimately replaces the forward-path transfer function $G_p(s)$ with a new transfer function $G_f(s)$. The design process then can be thought of as converting a $G_p(s)$ that is not suitable, to $G_f(s)$ that is more satisfactory for the proposed system.

In the following, we develop through selected design problems, the guidelines for cascade compensation design to satisfy the given frequency-domain specifications. Based on these guidelines, the parameter values of minor-loop compensation scheme can easily be determined by trial-and-error using a CAD facility [151–154].

10.2.1 Design Problem 1

Consider the system of Fig. 10.1 with the plant transfer function

$$G_p(s) = \frac{1}{s(s+2)}$$

We will assume that the phase margin ΦM and the velocity error constant K_v are our major design specifications. Impose the requirements of (i) $K_v \geq 10$, and (ii) $\Phi M \geq 60°$.

First we examine whether or not adjustment of gain alone (i.e., $D_c(s) = K$) can achieve the design.

$$K_v = \lim_{s \to 0} s\,KG_p(s) = \frac{K}{2}$$

In order to meet the K_v specification, we require that $K \geq 20$. We choose $K = 20$ and sketch the Bode plot of

$$G(s) = KG_p(s) = \frac{20}{s(s+2)} = \frac{10}{s(0.5s+1)}$$

in Fig. 10.3. We plot only the asymptotes. We see that the gain crossover frequency roughly equals 4.4 rad/sec, and the phase margin roughly equals 24°. This phase margin does not meet the specification. If K is the only parameter that can be adjusted to achieve the design, the only way to increase the phase margin is to decrease K. Decreasing K to 2.5 results in gain crossover frequency of 1.2 rad/sec and phase margin of 59° (refer Fig. 10.3). This, however, will violate the K_v specification. Thus for this problem, both the steady-state and transient performance requirements cannot be met by adjusting K alone.

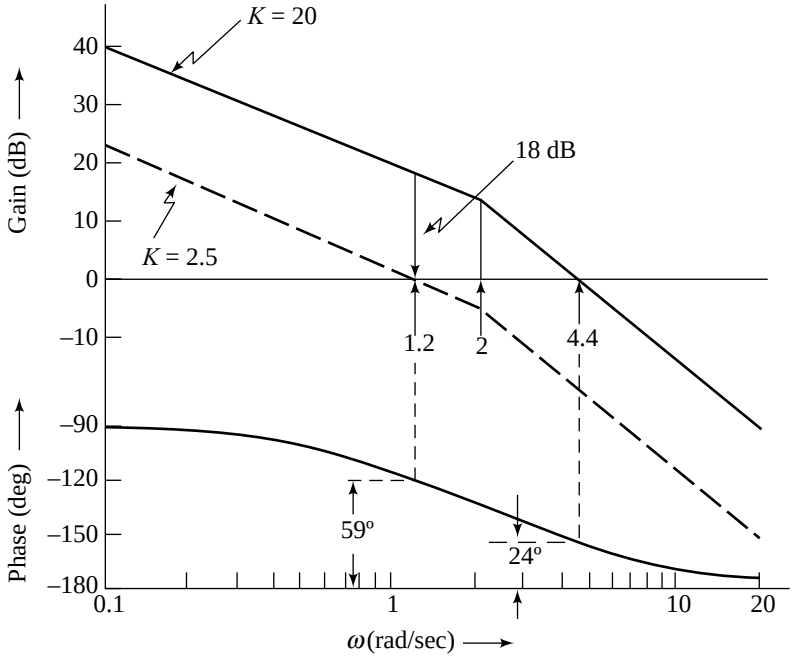

Fig. 10.3 Reshaping of the Bode plot by gain adjustment

The steady-state performance of the system is governed by low-frequency characteristics of the transfer function, and the transient performance of the system is governed by high-frequency characteristics. To simultaneously satisfy the transient and the steady-state performance requirements, the Bode plot of $G(j\omega)$ must be reshaped so that the high-frequency portion of the plot satisfies the phase margin requirement and the low-frequency portion satisfies the K_v requirement. When we inspect the Bode plot of Fig. 10.3 for $K = 20$, we see that we can meet the design objectives by adding more phase to the system in the positive direction in the high-frequency range around gain crossover frequency 4.4 rad/sec, while keeping the low-frequency region relatively unaltered. This reshaping of the Bode plot can be achieved using a cascade compensator $D_c(s)$ having frequency-response characteristics shown in Fig. 10.4. Figure 10.5 serves to illustrate the principle of this compensation. This figure shows Bode plots of gain-compensated system $G(j\omega) = 10/j\omega(j0.5\omega + 1)$ and $D_c(j\omega)G_p(j\omega)$ where $D_c(j\omega)$ is given by Fig. 10.4. The gain-compensated system has a phase margin of 24° and gain crossover frequency of 4.4 rad/sec. Using compensator $D_c(j\omega)$, the phase angle plot is raised for higher frequencies. Since the positive phase in the compensator is accompanied by an additional gain at high frequencies, the gain crossover frequency increases when this compensation is employed. From Fig. 10.5 we see that the compensated system has gain crossover frequency of 6.8 rad/sec, phase margin of 62° and $K_v = 10$.

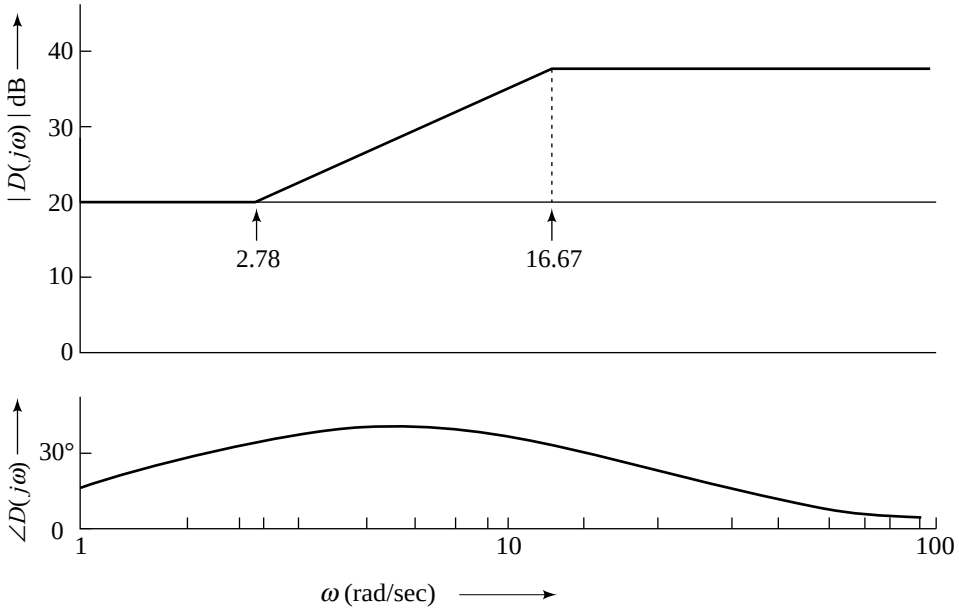

Fig. 10.4 Bode plot of a lead compensator

The transfer function of the compensator having frequency-response characteristics shown in Fig. 10.4, is of the form

$$D_c(s) = K\left(\frac{\tau s + 1}{\alpha\tau s + 1}\right);\ \alpha < 1,\ \tau > 0 \tag{10.6}$$

Note that $\alpha < 1$ ensures that the compensator adds positive phase to the system over some appropriate frequency range. Because of this property, the first-order compensator given by Eqn. (10.6) is called a *lead compensator* (also refer Eqns (7.45)).

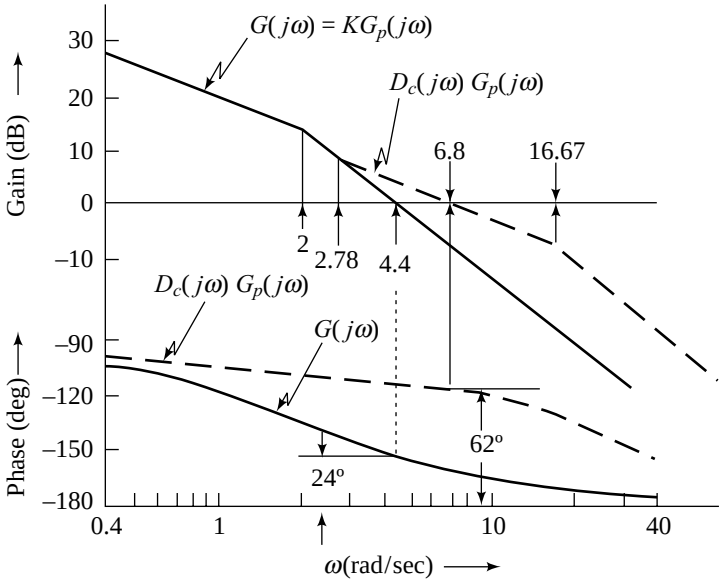

Fig. 10.5 Reshaping of the Bode plot by lead compensation

It is seen that $D_c(s)$ given by Eqn. (10.6) is a form of proportional plus derivative controller wherein the derivative action is bandwidth limited (refer Fig. 7.30):

$$D_c(s) = K\alpha + \frac{K\alpha\tau(1-\alpha)s}{\alpha\tau s + 1} = K_p + \frac{K_D s}{\tau_D s + 1} \tag{10.7a}$$

The design of compensator (controller) is basically a search problem in n-dimensional space where n is the number of design parameters of the compensator. The design of a lead compensator is a problem with three trial parameters; K, α, and τ. A lead compensator may meet the filtering requirement in addition to satisfying the specifications on transient response.

For feedback loops free from high-frequency noise problem, a PD compensator

$$D_c(s) = K_P + sK_D \tag{10.7b}$$

with only two trial parameters: K_P and K_D, is more appropriate choice. With the reduction in trial parameters, the design problem becomes simpler. However, real-life applications do have high-frequency noise problem. We have two choices for design; design a PD compensator, and a filter independently; or design a lead compensator as a total solution.

The guidelines developed for lead compensator are equally helpful for PD compensation, as we will see in Section 10.6.

10.2.2 Design Problem 2

Reconsider the design problem 1. We attempt an alternative solution.

In Fig. 10.3, we have seen that $K = 2.5$ meets the phase margin requirement. Apparently, we cannot set K to 2.5, since the velocity error constant would only be 1.25, and the steady-state performance requirement would not be satisfied. When we inspect the Bode plot of Fig. 10.3 for $K = 2.5$, we see that we can meet both the phase margin and the K_v requirements by reshaping the low-frequency portion of the plot to obtain $K_v = 10$, while keeping the plot near gain crossover frequency relatively unaltered. This reshaping requires increasing the gain in the low-frequency region. This is equivalent to increasing the gain for the entire frequency range

and then attenuating the magnitude curve in the high-frequency region. We can therefore meet the design objectives for the problem under consideration by starting with the plot of $G(j\omega)$ for $K = 20$, reducing the magnitude of $G(j\omega)$ in the high-frequency region in order to shift the gain crossover frequency to a lower value to meet the phase margin requirement, while keeping the low-frequency region of $G(j\omega)$ relatively unaltered. This reshaping of the Bode plot can be achieved using a compensator $D_c(s)$ having frequency-response characteristics shown in Fig. 10.6. Figure 10.7 serves to illustrate the principle of this compensation. This figure shows Bode plots of gain-compensated system $G(j\omega) = 10/j\omega\,(j0.5\omega + 1)$ and $D_c(j\omega)G_p(j\omega)$ where $D_c(j\omega)$ is given by Fig. 10.6. The gain-compensated system has a phase margin of 24° and gain crossover frequency of 4.4 rad/sec. Using compensator $D_c(j\omega)$, the gain crossover frequency reduces to 0.95 rad/sec, and the requirements on both the ΦM and the K_v are met.

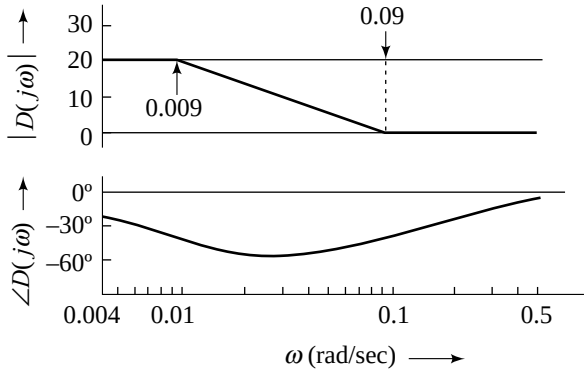

Fig. 10.6 Bode plot of a lag compensator

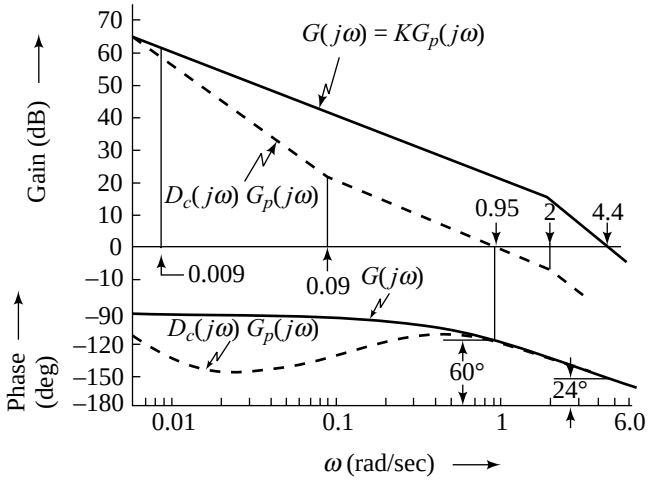

Fig. 10.7 Reshaping of the Bode plot by lag compensation

It should be noted that the attenuation characteristic of the compensator is accompanied by phase lag that tends to offset the increase in phase margin achieved due to reduction in gain crossover frequency. The loss in phase margin due to the phase lag characteristic of the compensator can be minimized by placing the frequency band over which the compensator has large phase lag much below the new gain crossover

frequency. From Fig. 10.6 we see that the upper corner frequency of the lag compensator is 0.09 rad/sec, which is nearly one decade below the new gain crossover frequency 0.95 rad/sec.

In general, it may not be possible to satisfy all the design specifications by simply using a lead or a lag compensator. Situations often arise when both the low-frequency and the high-frequency portions of the Bode plot of the controlled process need to be reshaped by using a *lag-lead compensator*, which is basically a lag compensator and a lead compensator in cascade.

It should be pointed out that the design of linear control systems is not an exact science. A number of compensation schemes and parameter values may satisfy the given set of performance specifications. Some degree of trial-and-error and fine tuning is inevitable. Therefore, a CAD facility for frequency-domain analysis should be invaluable [151–154].

The transfer function of the compensator having frequency-response characteristics shown in Fig. 10.6, is of the form

$$D_c(s) = K\left(\frac{\tau s + 1}{\beta\tau s + 1}\right);\ \beta > 1,\ \tau > 0 \tag{10.8}$$

The compensator gets its name *lag-compensator* for a reason similar to the lead compensator; it introduces phase lag (also refer Eqns (7.48)).

It is seen that $D_c(s)$ given by Eqn. (10.8) is a form of proportional plus integral controller wherein the integral action is low-frequency gain limited (refer Fig. 7.34):

$$D_c(s) = K + \frac{K(\beta - 1)}{\beta\tau s + 1} = K_P + \frac{K_I}{\tau_I s + 1} \tag{10.9a}$$

The design of a lag compensator is a problem with three trial parameters; K, β, and τ. For feedback loops wherein the primary requirement is to improve steady-state performance, a PI compensator

$$D_c(s) = K_P + \frac{K_I}{s} \tag{10.9b}$$

with only two trial parameters may be attempted. The limit on the low-frequency gain has now been relaxed. This compensator will, however, be useful if relaxing the limit does not degrade closed-loop stability appreciably.

The guidelines developed for lag compensator are equally helpful for PI compensation, as we will see in Section 10.6.

10.2.3 Concluding Comments

The purpose of reshaping of Bode plot generally falls in to one of these categories.

1. A given system is stable and its transient response is satisfactory, but its steady-state error is too large. Thus, the corresponding error constant must be increased while nearly preserving the transient response. This can be achieved by a cascade PI/lag compensator.
2. A given system is stable but its transient response is unsatisfactory. Thus the Bode plot must be reshaped to obtain acceptable phase margin, bandwidth, etc. This can be achieved by a cascade PD/lead compensator.
3. A PD/lead compensator system has satisfactory transient response but its steady-state error is too large. The steady-state error can be decreased by cascading a PI/lag compensator to the PD/lead compensated system.

Consider a cascade of lag and lead compensators:

$$D_c(s) = K\left(\frac{\tau_2 s + 1}{\beta\tau_2 s + 1}\right)\left(\frac{\tau_1 s + 1}{\alpha\tau_1 s + 1}\right);\ \beta > 1,\ \alpha < 1,\ \tau_2,\ \tau_1 > 0 \qquad (10.10)$$

This is a second-order *lag-lead compensator*. Expressed explicitly in the form of proportional, integral, and derivative actions, $D_c(s)$ looks like

$$D_c(s) = \left(K_{P1} + \frac{K_I}{\tau_I s + 1}\right)\left(K_{P2} + \frac{K_D s}{\tau_D s + 1}\right) \qquad (10.11a)$$

It is thus a cascade of gain-limited PI compensator with a bandwidth-limited PD compensator.

Consider now the cascade of PI and PD compensators:

$$D_c(s) = \left(K_1 + \frac{K_i}{s}\right)(K_2 + K_d s)$$

$$= K_1 K_2 + K_i K_d + \frac{K_1 K_i}{s} + K_2 K_d s$$

$$= K_P + \frac{K_I}{s} + K_D s \qquad (10.11b)$$

Thus cascading a PI compensator with a PD compensator is completely equivalent to a PID compensator.

In general, we can represent a dynamic compensator by the transfer function $D_c(s)$, given by

$$D_c(s) = \frac{K\prod_{i=1}^{m}(\tau_{zi} s + 1)}{\prod_{j=1}^{n}(\tau_{pj} s + 1)};\ m \le n,\ K > 0 \qquad (10.12a)$$

$$= KD(s) \qquad (10.12b)$$

The gain K is *zero-frequency gain* of the dynamic compensator $D_c(s)$, that has to be adjusted to improve steady-state accuracy.

For the purpose of simplifying the design procedure, we normally associate the adjustable gain parameter K with the plant transfer function and then design the compensator $D(s)$ given by Eqns (10.12) based on new plant transfer function $KG_p(s)$. At the implementation stage, the gain K is associated with the compensator and the transfer function $D_c(s)$ is realized. The configuration of Fig. 10.8a will accordingly be referred to as the *uncompensated system*, and that of Fig. 10.8b as *compensated system*.

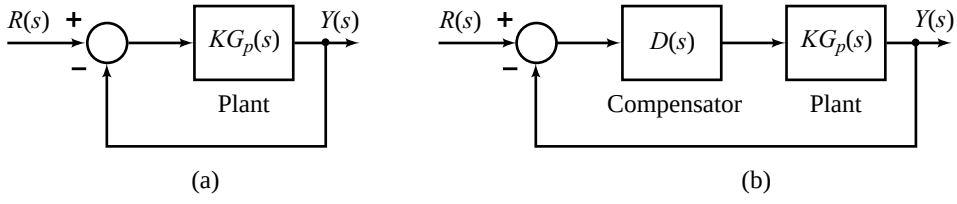

Fig. 10.8 (a) Uncompensated system, (b) Compensated system

10.3 CASCADE LEAD COMPENSATION

The primary function of a lead compensator is to reshape the frequency-domain plot by providing sufficient phase lead angle over some appropriate frequency range to offset the excessive phase lag associated with the plant.

10.3.1 Lead Compensator Frequency Response

Let us first look at the frequency-response characteristics of a lead compensator and derive some valuable relationships that will help us in the design process. The transfer function of a lead compensator with unity zero-frequency gain is of the form

$$D(s) = \frac{\tau s + 1}{\alpha\tau s + 1}\,;\ \alpha < 1,\ \tau > 0 \tag{10.13}$$

The sinusoidal transfer function is of the form

$$D(j\omega) = \frac{1 + j\omega\tau}{1 + j\omega\alpha\tau} \tag{10.14}$$

The Bode plot of $D(j\omega)$, shown in Fig. 10.9, has two corner frequencies at $\omega = 1/\tau$ and $\omega = 1/\alpha\tau$. The phase lead at any frequency ω is given by

$$\phi = \tan^{-1}\omega\tau - \tan^{-1}\omega\alpha\tau \tag{10.15}$$

Differentiating with respect to ω, we obtain

$$\frac{d\phi}{d\omega} = \frac{\tau}{1 + (\omega\tau)^2} - \frac{\alpha\tau}{1 + (\omega\alpha\tau)^2}$$

Setting $d\phi/d\omega$ equal to zero, we find that the frequency ω_m at which the maximum phase lead ϕ_m occurs, is

$$\omega_m = \frac{1}{\tau\sqrt{\alpha}} = \sqrt{\frac{1}{\tau}\left(\frac{1}{\alpha\tau}\right)} \tag{10.16}$$

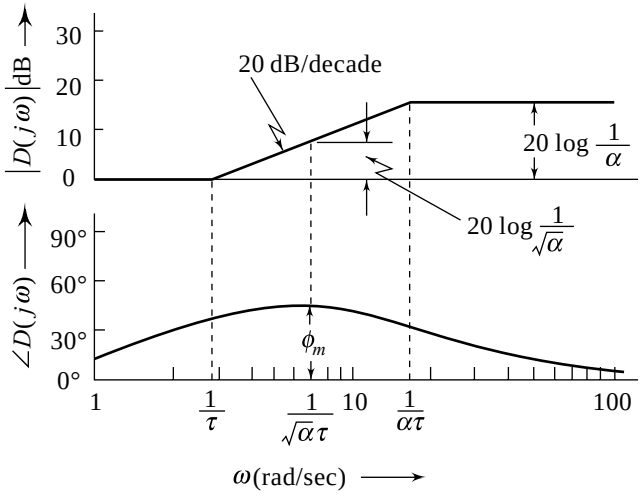

Fig. 10.9 Frequency response characteristics of lead compensators

As seen from Eqn. (10.16), ω_m is the geometric mean of the two corner frequencies of the compensator. At $\omega = \omega_m$, the maximum phase lead ϕ_m is given by (refer Eqn. (10.15))

$$\phi_m = \tan^{-1}\frac{1}{\sqrt{\alpha}} - \tan^{-1}\sqrt{\alpha}$$

Making use of the relation

$$\tan(\theta_1 - \theta_2) = \frac{\tan\theta_1 - \tan\theta_2}{1 + \tan\theta_1 \tan\theta_2},$$

we obtain

$$\tan\phi_m = \frac{1}{\sqrt{\alpha}} - \sqrt{\alpha} = \frac{1-\alpha}{\sqrt{\alpha}}$$

or

$$\sin\phi_m = \frac{1-\alpha}{1+\alpha} \tag{10.17}$$

This gives α in terms of ϕ_m as

$$\alpha = \frac{1-\sin\phi_m}{1+\sin\phi_m} \tag{10.18}$$

The magnitude of $D(j\omega)$ at $\omega = \omega_m$, the frequency of maximum phase lead, is

$$\left|D(j\omega_m)\right| = \frac{\left|1 + j\omega_m\tau\right|}{\left|1 + j\omega_m\alpha\tau\right|} = \frac{1}{\sqrt{\alpha}} \tag{10.19}$$

An important consideration governing the choice of α is the inherent noise in control systems. The noise is generally of high frequency nature relative to the frequencies of control signals that appear in the loop. We see from Fig. 10.9 that in a lead compensator, the high-frequency noise signals are amplified by a factor $(1/\alpha) > 1$, while the low-frequency control signals undergo unit amplification (0 dB gain). This means that the lead compensator boosts the noise signal level relative to the control signal, and the lower the value of α, the higher this boost. Thus, if noise is a problem in a particular system, one must be careful about choosing a value of α for a lead compensator. It is recommended that the value of α should not be less than 0.07. A common choice is $\alpha = 0.1$. Limiting the value of α amounts to limiting an increase in gain crossover frequency of the system due to addition of a lead compensator.

We are now ready to enumerate a design procedure for lead compensation.

10.3.2 Design Procedure

To illustrate the lead compensator design procedure, we reconsider the unity-feedback system of design problem 1, which was discussed earlier in Section 10.2. The design problem is to obtain the unity zero-frequency gain compensator

$$D(s) = \frac{\tau s + 1}{\alpha\tau s + 1};\ \alpha < 1,\ \tau > 0$$

for the plant with adjustable gain,

$$G(s) = \frac{K}{s(s+2)}$$

so that the closed-loop system has (i) $\Phi M \geq 60°$, and (ii) $K_v \geq 10$.

Since the lead compensator has negligible effect at low frequencies, we set the gain of the uncompensated system to a value that satisfies the steady-state error requirement. It is seen that $K = 20$ meets the K_v specification. The Bode plot of $G(j\omega)$ for $K = 20$ is shown in Fig. 10.10. From the plot we see that the uncompensated system has gain crossover frequency $\omega_g = 4.4$ rad/sec and phase margin = 24°. The required phase margin is 60°. If it were possible to simply add phase without affecting the magnitude, we would only need an additional 36° phase at the gain crossover frequency of $\omega_g = 4.4$. However, we know that insertion of lead compensator will maintain the same low-frequency gain but will affect the gain in high-frequency range; the gain crossover frequency will increase to a value $\omega_g' > \omega_g$. As the phase of most control processes decreases with increase in frequency, the phase of $G(j\omega)$ at ω_g' will be less than that at ω_g. Let this inevitable phase drop be equal to ε degrees. Therefore, to realize the specified phase margin, the lead compensator must provide a lead angle of $36° + \varepsilon$ at new gain crossover frequency ω_g'.

The value of ε depends upon ω_g', which in turn depends upon the parameters of the lead compensator. In the trial-and-error design procedure, we make a guess on the value of ε and design a lead compensator. If the characteristics of the feedback system are not acceptable after the design, then a redesign with a different value of ε may be necessary. The initial guess on ε depends upon the slope of the magnitude plot of the uncompensated system in the region of gain crossover frequency ω_g. For a slope of -40 dB/decade, as in the present example, $\varepsilon = 3°$ is a good guess. The guessed value may have to be as high as $15 - 20°$ for a slope of -60 dB/decade.

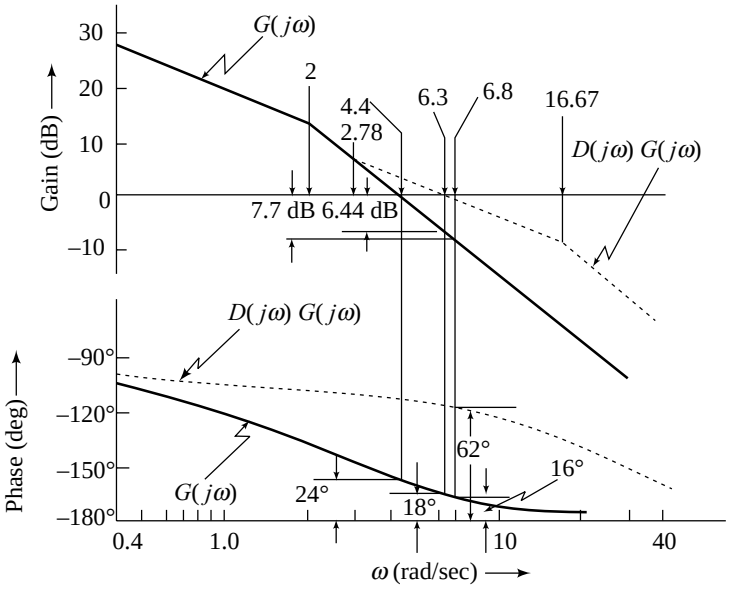

Fig. 10.10 Cascade lead compensation

In order to provide a phase lead angle of $36° + \varepsilon$ at ω_g' with the largest value of parameter α (this is desirable from signal/noise considerations), the frequency ω_m at which maximum phase lead occurs, must be made to coincide with ω_g'. Thus we get

$$\omega_m = \omega_g'; \; \phi_m = 36° + \varepsilon = 36° + 3° = 39°$$

The α-parameter of the compensator can then be computed from Eqn. (10.18).

$$\alpha = \frac{1 - \sin 39°}{1 + \sin 39°} = \frac{0.37}{1.63} = 0.227$$

Since at ω_m, the compensator provides a gain of $20 \log\left(1/\sqrt{\alpha}\right)$ dB (see Fig. 10.9), the new gain crossover frequency $\omega_g' = \omega_m$ can be determined as that frequency at which the uncompensated system has a gain of $-20 \log\left(1/\sqrt{\alpha}\right)$ dB. We draw a horizontal line at $-20 \log\left(1/\sqrt{\alpha}\right) = -6.44$ dB as shown in Fig. 10.10; its intersection with the magnitude plot yields the new gain crossover frequency as $\omega_g' = 6.3$. The corresponding phase margin of the uncompensated system is then read from the plot as 18°. The phase margin of uncompensated system at $\omega_g = 4.4$ was determined as 24°. Because 24° – 18° = 6°, which is larger than $\varepsilon = 3°$, the choice of $\varepsilon = 3°$ is not satisfactory. As a next try, we choose $\varepsilon = 7°$. Then we have $\phi_m = 36° + 7° = 43°$ and the corresponding α-parameter computed from Eqn. (10.18) is 0.17. Intersection of the horizontal line at $-20 \log\left(1/\sqrt{0{\cdot}17}\right)$ dB $= -7.7$ dB with the magnitude plot yields $\omega_g'' = 6.8$ rad/sec. The phase margin of the uncompensated system at ω_g'' is 16°. The phase drop due to increase in gain crossover frequency is 24° – 16° = 8° which nearly equals ε. Thus the choice of $\varepsilon = 7°$ is satisfactory and the corresponding $\alpha = 0.17$ can be used in the design.

Now we let $\omega_m = \omega_g''$. Using Eqn. (10.16),

$$\omega_m = \frac{1}{\sqrt{\alpha}\tau} = 6.8$$

which implies

$$\tau = \frac{1}{\sqrt{0.17} \times 6.8} = 0.36$$

Thus, the required lead compensator is

$$D(s) = \frac{\tau s + 1}{\alpha\tau s + 1} = \frac{0.36 s + 1}{0.06 s + 1}$$

The open-loop transfer function of the compensated system becomes

$$D(s)G(s) = \frac{10(0.36 s + 1)}{s(0.5 s + 1)(0.06 s + 1)}$$

The frequency-response characteristics of $D(s)G(s)$ in Fig. 10.10 can be seen to yield a phase margin of 62°. The compensated system, therefore, meets both the steady-state and the relative stability requirements.

The lead-compensation design procedure given above has been tailored to the set of two specifications: phase margin (measure of relative stability), and error constant (measure of steady-state performance). The resulting compensated system must be evaluated with respect to other performance requirements. It may become necessary to repeat the design procedure several times to meet all the specifications within acceptable bounds.

In many design problems, relative stability is adequately specified by the phase margin alone. However, if gain margin is also specified, we must check the gain margin from the Bode plot of $D(s)G(s)$ and repeat the design if the requirement is not satisfied. For the problem under consideration, specification on gain margin is not useful because the phase never crosses the $-180°$ line and the gain margin is always infinite.

Gain crossover frequency read from the Bode plot of $D(s)G(s)$ is an estimate of speed of response of the compensated system. We have seen that introduction of cascade lead compensator increases the gain crossover frequency and, consequently, the speed of response of the resulting system.

Bandwidth of the feedback system may be determined by transferring the data from Bode plot to Nichols chart. Since the gain crossover frequency is a rough measure of the bandwidth of a feedback system, we can say that the lead compensation increases the system bandwidth. It must of course be noted that too large an

increase in system bandwidth will include some of the noise frequencies; it is undesirable and must be guarded against in lead compensation design.

A summary of the lead compensation design procedure for designing compensator $D(s) = (\tau s + 1)/(\alpha\tau s + 1)$ for the plant $G(s)$ with adjustable gain K, is given below. This design procedure will apply to many cases; however, the designer should keep in mind that the specific procedure followed in any particular design may need to be tailored to its particular set of specifications.

1. Sketch the Bode plot of the uncompensated system with the gain K set according to the steady-state error requirement. Measure the gain crossover frequency ω_g, and phase margin of the uncompensated system.
2. Using the relation given below, determine the additional amount of phase lead needed at the new gain crossover frequency ω_g' to realize the specified phase margin.
   Additional phase lead required = specified phase margin – phase margin of the uncompensated system at $\omega_g + \varepsilon$.
   ε is a margin of safety required by the fact that the gain crossover frequency will increase due to compensation. A guess is made on the value of ε depending upon the slope of the magnitude plot in the region of gain crossover frequency. For a slope of –40 dB/decade, $\varepsilon = 5°$ is a good guess. The guessed value may have to be as high as 15–20° for a slope of – 60 dB/decade.
3. Set the maximum phase of the lead compensator,
   $$\phi_m = \text{additional phase lead required},$$
   and compute parameter α of the compensator using the following equation:
   $$\alpha = \frac{1 - \sin\phi_m}{1 + \sin\phi_m}$$
4. Locate the frequency at which the uncompensated system has a gain of $-20\log\left(1/\sqrt{\alpha}\right)$ dB. Select this frequency as the new gain crossover frequency ω_g'. Measure the phase margin of the uncompensated system at ω_g'. If the difference in phase margins of $G(j\omega)$ at ω_g and ω_g' is less than ε, go to the next step. Otherwise, choose a larger ε in step 2 and repeat steps 3 and 4.
5. Set $\omega_m = \omega_g'$ and compute parameter τ of the compensator using the following equation:
   $$\omega_m = \frac{1}{\sqrt{\alpha}\tau}$$
6. Sketch the frequency-response plots of compensated system in Bode and Nichols coordinate systems. Check any additional specifications on system performance, e.g., gain margin, bandwidth, etc. Redesign for another choice of ω_g', till all specifications are met. It may be noted that the additional specifications can only be met if they are consistent.

Example 10.1 Consider a type-1 unity-feedback system with an open-loop transfer function

$$G(s) = \frac{K}{s(s+1)}$$

It is desired to have the velocity error constant $K_v = 10$. Furthermore we desire that the phase margin of the system be atleast 45°.

The first step in the design procedure is to sketch the Bode plot of the uncompensated system with the gain K set according to the steady-state error requirement. $K = 10$ meets the K_v specification. The Bode plot of

$$G(j\omega) = \frac{10}{j\omega(j\omega + 1)}$$

is drawn in Fig. 10.11. The gain crossover frequency of the uncompensated system is $\omega_g = 3.16$ rad/sec, and the phase margin is 18 °.

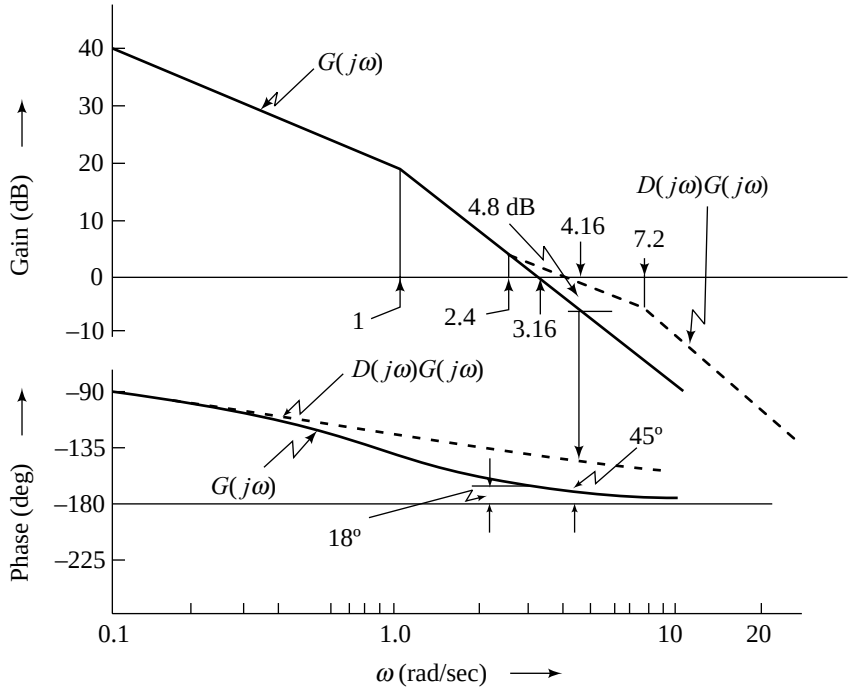

Fig. 10.11 Bode plot for Example 10.1

If cascade lead compensation scheme is employed to increase the phase margin to the specified value, the additional phase lead required at the new gain crossover frequency ω_g' is given by the following relation.

Additional phase lead required

= specified phase margin – phase margin of the uncompensated system at $\omega_g + \varepsilon$

= 45° – 18° + 3° = 30°

Setting the maximum phase ϕ_m of the lead compensator equal to the additional required phase lead of 30°, we obtain the α parameter of the lead compensator:

$$\alpha = \frac{1 - \sin\phi_m}{1 + \sin\phi_m} = \frac{1 - \sin 30°}{1 + \sin 30°} = 0.333$$

The uncompensated system has a gain of $-20 \log \left(1/\sqrt{\alpha}\right) = -4.8$ dB at $\omega_g' = 4.16$ rad/sec. Setting ω_m, the frequency at which the lead compensator has maximum phase ϕ_m, equal to ω_g', we obtain the τ parameter of the lead compensator:

$$\omega_m = \frac{1}{\sqrt{\alpha}\tau} = \omega_g' = 4.16$$

This gives $\tau = 0.416$

Therefore the lead compensator is

$$D(s) = \frac{\tau s + 1}{\alpha\tau s + 1} = \frac{0.416 s + 1}{0.139 s + 1}$$

and the compensated open-loop transfer function becomes

$$D(s)G(s) = \frac{10(0.416 s + 1)}{s(s + 1)(0.139 s + 1)}$$

The frequency-response plots of uncompensated and compensated systems in Bode and Nichols coordinate systems are shown in Figs 10.11 and 10.12, respectively. From these plots we observe the following:

1. Phase margin is increased from 18° to 45°.
2. Resonance peak is reduced from 10 dB to 3 dB.
3. Bandwidth is increased from 5 rad/sec to 7 rad/sec.

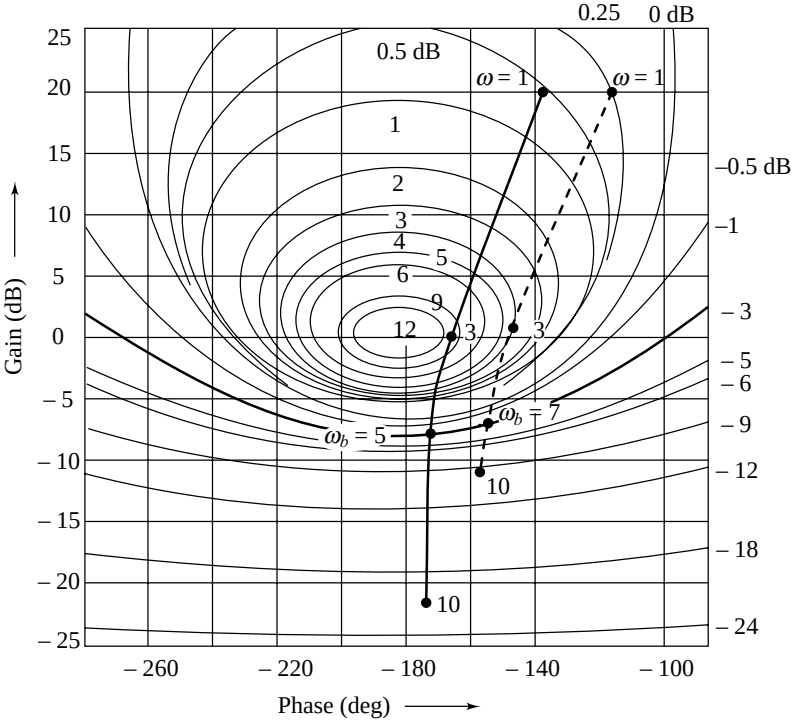

Fig. 10.12 Nichols chart for Example 10.1

Thus, in general, the effect of the lead compensation is to increase the margin of stability and speed of response (the design has been done here with the straightline asymptotic plots rather than the exact curves for the magnitude).

To reinforce these observations, we include the root locus and step response of the design just completed. To draw the root locus, we rearrange $D(s)G(s)$ in the form convenient for root-locus sketching:

$$D(s)G(s) = \frac{10(0.416s + 1)}{s(s + 1)(0.139s + 1)} = \frac{29.928(s + 2.404)}{s(s + 1)(s + 7.194)}$$

The root locus for this design is shown in Fig. 10.13a, with the root locations marked for root-locus gain 29.928. Note that the complex poles at $-2.55 \pm j3.85$, and the real-axis pole is at -3.1; it is close to the zero at $s = -2.404$. Reshaping of Bode plot has resulted in near-cancellation compensation.

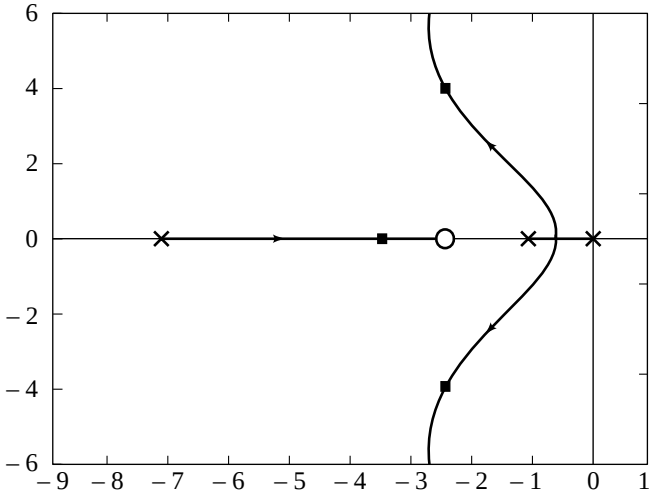

Fig. 10.13(a) Root locus for Example 10.1

For a phase margin of 40°, the value of ζ is 0.4 and the corresponding peak overshoot based on second-order approximation is 25.38 %.

The unit step response of the compensated closed-loop system shown in Fig. 10.13b, has an overshoot of 28.8%. This correlates reasonably well with the percent overshoot predicted by the formula $\zeta = 0.01 \times \Phi M$.

From the response curves of uncompensated and compensated systems shown in Fig. 10.13b, we observe that the speed of response of the compensated system (t_s = 1.8 sec) has increased due to the higher gain crossover incurred when we included the lead compensator. Peak overshoot has been reduced due to increase in phase margin.

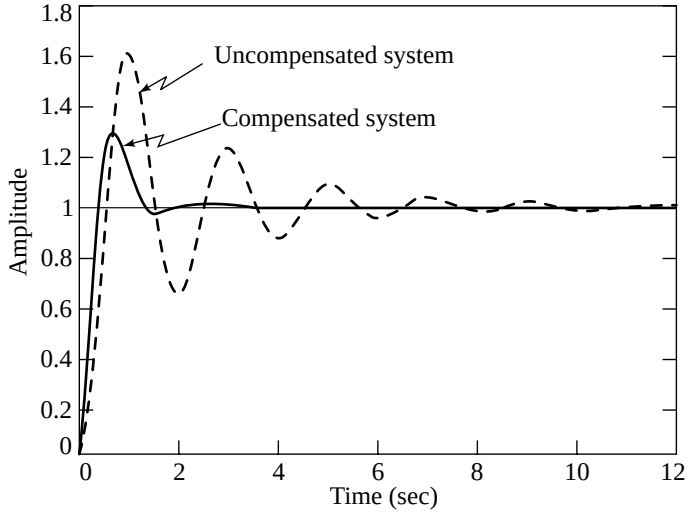

Fig. 10.13(b) Step responses for Example 10.1

Example 10.2 Consider now a unity-feedback control system with open-loop transfer function

$$G(s) = \frac{K}{s^2(0.2\,s + 1)}$$

Assume that the system is required to be compensated to meet the following specifications:

1. Acceleration error constant $K_a = 10$.
2. Phase margin $\geq 35°$.

From the steady-state requirement, we set $K = 10$. The Bode plot of $G(j\omega)$ when $K = 10$ is shown in Fig. 10.14. As observed from this plot, the gain crossover frequency $\omega_g = 3.16$ rad/sec, and the phase margin is $-32°$, which means that the uncompensated system is unstable. In fact, the uncompensated system is unstable for all values of K.

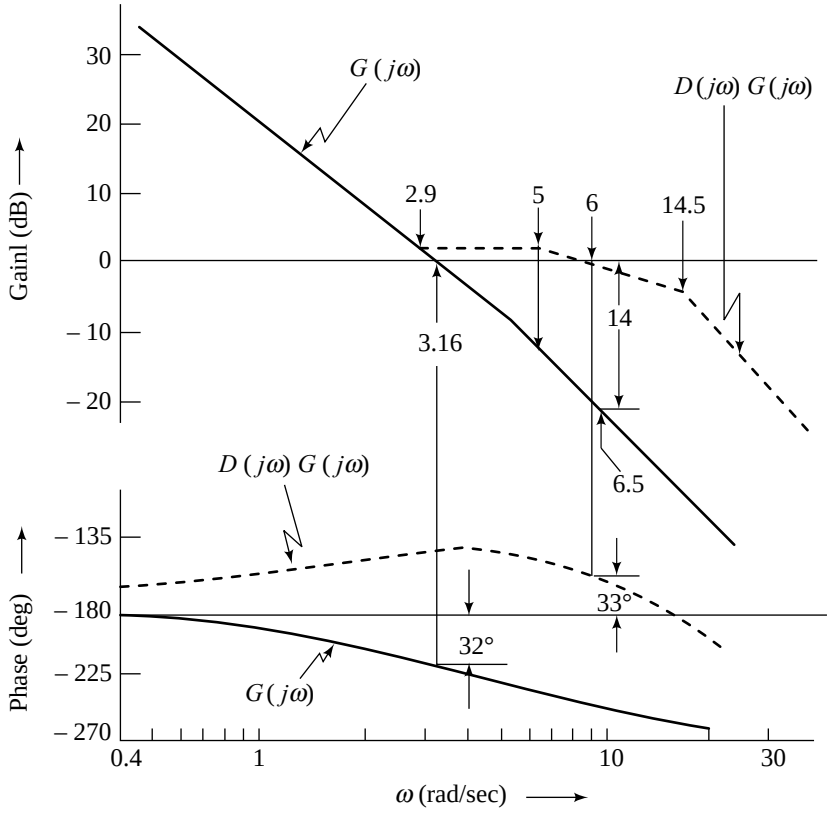

Fig. 10.14 Bode plot for Example 10.2

The phase lead needed at the new gain crossover frequency ω_g' is obtained as follows:

Additional phase lead required

= specified phase margin – phase margin of the uncompensated system at $\omega_g + \varepsilon$

= 35° + 32° + 15° = 82°

A large value of ε has been selected in this example because of rapid decrease of $\angle G(j\omega)$ in the region of gain crossover frequency ω_g.

Setting the maximun phase ϕ_m of the lead compensator equal to the additional required phase lead of 82°, we obtain the α parameter of the compensator as

$$\alpha = \frac{1 - \sin 82°}{1 + \sin 82°} = 0.005$$

Since the high-frequency noise signals are amplified by a factor of $1/\alpha$, the use of $\alpha = 0.005$ may not be acceptable.

Figure 10.15 shows the plot of ϕ_m *versus* $1/\alpha$, from which it is observed that to obtain phase leads more than 60° ($\alpha \cong 0.07$), $1/\alpha$ increases rather sharply, quite out of proportion to the increase in phase lead. Therefore, for phase leads greater than 60°, it is advisable to use two or more cascaded stages of lead compensator (described by Eqn. (10.13)) with moderate values of α rather than a single-stage lead compensator with too small a value of α.

For the design problem under consideration, using a single-stage lead compensator to give a phase lead of 82° is not advisable. We shall design a two-stage lead compensator (with an isolating amplifier), so that each stage has to provide maximum phase lead of 82/2 = 41°. The α parameter of each stage is

$$\alpha = \frac{1 - \sin 41°}{1 + \sin 41°} \cong 0.2$$

From the Bode plot of uncompensated system, it is seen that the gain $2\left(-20\log\left(1/\sqrt{\alpha}\right)\right) = -14$dB occurs at $\omega_g' = 6.5$ rad/sec (Fig. 10.14). This should be the gain crossover frequency of the system with single-stage lead compensator. Choosing $\omega_m = \omega_g'$, we obtain the τ parameter of one stage:

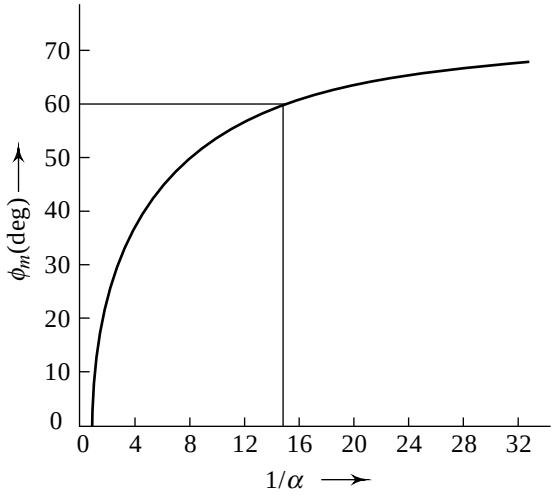

Fig. 10.15 ϕ_m versus $1/\alpha$ for a lead compensator

$$\omega_m = \frac{1}{\sqrt{\alpha}\tau} = \omega_g' = 6.5$$

This gives $\tau = 0.344$

By adding another identical stage of lead compensator, the open-loop transfer function of the compensated system becomes

$$D(s)G(s) = \frac{10(0.344s+1)^2}{s^2(0.2s+1)(0.069s+1)^2}$$

The Bode plot of $D(j\omega)G(j\omega)$ is shown in Fig. 10.14, from which it is found that the phase margin of the compensated system is 33°. This indicates that the system has become stable but the desired phase margin is not yet fully achieved. This is because of the excessive lag of the fixed part of the system at the new gain crossover frequency. If this phase margin is not acceptable, then the compensator should be redesigned with a higher value of ε.

Simulation of the closed-loop system corresponding to the design just completed shows a peak overshoot of 46.4% and settling time of 1.1 sec. The phase margin specification, when converted to time-domain measure on the basis of second-order correlations, gives $\zeta = 0.35$ (peak overshoot 30.92%). The actual response does not correlate well with the one predicted by second-order approximation. This time-response analysis dictates redesign if the actual performance is not in the acceptable range.

10.3.3 Concluding Remarks

1. The steady-state error of a feedback system is not affected by introduction of a unity zero-frequency gain lead compensator.
2. The phase of the open-loop transfer function in the vicinity of the gain crossover frequency is increased by lead compensation. This improves the phase margin of the closed-loop system.
3. Lead compensation increases the gain crossover frequency and bandwidth; consequently, the speed of response of the closed-loop system is increased.
4. The value of the α parameter of the lead compensator should not be smaller than 0.07, nor should the maximum phase lead ϕ_m be more than 60°, because such choices will need an additional gain of excessive value. If more than 60° phase lead is required, two (or more) lead networks may be used in series with an isolating amplifier.
5. If the uncompensated system has low stability margin, the additional phase lead required to obtain a certain desired phase margin may be excessive. This requires a relatively small value of α parameter of the compensator, which, as a result, will give rise to large bandwidth for the compensated system. Such a compensator may not be acceptable because of considerations of noise transmission. As we shall see later in this chapter, a lead compensator cascaded with a lag compensator may realize a large phase margin while limiting the increase in bandwidth of the closed-loop system.
6. If the phase angle of the uncompensated system decreases rapidly near the gain crossover frequency, lead compensation becomes less effective because the shift in the gain crossover frequency to the right makes it difficult to provide enough phase lead at the new gain crossover frequency.
7. The steady-state performance of a feedback system can be improved to any desired level by appropriately raising the open-loop gain K. Raising K results in amplification of signals at all frequencies. Introduction of a lead compensator provides additional gain for high-frequency signals, thereby boosting the noise signal level relative to the control signal. This imposes a limit on the improvement of steady-state error by raising gain K in a lead-compensated system.

10.4 CASCADE LAG COMPENSATION

The primary function of a lag compensator is to reshape the frequency-domain plot by providing sufficient attenuation over some appropriate frequency range. The phase lag characteristic is of no consequence in lag compensation.

10.4.1 Lag Compensator Frequency Response

The transfer function of a lag compensator with unity zero-frequency gain is of the form

$$D(s) = \frac{\tau s + 1}{\beta\tau s + 1} \quad \beta > 1,\ \tau > 0 \tag{10.20}$$

The sinusoidal transfer function is of the form

$$D(j\omega) = \frac{1 + j\omega\tau}{1 + j\omega\beta\tau} \tag{10.21}$$

The Bode plot of $D(j\omega)$, shown in Fig. 10.16, has two corner frequencies at $\omega = 1/\beta\tau$ and $\omega = 1/\tau$. The phase lag mainly occurs within and around the two corner frequencies. It must be recognized here that any phase lag at the gain crossover frequency of the compensated system is undesirable. To prevent detrimental effects of phase lag due to the lag compensator, the corner frequencies of the lag compensator must be located substantially lower than the gain crossover frequency of the compensated system.

Figure 10.16 also shows that in the high-frequency range, the lag compensator has an attenuation of 20 log β dB, which is the property that is utilized to give a system sufficient phase margin.

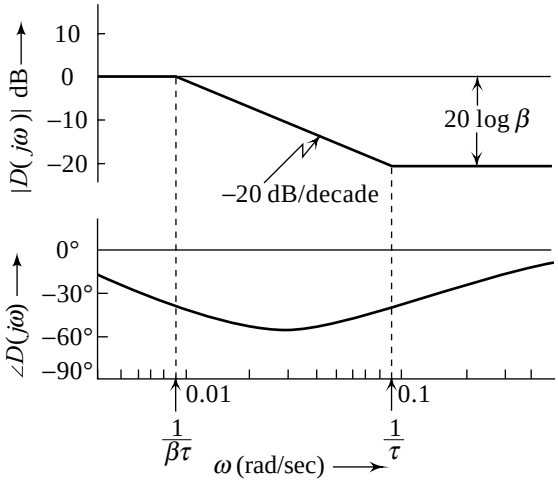

Fig. 10.16 Frequency response characteristics of lag compensators

The addition of a lag compensator results in an improvement in the ratio of control signal to noise signal in the loop. The high-frequency noise signals are attenuated by a factor $\beta > 1$, while the low-frequency control signals undergo unit amplification (0 dB gain). The choice of β is usually restricted because a very large β will appreciably reduce the gain crossover frequency and consequently speed of response of the system. A typical choice of β is 10.

We are now ready to enumerate a design procedure for lag compensation.

10.4.2 Design Procedure

To illustrate the lag-compensator design procedure, we reconsider the unity-feedback system of design problem 2, which was discussed earlier in Section 10.2. The design problem is to obtain the unity zero-frequency gain compensator

$$D(s) = \frac{\tau s + 1}{\beta \tau s + 1}; \beta > 1, \tau > 0$$

for the plant with adjustable gain,

$$G(s) = \frac{K}{s(s+2)}$$

so that the closed-loop system has (i) $\Phi M \geq 60°$, and (ii) $K_v \geq 10$.

The steady-state error requirement sets $K = 20$. The Bode plot of $G(j\omega)$ for $K = 20$ is shown in Fig. 10.17. From this plot we see that the uncompensated system has gain crossover frequency $\omega_g = 4.4$ rad/sec and phase margin = 24°. The required phase margin of 60° can be achieved by lowering the gain crossover frequency to a region where $G(j\omega)$ has more favourable phase characteristics. This can be achieved by introducing a lag compensator.

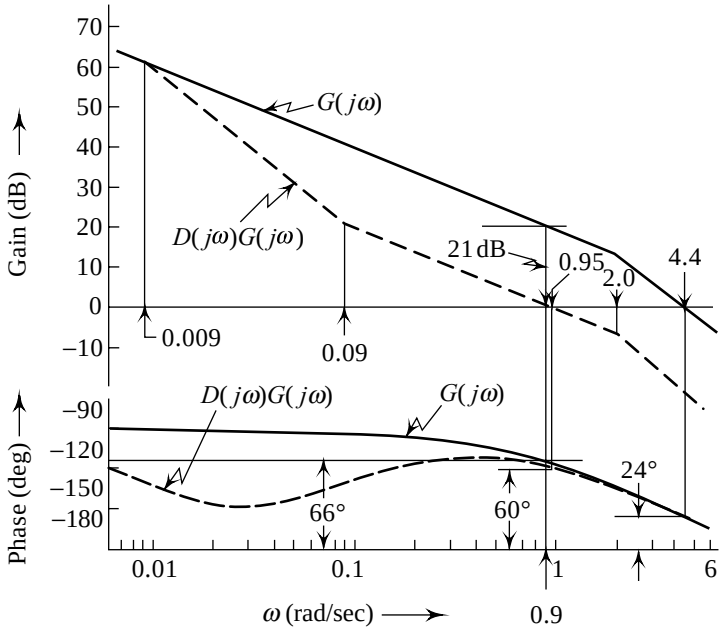

Fig. 10.17 Cascade lag compensation

First we search for a new gain crossover frequency that has a phase margin of 60° plus 6° (this will be explained later), or 66°. This can be found by drawing a horizontal line with 66° phase margin. Its intersection with the phase plot yields the new gain crossover frequency. It is read from Fig. 10.17 as $\omega_g' = 0.9$. We then draw a vertical line upward to the magnitude plot. We see that the magnitude at $\omega = \omega_g'$ is 21dB. To bring the magnitude curve down to 0 dB at ω_g', the lag compensator must provide 21 dB attenuation at ω_g'. From Fig. 10.16, we see that a lag compensator provides an attenuation of 20 log β for $\omega > 1/\tau$, the upper corner frequency. Therefore, a lag compensator with upper corner frequency $1/\tau < \omega_g'$, and the β parameter given by

$$20 \log \beta = 21 \tag{10.22}$$

will provide the required attenuation. From Eqn. (10.22), we get $\beta = 11$. We take $\beta = 10$ as the initial trial value.

Once the value of β is determined, it is necessary only to select the proper value of τ to complete the design. If the upper corner frequency $1/\tau$ is close to ω_g', the phase margin at ω_g' will be greatly reduced by

the phase lag of the compensator. If the upper corner frequency is very far away from ω_g' (on the left-hand side), then the phase margin will be hardly affected by the phase lag of the compensator. Therefore, it seems that we should choose τ so that $1/\tau$ is as small as possible. However, this will cause a different problem. If $1/\tau$ is very small, then $D(s)$ has a pole very close to the origin. If we plot the root locus of $1 + D(s)G(s)$, then we can see that the closed-loop system will have a pole very close to the origin and the corresponding time-constant will be very large. Due to this additional closed-loop pole, the speed of response of the resulting system may become slow. The magnitude of the response term contributed by the additional pole will not be too large because of the presence of compensator zero close to the additional closed-loop pole.

Usually, as a general guideline, the upper corner frequency, $1/\tau$, of the compensator should be approximately one octave to one decade below the new gain crossover frequency ω_g'. Taking

$$\frac{1}{\tau} = \frac{\omega_g'}{10}$$

we obtain

$$\tau = \frac{10}{0.9} = 11.1$$

Thus, the required lag compensator is

$$D(s) = \frac{\tau s + 1}{\beta\tau s + 1} = \frac{11.1s + 1}{111s + 1}$$

This lag compensator has a phase lag of 5.7° at $\omega_g' = 0.9$. Thus the phase of $G(s)$ will be reduced by roughly 6° after introducing $D(s)$. This is the reason for adding 6° to the required phase margin in determining ω_g'.

The open-loop transfer function of the compensated system becomes

$$D(s)G(s) = \frac{10(11.1s + 1)}{s(0.5s + 1)(111s + 1)}$$

The frequency-response characteristics of $D(s)G(s)$ in Fig. 10.17 can be seen to yield a phase margin of 60°. The compensated system, therefore, meets both the steady-state and the relative stability requirements.

A summary of the lag-compensation design procedure for designing compensator $D(s) = (\tau s + 1)/(\beta\tau s + 1)$ for the plant $G(s)$ with adjustable gain K, is given below.

1. Sketch the Bode plot of the uncompensated system with the gain K set according to the steady-state error requirement. Measure the gain crossover frequency ω_g, and the phase margin of the uncompensated system.
2. Determine the frequency at which the phase angle of the uncompensated system is:
   $$-180° + \text{specified phase margin} + \varepsilon$$
   Select this frequency as new gain crossover frequency ω_g'.
   ε is a margin of safety required by the fact that the compensator will contribute phase lag at ω_g'. A guess is made on the value of ε depending upon the value of ω_g'. If we can place upper corner frequency, $1/\tau$, of the compensator far below ω_g', a small value of ε is taken. If ω_g' is fairly low, the upper corner frequency $1/\tau$ cannot be taken far to its left to avoid large time-constants. In such cases, phase lag contribution of the compensator at ω_g' will be considerable; a large value of ε is taken to compensate for this detrimental effect.
   Allow for ε from 5° to 15° for phase lag contribution of the compensator at ω_g'.
3. To bring the magnitude curve down to 0 dB at ω_g', the lag compensator must provide the amount of attenuation equal to the value of gain of the uncompensated system at ω_g'. Measure the gain of the uncompensated system at ω_g' and equate it to 20 log β. Calculate therefrom, the parameter β of the compensator.

4. Choose the upper corner frequency of the compensator one octave to one decade below ω_g'. This gives the parameter τ of the compensator.
5. Calculate the phase lag of the compensator at ω_g'. If it is less than ε, go to the next step. Otherwise, choose a larger ε in step 2 and repeat steps 3 and 4.
6. Sketch the frequency-response plots of compensated system in Bode and Nichols coordinate system. Check any additional specification on system performance. Redesign for another choice of $1/\tau$ till all specifications are met. It may be noted that the additional specifications can only be met if they are consistent.

Example 10.3 Consider a type-1 unity-feedback system with an open-loop transfer function

$$G(s) = \frac{K}{s(s+1)}$$

It is desired to have the velocity error constant $K_v = 10$. Furthermore, we desire that the phase margin of the system be atleast 45°. Earlier in Example 10.1, a lead compensator was used to realize these specifications. We now attempt a lag compensation scheme.

The first step in the design procedure is to sketch the Bode plot of the uncompensated system with the gain K set according to the steady-state error requirement. $K = 10$ meets the K_v specification. The Bode plot of

$$G(j\omega) = \frac{10}{j\omega(j\omega+1)}$$

is drawn in Fig. 10.18. The gain crossover frequency of the uncompensated system is $\omega_g = 3.16$ rad/sec, and the phase margin is 18°.

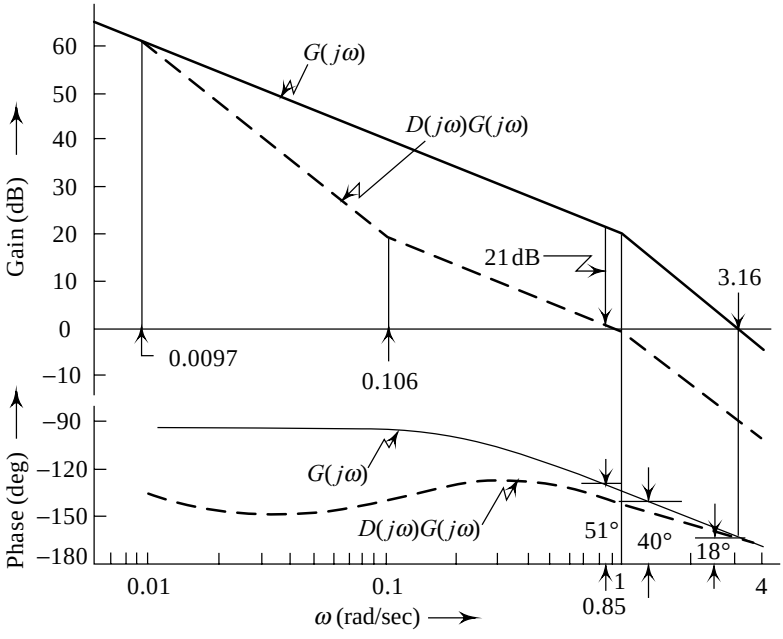

Fig. 10.18 Bode plot for Example 10.3

To realize a phase margin of 45°, the gain crossover frequency should be moved to ω_g' where the phase angle of the uncompensated system is:

$$-180° + \text{specified phase margin} + \varepsilon = -180° + 45° + 6° = -129°$$

From Fig. 10.18, we find that $\omega_g' = 0.85$. The gain of the uncompensated system at ω_g' is 21 dB. Therefore, to bring the magnitude curve down to 0 dB at ω_g', the lag compensator must provide an attenuation of 21 dB. The β parameter of the lag compensator can now be calculated.

$$20 \log \beta = 21$$

This gives $$\beta = 11$$

Placing the upper corner frequency of the compensator three octaves below ω_g', we obtain,

$$\frac{1}{\tau} = \frac{\omega_g'}{(2)^3} = \frac{0.85}{8}$$

which gives $$\tau = 9.4$$

The lower corner frequency is $\frac{1}{\beta\tau} = \frac{1}{103.4}$. Therefore the lag compensator $D(s) = \frac{9.4s + 1}{103.4s + 1}$, and the compensated open-loop transfer function

$$D(s)G(s) = \frac{10(9.4s + 1)}{s(s + 1)(103.4s + 1)}$$

The Bode plot of the compensated system is shown in Fig. 10.18. It is seen that the phase margin of the compensated system is approximately 40°. If this phase margin is not acceptable, then the compensator should be redesigned with a higher value of ε.

In Fig. 10.19, the log-magnitude *versus* phase shift plots of original and compensated systems are plotted on the Nichols chart. These plots are obtained by taking the values of magnitude and phase shift directly from the Bode plot of Fig. 10.18. From the Nichols chart, the bandwidth without compensation is found to be 5 rad/sec. The bandwidth after compensation is found to be 1.5 rad/sec, which means that the time response is slower with lag compensation.

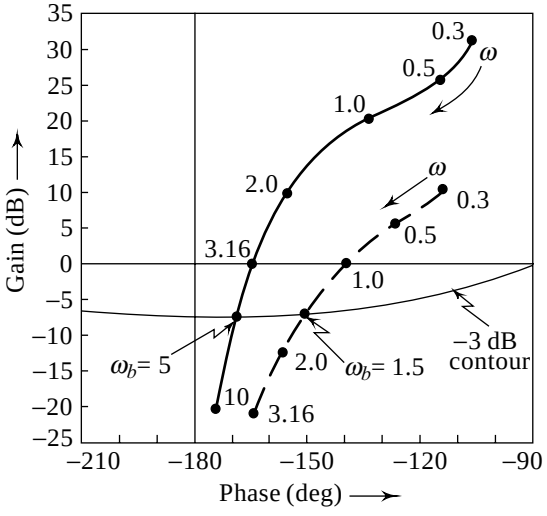

Fig. 10.19 Nichols chart for Example 10.3

To draw the root locus, we rearrange $D(s)G(s)$ as follows:

$$D(s)G(s) = \frac{10(9.4s+1)}{s(s+1)(103.4s+1)} = \frac{0.9091(s+0.1064)}{s(s+1)(s+0.0097)}$$

The root locus for this system is shown in Fig. 10.20. For root locus gain 0.9091, the complex poles are at $-0.445 \pm j\,0.784$, and the real pole is at -0.12, with a zero at $s = -0.1064$. Reshaping of Bode plot has resulted in near-cancellation compensation.

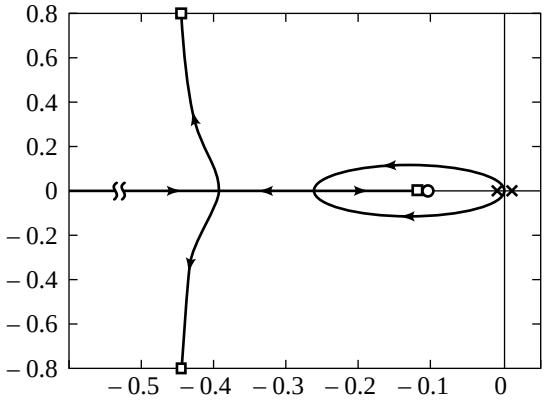

Fig. 10.20 Root locus for Example 10.3

The step response curves of compensated and uncompensated systems are shown in Fig. 10.21. The peak overshoot of compensated closed-loop system is 27.3%; it correlates reasonably well with the peak overshoot predicted by the formula $\zeta = 0.01 \times \Phi M$ (25.38%). We also note from Fig. 10.21, that the compensated system becomes slower corresponding to the decrease in gain crossover, giving a lower bandwidth for the system. The introduction of the slow root from the lag compensator has caused the response to require 15.6 sec settling time; the system 'creeps' towards the steady-state. Peak overshoot has been reduced due to increase in phase margin.

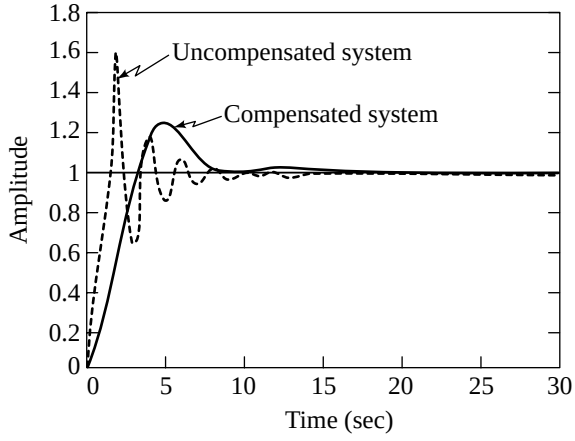

Fig. 10.21 Step responses for Example 10.3

A redesign might lower the phase margin, which may make the system response overshoot a bit; but this may reduce the creeping effect. In many applications, the long tail (creeping) in the system response is acceptable because the amplitude of its deviation from steady-state value is low.

Note that examples 10.1 and 10.3 meet an identical set of specifications for the same plant in very different ways. In the first case, the specifications are met with a lead compensation and a bandwidth $\omega_b = 7$ rad/sec, results. In the second case, the same specifications are met with a lag compensator and $\omega_b = 1.5$ rad/sec, results. Clearly, had there been specifications for rise time or bandwidth they would have influenced the choice of compensation (lead or lag). Likewise, if the slow settling (creeping) to the steady-state value was a problem, it might have suggested the use of lead compensation instead of lag.

10.4.3 Concluding Remarks

1. We utilize the attenuation characteristic of the lag compensator rather than its phase lag characteristic. The phase lag characteristic has no use for compensation purposes.
2. The steady-state error of a feedback system is not affected by introduction of a unity zero-frequency gain lag compensator.
3. Lag compensation reduces high-frequency gain for better phase margin.
4. Lag compensation decreases the gain crossover frequency and bandwidth; consequently, the closed-loop system becomes more sluggish.
5. Attenuation of high-frequency gain by lag compensation improves signal/noise ratio of the system.
6. If the uncompensated system has low stability margin, the high-frequency attenuation required to obtain a certain desired phase margin may be excessive. Such a compensator may not be acceptable because of consideration of speed of response. As we shall see later in this chapter, a lag compensator cascaded with a lead compensator may realize a large phase margin while limiting the loss of speed of response of the closed-loop system.
7. Steady-state performance of a feedback system can be improved to any desired level by appropriately raising the open-loop gain K. Raising K results in amplification of signals at all frequencies. Introduction of a lag compensator results in attenuation of the high-frequency signals, thereby reducing the noise signal level relative to the control signal. This feature of lag compensation allows a large value of K for significant improvement in steady-state performance of the feedback system.

10.5 CASCADE LAG-LEAD COMPENSATION

In general, there are two situations in which compensation is required. In the first case, the system is absolutely unstable and compensation is required to stabilize it, as well as to achieve a specified performance. In the second case, the system is stable but compensation is required to obtain the desired performance. The systems which are type-2 or higher, are usually absolutely unstable. The phase curve of such systems may lie entirely below the $-180°$ line in the Bode coordinate system. Under such situations, lag compensation cannot provide stability and required performance; lead compensation is the only answer.

In type-1 and type-0 systems, stable operation is always possible if the gain is sufficiently reduced. For such systems, phase margin can be improved to any level for a specified error constant by either lead or lag compensation. Decision on the choice of lead or lag compensation is based on performance requirements other than the relative stability and steady-state error. The lead compensation results in increased bandwidth and, consequently, faster speed of response. For higher-order systems and for systems with large specified error constants, large lead angles are required for compensation, resulting in excessively large bandwidth which is undesirable from noise transmission point of view. For such systems, lag compensation is preferred.

The lag compensation, on the other hand, reduces system bandwidth and, consequently, slows down the speed of response. For large specified error constant and moderately large desired bandwidth, it may not be possible to meet the specifications through either lead or lag compensation. Under such circumstances, we can use a lag-lead compensator.

10.5.1 Lag-Lead Compensator Frequency Response

As the name implies, the lag-lead compensator is basically just a lag compensator and a lead compensator in cascade. The transfer function of a lag-lead compensator with unity zero-frequency gain is of the form

$$D(s) = \underbrace{\left(\frac{\tau_1 s + 1}{\beta\tau_1 s + 1}\right)}_{\text{Lag section}} \underbrace{\left(\frac{\tau_2 s + 1}{\alpha\tau_2 s + 1}\right)}_{\text{Lead section}}; \beta > 1,\ \alpha < 1;\ \tau_1,\ \tau_2 > 0 \qquad (10.23)$$

The lead section alters the frequency-domain plot by adding phase lead angle and increasing the phase margin at the gain crossover frequency. The lag section provides attenuation near and above the gain crossover frequency and thereby allows an increase of gain in the low-frequency range to improve the steady-state performance.

For applications where independent choice of α and β is not essential (with the reduction in number of design parameters, the design problem becomes simpler), a lag-lead compensator of the form

$$D(s) = \frac{(\tau_1 s + 1)(\tau_2 s + 1)}{(\beta\tau_1 s + 1)\left(\frac{1}{\beta}\tau_2 s + 1\right)}; \beta > 1 \ \tau_1, \ \tau_2 > 0 \tag{10.24}$$

may be used. The sinusoidal transfer function of this compensator is

$$D(j\omega) = \frac{(1 + j\omega\tau_1)(1 + j\omega\tau_2)}{(1 + j\omega\beta\tau_1)(1 + j\omega\tau_2/\beta)} \tag{10.25}$$

Figure 10.22 shows the Bode plot of $D(j\omega)$. Note that the phase shift is a function of input frequency; phase angle varies from lag to lead as the frequency is increased. Thus, phase lag and phase lead occur in different frequency bands.

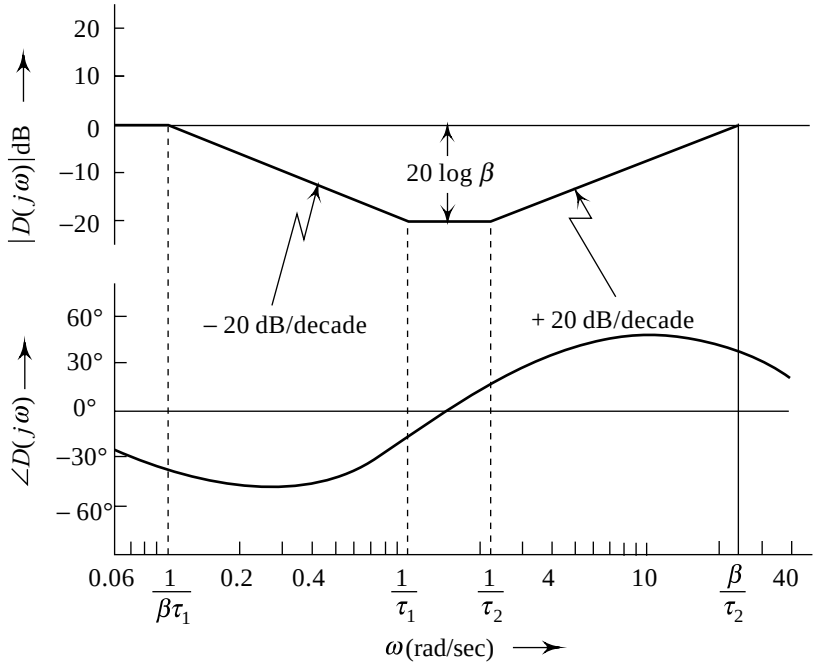

Fig. 10.22 Frequency response characteristics of lag-lead compensators

10.5.2 Design Procedure

To start with design, we check the phase margin and bandwidth of the uncompensated system with gain adjusted to meet the error constant specification. If the bandwidth is smaller than the specified value, lead compensation may be tried. However, if the bandwidth is larger than acceptable, lead compensation would

not be desirable; so we try lag compensation provided that the uncompensated system is not absolutely unstable. If the lag compensator design results in too low a bandwidth, the need for a lag-lead compensation is indicated.

Let us demonstrate the design procedure with an example.

Example 10.4 Consider the unity-feedback system whose open-loop transfer function is

$$G(s) = \frac{K}{s(0.1s+1)(0.2s+1)}$$

The system is to be compensated to meet the following specifications:

1. Velocity error constant $K_v = 30$.
2. Phase margin $\Phi M \geq 50°$.
3. Bandwidth $\omega_b = 12$ rad/sec.

It easily follows that $K = 30$ satisfies the specification on K_v. The Bode plot of $G(j\omega)$ with $K = 30$ is shown in Fig. 10.23 from which it is found that the uncompensated system has a gain crossover frequency $\omega_g = 11$ rad/sec and phase margin = – 23°.

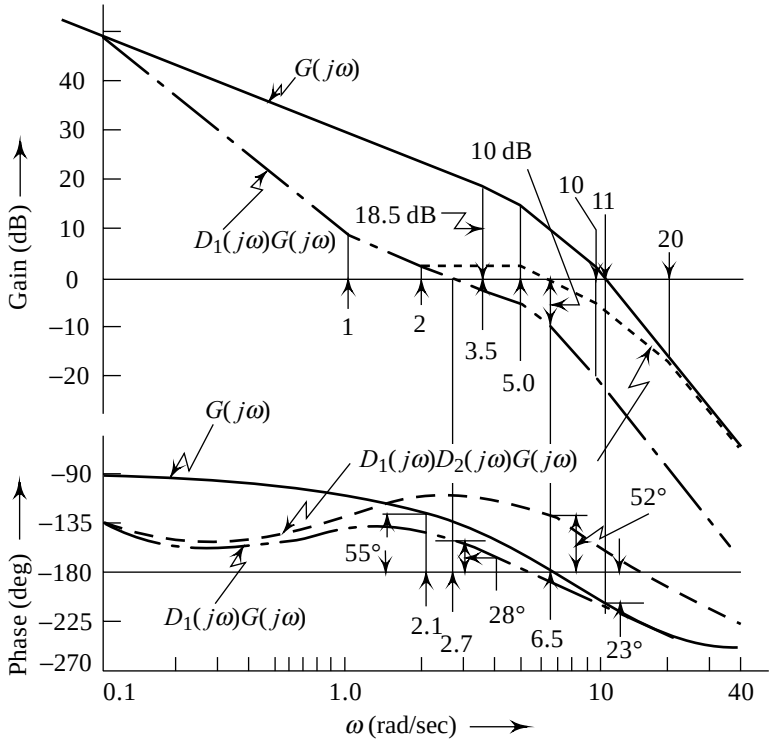

Fig. 10.23 Bode plot for Example 10.4

If lag compensation is employed for this system, the bandwidth will decrease sufficiently so as to fall short of the specified value of 12 rad/sec, resulting in a sluggish system. This fact can be verified by designing a lag compensator. If on the other hand, lead compensation is attempted, the bandwidth of the resulting system will be much higher than the specified value; the closed-loop system will be sensitive to noise which is undesirable.

This fact can also be verified by designing a lead compensation scheme. Owing to the large phase lead needed at the gain crossover frequency of the compensated system, two stages of lead compensator described by Eqn. (10.13), may be used.

Let us design a lag-lead compensator to overcome the difficulties mentioned above. Since a full lag compensator would reduce the system bandwidth excessively, the lag section of the lag-lead compensator must be designed to provide partial compensation only. The lag section design therefore proceeds by making a choice of the new gain crossover frequency which must be higher than the crossover frequency if the system were fully lag compensated. Full lag compensation demands that the gain crossover frequency should be shifted to a point where the phase angle of the uncompensated system is:

$$-180° + \text{specified phase margin} + \varepsilon = -180° + 50° + 5° = -125°$$

From Fig. 10.23, we find that this requirement is met at 2.1 rad/sec. For the design of lag section of lag-lead compensator, the selected gain crossover frequency should be higher than 2.1. The choice is made as $\omega_g' = 3.5$ rad/sec to start with.

From Fig. 10.23, we find that the gain of the uncompensated system at ω_g' is 18.5 dB. Therefore to bring the magnitude curve down to 0 dB at ω_g', the lag section must provide an attenuation of 18.5 dB. This gives the β parameter of the lag section as

$$20 \log \beta = 18.5$$

or

$$\beta = 8.41, \text{ say } 10$$

Let us now place the upper corner frequency of the lag section at 1 rad/sec. This gives the lag-section transfer function

$$D_1(s) = \frac{\tau_1 s + 1}{\beta \tau_1 s + 1} = \frac{s + 1}{10s + 1}$$

Bode plot of lag-section compensated system is shown in Fig. 10.23; the phase margin is 28°.

We now proceed to design the lead section. We choose $\alpha = 1/\beta = 0.1$. The maximum lead provided by the lead section is therefore (refer Eqn. (10.17))

$$\phi_m = \sin^{-1}\left(\frac{1-\alpha}{1+\alpha}\right) = 55°$$

The lag-compensated system has a gain of $-20 \log (1/\sqrt{\alpha}) = -10$ dB at $\omega_g'' = 6.5$ rad/sec. Setting ω_m, the frequency at which the lead section has maximum phase ϕ_m, equal to ω_g'', we obtain

$$\omega_m = \frac{1}{\sqrt{\alpha}\tau_2} = \omega_g'' = 6.5$$

This gives

$$\tau_2 = 0.5$$

The transfer function of the lead section, therefore, is

$$D_2(s) = \frac{\tau_2 s + 1}{\alpha \tau_2 s + 1} = \frac{0.5s + 1}{0.05s + 1}$$

Combining the transfer functions of the lead and lag sections, we obtain

$$D(s) = \frac{(s+1)(0.5s+1)}{(10s+1)(0.05s+1)}$$

The open-loop transfer function of the lag-lead compensated system is

$$D(s)G(s) = \frac{30(s+1)(0.5s+1)}{s(0{\cdot}1s+1)(0.2s+1)(10s+1)(0.05s+1)}$$

The Bode plot of $D(j\omega)G(j\omega)$ is shown in Fig. 10.23. The phase margin is found to be 52°.

The magnitude *versus* phase angle curve of the lag-lead compensated system is drawn on the Nichols chart in Fig. 10.24, from which the bandwidth of the system is found to be 9.6 rad/sec.

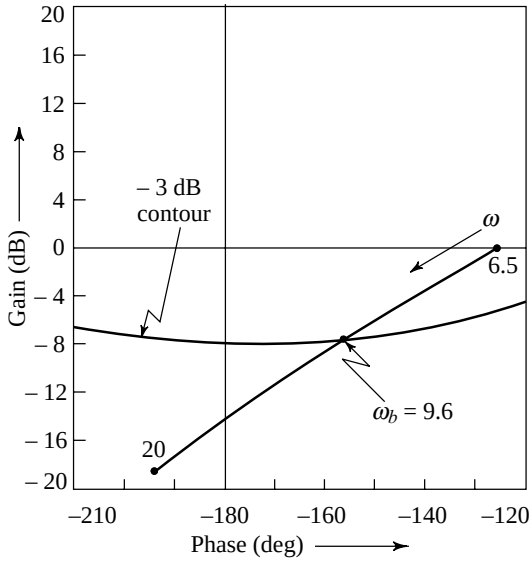

Fig. 10.24 Nichols chart for Example 10.4

The design does not meet the specifications laid down. We must, therefore, redesign by adjusting the initial choice of β and τ_1.

10.6 CASCADE PID COMPENSATION

The design of a controller is basically a search problem in n-dimensional parameter space, where n is the number of design parameters. Lesser the value of n, simpler is the design problem.

In the case of the design wherein the primary requirement is to improve transient response, we have recommended a lead compensator, which has three trial parameters. An alternative strategy is to design a PD compensator, which has two trial parameters. However, an independent design of a filter, to take care of high-frequency noise problem, will also be required.

When the primary requirement is to improve steady-state performance, we have recommended a lag compensator, which has three trial parameters. An alternative strategy is to design a PI compensator, which has two trial parameters. This compensator, however, will be useful if the pole at origin does not degrade closed-loop stability appreciably.

The design of PI, PD, and PID compensators follows in a straight forward way from the procedures of design of lag, lead and lag-lead compensators. Illustrative examples follow.

Example 10.5 A unity feedback system has forward-path transfer function

$$G(s) = \frac{4500K}{s(s+361.2)}$$

Our goal is to design a cascade PD compensator so that the closed-loop system meets the following specifications:

Steady-state error due to unit-ramp input ≤ 0.000443

Phase margin $\Phi M \geq 80°$

Bandwidth $\omega_b \leq 2000$ rad/sec

We want to achieve a steady-state response that has no more than 0.000443 error due to unit-ramp input. This, as we know, can be achieved by simple gain adjustment. We therefore first evaluate the 'uncompensated system' that meets the steady-state accuracy requirement.

Desired $$K_v = \frac{1}{0.000443}$$

Therefore

$$\frac{1}{0.000443} = \lim_{s\to 0} \frac{s(4500K)}{s(s+361.2)}$$

This gives

$$K = 181.17$$

Bode plot of uncompensated system with $K = 181.17$ is shown in Fig. 10.25, from which it is found that the gain crossover frequency $\omega_g = 868$ rad/sec and the phase margin $\Phi M = 22.6°$. In Fig. 10.26, the magnitude *versus* phase shift plot of the uncompensated system is drawn on the Nichols chart. It is seen that the bandwidth ω_b of the uncompensated system is 1400 rad/sec.

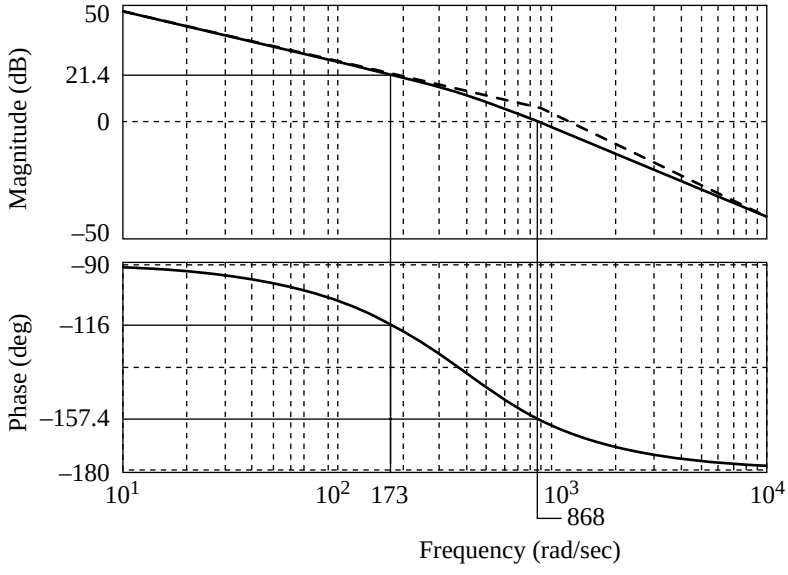

Fig. 10.25 Bode plot for Example 10.5

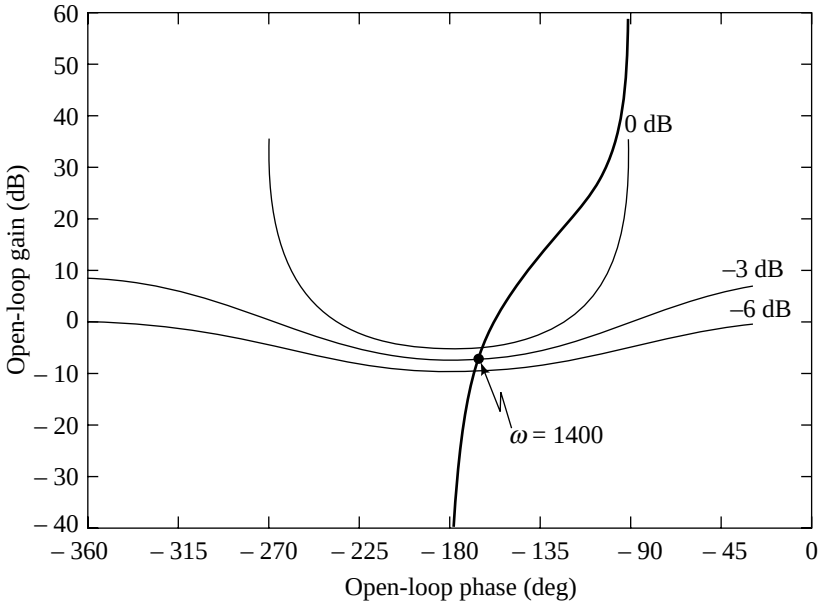

Fig. 10.26 Nichols chart for Example 10.5

A PD compensator with transfer function

$$D(s) = 1 + T_D s$$

has asymptotic Bode plot of the form shown in Fig. 10.27. The logical way to approach the design problem is to first examine how much additional phase is needed to realize a ΦM of 80°. Since the uncompensated system with the gain set to meet the steady-state requirement has ΦM of only 22.6°, the PD compensator must provide an additional phase of 80 – 22.6 = 57.4°. The additional phase must be placed at the desired gain crossover frequency of the compensated system in order to realize a ΦM of 80°.

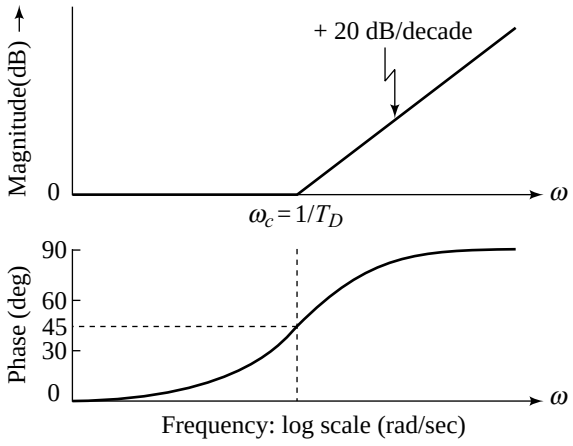

Fig. 10.27 Asymptolic Bode plot of PD compensator

Referring to the asymptotic Bode plot of PD compensator shown in Fig. 10.27, we see that the additional phase at frequencies > $1/T_D$ is always accompanied by a gain in the magnitude curve. As a result, the gain crossover of the compensated system will be pushed to a higher frequency. At new gain crossover, the phase of the uncompensated system would correspond to smaller ΦM. Thus we may run into the problem of diminishing returns.

Simple trial-and-error placement of corner frequency of the compensator around the gain crossover frequency can meet the design requirements. With T_D = 0.0017, the performance requirements in

frequency domain are satisfied. The reader is encouragd to verify this from the Bode plot and Nichols chart corresponding to the compensated system.

Example 10.6 Let us reconsider the system of Example 10.5. Let us now specify ΦM to be atleast 64°, bandwidth about 300 rad/sec, and e_{ss} (parabolic input) ≤ 0.2. We attempt a PI compensator to meet these requirements.

Initially we take $K = 181.17$ simply because the value was used in Example 10.5. We will tune the total loop gain later to meet the steady-state performance requirement. The uncompensated system with $K = 181.17$ has $\Phi M = 22.6°$, gain crossover frequency $\omega_g = 868$ rad/sec, and bandwidth $\omega_b = 1400$ rad/sec (refer Figs 10.25 and 10.26).

We know that PI compensator is an approximation for the lag compensator:

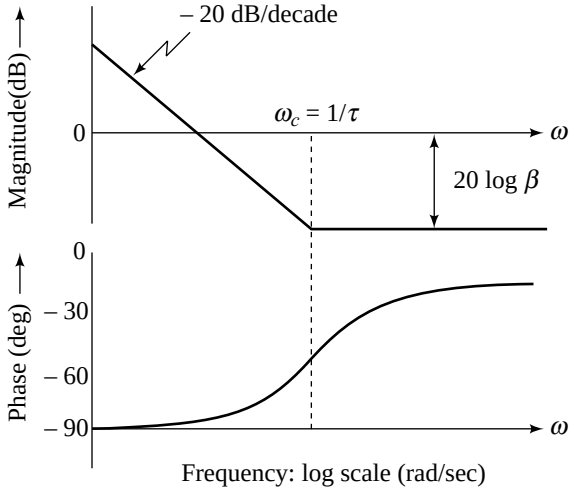

Fig. 10.28 Asymptotic Bode plot of PI compensator

$$D(s) = \frac{\tau s + 1}{\beta\tau s + 1};\ \beta > 1$$

$$\cong \frac{\tau s + 1}{\beta\tau s} = \frac{1}{\beta} + \frac{1}{\beta\tau s} = K_P + \frac{K_I}{s}$$

The asymptotic Bode plot of a PI compensator is shown in Fig. 10.28.

From the Bode plot of uncompensated system (Fig. 10.25), we find that the new gain crossover frequency ω_g' at which the phase margin is 64°, is 173 rad/sec. The magnitude of $G(j\omega)$ at this frequency is 21.4 dB. Thus the PI compensator should provide an attenuation of 21.4 dB at $\omega_g' = 173$ rad/sec.

$$20 \log(\beta) = 21.4;\ \beta = 1/0.0851.$$

This gives

$$K_P = \frac{1}{\beta} = 0.0851$$

A simple trial-and-error search for values of $\frac{1}{\tau} = \frac{K_I}{K_P}$ that are sufficiently small (low-frequency range) can meet the design requirements. With $1/\tau = 1$, the performance requirements in frequency domain are all satisfied. The reader is encouraged to verify this from the Bode plot and Nichols chart corresponding to the compensated system.

Let us now evaluate the steady-state performance.

$$D(s)\,G(s) = \frac{4500 \times 181.17 \times 0.0851(s+1)}{s^2(s+361.2)}$$

$$K_a = \frac{4500 \times 181.17 \times 0.0851}{361.2} = 192.0793$$

$$e_{ss} = 0.0052$$

Steady-state requirement is thus satisfied.

It should be noted that ΦM of the system can be improved further by increasing the value of β above 1/0.0851. However, the bandwidth of the system will be reduced. For example, for $\beta = 1/0.04$ and $1/\tau = 1$, the ΦM is increased to 75.7° but ω_b is reduced to 127 rad/sec.

Review Examples

Review Example 10.1 Consider a unity-feedback type-1 system with open-loop transfer function

$$G(s) = \frac{K}{s(s+1)(s+4)}$$

The system is to be compensated to meet the following specifications:

Velocity error constant	$K_v = 5$
Peak overshoot	$M_p = 25\%$
Settling time	$t_s = 10$ sec

Peak overshoot of 25% and settling time of 10 sec imply $\zeta = 0.4$ and $\omega_n = 1$ for the closed-loop dominant poles (refer Eqns (6.14) and (6.19)). Equation (10.1) yields a 40° phase margin for a damping ratio of 0.4, and from Eqn. (10.5) we find that with $\zeta = 0.4$ and $\omega_n = 1$, a closed-loop bandwidth of $\omega_b = 1.375$ rad/sec is required.

In order to meet the specification of $K_v = 5$, K must be set at 20, yielding

$$G(s) = \frac{5}{s(s+1)(0.25s+1)}$$

Bode plot of uncompensated system for $K = 20$ is shown in Fig. 10.29, from which it is found that the gain crossover frequency $\omega_g = 2.2$ rad/sec and the phase margin is –4°. If lead compensation is employed for this system, the gain crossover frequency of the compensated system will be more than 2.2 rad/sec and the bandwidth will exceed the specified value, making the system sensitive to noise. We, therefore, try lag compensation.

It is seen from the Bode plot that neglecting the phase-lag contribution of the compensator, the specified phase margin of 40° is obtained if the gain cross over frequency is 0.8 rad/sec. Since this is fairly low, the upper corner frequency of the lag compensator cannot be taken far to its left to avoid large time-constants. This indicates that phase-lag contribution of the compensator at the new gain crossover frequency ω_g will be considerable and may be guessed at $\varepsilon = 15°$. The uncompensated system must, therefore, have a phase angle of

$$-180° + \text{specified phase margin} + \varepsilon = -180° + 40° + 15° = -125°$$

at ω_g', which is found to be 0.52 rad/sec.

The gain of the uncompensated system at ω_g' is 20 dB. Therefore, to bring the magnitude curve down to 0 dB at ω_g', the lag compensator must provide an attenuation of 20 dB. The β parameter of the lag compensator can now be calculated.

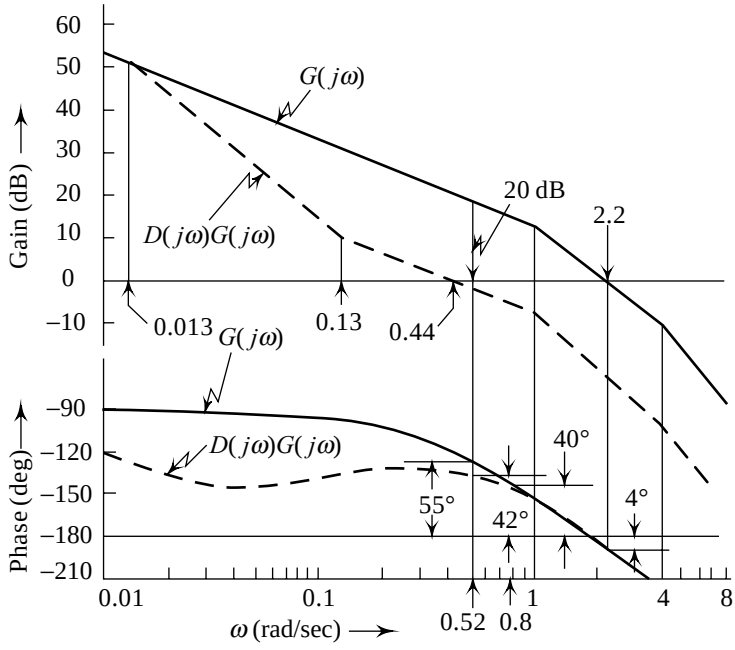

Fig. 10.29 Bode plot for Review Example 10.1

$$20 \log \beta = 20$$

This gives $\beta = 10$

Placing the upper corner frequency of the compensator two octaves below ω_g', we have

$$\frac{1}{\tau} = \frac{\omega_g'}{(2)^2} = 0.13 \text{ rad/sec} = \frac{1}{7.7}$$

The lower corner frequency of the compensator is then fixed at

$$\frac{1}{\beta\tau} = 0.013 \text{ rad/sec} = \frac{1}{77}$$

The transfer function of the lag compensator is then

$$D(s) = \frac{7.7s + 1}{77s + 1}$$

Phase-lag introduced by the lag compensator at ω_g' is

$$\tan^{-1}(7.7\omega_g') - \tan^{-1}(77\omega_g') = 76° - 88° = -12°$$

Therefore, the safety margin of $\varepsilon = 15°$ is justified.

The open-loop transfer function of the compensated system becomes

$$D(s)G(s) = \frac{5(7.7s + 1)}{s(s + 1)(0.25s + 1)(77s + 1)}$$

The Bode plot of $D(j\omega)G(j\omega)$ is shown in Fig. 10.29, from where the phase margin of the compensated system is found to be 42°.

In Fig. 10.30, the magnitude *versus* phase shift plot of the compensated system is drawn on the Nichols chart. It is seen that the bandwidth of the compensated system is 1 rad/sec. We must redesign by adjusting the initial choice of β and τ if an improvement in bandwidth is required.

Simulation of the closed-loop system corresponding to the design just completed gives peak overshoot of 31.7% and setting time of 18.7 sec.

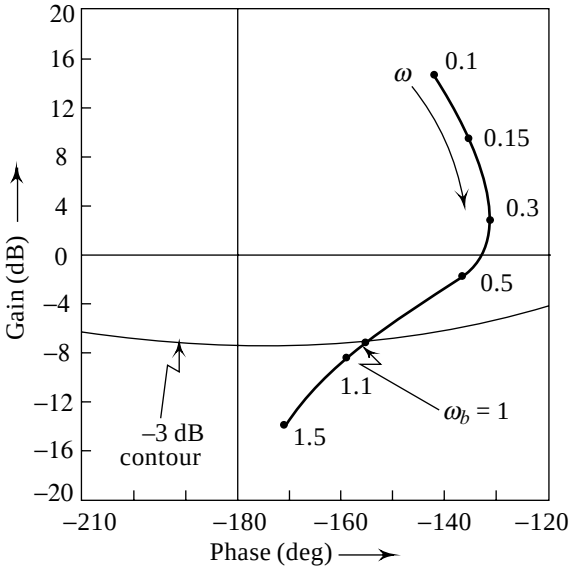

Fig. 10.30 Nichols chart for Review Example 10.1

Review Example 10.2 Consider the system shown in Fig. 10.31. Design a suitable compensator such that the closed-loop system will have a phase margin of 50°, a gain margin of not less than 10 dB and a gain crossover frequency of 1 rad/sec.

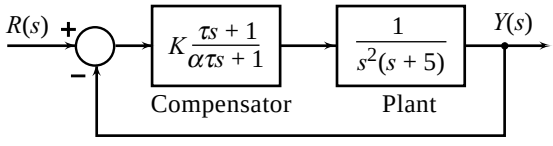

Fig. 10.31 Feedback system for Review Example 10.2

Solution The design problem may be reformulated as follows:

Design the unity zero-frequency gain compensator

$$D(s) = \frac{\tau s + 1}{\alpha\tau s + 1}$$

for the plant with adjustable gain,

$$G(s) = \frac{K}{s^2(s + 5)}$$

so that the closed-loop system meets the performance specifications.

Since the uncompensated system is unstable for all values of K, lag compensation scheme cannot be used. We attempt lead compensation. The gain crossover frequency of the compensated system is given to be $\omega_g = 1$ rad/sec. At ω_g, the phase angle of $G(j\omega)$ is $-191.3°$.

To realize a phase margin of 50°, the lead compensator must provide a phase lead of $50° + 11.3° = 61.3°$ at $\omega_g = 1$. Setting the maximum phase lead ϕ_m of the compensator equal to 61.3°, we obtain the α parameter of the lead compensator:

$$\alpha = \frac{1 - \sin\phi_m}{1 + \sin\phi_m} = 0.065$$

Noting that the maximum phase lead angle ϕ_m occurs at the geometric mean of the two corner frequencies of the compensator, we have

$$\omega_m = \sqrt{\frac{1}{\tau}\left(\frac{1}{\alpha\tau}\right)} = 1 = \frac{1}{\sqrt{\alpha}\tau}$$

This gives $\tau = 3.9$

Therefore the lead compensator $D(s) = \dfrac{\tau s + 1}{\alpha\tau s + 1} = \dfrac{3.9s + 1}{0.25s + 1}$

and the compensated open-loop transfer function

$$D(s)G(s) = \frac{K(3.9s + 1)}{s^2(s + 5)(0.25s + 1)} = \frac{0.2K(3.9s + 1)}{s^2(0.2s + 1)(0.25s + 1)}$$

A Bode plot of $D(j\omega)G(j\omega)/(0.2K)$ is shown in Fig. 10.32. From this plot we find that the magnitude curve must be lowered by 11.7 dB so that the magnitude equals 0 dB at $\omega = 1$ rad/sec. Hence

$$20 \log (0.2\,K) = -11.7 \quad \text{or} \quad 0.2\,K = 0.26$$

which yields $K = 1.3$

The Bode plot of compensated system (Fig. 10.32) shows that the system has phase margin of 50° and gain margin of 4.3 + 11.7 = 16 dB. Hence the design specifications are satisfied.

In this design problem, both the gain margin and phase margin have been specified. The two together qualitatively give a measure of the robustness property of the closed-loop system (refer Section 9.2).

Simulation of the closed-loop system corresponding to the design just completed gives peak overshoot of 25.5% and settling time of 9.59 sec.

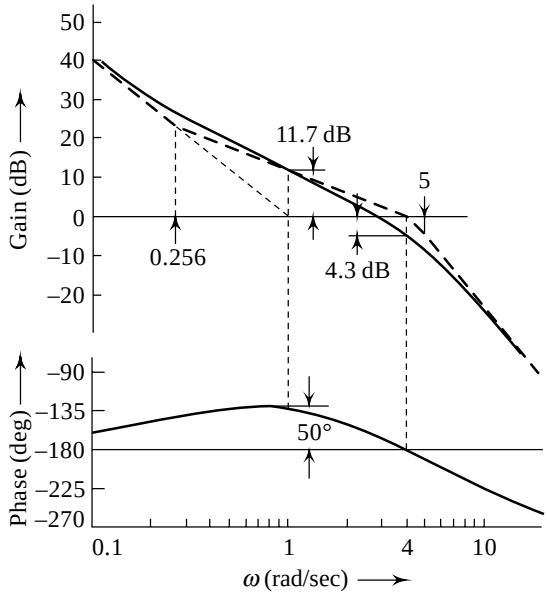

Fig. 10.32 Bode plot for Review Example 10.2

Review Example 10.3 The transfer function of the controlled process of a unity-feedback system is

$$G(s) = \frac{1.57e^{-0.785s}}{s(s+1)}$$

The Bode plot of $G(j\omega)$ is shown in Fig. 10.33. From the plot we see that the phase margin of the uncompensated system is approximately –5° and gain crossover frequency is $\omega_g = 1.1$ rad/sec.

Let us assume that the design specification calls for a phase margin of at least 45°. From Fig. 10.33 we see that the phase of $G(j\omega)$ decreases rapidly beyond 1 rad/sec. Therefore a cascade lead compensator may not be effective in improving the phase margin of the system. A cascade lag compensator seems to be more appropriate for this system.

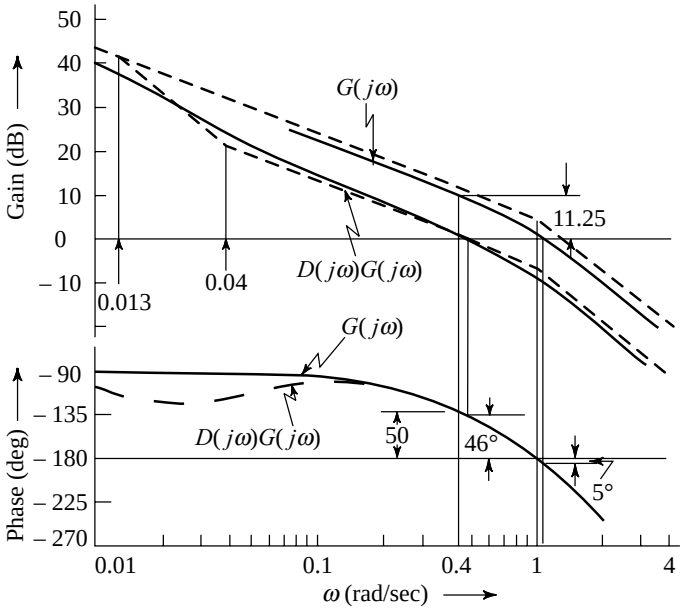

Fig. 10.33 Bode plot for Review Example 10.3

To realize a phase margin of 45°, the gain crossover frequency should be moved to ω_g' where the phase angle of the uncompensated system is:

$$-180° + \text{specified phase margin} + \varepsilon = -180° + 45° + 5° = -130°$$

From Fig. 10.33 we find that $\omega_g' = 0.4$ rad/sec. The gain of the uncompensated system at ω_g' is 11.25 dB. Therefore, to bring the magnitude curve down to 0 dB at ω_g', the lag compensator must provide an attenuation of 11.25 dB. The β parameter of the lag compensator can now be calculated.

$$20 \log \beta = 11.25$$

This gives

$$\beta = 3.65$$

Placing the upper corner frequency of the compensator one decade below ω_g', yields

$$\frac{1}{\tau} = \frac{\omega_g'}{10} = 0.04 \quad \text{or} \quad \tau = 25$$

Therefore the lag compensator $D(s) = \dfrac{25s + 1}{91.25s + 1}$

The Bode plot of the compensated system transfer function $D(j\omega)G(j\omega)$ is sketched in Fig. 10.33. The phase margin of the compensated system is as per specifications.

Review Example 10.4 The block diagram representation of an electromechanical servomechanism is sketched in Fig. 10.34. We assume that the servo has a mission requiring accurate positioning of the load.

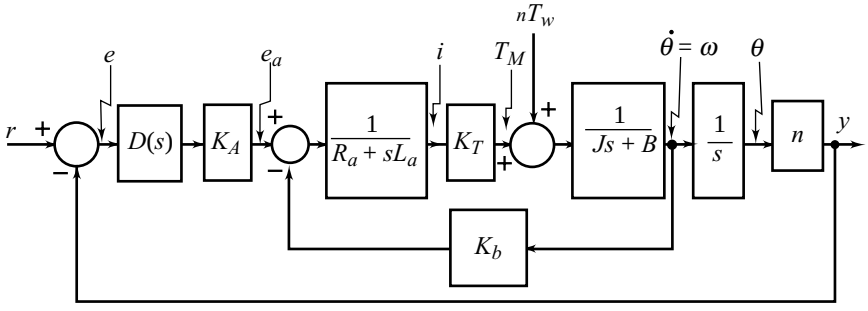

Fig. 10.34 Block diagram of an electromechanical servomechanism

The power amplifier is characterized by the parameter K_A. The possibility of loading problem is evident. We assume here that the amplifier has been tested and qualified for its $e(t)$ to $e_a(t)$ performance when it is loaded by the motor. In a position control application, the amplifier must be capable of supplying both positive and negative $e_a(t)$. This requirement demands careful electronic design to achieve a smooth transition between the positive and negative regions of operation without a *deadzone* (refer Chapter 14) in the static e_a–e relation in the transition region. The amplifier must also be capable of supplying the instantaneous power required to move the load. The current output of the amplifier is usually limited (*saturation* (refer Chapter 14)) in order to prevent damage to amplifier and motor.

R_a is the resistance of the circuit in which armature current circulates which includes the resistance of armature winding plus the contact resistance of the brushes wiping the sliding contacts. We assume R_a to be constant when the motor is turning (speed $\omega(t)$). L_a denotes the self-inductance of the armature circuit. $K_b\omega(t)$ is the back emf.

Let us now look at the mechanical side of the motor. Torque developed on the shaft is $K_T i(t)$. It drives the load through a single-mesh gear train of ratio n (We will neglect *backlash* (refer Chapter 14) introduced by the gear train). The load torque is assumed to be contributed by a rotating mass with moment of inertia J_L about the load axis. In addition to the load, the controlled plant will be subjected to unwanted disturbance T_w on the output shaft.

J_M is the moment of inertia of the motor shaft and all massive parts that are rigidly attached to it, excluding those of the load. B_M is viscous-damping coefficient resulting in velocity-dependent torque $B_M\omega(t)$ on the shaft. Note that the velocity-dependent torque is, in general, a nonlinear function of $\omega(t)$. Its approximation by a linear function is based on the following justification: servomotors which are machines intended for position control applications, are designed with low-friction bearings and with attention given to minimizing brush friction (*Coulomb friction* (refer Chapter 14)). In the moderate speed range, the torque-speed curve is nearly a straight line for most servomotors.

The numerical values of the physical parameters of the system are:

$$K_A = 4.1545 \text{ V/V}; \; R_a = 3.086 \; \Omega; \; L_a = 0.01 \text{ H}$$

$K_T = 0.0952$ N-m/amp; $K_b = 0.0952$ V/(rad/sec)

$J_M = 2.119 \times 10^{-5}$ kg-m^2; $B_M = B = 47.5 \times 10^{-5}$ N-m/(rad/sec)

$n = 1/10.5$; $J_L = 227.272 \times 10^{-5}$ kg-m^2

Moment of inertia reflected on the motor shaft

$$J = J_M + n^2 J_L = 4.1804 \times 10^{-5}$$

The moments of inertia of the gears are negligible. The position transducer on the output shaft has a scale factor of 1 V/rad.

Figure 10.35 shows the reduced block diagram model of the servomechanism (numerical values have been rounded slightly). This linear model produces analytical results that predict experimental behaviour to a satisfactory degree. Nevertheless, in some cases, the presence of *nonlinearities* and *uncertainties* in model parameters yields experimental dynamic behaviour that is substantially different from that predicted by analytical results based on linear model of the form shown in Fig. 10.34.

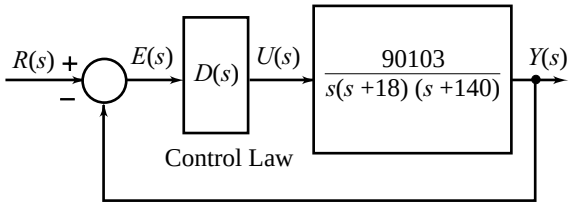

Fig. 10.35 Reduced block diagram obtained from Fig. 10.34 with $T_w = 0$

The nonlinearities we have neglected, are:

- Deadzone in amplifier characteristics
- Saturation in amplifier output
- Backlash in gears
- Coulomb friction

Simulation of the system model that includes one or more nonlinearities listed above may be used to predict experimental dynamic behaviour. Refer Chapter 14 for details.

In the model of Fig. 10.34, we have assumed that the physical parameters of the amplifier, motor, gears and load are known and fixed. In many practical cases, the numerical values of these parameters are not precisely known; also after the system is placed in service, the parameters may change owing to wear or variations in the operating environment. The system is *robust* if its performance remains satisfactory in the event of such uncertainties and changes. Considerable research effort is being expanded on the difficult problem of analytically representing the effects of uncertainties and changes in physical parameters in order to quantitatively assess the robustness of a control system.

In some cases, only a single parameter changes over a known range of values, and in such a case it is possible to calculate the robustness of the system with respect to the changes in the parameter if these changes occur slowly. As an example, consider the servomechanism of Fig. 10.34. One of the parameters is the moment of inertia of the load J_L, which is 227.272×10^{-5} kg-m^2. We consider this to be uncertain parameter whose actual value is $J_L = 227.272\Delta \times 10^{-5}$ kg-m^2. $\Delta = 1$ corresponds to the nominal plant model.

We begin the design process by examining the system of Fig. 10.35 with simplest form of control law; $D(s) = K_c$. Assume that overshoot is required to be less than 20%. The estimated value of K_c is obtained from the Bode plot, requiring $\Phi M \cong 48°$ (corresponding to $\zeta = 0.456$). We find $K_c = 19.4$. The bandwidth for this value of K_c is $\omega_b = 108$ rad/sec. From the transient response of the closed-loop system with $K_c = 19.4$, we find peak overshoot $M_p = 20.4\%$ and settling time $t_s = 0.103$ sec.

Let us now examine the steady-state behaviour corresponding to $K_c = 19.4$.

$$G(s) = \frac{90105 D(s)}{s(s+180)(s+140)}$$

$$K_v = \lim_{s\to 0} sG(s) = \frac{90105D(0)}{140 \times 180}$$

For $D(0) = 19.4$, $K_v = 69.3665$.

We have the following design criteria to judge the performance of our servomechanism:

- Phase margin (indicative of relative stability)
- Bandwidth (indicative of speed of response)
- Steady-state error in response to ramp command inputs (Steady-state error in response to step command inputs is zero).

We now examine steady-state error to disturbances. Suppose that the load shaft in our application is subjected to extraneous torque due to environmental conditions. This torque will displace the load shaft from its desired position. Assume that an assessment of the position error due to this disturbance torque shows that a new control law design providing a static gain $D(0) \geq 210$ will reduce the error to an acceptable level.

From Fig. 10.34, we get (numerical values have been rounded slightly)

$$\left.\frac{Y(s)}{T_w(s)}\right|_{R(s)=0} = \frac{217(s+309)}{s(s+140)(s+180)+90{,}105D(s)}$$

The steady-state error resulting from a step disturbances torque $T_w(s) = A/s$, can be determined by inspection of the equation:

$$y_{ss} = \frac{217 \times 309 \times A}{90{,}105\, D(0)} = \frac{0.74 \times A}{D(0)}$$

Since $K_v = 90{,}105D(0)/140 \times 180$, the requirement on $D(0)$ ($D(0) \geq 210$) is met if the new control law design provides $K_v \geq 750$.

Steady-state error e_{ss} to ramp command inputs will be less than 1/750, which we consider acceptable. The transient response achieved in the new design should be approximately as favourable as with the design with $D(s) = K_c = 19.4$.

For the nominal plant, the lag compensator

$$D(s) = \frac{17.05(s+5)}{(s+0.2)}$$

meets this requirement. It can be easily verified that for the lag-compensated system

$\Phi M = 46.8$; $\omega_b = 99.3$; $K_v = 1524.1$; $M_p = 25.7\%$; and $t_s = 0.286$ sec.

The K_v achieved here, which exceeds the required level by about 100%, is 22 times greater than the system with $D(s) = K_c = 19.4$; although the response is slightly slower in the compensated system. The slower response could be unsatisfactory in some applications. Because the lag compensator provided a remarkable increase in K_v, we wish to retain that feature in the design of the new control law. We may attempt to supplement that feature with a lead compensator that can meet the speed of response requirement.

Variations in performance parameters for Δ ranging from 0.25 to 3 are given below (obtained from Nichols chart).

Phase margin : 57.5° to 31.5°
Gain margin : 14.3 dB to 13.2 dB
Bandwidth : 113 rad/sec to 74.5 rad/sec

This gives a useful analysis of the robustness of the system with respect to a wide variation in the design value of J_L.

The performance features given above are valid only if the amplifier-motor operates in its linear range. The current output of the amplifier is usually limited in order to prevent damage to the amplifier and the motor. A limit of about 5 amps is typical for the amplifier-motor combination in this example. A MATLAB/Simulink simulation will be quite helpful for this analysis (Appendix A). Construct Simulink diagram for the electromechanical system of Fig. 10.34 with $D(s) = [17.05(s + 5)]/(s + 0.2)$. Connect the 'source' to the error point 'e' (with $r = 0$) and increase e in steps till the armature current i is found to exceed 5 amps. This value is 0.29 volts (refer Problem A.16 in Appendix A). The corresponding amplifier output e_a does not exceed 20.8 volts. Therefore the linearity range for which the armature current is limited to 5 amp is 0 – 0.29 volts. (This equivalently amounts to a limitation on step commands: 0 – 0.29 rad.)

Now simulate the closed-loop system of Fig. 10.34 after cascading a saturation block with the amplifier, i.e., replace K_A block with the blocks shown in Fig. 10.36. This simulation study will reveal the effect of exceeding linearity range on the performance of the closed-loop system (refer Problem A.17 in Appendix A).

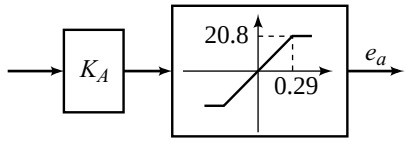

Fig. 10.36

Review Questions

10.1 Discuss the compensation characteristics of cascade lag and lead compensators using Bode plots. Show that

(a) lead compensation is suitable for systems having unsatisfactory transient response, and it provides a limited improvement in steady-state performance; and
(b) lag compensation is suitable for systems with satisfactory transient response but unsatisfactory steady-state response.

10.2 Sketch op amp circuits capable of providing

(a) phase lead;
(b) phase lag; and
(c) phase lead and lag over different frequency bands.

Determine transfer function model of each circuit and draw Bode plot for each model.

10.3 The transfer function of a lag-lead compensator is given by

$$D(s) = \underbrace{\left[\frac{\tau_1 s + 1}{\beta\tau_1 s + 1}\right]}_{\text{Lag Section}}\underbrace{\left[\frac{\tau_2 s + 1}{\alpha\tau_2 s + 1}\right]}_{\text{Lead Section}}; \beta > 1,\ \alpha < 1,\ \tau_1,\ \tau_2 > 0$$

Give an op amp circuit that realizes this $D(s)$.

10.4 Sketch op amp circuits capable of realizing

(a) PD control action;
(b) PI control action; and
(c) PID control action.

Determine transfer function model of each circuit and draw Bode plot for each model.

Problems

10.1 The open-loop transfer function of a control system is

$$G(s)H(s) = \frac{1}{s(1+0.5s)(1+2s)}$$

(a) Determine approximate values of gain margin and phase margin.
(b) If a lag compensator with transfer function $D(s) = K_c(1 + 3s)/(1 + 5s)$ is inserted in the forward path, find the value of K_c to keep the gain margin unchanged.

MATLAB Exercise After solving the problem using hand sketches, attempt it using MATLAB. Determine settling time and peak overshoot of the compensated and uncompensated systems.

10.2 The open-loop transfer function of a control system is

$$G(s)H(s) = \frac{10}{s(1+0.5s)(1+0.1s)}$$

(a) Draw the Bode plot and determine gain crossover frequency, and phase and gain margins.
(b) A lead compensator with transfer function $D(s) = (1 + 0.23s)/(1 + 0.023s)$ is now inserted in the forward path. Determine the new gain crossover frequency, and phase and gain margins. Comment upon the effects of lead compensation on system performance.

MATLAB Exercise After completing the hand sketches, verify your results using MATLAB. Determine the bandwidth, resonance peak and resonance frequency of the uncompensated and compensated systems.

10.3 The block diagram of Fig. P10.3 represents a position control system. You have been given the task of designing the compensation $D(s)$.

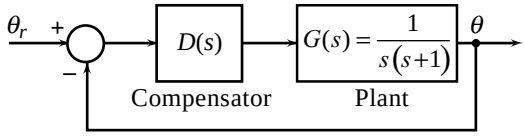

Fig. P10.3

(a) Consider first $D(s) = K$. What value of K would provide velocity error constant $K_v = 12$?
(b) For the value of K in part (a), determine phase margin ΦM, bandwidth ω_b, resonance peak M_r, and resonance frequency ω_r.
(c) Next consider $D(s) = K\dfrac{\tau s + 1}{\alpha\tau s + 1}$. With the parameter K set for K_v of 12, choose $\tau > 0$, and $\alpha < 1$ so that ΦM is greater than 40°.
(d) For the value of $D(s)$ in part (c), determine ΦM, ω_b, M_r, and ω_r.

MATLAB Exercise Verify and refine your design using MATLAB. Determine settling time and peak overshoot of the compensated system.

10.4 Consider the system shown in Fig. P10.3. It is desired to obtain a phase margin greater than 45°, and steady-state error less than 0.1 for a unit ramp input.

(a) Design a cascade lead compensator that meets the given specifications.
(b) Design a cascade lag compensator that meets the given specifications.
(c) Since an identical set of specifications can be met by lead as well as lag compensation, how do we make a choice of the compensation scheme?

MATLAB Exercise Verify and refine your designs using MATLAB. Determine settling time and peak overshoot of the compensated systems.

10.5 A unity-feedback control system has open-loop transfer function

$$G(s) = 1/s^2$$

The specifications for the system are:
Settling time $t_s \leq 4$ sec
Peak overshoot for a step input $\leq$ 20%

(a) Design a suitable cascade lead, lag, or lag-lead compensator to realize the given objectives.
(b) Design a suitable PD, PI, or PID compensator to realize the given objectives.

MATLAB Exercise Convert the specifications to frequency domain using second-order correlations. After completing the design by hand sketches, verify the design using MATLAB. Obtain the time response of the compensated system and check whether time-domain requirements are satisfied. If found necessary, refine the design.

10.6 An uncompensated control system with unity feedback has a plant transfer function

$$G(s) = \frac{K}{s(s+2)}$$

It is desired to have a steady-state error for a ramp input less than five per cent of the magnitude of ramp. It is also desired that the phase margin of the system be at least 45° and the closed-loop bandwidth greater than 10 rad/sec. Design a cascade lead compensator to yield the desired specifications.

MATLAB Exercise Verify and refine your design using MATLAB. Determine settling time and peak overshoot of the compensated system.

10.7 For the system of Problem 10.6, design a cascade lag compensator to yield the desired specifications, with the exception that a bandwidth equal to or greater than 2 rad/sec will be acceptable.

MATLAB Exercise Attempt this problem using MATLAB dialogues.

10.8 An uncompensated control system with unity feedback has a plant transfer function

$$G(s) = \frac{K}{s(1+0.1s)(1+0.2s)}$$

The system must satisfy the following performance specifications:

(i) The magnitude of the steady-state error of the system due to a unit ramp function input is 0.01.
(ii) Phase margin $\geq 40°$.

Use two identical cascaded lead compensators to compensate the system. Justify the use of two-stage lead compensator.

MATLAB Exercise Attempt this problem using MATLAB dialogues. Include root-locus analysis and simulation study of your design. Redesign if found necessary.

10.9 Consider the problem of design of angular control system of a robot's joint. A block diagram of the system is shown in Fig. P10.9. The performance specifications of the system are as follows:

(i) The steady-state error due to ramp input should be less than or equal to one per cent.
(ii) The phase margin of the system should be greater than 45°.

Design a cascade lead compensator to yield the desired specifications. Determine the resonance peak M_r, and the bandwidth ω_b of the compensated system.

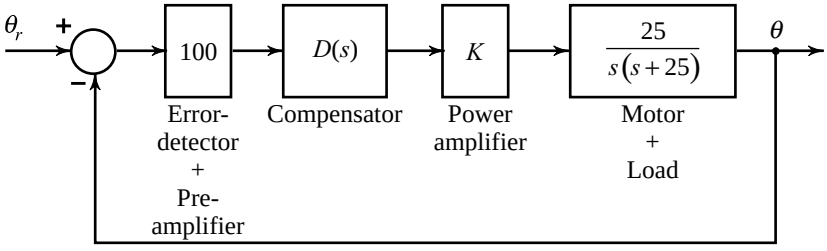

Fig. P10.9

MATLAB Exercise (i)You have neglected the time-constant of the power amplifier. Check the robustness of your design with respect to this modelling approximation. Determine the range of amplifier time-constant for which your design gives acceptable performance (ii) Set up block diagram of the system in Simulink window and study the saturation effects of the amplifier. Determine the linear range of the amplifier for which your design gives acceptable performance.

10.10 For the system of Problem 10.9, design a cascade lag compensator to yield the desired specifications. Determine the resonance peak M_r, and the bandwidth ω_b of the compensated system.

MATLAB Exercise Attempt this problem using MATLAB dialogues. Include root-locus analysis and simulation study of your design. Redesign if found necessary.

10.11 A unity-feedback system has an open-loop transfer function

$$G(s) = \frac{5}{s(s+1)(0.5s+1)}$$

It is desired to obtain the phase margin of atleast 40° and the gain margin of atleast 10 dB without sacrificing the velocity error constant of the system.

(a) Design a suitable cascade lead, lag, or lag-lead compensator to realize the given objective. Give reasons for your choice of the compensation scheme.
(b) Design a suitable PD, PI or PID compensator to realize the given objectives. Give reasons for your choice of the compensation scheme.

MATLAB Exercise Attempt this problem using MATLAB dialogues. Include root-locus analysis and simulation study of your design. Redesign if found necessary.

10.12 The block diagram of Fig. P10.12 represents a position control system. You have been given the task of designing the compensation $D(s)$ to meet the following specifications:
Velocity error constant, $K_v = 30$.
Phase margin, $\Phi M \geq 50°$.
Bandwidth, $\omega_b = 12$ rad/sec.

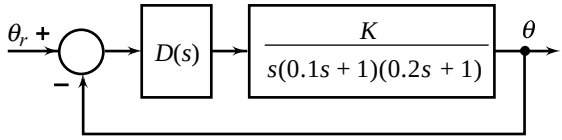

Fig. P10.12

(a) Show that if lead compensation is employed to meet the K_v and ΦM requirements, the bandwidth will be larger than the specified value, resulting in a system sensitive to noise.
(b) Show that if lag compensation is attempted to meet the K_v and ΦM requirements, the bandwidth will fall short of the specified value, resulting in a sluggish system.
(c) Design a suitable lag-lead compensator that meets the specifications on K_v, ΦM, and ω_b.

MATLAB Exercise Attempt this design problem using MATLAB dialogues. Many iterations may be required to meet the design objectives.

10.13 For the position control system shown in Fig. P10.13, design a lead compensator to yield a $K_v = 40$, and a 20% overshoot in the transient response for a step input, with a peak time of 0.1 second. Use only frequency domain methods.

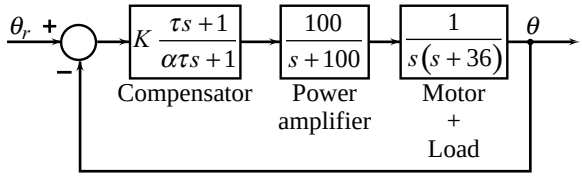

Fig. P10.13

MATLAB Exercise You have employed second-order correlations to solve this problem using hand sketches. Verify your solution using MATLAB, and if required refine your design. Due to uncertainties in the load, the time-constant of motorload may vary by 10%. Check the robustness of your design determining transient and steady-state performance for various values of this time-constant.

10.14 The open-loop transfer function of a unity-feedback system is

$$G(s) = \frac{K}{s(s+10)^2}$$

It is specified that the velocity error constant of this system be equal to 20, while the damping ratio of the dominant roots be equal to 0.707.

(a) It is not advisable to compensate this system by a single-stage cascade lead compensator. Why?
(b) Design a cascade lag compensator to meet the given performance specifications. Use only frequency-domain methods.
(c) Determine the bandwidth of the compensated system.

The –3 dB contour of the Nichols chart may be constructed using the following table.

Phase, degrees	0	– 30	– 60	– 90	– 120	– 150	– 180	– 210
Magnitude, dB	7.66	6.8	4.18	0	– 4.18	– 6.8	– 7.66	– 6.8

10.15 A unity-feedback type-0 system with dead-time has a forward path transfer function

$$G(s) = \frac{10\,e^{-0.02s}}{(0.5\,s+1)(0.1\,s+1)(0.05\,s+1)}$$

Design a suitable compensation scheme so that the system acquires a damping ratio of 0.4 without loss of steady-state accuracy. Use only frequency-domain methods.
Estimate the bandwidth and the settling time of the compensated system.

MATLAB Exercise You have employed second-order correlations to solve this problem using hand sketches. Verify your solution using MATLAB, and if required refine your design.

10.16 Consider the servo system shown in Fig. P10.16.

(a) Sketch the Bode plot of $G(s)$ when $D(s) = 1$. Find the phase margin of the uncompensated system.

(b) The second-order compensator

$$D(s) = \frac{s^2 + 0.8\,s + 4}{(s+0.384)(s+10.42)}$$

cancels the complex poles of the process transfer function $G(s)$. Find the phase margin of the compensated system. What is the effect of $D(s)$ on the steady-state performance of the system?

(c) The closed-loop system is required to have a phase margin of at least 70° without sacrificing the steady-state performance of the system. If the cancellation-compensation proposed in part (b) cannot meet the phase-margin requirement, add a stage of lead compensator to further improve the relative stability of the system.

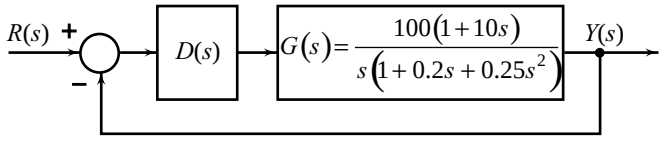

Fig. P10.16

MATLAB Exercise The parameter K_t is subject to variations by 10%. Check by simulation the robustness of the closed-loop system to these variations by determining phase margin and K_v for various values of K_t.

10.17 Consider the position control system of Fig. P10.17.

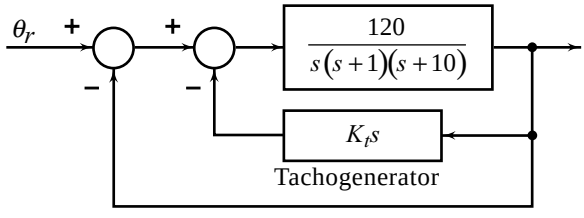

Fig. P10.17

Show that $K_t = \frac{1}{8}$ provides approximately 25° phase margin. Find K_v of the compensated system.

Digital Control Systems

11

11.1 INDUSTRIAL AND EMBEDDED CONTROL

A control system is an implemented strategy used to cause a physical system, or *plant*, to behave in a desired manner. Closed-loop control uses feedback measurements to correct error between the plant output and a reference input, *i.e.*, to provide the desired behaviour. As the feedback control strategy increases in complexity, it becomes more difficult to apply analog components for its implementation. In modern control systems, the control strategy is thus typically implemented in software. A digital computer determines the input to manipulate the plant; and this requires facilities to apply this input to the physical world. In addition, the control strategy typically relies on measured values of the plant behaviour that have to be made available to the computing resources.

Because the controller operates in the low-power electronics domain and the plant operates in high-power hydraulics, mechanics, thermal, and other physical domains, transducers are needed to convert between controllers and plant. These transducers are used either by *actuators*, to drive the plant with controller-computed values, or by *sensors*, to provide measurements to the low-power electronics domain. In addition to the transformation between high- and low-power domains, transformations between discrete-time and continuous-time behaviour are required. The plant dynamics change continuously with time. The controller, however, has a discrete clock that governs its behavior, and so its values change only at discrete points in time. To ensure data integrity, the sensor must include a mechanism to sample continuous data from the plant at discrete points in time, while the actuators need to provide a continuous value between the time points of discrete-time data from the controller.

Computer interfacing for data acquisition consists of analog-to-digital (A/D) conversion of input (to the controller) analog signals. Prior to the conversion, the analog signal has to be conditioned to meet the input requirements of the A/D converter. Signal conditioning consists of amplification (for sensors generating very low power signals), and filtering (to limit the amount of noise in the signal). Conversion of a digital signal to on analog signal (D/A) at the output (of the controller) is to be carried out to send this signal to an actuator which requires an analog signal. The signal has to be amplified by a transistor or solid state relay or

power amplifier. Most manufacturers of electronic instrumentation devices are producing signal conditioners as modules. The immersion of the computing power into the physical world has changed the scene of control system design. A comprehensive theory of digital control has been developed.

The broad space of control applications can be roughly divided into two categories: *industrial control* and *embedded control*. Industrial or process control applications are those in which control is used as part of the process of creating or producing an end-product. The control system is not a part of the actual end-product itself. Examples include the manufacture of pharmaceuticals and the refining of oil. In the case of industrial process control, the control system must be robust and reliable, since the processes typically run continuously for days, weeks or years.

Embedded control applications are those in which the control system is a component of the end-product itself. For example, Electronic Control Units (ECUs) are found in a wide variety of products including automobiles, airplanes, and home appliances. Most of these ECUs implement different feedback control tasks, for instance, engine control, traction control, anti-lock braking, active stability control, cruise control, and climate control. While embedded control systems must also be reliable, cost is a more significant factor, since the components of the control system contribute to the overall cost of manufacture of the product. In this case, much more time and effort is usually spent in the design phase of the control system to ensure reliable performance without requiring any unnecessary excess of processing power, memory, sensors, actuators etc., in the digital control system. Our focus in this book has been on industrial control applications.

Perhaps more than any other factor, the development of microprocessors has been responsible for the explosive growth of the computer industry. A microprocessor is a computer on a chip. While early microprocessors required many additional components in order to perform any useful task, the increasing use of large-scale integration (LSI) and very large-scale integration (VLSI) semiconductor fabrication techniques has led to the production of microcomputers, where all of the required circuitry is embedded on one or a small number of integrated circuits. A further extension of the integration is the single chip microcontroller, which adds analog and binary I/O, timers and counters, so as to be able to carry out real-time control functions with almost no additional hardware. The major types of microcontrollers are (i) embedded 8-bit microcontrollers, (ii) 16-to-32-bit microcontrollers, and (iii) digital signal processors (DSPs). Because of DSP's special architecture, it is more useful than a general-purpose microprocessor for high-speed processing applications.

Why would any one want to use a microcontroller when there exists a powerful PC that can be programmed to perform almost any computer-related task? The main reasons for selecting microcontrollers over PCs are the cost and the size. For many applications, a moderate amount of local computer-processing power is required. A PC would not be a good choice for such applications. Cost-effective microcontrollers are ideal for such applications. Attractive compactness of microcontrollers is another factor which dictates the choice.

Today, most complex industrial processes are under computer control. We call a complete installation (hardware and software) a SCADA (*Supervisory Control and Data Acquisition*) system. SCADA systems adopt a multilevel or hierarchical view point of control strategy. The multilevel approach subdivides the system into a hierarchy of simpler control design problems. On the lowest level of control (*direct process control level*), closed-loop control functions based on directives from the next 'higher' level are handled. The higher levels are: *supervisory level, production scheduling and control level, and plant management level*; the plant management level being the 'highest' hierarchical level of the plant automation system. The direct process control functions are delegated to special control units connected to the SCADA systems. Hierarchical, distributed, flexible and extremely powerful *Computer Integrated Process System* (CIPS) is now a technical reality.

A quiet revolution is going on in the manufacturing world as well, that is changing the look of the factory. Computers are controlling and monitoring the manufacturing processes. The high degree of automation that until recently was reserved for mass production only, is applied now also to small batches. This requires a change from hard automation in the production line to a *flexible manufacturing system* which can be more readily rearranged to handle new market requirements. Flexible manufacturing systems, combined with automatic assembly and product inspection on one hand, and CAD/CAM systems (Computer-Aided Design/ Computer-Aided Manufacturing) on the other, are the basic components of the modern *Computer Integrated Manufacturing System* (CIMS). In a CIMS, the production flow, from the conceptual design to the finished product, is entirely under computer control and management. CIMS also adapts a multilevel or hierarchical view point of control strategy which subdivides the system into a hierarchy of simpler control design problems. The lowest level of this structure contains stand-alone control systems of manufacturing processes and industrial robots. This includes all types of machine tools, welding, electrochemical machining, etc. The stand-alone control systems have a proper interfacing with the higher levels of hierarchy: *supervisory level*, *production scheduling* and *control level*, and *plant management level*.

The strength of PC-based solutions comes from being able to provide an extremely wide range of measurements and record, and analyze the resultant data with high real-time speed. The CIPS and CIMS employ such solutions. Plug-in (in expansion slots) data acquisition and control boards (called add-on boards) are available for many popular computers.

PC-based monitoring and control systems using textual and graphical programming are today in use. The user familiarity with a computer-aided package like MATLAB allows easy adaptation of textual programming. Graphical programming permits the utilization of graphical components for assembling systems, and simplifies the development of monitoring and control programs. LabVIEW Real-Time provides a single software development tool that can implement the functions of PC-based control systems.

With the option of calculating the control signal in software (microcontrollers) rather than hardware (op amps), a digital controller gives the designer much more flexibility in making modifications to the control law after the hardware design (actuators, sensors, etc.) is fixed. In many applications, hardware and software designs can proceed almost independently.

In general, the design of control systems using a microcontroller requires a sophisticated use of new concepts such as z-transform. It is however quite straight forward to translate an analog design into a digital equivalent. Digital controller differs from analog control in that the signals must be *sampled* and *quantized.* A continuous-time signal to be used in digital logic needs to be sampled first (with sampling period T sec), and then each sample needs to be converted into a quantized digital number by an A/D converter. Once the digital computer has calculated the proper next control signal value, this value needs to be converted back to an analog signal by a D/A converter in order to be applied to the actuator of the process.

In Sections 11.2–11.6 of this chapter, we will describe a simple technique for finding a sampled equivalent to a given analog compensator. Finding a discrete equivalent to a given analog compensator is equivalent to finding a recurrence equation for the samples of the controller which will approximate the transfer function of the analog device. The method requires the sampling period T sec being short enough so that the reconstructed (output of D/A converter) control signal is close to the signal that the original analog compensator would have produced. The rest of the chapter deals with direct digital design using z-transforms. This route of design, as we shall see, relaxes the need for a very short sampling interval; thereby giving us flexibility in terms of selection of digital hardware for implementation of design.

11.2 USE OF DIGITAL COMPUTER AS A COMPENSATOR DEVICE

In recent years, there has been a rapid increase in the use of digital computers in control systems. In fact, many industrial control systems include digital computers as an integral part of their operation. Also the availability of low-cost microprocessors and microcomputers has established a new trend towards the use of digital computers even in small-scale control systems, including those for automobiles and household appliances.

11.2.1 Advantages Offered by Digital Control

1. The accuracy of analog control systems is often limited. For example, if an analog compensator is to be built using a resistor with resistance 980.5 ohms and a capacitor with capacitance 81.33 microfarads, it would be difficult and expensive to obtain components with exactly these values. In digital control systems, the accuracy of a digital compensator can be increased simply by increasing the number of bits.
2. Digital signals are coded in sequences of '0' and '1', which represent ranges of voltages. This representation is less susceptible to noise and drift of power supply.
3. Due to the growth of very large scale integration (VLSI) technology, the price of digital systems has been constantly decreasing during the last decade. Now the use of a digital computer or microprocessor is cost-effective even for small control systems.
4. An important advantage offered by digital control is in flexibility of modifying controller characteristics, or of adapting the controller if plant dynamics change with operating conditions. The ability to 'redesign' the controller by changing software (rather than hardware) is an important feature of digital control over analog control.
5. If a digital computer is used, it can be used not only as a compensator but also to collect data, to carry out complex computations, and to monitor the status of the controlled system. To enable the computer to meet the variety of demands imposed on it, it is time-shared among its tasks.
6. Implementation of nonlinear and/or time-varying control laws, and adaptive control schemes was earlier constrained by the limitations of analog controllers and high cost of digital computers. However, with the advent of inexpensive digital computers with virtually limitless computing power, advanced control techniques are now being put to practice.
7. The study of emerging applications shows that artificial-intelligence (AI) will affect design and application of control systems as profoundly as the impact of microprocessor has been in the last decade. It is clear that future generation control systems will have a significant AI component; the list of applications of computer-based control will continue to expand.

11.2.2 Implementation Problems in Digital Control

The main problems associated with the implementation of digital control are related to the effects of sampling and quantization.

Most processes that we are called upon to control operate in continuous time. This implies that we are dealing largely with an analog environment; to this environment we must interface the digital computer through which we seek to influence the process.

The interface is accomplished by a system of the form shown in Fig. 11.1. It is a cascade of the A/D conversion system followed by a computer

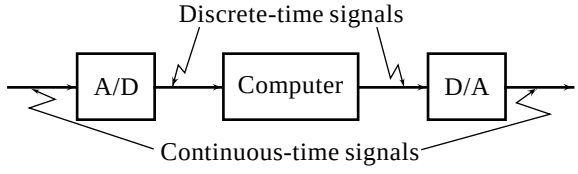

Fig. 11.1 Discrete-time processing of continuous-time signals

followed by a D/A conversion system. The A/D conversion process involves deriving samples of the analog signal at discrete instants of time separated by sampling period T sec. The D/A conversion process involves reconstructing a continuous-time signal from the samples given out by the digital computer.

Quantization Effects The conversion of signals from analog into digital form and *vice versa* is performed by electronic devices (A/D and D/A converters) of finite resolution. A device of n-bit resolution has 2^n quantization levels and the analog signal gets tied to these finite number of quantization levels in the process of conversion to digital form. Therefore, by the sheer act of conversion, a valuable part of information about the signal is lost.

Furthermore, any computer employed as a real-time controller must perform all of the necessary calculations with a limited precision, thus introducing a truncation error after each arithmetic operation has been performed. As the computational accuracy is normally much higher than the resolution of real converters, a further truncation must take place before the computed data are converted into the analog form. The repeated process of approximate conversion—computation—conversion may be costly, if not disastrous, in terms of control system performance.

Sampling Effects Selection of sampling period T is a fundamental problem in digital control systems. The *sampling theorem* (refer Section 11.10) states that a continuous-time signal whose frequency spectrum is bounded by upper limit ω_m, can be completely reconstructed from its samples when the sampling frequency $\omega_s = 2\pi/T > 2\omega_m$. There are two problems associated with the use of sampling theorem in practical control systems.

1. Frequency spectra of real signals do not possess strictly defined bandwidth ω_m. There are almost always frequency components outside the 3 dB-bandwidth ω_b. Therefore, the selection of the sampling frequency ω_s using the sampling theorem on the basis of system bandwidth ($\omega_b = \omega_m$) will result in information loss due to sampling.
2. Ideal lowpass filter needed for distortionless reconstruction of the continuous-time signal from its samples, is not physically realizable. Practical devices, such as D/A converters, introduce distortions.

Thus the process of sampling and reconstruction affects the amount of information available to the plant, and degrades control system performance. The ill-effects of sampling can be reduced, if not eliminated completely, by sampling at a very high rate. As a signal is sampled more frequently, adjacent samples have more or less similar magnitudes. In order to realize the beneficial effects of shorter sampling, longer word lengths are needed to resolve the differences between adjacent samples. Excessively fast sampling ($T \to 0$) may, however, result in numerical ill-conditioning in implementation of recursive control algorithms.

With the availability of low-cost, high-performance digital computers and interfacing hardware, the implementation problems in digital control do not pose a serious threat to its usefulness; the advantages of digital control outweigh its disadvantages for most of the applications.

11.3 CONFIGURATION OF THE BASIC COMPUTER-CONTROL SCHEME

Figure 11.2 depicts a block diagram of a computer-controlled system showing a configuration of the basic control scheme. The basic elements of the system are shown by the blocks.

The analog feedback signal coming from the sensor is converted into digital form by an A/D converter. The A/D converter converts a voltage (or current) amplitude at its input into a binary code representing a quantized amplitude value closest to the amplitude of the input.

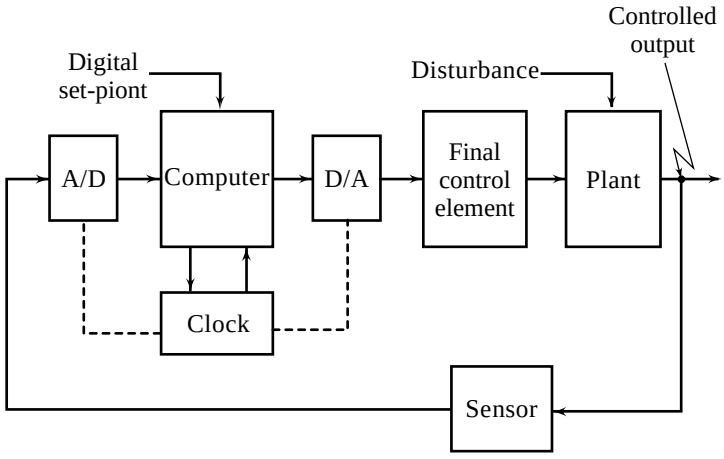

Fig. 11.2 Configuration of the basic digital control scheme

The digital computer processes the sequence of numbers by means of an algorithm and produces a new sequence of numbers. Since data conversions and computations take time, there will always be a delay when a control law is implemented using a digital computer. The delay, which is called the *computational delay*, degrades the control system performance. It should be minimized by a proper choice of hardware and by a proper design of software for the control algorithm. Floating-point operations take a considerably longer time to perform (even when carried out by arithmatic co-processor) than the fixed-point ones. We therefore try to execute fixed-point operations whenever possible.

The D/A conversion system in Fig. 11.2 converts the sequence of numbers in numerical code into a piece-wise continuous-time signal. The output of the D/A converter is fed to the plant through the actuator (final control element) to control its dynamics.

The basic control scheme of Fig. 11.2 assumes a uniform sampling operation, i.e., only one sampling rate exists in the system and the sampling period is constant. The real-time clock in the computer synchronizes all the events of A/D conversion → computation → D/A conversion.

The overall system in Fig. 11.2 is hybrid in nature; the signals are in a *sampled form* (*discrete-time signals*/*digital signals*) in the computer and in continuous-time form in the plant. Such systems have traditionally been called sampled-data control systems; we will use this term as a synonym to *computer control systems*/*digital control systems*.

11.4 PRINCIPLES OF SIGNAL CONVERSION

Figure 11.3a shows an analog signal $y(t)$—it is defined at a continuum of times, and its amplitudes assume a continuous range of values. Such a signal cannot be stored in digital computers; the signal therefore must be converted to a form that will be accepted by digital computers. One very common way to do this is to record sample values of this signal at equally spaced instants. If we sample the signal every 10 msec, for example, we obtain the *discrete-time signal* sketched in Fig. 11.3b. This *sampling interval* corresponds to a *sampling rate* of 100 samples/sec. The choice of sampling rate is an important one, since it determines how accurately the discrete-time signal can represent the original signal.

Notice that the time axis of the discrete-time signal in Fig. 11.3b is labelled simply ‘sample number’ and index k has been used to denote this number; $k = 0, 1, 2, \ldots$. Corresponding to different values of sample

number k, the discrete-time signal assumes the same continuous range of values assumed by the analog signal $y(t)$. We can represent the sample values by a sequence of numbers y_s (refer Fig. 11.3b):

$$y_s = \{1.7, 2.4, 2.8, 1.4, 0.4, \ldots\}$$

In general,

$$y_s = \{y(k)\},\ 0 \le k < \infty$$

where $y(k)$ denotes the kth number in the sequence.

The sequence defined above is a *one-sided sequence*; $y_s = 0$ for $k < 0$. In digital control applications, we normally encounter one-sided sequences.

Although, strictly speaking, $y(k)$ denotes the kth number in the sequence, the notation given above is often unnecessarily cumbersome, and it is convenient and unambiguous to refer to $y(k)$ itself as a sequence.

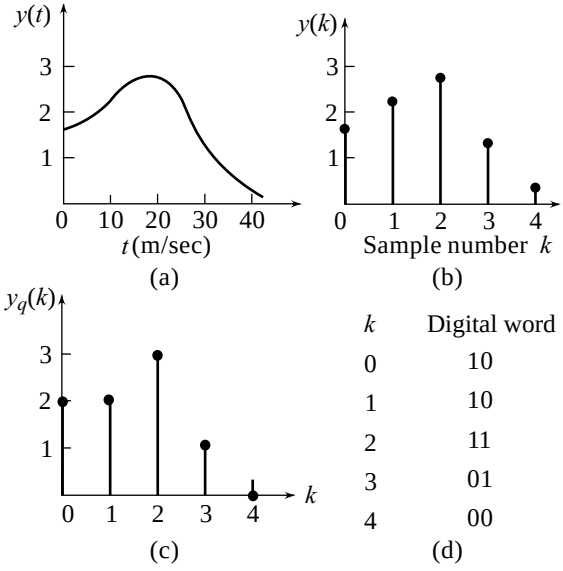

Fig. 11.3 Sampling, quantization, and coding of an analog signal

Throughout our discussion on digital control, we will assume *uniform sampling*, i.e., sample values of the analog signal are extracted at equally spaced sampling instants. If the physical time corresponding to the sampling interval is T seconds, then the kth sample $y(k)$ gives the value of the discrete-time signal at $t = kT$ seconds. We may, therefore, use $y(kT)$ to denote a sequence wherein the independent variable is physical time.

The signal of Fig. 11.3b is defined at discrete instants of time; the sample values are however tied to a continuous range of numbers. Such a signal, in principle, can be stored in an infinite-bit machine because a finite-bit machine can store only a finite set of numbers.

A simplified hypothetical two-bit machine can store four numbers given below:

Binary number	*Decimal equivalent*
00	0
01	1
10	2
11	3

The signal of Fig. 11.3b can therefore be stored in such a machine if the sample values are quantified to four *quantization levels*. Figure 11.3c shows a quantized discrete-time signal for our hypothetical machine. We have assumed that any value in the interval [0.5, 1.5) is rounded to 1, and so forth. The signals for which both time and amplitude are discrete, are called *digital signals*.

After sampling and quantization, the final step required in converting an analog signal to a form acceptable to digital computer is *coding* (or *encoding*). The encoder maps each quantized sample value into a digital word. Figure 11.3d gives a coded digital signal corresponding to the analog signal of Fig. 11.3a for our hypothetical two-bit machine.

The device that performs the sampling, quantization and coding is an *analog-to-digital* (A/D) *converter.* Figure 11.4 is a block diagram representation of the operations performed by an A/D converter.

It may be noted that the quantized discrete-time signal of Fig. 11.3c and the coded signal of Fig. 11.3d carry exactly the same information. For the purpose of an analytical study of digital systems, we will use the quantized discrete-time form for digital signals.

The number of binary digits carried by a device is its *word length*, and this is obviously an important characteristic related to the *resolution* of the device —the smallest change in the input signal that will produce a change in the output signal. The A/D converter that generates signals of Fig. 11.3 has two binary digits and thus four quantization levels. Any change, therefore, in the input over the interval [0.5, 1.5) produces no change in the output. With three binary digits, 2^3 quantization levels can be obtained, and the resolution of the converter would improve.

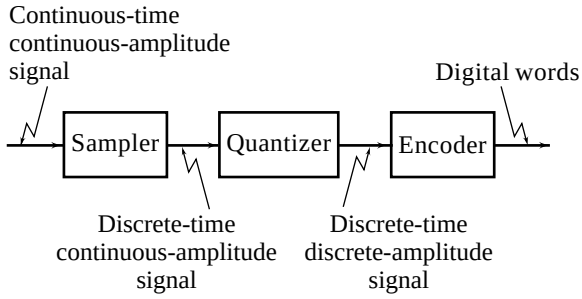

Fig. 11.4 Operations performed by an A/D converter

The A/D converters in common use have word length of 8 to 16 bits. For an A/D converter with a word length of eight-bits, an input signal can be resolved to one part in 2^8, or 1 in 256. If the input signal has a range of 10 V, the resolution is 10/256, or approximately 0.04 V. Thus, the input signal must change by at least 0.04 V in order to produce a change in the output.

With the availability of converters with resolution ranging from 8 to 16 bits, the quantization errors do not pose a serious threat in computer control of industrial processes. In our treatment of the subject, we assume quantization errors to be zero. This is equivalent to assuming infinite-bit digital devices. Thus, we treat digital signals as if they are discrete-time signals with amplitudes assuming a continuous range of values. In other words, we make no distinction between the words 'discrete-time' and 'digital'.

A typical topology of a single-loop digital control system is shown in Fig. 11.2. It has been assumed that the measuring transducer and the actuator (final control element) are analog devices requiring, respectively, A/D and D/A conversion at the computer input and output. The D/A conversion is a process of producing an analog signal from a digital signal and is, in some sense, the reverse of the sampling process discussed above.

The *digital-to-analog* (D/A) *converter* performs two functions; first, generation of output samples from the binary-form digital signals produced by the machine, and second, conversion of these samples to analog form. Figure 11.5 is a block diagram representation of the operations performed by a D/A converter. The decoder maps each digital word into a sample value of the signal in discrete-time form. It is usually not possible to drive a load, such as a motor, with these samples. In order to deliver sufficient energy, the sample amplitude might have to be so large that it is infeasible to be generated. Also, large-amplitude signals might saturate the system being driven.

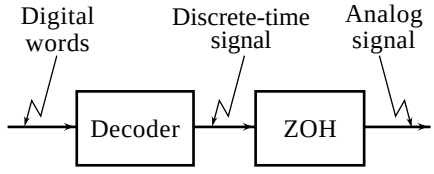

Fig. 11.5 Operations performed by a D/A converter

The solution to this problem is to smooth the output samples to produce a signal in analog form. The simplest way of converting a sample sequence into a continuous-time signal is to hold the value of the sample until the next one arrives. The net effect is to convert a sample to a pulse of duration T, the sampling period. This function of a D/A converter is referred to as a *zero-order hold* (ZOH) operation. The term *zero order* refers to the zero-order polynomial used to extrapolate between the sampling times. Figure 11.6 shows a typical sampled sequence produced by the decoder, and the analog signal resulting from the ZOH operation.

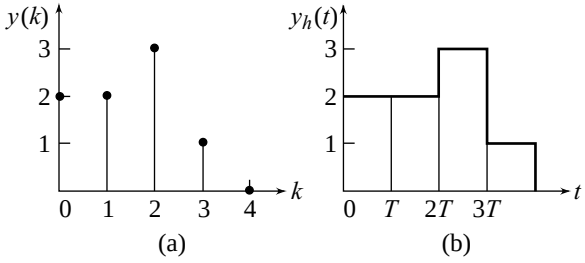

Fig. 11.6 (a) Sampled sequence; (b) Analog output from ZOH

Figure 11.7 represents a model of a unity-feedback digital control system. This representation is useful for the purpose of analytical study of digital control systems. The sampler which samples continuous-time signal $e(t)$ every T secs, is a model of A/D converter, and the ZOH which constructs a continuous-time signal from a discrete-time output of digital control algorithm, is a model of D/A converter.

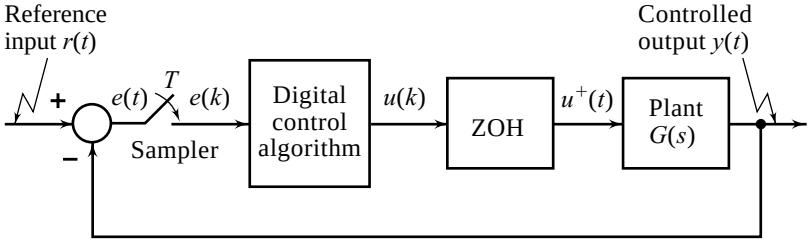

Fig. 11.7 Analytical model of a unity-feedback digital control system

11.5 SHAFT-ANGLE ENCODERS FOR DIGITAL MEASUREMENT OF SHAFT POSITION/SPEED

Recall the configuration of the basic digital control scheme given in Fig. 11.2. In most cases, the measuring transducer (sensor) and the actuator (final control element) are analog devices requiring, respectively, A/D and D/A conversion at the computer input and output. There are, of course, exceptions; sensors which combine the functions of the transducer and the A/D converter, and actuators which combine the functions of the D/A converter and the final control element are available. In the control scheme of Fig. 1.14, the control signal from the digital computer is processed by the SCR trigger control circuit to control the firing angle of the SCR (D/A conversion and the power conversion by the final control element are embedded in the scheme). In the control scheme of Fig. 1.12, the measurement of shaft position and processing of signals (calculation of control signal) are digital in nature (A/D function and the transducer function are embedded in the scheme).

In this section, we present the functional details of *shaft-angle encoders* for digital measurement of shaft position/speed.

The digital measurement of shaft position requires conversion from the analog quantity 'shaft angle' to a binary number. One way of doing this would be to change shaft angle to a voltage using a potentiometer, and then to convert it to a binary number through an electronic A/D converter. This is perfectly feasible but is not sensible because:

(i) high quality potentiometers of good accuracy are expensive and subject to wear; and
(ii) the double conversion is certain to introduce more errors than a single conversion would do.

We can go straight from angle to number using an optical angular *absolute-position encoder*. It consists of a rotary disk made of a transparent material. The disk is divided into a number of equal angular sectors depending on the resolution required. Several tracks, which are transparent in certain sectors but opaque in others, are laid out. Each track represents one digit of a binary number. Detectors on these tracks sense whether the digit is a '1' or a '0'. Figure 11.8 gives an example. Here the disk is divided into eight 45º sectors. To represent eight angles in binary code requires three digits ($2^3 = 8$), hence there are three tracks. Each track has a light source sending a beam on the disk, and on the opposite side a photoelectric sensor receiving this beam. Depending upon the angular sector momentarily facing the sensors, they transmit a bit pattern representing the angular disk position. For example, if the bit pattern is 010, then Sector IV is facing the sensors.

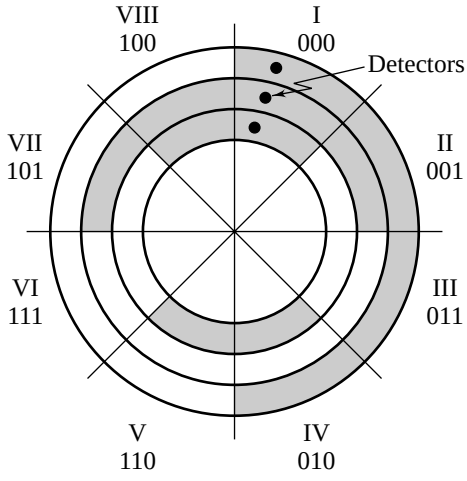

Fig. 11.8 Absolute encoder

Figure 11.8 is an example of an 'absolute encoder', so called because for a given angle the digital output must always be the same. Note that a cyclic (Gray) binary code is normally used on absolute encoders (in cyclic codes, only one bit changes between adjacent numbers). If a natural binary-code pattern were used, a transition from, say 001 to 010, would produce a race between the two right-hand bits. Depending on which photosensor responded faster, the output would go briefly through 011 or 000. In either case, a momentary false bit pattern would be sent. Cyclic codes avoid such races. A cyclic code can be converted into natural binary code by either hardware or computer software.

Encoders similar to Fig. 11.8 have been widely used. But they have certain disadvantages.

(i) The resolution obtainable with these encoders is limited by the number of tracks on the encoder disk. The alignment of upto ten detectors and the laying out of ten tracks is still quite difficult and thus expensive.

(ii) The resulting digital measurement is in a cyclic code and must usually be converted to natural binary before use.

(iii) The large number of tracks and detectors inevitably increases the chance of mechanical and/or electrical failure.

For these reasons, another form of encoder is commonly used today and is known as the *incremental encoder*. The basis of an incremental encoder is a single track served by a single detector and laid out in equal segments of '0' and '1' as in Fig. 11.9. As the track moves relative to the detector, a pulse train is generated, and can be fed to a counter to record how much motion has occurred. With regard to this scheme of measurement, the following questions may be raised.

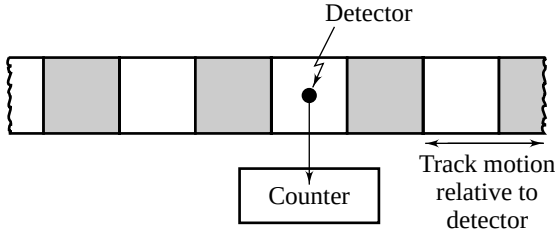

Fig. 11.9 Incremental encoder

(i) How do we know which direction the motion was?

(ii) If we can record only the distance moved, how do we know where we were?

The answer to the first question involves the addition of a second detector. Figure 11.10a shows two detectors, spaced one half of a segment apart. As the track moves relative to the detectors (we assume at a constant rate), the detector outputs vary with time as shown in the waveforms of Fig. 11.10b. We can see that the relative 'phasing' of the *A* and *B* signals depends upon the direction of motion and so gives us a means of detecting the direction.

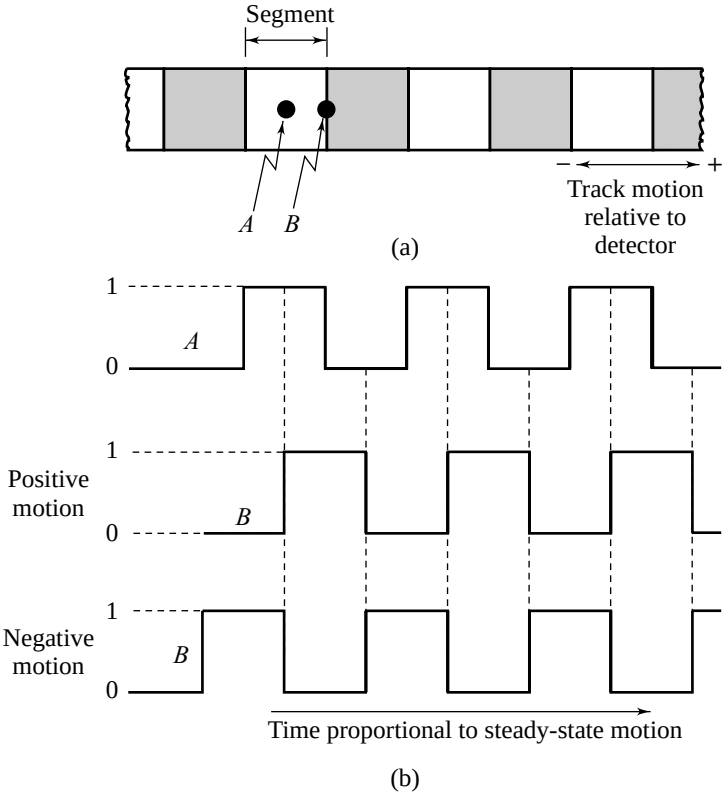

Fig. 11.10 Quadrature encoding

For example, if signal *B* goes from '0' to '1' while signal *A* is at '1', the motion is positive. For the same direction, we see that *B* goes from '1' to '0' whilst *A* is at '0'. For negative motion, a similar but different pair of statements can be made. By application of some fairly simple logic, it is possible to control a reversible counter as is indicated in Fig. 11.11.

This method of direction sensing is referred to as *quadrature encoding*. The detectors are one half of a segment apart, but reference to the waveforms of Fig. 11.10 shows that there are two segments to one cycle; so the detectors are one-quarter of a cycle apart, and hence the name.

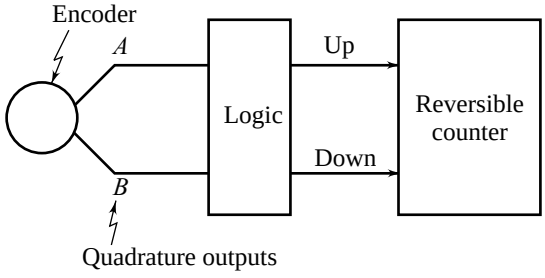

Fig. 11.11 Direction-detecting circuit for an incremental encoder

The solution to the second problem also requires an additional detector working on a datum track as shown in Fig. 11.12. The datum resets the counter every time it goes by.

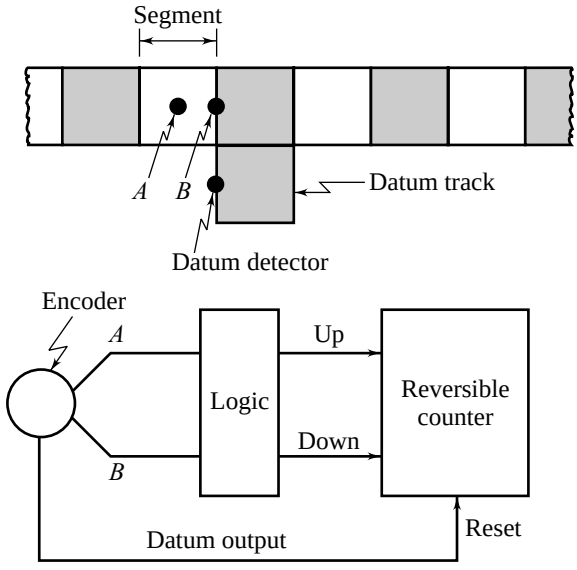

Fig. 11.12 Datum detector in an incremental encoder

We have thus three detectors in an incremental encoder. But this is still a lot less than on an absolute encoder.

In an analog system, speed is usually measured by a tachogenerator attached to the motor shaft. This is because the time differentiation of analog position signal presents practical problems.

In a digital system, however, it is relatively easy to carry out step-by-step calculation of the 'slope' of the position/time curve. We have the position data in digital form from the shaft encoder, so the rest is fairly straightforward.

11.6 DIGITAL IMPLEMENTATION OF ANALOG COMPENSATORS

Plants of control systems are mostly analog systems. However, because digital compensators have many advantages over analog ones, we may be asked to design digital compensators to control analog plants. There are two approaches to carrying out the design. The first approach uses the design methods discussed in the preceding chapters to design an analog compensator and then transforms it into a digital one. The second approach first transforms analog plants into digital plants and then carries out design using digital techniques. We consider in this section the first approach. The rest of the chapter deals with second approach.

Consider the analog compensator with a proper transfer function $D(s)$ shown in Fig. 11.13a. The arrangement in Fig. 11.13b implements the analog compensator digitally. It consists of three parts: a sampler, a digital control algorithm, and a ZOH . The problem is to find a digital algorithm such that for any input $e(t)$, the output $u(t)$ of the analog compensator and the output $u^+(t)$ of the digital compensator are roughly equal. From Fig. 11.13b, we see that the output of the sampler is $e(k) \triangleq e(t = kT)$, the sample of $e(t)$ with sampling period T. We then search for a digital algorithm which operates on $e(k)$ to yield a sequence $u(k)$. The ZOH

then holds the value of u constant until the arrival of next data. Thus, the output $u^+(t)$ of the digital compensator is stepwise as shown. The output of analog compensator is generally not stepwise; the best we can achieve is that $u^+(t)$ approximately equals $u(t)$.

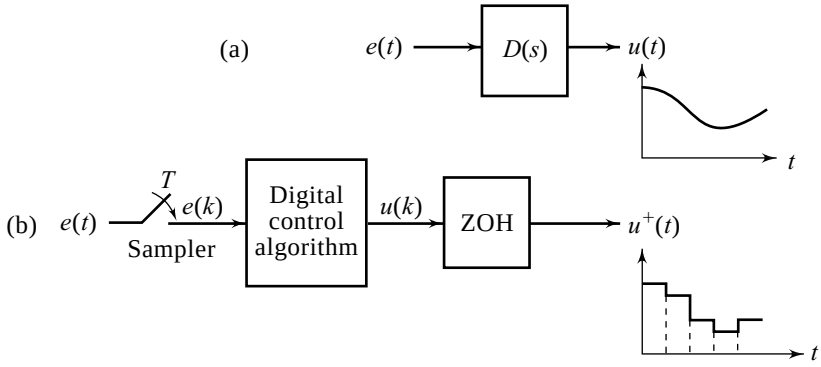

Fig. 11.13 (a) Analog compensator; (b) Digital compensator

Computer processing of input samples $e(k)$ to produce output samples $u(k)$ may be described by difference equations, analogous to differential equations that characterize continuous-time systems. The general form of nth-order linear difference equation relating output $u(k)$ to input $e(k)$ is given below.

$$u(k) + a_1u(k-1) + \cdots + a_nu(k-n) = b_0e(k) + b_1e(k-1) + \cdots + b_me(k-m) \quad (11.1)$$

The coefficients a_i and b_j are real constants; m and n are integers with $m \le n$.

We will consider the general linear difference equation in the following form:

$$u(k) + a_1u(k-1) + \cdots + a_nu(k-n) = b_0e(k) + b_1e(k-1) + \cdots + b_ne(k-n) \quad (11.2)$$

There is no loss of generality in this assumption; the results for $m = n$ can be used for the case of $m < n$ by setting appropriate b_j coefficients to zero.

If the input is assumed to be switched on at $k = 0$ ($e(k) = 0$ for $k < 0$), then the difference equation model (11.2) gives the output at instant '0' in terms of the past values of the output; $u(-1), u(-2), \ldots, u(-n)$, and the present input $e(0)$. Thus the initial conditions of the model (11.2) are $\{u(-1), u(-2), \ldots, u(-n)\}$.

Since the difference equation model (11.2) represents a time-invariant system, the choice of the initial point on the time scale is simply a matter of convenience in analysis. Shifting the origin from $k = 0$ to $k = n$, we get the equivalent difference equation model:

$$u(k+n) + a_1u(k+n-1) + \cdots + a_nu(k) = b_0e(k+n) + b_1e(k+n-1) + \cdots + b_0e(k) \quad (11.3)$$

Substituting $k = 0$ in Eqn. (11.3), we observe that the output at instant 'n' is expressed in terms of n values of the past outputs: $u(0), u(1), \ldots, u(n-1)$ and in terms of inputs : $e(0), e(1), \ldots, e(n)$. If k is incremented to take on values $k = 0,1,2,\ldots$, *etc*., the $u(k)$; $k = n, n+1,\ldots$, can easily be generated by the iterative procedure. Given $\{u(-1), u(-2), \ldots, u(-n)\}$, the initial conditions $\{u(0), u(1), \ldots, u(n-1)\}$ of the model (11.3) can be determined by successively substituting $k = -n, -n+1, \ldots, -2, -1$ in Eqn. (11.3).

Consider, for example, the computer processing of the input samples $e(k) \triangleq e(kT)$ to generate output sequence $u(k) \triangleq u(kT)$ as per the algorithm described by second-order difference equation

$$u(k+2) - 3u(k+1) + 2u(k) = 2e(k+1) - e(k) \tag{11.4}$$

The input is applied at $k = 0$ ($e(k) = 0$ for $k < 0$). We assume zero initial conditions, i.e., $u(k) = 0$ for $k < 0$. If we write Eqn. (11.4) as

$$u(k) = 3u(k-1) - 2u(k-2) + 2e(k-1) - e(k-2)$$

then its response to the given input sequence $e(k)$; $k \geq 0$, can be computed recursively as

$$u(0) = 0$$
$$u(1) = 3u(0) + 2e(0)$$
$$u(2) = 3u(1) - 2u(0) + 2e(1) - e(0)$$
$$u(3) = 3u(2) - 2u(1) + 2e(2) - e(1)$$
$$\vdots$$

and so forth.

The discretization problem, therefore, amounts to conversion of the transfer function

$$\frac{U(s)}{E(s)} = D(s)$$

to an equivalent difference equation. There is no exact solution to this problem because $D(s)$ responds to the complete history of $e(t)$, whereas the digital control algorithm has access only to the samples $e(k)$. In a sense, various discretization procedures simply make different assumptions about what happens to $e(k)$ between the sample points. A simple discretization approach is based on numerical integration scheme:

$$\int_{(k-1)T}^{kT} e(t)dt \cong \frac{T}{2}\,[e(k) + e(k-1)] \tag{11.5}$$

where $e(k) \triangleq e(t = kT)$.

In Eqn. (11.5), the area in question has been approximated by that of a trapezoid formed by the base T and vertices $e(k)$ and $e(k-1)$, as shown in Fig. 11.14. The area can also be approximated by the rectangle of amplitude $e(k-1)$ or $e(k)$ to give

$$\int_{(k-1)T}^{kT} e(t)dt \cong T\,[e(k-1)] \tag{11.6}$$

or

$$\int_{(k-1)T}^{kT} e(t)dt \cong T\,[e(k)] \tag{11.7}$$

In this chapter, we will employ *trapezoidal rule for integration*, given by Eqn. (11.5). Refer [155] for the characteristics of rectangular rules for integration, given by Eqns (11.6) and (11.7).

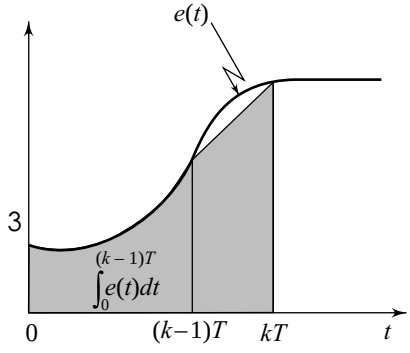

Fig. 11.14 Trapezoidal rule for integral approximation

Example 11.1 The simplest formula for the PID or three-mode controller is the addition of the proportional, integral, and derivative modes:

$$u(t) = K_c\left[e(t) + \frac{1}{T_I}\int_0^t e(t)dt + T_D\frac{de(t)}{dt}\right] \tag{11.8}$$

where

u = controller output signal
e = error (controller input) signal
K_c = controller gain
T_I = integral or reset time
T_D = derivative or rate time

For the digital realization of the PID controller, it is necessary to approximate each mode in Eqn. (11.8) using the sampled values of $e(t)$.

The proportional mode requires no approximation since it is purely static part:

$$u_P(k) = K_c e(k) \tag{11.9}$$

The integral mode may be approximated by trapezoidal rule for integration:

$$u_I(k) = \frac{K_c}{T_I}\int_0^{kT} e(t)dt$$

$$= \frac{K_c}{T_I}\int_0^{(k-1)T} e(t)\,dt + \frac{K_c}{T_I}\int_{(k-1)T}^{kT} e(t)dt$$

$$\cong u_I(k-1) + \left(\frac{K_c}{T_I}\right)\frac{T}{2}[e(k) + e\,(k-1)] \tag{11.10}$$

In the derivative-mode term, the values of u and e are reversed from integral-mode term, and the consistent approximation can be written down at once from Eqns (11.8) and (11.10):

$$u_D(t) = K_c T_D \frac{de(t)}{dt}$$

Therefore

$$K_c T_D e(k) \cong K_c T_D e(k-1) + \frac{T}{2}[u_D(k) + u_D(k-1)]$$

or

$$u_D(k) = (K_c T_D)\frac{2}{T}[e(k) - e(k-1)] - u_D(k-1) \tag{11.11}$$

Bringing all the three modes together results in the following PID algorithm:

$$u(k) = u_P(k) + u_I(k) + u_D(k) \tag{11.12}$$

11.6.1 Sampling Rate Selection

The selection of the best sampling rate for a digital control system is the result of a compromise among many factors. The basic motivation to lower the sampling rate is cost. A decrease in sampling rate means more time is available for the control calculations; hence slower computers can be used for a given control function or more control capability can be achieved from a given computer. Either way, the cost per function is lowered. For systems with A/D converters, less demand on conversion speed will also lower cost. These economic arguments indicate that the best engineering choice is the slowest possible sampling rate that still meets all performance specifications.

With excessive reduction in sampling rate, a number of potentially degrading effects start to become significant. For a particular application, one or more of these degrading effects set the lower limit for the sampling rate. The process dynamics, the type of algorithm and control requirements, and the characteristics of input and noise signals, all interact to set the maximum usable value for sampling period T.

How to find an adequate sampling interval, has been widely discussed in the literature. Some commonly used empirical rules are reported below.

Empirical Rules for the Selection of Sampling Rate Practical experience and simulation results have produced a number of useful approximate rules for the specification of minimum sampling rate/ maximum sampling interval.

1. The following recommendations for the most common process variables follow from the experience of process industries:

Type of variable	*Sampling time (sec)*
Flow	1 – 3
Level	5 – 10
Pressure	1 – 5
Temperature	10 – 20

2. Fast-acting electromechanical systems require much shorter sampling intervals, perhaps down to a few milliseconds.
3. A rule of thumb says that select a sampling period that is much shorter than any of the time-constants in the continuous-time plant to be controlled digitally. Sampling interval equal to one-tenth of the smallest time-constant or the inverse of the largest real pole (or real part of complex pole) has been recommended.
4. For complex poles with imaginary part ω_d, the frequency of transient oscillations corresponding to the poles is ω_d. A convenient rule suggests sampling at the rate of 6 to 10 times per cycle. Thus, if the largest imaginary part in the poles of the continuous-time plant is 1 rad/sec, which corresponds to transient oscillations with a frequency of 1/6.28 cycles per second, $T = 1$ sec may be satisfactory.
5. Rules of thumb based on open-loop plant model are full of danger under the conditions where high closed-loop performance is forced from a plant with a low open-loop performance. The rational choice of the sampling rate should be based on an understanding of its influence on the closed-loop performance of the control system. It seems reasonable that the highest frequency of interest should be closely related to the 3 dB-bandwidth of the closed-loop system. The selection of sampling rates can then be based on the bandwidth of the closed-loop system. Reasonable sampling rates are 10 to 30 times the bandwidth.
6. Another rule of thumb based on closed-loop performance is to select sampling interval T equal to or less than one-tenth of the desired settling time.

Example 11.2 Consider the analog control system shown in Fig. 11.15. The specifications for the system are that the damping ratio ζ of the pair of dominant closed-loop poles be 0.7, and the natural frequency ω_n be 0.3 rad/sec. The specifications can be met with

$$D(s) = \frac{0.81(s + 0.2)}{s + 2}$$

as can be verified by the root locus plot.

To digitize this $D(s)$, we first need to select a sampling rate. For a system with $\omega_n = 0.3$ rad/sec, a very 'safe' sampling rate would be a factor of 20 faster than ω_n, yielding $\omega_s = 0.3 \times 20 = 6$ rad/sec, or 1 Hz .

Thus, let us pick $T = 1$ sec. Using the trapezoidal rule for integration, a digital control algorithm is obtained as follows:

$$D(s) = \frac{0.81(s + 0.2)}{s + 2} = \frac{U(s)}{E(s)} \tag{11.13}$$

gives $$\dot{u}(t) + 2u(t) = 0.81\,\dot{e}(t) + 0.162\,e(t)$$

or $$\dot{u}(t) = -2u(t) + 0.81\,\dot{e}(t) + 0.162e(t)$$

Therefore $$u(t) = u(0) - 2\int_0^t u(\tau)d\tau + 0.81e(t)$$

$$-0.81e(0) + 0.162\int_0^t e(\tau)d\tau$$

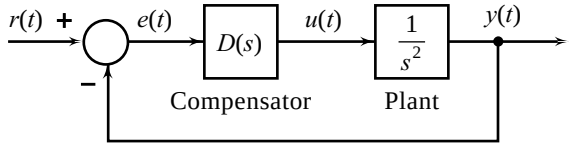

Fig. 11.15 An analog control system

Using the trapezoidal rule for integration, the following recursive algorithm follows from this equation.

$$u(k) = u(k-1) - 2\left[\frac{u(k)+u(k-1)}{2}\right]T + 0.81e(k) - 0.81e(k-1)$$

$$+ 0.162\left[\frac{e(k)+e(k-1)}{2}\right]T$$

or $$u(k) = 0.4455e(k) - 0.3645e(k-1) \qquad (11.14)$$

where $$e(k) = r(k) - y(k)$$

This completes the digital algorithm design. The complete digital control system is shown in Fig. 11.16.

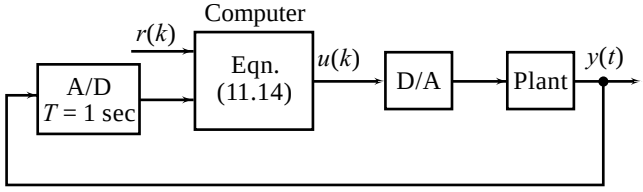

Fig. 11.16 A digital control system

11.6.2 Applicability Limits of Digital Implementation of Analog Compensators

When a continuous-time signal is sampled at regular intervals of time and is then reconstructed by holding the sampled values constant for each sampling interval, the reconstructed signal is effectively delayed by approximately one half of the sampling interval, as shown in Fig. 11.17.

In digital control configuration of Fig. 11.7, the ZOH holds the output of the digital controller constant between updates, thus introducing a delay of $T/2$ sec into the loop. This dead-time introduces a phase lag, and thus reduces the stability margin in a closed-loop system. If an exact discrete-time analysis or a simulation of a digital control system obtained by discretization

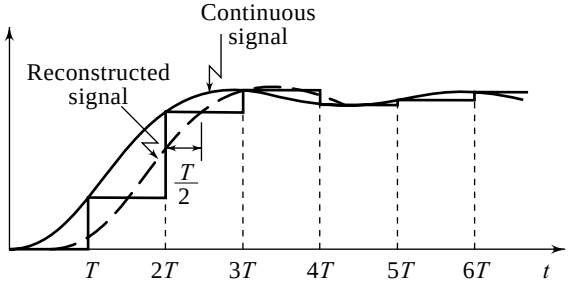

Fig. 11.17 Time delay introduced by sampling and reconstruction

of analog design were performed, and the discretization determined for a wide range of sampling rates, the system would be unstable for sampling rates lower than approximately $5 \times \omega_b$, and the damping would be substantially degraded for sampling rates lower than $10 \times \omega_b$. At sampling rates of the order of $20 \times \omega_b$, this design method will yield reasonable results, and can be used with confidence for sampling rates of $30 \times \omega_b$ or higher.

Thus, a fictitious limit on the sampling rate occurs when using digital implementation of analog design. The inherent approximation in the method may give rise to system instabilities as the sampling rate is lowered, and this can lead the designer to conclude that a lower limit on ω_s has been reached when, in fact, the proper conclusion is that the approximations are invalid; the solution is not to sample faster but to refine the design.

A simple way to refine the design is to account for the lagging effect of the ZOH in the analog design itself. We introduce the transfer function

$$G_h(s) = e^{-sT/2} \tag{11.15}$$

in analog control loop (refer Fig. 11.18) in anticipation of the conversion from an analog controller to a digital controller. Note that $G_h(s)$ is a pure time delay with dead time of $T/2$ and a dc gain of unity. Considering $G_h(s)G(s)$ as the plant model, we design the analog compensator $D(s)$. Discretization of this $D(s)$ will allow for higher values of sampling interval.

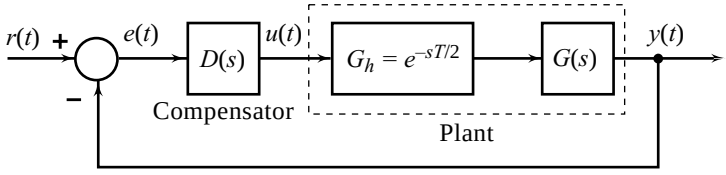

Fig. 11.18 Analog compensator design for digital implementation

11.7 FORMULATION OF DIRECT DIGITAL CONTROL DESIGN PROBLEM

There are two basic routes to the design of digital controllers for continuous-time processes. The route: *continuous-time modelling → continuous-time control design → discrete-time approximation of the controller*, was considered in earlier sections of this chapter. This approach is based on the fact that a digital system with a high sampling rate approximates to an analog system. However, the use of high sampling rates wastes computer power, and can lead to problems of arithmetic precision, etc. One is therefore driven to find methods of design which take account of the sampling process. The rest of the chapter is devoted to the following route, which takes sampling process into account: *continuous-time modelling → discrete-time approximation of the model → discrete-time control design.*

An actual design process is often a combination of the two methods. First iteration to a digital design may be obtained using discretization of an analog design. Then the result is tuned up using direct digital analysis and design.

Consider an analytical model of a unity-feedback digital control system shown in Fig. 11.7. This representation is useful for direct digital control design. The sampler which samples continuous-time signals $e(t)$ every T secs to generate the sequence $e(k)$, is a model of A/D converter, and the zero-order hold(ZOH) which constructs a continuous-time signal $u^+(t)$ from a discrete-time output $u(k)$ of the digital computer (digital control algorithm), is a model of D/A converter. Direct digital control design begins with sufficiently accurate mathematical models of sampling and hold operations.

11.7.1 A Mathematical Model of Sampling Operation

We assume that the sampler in Fig. 11.7 is an ideal switch that closes and reopens instantaneously. Of course, no switch opens and closes instantaneously, but the modern A/D converter comes very close. A/D converters with a conversion rate of 100 kHz are fairly inexpensive, and conversion rates in the megahertz range are available (In control applications, the sampling rate is usually less than 100 Hz). If the conversion rate is 100 kHz, the conversion is completed in less than one one-thousand of the typical sample period. Thus the conversion rate of A/D converter is close enough to instantaneous.

To establish a relationship of the sequence $e(k)$ to the continuous-time function $e(t)$ from which this sequence is derived, we take the following approach. We treat each sample of the sequence $e(k)$ as an impulse function of strength equal to the value of the sample (Impulse function $A\,\delta(t - t_0)$ is an impulse of strength A occurring at $t = t_0$). The idea is to give a mathematical description to periodic samples of a continuous-time function in such a way that we can analyze the samples and the function simultaneously using the same tool (Laplace transform). The sequence $e(k)$ can be viewed as a train of impulses, represented by the continuous-time function $e^*(t)$:

$$e^*(t) = e(0)\,\delta(t) + e(1)\,\delta(t - T) + e(2)\,\delta(t - 2T) + \cdots$$

$$= \sum_{k=0}^{\infty} e(k)\delta(t - kT) \tag{11.16}$$

Typical signals $e(t)$, $e(k)$ and $e^*(t)$ are shown in Fig. 11.19. The sampler of Fig. 11.7 can thus be viewed as an 'impulse modulator' with the carrier signal

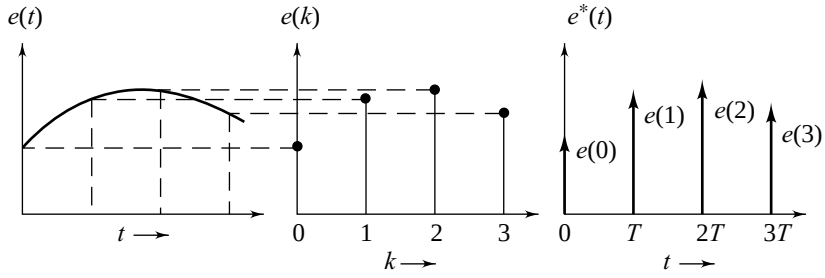

Fig. 11.19 Conversion of a continuous-time signal to a sequence

$$\delta_T(t) = \sum_{k=0}^{\infty} \delta(t - kT) \tag{11.17}$$

and modulating signal $e(t)$. The modulation process is schematically represented in Fig. 11.20a, and the *impulse train* $\delta_T(t)$ in Fig. 11.20b:

$$e^*(t) = e(t)\delta_T(t) \tag{11.18a}$$

We will eliminate the delta function by simply taking the Laplace transform of $e^*(t)$ to obtain (refer Eqn. (2.24))

$$\mathscr{L}[e^*(t)] \triangleq E^*(s)$$

$$= \int_0^{\infty} e(t)\delta_T(t)e^{-st}\,dt$$

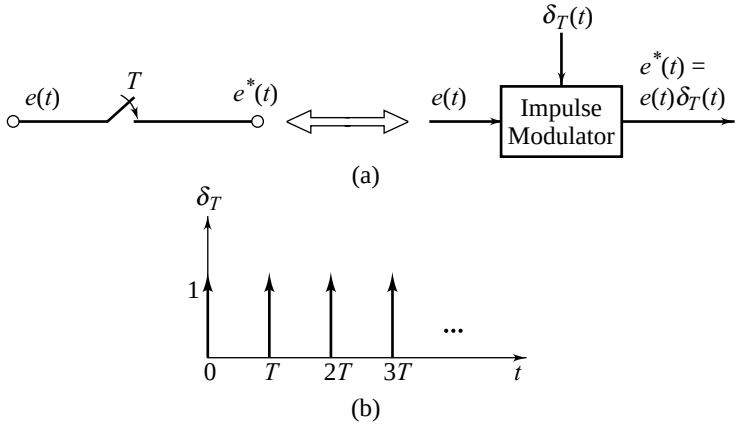

Fig. 11.20 (a) Representation of sampling as impulse modulator
(b) Representation of impulse train

$$= \sum_{k=0}^{\infty} \int_{0}^{\infty} e(t)\,\delta(t - kT) e^{-st}\,dt$$

$$= \sum_{k=0}^{\infty} e(kT) e^{-skT} \tag{11.18b}$$

We see that by applying Laplace transform to $e^*(t)$, we have sifted out the values $e(0)$, $e(T)$, $e(2T)$,…, $e(kT)$, … . These are simply the values of $e(t)$ at the output of the A/D converter.

The expression (11.18b) for $E^*(s)$ represents a Laplace transform, but it is not a transform that is easy to use because the complex variable s occurs in the exponent of the transcendental function e. By contrast, the Laplace transforms that we have used previously in this book , have mostly been ratios of polynomials in the Laplace variable s, with real coefficients. These latter transforms are easy to manipulate and interpret. Ultimately, we will be able to achieve these same ratios of polynomials in a new complex variable z by transforming $E^*(s)$ to reach what we call the z-plane.

The expression $E^*(s)$, given by (11.18b), contains the term e^{-Ts}; T is the fixed sampling period. To transform the irrational function $E^*(s)$ into a rational function, we use a transformation from the complex variable s to another complex variable z. An obvious choice for this transformation is

$$z = e^{Ts} \tag{11.19a}$$

although $z = e^{-Ts}$ would be just as acceptable.

Solving for s in Eqn. (11.19a), we obtain

$$s = \frac{1}{T} \ln z \tag{11.19b}$$

The relationship between s and z in Eqns (11.19) may be defined as the *z-transformation*.

When Eqns (11.19) are substituted in Eqn. (11.18b), we have

$$E^*\left(s = \frac{1}{T} \ln z\right) = E(z) = \sum_{k=0}^{\infty} e(kT) z^{-k} = \sum_{k=0}^{\infty} e(k) z^{-k} \tag{11.20}$$

The mapping (11.20) is often used as the definition of *z-transform*.

11.7.2 A Mathematical Model of Zero-Order Hold

We have replaced the D/A converter with a zero-order hold (ZOH) in the analytical model of Fig. 11.7. A ZOH clamps the output signal to a value equal to that of the input signal at the sampling instant. If a discrete-time signal $u(k)$ is applied at $t = kT$, the ZOH immediately puts out a value of $u(k)$ and holds it for T units of time. No physical device behaves exactly like this, but a modern D/A converter can convert a digital input to an analog signal in roughly 10^{-5} sec. This is nearly the ideal behaviour (instantaneous response).

In an actual operation, the digital output $e(k)$ of the A/D converter (refer Fig. 11.7) is processed by the digital control algorithm, and the computer outputs digital signal $u(k)$ which is converted to an analog signal $u^+(t)$ by the D/A converter (refer Fig. 11.13). For mathematical modelling, we have assumed that the sampler (A/D converter) generates impulse signals $e^*(t)$ (refer Fig. 11.19). To continue with this school of thought, we may assume that the computer algorithm has a transfer function $D^*(s)$ and has been designed to process impulse signals $e^*(t)$ and outputs impulse signals $u^*(t)$, which are then converted to $u^+(t)$ by the ZOH as shown in Fig.11.21.

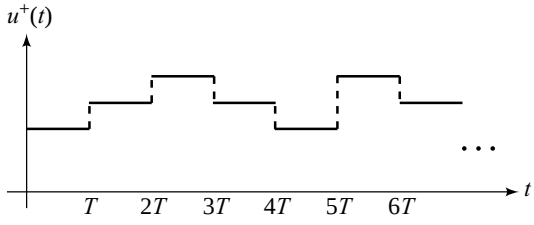

Fig. 11.21 Output of a zero-order hold

We can therefore write the ZOH output as

$$u^+(t) = \sum_{k=0}^{\infty} u(kT)\left[\mu(t-kT) - \mu\left(t-\overline{k+1}\right)T\right] \tag{11.21a}$$

Taking the Laplace transform, we have

$$U^+(s) = \sum_{k=0}^{\infty} u(kT)\left[\frac{e^{-skT}}{s} - \frac{e^{-s(k+1)T}}{s}\right]$$

$$= \left[\frac{1-e^{-sT}}{s}\right]\left[\sum_{k=0}^{\infty} u(kT)e^{-skT}\right] \tag{11.21b}$$

The second factor in Eqn. (11.21b) is the Laplace transform of the input signal $u^*(t)$ (refer Eqn. (11.18b)). We can therefore write Eqn. (11.21b) as

$$U^+(s) = G_{h0}(s)U^*(s)$$

where

$$G_{h0}(s) = \frac{1-e^{-sT}}{s} \tag{11.22}$$

is the transfer function of zero-order hold.

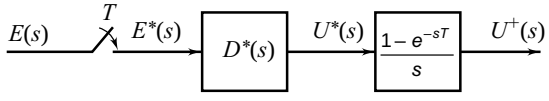

Fig. 11.22 Mathematical representation of sampler and zero-order hold

It should be remembered that $U^*(s)$ is not present in the physical system but appears in the mathematical model as a result of Eqn. (11.22). Also the sampler with model given by Eqns (11.18) is not present in the physical system. However the combination shown in Fig. 11.22, does accurately model the sampling and reconstruction operation in a physical system.

If we make the substitution $s = \ln z/T$, we get the mathematical representation of sampled-data system on the z-plane. This transformation enables us to preserve, in large part, the frequency-domain techniques developed in the previous chapters. The design approaches that follow in this chapter use z-transform as the background tool. In Chapter 13, we will solve the identical problems using state-space formulation.

11.8 THE z-TRANSFORM

11.8.1 Definition of the z-Transform

The z-transform is a technique of expressing a sequence $x(k)$ as a sum of functions of the form z^{-k}, where z is a complex variable. Recall the mapping (11.20) introduced in the previous section. The expression

$$X(z) = \sum_{k=0}^{\infty} x(k)z^{-k}$$

is used as the definition of the z-transform of sequence $x(k)$, denoted symbolically as $\mathcal{Z}[x(k)]$:

$$X(z) \triangleq \mathcal{Z}[x(k)] = \sum_{k=0}^{\infty} x(k)z^{-k};\ x(k) = 0 \text{ for } k < 0 \tag{11.23}$$

where the variable z is a complex variable:

$$z = a + jb = r\,e^{j\Omega} \tag{11.24}$$

For a fixed value of r, the locus of z is a circle of radius r in the complex z-plane. Circle of radius unity in the complex z-plane will be of specific interest to us. This circle is called a *unit circle* (Fig.11.23).

The summation in Eqn. (11.23) does not converge for all functions; and when it does, it does so for restricted values of z in the z-plane. Therefore, for each sequence for which the summation converges, there is an associated *convergence region* in the complex z-plane (Examples of z-plane convergence regions will shortly follow).

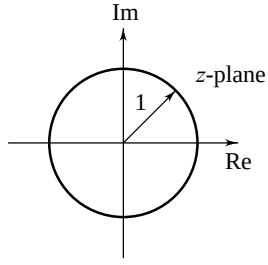

Fig. 11.23 Unit circle in z-plane

11.8.2 z-Transforms of Functions Useful for Control System Analysis

In this section, our goal is to find the z-transform of the functions we will subsequently need for our analysis of control systems.

Unit Sample Sequence The unit sample sequence (*discrete-time impulse*) contains only one nonzero element and is defined by

$$\delta(k) = \begin{cases} 1 \text{ for } k = 0 \\ 0 \text{ otherwise} \end{cases} \tag{11.25a}$$

The z-transform of this elementary signal is

$$\mathcal{Z}[\delta(k)] = \sum_{k=0}^{\infty} \delta(k)z^{-k} = z^0 = 1; |z| > 0 \tag{11.25b}$$

Unit Step Sequence The unit step sequence is defined as

$$\mu(k) = \begin{cases} 1 \text{ for } k \geq 0 \\ 0 \text{ otherwise} \end{cases} \tag{11.26a}$$

The z-transform is

$$\mathcal{Z}[\mu(k)] = \sum_{k=0}^{\infty} \mu(k)z^{-k} = \sum_{k=0}^{\infty} z^{-k}$$

Using the geometric series formula

$$\sum_{k=0}^{\infty} x^k = \frac{1}{1-x}; |x| < 1,$$

this becomes

$$\mathcal{Z}[\mu(k)] = \frac{1}{1-z^{-1}} = \frac{z}{z-1} \tag{11.26b}$$

Note that this equation holds only if the infinite sum converges, that is if $|z^{-1}| < 1$ or $|z| > 1$. Thus, the region of convergence is the area outside the unit circle in the z-plane.

Sampled Ramp Function Discrete form of $y(t) = t\mu(t)$ is

$$y(k) = \begin{cases} kT \text{ for } k \geq 0 \\ 0 \text{ otherwise} \end{cases} \tag{11.27}$$

Given the z-transform of $x(k)$, we can obtain z-transform of $\{kT\,x(k)\}$using the following property of z-transforms. From the basic definition (11.23),

$$\frac{dX(z)}{dz} = \sum_{k=0}^{\infty} \frac{d}{dz}[x(k)z^{-k}] = \sum_{k=0}^{\infty} (-k)x(k)z^{-k-1}$$

Consequently

$$-z\frac{dX(z)}{dz} = \sum_{k=0}^{\infty} k\,x(k)z^{-k}$$

or

$$\mathcal{Z}[kT\,x(k)] = -Tz\frac{dX(z)}{dz} \tag{11.28}$$

For $x(k) = \mu(k)$, we obtain

$$\mathcal{Z}[kT\mu(k)] = \mathcal{Z}[\,y(k)] = Y(z) = -Tz\frac{d}{dz}\left(\frac{z}{z-1}\right) \tag{11.29}$$

$$= -Tz\left[\frac{-z}{(z-1)^2} + \frac{1}{z-1}\right] = \frac{Tz}{(z-1)^2}; |\,z\,| > 1$$

Sampled Exponential Function Discrete form of $x(t) = e^{-at}$ is

$$x(k) = \begin{cases} e^{-akT} \text{ for } k \geq 0 \\ 0 \text{ otherwise} \end{cases} \tag{11.30a}$$

Then

$$X(z) = \sum_{k=0}^{\infty} e^{-akT}z^{-k} = \sum_{k=0}^{\infty} (e^{aT}z)^{-k} = \sum_{k=0}^{\infty} \alpha^{-k}; \alpha = e^{aT}z$$

$$= \frac{1}{1-\alpha^{-1}} = \frac{e^{aT}z}{e^{aT}z-1} = \frac{z}{z-e^{-aT}} \tag{11.30b}$$

This equation holds only if the infinite sum converges, that is if $|e^{-aT}z^{-1}| < 1$ or $|z| > |e^{-aT}|$. This result holds for both real and complex a. The transform of sampled sinusoid $A\cos(\omega kT + \phi)$ can be found by expanding

the sequence into complex exponential components. Given the z-transform of $A\cos(\omega kT+\phi)$, we can obtain z-transform of $Ae^{-akT}\cos(\omega kT+\phi)$using the following property of z-transforms:

$$\mathcal{Z}[e^{-akT}x(k)] = \sum_{k=0}^{\infty} x(k)e^{-akT}z^{-k} = \sum_{k=0}^{\infty} x(k)(ze^{aT})^{-k} = X(ze^{aT}) \tag{11.31}$$

We summarize the z-transforms we have derived to this point plus some additional transforms in Table 11.1. The table lists commonly encountered functions $x(t)$; $t \geq 0$ and z-transforms of sampled version of these functions, given by $x(kT)$. We also include in this table the Laplace transforms $X(s)$ corresponding to the selected functions $x(t)$. Whenever a function in s is given, one approach for finding the corresponding z-transform is to convert $X(s)$ into $x(t)$ and then find z-transform of $x(kT)$. Another approach is to expand $X(s)$ into partial fractions and directly use a z-transform table to find the z-transforms of the expanded terms. Table 11.1 will be helpful for this second approach.

All the transforms listed in the table can easily be derived from first principles. It may be noted that in this transform table, regions of convergence have not been specified. In our applications of systems analysis, which involve transformation from time-domain to z-domain and inverse transformation, the variable z acts as a dummy operator. If transform pairs for sequences of interest to us are available, we are not concerned with the region of convergence.

Table 11.1 Abbreviated table of z-transforms

$X(s)$	$x(t);\ t \geq 0$	$x(k);\ k = 0, 1, 2\ldots$	$X(z)$
–	–	$\delta(k)$	1
$\frac{1}{s}$	$\mu(t)$	$\mu(k)$	$\frac{z}{z-1}$
$\frac{1}{s+a}$	e^{-at}	e^{-akT}	$\frac{z}{z-e^{-aT}}$
$\frac{1}{s^2}$	t	kT	$\frac{Tz}{(z-1)^2}$
$\frac{1}{(s+a)^2}$	te^{-at}	kTe^{-akT}	$\frac{Te^{-aT}z}{(z-e^{-aT})^2}$
$\frac{a}{s(s+a)}$	$1-e^{-at}$	$1-e^{-akT}$	$\frac{(1-e^{-aT})z}{(z-1)(z-e^{-aT})}$
$\frac{\omega}{s^2+\omega^2}$	$\sin\omega t$	$\sin\omega kT$	$\frac{(\sin\omega T)z}{z^2-(2\cos\omega T)z+1}$
$\frac{s}{s^2+\omega^2}$	$\cos\omega t$	$\cos\omega kT$	$\frac{z^2-(\cos\omega T)z}{z^2-(2\cos\omega T)z+1}$
$\frac{\omega}{(s+a)^2+\omega^2}$	$e^{-at}\sin\omega t$	$e^{-akT}\sin\omega kT$	$\frac{(e^{-aT}\sin\omega T)z}{z^2-(2e^{-aT}\cos\omega T)z+e^{-2aT}}$
$\frac{s+a}{(s+a)^2+\omega^2}$	$e^{-at}\cos\omega t$	$e^{-akT}\cos\omega kT$	$\frac{z^2-(e^{-aT}\sin\omega T)z}{z^2-(2e^{-aT}\cos\omega T)z+e^{-2aT}}$

11.8.3 Useful Operations with z-Transforms

Shifting Theorem: Advance (forward shift) z-transformation of difference equations written in terms of advanced versions of the input and output variables (refer Eqn. (11.3)) requires the following results.

$$\mathcal{Z}[y(k+1)] = \sum_{k=0}^{\infty} y(k+1)z^{-k} = z\sum_{k=0}^{\infty} y(k+1)z^{-(k+1)}$$

Letting $k+1 = m$, yields

$$\mathcal{Z}[y(k+1)] = z\sum_{m=1}^{\infty} y(m)z^{-m} = z\left[\sum_{m=0}^{\infty} y(m)z^{-m} - y(0)\right]$$

$$= zY(z) - zy(0) \tag{11.32a}$$

Use of this result in a recursive manner results in the general transform formula:

$$\mathcal{Z}[y(k+n)] = z^n Y(z) - z^n y(0) - z^{n-1}y(1) - \cdots - z^2 y(n-2) - zy(n-1) \tag{11.32b}$$

Shifting Theorem: Delay (backward shift) z-transformation of difference equations written in terms of delayed versions of input and output variables (refer Eqn. (11.2)) requires the following results.

$$\mathcal{Z}[y(k-1)] = \sum_{k=0}^{\infty} (k-1)z^{-k} = y(-1)z^0 + y(0)z^{-1} + y(1)z^{-2} + \cdots$$

$$= z^{-1}\left[\sum_{k=0}^{\infty} y(k)z^{-k}\right] + y(-1) = z^{-1}Y(z) + y(-1) \tag{11.33a}$$

If $y(k)$=0 for k<0, we have

$$\mathcal{Z}[y(k-n)] = z^{-n}Y(z) \tag{11.33b}$$

Remember that multiplication of the z-transform $X(z)$ by z has the effect of advancing the signal $x(k)$ by one sampling period, and that multiplication of the z-transform $X(z)$ by z^{-1} has the effect of delaying the signal $x(k)$ by one sampling period. In control engineering and signal processing, $X(z)$ is frequently expressed as a ratio of polynomials in z^{-1} ; z^{-1} is interpreted as the *unit delay operator*.

11.8.4 z-Transform Inversion

We will obtain the inverse z-transform in exactly the same way that we obtained the inverse Laplace transform (Chapter 2), namely, by partial fraction expansion. The reason that the partial fraction expansion method works is that we frequently encounter transforms that are rational functions, i.e., ratio of two polynomials in z with real coefficients:

$$X(z) = \frac{b_0 z^m + b_1 z^{m-1} + \cdots + b_m}{z^n + a_1 z^{n-1} + \cdots + a_n};\ m \le n \tag{11.34a}$$

$$= \frac{K\prod_{i=1}^{m}(z-\beta_i)}{\prod_{j=1}^{n}(z-\alpha_j)} \tag{11.34b}$$

where the β_i and α_j are either real or complex-conjugate pairs.

The z-transform *zeros* are the values of z for which the transform is zero; $z = \beta_i$ are the zeros of $X(z)$.The z-transform *poles* are the values of z for which the transform is infinite; $z = \alpha_j$ are the poles of $X(z)$.

The transform pairs encountered using the partial fraction expansion technique will usually be those found in Table 11.1. Those not found in the table can easily be derived by using basic properties of z-transformation. The partial fraction expansion method for z-transforms is very straightforward and similar in most respects to the partial fraction expansion in Laplace transforms. We illustrate the method with some examples.

Example 11.3 We observe that the transforms of the elementary functions (see Table 11.1) contain a factor of z in the numerator. To ensure that the partial fraction expansion will yield terms corresponding to those tabulated, it is customary to first expand the function $Y(z)/z$ if $Y(z)$ has one or more roots at the origin, and then multiply the resulting expansion by z. For instance, if $Y(z)$ is given:

$$Y(z) = \frac{2z^2 - 1.5z}{z^2 - 1.5z + 0.5} = \frac{z(2z - 1.5)}{(z - 0.5)(z - 1)},$$

we are justified in writing

$$\frac{Y(z)}{z} = \frac{2z - 1.5}{(z - 0.5)(z - 1)} = \frac{A_1}{z - 0.5} + \frac{A_2}{z - 1}$$

Constants A_1 and A_2 can be evaluated by applying the conventional partial fraction expansion rules.

$$A_1 = (z - 0.5)\left[\frac{Y(z)}{z}\right]_{z=0.5} = 1$$

$$A_2 = (z - 1)\left[\frac{Y(z)}{z}\right]_{z=1} = 1$$

$$\frac{Y(z)}{z} = \frac{1}{z - 0.5} + \frac{1}{z - 1} \text{ or } Y(z) = \frac{z}{z - 0.5} + \frac{z}{z - 1}$$

Using the transform pairs from Table 11.1,

$$y(k) = (0.5)^{kT} + 1;\ k \geq 0$$

Example 11.4 When $Y(z)$ does not have one or more zeros at the origin, we expand $Y(z)$, instead of $Y(z)/z$, into partial fractions and utilize shifting theorem given by Eqn. (11.33b) to obtain inverse z-transform.

Let us consider an example:

$$Y(z) = \frac{10}{(z - 1)(z - 0.2)} = \frac{12.5}{z - 1} - \frac{12.5}{z - 0.2}$$

Notice that the inverse z-transform of $1/(z–1)$ is not available in Table 11.1. However, using the shifting theorem, we find that

$$\mathcal{Z}^{-1}\left[\frac{1}{z - 1}\right] = \mathcal{Z}^{-1}\left[z^{-1}\left(\frac{z}{z - 1}\right)\right] = \begin{cases} 1; k = 1, 2, \ldots \\ 0; k \leq 0 \end{cases}$$

Also

$$\mathcal{Z}^{-1}\left[\frac{1}{z - 0.2}\right] = \mathcal{Z}^{-1}\left[z^{-1}\left(\frac{z}{z - 0.2}\right)\right] = \begin{cases} (0.2)^{k-1}; k\ 1, 2, \ldots \\ 0 \qquad\quad ; k \leq 0 \end{cases}$$

Therefore

$$y(k) = \mathcal{Z}^{-1}[Y(z)] = \begin{cases} 12.5[1-(0.2)^{k-1}]; k = 1, 2, \ldots \\ 0 \qquad\qquad\qquad\quad ; k \le 0 \end{cases}$$

which can be rewritten as

$$y(k) = 12.5\ [1-(0.2)^{k-1}]\mu(k-1)$$

11.8.5 Final Value Theorem

The final value theorem is concerned with the evaluation of $y(k)$ as $k \to \infty$ assuming, of course, that $y(k)$ does approach a limit. Using partial fraction expansion for inverting z-transforms, it is a simple matter to show that $y(k)$ approaches a limit as $k \to \infty$ if all the poles of $Y(z)$ lie inside the *unit circle* ($|z| < 1$) in the complex z-plane. The unit circle boundary is, however, excluded except for a single pole at $z = 1$. This is because purely sinusoidal signals whose transforms will have poles on the unit circle, do not settle to a constant value as $k \to \infty$. Multiple poles at $z = 1$ are also excluded because, as we have already seen in the table of z-transforms, these correspond to unbounded signals like ramps. A more compact way of phrasing these conditions is to say that $(z-1)Y(z)$ must be *analytic* on the boundary and outside the unit circle in the complex z-plane. The final value theorem states that when this condition on $(z-1)Y(z)$ is satisfied, then

$$\lim_{k\to\infty} y(k) = \lim_{z\to 1} (z-1)Y(z) \tag{11.35}$$

The proof is as follows:

$$\mathcal{Z}[y(k+1) - y(k)] = \lim_{m\to\infty} \sum_{k=0}^{m} [y(k+1) - y(k)]z^{-k}$$

or

$$z\,Y(z) - z\,y(0) - Y(z) = \lim_{m\to\infty} \sum_{k=0}^{m} [y(k+1) - y(k)]z^{-k}$$

Letting $z \to 1$ on both sides,

$$\lim_{z\to 1} [(z-1)Y(z) = y(0) + \lim_{z\to 1} \lim_{m\to\infty} \sum_{k=0}^{m} [y(k+1 - y(k)]z^{-k}$$

Interchanging the order of limits on the right-hand side, we have

$$\lim_{z\to 1} [(z-1)Y(z)] = y(0) + \lim_{m\to\infty} \sum_{k=0}^{m} [y(k+1) - y(k)] = y(\infty)$$

11.9 CLOSED-LOOP SAMPLED-DATA SYSTEMS: TRANSFER FUNCTION MODELS AND DYNAMIC RESPONSE

The very first step in the analytical study of a system is to set up mathematical equations to describe the system. Because of different analytical methods used, or because of different questions asked, we may often set up different mathematical models to describe the same system. In this chapter, our focus is on transfer function models; state variable representation will be given in later chapters.

11.9.1 Transfer Function Models of Digital Control Algorithms

Computer processing of input samples $e(k)$ to produce output samples $u(k)$ (refer Fig. 11.7) is generally described by difference equations of the form (11.2) or (11.3). Given the model of the form (11.3), we can shift the origin from $k = n$ to $k = 0$ to obtain a model of the form (11.2), reproduced below.

$$u(k) + a_1u(k-1) + \cdots + a_nu(k-n) = b_0e(k) + b_1e(k-1) + \cdots + b_ne(k-n)$$

We assume that the input is switched on at $k = 0$ ($e(k) = 0$ for $k < 0$) and the initial conditions $u(-1)$, $u(-2)$,..., $u(-n)$ are all zero. The z-transform operation on Eqn. (11.2) gives (using the shifting theorem given by Eqn. (11.33b))

$$U(z) + a_1z^{-1}U(z) + \cdots + a_nz^{-n}U(z) = b_0E(z) + b_1z^{-1}E(z) + \cdots + b_nz^{-n}E(z)$$

or

$$(1 + a_1z^{-1} + \cdots + a_nz^{-n})U(z) = (b_0 + b_1z^{-1} + \cdots + b_nz^{-n})E(z)$$

Therefore

$$D(z) = \frac{U(z)}{E(z)} = \frac{b_0 + b_1z^{-1} + \cdots + b_nz^{-n}}{1 + a_1z^{-1} + \cdots + a_nz^{-n}} \tag{11.36a}$$

This transfer function can be equivalently expressed as

$$D(z) = \frac{U(z)}{E(z)} = \frac{b_0z^n + b_1z^{n-1} + \cdots + b_n}{z^n + a_1z^{n-1} + \cdots + a_n} \tag{11.36b}$$

11.9.2 Transfer Function Model of Plant

Consider the sampled-data system of Fig. 11.7. The plant is a continuous-time system with transfer function $G(s)$, and the ZOH operation has been approximated by a transfer function model $G_{h0}(s) = ((1 - e^{-sT})/s)$. The two are in cascade and are not separated by a sampler; we can treat the two together as a single system with transfer function $G_{h0}(s)G(s)$.

We therefore consider $G_{h0}G(s) \triangleq G_{h0}(s)G(s)$ as the continuous-time system with input $u(k)$ and the output $y(t)$ as shown in Fig. 11.24a. Note that the input is a discrete-time signal and the output is a continuous-time signal. If, however, we are satisfied with finding the output at the sampling instants and not in between, the representation of the sampled-data system of Fig. 11.24a can be greatly simplified. Our assumption is visually described in Fig. 11.24b where the output is conceptually sampled in synchronization with the input by a *mathematical sampler* $T(M)$. The block represented by dotted lines has now discrete-time signals both at the input and the output and therefore a z-domain transfer function model can be derived.

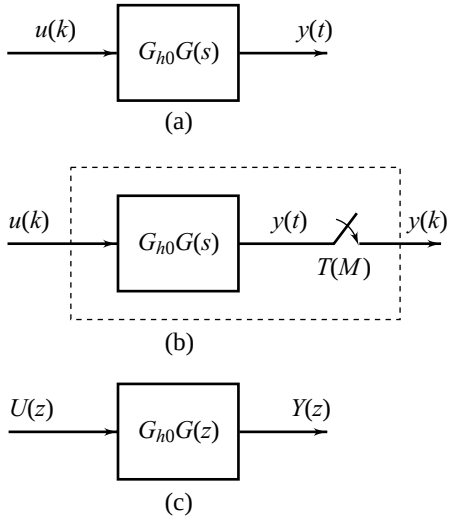

Fig. 11.24 Sampled-data systems

$$G_{h0}G(s) = \left(\frac{1 - e^{-sT}}{s}\right)G(s) = (1 - e^{-sT})\frac{G(s)}{s}$$

Let $$\mathscr{L}^{-1}\left[\frac{G(s)}{s}\right] = g_1(t), \text{ and } \mathscr{Z}[g_1(kT)] = G_1(z)$$

Then $$\mathscr{L}^{-1}\left[e^{-sT}\frac{G(s)}{s}\right] = g_1(t-T), \text{ and } \mathscr{Z}[g_1(kT-T)] = z^{-1}G_1(z)$$

Therefore

$$G_{h0}G(z) \triangleq \mathscr{Z}[G_{h0}G(s)] = \mathscr{Z}\left[\frac{G(s)}{s} - e^{-sT}\frac{G(s)}{s}\right] = (1-z^{-1})\,\mathscr{Z}\left[\frac{G(s)}{s}\right] \tag{11.37}$$

Expanding $\frac{G(s)}{s}$ into partial fractions, $\mathscr{Z}\left[\frac{G(s)}{s}\right]$ can be found by using the entries in Table 11.1. Figure 11.24c gives the z-domain equivalent of Fig. 11.24b.

Example 11.5 Let $$G(s) = \frac{ae^{-\tau_D s}}{s+a} \tag{11.38}$$

The dead-time τ_D can be expressed as

$$\tau_D = NT + \Delta T \tag{11.39a}$$

where N is an integer and $0 < \Delta < 1$. We can find $G_{h0}G(z)$ using this formulation (refer the companion book [155]). However, given the capabilities of the modern microprocessor, we can always adjust the sampling interval slightly so that

$$\tau_D = NT \tag{11.39b}$$

This assumption would simplify the model $G_{h0}G(z)$, and in most cases we make this adjustment in the sampling frequency. Under this assumption (using Table 11.1),

$$\begin{aligned} G_{h0}G(z) &= (1-z^{-1})\,\mathscr{Z}\left[\frac{G(s)}{s}\right] = (1-z^{-1})\,\mathscr{Z}\left[\frac{ae^{-NTs}}{s(s+a)}\right] \\ &= (1-z^{-1})z^{-N}\,\mathscr{Z}\left[\frac{a}{s(s+a)}\right] = (1-z^{-1})z^{-N}\,\mathscr{Z}\left[\frac{1}{s} - \frac{1}{s+a}\right] \\ &= \frac{z-1}{z(z^N)}\left[\frac{z}{z-1} - \frac{z}{z-e^{-aT}}\right] = \frac{1-e^{-aT}}{z^N(z-e^{-aT})} \end{aligned} \tag{11.40}$$

11.9.3 Transfer Function Model of Closed-loop Sampled-Data System

Consider now the closed-loop sampled-data system of Fig. 11.7, reproduced in Fig. 11.25a. It has $r(t)$ as its input and $y(t)$ is the output. The system of Fig. 11.25b is functionally equivalent to that of Fig. 11.25a; the manipulation of the block diagram from Fig. 11.25a to Fig. 11.25b helps us to use the relations previously established in this section. The following equations easily follow:

$$U(z) = D(z)E(z) \tag{11.41a}$$

$$Y(z) = G_{h0}G(z)U(z) \tag{11.41b}$$

Since $$e(kT) = r(kT) - y(kT), \tag{11.41c}$$

we have $$E(z) = R(z) - Y(z)$$

Combining Eqns (11.41a), (11.41b), and (11.41c), gives

$$\frac{E(z)}{R(z)} = \frac{1}{1 + D(z)G_{h0}G(z)} \tag{11.42}$$

$$M(z) = \frac{Y(z)}{R(z)} = \frac{D(z)G_{h0}G(z)}{1 + D(z)G_{h0}G(z)} \tag{11.43}$$

Figure 11.25c gives the z-domain equivalent of Fig. 11.25b.

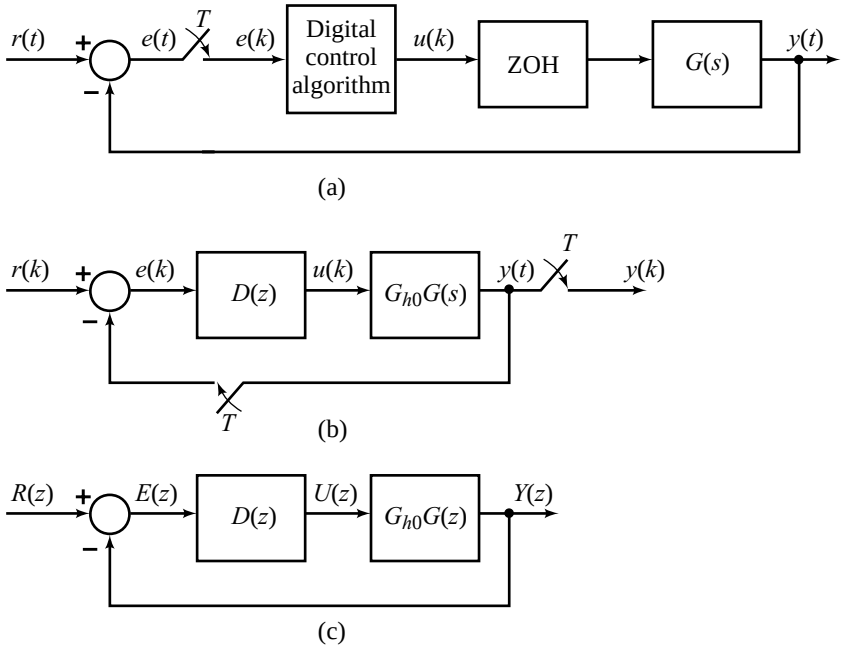

Fig.11.25 Closed.loop sampled-data system

Example 11.6 Consider the sampled-data feedback system of Fig. 11.26a where the sensor dynamics is represented by transfer function $H(s)$. Figure 11.26b shows a functionally equivalent system. The following equations easily follow:

$$E(z) = R(z) - B(z) \tag{11.44a}$$

$$Y(z) = G_{h0}G(z)E(z) = \mathscr{Z}[G_{h0}(s)G(s)]E(z) \tag{11.44b}$$

$$B(z) = G_{h0}GH(z)E(z) = \mathscr{Z}[G_{h0}(s)G(s)H(s)]E(z) \tag{11.44c}$$

Equations (11.44a), (11.44b), and (11.44c) give

$$\frac{E(z)}{R(z)} = \frac{1}{1 + G_{h0}GH(z)} \tag{11.45a}$$

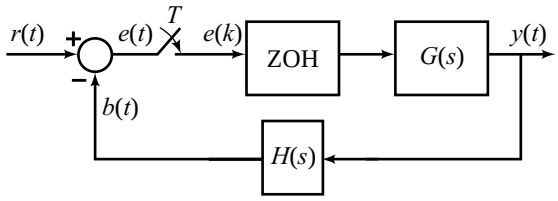

(a)

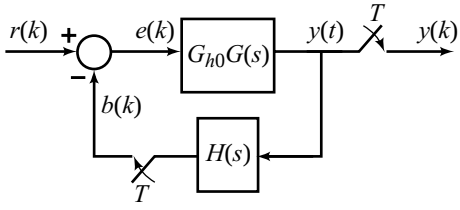

(b)

Fig.11.26 A non-unity feedback sampled-data system

$$M(z) = \frac{Y(z)}{R(z)} = \frac{G_{h0}G(z)}{1 + G_{h0}GH(z)} \tag{11.45b}$$

Having become familiar with the technique, from now onwards we may directly write z-domain relationships without manipulating the block diagrams of sampled-data systems.

11.9.4 Dynamic Response

A standard problem in control engineering is to find the response, $y(k)$, of a system given the input, $r(k)$, and a model of the system. With z-transforms, we have a means for easily computing the response of linear time-invariant systems to quite general inputs.

Given a general relaxed, closed-loop sampled-data system and an input signal $r(k)$, the procedure for determining the output $y(k)$ is given by the following steps.

STEP1: Determine the transfer function $M(z)$ of the sampled-data system.
STEP2: Determine the z-transform of the input signal; $R(z) = \mathcal{Z}[r(k)]$.
STEP3: Determine the z-transform of the output; $Y(z) = M(z)R(z)$.
STEP4: Break-up $Y(z)$ by partial-fraction expansion.
STEP5: Invert $Y(z)$ to get $y(k)$: look-up the components of $y(k)$ in a table of transform pairs and combine the components to get the total solution in the desired form.

Example 11.7 A sampled-data system is described by the transfer function

$$M(z) = \frac{Y(z)}{R(z)} = \frac{1}{z^2 + a_1 z + a_2}; \; a_1 = -\frac{3}{4}, \; a_2 = \frac{1}{8}$$

Find the response $y(k)$ to the input (i) $r(k) = \delta(k)$, (ii) $r(k) = \mu$(k)

Solution

The transfer function $M(z)$ expressed as a ratio of polynomials in z^{-1} :

$$M(z) = \frac{z^{-2}}{1 - \frac{3}{4}z^{-1} + \frac{1}{8}z^{-2}}$$

Since z^{-1} is a unit delay operator, we can immediately write the corresponding difference equation:

$$y(k) - \frac{3}{4}y(k-1) + \frac{1}{8}y(k-2) = r(k-2)$$

The difference equations can be solved easily by means of recursion procedure. The recursion procedure is quite simple and convenient for digital computations. In the following, we obtain the closed-form solutions.

(i) The z-transform of $\delta(k)$ is (refer Table 11.1): $\mathcal{Z}[\delta(k)] = 1$

Letting $R(z)=1$, we obtain

$$Y(z) = M(z) = \frac{1}{z^2 - \frac{3}{4}z + \frac{1}{8}} = \frac{1}{\left[z - \frac{1}{4}\right]\left[z - \frac{1}{2}\right]} = \frac{4}{z - \frac{1}{2}} - \frac{4}{z - \frac{1}{4}}$$

The response $y(k)$ is therefore (refer Table 11.1)

$$y(k) = \mathcal{Z}^{-1} = \left[z^{-1}\left(\frac{4z}{z - \frac{1}{2}}\right)\right] - \mathcal{Z}^{-1}\left[z^{-1}\left(\frac{4z}{z - \frac{1}{4}}\right)\right] = 4\left(\frac{1}{2}\right)^{k-1} - 4\left(\frac{1}{4}\right)^{k-1};\ k \geq 1$$

The discrete-time impulse input thus excites the system poles without creating any additional response term.

(ii) The z-transform of $\mu(k)$ is (refer Table 11.1)

$$\mathcal{Z}[\mu(k)] = \frac{z}{z-1}$$

Letting $R(z) = \frac{z}{z-1}$, we obtain

$$Y(z) = \frac{1}{\left(z - \frac{1}{4}\right)\left(z - \frac{1}{2}\right)}\left[\frac{z}{z-1}\right] = \frac{z}{\left(z - \frac{1}{4}\right)\left(z - \frac{1}{2}\right)(z-1)}$$

$$= \underbrace{\frac{\frac{16}{3}z}{z - \frac{1}{4}} + \frac{-8z}{z - \frac{1}{2}}}_{\text{System poles}} + \underbrace{\frac{\frac{8}{3}z}{z-1}}_{\text{Excitation pole}}$$

The inverse transform operation gives (refer Table 11.1)

$$y(k) = \left[\underbrace{\frac{16}{3}\left(\frac{1}{4}\right)^k - 8\left(\frac{1}{2}\right)^k}_{\text{Transient response}} + \underbrace{\frac{8}{3}(1)^k}_{\text{Steady-state response}}\right]$$

The *transient response* terms correspond to system poles excited by the input $\mu(k)$. These terms vanish as $k \to \infty$. The second response term arises due to the excitation pole, and has the same nature as the input itself except for a modification in magnitude caused by the system's behaviour to the specified input. Since the input exists as $k \to \infty$, the second response term does not vanish and is called the *steady-state response* of the system.

The steady-state response can be quickly obtained without doing the complete inverse transform operation by use of the final value theorem (Eqn. (11.35)):

$$\lim_{k\to\infty} y(k) = \lim_{z\to 1} (z-1)Y(z)$$

if $(z\text{-}1)Y(z)$ has no poles on the boundary and outside of the unit circle in the complex z-plane.

11.10 s-PLANE TO z-PLANE MAPPING

11.10.1 The $z = e^{sT}$ Mapping

For continuous-time systems, we saw in earlier chapters that certain behaviours result from different pole locations in the s-plane: oscillatory behaviour for poles near the imaginary axis, exponential decay for poles on the negative real axis, and unstable behaviour for poles with positive real part. A similar kind of association would also be useful to know when designing sampled-data systems.

The mapping (11.19a):

$$z = e^{sT};\ T = \text{sampling period} \tag{11.46}$$

defines z in terms of s, and is therefore a mapping from the s-plane to the z-plane. The equivalent characteristics in the z-plane are related to those in the s-plane by the mapping (11.46). Consider for example, a continuous-time signal

$$f(t) = e^{-at};\ t > 0$$

which has the Laplace transform

$$F(s) = \frac{1}{s+a}$$

that corresponds to the pole at $s = -a$. The z-transform of $f(kT)$ is (refer Table 11.1)

$$F(z) = \mathcal{Z}[e^{-akT}] = \frac{z}{z - e^{-aT}}$$

which corresponds to a pole at $z = e^{-aT}$. This means that a pole at $s = -a$ in the s-plane corresponds to a pole at $z = e^{-aT}$ in the z-plane. The relationship $z = e^{sT}$ is, in fact, true in general for the poles of Laplace transform and z-transform functions, as is demonstrated by the entries in Table 11.1.

In Fig. 11.27a, the s-plane has been divided into strips of width ω_s where $\omega_s = 2\pi/T$ is the sampling frequency. The primary strip extends from $\omega = -\frac{\omega_s}{2}\left(=\frac{-\pi}{T}\right)$ to $+\frac{\omega_s}{2}\left(=\frac{\pi}{T}\right)$, and the complimentary strips extend from $-\frac{\omega_s}{2}\left(=\frac{-\pi}{T}\right)$ to $-\frac{3\omega_s}{2}\left(=\frac{-3\pi}{T}\right)$,..., for negative frequencies, and from $\frac{\omega_s}{2}\left(=\frac{\pi}{T}\right)$ to $\frac{3\omega_s}{2}\left(=\frac{3\pi}{T}\right)$,..., for positive frequencies.

It can easily be demonstrated that the primary strip, shown shaded in Fig. 11.27a, maps into the entire z-plane. The points in the shaded strip belonging to the left-half of the s-plane map into the interior of the unit circle; the points in the strip belonging to $j\omega$-axis of the s-plane map onto the boundary of the unit circle; and the points in the strip belonging to the right-half of the s-plane map into the exterior of the unit circle in the complex z-plane (Fig. 11.27b).

An important observation on the mapping $z = e^{sT}$ is that each of the complimentary strips maps into the entire z-plane the way the primary strip maps. Consider poles at $s = -a \pm j2n\pi/T$; $n = 1, 2,...$ (For $n = 1$, the poles lie in the complimentary strip that extends from π/T to $3\pi/T$, as shown in Fig. 11.27a). The corresponding pole locations in the z-plane are $z = e^{-aT}e^{\pm j2n\pi} = e^{-aT}$, which is the mapping of the pole $s = -a$ in the primary strip. This means that with the mapping $z = e^{sT}$,we cannot distinguish the poles in the primary strip from the poles in the secondary strips. Thus the largest frequency we can distinguish is $\omega = \pi/T$, which is half the sampling frequency $\omega_s = 2\pi/T$.

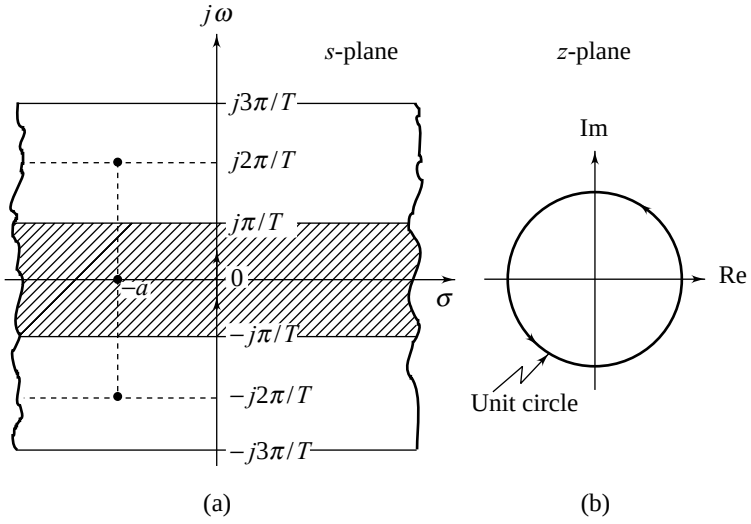

Fig. 11.27 Mapping of the s-plane to the z-plane using the $z = e^{sT}$ transformation

While sampling a continuous-time signal to produce the discrete-time sequence, we want to ensure that all the information in the original signal is retained in the samples. There will be no information loss if we can exactly recover the continuous-time signal from the samples. To determine the condition under which there is no information loss, let us consider the continuous-time signal to be band-limited signal with maximum frequency ω_m. From Fig. 11.27 we observe that there is no information loss if

$$\frac{\pi}{T} > \omega_m \quad \text{or,} \quad \omega_s > 2\omega_m$$

This, in fact, is the *sampling theorem*: Let $x(t)$ be a band-limited signal with $X(j\omega) = 0$ for $|\omega| > \omega_m$, then $x(t)$ is uniquely determined from its samples $x(kT)$ if the sampling frequency $\omega_s \left(= \frac{2\pi}{T}\right) > 2\omega_m$, i.e., the *sampling frequency must be at least twice the highest frequency present in the signal.*

11.10.2 Stability on the z-Plane

From Fig. 11.27, the following conclusions can easily be drawn (Revisiting Chapter 5 will be helpful).
A sampled-data control system with closed-loop transfer function $M(z)$ is

(a) stable if all the poles of $M(z)$ are inside the unit circle;
(b) unstable if any pole of $M(z)$ is outside the unit circle and/or there are poles of multiplicity greater than one on the unit circle; and
(c) marginally stable if the poles on the unit circle are of multiplicity one and all other poles are inside the unit circle.

The determination of stability hinges upon our ability to determine whether the roots of the denominator of the closed-loop transfer function $M(z)$ are in the stable region of the z-plane. The problem for high-order systems is complicated because of the fact that the denominator of $M(z)$ is in polynomial form, not in factored form. Tabular methods for determining stability for high-order sampled-data systems exist (Jury's stability test is a well-known tabular method). For want of space, these methods are not covered in this introductory chapter on digital control (refer the companion book [155]).

The approach of stability analysis by tabular methods (such as Jury's criterion) is purely algebraic. The methods lack the ability to give an overall picture of how the closed-loop response would vary with changes in gain. The key to achieving this global picture is to rethink the solution in terms of geometry. The root locus technique is intrinsically geometric as opposed to algebraic approach of the tabular methods. In chapter 7, we have discussed relative stability analysis of continuous-time systems by the root-locus technique. The analysis was centred around some particular patterns in the s-plane: (i) loci of points in the s-plane with constant damping ratio ζ; and (ii) loci of points in the s-plane with constant undamped natural frequency ω_n. Correlating these patterns of the s-plane with particular features of system behaviour on the z-plane will be of great value in relative stability analysis of sampled-data systems using the root locus technique. The correlations based on the mapping $z = e^{sT}$ are described below, and the root locus analysis will appear in the next section.

Complex-conjugate pair of s-plane poles:

$$s_{1,2} = -\zeta\omega_n \pm j\omega_n \sqrt{1-\zeta^2} = -\zeta\omega_n \pm j\omega_d \tag{11.47a}$$

is transformed to

$$z_{1,2} = e^{-\zeta\omega_n T}\, e^{\pm j\omega_n T\sqrt{1-\zeta^2}} = re^{\pm j\theta} \tag{11.47b}$$

We know from earlier chapters that as ω_n is varied for constant ζ, the poles given by (11.47a) lie along a radial line in the s-plane (Fig.11.28a). In the z-plane, the magnitude of z (i.e., the distance to the origin) is $r = e^{-\zeta\omega_n T}$ and the angles with the positive real axis of the z-plane, measured positive in the counterclockwise direction, are $\theta = \omega_n T\sqrt{1-\zeta^2}$. As ω_n increases for a constant ζ, the magnitude of z decreases and the phase angle increases; constant ζ locus is a logarithmic spiral in the z-plane (Fig.11.28c). This, in fact, is one-to-one map of constant-ζ line in the primary strip.

Consider now the locus of the poles in Eqn. (11.47a) when ζ is varied but ω_d is held constant (Fig. 11.28b). We assume that ω_d is in the primary strip. Note that we are considering constant-ω_d locus instead of constant-ω_n locus. As we shall see, this helps us to extract the information on system behaviour using a simple straight line locus. The constant-ω_n locus is nonlinear [155].

From Eqns (11.47),

$$z_{1,2} = e^{-\zeta\omega_n T}\, e^{\pm j\omega_d T} = re^{\pm j\theta}$$

For a constant ω_d, the angle θ is fixed. Therefore a radial line at an angle $\theta°$ with the real axis is a constant-ω_d locus (Fig. 11.28d):

$$\omega_d T = \frac{\theta° \times \pi}{180} \text{ rad} \tag{11.47c}$$

Figure 11.28e illustrates the translation of specifications on ζ and ω_n to the characteristic root locations in the z-plane. The z-plane poles for constant ζ lie along a spiral, and the z-plane poles for constant ω_d (value of ω_d derived from specified values of ζ and ω_n) lie along a straight line. The intersection of the two curves provides the z-plane pole locations for specified values of ζ and ω_n.

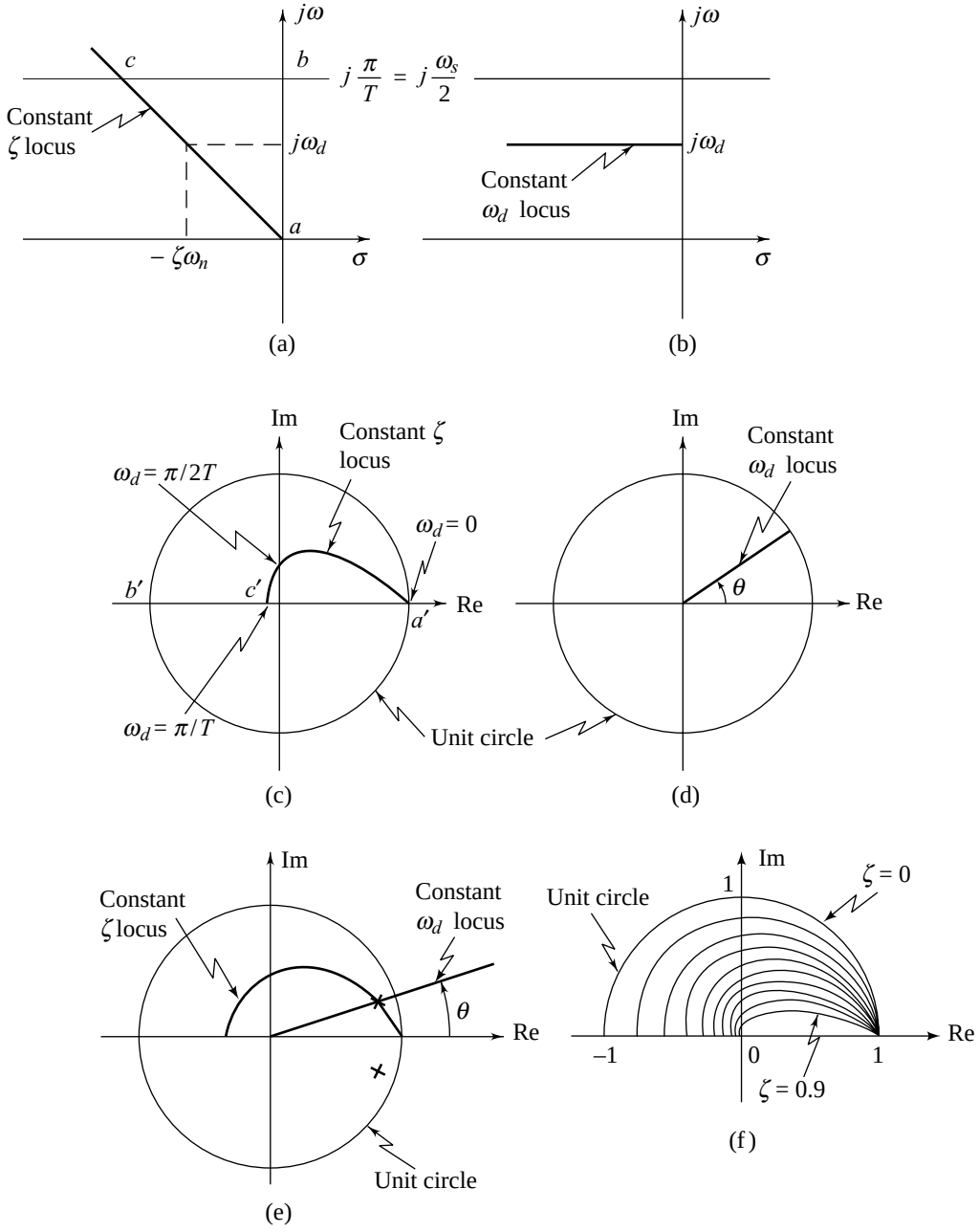

Fig. 11.28 Mapping of s-plane patterns onto z-plane

For a given ζ, the constant-ζ curve on the z-plane may be constructed using Eqn. (11.47b). Table 11.2 gives the real and imaginary coordinates of points on some constant-ζ curves. Figure 11.28f shows a plot of constant-ζ curves. Constant-ω_d curves are radial lines which are relatively easy to construct for given values of ω_d.

Table 11.2 Coordinates of points on some constant-ζ curves.

$\zeta = 0.3$	Re	0.932	0.735	0.360	0	–0.259	–0.380	–0.373
	Im	0.164	0.424	0.623	0.610	0.448	0.220	0
$\zeta = 0.4$	Re	0.913	0.689	0.317	0	–0.201	–0.276	–0.254
	Im	0.161	0.398	0.549	0.504	0.347	0.160	0
$\zeta = 0.5$	Re	0.891	0.640	0.273	0	–0.149	–0.191	–0.163
	Im	0.157	0.370	0.473	0.404	0.259	0.110	0
$\zeta = 0.6$	Re	0.864	0.585	0.228	0	–0.104	–0.122	–0.095
	Im	0.152	0.338	0.395	0.308	0.180	0.070	0
$\zeta = 0.7$	Re	0.830	0.519	0.179	0	–0.064	–0.067	–0.046
	Im	0.146	0.299	0.310	0.215	0.111	0.039	0
$\zeta = 0.8$	Re	0.780	0.431	0.124	0	–0.031	–0.026	–0.015
	Im	0.138	0.249	0.215	0.123	0.053	0.015	0

11.10.3 The Bilinear Mapping

In Section 11.6, we discussed a numerical integration scheme: trapezoidal rule for integration, for performing the discretization of analog compensators. Armed with an understanding of the z-transform, we now revisit this discretization method.

Assume we are given an analog compensator $D(s)$, shown in Fig. 11.13a. We wish to find a set of difference equations (or $D(z)$) for the digital implementation of that compensation in Fig. 11.13b. We rephrase the problem as one of finding the best $D(z)$ in the digital implementation shown in Fig. 11.29a to match the analog system represented by $D(s)$ in Fig. 11.29b. The technique followed in Section 11.6 is to approach the problem as one of numerical integration. Suppose

$$\frac{U(s)}{E(s)} = D(s) = \frac{1}{s}$$

Therefore

$$u(kT) = \int_0^{kT-T} e(t)\,dt + \int_{kT-T}^{kT} e(t)\,dt$$

which can be rewritten as

$$u(kT) = u(kT - T) + (\text{area under the } e(t) \text{ curve over } t = kT - T \text{ to } t = kT) \tag{11.48}$$

where T is the sampling period.

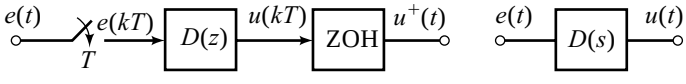

(a) (b)

Fig. 11.29 (a) Digital compensator; (b) Analog compensator

The trapezoidal rule for integration approximates $e(t)$ by a straight line between the two samples (Fig. 11.14). Writing $u(kT)$ as $u(k)$ and $u(kT - T)$ as $u(k - 1)$ for short, we approximate Eqn. (11.48) to

$$u(k) = u(k-1) + \frac{T}{2}[e(k-1) + e(k)] \tag{11.49}$$

z-transformation of this equation gives

$$\frac{U(z)}{E(z)} = \frac{T}{2}\left(\frac{1+z^{-1}}{1-z^{-1}}\right) = \frac{1}{\frac{2}{T}\left(\frac{1-z^{-1}}{1+z^{-1}}\right)} = D(z)$$

For $D(s) = \dfrac{a}{s+a}$, applying the same integration procedure yields

$$D(z) = \frac{a}{\frac{2}{T}\left(\frac{1-z^{-1}}{1+z^{-1}}\right) + a}$$

In fact, substituting

$$s = \frac{2}{T}\left(\frac{1-z^{-1}}{1+z^{-1}}\right) \tag{11.50}$$

for every occurrence of s in any $D(s)$ yields a $D(z)$ based on the trapezoidal integration rule. This is called the *bilinear mapping*.

11.11 TRANSFORM DESIGN OF DIGITAL CONTROLS

The transform design of digital compensators is very similar to the design of analog compensators discussed is earlier chapters; in fact, all the same rules apply.

11.11.1 Design Using Root-Locus Plots

A closed-loop sampled-data system with a digital control algorithm used to improve the performance is shown in Fig. 11.25. The closed-loop transfer function is (refer Eqn. (11.43))

$$\frac{Y(z)}{R(z)} = M(z) = \frac{D(z)G_{h0}G(z)}{1 + D(z)G_{h0}G(z)} \tag{11.51}$$

The transient behaviour of the closed-loop system is given by the factors in the denominator of Eqn. (11.51), that is, the roots of the characteristic equation

$$1 + D(z)G_{h0}G(z) = 0 \tag{11.52}$$

The root-locus techniques used in continuous-time systems (Chapter 7) to find roots of a polynomial in s apply equally well and without modification to the polynomial in z; however, the interpretation of the results is quite different as we saw in Fig. 11.28. A major difference is that the stability boundary is now the unit circle instead of the imaginary axis.

We use Table 7.1 with s replaced by z for sketching the root locus plot for sampled-data systems. All the rules in the table apply for sampled-data systems without modification. For stability analysis and design of digital compensator, we superimpose a unit circle on the root locus plot and determine the characteristics of the closed-loop sampled-data systems. Examples that follow will illustrate the procedure.

Transient Accuracy The specifications on peak overshoot, settling time, etc., of the closed-loop transient response are translated into the parameters ζ and ω_n of the standard second-order transfer function (refer Chapter 6), the poles of the standard second-order transfer function are mapped onto the z-plane (revisit Section 11.10), and a digital compensator that matches the dominant roots of the characteristic equation (11.52) with the z-plane poles of the standard second-order transfer function is selected.

On the z plane root locus, a finite zero/additional pole has only a small effect when located in the range 0 to -1. This can be seen from Fig. 11.28f. For $\zeta = 0$, the s-plane point $j\omega_s/2$ maps to z-plane point -1. As $\zeta \to 1$, the point given by intersection of ζ-line and boundary $j\omega_s/2$ of the primary strip maps to a point on the negative real axis of the z-plane between -1 and 0. Figure 11.28c shows mapping of one such point.

Steady-State Accuracy The steady-state behaviour of the closed-loop sampled-data system of Fig. 11.25 may be determined from the relation (refer Eqn. (11.42))

$$E(z) = \frac{R(z)}{1 + D(z)G_{h0}G(z)} \tag{11.53}$$

The final value theorem given by Eqn. (11.35) states that when $(z-1)E(z)$ is analytic,

$$e_{ss}^{*} = \lim_{z \to 1} (1 - z^{-1})E(z) \tag{11.54a}$$

where e_{ss}^{*} is the final sampled value of $e(t)$, i.e., the final value of $e(kT)$.

Using the final value theorem on Eqn. (11.53), we find that the sampled steady-state error for the system of Fig. 11.25 is

$$e_{ss}^{*} = \lim_{z \to 1} (z - 1) \frac{R(z)}{1 + D(z)G_{h0}G(z)} \tag{11.54b}$$

For a unit step input (from Table 11.1),

$$R(z) = \frac{z}{z - 1}$$

Substituting into Eqn. (11.54b), we have

$$e_{ss}^{*} = \frac{1}{1 + \lim_{z \to 1} D(z)G_{h0}G(z)} = \frac{1}{1 + K_p} \tag{11.55a}$$

where the *position error constant*

$$K_p = \lim_{z \to 1} [D(z)G_{h0}G(z)] \tag{11.55b}$$

For a unit ramp input,

$$R(z) = \frac{Tz}{(z - 1)^2}$$

Following the procedure for the step input, we get

$$e_{ss}^{*} = \frac{1}{K_v} \tag{11.56a}$$

where the *velocity error constant*

$$K_v = \frac{1}{T} \lim_{z \to 1} [(z - 1)D(z)G_{h0}G(z)] \tag{11.56b}$$

For a unit parabolic input,

$$R(z) = \frac{T^2 z(z+1)}{2(z-1)^3}$$

and

$$e_{ss}^{*} = \frac{1}{K_a} \tag{11.57a}$$

where the *acceleration error constant*

$$K_a = \frac{1}{T^2} \lim_{z \to 1} [(z-1)^2 D(z) G_{h0} G(z)] \tag{11.57b}$$

We can always express the forward path transfer function $D(z)G_{h0}G(z)$ as

$$D(z)\ G_{h0}G(z) = \frac{K \prod_i (z - z_i)}{(z-1)^N \prod_j (z - p_j)}\ ;\ p_j \neq 1,\ z_i \neq 1 \tag{11.58}$$

$D(z)G_{h0}G(z)$ in Eqn. (11.58) involves the term $(z-1)^N$ in the denominator. As $z \to 1$, this term dominates in determining the steady-state error. Digital control systems are, therefore, classified in accordance with the number of poles at $z = 1$ in the forward-path transfer function. From Eqns (11.55)–(11.57) we see that a system with $N = 0$ (called a type-0 system) has a finite non-zero position error, infinite velocity and acceleration errors at steady-state. A system with $N = 1$ (called a type-1 system) has zero position error, a finite non-zero velocity error and infinite acceleration error at steady-state. A system with $N - 2$ (called a type-2 system) has zero position and velocity errors and a finite non-zero acceleration error at steady-state.

Lead Compensator A simple lead compensator model in the s-plane is described by a transfer function

$$D(s) = \frac{1 + s\tau}{1 + \alpha s\tau}\ ;\ \alpha < 1,\ \tau > 0 \tag{11.59a}$$

The pole and zero of $D(s)$ always lie on the real axis in the left-half of s-plane; the zero is always to the right of the pole. On the z-plane, the pole and zero of $D(z)$ will always lie on the real axis inside the unit circle; with the zero always to the right of the pole (by s-plane to z-plane mapping). A typical pole-zero configuration of a lead compensator

$$D(z) = K_{c1} \frac{z - \alpha_1}{z - \alpha_2} \tag{11.59b}$$

is shown in Fig. 11.30a.

Lag Compensator A simple lag compensator model in the s-plane is described by a transfer function

$$D(s) = \frac{1 + s\tau}{1 + \beta s\tau}\ ;\ \beta > 1,\ \tau > 0 \tag{11.60a}$$

The pole and zero of $D(s)$ always lie on the real axis in the left half of s-plane; the pole is always to the right of the zero. On the z-plane, the pole and the zero of $D(z)$ will always lie on the real axis inside the unit circle; with pole always to the right of the zero (by s-plane to z-plane mapping). A typical pole-zero configuration of a lag compensator

$$D(z) = K_{c2} \frac{z - \beta_1}{z - \beta_2} \tag{11.60b}$$

is shown in Fig. 11.30b.

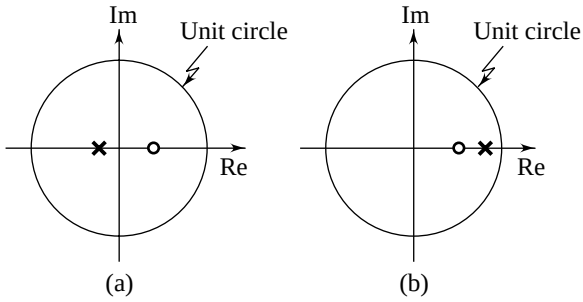

Fig. 11.30 Pole-zero configurations of compensators

Example 11.8 To study the effect of a lead compensator on the root loci, we consider a unity feedback sampled-data system with open-loop transfer function

$$G_{h0}G(z) = \frac{K(z+0.368)}{(z-0.368)(z-0.135)}\,;\; T = 1 \text{ sec} \qquad (11.61)$$

The root locus plot of the uncompensated system is shown in Fig. 11.31a. The plot intersects the $\zeta = 0.5$ locus at point P. The value of gain K at this point is determined to be 0.3823.

Constant-ω_d locus passing through point P is a radial line at an angle of 82º with the real axis (Fig. 11.31a). Therefore

$$\omega_d T = \omega_n T\sqrt{1-\zeta^2} = \frac{82\pi}{180}$$

This gives $\omega_n = 1.65$ rad/sec

Since $G_{h0}G(z)$ given by Eqn. (11.61) is a type-0 system, we will consider position error constant K_p to study steady-state accuracy. For $K = 0.3823$,

$$K_p = \lim_{z\to 1} G_{h0}G(z) = \frac{0.3823(1+0.368)}{(1-0.368)(1-0.135)} = 0.957$$

We now cancel the pole of $G_{h0}G(z)$ at $z = 0.135$ by the zero of the lead compensator and add a pole at $z = -0.135$, i.e., we select

$$D(z) = \frac{z-0.135}{z+0.135}$$

Figure 11.31b shows the root locus plot of lead compensated system. The modified locus has moved to the left, toward the more stable part of the plane. The intersection of the locus with the $\zeta = 0.5$ line is at point Q. The value of ω_n at this point is determined to be 2.2 rad/sec. The lead compensator has thus increased ω_n and hence the speed of response of the system. The gain K at point Q is determined to be 0.433. The position error constant of the lead compensated system is given by

$$K_p = \lim_{z\to 1} D(z)G_{h0}G(z) = \lim_{z\to 1} \frac{0.433(z+0.368)}{(z-0.368)(z+0.135)} = 0.826$$

The lead compensator has thus given satisfactory dynamic response, but the position error constant is too low. We will shortly see how K_p can be increased by lag compensation.

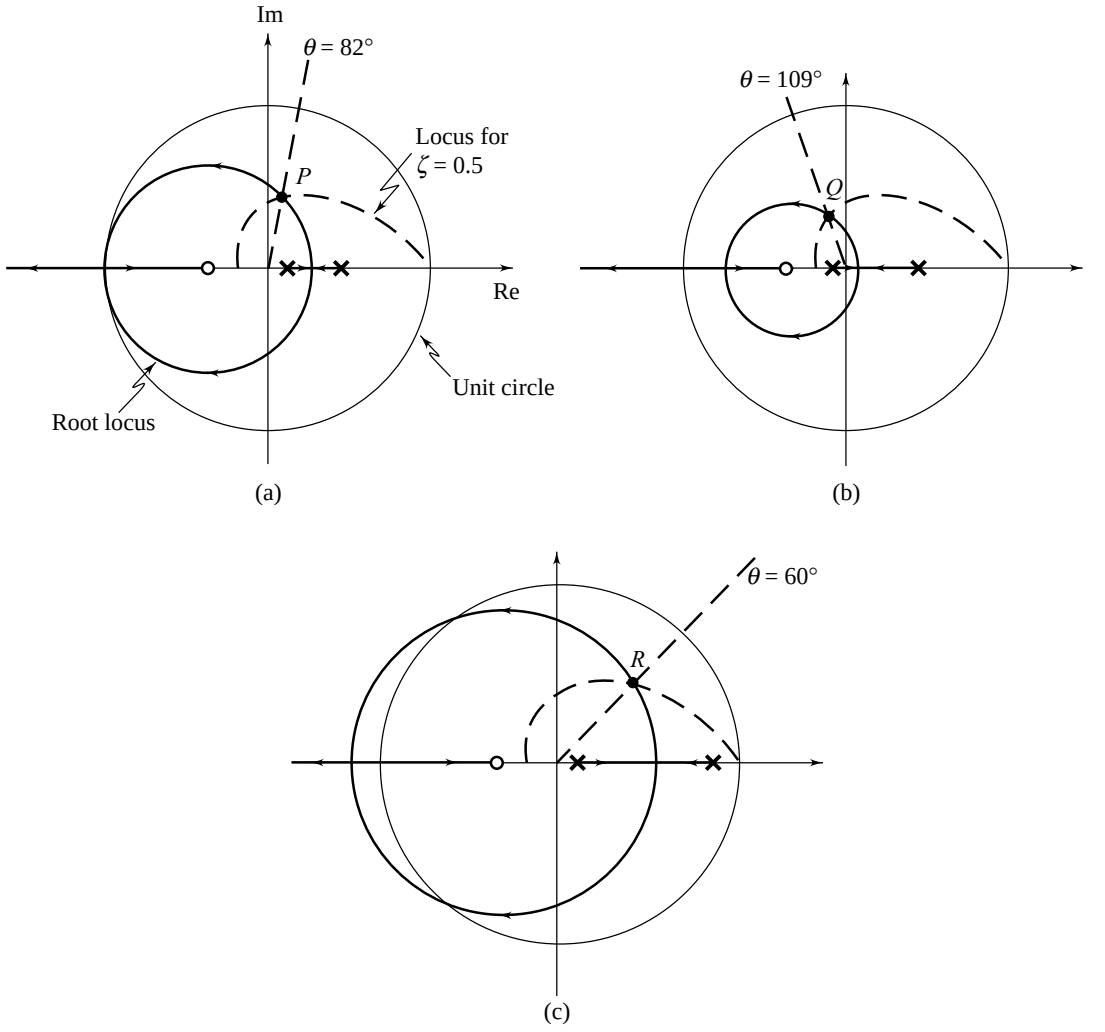

Fig 11.31 Root locus plot for (a) uncompensated; (b) lead compensated; and (c) lag compensated system

The selection of the exact values of pole and zero of the lead compensator is done by experience and by trial-and-error. In general, the zero is placed in the neighbourhood of the desired dominant closed-loop poles, and the pole is located at a reasonable distance to the left of the zero location.

Example 11.9 To study the effect of lag compensator on the root loci, we reconsider the system described by Eqn. (11.61):

$$G_{h0}G(z) = \frac{K(z+0.368)}{(z-0.368)(z-0.135)}\,;\; T = 1 \text{ sec}$$

The root locus plot of the uncompensated system is shown in Fig. 11.31a. At point P, $\zeta = 0.5$, $\omega_n = 1.65$ and $K = 0.3823$ ($K_p = 0.957$).

We now cancel the pole of $G_{h0}G(z)$ at $z = 0.368$ by the zero of the lag compensator and add a pole at $z = 0.9$, i.e., we select

$$D(z) = \frac{z - 0.368}{z - 0.9}$$

Figure 11.31c shows the root locus plot of the lag compensated system. The intersection of the locus with $\zeta = 0.5$ line is at point R. The value of ω_n at this point is determined to be 1.2 rad/sec. The lag compensator has thus reduced ω_n and hence the speed of response. The value of the gain K at point R is determined to be 0.478. The position error constant of the lag compensated system is

$$K_p = \lim_{z \to 1} D(z)\, G_{h0}G(z) = \lim_{z \to 1} \frac{0.478(z + 0.368)}{(z - 0.135)(z - 0.9)} = 7.56$$

Thus we have been able to increase position error constant appreciably by lag compensation.

If both the pole and the zero of the lag compensator are moved close to $z = 1$, then the root locus plot of the lag compensated system moves back towards its uncompensated shape. Consider the root locus plot of the uncompensated system shown in Fig. 11.31a. The angle contributed at point P by additional pole-zero pair close to $z = 1$ (called a *dipole*) will be negligibly small; therefore the point P will continue to lie on the lag compensated root locus plot. However, the lag compensator

$$D(z) = \frac{z - \beta_1}{z - \beta_2}$$

will raise the system K_p by a factor of $(1 - \beta_1)/(1 - \beta_2)$.

11.11.2 Design using Frequency-Response Plots

For a system of the form shown in Fig. 11.25, having closed-loop transfer function (11.51), the frequency-domain performance can be investigated by making the frequency response plots of open-loop transfer function $G_{h0}G(z)$. The frequency response plots of $G_{h0}G(z)$ can be obtained by setting

$$z = e^{j\omega T};\ T = \text{sampling interval} \tag{11.62}$$

and then letting the frequency ω vary from $-\omega_s/2$ to $+\omega_s/2$; $\omega_s = 2\pi/T$.

Since the frequency appears in the form $e^{j\omega T}$, the discrete-time transfer functions are typically not rational functions and the simplicity of Bode's design techniques (refer Chapter 10) is altogether lost in the z-plane. Computer assistance is normally required to make the frequency response plots.

The following sequential steps are quite helpful for designing digital compensators.

(i) Design an analog compensator $D(s)$ for the given continuous-time plant model using the procedure detailed in Chapter 10.

(ii) Discretize the analog compensator using bilinear transformation; this will yield $D(z)$. Note that bilinear transformation will result in rational transfer function $D(z)$.

(iii) Analyze in time domain the sampled-data feedback system composed of discretized plant model and the compensator $D(z)$ obtained from step (ii).

(iv) Obtain frequency response plots of discrete-time open-loop transfer function and fine-tune the digital compensator of step (ii) using frequency-domain design preocedures.

Refer the companion book [155] for more details.

Review Examples

Review Example 11.1 Consider the sampled-data system shown in Fig. 11.32a. From the block diagram we obtain (refer Eqn. (11.43))

$$\frac{Y(z)}{R(z)} = \frac{G_{h0}G(z)}{1+G_{h0}G(z)} \tag{11.63}$$

Figure 11.32b gives the z-domain equivalent of Fig. 11.32a. The forward path transfer function

$$G_{h0}G(z) = \mathcal{Z}[G_{h0}(s)G(s)]$$

$$= (1-z^{-1})\,\mathcal{Z}\left[\frac{G(s)}{s}\right] = (1-z^{-1})\,\mathcal{Z}\left[\frac{1}{s^2(s+1)}\right]$$

$$= (1-z^{-1})\,\mathcal{Z}\left[\frac{1}{s^2}-\frac{1}{s}+\frac{1}{s+1}\right] = (1-z^{-1})\left[\frac{Tz}{(z-1)^2}-\frac{z}{z-1}+\frac{z}{z-e^{-T}}\right]$$

$$= \frac{z(T-1+e^{-T})+(1-e^{-T}-Te^{-T})}{(z-1)(z-e^{-T})}$$

When $T = 1$, we have

$$G_{h0}G(z) = \frac{ze^{-1}+1-2e^{-1}}{(z-1)(z-e^{-1})} = \frac{0.3679z+0.2642}{z^2-1.3679z+0.3679}$$

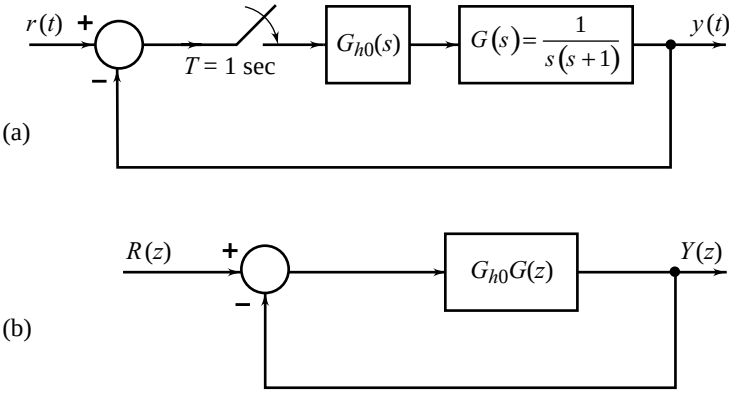

Fig. 11.32 A closed-loop sampled-data system

Substituting in Eqn. (11.63), we obtain

$$\frac{Y(z)}{R(z)} = \frac{0.3679z+0.2642}{z^2-z+0.6321}$$

For a unit-step input,

$$R(z) = \frac{z}{z-1}$$

and therefore

$$Y(z) = \frac{z(0.3679z + 0.2642)}{(z-1)(z^2 - z + 0.6321)} = \frac{0.3679z^2 + 0.2642z}{z^3 - 2z^2 + 1.6321z - 0.6321}$$

$$= \frac{0.3679\, z^{-1} + 0.2642\, z^{-2}}{1 - 2z^{-1} + 1.6321\, z^{-2} - 0.6321\, z^{-3}}$$

By long-division process, we get

$$Y(z) = 0.3679\, z^{-1} + z^{-2} + 1.3996\, z^{-3} + 1.3996\, z^{-4} + 1.1469\, z^{-5} + 0.8944\, z^{-6} + 0.8015\, z^{-7} + \cdots$$

Therefore, the sequence ($k = 1, 2, ...$)

$$y(kT) = \{0.3679, 1, 1.3996, 1.3996, 1.1469, 0.8944, 0.8015, ...\}$$

Note that the final value of $y(kT)$ is (refer Eqn. (11.35)),

$$\lim_{k\to\infty} y(kT) = \lim_{z\to 1} (z-1)Y(z) = \frac{0.3679 + 0.2642}{0.6321} = 1$$

The unit-step response is shown in Fig. 11.33. Also shown in this figure is the unit-step response of the continuous-time system (i.e., when $T = 0$). The overshoot of the sampled system is 45%, in contrast to 17% for the continuous-time system.

The performance of the digital system is thus dependent on the sampling period T. Larger sampling periods usually give rise to higher overshoots in the step response, and may eventually cause instability if the sampling period is too large.

For the continuous-time feedback system with process transfer function $G(s)$, the velocity error constant

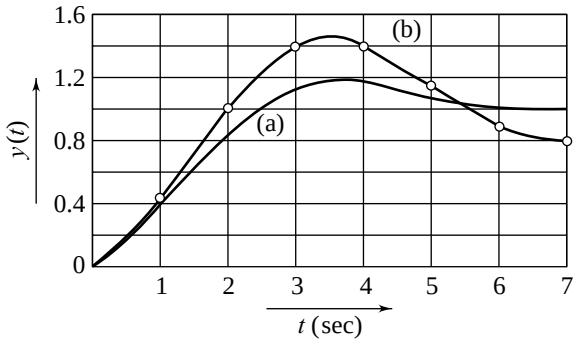

Fig. 11.33 The response of a second-order system: (a) analog; (b) sampled

$$K_v = \lim_{s\to 0} sG(s) = \lim_{s\to 0} s\left[\frac{1}{s(s+1)}\right] = 1$$

When the sampler and the ZOH are introduced in the feedback loop (Fig. 11.32a), the velocity error constant becomes

$$K_v = \frac{1}{T}\lim_{z\to 1}\left[(z-1)G_{h0}G(z)\right]$$

$$= \frac{1}{T}\lim_{z\to 1}\left\{(z-1)\left[\frac{z(T-1+e^{-T}) + (1-e^{-T} - Te^{-T})}{(z-1)(z-e^{-T})}\right]\right\}$$

$$= 1$$

Thus for a type-1 system, the system with sampler and zero-order hold has exactly the same steady-state error as the continuous-time system with the same process transfer function. This, in fact, is true for type-0 and type-2 systems also.

Review Example 11.2 Consider the block diagram of a digital control system shown in Fig. 11.34; *r(t)* stands for reference input and *w(t)* stands for disturbance.

For $r = 0$, the block diagram reduces to the one shown in Fig. 11.35. From this figure it immediately follows that (note that functional equivalence will be lost if we introduce a sampler to discretize disturbance input)

$$Y(s) = G(s)W(s) - G_{h0}(s)G(s)U^*(s)$$
$$\triangleq WG(s) - G_{h0}G(s)U^*(s)$$

Therefore,

$$Y(z) = \mathcal{Z}[WG(s)] - \mathcal{Z}[G_{h0}G(s)]U(z)$$
$$= WG(z) - G_{h0}G(z)U(z)$$

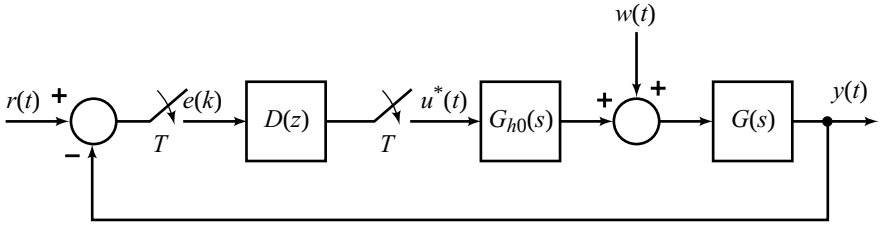

Fig. 11.34

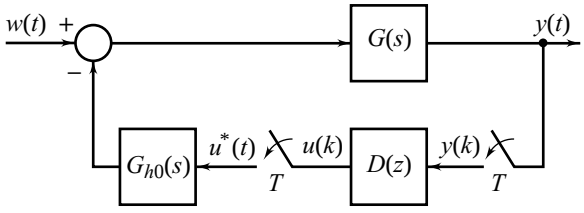

Fig. 11.35

Also,

$$U(z) = D(z)Y(z)$$

This gives

$$Y(z) = WG(z) - D(z)G_{h0}G(z)Y(z)$$

or

$$Y(z) = \frac{WG(z)}{1 + D(z)G_{h0}G(z)} \tag{11.64}$$

Review Example 11.3 Let us reconsider the problem of discretization of a PID controller discussed earlier in Example 11.1. Equation (11.8) is equivalent to:

$$U(s) = K_c\left[1 + \frac{1}{T_I s} + T_D s\right]E(s) = D(s)E(s) \tag{11.65}$$

Discretization of $D(s)$ using bilinear mapping (11.50) gives

$$U(z) = K_c\left[1+\left(\frac{1}{T_I}\right)\frac{T}{2}\left(\frac{z+1}{z-1}\right)+(T_D)\frac{2}{T}\left(\frac{z-1}{z+1}\right)\right]E(z) \tag{11.66}$$

$$= U_P(z) + U_I(z) + U_D(z)$$

The first term in (11.66) is

$$U_P(z) = K_c E(z)$$

This gives

$$u_P(k) = K_c e(k) \tag{11.67a}$$

The second term in (11.66) is

$$U_I(z) = \left(\frac{K_c}{T_I}\right)\frac{T}{2}\left[\frac{z+1}{z-1}\right]E(z)$$

or

$$zU_I(z) = U_I(z)+\left(\frac{K_c}{T_I}\right)\frac{T}{2}\left[zE(z)+E(z)\right]$$

Therefore

$$U_I(z) = z^{-1}U_I(z)+\left(\frac{K_c}{T_I}\right)\frac{T}{2}\left[E(z)+z^{-1}E(z)\right]$$

This gives

$$u_I(k) = u_I(k-1)+\left(\frac{K_c}{T_I}\right)\frac{T}{2}\left[e(k)+e(k-1)\right] \tag{11.67b}$$

The third term in (11.66) is

$$U_D(z) = (K_c T_D)\frac{2}{T}\left[\frac{z-1}{z+1}\right]E(z)$$

or

$$zU_D(z) = -U_D(z) + (K_c T_D)\frac{2}{T}[zE(z) - E(z)]$$

Therefore

$$U_D(z) = -z^{-1}U_D(z)+(K_c T_D)\frac{2}{T}\left[E(z)-z^{-1}E(z)\right]$$

This gives

$$u_D(k) = (K_c T_D)\frac{2}{T}\left[e(k)-e(k-1)\right]-u_D(k-1) \tag{11.67c}$$

From (11.67a), (11.67b) and (11.67c), we obtain

$$u(k) = u_P(k) + u_I(k) + u_D(k) \tag{11.68}$$

Review Questions

11.1 Describe important advantages offered by the use of digital computers as compensator device in a control system. What are the main problems associated with implementation of digital control?

11.2 Sketch a schematic diagram of a speed control system using the following units: motor, tachogenerator, A/D convertor, digital computer, D/A convertor, and power amplifier. Explain the function of each section of the diagram. How do we select the sampling rate?

11.3 Explain with the aid of appropriate diagrams the construction and operation of a shaft encoder. Give a schematic diagram showing how the shaft encoder would be embodied in a digital position control system.

11.4 Given the tuning rules for analog controllers, how do we obtain tuning rules for digital controllers?

11.5 Viewing sampler as an 'impulse modulator', derive suitable mathematical models of A/D and D/A convertors.

11.6 State and prove the final value theorem of the z-transform. What is the condition under which the theorem is valid?

11.7 The sampling theorem states that a continuous-time signal whose frequency spectrum is bounded by upper limit ω_m, can be completely reconstructed from its samples when the sampling frequency $\omega_s > 2\omega_m$. Explain the theorem using $z = e^{sT}$ mapping.

11.8 (a) Given a desired second-order characteristic equation on the s-plane, how can one find the associated desired characteristic equation on the z-plane?

(b) Given a second-order characteristic equation on the z-plane, how can one determine the associated percent overshoot, settling time, and peak time?

11.9 Define the regions of stability, marginal stability, and instability on the s-plane. How are these regions translated to z-plane by the mapping: $z = e^{sT}$?

11.10 Explain bilinear mapping for conversion of analog compensator $D(s)$ to an equivalent digital compensator $D(z)$.

11.11 Using appropriate examples, show that sampling has detrimental effect on the transient response of a closed-loop system, but the steady state response remains unaffected.

Problems

11.1 A PID controller is described by the following relation between input $e(t)$ and output $y(t)$:

$$u(t) = K_c\left[e(t) + \frac{1}{T_I}\int_0^t e(t)\,dt + T_D\frac{de(t)}{dt}\right]$$

Using the trapezoidal rule for integration, obtain the difference equation model for the PID algorithm.

11.2 Consider the analog control system shown in Fig. P11.2. By root-locus analysis, it is found that the closed-loop natural frequency $\omega_n \cong 0.6$ rad/sec, and damping ratio $\zeta = 0.5$.

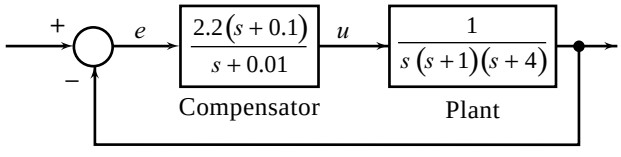

Fig. P11.2

We wish to replace the analog compensator by a digital one. Select a suitable sampling interval and obtain an equivalent digital control algorithm using bilinear mapping. Give a block diagram of the digital control system.

11.3 Figure P11.3 shows a minor-loop feedback compensation scheme. We wish to realize the control action by a digital controller with a uniform sampling interval of T sec. Obtain digital control algorithm using trapezoidal rule for integration. Give a block diagram of the digital control system.

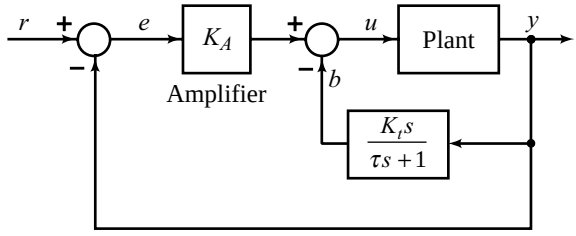

Fig. P11.3

11.4 The most widely used approach for tuning digital PID controllers, is to apply rules given in Table 6.2 developed for analog PID controllers with a simple correction to account for the effect of A/D sampling; the D/A reconstructed signal is effectively delayed by approximately one-half of the sampling interval T. The correction for sampling is then simply to add $T/2$ to the dead-time τ_D. The tuning formulas of Table 6.2 can directly be used for digital PID controllers with τ_D replaced by corrected dead-time.

A process has a gain of 2, a time-constant of 10 min, and a dead-time of 2 min.

(a) Calculate the QDR tuning parameters for a PID controller.

(b) Readjust the tuning parameters calculated in (a) if the PID control is to be carried out with a processing period of 8 sec on a computer control installation.

11.5 Table 6.3 can be directly used for tuning of digital PID controllers; correction for sampling is not required if the test has been conducted on a computer-controlled loop.

In a low-pass process, the following critical quantities were determined by an oscillation test conducted on a computer-controlled loop with sample time $T = 4$ sec.

Ultimate gain, $K_{cu} = 5$

Ultimate period, $T_u = 34$ sec

Determine tuning parameters for a digital PI controller.

11.6 Consider the discrete-time system shown in Fig. P11.6

(a) Obtain the difference equation model and therefrom the transfer function model of the system.

(b) Find the impulse response of the system.

(c) Find the response of the system to unit step input $\mu(k)$.

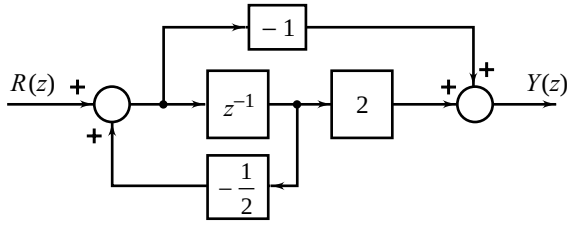

Fig. P11.6

11.7 Solve the following difference equation using z-transform approach:

$$2y(k) - 2y(k-1) + y(k-2) = r(k);\ y(k) = 0 \text{ for } k < 0, \text{ and}$$

$$r(k) = \begin{cases} 1; & k = 0, 1, 2, \ldots \\ 0; & k < 0 \end{cases}$$

11.8 Solve the following difference equation using z-transforms:

$$y(k) - 3y(k-1) + 2y(k-2) = r(k)$$

where

$$r(k) = \begin{cases} 1 \text{ for } k = 0, 1 \\ 0 \text{ for } k \geq 2 \end{cases};\ y(-2) = y(-1) = 0$$

Will the final value theorem give the correct value of $y(k)$ as $k \to \infty$? Why?

11.9 For the transfer function models and inputs given below, find the response $y(k)$ as a function of k:

(a) $G(z) = \dfrac{Y(z)}{R(z)} = \dfrac{2z-3}{(z-0.5)(z+0.3)}$

$r(k) = \begin{cases} 1; & k = 1 \\ 0; & k = 0, 2, 3, 4, \ldots \end{cases}$

(b) $G(z) = \dfrac{Y(z)}{R(z)} = \dfrac{-6z+1}{\left(z-\frac{1}{2}+j\frac{1}{4}\right)\left(z-\frac{1}{2}-j\frac{1}{4}\right)}$

$r(k) = \begin{cases} 0; & k < 0 \\ 1; & k = 0, 1, 2, 3, \ldots \end{cases}$

11.10 For the transfer function models and inputs given below, find the response $y(k)$ as a function of k:

(a) $G(z) = \dfrac{Y(z)}{R(z)} = \dfrac{1}{(z-0.5)(z+0.3)}$

$r(k) = \begin{cases} 1; & k \text{ even} \\ 0; & k \text{ odd} \end{cases}$

(b) $G(z) = \dfrac{Y(z)}{R(z)} = \dfrac{1}{(z-0.5)^2(z-0.1)}$

$r(k) = \begin{cases} 0; & k < 0 \\ 1; & k = 0, 1, 2, 3, \ldots \end{cases}$

11.11 Figure P11.11 shows a discrete-time system. Determine the transfer function of this system assuming that the samplers operate synchronously at intervals of T sec. Also find the unit-step response of the system.

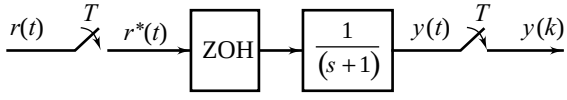

Fig. P11.11

11.12 Figure P11.12 shows the model of a plant driven by a D/A converter. Derive the transfer function model relating $r(kT)$ and $y(kT)$; $T = 0.4$ sec.

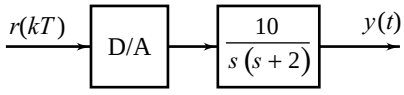

Fig. P11.12

11.13 Shown in Fig. P11.13 is the block diagram of the servo control system for one of the joints of a robot. With $D(z) = 1$, find the transfer function model of the closed-loop system. Sampling period $T = 0.25$ sec.

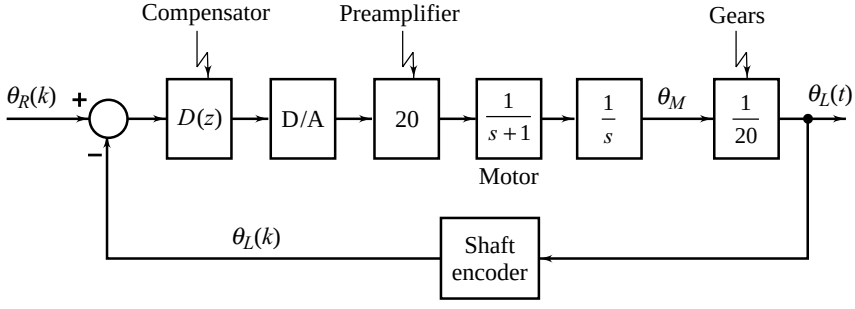

Fig. P11.13

11.14 For the system shown in Fig. P11.14, the computer solves the difference equation $u(k) = u(k-1) + 0.5\,e(k)$, where $e(k)$ is the filter input and $u(k)$ is the filter output. If the sampling rate $f_s = 5$ Hz, find $Y(z)/R(z)$.

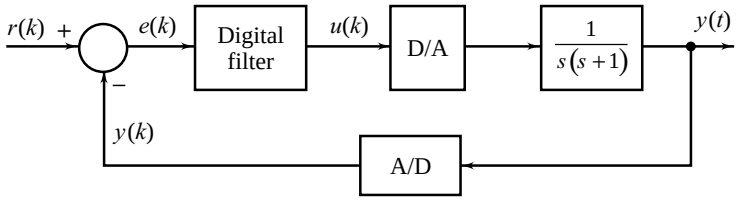

Fig. P11.14

11.15 For the sampled-data system shown in Fig. P11.15, find the output $y(k)$ for $r(t)$ = unit step.

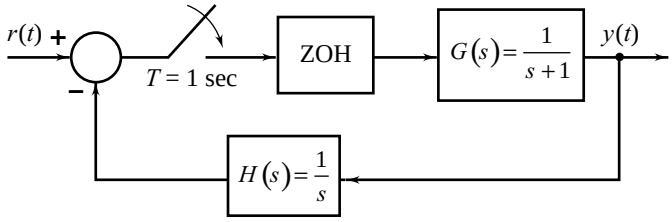

Fig. P11.15

11.16 For the sampled-data system of Fig. P11.16, find the response $y(kT)$; $k = 0, 1, 2, ...$, to a unit-step input $r(t)$.

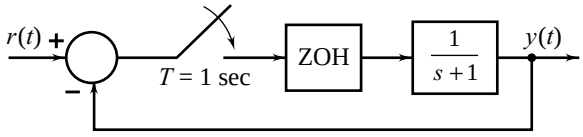

Fig. P11.16

11.17 For the system shown in Fig. P11.17, find

(i) position error constant, K_p,

(ii) velocity error constant, K_v, and

(iii) acceleration error constant, K_a.

Express the results in terms of K_1, K_2, J, and T.

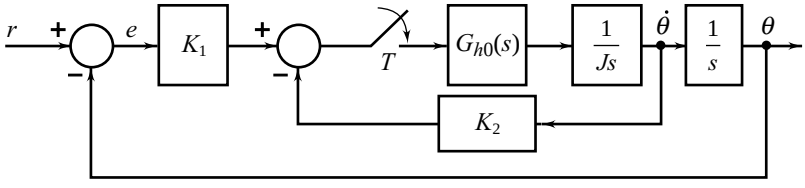

Fig. P11.17

11.18 A unity feedback system is characterized by the open-loop transfer function

$$G_{h0}G(z) = \frac{0.2385(z+0.8760)}{(z-1)(z-0.2644)}$$

The sampling period $T = 0.2$ sec.

Determine steady-state errors for unit-step, unit-ramp, and unit-acceleration inputs.

11.19 Predict the nature of the transient response of a discrete-time system whose characteristic equation is given by

$$z^2 - 1.9z + 0.9307 = 0$$

The sampling interval $T = 0.02$ sec.

11.20 Consider the system of Fig. P11.20. The design specifications for the system require that

(i) the steady-state error to a unit-ramp reference input be less than 0.01,

(ii) a constant disturbance w should not affect the steady-state value of the output.

Show that these objectives can be met if $D(z)$ is a proportional-plus-integral compensator.

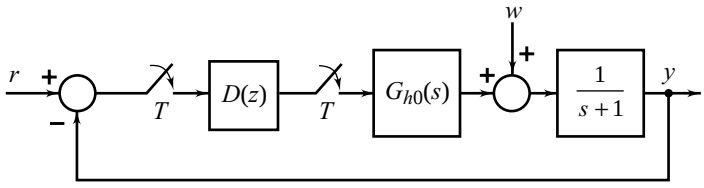

Fig. P11.20

11.21 Given $$G_{h0}G(z) = \frac{K(z-0.9048)}{(z-1)^2}$$

Sketch the root locus plot for $0 \le K < \infty$. Using the information in the root locus plot, determine the range of values of K for which the closed-loop system is stable. Also determine the value of K for which the system closed-loop poles are real and multiple.

11.22 A sampled-data feedback control system is shown in Fig. P11.22. The controlled process of the system is described by the transfer function

$$G(s) = \frac{K}{s(s+1)}; \; 0 \le K < \infty$$

The sampling period $T = 1$ sec.

(a) Sketch the root locus plot for the system on the z-plane and from there obtain the value of K that results in marginal stability.

(b) Repeat part (a) for (i) $T = 2$ sec, (ii) $T = 4$ sec, and compare the stability properties of the system with different values of sampling interval.

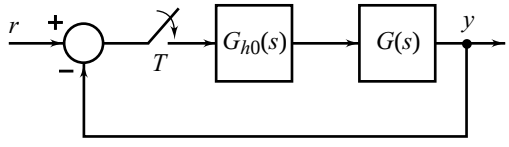

Fig. P11.22

11.23 Consider the system shown in Fig. P11.23. Using root-locus analysis, find the range of $K > 0$ for which the system is stable.

11.24 The digital process of a unity feedback system is described by the transfer function

$$G_{h0}G(z) = \frac{K(z+0.717)}{(z-1)(z-0.368)}; \; T = 1 \text{ sec}$$

Sketch the root locus plot for $0 \le K < \infty$ and from there obtain the following information:

(a) The value of K that results in marginal stability. Also find the frequency of oscillations.

(b) The value of K that results in $\zeta = 1$. What are the time-constants of the closed-loop poles?

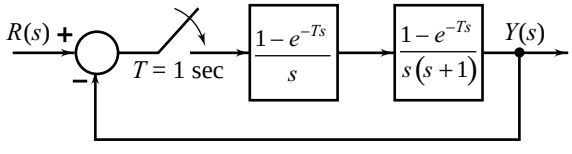

Fig. P11.23

(c) The value of K that results in $\zeta = 0.5$. Also find the natural frequency ω_n for this value of K. You may use the following table to construct a constant-ζ locus on the z-plane corresponding to $\zeta = 0.5$.

Re	0.891	0.64	0.389	0.169	0	–0.113	–0.174	–0.188	–0.163
Im	0.157	0.37	0.463	0.464	0.404	0.310	0.207	0.068	0

11.25 The characteristic equation of a feedback control system is

$$z^2 + 0.2A\,z - 0.1\,A = 0$$

Sketch the root loci for $0 \le A < \infty$, and therefrom obtain the range of parameter A for which the system is stable.

11.26 Consider the system shown in Fig. P11.26 with $G(s) = \dfrac{1}{s(s+1)}$ and $T = 0.2$ sec.

(a) Design a lead compensator so that the dominant closed-loop poles of the system will have $\zeta = 0.5$ and $\omega_n = 4.5$.

(b) Obtain the velocity error constant K_v of the lead compensated system.

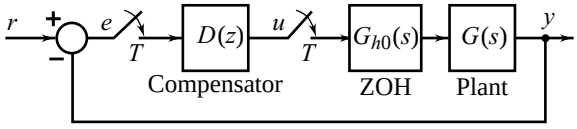

Fig. P11.26

11.27 Consider the system shown in Fig. P11.26 with

$$G(s) = \frac{1}{(s+1)(s+2)}\,;\; T = 1 \text{ sec}$$

Design a compensator $D(z)$ that meets the following specifications on system performance:

(a) $\zeta = 0.5$

(b) $\omega_n = 1.5$, and

(c) $K_p \ge 7.5$

Use root locus method.

12 Control System Analysis Using State Variable Methods

12.1 INTRODUCTION

In the preceding chapters, we showed that the root-locus and the frequency-response methods are quite powerful for the analysis and design of feedback control systems. The analysis and design are carried out using transfer functions, together with a variety of graphical tools such as root-locus plots, Nyquist plots, Bode plots, Nichols chart, etc. These techniques of the so-called *classical control theory* have been greatly enhanced by the availability and low cost of digital computers for system analysis and simulation. The graphical tools can now be more easily used with computer graphics.

The classical design methods suffer from certain limitations due to the fact that the transfer function model is applicable only to linear time-invariant systems, and there too it is generally restricted to SISO systems, as the classical design approach becomes highly cumbersome for use in MIMO systems. Another limitation of the transfer function technique is that it reveals only the system output for a given input and provides no information about the internal behaviour of the system. There may be situations where the output of a system is stable and yet some of the system elements may have a tendency to exceed their specified ratings. In addition to this, it may sometimes be necessary and advantageous to provide a feedback proportional to the internal variables of a system, rather than the output alone, for the purpose of stabilizing and improving the performance of a system.

The limitations of classical methods based on transfer function models, have led to the development of a state space approach of analysis and design. It is a direct time-domain approach which provides a basis for *modern control theory.* It is a powerful technique for the analysis and design of linear and nonlinear, time-invariant or time-varying MIMO systems. The organization of the state space approach is such that it is easily amenable to solution through digital computers.

It will be incorrect to conclude from the foregoing discussion that the state variable design methods can completely replace the classical design methods. In fact, the classical control theory comprising a large body of use-tested knowledge is going strong. State variable design methods prove their mettle in applications which are intractable by classical methods.

The state variable formulation contributes to the application areas of classical control theory in a different way. It is the most efficient form of system representation from the standpoint of computer simulation. To compute the response of $G(s)$ to an input $R(s)$ requires expansion of $\{G(s)R(s)\}$ into partial fractions; which, in turn, requires computation of all the poles of $\{G(s)R(s)\}$, or all the roots of a polynomial. The roots of a polynomial are very sensitive to their coefficients. Furthermore, to develop a computer program to carry out partial fraction expansion is not simple. On the other hand, the response of state variable equations is easy to program. Its computation does not require computation of roots or eigenvalues; therefore, it is less sensitive to parameter variations. For these reasons, it is desirable to compute the response of $G(s)$ through state variable equations.

Many CAD packages handling both the classical and the modern tools of control system design use state variable formulation. It is, therefore, helpful for the control engineer to be familiar with state variable methods of system representation and analysis. This chapter introduces the main concepts of state variable analysis. This material may be used as a brief terminating study or as an introduction to a more in-depth discussion of state variable methods in Chapter 13.

We have been mostly concerned with SISO systems in the text so far. In this chapter also our emphasis will be on SISO systems. However, many of the methods based on state variable concepts are applicable to both SISO and MIMO systems with almost equal convenience; the only difference being the additional computational effort for MIMO systems which is taken care of by CAD packages.

12.2 MATRICES

This section is intended to be a concise summary of facts about matrices[1] that the reader will need to know in reading the present chapter. Having them all at hand will minimize the need to consult a book on matrix theory. It also serves to define the notation and terminology which are, regrettably, not entirely standard.

No attempt has been made at proving every statement made in this section. The interested reader is urged to consult a suitable book (for example [27, 28]) for details of proofs.

Basic definitions and algebraic operations associated with matrices are given below.

Matrix

The matrix

$$\mathbf{A} = \begin{bmatrix} a_{11} & a_{12} & \cdots & a_{1m} \\ a_{21} & a_{22} & \cdots & a_{2m} \\ \vdots & \vdots & & \vdots \\ a_{n1} & a_{n2} & \cdots & a_{nm} \end{bmatrix} = \begin{bmatrix} a_{ij} \end{bmatrix} \tag{12.1}$$

is a rectangular array of nm elements. It has n rows and m columns. a_{ij} denotes (i, j)th element, i.e., the element located in ith row and jth column. $\mathbf{A}$ is said to be a *rectangular matrix* of order $n \times m$.

When $m = n$, i.e., the number of columns is equal to that of rows, the matrix is said to be a *square matrix* of order n.

An $n \times 1$ matrix, i.e., a matrix having only one column is called a *column matrix*. A $1 \times n$ matrix, i.e., a matrix having only one row is called a *row matrix*.

Diagonal matrix A diagonal matrix is a square matrix whose elements off the *principal diagonal* are all zeros ($a_{ij} = 0$ for $i \neq j$). The following matrix is a diagonal matrix.

[1]We will use upper case bold letters to represent matrices and lower case bold letters to represent vectors.

$$\mathbf{\Lambda} = \begin{bmatrix} a_{11} & 0 & \cdots & 0 \\ 0 & a_{22} & \cdots & 0 \\ \vdots & \vdots & & \vdots \\ 0 & 0 & \cdots & a_{nn} \end{bmatrix} \tag{12.2}$$

Unit (identity) matrix A unit matrix **I** is a diagonal matrix whose diagonal elements are all equal to unity ($a_{ii} = 1$, $a_{ij} = 0$ for $i \neq j$).

$$\mathbf{I} = \begin{bmatrix} 1 & 0 & \cdots & 0 \\ 0 & 1 & \cdots & 0 \\ \vdots & \vdots & & \vdots \\ 0 & 0 & \cdots & 1 \end{bmatrix}$$

Whenever necessary, an $n \times n$ unit matrix will be denoted by $\mathbf{I}_n$.

Null (zero) matrix A null matrix **0** is a matrix whose elements are all equal to zero.

$$\mathbf{0} = \begin{bmatrix} 0 & 0 & \cdots & 0 \\ 0 & 0 & \cdots & 0 \\ \vdots & \vdots & & \vdots \\ 0 & 0 & \cdots & 0 \end{bmatrix}$$

Whenever necessary, the dimensions of the null matrix will be indicated by two subscripts: $\mathbf{0}_{nm}$.

Matrix transpose If the rows and columns of an $n \times m$ matrix **A** are interchanged, the resulting $m \times n$ matrix, denoted as $\mathbf{A}^T$, is called the *transpose* of the matrix **A**. Namely, if **A** is given by Eqn. (12.1), then

$$\mathbf{A}^T = \begin{bmatrix} a_{11} & a_{21} & \cdots & a_{n1} \\ a_{12} & a_{22} & \cdots & a_{n2} \\ \vdots & \vdots & & \vdots \\ a_{1m} & a_{2m} & \cdots & a_{nm} \end{bmatrix}$$

Some properties of the matrix transpose are

(i) $(\mathbf{A}^T)^T = \mathbf{A}$

(ii) $(k\mathbf{A})^T = k\mathbf{A}^T$, where k is a scalar

(iii) $(\mathbf{A} + \mathbf{B})^T = \mathbf{A}^T + \mathbf{B}^T$

(iv) $(\mathbf{AB})^T = \mathbf{B}^T\mathbf{A}^T$

Determinant of a matrix Determinants are defined for square matrices only. The determinant of the $n \times n$ matrix **A**, written as $|\mathbf{A}|$ or *det* **A**, is a scalar-valued function of **A**. It is found through the use of minors and cofactors.

The *minor* m_{ij} of the element a_{ij} is the determinant of a matrix of order $(n-1) \times (n-1)$ obtained from **A** by removing the row and the column containing a_{ij}.

The *cofactor* c_{ij} of the element a_{ij} is defined by the equation

$$c_{ij} = (-1)^{i+j} m_{ij}$$

Determinants can be evaluated by the method of *Laplace expansion*. If **A** is an $n \times n$ matrix, any arbitrary row k can be selected and $|\mathbf{A}|$ is then given by

$$|\mathbf{A}| = \sum_{j=1}^{n} a_{kj} c_{kj}$$

Similarly, Laplace expansion can be carried out with respect to any arbitrary column l, to obtain

$$|\mathbf{A}| = \sum_{i=1}^{n} a_{il}\, c_{il}$$

Laplace expansion reduces the evaluation of an $n \times n$ determinant down to the evaluation of a string of $(n-1)\times(n-1)$ determinants, namely the cofactors.

Some properties of determinants are

(i) $det\ \mathbf{AB} = (det\ \mathbf{A})(det\ \mathbf{B})$ (ii) $det\ \mathbf{A}^T = det\ \mathbf{A}$

(iii) $det\ k\mathbf{A} = k^n det\ \mathbf{A}$; $\mathbf{A}$ is $n \times n$ matrix and k is scalar

(iv) The determinant of any diagonal matrix is the product of its diagonal elements.

Singular matrix A square matrix is called singular if the associated determinant is zero.

Nonsingular matrix A square matrix is called nonsingular if the associated determinant is non-zero.

Adjoint matrix The adjoint matrix of a square matrix $\mathbf{A}$ is found by replacing each element a_{ij} of matrix $\mathbf{A}$ by its cofactor c_{ij} and then transposing.

$$adj\ \mathbf{A} = \mathbf{A}^{+}$$

$$= \begin{bmatrix} c_{11} & c_{21} & \cdots & c_{n1} \\ c_{12} & c_{22} & \cdots & c_{n2} \\ \vdots & \vdots & & \vdots \\ c_{1n} & c_{2n} & \cdots & c_{nn} \end{bmatrix} = [c_{ji}]$$

Note that

$$\mathbf{A}(adj\ \mathbf{A}) = (adj\ \mathbf{A})\mathbf{A} = |\mathbf{A}|\ \mathbf{I} \tag{12.3}$$

Matrix inverse The inverse of a square matrix is written as $\mathbf{A}^{-1}$, and is defined by the relation

$$\mathbf{A}^{-1}\mathbf{A} = \mathbf{A}\mathbf{A}^{-1} = \mathbf{I}$$

From Eqn. (12.3) and the definition of the inverse matrix, we have

$$\mathbf{A}^{-1} = \frac{adj\ \mathbf{A}}{|\mathbf{A}|} \tag{12.4}$$

Some properties of matrix inverse are

(i) $(\mathbf{A}^{-1})^{-1} = \mathbf{A}$ (ii) $(\mathbf{A}^T)^{-1} = (\mathbf{A}^{-1})^T$

(iii) $(\mathbf{AB})^{-1} = \mathbf{B}^{-1}\mathbf{A}^{-1}$ (iv) $det\ \mathbf{A}^{-1} = \dfrac{1}{det\ \mathrm{A}}$

(v) $det\ \mathbf{P}^{-1}\mathbf{AP} = det\ \mathbf{A}$

(vi) Inverse of diagonal matrix given by Eqn. (12.2) is

$$\mathbf{\Lambda}^{-1} = \begin{bmatrix} 1/a_{11} & 0 & \cdots & 0 \\ 0 & 1/a_{22} & \cdots & 0 \\ \vdots & \vdots & & \vdots \\ 0 & 0 & \cdots & 1/a_{nn} \end{bmatrix}$$

Rank of a matrix The rank $\rho(\mathbf{A})$ of a matrix $\mathbf{A}$ is the dimension of the largest array in $\mathbf{A}$ with a non-zero determinant. Some properties of rank are

(i) $\rho(\mathbf{A}^T) = \rho(\mathbf{A})$

(ii) The rank of a rectangular matrix cannot exceed the lesser of the number of rows or the number of columns. A matrix whose rank is equal to the lesser of the number of rows and number of columns is said to be of *full rank*.

$$\rho(\mathbf{A}) \leq \min(n, m); \ \mathbf{A} \text{ is } n \times m \text{ matrix}$$

(iii) The rank of a product of two matrices cannot exceed the rank of the either:

$$\rho(\mathbf{AB}) \leq \min[\rho(\mathbf{A}), \rho(\mathbf{B})]$$

Partitioned matrix A matrix can be partitioned into submatrices. Broken lines are used to show the partitioning when the elements of the submatrices are explicitly shown. For example

$$\mathbf{A} = \left[\begin{array}{cc:c} a_{11} & a_{12} & a_{13} \\ a_{21} & a_{22} & a_{23} \\ \hdashline a_{31} & a_{32} & a_{33} \end{array}\right]$$

The broken lines indicating the partitioning are sometimes omitted when the context makes it clear that partitioned matrices are being considered.

We will be frequently using the following forms of partitioning.

(i) Matrix $\mathbf{A}$ partitioned into its columns:

$$\mathbf{A} = [\mathbf{a}_1 \ \mathbf{a}_2 \ \ldots \ \mathbf{a}_m] \tag{12.5a}$$

where

$$\mathbf{a}_i = \begin{bmatrix} a_{1i} \\ a_{2i} \\ \vdots \\ a_{ni} \end{bmatrix} = i\text{th column in } \mathbf{A}$$

(ii) Matrix $\mathbf{A}$ partitioned into its rows:

$$\mathbf{A} = \begin{bmatrix} \boldsymbol{\alpha}_1 \\ \boldsymbol{\alpha}_2 \\ \vdots \\ \boldsymbol{\alpha}_n \end{bmatrix} \tag{12.5b}$$

where

$$\boldsymbol{\alpha}_i = [a_{i1} \ a_{i2} \ \ldots \ a_{im}] = i\text{th row in } \mathbf{A}$$

(iii) A *block diagonal matrix* is a square matrix that can be partitioned so that the non-zero elements are contained only in square submatrices along the main diagonal,

$$\mathbf{A} = \begin{bmatrix} \mathbf{A_1} & \mathbf{0} & \cdots & \mathbf{0} \\ \mathbf{0} & \mathbf{A_2} & \cdots & \mathbf{0} \\ \vdots & \vdots & & \vdots \\ \mathbf{0} & \mathbf{0} & \cdots & \mathbf{A}_m \end{bmatrix} \tag{12.6a}$$

$$= \text{diag}[\mathbf{A}_1 \ \mathbf{A}_2 \ \ldots \ \mathbf{A}_m]$$

For this case

(a) $|\mathbf{A}| = |\mathbf{A}_1|\,|\mathbf{A}_2| \ldots |\mathbf{A}_m|$

(b) $\mathbf{A}^{-1} = \text{diag}\,[\mathbf{A}_1^{-1}\ \mathbf{A}_2^{-1} \cdots \mathbf{A}_m^{-1}]$, provided that $\mathbf{A}^{-1}$ exists.

(iv) A square matrix which has all of its elements *below* (*above*) the main diagonal equal to zero, is called an *upper triangular* (*lower triangular*) matrix. The determinant of any triangular matrix is the product of its diagonal elements.

The determinant of *block triangular* matrices is the product of determinants of square submatrices along the main diagonal. For example, for

$$\mathbf{A} = \begin{bmatrix} \mathbf{A}_{11} & \mathbf{A}_{12} \\ \mathbf{0} & \mathbf{A}_{22} \end{bmatrix}; \quad |\mathbf{A}| = |\mathbf{A}_{11}|\,|\mathbf{A}_{22}| \tag{12.6b}$$

Quadratic forms and definiteness of matrices An expression such as

$$V(x_1, x_2, \ldots, x_n) = \sum_{i=1}^{n}\sum_{j=1}^{n} q_{ij} x_i x_j$$

involving terms of second degree in x_i and x_j is known as the *quadratic form* of n variables. When x_i, x_j and q_{ij} are all real, the value of V is real, and the quadratic form can be expressed in the vector-matrix notation as [155]

$$V(\mathbf{x}) = \mathbf{x}^T\mathbf{Q}\mathbf{x} \tag{12.7a}$$

where

$$\mathbf{x} = \begin{bmatrix} x_1 \\ x_2 \\ \vdots \\ x_n \end{bmatrix}; \quad (n \times 1) \text{ vector of variables}$$

$$\mathbf{Q} = \begin{bmatrix} q_{11} & q_{12} & \cdots & q_{1n} \\ q_{21} & q_{22} & \cdots & q_{2n} \\ \vdots & \vdots & & \vdots \\ q_{n1} & q_{n2} & \cdots & q_{nn} \end{bmatrix}; \quad (n \times n)\text{constant } \textit{symmetric matrix } (\mathbf{Q} = \mathbf{Q}^T).$$

If for all $\mathbf{x} \neq \mathbf{0}$,

(i) $V(\mathbf{x}) = \mathbf{x}^T\mathbf{Q}\mathbf{x} \geq 0$, then $V(\mathbf{x})$ is called a *positive semidefinite function* and $\mathbf{Q}$ is called a *positive semidefinite matrix*;

(ii) $V(\mathbf{x}) = \mathbf{x}^T\mathbf{Q}\mathbf{x} > 0$, then $V(\mathbf{x})$ is called a *positive definite function* and $\mathbf{Q}$ is called a *positive definite matrix*.

The Sylvester's criterion states that the necessary and sufficient conditions for $\mathbf{Q}$ to be positive definite are that all the successive *principal minors* of $\mathbf{Q}$ be positive, i.e.,

$$q_{11} > 0; \quad \begin{vmatrix} q_{11} & q_{12} \\ q_{21} & q_{22} \end{vmatrix} > 0; \quad \begin{vmatrix} q_{11} & q_{12} & q_{13} \\ q_{21} & q_{22} & q_{23} \\ q_{31} & q_{32} & q_{33} \end{vmatrix} > 0; \cdots; |\mathbf{Q}| > 0 \tag{12.7b}$$

The necessary and sufficient conditions for **Q** to be positive semidefinite are that **Q** is singular and all the other principal minors of **Q** are non-negative.

12.3 STATE VARIABLE REPRESENTATION

12.3.1 State Variable Modelling

We have already seen in Chapter 2 (refer Eqns (2.4)) that the application of physical laws to mechanical, electrical, thermal, liquid-level, and other physical processes results in state variable models of the form

$$\dot{\mathbf{x}}(t) = \mathbf{A}\mathbf{x}(t) + \mathbf{b}u(t);\ \mathbf{x}(t_0) \triangleq \mathbf{x}^0 : \textit{State equation} \tag{12.8a}$$

$$y(t) = \mathbf{c}\mathbf{x}(t) + du(t): \textit{output equation} \tag{12.8b}$$

where

$\mathbf{x}(t) = n \times 1$ state vector of nth-order dynamic system
$u(t)$ = system input
$y(t)$ = defined output
$\mathbf{A} = n \times n$ matrix
$\mathbf{b} = n \times 1$ column matrix
$\mathbf{c} = 1 \times n$ row matrix
d = scalar, representing direct coupling between input and output (direct coupling is rare in control systems, i.e., usually $d = 0$)

A review through couple of examples of the basic concepts of state variable modelling presented earlier in Section 2.2, will be helpful.

Example 12.1 Two very usual applications of dc motors are in speed and position control systems.

Figure 12.1 gives the basic block diagram of a speed control system. A separately excited dc motor drives the load. A dc tachogenerator is attached to the motor shaft; speed signal is fedback and the error signal is used to control the armature voltage of the motor.

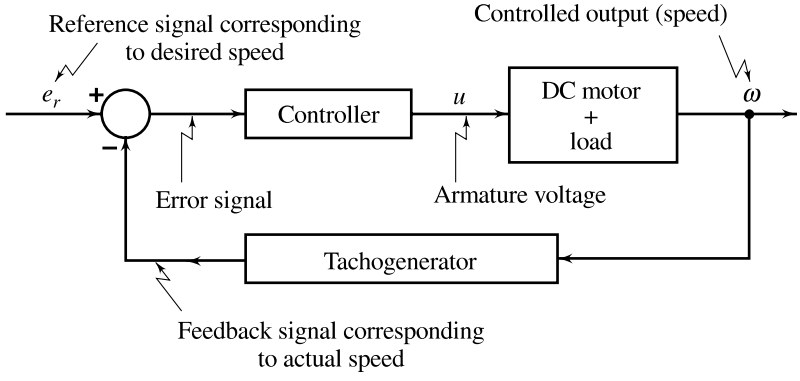

Fig. 12.1 Basic block diagram of a closed-loop speed control system

In the following, we derive the plant model for the speed control system. A separately excited dc motor with armature voltage control is shown in Fig. 12.2.

The loop equation for the armature circuit is

$$u(t) = L_a \frac{d\, i_a(t)}{d\, t} + R_a\, i_a(t) + e_b(t) \qquad (12.9a)$$

where

L_a = inductance of armature winding (henrys)
R_a = resistance of armature winding (ohms)
i_a = armature current (amperes)
e_b = back emf (volts)
u = applied armature voltage (volts)

The torque balance equation is

$$T_M(t) = J \frac{d\omega(t)}{dt} + B\, \omega(t) \qquad (12.9b)$$

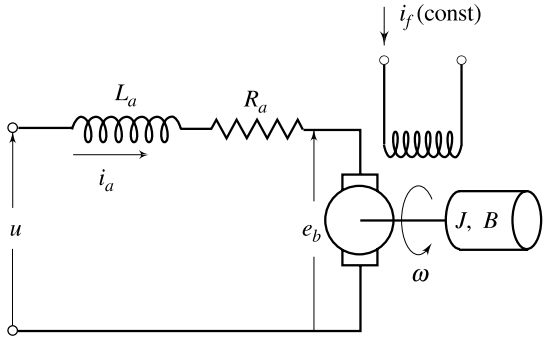

Fig. 12.2 Model of a separately excited dc motor

where

T_M = torque developed by the motor (newton-m)
J = equivalent moment of inertia of motor and load referred to motor shaft (kg-m^2)
B = equivalent viscous friction coefficient of motor and load referred to motor shaft (newton-m/(rad/sec))
ω = angular velocity of motor shaft (rad/sec)

In servo applications, the dc motors are generally used in the linear range of the magnetization curve. Therefore, the air gap flux ϕ is proportional to the field current. For the armature controlled motor, the field current i_f is held constant. Therefore, the torque T_M developed by the motor, which is proportional to the product of the armature current and the air gap flux, can be expressed as

$$T_M(t) = K_T\, i_a(t) \qquad (12.9c)$$

where

K_T = motor torque constant (newton-m/amp)

The counter electromotive force e_b, which is proportional to ϕ and ω, can be expressed as

$$e_b(t) = K_b\, \omega(t) \qquad (12.9d)$$

where

K_b = back emf constant[2] (volts/(rad/sec))

Equations (12.9) can be reorganized as

$$\begin{aligned} \frac{di_a(t)}{dt} &= -\frac{R_a}{L_a}\, i_a(t) - \frac{K_b}{L_a}\, \omega(t) + \frac{1}{L_a}\, u(t) \\ \frac{d\omega(t)}{dt} &= \frac{K_T}{J}\, i_a(t) - \frac{B}{J}\, \omega(t) \end{aligned} \qquad (12.10)$$

$x_1(t) = \omega(t)$, and $x_2(t) = i_a(t)$ is the obvious choice for state variables. The output variable is $y(t) = \omega(t)$.

[2]In MKS units, $K_b = K_T$. Refer Section 3.5.

The plant model of the speed control system, organized into the vector-matrix notation, is given below:

$$\begin{bmatrix} \dot{x}_1(t) \\ \dot{x}_2(t) \end{bmatrix} = \begin{bmatrix} -\frac{B}{J} & \frac{K_T}{J} \\ -\frac{K_b}{L_a} & -\frac{R_a}{L_a} \end{bmatrix} \begin{bmatrix} x_1(t) \\ x_2(t) \end{bmatrix} + \begin{bmatrix} 0 \\ \frac{1}{L_a} \end{bmatrix} u(t)$$

$$y(t) = x_1(t)$$

Let us assign numerical values to the system parameters.
For the parameters[3]

$$\begin{aligned} R_a &= 1 \text{ ohm}, L_a = 0.1 \text{ H}, J = 0.1 \text{ kg-m}^2, \\ B &= 0.1 \text{ newton-m/(rad/sec)}, K_b = K_T = 0.1 \end{aligned} \tag{12.11}$$

the plant model becomes

$$\begin{aligned} \dot{\mathbf{x}}(t) &= \mathbf{A}\mathbf{x}(t) + \mathbf{b}u(t) \\ y(t) &= \mathbf{c}\mathbf{x}(t) \end{aligned} \tag{12.12}$$

where $\mathbf{A} = \begin{bmatrix} -1 & 1 \\ -1 & -10 \end{bmatrix}$; $\mathbf{b} = \begin{bmatrix} 0 \\ 10 \end{bmatrix}$; $\mathbf{c} = [1 \quad 0]$

Example 12.2 Figure 12.3 gives the basic block diagram of a position control system. The controlled variable is now the angular position $\theta(t)$ of the motor shaft:

$$\frac{d\theta(t)}{dt} = \omega(t) \tag{12.13}$$

We make the following choice for state and output variables.

$$x_1(t) = \theta(t), x_2(t) = \omega(t), x_3(t) = i_a(t), y(t) = \theta(t)$$

For this choice, we obtain the following plant model from Eqns (12.10) and (12.13).

$$\begin{bmatrix} \dot{x}_1(t) \\ \dot{x}_2(t) \\ \dot{x}_3(t) \end{bmatrix} = \begin{bmatrix} 0 & 1 & 0 \\ 0 & -\frac{B}{J} & \frac{K_T}{J} \\ 0 & -\frac{K_b}{L_a} & -\frac{R_a}{L_a} \end{bmatrix} \begin{bmatrix} x_1(t) \\ x_2(t) \\ x_3(t) \end{bmatrix} + \begin{bmatrix} 0 \\ 0 \\ \frac{1}{L_a} \end{bmatrix} u(t)$$

$$y(t) = x_1(t)$$

For the system parameters given by (12.11), the plant model for position control system becomes

$$\begin{aligned} \dot{\mathbf{x}}(t) &= \mathbf{A}\mathbf{x}(t) + \mathbf{b}\mathbf{u}(t) \\ y(t) &= \mathbf{c}\mathbf{x}(t) \end{aligned} \tag{12.14}$$

[3]These parameters have been chosen for computational convenience.

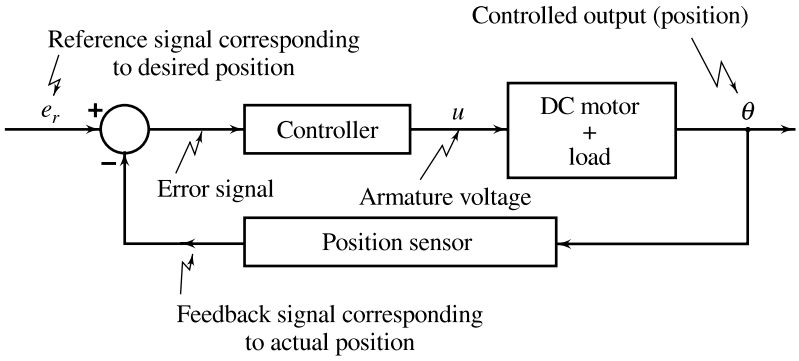

Fig. 12.3 Basic block diagram of a closed-loop position control system

where

$$\mathbf{A} = \begin{bmatrix} 0 & 1 & 0 \\ 0 & -1 & 1 \\ 0 & -1 & -10 \end{bmatrix}; \mathbf{b} = \begin{bmatrix} 0 \\ 0 \\ 10 \end{bmatrix}; \mathbf{c} = \begin{bmatrix} 1 & 0 & 0 \end{bmatrix}$$

In Examples 12.1 and 12.2 discussed above, the selected state variables are the physical quantities of the systems, which can be measured. It may sometimes be necessary and advantageous to provide a feedback proportional to the state variables of a system, rather than the output alone, for the purpose of stabilizing and improving the performance of a system (refer Chapter 13). The implementation of design with state variable feedback becomes straightforward if the state variables are available for feedback. The choice of physical variables of a system as state variables therefore helps in the implementation of design. Another advantage of selecting physical variables for state variable formulation is that the solution of state equation gives time variation of variables which have direct relevance to the physical system.

12.3.2 Transformation of State Variables

It frequently happens that the state variables used in the original formulation of the dynamics of a system are not as convenient as another set of state variables. Instead of having to reformulate the system dynamics, it is possible to transform the set $\{\mathbf{A}, \mathbf{b}, \mathbf{c}, d\}$ of the original formulation (12.8) to a new set $\{\bar{\mathbf{A}}, \bar{\mathbf{b}}, \bar{\mathbf{c}}, \bar{d}\}$. The change of variables is represented by a linear transformation

$$\mathbf{x} = \mathbf{P}\bar{\mathbf{x}} \tag{12.15a}$$

where $\bar{\mathbf{x}}$ is a state vector in the new formulation and $\mathbf{x}$ is the state vector in the original formulation. It is assumed that the transformation matrix $\mathbf{P}$ is a nonsingular $n \times n$ matrix, so that we can always write

$$\bar{\mathbf{x}} = \mathbf{P}^{-1}\mathbf{x} \tag{12.15b}$$

We assume, moreover, that $\mathbf{P}$ is a constant matrix.

The original dynamics are expressed by

$$\dot{\mathbf{x}}(t) = \mathbf{A}\mathbf{x}(t) + \mathbf{b}u(t); \mathbf{x}(t_0) \triangleq \mathbf{x}^0 \tag{12.16a}$$

and the output by

$$y(t) = \mathbf{c}\mathbf{x}(t) + du(t) \tag{12.16b}$$

Substitution of $\mathbf{x}$ as given by Eqn. (12.15a) into these equations, gives

$$\mathbf{P}\dot{\bar{\mathbf{x}}}(t) = \mathbf{AP}\,\bar{\mathbf{x}}(t) + \mathbf{b}u(t)$$

$$y(t) = \mathbf{cP}\,\bar{\mathbf{x}}(t) + du(t)$$

or

$$\dot{\bar{\mathbf{x}}}(t) = \bar{\mathbf{A}}\,\bar{\mathbf{x}}(t) + \bar{\mathbf{b}}\,u(t);\ \bar{\mathbf{x}}(t_0) = \mathbf{P}^{-1}\mathbf{x}(t_0) \tag{12.17a}$$

$$y(t) = \bar{\mathbf{c}}\,\bar{\mathbf{x}}(t) + \bar{d}\,u(t) \tag{12.17b}$$

with

$$\bar{\mathbf{A}} = \mathbf{P}^{-1}\mathbf{AP},\ \bar{\mathbf{b}} = \mathbf{P}^{-1}\mathbf{b},\ \bar{\mathbf{c}} = \mathbf{cP},\ \bar{d} = d$$

In the next section, we will prove that both the linear systems (12.16) and (12.17) have identical output responses for the same input. The linear system (12.17) is said to be *equivalent* to the linear system (12.16), and $\mathbf{P}$ is called an *equivalence* or *similarity transformation.*

It is obvious that there exist an infinite number of equivalent systems since the transformation matrix $\mathbf{P}$ can be arbitrarily chosen. Some transformations have been extensively used for the purposes of analysis and design. Five of such special (*canonical*) transformations will be introduced in this chapter.

Example 12.3 *Example* 12.1 *revisited*

For the system of Fig. 12.2, we have taken angular velocity $\omega(t)$ and armature current $i_a(t)$ as state variables:

$$\mathbf{x} = \begin{bmatrix} x_1 \\ x_2 \end{bmatrix} = \begin{bmatrix} \omega \\ i_a \end{bmatrix}$$

We now define new state variables as

$$\bar{x}_1 = \omega,\ \bar{x}_2 = -\omega + i_a$$

or

$$\bar{\mathbf{x}} = \begin{bmatrix} \bar{x}_1 \\ \bar{x}_2 \end{bmatrix} = \begin{bmatrix} x_1 \\ -x_1 + x_2 \end{bmatrix} = \begin{bmatrix} 1 & 0 \\ -1 & 1 \end{bmatrix}\begin{bmatrix} x_1 \\ x_2 \end{bmatrix}$$

We can express velocity $x_1(t)$ and armature current $x_2(t)$ in terms of the variables $\bar{x}_1(t)$ and $\bar{x}_2(t)$:

$$\mathbf{x} = \mathbf{P}\,\bar{\mathbf{x}} \tag{12.18}$$

with

$$\mathbf{P} = \begin{bmatrix} 1 & 0 \\ 1 & 1 \end{bmatrix}$$

Using Eqns (12.17)and (12.12), we obtain the following state variable model for the system of Fig. 12.2 in terms of the transformed state vector $\bar{\mathbf{x}}(t)$:

$$\dot{\bar{\mathbf{x}}}(t) = \bar{\mathbf{A}}\,\bar{\mathbf{x}}(\mathrm{t}) + \bar{\mathbf{b}}\,u(t)$$

$$y(t) = \bar{\mathbf{c}}\,\bar{\mathbf{x}}(t) \tag{12.19}$$

where

$$\bar{\mathbf{A}} = \mathbf{P}^{-1}\mathbf{A}\,\mathbf{P} = \begin{bmatrix} 1 & 0 \\ -1 & 1 \end{bmatrix}\begin{bmatrix} -1 & 1 \\ -1 & -10 \end{bmatrix}\begin{bmatrix} 1 & 0 \\ 1 & 1 \end{bmatrix} = \begin{bmatrix} 0 & 1 \\ -11 & -11 \end{bmatrix}$$

$$\bar{\mathbf{b}} = \mathbf{P}^{-1}\mathbf{b} = \begin{bmatrix} 1 & 0 \\ -1 & 1 \end{bmatrix}\begin{bmatrix} 0 \\ 10 \end{bmatrix} = \begin{bmatrix} 0 \\ 10 \end{bmatrix}$$

$$\bar{\mathbf{c}} = \mathbf{cP} = \begin{bmatrix} 1 & 0 \end{bmatrix}\begin{bmatrix} 1 & 0 \\ 1 & 1 \end{bmatrix} = \begin{bmatrix} 1 & 0 \end{bmatrix}$$

$$\bar{x}_1(t_0) = x_1(t_0);\ \bar{x}_2(t_0) = -x_1(t_0) + x_2(t_0) \tag{12.20}$$

Equation (12.19) give an alternative state variable model of the system previously represented by Eqns (12.12). $\bar{\mathbf{x}}(t)$ and $\mathbf{x}(t)$ both qualify to be state vectors of the given system (the two vectors individually characterize the system completely at time t), and the output $y(t)$, as we shall see shortly, is uniquely determined from either of the models (12.12) and (12.19). State variable model (12.19) is thus *equivalent* to the model (12.12), and the matrix **P** given by Eqn. (12.18) is an equivalence or similarity transformation.

The state variable model given by Eqn. (12.19) is in a *canonical* (special) form.

12.4 CONVERSION OF STATE VARIABLE MODELS TO TRANSFER FUNCTIONS

We shall derive the transfer function of a SISO system from the Laplace-transformed version of the state and output equations. Refer Section 12.2 for the matrix operations used in the derivation.

Consider the state variable model (Eqns (12.8)):

$$\begin{aligned} \dot{\mathbf{x}}(t) &= \mathbf{A}\mathbf{x}(t) + \mathbf{b}u(t);\ \mathbf{x}(t_0) \triangleq \mathbf{x}^0 \\ y(t) &= \mathbf{c}\mathbf{x}(t) + du(t) \end{aligned} \tag{12.21}$$

Taking the Laplace transform of Eqns (12.21), we obtain

$$\begin{aligned} s\mathbf{X}(s) - \mathbf{x}^0 &= \mathbf{A}\mathbf{X}(s) + \mathbf{b}U(s) \\ Y(s) &= \mathbf{c}\mathbf{X}(s) + dU(s) \end{aligned}$$

where

$$\mathbf{X}(s) \triangleq \mathscr{L}[\mathbf{x}(t)];\ U(s) \triangleq \mathscr{L}[u(t)];\ Y(s) \triangleq \mathscr{L}[y(t)]$$

Manipulation of these equations gives

$$(s\mathbf{I} - \mathbf{A})\mathbf{X}(s) = \mathbf{x}^0 + \mathbf{b}U(s);\ \mathbf{I} \text{ is } n \times n \text{ identity matrix}$$

or

$$\mathbf{X}(s) = (s\mathbf{I} - \mathbf{A})^{-1}\mathbf{x}^0 + (s\mathbf{I} - \mathbf{A})^{-1}\mathbf{b}U(s) \tag{12.22a}$$

$$Y(s) = \mathbf{c}(s\mathbf{I} - \mathbf{A})^{-1}\mathbf{x}^0 + [\mathbf{c}(s\mathbf{I} - \mathbf{A})^{-1}\mathbf{b} + d]U(\mathrm{s}) \tag{12.22b}$$

Equations (12.22) are algebraic equations. If $\mathbf{x}^0$ and $U(s)$ are known, $\mathbf{X}(s)$ and $Y(s)$ can be computed from these equations.

In the case of a zero initial state (i.e., $\mathbf{x}^0 = \mathbf{0}$), the input–output behaviour of the system (12.21) is determined entirely by the transfer function

$$\frac{Y(s)}{U(s)} = G(s) = \mathbf{c}(s\mathbf{I} - \mathbf{A})^{-1}\mathbf{b} + d \tag{12.23}$$

We can express the inverse of the matrix $(s\mathbf{I} - \mathbf{A})$ as

$$(s\mathbf{I} - \mathbf{A})^{-1} = \frac{(s\mathbf{I} - \mathbf{A})^{+}}{|s\mathbf{I} - \mathbf{A}|} \tag{12.24}$$

where

$|s\mathbf{I} - \mathbf{A}|$ = determinant of the matrix $(s\mathbf{I} - \mathbf{A})$

$(s\mathbf{I} - \mathbf{A})^{+}$ = adjoint of the matrix $(s\mathbf{I} - \mathbf{A})$

Using Eqn. (12.24), the transfer function $G(s)$ given by Eqn. (12.23) can be written as

$$G(s) = \frac{\mathbf{c}(s\mathbf{I} - \mathbf{A})^{+}\mathbf{b}}{|s\mathbf{I} - \mathbf{A}|} + d \tag{12.25}$$

12.4.1 Eigenvalues of a Matrix

For a general nth-order matrix

$$\mathbf{A} = \begin{bmatrix} a_{11} & a_{12} & \cdots & a_{1n} \\ a_{21} & a_{22} & \cdots & a_{2n} \\ \vdots & \vdots & & \vdots \\ a_{n1} & a_{n2} & \cdots & a_{nn} \end{bmatrix},$$

the matrix $(s\mathbf{I} - \mathbf{A})$ has the following appearance:

$$(s\mathbf{I} - \mathbf{A}) = \begin{bmatrix} s - a_{11} & -a_{12} & \cdots & -a_{1n} \\ -a_{21} & s - a_{22} & \cdots & -a_{2n} \\ \vdots & \vdots & & \vdots \\ -a_{n1} & -a_{n2} & \cdots & s - a_{nn} \end{bmatrix}$$

If we imagine calculating *det* $(s\mathbf{I} - \mathbf{A})$, we see that one of the terms will be the product of diagonal elements of $(s\mathbf{I} - \mathbf{A})$:

$$(s - a_{11})(s - a_{22}) \cdots (s - a_{nn}) = s^n + \alpha_1' s^{n-1} + \cdots + \alpha_n',$$

a polynomial of degree n with the leading coefficient of unity. There will be other terms coming from the off-diagonal elements of $(s\mathbf{I} - \mathbf{A})$, but none will have a degree as high as n. Thus $|s\mathbf{I} - \mathbf{A}|$ will be of the following form:

$$|s\mathbf{I} - \mathbf{A}| = \Delta(s) = s^n + \alpha_1 s^{n-1} + \cdots + \alpha_n \tag{12.26}$$

where α_i are constant scalars.

This is known as the *characteristic polynomial* of the matrix $\mathbf{A}$. It plays a vital role in the dynamic behaviour of the system. The roots of this polynomial are called the *characteristic roots* or *eigenvalues* of matrix $\mathbf{A}$. These roots, as we shall see in Section 12.6, determine the essential features of the unforced dynamic behaviour of the system (12.21).

The adjoint of an $n \times n$ matrix is itself an $n \times n$ matrix whose elements are the cofactors of the original matrix. Each cofactor is obtained by computing the determinant of the matrix that remains when a row and a column of the original matrix are deleted. It thus follows that each element in $(s\mathbf{I} - \mathbf{A})^{+}$ is a polynomial in s of maximum degree $(n - 1)$. Adjoint of $(s\mathbf{I} - \mathbf{A})$ can therefore be expressed as

$$(s\mathbf{I} - \mathbf{A})^{+} = \mathbf{Q}_1 s^{n-1} + \mathbf{Q}_2 s^{n-2} + \cdots + \mathbf{Q}_{n-1} s + \mathbf{Q}_n \tag{12.27}$$

where $\mathbf{Q}_i$ are constant $n \times n$ matrices. We can express transfer function $G(s)$ given by Eqn. (12.25) in the following form:

$$G(s) = \frac{\mathbf{c}[\mathbf{Q}_1 s^{n-1} + \mathbf{Q}_2 s^{n-2} + \cdots + \mathbf{Q}_{n-1} s + \mathbf{Q}_n]\mathbf{b}}{s^n + \alpha_1 s^{n-1} + \cdots + \alpha_{n-1} s + \alpha_n} + d \qquad (12.28)$$

$G(s)$ is thus a rational function of s. When $d = 0$, the degree of numerator polynomial of $G(s)$ is strictly less than the degree of the denominator polynomial and therefore the resulting transfer function is a *strictly proper transfer function*. When $d \neq 0$, the degree of numerator polynomial of $G(s)$ will be equal to the degree of the denominator polynomial, giving a *proper transfer function*. Further,

$$d = \lim_{s \to \infty} [G(s)] \qquad (12.29)$$

From Eqns (12.26) and (12.28) we observe that the characteristic polynomial of matrix **A** of the system (12.21) is same as the denominator polynomial of the corresponding transfer function $G(s)$. If there are no cancellations between the numerator and denominator polynomials of $G(s)$ in Eqn. (12.28), the *eigenvalues* of matrix **A** are same as the *poles* of $G(s)$. We will take up in Section 12.8, this aspect of the correspondence between state variable models and transfer functions. It will be proved that for a completely controllable and completely observable state variable model, the eigenvalues of matrix **A** are same as the poles of the corresponding transfer function.

12.4.2 Invariance Property

It is recalled that the state variable model for a system is not unique, but depends on the choice of a set of state variables. A transformation

$$\mathbf{x}(t) = \mathbf{P}\,\bar{\mathbf{x}}(t);\ \mathbf{P} \text{ is a nonsingular matrix} \qquad (12.30)$$

results in the following alternative state variable model (refer Eqns (12.17)) for the system (12.21):

$$\dot{\bar{\mathbf{x}}}(t) = \bar{\mathbf{A}}\,\bar{\mathbf{x}}(t) + \bar{\mathbf{b}}\,u(t);\ \bar{\mathbf{x}}(t_0) = \mathbf{P}^{-1}\mathbf{x}(t_0) \qquad (12.31a)$$

$$y(t) = \bar{\mathbf{c}}\,\bar{\mathbf{x}}(t) + du(t) \qquad (12.31b)$$

where $\bar{\mathbf{A}} = \mathbf{P}^{-1}\mathbf{A}\mathbf{P},\ \bar{\mathbf{b}} = \mathbf{P}^{-1}\mathbf{b},\ \bar{\mathbf{c}} = \mathbf{c}\mathbf{P}$

The definition of new set of internal state variables should evidently not affect the eigenvalues or input-output behaviour. This may be verified by evaluating the characteristic polynomial and the transfer function of the transformed system.

(i)
$$|s\mathbf{I} - \bar{\mathbf{A}}| = |s\mathbf{I} - \mathbf{P}^{-1}\mathbf{A}\mathbf{P}| = |s\mathbf{P}^{-1}\mathbf{P} - \mathbf{P}^{-1}\mathbf{A}\mathbf{P}|$$
$$= |\mathbf{P}^{-1}(s\mathbf{I} - \mathbf{A})\mathbf{P}| = |\mathbf{P}^{-1}|\,|s\mathbf{I} - \mathbf{A}|\,|\mathbf{P}| = |s\mathbf{I} - \mathbf{A}| \qquad (12.32)$$

(ii) System output in response to input $u(t)$ is given by the transfer function

$$\bar{G}(s) = \bar{\mathbf{c}}\,(s\mathbf{I} - \bar{\mathbf{A}})^{-1}\,\bar{\mathbf{b}} + d$$
$$= \mathbf{c}\mathbf{P}(s\mathbf{I} - \mathbf{P}^{-1}\mathbf{A}\mathbf{P})^{-1}\mathbf{P}^{-1}\mathbf{b} + d$$
$$= \mathbf{c}\mathbf{P}(s\mathbf{P}^{-1}\mathbf{P} - \mathbf{P}^{-1}\mathbf{A}\mathbf{P})^{-1}\mathbf{P}^{-1}\mathbf{b} + d$$
$$= \mathbf{c}\mathbf{P}[\mathbf{P}^{-1}(s\mathbf{I} - \mathbf{A})\mathbf{P}]^{-1}\mathbf{P}^{-1}\mathbf{b} + d$$
$$= \mathbf{c}\mathbf{P}\mathbf{P}^{-1}(s\mathbf{I} - \mathbf{A})^{-1}\mathbf{P}\mathbf{P}^{-1}\,\mathbf{b} + d$$
$$= \mathbf{c}(s\mathbf{I} - \mathbf{A})^{-1}\mathbf{b} + d = G(s) \qquad (12.33)$$

(iii) System output in response to initial state $\bar{\mathbf{x}}(t_0)$ is given by (refer Eqn. (12.22b))

$$\begin{aligned}\bar{\mathbf{c}}(s\mathbf{I}-\mathbf{A})^{-1}\bar{\mathbf{x}}(t_0) &= \mathbf{cP}(s\mathbf{I}-\mathbf{P}^{-1}\mathbf{AP})^{-1}\mathbf{P}^{-1}\mathbf{x}(t_0)\\ &= \mathbf{c}(s\mathbf{I}-\mathbf{A})^{-1}\mathbf{x}(t_0)\end{aligned} \tag{12.34}$$

The input-output behaviour of the system (12.21) is thus *invariant* under the transformation (12.30).

Example 12.4 Consider the position control system of Example 12.2. The plant model of the system is reproduced below:

$$\begin{aligned}\dot{\mathbf{x}}(t) &= \mathbf{Ax}(t) + \mathbf{b}u(t)\\ y(t) &= \mathbf{cx}(t)\end{aligned} \tag{12.35}$$

with $$\mathbf{A} = \begin{bmatrix}0 & 1 & 0\\ 0 & -1 & 1\\ 0 & -1 & -10\end{bmatrix};\ \mathbf{b} = \begin{bmatrix}0\\ 0\\ 10\end{bmatrix};\ \mathbf{c} = \begin{bmatrix}1 & 0 & 0\end{bmatrix}$$

The characteristic polynomial of matrix **A** is

$$|s\mathbf{I}-\mathbf{A}| = \begin{vmatrix}s & -1 & 0\\ 0 & s+1 & -1\\ 0 & 1 & s+10\end{vmatrix} = s(s^2+11s+11)$$

The transfer function

$$\begin{aligned}G(s) = \frac{Y(s)}{U(s)} &= \frac{\mathbf{c}(s\mathbf{I}-\mathbf{A})^{+}\mathbf{b}}{|s\mathbf{I}-\mathbf{A}|}\\ &= \frac{\begin{bmatrix}1 & 0 & 0\end{bmatrix}\begin{bmatrix}s^2+11s+11 & s+10 & 1\\ 0 & s(s+10) & s\\ 0 & -s & s(s+1)\end{bmatrix}\begin{bmatrix}0\\ 0\\ 10\end{bmatrix}}{s(s^2+11s+11)}\\ &= \frac{10}{s(s^2+11s+11)}\end{aligned} \tag{12.36}$$

12.5 CONVERSION OF TRANSFER FUNCTIONS TO CANONICAL STATE VARIABLE MODELS

In the last section, we studied the problem—finding the transfer function from the state variable model of a system. The converse problem—finding a state variable model from the transfer function of a system, is the subject of discussion in this section. This problem is quite important because of the following reasons:

(i) Quite often the system dynamics is determined experimentally using standard test signals like a step, impulse, or sinusoidal signal. A transfer function is conveniently fitted to the experimental data in some best possible manner.

There are, however, many design techniques developed exclusively for state variable models. In order to apply these techniques, experimentally obtained transfer function descriptions must be realized into state variable models.

(ii) Realization of transfer functions into state variable models is needed even if the control system design is based on frequency-domain design methods. In these cases the need arises for the purpose of transient response simulation. Many algorithms and numerical integration computer programs designed for solution of systems of first-order equations are available, but there is not much software for the numerical inversion of Laplace transforms. Thus, if a reliable method is needed for calculating the transient response of a system, one may be better off converting the transfer function of the system to state variable description and numerically integrating the resulting differential equations rather than attempting to compute the inverse Laplace transform by numerical methods.

We shall discuss here the problem of realization of transfer function into state variable models. Note the use of the term 'realization'. A state variable model that has a prescribed rational function $G(s)$ as its transfer function, is the *realization* of $G(s)$. The term 'realization' is justified by the fact that by using the *state diagram,* a pictorial representation of the state variable model, the system with the transfer function $G(s)$ can be built in the real world by an op amp circuit. We shall see shortly that a state diagram is essentially an analog-computer program for the given system, which is characterized by three basic operations: (i) multiplication of a variable by a constant, (ii) addition of several variables, and (iii) integration of variables.

The following three problems are involved in the realization of a given transfer function into state variable models:

(i) Is it possible at all to obtain state variable description from the given transfer function?
(ii) If yes, is the state variable description unique for a given transfer function?
(iii) How do we obtain the state variable description from the given transfer function?

The answer to the first problem has been given in the last section. A rational function $G(s)$ is realizable by a finite dimensional linear time-invariant state model if and only if $G(s)$ is a proper rational function. A proper rational function will have state model of the form:

$$\begin{aligned} \dot{\mathbf{x}}(t) &= \mathbf{A}\mathbf{x}(t) + \mathbf{b}u(t) \\ y(t) &= \mathbf{c}\mathbf{x}(t) + du(t) \end{aligned} \tag{12.37}$$

where $\mathbf{A}$, $\mathbf{b}$, $\mathbf{c}$ and d are constant matrices of appropriate dimensions. A strictly proper rational function will have state model of the form

$$\begin{aligned} \dot{\mathbf{x}}(t) &= \mathbf{A}\mathbf{x}(t) + \mathbf{b}u(t) \\ y(t) &= \mathbf{c}\mathbf{x}(t) \end{aligned} \tag{12.38}$$

Let us now turn to the second problem. In the last section, we saw that there are innumerable systems that have the same transfer function. Hence, the representation of a transfer function in state variable form is obviously not unique. However, all these representations will be equivalent.

In the remaining part of this section, we deal with the third problem. We shall develop three standard, or 'canonical' representations of transfer functions.

A linear time-invariant SISO system is described by transfer function of the form

$$G(s) = \frac{\beta_0 s^m + \beta_1 s^{m-1} + \cdots + \beta_m}{s^n + \alpha_1 s^{n-1} + \cdots + \alpha_n} \; ; \; m \le n$$

where the coefficients α_i and β_i are real constant scalars. Note that there is no loss in generality to assume the coefficient of s^n to be unity.

In the following, we derive results for $m = n$; these results may be used for the case $m < n$ by setting appropriate β_i coefficients equal to zero. Therefore, our problem is to obtain a state variable model corresponding to the transfer function

$$G(s) = \frac{\beta_0 s^n + \beta_1 s^{n-1} + \cdots + \beta_n}{s^n + \alpha_1 s^{n-1} + \cdots + \alpha_n} \tag{12.39}$$

12.5.1 First Companion Form

Our development starts with a transfer function of the form

$$\frac{Z(s)}{U(s)} = \frac{1}{s^n + \alpha_1 s^{n-1} + \cdots + \alpha_n} \tag{12.40}$$

which can be written as

$$(s^n + \alpha_1 s^{n-1} + \cdots + \alpha_n)\, Z(s) = U(s)$$

The corresponding differential equation is

$$p^n z(t) + \alpha_1 p^{n-1} z(t) + \cdots + \alpha_n z(t) = u(t)$$

where

$$p^k z(t) \triangleq \frac{d^k z(t)}{dt^k}$$

Solving for highest derivative of $z(t)$, we obtain

$$p^n z(t) = -\alpha_1 p^{n-1} z(t) - \alpha_2 p^{n-2} z(t) - \cdots - \alpha_n z(t) + u(t) \tag{12.41}$$

Now consider a chain of n integrators as shown in Fig. 12.4. Suppose that the output of the last integrator is $z(t)$. Then the output of the just previous integrator is $p\,z = dz/dt$, and so forth. The output from the first integrator is $p^{n-1}z(t)$, and the input to this integrator is thus $p^n z(t)$. This leaves only the problem of obtaining $p^n z(t)$ for use as input to the first integrator. In fact, this is already specified by Eqn. (12.41). Realization of this equation is shown in Fig. 12.4.

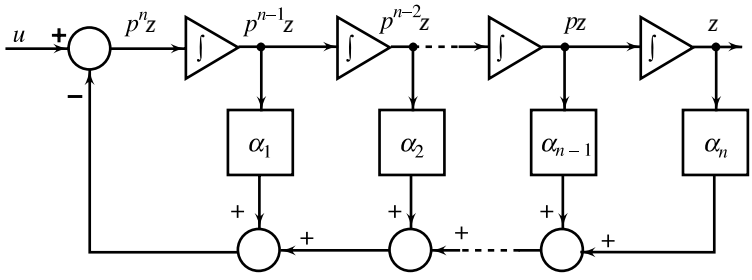

Fig. 12.4 Realization of the system (12.41)

Having developed a realization of the simple transfer function (12.40), we are now in a position to consider the more general transfer function (12.39). We decompose this transfer function into two parts, as shown in Fig. 12.5. The output $Y(s)$ can be written as

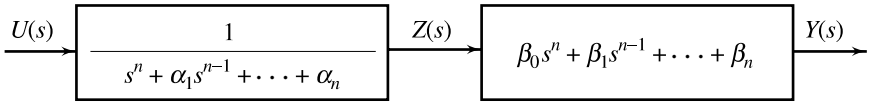

Fig. 12.5 Decomposition of the transfer function (12.39)

$$Y(s) = (\beta_0 s^n + \beta_1 s^{n-1} + \cdots + \beta_n)\, Z(s) \tag{12.42a}$$

where $Z(s)$ is given by

$$\frac{Z(s)}{U(s)} = \frac{1}{s^n + \alpha_1 s^{n-1} + \cdots + \alpha_n} \tag{12.42b}$$

A realization of the transfer function (12.42b) has already been developed. Figure 12.4 shows this realization. The output of the last integrator is $z(t)$ and the inputs to the integrators in the chain from the last to the first are the n successive derivatives of $z(t)$.

Realization of the transfer function (12.42a) is now straightforward. The output

$$y(t) = \beta_0\, p^n z(t) + \beta_1\, p^{n-1} z(t) + \cdots + \beta_n\, z(t),$$

is nothing but the sum of the scaled versions of the inputs to the n integrators. Figure 12.6 shows complete realization of the transfer function (12.39). All that remains to be done is to write the corresponding differential equations.

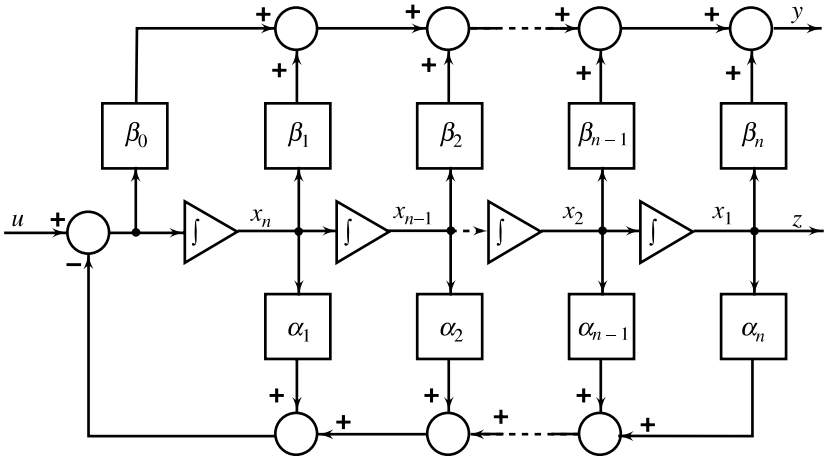

Fig. 12.6 Realization (state diagram) of the system (12.39)

To get one state variable model of the system, we identify the output of each integrator in Fig. 12.6 with a state variable, starting at the right and proceeding to the left. The corresponding differential equations, using this identification of state variables are

$$\begin{aligned}
\dot{x}_1 &= x_2 \\
\dot{x}_2 &= x_3 \\
&\vdots \\
\dot{x}_{n-1} &= x_n \\
\dot{x}_n &= -\alpha_n x_1 - \alpha_{n-1} x_2 - \cdots - \alpha_1 x_n + u
\end{aligned} \tag{12.43a}$$

The output equation is found by careful examination of the block diagram of Fig. 12.6. Note that there are two paths from the output of each integrator to the system output—one path upward through the box labelled β_i, and a second path down through the box labelled α_i and thence through the box labelled β_0. As a consequence,

$$y = (\beta_n - \alpha_n \beta_0)\, x_1 + (\beta_{n-1} - \alpha_{n-1}\beta_0)\, x_2 + \cdots + (\beta_1 - \alpha_1 \beta_0)\, x_n + \beta_0\, u \tag{12.43b}$$

The state and output Eqns (12.43), organized in vector-matrix form, are given below:

$$\begin{aligned} \dot{\mathbf{x}}(t) &= \mathbf{A}\mathbf{x}(t) + \mathbf{b}u(t) \\ y(t) &= \mathbf{c}\mathbf{x}(t) + du(t) \end{aligned} \tag{12.44}$$

with

$$\mathbf{A} = \begin{bmatrix} 0 & 1 & 0 & \cdots & 0 \\ 0 & 0 & 1 & \cdots & 0 \\ \vdots & \vdots & \vdots & & \vdots \\ 0 & 0 & 0 & \cdots & 1 \\ -\alpha_n & -\alpha_{n-1} & -\alpha_{n-2} & \cdots & -\alpha_1 \end{bmatrix}; \mathbf{b} = \begin{bmatrix} 0 \\ 0 \\ \vdots \\ 0 \\ 1 \end{bmatrix}$$

$$\mathbf{c} = [\beta_n - \alpha_n\beta_0, \quad \beta_{n-1} - \alpha_{n-1}\beta_0, \ldots, \beta_1 - \alpha_1\beta_0]; \; d = \beta_0$$

If the direct path through β_0 is absent (refer Fig. 12.6), then the scalar d is zero and the row matrix **c** contains only the β_i coefficients.

The matrix **A** in Eqns (12.44) has a very special structure: the coefficients of the denominator of the transfer function preceded by minus signs form a string along the bottom row of the matrix. The rest of the matrix is zero except for the 'superdiagonal' terms which are all unity. In matrix theory, a matrix with this structure is said to be in *companion form*. For this reason, we identify the realization (12.44) as *companion-form realization* of the transfer function (12.39). We call this the *first companion form*: another companion form follows.

12.5.2 Second Companion Form

In the first companion form, the coefficients of the denominator of the transfer function appear in one of the rows of the **A** matrix. There is another companion form in which the coefficients appear in a column of the **A** matrix. This can be obtained by writing Eqn. (12.39) as

$$(s^n + \alpha_1 s^{n-1} + \cdots + \alpha_n)\, Y(s) = (\beta_0 s^n + \beta_1 s^{n-1} + \cdots + \beta_n)\, U(s)$$

or $\quad s^n [Y(s) - \beta_0 U(s)] + s^{n-1}[\alpha_1 Y(s) - \beta_1 U(s)] + \cdots + [\alpha_n Y(s) - \beta_n U(s)] = 0$

On dividing by s^n and solving for $Y(s)$, we obtain

$$Y(s) = \beta_0 U(s) + \frac{1}{s}\,[\beta_1 U(s) - \alpha_1 Y(s)] + \cdots + \frac{1}{s^n}\,[\beta_n U(s) - \alpha_n Y(s)] \tag{12.45}$$

Note that $1/s^n$ is the transfer function of a chain of n integrators. Realization of $\frac{1}{s^n}\,[\beta_n U(s) - \alpha_n Y(s)]$ requires a chain of n integrators with an input $[\beta_n u - \alpha_n y]$ to the first integrator in the chain from left-to-right. Realization of $\frac{1}{s^{n-1}}\,[\beta_{n-1} U(s) - \alpha_{n-1} Y(s)]$ requires a chain of $(n-1)$ integrators with input $[\beta_{n-1} u - \alpha_{n-1} y]$ to the first integrator in the chain from left-to-right, and so forth. This immediately leads to the structure shown in Fig. 12.7. The signal y is fed back to each of the integrators in the chain and the signal u is fed forward. Thus the signal $[\beta_n u - \alpha_n y]$ passes through n integrators; the signal $[\beta_{n-1} u - \alpha_{n-1} y]$ passes through $(n-1)$ integrators and so forth to complete the realization of Eqn. (12.45). The structure retains the ladder-like shape of the first companion form, but the feedback paths are in different directions.

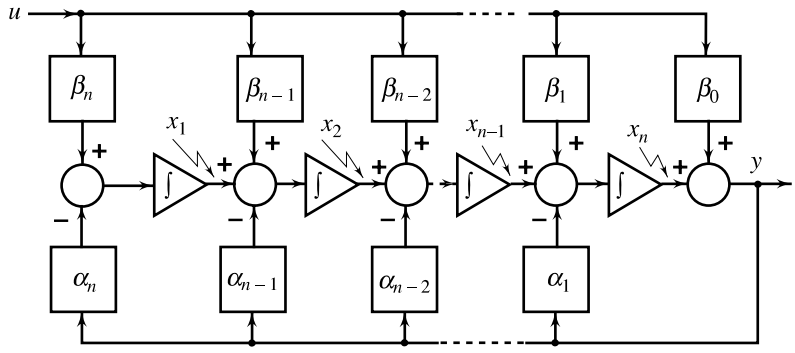

Fig. 12.7 Realization (state diagram) of Eqn. (12.45)

We can now write differential equations for the realization given by Fig. 12.7. To get one state variable model, we identify the output of each integrator in Fig. 12.7 with a state variable starting at the left and proceeding to the right. The corresponding differential equations are

$$\begin{aligned}
\dot{x}_n &= x_{n-1} - \alpha_1(x_n + \beta_0 u) + \beta_1 u \\
\dot{x}_{n-1} &= x_{n-2} - \alpha_2(x_n + \beta_0 u) + \beta_2 u \\
&\vdots \\
\dot{x}_2 &= x_1 - \alpha_{n-1}(x_n + \beta_0 u) + \beta_{n-1} u \\
\dot{x}_1 &= -\alpha_n(x_n + \beta_0 u) + \beta_n u
\end{aligned}$$

and the output equation is

$$y = x_n + \beta_0 u$$

The state and output equations organized in vector-matrix form are given below:

$$\begin{aligned}
\dot{\mathbf{x}}(t) &= \mathbf{A}\mathbf{x}(t) + \mathbf{b}u(t) \\
y(t) &= \mathbf{c}\mathbf{x}(t) + du(t)
\end{aligned} \tag{12.46}$$

with $\mathbf{A} = \begin{bmatrix} 0 & 0 & \cdots & 0 & -\alpha_n \\ 1 & 0 & \cdots & 0 & -\alpha_{n-1} \\ 0 & 1 & \cdots & 0 & -\alpha_{n-2} \\ \vdots & \vdots & & \vdots & \vdots \\ 0 & 0 & \cdots & 1 & -\alpha_1 \end{bmatrix}$; $\mathbf{b} = \begin{bmatrix} \beta_n - \alpha_n\beta_0 \\ \beta_{n-1} - \alpha_{n-1}\beta_0 \\ \\ \vdots \\ \beta_1 - \alpha_1\beta_0 \end{bmatrix}$

$\mathbf{c} = [0\ 0\ \ldots\ 0\ 1]$; $d = \beta_0$

Compare **A**, **b**, and **c** matrices of the second companion form with that of the first. We observe that **A**, **b**, and **c** matrices of one companion form correspond to the transpose of the **A**, **c**, and **b** matrices, respectively, of the other.

There are many benefits derived from the companion forms of state variable models. One obvious benefit is that both the companion forms lend themselves easily to simple analog computer models. Both the companion forms also play an important role in pole-placement design through state feedback.(refer Chapter 13)

12.5.3 Jordan Canonical Form

In the two canonical forms (12.44) and (12.46), the coefficients of the denominator of the transfer function appear in one of the rows or columns of matrix **A**. In another of the canonical forms, the poles of the transfer function form a string along the main diagonal of the matrix. This canonical form follows directly from the partial fraction expansion of the transfer function.

The general transfer function under consideration is (refer Eqn. (12.39))

$$G(s) = \frac{\beta_0 s^n + \beta_1 s^{n-1} + \cdots + \beta_n}{s^n + \alpha_1 s^{n-1} + \cdots + \alpha_n}$$

By long division, $G(s)$ can be written as

$$G(s) = \beta_0 + \frac{\beta_1' s^{n-1} + \beta_2' s^{n-2} + \cdots + \beta_n'}{s^n + \alpha_1 s^{n-1} + \cdots + \alpha_n} = \beta_0 + G'(s)$$

The results are simplest when the poles of the transfer function are all distinct. The partial fraction expansion of the transfer function then has the form:

$$G(s) = \frac{Y(s)}{U(s)} = \beta_0 + \frac{r_1}{s - \lambda_1} + \frac{r_2}{s - \lambda_2} + \cdots + \frac{r_n}{s - \lambda_n} \tag{12.47}$$

The coefficients r_i ($i = 1, 2, ..., n$) are the residues of the transfer function $G'(s)$ at the corresponding poles at $s = \lambda_i$ ($i = 1, 2, ..., n$). In the form of Eqn. (12.47), the transfer function consists of a direct path with gain β_0, and n first-order transfer functions in parallel. A block diagram representation of Eqn. (12.47) is shown in Fig. 12.8. The gains corresponding to the residues have been placed at the outputs of the integrators. This is quite arbitrary. They could have been located on the input side, or indeed split between the input and the output.

Identifying the outputs of the integrators with the state variables results in the following state and output equations:

$$\dot{\mathbf{x}}(t) = \mathbf{\Lambda x}(t) + \mathbf{b}u(t)$$
$$y(t) = \mathbf{cx}(t) + du(t) \tag{12.48}$$

with $\mathbf{\Lambda} = \begin{bmatrix} \lambda_1 & 0 & \cdots & 0 \\ 0 & \lambda_2 & \cdots & 0 \\ \vdots & \vdots & & \vdots \\ 0 & 0 & \cdots & \lambda_n \end{bmatrix}$; $\mathbf{b} = \begin{bmatrix} 1 \\ 1 \\ \vdots \\ 1 \end{bmatrix}$

$\mathbf{c} = \begin{bmatrix} r_1 & r_2 & \cdots & r_n \end{bmatrix}$; $d = \beta_0$

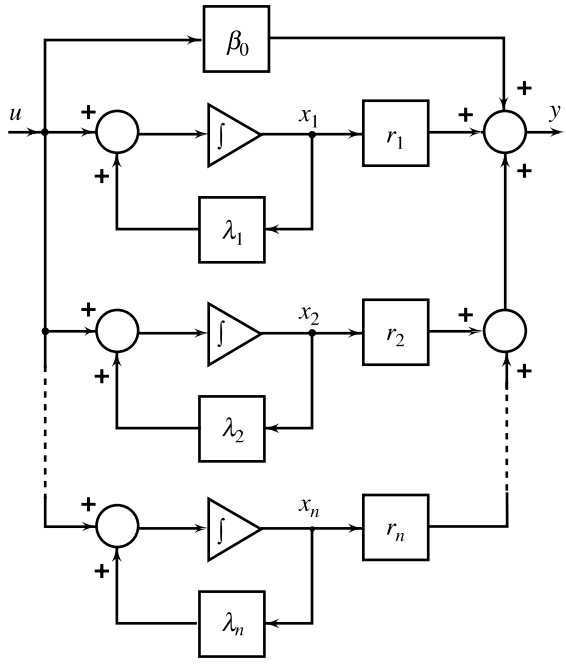

Fig. 12.8 Realization (state diagram) of $G(s)$ in Eqn. (12.47)

It is observed that for this canonical state variable model, the matrix $\mathbf{\Lambda}$ is a diagonal matrix with the poles of $G(s)$ as its diagonal elements. The unique *decoupled* nature of the canonical model is obvious from Equations (12.48); the n first-order differential equations are independent of each other:

$$\dot{x}_i(t) = \lambda_i x_i(t) + u(t);\ i = 1, 2, ..., n \tag{12.49}$$

This decoupling feature greatly helps in system analysis (refer [155]).

The block diagram representation of Fig. 12.8 can be turned into hardware only if all the poles at $s = \lambda_1$, λ_2, ..., λ_n are real. If they are complex, the feedback gains and the gains corresponding to the residues are complex. In this case, the representation must be considered as being purely conceptual; valid for theoretical studies, but not physically realizable. A realizable representation can be obtained by introducing an equivalence transformation.

Suppose that $s = \sigma + j\omega$, $s = \sigma - j\omega$ and $s = \lambda$ are the three poles of a transfer function. The residues at the pair of complex conjugate poles must be themselves complex conjugates. Partial fraction expansion of the transfer function with a pair of complex conjugate poles and a real pole has the form

$$G(s) = d + \frac{p + jq}{s - (\sigma + j\omega)} + \frac{p - jq}{s - (\sigma - j\omega)} + \frac{r}{s - \lambda}$$

A state variable model for this transfer function is given below (refer Eqns (12.48)):

$$\begin{aligned} \dot{\mathbf{x}} &= \mathbf{\Lambda x} + \mathbf{b}u \\ y &= \mathbf{cx} + du \end{aligned} \tag{12.50}$$

with $$\mathbf{\Lambda} = \begin{bmatrix} \sigma + j\omega & 0 & 0 \\ 0 & \sigma - j\omega & 0 \\ 0 & 0 & \lambda \end{bmatrix}; \mathbf{b} = \begin{bmatrix} 1 \\ 1 \\ 1 \end{bmatrix}$$

$$\mathbf{c} = [p + jq \quad p - jq \quad r]$$

Introducing an equivalence transformation

$$\mathbf{x} = \mathbf{P}\,\bar{\mathbf{x}}$$

with $$\mathbf{P} = \begin{bmatrix} 1/2 & -j1/2 & 0 \\ 1/2 & j1/2 & 0 \\ 0 & 0 & 1 \end{bmatrix}$$

we obtain (refer Eqns (12.17))

$$\begin{aligned} \dot{\bar{\boldsymbol{x}}}(t) &= \bar{\mathbf{A}}\,\bar{\mathbf{x}}(t) + \bar{\mathbf{b}}\,u(t) \\ y(t) &= \bar{\mathbf{c}}\,\bar{\mathbf{x}}(t) + du(t) \end{aligned} \tag{12.51}$$

where

$$\bar{\mathbf{A}} = \mathbf{P}^{-1}\mathbf{\Lambda P} = \begin{bmatrix} 1 & 1 & 0 \\ j & -j & 0 \\ 0 & 0 & 1 \end{bmatrix} \begin{bmatrix} \sigma + j\omega & 0 & 0 \\ 0 & \sigma - j\omega & 0 \\ 0 & 0 & \lambda \end{bmatrix} \begin{bmatrix} 1/2 & -j1/2 & 0 \\ 1/2 & j1/2 & 0 \\ 0 & 0 & 1 \end{bmatrix} = \begin{bmatrix} \sigma & \omega & 0 \\ -\omega & \sigma & 0 \\ 0 & 0 & \lambda \end{bmatrix}$$

$$\bar{\mathbf{b}} = \mathbf{P}^{-1}\mathbf{b} = \begin{bmatrix} 2 \\ 0 \\ 1 \end{bmatrix}$$

$$\bar{\mathbf{c}} = \mathbf{cP} = [p \quad q \quad r]$$

When the transfer function $G(s)$ has repeated poles, the partial fraction expansion will not be as simple as Eqn. (12.47). Assume that $G(s)$ has m distinct poles at $s = \lambda_1, \lambda_2, \ldots, \lambda_m$ of multiplicity $n_1, n_2, \ldots, n_m$ respectively; $n = n_1 + n_2 + \cdots + n_m$. That is, $G(s)$ is of the form

$$G(s) = \beta_0 + \frac{\beta_1' s^{n-1} + \beta_2' s^{n-2} + \cdots + \beta_n'}{(s-\lambda_1)^{n_1}(s-\lambda_2)^{n_2}\cdots(s-\lambda_m)^{n_m}} \tag{12.52}$$

The partial fraction expansion of $G(s)$ is of the form:

$$G(s) = \beta_0 + H_1(s) + \cdots + H_m(s) = \frac{Y(s)}{U(s)} \tag{12.53}$$

where

$$H_i(s) = \frac{r_{i1}}{(s-\lambda_i)^{n_i}} + \frac{r_{i2}}{(s-\lambda_i)^{n_i-1}} + \cdots + \frac{r_{in_i}}{(s-\lambda_i)} = \frac{Y_i(s)}{U(s)}$$

The first term in $H_i(s)$ can be synthesized as a chain of n_i identical, first-order systems, each having transfer function $1/(s-\lambda_i)$. The second term can be synthesized by a chain of $(n_i - 1)$ first-order systems, and so forth. The entire $H_i(s)$ can be synthesized by the system having the block diagram shown in Fig. 12.9.

We can now write differential equations for the realization of $H_i(s)$ given by Fig. 12.9. To get one state variable formulation, we identify the output of each integrator with a state variable starting at the right and proceeding to the left. The corresponding differential equations are

$$\begin{aligned} \dot{x}_{i1} &= \lambda_i x_{i1} + x_{i2} \\ \dot{x}_{i2} &= \lambda_i x_{i2} + x_{i3} \\ &\vdots \\ \dot{x}_{in_i} &= \lambda_i x_{in_i} + u \end{aligned} \tag{12.54a}$$

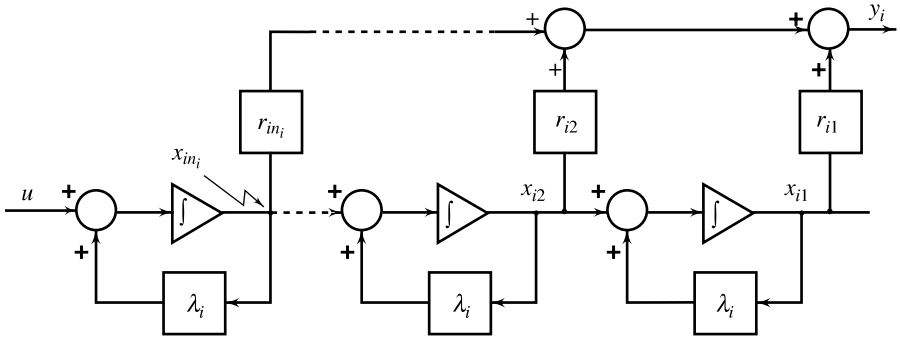

Fig. 12.9 Realization (state diagram) of $H_i(s)$ in Eqn. (12.53)

and the output is given by

$$y_i = r_{i1} x_{i1} + r_{i2} x_{i2} + \cdots + r_{in_i} x_{in_i} \tag{12.54b}$$

If the state vector for the subsystem is defined by

$$\mathbf{x}_i = [x_{i1} \quad x_{i2} \cdots x_{in_i}]^T$$

then Eqns (12.54) can be written in the standard form

$$\dot{\mathbf{x}}_i = \mathbf{\Lambda}_i \mathbf{x}_i + \mathbf{b}_i u$$
$$y_i = \mathbf{c}_i \mathbf{x}_i \tag{12.55}$$

where

$$\mathbf{\Lambda}_i = \begin{bmatrix} \lambda_i & 1 & 0 & \cdots & 0 & 0 \\ 0 & \lambda_i & 1 & \cdots & 0 & 0 \\ \vdots & \vdots & \vdots & & \vdots & \vdots \\ 0 & 0 & 0 & \cdots & \lambda_i & 1 \\ 0 & 0 & 0 & \cdots & 0 & \lambda_i \end{bmatrix}; \mathbf{b}_i = \begin{bmatrix} 0 \\ 0 \\ \vdots \\ 0 \\ 1 \end{bmatrix}$$

$$\mathbf{c}_i = \begin{bmatrix} r_{i1} & r_{i2} & \cdots & r_{in_i} \end{bmatrix}$$

Note that matrix $\mathbf{\Lambda}_i$ has two diagonals—the principal diagonal has the corresponding characteristic root (pole) and the superdiagonal has all 1's. In matrix theory, a matrix having this structure is said to be in *Jordan form*. For this reason, we identify the realization (12.55) as *Jordan canonical form*.

According to Eqn. (12.53), the overall transfer function $G(s)$ consists of a direct path with gain β_0 and m subsystems, each of which is in the Jordan canonical form as shown in Fig. 12.10. The state vector of the overall system consists of the concatenation of the state vectors of each of the *Jordan blocks*:

$$\mathbf{x} = \begin{bmatrix} \mathbf{x}_1 \\ \mathbf{x}_2 \\ \vdots \\ \mathbf{x}_m \end{bmatrix} \tag{12.56a}$$

Since there is no coupling between any of the subsystems, the $\mathbf{\Lambda}$ matrix of the overall system is 'block diagonal':

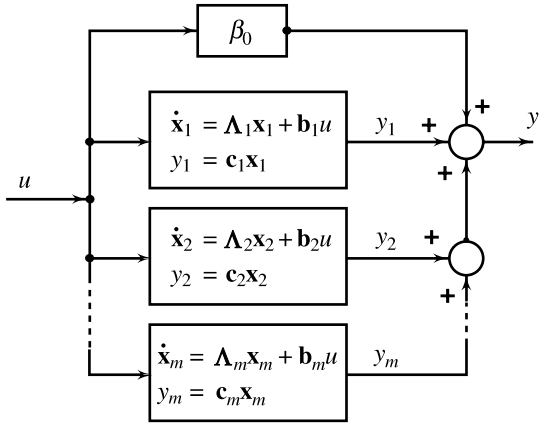

Fig. 12.10 Subsystems in Jordan canonical form combined into overall system

$$\mathbf{\Lambda} = \begin{bmatrix} \mathbf{\Lambda}_1 & \mathbf{0} & \cdots & \mathbf{0} \\ \mathbf{0} & \mathbf{\Lambda}_2 & \cdots & \mathbf{0} \\ \vdots & \vdots & & \vdots \\ \mathbf{0} & \mathbf{0} & \cdots & \mathbf{\Lambda}_m \end{bmatrix} \tag{12.56b}$$

where each of the submatrices $\mathbf{\Lambda}_i$ is in the Jordan canonical form (12.55). The $\mathbf{b}$ and $\mathbf{c}$ matrices of the overall system are the concatenations of the $\mathbf{b}_i$ and $\mathbf{c}_i$ matrices respectively of each of the subsystems:

$$\mathbf{b} = \begin{bmatrix} \mathbf{b}_1 \\ \mathbf{b}_2 \\ \vdots \\ \mathbf{b}_m \end{bmatrix}; \ \mathbf{c} = [\mathbf{c}_1 \quad \mathbf{c}_2 \cdots \mathbf{c}_m]; \ d = \beta_0 \tag{12.56c}$$

The state variable model (12.48) derived for the case of distinct poles, is a special case of Jordan canonical form (12.56) where each Jordan block is of 1×1 dimension.

Example 12.5 In the following, we obtain three different realizations for the transfer function

$$G(s) = \frac{s+3}{s^3 + 9s^2 + 24s + 20} = \frac{Y(s)}{U(s)}$$

First companion form Note that the given $G(s)$ is a strictly proper fraction; the realization will therefore be of the form (12.38), i.e., the parameter d in the realization $\{\mathbf{A}, \mathbf{b}, \mathbf{c}, d\}$ is zero.

The state variable formulation in the first companion form can be written just by inspection of the given transfer function. Referring to Eqns (12.44), we obtain

$$\begin{bmatrix} \dot{x}_1 \\ \dot{x}_2 \\ \dot{x}_3 \end{bmatrix} = \begin{bmatrix} 0 & 1 & 0 \\ 0 & 0 & 1 \\ -20 & -24 & -9 \end{bmatrix} \begin{bmatrix} x_1 \\ x_2 \\ x_3 \end{bmatrix} + \begin{bmatrix} 0 \\ 0 \\ 1 \end{bmatrix} u$$

$$y = \begin{bmatrix} 3 & 1 & 0 \end{bmatrix} \begin{bmatrix} x_1 \\ x_2 \\ x_3 \end{bmatrix}$$

Figure 12.11a shows the state diagram in signal flow graph form.

Second companion form Referring to Eqns (12.46), we obtain

$$\begin{bmatrix} \dot{x}_1 \\ \dot{x}_2 \\ \dot{x}_3 \end{bmatrix} = \begin{bmatrix} 0 & 0 & -20 \\ 1 & 0 & -24 \\ 0 & 1 & -9 \end{bmatrix} \begin{bmatrix} x_1 \\ x_2 \\ x_3 \end{bmatrix} + \begin{bmatrix} 3 \\ 1 \\ 0 \end{bmatrix} u$$

$$y = x_3$$

Figure 12.11b shows the state diagram.

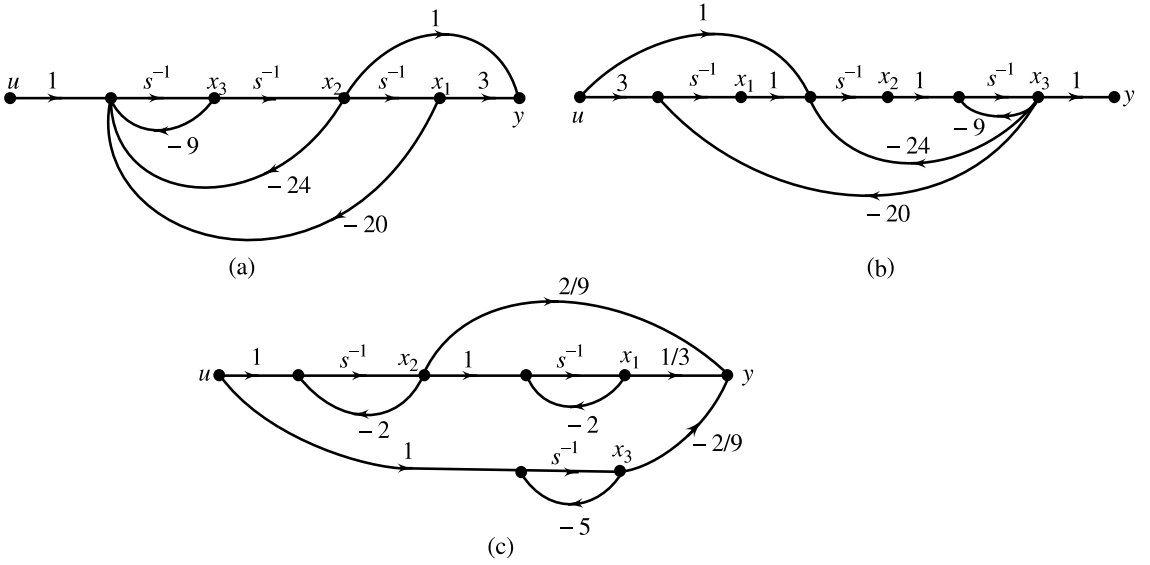

Fig. 12.11 Three realizations of given $G(s)$

Jordan canonical form The given transfer function $G(s)$ in the factored form:

$$G(s) = \frac{s+3}{(s+2)^2(s+5)}$$

Using partial fraction expansion, we obtain

$$G(s) = \frac{1/3}{(s+2)^2} + \frac{2/9}{s+2} + \frac{-2/9}{s+5}$$

A matrix of the state variable model in Jordan canonical form will be block-diagonal; consisting of two Jordan blocks (refer Eqns (12.55)):

$$\mathbf{\Lambda}_1 = \begin{bmatrix} -2 & 1 \\ 0 & -2 \end{bmatrix},$$

$$\mathbf{\Lambda}_2 = [-5]$$

The corresponding $\mathbf{b}_i$ and $\mathbf{c}_i$ vectors are (refer Eqns (12.55)):

$$\mathbf{b}_1 = \begin{bmatrix} 0 \\ 1 \end{bmatrix}; \mathbf{c}_1 = \begin{bmatrix} \frac{1}{3} & \frac{2}{9} \end{bmatrix}$$

$$\mathbf{b}_2 = [1]\ ; \mathbf{c}_2 = \begin{bmatrix} -\frac{2}{9} \end{bmatrix}$$

The state variable model of the given $G(s)$ in Jordan canonical form is therefore given by (refer Eqns (12.56))

$$\begin{bmatrix} \dot{x}_1 \\ \dot{x}_2 \\ \dot{x}_3 \end{bmatrix} = \left[\begin{array}{cc:c} -2 & 1 & 0 \\ 0 & -2 & 0 \\ \hdashline 0 & 0 & -5 \end{array}\right] \begin{bmatrix} x_1 \\ x_2 \\ x_3 \end{bmatrix} + \left[\begin{array}{c} 0 \\ 1 \\ \hdashline 1 \end{array}\right] u$$

$$y = \left[\begin{array}{cc:c} \frac{1}{3} & \frac{2}{9} & -\frac{2}{9} \end{array}\right] \begin{bmatrix} x_1 \\ x_2 \\ x_3 \end{bmatrix}$$

Figure 12.11c shows the state diagram. We note that Jordan canonical state variables are not completely decoupled. The decoupling is blockwise; state variables of one block are independent of state variables of all other blocks. However, the state variables of one block among themselves are coupled; the coupling is unique and simple.

12.6 SOLUTION OF STATE EQUATIONS

In this section, we investigate the solution of the state equation

$$\dot{\mathbf{x}}(t) = \mathbf{A}\mathbf{x}(t) + \mathbf{b}u(t);\ \mathbf{x}(t_0) \triangleq \mathbf{x}^0 \tag{12.57}$$

where $\mathbf{x}$ is $n \times 1$ state vector, u is a scalar input, $\mathbf{A}$ is $n \times n$ constant matrix, and $\mathbf{b}$ is $n \times 1$ constant vector.

12.6.1 Matrix Exponential

Functions of square matrices arise in connection with the solution of vector differential equations. Of immediate interest to us are matrix infinite series.

Consider the infinite series in a scalar variable x:

$$f(x) = \alpha_0 + \alpha_1 x + \alpha_2 x^2 + \cdots = \sum_{i=0}^{\infty} \alpha_i x^i \tag{12.58a}$$

with the radius of convergence r.

We can define infinite series in a matrix variable $\mathbf{A}$ as

$$f(\mathbf{A}) = \alpha_0 \mathbf{I} + \alpha_1 \mathbf{A} + \alpha_2 \mathbf{A}^2 + \cdots = \sum_{i=0}^{\infty} \alpha_i \mathbf{A}^i \tag{12.58b}$$

An important relation between the scalar power series (12.58a) and the matrix power series (12.58b) is that if the absolute values of eigenvalues of $\mathbf{A}$ are smaller than r, then the matrix power series (12.58b) converges (for proof, refer Lefschetz [33]).

Consider, in particular, the scalar power series

$$f(x) = 1 + x + \frac{1}{2!}x^2 + \cdots + \frac{1}{k!}x^k + \cdots = \sum_{i=0}^{\infty} \frac{1}{i!} x^i \tag{12.59a}$$

It is well-known that this power series converges on to the exponential e^x for a finite x, so that

$$f(x) = e^x \tag{12.59b}$$

It follows from this result that the matrix power series

$$f(\mathbf{A}) = \mathbf{I} + \mathbf{A} + \frac{1}{2!}\mathbf{A}^2 + \cdots + \frac{1}{k!}\mathbf{A}^k + \cdots = \sum_{i=0}^{\infty} \frac{1}{i!}\mathbf{A}^i$$

converges for all **A**. By analogy with the power series in Eqns (12.59) for the ordinary exponential function, we adopt the following nomenclature:

If **A** is an $n \times n$ matrix, the *matrix exponential* of **A** is

$$e^{\mathbf{A}} \triangleq \mathbf{I} + \mathbf{A} + \frac{1}{2!}\mathbf{A}^2 + \cdots + \frac{1}{k!}\mathbf{A}^k + \cdots = \sum_{i=0}^{\infty} \frac{1}{i!}\mathbf{A}^i$$

The following matrix exponential will appear in the solution of state equations:

$$e^{\mathbf{A}t} = \mathbf{I} + \mathbf{A}t + \frac{1}{2!}\mathbf{A}^2t^2 + \cdots + \frac{1}{k!}\mathbf{A}^kt^k + \cdots = \sum_{i=0}^{\infty} \frac{1}{k!}\mathbf{A}^it^i \qquad (12.60)$$

It converges for all **A** and all finite t.

In the following we examine some of the properties of the matrix exponential.

1. $$e^{\mathbf{A}0} = \mathbf{I} \qquad (12.61)$$

This is easily verified by setting $t = 0$ in Eqn. (12.60).

2. $$e^{\mathbf{A}(t+\tau)} = e^{\mathbf{A}t}e^{\mathbf{A}\tau} = e^{\mathbf{A}\tau}e^{\mathbf{A}t} \qquad (12.62)$$

This is easily verified by multiplying out the first few terms for $e^{\mathbf{A}t}$ and $e^{\mathbf{A}\tau}$.

3. $$(e^{\mathbf{A}t})^{-1} = e^{-\mathbf{A}t} \qquad (12.63)$$

Setting $\tau = -t$ in Eqn. (12.62), we obtain

$$e^{\mathbf{A}t}e^{-\mathbf{A}t} = e^{\mathbf{A}0} = \mathbf{I}$$

Thus the inverse of $e^{\mathbf{A}t}$ is $e^{-\mathbf{A}t}$.

Since the inverse of $e^{\mathbf{A}t}$ always exists, the matrix exponential is nonsingular for all finite values of t.

4. $$\frac{d}{dt}e^{\mathbf{A}t} = \mathbf{A}e^{\mathbf{A}t} = e^{\mathbf{A}t}\mathbf{A} \qquad (12.64)$$

Term-by-term differentiation of Eqn. (12.60) gives

$$\frac{d}{dt}e^{\mathbf{A}t} = \mathbf{A} + \mathbf{A}^2t + \frac{1}{2!}\mathbf{A}^3t^2 + \cdots + \frac{1}{(k-1)!}\mathbf{A}^kt^{k-1} + \cdots$$

$$= \mathbf{A}[\mathbf{I} + \mathbf{A}t + \frac{1}{2!}\mathbf{A}^2t^2 + \cdots + \frac{1}{(k-1)!}\mathbf{A}^{k-1}t^{k-1} + \cdots] = \mathbf{A}e^{\mathbf{A}t}$$

$$= [\mathbf{I} + \mathbf{A}t + \frac{1}{2!}\mathbf{A}^2t^2 + \cdots + \frac{1}{(k-1)!}\mathbf{A}^{k-1}t^{k-1} + \cdots]\mathbf{A} = e^{\mathbf{A}t}\mathbf{A}$$

12.6.2 Solution of Homogeneous State Equation

The simplest form of the general differential Eqn. (12.57) is the homogeneous, i.e., unforced equation

$$\dot{\mathbf{x}}(t) = \mathbf{A}\mathbf{x}(t);\ \mathbf{x}(t_0) \triangleq \mathbf{x}^0 \qquad (12.65)$$

We assume a solution $\mathbf{x}(t)$ of the form

$$\mathbf{x}(t) = e^{\mathbf{A}t}\mathbf{k} \tag{12.66}$$

where $e^{\mathbf{A}t}$ is the matrix exponential function defined in Eqn. (12.60) and $\mathbf{k}$ is a suitably chosen constant vector.

The assumed solution is, in fact, the true solution since it satisfies the differential Eqn. (12.65) as is seen below.

$$\dot{\mathbf{x}}(t) = \frac{d}{dt}[e^{\mathbf{A}t}\mathbf{k}] = \frac{d}{dt}[e^{\mathbf{A}t}]\mathbf{k}$$

Using property (12.64) of the matrix exponential, we obtain

$$\dot{\mathbf{x}}(t) = \mathbf{A}e^{\mathbf{A}t}\,\mathbf{k} = \mathbf{A}\mathbf{x}(t)$$

To evaluate the constant $\mathbf{k}$ in terms of the known initial state $\mathbf{x}(t_0)$, we substitute $t = t_0$ in Eqn. (12.66):

$$\mathbf{x}(t_0) = e^{\mathbf{A}t_0}\,\mathbf{k}$$

Using property (12.63) of the matrix exponential, we obtain

$$\mathbf{k} = (e^{\mathbf{A}t_0})^{-1}\mathbf{x}(t_0) = e^{-\mathbf{A}t_0}\,\mathbf{x}(t_0)$$

Thus the general solution to Eqn. (12.65) for the state $\mathbf{x}(t)$ at time t, given the state $\mathbf{x}(t_0)$ at time t_0, is

$$\mathbf{x}(t) = e^{\mathbf{A}t}e^{-\mathbf{A}t_0}\,\mathbf{x}(t_0) = e^{\mathbf{A}(t-t_0)}\,\mathbf{x}(t_0) \tag{12.67a}$$

We have used the property (12.62) of the matrix exponential to express the solution in this form.

If the initial time $t_0 = 0$, i.e., the initial state $\mathbf{x}^0$ is known at $t = 0$, we have from Eqn. (12.67a):

$$\mathbf{x}(t) = e^{\mathbf{A}t}\mathbf{x}(0) \tag{12.67b}$$

From Eqn. (12.67b) it is observed that the initial state $\mathbf{x}(0) \triangleq \mathbf{x}^0$ at $t = 0$ is driven to a state $\mathbf{x}(t)$ at time t. This transition in state is carried out by the matrix exponential $e^{\mathbf{A}t}$. Due to this property, $e^{\mathbf{A}t}$ is known as the *state transition matrix*, and is denoted by $\boldsymbol{\phi}(t)$.

Properties of state transition matrix Properties of the matrix exponential, given earlier in Eqns (12.61) – (12.64), are restated below in terms of state transition matrix $\boldsymbol{\phi}(t)$.

1. $\dfrac{d}{dt}\boldsymbol{\phi}(t) = \mathbf{A}\boldsymbol{\phi}(t);\ \boldsymbol{\phi}(0) = \mathbf{I}$
2. $\boldsymbol{\phi}(t_2 - t_1)\,\boldsymbol{\phi}(t_1 - t_0) = \boldsymbol{\phi}(t_2 - t_0)$ for any t_0, t_1, t_2

   This property of the state transition matrix is important since it implies that a state transition process can be divided into a number of sequential transitions. The transition form t_0 to t_2:

   $$\mathbf{x}(t_2) = \boldsymbol{\phi}(t_2 - t_0)\,\mathbf{x}(t_0);$$

   is equal to the transition from t_0 to t_1 and then from t_1 to t_2:

   $$\mathbf{x}(t_1) = \boldsymbol{\phi}(t_1 - t_0)\mathbf{x}(t_0)$$

   $$\mathbf{x}(t_2) = \boldsymbol{\phi}(t_2 - t_1)\mathbf{x}(t_1)$$
3. $\boldsymbol{\phi}^{-1}(t) = \boldsymbol{\phi}(-t)$
4. $\boldsymbol{\phi}(t)$ is a nonsingular matrix for all finite t.

Evaluation of state transition matrix Taking the Laplace transform on both sides of Eqn. (12.65) yields

$$s\mathbf{X}(s) - \mathbf{x}^0 = \mathbf{A}\mathbf{X}(s)$$

where $\mathbf{X}(s) \triangleq \mathscr{L}[\mathbf{x}(t)]$

$\mathbf{x}^0 \triangleq \mathbf{x}(0)$

Solving for $\mathbf{X}(s)$, we get

$$\mathbf{X}(s) = (s\mathbf{I} - \mathbf{A})^{-1}\mathbf{x}^0$$

The state vector $\mathbf{x}(t)$ can be obtained by inverse transforming $\mathbf{X}(s)$:

$$\mathbf{x}(t) = \mathscr{L}^{-1}[(s\mathbf{I} - \mathbf{A})^{-1}]\mathbf{x}^0$$

Comparing this equation with Eqn. (12.67b), we get

$$e^{\mathbf{A}t} = \boldsymbol{\phi}(t) = \mathscr{L}^{-1}[(s\mathbf{I} - \mathbf{A})^{-1}] \tag{12.68}$$

The matrix $(s\mathbf{I} - \mathbf{A})^{-1} = \boldsymbol{\Phi}(s)$ is known in mathematical literature as the resolvent of $\mathbf{A}$. The entries of the resolvent matrix $\boldsymbol{\Phi}(s)$ are rational functions of s.

Example 12.6 Consider the system

$$\dot{\mathbf{x}} = \begin{bmatrix} 0 & 0 & -2 \\ 0 & 1 & 0 \\ 1 & 0 & 3 \end{bmatrix} \mathbf{x} \; ; \; \mathbf{x}(0) = \begin{bmatrix} 0 \\ 1 \\ 0 \end{bmatrix}$$

The resolvent matrix

$$\boldsymbol{\Phi}(s) = (s\mathbf{I} - \mathbf{A})^{-1} = \begin{bmatrix} s & 0 & 2 \\ 0 & s-1 & 0 \\ -1 & 0 & s-3 \end{bmatrix}^{-1} = \frac{(s\mathbf{I} - \mathbf{A})^{+}}{|\, s\mathbf{I} - \mathbf{A}\,|}$$

$$|s\mathbf{I} - \mathbf{A}| = (s-1)^2\,(s-2)$$

$$(s\mathbf{I} - \mathbf{A})^{+} = \begin{bmatrix} (s-1)(s-3) & 0 & -2(s-1) \\ 0 & (s-1)(s-2) & 0 \\ (s-1) & 0 & s\,(s-1) \end{bmatrix}$$

$$e^{\mathbf{A}t} = \mathscr{L}^{-1}\,[\boldsymbol{\Phi}(s)] = \mathscr{L}^{-1}\,[(s\mathbf{I} - \mathbf{A})^{-1}]$$

$$= \mathscr{L}^{-1} \begin{bmatrix} \dfrac{(s-3)}{(s-1)(s-2)} & 0 & \dfrac{-2}{(s-1)(s-2)} \\ 0 & \dfrac{1}{(s-1)} & 0 \\ \dfrac{1}{(s-1)(s-2)} & 0 & \dfrac{s}{(s-1)(s-2)} \end{bmatrix}$$

$$= \begin{bmatrix} 2e^{t} - e^{2t} & 0 & 2e^{t} - 2e^{2t} \\ 0 & e^{t} & 0 \\ -e^{t} + e^{2t} & 0 & 2e^{2t} - e^{t} \end{bmatrix}$$

Consequently, the free response of the system is

$$\mathbf{x}(t) = e^{\mathbf{A}t}\mathbf{x}(0) = \begin{bmatrix} 0 \\ e^{t} \\ 0 \end{bmatrix}$$

Note that $\mathbf{x}(t)$ could be more easily computed by taking the inverse Laplace transform of

$$\mathbf{X}(s) = [(s\mathbf{I} - \mathbf{A})^{-1}\mathbf{x}(0)]$$

12.6.3 Solution of Nonhomogeneous State Equation

When an input $u(t)$ is present, the complete solution $\mathbf{x}(t)$ is obtained from the nonhomogeneous Eqn. (12.57). By writing Eqn. (12.57) as

$$\dot{\mathbf{x}}(t) - \mathbf{A}\mathbf{x}(t) = \mathbf{b}u(t)$$

and premultiplying both sides of this equation by $e^{-\mathbf{A}t}$, we obtain

$$e^{-\mathbf{A}t}[\dot{\mathbf{x}}(t) - \mathbf{A}\mathbf{x}(t)] = e^{-\mathbf{A}t}\mathbf{b}u(t) \tag{12.69}$$

By applying the rule for the derivative of the product of two matrices, we can write (refer Eqn. (12.64))

$$\begin{aligned} \frac{d}{dt}[e^{-\mathbf{A}t}\mathbf{x}(t)] &= e^{-\mathbf{A}t}\frac{d}{dt}(\mathbf{x}(t)) + \frac{d}{dt}(e^{-\mathbf{A}t})\mathbf{x}(t) \\ &= e^{-\mathbf{A}t}\dot{\mathbf{x}}(t) - e^{-\mathbf{A}t}\mathbf{A}\mathbf{x}(t) \\ &= e^{-\mathbf{A}t}[\dot{\mathbf{x}}(t) - \mathbf{A}\mathbf{x}(t)] \end{aligned}$$

Use of this equality in Eqn. (12.69) gives

$$\frac{d}{dt}[e^{-\mathbf{A}t}\mathbf{x}(t)] = e^{-\mathbf{A}t}\mathbf{b}u(t)$$

Integrating both sides with respect to t between the limits 0 and t, we get

$$e^{-\mathbf{A}t}\mathbf{x}(t)\Big|_0^t = \int_0^t e^{-\mathbf{A}\tau}\mathbf{b}u(\tau)d\tau$$

or

$$e^{-\mathbf{A}t}\mathbf{x}(t) - \mathbf{x}(0) = \int_0^t e^{-\mathbf{A}\tau}\mathbf{b}u(\tau)d\tau$$

Now premultiplying both sides by $e^{\mathbf{A}t}$, we have

$$\mathbf{x}(t) = e^{\mathbf{A}t}\mathbf{x}(0) + \int_0^t e^{\mathbf{A}(t-\tau)}\mathbf{b}u(\tau)d\tau \tag{12.70}$$

If the initial state is known at $t = t_0$, rather than $t = 0$, Eqn. (12.70) becomes

$$\mathbf{x}(t) = e^{\mathbf{A}(t-t_0)}\mathbf{x}(t_0) + \int_{t_0}^t e^{\mathbf{A}(t-\tau)}\mathbf{b}u(\tau)d\tau \tag{12.71}$$

Equation (12.71) can also be written as

$$\mathbf{x}(t) = \boldsymbol{\phi}(t - t_0)\,\mathbf{x}(t_0) + \int_{t_0}^{t} \boldsymbol{\phi}(t - \tau)\,\mathbf{b}u(\tau)\,d\tau \tag{12.72}$$

where $\boldsymbol{\phi}(t) = e^{\mathbf{A}t}$

Equation (12.72) is the solution of Eqn. (12.57). This equation is called the *state transition equation*. It describes the change of state relative to the initial conditions $\mathbf{x}(t_0)$ and the input $u(t)$.

Example 12.7 For the speed control system of Fig. 12.1, the following plant model was derived in Example 12.1 (refer Eqns (12.12)):

$$\dot{\mathbf{x}} = \mathbf{A}\mathbf{x} + \mathbf{b}u$$
$$y = \mathbf{c}\mathbf{x}$$

with

$$\mathbf{A} = \begin{bmatrix} -1 & 1 \\ -1 & -10 \end{bmatrix};\ \mathbf{b} = \begin{bmatrix} 0 \\ 10 \end{bmatrix};\ \mathbf{c} = [1\ 0]$$

State variables x_1 and x_2 are the physical variables of the system:

$x_1(t) = \omega(t)$, angular velocity of the motor shaft

$x_2(t) = i_a(t)$, armature current

The output

$$y(t) = x_1(t) = \omega(t)$$

In the following, we evaluate the response of this system to a unit step input under zero initial conditions.

$$(s\mathbf{I} - \mathbf{A})^{-1} = \begin{bmatrix} s+1 & -1 \\ 1 & s+10 \end{bmatrix}^{-1}$$

$$= \frac{1}{s^2 + 11s + 11}\begin{bmatrix} s+10 & 1 \\ -1 & s+1 \end{bmatrix}$$

$$= \begin{bmatrix} \dfrac{s+10}{(s+a_1)(s+a_2)} & \dfrac{1}{(s+a_1)(s+a_2)} \\ \dfrac{-1}{(s+a_1)(s+a_2)} & \dfrac{s+1}{(s+a_1)(s+a_2)} \end{bmatrix};\ a_1 = 1.1125,\ a_2 = 9.8875$$

$$e^{\mathbf{A}t} = \mathscr{L}^{-1}[(s\mathbf{I} - \mathbf{A})^{-1}]$$

$$= \begin{bmatrix} 1.0128\,e^{-a_1 t} - 0.0128\,e^{-a_2 t} & 0.114\,e^{-a_1 t} - 0.114\,e^{-a_2 t} \\ -0.114\,e^{-a_1 t} + 0.114\,e^{-a_2 t} & -0.0128\,e^{-a_1 t} + 1.0128\,e^{-a_2 t} \end{bmatrix}$$

$$u(t) = 1;\ t \geq 0$$

$$\mathbf{x}(0) = \mathbf{0}$$

Therefore,

$$\mathbf{x}(t) = \int_0^t e^{\mathbf{A}(t-\tau)}\mathbf{b}\,d\tau = \int_0^t \begin{bmatrix} 1.14\left(e^{-a_1(t-\tau)} - e^{-a_2(t-\tau)}\right) \\ 1.14\left(-0.1123\,e^{-a_1(t-\tau)} + 8.8842\,e^{-a_2(t-\tau)}\right) \end{bmatrix} d\tau$$

$$= \begin{bmatrix} 0.9094 - 1.0247\,e^{-a_1 t} + 0.1153\,e^{-a_2 t} \\ -0.0132 + 0.1151\,e^{-a_1 t} - 0.1019\,e^{-a_2 t} \end{bmatrix}$$

The output

$$y(t) = \omega(t) = 0.9094 - 1.0247\,e^{-1.1125t} + 0.1153e^{-9.8875t};\ t \geq 0$$

12.6.4 Discrete-Time Solution

As illustrated in Fig. 12.12, the time axis is discretized into intervals of width T, and $u(t)$ is approximated by a staircase function, constant over the intervals. For the k^{th} interval,

$$u(t) = u(kT);\ kT \leq t < (k+1)\,T;\ k = 0, 1, 2, \ldots \tag{12.73}$$

Using Eqn. (12.71) for $t_0 = kT$,

$$\mathbf{x}(t) = e^{\mathbf{A}(t-kT)}\mathbf{x}(kT) + \left[\int_{kT}^{t} e^{\mathbf{A}(t-\tau)}\mathbf{b}\,d\tau\right] u(kT);\ kT \leq t < (k+1)T \tag{12.74}$$

In response to the input $u(kT)$, the state settles to the value $\mathbf{x}((k+1)T)$, where

$$\mathbf{x}((k+1)T) = e^{\mathbf{A}T}\mathbf{x}(kT) + \left[\int_{kT}^{(k+1)T} e^{\mathbf{A}[(k+1)T-\tau]}\mathbf{b}\,d\tau\right] u(kT)$$

Letting $\sigma = (\tau - kT)$, we have

$$\mathbf{x}((k+1)T) = e^{\mathbf{A}T}\mathbf{x}(kT) + \left[\int_0^T e^{\mathbf{A}(T-\sigma)}\mathbf{b}\,d\sigma\right] u(kT)$$

With $\theta = T - \sigma$, we get

$$\mathbf{x}((k+1)T) = e^{\mathbf{A}T}\mathbf{x}(kT) + \left[\int_0^T e^{\mathbf{A}\theta}\mathbf{b}\,d\theta\right] u(kT)$$

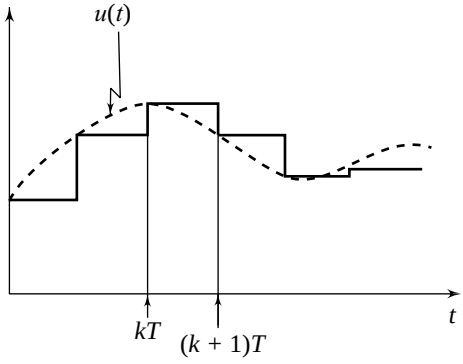

Fig. 12.12 Time discretization

Therefore, for the k^{th} interval,

$$\mathbf{x}((k+1)T) = \mathbf{F}\mathbf{x}(kT) + \mathbf{g}u(kT) \tag{12.75a}$$

where

$$\mathbf{F} = e^{\mathbf{A}T} \tag{12.75b}$$

$$\mathbf{g} = \int_0^T e^{\mathbf{A}\theta}\mathbf{b}\,d\theta \tag{12.75c}$$

This permits the solution to be calculated forward in time.

The infinite series (12.60) may be used to compute **F** and **g**.

$$\mathbf{F} = e^{\mathbf{A}T} = \mathbf{I} + \mathbf{A}T + \frac{1}{2!}\mathbf{A}^2T^2 + \frac{1}{3!}\mathbf{A}^3T^3 + \cdots$$

$$= \sum_{i=0}^{\infty} \frac{\mathbf{A}^i T^i}{i!}; \mathbf{A}^0 = \mathbf{I} \tag{12.76}$$

For a finite T, this series is uniformly convergent. It is therefore possible to evaluate **F** within prescribed accuracy. If the series is truncated at $i = N$, then we may write the finite series sum as

$$\mathbf{F} \cong \sum_{i=0}^{N} \frac{\mathbf{A}^i T^i}{i!} \tag{12.77}$$

which represents the infinite series approximation. The larger the N, the better is the approximation.

The integral in Eqn. (12.75c) can be evaluated term by term to give

$$\mathbf{g} = \left[\int_0^T \left(\mathbf{I} + \mathbf{A}\theta + \frac{1}{2!}\mathbf{A}^2\theta^2 + \cdots\right) d\theta\right]\mathbf{b}$$

$$= \sum_{i=0}^{\infty} \frac{\mathbf{A}^i T^{i+1}}{(i+1)!}\mathbf{b} \tag{12.78}$$

g may also be computed by the approximation technique described above.

Example 12.8 Consider the state variable model

$$\dot{\mathbf{x}}(t) = \mathbf{A}\mathbf{x}(t) + \mathbf{b}\,u(t)$$

$$y(t) = \mathbf{c}\mathbf{x}(t)$$

with

$$\mathbf{A} = \begin{bmatrix} 0 & 1 \\ 0 & -5 \end{bmatrix}; \mathbf{b} = \begin{bmatrix} 0 \\ 1 \end{bmatrix}; \mathbf{c} = \begin{bmatrix} 1 & 0 \end{bmatrix}$$

The state transition matrix

$$e^{\mathbf{A}t} = \mathscr{L}^{-1}[(s\mathbf{I} - \mathbf{A})^{-1}] = \mathscr{L}^{-1}\begin{bmatrix} \frac{1}{s} & \frac{1}{s(s+5)} \\ 0 & \frac{1}{s+5} \end{bmatrix} = \begin{bmatrix} 1 & \frac{1}{5}(1 - e^{-5t}) \\ 0 & e^{-5t} \end{bmatrix}$$

Discretizing time axis into intervals of width $T = 0.1$ sec, we get the following state transition equation, that yields discrete-time solution:

$$\mathbf{x}((k+1)T) = \mathbf{F}\mathbf{x}(kT) + \mathbf{g}u(kT)$$

where

$$\mathbf{F} = e^{\mathbf{A}t} = \begin{bmatrix} 1 & \frac{1}{5}(1 - e^{-5T}) \\ 0 & e^{-5T} \end{bmatrix} = \begin{bmatrix} 1 & 0{\cdot}0787 \\ 0 & 0{\cdot}6065 \end{bmatrix}$$

$$\mathbf{g} = \int_0^T e^{\mathbf{A}\theta}\mathbf{b}\,d\theta = \begin{bmatrix} \int_0^T \frac{1}{5}(1-e^{-5\theta})\,d\theta \\ \int_0^T e^{-5\theta}\,d\theta \end{bmatrix} = \begin{bmatrix} \frac{1}{5}(T-\frac{1}{5}+\frac{1}{5}e^{-5T}) \\ \frac{1}{5}(1-e^{-5T}) \end{bmatrix} = \begin{bmatrix} 0{\cdot}0043 \\ 0{\cdot}0787 \end{bmatrix}$$

For a given initial state $\mathbf{x}(0)$, and input $u(t)$; $t \geq 0$,

$$\mathbf{x}(T) = \mathbf{F}\mathbf{x}(0) + \mathbf{g}u(0)$$
$$\mathbf{x}(2T) = \mathbf{F}\mathbf{x}(T) + \mathbf{g}u(T)$$
$$\mathbf{x}(3T) = \mathbf{F}\mathbf{x}(2T) + \mathbf{g}u(2T)$$
$$\vdots$$

The output

$$y(kT) = \mathbf{c}\mathbf{x}\,(kT)$$

12.7 CONCEPTS OF CONTROLLABILITY AND OBSERVABILITY

Controllability and observability are properties which describe structural features of a dynamic system. These properties play an important role in modern control system design theory; the conditions on controllability and observability often govern the control solution.

To illustrate the motivation of investigating controllability and observability properties, we consider the problem of the stabilization of an inverted pendulum on a motor-driven cart.

Example 12.9 Figure 12.13 shows an inverted pendulum with its pivot mounted on a cart. The cart is driven by an electric motor. The motor drives a pair of wheels of the cart; the whole cart and the pendulum become the 'load' on the motor. The motor at time t exerts a torque $T(t)$ on the wheels. The linear force applied to the cart is $u(t)$; $T(t) = Ru(t)$, where R is the radius of the wheels.

The pendulum is obviously unstable. It can, however, be kept upright by applying a proper control force $u(t)$. This somewhat artificial system example represents a dynamic model of a space booster on take off—the booster is balanced on top of the rocket engine thrust vector.

From inspection of Fig. 12.13, we construct the differential equations describing the dynamics of the inverted pendulum and the cart. The horizontal displacement of the pivot on the cart with respect to the fixed nonrotating coordinate frame, is $z(t)$, while the rotational angle of the pendulum is $\theta(t)$. The parameters of the system are as follows.

M = the mass of the cart
L = the length of the pendulum = $2l$
m = the mass of the pendulum
J = the moment of inertia of the pendulum with

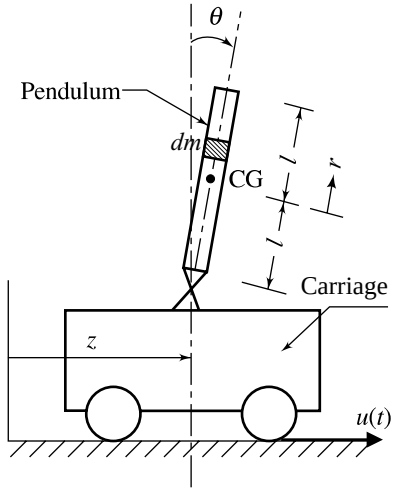

Fig. 12.13 Inverted pendulum system

respect to centre of gravity (CG)

$$J = \int_{-\ell}^{\ell} r^2 dm = \int_{-\ell}^{\ell} r^2 (\rho A dr) = \rho A \left[\frac{r^3}{3}\right]_{-\ell}^{\ell} = \rho A \left(\frac{2\ell^3}{3}\right)$$

$$= \rho A (2\ell)\left(\frac{\ell^2}{3}\right) = \frac{m\ell^2}{3}$$

A = area of cross-section; and ρ = density.

The horizontal and vertical positions of the CG of the pendulum are given by $(z + l \sin\theta)$ and $(l \cos\theta)$ respectively.

The forces exerted on the pendulum are the force mg on the centre of gravity, a horizontal reaction force H and a vertical reaction force V (Fig. 12.14). H is the horizontal reaction force that the cart exerts on the pendulum, whereas $-H$ is the force exerted by the pendulum on the cart. Similar convention applies to forces V and $-V$. Taking moments around CG of the pendulum, we get

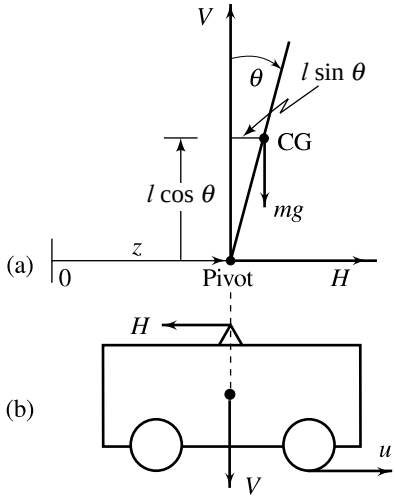

Fig. 12.14

$$J\frac{d^2\theta(t)}{dt^2} = V(t)\, l \sin\theta(t) - H(t)\, l \cos\theta(t) \qquad (12.79a)$$

Summing up all forces on the pendulum in vertical and horizontal directions, we obtain

$$m\frac{d^2}{dt^2}(l\cos\theta(t)) = V(t) - mg \qquad (12.79b)$$

$$m\frac{d^2}{dt^2}(z(t) + l\sin\theta(t)) = H(t) \qquad (12.79c)$$

Summing up all forces on the cart in the horizontal direction, we get

$$M\frac{d^2 z(t)}{dt^2} = u(t) - H(t) \qquad (12.79d)$$

In our problem, since the objective is to keep the pendulum upright, it seems reasonable to assume that $\dot{\theta}(t)$ and $\theta(t)$ will remain close to zero. In view of this, we can set with sufficient accuracy $\sin\theta \cong \theta$; $\cos\theta \cong 1$. With this approximation, we get from Eqns (12.79),

$$ml\ \ddot{\theta}(t) + (m + M)\ddot{z}(t) = u(t)$$

$$(J + ml^2)\ddot{\theta}(t) + ml\ \ddot{z}(t) - mgl\ \theta(t) = 0$$

These equations may be rearranged as

$$\ddot{\theta}(t) = \frac{ml(M+m)g}{\Delta}\ \theta(t) - \frac{ml}{\Delta}u(t) \qquad (12.80a)$$

$$\ddot{z}(t) = -\frac{m^2 l^2 g}{\Delta}\ \theta(t) + \frac{(J + ml^2)}{\Delta}u(t) \qquad (12.80b)$$

where

$$\Delta = (M + m)J + Mm\, l^2$$

Suppose that the system parameters are $M = 1$ kg, $m = 0.15$ kg, and $l = 0.5$ m. Recall that $g = 9.81$ m/sec^2 For these parameters, we have from Eqns (12.80),

$$\ddot{\theta}(t) = 16.3106\,\theta(t) - 1.4458\,u(t) \tag{12.81a}$$

$$\ddot{z}(t) = -1.0637\,\theta(t) + 0.9639\,u(t) \tag{12.81b}$$

Choosing the states $x_1 = \theta$, $x_2 = \dot{\theta}$, $x_3 = z$, and $x_4 = \dot{z}$, we obtain the following state model for the inverted pendulum on moving cart.

$$\dot{\mathbf{x}} = \mathbf{A}\mathbf{x} + \mathbf{b}u \tag{12.82}$$

with

$$\mathbf{A} = \begin{bmatrix} 0 & 1 & 0 & 0 \\ 16.3106 & 0 & 0 & 0 \\ 0 & 0 & 0 & 1 \\ -1.0637 & 0 & 0 & 0 \end{bmatrix}; \quad \mathbf{b} = \begin{bmatrix} 0 \\ -1.4458 \\ 0 \\ 0.9639 \end{bmatrix}$$

The plant (12.82) is said to be *completely controllable* if every state $\mathbf{x}(t_0)$ can be affected or controlled to reach a desired state in finite time by some unconstrained control $u(t)$. Shortly we will see that the plant (12.82) satisfies this condition and therefore a solution exists to the following control problem:

Move the cart from one location to another without causing the pendulum to fall.

The solution to this control problem is not unique. We normally look for a feedback control scheme so that the destabilizing effects of disturbance forces (due to wind, for example) are filtered out. Figure 12.15a shows a state-feedback control scheme for stabilizing the inverted pendulum. The closed-loop system is formed by feeding back the state variables through a real constant matrix $\mathbf{k}$;

$$u(t) = -\mathbf{k}\mathbf{x}(t)$$

The closed-loop system is thus described by

$$\dot{\mathbf{x}}(t) = (\mathbf{A} - \mathbf{b}\mathbf{k})\mathbf{x}(t)$$

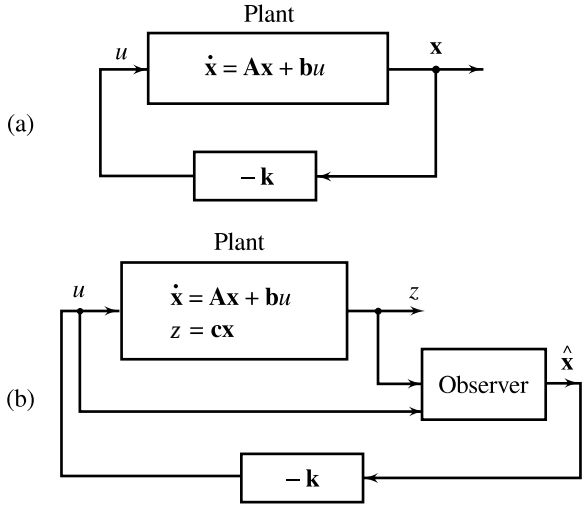

Fig. 12.15 Control system with state feedback

The design objective in this case is to find the feedback matrix **k** such that the closed-loop system is stable. The existence of solution to this design problem is directly based on the controllability property of the plant (12.82).

Implementation of the state-feedback control solution requires access to all the state variables of the plant model. In many control situations of interest, it is possible to install sensors to measure all the state variables. This may not be possible or practical in some cases. For example, if the plant model includes non-physical state variables, measurement of these variables using physical sensors is not possible. Accuracy requirements or cost considerations may prohibit the use of sensors for some physical variables also.

The input and the output of a system are always physical quantities, and are normally easily accessible to measurement. We therefore need a subsystem that performs the estimation of state variables based on the information received from the input $u(t)$ and the output $y(t)$. This subsystem is called an *observer* whose design is based on *observability property* of the controlled system.

The plant (12.82) is said to be *completely observable* if all the state variables in $\mathbf{x}(t)$ can be observed from the measurements of the output $y(t) = \theta(t)$ and the input $u(t)$. Shortly we will see that the plant (12.82) does not satisfy this condition, and therefore a solution to the observer-design problem does not exist when the inputs to the observer subsystem are $u(t)$ and $\theta(t)$.

Cart position $z(t)$ is easily accessible to measurement and, as we shall see, the observability condition is satisfied with this choice of input information to the observer subsystem. Figure 12.15b shows the block diagram of the closed-loop system with an observer that estimates the state vector from measurements of $u(t)$ and $z(t)$. The observed or estimated state vector, designated as $\hat{\mathbf{x}}$, is then used to generate the control u through the feedback matrix **k**.

A study of controllability and observability properties, presented in this section, provides a basis for the state-feedback design problems (Chapter 13). Further, these properties establish the conditions for complete equivalence between the state variable and transfer function representations (Section 12.8).

12.7.1 Definitions of Controllability and Observability

In this section, we study the controllability and observability of linear time-invariant systems described by state variable model of the following form:

$$\dot{\mathbf{x}}(t) = \mathbf{A}\mathbf{x}(t) + \mathbf{b}u(t) \tag{12.83a}$$

$$y(t) = \mathbf{c}\mathbf{x}(t) + du(t) \tag{12.83b}$$

where **A**, **b**, **c** and d are respectively $n \times n$, $n \times 1$, $1 \times n$ and 1×1 matrices, $\mathbf{x}(t)$ is $n \times 1$ state vector, $y(t)$ and $u(t)$ are, respectively, output and input variables.

Controllability For the linear system given by (12.83), if there exists an input $u_{[0, t_1]}$ which transfers the initial state $\mathbf{x}(0) \triangleq \mathbf{x}^0$ to the state $\mathbf{x}^1$ in a finite time t_1, the state $\mathbf{x}^0$ is said to be controllable. If all initial states are controllable, the system is said to be *completely controllable*, or simply *controllable*. Otherwise, the system is said to be *uncontrollable*.

From Eqn. (12.70), the solution of Eqn. (12.83a) is

$$\mathbf{x}(t) = e^{\mathbf{A}t}\mathbf{x}^0 + \int_0^t e^{\mathbf{A}(t-\tau)}\,\mathbf{b}u(\tau)\,d\tau$$

To study the controllability property, we may assume without loss of generality that $\mathbf{x}^1 \equiv \mathbf{0}$. Therefore if the system (12.83) is controllable, there exists an input $u_{[0, t_1]}$ such that

$$-\mathbf{x}^0 = \int_0^{t_1} e^{-\mathbf{A}\tau}\,\mathbf{b}u(\tau)\,d\tau \tag{12.84}$$

From this equation, we observe that complete controllability of a system depends on **A** and **b**, and is independent of output matrix **c**. The controllability of the system (12.83) is frequently referred to as the controllability of the pair {**A**, **b**}.

It may be noted that according to the definition of controllability, there is no constraint imposed on the input or on the trajectory that the state should follow. Further, the system is said to be uncontrollable although it may be 'controllable in part'.

From the definition of controllability, we observe that by complete controllability of a plant, we mean that we can make the plant do whatever we please. Perhaps this definition is too restrictive in the sense that we are asking too much of the plant. But if we are able to show that system equations satisfy this definition, certainly there can be no intrinsic limitation on the design of the control system for the plant. However, if the system turns out to be uncontrollable, it does not necessarily mean that the plant can never be operated in a satisfactory manner. Provided that a control system will maintain the important variables in an acceptable region, the fact that the plant is not completely controllable is immaterial.

Another important point which the reader must bear in mind is that almost all physical systems are nonlinear in nature to a certain extent and a linear model is obtained after making certain approximations. Small perturbations of the elements of **A** and **b** may cause an uncontrollable system to become controllable.

A common source of uncontrollable state variable models arises when redundant state variables are defined. No one would intentionally use more state variables than the minimum number needed to characterize the behaviour of the dynamic system. In a complex system with unfamiliar physics, one may be tempted to write down differential equations for everything in sight and in doing so, may write down more equations than are necessary. This will invariably result in an uncontrollable model for the system.

Observability For the linear system given by Eqns (12.83), if the knowledge of the output y and the input u over a finite interval of time $[0, t_1]$ suffices to determine the state $\mathbf{x}(0) \triangleq \mathbf{x}^0$, the state $\mathbf{x}^0$ is said to be observable. If all initial states are observable, the system is said to be *completely observable*, or simply *observable*. Otherwise, the system is said to be *unobservable*.

The output of the system (12.83) is given by

$$y(t) = \mathbf{c}\,e^{\mathbf{A}t}\mathbf{x}^0 + \mathbf{c}\int_0^t e^{\mathbf{A}(t-\tau)}\mathbf{b}u(\tau)d\tau + du(t)$$

The output and the input can be measured and used, so that the following signal $\eta(t)$ can be obtained from u and y.

$$\eta(t) \triangleq y(t) - \mathbf{c}\int_0^t e^{\mathbf{A}(t-\tau)}\mathbf{b}\,u(\tau)d\tau - d\,u(t) = \mathbf{c}\,e^{\mathbf{A}t}\mathbf{x}^0 \tag{12.85}$$

Premultiplying by $e^{\mathbf{A}^T t}\,\mathbf{c}^T$ and integrating from 0 to t_1, gives

$$\left\{\int_0^{t_1} e^{\mathbf{A}^T t}\mathbf{c}^T\mathbf{c}\,e^{\mathbf{A}t}\,dt\right\}\mathbf{x}^0 = \int_0^{t_1} e^{\mathbf{A}^T t}\mathbf{c}^T\eta(t)dt \tag{12.86}$$

When the signal $\eta(t)$ is available over a time interval $[0, t_1]$, and the system (12.83) is observable, then the initial state $\mathbf{x}^0$ can be uniquely determined from Eqn. (12.86).

From Eqn. (12.86) we see that complete observability of a system depends on **A** and **c**, and is independent of **b**. The observability of the system (12.83) is frequently referred to as the observability of the pair {**A**, **c**}.

Note that the system is said to be unobservable, although it may be 'observable in part'. For plants that are not completely observable, one may examine feedback control schemes which do not require complete state feedback.

12.7.2 Controllability Test

It is difficult to guess whether a system is controllable or not from the defining Eqn. (12.84). Some simple mathematical tests which answer the question of controllability have been developed. The following theorem gives a simple controllability test[4].

***Theorem* 12.1** The necessary and sufficient condition for the system (12.83) to be completely controllable is that the $n \times n$ *controllability matrix*

$$\mathbf{U} \triangleq [\mathbf{b} \quad \mathbf{Ab} \quad \mathbf{A}^2\mathbf{b} \cdots \mathbf{A}^{n-1}\mathbf{b}] \tag{12.87}$$

has rank equal to n, i.e., $\rho(\mathbf{U}) = n$.

Example 12.10 Recall the inverted pendulum of Example 12.9, shown in Fig. 12.13, in which the object is to apply a force $u(t)$ so that the pendulum remains balanced in the vertical position. We found the linearized equations governing the system to be:

$$\dot{\mathbf{x}} = \mathbf{Ax} + \mathbf{b}u$$

where

$$\mathbf{x} = [\theta \ \dot{\theta} \ z \ \dot{z}]^T$$

$$\mathbf{A} = \begin{bmatrix} 0 & 1 & 0 & 0 \\ 16.3106 & 0 & 0 & 0 \\ 0 & 0 & 0 & 1 \\ -1.0637 & 0 & 0 & 0 \end{bmatrix}; \ \mathbf{b} = \begin{bmatrix} 0 \\ -1.4458 \\ 0 \\ 0.9639 \end{bmatrix}$$

$z(t) =$ horizontal displacement of the pivot on the cart

$\theta(t) =$ rotational angle of the pendulum.

To check the controllability of this system, we compute the controllability matrix **U**:

$$\mathbf{U} = [\mathbf{b} \ \ \mathbf{Ab} \ \ \mathbf{A}^2\mathbf{b} \ \ \mathbf{A}^3\mathbf{b}] = \begin{bmatrix} 0 & -1.4458 & 0 & -23.5816 \\ -1.4458 & 0 & -23.5816 & 0 \\ 0 & 0.9639 & 0 & 1.5379 \\ 0.9639 & 0 & 1.5379 & 0 \end{bmatrix}$$

Since $|\mathbf{U}| = 420.4851$, **U** has full rank, and by Theorem 12.1, the system is completely controllable. Thus if the angle θ departs from equilibrium by a small amount, a control always exists which will drive it back to zero.[5] Moreover, a control also exists which will drive both θ and z, as well as their derivatives, to zero.

[4]For proof, refer Chapter 5 of reference [155].

[5]This justifies the assumption that $\theta(t) \cong 0$, provided we choose an appropriate control strategy.

Example 12.11 Consider the electrical network shown in Fig. 12.16. Differential equations governing the dynamics of this network can be obtained by various standard methods. By use of nodal analysis, for example, we get

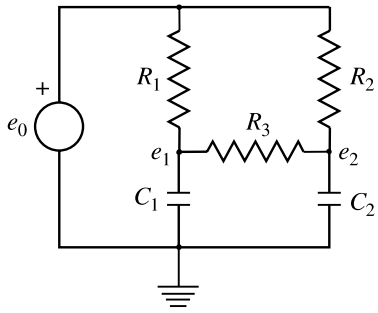

Fig. 12.16

$$C_1\frac{de_1}{dt}+\frac{e_1-e_2}{R_3}+\frac{e_1-e_0}{R_1}=0$$

$$C_2\frac{de_2}{dt}+\frac{e_2-e_1}{R_3}+\frac{e_2-e_0}{R_2}=0$$

The appropriate state variables for the network are the capacitor voltages e_1 and e_2. Thus, the state equations of the network are

$$\dot{\mathbf{x}} = \mathbf{A}\mathbf{x} + \mathbf{b}e_0$$

where $\mathbf{x} = [e_1\ e_2]^T$

$$\mathbf{A}=\begin{bmatrix} -\left(\frac{1}{R_1}+\frac{1}{R_3}\right)\frac{1}{C_1} & \frac{1}{R_3C_1} \\ \frac{1}{R_3C_2} & -\left(\frac{1}{R_2}+\frac{1}{R_3}\right)\frac{1}{C_2}\end{bmatrix};\ \mathbf{b}=\begin{bmatrix}\frac{1}{R_1C_1}\\ \frac{1}{R_2C_2}\end{bmatrix}$$

The controllability matrix of the system is

$$\mathbf{U}=[\mathbf{b}\quad \mathbf{A}\mathbf{b}]=\begin{bmatrix}\frac{1}{R_1C_1} & -\frac{1}{(R_1C_1)^2}+\frac{1}{R_3C_1}\left(\frac{1}{R_2C_2}-\frac{1}{R_1C_1}\right)\\ \frac{1}{R_2C_2} & -\frac{1}{(R_2C_2)^2}+\frac{1}{R_3C_2}\left(\frac{1}{R_1C_1}-\frac{1}{R_2C_2}\right)\end{bmatrix}$$

We see that under the condition

$$R_1C_1 = R_2C_2,$$

$\rho(\mathbf{U}) = 1$ and the system becomes 'uncontrollable'. This condition is the one required to balance the bridge, and in this case, the voltage across the terminals of R_3 cannot be influenced by the input e_0.

12.7.3 Observability Test

The following theorem gives a simple observability test[6].

***Theorem* 12.2** The necessary and sufficient condition for the system (12.83) to be completely observable is that the $n \times n$ *observability matrix*

$$\mathbf{V} \triangleq \begin{bmatrix}\mathbf{c}\\ \mathbf{c}\mathbf{A}\\ \vdots\\ \mathbf{c}\mathbf{A}^{n-1}\end{bmatrix} \tag{12.88}$$

has rank equal to n, i.e., $\rho(\mathbf{V}) = n$.

[6]For proof, refer Chapter 5 of reference [155].

Example 12.12 We now return to the inverted pendulum of Example 12.10. Assuming that the only output variable for measurement is $\theta(t)$, the position of the pendulum, then the linearized equations governing the system are

$$\dot{\mathbf{x}} = \mathbf{A}\mathbf{x} + \mathbf{b}u$$
$$y = \mathbf{c}\mathbf{x}$$

where
$$\mathbf{A} = \begin{bmatrix} 0 & 1 & 0 & 0 \\ 16.3106 & 0 & 0 & 0 \\ 0 & 0 & 0 & 1 \\ -1.0637 & 0 & 0 & 0 \end{bmatrix}; \mathbf{b} = \begin{bmatrix} 0 \\ -1.4458 \\ 0 \\ 0.9639 \end{bmatrix}$$
$$\mathbf{c} = [\,1\ 0\ 0\ 0\,]$$

The observability matrix

$$\mathbf{V} = \begin{bmatrix} \mathbf{c} \\ \mathbf{cA} \\ \mathbf{cA}^2 \\ \mathbf{cA}^3 \end{bmatrix} = \begin{bmatrix} 1 & 0 & 0 & 0 \\ 0 & 1 & 0 & 0 \\ 16.3106 & 0 & 0 & 0 \\ 0 & 16.3106 & 0 & 0 \end{bmatrix}$$

$|\mathbf{V}| = 0$, and therefore by Theorem 12.2, the system is not completely observable.

Consider now the displacement $z(t)$ of the cart as the output variable. Then

$$\mathbf{c} = [0\ 0\ 1\ 0]$$

and the observability matrix

$$\mathbf{V} = \begin{bmatrix} 0 & 0 & 1 & 0 \\ 0 & 0 & 0 & 1 \\ -1.0637 & 0 & 0 & 0 \\ 0 & -1.0637 & 0 & 0 \end{bmatrix}$$

$|\mathbf{V}| = 1.1315 \neq 0$; the system is therefore completely observable. The values of $\dot{z}(t)$, $\theta(t)$ and $\dot{\theta}(t)$ can all be determined by observing $z(t)$ over an arbitrary time interval.

12.7.4 Invariance Property

It is recalled that the state variable model for a system is not unique, but depends on the choice of a set of state variables. A transformation

$$\mathbf{x}(t) = \mathbf{P}\,\overline{\mathbf{x}}\,(t);\ \mathbf{P} \text{ is a nonsingular constant matrix,}$$

results in the following alternative state variable model (refer Eqns (12.17)) for the system (12.83):

$$\dot{\overline{\mathbf{x}}}\,(t) = \overline{\mathbf{A}}\,\overline{\mathbf{x}}\,(t) + \overline{\mathbf{b}}\,u(t);\ \overline{\mathbf{x}}\,(t_0) = \mathbf{P}^{-1}\mathbf{x}(t_0)$$
$$y(t) = \overline{\mathbf{c}}\,\overline{\mathbf{x}}\,(t) + du(t)$$

where

$$\overline{\mathbf{A}} = \mathbf{P}^{-1}\mathbf{A}\mathbf{P},\ \overline{\mathbf{b}} = \mathbf{P}^{-1}\mathbf{b},\ \overline{\mathbf{c}} = \mathbf{c}\mathbf{P}$$

The definition of a new set of internal state variables should evidently not affect the controllability and observability properties. This may be verified by evaluating the controllability and observability matrices of the transformed system.

I.
$$\bar{\mathbf{U}} = [\bar{\mathbf{b}} \quad \bar{\mathbf{A}}\bar{\mathbf{b}} \quad \cdots \quad (\bar{\mathbf{A}})^{n-1}\bar{\mathbf{b}}]$$
$$\bar{\mathbf{b}} = \mathbf{P}^{-1}\mathbf{b}$$
$$\bar{\mathbf{A}}\bar{\mathbf{b}} = \mathbf{P}^{-1}\mathbf{A}\mathbf{P}\mathbf{P}^{-1}\mathbf{b} = \mathbf{P}^{-1}\mathbf{A}\mathbf{b}$$
$$(\bar{\mathbf{A}})^2\bar{\mathbf{b}} = (\bar{\mathbf{A}})\left(\bar{\mathbf{A}}\bar{\mathbf{b}}\right) = \mathbf{P}^{-1}\mathbf{A}\mathbf{P}\mathbf{P}^{-1}\mathbf{A}\mathbf{b} = \mathbf{P}^{-1}\mathbf{A}^2\mathbf{b}$$
$$\vdots$$
$$(\bar{\mathbf{A}})^{n-1}\bar{\mathbf{b}} = \mathbf{P}^{-1}\mathbf{A}^{n-1}\mathbf{b}$$

Therefore,
$$\bar{\mathbf{U}} = [\mathbf{P}^{-1}\mathbf{b} \quad \mathbf{P}^{-1}\mathbf{A}\mathbf{b} \cdots \mathbf{P}^{-1}\mathbf{A}^{n-1}\mathbf{b}] = \mathbf{P}^{-1}\mathbf{U}$$
where
$$\mathbf{U} = [\mathbf{b} \quad \mathbf{A}\mathbf{b} \cdots \mathbf{A}^{n-1}\mathbf{b}]$$
Since $\mathbf{P}^{-1}$ is nonsingular,
$$\rho(\bar{\mathbf{U}}) = \rho(\mathbf{U})$$

II. A similar relationship can be shown for the observability matrices.

12.8 EQUIVALENCE BETWEEN TRANSFER FUNCTION AND STATE VARIABLE REPRESENTATIONS

In frequency-domain analysis, it is tacitly assumed that the dynamic properties of a system are completely determined by the transfer function of the system. That this is not always the case is illustrated by the following examples.

Example 12.13 Consider the system

$$\dot{\mathbf{x}} = \mathbf{A}\mathbf{x} + \mathbf{b}u$$
$$y = \mathbf{c}\mathbf{x} \tag{12.89}$$

with
$$\mathbf{A} = \begin{bmatrix} -2 & 1 \\ 1 & -2 \end{bmatrix}; \quad \mathbf{b} = \begin{bmatrix} 1 \\ 1 \end{bmatrix}; \quad \mathbf{c} = [0 \quad 1]$$

The controllability matrix
$$\mathbf{U} = [\mathbf{b} \quad \mathbf{A}\mathbf{b}] = \begin{bmatrix} 1 & -1 \\ 1 & -1 \end{bmatrix}$$

Since $\rho(\mathbf{U}) = 1$, the second-order system (12.89) is not completely controllable.
The eigenvalues of matrix $\mathbf{A}$ are the roots of the characteristic equation
$$|s\mathbf{I} - \mathbf{A}| = \begin{vmatrix} s+2 & -1 \\ -1 & s+2 \end{vmatrix} = 0$$

The eigenvalues are obtained as $-1, -3$. The *modes* of the transient response are therefore e^{-t} and e^{-3t}.

The transfer function of the system (12.89) is calculated as

$$G(s) = \mathbf{c}(s\mathbf{I} - \mathbf{A})^{-1}\mathbf{b} = [0 \quad 1]\begin{bmatrix} s+2 & -1 \\ -1 & s+2 \end{bmatrix}^{-1}\begin{bmatrix} 1 \\ 1 \end{bmatrix}$$

$$= [0 \quad 1]\begin{bmatrix} \dfrac{s+2}{(s+1)(s+3)} & \dfrac{1}{(s+1)(s+3)} \\ \dfrac{1}{(s+1)(s+3)} & \dfrac{s+2}{(s+1)(s+3)} \end{bmatrix}\begin{bmatrix} 1 \\ 1 \end{bmatrix} = \frac{1}{s+1}$$

We find that because of pole-zero cancellation, both the eigenvalues of matrix **A** do not appear as poles in $G(s)$. The dynamic mode e^{-3t} of the system (12.89) does not show up in input-output characterization given by the transfer function $G(s)$. Note that the system under consideration is not a completely controllable system.

Example 12.14 Consider the system

$$\begin{aligned} \dot{\mathbf{x}} &= \mathbf{A}\mathbf{x} + \mathbf{b}u \\ y &= \mathbf{c}\mathbf{x} \end{aligned} \tag{12.90}$$

with

$$\mathbf{A} = \begin{bmatrix} -2 & 1 \\ 1 & -2 \end{bmatrix}; \ \mathbf{b} = \begin{bmatrix} 1 \\ 0 \end{bmatrix}; \ \mathbf{c} = [1 \quad -1]$$

The observability matrix

$$\mathbf{V} = \begin{bmatrix} \mathbf{c} \\ \mathbf{cA} \end{bmatrix} = \begin{bmatrix} 1 & -1 \\ -3 & 3 \end{bmatrix}$$

Since $\rho(\mathbf{V}) = 1$, the second-order system (12.90) is not completely observable.

The eigenvalues of matrix **A** are $-1, -3$. The transfer function of the system (12.90) is calculated as

$$G(s) = \mathbf{c}(s\mathbf{I} - \mathbf{A})^{-1}\mathbf{b}$$

$$= [1 \quad -1]\begin{bmatrix} \dfrac{s+2}{(s+1)(s+3)} & \dfrac{1}{(s+1)(s+3)} \\ \dfrac{1}{(s+1)(s+3)} & \dfrac{s+2}{(s+1)(s+3)} \end{bmatrix}\begin{bmatrix} 1 \\ 0 \end{bmatrix} = \frac{1}{s+3}$$

The dynamic mode e^{-t} of the system (12.90) does not show up in the input-output characterization given by the transfer function $G(s)$. Note that the system under consideration is not a completely observable system.

In the following, we give two specific state transformations to reveal the underlying structure imposed upon a system by its controllability and observability properties (for proof, refer [105]). These results are then used to establish equivalence between transfer function and state variable representations.

***Theorem* 12.3** Consider an nth-order system

$$\begin{aligned} \dot{\mathbf{x}} &= \mathbf{A}\mathbf{x} + \mathbf{b}u \\ y &= \mathbf{c}\mathbf{x} \end{aligned} \tag{12.91a}$$

Assume that

$$\rho(\mathbf{U}) = \rho[\mathbf{b} \quad \mathbf{A}\mathbf{b} \cdots \mathbf{A}^{n-1}\mathbf{b}] = m < n$$

There exists an equivalence transformation

$$\mathbf{x} = \mathbf{P}\,\bar{\mathbf{x}} \tag{12.91b}$$

that transforms the system (12.91a) to the following form:

$$\begin{aligned} \begin{bmatrix} \dot{\bar{\mathbf{x}}}_1 \\ \dot{\bar{\mathbf{x}}}_2 \end{bmatrix} &= \begin{bmatrix} \bar{\mathbf{A}}_c & \bar{\mathbf{A}}_{12} \\ \mathbf{0} & \bar{\mathbf{A}}_{22} \end{bmatrix} \begin{bmatrix} \bar{\mathbf{x}}_1 \\ \bar{\mathbf{x}}_2 \end{bmatrix} + \begin{bmatrix} \bar{\mathbf{b}}_c \\ \mathbf{0} \end{bmatrix} u \\ &= \bar{\mathbf{A}}\,\bar{\mathbf{x}} + \bar{\mathbf{b}}\,u \end{aligned} \tag{12.91c}$$

$$y = [\bar{\mathbf{c}}_1 \quad \bar{\mathbf{c}}_2] \begin{bmatrix} \bar{\mathbf{x}}_1 \\ \bar{\mathbf{x}}_2 \end{bmatrix} = \bar{\mathbf{c}}\,\bar{\mathbf{x}}$$

where the m-dimensional subsystem

$$\dot{\bar{\mathbf{x}}}_1 = \bar{\mathbf{A}}_c\,\bar{\mathbf{x}}_1 + \bar{\mathbf{b}}_c\,u + \bar{\mathbf{A}}_{12}\,\bar{\mathbf{x}}_2$$

is controllable from u (the additional driving term $\bar{\mathbf{A}}_{12}\bar{\mathbf{x}}_2$ has no effect on controllability), and the $(n - m)$ dimensional subsystem

$$\dot{\bar{\mathbf{x}}}_2 = \bar{\mathbf{A}}_{22}\,\bar{\mathbf{x}}_2$$

is not affected by the input, and is therefore entirely uncontrollable.

This theorem shows that any system which is not completely controllable can be decomposed into controllable and uncontrollable subsystems shown in Fig. 12.17. The state model (12.91c) is said to be in *controllability canonical form*.

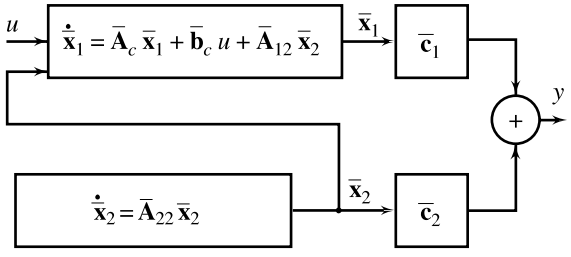

Fig. 12.17 The controllability canonical form of a state variable model

In Section 12.4, it was shown that the characteristic equations and transfer functions of equivalent systems are identical. Thus, the set of eigenvalues of matrix **A** of system (12.91a) is same as the set of eigenvalues of matrix **A** of system (12.91c), which is a union of the subsets of eigenvalues of matrices $\bar{\mathbf{A}}_c$ and $\bar{\mathbf{A}}_{22}$. Also

the transfer function of system (12.91a) must be the same as that of (12.91c). The transfer function of (12.91a) is calculated from Eqn. (12.91c) as[7]

$$G(s) = \begin{bmatrix} \bar{\mathbf{c}}_1 & \bar{\mathbf{c}}_2 \end{bmatrix} \begin{bmatrix} s\mathbf{I} - \bar{\mathbf{A}}_c & -\bar{\mathbf{A}}_{12} \\ \mathbf{0} & s\mathbf{I} - \bar{\mathbf{A}}_{22} \end{bmatrix}^{-1} \begin{bmatrix} \bar{\mathbf{b}}_c \\ \mathbf{0} \end{bmatrix}$$

$$= \begin{bmatrix} \bar{\mathbf{c}}_1 & \bar{\mathbf{c}}_2 \end{bmatrix} \begin{bmatrix} (s\mathbf{I} - \bar{\mathbf{A}}_c)^{-1} & (s\mathbf{I} - \bar{\mathbf{A}}_c)^{-1} \bar{\mathbf{A}}_{12} (s\mathbf{I} - \bar{\mathbf{A}}_{22})^{-1} \\ \mathbf{0} & (s\mathbf{I} - \bar{\mathbf{A}}_{22})^{-1} \end{bmatrix} \begin{bmatrix} \bar{\mathbf{b}}_c \\ \mathbf{0} \end{bmatrix}$$

$$= \bar{\mathbf{c}}_1 (s\mathbf{I} - \bar{\mathbf{A}}_c)^{-1} \bar{\mathbf{b}}_c$$

Therefore, the input–output relationship for the system is dependent only on the controllable part of the system. We will refer to the eigenvalues of $\bar{\mathbf{A}}_c$ as *controllable poles* and the eigenvalues of $\bar{\mathbf{A}}_{22}$ as *uncontrollable poles*.

Only the controllable poles appear in the transfer function model; the uncontrollable poles are cancelled by the zeros.

***Theorem* 12.4** Consider the *n*th order system

$$\begin{aligned} \dot{\mathbf{x}} &= \mathbf{A}\mathbf{x} + \mathbf{b}u \\ y &= \mathbf{c}\mathbf{x} \end{aligned} \tag{12.92a}$$

Assume that

$$\rho(\mathbf{V}) = \rho \begin{bmatrix} \mathbf{c} \\ \mathbf{cA} \\ \vdots \\ \mathbf{cA}^{n-1} \end{bmatrix} = l < n$$

There exits an equivalence transformation

$$\bar{\mathbf{x}} = \mathbf{Q}\mathbf{x} \tag{12.92b}$$

that transforms the system (12.92a) to the following form:

$$\begin{bmatrix} \dot{\bar{\mathbf{x}}}_1 \\ \dot{\bar{\mathbf{x}}}_2 \end{bmatrix} = \begin{bmatrix} \bar{\mathbf{A}}_0 & \mathbf{0} \\ \bar{\mathbf{A}}_{21} & \bar{\mathbf{A}}_{22} \end{bmatrix} \begin{bmatrix} \bar{\mathbf{x}}_1 \\ \bar{\mathbf{x}}_2 \end{bmatrix} + \begin{bmatrix} \bar{\mathbf{b}}_1 \\ \bar{\mathbf{b}}_2 \end{bmatrix} u = \bar{\mathbf{A}}\bar{\mathbf{x}} + \bar{\mathbf{b}}u \tag{12.92c}$$

$$y = \begin{bmatrix} \bar{\mathbf{c}}_0 & \mathbf{0} \end{bmatrix} \begin{bmatrix} \bar{\mathbf{x}}_1 \\ \bar{\mathbf{x}}_2 \end{bmatrix} = \bar{\mathbf{c}}\bar{\mathbf{x}}$$

---

[7] $\left[\begin{array}{c|c} \mathbf{A}_1 & \mathbf{A}_2 \\ \hline \mathbf{0} & \mathbf{A}_3 \end{array}\right] \left[\begin{array}{c|c} \mathbf{B}_1 & \mathbf{B}_2 \\ \hline \mathbf{B}_3 & \mathbf{B}_4 \end{array}\right] = \left[\begin{array}{c|c} \mathbf{I} & \mathbf{0} \\ \hline \mathbf{0} & \mathbf{I} \end{array}\right]$

gives $\left[\begin{array}{c|c} \mathbf{B}_1 & \mathbf{B}_2 \\ \hline \mathbf{B}_3 & \mathbf{B}_4 \end{array}\right] = \left[\begin{array}{c|c} \mathbf{A}_1^{-1} & -\mathbf{A}_1^{-1}\mathbf{A}_2\mathbf{A}_3^{-1} \\ \hline \mathbf{0} & \mathbf{A}_3^{-1} \end{array}\right]$

where the l-dimensional subsystem

$$\dot{\bar{\mathbf{x}}}_1 = \bar{\mathbf{A}}_0 \bar{\mathbf{x}}_1 + \bar{\mathbf{b}}_1 u$$

$$y = \bar{\mathbf{c}}_0 \bar{\mathbf{x}}_1$$

is observable from y, and the $(n - l)$-dimensional subsystem

$$\dot{\bar{\mathbf{x}}}_2 = \bar{\mathbf{A}}_{22} \bar{\mathbf{x}}_2 + \bar{\mathbf{b}}_2 u + \bar{\mathbf{A}}_{21} \bar{\mathbf{x}}_1$$

has no effect upon the output y, and is therefore entirely unobservable, i.e., nothing about $\bar{\mathbf{x}}_2$ can be inferred from output measurement.

This theorem shows that any system which is not completely observable can be decomposed into the observable and unobservable sub-systems shown in Fig. 12.18. The state model (12.92c) is said to be in *observability canonical form*.

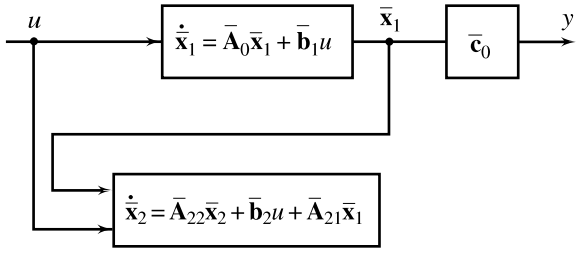

Fig. 12.18 The observability canonical form of a state variable model

Since systems (12.92a) and (12.92c) are equivalent, the set of eigenvalues of matrix $\mathbf{A}$ of system (12.92a) is same as the set of eigenvalues of matrix $\bar{\mathbf{A}}$ of system (12.92c), which is a union of the subsets of eigenvalues of matrices $\bar{\mathbf{A}}_0$ and $\bar{\mathbf{A}}_{22}$. The transfer function of the system (12.92a) may be calculated from (12.92c) as follows:

$$\begin{aligned} G(s) &= \begin{bmatrix} \bar{\mathbf{c}}_0 & \mathbf{0} \end{bmatrix} \begin{bmatrix} s\mathbf{I} - \bar{\mathbf{A}}_0 & \mathbf{0} \\ -\bar{\mathbf{A}}_{21} & s\mathbf{I} - \bar{\mathbf{A}}_{22} \end{bmatrix}^{-1} \begin{bmatrix} \bar{\mathbf{b}}_1 \\ \bar{\mathbf{b}}_2 \end{bmatrix} \\ &= \begin{bmatrix} \bar{\mathbf{c}}_0 & \mathbf{0} \end{bmatrix} \begin{bmatrix} (s\mathbf{I} - \bar{\mathbf{A}}_0)^{-1} & \mathbf{0} \\ (s\mathbf{I} - \bar{\mathbf{A}}_{22})^{-1} \bar{\mathbf{A}}_{21} (s\mathbf{I} - \bar{\mathbf{A}}_0)^{-1} & (s\mathbf{I} - \bar{\mathbf{A}}_{22})^{-1} \end{bmatrix} \begin{bmatrix} \bar{\mathbf{b}}_1 \\ \bar{\mathbf{b}}_2 \end{bmatrix} \\ &= \bar{\mathbf{c}}_0 (s\mathbf{I} - \bar{\mathbf{A}}_0)^{-1} \bar{\mathbf{b}}_1 \end{aligned} \tag{12.93}$$

which shows that the unobservable part of the system does not affect the input–output relationship. We will refer to the eigenvalues of $\bar{\mathbf{A}}$ as *observable poles* and the eigenvalues of $\bar{\mathbf{A}}_{22}$ as unobservable poles.

We now examine the use of state variable and transfer function models of a system to study its dynamic properties.

We know that a system is asymptotically stable if all the eigenvalues of the characteristic matrix $\mathbf{A}$ of its state variable model are in the left-half of complex plane. Also we know that a system is (bounded-input bounded-output) BIBO stable if all the poles of its transfer function model are in the left-half of complex plane. Since, in general, the poles of the transfer function model of a system are a subset of the eigenvalues of the characteristic matrix $\mathbf{A}$ of the system, *asymptotic stability always implies BIBO stability*.

The reverse, however, may not always be true because the eigenvalues of the uncontrollable and/or unobservable part of the system are hidden from the BIBO stability analysis. These may lead to instability of a BIBO stable system. When a state variable model is both controllable and observable, all the eigenvalues of characteristic matrix $\mathbf{A}$ appear as poles in the corresponding transfer function. Therefore *BIBO stability implies asymptotic stability only for completely controllable and completely observable system*.

To conclude, we may say that the transfer function model of a system represents its complete dynamics only if the system is both controllable and observable.

Review Examples

Review Example 12.1 A feedback system has a closed-loop transfer function

$$\frac{Y(s)}{R(s)} = \frac{10(s+4)}{s(s+1)(s+3)}$$

Construct three different state models for this system:
(a) One where the system matrix **A** is a diagonal matrix.
(b) One where **A** is in first companion form.
(c) One where **A** is in second companion form.

Solution

(a) The given transfer function can be expressed as

$$\frac{Y(s)}{R(s)} = \frac{10(s+4)}{s(s+1)(s+3)} = \frac{40/3}{s} + \frac{-15}{s+1} + \frac{5/3}{s+3}$$

Therefore,

$$Y(s) = \frac{40/3}{s} R(s) + \frac{-15}{s+1} R(s) + \frac{5/3}{s+3} R(s)$$

Let $X_1(s) = \frac{40}{3} R(s)$; this gives $\dot{x}_1 = \frac{40}{3} r$

$X_2(s) = \frac{-15}{s+1} R(s)$; this gives $\dot{x}_2 + x_2 = -15\, r$

$X_3(s) = \frac{5/3}{s+3} R(s)$; this gives $\dot{x}_3 + 3x_3 = \frac{5}{3} r$

In terms of x_1, x_2 and x_3, the output $y(t)$ is given by

$$y(t) = x_1(t) + x_2(t) + x_3(t)$$

A state variable formulation for the given transfer function is defined by the following matrices:

$$\mathbf{\Lambda} = \begin{bmatrix} 0 & 0 & 0 \\ 0 & -1 & 0 \\ 0 & 0 & -3 \end{bmatrix}; \mathbf{b} = \begin{bmatrix} 40/3 \\ -15 \\ 5/3 \end{bmatrix}; \mathbf{c} = [\,1 \quad 1 \quad 1\,]; d = 0$$

Note that the coefficient matrix $\mathbf{\Lambda}$ is diagonal, and the state model is in Jordan canonical form.

We now construct two state models for the given transfer function in companion form. To do this, we express the transfer function as

$$\frac{Y(s)}{R(s)} = \frac{10(s+4)}{s(s+1)(s+3)} = \frac{10s+40}{s^3+4s^2+3s} = \frac{\beta_0 s^3 + \beta_1 s^2 + \beta_2 s + \beta_3}{s^3 + \alpha_1 s^2 + \alpha_2 s + \alpha_3};$$

$$\beta_0 = \beta_1 = 0,\ \beta_2 = 10,\ \beta_3 = 40,\ \alpha_1 = 4,\ \alpha_2 = 3,\ \alpha_3 = 0$$

(b) With reference to Eqns (12.44), we obtain the following state model in the first companion form:

$$\mathbf{A} = \begin{bmatrix} 0 & 1 & 0 \\ 0 & 0 & 1 \\ 0 & -3 & -4 \end{bmatrix}; \mathbf{b} = \begin{bmatrix} 0 \\ 0 \\ 1 \end{bmatrix}; \mathbf{c} = [40\ 10\ 0]; d = 0$$

(c) With reference to Eqns (12.46), the state model in second companion form becomes

$$\mathbf{A} = \begin{bmatrix} 0 & 0 & 0 \\ 1 & 0 & -3 \\ 0 & 1 & -4 \end{bmatrix}; \mathbf{b} = \begin{bmatrix} 40 \\ 10 \\ 0 \end{bmatrix}, \mathbf{c} = [0\ 0\ 1]; d = 0$$

Review Example 12.2 A linear time-invariant system is characterized by the homogeneous state equation

$$\begin{bmatrix} \dot{x}_1 \\ \dot{x}_2 \end{bmatrix} = \begin{bmatrix} 0 & 1 \\ 0 & -2 \end{bmatrix} \begin{bmatrix} x_1 \\ x_2 \end{bmatrix}$$

(a) Compute the solution of the homogeneous equation assuming the initial state vector

$$\mathbf{x}(0) = \begin{bmatrix} 1 \\ 0 \end{bmatrix}$$

(b) Consider now that the system has a forcing function and is represented by the following nonhomogeneous state equation:

$$\begin{bmatrix} \dot{x}_1 \\ \dot{x}_2 \end{bmatrix} = \begin{bmatrix} 0 & 1 \\ 0 & -2 \end{bmatrix} \begin{bmatrix} x_1 \\ x_2 \end{bmatrix} + \begin{bmatrix} 0 \\ 1 \end{bmatrix} u$$

where u is a unit step input.

Compute the solution of this equation assuming initial conditions of part (a).

Solution

(a) Since

$$(s\mathbf{I} - \mathbf{A}) = \begin{bmatrix} s & -1 \\ 0 & s+2 \end{bmatrix}$$

we obtain

$$(s\mathbf{I} - \mathbf{A})^{-1} = \begin{bmatrix} \dfrac{1}{s} & \dfrac{1}{s(s+2)} \\ 0 & \dfrac{1}{s+2} \end{bmatrix}$$

Hence

$$e^{\mathbf{A}t} = \mathscr{L}^{-1}[(s\mathbf{I} - \mathbf{A})^{-1}] = \begin{bmatrix} 1 & \frac{1}{2}(1 - e^{-2t}) \\ 0 & e^{-2t} \end{bmatrix}$$

$$\mathbf{x}(t) = e^{\mathbf{A}t}\mathbf{x}(0) = \begin{bmatrix} 1 \\ 0 \end{bmatrix}$$

(b) $$\mathbf{x}(t) = e^{\mathbf{A}t}\mathbf{x}(0) + \int_0^t e^{\mathbf{A}(t-\tau)}\,\mathbf{b}u(\tau)d\tau$$

Now

$$\int_0^t e^{\mathbf{A}(t-\tau)}\,\mathbf{b}u(\tau)d\tau = \begin{bmatrix} \frac{1}{2}\int_0^t [1 - e^{-2(t-\tau)}]d\tau \\ \int_0^t e^{-2(t-\tau)}d\tau \end{bmatrix} = \begin{bmatrix} -\frac{1}{4} + \frac{1}{2}t + \frac{1}{4}e^{-2t} \\ \frac{1}{2}\left(1 - e^{-2t}\right) \end{bmatrix}$$

Therefore,

$$x_1(t) = \tfrac{3}{4} + \tfrac{1}{2}t + \tfrac{1}{4}e^{-2t}$$

$$x_2(t) = \tfrac{1}{2}(1 - e^{-2t})$$

Review Example 12.3 The motion of a satellite in the equatorial (r, θ) plane is given by the state equation [122]

$$\begin{bmatrix} \dot{x}_1 \\ \dot{x}_2 \\ \dot{x}_3 \\ \dot{x}_4 \end{bmatrix} = \begin{bmatrix} 0 & 1 & 0 & 0 \\ 3\omega^2 & 0 & 0 & 2\omega \\ 0 & 0 & 0 & 1 \\ 0 & -2\omega & 0 & 0 \end{bmatrix} \begin{bmatrix} x_1 \\ x_2 \\ x_3 \\ x_4 \end{bmatrix} + \begin{bmatrix} 0 \\ 1 \\ 0 \\ 0 \end{bmatrix} u_1 + \begin{bmatrix} 0 \\ 0 \\ 0 \\ 1 \end{bmatrix} u_2$$

where ω is the angular frequency of the satellite in circular, equatorial orbit, $x_1(t)$ and $x_3(t)$ are, respectively, the deviations in position variables $r(t)$ and $\theta(t)$ of the satellite, and $x_2(t)$ and $x_4(t)$ are, respectively, the deviations in velocity variables $\dot{r}(t)$ and $\dot{\theta}(t)$. The inputs $u_1(t)$ and $u_2(t)$ are the thrusts u_r and u_θ in the radial and tangential directions respectively, applied by small rocket engines or gas jets ($\mathbf{u} = \mathbf{0}$ when $\mathbf{x} = \mathbf{0}$). Sensors have been installed for measuring $r(t)$ and $\theta(t)$.

(a) Suppose that the tangential thruster becomes inoperable. Determine the controllability of the system with the radial thruster alone.

(b) Suppose that the radial thruster becomes inoperable. Determine the controllability of the system with the tangential thruster alone.

(c) Suppose that the tangential measuring device becomes inoperable. Determine the observability of the system from radial position measurement ($x_1 = r$) alone.

(d) Suppose that the radial measurements are lost. Determine the observability of the system from tangential position measurement ($x_3 = \theta$) alone.

Solution

(a) With $u_2 = 0$,

$$\mathbf{b} = \begin{bmatrix} 0 \\ 1 \\ 0 \\ 0 \end{bmatrix}$$

The controllability matrix

$$\mathbf{U} = [\mathbf{b} \quad \mathbf{Ab} \quad \mathbf{A}^2\mathbf{b} \quad \mathbf{A}^3\mathbf{b}] = \begin{bmatrix} 0 & 1 & 0 & -\omega^2 \\ 1 & 0 & -\omega^2 & 0 \\ 0 & 0 & -2\omega & 0 \\ 0 & -2\omega & 0 & 2\omega^3 \end{bmatrix}$$

$$|\mathbf{U}| = - \begin{vmatrix} 1 & 0 & -\omega^2 \\ 0 & -2\omega & 0 \\ -2\omega & 0 & 2\omega^2 \end{vmatrix} = -[-2\omega(2\omega^3 - 2\omega^3)] = 0$$

Therefore, $\rho(\mathbf{U}) < 4$, and the system is not completely controllable with u_1 alone.

(b) With $u_1 = 0$,

$$\mathbf{b} = \begin{bmatrix} 0 \\ 0 \\ 0 \\ 1 \end{bmatrix}$$

The controllability matrix

$$\mathbf{U} = \begin{bmatrix} 0 & 0 & 2\omega & 0 \\ 0 & 2\omega & 0 & -2\omega^3 \\ 0 & 1 & 0 & -4\omega^2 \\ 1 & 0 & -4\omega^2 & 0 \end{bmatrix}$$

$$|\mathbf{U}| = 2\omega \begin{vmatrix} 0 & 2\omega & -2\omega^3 \\ 0 & 1 & -4\omega^2 \\ 1 & 0 & 0 \end{vmatrix} = -12\omega^4 \neq 0$$

Therefore, $\rho(\mathbf{U}) = 4$, and the system is completely controllable with u_2 alone.

(c) With $y = x_1$,

$$\mathbf{c} = [1 \quad 0 \quad 0 \quad 0]$$

The observability matrix

$$\mathbf{V} = \begin{bmatrix} \mathbf{c} \\ \mathbf{cA} \\ \mathbf{cA}^2 \\ \mathbf{cA}^3 \end{bmatrix} = \begin{bmatrix} 1 & 0 & 0 & 0 \\ 0 & 1 & 0 & 0 \\ 3\omega^2 & 0 & 0 & 2\omega \\ 0 & -\omega^2 & 0 & 0 \end{bmatrix}$$

$$|\mathbf{V}| = 0$$

Therefore, $\rho(\mathbf{V}) < 4$, and the system is not completely observable from $y = x_1$ alone.

(d) With $y = x_3$,

$$\mathbf{c} = [0 \quad 0 \quad 1 \quad 0]$$

The observability matrix

$$\mathbf{V} = \begin{bmatrix} 0 & 0 & 1 & 0 \\ 0 & 0 & 0 & 1 \\ 0 & -2\omega & 0 & 0 \\ -6\omega^3 & 0 & 0 & -4\omega^2 \end{bmatrix}$$

$$|\mathbf{V}| = -12\omega^4 \neq 0$$

Therefore, $\rho(\mathbf{V}) = 4$, and the system is completely observable from $y = x_3$ alone.

Review Example 12.4 Consider state equation of a single-input system which includes delay in control action:

$$\dot{\mathbf{x}}(t) = \mathbf{A}\mathbf{x}(t) + \mathbf{b}u(t - \tau_D) \tag{12.94a}$$

where $\mathbf{x}$ is $n \times 1$ state vector, u is scalar input, τ_D is the dead-time, and $\mathbf{A}$ and $\mathbf{b}$ are, respectively, $n \times n$ and $n \times 1$ real constant matrices.

For discrete-time solution, the time axis is discretized (sampled) into intervals of width T; $t = kT$, $k = 0, 1, 2, ...$; and $u(t)$ is approximated by a staircase function, constant over the intervals. Given the capabilities of the modern microprocessor, we can always adjust the sampling frequency slightly so that

$$\tau_D = NT \tag{12.94b}$$

where N is an integer.

For the k^{th} interval, $u(t) = u(kT - NT); kT \le t < (k+1)T;\ k = 0,1,2,....$ Following the steps given in Eqns (12.73)–(12.75), we obtain

$$\mathbf{x}((k+1)T) = \mathbf{F}\mathbf{x}(kT) + \mathbf{g}u(kT - NT) \tag{12.95}$$

where

$$\mathbf{F} = e^{\mathbf{A}T} \text{ and } \mathbf{g} = \int_0^T e^{\mathbf{A}\theta}\mathbf{b}\,d\theta$$

Let us introduce N new state variables defined below.

$$\begin{aligned} x_{n+1}(k) &= u(k-N) \\ x_{n+2}(k) &= u(k-N+1) \\ &\vdots \\ x_{n+N}(k) &= u(k-1) \end{aligned}$$

The augmented state equation becomes

$$\begin{bmatrix} \mathbf{x}(k+1) \\ x_{n+1}(k+1) \\ x_{n+2}(k+1) \\ \vdots \\ x_{n+N-1}(k+1) \\ x_{n+N}(k+1) \end{bmatrix} = \begin{bmatrix} \mathbf{F} & \mathbf{g} & \mathbf{0} & \mathbf{0} & \cdots & \mathbf{0} \\ \mathbf{0} & 0 & 1 & 0 & \cdots & 0 \\ \mathbf{0} & 0 & 0 & 1 & \cdots & 0 \\ \vdots & \vdots & \vdots & \vdots & & \vdots \\ \mathbf{0} & 0 & 0 & 0 & \cdots & 1 \\ \mathbf{0} & 0 & 0 & 0 & \cdots & 0 \end{bmatrix} \begin{bmatrix} \mathbf{x}(k) \\ x_{n+1}(k) \\ x_{n+2}(k) \\ \vdots \\ x_{n+N-1}(k) \\ x_{n+N}(k) \end{bmatrix} + \begin{bmatrix} \mathbf{0} \\ 0 \\ 0 \\ \vdots \\ 0 \\ 1 \end{bmatrix} u(k) \tag{12.96}$$

Review Questions

12.1 Given a single-input single-output state variable model

$$\dot{\mathbf{x}} = \mathbf{A}\mathbf{x} + \mathbf{b}u$$
$$y = \mathbf{c}\mathbf{x}$$

Prove that the eigenvalues of matrix **A** are invariant under state transformation $\mathbf{x} = \mathbf{P}\,\bar{\mathbf{x}}$; **P** is a constant nonsingular matrix.

12.2 Given a single-input single-output state variable model

$$\dot{\mathbf{x}} = \mathbf{A}\mathbf{x} + \mathbf{b}u$$
$$y = \mathbf{c}\mathbf{x}$$

(a) Prove that $\dfrac{Y(s)}{U(s)} = G(s) = \mathbf{c}(s\mathbf{I} - \mathbf{A})^{-1}\mathbf{b}$.

(b) Prove that $G(s)$ is invariant under state transformation $\mathbf{x} = \mathbf{P}\,\bar{\mathbf{x}}$; **P** is a constant nonsingular matrix.

12.3 Is the state variable description for a given transfer function

$$G(s) = \frac{\beta_0 s^n + \beta_1 s^{n-1} + \cdots + \beta_{n-1} s + \beta_n}{s^n + \alpha_1 s^{n-1} + \cdots + \alpha_{n-1} s + \alpha_n}$$

unique? If not, explain how three different state variable descriptions for the given transfer function can be obtained.

12.4 (a) Write two $n \times n$ general matrices, one having companion form and the other having Jordan form structure.

(b) An nth-order state variable model in Jordan canonical form always yields n decoupled first-order differential equations. Is the statement true? Justify your answer.

12.5 Given a single-input state variable equation

$$\dot{\mathbf{x}} = \mathbf{A}\mathbf{x} + \mathbf{b}u$$

Prove that

$$\mathbf{x}(t) = e^{\mathbf{A}t}\,\mathbf{x}(0) + \int_0^t e^{\mathbf{A}(t-\tau)}\mathbf{b}\,u(\tau)\,d\tau$$

12.6 List the properties of the state transition matrix

$$\boldsymbol{\phi}(t) = e^{\mathbf{A}t}$$

of the system

$$\dot{\mathbf{x}} = \mathbf{A}\mathbf{x};\ \mathbf{x}(0) \triangleq \mathbf{x}^0$$

Prove that

$$e^{\mathbf{A}t} = \mathscr{L}^{-1}\left[(s\mathbf{I} - \mathbf{A})^{-1}\right]$$

Why is the matrix exponential $e^{\mathbf{A}t}$ called the state transition matrix?

12.7 Given a single-input state equation

$$\dot{\mathbf{x}} = \mathbf{A}\mathbf{x} + \mathbf{b}u$$

For discrete-time solution, the equation can be discretized to the following form:

$$\mathbf{x}(kT + T) = \mathbf{F}\mathbf{x}(kT) + \mathbf{g}u(kT);\ T = \text{sampling interval}$$

Find the matrices **F** and **g**.

12.8 A system is described by the single-input single-output state variable model

$$\dot{\mathbf{x}} = \mathbf{A}\mathbf{x} + \mathbf{b}u$$
$$y = \mathbf{c}\mathbf{x}$$

What is the motivation behind the concept of controllability of the system? Give a precise definition of controllability and describe a controllability test in terms of matrices **A** and **b**.

Prove that controllability property is invariant under state transformation $\mathbf{x} = \mathbf{P}\,\overline{\mathbf{x}}$; **P** is a constant nonsingular matrix.

12.9 A system is described by the single-input single-output state variable model

$$\dot{\mathbf{x}} = \mathbf{A}\mathbf{x} + \mathbf{b}u$$
$$y = \mathbf{c}\mathbf{x}$$

What is the motivation behind the concept of observability? Give a precise definition of observability and describe an observability test in terms of matrices **A** and **c**.

Prove that observability property is invariant under state transformation $\mathbf{x} = \mathbf{P}\,\overline{\mathbf{x}}$; **P** is a constant nonsingular matrix.

12.10 (a) Show that if a continuous-time linear time-invariant system is asymptotically stable, it is also BIBO stable.

(b) Show that a BIBO stable continuous-time linear time-invariant system is asymptotically stable only if the system is completely controllable and completely observable.

12.11 Prove that the transfer function model of the single-input single-output system

$$\dot{\mathbf{x}} = \mathbf{A}\mathbf{x} + \mathbf{b}u$$
$$y = \mathbf{c}\mathbf{x}$$

is a complete characterization of the system only if the system is both controllable and observable.

Problems

12.1 Figure P12.1 shows a control scheme for controlling the azimuth angle of a rotating antenna. The plant consists of an armature-controlled dc motor with dc generator used as an amplifier. The parameters of the plant are given below:

Motor torque constant, $K_T = 1.2$ N-m/amp

Motor back emf constant, $K_b = 1.2$ V/(rad/sec)

Generator gain constant, $K_g = 100$ V/amp

Motor to load gear ratio, $n = \left(\dot{\theta}_L / \dot{\theta}_M\right) = 1/2$

$R_f = 21\Omega$, $L_f = 5$H, $R_g = 9\Omega$, $L_g = 0.06$ H, $R_a = 10\Omega$, $L_a = 0.04$ H,

$J = 1.6$ N-m/(rad/sec^2), $B = 0.04$ N-m/(rad/sec), motor inertia and friction are negligible.

Taking physically meaningful and measurable variables as state variables, derive a state model for the system.

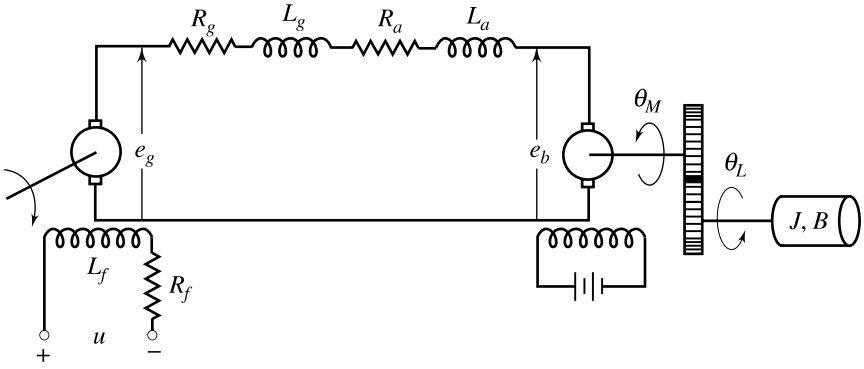

Fig. P12.1

12.2 Figure P12.2 shows a position control system with state variable feedback. The plant consists of a field-controlled dc motor with a dc amplifier. The parameters of the plant are given below:

Amplifier gain, $K_A = 50$ volt/volt
Motor field resistance, $R_f = 99\ \Omega$
Motor field inductance, $L_f = 20$ H
Motor torque constant, $K_T = 10$ N-m/amp
Moment of inertia of load, $J = 0.5$ N-m/(rad/sec^2)
Coefficient of viscous friction of load, $B = 0.5$ N-m/(rad/sec)
Motor inertia and friction are negligible.

Taking $x_1 = \theta$, $x_2 = \dot{\theta}$, and $x_3 = i_f$ as the state variables, $u = e_f$ as the input, and $y = \theta$ as the output, derive a state variable model for the plant.

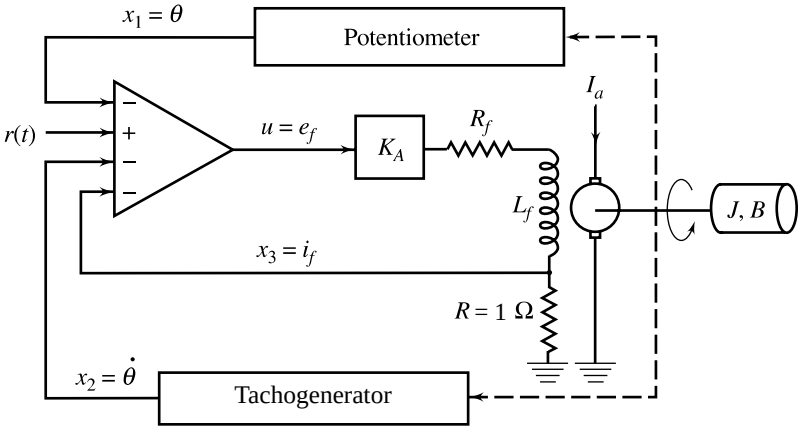

Fig. P12.2

12.3 Figure P12.3 shows the block diagram of a motor-driven single-link robot manipulator with position and velocity feedback. The drive motor is an armature controlled dc motor; e_a is armature voltage, i_a is armature current, θ_M is the motor shaft position and $\dot{\theta}_M$ is motor shaft velocity. θ_L is the position of the robot arm.

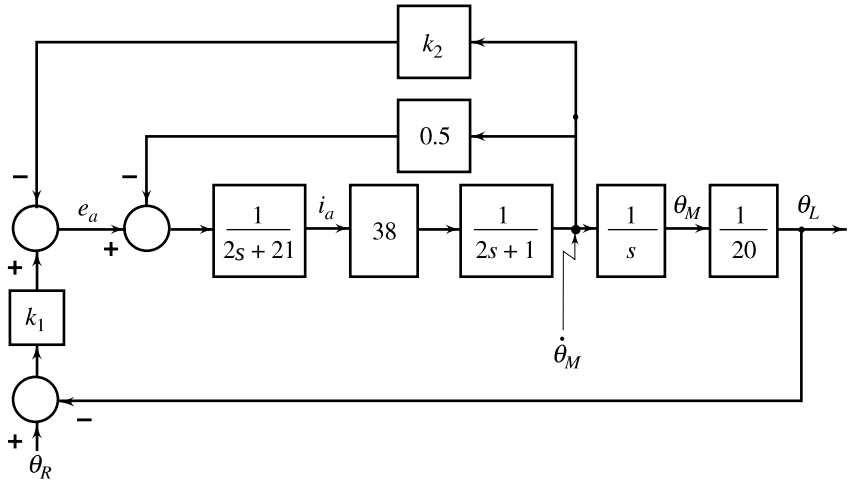

Fig. P12.3

Taking θ_M, $\dot{\theta}_M$ and i_a as state variables, derive a state model for the feedback system.

12.4 Figure P12.4 shows the block diagram of a speed control system with state variable feedback. The drive motor is an armature-controlled dc motor with armature resistance R_a, armature inductance L_a, motor torque constant K_T, inertia referred to motor shaft J, viscous friction coefficient referred to motor shaft B, back emf constant K_b, and tachogenerator constant K_t. The applied armature voltage is controlled by a three-phase full-converter. We have assumed a linear relationship between the control voltage e_c and the armature voltage e_a . e_r is the reference voltage corresponding to the desired speed.

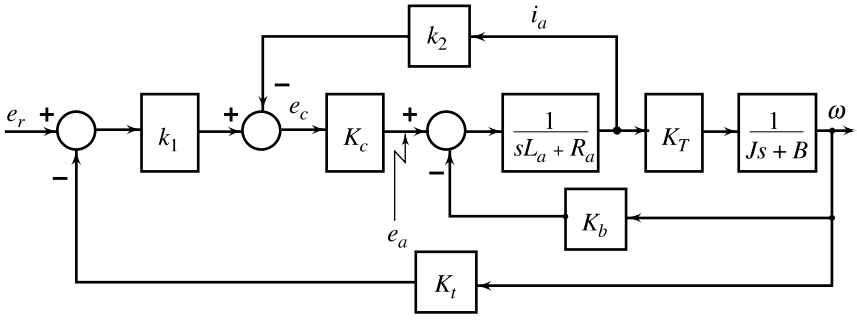

Fig. P12.4

Taking $x_1 = \omega$ (speed) and $x_2 = i_a$ (armature current) as the state variables, $u = e_r$ as the input, and $y = \omega$ as the output, derive a state variable model for the feedback system.

12.5 Consider the system

$$\dot{\mathbf{x}} = \begin{bmatrix} -3 & 1 \\ -2 & 0 \end{bmatrix} \mathbf{x} + \begin{bmatrix} 0 \\ 1 \end{bmatrix} u$$

$$y = [1 \quad 0]\, \mathbf{x}$$

A similarity transformation is defined by

$$\mathbf{x} = \mathbf{P}\,\bar{\mathbf{x}} = \begin{bmatrix} 2 & -1 \\ -1 & 1 \end{bmatrix} \bar{\mathbf{x}}$$

(a) Express the state model in terms of the states $\bar{\mathbf{x}}(t)$.
(b) Draw state diagrams in signal flow graph form for the state models in $\mathbf{x}(t)$ and $\bar{\mathbf{x}}(t)$.
(c) Show by Mason's gain formula that the transfer functions for the two state diagrams in (b) are equal.

12.6 Consider a double-integrator plant described by the differential equation

$$\frac{d^2\theta(t)}{dt^2} = u(t)$$

(a) Develop a state equation for this system with u as the input, and θ and $\dot{\theta}$ as the state variables x_1 and x_2 respectively.
(b) A similarity transformation is defined as

$$\mathbf{x} = \mathbf{P}\,\bar{\mathbf{x}} = \begin{bmatrix} 1 & 0 \\ 1 & 1 \end{bmatrix} \bar{\mathbf{x}}$$

Express the state equation in terms of the states $\bar{\mathbf{x}}(t)$.
(c) Show that the eigenvalues of the system matrices of the two state equations in (a) and (b) are equal.

12.7 A system is described by the state equation

$$\dot{\mathbf{x}} = \begin{bmatrix} 0 & 1 & 0 \\ 0 & 0 & 1 \\ -1 & 0 & -3 \end{bmatrix} \mathbf{x} + \begin{bmatrix} 0 \\ 0 \\ 1 \end{bmatrix} u \; ; \; \mathbf{x}(0) = \mathbf{x}^0$$

Using the Laplace transform technique, transform the state equation into a set of linear algebraic equations in the form

$$\mathbf{X}(s) = \mathbf{G}(s)\mathbf{x}^0 + \mathbf{H}(s)\,U(s)$$

12.8 Give a block diagram for the programming of the system of Problem 12.7 on an analog computer.

12.9 The state diagram of a linear system is shown in Fig. P12.9. Assign the state variables and write the dynamic equations of the system.

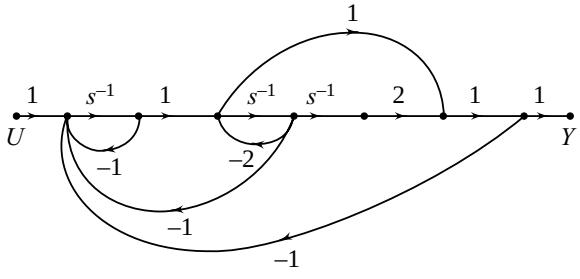

Fig. P 12.9

12.10 Derive transfer functions corresponding to the following state models:

(a) $\dot{\mathbf{x}} = \begin{bmatrix} 0 & 1 \\ -2 & -3 \end{bmatrix} \mathbf{x} + \begin{bmatrix} 1 \\ 0 \end{bmatrix} u;\ y = [1\ \ 0]\,\mathbf{x}$

(b) $\dot{\mathbf{x}} = \begin{bmatrix} -3 & 1 \\ -2 & 0 \end{bmatrix} \mathbf{x} + \begin{bmatrix} 0 \\ 1 \end{bmatrix} u;\ y = [1\ \ 0]\mathbf{x}$

12.11 Figure P12.11 shows the block diagram of a control system with state variable feedback and integral control. The plant model is:

$$\begin{bmatrix} \dot{x}_1 \\ \dot{x}_2 \end{bmatrix} = \begin{bmatrix} -3 & 2 \\ 4 & -5 \end{bmatrix} \begin{bmatrix} x_1 \\ x_2 \end{bmatrix} + \begin{bmatrix} 1 \\ 0 \end{bmatrix} u$$

$$y = [\,0 \quad 1]\mathbf{x}$$

(a) Derive a state model of the feedback system.
(b) Derive the transfer function $Y(s)/R(s)$.

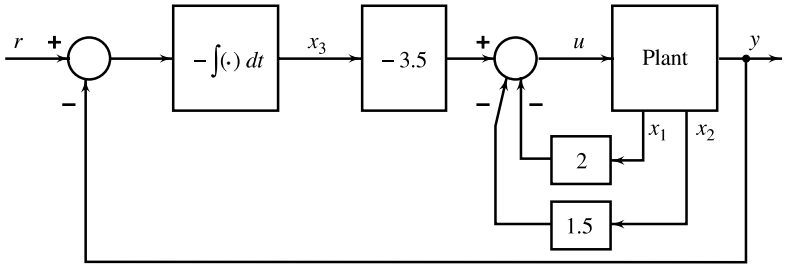

Fig. P12.11

12.12 Construct state models for the systems of Fig. P12.12a and Fig. P12.12b, taking outputs of simple lag blocks as state variables.

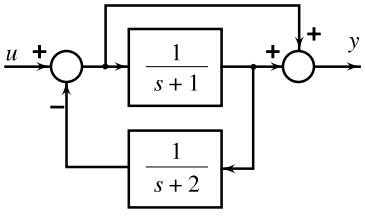

Fig. P12.12a

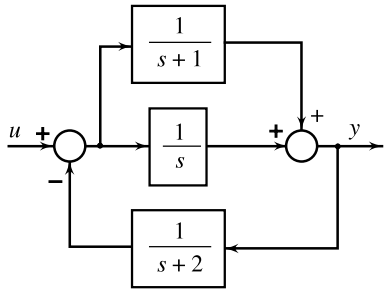

Fig. P12.12b

12.13 Construct state models for the following transfer functions. Obtain different canonical form for each system.

(i) $\dfrac{s+3}{s^2+3s+2}$ (ii) $\dfrac{5}{(s+1)^2(s+2)}$ (iii) $\dfrac{s^3+8s^2+17s+8}{(s+1)(s+2)(s+3)}$

Give block diagrams for the analog computer simulation of these transfer functions.

12.14 Construct state models for the following differential equations. Obtain a different canonical form for each system.

(i) $\dddot{y} + 3\ddot{y} + 2\dot{y} = \dot{u} + u$ (ii) $\dddot{y} + 6\ddot{y} + 11\dot{y} + 6y = u$

(iii) $\dddot{y} + 6\ddot{y} + 11\dot{y} + 6y = \dddot{u} + 8\ddot{u} + 17\dot{u} + 8u$

12.15 Derive two state models for the system with transfer function

$$\frac{Y(s)}{U(s)} = \frac{50(1 + s/5)}{s(1 + s/2)(1 + s/50)}$$

(a) One for which the system matrix is a companion matrix.

(b) One for which the system matrix is diagonal.

12.16 (a) Obtain state variable model in Jordan canonical form for the system with transfer function

$$\frac{Y(s)}{U(s)} = \frac{2s^2 + 6s + 5}{(s+1)^2(s+2)}$$

(b) Find the response $y(t)$ to a unit-step input using the state variable model in (a)

(c) Give a block diagram for analog computer simulation of the transfer function.

12.17 Consider a continuous-time system

$$\dot{\mathbf{x}}(t) = \begin{bmatrix} -2 & 2 \\ 1 & -3 \end{bmatrix} \mathbf{x}(t) + \begin{bmatrix} -1 \\ 5 \end{bmatrix} u(t)$$

$$y(t) = [2 \quad -4]\, \mathbf{x}(t) + 6u(t)$$

Discretizing time axis into intervals of $T = 0.2$ sec, obtain state transition and output equations that yield discrete-time solutions for $\mathbf{x}(t)$ and $y(t)$.

12.18 The mathematical model of the plant of a control system is given below:

$$\frac{Y(s)}{U(s)} = G(s) = \frac{e^{-0.4s}}{s+1}$$

For digital simulation of the plant, obtain a difference equation model with $T = 0.4$ sec as the sampling interval.

12.19 Given the system

$$\dot{\mathbf{x}} = \begin{bmatrix} -2 & 1 \\ 1 & -2 \end{bmatrix} \mathbf{x} + \begin{bmatrix} 1 \\ 1 \end{bmatrix} u$$

(a) Obtain a state diagram in signal flow graph form.

(b) From the signal flow graph, determine the state equation in the form

$$\mathbf{X}(s) = \mathbf{G}(s)\mathbf{x}(0) + \mathbf{H}(s)U(s)$$

(c) Using inverse Laplace transformation, obtain the

(i) zero-input response to initial condition

$$\mathbf{x}(0) = \begin{bmatrix} x_1^0 & x_2^0 \end{bmatrix}^T \text{; and}$$

(ii) zero-state response to unit-step input.

12.20 Consider the system

$$\dot{\mathbf{x}} = \begin{bmatrix} 0 & 1 \\ -2 & -3 \end{bmatrix} \mathbf{x} + \begin{bmatrix} 0 \\ 1 \end{bmatrix} u \text{ ; } \mathbf{x}(0) = \begin{bmatrix} 1 \\ 1 \end{bmatrix}$$

$$y = [1 \quad 0]\mathbf{x}$$

(a) Determine the stability of the system.
(b) Find the output response of the system to unit-step input.

12.21 Figure P12.21 shows the block diagram of a control system with state variable feedback and feedforward control. The plant model is

$$\dot{\mathbf{x}} = \begin{bmatrix} -3 & 2 \\ 4 & -5 \end{bmatrix} \mathbf{x} + \begin{bmatrix} 1 \\ 0 \end{bmatrix} u$$

$$y = [0 \quad 1]\mathbf{x}$$

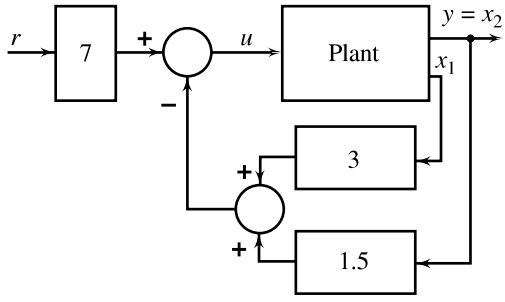

Fig. P12.21

(a) Derive a state model for the feedback system.
(b) Find the output $y(t)$ of the feedback system to a unit-step input $r(t)$; the initial state is assumed to be zero.

12.22 Consider the state equation

$$\dot{\mathbf{x}} = \begin{bmatrix} 0 & 1 \\ -1 & -2 \end{bmatrix} \mathbf{x}$$

Find a set of states $x_1(1)$ and $x_2(1)$ such that $x_1(2) = 2$.

12.23 The following facts are known about the linear system

$$\dot{\mathbf{x}}(t) = \mathbf{A}\mathbf{x}(t)$$

$$\text{If } \mathbf{x}(0) = \begin{bmatrix} 1 \\ -2 \end{bmatrix}, \text{ then } \mathbf{x}(t) = \begin{bmatrix} e^{-2t} \\ -2e^{-2t} \end{bmatrix}$$

$$\text{If } \mathbf{x}(0) = \begin{bmatrix} 1 \\ -1 \end{bmatrix}, \text{ then } \mathbf{x}(t) = \begin{bmatrix} e^{-t} \\ -e^{-t} \end{bmatrix}$$

Find $e^{\mathbf{A}t}$ and hence $\mathbf{A}$.

12.24 Show that the pair $\{\mathbf{A}, \mathbf{c}\}$ is completely observable for all values of α_i's.

$$\mathbf{A} = \begin{bmatrix} 0 & 0 & 0 & \cdots & 0 & -\alpha_n \\ 1 & 0 & 0 & \cdots & 0 & -\alpha_{n-1} \\ 0 & 1 & 0 & \cdots & 0 & -\alpha_{n-2} \\ \vdots & \vdots & \vdots & & \vdots & \vdots \\ 0 & 0 & 0 & \cdots & 0 & -\alpha_2 \\ 0 & 0 & 0 & \cdots & 1 & -\alpha_1 \end{bmatrix}$$

$$\mathbf{c} = [0 \quad 0 \cdots 0 \quad 1]$$

12.25 Show that the pair {**A**, **b**} is completely controllable for all values of α_i's.

$$\mathbf{A} = \begin{bmatrix} 0 & 1 & 0 & \cdots & 0 \\ 0 & 0 & 1 & \cdots & 0 \\ \vdots & \vdots & \vdots & & \vdots \\ 0 & 0 & 0 & \cdots & 1 \\ -\alpha_n & -\alpha_{n-1} & -\alpha_{n-2} & \cdots & -\alpha_1 \end{bmatrix}; \mathbf{b} = \begin{bmatrix} 0 \\ 0 \\ \vdots \\ 0 \\ 1 \end{bmatrix}$$

12.26 Determine the controllability and observability properties of the following systems:

(i) $\mathbf{A} = \begin{bmatrix} -2 & 1 \\ 1 & -2 \end{bmatrix}; \mathbf{b} = \begin{bmatrix} 1 \\ 0 \end{bmatrix}; \mathbf{c} = [1 \quad -1]$

(ii) $\mathbf{A} = \begin{bmatrix} -1 & 0 \\ 0 & -2 \end{bmatrix}; \mathbf{b} = \begin{bmatrix} 2 \\ 5 \end{bmatrix}; \mathbf{c} = [0 \quad 1]$

(iii) $\mathbf{A} = \begin{bmatrix} 0 & 1 & 0 \\ 0 & 0 & 1 \\ 0 & -2 & -3 \end{bmatrix}; \mathbf{b} = \begin{bmatrix} 0 \\ 0 \\ 1 \end{bmatrix}; \mathbf{c} = [10 \quad 0 \quad 0]$

(iv) $\mathbf{A} = \begin{bmatrix} 0 & 0 & 0 \\ 1 & 0 & -3 \\ 0 & 1 & -4 \end{bmatrix}; \mathbf{b} = \begin{bmatrix} 40 \\ 10 \\ 0 \end{bmatrix}; \mathbf{c} = [0 \quad 0 \quad 1]$

12.27 The following models realize the transfer function $G(s) = \dfrac{1}{s+1}$.

(i) $\mathbf{A} = \begin{bmatrix} -2 & 1 \\ 1 & -2 \end{bmatrix}; \mathbf{b} = \begin{bmatrix} 1 \\ 1 \end{bmatrix}; \mathbf{c} = [0 \quad 1]$

(ii) $\mathbf{A} = \begin{bmatrix} -1 & 0 \\ 0 & -3 \end{bmatrix}; \mathbf{b} = \begin{bmatrix} 1 \\ 1 \end{bmatrix}; \mathbf{c} = [1 \quad 0]$

(iii) $\mathbf{A} = \begin{bmatrix} -2 & 0 \\ 0 & -1 \end{bmatrix}; \mathbf{b} = \begin{bmatrix} 0 \\ 1 \end{bmatrix}; \mathbf{c} = [0 \quad 1]$

Investigate the controllability and observability properties of these models. Find a state variable model for the given transfer function which is both controllable and observable.

12.28 Consider the systems

(i) $\mathbf{A} = \begin{bmatrix} 0 & -2 \\ 1 & -3 \end{bmatrix}; \mathbf{b} = \begin{bmatrix} 1 \\ 1 \end{bmatrix}; \mathbf{c} = [0 \quad 1]$

(ii) $\mathbf{A} = \begin{bmatrix} 0 & 1 & 0 \\ 0 & 0 & 1 \\ -6 & -11 & -6 \end{bmatrix}; \mathbf{b} = \begin{bmatrix} 0 \\ 0 \\ 1 \end{bmatrix}; \mathbf{c} = [4 \quad 5 \quad 1]$

Determine the transfer function in each case. What can we say about controllability and observability properties without making any further calculations?

12.29 Consider the system

$$\dot{\mathbf{x}} = \begin{bmatrix} 1 & 1 & 0 \\ 0 & -2 & 1 \\ 0 & 0 & -1 \end{bmatrix} \mathbf{x} + \begin{bmatrix} 0 \\ 1 \\ -2 \end{bmatrix} u \; ; \; y = [1 \quad 0 \quad 0] \, \mathbf{x}$$

(a) Find the eigenvalues of **A** and from there determine the stability of the system.
(b) Find the transfer function model and from there determine the stability of the system.
(c) Are the two results same? If not, why?

12.30 Given a transfer function

$$G(s) = \frac{10}{s(s+1)} = \frac{Y(s)}{U(s)}$$

Construct three different state models for this system:
(a) One which is both controllable and observable.
(b) One which is controllable but not observable.
(c) One which is observable but not controllable.

13 Control System Design Using State Variable Methods

13.1 INTRODUCTION

State variable methods have provided control theory with a deep and satisfying mathematical basis. With state variable models, we use an internal description of the system dynamics as opposed to a straightforward input-output transfer function model. We will see in this chapter that we gain from the knowledge of these internal states, and benefit from the use of this information in control system design.

The very fact that we describe a system using a state variable model leads directly to new terms and analysis/design methods. In the previous chapter on state variable analysis, we used system eigenvalues when we discussed system stability. These eigenvalues were found to be the same as system poles for systems that are both controllable and observable. When we looked at the initial condition and forced system responses, we found that these naturally occurred in the state variable framework.

When we discuss the control of a plant or process using state variable model, we will find many new fundamental insights about control theory. We will learn how state variable models lead to new methods for the design of compensators. These developments are relatively new; whereas PID control dates from 1940 onwards, state variable methods emerged from around 1960 and underwent many refinements before reaching the highly developed level available today. In this chapter, we introduce state variable control methods.

Before we begin our introduction to state variable control methods, a recapitulation of (Eqns (12.8)) the general state variable system structure will be in order here. Consider the general state variable system diagram shown in Fig. 13.1. The link between the real world and this rather abstract representation of a system is through the system input, output, and states.

The *system states* are the important set of system variables. It is the $n \times 1$ state vector $\mathbf{x}$ and the $n \times n$ system matrix $\mathbf{A}$ that governs how the system internal dynamics will operate. This means that $\mathbf{x}(t)$ is the key *information-carrying vector* in a state variable system model.

The *system inputs* are the control inputs to the system. They are able to influence and shape the dynamical behaviour of the system. In the system structure of Fig. 13.1, we have assumed that there is only one control input $u(t)$ available to us to manipulate. The input is connected to the system state through the $n \times 1$ input matrix $\mathbf{b}$.

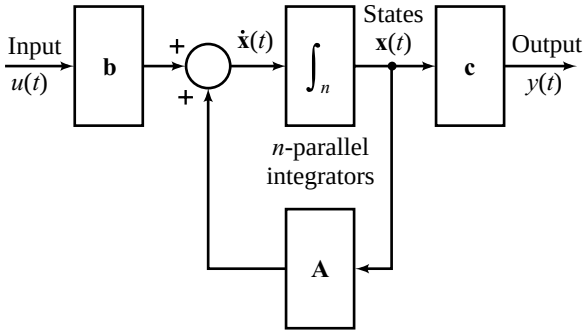

Fig. 13.1 General state variable system structure

The *system outputs* are generally those variables we can measure and wish to control. In the structure of Fig. 13.1, we have assumed that there is only one output $y(t)$ we can measure and wish to control. The state is connected to the output via the $1 \times n$ output matrix **c**. Thus **c** is *information-reducing matrix* in the sense that it specifies just how much we are able to view of the whole system state vector $\mathbf{x}(t)$.

In the structure of Fig. 13.1, we have assumed that there is no direct coupling between output y and input u (i.e., $d = 0$ in Eqns (12.8)). Direct coupling is rare in control systems.

The state variable model for the SISO system of Fig. 13.1 takes the form:

$$\dot{\mathbf{x}}(t) = \mathbf{A}\mathbf{x}(t) + \mathbf{b}u(t) \tag{13.1a}$$

$$y(t) = \mathbf{c}\mathbf{x}(t) \tag{13.1b}$$

13.2 STATE VARIABLE FEEDBACK STRUCTURE

Output feedback and the use of a compensator has been the common structure applied in this book so far. The compensators were used in the context of input-output transfer function model. The solution of the design problem was based on the choice of the parameters of the compensator to move poles of the closed-loop system to new locations to maintain stability of the closed-loop, and achieve some desired performance measures on speed of response and steady-state accuracy. The performance measures on speed of response were translated to specifying two dominant closed-loop poles. The locations of the other $(n - 2)$ poles of the n^{th}-order closed-loop system were not specified; however, it was required to push these poles to the regions in the complex plane from where the contribution of these poles to the dynamics of the closed-loop system is insignificant.

One obvious question may be raised here. Why did we not specify all the n closed-loop poles to shape the dynamics of the closed-loop system? The answer to this question is straightforward: with output feedback and the selected compensator structures (PID, Lag/Lead), a full pole-placement solution cannot be obtained, and we settle for the partial control over the closed-loop pole locations.

An important constraint here is that the output y is only a partial view of the state vector **x**; the state passes through the output matrix **c** to give the output variable y. We now investigate what happens if we can remove this constraint and have direct access to all the state variables, i.e., instead of using output in a feedback control law, we investigate the outcome of using the state vector *directly* in the feedback control law. We assume that we have a set of measurements available that allow a *full* view of the state vector.

Figure 13.2 shows a structure of state-feedback control for tracking the constant reference signal r. It is the structure of a *servo system*. When $r = 0$, the structure corresponds to a *regulator system*. The state-feedback law is of the form

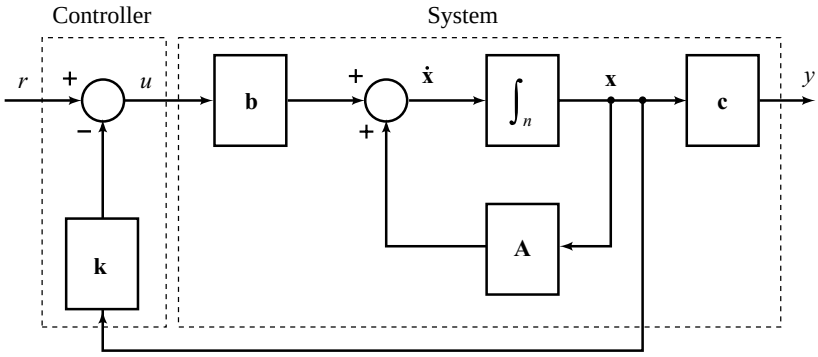

Fig. 13.2 State-feedback control structure

$$u(t) = r - \mathbf{k}\mathbf{x}(t) \tag{13.2}$$

The gain $\mathbf{k}$ is a $1 \times n$ row matrix with n tunable design parameters $k_1, k_2, ..., k_n$. We anticipate that we should be able to achieve more with state feedback. Closed-loop system analysis for the general state-feedback system of Fig. 13.2 is as follows:

Direct substitution of the control law (13.2) into the system Eqn. (13.1a) gives

$$\begin{aligned}\dot{\mathbf{x}}(t) &= \mathbf{A}\mathbf{x}(t) + \mathbf{b}[r - \mathbf{k}\mathbf{x}(t)] \\ &= (\mathbf{A} - \mathbf{b}\mathbf{k})\,\mathbf{x}(t) + \mathbf{b}r\end{aligned} \tag{13.3}$$

where $(\mathbf{A} - \mathbf{b}\mathbf{k})$ is the closed-loop system matrix.

We assume that a state-feedback gain $\mathbf{k}$ can be found to stabilize the closed-loop, so that all the eigenvalues of $(\mathbf{A} - \mathbf{b}\mathbf{k})$ have a strictly negative real part. As we shall see shortly, this is possible if the system (13.1) is controllable.

We have earlier observed in Chapter 2 that the transient response of a stable system vanishes as $t \to \infty$, and the steady-state response has the same nature as the input itself except for a modification in magnitude caused by the system's behavior to the specified input. Therefore, with the state-feedback gain $\mathbf{k}$ that stabilizes the closed-loop system of Fig. 13.2, the constant reference signal r causes the output y to reach constant level as $t \to \infty$. We denote this steady level as y_s.This output is connected to the state $\mathbf{x}_s$ via the output matrix $\mathbf{c}$.

Equation (13.3), as $t \to \infty$, becomes

$$\dot{\mathbf{x}}_s = (\mathbf{A} - \mathbf{b}\mathbf{k})\mathbf{x}_s + \mathbf{b}r = \mathbf{0}$$

which gives

$$\mathbf{x}_s = -(\mathbf{A} - \mathbf{b}\mathbf{k})^{-1}\mathbf{b}r$$

and

$$y_s = \mathbf{c}[-(\mathbf{A} - \mathbf{b}\mathbf{k})^{-1}]\mathbf{b}r \tag{13.4}$$

Thus, with the stabilizing feedback matrix $\mathbf{k}$, the state-feedback control structure of Fig. 13.2 results in a finite steady-state error.

We have two design issues in hand:

1. Find the gain matrix $\mathbf{k}$ so that the eigenvalues of $(\mathbf{A} - \mathbf{b}\mathbf{k})$ are at the desired locations in the complex plane. Iterate on the desired locations to obtain acceptable transient as well as steady-state response.
2. Another design issue arises when finite steady-state error resulting from solution to the first design problem is not acceptable, and it is desired to reduce the error to zero. This requires modifying the control structure of Fig. 13.2.

We first take up design problem 1. Consideration of design problem 2 will follow subsequently.

13.3 POLE-PLACEMENT DESIGN USING STATE FEEDBACK

Consider that the process/plant is described by the following state equation:

$$\dot{\mathbf{x}}(t) = \mathbf{A}\mathbf{x}(t) + \mathbf{b}u(t) \tag{13.5}$$

where $\mathbf{x}(t)$ is the $n \times 1$ state vector and $u(t)$ is the scalar control. The state-feedback control law is

$$u(t) = -\mathbf{k}\mathbf{x}(t) + r \tag{13.6}$$

where $\mathbf{k}$ is the $1 \times n$ feedback matrix with constant gain elements.

By substituting Eqn. (13.6) into Eqn. (13.5), the closed-loop system is represented by the state equation

$$\dot{\mathbf{x}}(t) = (\mathbf{A} - \mathbf{b}\mathbf{k})\mathbf{x}(t) + \mathbf{b}r \tag{13.7}$$

It will be shown in the following that if the pair $\{\mathbf{A}, \mathbf{b}\}$ is completely controllable, then a matrix $\mathbf{k}$ exists that can give an arbitrary set of eigenvalues of $(\mathbf{A} - \mathbf{b}\mathbf{k})$, i.e., the roots of the characteristic equation (poles of the closed-loop system)

$$\left|s\mathbf{I} - (\mathbf{A} - \mathbf{b}\mathbf{k})\right| = 0 \tag{13.8}$$

can be arbitrarily placed.

To show that this is true, we refer to the findings in Chapter 12 that a state equation in first companion form (refer Eqns (12.44)) is always completely controllable (refer Problem 12.25). For this reason, the companion-form realization given by Eqns (12.44) is referred to as *controllable canonical form*[1]. It implies that if a system is completely controllable, it can always be represented in the controllable canonical form.

We assume that there exists a transformation

$$\bar{\mathbf{x}} = \mathbf{P}\mathbf{x} \tag{13.9}$$

$$= \begin{bmatrix} p_{11} & p_{12} & \cdots & p_{1n} \\ p_{21} & p_{22} & \cdots & p_{2n} \\ \vdots & \vdots & & \vdots \\ p_{n1} & p_{n2} & \cdots & p_{nn} \end{bmatrix} \mathbf{x} = \begin{bmatrix} \mathbf{p}_1 \\ \mathbf{p}_2 \\ \vdots \\ \mathbf{p}_n \end{bmatrix} \mathbf{x}$$

$$\mathbf{p}_i = \begin{bmatrix} p_{i1} & p_{i2} & \ldots & p_{in} \end{bmatrix}; \; i = 1, 2, \ldots, n$$

which transforms system (13.5) to the following controllable canonical model:

$$\dot{\bar{\mathbf{x}}} = \bar{\mathbf{A}}\bar{\mathbf{x}} + \bar{\mathbf{b}}\,u \tag{13.10}$$

where

$$\bar{\mathbf{A}} = \mathbf{P}\mathbf{A}\mathbf{P}^{-1} = \begin{bmatrix} 0 & 1 & 0 & \cdots & 0 \\ 0 & 0 & 1 & \cdots & 0 \\ \vdots & \vdots & \vdots & & \vdots \\ 0 & 0 & 0 & & 1 \\ -\alpha_n & -\alpha_{n-1} & -\alpha_{n-2} & \cdots & -\alpha_1 \end{bmatrix}$$

[1]A state model in second companion form (refer Eqns (12.46)) is always completely observable (refer Problem 12.24). For this reason, the companion form realization given by Eqns (12.46) is referred to as *observable canonical form.*

$$\bar{\mathbf{b}} = \mathbf{Pb} = \begin{bmatrix} 0 \\ 0 \\ \vdots \\ 0 \\ 1 \end{bmatrix}$$

$$|s\mathbf{I} - \bar{\mathbf{A}}| = s^n + \alpha_1 s^{n-1} + \cdots + \alpha_{n-1} s + \alpha_n = |s\mathbf{I} - \mathbf{A}|$$

(Characteristic polynomial is invariant under equivalence transformation)
The first equation in the set (13.9) is given by

$$\bar{x}_1 = p_{11} x_1 + p_{12} x_2 + \cdots + p_{1n} x_n = \mathbf{p}_1 \mathbf{x}$$

Taking the derivative on both sides of this equation, we get

$$\dot{\bar{x}}_1 = \mathbf{p}_1 \dot{\mathbf{x}} = \mathbf{p}_1 \mathbf{A}\mathbf{x} + \mathbf{p}_1 \mathbf{b} u$$

But $\dot{\bar{x}}_1$ $(= \bar{x}_2)$ is a function of $\mathbf{x}$ only as per the canonical model (13.10).
Therefore

$$\mathbf{p}_1 \mathbf{b} = 0 \text{ and } \bar{x}_2 = \mathbf{p}_1 \mathbf{A}\mathbf{x}$$

Taking derivative on both sides once again, we get

$$\mathbf{p}_1 \mathbf{A}\mathbf{b} = 0 \text{ and } \bar{x}_3 = \mathbf{p}_1 \mathbf{A}^2 \mathbf{x}$$

Continuing the process, we obtain

$$\mathbf{p}_1 \mathbf{A}^{n-2} \mathbf{b} = 0 \text{ and } \bar{x}_n = \mathbf{p}_1 \mathbf{A}^{n-1} \mathbf{x}$$

Taking derivative once again, we obtain

$$\mathbf{p}_1 \mathbf{A}^{n-1} \mathbf{b} = 1$$

Thus

$$\bar{\mathbf{x}} = \mathbf{Px} = \begin{bmatrix} \mathbf{p}_1 \\ \mathbf{p}_1 \mathbf{A} \\ \vdots \\ \mathbf{p}_1 \mathbf{A}^{n-1} \end{bmatrix} \mathbf{x}$$

where $\mathbf{p}_1$ must satisfy the conditions

$$\mathbf{p}_1 \mathbf{b} = \mathbf{p}_1 \mathbf{A}\mathbf{b} = \cdots = \mathbf{p}_1 \mathbf{A}^{n-2} \mathbf{b} = 0, \mathbf{p}_1 \mathbf{A}^{n-1} \mathbf{b} = 1$$

From Eqn. (13.10), we have

$$\mathbf{Pb} = \begin{bmatrix} 0 \\ 0 \\ \vdots \\ 0 \\ 1 \end{bmatrix} = \begin{bmatrix} \mathbf{p}_1 \mathbf{b} \\ \mathbf{p}_1 \mathbf{A}\mathbf{b} \\ \vdots \\ \mathbf{p}_1 \mathbf{A}^{n-2} \mathbf{b} \\ \mathbf{p}_1 \mathbf{A}^{n-1} \mathbf{b} \end{bmatrix}$$

or $\mathbf{p}_1[\mathbf{b} \quad \mathbf{Ab} \cdots \mathbf{A}^{n-2}\mathbf{b} \quad \mathbf{A}^{n-1}\mathbf{b}] = [0 \quad 0 \cdots 0 \quad 1]$

This gives

$$\mathbf{p}_1 = [0 \quad 0 \cdots 0 \quad 1]\mathbf{U}^{-1}$$

where

$$\mathbf{U} = [\mathbf{b} \quad \mathbf{Ab} \cdots \mathbf{A}^{n-1}\mathbf{b}]$$

is the controllability matrix, which is nonsingular because of the assumption of controllability of the system (13.5).

Therefore, the controllable state model (13.5) can be transformed to the canonical form (13.10) by the transformation

$$\bar{\mathbf{x}} = \mathbf{P}\mathbf{x} \tag{13.11}$$

where $$\mathbf{P} = \begin{bmatrix} \mathbf{p}_1 \\ \mathbf{p}_1\mathbf{A} \\ \vdots \\ \mathbf{p}_1\mathbf{A}^{n-1} \end{bmatrix}; \quad \mathbf{p}_1 = [0 \quad 0 \cdots 0 \quad 1]\mathbf{U}^{-1}$$

Under the equivalence transformation (13.11), the state-feedback control law (13.6) becomes

$$u = -\mathbf{k}\mathbf{x} + r = -\bar{\mathbf{k}}\,\bar{\mathbf{x}} + r \tag{13.12a}$$

where $$\bar{\mathbf{k}} = \mathbf{k}\mathbf{P}^{-1} = [\bar{k}_1 \quad \bar{k}_2 \quad \ldots \quad \bar{k}_n] \tag{13.12b}$$

With this control law, system (13.10) becomes

$$\dot{\bar{\mathbf{x}}} = (\bar{\mathbf{A}} - \bar{\mathbf{b}}\,\bar{\mathbf{k}})\,\bar{\mathbf{x}} + \bar{\mathbf{b}}\,r$$

$$= \begin{bmatrix} 0 & 1 & 0 & \cdots & 0 & 0 \\ 0 & 0 & 1 & \cdots & 0 & 0 \\ \vdots & \vdots & \vdots & & \vdots & \vdots \\ 0 & 0 & 0 & \cdots & 0 & 1 \\ \vdots & \vdots & \vdots & & \vdots & \vdots \\ -\alpha_n - \bar{k}_1 & -\alpha_{n-1} - \bar{k}_2 & -\alpha_{n-2} - \bar{k}_3 & \cdots & -\alpha_2 - \bar{k}_{n-1} & -\alpha_1 - \bar{k}_n \end{bmatrix} \bar{\mathbf{x}} + \begin{bmatrix} 0 \\ 0 \\ \vdots \\ 0 \\ 1 \end{bmatrix} r \tag{13.13}$$

$$|s\mathbf{I} - (\bar{\mathbf{A}} - \bar{\mathbf{b}}\,\bar{\mathbf{k}})| = s^n + (\alpha_1 + \bar{k}_n))s^{n-1} + (\alpha_2 + \bar{k}_{n-1})s^{n-2} +$$

$$\cdots + (\alpha_{n-1} + \bar{k}_2)\,s + (\alpha_n + \bar{k}_1) \tag{13.14}$$

Since the coefficients $\bar{k}_i$ are arbitrarily chosen real numbers, the coefficients of the characteristic polynomial of $(\mathbf{A} - \mathbf{bk})$ can be given any desired values. Hence, the closed-loop poles can be placed at any desired locations in the complex plane (subject to conjugate pairing: coefficients of a characteristic polynomial will be real only if the complex poles are present in conjugate pairs).

Assume that the desired characteristic polynomial of $(\mathbf{A} - \mathbf{bk})$, and hence $(\bar{\mathbf{A}} - \bar{\mathbf{b}}\,\bar{\mathbf{k}})$, is

$$s^n + a_1 s^{n-1} + \cdots + a_n$$

From Eqn. (13.14), it is obvious that this requirement is met if $\bar{\mathbf{k}}$ is chosen as

$$\bar{\mathbf{k}} = [a_n - \alpha_n \quad a_{n-1} - \alpha_{n-1} \cdots a_1 - \alpha_1]$$

Transforming this feedback controller to the original coordinates, we obtain

$$\mathbf{k} = \bar{\mathbf{k}}\,\mathbf{P} = [a_n - \alpha_n \quad a_{n-1} - \alpha_{n-1} \cdots a_1 - \alpha_1]\mathbf{P} \tag{13.15}$$

This proves that if (13.5) is controllable, the closed-loop poles can be arbitrarily assigned

We can find the parameters of the feedback matrix **k** by matching the coefficients of $|s\mathbf{I} - (\mathbf{A} - \mathbf{bk})|$ with the coefficients of the desired characteristic polynomial of the closed-loop system. This technique, in general, leads to difficult calculations of the feedback gains, especially for higher-order systems not represented in controllable canonical form. For higher-order systems represented in controllable canonical form, the feedback gains **k** can be easily determined by matching the coefficients. However, the physics of the problem generally requires feedback from state variables that are not canonical. This requires transforming the system to controllable canonical form, designing the feedback gains, and transforming the designed system back to the original state variable representation. This technique, derived earlier in this section, is summarized below:

Characteristic polynomial of the plant:

$$|s\mathbf{I} - \mathbf{A}| = s^n + \alpha_1 s^{n-1} + \cdots + \alpha_{n-1}s + \alpha_n \tag{13.16a}$$

Desired characteristic polynomial of the feedback system:

$$\Delta(s) = s^n + a_1 s^{n-1} + \cdots + a_{n-1}s + a_n \tag{13.16b}$$

The feedback matrix

$$\mathbf{k} = [a_n - \alpha_n \quad a_{n-1} - \alpha_{n-1} \cdots a_1 - \alpha_1]\mathbf{P} \tag{13.16c}$$

$$\mathbf{P} = \begin{bmatrix} \mathbf{p}_1 \\ \mathbf{p}_1\mathbf{A} \\ \vdots \\ \mathbf{p}_1\mathbf{A}^{n-1} \end{bmatrix}; \quad \begin{matrix} \mathbf{p}_1 = [0 \quad 0 \quad \cdots \quad 0 \quad 1]\mathbf{U}^{-1} \\ \mathbf{U} = [\mathbf{b} \quad \mathbf{Ab} \quad \cdots \quad \mathbf{A}^{n-1}\mathbf{b}] \end{matrix} \tag{13.16d}$$

Example 13.1 Consider the problem of designing an attitude control system for a rigid satellite. Satellites usually require attitude control so that antennas, sensors, and solar panels are properly oriented. For example, antennas are usually pointed towards a particular location on the earth while solar panels need to be oriented towards the sun for maximum power generation. To gain an insight into the full three-axis attitude-control system, we often consider one axis at a time. Figure 13.3 depicts this case. The angle θ that describes the satellite orientation must be measured with respect to an 'inertial' reference, that is, a reference that has no angular acceleration. The control signal comes from the reaction jets that produce a torque $T(t)$ $(= Fd)$ about the mass centre.

The satellite is assumed to be in frictionless environment. If $T(t)$ is the system input and $\theta(t)$ is the system output, we have

$$T(t) = J\,\frac{d^2\theta(t)}{dt^2}$$

where J is the moment of inertia of the satellite. Normalizing, we define

$$u = T(t)/J$$

and obtain

$$\ddot{\theta} = u \text{ or } \frac{\theta(s)}{U(s)} = \frac{1}{s^2}$$

This is a reasonably accurate model of a rigid satellite in a frictionless environment, and is useful in examples because of its simplicity.

Choosing $x_1 = \theta$ and $x_2 = \dot{\theta}$ as state variables, we obtain the following state equation for the system.

$$\dot{\mathbf{x}} = \mathbf{A}\mathbf{x} + \mathbf{b}u = \begin{bmatrix} 0 & 1 \\ 0 & 0 \end{bmatrix} \mathbf{x} + \begin{bmatrix} 0 \\ 1 \end{bmatrix} u \quad (13.17)$$

It is desired to maintain the attitude of the satellite at $\theta = 0$ (i.e., $r = 0$). This is a regulator problem.
To stabilize the system, the input signal is chosen to be of the form

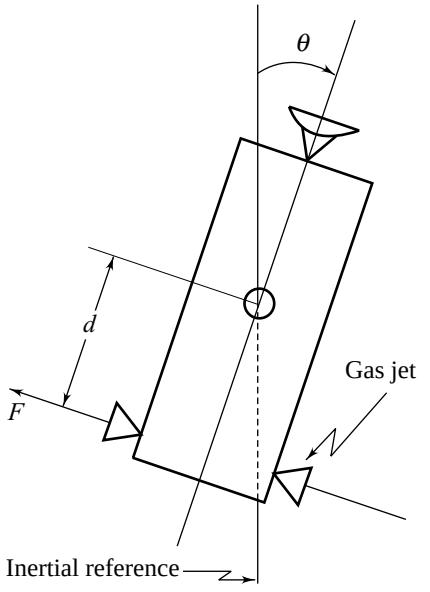

Fig. 13.3 Satellite control schematic

$$u(t) = -k_1 x_1(t) - k_2 x_2(t) = -\mathbf{k}\mathbf{x}(t)$$

The state equation for the closed-loop system (Fig. 13.4), then becomes

$$\dot{\mathbf{x}} = (\mathbf{A} - \mathbf{b}\mathbf{k})\mathbf{x} = \left(\begin{bmatrix} 0 & 1 \\ 0 & 0 \end{bmatrix} - \begin{bmatrix} 0 \\ 1 \end{bmatrix} [k_1 \quad k_2] \right) \mathbf{x} = \begin{bmatrix} 0 & 1 \\ -k_1 & -k_2 \end{bmatrix} \mathbf{x}$$

The characteristic equation of the closed-loop system is

$$|s\mathbf{I} - (\mathbf{A} - \mathbf{b}\mathbf{k})| = s^2 + k_2 s + k_1 = 0 \quad (13.18a)$$

Suppose that the design specifications for this system require $\zeta = 0.707$ with a settling time of 1 sec $\left(\dfrac{4}{\zeta\omega_n} = 1 \text{ or } \zeta\omega_n = 4 \right)$. The closed-loop pole locations needed are at $s = -4 \pm j4$. The desired characteristic equation is

$$(s + 4 + j4)(s + 4 - j4) = s^2 + 8s + 32 \quad (13.18b)$$

Equating the coefficients with like powers of s in Eqns (13.18a) and (13.18b) yields

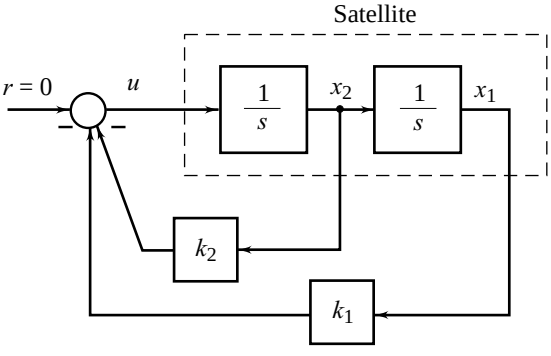

Fig. 13.4 Simulation diagram for the satellite control system

$$k_1 = 32, k_2 = 8$$

Example 13.2 The plant of a servo system is described by the equations

$$\dot{\mathbf{x}} = \mathbf{A}\mathbf{x} + \mathbf{b}u$$
$$y = \mathbf{c}\mathbf{x} \quad (13.19)$$

where

$$\mathbf{A} = \begin{bmatrix} -3 & 2 \\ 4 & -5 \end{bmatrix}; \quad \mathbf{b} = \begin{bmatrix} 1 \\ 0 \end{bmatrix}; \quad \mathbf{c} = \begin{bmatrix} 0 & 1 \end{bmatrix}$$

The characteristic polynomial of this system is

$$|s\mathbf{I} - \mathbf{A}| = s^2 + 8s + 7 = s^2 + \alpha_1 s + \alpha_2$$

The desired characteristic polynomial is

$$(s + 4)\,(s + 7) = s^2 + 11s + 28 = s^2 + a_1 s + a_2$$

A control law of the form

$$u = -\mathbf{k}\mathbf{x} + r \tag{13.20a}$$

is proposed; r is a unit-step reference input. The gain matrix (refer Eqns (13.16))

$$\mathbf{k} = [a_2 - \alpha_2 \quad a_1 - \alpha_1]\mathbf{P} = [21 \quad 3]\mathbf{P}$$

where

$$\mathbf{P} = \begin{bmatrix} \mathbf{p}_1 \\ \mathbf{p}_1\mathbf{A} \end{bmatrix}$$

$$\mathbf{p}_1 = [0 \quad 1][\mathbf{b} \quad \mathbf{A}\mathbf{b}]^{-1} = [0 \quad 1]\begin{bmatrix} 1 & \frac{3}{4} \\ 0 & \frac{1}{4} \end{bmatrix} = \begin{bmatrix} 0 & \frac{1}{4} \end{bmatrix}; \quad \mathbf{p}_1\mathbf{A} = \begin{bmatrix} 1 & \frac{-5}{4} \end{bmatrix}$$

This gives

$$\mathbf{k} = [3 \quad 1.5] \tag{13.20b}$$

Substituting the control law (13.20) into (13.19), we get the state equations of the feedback system:

$$\dot{\mathbf{x}} = (\mathbf{A} - \mathbf{b}\mathbf{k})\mathbf{x} + \mathbf{b}r = \begin{bmatrix} -6 & 0.5 \\ 4 & -5 \end{bmatrix}\mathbf{x} + \begin{bmatrix} 1 \\ 0 \end{bmatrix} r \tag{13.21}$$

At steady state, $\dot{\mathbf{x}} = \mathbf{0}$. This gives (for $r = 1$)

$$4x_{1s} - 5x_{2s} = 0$$

and

$$-6x_{1s} + 0.5x_{2s} = 1$$

From these equations we get

$$x_{2s} = y_s = \tfrac{1}{7}$$

Steady-state error $= r - y_s = \tfrac{6}{7}$

13.4 STATE FEEDBACK WITH INTEGRAL CONTROL

This section is concerned with steady-state error design via integral control. Recall that state-feedback control structure of Fig. 13.2 results in a finite steady-state error to step commands. We modify this control structure to the one shown in Fig. 13.5. A feedback path from the output has been added to form the error e,

which is fed forward to the controlled plant via an integrator. The integrator increases the system type and reduces the finite steady-state error to zero. We will now derive the form of the state equations for the system of Fig. 13.5, and then use that form to design a controller. Thus, we will be able to design a system for zero steady-state error to step input, as well as obtain the desired transient response.

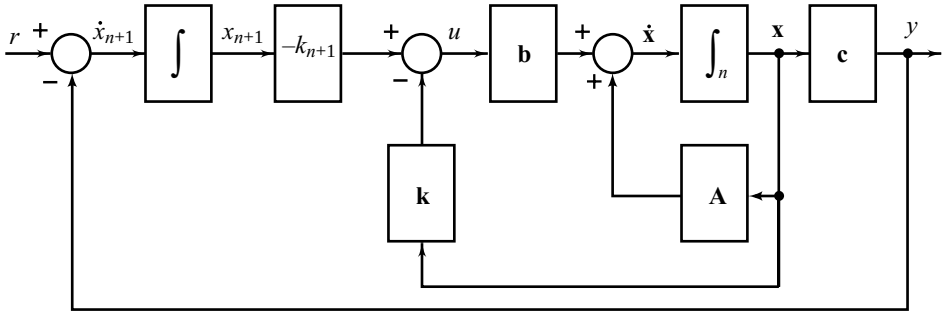

Fig. 13.5 State feedback with integral control

An additional state variable x_{n+1} has been added at the output of the left-most integrator. The error e is the derivative of this variable. Now from Fig.13.5,

$$\dot{x}_{n+1}(t) = r - \mathbf{c}\mathbf{x}(t)$$

Writing the state equations from Fig. 13.5, we have

$$\begin{aligned} \dot{\mathbf{x}}(t) &= \mathbf{A}\mathbf{x}(t) + \mathbf{b}u(t) \\ \dot{x}_{n+1}(t) &= -\mathbf{c}\mathbf{x}(t) + r \\ y(t) &= \mathbf{c}\mathbf{x}(t) \end{aligned} \tag{13.22}$$

These equations can be written as augmented vectors and matrices. Hence

$$\begin{bmatrix} \dot{\mathbf{x}} \\ \dot{x}_{n+1} \end{bmatrix} = \begin{bmatrix} \mathbf{A} & \mathbf{0} \\ -\mathbf{c} & 0 \end{bmatrix} \begin{bmatrix} \mathbf{x} \\ x_{n+1} \end{bmatrix} + \begin{bmatrix} \mathbf{b} \\ 0 \end{bmatrix} u + \begin{bmatrix} \mathbf{0} \\ 1 \end{bmatrix} r$$

$$y = [\mathbf{c} \quad 0] \begin{bmatrix} \mathbf{x} \\ x_{n+1} \end{bmatrix} \tag{13.23a}$$

or

$$\begin{aligned} \dot{\bar{\mathbf{x}}}(t) &= \bar{\mathbf{A}}\bar{\mathbf{x}}(t) + \bar{\mathbf{b}}u(t) + \begin{bmatrix} \mathbf{0} \\ 1 \end{bmatrix} r \\ y(t) &= \bar{\mathbf{c}}\,\bar{\mathbf{x}}(t) \end{aligned} \tag{13.23b}$$

where $\bar{\mathbf{x}}(t)$ is the $(n+1)\times 1$ state vector, $u(t)$ and $y(t)$ are the scalar control signal and output, respectively; r is the scalar constant reference input. The coefficient matrices are represented by $(n+1)\times(n+1)$ matrix $\bar{\mathbf{A}}$, $(n+1)\times 1$ matrix $\bar{\mathbf{b}}$, and $1\times(n+1)$ matrix $\bar{\mathbf{c}}$.

The control signal $u(t)$ is related to the state variables through state and integral feedback:

$$u(t) = -\mathbf{k}\mathbf{x}(t) - k_{n+1}x_{n+1} = -\bar{\mathbf{k}}\bar{\mathbf{x}}(t) \tag{13.24a}$$

where

$$\mathbf{k} = [k_1 \quad k_2 \quad \cdots \quad k_n] \tag{13.24b}$$

is the state-feedback gain vector, and k_{n+1} is the scalar integral-feedback gain; and

$$\bar{\mathbf{k}} = [k_1 \quad k_2 \quad \cdots \quad k_n \quad k_{n+1}] \tag{13.24c}$$

Substituting Eqn. (13.24a) into Eqn. (13.23b), the $n + 1$ state equations of the feedback system are written as

$$\begin{aligned} \dot{\bar{\mathbf{x}}}(t) &= (\bar{\mathbf{A}} - \bar{\mathbf{b}}\bar{\mathbf{k}})\bar{\mathbf{x}}(t) + \begin{bmatrix} \mathbf{0} \\ 1 \end{bmatrix} r \\ y(t) &= \bar{\mathbf{c}}\,\bar{\mathbf{x}} \end{aligned} \tag{13.25}$$

We can use the characteristic equation associated with system (13.25) to design $\bar{\mathbf{k}}$ to yield the desired transient response. The $(n + 1)$ eigenvalues of the system matrix in Eqn. (13.25) are placed at desired locations. Of course, for this to be possible, the pair $\{\bar{\mathbf{A}}, \bar{\mathbf{b}}\}$ must be completely controllable.

At steady-state, $\dot{\mathbf{x}}_s = \mathbf{0}$ and $\dot{x}_{(n+1)s} = 0$. The $(n + 1)^{th}$ equation in the set (13.25) gives

$$\dot{x}_{(n+1)s} = -\mathbf{c}\mathbf{x}_s + r = 0$$

ensuring zero steady-state error to step input r.

Example 13.3 Suppose the system is given by

$$\frac{Y(s)}{U(s)} = \frac{1}{s+3}$$

with a constant reference command signal. We wish to have integral control with closed-loop poles at $\omega_n = 5$ and $\zeta = 0.5$, which is equivalent to asking for a desired characteristic equation

$$s^2 + 5s + 25 = 0$$

The plant model is

$$\begin{aligned} \dot{x}_1 &= -3x_1 + u \\ y &= x_1 \end{aligned}$$

Augmenting the plant state x_1 with the integral state x_2 defined by the equation

$$x_2(t) = \int_0^t (r - y(t))dt$$

we obtain

$$\begin{bmatrix} \dot{x}_1 \\ \dot{x}_2 \end{bmatrix} = \begin{bmatrix} -3 & 0 \\ -1 & 0 \end{bmatrix} + \begin{bmatrix} x_1 \\ x_2 \end{bmatrix} + \begin{bmatrix} 1 \\ 0 \end{bmatrix} u + \begin{bmatrix} 0 \\ 1 \end{bmatrix} r$$

We can find **k** from

$$det\left(s\mathbf{I}-\begin{bmatrix}-3 & 0\\ -1 & 0\end{bmatrix}+\begin{bmatrix}1\\ 0\end{bmatrix}\mathbf{k}\right)=s^2+5s+25$$

or $$s^2+(3+k_1)s-k_2=s^2+5s+25$$

Therefore

$$\mathbf{k}=[2 \quad -25]=[k_1 \quad k_2]$$

The control

$$u=-k_1x_1-k_2x_2=-2x_1+25\int_0^t(r-y(t))dt$$

The control configuration is shown in Fig. 13.6. This system will behave according to the desired closed-loop roots ($\omega_n=5$, $\zeta=0.5$) and will exhibit the characteristics of integral control: zero steady-state error to a step r.

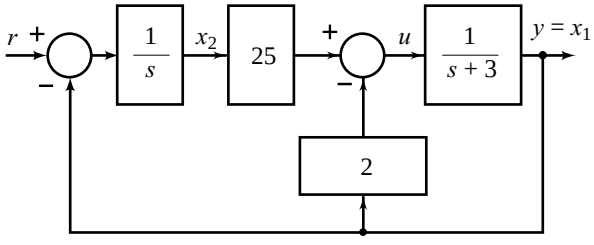

Fig. 13.6 Integral control example

13.5 CRITIQUE OF POLE-PLACEMENT STATE FEEDBACK CONTROL

Chapters 1–10 of this book were devoted to the classical methods of control design using output feedback. From Chapters 7 and 10, we have observed that the output-feedback control law is restricted in design achievements; by trial-and-error we place the two dominant poles of the closed-loop system at the desired locations, and all other poles are made insignificant by pole-zero cancellation and/or by shifting them to the region of insignificance on the complex plane. Rigorous trial-and-error is involved in the design procedure and many a times we terminate trials when dominant poles *close to* the desired locations (not *at* the desired locations) have been achieved.

The state-feedback control law is able to give total control over the system dynamics; all the poles of the closed-loop system can be placed exactly at the desired locations. Also there is no trial-and-error involved; state variable methods provide control theory with deep and satisfying mathematical design tools.

The important step in the pole-placement design approach using state-feedback is to choose the locations of the desired closed-loop poles. The design procedure, however, gives no guidance as to where in the left-half complex plane, the closed-loop poles should be placed. It appears that we can choose the magnitude of the real part of the closed-loop poles arbitrarily large, making the system response arbitrarily fast. However, to increase the rate at which the plant responds, the input signal to the plant must become larger, requiring large values of gains. As the magnitudes of the signals in a system increase, the likelihood of the system

entering nonlinear regions of operation increases. For very large signals, this nonlinear operation will occur for almost every physical system. Hence, the linear model that is used in design no longer accurately models the physical system.

Thus, the selection of desired closed-loop poles requires a proper balance of bandwidth, overshoot, control effort, and other design requirements. If the system is of second-order, then the system dynamics (response characteristics) can be precisely correlated to the locations of the desired closed-loop poles. For higher-order systems, the locations of the closed-loop poles and the response characteristics are not easily correlated. Hence, in determining the state-feedback gain matrix **k** for a given system, it is desirable to examine by computer simulations, the response characteristics for several different matrices **k** (based on several different characteristic equations), and choose the one that gives the best overall performance. In fact, if critically examined, we observe that the trial-and-error involved in classical design procedures is also involved in state-variable methods, though in a different form.

Therefore, theory is always what it says it is: *just theory*, which has to be matched against the practical reality of the real world. State variable methods provide control theory with mathematical design tools that don't involve trial-and-error iterations, and that guarantee the design properties: all the poles of the closed-loop systems can be placed exactly at the desired locations. The design flexibility of state feedback is achieved because it has been assumed that

- we can access each state variable; and
- performance requirements have been translated into desired locations for all the closed-loop poles.

The assumption of accessibility of each state variable, in practice, means that we must be able to measure every state variable, or we must have a more complicated control system when we include the model of the estimator which provides us with the state information. *Observer-based state-feedback controllers* incorporate model of the state estimator and are used when all the states are not able to be measured and we have a good model of the process.

Most individual control systems will have many unmeasurable system states and, further, industrial process models are not usually so well known or accurate. Adequate stability margins are required to protect against the model uncertainties. In some situations we may design a controller that works perfectly under computer simulations but turns out to be unstable in practice. Therefore, any design must be tested thoroughly to prevent disastrous results.

The assumption of availability of performance specifications in the form of exact locations for desired poles of the closed-loop system does not match against the practical reality. With the freedom of choice rendered by state feedback (of relocating all the closed-loop poles at desired locations, in contrast with classical design whereby the designer may only hope to achieve a pair of complex conjugate poles that are dominant) comes with the responsibility of selecting closed-loop poles judiciously. An obvious temptation of pushing the poles too far into the left-hand complex plane to get a faster system, is costlier because a faster system may require accurate sensors and a larger or stronger actuator (such as a motor) to perform the task. Also the system bandwidth increases, and the system becomes sensitive to noise. Further, the signals in the system may become very large, with the result that the system may become nonlinear. No magic choice of closed-loop poles is possible; trial-and-error involved in classical design procedure gets shifted to trial-and-error in selection of closed-loop poles when state-feedback freedom is utilized.

Another approach is based in *linear quadratic optimal control*. This approach will determine the desired closed-loop poles such that it balances between the acceptable response and the amount of control energy required. The linear quadratic optimal control approach, as we shall see in this chapter, also involves trial-and-error but the number of trials are drastically reduced. The task of the designer shifts from selection of closed-loop poles to one of specifying various parameters in the performance index.

The classical output feedback procedures have more tolerance on uncertainity of the process models. State variable methods require 'good' models. Inspite of this we can say that state variable methods provide control theory with a deep mathematical basis. Of course, there is a gap between theory and practice, but it is the interplay between them that makes the practical outcomes so interesting and useful. We need the precision of mathematical control tools to illuminate control application problems in industry.

In the following, we present an introduction to observer-based state-feedback control design. Formulation of linear quadratic optimal control will also be given; however, for want of space we refer the reader to the companion book [155] for the solution of optimal control problem.

13.6 OBSERVER-BASED STATE FEEDBACK CONTROL

The control law designed in Section 13.3 assumed that all the state variables are available for feedback. In most cases, not all the state variables are measured. The cost of the required sensors may be prohibitive, or it may not be physically possible to measure all the state variables.

In this section, we demonstrate how to reconstruct all the state variables of a system from a few measurements. If the estimate of the state is denoted by $\hat{\mathbf{x}}$, it would be convenient if we could replace the true value in the control law given in Eqn.(13.6) with the estimate so that the control law becomes

$$u(t) = -\mathbf{k}\hat{\mathbf{x}}(t) + r \tag{13.26}$$

This is indeed possible, as we shall see in this section. So the construction of a state estimate is a key part of state feedback control design.

A device (or a computer program) that estimates the state variables is called a *state observer*, or simply an *observer*. If the state observer estimates all the state variables of the system, regardless of whether some state variables are available for direct measurement, it is called a *full-order state observer*. However, if accurate measurements of certain states are possible, we may estimate only the remaining states, and the accurately measured signals are then used directly for feedback. The resulting observer is called a *reduced-order state observer*. In this chapter, we discuss full-order observers. Refer the companion book [155] for reduced-order observers.

13.6.1 Full-Order State Observer

Consider a process described by the state equation

$$\dot{\mathbf{x}}(t) = \mathbf{A}\mathbf{x}(t) + \mathbf{b}u(t) \tag{13.27a}$$

where $\mathbf{A}$ and $\mathbf{b}$ are, respectively, $n \times n$ and $n \times 1$ real constant matrices. The measurement $y(t)$ is related to the state by the equation

$$y(t) = \mathbf{c}\mathbf{x}(t) \tag{13.27b}$$

where $\mathbf{c}$ is $1 \times n$ real constant matrix. Without loss of generality, the direct transmission part has been assumed to be zero.

One method of estimating all the state variables that we may consider is to construct a model of the plant dynamics:

$$\dot{\hat{\mathbf{x}}}(t) = \mathbf{A}\hat{\mathbf{x}}(t) + \mathbf{b}u(t) \tag{13.28}$$

where $\hat{\mathbf{x}}$ is the estimate of the actual state $\mathbf{x}$. We know $\mathbf{A}$, $\mathbf{b}$ and $u(t)$, and hence this estimator is satisfactory if we can obtain the correct initial condition $\mathbf{x}(0)$ and set $\hat{\mathbf{x}}(0)$ equal to it. Figure 13.7 depicts this 'open-loop' estimator. However, it is precisely the lack of information on $\mathbf{x}(0)$ that requires the construction of an

estimator. If $\hat{\mathbf{x}}(0) \neq \mathbf{x}(0)$, the estimated state $\hat{\mathbf{x}}(t)$ obtained from the open-loop scheme of Fig. 13.7 would have a continually growing error, or an error that goes to zero too slowly to be of any use. Furthermore, small errors in our knowledge of the system (**A**, **b**), and the disturbances that enter the system but not the model would also cause the estimate to slowly diverge from the true state.

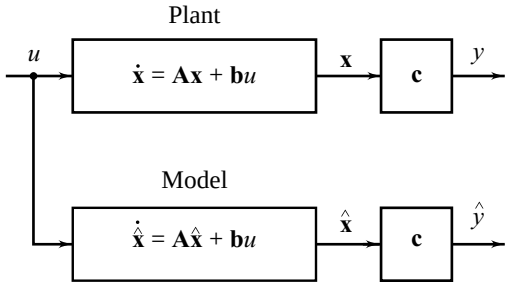

Fig. 13.7 Open-loop estimator

In order to speed up the estimation process and provide a useful state estimate, we feedback the difference between the measured and the estimated outputs and correct the model continuously with this error signal. This scheme, commonly known as 'Luenberger state observer', is shown in Fig. 13.8, and the equation for it is

$$\dot{\hat{\mathbf{x}}}(t) = \mathbf{A}\,\hat{\mathbf{x}}(t) + \mathbf{b}u(t) + \mathbf{m}(y(t) - \hat{y}(t)) \tag{13.29}$$

where **m** is an $n \times 1$ real constant gain matrix.
The state error vector

$$\tilde{\mathbf{x}}(t) = \mathbf{x}(t) - \hat{\mathbf{x}}(t) \tag{13.30}$$

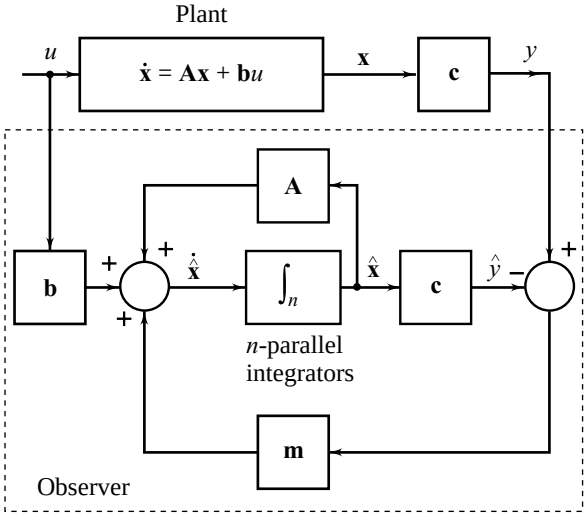

Fig. 13.8 Luenberger state observer

Differentiating both sides, we get

$$\dot{\tilde{\mathbf{x}}}(t) = \dot{\mathbf{x}}(t) - \dot{\hat{\mathbf{x}}}(t)$$

Substituting for $\dot{\mathbf{x}}(t)$ and $\dot{\hat{\mathbf{x}}}(t)$ from Eqns (13.27) and (13.29) respectively, we get

$$\begin{aligned}\dot{\tilde{\mathbf{x}}}(t) &= \mathbf{A}\mathbf{x}(t) + \mathbf{b}u(t) - \mathbf{A}\,\hat{\mathbf{x}}(t) - \mathbf{b}u(t) - \mathbf{mc}(\mathbf{x}(t) - \hat{\mathbf{x}}(t)) \\ &= (\mathbf{A} - \mathbf{mc})\,\tilde{\mathbf{x}}(t)\end{aligned} \tag{13.31}$$

The characteristic equation of the error is given by

$$|s\mathbf{I} - (\mathbf{A} - \mathbf{mc})| = 0 \tag{13.32a}$$

If **m** can (we hope) be chosen so that (**A** – **mc**) has stable and reasonably fast roots, $\tilde{\mathbf{x}}(t)$ will decay to zero irrespective of $\tilde{\mathbf{x}}(0)$. This means that $\hat{\mathbf{x}}(t)$ will converge to $\mathbf{x}(t)$ regardless of the value of $\hat{\mathbf{x}}(0)$, and furthermore, the dynamics of the error can be chosen to be faster than the open-loop dynamics. Note that Eqn. (13.31) is independent of applied control. This is a consequence of assuming **A**, **b** and **c** to be identical in the plant and the observer. Therefore, the estimation error $\tilde{\mathbf{x}}$ converges to zero and remains there, independent of any known forcing function $u(t)$ on the plant and its effect on the state $\mathbf{x}(t)$. If we do not have a very accurate model of the plant (**A**, **b**, **c**), the dynamics of the error are no longer governed by Eqn. (13.31). However, **m** can typically be chosen so that the error system is stable and the error is acceptably small, even with small modelling errors and disturbance inputs.

The selection of **m** can be approached in exactly the same fashion as the selection of **k** is in the control law design. If we specify the desired location of the observer error roots as

$$s = \lambda_1, \lambda_2, \ldots, \lambda_n,$$

the desired observer characteristic equation is

$$(s - \lambda_1)(s - \lambda_2) \cdots (s - \lambda_n) = 0 \tag{13.32b}$$

and one can solve for **m** by comparing coefficients in Eqns (13.32a) and (13.32b). However, as we shall see shortly, this can be done only if the system (13.27) is completely observable.

We can directly use the equations of the control-law design for computing the observer gain matrix **m** if we examine the resemblance between the estimation and control problems. In fact, the two problems are mathematically equivalent. This property is called *duality*. The design of a full-order observer requires the determination of the gain matrix **m** such that (**A** – **mc**) has desired eigenvalues λ_i; $i = 1, 2, \ldots, n$. This is mathematically equivalent to designing a full state-feedback controller for the 'transposed auxiliary system',

$$\dot{\boldsymbol{\zeta}}(t) = \mathbf{A}^T\boldsymbol{\zeta}(t) + \mathbf{c}^T\eta(t) \tag{13.33a}$$

with feedback

$$\eta(t) = -\mathbf{m}^T\boldsymbol{\zeta}(t) \tag{13.33b}$$

so that the closed-loop auxiliary system

$$\dot{\boldsymbol{\zeta}}(t) = (\mathbf{A}^T - \mathbf{c}^T\mathbf{m}^T)\boldsymbol{\zeta}(t) \tag{13.34}$$

has eigenvalues λ_i; $i = 1, 2, \ldots, n$.

Since

$$det\ \mathbf{W} = det\ \mathbf{W}^T,$$

one obtains

$$det\ [s\mathbf{I} - (\mathbf{A}^T - \mathbf{c}^T\mathbf{m}^T)] = det\ [s\mathbf{I} - (\mathbf{A} - \mathbf{mc})]$$

i.e., the eigenvalues of $(\mathbf{A}^T - \mathbf{c}^T\mathbf{m}^T)$ are same as the eigenvalues of (**A** – **mc**).

By comparing the characteristic equation of the closed-loop system (13.7) and that of the auxiliary system (13.34), we obtain the duality relations given in Table 13.1 between the control and estimation problems. The control-design relations given by Eqns (13.16) become the observer-design relations if the substitutions of Table 13.1 are made.

Table 13.1 Duality between control and estimation

Control	*Estimation*
$\mathbf{A}$	$\mathbf{A}^T$
$\mathbf{b}$	$\mathbf{c}^T$
$\mathbf{k}$	$\mathbf{m}^T$

A necessary and sufficient condition for determination of the observer gain matrix $\mathbf{m}$ for the desired eigenvalues of $(\mathbf{A} - \mathbf{mc})$ is that the auxiliary system (13.33) be completely controllable. The controllability condition for this system is that the rank of

$$[\mathbf{c}^T \; \mathbf{A}^T\mathbf{c}^T \cdots (\mathbf{A}^T)^{n-1} \; \mathbf{c}^T]$$

is n. This is the condition for complete observability of the original system defined by Eqns (13.27). This means that a necessary and sufficient condition for estimation of the state of the system defined by Eqns (13.27) is that the system be completely observable.

Example 13.4 We will consider the satellite control system of Example 13.1. The state equation of the plant is

$$\dot{\mathbf{x}} = \mathbf{A}\mathbf{x} + \mathbf{b}u$$

with

$$\mathbf{A} = \begin{bmatrix} 0 & 1 \\ 0 & 0 \end{bmatrix}; \; \mathbf{b} = \begin{bmatrix} 0 \\ 1 \end{bmatrix}$$

$x_1 = \theta$, the orientation of the satellite

$x_2 = \dot{\theta}$

We assume that the orientation θ can be accurately measured from the antenna signal; therefore

$$y = \mathbf{c}\mathbf{x}(t)$$

with

$$\mathbf{c} = [1 \quad 0]$$

Let us design a state observer for the system. We choose the observer to be critically damped with a settling time of 0.4 sec $\left(\dfrac{4}{\zeta\omega_n} = 0.4; \zeta\omega_n = 10\right)$. To satisfy these specifications, the observer poles will be placed at $s = -10, -10$.

The transposed auxiliary system is given by

$$\dot{\boldsymbol{\zeta}} = \mathbf{A}^T\boldsymbol{\zeta} + \mathbf{c}^T\eta$$

$$\eta = -\mathbf{m}^T\boldsymbol{\zeta}$$

The desired characteristic equation of the closed-loop auxiliary system is

$$s^2 + a_1 s + a_2 = (s + 10)(s + 10) = s^2 + 20s + 100$$

To apply pole-placement relations given by Eqns (13.16), we compute

$$\mathbf{U}^{-1} = [\mathbf{c}^T \quad \mathbf{A}^T\mathbf{c}^T]^{-1} = \begin{bmatrix} 1 & 0 \\ 0 & 1 \end{bmatrix}$$

$$\mathbf{p}_1 = [0 \quad 1]\mathbf{U}^{-1} = [0 \quad 1]$$

$$\mathbf{p}_1\mathbf{A}^T = [0 \quad 1]\begin{bmatrix} 0 & 0 \\ 1 & 0 \end{bmatrix} = [1 \quad 0]$$

$$\mathbf{P} = \begin{bmatrix} 0 & 1 \\ 1 & 0 \end{bmatrix}$$

$$\left| s\mathbf{I} - \mathbf{A}^T \right| = s^2 = s^2 + \alpha_1 s + \alpha_2$$

$$\Delta(s) = s^2 + 20s + 100$$

$$\mathbf{m}^T = [a_2 - \alpha_2 \quad a_1 - \alpha_1]\mathbf{P} = [100 \quad 20]\begin{bmatrix} 0 & 1 \\ 1 & 0 \end{bmatrix} = [20 \quad 100]$$

Therefore

$$\mathbf{m} = \begin{bmatrix} 20 \\ 100 \end{bmatrix}$$

13.6.2 Effects of the Addition of an Observer on a Closed-Loop System

In the pole-placement design process, we assumed that the actual state $\mathbf{x}(t)$ was available for feedback. In practice, however, the actual state $\mathbf{x}(t)$ may not be measurable; so we will need to design an observer and use the observed state $\hat{\mathbf{x}}(t)$ for feedback. The design process therefore becomes a two-stage process; the first stage being the determination of the feedback gain matrix $\mathbf{k}$ to yield the desired characteristic equation of the closed-loop system, and the second stage being the determination of the observer gain matrix $\mathbf{m}$ to yield the desired observer characteristic equation.

Let us now investigate the effects of the use of the observed state $\hat{\mathbf{x}}(t)$, rather than the actual state $\mathbf{x}(t)$, on the characteristic equation of the closed-loop system.

Consider the completely controllable and completely observable system defined by the equations

$$\begin{aligned} \dot{\mathbf{x}} &= \mathbf{A}\mathbf{x} + \mathbf{b}u \\ y &= \mathbf{c}\mathbf{x} \end{aligned} \tag{13.35}$$

Suppose we have designed a state-feedback control law

$$u = -\mathbf{k}\mathbf{x} + r \tag{13.36}$$

using the method of Section 13.3. And also suppose we have designed a full-order observer

$$\dot{\hat{\mathbf{x}}} = \mathbf{A}\hat{\mathbf{x}} + \mathbf{b}u + \mathbf{m}(y - \mathbf{c}\hat{\mathbf{x}}) \tag{13.37}$$

using the method described earlier in this section.

For the state-feedback control based on the observed state $\hat{\mathbf{x}}$,

$$u = -\mathbf{k}\hat{\mathbf{x}} + r \tag{13.38}$$

The control system based on combining the state-feedback control law and state observer, has the configuration shown in Fig. 13.9. Note that the number of state variables in the compensator is equal to the order

of the embedded observer and hence is equal to the order of the plant. Thus, the order of the overall closed-loop system, when a full-order observer is used in the compensator, is $2n$ for a plant of order n. We are interested in the dynamic behaviour of the $2n$th-order system comprising the plant and the compensator. With the control law (13.38) used, the plant dynamics become

$$\dot{\mathbf{x}} = \mathbf{A}\mathbf{x} - \mathbf{b}\mathbf{k}\hat{\mathbf{x}} + \mathbf{b}r = (\mathbf{A} - \mathbf{b}\mathbf{k})\mathbf{x} + \mathbf{b}\mathbf{k}(\mathbf{x} - \hat{\mathbf{x}}) + \mathbf{b}r \tag{13.39}$$

The difference between the actual state $\mathbf{x}$ and observed state $\hat{\mathbf{x}}$ has been defined as the error $\tilde{\mathbf{x}}$:

$$\tilde{\mathbf{x}} = \mathbf{x} - \hat{\mathbf{x}}$$

Substitution of the error vector into Eqn. (13.39) gives

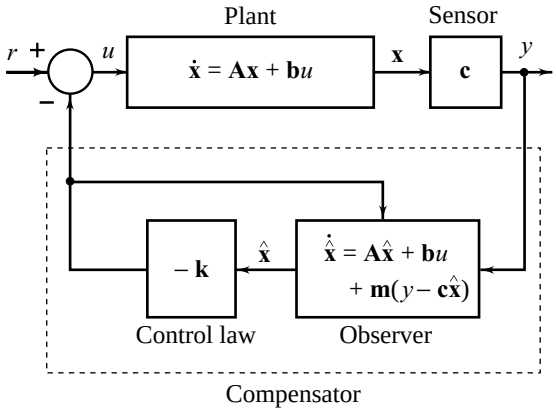

Fig. 13.9 Combined state-feedback control and state estimation

$$\dot{\mathbf{x}} = (\mathbf{A} - \mathbf{b}\mathbf{k})\mathbf{x} + \mathbf{b}\mathbf{k}\tilde{\mathbf{x}} + \mathbf{b}r \tag{13.40}$$

Note that the observer error was given by Eqn. (13.31), repeated here:

$$\dot{\tilde{\mathbf{x}}} = (\mathbf{A} - \mathbf{m}\mathbf{c})\tilde{\mathbf{x}} \tag{13.41}$$

Combining Eqns (13.40) and (13.41), we obtain

$$\begin{bmatrix} \dot{\mathbf{x}} \\ \dot{\tilde{\mathbf{x}}} \end{bmatrix} = \begin{bmatrix} \mathbf{A} - \mathbf{b}\mathbf{k} & \mathbf{b}\mathbf{k} \\ \mathbf{0} & \mathbf{A} - \mathbf{m}\mathbf{c} \end{bmatrix} \begin{bmatrix} \mathbf{x} \\ \tilde{\mathbf{x}} \end{bmatrix} \tag{13.42}$$

Equation (13.42) describes the dynamics of the $2n$-dimensional system of Fig. 13.9. The characteristic equation for the system is

$$|s\mathbf{I} - (\mathbf{A} - \mathbf{b}\mathbf{k})|\,|s\mathbf{I} - (\mathbf{A} - \mathbf{m}\mathbf{c})| = 0$$

In other words, the closed-loop poles of the observed state-feedback control system consist of the poles due to the pole-placement design alone and the poles due to the observer design alone. This means that the pole-placement design and the observer design are independent of each other. They can be designed separately and combined to form the observed state feedback control system. If the order of the plant is n, then the observer is also of n^{th} order (if full-order state observer is used) and the resulting characteristic equation for the entire closed-loop system becomes of order $2n$.

The poles of the observer are usually chosen so that the observer response is much faster than the system response. A rule of thumb is to choose an observer response atleast two to five times faster than the system response. This is to ensure a faster decay of estimation errors compared with the desired dynamics, thus causing the closed-loop poles generated by state feedback to determine the total response.

13.7 DIGITAL CONTROL DESIGN USING STATE FEEDBACK

We have seen in Chapter 12 that linear time-invariant SISO sampled-data systems can be represented by a first-order matrix difference equation of the form (refer Eqns (12.75) and (12.96))

$$\mathbf{x}(k+1) = \mathbf{F}\mathbf{x}(k) + \mathbf{g}u(k) \tag{13.43a}$$

The $n \times 1$ vector $\mathbf{x}(k)$ is the system state, and the $n \times n$ matrix $\mathbf{F}$ is the system matrix that governs how the system internal dynamics will operate. The scalar input $u(k)$ is connected to the system state through $n \times 1$ input matrix $\mathbf{g}$.

The output equation can be expressed as

$$y(k) = \mathbf{c}\mathbf{x}(k) \tag{13.43b}$$

The state $\mathbf{x}(k)$ is connected to the scalar output $y(k)$ through the $1 \times n$ output matrix $\mathbf{c}$.

Much of the algebra for state-space design of sampled-data systems is the same as for the continuous-time case discussed in earlier sections of this chapter. Figure 13.10 shows a structure of state-feedback control for tracking the constant signal r. The poles of the closed-loop sampled-data system can be moved to the desired locations by state-feedback control law of the form

$$u(k) = r - \mathbf{k}\mathbf{x}(k);\ \mathbf{k} = [k_1 \quad k_2 \quad \cdots \quad k_n] \tag{13.44a}$$

such that

$$\left|z\mathbf{I} - (\mathbf{F} - \mathbf{g}\mathbf{k})\right| = \text{desired characteristic polynomial } \Delta(z) \tag{13.44b}$$

provided the system is controllable.

The system is controllable if the controllability matrix

$$\mathbf{U} = [\mathbf{g} \quad \mathbf{F}\mathbf{g} \quad \cdots \quad \mathbf{F}^{n-1}\mathbf{g}] \tag{13.45}$$

is of rank n.

Given the desired characteristic polynomial

$$\begin{aligned}\Delta(z) &= (z - \lambda_1)(z - \lambda_2)\cdots(z - \lambda_n) \\ &= z^n + a_1 z^{n-1} + \cdots + a_{n-1} z + a_n\end{aligned} \tag{13.46a}$$

the required elements of $\mathbf{k}$ are obtained from the following equations (refer Eqns (13.16))

$$\left|z\mathbf{I} - \mathbf{F}\right| = z^n + \alpha_1 z^{n-1} + \cdots + \alpha_{n-1} z + \alpha_n \tag{13.46b}$$

$$\mathbf{k} = [a_n - \alpha_n \quad a_{n-1} - \alpha_{n-1} \quad \cdots \quad a_1 - \alpha_1]\mathbf{P} \tag{13.46c}$$

$$\mathbf{P} = \begin{bmatrix} \mathbf{p}_1 \\ \mathbf{p}_1\mathbf{F} \\ \vdots \\ \mathbf{p}_1\mathbf{F}^{n-1} \end{bmatrix};\ \mathbf{p}_1 = [0 \quad 0 \quad \cdots \quad 0 \quad 1]\mathbf{U}^{-1} \tag{13.46d}$$

Direct substitution of control law (13.44a) into the system equation (13.43a) gives

$$\mathbf{x}(k+1) = (\mathbf{F} - \mathbf{g}\mathbf{k})\,\mathbf{x}(k) + \mathbf{g}\,r \tag{13.47a}$$

As $k \to \infty$, $\mathbf{x}(k+1) - \mathbf{x}(k) \to \mathbf{0}$; $\mathbf{x}(k+1) = \mathbf{x}(k) = \mathbf{x}_s$. At steady state, Eqn. (13.47a) becomes

$$\mathbf{x}_s = (\mathbf{F} - \mathbf{g}\mathbf{k})\mathbf{x}_s + \mathbf{g}\,r$$

which gives

$$\mathbf{x}_s = -(\mathbf{F} - \mathbf{g}\mathbf{k} - \mathbf{I})^{-1}\mathbf{g}\,r \tag{13.47b}$$

or

$$y_s = \mathbf{c}[-(\mathbf{F} - \mathbf{g}\mathbf{k} - \mathbf{I})^{-1}]\mathbf{g}\,r \tag{13.47c}$$

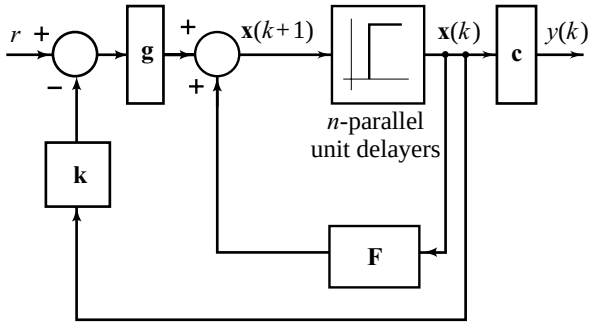

Fig. 13.10 State-feedback control structure for sampled-data systems

A discrete-time state observer has the form

$$\hat{\mathbf{x}}(k+1) = \mathbf{F}\hat{\mathbf{x}}(k) + \mathbf{g}u(k) + \mathbf{m}\big(y(k) - \mathbf{c}\hat{\mathbf{x}}(k)\big) \tag{13.48a}$$

where $\hat{\mathbf{x}}$ is the state estimate, and

$$\mathbf{m} = [m_1 \quad m_2 \quad \cdots \quad m_n]^T \tag{13.48b}$$

are the observer gains.
The error equation

$$\tilde{\mathbf{x}}(k+1) = (\mathbf{F} - \mathbf{mc})\tilde{\mathbf{x}}(k)\,; \quad \tilde{\mathbf{x}} = \mathbf{x} - \hat{\mathbf{x}} \tag{13.48c}$$

can be given any arbitrary dynamics, provided that the system (13.43) is observable, which requires that the observability matrix

$$\mathbf{V} = \begin{bmatrix} \mathbf{c} \\ \mathbf{cF} \\ \vdots \\ \mathbf{cF}^{n-1} \end{bmatrix} \tag{13.49}$$

be of rank n.

To introduce integrator in the control scheme shown in Fig. 13.10, we augment the plant state vector $\mathbf{x}$ with the 'integral state' x_{n+1} that integrates the difference between the output $y(k)$ and the constant reference input r (Fig. 13.11). The 'integral state' x_{n+1} is defined by

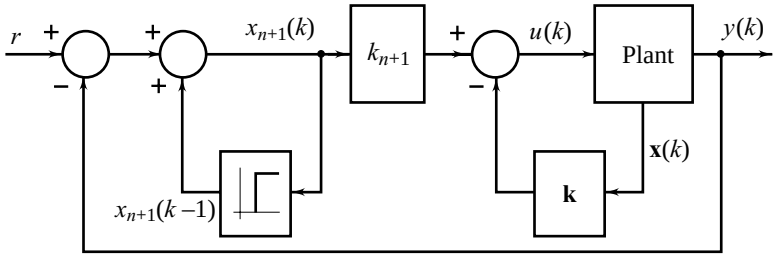

Fig. 13.11 State feedback with integral control for sampled-data systems

$$x_{n+1}(k) = x_{n+1}(k-1) + r - y(k)$$

This equation may be rewritten as

$$\begin{aligned} x_{n+1}(k+1) &= x_{n+1}(k) + r - y(k+1) \\ &= x_{n+1}(k) - \mathbf{c}\left[\mathbf{F}\mathbf{x}(k) + \mathbf{g}u(k)\right] + r \\ &= -\mathbf{c}\mathbf{F}\mathbf{x}(k) + x_{n+1}(k) - \mathbf{c}\mathbf{g}u(k) + r \end{aligned} \tag{13.50}$$

From Eqns (13.43) and (13.50), we obtain

$$\begin{bmatrix} \mathbf{x}(k+1) \\ x_{n+1}(k+1) \end{bmatrix} = \begin{bmatrix} \mathbf{F} & \mathbf{0} \\ -\mathbf{c}\mathbf{F} & 1 \end{bmatrix} \begin{bmatrix} \mathbf{x}(k) \\ x_{n+1}(k) \end{bmatrix} + \begin{bmatrix} \mathbf{g} \\ -\mathbf{c}\mathbf{g} \end{bmatrix} u(k) + \begin{bmatrix} \mathbf{0} \\ 1 \end{bmatrix} r \tag{13.51a}$$

or

$$\bar{\mathbf{x}}(k+1) = \bar{\mathbf{F}}\bar{\mathbf{x}}(k) + \bar{\mathbf{g}}u(k) + \begin{bmatrix} \mathbf{0} \\ 1 \end{bmatrix} r \tag{13.51b}$$

The control

$$u(k) = -\mathbf{k}\mathbf{x}(k) - k_{n+1}x_{n+1}(k) = -\bar{\mathbf{k}}\bar{\mathbf{x}}(k) \tag{13.52}$$

may be obtained from the equations

$$\left|z\mathbf{I} - \left(\bar{\mathbf{F}} - \bar{\mathbf{g}}\bar{\mathbf{k}}\right)\right| = \text{desired } (n+1)^{\text{th}}\text{-order characteristic polynomial} \tag{13.53}$$

Example 13.5 Consider the problem of attitude control of a rigid satellite. A state variable model of the plant is (refer Example (13.1))

$$\dot{\mathbf{x}} = \mathbf{A}\mathbf{x} + \mathbf{b}u = \begin{bmatrix} 0 & 1 \\ 0 & 0 \end{bmatrix} \mathbf{x} + \begin{bmatrix} 0 \\ 1 \end{bmatrix} u$$

where $x_1 = \theta$ is the attitude angle and u is the system input.

The discrete-time description of the plant (assuming that the input u is applied through a zero-order hold (ZOH)) is given below (refer Eqn. (12.75)):

$$\mathbf{x}(k+1) = \mathbf{F}\mathbf{x}(k) + \mathbf{g}u(k) \tag{13.54}$$

where

$$\mathbf{F} = e^{\mathbf{A}T} = \begin{bmatrix} 1 & T \\ 0 & 1 \end{bmatrix}$$

$$\mathbf{g} = \int_0^T e^{\mathbf{A}\tau}\mathbf{b}\,d\tau = \begin{bmatrix} T^2/2 \\ T \end{bmatrix}$$

The characteristic equation of the open-loop system is

$$|z\mathbf{I} - \mathbf{F}| = \begin{vmatrix} z-1 & -T \\ 0 & z-1 \end{vmatrix} = (z-1)^2 = 0$$

It is desired to maintain the attitude of the satellite at $\theta = 0$ (i.e., $r = 0$). This is a regulator problem. With the control law

$$u(k) = -\mathbf{k}\mathbf{x}(k) = -[k_1 \quad k_2]\,\mathbf{x}(k)$$

the closed-loop system becomes

$$\mathbf{x}(k+1) = (\mathbf{F} - \mathbf{g}\mathbf{k})\mathbf{x}(k)$$

The characteristic equation of the closed-loop system is

$$|z\mathbf{I} - (\mathbf{F} - \mathbf{g}\mathbf{k})| = z^2 + (Tk_2 + (T^2/2)k_1 - 2)\,z + (T^2/2)k_1 - Tk_2 + 1 = 0 \quad (13.55a)$$

We assume that $T = 0.1$ sec, and the desired characteristic roots of the closed-loop system are $z_{1,2} = 0.875 \angle \pm 17.9^{\circ}$.

Note that these roots correspond to $\zeta = 0.5$, and $\omega_n = 3.6$ (refer Eqn. (11.47b)):

$$z_{1,2} = e^{-\zeta\omega_n T} e^{\pm j\omega_n T\sqrt{1-\zeta^2}}$$

The desired characteristic equation is then (approximately)

$$z^2 - 1.6z + 0.70 = 0 \quad (13.55b)$$

Matching coefficients in Eqns (13.55a) and (13.55b), we obtain

$$k_1 = 10,\ k_2 = 3.5$$

Example 13.6 Consider the problem of digital control of a plant described by the transfer function

$$G(s) = \frac{1}{s+3}$$

Discretization of the plant model gives (refer Chapter 11)

$$G_{h0}G(z) = \frac{Y(z)}{U(z)} = \mathcal{Z}\left[\left(\frac{1-e^{-sT}}{s}\right)\left(\frac{1}{s+3}\right)\right]$$

$$= (1 - z^{-1})\,\mathcal{Z}\left[\frac{1}{s(s+3)}\right] = \frac{1}{3}\left(\frac{1-e^{-3T}}{z-e^{-3T}}\right)$$

For a sampling interval $T = 0.1$ sec,

$$G_{h0}G(z) = \frac{0.0864}{z-0.741}$$

The difference equation model of the plant is

$$y(k+1) = 0.741y(k) + 0.0864u(k)$$

The plant has a constant reference command signal. We wish to design a PI control algorithm that results in system response characteristics: $\zeta = 0.5$, $\omega_n = 5$. This is equivalent to asking for the closed-loop poles at

$$z_{1,2} = e^{-\zeta\omega_n T} e^{\pm j\omega_n T\sqrt{1-\zeta^2}} = 0.7788 \angle \pm 24.82^{\circ} = 0.7068 \pm j0.3269$$

The desired characteristic equation is therefore

$$(z - 0.7068 - j0.3269)(z - 0.7068 + j0.3269)$$

$$= z^2 - 1.4136z + 0.6065 = z^2 + a_1 z + a_2 = 0$$

Augmenting the plant state $x_1(k) = y(k)$ with the 'integral state' $x_2(k)$ defined by

$$x_2(k) = x_2(k-1) + r - y(k),$$

we obtain

$$\begin{bmatrix} x_1(k+1) \\ x_2(k+1) \end{bmatrix} = \begin{bmatrix} 0.741 & 0 \\ -0.741 & 1 \end{bmatrix} + \begin{bmatrix} x_1(k) \\ x_2(k) \end{bmatrix} u(k) + \begin{bmatrix} 0 \\ 1 \end{bmatrix} r$$

or

$$\bar{\mathbf{x}}(k+1) = \bar{\mathbf{F}}\bar{\mathbf{x}}(k) + \bar{\mathbf{g}}u(k) + \begin{bmatrix} \mathbf{0} \\ 1 \end{bmatrix} r$$

Following the pole-placement relations given by Eqns (13.46), we get

$$\mathbf{U}^{-1} = \begin{bmatrix} \bar{\mathbf{g}} & \bar{\mathbf{F}}\bar{\mathbf{g}} \end{bmatrix}^{-1} = \begin{bmatrix} 0.0864 & 0.064 \\ -0.0864 & -0.15 \end{bmatrix}^{-1} = \begin{bmatrix} 20.1873 & 8.6133 \\ -11.628 & -11.628 \end{bmatrix}$$

$$\mathbf{p}_1 = [0 \quad 1]\mathbf{U}^{-1} = [-11.628 \quad -11.628]$$

$$\mathbf{p}_1\bar{\mathbf{F}} = [0 \quad -11.628]$$

$$\mathbf{P} = \begin{bmatrix} \mathbf{p}_1 \\ \mathbf{p}_1\bar{\mathbf{F}} \end{bmatrix}$$

$$\left| z\mathbf{I} - \bar{\mathbf{F}} \right| = z^2 - 1.741z + 0.741 = z^2 + \alpha_1 z + \alpha_2$$

$$\mathbf{k} = [a_2 - \alpha_2 \quad a_1 - \alpha_1]\mathbf{P} = [-0.1345 \quad 0.328]\mathbf{P}$$

$$= [1.564 \quad -2.25]$$

13.8 FORMULATION OF THE OPTIMAL CONTROL PROBLEM

The command following control structure of Fig.13.2 controls the plant

$$\dot{\mathbf{x}}(t) = \mathbf{A}\mathbf{x}(t) + \mathbf{b}u(t) \tag{13.56a}$$

with the control law

$$u(t) = -\mathbf{k}\mathbf{x}(t) + r \tag{13.56b}$$

The feedback control system obeys the equation

$$\dot{\mathbf{x}}(t) = (\mathbf{A} - \mathbf{b}\mathbf{k})\mathbf{x}(t) + \mathbf{b}r \tag{13.56c}$$

13.8.1 Regulator Problem

In the *regulator problem*, the reference input $r = 0$; the control law for the plant (13.56a) is therefore

$$u(t) = -\mathbf{k}\,\mathbf{x}(t) \tag{13.57a}$$

and the feedback system obeys the equation

$$\dot{\mathbf{x}}(t) = (\mathbf{A} - \mathbf{b}\mathbf{k})\mathbf{x}(t) \tag{13.57b}$$

$\dot{\mathbf{x}}(t) = \mathbf{0}$ in steady-state provided that the feedback system is stable. This means that as $t \to \infty$, the state $\mathbf{x}(t)$ of the regulator (13.57b) must approach the origin of the state space. Therefore at any time t, the state $\mathbf{x}(t)$ represents a deviation of the state dynamics from this desired value, i.e., $\mathbf{x}(t)$ is an error vector. It is desired that the state $\mathbf{x}(t)$, for all possible initial states, asymptotically decays to zero as $t \to \infty$.

The dynamics (speed of response, overshoot, etc.) of the decay, as we have seen earlier in this chapter, can be manipulated by locating the eigenvalues of $(\mathbf{A} - \mathbf{bk})$ at appropriate locations in the complex plane. Here in this section, a somewhat different approach to design is taken. The performance of the system (the decay of state $\mathbf{x}(t)$ to zero as $t \to \infty$) is measured with a single scalar quantity—the *performance index*. The free parameters $\mathbf{k}$ in the state-feedback configuration that optimize the performance index are determined.

Selection of an appropriate performance index is as much a part of the design process as the optimization of the index. We know that the performance of a control system can be adequately specified in terms of settling time, peak overshoot, and steady-state error. An index which is a function of these performance parameters may be selected and optimization (minimization) of this index should lead to an optimal control strategy. Such an index looks quite reasonable; however it is not trackable analytically. A compromise must be made between specifying a performance index which includes all the desired system characteristics, and a performance index which can be minimized with a reasonable amount of computation.

In the following, we present a performance index which includes the desired system characteristics and in addition has good mathematical trackability. This index involves integrating square of system error, and is therefore called *quadratic performance index*:

$$J = \int_0^\infty \left[\mathbf{x}^T(t)\mathbf{x}(t) \right] dt$$

$$= \int_0^\infty \left[x_1^2(t) + x_2^2(t) + \cdots + x_n^2(t) \right] dt$$

where $\mathbf{x}(t)$, a deviation of the system state from the origin of the state space (equilibrium point), is the system error at time t.

In practical systems, the regulation of all the states of the system is not equally important. To be more general,

$$J = \int_0^\infty \left[\mathbf{x}^T(t)\mathbf{Q}\mathbf{x}(t) \right] dt \tag{13.58a}$$

with $\mathbf{Q}$, a $n \times n$ real, symmetric, positive definite constant matrix (refer Chapter 12 for matrix definitions), can be used as a performance measure (A positive semidefinite matrix $\mathbf{Q}$ may also be selected for some control problems (reference [155])).

The simplest form of $\mathbf{Q}$ one can use is a diagonal matrix:

$$\mathbf{Q} = \begin{bmatrix} q_1 & 0 & \cdots & 0 \\ 0 & q_2 & \cdots & 0 \\ \vdots & \vdots & & \vdots \\ 0 & 0 & \cdots & q_n \end{bmatrix} \tag{13.58b}$$

The i^{th} entry of $\mathbf{Q}$ represents the weight the designer places on the constraint on the i^{th} variable. The larger the value of q_i relative to the other values of q, the more control effort is spent to regulate $x_i(t)$.

The design of systems carried out to meet time response specifications through minimization of performance index (13.58a), may be unsatisfactory because it may lead to excessively large control signals. A more realistic solution to the problem is reached if the performance specifications also account for the constraint: $|u(t)| \leq M$, for some constant M.

In the pole-placement design method, the control effort constraints cannot be embedded in the design procedure. Trial-and-error on the selection of poles of the closed-loop system is done and design for each selection is carried out; the design that meets the control effort constraints becomes the outcome of the design procedure. The optimal control techniques, however, allow for the inclusion of control effort constraints in the performance index in the following way:

$$J = \int_0^\infty \left[\mathbf{x}^T(t)\mathbf{Q}\mathbf{x}(t) + \lambda u^2(t) \right] dt \tag{13.58c}$$

where λ, a positive constant, is called the weighting factor. By adjusting λ, we can weigh the relative importance of regulation of $x_i(t)$ and the control effort. By increasing λ, i.e., by giving sufficient weight to control effort, the amplitude of the control signal which minimizes the overall performance index may be kept within practical bounds, although at the expense of poor regulation of $\mathbf{x}(t)$ to the origin.

Compared to state feedback design procedure based on pole placement, in the quadratic optimal control design procedure, the trial-and-error in the selection of the desired closed-loop poles reduces to the trial-and-error in the selection of $\mathbf{Q}$ and λ. For each selection of {$\mathbf{Q}$, λ}, state feedback matrix $\mathbf{k}$ that minimizes the performance index is calculated; the eigenvalues of the matrix $(\mathbf{A} - \mathbf{bk})$ are the corresponding closed-loop poles. In practice, a faster convergence to acceptable performance is achieved this way. This is followed by observer-based state feedback design according to the procedure of Section 13.6, if the assumption of accessibility of each state variable is not satisfied.

13.8.2 Servo Problem/Shifted Regulator Problem

The command-following feedback system is given by Eqn. (13.56c). For a constant r, $\dot{\mathbf{x}}(t) = \mathbf{0}$ in steady-state provided that the system is stable. This means that steady-state solution $\mathbf{x}_s$ must satisfy the equation

$$\mathbf{x}_s = -(\mathbf{A} - \mathbf{bk})^{-1}\mathbf{b}r \tag{13.59}$$

Therefore at any time t, $(\mathbf{x}(t) - \mathbf{x}_s)$ represents a deviation of the state dynamics from the desired value, i.e., $\mathbf{x}(t) - \mathbf{x}_s = \tilde{\mathbf{x}}(t)$ is an error vector.

We can formulate this servo problem as a shifted regulator problem by shifting the origin of the state space to the steady-state point $\mathbf{x}_s$. The resulting regulator system has state $\tilde{\mathbf{x}}(t)$ and it is desired that $\tilde{\mathbf{x}}(t)$ decays to the origin of the state space asymptotically.

13.8.3 Solution of Regulator Problem

For want of space, the solution of the linear quadratic optimal control problem is not being covered in this chapter; the detailed account of the subject is given in the companion book [155].

A method suitable for computer calculation is stated without proof in the following paragraph. Consider the uncompensated single-input system

$$\dot{\mathbf{x}} = \mathbf{A}\mathbf{x} + \mathbf{b}u,$$

with feedback

$$u = -\mathbf{kx}$$

The performance index is

$$J = \int_0^\infty (\mathbf{x}^T\mathbf{Q}\mathbf{x} + \lambda u^2)dt$$

The index is minimized when

$$\mathbf{k} = \lambda^{-1}\mathbf{b}^T\mathbf{P}$$

The $(n \times n)$ matrix $\mathbf{P}$ is determined from the solution of the equation

$$\mathbf{A}^T\mathbf{P} + \mathbf{PA} - \mathbf{Pb}\lambda^{-1}\mathbf{b}^T\mathbf{P} + \mathbf{Q} = \mathbf{0} \tag{13.60}$$

Equation (13.60) can be easily programmed for a computer or solved using MATLAB refer Appendix A. Equation (13.60) is often called the *Riccati equation*.

Review Examples

Review Example 13.1 In the following, we consider the problem of design of a type-1 servo system when the plant has an integrator. General configuration of such a system is shown in Fig. 13.12. Here we assumed that $y = x_1$ (by a proper choice of a set of state variables, it is possible to choose the output equal to one of the state variables; refer Chapter 12).

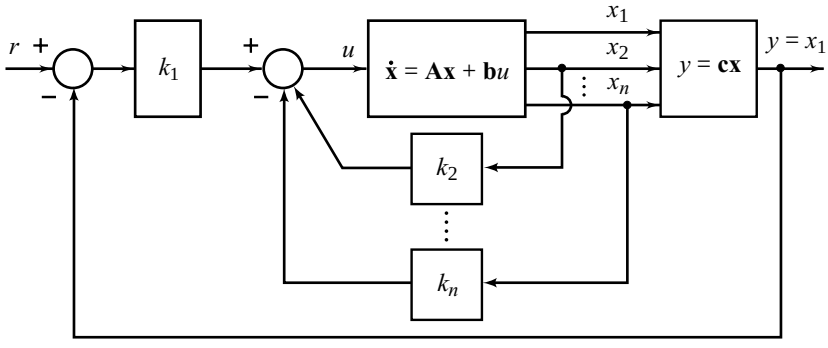

Fig.13.12 Design of a type-1 servo system when the plant has an integrator

The state feedback control law for the configuration of Fig. 13.12 is

$$\begin{aligned} u &= k_1(r - x_1) - k_2x_2 - \cdots - k_nx_n \\ &= -\mathbf{kx} + k_1r; \quad \mathbf{k} = \begin{bmatrix} k_1 & k_2 & \cdots & k_n \end{bmatrix} \end{aligned} \tag{13.61}$$

For a constant reference input r, the desired steady state is

$$\mathbf{x}_s = [r \quad 0 \quad 0 \cdots 0]^T \tag{13.62}$$

which is a non-null state.

As the plant has integrating property, the steady-state value u_s of the input u must be zero (otherwise the output cannot stay constant).

The state error vector

$$\tilde{\mathbf{x}}(t) = \mathbf{x}(t) - \mathbf{x}_s \tag{13.63a}$$

Differentiating both sides we get

$$\dot{\tilde{\mathbf{x}}}(t) = \dot{\mathbf{x}}(t) - \dot{\mathbf{x}}_s = \mathbf{A}\mathbf{x}(t) + \mathbf{b}u(t) - \mathbf{A}\mathbf{x}_s - \mathbf{b}u_s$$

Since $u_s = 0$, we have

$$\dot{\tilde{\mathbf{x}}}(t) = \mathbf{A}\tilde{\mathbf{x}}(t) + \mathbf{b}u(t) \tag{13.63b}$$

In terms of the state error vector $\tilde{\mathbf{x}}$, the state-feedback control law (13.61) becomes

$$u(t) = -\mathbf{k}\tilde{\mathbf{x}}(t) \tag{13.64}$$

The dynamics of $\tilde{\mathbf{x}}$ is thus given by

$$\dot{\tilde{\mathbf{x}}}(t) = (\mathbf{A} - \mathbf{b}\mathbf{k})\tilde{\mathbf{x}}(t) \tag{13.65}$$

We shall design the type-1 servo system such that the eigenvalues of $(\mathbf{A} - \mathbf{b}\mathbf{k})$ are located at desired positions. The designed system will be an asymptotically stable system: as $t \to \infty$, $\tilde{\mathbf{x}} \to \mathbf{0}$, $(\mathbf{x} \to [r \;\; 0 \cdots 0])$, $y = x_1 \to r$ and $u \to 0$.

As an example, consider the attitude control system for a rigid satellite. The plant equations are (refer Example 13.1)

$$\dot{\mathbf{x}} = \mathbf{A}\mathbf{x} + \mathbf{b}u$$
$$y = \mathbf{c}\mathbf{x}$$

where

$$\mathbf{A} = \begin{bmatrix} 0 & 1 \\ 0 & 0 \end{bmatrix}; \quad \mathbf{b} = \begin{bmatrix} 0 \\ 1 \end{bmatrix}; \quad \mathbf{c} = [1 \;\; 0]$$

$$x_1(t) = \text{position } \theta(t); \quad x_2(t) = \text{velocity } \dot{\theta}(t)$$

The reference input $r = \theta_r$, is a step function. It is a servo problem.

In Example 13.1, we found that the eigenvalues of $(\mathbf{A} - \mathbf{b}\mathbf{k})$ are placed at the desired locations $-4 \pm j4$ when

$$\mathbf{k} = [k_1 \quad k_2] = [32 \quad 8]$$

In terms of the shifted state variables,

$$\tilde{x}_1 = x_1 - \theta_r, \; \tilde{x}_2 = x_2,$$

the control law is

$$u = -k_1\tilde{x}_1 - k_2\tilde{x}_2$$

In terms of original state variables,

$$u = -k_1x_1 - k_2x_2 + k_1\theta_r = -\mathbf{k}\mathbf{x} + k_1\theta_r$$

Figure 13.13 shows a configuration for attitude control of the satellite.

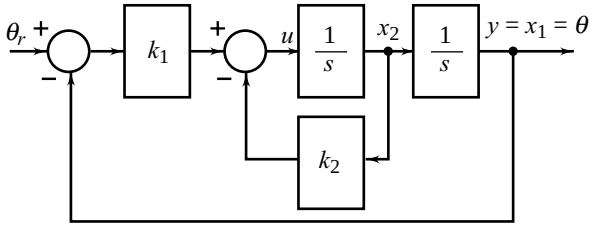

Fig. 13.13 Attitude control of a satellite

Review Example 13.2 The system considered in this example is the attitude control system for a rigid satellite. The plant equations are (refer Example 13.5)

$$\mathbf{x}(k+1) = \mathbf{F}\mathbf{x}(k) + \mathbf{g}u(k)$$

where

$$\mathbf{F} = \begin{bmatrix} 1 & T \\ 0 & 1 \end{bmatrix}; \mathbf{g} = \begin{bmatrix} T^2/2 \\ T \end{bmatrix}; T = 0.1 \text{ sec}$$

$$x_1(k) = \text{position state } \theta$$

$$x_2(k) = \text{velocity state } \omega$$

The reference input $r = \theta_r$, a step function. The desired steady-state

$$\mathbf{x}_s = [\theta_r \quad 0]^T$$

which is a non-null state. It is a servo problem.

As the plant has integrating property, the steady-state value u_s of the input must be zero (otherwise the output cannot stay constant). For this case, the shifted regulator problem may be formulated as follows:

$$\tilde{x}_1 = x_1 - \theta_r$$

$$\tilde{x}_2 = x_2$$

Shifted state variables satisfy the equations

$$\tilde{\mathbf{x}}(k+1) = \mathbf{F}\tilde{\mathbf{x}}(k) + \mathbf{g}u(k)$$

The state-feedback control

$$u(k) = -\mathbf{k}\tilde{\mathbf{x}}(k)$$

results in the dynamics of $\tilde{\mathbf{x}}$ given by

$$\tilde{\mathbf{x}}(k+1) = (\mathbf{F} - \mathbf{g}\mathbf{k})\tilde{\mathbf{x}}(k)$$

We now determine the gain matrix $\mathbf{k}$ such that the desired characteristic equation is

$$z^2 = 0 = z^2 + a_1 z + a_2$$

$$\mathbf{U}^{-1} = [\mathbf{g} \quad \mathbf{F}\mathbf{g}]^{-1} = \begin{bmatrix} 0.005 & 0.015 \\ 0.1 & 0.1 \end{bmatrix}^{-1} = \begin{bmatrix} -100 & 15 \\ 100 & -5 \end{bmatrix}$$

$$\mathbf{p}_1 = [0 \quad 1]\mathbf{U}^{-1} = [100 \quad -5]$$

$$\mathbf{p}_1\mathbf{F} = [100 \quad 5]$$

$$\mathbf{p} = \begin{bmatrix} 100 & -5 \\ 100 & 5 \end{bmatrix}$$

$$|z\mathbf{I} - \mathbf{F}| = z^2 - 2z + 1 = z^2 + \alpha_1 z + \alpha_2$$

$$\mathbf{k} = [a_2 - \alpha_2 \quad a_1 - \alpha_1]\mathbf{P} = [-1 \quad 2]\mathbf{p}$$

$$= [100 \quad 15]$$

The control law expressed in terms of original state variables is given as

$$u(k) = -k_1 \tilde{x}_1(k) - k_2 \tilde{x}_2(k) = -100(x_1(k) - \theta_r) - 15x_2(k)$$

Review Example 13.3 Reconsider the problem of attitude control of a satellite. For implementation of the design of the previous review example, we require the states $x_1(k)$ and $x_2(k)$ to be measurable. Assuming that the output $y(k) = x_1(k)$ is the only state variable that can be measured, we design a state observer for the system. It is desired that the error vector exhibit response given by the characteristic equation $z^2 = 0 = z^2 + a_1 z + a_2$.

The measurement equation is

$$y(k) = \mathbf{cx}(k) = [1 \quad 0]\mathbf{x}(k)$$

The state observer for the system is given as

$$\hat{\mathbf{x}}(k+1) = \mathbf{F}\hat{\mathbf{x}}(k) + \mathbf{g}u(k) + \mathbf{m}(y(k) - \mathbf{c}\hat{\mathbf{x}}(k))$$

The gains **m** may be calculated by solving the state regulator design problem for the 'transposed auxiliary system'

$$\boldsymbol{\zeta}(k+1) = \mathbf{F}^T\boldsymbol{\zeta}(k) + \mathbf{c}^T\eta(k)$$

$$\eta(k) = -\mathbf{m}^T\boldsymbol{\zeta}(k)$$

$$\mathbf{p}_1 = [0 \quad 1]\mathbf{U}^{-1} = [0 \quad 10]$$

$$\mathbf{p}_1\mathbf{F}^T = [1 \quad 10]$$

$$\mathbf{P} = \begin{bmatrix} 0 & 10 \\ 1 & 10 \end{bmatrix}$$

$$\left|z\mathbf{I} - \mathbf{F}^T\right| = z^2 - 2z + 1 = z^2 + \alpha_1 z + \alpha_2$$

$$\mathbf{m}^T = [a_2 - \alpha_2 \quad a_1 - \alpha_1]\mathbf{P} = [-1 \quad 2]\mathbf{P} = [2 \quad 10]$$

Review Questions

1. Briefly describe the configuration of a state feedback control system. What is the advantage that state variable methods have over the root-locus techniques in the placement of closed-loop poles for transient response design? What are the associated problems to be tackled to utilize this advantage?
2. Under what conditions can the state feedback matrix be selected so that the roots of the characteristic equation of the closed-loop system are arbitrarily placed? What is the advantage of using the linear quadratic optimal control in designing the state feedback matrix?
3. A high-order plant is controllable but state variables have not been selected in controllable canonical form. Derive an algorithm for state feedback design of such a system.
4. Pole-placement design of a servo system using state feedback leads to an unacceptable steady-state error. Describe a configuration employing state feedback with integral control for improving the steady-state performance.
5. What is an observer? Under what conditions would you use an observer in your state feedback design of a control system? Briefly describe the configuration of an observer.

6. An observer-based state feedback control system has a characteristic equation of order $2n$. Show that the placement of $2n$ roots of this equation can be done in a two-stage process: the first stage being the determination of the feedback gain matrix to yield the desired n^{th}-order characteristic equation of the closed-loop system, and the second stage being determination of the observer gain matrix to yield the desired n^{th}-order observer characteristic equation.
7. Briefly describe the configuration of a sampled-data system employing state feedback. Modify this configuration by introducing 'integral state' to improve steady-state performance.

Problems

13.1 A regulator system has the plant

$$\dot{\mathbf{x}} = \begin{bmatrix} 0 & 1 & 0 \\ 0 & 0 & 1 \\ -6 & -11 & -6 \end{bmatrix} \mathbf{x} + \begin{bmatrix} 0 \\ 0 \\ 1 \end{bmatrix} u$$

$$y = [1 \quad 0 \quad 0]\,\mathbf{x}$$

(a) Design a state-feedback controller which will place the closed-loop poles at $-2 \pm j3.464, -5$. Give a block diagram of the control configuration.

(b) Design a full-order state observer; the observer-error poles are required to be located at $-2 \pm j3.464, -5$. Give all the relevant observer equations and a block diagram description of the observer structure.

13.2 A regulator system has the plant

$$\dot{\mathbf{x}} = \mathbf{A}\mathbf{x} + \mathbf{b}u$$

$$y = \mathbf{c}\mathbf{x}$$

with

$$\mathbf{A} = \begin{bmatrix} 0 & 0 & -6 \\ 1 & 0 & -11 \\ 0 & 1 & -6 \end{bmatrix}; \mathbf{b} = \begin{bmatrix} 1 \\ 0 \\ 0 \end{bmatrix}; \mathbf{c} = [0 \quad 0 \quad 1]$$

(a) Compute $\mathbf{k}$ so that the control law $u = -\mathbf{k}\mathbf{x}$ places the closed-loop poles at $-2 \pm j3.464, -5$. Give the state variable model of the closed-loop system.

(b) For the estimation of the state vector $\mathbf{x}$, we use an observer defined by

$$\dot{\hat{\mathbf{x}}} = (\mathbf{A} - \mathbf{mc})\,\hat{\mathbf{x}} + \mathbf{b}u + \mathbf{m}y$$

Compute $\mathbf{m}$ so that the eigenvalues of $(\mathbf{A} - \mathbf{mc})$ are located at $-2 \pm j3.464, -5$.

13.3 Consider the system with the transfer function

$$\frac{Y(s)}{U(s)} = \frac{9}{s^2 - 9}$$

(a) Find $(\mathbf{A}, \mathbf{b}, \mathbf{c})$ for this system in observable canonical form.

(b) Compute $\mathbf{k}$ so that the control law $u = -\mathbf{k}\mathbf{x}$ places the closed-loop poles at $-3 \pm j3$.

(c) Design a full-order observer such that the observer-error poles are located at $-6 \pm j6$. Give all the relevant observer equations.

13.4 The equation of motion of an undamped oscillator with frequency ω_0 is

$$\ddot{y} + \omega_0^2 y = u$$

(a) Write the equations of motion in the state variable form with $x_1 = y$ and $x_2 = \dot{y}$ as the state variables.

(b) Find k_1 and k_2 such that $u = -k_1 x_1 - k_2 x_2$ gives closed-loop characteristic roots with $\omega_n = 2\omega_0$ and $\zeta = 1$.

(c) Design a second-order observer that estimates x_1 and x_2, given measurements of x_1. Pick the characteristic roots of the state-error equation with $\omega_n = 10\omega_0$ and $\zeta = 1$. Give a block diagram of the observer-based state-feedback control system.

13.5 A regulator system has the plant

$$\dot{\mathbf{x}} = \begin{bmatrix} 0 & 1 \\ 20.6 & 0 \end{bmatrix} \mathbf{x} + \begin{bmatrix} 0 \\ 1 \end{bmatrix} u$$

$$y = [1 \quad 0]\, \mathbf{x}$$

(a) Design a control law $u = -\mathbf{k}\mathbf{x}$ so that the closed-loop system has eigenvalues at $-1.8 \pm j2.4$.

(b) Design a full-order state observer to estimate the state vector. The observer matrix is required to have eigenvalues at $-8, -8$.

13.6 A regulator system has the double integrator plant

$$\frac{Y(s)}{U(s)} = \frac{1}{s^2}$$

(a) Taking $x_1 = y$ and $x_2 = \dot{y}$ as state variables, obtain the state variable model of the plant.

(b) Compute $\mathbf{k}$ such that $u = -\mathbf{k}\mathbf{x}$ gives closed-loop characteristic roots with $\omega_n = 1$, $\zeta = \sqrt{2}/2$.

(c) Design a full-order observer that estimates x_1 and x_2, given measurements of x_1. Pick the characteristic roots of the state-error equation with $\omega_n = 5$, $\zeta = 0.5$.

13.7 A servo system has the type-1 plant described by the equation

$$\dot{\mathbf{x}} = \mathbf{A}\mathbf{x} + \mathbf{b}u$$

$$y = \mathbf{c}\mathbf{x}$$

where

$$\mathbf{A} = \begin{bmatrix} 0 & 1 & 0 \\ 0 & -1 & 1 \\ 0 & 0 & -2 \end{bmatrix}; \mathbf{b} = \begin{bmatrix} 0 \\ 0 \\ 1 \end{bmatrix}; \mathbf{c} = [1 \quad 0 \quad 0]$$

(a) If $u = -\mathbf{k}\mathbf{x} + Nr$, compute $\mathbf{k}$ and N so that the closed-loop poles are located at $-1 \pm j\,1, -2$; and $y(\infty) = r$, a constant reference input.

(b) For the estimation of the state vector $\mathbf{x}$, we use a full-order observer

$$\dot{\hat{\mathbf{x}}} = (\mathbf{A} - \mathbf{m}\mathbf{c})\,\hat{\mathbf{x}} + \mathbf{b}u + \mathbf{m}y$$

Compute $\mathbf{m}$ so that observer-error poles are located at $-2 \pm j2, -4$.

(c) Replace the control law in (a) by $u = -\mathbf{k}\,\hat{\mathbf{x}} + Nr$, and give a block diagram of the observer-based servo system.

13.8 A plant is described by the equation

$$\dot{\mathbf{x}} = \begin{bmatrix} -1 & 0 \\ 0 & -2 \end{bmatrix} \mathbf{x} + \begin{bmatrix} 1 \\ 1 \end{bmatrix} u$$

$$y = [1 \quad 3]\,\mathbf{x}$$

Add to the plant equations an integrator $\dot{x}_3 = r - y$ (r is a constant reference input) and select gains $\mathbf{k}$, k_3 so that if $u = -\mathbf{kx} - k_3 x_3$, the closed-loop poles are at $-2, -1 \pm j\sqrt{3}$. Give a block diagram of the control configuration.

13.9 Figure P13.9 shows control configuration of a type-1 servo system. Both the state variables x_1 and x_2 are assumed to be measurable. It is desired to regulate the output y to a constant value $r = 5$. Find the values of k_1, k_2 and N so that

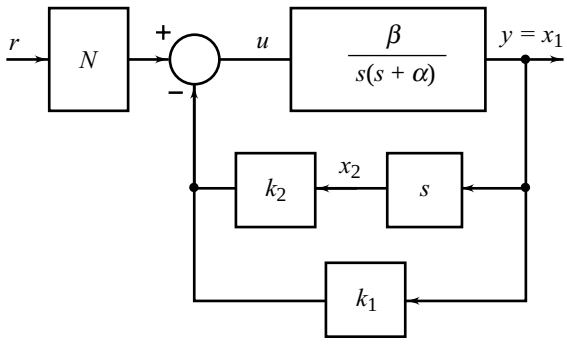

Fig. P13.9

(i) $y(\infty) = r = 5$

(ii) The closed-loop characteristic equation is

$$s^2 + a_1 s + a_2 = 0$$

13.10 The plant of a servo system is described by the equations

$$\dot{\mathbf{x}} = \mathbf{Ax} + \mathbf{b}u$$

$$y = \mathbf{cx}$$

where

$$\mathbf{A} = \begin{bmatrix} -3 & 2 \\ 4 & -5 \end{bmatrix}; \quad \mathbf{b} = \begin{bmatrix} 1 \\ 0 \end{bmatrix}; \quad \mathbf{c} = [0 \quad 1]$$

A control law of the form $u = -\mathbf{kx} + r$ is proposed; r is a constant reference input.

(a) Compute $\mathbf{k}$ so that the eigenvalues of $(\mathbf{A} - \mathbf{bk})$ are $-4, -7$.

(b) Show that the steady-state error to a constant input r is non-zero.

(c) Add to the plant equation, an integrator equation ($x_3(t)$ being the state of the integrator):

$$\dot{x}_3(t) = r - y(t)$$

and select gains k_1, k_2 and k_3 so that the control law $u = -k_1 x_1(t) - k_2 x_2(t) - k_3 x_3(t)$ places the eigenvalues of closed-loop system matrix at $-1, -2, -7$.

(d) Draw a block diagram of the control scheme employing integral control and show that the steady-state error to constant reference input is zero.

13.11 A discrete-time regulator system has the plant

$$\mathbf{x}(k+1) = \begin{bmatrix} 0 & 1 & 0 \\ 0 & 0 & 1 \\ -4 & -2 & -1 \end{bmatrix} \mathbf{x}(k) + \begin{bmatrix} 0 \\ 0 \\ 1 \end{bmatrix} u(k)$$

Design a state-feedback controller which will place the closed-loop poles at $-\frac{1}{2} \pm j\frac{1}{2}$, 0. Give a block diagram of the control configuration.

13.12 Consider the system defined by

$$\mathbf{x}(k+1) = \begin{bmatrix} 0 & 1 & 0 \\ 0 & 0 & 1 \\ -0.5 & -0.2 & 1.1 \end{bmatrix} \mathbf{x}(k) + \begin{bmatrix} 0 \\ 0 \\ 1 \end{bmatrix} u(k)$$

Determine the state-feedback gain matrix **k** such that when the control signal is given by $u(k) = -\mathbf{k}\mathbf{x}(k)$, the closed-loop system will have all poles at $z = 0$. Give the state variable model of the closed-loop system.

13.13 A discrete-time regulator system has the plant

$$\mathbf{x}(k+1) = \begin{bmatrix} 2 & -1 \\ -1 & 1 \end{bmatrix} \mathbf{x}(k) + \begin{bmatrix} 4 \\ 3 \end{bmatrix} u(k)$$

$$y(k) = [1 \quad 1]\, \mathbf{x}(k)$$

(a) Design a state-feedback control algorithm $u(k) = -\mathbf{k}\mathbf{x}(k)$ which places the closed-loop characteristic roots at $\pm j\frac{1}{2}$.

(b) Design a state observer which has both the characteristic roots at $z = 0$. Give the relevant observer equations.

13.14 A regulator system has the plant with transfer function

$$\frac{Y(z)}{U(z)} = \frac{z^{-2}}{(1+0.8z^{-1})(1+0.2z^{-1})}$$

(a) Find (**F**, **g**, **c**) for the plant in controllable canonical form.

(b) Find k_1 and k_2 such that $u(k) = -k_1x_1(k) - k_2x_2(k)$ gives closed-loop characteristic roots at $0.6 \pm j0.4$.

13.15 A double integrator plant is to be controlled by a digital computer employing state-feedback. Figure P13.15 shows a model of the control scheme. Both the state variables x_1 and x_2 are assumed to be measurable.

(a) Obtain the discrete-time state variable model of the plant.

(b) Compute k_1 and k_2 so that the response $y(t)$ of the closed-loop system has the parameters: $\zeta = 0.5$, $\omega_n = 4$.

(c) Assume now that only x_1 is measurable. Design a state observer to estimate the state vector **x**; both the characteristic roots of the observer are required to be at $z = 0$.

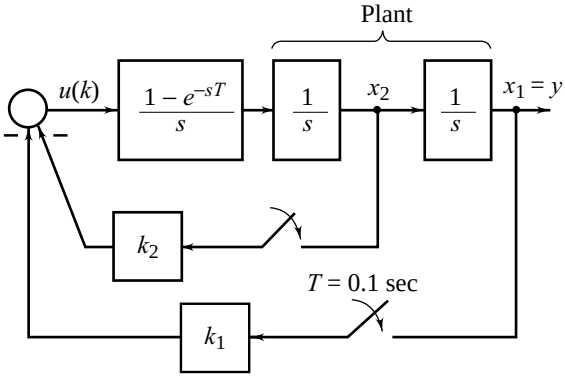

Fig. P13.15

13.16 Figure P13.16 shows the block diagram of a digital positioning system. The plant is a dc motor driving inertia load. Both the position θ and velocity $\dot{\theta}$ are measurable.

(a) Obtain matrices (**F**, **g**, **c**) of the discrete-time state variable model of the plant.

(b) Compute k_1 and k_2 so that the closed-loop system has all characteristic roots at $z = 0$.

(c) Assume now that the position θ is measured by a shaft encoder and a second-order state observer is used to estimate the state vector $\mathbf{x}$ from plant input u and measurements of θ. Design a state observer with characteristic roots at $z = 0$. Give a block diagram of the observer-based digital positioning system.

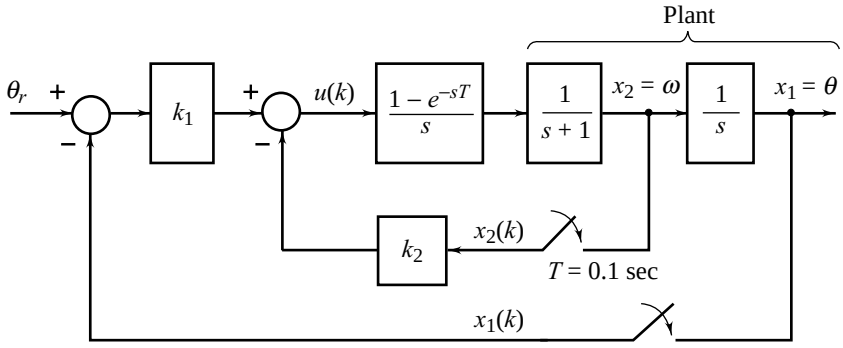

Fig. P13.16

13.17 A continuous-time plant described by the equation

$$\dot{y} = -y + u$$

is to be controlled by a digital computer; y is the output, and u is the input. Sampling interval $T = 1$ sec.

(a) Obtain a discrete-time state variable model of the plant.

(b) Compute K so that the control law

$$u(k) = -Ky(k) + r$$

results in a response $y(t)$ with time constant 0.5 sec.

(c) Show that the steady-state error to a constant reference input r is non-zero for the above choice of the control scheme.

(d) Add to the plant equation, an integrator equation ($x_2(k)$ being the integral state; $x_1(k) = y(k)$)

$$x_2(k) = x_2(k-1) + r - x_1(k)$$

and select gains K_1 and K_2 so that the control law

$$u = -K_1 x_1(k) - K_2 x_2(k)$$

results in a response $y(t)$ with parameters: $\zeta = 0.5$, $\omega_n = 4$.

(e) Give a block diagram depicting the control configuration employing integral control and show that the steady-state error to constant input r is zero.

Nonlinear Systems Analysis

14

14.1 INTRODUCTION

As we have tried to make clear in the previous chapters, every real control system is nonlinear, and the linear analysis and design methods we have described use linear approximations to the real models. The linear control design relies on the key assumption of a small range of operation for the linear model to be valid. In practice, because of unforeseen reasons, when the operation range exceeds and invalidates the key assumption of design, the linear controller is likely to perform very poor or to be unstable, because the nonlinearities in the system cannot be properly compensated for. Also, in designing linear controllers it is usually necessary to assume that the parameters of the system model are reasonably well known. However, as we have seen in earlier chapters, many control problems involve uncertainties in the model parameters. A linear controller based on inaccurate values of the model parameters may exhibit significant performance degradation or even instablility in practice. Thus, the design based on approximation of the real models requires rigorous analysis before it is put to practice. The analysis must be carried out to determine tolerance bounds on uncertainties in models used for design, i.e., the analysis must determine a family of models for which the design gives an acceptable performance. The analysis must also consider the situations wherein the linearity range is violated in practice.

Perhaps the single most valuable asset in the field of engineering is the simulation tool—constructing a model of the proposed or actual system and using a numerical solution of the model to reveal the behaviour of the system. Simulation is the only general method of analysis applicable to finding effects of uncertainties and/or nonlinearities on the performance of a control system. Of course, simulation finds *specific* solutions; that is, solutions to the system response with specific inputs, initial conditions; and parametric conditions. Important properties such as stability and conditional stability are not *proven* with simulations. When the complexity of a system precludes the use of any analytical approach, simulation will be the only way to obtain necessary information for design purposes. Throughout the book so for, we have been dependent on simulations for the analysis of the effects of uncertainties and/or nonlinearities.

This chapter also does not provide a magic solution to the analysis problem. In fact, no universal analytical technique exists that can cater to our demand on analysis of the effects of uncertainties and/or

nonlinearities. Our focus in this chapter is only on some important categories of nonlinear systems for which significant analysis (and design) can be done.

Describing Function Analysis For the so-called *separable* systems, which comprise a linear part defined by its transfer function, and a nonlinear part defined by a time-independent relationship between its input and output variables, the *describing function method* is most practically useful for analysis. It is an approximate method but experience with real systems and computer simulation results shows adequate accuracy in many cases. Basically the method is an approximate extension of frequency response methods (including Nyquist stability criterion) to nonlinear systems.

In terms of mathematical properties, nonlinearities may be categorized as *continuous* and *discontinuous*. Because discontinuous nonlinearities cannot be locally approximated by linear functions, they are also called "hard" nonlinearities. Hard nonlinearities are commonly found in control systems, both in small range operation and large range operation (Review Example 10.4 shows separable nonlinearities: saturation, deadzone, backlash, Coulomb friction, in a servo system). Whether a system in small range operation should be regarded as nonlinear or linear depends on the magnitude of the hard nonlinearities and on the extent of their effects on the system performance.

The continuous or so-called "soft" nonlinearities are present in every control system, though not visible because these are not separable. Throughout the book we have neglected these nonlinearities in our derivations of transfer function and state variable models. For example, we have assumed linear restoring force of a spring, a constant damping coefficient independent of the position of the mass, etc. In practice, none of these assumptions is true for a large range operation. Also there are situations, not covered in this book, wherein the linearity assumption gives too small range of operation to be useful; linear design methods cannot be applied for such systems. If the controlled systems are not too complex and the performance requirements are not too stringent, the linearity assumptions made in this book give satisfactory results in practice.

For the category of separable systems, as we shall see later in this chapter, the predictions of describing function analysis usually are a good approximation to actual behaviour when the linear part of the system provides a sufficiently strong filtering effect. Filtering characteristics of the linear part of a system improve as the order of the system goes up. The 'lowpass filtering' requirement is never completely satisfied; for this reason the describing function method is mainly used for stability analysis and is not directly applied to the optimization of system design.

Phase Plane Analysis Another practically useful method for nonlinear system analysis is the *phase-plane method*. While phase-plane analysis does not suffer from any approximations and hence can be used for stability analysis as well as optimization of system design, its main limitation is that it is applicable to systems which can be well approximated by second-order dynamics. Its basic idea is to solve second-order differential equation and graphically display the result as a family of system motion trajectories on a two-dimensional plane, called the *phase-plane*, which allows us to visually observe the motion patterns of the system. The method is equally applicable to both hard and soft nonlinearities.

Lyapunov Stability Analysis The most fundamental analysis tool is the concept of a Lyapunov function and its use in nonlinear stability analysis. The power of the method comes from its generality; it is applicable to all kinds of control systems; systems with hard or soft nonlinearities, and of second-order or higher-order. The limitation of the method lies in the fact that it is often difficult to find a Lyapunov function for a given system.

The aim of this chapter is to introduce the two classical, yet practically important tools—the describing function method and the phase-plane method—for a class of nonlinear systems. The two methods are

complementary to a large extent, each being available for the study of the systems which are most likely to be beyond the scope of the other. The phase-plane analysis applies primarily to systems described by second-order differential equations. Systems of order higher than the second are likely to be well filtered and tractable by the describing function method.

A brief introduction to Lyapunov stability analysis will also be given in this chapter.

14.2 SOME COMMON NONLINEAR SYSTEM BEHAVIOURS

As a minimum, it is important to be aware of the main characteristics of nonlinear behaviour, only to permit recognition if these are encountered experimentally or in system simulations.

The previous chapters have been predominantly concerned with the study of linear time-invariant control systems. We have observed that these systems have quite simple properties, such as

- a linear system $\dot{\mathbf{x}} = \mathbf{A}\mathbf{x}$, with $\mathbf{x}$ being the vector of states and $\mathbf{A}$ being the system matrix, has a *unique equilibrium point* (if $\mathbf{A}$ is nonsingular; normally true for feedback system matrices);
- the equilibrium point is stable if all eigenvalues of $\mathbf{A}$ have negative real parts, *regardless of initial conditions*;
- the transient response is composed of the natural modes of the system, and the general solution can be solved analytically;
- in the presence of the external input $u(t)$, the system response has a number of interesting properties: (i) it satisfies the *principle of superposition*, (ii) the asymptotic stability of the system implies bounded-input bounded-output stability, and (iii) a sinusoidal input leads to a sinusoidal output of the same frequency.

The behaviour of nonlinear systems, however, is much more complex. Due to the lack of superposition property, nonlinear systems respond to external inputs and initial conditions quite differently from linear systems. Some common nonlinear system properties are as follows [126]:

1. Nonlinear systems frequently have more than one equilibrium point. For a linear system, stability is seen by noting that for *any* initial condition, the motion of a stable system always converges to the equilibrium point. However, a nonlinear system may converge to an equilibrium point starting with one set of the initial conditions, and may go to infinity starting with another set of initial conditions. This means that the stability of nonlinear systems may depend on initial conditions. In the presence of a bounded external input, unlike linear systems, stability of nonlinear systems may also be dependent on the input value.
2. Nonlinear systems can display oscillations of fixed amplitude and fixed period without external excitation. These oscillations are called *limit cycles*. Consider the well-known *Van der Pol's differential equation*

$$M\ddot{y} + B(y^2 - 1)\dot{y} + Ky = 0; M > 0, B > 0, K > 0 \tag{14.1}$$

which describes physical situations in many nonlinear systems. It can be regarded as describing a mass-spring-damper system with a position-dependent damping coefficient $B(y^2 - 1)$. For large values of y, the damping coefficient is positive and the damper removes energy from the system. This implies that the system motion has a convergent tendency. However, for small values of y, the damping coefficient is negative and the damper adds energy into the system. This suggests that the system motion has a divergent tendency. Therefore, because the nonlinear damping varies with y, the system motion can neither grow unboundedly nor decay to zero. Instead, it displays a sustained oscillation independent of initial conditions, as illustrated in Fig. 14.1.

Of course, sustained oscillations can also be found in linear systems, e.g., in the case of marginally stable linear systems. However, the oscillation of a marginally stable linear system has its amplitude determined by its initial conditions, and such a system is very sensitive to changes in system parameters (a slight change in parameters is capable of leading either to stable convergence or to instability). In nonlinear systems, on the other hand, the amplitude of sustained oscillations is independent of the initial conditions, and limit cycles are not easily affected by parameter changes.

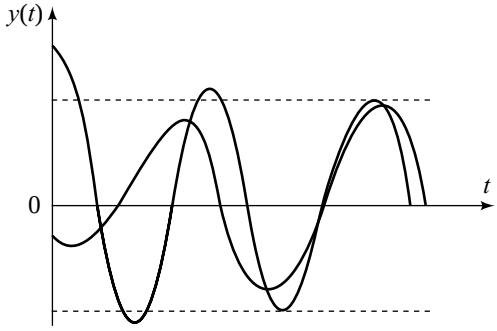

Fig. 14.1 Responses of the van der Pol oscillator

3. A nonlinear system with a periodic input may exhibit a periodic output whose frequency is either a subharmonic or a harmonic of the input frequency. For example, an input of frequency of 10 Hz may result in an output of 5 Hz for the subharmonic case or 30 Hz for the harmonic case.
4. A nonlinear system can display *jump resonance*, a form of hysteresis, in its frequency response. Consider a mass-spring-damper system

$$M\ddot{y} + B\dot{y} + K_1 y + K_2 y^3 = F\cos\omega t;\ M>0,\ B>0,\ K_1>0,\ K_2>0 \tag{14.2}$$

Note that the restoring force of the spring is assumed to be nonlinear. If in an experiment, the frequency ω is varied and the input amplitude F is held constant, frequency-response curve of the form shown in Fig. 14.2 may be obtained. As the frequency ω is increased, the response y follows the curve through the points A, B and C. At point C, a small change in frequency results in a discontinuous jump to point D. The response then follows the curve to point E upon further increase in frequency. As the frequency is decreased from point E, the response follows the curve through points D and F. At point F, a small change in frequency results in a discontinuous jump to point B. The response follows the curve to point A for further decrease in frequency. Observe from this description that the response never actually follows the segment CF. This portion of the curve represents a condition of unstable equilibrium.

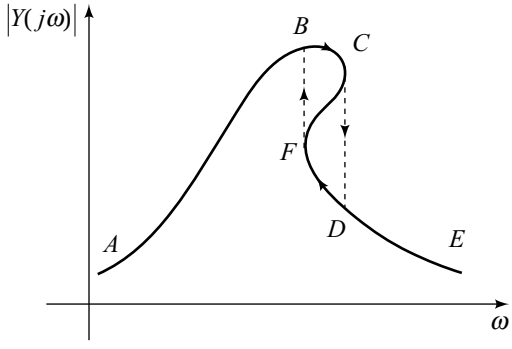

Fig. 14.2 Frequency response of a system with jump resonance

14.3 COMMON NONLINEARITIES IN CONTROL SYSTEMS

In this section, we take a closer look at the nonlinearities found in control systems. Consider the typical block diagram of closed-loop system shown in Fig. 14.3. It is composed of four parts: a plant to be controlled, sensors for measurements, actuators for control action, and a control law usually implemented on a computer. Nonlinearities may occur in any part of the system.

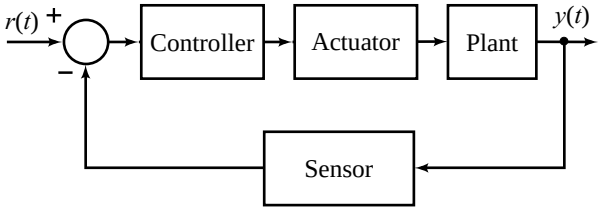

Fig. 14.3 General block diagram of a control system

Saturation Saturation is probably the most commonly encountered nonlinearity in control systems. It is often associated with amplifiers and actuators. In transistor amplifiers, the output varies linearly with the input only for small amplitude limits. When the input amplitude gets out of the linear range of the amplifier, the output changes very little and stays close to its maximum value. Figure 14.4a shows a linear-segmented approximation of saturation nonlinearity.

Most actuators display saturation characteristics. For example, the output torque of a servo motor cannot increase infinitely and tends to saturate due to the properties of the magnetic material. Similarly, valve-controlled hydraulic actuators are saturated by the maximum flow rate.

Deadzone A deadzone nonlinearly may occur in sensors, amplifiers and actuators. In a dc motor, we assume that any voltage applied to the armature windings will cause the armature to rotate if the field current is maintained constant. In reality, due to static friction at the motor shaft, rotation will occur only if the torque provided by the motor is sufficiently large. This corresponds to a so-called deadzone for small voltage signals. Similar deadzone phenomena occur in valve-controlled pneumatic and hydraulic actuators. Figure 14.4b shows linear-segmented approximation of deadzone nonlinearity.

Backlash A backlash nonlinearity commonly occurs in mechanical components of control systems. In gear trains, small gaps exist between a pair of mating gears (refer Fig. 14.4c). As a result, when the driving gear rotates a smaller angle than the gap H, the driven gear does not move at all, which corresponds to the deadzone (OA segment in Fig. 14.4c); after contact has been established between the two gears, the driven gear follows the rotation of the driving gear in a linear fashion (AB segment). When the driving gear rotates in the reverse direction by a distance of $2H$, the driven gear again does not move, corresponding to the segment BC in Fig. 14.4c. After the contact between the two gears is re-established, the driven gear linearly follows the rotation of the driving gear in the reverse direction (CD segment). Therefore, if the driving gear is in periodic motion, the driven gear will move in the fashion represented by the closed path $EBCD$.

A critical feature of backlash, a form of hysteresis, is its multi-valued nature. Corresponding to each input, two output values are possible. Which one of the two occurs depends on the history of the input.

Coulomb Friction In any system where there is a relative motion between contacting surfaces, there are several types of friction: all of them nonlinear except the viscous components. Coulomb friction is, in essence, a drag (reaction) force which opposes motion, but is essentially constant in magnitude regardless of velocity (Fig. 14.4d). The common example is an electric motor in which we find Coulomb friction drag due to the rubbing contact between the brushes and the commutator.

On-Off Nonlinearity In this book we have primarily covered three *modes of control*:

(i) proportional control;
(ii) integral control; and
(iii) derivative control.

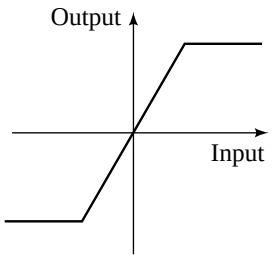

(a) Saturation nonlinearity

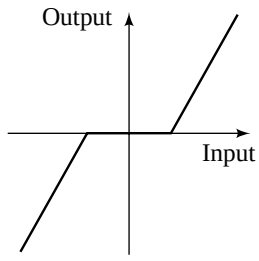

(b) Deadzone nonlinearity

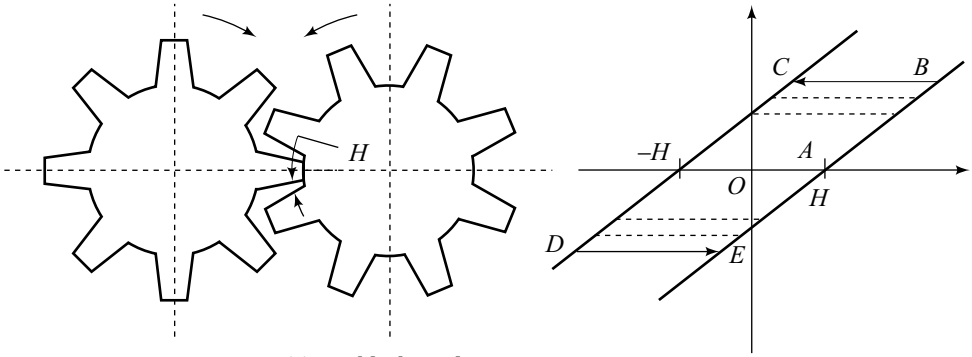

(c) Backlash nonlinearity

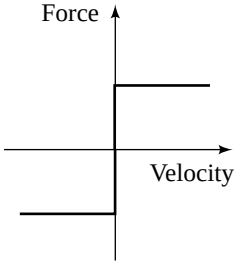

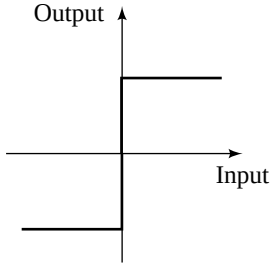

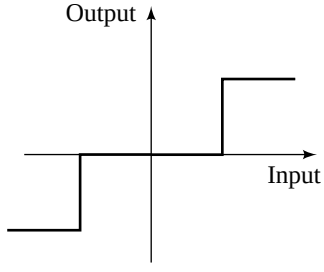

(d) Coulomb friction nonlinearity

(e) On-Off (two position/three position) control nonlinearities

Fig. 14.4

Another important mode of feedback control is the *on-off control*. This class of controllers have only two fixed states rather than a continuous output. In its wider application, the states of an *on-off controller* may not be simply on and off however, but could represent any two values of a control variable. Oscillatory behaviour is a typical response characteristic of a system under *two-position control,* also called *bang-bang control*. The oscillatory behaviour may be avoided using a *three-position control*(*on-off controller with a deadzone*).

The on-off mode of control results in a *variable structure system* whose structure changes in accordance with the current value of its state. A variable structure system can be viewed as a system composed of independent structures together with a switching logic between each of the structures. With appropriate switching logic, a variable structure system can exploit the desirable properties of each of the structures the

system is composed of. Even more, a variable structure system may have a property that is not a property of any of its structures. The variable structure sliding mode control law is usually implemented on a computer.

In this chapter, due to space considerations, we cannot introduce the reader to variable structure sliding mode control systems. This, however, is a highly important and widely practiced robust control strategy. The companion book [155] covers this subject.

We accommodate in this chapter the analysis of nonlinear systems with on-off controllers in the feedback loop. Figure 14.4e shows the characteristics of these controllers.

We may classify the nonlinearities as *inherent* and *intentional*. Inherent nonlinearities naturally come with the system's hardware (saturation, deadzone, backlash, coulomb friction). Usually such nonlinearities have undesirable effects, and control systems have to properly compensate for them. Intentional nonlinearities, on the other hand, are artificially introduced by the designer. Nonlinear control laws, such as bang-bang optimal control laws [155] and adaptive control laws [155], are typical examples of intentional nonlinearities.

14.4 DESCRIBING FUNCTION FUNDAMENTALS

Of all the analytical methods developed over the years for nonlinear systems, the describing function method is generally agreed upon as being the most practically useful. It is an approximate method but experience with real systems and computer simulation results shows adequate accuracy in many cases. The method predicts whether limit cycle oscillations will exist or not, and gives numerical estimates of oscillation frequency and amplitude when limit cycles are predicted. Basically the method is an approximate extension of frequency-response methods (including Nyquist stability criterion) to nonlinear systems.

To discuss the basic concept underlying the describing function analysis, let us consider the block diagram of a nonlinear system shown in Fig. 14.5, where the blocks $G_1(s)$ and $G_2(s)$ represent the linear elements, while the block N represents the nonlinear element.

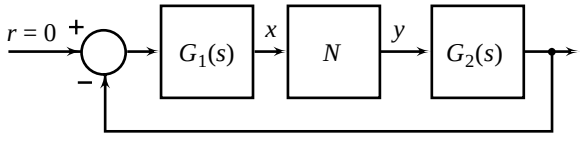

Fig. 14.5 A nonlinear system

The describing function method provides a "linear approximation" to the nonlinear element based on the assumption that the input to the nonlinear element is a sinusoid of known, constant amplitude. The fundamental harmonic of the element's output is compared with the input sinusoid to determine the steady-state amplitude and phase relation. This relation is the describing function for the nonlinear element. The method can thus be viewed as "harmonic linearization" of a nonlinear element.

The describing function method is based on the Fourier series. A review of the Fourier series will be in order here.

14.4.1 Fourier Series

We begin with the definition of a periodic signal. A signal $y(t)$ is said to be periodic with the period T if $y(t + T) = y(t)$ for every value of t. The smallest positive value of T for which $y(t + T) = y(t)$, is called fundamental period of $y(t)$. We denote the fundamental period as T_0. Obviously, $2T_0$ is also a period of $y(t)$, and so is any integer multiple of T_0.

A periodic signal $y(t)$ may be represented by the series [31]:

$$y(t) = \frac{a_0}{2} + \sum_{n=1}^{\infty} [a_n \cos n\omega_0 t + b_n \sin n\omega_0 t] \qquad (14.3a)$$

$$= \frac{a_0}{2} + \sum_{n=1}^{\infty} Y_n \sin(n\omega_0 t + \phi_n) \tag{14.3b}$$

where

$$a_n = \frac{2}{T_0}\int_0^{T_0} y(t) \cos n\omega_0 t \, dt;\ n = 0, 1, 2, \ldots \tag{14.3c}$$

$$b_n = \frac{2}{T_0}\int_0^{T_0} y(t) \sin n\omega_0 t \, dt;\ n = 1, 2, \ldots \tag{14.3d}$$

$$Y_n = \sqrt{a_n^2 + b_n^2} \tag{14.3e}$$

$$\phi_n = \tan^{-1}\left(\frac{a_n}{b_n}\right) \tag{14.3f}$$

In Eqn. (14.3b), the term for $n = 1$ is called *fundamental* or *first-harmonic* and always has the same frequency as the repetition rate of the original periodic waveform; whereas $n = 2, 3, \ldots$, give second, third, and so forth harmonic frequencies as integer multiples of the fundamental frequency.

Introducing a change of variable, $\psi = \omega_0 t$, we obtain the following alternative equations for the coefficients of Fourier series:

$$a_n = \frac{1}{\pi}\int_0^{2\pi} y(t) \cos n\omega_0 t \, d(\omega_0 t);\ n = 0, 1, 2, \ldots \tag{14.4a}$$

$$b_n = \frac{1}{\pi}\int_0^{2\pi} y(t) \sin n\omega_0 t \, d(\omega_0 t);\ n = 1, 2, \ldots \tag{14.4b}$$

Certain simplifications are possible when $y(t)$ has a symmetry of one type or another.

(i) Even symmetry: $y(t) = y(-t)$ results in

$$b_n = 0;\ n = 1, 2, \ldots \tag{14.4c}$$

(ii) Odd symmetry: $y(t) = -y(-t)$ results in

$$a_n = 0;\ n = 0, 1, 2, \ldots \tag{14.4d}$$

(iii) Odd half-wave symmetry: $y(t \pm T_0/2) = -y(t)$ results in

$$a_n = b_n = 0;\ n = 0, 2, 4, \ldots \tag{14.4e}$$

14.4.2 Describing Function for the Nonlinear Element

Let us assume that input x to the nonlinearity in Fig. 14.5 is sinusoidal, i.e.,

$$x = X \sin \omega t$$

With such an input, the output y of the nonlinear element will in general be a nonsinusoidal periodic function which may be expressed in terms of Fourier series as follows (refer Eqns (14.3)–(14.4)):

$$y = Y_0 + A_1 \cos \omega t + B_1 \sin \omega t + A_2 \cos 2\omega t + B_2 \sin 2\omega t + \cdots$$

The nonlinear characteristics listed in the previous section are all odd-symmetrical/odd half-wave symmetrical; the mean value Y_0 for all such cases is zero and therefore the output

$$y = A_1\cos\,\omega t + B_1\sin\,\omega t + A_2\cos\,2\omega t + B_2\sin\,2\omega t + \cdots$$

In the absence of an external input (i.e., $r = 0$ in Fig. 14.5), the output y of the nonlinear element N is fedback to its input through the linear elements $G_2(s)$ and $G_1(s)$ in tandem. If $G_2(s)G_1(s)$ has lowpass characteristics (this is usually the case in control systems), it can be assumed to a good degree of approximation that all the higher harmonics of y are filtered out in the process, and the input x to the nonlinear element N is mainly contributed by the fundamental component (first harmonic) of y, i.e., x remains sinusoidal. Under such conditions, the second and higher harmonics of y can be thrown away for the purpose of analysis and the fundamental component of y, i.e.,

$$y_1 = A_1\cos\,\omega t + B_1\sin\,\omega t$$

need only be considered.

The above procedure heuristically linearizes the nonlinearity since for a sinusoidal input, only a sinusoidal output of the same frequency is now assumed to be produced. This type of linearization, called the *first harmonic approximation*, is valid for large signals as well, so long as the filtering condition is satisfied.

We can write $y_1(t)$ in the form

$$y_1(t) = A_1\sin(\omega t + 90°) + B_1\sin\,\omega t = Y_1\sin(\omega t + \phi_1) \tag{14.5a}$$

where, by using phasors,

$$Y_1\angle\,\phi_1 = B_1 + jA_1 = \sqrt{B_1^2 + A_1^2}\;\angle\,\tan^{-1}(A_1/B_1) \tag{14.5b}$$

The coefficients A_1 and B_1 of the Fourier series are given by (refer Eqns (14.3))

$$A_1 = \frac{1}{\pi}\int_0^{2\pi} y\cos\,\omega t\,d(\omega t) \tag{14.5c}$$

$$B_1 = \frac{1}{\pi}\int_0^{2\pi} y\sin\,\omega t\,d(\omega t) \tag{14.5d}$$

As we shall see shortly, the amplitude Y_1 and the phase shift ϕ_1 are both functions of X, but independent of ω. We may combine the amplitude ratio and the phase shift in a *complex equivalent gain* $N(X)$ such that

$$N(X) = \frac{Y_1(X)}{X}\angle\phi_1(X) = \frac{B_1 + jA_1}{X} \tag{14.6}$$

Under first-harmonic approximation, the nonlinear element is completely characterized by the function $N(X)$; this function is usually referred to as the *describing function* of the nonlinearity.

The describing function differs from a linear system transfer function in that its numerical value will vary with input amplitude X. Also, it does not depend on frequency ω (there are, however, a few situations in which the describing function for the nonlinearity is a function of both the input amplitude X and the frequency ω (refer [128 – 129]). When embedded in an otherwise linear system (Fig. 14.6), the describing function can be combined with the 'ordinary' sinusoidal transfer function of the rest of the system to obtain the complete open-loop function; however, we will get a different open-loop function for every different amplitude X. We can check all of these open-loop functions for closed-loop stability using Nyquist stability criterion.

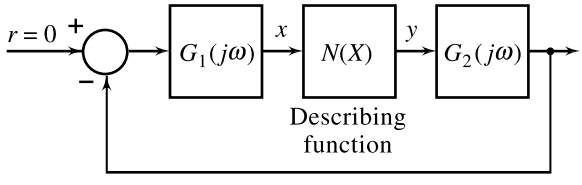

Fig. 14.6 Nonlinear system with nonlinearity replaced by describing function

It is important to remind ourselves here that the simplicity in analysis of nonlinear systems using describing functions has been achieved at the cost of certain limitations, the foremost being the assumption that in traversing the path through the linear parts of the system from nonlinearity output back to nonlinearity input, the higher harmonics will have been effectively lowpass filtered, relative to the first harmonic. When the linear part of the system does indeed provide a sufficiently strong filtering effect, then the predictions of describing function analysis usually are a good approximation to actual behaviour. Filtering characteristics of the linear part of the system improve as the order of the system goes up.

The 'lowpass filtering' requirement is never completely satisfied; for this reason the describing function method is mainly used for stability analysis and is not directly applied to the optimization of system design. Usually the describing function analysis will correctly predict the existence and characteristics of limit cycles. However, false indications cannot be ruled out; therefore the results must be verified by simulation. Simulation, in fact, is an almost indispensable tool for analysis and design of nonlinear systems; describing function and other analytical methods provide the background for intelligent planning of the simulations.

We will limit our discussion to separable nonlinear systems with reference input $r = 0$, and with symmetrical nonlinearities (listed in Section 14.3) in the loop. Refer [128–129] for situations wherein dissymmetrical nonlinearities are present, and/or the reference input is non-zero.

14.5 DESCRIBING FUNCTIONS OF COMMON NONLINEARITIES

Before coming to the stability study by the describing function method, it is worthwhile to derive the describing functions of some common nonlinearities. Our first example is an on–off controller with a deadzone as in Fig. 14.7. If X is less than deadzone Δ, then the controller produces no output; the first harmonic component of the Fourier series is of course zero, and the describing function is also zero. If $X > \Delta$, the controller produces the 'square wave' output y. One cycle of this periodic function of period 2π is described as follows:

$$y = \begin{cases} 0\ ; & 0 \le \omega t < \alpha \\ M\ ; & \alpha \le \omega t < (\pi - \alpha) \\ 0\ ; & (\pi - \alpha) \le \omega t < (\pi + \alpha) \\ -M\ ; & (\pi + \alpha) \le \omega t < (2\pi - \alpha) \\ 0\ ; & (2\pi - \alpha) \le \omega t \le 2\pi \end{cases} \tag{14.7}$$

where $X \sin \alpha = \Delta$; or $\alpha = \sin^{-1}(\Delta / X)$

This periodic function has odd symmetry:

$$y(\omega t) = -y(-\omega t)$$

Therefore, the fundamental component of y is given by (refer Eqn. (14.4d))

$$y_1 = B_1 \sin \omega t$$

where $$B_1 = \frac{1}{\pi} \int_0^{2\pi} y \sin \omega t \, d(\omega t)$$

Due to the symmetry of y (refer Fig. 14.7), the coefficient B_1 can be calculated as follows:

$$B_1 = \frac{4}{\pi} \int_0^{\frac{\pi}{2}} y \sin \omega t \, d(\omega t) = \frac{4M}{\pi} \int_{\alpha}^{\frac{\pi}{2}} \sin \omega t \, d(\omega t) = \frac{4M}{\pi} \cos \alpha \tag{14.8}$$

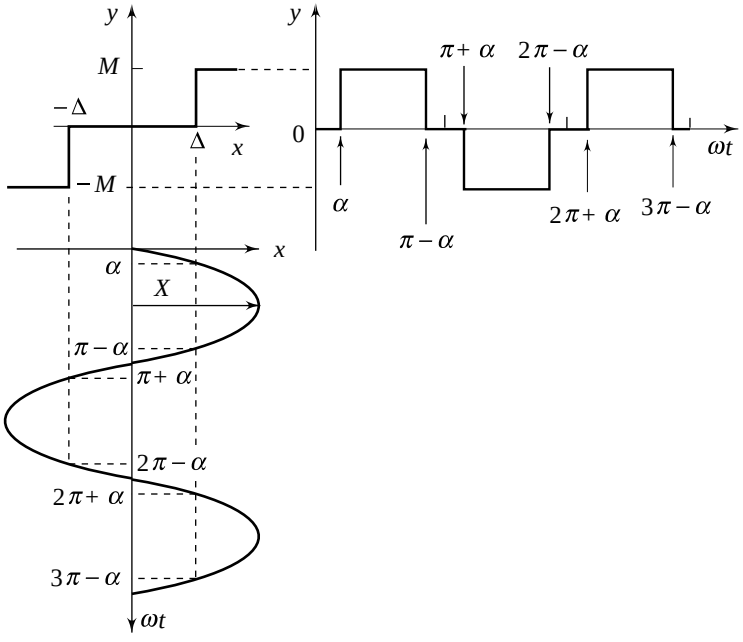

Fig. 14.7 Fourier-series analysis of an on–off controller with deadzone

Since A_1 (the Fourier series cosine coefficient) is zero, the first harmonic component of y is exactly in phase with $X \sin \omega t$, and the describing function $N(X)$ is given by (refer Eqns (14.6)–(14.8))

$$N(X) = \begin{cases} 0 & ; X < \Delta \\ \dfrac{4M}{\pi X}\sqrt{1-\left(\dfrac{\Delta}{X}\right)^2} & ; X \geq \Delta \end{cases} \qquad (14.9)$$

For a given controller, M and Δ are fixed and the describing function is a function of input amplitude X, which is graphed in Fig. 14.8a together with peak location and value found by standard calculus maximization procedure. Note that for a given X, $N(X)$ is just a pure real positive number, and thus plays the role of a steady-state gain in a block diagram of the form shown in Fig. 14.6. However, this gain term is unusual in that it changes when X changes.

A describing function $N(X)$ may be equivalently represented by a plot of

$$-\frac{1}{N(X)} = \left|-\frac{1}{N(X)}\right| \angle(-1/N(X)) \qquad (14.10)$$

as a function of X on the polar plane. We will use this form of representation in the next section for stability analysis.

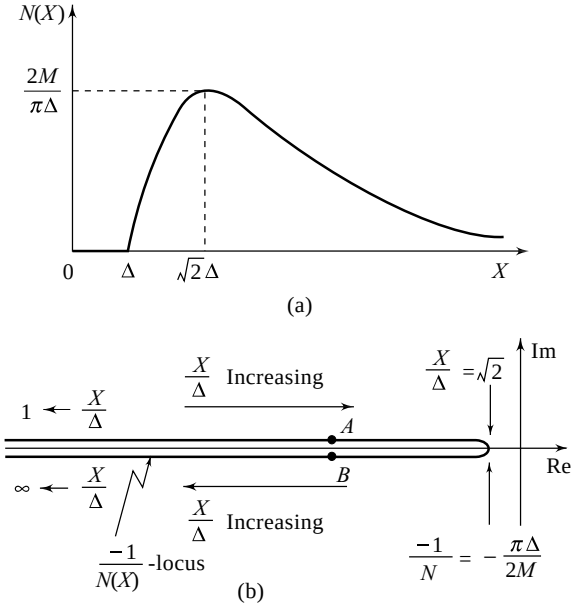

Fig. 14.8 Describing function of an on–off controller with deadzone

Rearrangement of Eqn. (14.9) gives

$$-\frac{1}{N(X)} = -\frac{\pi\Delta}{4M}\frac{(X/\Delta)^2}{\sqrt{(X/\Delta)^2-1}} \tag{14.11}$$

Figure 14.8b gives the representation on the polar plane of the describing function for an on–off controller with deadzone. It may be noted that though the points A and B lie at the same place on the negative real axis, they belong to different values of X/Δ.

We choose as another example the backlash since its behaviour brings out certain features not encountered in our earlier example. The characteristics of backlash nonlinearity and its response to sinusoidal input are shown in Fig. 14.9. The output y is again a periodic function of period 2π ; one cycle of this function is described as follows:

$$y = \begin{cases} x - H\,; & 0 \le \omega t < \pi/2 \\ X - H\,; & \pi/2 \le \omega t < (\pi - \beta) \\ x + H\,; & (\pi - \beta) \le \omega t < 3\pi/2 \\ -X + H\,; & 3\pi/2 \le \omega t < (2\pi - \beta) \\ x - H\,; & (2\pi - \beta) \le \omega t \le 2\pi \end{cases} \tag{14.12}$$

where $X \sin\beta = X - 2H$; or $\beta = \sin^{-1}\left(1 - \dfrac{2H}{X}\right)$.

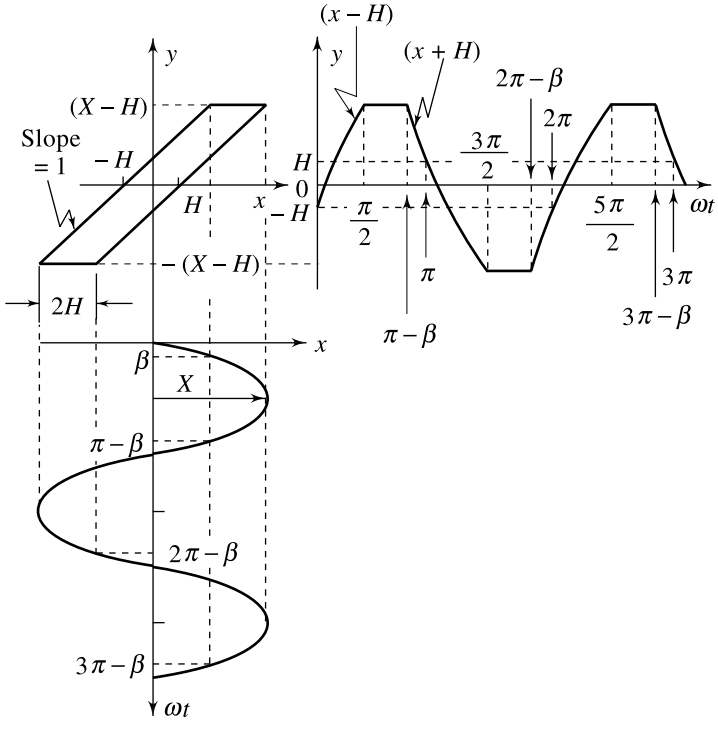

Fig. 14.9 Fourier-series analysis of backlash

The periodic function does not possess odd symmetry:

$$y(\omega t) \neq -y(-\omega t),$$

but possesses odd half-wave symmetry:

$$y(\omega t \pm \pi) = -y(\omega t)$$

Therefore, the fundamental component of y is given by (refer Eqn. (14.4e))

$$y_1 = A_1 \cos\omega t + B_1 \sin\omega t$$

where

$$A_1 = \frac{1}{\pi}\int_0^{2\pi} y \cos\omega t \, d(\omega t)$$

$$B_1 = \frac{1}{\pi}\int_0^{2\pi} y \sin\omega t \, d(\omega t)$$

Due to the symmetry of y, only the positive half wave need be considered (Fig. 14.9):

$$A_1 = \frac{2}{\pi}\left[\int_0^{\frac{\pi}{2}} (X\sin\omega t - H)\cos\omega t \, d(\omega t) + \int_{\frac{\pi}{2}}^{(\pi-\beta)} (X - H)\cos\omega t \, d(\omega t)\right.$$

$$\left. + \int_{(\pi-\beta)}^{\pi} (X\sin\omega t + H)\cos\omega t \, d(\omega t)\right]$$

$$= \frac{2X}{\pi}\int_0^{\frac{\pi}{2}} \sin\theta\cos\theta \, d\theta - \frac{2H}{\pi}\int_0^{\frac{\pi}{2}} \cos\theta \, d\theta + \frac{2(X-H)}{\pi}\int_{\frac{\pi}{2}}^{(\pi-\beta)} \cos\theta \, d\theta$$

$$+ \frac{2X}{\pi}\int_{(\pi-\beta)}^{\pi} \sin\theta\cos\theta \, d\theta + \frac{2H}{\pi}\int_{(\pi-\beta)}^{\pi} \cos\theta \, d\theta$$

$$= -\frac{3X}{2\pi} + \frac{2(X-2H)}{\pi}\sin\beta + \frac{X}{2\pi}\cos 2\beta$$

$$= -\frac{3X}{2\pi} + \frac{2X}{\pi}\sin^2\beta + \frac{X}{2\pi}\cos 2\beta = -\frac{X}{\pi}\cos^2\beta \qquad (14.13a)$$

$$B_1 = \frac{2}{\pi}\left[\int_0^{\frac{\pi}{2}} (X\sin\omega t - H)\sin\omega t \, d(\omega t) + \int_{\frac{\pi}{2}}^{(\pi-\beta)} (X - H)\sin\omega t \, d(\omega t)\right.$$

$$\left. + \int_{(\pi-\beta)}^{\pi} (X\sin\omega t + H)\sin\omega t \, d(\omega t)\right]$$

$$= \frac{2X}{\pi}\int_0^{\frac{\pi}{2}} \sin^2\theta\, d\theta - \frac{2H}{\pi}\int_0^{\frac{\pi}{2}} \sin\theta d\theta + \frac{2(X-H)}{\pi}\int_{\frac{\pi}{2}}^{(\pi-\beta)} \sin\theta d\theta$$

$$+ \frac{2X}{\pi}\int_{(\pi-\beta)}^{\pi} \sin^2\theta d\theta + \frac{2H}{\pi}\int_{(\pi-\beta)}^{\pi} \sin\theta d\theta$$

$$= \frac{X}{\pi}\left[\frac{\pi}{2}+\beta\right] + \frac{2(X-2H)}{\pi}\cos\beta - \frac{X}{2\pi}\sin 2\beta$$

$$= \frac{X}{\pi}\left[\frac{\pi}{2}+\beta\right] + \frac{2X}{\pi}\sin\beta\cos\beta - \frac{X}{2\pi}\sin 2\beta = \frac{X}{\pi}\left[\frac{\pi}{2}+\beta+\frac{1}{2}\sin 2\beta\right] \qquad (14.13b)$$

It is clear that the fundamental component of y will have a phase shift with respect to $X \sin \omega t$ (a feature not present in our earlier example). The describing function $N(X)$ is given by (refer Eqns (14.6), (14.12), (14.13))

$$N(X) = \frac{1}{X}(B_1 + jA_1) = \frac{1}{\pi}\left[\frac{\pi}{2}+\beta+\frac{1}{2}\sin 2\beta - j\cos^2\beta\right] \qquad (10.14)$$

$$\beta = \sin^{-1}\left(1-\frac{2H}{X}\right)$$

Note that $N(X)$ is a function of the non-dimensional ratio H/X; we can thus tabulate or plot a single graph of $N(X)$ that will be usable for any numerical value of H (see Table 14.1, and Fig. 14.10).

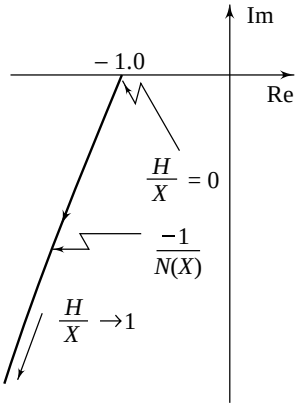

Fig. 14.10 Describing function for backlash

Table 14.1 Describing function for backlash

H/X	$\lvert -1/N(X)\rvert$	$\angle(N(X))$
0.000	1.000	180.0
0.050	1.017	183.5
0.125	1.066	188.5
0.200	1.134	193.4
0.300	1.259	199.7
0.400	1.435	206.0
0.500	1.687	212.5
0.600	2.072	219.3
0.700	2.720	226.7
0.800	4.024	235.1
0.850	5.330	239.9
0.900	7.946	245.6
0.925	10.560	248.9
0.950	15.800	252.8
0.975	31.500	257.9

We have so far given illustrative derivations of describing functions for on–off controller with deadzone, and backlash. By similar procedures, the describing functions of other common nonlinearities can be derived; some of these are tabulated in Table 14.2.

Table 14.2 Describing functions of common nonlinearities

Nonlinearity	*Describing function (input = $X \sin \omega t$)*
1. 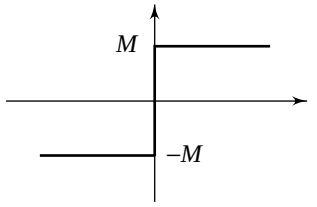	$N(X) = \dfrac{4M}{\pi X}$
2. 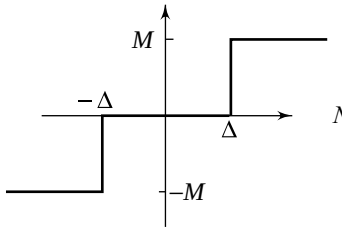	$N(X) = \begin{cases} 0 & ; X < \Delta \\ \dfrac{4M}{\pi X}\sqrt{1-\left(\dfrac{\Delta}{X}\right)^2} & ; X \geq \Delta \end{cases}$
3. 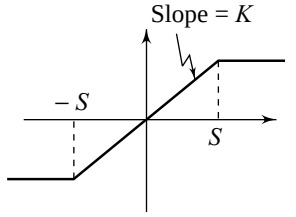	$N(X) = \begin{cases} K & ; X < S \\ \dfrac{2K}{\pi}\left[\sin^{-1}\dfrac{S}{X} + \dfrac{S}{X}\sqrt{1-\left(\dfrac{S}{X}\right)^2}\right] & ; X \geq S \end{cases}$
4. 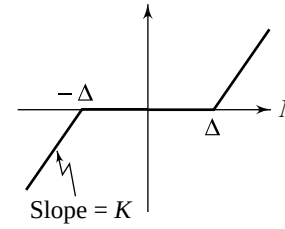	$N(X) = \begin{cases} 0 & ; X < \Delta \\ \dfrac{2K}{\pi}\left[\dfrac{\pi}{2} - \sin^{-1}\dfrac{\Delta}{X} - \dfrac{\Delta}{X}\sqrt{1-\left(\dfrac{\Delta}{X}\right)^2}\right] & ; X \geq \Delta \end{cases}$
5. 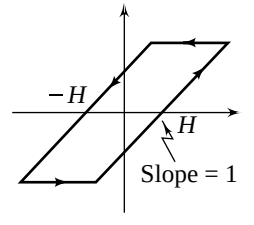	$N(X) = \dfrac{1}{\pi}\left[\dfrac{\pi}{2} + \beta + \dfrac{1}{2}\sin 2\beta - j\cos^2\beta\right]$ $\beta = \sin^{-1}\left(1 - \dfrac{2H}{X}\right)$

14.6 STABILITY ANALYSIS BY THE DESCRIBING FUNCTION METHOD

Consider the linear system of Fig. 14.11a. Application of Nyquist stability criterion (refer Chapter 8) to this system involves the following steps.

1. Define the Nyquist contour in the s-plane that encloses the entire right-hand side (unstable region) of the s-plane (Fig. 14.11b).
2. Sketch the Nyquist plot, which is the locus of $KG(s)H(s)$ when s takes on values along the Nyquist contour (Fig. 14.11c).
3. The characteristic equation of the system is

$$1 + KG(s)H(s) = 0$$

or

$$KG(s)H(s) = -1 \tag{14.15}$$

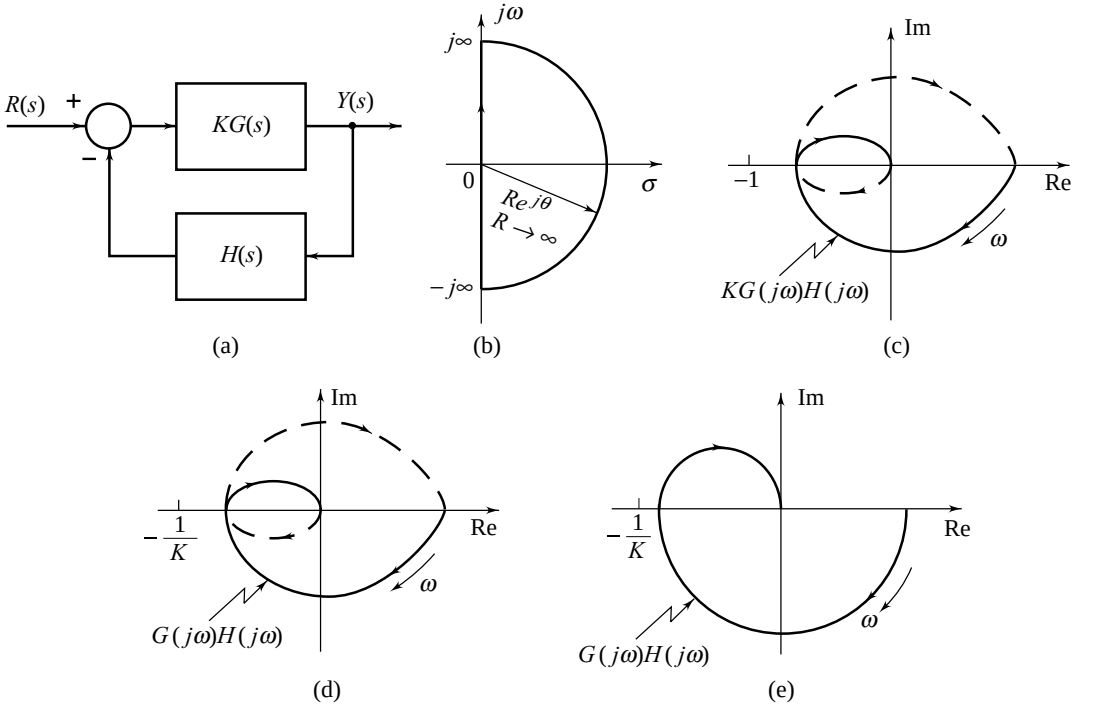

Fig. 14.11 Application of the Nyquist stability criterion

The stability of the closed-loop system is determined by investigating the behaviour of the Nyquist plot of $KG(s)H(s)$ with respect to the *critical point* $(-1 + j0)$ in the $KG(s)H(s)$-plane.

For the predominant case of systems wherein open-loop transfer function $KG(s)H(s)$ has no poles in the right-half of s-plane, the Nyquist stability criterion is stated below:

If the Nyquist plot of the open-loop transfer function $KG(s)H(s)$ corresponding to the Nyquist contour in the s-plane does not encircle the critical point $(-1 + j0)$, *the closed-loop system is stable.*

4. The characteristic Eqn. (14.15) may be rearranged as follows:

$$G(s)H(s) = -1/K \tag{14.16}$$

For the linear system with open-loop transfer function $KG(s)H(s)$, we can count the number of encirclements of $(-1/K + j0)$ point if the Nyquist plot of $G(s)H(s)$ is constructed (Fig. 14.11d).

5. When the Nyquist plot of $G(s)H(s)$ passes through $(-1/K + j0)$ point, the number of encirclements is indeterminate. This corresponds to the condition where $1 + KG(s)H(s)$ has zeros on the imaginary axis (i.e., the closed-loop system has poles on the imaginary axis). The gain corresponding to this situation will yield oscillatory behaviour (we have assumed that the zeros are non-repeated).
6. The most commonly occurring situation in control system design is that the system becomes unstable if the gain increases past a certain critical value. Stability condition for such systems becomes

$$|G(j\omega)H(j\omega)| < 1/K \text{ at } \angle G(j\omega)H(j\omega) = -180^\circ$$

The stability may therefore be examined from polar plot (plot of $G(j\omega)H(j\omega)$ on polar plane with ω varying from 0 to ∞) only (Fig. 14.11e).

Consider now a nonlinear system of Fig. 14.12; $N(X)$ is the describing function of the nonlinear element and $G(s)$ is the transfer function of the linear part of the system. $G(s)$ is assumed to have no poles in the right half s-plane.

The validity of the block diagram shown in Fig. 14.12 is based on the assumption that the input to the nonlinearity is a pure sinusoid $x = X \sin \omega t$. This necessarily requires that r is zero, since non-zero values of the system input usually result in the nonlinearity input signal containing components in addition to the assumed sine wave. So the describing function approach is applicable when the input r is zero and the system is excited by some initial conditions. For different values of the initial conditions, a signal of the form $x = X \sin \omega t$ will be generated at the input of an odd-symmetrical/odd half-wave symmetrical nonlinearity, with X varying from 0 to ∞. This is true only if the linear part of the system possesses the required lowpass characteristics (for situations where the nonlinearity input signal contains components in addition to $X \sin \omega t$ (such as r not being zero), the method of dual-input describing functions may be useful (refer [128–129]).

For a given X, $N(X)$ in Fig. 14.12 is just a real/complex number; the condition (14.16) therefore becomes

$$G(s) = -1/N(X) \tag{14.17}$$

This modified condition differs from the condition (14.16) in the fact that the critical point $(-1/K + j0)$ now becomes the critical locus $-1/N(X)$ as a function of X. The stability analysis can be carried out by examining the relative position of the following plots on polar plane.

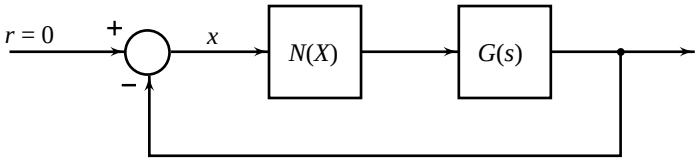

Fig. 14.12 A nonlinear system

1. Plot of $G(j\omega)$ with ω varying from 0 to ∞, called the polar plot of $G(j\omega)$ (note that the Nyquist plot is the plot of $G(j\omega)$ with ω varying from $-\infty$ to $+\infty$).
2. Plot of $-1/N(X)$ with X varying from 0 to ∞.

When the critical points of $-1/N(X)$ lie to the left of the polar plot of $G(j\omega)$ (or are not encircled by the Nyquist plot of $G(j\omega)$), the closed-loop system is stable; any disturbances which appear in the system will tend to die out. Conversely, if any part of the $-1/N(X)$ locus lies to the right of the polar plot of $G(j\omega)$ (or is enclosed by the Nyquist plot of $G(j\omega)$), it implies that any disturbances which are characterized by the values of X corresponding to the enclosed critical points will provide unstable operations. The intersection of $G(j\omega)$ and $-1/N(X)$ loci corresponds to the possibility of a periodic oscillation (limit cycle) characterized by the value of X on the $-1/N(X)$ locus and the value of ω on the $G(j\omega)$ locus.

Figure 14.13a shows a $G(j\omega)$ plot superimposed on a $-1/N(X)$ locus. The values of X for which the $-1/N(X)$ locus lies in the region to the right of an observer traversing the polar plot of $G(j\omega)$ in the direction of increasing ω, correspond to unstable conditions. Similarly, the values of X for which the $-1/N(X)$ locus lies in the region to the left of an observer traversing the polar plot of $G(j\omega)$ in the direction of increasing ω, correspond to the stable conditions. The locus of $-1/N(X)$ and the polar plot of $G(j\omega)$ intersect at the point $A(\omega = \omega_2, X = X_2)$ which corresponds to the condition of limit cycle. The system is unstable for $X < X_2$ and is stable for $X > X_2$. The stability of the limit cycle can be judged by the perturbation technique described below.

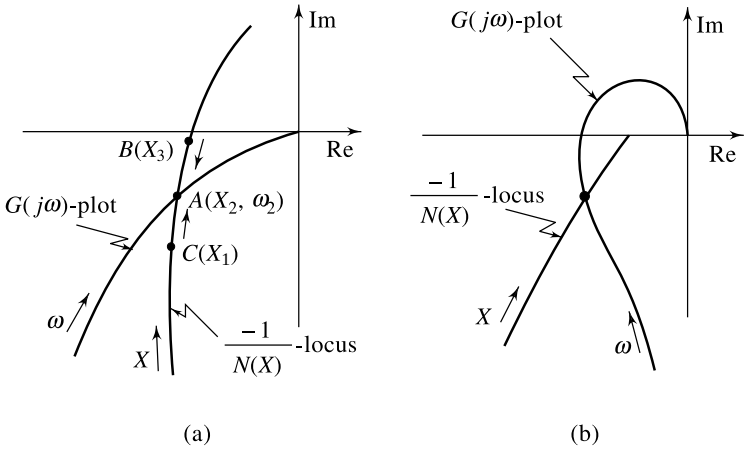

Fig. 14.13 Prediction and stability of limit cycles

Suppose that the system is originally operating at A under the state of a limit cycle. Assume that a slight perturbation is given to the system so that the input to the nonlinear element increases to X_3, i.e., the operating point is shifted to B. Since B is in the range of stable operation, the amplitude of the input to the nonlinear element progressively decreases and hence the operating point moves back towards A. Similarly, a perturbation which decreases the amplitude of input to the nonlinearity shifts the operating point to C which lies in the range of unstable operation. The input amplitude now progressively increases and the operating point again returns to A. Therefore, the system has a stable limit cycle at A.

Figure 14.13b shows the case of an unstable limit cycle. For systems having $G(j\omega)$ plots and $-1/N(X)$ loci as shown in Figs 14.14a and 14.14b, there are two limit cycles; one stable and the other unstable.

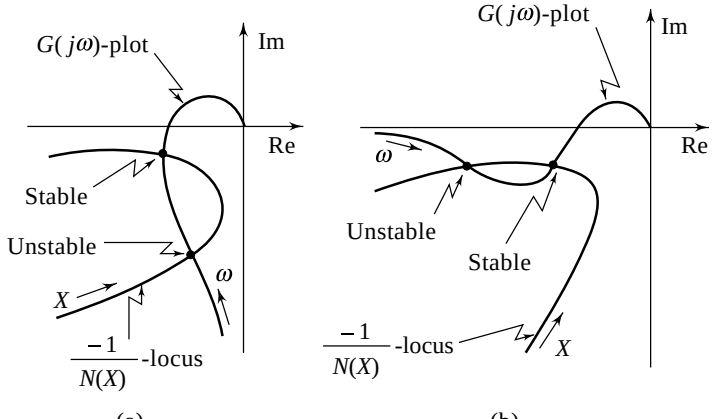

Fig. 14.14 Prediction and stability of limit cycles

Describing function method usually gives sufficiently accurate information about stability and limit cycles. This analysis is invariably followed by a simulation study.

Example 14.1 Let us investigate the stability of a system with on-off controller, shown in Fig. 14.15. Using the describing function of an on-off nonlinearity given in Table 14.2, we have

$$-\frac{1}{N(E)} = -\frac{\pi E}{4} \tag{14.18}$$

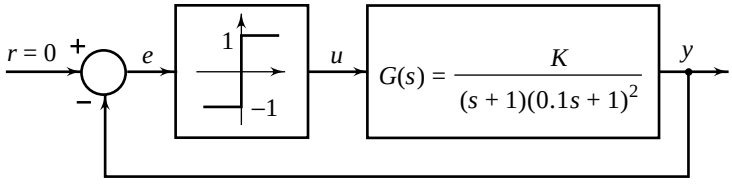

Fig. 14.15 A system with on-off controller

where E is the maximum amplitude of the sinusoidal signal e. Figure 14.16 shows the locus of $-1/N(E)$ as a function of E and the plot of $G(j\omega)$ for $K = 5$. Equation (14.17) is satisfied at A since the two graphs intersect at this point.

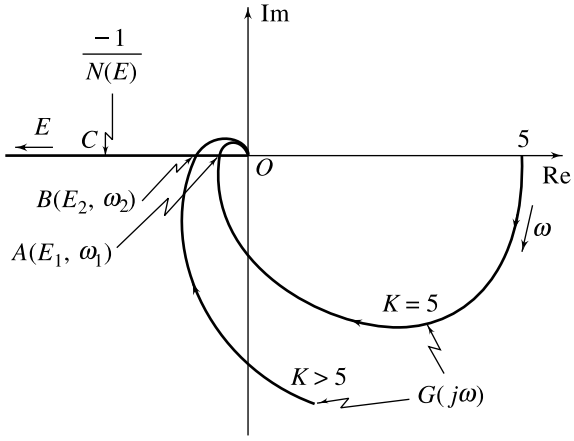

Fig. 14.16 Stability analysis of the system in Fig. 14.15

The point of intersection on the $G(j\omega)$ plot gives a numerical value ω_1 for the frequency of the limit cycle; whereas the same point on the $-1/N(E)$ locus gives us the predicted amplitude E_1 of the oscillation. As an observer traverses the $G(j\omega)$ plot in the direction of increasing ω, the portion O-A of the $-1/N(E)$ locus lies to its right and the portion A-C lies to its left. Using the arguments presented previously, we can conclude that the limit cycle is a stable one.

Since $-1/N(E)$ is a negative real number, it is clear that intersection occurs at $-180°$ phase angle. The frequency ω_1 that gives $\angle G(j\omega_1) = -180°$ is 10.95 rad/sec. Furthermore, at point A

$$|G(j\omega_1)| = \left|-\frac{1}{N(E_1)}\right|$$

At $\omega_1 = 10.95$, $|G(j\omega_1)| = 0.206$ and therefore (refer Eqn. (14.18)).

$$\left|-\frac{1}{N(E_1)}\right| = \frac{\pi E_1}{4} = 0.206$$

This gives $E_1 = 0.262$.

The describing function analysis thus predicts a limit cycle (sustained oscillation)

$$y(t) = -e(t) = -0.262 \sin 10.95t$$

For $K > 5$, the intersection point shifts to B (Fig. 14.16) resulting in a limit cycle of amplitude $E_2 > E_1$ and frequency $\omega_2 = \omega_1$. It should be observed that the system has a limit cycle for all positive values of gain K.

To gain some further insight into on–off control behaviour and describing function analysis, let us modify the system of Fig. 14.15 by letting the linear portion be of second-order with

$$G(s) = \frac{5}{(s+1)(0.1s+1)}$$

Figure 14.17 shows the plot of $G(j\omega)$ superimposed on the locus of $-1/N(E)$. The intersection of the two graphs is now impossible since the phase angle of neither $G(j\omega)$ nor $-1/N(E)$ can be more lagging than –180°. Describing function analysis thus seems to predict no limit cycling, whereas the fact that the control signal u must be either +1.0 or –1.0 dictates that the system oscillate. One possible interpretation to this analysis would be that the second-order linear system provides less of the lowpass filtering assumed in the describing function method than did the third-order system and thus the approximation has become inaccurate to the point of predicting no limit cycle when actually one occurs. Another interpretation would be that the curves actually do 'intersect' at the origin, predicting a limit cycle of infinite frequency and infinitesimal amplitude. This latter interpretation, even though it predicts a physically impossible result, agrees with the rigorous mathematical solution of the differential equations: for some non-zero initial value of y, we find that $y(t)$ oscillates about zero with ever-decreasing amplitude and ever-increasing frequency. We will examine this solution on the phase plane in a later section.

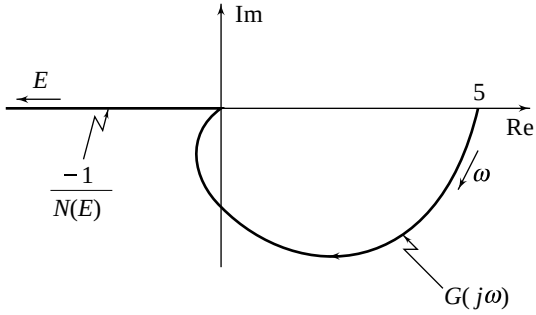

Fig. 14.17 Describing function analysis of a system with second-order plant and on-off controller

Let us now modify the system of Fig. 14.15 by giving the controller a deadzone Δ, as shown in Fig. 14.18. The $-1/N(E)$ locus for this type of controller is given by Fig. 14.8b. Plots of $G(j\omega)$ for different values of K, superimposed on $-1/N(E)$ locus, are shown in Fig. 14.19. From this figure, we observe that for $K = K_1$, the $G(j\omega)$ plot crosses the negative real axis at a point to the right of $-\pi\Delta/2$ such that no intersection takes place between the graphs of $G(j\omega)$ and $-1/N(E)$, and therefore no limit cycle results. With such a gain, the $-1/N(E)$ locus lies entirely to the left of the $G(j\omega)$ plot; the system is therefore stable, i.e., it has effectively positive damping.

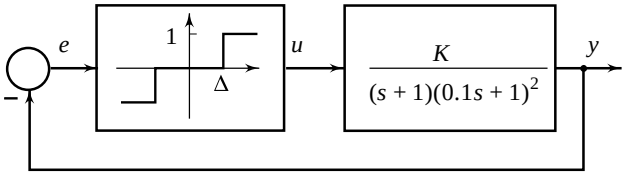

Fig. 14.18 A system controlled by on-off controller with deadzone

If the gain K is now increased to a value K_2 such that the $G(j\omega)$ plot intersects the $-1/N(E)$ locus at the point A(i.e., on the negative real axis at $-\pi\Delta/2$), then there exists a limit cycle. Now suppose that the system is operating at the point A. Any increase in the amplitude of E takes the operating point to the left so that it is not enclosed by the $G(j\omega)$ plot, which means that the system has positive damping. This reduces E till the operating point comes back to A. Any decrease in the amplitude of E again takes the operating point to the left of the $G(j\omega)$ plot, i.e., the system has positive damping which further reduces E, finally driving the system to rest. Since random disturbances are always present in any system, the system under discussion cannot remain at A. Therefore, the limit cycle represented by A is unstable.

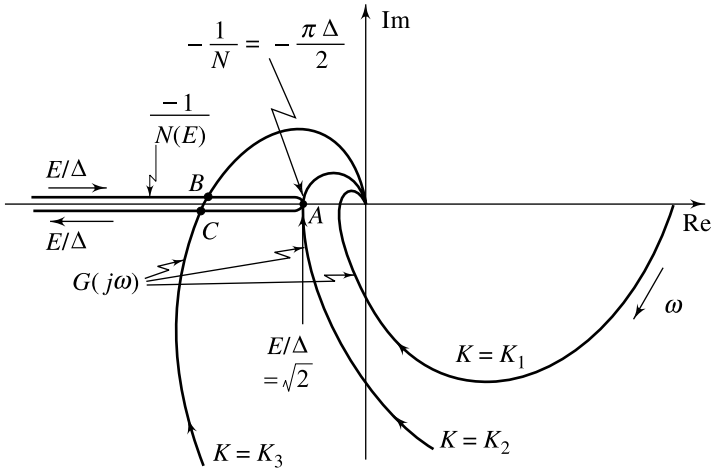

Fig. 14.19 Stability analysis of the system of Fig. 14.18

When the gain K is further increased to K_3, the graphs of $G(j\omega)$ and $-1/N(E)$ intersect at two points B and C. By arguments similar to those advanced earlier, it can be shown that the point B represents an unstable limit cycle and C represents a stable limit cycle. It may be noted that though the points B and C lie at the same place on the negative real axis, they belong to different values of E/Δ.

It is also clear that limit cycling is predicted only for deadzone Δ smaller than the value given by

$$\frac{\pi\Delta}{2} = |G(j\omega_1)|$$

where ω_1 is the frequency at which the plot $G(j\omega)$ intersects the negative real axis. A deadzone in on-off controllers appears to be a desirable feature to avoid limit cycling. However, as we shall see later in this chapter, a large value of Δ would cause the steady-state performance of the system to deteriorate.

Example 14.2 Figure 14.20a shows a block diagram for a servo system consisting of an amplifier, a motor, a gear train, and a load (gear 2 shown in the diagram includes the load element). It is assumed that the inertia of the gears and load element is negligible compared with that of the motor, and backlash exists between gear 1 and gear 2. The gear ratio between gear 1 and gear 2 is unity.

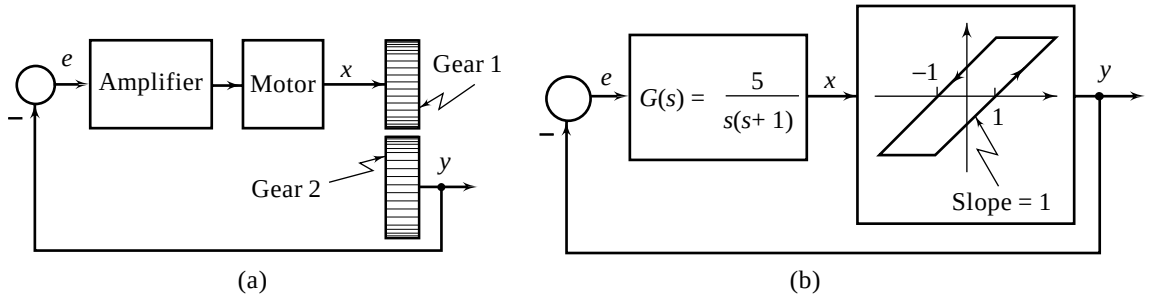

Fig. 14.20 A servo system with backlash in gears

The transfer function of the amplifier-motor combination is given by $5/s(s+1)$ and the backlash amplitude is given as unity ($H = 1$).

From the problem statement, the block diagram of the system may be redrawn as shown in Fig. 14.20b. Let us investigate the stability of this system. The $-1/N(X)$ locus for the backlash nonlinearity is given by Fig. 14.10 (Table 14.1). Plot of $G(j\omega)$ superimposed on $-1/N(X)$ locus is shown in Fig. 14.21. As seen from this figure, there are two intersections of the two loci. Applying the stability test for the limit cycle reveals that point A corresponds to a stable limit cycle and point B corresponds to an unstable limit cycle. The stable limit cycle has a frequency of 1.6 rad/sec and an amplitude of 2 (the unstable limit cycle cannot physically occur). To avoid limit-cycle behaviour, the gain of the amplifier must be decreased sufficiently so that the entire $G(j\omega)$ plot lies to the left of $-1/N(X)$ locus.

Note that checking for an intersection must be done graphically/numerically since no analytical solution for limit-cycle amplitude or frequency is possible. A computer program that tabulates $G(j\omega)$ and $-1/N(X)$ is useful in searching for intersections and is not difficult to write. Once the general region of an intersection is found, we can use smaller increments of H/X and ω to pinpoint the intersection as accurately as we wish.

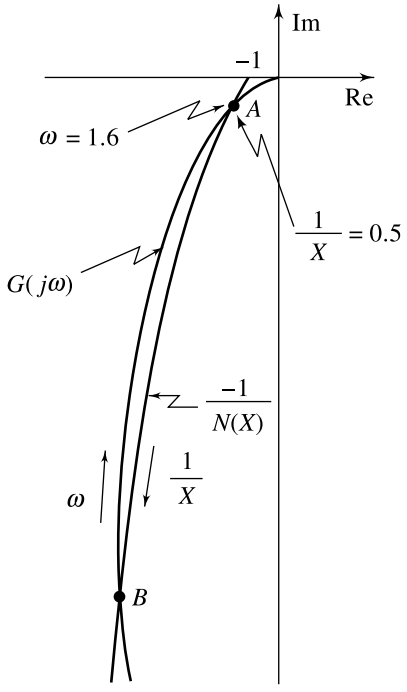

Fig. 14.21 Stability analysis of the system of Fig. 14.20

14.7 CONCEPTS OF PHASE PLANE ANALYSIS

The free motion of any second-order nonlinear system can always be described by an equation of the form

$$\ddot{y} + g(y, \dot{y})\dot{y} + h(y, \dot{y})y = 0 \tag{14.19}$$

The state of the system at any moment can be represented by a point of coordinates $(y, \dot{y})$ in a system of rectangular coordinates. Such a coordinate plane is called a 'phase plane'.

In terms of the state variables

$$x_1 = y,\ x_2 = \dot{y}, \tag{14.20a}$$

second-order system (14.19) is equivalent to the following canonical set of state equations:

$$\begin{aligned} \dot{x}_1 &= \frac{dx_1}{dt} = x_2 \\ \dot{x}_2 &= \frac{dx_2}{dt} = -g(x_1, x_2)x_2 - h(x_1, x_2)x_1 \end{aligned} \tag{14.20b}$$

By division, we obtain a first-order differential equation relating the variables x_1 and x_2:

$$\frac{dx_2}{dx_1} = -\frac{g(x_1, x_2)x_2 + h(x_1, x_2)x_1}{x_2} \tag{14.21}$$

Thus, we have eliminated the independent variable t from the set of first-order differential equations given by (14.20b). In Eqn. (14.21), we consider x_1 and x_2 as independent and dependent variables respectively.

For a given set of initial conditions $\{x_1(0), x_2(0)\}$, the solution to Eqn. (14.21) may be represented by a single curve in the phase plane for which the coordinates are x_1 and x_2. The curve traced out by the state point $\{x_1(t), x_2(t)\}$ as time t is varied from 0 to ∞ is called the *phase trajectory*, and the family of all possible curves for different initial conditions is called the *phase portrait*. Normally, a finite number of trajectories, defined in a finite region, is considered a portrait.

One may obviously raise the question that when time solutions $x_1(t)$ and $x_2(t)$ as time t is varied from 0 to ∞, may be obtained by direct integration of Eqns (14.20b) analytically or numerically, where is the necessity of drawing phase portraits? In fact, as we shall see, the phase portraits provide a powerful qualitative aid for investigating system behaviour and the design of system parameters to achieve a desired response. Furthermore, the existence of limit cycles is sharply brought into focus by the phase portrait.

Figure 14.22 shows the output response and the corresponding phase trajectory for a linear second-order servo system described by the differential equation

$$\ddot{y} + 2\zeta\dot{y} + y = 0; y(0) = y^0, \ \dot{y}(0) = 0, \ 0 < \zeta < 1$$

In terms of the state variables $x_1 = y$ and $x_2 = \dot{y}$, the system model is given by the equations

$$\dot{x}_1 = x_2; \ \dot{x}_2 = -2\zeta x_2 - x_1; x_1(0) = y^0, x_2(0) = 0$$

The origin of the phase plane ($x_1 = 0, x_2 = 0$) is the *equilibrium point* of the system since at this point the derivatives $\dot{x}_1$ and $\dot{x}_2$ are zero (the system continues to lie at the equilibrium point unless otherwise disturbed). The nature of the transient can be readily inferred from the phase trajectory of Fig. 14.22; starting from the point P, i.e., with initial deviation but no initial velocity, the system returns to rest, i.e., to the origin, with damped oscillatory behaviour.

Consider now the well-known *Van der Pol's differential equation* (refer Eqn. (14.1))

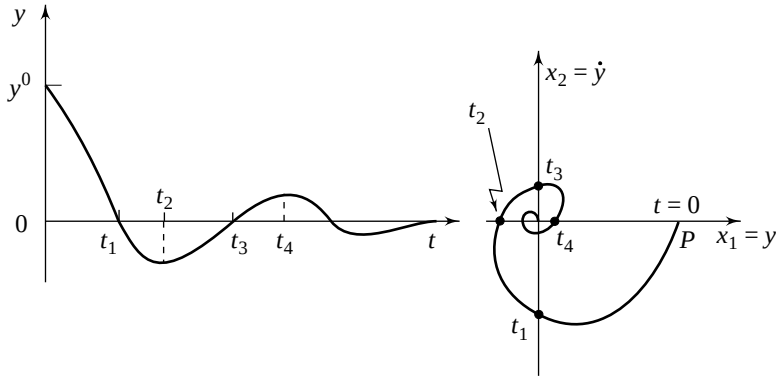

Fig. 14.22 A second-order linear system on the phase plane

$$\ddot{y} - \mu(1 - y^2)\dot{y} + y = 0$$

which describes physical situations in many nonlinear systems. In terms of the state variables $x_1 = y$ and $x_2 = \dot{y}$, we obtain

$$\dot{x}_1 = x_2; \ \dot{x}_2 = \mu(1 - x_1^2)x_2 - x_1$$

Origin of the phase plane is the equilibrium point of the system. Figure 14.23 shows phase portraits for (i) $\mu > 0$, (ii) $\mu < 0$. In the case of $\mu > 0$, we observe that for large values of $x_1(0)$, the system response is damped and the amplitude of $x_1(t) = y(t)$ decreases till the system state enters the limit cycle as shown by the outer trajectory. On the other hand, if initially $x_1(0)$ is small, the damping is negative, hence the amplitude of $x_1(t) = y(t)$ increases till the system state enters the limit cycle as shown by the inner trajectory. The limit cycle is a stable one, since the paths in its neighbourhood converge toward the limit cycle. Figure 14.23 shows an unstable limit cycle for $\mu < 0$.

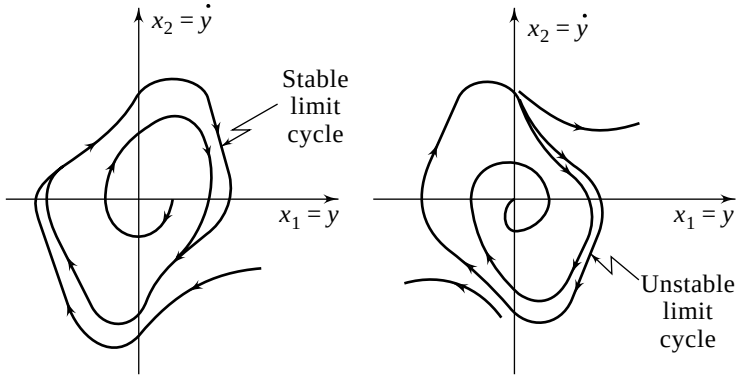

(i) $\mu > 0$ (ii) $\mu < 0$

Fig. 14.23 A second-order nonlinear system on the phase plane

The *phase plane* for second-order systems is indeed a special case of *phase space* or *state space* defined for *n*th-order systems. Much work has been done to extend this approach of analysis to third-order systems. Though a phase trajectory for a third-order system can be graphically visualized through its projections on two planes, say (x_1, x_2) and (x_2, x_3) planes, this complicacy causes the technique to lose its major power of quick graphical visualization of the total system response. The phase trajectories are therefore generally restricted to second-order systems only.

For time-invariant systems, the entire phase plane is covered with trajectories with one and only one curve passing through each point of the plane except for certain critical points through which either infinite number or none of the trajectories pass. Such points (called *singular points*) are discussed later in Section 14.9.

If the parameters of a system vary with time, or if a time-varying driving function is imposed, two or more trajectories may pass through a single point in a phase plane. In such cases, the phase portrait becomes complex and more difficult to work with and interpret. Therefore, the use of phase-plane analysis is restricted to second-order systems with constant parameters and constant or zero input. However, it may be mentioned that investigators have made fruitful use of the phase-plane method in investigating second-order time-invariant systems under simple time-varying inputs such as ramp. Some simple time-varying systems have also been analysed by this method. Our discussion will be limited to second-order time-invariant systems with constant or zero input.

From the above discussion, we observe that the phase-plane analysis applies primarily to systems described by second-order differential equations. In the case of feedback control systems, systems of order higher than the second are likely to be well filtered and tractable by the describing-function method discussed earlier in this chapter. The two methods of the phase plane and of the describing function are therefore complementary to a large extent, each being available for the study of the systems which are most likely to be beyond the scope of the other.

14.8 CONSTRUCTION OF PHASE PORTRAITS

Today, phase portraits are routinely computer-generated. However (as for example, in the case of root locus for linear systems), it is still practically useful to learn how to roughly sketch phase portraits or quickly verify the plausibility of computer outputs.

For some special nonlinear systems, particularly piecewise linear systems (whose phase portraits can be constructed by piecing together the phase portraits of the related linear systems), phase portraits can be constructed analytically. Analytical methods are useful for systems modelled by differential equations that can be easily solved. If the system of differential equations cannot be solved analytically, we can use graphical methods. A number of graphical methods for constructing phase-plane trajectories are now available; we will describe in this section the method of isoclines.

14.8.1 Analytical Method

Most nonlinear systems cannot be easily solved by analytical techniques. However for piecewise linear systems, an important class of nonlinear systems, this method can be conveniently used, as the following examples show.

Example 14.3 In this example, we consider a model of a satellite shown in Fig. 13.3. We assume that the satellite is rigid and is in a frictionless environment. It can rotate about the reference axis as a result of torque T applied to the satellite about its mass centre by firing the thrusters ($T = Fd$). The system input is the applied torque T and the system output is the attitude angle θ. The satellite's moment of inertia is J. The input-output model of the system is

$$J\frac{d^2\theta}{dt^2} = T \tag{14.22a}$$

We assume that when the thrusters fire, the thrust is constant; that is, $T = A$, a constant greater than or less than zero. In terms of output variable $y(=\theta)$, we obtain the equation

$$J\ddot{y} = A \tag{14.22b}$$

In terms of the state variables $x_1 = y$ and $x_2 = \dot{y}$, the state equations become

$$\dot{x}_1 = x_2; \quad \dot{x}_2 = \frac{A}{J} \tag{14.22c}$$

Elimination of t by division yields the equation of the trajectories:

$$\frac{dx_2}{dx_1} = \frac{A}{Jx_2} \tag{14.23}$$

or $$Jx_2\,dx_2 = A\,dx_1$$

This equation is easily integrated; the general solution is

$$x_1(t) = \frac{Jx_2^2(t)}{2A} + C \tag{14.24a}$$

where C is a constant of integration and is determined by initial conditions, i.e.,

$$C = x_1(0) - \frac{Jx_2^2(0)}{2A} \tag{14.24b}$$

For an initial state point $(x_1(0), x_2(0))$, the trajectory is a parabola passing through the point $x_1 = C$ on the x_1-axis where C is defined by Eqn. (14.24b).

A family of parabolas in the (x_1, x_2) plane is shown in Fig. 14.24a for $A > 0$. As time t increases, each trajectory is described in the clockwise direction as indicated by the arrows. The direction of the phase trajectories is dictated by the relationship $\dot{x}_1 = x_2$: x_1 increases with time in the upper half of the phase plane and the state point therefore moves from left to right ($\rightarrow$); in the lower half of the phase plane, x_1 decreases with time and the state point must therefore move from right to left ($\leftarrow$).

The time interval between two points of a trajectory is given by $\Delta t = \Delta x_1 / x_{2av}$. The trajectories may be provided with a time scale by means of this equation. This operation is, however, often unnecessary since the phase portrait is mainly used to display the general features of the system transients.

The phase portrait for $A < 0$ is shown in Fig. 14.24b. In the special case of $A = 0$ (no driving torque), the integration of the trajectory equation (14.23) gives $x_2(t) = x_2(0)$. The trajectories are therefore straight lines parallel to x_1-axis.

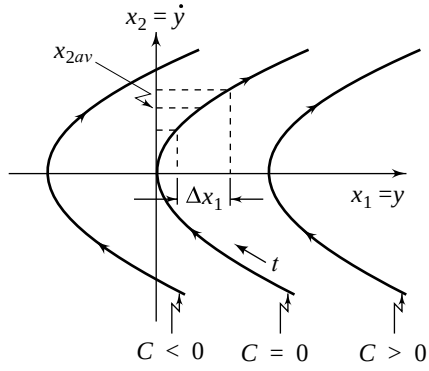

(a) $A > 0$

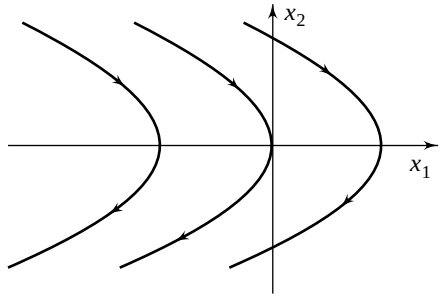

(b) $A < 0$

Fig. 14.24 Phase potraits for system (14.22)

Example 14.4 Consider now the equation

$$J\ddot{\theta} + B\dot{\theta} = T \tag{14.25a}$$

corresponding to a torque T driving a load comprising inertia J and viscous friction B. For a constant torque, the equation may be expressed as

$$\tau\ddot{y} + \dot{y} = A \tag{14.25b}$$

where $y = \theta$ is the system output and A represents normalized torque; a constant greater than or less than zero. The equivalent system is

$$\dot{x}_1 = x_2; \quad \tau\dot{x}_2 = A - x_2 \tag{14.25c}$$

Let us take a new variable z such that

$$A - x_2 = z;\ dx_2 = -dz$$

Eliminating the time variable by division, we obtain

$$\frac{1}{\tau}\frac{dx_1}{dz} = -\frac{A - z}{z} = 1 - \frac{A}{z}$$

This first-order equation is readily integrated.

$$\frac{1}{\tau}x_1 = z - A \ln z + C$$

or $$\frac{1}{\tau}x_1(t) = A - x_2(t) - A\ln(A - x_2(t)) + C \qquad (14.26a)$$

where the constant of integration C is determined by the initial conditions, i.e.,

$$C = \frac{1}{\tau}x_1(0) - A + x_2(0) + A\ln(A - x_2(0)) \qquad (14.26b)$$

Therefore, the trajectory equation becomes

$$\frac{1}{\tau}(x_1 - x_1(0)) = -(x_2 - x_2(0)) - A\ln\left(\frac{A - x_2}{A - x_2(0)}\right) \qquad (14.26c)$$

The phase portrait is shown in Fig. 14.25a for $A > 0$.

For the case of initial state point at the origin ($x_1(0) = x_2(0) = 0$), Eqn. (14.26c) reads

$$\frac{1}{\tau}x_1 = -x_2 - A\ln\left(\frac{A - x_2}{A}\right) \qquad (14.26d)$$

The phase trajectory described by this equation is shown in Fig. 14.25a as the curve Γ_0. It is seen that the trajectory is asymptotic to the line $x_2 = A$, which is the final velocity.

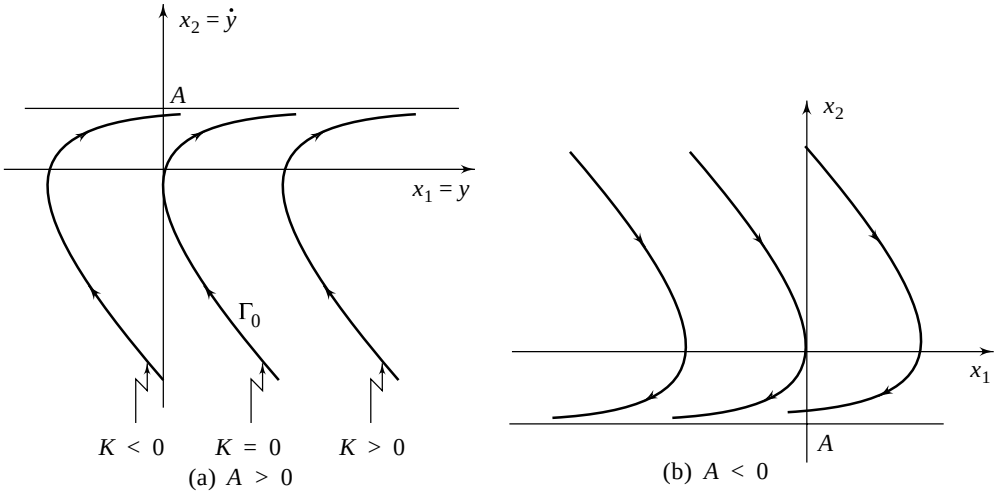

Fig. 14.25 Phase portraits for system (14.25)

For an initial state point $(x_1(0), x_2(0))$, the trajectory will have the same shape as the curve Γ_0, except that it is shifted horizontally so that it passes through the point $(x_1(0), x_2(0))$. This is obvious from Eqn. (14.26c) which can be written as

$$\frac{1}{\tau}(x_1 - K) = -x_2 - A\ln\left(\frac{A - x_2}{A}\right)$$

where $$K = x_1(0) + \tau x_2(0) + \tau A\ln\left(\frac{A - x_2(0)}{A}\right)$$

For an initial state point $(x_1(0), x_2(0))$, the trajectory is Γ_0 shifted horizontally by K units. The phase portrait for $A < 0$ is shown in Fig. 14.25b. In the special case of $A = 0$, the phase portrait consists of a family of straight lines of slope $-1/\tau$.

14.8.2 The Method of Isoclines

Consider a time-invariant second-order system described by equations of the form (refer Eqns (14.20b))

$$\begin{aligned} \dot{x}_1 &= x_2 \\ \dot{x}_2 &= f(x_1, x_2) \end{aligned} \tag{14.27}$$

The equation of the trajectories is

$$\frac{dx_2}{dx_1} = \frac{f(x_1, x_2)}{x_2}, \tag{14.28}$$

At a point (x_1^*, x_2^*) in the phase plane, the slope m^* of the tangent to the trajectory can be determined from

$$\frac{f(x_1^*, x_2^*)}{x_2^*} = m^* \tag{14.29}$$

An *isocline* is defined to be the locus of the points corresponding to a given constant slope m of the trajectories on the phase plane. All trajectories passing through the points on the curve

$$f(x_1, x_2) = mx_2 \tag{14.30}$$

will have the same tangent slope m at the points on the curve; the curve thus represents an isocline corresponding to trajectories of slope m. All trajectories crossing this isocline will have tangent slope m at the points on the isocline.

The idea of the method of isoclines is to construct several isoclines and a field of local tangents m. Then, the trajectory passing through any given point in the phase plane is obtained by drawing a continuous curve following the directions of the field.

Consider the Van der Pol equation (refer Eqn. (14.1))

$$\ddot{y} + \mu\left(y^2 - 1\right)\dot{y} + y = 0 \tag{14.31}$$

With $x_1 = y$ and $x_2 = \dot{y}$, the equation of the trajectories becomes

$$\frac{dx_2}{dx_1} = \frac{-\mu(x_1^2 - 1)x_2 - x_1}{x_2}$$

Therefore, the points on the curve

$$\frac{-\mu(x_1^2 - 1)x_2 - x_1}{x_2} = m$$

all have the same slope m. The isocline equation becomes

$$x_2 = \frac{x_1}{\left(\mu - \mu x_1^2\right) - m}$$

By taking m of different values, different isoclines can be obtained. Short line segments are drawn on the isoclines to generate a field of tangent directions. A trajectory starting at any point can be constructed by drawing short lines from one isocline to another at average slope corresponding to the two adjoining isoclines as shown in Fig. 14.26.

Of course, the construction is much simpler if isoclines are straight lines.

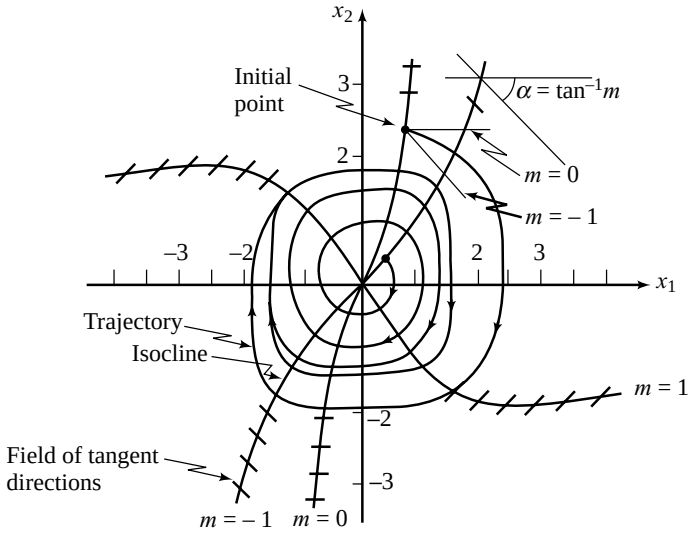

Fig. 14.26 Phase portrait of the Van der Pol equation

Example 14.5 The satellite in Example 14.3 is now placed in a feedback configuration in order to maintain the attitude θ at 0°. This feedback control system, called an attitude control system, is shown in Fig. 14.27. When θ is other than 0°, the appropriate thruster will fire to force θ towards 0°. When $\theta = x_1$ is greater than 0°, u (torque T) = $-U$, and the trajectories of Fig. 14.24b (corresponding to $A < 0$) apply. When $\theta = x_1$ is less than 0°, u (torque T) = U, and the trajectories of Fig. 14.24a (corresponding to $A > 0$) apply. Note that the switching of u occurs at $x_1 = 0$. Thus the line $x_1 = 0$ (the x_2-axis) is called the *switching line*. From this discussion we see that Fig. 14.28a illustrates a typical trajectory for the system corresponding to the initial condition (x_1^0, x_2^0). The system response is thus a periodic motion. Figure 14.28b shows many closed curves for different initial conditions.

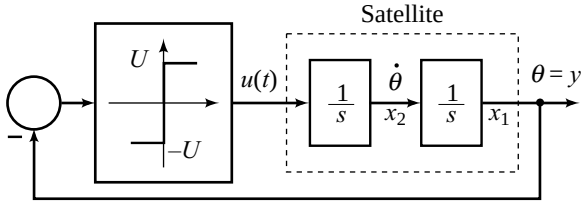

Fig. 14.27 A satellite-attitude control system

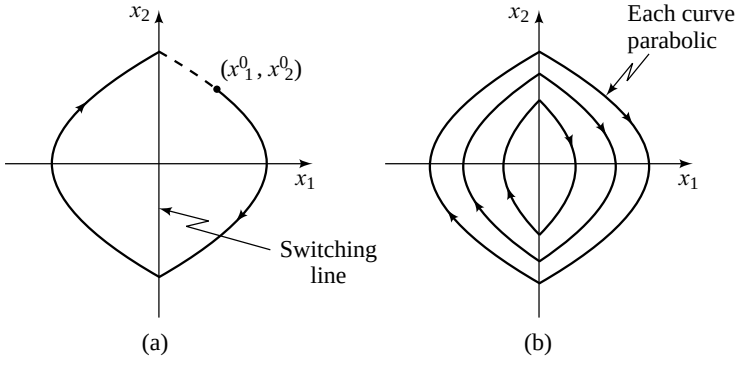

Fig. 14.28 Typical trajectories for the system of Fig.14.27

By controlling the switching line in the phase plane, we can control the performance of the attitude control system. This simple control strategy leads to a robust nonlinear control structure: the *variable structure sliding mode control*. Refer the companion book [155] for details.

In the following we obtain the phase portrait of the closed-loop system of Fig. 14.27 using the method of isoclines. The purpose here is to illustrate the method of isoclines.

The state equations are

$$\dot{x}_1 = x_2$$

$$\dot{x}_2 = -U \operatorname{sgn} x_1$$

where

$$\operatorname{sgn} x_1 = \begin{cases} 1, & x_1 > 0 \\ -1, & x_1 < 0 \end{cases}$$

Then

$$m = \frac{dx_2}{dx_1} = \frac{-U \operatorname{sgn} x_1}{x_2}$$

Suppose that U is normalized to a value of unity for convenience. Then

$$x_2 = -\frac{1}{m} \operatorname{sgn} x_1$$

For $x_1 > 0$, $\operatorname{sgn} x_1 = 1$, and the isocline equation is

$$x_2 = -\frac{1}{m}; \; x_1 > 0$$

For $x_1 < 0$, $\operatorname{sgn} x_1 = -1$, and the isocline equation is

$$x_2 = \frac{1}{m}; \; x_1 < 0$$

Given in Fig. 14.29 is the phase plane showing the isoclines and a typical phase trajectory. Note the parabolic shape, as was determined analytically earlier in this example.

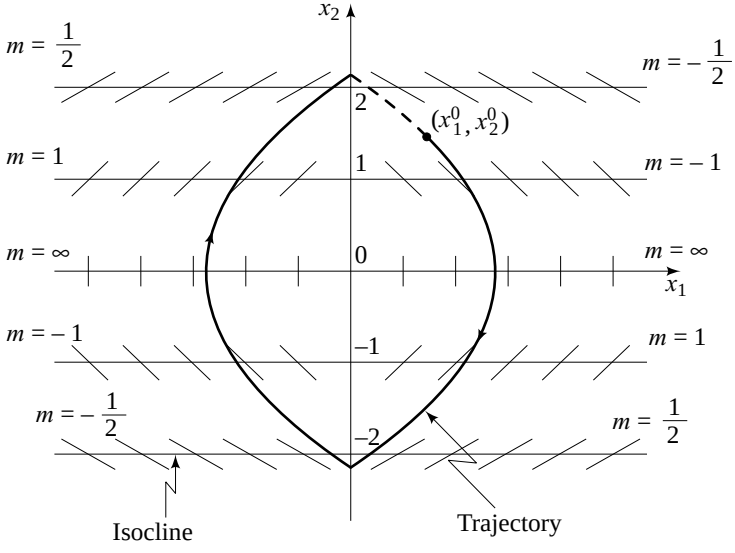

Fig.14.29 The isoclines and a typical trajectory for the system of Fig. 14.27

14.9 SYSTEM ANALYSIS ON THE PHASE PLANE

In the phase plane analysis of nonlinear systems, two points should be kept in mind:

- Phase plane analysis of nonlinear systems is related to that of linear systems because the local behaviour of a nonlinear system can be approximated by a linear system behaviour.
- Still, nonlinear systems can display much more complicated patterns on the phase plane, such as multiple equilibrium points, and limit cycles.

Consider a time-invariant second-order system described by equations of the form (refer Eqns (14.27))

$$\dot{x}_1 = x_2 \; ; \; \dot{x}_2 = f(x_1, x_2) \tag{14.32}$$

Elimination of independent variable t gives the equation of the trajectories of phase plane (refer Eqn. (14.28)):

$$\frac{dx_2}{dx_1} = \frac{f(x_1, x_2)}{x_2} \tag{14.33}$$

In this equation, x_1 and x_2 are independent and dependent variables, respectively. Integration of the equation, analytically, graphically or numerically, for various initial conditions yields a family of phase trajectories which displays the general features of the system transients.

14.9.1 Singular Points

Every point (x_1, x_2) of the phase plane has associated with it the slope of the trajectory which passes through that point. The slope m at the point (x_1, x_2) is given by the equation

$$m = \frac{dx_2}{dx_1} = \frac{f(x_1, x_2)}{x_2}$$

With the function $f(x_1, x_2)$ assumed to be single valued, there is usually a definite value for this slope at any given point in phase plane. This implies that the phase trajectories will not intersect. The only exceptions are the *singular points* at which the trajectory slope is indeterminate:

$$\frac{dx_2}{dx_1} = \frac{0}{0} = \frac{f(x_1, x_2)}{x_2} \tag{14.34a}$$

Many trajectories may intersect at such points. This indeterminacy of the slope accounts for the adjective 'singular'.

Singular points are very important features on the phase plane. Examination of the singular points can reveal a great deal of information about the properties of a system. In fact, the stability of linear systems is uniquely characterized by the nature of their singular points. For nonlinear systems, besides singular points, there may be more complex features such as limit cycles.

We need to know the following:

1. Where will the singular points be and how many will be there?
2. What is the behaviour of trajectories (i.e., the system) in the vicinity of a singular point?

The first question is answered by our definition of the singular point. There will be singular points at all the points of the phase plane for which the slope of the trajectory is undefined. These points are given by the solution of the equations

$$x_2 = 0; f(x_1, x_2) = 0 \tag{14.34b}$$

Singular points of the nonlinear system (14.32), thus, lie on the x_1-axis of the phase plane.

Since at singular points on the phase plane, $\dot{x}_1 = \dot{x}_2 = 0$, these points in fact correspond to the *equilibrium states* of the nonlinear system. We know a nonlinear system often has multiple equilibrium states.

To determine the behaviour of the trajectories in the vicinity of a singular point (equilibrium state of the nonlinear system), we first linearize the nonlinear equations at the singular point and then determine the nature of phase trajectories around the singular point by linear system analysis. If the singular point of interest is not at the origin, by defining the difference between the original state and the singular point as a new set of state variables, one can always shift the singular point to the origin. Therefore, without loss of generality, we can simply consider Eqns (14.32) with a singular point at **0**. Using Taylor series expansion, Eqns (14.32) can be rewritten as

$$\dot{x}_1 = x_2$$
$$\dot{x}_2 = ax_1 + bx_2 + g_2(x_1, x_2)$$

where $g_2(\bullet)$ contains higher-order terms.

In the vicinity of the origin, the higher-order terms can be neglected and therefore the nonlinear system trajectories essentially satisfy the linearized equations

$$\dot{x}_1 = x_2$$
$$\dot{x}_2 = ax_1 + bx_2$$

Transforming these equations into a scalar second-order equation, we get

$$\ddot{x}_1 = a x_1 + b\dot{x}_1$$

Therefore, we will simply consider the second-order linear system described by

$$\ddot{y} + 2\zeta\omega_n \dot{y} + \omega_n^2 y = 0 \tag{14.35a}$$

The characteristic roots of this equation are assumed to be $\lambda_1$and λ_2:

$$\ddot{y} + 2\zeta\omega_n \dot{y} + \omega_n^2 y = (s - \lambda_1)(s - \lambda_2) = 0 \tag{14.35b}$$

The corresponding canonical state model is

$$\dot{x}_1 = x_2; \quad \dot{x}_2 = -2\zeta\omega_n x_2 - \omega_n^2 x_1 \tag{14.35c}$$

and the differential equation of the trajectories is

$$\frac{dx_2}{dx_1} = \frac{-2\zeta\omega_n x_2 - \omega_n^2 x_1}{x_2} \tag{14.35d}$$

By inspection of this equation it is easily seen that at $x_1 = x_2 = 0$, the slope dx_2/dx_1 is indeterminate:

$$\frac{dx_2}{dx_1} = \frac{0}{0}$$

In the following, we discuss the behaviour of the trajectories in the vicinity of this point with undefined slope (the *singular point*).

According to the values of λ_1 and λ_2, one is led to distinguish between the six types of singular points shown in Fig. 14.30. Let us examine each of these cases in detail.

1. Stable system with complex roots

$$\lambda_1 = -\alpha + j\beta, \quad \lambda_2 = -\alpha - j\beta; \quad \alpha > 0, \beta > 0$$

The response $$y(t) = C_1 e^{-\alpha t} \sin(\beta t + C_2) \tag{14.36}$$

where the constants C_1 and C_2 are determined by the initial conditions.

Using Eqn. (14.36), we can construct a phase portrait on the (x_1, x_2)-plane with $x_1 = y$ and $x_2 = \dot{y}$. A typical phase trajectory is shown in Fig. 14.30a which is a logarithmic spiral into the singular point. This type of singular point is called a *stable focus*.

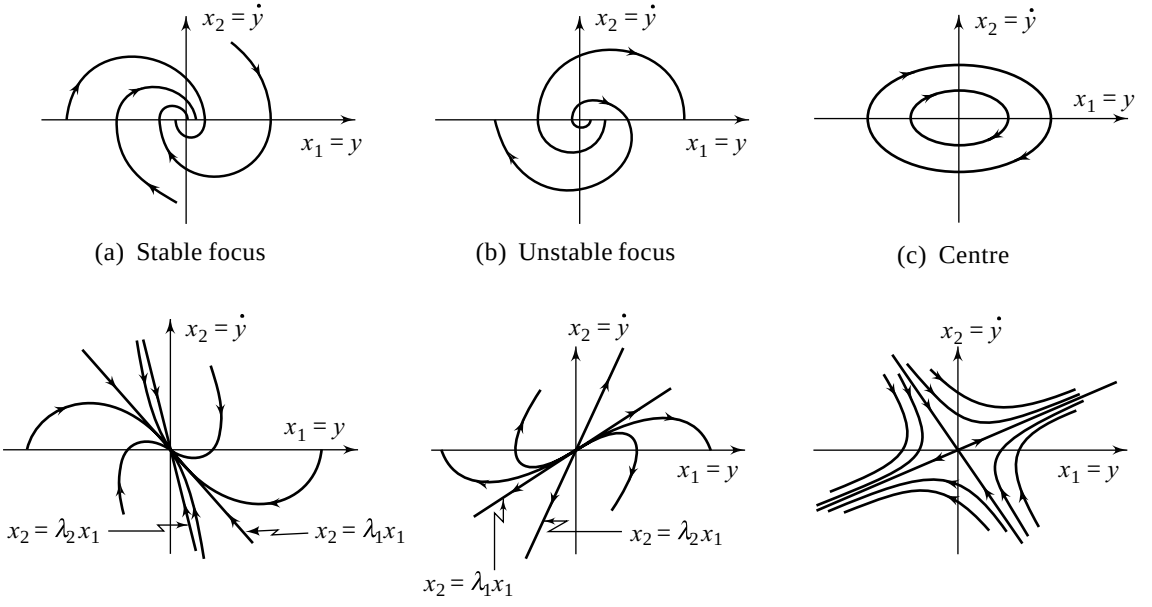

(a) Stable focus (b) Unstable focus (c) Centre

(d) Stable node (e) Unstable node (f) Saddle point

Fig. 14.30 Phase portraits for system (14.35)

2. Unstable system with complex roots

$$\lambda_1 = \alpha + j\beta, \quad \lambda_2 = \alpha - j\beta; \quad \alpha > 0, \beta > 0$$

The response $$y(t) = C_1 e^{\alpha t} \sin(\beta t + C_2) \tag{14.37}$$

The transient is an exponentially increasing sinusoid; the phase trajectory on the $(x_1 = y, x_2 = \dot{y})$-plane is a logarithmic spiral expanding out of the singular point (Fig. 14.30b). This type of singular point is called an *unstable focus*.

3. Marginally stable system with complex roots

$$\lambda_1 = j\beta, \lambda_2 = -j\beta; \quad \beta > 0$$

The response $$y(t) = C_1 \sin(\beta t + C_2) \tag{14.38}$$

The phase trajectories are closed curves (elliptical) concentric with the singular point (Fig. 14.30c). This type of singular point is called a *centre*, or a *vortex*.

4. *Stable system with real roots* Assume that λ_1 and λ_2 are two real, distinct roots in the left half of the s-plane; λ_1 is the root with the smaller modulus. The response

$$y(t) = C_1 e^{\lambda_1 t} + C_2 e^{\lambda_2 t} \tag{14.39a}$$

It is an overdamped system. The phase portrait in the vicinity of the singular point on the $(x_1 = y, x_2 = \dot{y})$-plane is shown in Fig. 14.30d. Such a singular point is called a *stable node*.

The phase portrait has two straightline trajectories defined by the equations

$$x_2(t) = \lambda_1 x_1(t); \quad x_2(t) = \lambda_2 x_1(t) \tag{14.39b}$$

It can easily be verified that these trajectories satisfy the differential equation of the given system.

The transient term $e^{\lambda_2 t}$ decays faster than the term $e^{\lambda_1 t}$. Therefore as t increases indefinitely, $x_1 \to C_1 e^{\lambda_1 t} \to 0$, and $x_2 \to \lambda_1 C_1 e^{\lambda_1 t} \to 0$, so that all the trajectories are tangential at the origin to the straightline trajectory $x_2(t) = \lambda_1 x_1(t)$. The other straightline trajectory, $x_2(t) = \lambda_2 x_1(t)$, is described only if the initial conditions are such that $x_2(0) = \lambda_2 x_1(0)$.

For stable systems with repeated real roots, the two straightline trajectories coalesce into a single trajectory, again with the slope determined by the root value.

5. *Unstable system with positive real roots* Assume that λ_1 and λ_2 are two real distinct roots in the right half of the s-plane; λ_1 is the smaller root. The phase portrait in the vicinity of the singular point on the $(x_1 = y, x_2 = \dot{y})$-plane is shown in Fig. 14.30e. Such a singular point is called an *unstable node*.

All trajectories emerge from the singular point and go to infinity. The trajectories are tangential at the origin to the straightline trajectory, $x_2(t) = \lambda_1 x_1(t)$.

6. *Unstable system with one negative real root and one positive real root* The phase portrait in the vicinity of the singular point on the $(x_1 = y, x_2 = \dot{y})$-plane is shown in Fig. 14.30f. Such a singular point is called a *saddle*.

There are two straightline trajectories with slopes defined by the root values. The straightline due to the negative root provides a trajectory that *enters* the singular point, while the straightline trajectory due to the positive root *leaves* the singular point. All other trajectories approach the singular point adjacent to the incoming straight line, then curve away and leave the vicinity of the singular point, eventually approaching the second straight line asymptotically.

Example 14.6 Consider the nonlinear system shown in Fig. 14.31. The nonlinear element is an on-off controller with deadzone whose characteristics are shown in the figure.

The differential equation governing the dynamics of the system is given by

$$\ddot{y} + \dot{y} = u; \qquad \text{or} \qquad \ddot{e} + \dot{e} = -\phi(e) \tag{14.40}$$

where $e = r - y$; r is constant, and

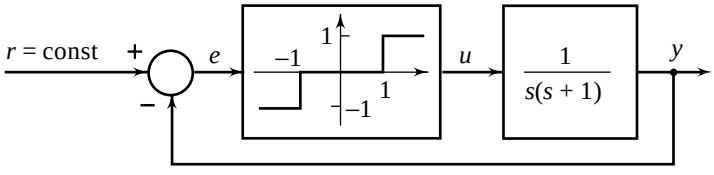

Fig. 14.31 A system controlled by on-off controller with deadzone

$$\phi(e) = \begin{cases} +1\,;\ e>1 \\ 0\,;\ -1<e<1 \\ -1\ ;\ e<-1 \end{cases}$$

Choosing the state variables $x_1 = e$ and $x_2 = \dot{e}$, we obtain the following first-order equations:

$$\dot{x}_1 = x_2; \quad \dot{x}_2 = -x_2 - \phi(x_1)$$

These equations are same as Eqns (14.25c) with $\tau = 1$ and $A = -\phi(x_1)$.
The phase plane may be divided into three regions:

1. *Region* I (defined by $x_1 > 1$): The trajectories in this region are given by the equation (refer Eqn. (14.26c): $\tau = 1$, $A = -1$)

$$x_1 - x_1(0) = -(x_2 - x_2(0)) + \ln\left(\frac{1+x_2}{1+x_2(0)}\right) \tag{14.41a}$$

   The trajectories are asymptotic to the ordinate -1.
2. *Region* II (defined by $-1 < x_1 < 1$): The trajectories in this region are given by the equation (refer Eqn. (14.26c): $\tau = 1$, $A = 0$)

$$x_1 - x_1(0) = -(x_2 - x_2(0)) \tag{14.41b}$$

   The trajectories are straightlines of slope -1.
3. *Region* III (defined by $x_1 < -1$): The trajectories in this region are given by the equation (refer Eqn. (14.26c): $\tau = 1$, $A = 1$)

$$x_1 - x_1(0) = -(x_2 - x_2(0)) - \ln\left(\frac{1-x_2}{1-x_2(0)}\right) \tag{14.41c}$$

The trajectories are asymptotic to the ordinate $+1$.

For a step input $r = 3$ and zero initial conditions, the initial point of the phase trajectory is located at P in Fig. 14.32. The figure also shows a phase trajectory, constructed using Eqns (14.41).

It is important to note that a small deadzone region is not always undesirable in on-off controllers. Let us investigate the behaviour of the system of Fig. 14.31 using on-off with no deadzone as a controller. For such a controller, the width of region II (corresponding to deadzone) in the phase plane reduces to zero. The phase trajectory of such a system with $r = 3$ is shown in Fig. 14.33 : $e(t)$ oscillates about the origin with ever-decreasing amplitude and ever-increasing frequency.

Comparison of Figs 14.32 and 14.33 reveals that deadzone in on-off controller characteristic helps to reduce system oscillations, thereby reducing settling time. However the on-off controller with deadzone drives the system to a point within the deadzone width. A large deadzone would of course cause the steady-state performance of the system to deteriorate.

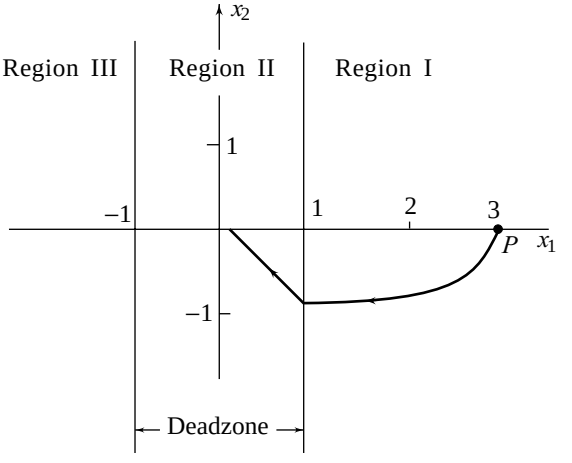

Fig. 14.32 A typical trajectory for the system in Fig. 14.31

Example 14.7 Let us investigate the performance of a second-order position control system with Coulomb friction. Figure 14.34 is a model for a motor position servo with Coulomb friction on the motor shaft. The dynamics of the system is described by the following differential equation:

$$K e - T_c \operatorname{sgn}(\dot{y}) = J\ddot{y} + B\dot{y}$$

where T_c is the Coulomb frictional torque.

For constant input r, $\dot{y} = -\dot{e}$ and $\ddot{y} = -\ddot{e}$. Therefore

$$J\ddot{e} + B\dot{e} + T_c \operatorname{sgn}(\dot{e}) + Ke = 0$$

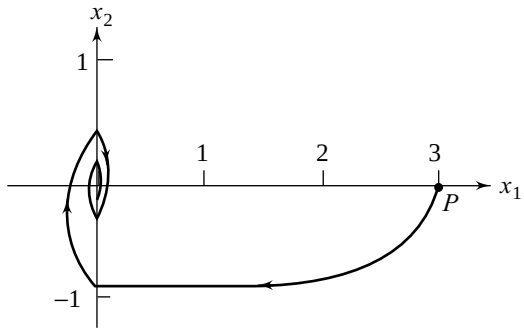

Fig. 14.33 Phase trajectory for the system in Fig. 14.31 when the deadzone is absent

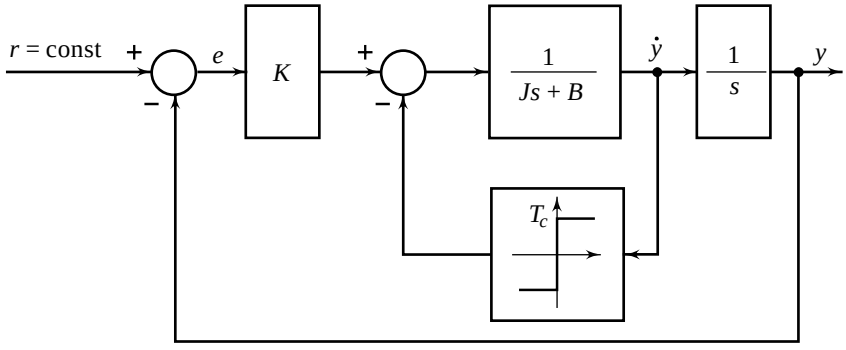

Fig. 14.34 A motor position servo with Coulomb friction on the motor shaft

or
$$\frac{J}{B}\ddot{e} + \dot{e} + \frac{T_c}{B}\operatorname{sgn}(\dot{e}) + \frac{K}{B}e = 0 \tag{14.42}$$

Letting $J/B = \tau$, we get

$$\tau\ddot{e} + \dot{e} + \frac{T_c}{B}\operatorname{sgn}(\dot{e}) + \frac{K}{B}e = 0 \tag{14.43}$$

In terms of state variables

$$x_1 = e;\ x_2 = \dot{e}$$

we get the following description of the system:

$$\dot{x}_1 = x_2; \quad \tau\dot{x}_2 = -\frac{K}{B}x_1 - x_2 - \frac{T_c}{B}\operatorname{sgn}(x_2) \tag{14.44}$$

The singular points are given by the solution of the equations (refer Eqns (14.34b))

$$0 = x_2; \quad 0 = -\frac{K}{B}x_1 - x_2 - \frac{T_c}{B}\operatorname{sgn}(x_2)$$

The solution gives

$$x_1 = -\frac{T_c}{K}\operatorname{sgn}(x_2)$$

Thus, there are two singular points. Their location can be interpreted physically—they are at a value of $e = x_1$, such that $|K\,e| = |T_c|$, i.e., the drive torque is exactly equal to the Coulomb-friction torque. We note that both the singular points are on the x_1-axis ($x_2 \equiv 0$) and that the singular point given by $x_1 = T_c/K$ is related to the lower-half phase plane (x_2 negative) and the singular point given by $x_1 = -T_c/K$ is related to the upper-half phase plane (x_2 positive).

Let us now investigate the stability of the singular points. For $\dot{e} > 0$, Eqn. (14.43) may be expressed as

$$\tau \frac{d^2}{dt^2}\left(e + \frac{T_c}{K}\right) + \frac{d}{dt}\left(e + \frac{T_c}{K}\right) + \frac{K}{B}\left(e + \frac{T_c}{K}\right) = 0 \tag{14.45}$$

This is a linear second-order system with the singular point at $(-T_c/K,\ 0)$ on the $(e,\ \dot{e}\,)$-plane. The characteristic equation of this system is given by

$$\lambda^2 + \frac{1}{\tau}\lambda + \frac{K}{\tau B} = 0$$

Let us assume the following parameter values for the system under consideration:

$$(K/B) = 5,\ \tau = 4 \tag{14.46}$$

With these parameters, the roots of the characteristic equation are complex conjugate with negative real parts; the singular point is therefore a stable focus (refer Fig. 14.30a).

Let us now investigate the system behaviour when large inputs are applied. Phase trajectories may be obtained by solving the following second-order differential equations for given initial state points (refer Eqns (14.35b)–(14.36)).

Region I (defined by $x_2 > 0$):

$$4\,\ddot{z} + \dot{z} + 5z = 0;\ z = x_1 + \frac{T_c}{K};\ x_2 = \dot{x}_1$$

Region II (defined by $x_2 < 0$):

$$4\,\ddot{z} + \dot{z} + 5z = 0;\ z = x_1 - \frac{T_c}{K};\ x_2 = \dot{x}_1$$

Figure 14.35 shows a few phase trajectories. It is observed that for small as well as large inputs, the resulting trajectories terminate on a line along the x_1-axis from $-T_c/K$ to $+T_c/K$, i.e., the line joining the singular points. Therefore, the system with Coulomb friction is stable; however, there is a possibility of large steady-state error.

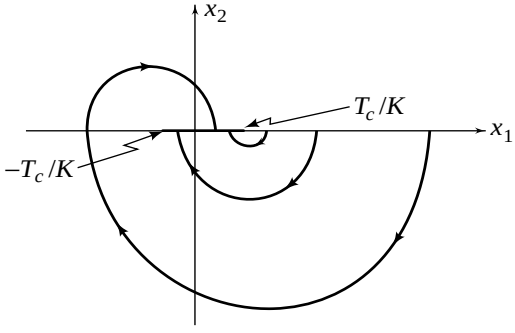

Fig. 14.35 Phase portrait for the system in Fig. 14.34

14.9.2 Limit Cycles

In the phase portrait of the nonlinear Van der Pol equation, shown in Fig. 14.26 , one observes that there is a closed-curve in the phase portrait. Trajectories inside the curve and those outside the curve all tend to this curve, while a motion started on this curve will stay on it forever. This curve is an instance of the so-called "limit cycle" phenomenon. Limit cycles are unique features of nonlinear systems.

On the phase plane, *a limit cycle is defined as an isolated closed curve*. The trajectory has to be both closed, indicating the periodic nature of motion, and isolated, indicating the limiting nature of the cycle (with neighboring trajectories converging to or diverging from it). Thus while there are many closed curves in Fig. 14.28b (in the satellite system in Example 14.5), these are not limit cycles because they are not isolated.

A limit cycle is stable if all trajectories in the vicinity of the limit cycle converge to it as $t \to \infty$ (Fig. 14.23a). A limit cycle is unstable if all trajectories in the vicinity of the limit cycle diverge from it as $t \to \infty$ (Fig. 14.23b).

14.10 LYAPUNOV STABILITY

It should be obvious by now that stability plays a major role in control systems design. We have introduced earlier in Chapters 5 and 12, the concept of stability based on the dynamic evolution of the system state in response to arbitrary initial state, representing initial energy storage. State variable model

$$\dot{\mathbf{x}}(t) = \mathbf{A}\mathbf{x}(t); \mathbf{x}(t=0) \triangleq \mathbf{x}^0 \tag{14.47}$$

is most appropriate to study dynamic evolution of the state $\mathbf{x}(t)$ in response to the initial state $\mathbf{x}^0$ with zero external input. At the origin of the state space, $\dot{\mathbf{x}}(t) = \mathbf{0}$ for all t; the origin is thus the *equilibrium point* of the system, and $\mathbf{x}^e = \mathbf{0}$ is the *equilibrium state*. This system is *marginally stable* if for all possible initial states $\mathbf{x}^0$, $\mathbf{x}(t)$ remains thereafter within finite bounds for $t > 0$. This is true if none of the eigenvalues of $\mathbf{A}$ are in the right half of the complex plane and eigenvalues on the imaginary axis, if any, are simple (A multiple eigenvalue on the imaginary axis would have a response that grows in time and could not be stable). Furthermore, the system is *asymptotically stable* if for all possible initial states $\mathbf{x}^0$, $\mathbf{x}(t)$ eventually decays to zero as t approaches infinity. This is true if all the eigenvalues of $\mathbf{A}$ are inside the left half of the complex plane.

This concept of stability, in fact, follows from Lyapunov stability theory. A.M. Lyapunov considered the stability of general nonlinear systems described by state equation of the form

$$\dot{\mathbf{x}}(t) = \mathbf{f}(\mathbf{x}(t)); \mathbf{x}(0) \triangleq \mathbf{x}^0 \tag{14.48}$$

If $\mathbf{f}(\mathbf{x}) = \mathbf{A}\mathbf{x}$, then we have the linear case considered in earlier chapters of the book. We assume that the equation has been written so that $\mathbf{x} = \mathbf{0}$ is an *equilibrium point*, which is to say that $\mathbf{f}(\mathbf{0}) = \mathbf{0}$, i.e., the system will continue to be in *equilibrium state* $\mathbf{x}^e = \mathbf{0}$ for all time. This equilibrium point is said to be *stable in the sense of Lyapunov* if we are able to select a bound on initial condition $\mathbf{x}^0$ that will result in state trajectories $\mathbf{x}(t)$ that remain within a chosen finite limit. More formally, the system described by Eqn. (14.48) is stable in the sense of Lyapunov at $\mathbf{x} = \mathbf{0}$ if, for every real number $\varepsilon > 0$ there exists a real number $\delta > 0$, such that[1] $\|\mathbf{x}(0)\| < \delta$ results in $\|\mathbf{x}(t)\| < \varepsilon$ for all $t \geq 0$. The system is asymptotically stable at $\mathbf{x} = \mathbf{0}$ if it is stable in the sense of Lyapunov and in addition, the state $\mathbf{x}(t)$ approaches zero as time t approaches infinity. Responses that are stable in the sense of Lyapunov, and asymptotically stable are shown in Figs 14.36. The term 'marginally stable' used in earlier chapters of the book, in fact, is an adaptation of the term "stable in the sense of Lyapunov", for our specific needs in linear system analysis.

No new results are obtained by the use of Lyapunov's method for the stability analysis of linear time-invariant systems. Simple and powerful methods discussed in earlier chapters are adequate for such systems. However, Lyapunov functions supply certain performance indices and synthesis data of linear time-invariant systems [155].

The Lyapunov's method of stability analysis, in principle, is the most general method for determination of stability of nonlinear systems. The major drawback which seriously limits its use in practice is the difficulty often associated with the construction of the Lyapunov function required by the method. Unfortunately, there is no universal method for selecting the Lyapunov function which is unique for a given nonlinear

[1] $\|\mathbf{x}\| = a$ *norm* of vector $\mathbf{x} = \left(\sum_{i=1}^{n} x_i^2\right)^{1/2} = \left(\mathbf{x}^T\mathbf{x}\right)^{1/2}$

is a measure of the length of vector $\mathbf{x}$.

system. Several techniques have been devised for the systematic construction of Lyapunov functions; each is applicable to a particular class of systems. If a Lyapunov function cannot be found, it in no way implies that the system is unstable. It only means that our attempt in trying to establish the stability of an equilibrium state has failed. Therefore, faced with specific systems, one has to use experience, intuition, and physical insights to search for an appropriate Lyapunov function. An elegant and powerful Lyapunov analysis may be possible for complex systems if engineering insight and physical properties are properly exploited. Inspite of these limitations, Lyapunov's method is the most powerful technique available today for the stability analysis of nonlinear systems. For linear time-invariant systems, the quadratic function (refer Eqn. (12.7a)) is adequate for demonstrating Lyapunov stability.

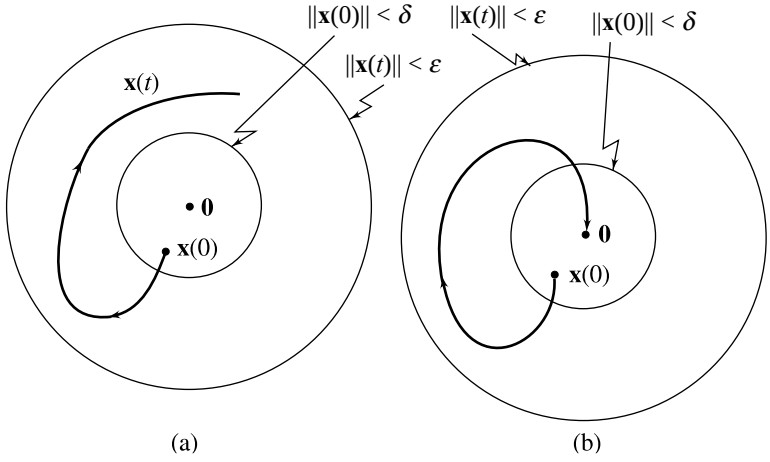

Fig. 14.36 Stability definitions

Since our brief presentation is meant as a first exposure of the student to Lyapunov stability, we restrict our choice of Lyapunov functions to quadratic form in our examples on stability analysis of both linear and nonlinear systems. For further details on the subject, refer the companion book [155].

14.10.1 Lyapunov Stability Theorem

To prove stability results for nonlinear systems, Lyapunov introduced a function that has many of the properties of energy. For the system (14.48), sufficient conditions of stability are as follows.

Suppose that there exists a scalar function $V(\mathbf{x})$ which satisfies the following properties:

(1) $V(\mathbf{x}) > 0;\ \mathbf{x} \neq \mathbf{0}$

(2) $V(\mathbf{0}) = 0$ (14.49)

(3) $V(\mathbf{x})$ is continuous and has continuous partial derivatives with respect to all components of $\mathbf{x}$.

(4) $\dot{V}(\mathbf{x}) \leq 0$ along trajectories of Eqn. (14.48)

We call $V(\mathbf{x})$ having these properties a *Lyapunov function* for the system. Properties (1) and (2) mean that, like energy, $V(\mathbf{x}) > 0$ if any state is different from zero, but $V(\mathbf{x}) = 0$ when the state is zero. Property (3) ensures that $V(\mathbf{x})$ is a smooth function and generally has the shape of a bowl near the equilibrium.

A visual analysis may be obtained by considering the surface

$$V(x_1, x_2) = \frac{1}{2} p_1 x_1^2 + \frac{1}{2} p_2 x_2^2;\ p_1 > 0,\ p_2 > 0 \tag{14.50}$$

This is a paraboloid (a solid generated by rotation of parabola about its axis of symmetry) surface as shown in Fig. 14.37. The value $V(x_1, x_2) = k_i$ (a constant) is represented by the intersection of $V(x_1, x_2)$ surface and the plane $z = k_i$. This intersection results in a closed curve; an oval. If one plots a trajectory from the point $(x_1^0, x_2^0, V(\mathbf{x}^0))$, the trajectory crosses the ovals $V(x_1, x_2) = k_i$ for successively smaller values of $V(x_1, x_2)$ and moves towards the point corresponding to $V(x_1, x_2) = 0$, which is the equilibrium point. Figure 14.37 shows a typical trajectory.

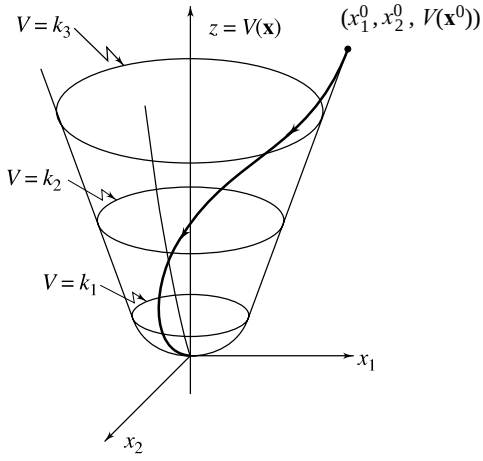

Fig. 14.37 Constant-*V* curves

Property (4) guarantees that any trajectory moves so as never to climb higher on the bowl than where it started out. If property (4) was made stronger so that $\dot{V}(\mathbf{x}) < 0$ for $\mathbf{x} \neq \mathbf{0}$, then the trajectory must be drawn to the origin (The trajectory in Fig. 14.37, in fact, corresponds to this case, i.e., $\dot{V}(\mathbf{x}) < 0$).

The *Lyapunov stability theorem states that, given the system of equations* $\dot{\mathbf{x}} = \mathbf{f}(\mathbf{x})$ *with* $\mathbf{f}(\mathbf{0}) = \mathbf{0}$, *if there exists a Lyapunov function for this equation, then the origin is stable in the sense of Lyapunov*; *in addition, if* $\dot{V}(\mathbf{x}) < 0$ for $\mathbf{x} \neq \mathbf{0}$, *then the stability is asymptotic.*

14.10.2 Lyapunov Function for Linear Systems

For linear time-invariant systems, the quadratic function is adequate for demonstrating Lyapunov stability. Consider the function

$$V(\mathbf{x}) = \mathbf{x}^T \mathbf{P} \mathbf{x} \tag{14.51}$$

where **P** is a symmetric positive definite matrix. The quadratic function (14.51) satisfies properties (1), (2) and (3) of a Lyapunov function. We need to consider property (4), the derivative condition. To compute the derivative of $V(\mathbf{x})$, we use the chain rule to get

$$\begin{aligned} \dot{V}(\mathbf{x}) &= \frac{d}{dt}(\mathbf{x}^T \mathbf{P} \mathbf{x}) \\ &= \dot{\mathbf{x}}^T \mathbf{P} \mathbf{x} + \mathbf{x}^T \mathbf{P} \dot{\mathbf{x}} \end{aligned} \tag{14.52}$$

Using Eqns (14.47) and (14.52), we get

$$\dot{V}(\mathbf{x}) = \mathbf{x}^T \mathbf{A}^T \mathbf{P} \mathbf{x} + \mathbf{x}^T \mathbf{P} \mathbf{A} \mathbf{x} = \mathbf{x}^T (\mathbf{A}^T \mathbf{P} + \mathbf{P} \mathbf{A}) \mathbf{x} = -\mathbf{x}^T \mathbf{Q} \mathbf{x}$$

where **Q** is defined by

$$\mathbf{A}^T \mathbf{P} + \mathbf{P} \mathbf{A} = -\mathbf{Q} \tag{14.53}$$

Lyapunov showed that for any positive definite **Q**, the solution **P** of the *Lyapunov Eqn.* (14.53) is positive definite if and only if all the eigenvalues of **A** have negative real parts. In other words, given the system matrix **A**, we can select a positive definite **Q** (such as identify matrix **I**), solve the Lyapunov equation (which is simply a system of linear equations in $n(n-1)/2$ unknowns), and test to see whether **P** is positive definite by looking at the determinants of the n principal minors (refer inequalities (12.7b)). From this process, we can determine the stability of the system (14.47) without finding the eigenvalues of matrix **A**.

Example 14.8 Consider a nonlinear system governed by the equations

$$\dot{x}_1 = -x_1 + 2x_1^2 x_2$$

$$\dot{x}_2 = -x_2$$

Note that $\mathbf{x} = \mathbf{0}$ is the equilibrium point.

A candidate for a Lyapunov function is

$$V = p_{11}x^2{}_1 + p_{22}x_2^2 \,;\, p_{11} > 0, p_{22} > 0$$

which is a positive definite function.
Then

$$\frac{dV}{dt} = 2p_{11}x_1\dot{x}_1 + 2p_{22}x_2\dot{x}_2 = 2p_{11}x_1(-x_1 + 2x_1^2x_2) + 2p_{22}x_2(-x_2)$$

$$= -2p_{11}x_1^2(1 - 2x_1x_2) - 2p_{22}x_2^2$$

dV/dt is negative definite if

$$1 - 2x_1x_2 > 0 \qquad (14.54)$$

Therefore, for asymptotic stability we require that the condition (14.54) is satisfied. The region of state space where this condition is not satisfied is *possibly* the region of instability. Let us concentrate on the region of state space where this condition is satisfied. The limiting condition for such a region is

$$1 - 2x_1x_2 = 0$$

The dividing lines lie in the first and the third quadrants and are rectangular hyperbolas as shown in Fig. 14.38. In the second and the fourth quadrants, the inequality is satisfied for all values of x_1 and x_2. Figure 14.38 shows the regions of stability and possible instability. Since the choice of the Lyapunov function is not unique, it may be possible to choose another Lyapunov function for the system under consideration which yields a larger region of stability.

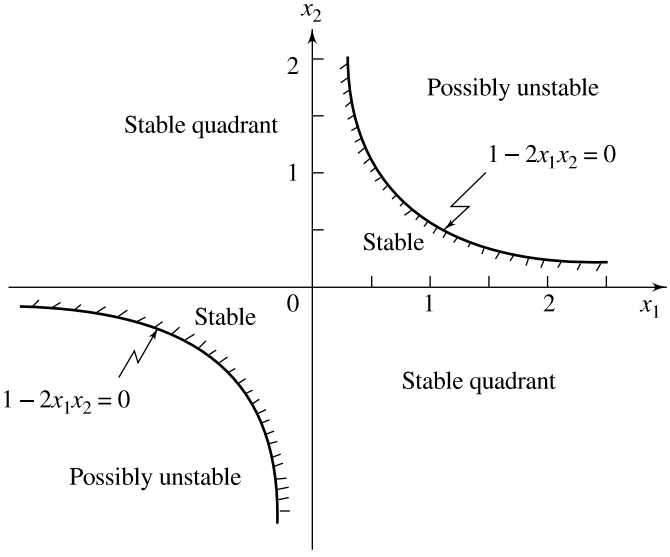

Fig. 14.38 Stability regions for the nonlinear system of Example 14.8

Example 14.9 Let us determine the stability of the system described by the following equation:

$$\dot{\mathbf{x}} = \mathbf{A}\mathbf{x}$$

with

$$\mathbf{A} = \begin{bmatrix} -1 & -2 \\ 1 & -4 \end{bmatrix}$$

We will first solve Eqn. (14.53) for **P** for an arbitrary choice of real symmetric positive definite matrix **Q**. We may choose **Q** = **I**, the identity matrix. Equation (14.53) then becomes

$$\mathbf{A}^T\mathbf{P} + \mathbf{P}\mathbf{A} = -\mathbf{I}$$

or

$$\begin{bmatrix} -1 & 1 \\ -2 & -4 \end{bmatrix}\begin{bmatrix} p_{11} & p_{12} \\ p_{12} & p_{22} \end{bmatrix} + \begin{bmatrix} p_{11} & p_{12} \\ p_{12} & p_{22} \end{bmatrix}\begin{bmatrix} -1 & -2 \\ 1 & -4 \end{bmatrix} = \begin{bmatrix} -1 & 0 \\ 0 & -1 \end{bmatrix} \tag{14.55}$$

Note that we have taken $p_{12} = p_{21}$. This is because the solution matrix **P** is known to be a positive definite real symmetric matrix for a stable system.

From Eqn. (14.55), we get

$$\begin{aligned} -2p_{11} + 2p_{12} &= -1 \\ -2p_{11} - 5p_{12} + p_{22} &= 0 \\ -4p_{12} - 8p_{22} &= -1 \end{aligned}$$

Solving for p_{ij}'s, we obtain

$$\mathbf{P} = \begin{bmatrix} p_{11} & p_{12} \\ p_{12} & p_{22} \end{bmatrix} = \begin{bmatrix} \frac{23}{60} & -\frac{7}{60} \\ -\frac{7}{60} & \frac{11}{60} \end{bmatrix}$$

Using Sylvester's test (inequalities (12.7b)), we find that **P** is positive definite. Therefore, the system under consideration is asymptotically stable.

Review Examples

Review Example 14.1 Figure 14.39 shows the input-output waveforms of a saturating element or a limiter. For small input signals ($X < S$), the output is proportional to the input. However, if the input amplitude is sufficiently large to cause saturation ($X > S$), the output is a clipped sine wave. One cycle of the output, which is a periodic function of period 2π, is described as follows:

$$y = \begin{cases} Kx; & 0 \le \omega t < \alpha \\ KS; & \alpha \le \omega t < (\pi - \alpha) \\ Kx; & (\pi - \alpha) \le \omega t < (\pi + \alpha) \\ -KS; & (\pi + \alpha) \le \omega t < (2\pi - \alpha) \\ Kx; & (2\pi - \alpha) \le \omega t \le 2\pi \end{cases}$$

where $\alpha = \sin^{-1}(S/X)$

This periodic function has odd symmetry:

$$y(\omega t) = -y(-\omega t)$$

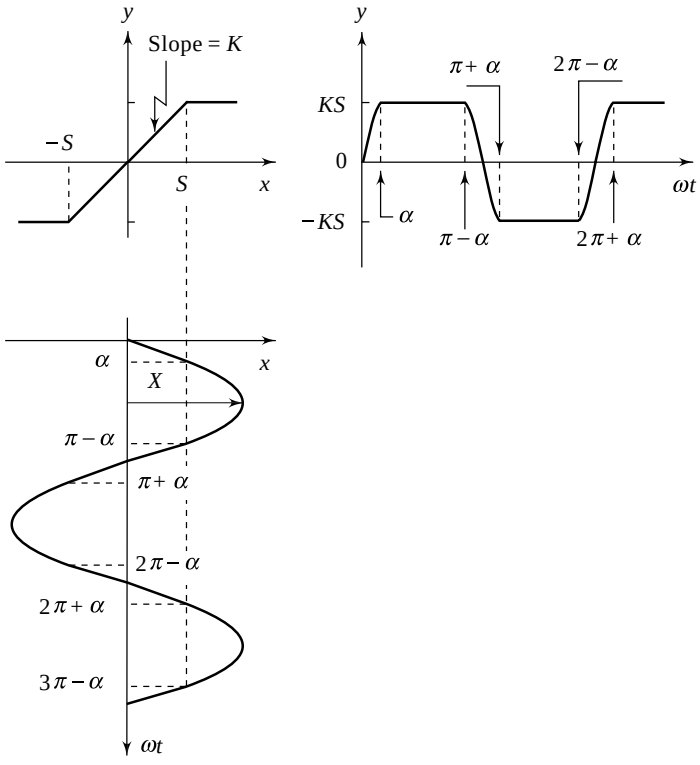

Fig. 14.39 Fourier-series analysis of a saturating element

Therefore, the fundamental component of y is given by (refer Eqn. (14.4d))

$$y_1 = B_1 \sin \omega t$$

where

$$B_1 = \frac{1}{\pi} \int_0^{2\pi} y \sin \omega t \, d(\omega t)$$

Due to symmetry of y (refer Fig. 14.39), the coefficient B_1 can be calculated as follows:

$$B_1 = \frac{4}{\pi} \int_0^{\frac{\pi}{2}} y \sin\theta \, d\theta = \frac{4K}{\pi} \left[\int_0^{\alpha} X \sin^2\theta \, d\theta + \int_{\alpha}^{\frac{\pi}{2}} S \sin\theta \, d\theta \right] = \frac{4K}{\pi} \left[\frac{X}{2}(\alpha - \sin\alpha\cos\alpha) + S\cos\alpha \right]$$

$$\frac{B_1}{X} = \frac{2K}{\pi} \left[\sin^{-1}\frac{S}{X} - \frac{S}{X}\sqrt{1-\left(\frac{S}{X}\right)^2} + \frac{2S}{X}\sqrt{1-\left(\frac{S}{X}\right)^2} \right]$$

Therefore

$$N(X) = \begin{cases} \dfrac{2K}{\pi} \left[\sin^{-1}\dfrac{S}{X} + \dfrac{S}{X}\sqrt{1-\left(\dfrac{S}{X}\right)^2} \right] & ; X \geq S \\ K & ; X < S \end{cases} \qquad (14.56)$$

The describing functions given by Eqn. (14.56) and for nonlinearity 4 in Table 14.2 have a common term of the form

$$N_c(z) = \frac{2}{\pi}\left[\sin^{-1}\frac{1}{z} + \frac{1}{z}\sqrt{1-\left(\frac{1}{z}\right)^2}\right] \tag{14.57}$$

In terms of $N_c(z)$, the describing function (14.56) may be expressed as

$$N(X) = KN_c\left(\frac{X}{S}\right) \tag{14.58}$$

The function $N_c(z)$ is listed in Table 14.3.

Table 14.3 Values of $N_C(z)$ given by Eqn. (14.56)

z	$N_c(z)$	z	$N_c(z)$	z	$N_c(z)$
1.0	1.000	6.0	0.211	11.0	0.116
1.5	0.781	6.5	0.195	11.5	0.111
2.0	0.609	7.0	0.181	12.0	0.106
2.5	0.495	7.5	0.169	12.5	0.102
3.0	0.416	8.0	0.159	13.0	0.0978
3.5	0.359	8.5	0.149	14.0	0.0909
4.0	0.315	9.0	0.141	15.0	0.0848
4.5	0.281	9.5	0.134	19.0	0.0670
5.0	0.253	10.0	0.127	25.0	0.0509
5.5	0.230	10.5	0.121	30.0	0.0424
				50.0	0.0255
				100.0	0.0127

Review Example 14.2 Consider the nonlinear system of Fig. 14.40a, with a saturating amplifier having gain K in its linear region. Determine the largest value of gain K for the system to stay stable. What would be the frequency, amplitude and nature of the limit cycle for a gain $K = 3$?

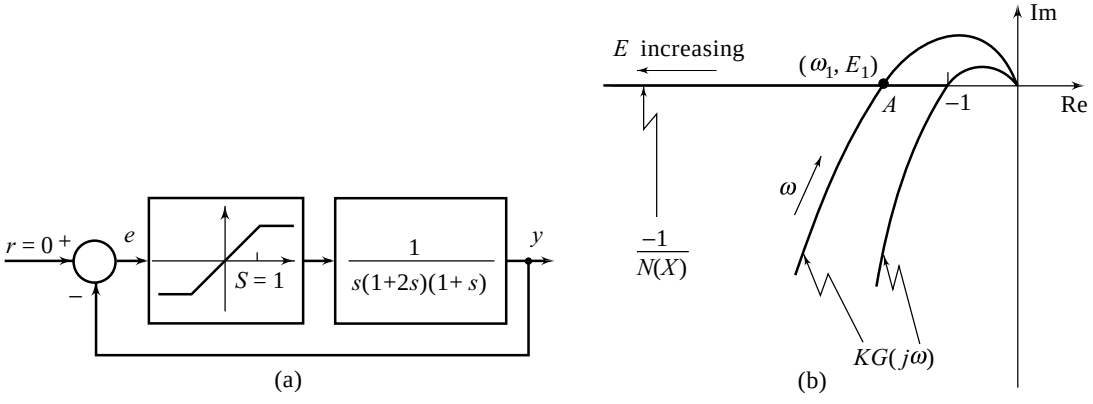

Fig. 14.40 Nonlinear system with saturating amplifier

Solution

It is convenient to regard the amplifier to have unit gain and the gain K to be attached to the linear part. From Eqn. (14.57), we obtain for $S = 1$ and $K = 1$,

$$N(E) = N_c(E);$$

the function $N_c(E)$ is listed in Table 14.3.

The locus of $-1/N(E)$ thus starts from $(-1 + j0)$ and travels along the negative real axis for increasing E, as shown in Fig. 14.40b. Now, for the equation

$$KG(j\omega) = -1/N(X)$$

to be satisfied, $G(j\omega)$ must have an angle of $-180°$:

$$\angle G(j\omega) = -90° - \tan^{-1}2\omega - \tan^{-1}\omega = -180°$$

This gives

$$\frac{2\omega + \omega}{1 - 2\omega^2} = \tan 90° = \infty \quad \text{or} \quad \omega = 1/\sqrt{2} \text{ rad/sec.}$$

The largest value of K for stability is obtained when $KG(j\omega)$ passes through $(-1 + j0)$, i.e.,

$$\left|KG(j\omega)\right|_{\omega = 1/\sqrt{2}} = 1 \quad \text{or} \quad \frac{K}{\left(\frac{1}{\sqrt{2}}\right)\left(\sqrt{3}\right)\left(\frac{\sqrt{3}}{\sqrt{2}}\right)} = 1 \text{ or } K = 3/2$$

For $K = 3$, $KG(j\omega)$ plot intersects $-1/N(X)$ locus resulting in a limit cycle at (ω_1, E_1) where $\omega_1 = 1/\sqrt{2}$, while E_1 is obtained from the relation

$$|-1/N(E_1)| = |3G(j\omega_1)| = 2 \quad \text{or} \quad |N(E_1)| = 0.5$$

From Table 14.3, we obtain

$$E_1 \cong 2.5$$

Applying the stability test for the limit cycle reveals that point A in Fig. 14.40b corresponds to a stable limit cycle.

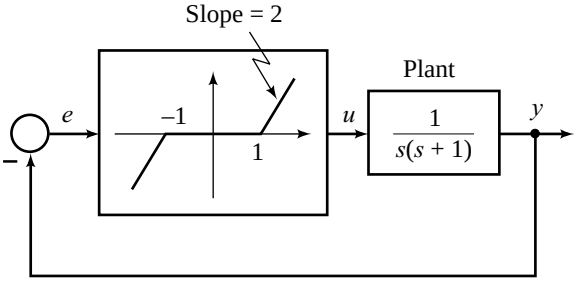

Fig. 14.41 A system with deadzone nonlinearity

Review Example 14.3 Consider the servomechanism of Fig. 14.41, having a deadzone nonlinearity in the feedback loop. With $x_1 = y$ and $x_2 = \dot{y}$, we get

$$\dot{x}_1 = x_2$$

$$\dot{x}_2 = \begin{cases} -x_2 & ; -1 < x_1 < 1 \\ -x_2 - 2(x_1 - 1) & ; x_1 > 1 \\ -x_2 - 2(x_1 + 1) & ; x_1 < -1 \end{cases}$$

The phase plane may be divided into three regions:

1. *Region I* (defined by $-1 < x_1 < 1$): The isocline equation is

$$m = \frac{-x_2}{x_2} = -1$$

Since m is the slope of phase trajectories, all trajectories in Region I have a slope of -1. Typical trajectories are shown in Fig. 14.42.

2. *Region II* (defined by $x_1 > 1$): The isocline equation is

$$m = \frac{-x_2 - 2(x_1 - 1)}{x_2}$$

or

$$x_2 = \frac{-2(x_1 - 1)}{m + 1}$$

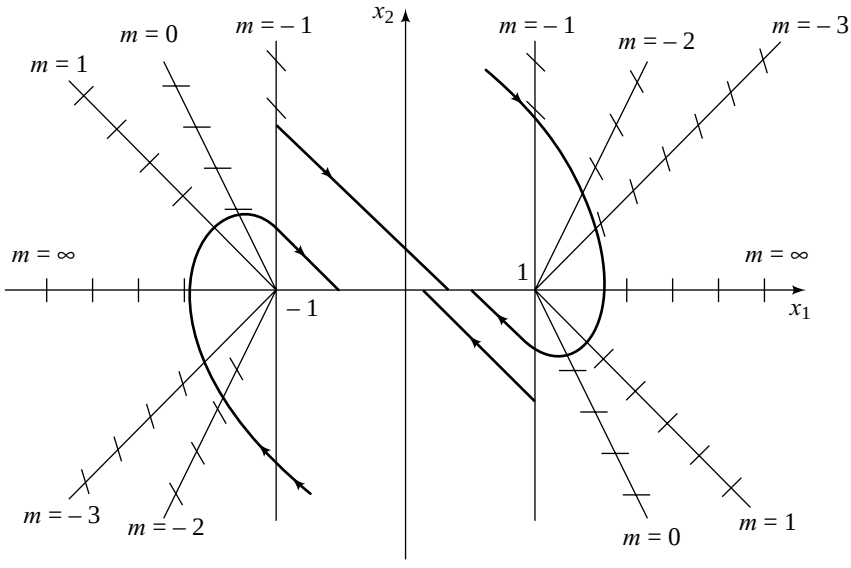

Fig. 14.42 Isoclines and typical trajectories for the system of Fig. 14.41

The isoclines are straightlines intersecting the x_1-axis at $x_1 = 1$, with slope equal to $-2 / (m + 1)$. Some of these isoclines are shown in Fig. 14.42.

3. *Region III* (defined by $x_1 < -1$): The isocline equation is

$$x_2 = \frac{-2(x_1 + 1)}{m + 1}$$

These isoclines are straight lines intersecting the x_1-axis at $x_1 = -1$ with slope equal to $-2 / (m + 1)$. Some of these isoclines are shown in Fig. 14.42.

Some typical phase trajectories are also shown in Fig. 14.42. Note that for the given system, we have an *equilibrium zone*, $-1 \le x_1 \le 1$ with $x_2 = 0$. The system comes to rest at any point within this zone.

Review Questions

1. Describe the following common nonlinear system behaviours:
   (a) Limit cycles
   (b) Jump resonance
2. Phase plane analysis applies primarily to second-order systems while the describing function method gives satisfactory results for higher-order systems. Why?
3. Phase portraits are today routinely computer generated. It is still practically useful to learn how to roughly sketch phase portraits. Describe the isoclines method of construction of phase portraits. Illustrate through an example.
4. What are singular points on phase plane? Describe the behaviour of trajectories in the vicinity of commonly found singular points in phase portraits.
5. State and explain Lyapunov stability theorem. How do we generate Lyapunov functions for nonlinear systems?
6. State and derive Lyapunov equation for stability analysis of linear systems.

Problems

14.1 For a sinusoidal input $x = X \sin \omega t$, find the output waveforms for each of the nonlinearities listed in Table 14.2. By Fourier-series analysis of the output waveforms, derive the describing function for each entry of the table.

14.2 Consider the system shown in Fig. P14.2. Using the describing-function analysis, show that a stable limit cycle exists for all values of $K > 0$. Find the amplitude and frequency of the limit cycle when $K = 4$, and plot $y(t)$ versus t.

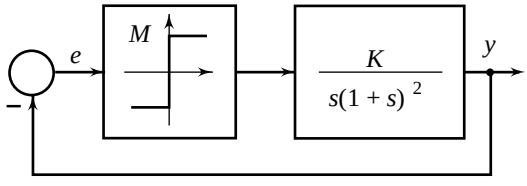

Fig. P14.2

14.3 Consider the system shown in Fig. P14.3. Use the describing function technique to investigate the possibility of limit cycles in this system. If a stable limit cycle is predicted, determine its amplitude and frequency.

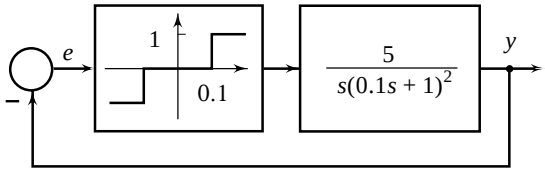

Fig. P14.3

14.4 Using the describing-function analysis, prove that no limit cycle exists in the system shown in Fig. P14.4. Find the range of values of the deadzone of the on-off controller for which limit cycling will be predicted.

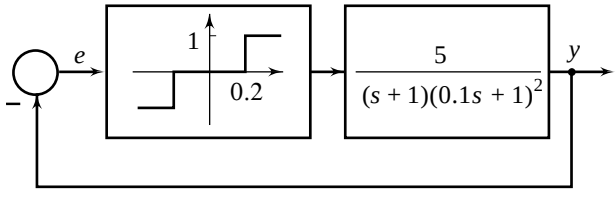

Fig. P14.4

14.5 Consider the system shown in Fig. P14.5. Using the describing-function technique, show that a stable limit cycle cannot exist in this system for any $K > 0$.

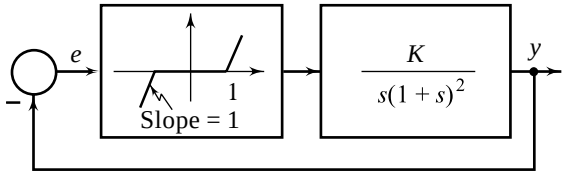

Fig. P14.5

14.6 Consider the system shown in Fig. P14.6. Using the describing-function analysis, investigate the possibility of a limit cycle in the system. If a limit cycle is predicted, determine its amplitude and frequency, and investigate its stability.

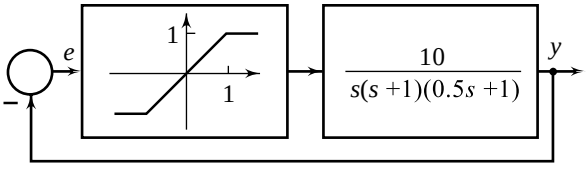

Fig. P14.6

14.7 An instrument servo system used for positioning a load may be adequately represented by the block diagram in Fig. P14.7a. The backlash characteristic is shown in Fig. P14.7b. Show that the system is stable for $K = 1$. If the value of K is now raised to 2, show that limit cycles exist. Investigate the stability of these limit cycles. Determine the amplitude and frequency of the stable limit cycle.

Given:

H/X	0	0.1	0.2	0.5	0.7	0.8	0.9	0.95	1.0
$\lvert N(X)\rvert$	1	0.954	0.882	0.593	0.367	0.249	0.126	0.063	0
$\angle N(X)$	0	– 6.7°	– 13.4°	– 32.5°	– 46.6°	– 55.1°	– 65.6°	– 72.8°	– 90°

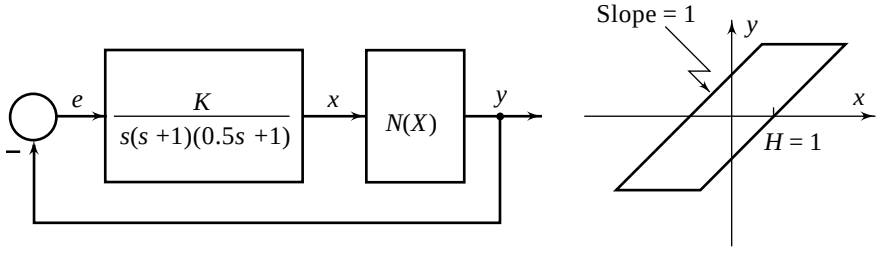

Fig. P14.7

14.8 Determine the kind of singularity for each of the following differential equations. Also locate the singular points on the phase plane.

(a) $\ddot{y} + 3\dot{y} + 2y = 0$ (b) $\ddot{y} + 5\dot{y} + 6y = 6$ (c) $\ddot{y} - 8\dot{y} + 17y = 34$

14.9 Consider the position control system shown in Fig. P14.9. The feedback action is provided by synchros which generate the actuating signal $e = \sin(\theta_R - \theta)$. Prove that this nonlinear system has multiple singular points. Linearize the system around the singular points (0,0) and $(\pi,0)$, and identify the kind of singularity at each point.

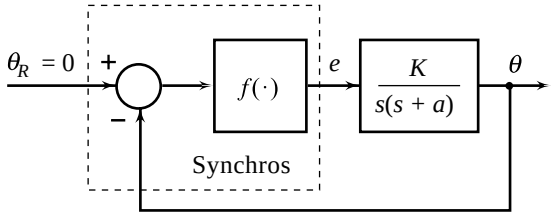

Fig. P14.9

14.10 A linear second-order servo is described by the equation

$$\ddot{y} + 2\zeta\omega_n \dot{y} + \omega_n^2 y = \omega_n^2$$

where $\omega_n = 1, y(0) = 2.0, \dot{y}(0) = 0$

Determine the singular points when (i) $\zeta = 0$, (ii) $\zeta = 0.15$. Construct the phase trajectory in each case.

14.11 Consider the block diagram of a system, shown in Fig. P14.11.

(a) Derive state variable model with $x_1 = e$ and $x_2 = \dot{e}$.

(b) Write equations of the isoclines on the x_1 versus x_2 plane.

(c) Given: $x_1(0) = 1$, $x_2(0) = 0$, obtain a trajectory on the x_1 versus x_2 plane. Show singular points (if any) and some isoclines.

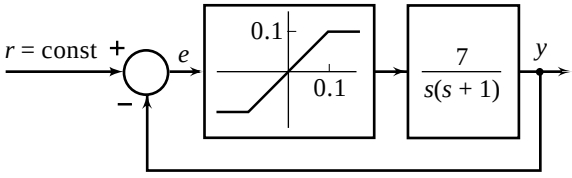

Fig. P14.11

14.12 Consider the block diagram of a system, shown in Fig. P14.12.

(a) Derive state variable model with $x_1 = e$ and $x_2 = \dot{e}$.

(b) Write equations of the isoclines on the x_1 versus x_2 plane.

(c) Given: $x_1(0) = 1$, $x_2(0) = 0$, obtain a trajectory on the x_1 versus x_2 plane. Show singular points (if any) and some isoclines.

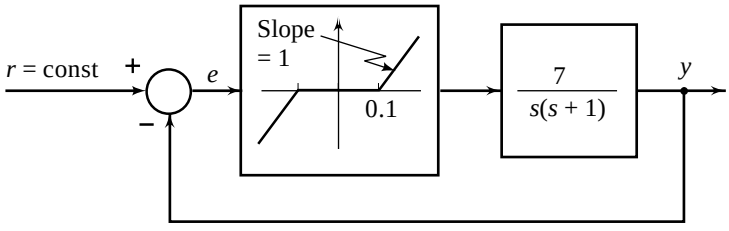

Fig. P14.12

14.13 Consider the block diagram of a system, shown in Fig. P14.13.

(a) Derive state variable model with $x_1 = e$ and $x_2 = \dot{e}$.

(b) Write equations of the isoclines on the x_1 versus x_2 plane.

(c) Given: $x_1(0) = 1$, $x_2(0) = 0$, obtain a trajectory on the x_1 versus x_2 plane. Show singular points (if any) and some isoclines.

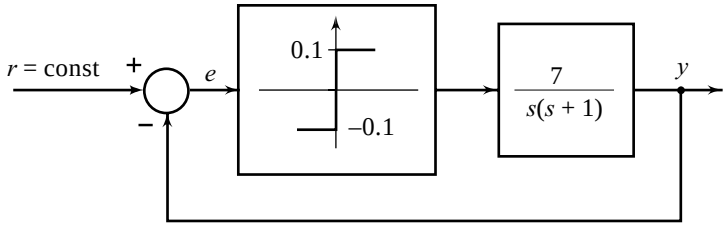

Fig. P14.13

14.14 Consider the block diagram of a system, shown in Fig. P14.14.

(a) Derive state variable model with $x_1 = e$ and $x_2 = \dot{e}$.

(b) Write equations of the isoclines on the x_1 versus x_2 plane.

(c) Given: $x_1(0) = 1$, $x_2(0) = 0$, obtain a trajectory on the x_1 versus x_2 plane. Show singular points (if any) and some isoclines.

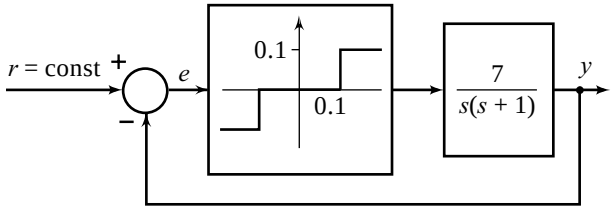

Fig. P14.14

14.15 Consider the block diagram of a system, shown in Fig. P14.15.

(a) Derive state variable model with $x_1 = e$ and $x_2 = \dot{e}$.

(b) Write equations of the isoclines on the x_1 versus x_2 plane.

(c) Given: $x_1(0) = 1$, $x_2(0) = 0$, obtain a trajectory on the x_1 versus x_2 plane. Show singular points (if any) and some isoclines.

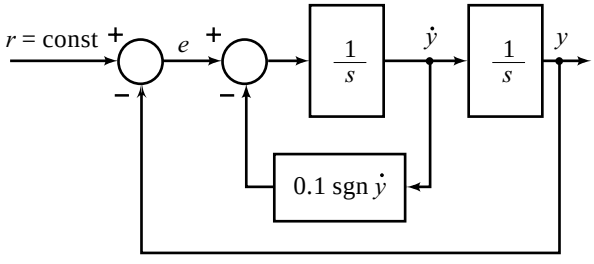

Fig. P14.15

14.16 The position control system shown in Fig. P14.16 has Coulomb friction T_c sgn($\dot{\theta}$) at the output shaft. Prove that the phase trajectories on $(e, \dot{e}/\omega_n)$-plane are semicircles with the centre on horizontal axis at $+T_c/K$ for $\dot{e} < 0$ and $-T_c/K$ for $\dot{e} > 0$.

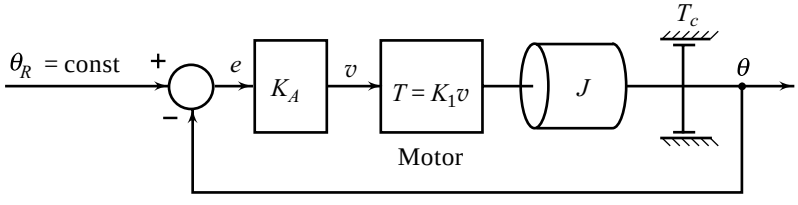

Fig. P14.16

Examine the phase trajectory corresponding to θ_R = unit step, $\dot{\theta}(0) = \theta(0) = 0$; and find the value of the steady-state error. What is the largest possible steady-state error which the system in Fig. P14.16 can possess?

Given:

$$\omega_n = \sqrt{K/J} = 1.2 \text{ rad/sec}; \quad T_c/K = 0.3 \text{ rad where} \quad K = K_A K_1.$$

14.17 Consider the nonlinear system with deadzone shown in Fig. P14.17. Using the method of isoclines, sketch some typical phase trajectories with and without deadzone, and comment upon the effect of deadzone on transient and steady-state behaviour of the system.

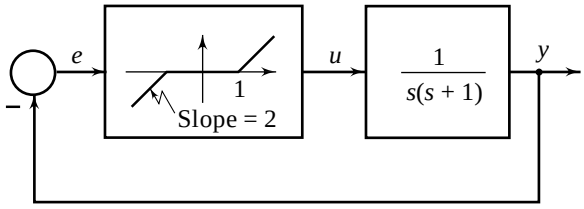

Fig. P14.17

14.18 Consider the system shown in Fig. P14.18 in which the nonlinear element is a power amplifier with gain equal to 1.0, which saturates for error magnitudes greater than 0.4. Given the initial condition: $e(0) = 1.6$, $\dot{e}(0) = 0$, plot phase trajectories with and without saturation, and comment upon the effect of saturation on the transient behaviour of the system.

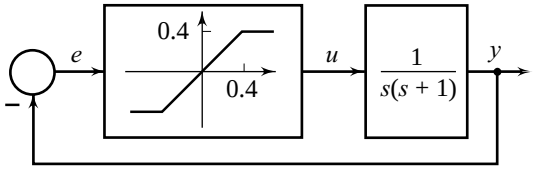

Fig. P14.18

14.19 Consider the linear autonomous system

$$\dot{\mathbf{x}} = \begin{bmatrix} 0 & 1 \\ -1 & -1 \end{bmatrix} \mathbf{x}$$

Using Lyapunov analysis, determine the stability of the equilibrium state.

14.20 Using Lyapunov analysis, determine the stability of the equilibrium state of the system

$$\dot{\mathbf{x}} = \mathbf{A}\mathbf{x}$$

with

$$\mathbf{A} = \begin{bmatrix} 0 & 1 \\ -1 & 1 \end{bmatrix}$$

14.21 Consider the nonlinear system described by the equations

$$\dot{x}_1 = x_2$$
$$\dot{x}_2 = -(1 - |x_1|)x_2 - x_1$$

Find the region in the state plane for which the equilibrium state of the system is asymptotically stable.

14.22 Check the stability of the equilibrium state of the system described by

$$\dot{x}_1 = x_2$$
$$\dot{x}_2 = -x_1 - x_1^2 x_2$$

References

APPLICATIONS

1. Siouris, G.M.; *Missile Guidance and Control Systems*: New York: Springer-Verlag, 2004.
2. Lawrence, A.; *Modern Inertial Technology: Navigation, Guidance, and Control;* 2nd Edition, New York: Springer-Verlag, 1998.
3. Leonhard, W.; *Control of Electric Drives*; 3rd Edition, New York: Springer-Verlag, 2001.
4. Bose, B.K.; *Modern Power Electronics and AC Drives*: Englewood Cliffs, NJ: Prentice-Hall, 2001.
5. Sen, P.C.; *Thyristor DC Drives*; 2nd Edition, New York: Wiley-Interscience, 1991.
6. Seborg, D.E., T.F. Edgar, and D.A. Mellichamp; *Process Dynamics and Control*; 2nd Edition, New York: John Wiley, 2004.
7. Bequette, B.W.; *Process Control: Modeling, Design and Simulation*; Upper Saddle Drive, NJ: Pearson Education, 2003.
8. Marlin, T.E.; *Process Control: Designing Processes and Control Systems for Dynamic Performance*: 2nd Edition, New York : McGraw-Hill, 2000.
9. Smith, C.A., and A.B. Corripio: *Principles and Practice of Automatic Process Control*; 2nd Edition, New York: John Wiley, 1997.
10. Shinskey, F.G.; *Process Control Systems*; 4th Edition, New York: McGraw-Hill, 1996.
11. Astrom, K.J., and T. Hagglund; *PID Controllers: Theory, Design, and Tuning*; 2nd Edition, Seattle, WA: International Society for Measurement and Control, 1995.
12. Corripio, A.B.; *Tuning of Industrial Control Systems*; Research Tringle Park, North Carolina : Instrument Society of America, 1990.
13. Stephanopoulos, G.; *Chemical Process Control—An Introduction to Theory and Practice*; Englewood Cliffs, NJ: Prentice-Hall, 1984.
14. Steven, B., and F. Lewis; *Aircraft Control and Simulation*; New York: Wiley Interscience, 2003.
15. Nelson, R.C.; *Flight Stability and Automatic Control*, 2nd Edition, New York: McGraw-Hill, 1997.
16. Etkin,B., and L.D. Reid; *Dynamics of Flight: Stability and Control*; 3rd Edition, New York : John Wiley, 1996.
17. Craig, J.J.; *Introduction to Robotics: Mechanics and Control*; 3rd Edition, Englewood Cliffs, NJ: Prentice-Hall, 2003.
18. Koivo, A.J.; *Fundamentals for Control of Robotics Manipulators*; New York; John Wiley, 1989.
19. Asda, H., and K. Youcef-Touni, *Direct Drive Robots*: *Theory and Practice*, Cambridge, Massachusetts: The MIT Press, 1987.

20. Valentino, J.V., and J. Goldenberg; *Introduction to Computer Numerical Control* (CNC); 3rd Edition, Englewood Cliffs, NJ: Prentice-Hall, 2002.
21. Groover, M.K; *Automation, Production Systems, and Computer-Integrated Manufacturing*; 2nd Edition, Englewood Cliffs, NJ: Prentice-Hall, 2000.
22. Olsson, G., and G. Piani; *Computer Systems for Automation and Control*; London: Prentice-Hall International, 1992.
23. Hughes, T.A.; *Programmable Controllers*; 4th Edition, North Carolina: The Instrumentation, Systems, and Automation Society, 2004.
24. Petruzella, F.D.; *Programmable Logic Controllers*; 3rd Edition, New York : McGraw-Hill, 2004.
25. Bolton, W.; *Programmable Logic Controllers*; 3rd Edition, Burlington, MA: Newnes Publications, 2003.
26. Beards, C.F.; *Vibration Analysis and Control System Dynamics*; 2nd Edition, Englewood Cliffs, NJ : Prentice-Hall, 1995.

MATHEMATICAL BACKGROUND

27. Noble, B; and J.W. Daniel, *Applied Linear Algebra*, 3rd Edition, Englewood Cliffs, NJ: Prentice-Hall 1988.
28. Lancaster, P., and M. Tismenetsky, *The Theory of Matrices*, 2nd Edition, Orlando, Florida: Academic Press, 1985.
29. Nash, S.G., and A. Sofer, *Linear and Nonlinear Programming,* Singapore: McGraw-Hill, 1996.
30. Oppenheim, A.V., R.W. Shafer, and J.R. Buck; *Discrete-Time Signal Processing*; 2nd Edition, Englewood Cliffs, NJ: Prentice-Hall, 1999.
31. Oppenheim, A.V., A.S. Willsky and S. Hamid Nawab; *Signals and Systems*; 2nd Edition, Upper Saddle River, NJ: Prentice-Hall, 1997.
32. Brown, J.W., and R.V. Churchill; *Complex Variables and Applications*; 7th Edition, New York: McGraw-Hill, 2003.
33. Lefschetz, S., *Differential Equations: Geometric Theory*; 2nd Edition, New York: Dover Publications, 1977.

DYNAMICAL SYSTEMS AND MODELLING

34. Palm, W.J., III; *System Dynamics*; New York : McGraw-Hill, 2004.
35. Zak, S.H.; *Systems and Control*; New York: Oxford University Press, 2003.
36. Ogata, K.; *System Dynamics*; 4th Edition, Englewood Cliffs, NJ: Prentice-Hall, 2003.
37. Clark, R.N.; *Control System Dynamics*; New York: Cambridge University Press, 1996.
38. Belanger, P.R., *Control Engineering*: *A Modern Approach*; Orlando, Florida: Saunders College Publishing, 1995.
39. Moschytz, G.S., *Linear Integrated Networks: Fundamentals*, New York: Van Nostrand Reinhold, 1974.
40. Schwarz, R.J., and B. Friedland, *Linear Systems*, New York: McGraw-Hill, 1965.
41. Mason, S.J., "Feedback Theory: Further Properties of Signal Flow Graphs", *Proc. IRE*, Vol. 44, No. 7, pp. 920-926, July 1956.
42. Mason, S.J., "Feedback Theory: Some Properties of Signal Flow Graphs", *Proc. IRE*, Vol. 41, No. 9, pp. 1144-1156, Sept. 1953.

INDUSTRIAL CONTROL DEVICES

43. Necsulescu, D.; *Mechatronics*; Singapore: Pearson Education, 2002.
44. Gupta, S.; *Elements of Control Systems*; Upper Saddle River, N.J: Pearson Education, 2002.
45. Kilian, C.T., *Modern Control Technology: Components and Systems*; 2nd Edition, Singapore: Delmar Publishers, 2001.
46. Morris, N.M.; *Control Engineering*; 4th Edition, London: McGraw-Hill, 1991.
47. De Silva, C.W., *Control Sensors and Actuators*, Englewood Cliffs, NJ: Prentice-Hall, 1989.
48. Anderson, W.R., *Controlling Electrohydraulic Systems*, New York: Marcel Dekker, 1988.

49. Parr, E.A., *Industrial Control Handbook*, Vol.1-Vol.3, Oxford: BSP Professional Books, 1987.
50. Schuler, C.A., and W.L. McNamee, *Industrial Electronics and Robotics*, New York: McGraw-Hill, 1986.
51. Kenjo, T., and S. Nagamori, *Permanent-magnet and Brushless DC Motors*, Oxford: Clarendon Press, 1985.
52. Kenjo, T. *Stepping Motors and their Microprocessor Controls*, Oxford: Clarendon Press, 1984.
53. Ahrendt, W.R., and C.J. Savant Jr., *Servomechanism Practice*, 2nd Edition, New York: McGraw-Hill, 1960.
54. Kuo, S., and W.S. Gan; *Digital Signal Processors: Architectures, Implementations, and Applications*; Upper Saddle River, NJ: Pearson Education, 2005.
55. Pack, D., and S. Barrett; *68HCI2 Microcontroller: Theory and Applications*; Upper Saddle River, NJ: Prentice-Hall, 2002.
56. Wolf, W.; *Computers as Components: Principles of Embedded Computing System Design*; San Franscisco: Morgan Kaufmann, 2001.
57. Mackenzie, I.; *The 8051 Microcontroller*; Upper Saddle River, NJ: Prentice-Hall, 1998.

FEEDBACK CONTROL THEORY

58. Franklin, G.F., J.D. Powell, and A. Emami-Naeini; *Feedback Control of Dynamical Systems*; 5th Edition, Upper Saddle River, NJ: Pearson Education, 2005.
59. Dorf, R.C., and R.H. Brishop; *Modern Control Systems*, 10th Edition, Upper Saddle River, NJ: Pearson Education, 2004.
60. Nise, N.S.; *Control Systems Engineering;* 4th Edition, Danvers, MA: John Wiley, 2003.
61. Kuo, B.C., and F. Golnaraghi: *Automatic Control systems*; 8th Edition, Danvers, MA: John Wiley, 2003.
62. D'Azzo, J.J., C.H. Houpis, and S.N. Sheldon; *Linear Control System Analysis and Design with MATLAB*, 5th Edition, New York: Marcel Dakker, 2003.
63. Wilkie, J.,M. Johnson, and R. Ketabi; *Control Engineering: An Introductory Course*; New York: Palgrave, 2003.
64. Dorsey, J.; *Continuous and Discrete Control Systems*; New York: McGraw-Hill, 2002.
65. Stefani, R.T., B. Shahian, C.J. Savant, and G.H. Hostetter; *Design of Feedback Control Systems*; 4th Edition, New York: Oxford University Press, 2002.
66. Ogata, K.; *Modern Control Engineering*; 4th Edition, Englewood Cliffs, NJ: Prentice-Hall, 2001.
67. Goodwin, G.C., S.F. Graebe, and M.E. Salgado; *Control System Design*; Upper Saddle River, NJ: Pearson Education, 2001.
68. Phillips, C.L., and R.D. Harbor; *Feedback Control Systems*; 4th Edition, Englewood Cliffs, NJ: Prentice-Hall, 1999.
69. Shinners, S.M.; *Modern Control System Theory and Design*; 2nd Edition, New York: John Wiley, 1998.
70. Raven, F.H.; *Automatic Control Engineering*; 5th Edition, New York: McGraw-Hill, 1995.
71. Wolovich, W.A.; *Automatic Control Systems: Basic Analysis and Design*; Orlando, Florida: Saunders College Publishing, 1994.
72. Doebelin, E.O., *Control System Principles and Design*, New York: John Wiley, 1986.
73. Truxal, J. G., *Automatic Feedback Control System Synthesis*, New York: McGraw-Hill, 1955.

ROBUST CONTROL

74. Dullerud, G.E., and F. Paganini; *A Course in Robust Control Theory*; New York: Springer-Verlag, 2000.
75. Zhou, K., and J.C. Doyle; *Essentials of Robust Control*; Englewood Cliffs, NJ: Prentice-Hall, 1997.
76. Saberi, A., B.M. Chen, and P. Sannuti, *Loop Transfer Recovery—Analysis and Design*, London: Springer-Verlag, 1993.
77. Doyle, J.C., B.A. Francis, and A.R. Tannenbaum, *Feedback Control Theory*, New York: MacMillan, 1992.
78. Francis, B.A., *A Course in Control Theory*, *Lecture Notes in Control and Information Sciences*, No. 88, Berlin: Springer-Verlag, 1987.
79. Rosenwasser, E., and R. Yusupov; *Sensitivity of Automatic Control Systems*; Boca Raton, FL: CRC Press, 2004.

DIGITAL CONTROL

80. Franklin, G.F., J.G. Powell, and M.L. Workman; *Digital Control of Dynamic Systems*; 3rd Edition, San Diego, CA: Addison-Wesley, 1997.
81. Astrom, K.J., and B. Wittenmark; *Computer-Controlled Systems*; 3rd Edition, Englewood Cliffs, NJ: Prentice-Hall, 1996.
82. Santina, M.S., and A.R. Stubberud; *Sample-Rate Selection*, Boca Raton, FL: CRC Press, 1996.
83. Santina, M.S., and A.R. Stubberud; *Quantization Effects*; Boca Raton, FL: CRC Press, 1996.
84. Ogata, K.; *Discrete-Time Control Systems*; 2nd Edition, Upper Saddle River, NJ: Pearson Education, 1995.
85. Santina, M.S., A.R. Stubberud, and G.H. Hostetter; *Digital Control System Design*; 2nd Edition, Stamford, CT: International Thomson Publishing, 1994.
86. Phillips, C.L., and H.T. Nagle, Jr.; *Digital Control System Analysis and Design*; 3rd Edition, Upper Saddle River, NJ: Pearson Education, 1994.
87. Kuo, B.C.; *Digital Control Systems*; 2nd Edition, Orlando, Florida: Saunders College Publishing, 1992.
88. Houpis, C.H., and G.B. Lemont; *Digital Control Systems: Theory, Hardware, and Software*; 2nd Edition, New York: McGraw-Hill, 1992.
89. Hristu-Varsakelis, D., and W.S. Levine (eds); *Handbook of Networked and Embedded Control Systems*; Boston: Birkhauser Publishers, 2005.
90. Ibrahim, D.; *Microcontroller Based Temperature Monitoring and Control*; Woburn, MA: Newnes Publications, 2002.
91. Chidambaram, M.; *Computer Control of Processes*; New Delhi: Narosa Publishers, 2002.
92. Ozkul, T.; *Data Acquisition and Process Control using Personal Computers*; New York: Marcel Dekkar, 1996.
93. Rigby, W.H., and T. Delby; *Computer Interfacing: A Practical Approach to Data Acquisition and Control*; Englewood Cliffs, NJ: Prentice-Hall, 1995.
94. Tooly, M.; *PC-Based Instrumentation and Control*; 2nd Edition, Oxford: Newnes Publications, 1995.
95. Gupta, S., and J.P. Gupta; *PC Interfacing for Data Acquisition and Process Control*, 2nd Edition, Research Triangle Park, North Carolina: Instrument Society of America, 1994.
96. Gopal, M., *Digital Control Engineering*; New Delhi: New Age International, 1988.
97. Rao, M.V.C, and A.K. Subramanium "Elimination of singular cases in Jury's test" *IEEE Trans. Automatic Control*, Vol. AC-21, pp.114-115, February 1976.
98. Jury, E.I., and J. Blanchard, "A Stability Test for Linear Discrete-time Systems in Table Form", *Proc. IRE*, Vol. 49, pp. 1947-1948, 1961.

STATE SPACE AND LINEAR SYSTEMS

99. Tewari, A.; *Modern Control Design with MATLAB and Simulink*; Singapore: John Wiley, 2003.
100. Chen, C-T.; *Linear System Theory and Design*; 3rd Edition, New York : Oxford University Press, 1998.
101. DeRusso, P.M., R.J. Roy, C.M. Close, and A.A. Desrochers; *State Variables for Engineers;* 2nd Edition, New York : John Wiley, 1998.
102. Szidarovszky, F., and A.T. Bahill; *Linear System Theory*; 2nd Edition, Boca Raton, FL: CRC Press, 1998.
103. Antsaklis, P.J., and A.N. Michel; *Linear Systems*; New York: McGraw-Hill, 1997.
104. Rugh, W.J.; *Linear System Theory*; 2nd Edition, Upper Saddle River, NJ: Prentice-Hall, 1995.
105. Gopal, M.; *Modern Control System Theory*; 2nd Edition, New Delhi: New Age International, 1993.
106. Brogan, W.L.; *Modern Control Theory;* 3rd Edition, Englewood Cliffs, NJ: Prentice-Hall, 1991.
107. Friedland, B., *Control System Design*: *An Introduction to State-Space Methods*, New York: McGraw-Hill, 1986.
108. Zadeh, L.A., and C.A. Desoer, *Linear System Theory: A State Space Approach*, New York: McGraw-Hill, 1963.

MULTIVARIABLE AND OPTIMAL CONTROL

109. Bertsekas, D.P.; *Dynamic Programming and Optical Control;* 3rd Edition, Belmont: Athena Scientific, 2005.
110. Naidu, D.S., *Optimal Control Systems;* Boca Raton, FL: CRC Press, 2003.

111. Camacho, E.F., and C. Bordons; *Model Predictive Control*; 2nd Edition, London: Springer-Verlag, 2003.
112. Bryson, A.E.; *Applied Linear Optimal Control: Examples and Algorithms*; Cambridge, UK: Cambridge University Press, 2002.
113. Locatelli, A.; *Optimal Control: An Introduction*; Basel, Switzerland: Birkhauser Verlag, 2001.
114. Chen, T., and B. Francis; *Optimal Sampled-Data Control Systems*; 2nd Edition, London: Springer, 1996.
115. Lewis, F.L., and V.L. Syrmos; *Optimal Control*; 2nd Edition, New York : John Wiley, 1995.
116. Zhou, K., J.C. Doyle, and K. Glover; *Robust and Optimal Control*; Upper Saddle River, NJ: Prentice-Hall, 1996.
117. Anderson, B.D.O., and J.B. Moore, *Optimal Control: Linear Quadratic Methods*, Englewood Cliffs, NJ: Prentice-Hall, 1990.
118. Grimble, M.J., and M.A. Johnson, *Optimal Control and Stochastic Estimation: Theory and Applications*, Vol.I, Chichester: John Wiley, 1988.
119. Albertos, P., and A. Sala; *Multivariable Control Systems: An Engineering Approach*; Springer, 2004.
120. Clarke, D.W., C. Mothadi, and P.S. Tuffs, "Generalized predictive control–Part I. The basic algorithm", *Automatica*, Vol. 23, No. 2, pp. 137–148, 1987.
121. Clarke, D.W., C. Mothadi, and P.S. Tuffs, "Generalized predictive control–Part II. Extensions and interpretations", *Automatica,* Vol. 23, No. 2, pp. 149–160, 1987.
122. Fortman, T.E., and K.L. Hitz, *An Introduction to Linear Control Systems,* New York: Marcel Dekker, 1977.
123. Kautsky, J., N.K., Nichols, and P. Dooren, "Robust pole assignment by linear state feedback", *Int. J. Control*, Vol. 41, No. 5, pp.1129-1155, 1985.
124. Doyle, J.C., and G. Stein, "Robustness with Observers*", IEEE Trans. Automatic Control*, Vol. AC-24, No. 4, pp. 607-611, Aug.1979.

NONLINEAR CONTROL SYSTEMS

125. Khalil, H.K.; *Nonlinear Systems*; 3rd Edition, Upper Saddle River, NJ: Prentice-Hall, 2001.
126. Slotine, J.J.E., and W. Li., *Applied Nonlinear Control*, Englewood Cliffs, NJ: Prentice-Hall, 1991.
127. Itkis, U., *Control Systems of Variable Structure*, New York:John Wiley, 1976.
128. Atherton, D.P., *Nonlinear Control Engineering*, London: Van Nostrand Reinhold Company, 1975.
129. Minorsky N., *Theory of Nonlinear Control System,* New York: McGraw-Hill, 1969.

SYSTEM IDENTIFICATION AND ADAPTIVE CONTROL

130. Narendra, K.S., and A.M. Annaswamy; *Stable Adaptive Systems*; New York: Dover Publications, 2005.
131. Ljung, L.; *System Identification: Theory for the User*; 2nd Edition, Englewood Cliffs, NJ: Prentice-Hall, 1998.
132. Astrom, K.J., and B. Wittenmark; *Adaptive Control*; 2nd Edition, Reading, MA: Prentice-Hall, 1994.
133. Landau, I.D., *System Identification and Control Design*, Englewood Cliffs, NJ: Prentice-Hall, 1990.
134. Sastry, S., and M. Bodson, *Adaptive Control: Stability*, *Convergence and Robustness*, Englewood Cliffs, NJ: Prentice-Hall, 1989.
135. Grimble, M.J., and M.A. Johnson, *Optimal Control and Stochastic Examination: Theory and Applications*, Vol.II, Chichester: John Wiley, 1988.
136. Harris, C.J., and S.A. Billings (eds); *Self-Tuning and Adaptive Control: Theory and Applications;* 2nd Edition, London: Peter Peregrinus, 1985.

INTELLIGENT CONTROL

137. Negnevitsky, M.; *Artificial Intelligence: A Guide to Intelligent Systems*; 2nd Edition, Essex, UK: Pearson Education, 2005.
138. Kecman, V.; *Learning and Soft Computing;* Cambridge, MA: The MIT Press, 2001.
139. Norgaard, M., O. Ravn, N.K. Poulsen, and L.K. Hansen, *Neural Networks for Modeling and Control of Dynamic Systems*, London: Springer-Verlag, 2000.

140. Lewis, F.L., S. Jagannathan, and A. Yesildirek, *Neural Network Control of Robot Manipulators and Nonlinear Systems*, London: Taylor & Francis, 1999.
141. Haykin, S., *Neural Networks: A Comprehensive Foundation*, 2nd Edition, Prentice-Hall, 1998.
142. Jang, J.S.R., C-T Sun, and E. Mizutani; *Neuro-Fuzzy and Soft Computing: A Computational Approach to Learning and Machine Intelligence*; Upper Saddle River, NJ: Pearson Education, 1997.
143. Lin C-T, and C.S. George Lee, *Neural Fuzzy Systems*, Upper Saddle River, NJ: Prentice-Hall, 1996.
144. Ying, Hao, *Fuzzy Control and Modeling: Analytical Foundations and Applications*, New York: IEEE Press, 2000.
145. Passino, K.M., and S. Yurkovich, *Fuzzy Control*, California: Addison-Wesley, 1998.
146. Goldberg, D.E., *Genetic Algorithms in Search Optimization, and Machine Learning*, Reading, Massachusetts: Addison-Wesley, 1989.
147. Werbos, P., *A Handbook of Learning and Approximate Dynamic Programming*, New York: Wiley-IEEE Press, August 2004.
148. Sutton, R.S., and A.G. Barto, *Reinforcement Learning: An Introduction,* Cambridge, Mass.: MIT Press, 1998.
149. Mitchell, T.M., *Machine Learning*, Singapore: McGraw-Hill, 1997.
150. Bertsekas, D.P., and J.N. Tsitsiklis, *Neuro-Dynamic Programming*, Belmont, Mass: Athena Scientific, 1996.

TECHNICAL COMPUTING

151. NATIONAL PROGRAMME ON TECHNOLOGY ENHANCEMENT LEARNING
Course: Electrical Engineering (Control Engineering)
Faculty Coordinator: Prof. M. Gopal
Web Content: MATLAB Modules for Control System Principles and Design
www.nptel.iitm.ac.in
152. MATLAB & Simulink Software
www.mathworks.com
The MathWorks, Inc.
3 Apple Hill Drive
Natick, MA 01760-2098, USA
153. MATHEMATICA Software
www.wolfram.com
Wolfram Research, Inc.
100 Trade Center Drive
Champaign, IL 61820-7237, USA
154. MAPLESOFT Software
www.maplesoft.com
Maplesoft
615 Kumpf Drive
Waterloo, Ontario
Canada N2V1K8

COMPANION BOOK

155. Gopal, M., *Digital Control and State Variable Methods: Conventional and Intelligent Control Systems,* 3rd Edition, New Delhi: Tata McGraw-Hill, 2008.

Answers to Problems

2.1 (a) (i) $y(t) = \dfrac{KA}{\tau}\ e^{-t/\tau};\ y_{ss} = 0$ (ii) $y(t) = KA(1 - e^{-t/\tau});\ y_{ss} = KA$

(iii) $y(t) = KA(t - \tau + \tau e^{-t/\tau});\ y_{ss} = KA(t - \tau)$

(iv) $y(t) = \dfrac{KA\omega\tau}{\tau^2\omega^2 + 1}\ e^{-t/\tau} + \dfrac{KA}{\sqrt{\tau^2\omega^2 + 1}}\ \sin(\omega t - \tan^{-1}\omega\tau)$

$$y_{ss} = \frac{KA}{\sqrt{\tau^2\omega^2 + 1}}\ \sin(\omega t - \tan^{-1}\omega\tau)$$

(b) (i) $y(t) = 1 - \dfrac{e^{-\zeta\omega_n t}}{\sqrt{1-\zeta^2}}\ \sin\left(\omega_d t + \tan^{-1}\dfrac{\sqrt{1-\zeta^2}}{\zeta}\right)$

$\omega_d = \omega_n\sqrt{1-\zeta^2}$

$y_{ss} = 1$

(ii) $y(t) = t - \dfrac{2\zeta}{\omega_n} + \dfrac{e^{-\zeta\omega_n t}}{\omega_d}\ \sin\left(\omega_d t + 2\tan^{-1}\dfrac{\sqrt{1-\zeta^2}}{\zeta}\right);\ y_{ss} = t - \dfrac{2\zeta}{\omega_n}$

2.3 (a) $\dfrac{s^2 + s + 1}{(s+1)(s^2 + 2s + 2)};\ y_{ss} = 0.5$ (b) $\dfrac{1}{4} + \dfrac{1}{2}t - \dfrac{1}{4}e^{-2t};\ y_{ss} = \dfrac{1}{4} + \dfrac{1}{2}t$

2.4 Steady-state error = 1.5

2.5 $\zeta = 0.5;\ \omega_n = 10;\ \omega_d = 5\sqrt{3}\ ;\ y(t) = 0.01\left[1 - \frac{2}{\sqrt{3}}\, e^{-5t} \sin\left(5\sqrt{3}\, t + \tan^{-1}\sqrt{3}\right)\right]$

2.6 (b) $0.707 \sin(2t - 135°)$

2.7 (a) $y(t) = \frac{1}{2}\, e^{-t} - \frac{1}{3}\, e^{-2t} - \frac{1}{6}\, e^{-5t}$ (b) $y(t) = \frac{1}{2}\, e^{-t} + \frac{3}{2}\, e^{-2t} - e^{-5t}$

2.9 $\dfrac{X(s)}{Y(s)} = \dfrac{0.1667}{(0.0033s + 1)(0.0217s + 1)}$; x(peak) = 1.2113 cm

2.10 (a) Peak amplitude of the force transmitted to the foundation
(b) Peak amplitude of machine vibration

$$= \frac{A\sqrt{1 + \left(\dfrac{B\omega}{K}\right)^2}}{\sqrt{\left(1 - \dfrac{M\omega^2}{K}\right)^2 + \left(\dfrac{B\omega}{K}\right)^2}} = \frac{A\sqrt{1 + \left(\dfrac{B\gamma}{K}\right)^2}}{\sqrt{\left(1 - \dfrac{M\gamma^2}{K}\right)^2 + \left(\dfrac{B\gamma}{K}\right)^2}}$$

2.11 $M_1\, \ddot{y}_1 + K_1(y_1 - y_0) + B_1(\dot{y}_1 - \dot{y}_0) + K_2(y_1 - y_2) + B_2(\dot{y}_1 - \dot{y}_2) = 0$

$M_2\, \ddot{y}_2 + K_2(y_2 - y_1) + B_2(\dot{y}_2 - \dot{y}_1) = 0$

2.12 $\left.\dfrac{\theta_2(s)}{Q_m(s)}\right|_{\theta_i = 0} = \dfrac{0.348}{s^2 + 1.94s + 0.234}$; $\left.\dfrac{\theta_2(s)}{\theta_i(s)}\right|_{q_m = 0} = \dfrac{0.125(s + 1.92)}{s^2 + 1.94s + 0.234}$

2.13 $\bar{Q}_m = 17.26$ kg/min

2.14 $\dfrac{H_2(s)}{X_1(s)} = \dfrac{4}{s^2 + 8s + 7}$; $\dfrac{H_1(s)}{X_1(s)} = \dfrac{s + 5}{s^2 + 8s + 7}$

2.15 $\dfrac{Adh(t)}{dt} = K_v x(t) - \dfrac{\rho g h(t) - p_w(t)}{R} - q_w(t)$

3.1 $\dfrac{Y(s)}{R(s)} = \dfrac{G_1(G_2G_3 + G_4)}{1 + (G_2G_3 + G_4)(G_1 + H_2) + G_1H_1G_2}$

3.2 $\dfrac{Y(s)}{R(s)} = G_4 + \dfrac{G_1G_2G_3}{1 + G_2G_3H_2 + G_2H_1(1 - G_1)}$

3.3 $\dfrac{Y(s)}{R(s)} = \dfrac{(1+G_4H_2)(G_2+G_3)G_1}{1+G_1H_1H_2(G_2+G_3)}$

3.4 $M(s) = \dfrac{G_1G_2G_3}{1+G_2H_3+G_3H_2+G_1G_2G_3H_1}$; $M_w(s) = \dfrac{G_3(1+H_3G_2)}{1+H_3G_2+G_3(G_1H_1G_2+H_2)}$

3.5 (a) $\dfrac{\theta_L(s)}{\theta_R(s)} = \dfrac{G_1G_2G_3}{1+G_1G_2G_3}$; $\dfrac{\theta_L(s)}{nT_w(s)} = -\dfrac{NG_3}{1+G_1G_2G_3}$; $G = K_PK_AR_f/R$;

$G_2 = \dfrac{K_T/R_a}{Js+B+K_TK_b/R_a}$; $G_3 = n/s$

(b) $\dfrac{\theta_2(s)}{\theta_r(s)} = \dfrac{K_sK_AK_eK_vG_p(s)}{1+K_sK_AK_eK_vG_p(s)}$; $\dfrac{\theta_2(s)}{\theta_i(s)} = \dfrac{N(s)}{1+K_sK_AK_eK_vG_p(s)}$

3.6 $\dfrac{\omega(s)}{E_r(s)} = \dfrac{50}{s+10.375}$; $\omega(t) = 481.8\,(1-e^{-10.375t})$

3.7 $\dfrac{\theta_L(s)}{\theta_R(s)} = \dfrac{1}{s(0.1s+1)(0.2s+1)+1}$

3.8 $\dfrac{\theta_L(s)}{E_c(s)} = \dfrac{1}{s(0.32s+1)}$

3.9 (i) $\dfrac{\theta_M(s)}{E_a(s)} = \dfrac{16.7}{s(s^2+100s+19.2)}$

3.10 $\dfrac{\theta_M(s)}{\theta_R(s)} = \dfrac{13.33}{s^2+3.55s+13.33}$

3.11 (a) $\dfrac{\omega(s)}{E_r(s)} = \dfrac{K}{\dfrac{1}{\omega_n^2}s^2+\dfrac{2\zeta}{\omega_n}s+1}$; $K = 17.2$, $\zeta = 1.066$, $\omega_n = 61.2$

3.12 (b) $\dfrac{\theta_L(s)}{\theta_R(s)} = \dfrac{K_PK_AK_T\,G(s)}{1+K_PK_AK_T\,G(s)}$; $\dfrac{\theta_L(s)}{-T_w(s)} = \dfrac{N(s)}{1+K_PK_AK_T\,G(s)}$

$$G(s) = \frac{Bs + K}{s^2\left[J_M J_L s^2 + (J_M + J_L) Bs + (J_M + J_L) K\right]};$$

$$N(s) = \frac{J_M s^2 + Bs + K}{s^2\left[J_M J_L s^2 + (J_M + J_L) Bs + (J_M + J_L) K\right]}$$

3.13 $\dfrac{Y(s)}{R(s)} = \dfrac{2}{s^2 + 0.02s + 2}$

3.14 $\dfrac{Y(s)}{E_r(s)} = \dfrac{G(s)}{1 + G(s)\,H(s)}$; $G(s) = \dfrac{(K_A K_v K_1 A/K_2)e^{-s\tau_D}}{s(Ms + B + A^2/K_2)}$; $\tau_D = d/v$; $H(s) = K_s$

3.15 $G(s) = \dfrac{R_2/\rho g}{(\tau_1 s + 1)(\tau_2 s + 1)}$; $\tau_1 = A_1 R_1/\rho g, \tau_2 = A_2 R_2/\rho g$; $\dfrac{H_2(s)}{H_r(s)} = \dfrac{G(s)K_v K_e K_a K_s}{1 + G(s)K_v K_e K_a K_s}$

3.16 $G(s) = \dfrac{R_t}{\tau s + 1}$; $\tau = R_t C_t$; $\dfrac{\theta(s)}{E_r(s)} = \dfrac{G(s)K_h R_f R_1}{RR_1 + G(s)K_h K_t R_f R_2}$

3.17 $G(s) = \dfrac{K_g}{\dfrac{1}{\omega_n^2}s^2 + \dfrac{2\zeta}{\omega_n}s + 1}$; $K_g = \dfrac{1}{Q\rho c}$, $\omega_n = \sqrt{\dfrac{Q}{R_1 C_1 V}}$; $2\zeta\omega_n = \dfrac{R_1 C_1 Q\rho c + V\rho c + C_1}{VR_1 C_1 \rho c}$

$$\frac{\theta(s)}{\theta_r(s)} = \frac{G(s)K_h K_A K_s}{1 + G(s)K_h K_A K_s}; \quad \frac{\theta(s)}{\theta_i(s)} = \frac{G(s)[(\tau s + 1)/K_g]}{1 + G(s)K_h K_A K_s}; \quad \tau = R_1 C_1$$

4.1 $\left|S_G^M\right| = 0.0289$; $\left|S_H^M\right| = 1.02$

4.2 $\dfrac{Y(s)}{R(s)} = M(s) = \dfrac{5K_1}{s^2(s + 1 + 5K_1) + 5K_1 + 5}$; $S_{K_1}^M = 0.5$

4.3 $y(t)|_{\text{open-loop}} = 20(1 - e^{-t})$; $y(t)|_{\text{closed-loop}} = \dfrac{20}{21}(1 - e^{-21t})$

$y'(t)|_{\text{open-loop}} = 50(1 - e^{-0.4t})$; $y'(t)|_{\text{closed-loop}} = \dfrac{20}{20.4}(1 - e^{-20.4t})$

4.4 $e_{ss}|_{\text{open-loop}} = 0$; $e_{ss}|_{\text{closed-loop}} = 0.0099$
$e'_{ss}|_{\text{open-loop}} = -0.1$; $e'_{ss}|_{\text{closed-loop}} = 0.009$

4.5 $K = 3.9$

4.6 Case I: $y_{ss} = 0$; Case II: $y_{ss} = 1$

4.7 (i) $e_{ss} = 1/3$ (ii) $e_{ss} = 0$ (iii) $e_{ss} = 1/3$

4.8 (i) Oscillatory (ii) stable (iii) unstable

4.9 (a) $\omega_0(t) = \frac{125}{13}(1 - e^{-130t})$; $\omega_{0ss} = 9.61$ rad/sec

(b) $\omega_0(t) = 9.61(1 - e^{-5t})$

(c) $\dfrac{\omega_0(s)}{\omega_r(s)} = M(s)$ with feedback; $\dfrac{\omega_0(s)}{\omega_r(s)} = G(s)$ without feedback

$$\left|S_{K_A}^{M}\right| = \frac{2s+10}{2s+10+K_A K_g} = S_{\omega_g}^{M};\ S_{K_A}^{G} = 1 = S_{\omega_g}^{G}$$

4.10 (b) $\left|S_{K_g}^{M}\right| = 4 \times 10^{-4}$ (c) $\theta_{L\,ss} = 0.1$ rad

4.11 (c) $S_R^M = \dfrac{1}{1+KR}$; $M(s) = \dfrac{H(s)}{H_r(s)}$ (d) $e_{ss} = \dfrac{1}{1+KR}$

4.12 (b) Open-loop case: (i) $S_K^G = 1$, $G(s) = \dfrac{\theta(s)}{E_r(s)}$ (ii) $\theta_{ss} = 1$ (iii) $\tau = R_1 C$

Closed-loop case: (i) $S_K^M = \dfrac{R_1 Cs + 1}{R_1 Cs + 1 + KK_t R_1}$, $M(s) = \dfrac{\theta(s)}{E_r(s)}$

(ii) $\theta_{ss} = \dfrac{1}{1+KK_t R_1}$ (iii) $\tau = \dfrac{R_1 C}{1+KK_t R_1}$

(c) $\theta_{ss}|_{\text{open-loop}} = \dfrac{R_1}{R_1+R_2}$; $R_2 = \dfrac{1}{UA}$; $\theta_{ss}|_{\text{closed-loop}} = \dfrac{R_1}{R_1+R_2+KK_t R_1 R_2}$

4.13 (a) $\tau|_{\text{without current feedback}} = \dfrac{L_f}{R_f+1}$; $\tau|_{\text{with current feedback}} = \dfrac{L_f}{R_f+K_A+1}$

4.14 (a) $K_c = 4$; $T_D = 0.5$

4.15 $\left|S_K^M\right| = 1.41$ for Fig. P4.15a; $\left|S_K^M\right| = 1$ for Fig. P4.15b

5.1 (a) All roots in the left-half plane
(b) Two roots in the right-half plane, and the rest in the left-half plane
(c) Two roots in the right-half plane, and the rest in the left-half plane
(d) Two roots on the imaginary axis, and the rest in the left-half plane
(e) One root in the right-half plane, and the rest in the left-half plane
(f) Two roots in the right-half plane, and the rest in the left-half plane

5.2 (a) $(s+j3)\,(s-j3)\,(s+1+j1)\,(s+1-j1)=0$
(b) $(s+2)\,(s+1)\,(s-1)\,(s+j5)\,(s-j5)=0$
(c) $(s+1)\,(s+2)\,(s+j1)\,(s-j1)\,\left(s+j\sqrt{2}\right)\left(s-j\sqrt{2}\right)=0$

5.3 The largest time-constant is equal to 1.0 sec.

5.4 (a) Unstable for all values of K (b) Unstable for all values of K
(c) $K<14/9$ (d) $K>0.528$

5.5 $K>0.528$

5.6 $K<43.3$

5.7 (i) $K<45$ (ii) $K<7.5$ (iii) $K<10.1$

5.8 (a) (i) $K<70$ (ii) $K=70$ (iii) $\Delta(s)=(s+j9.54)\,(s-j9.54)\,(s+10)$
(b) (i) $K>7.5$ (ii) $K=7.5$ (iii) $\Delta(s)=(s+j1.223)\,(s-j1.223)\,(s+5)$
(c) (i) $K<28.1$ (ii) $K=28.1$ (iii) $\Delta(s)=(s+j2.75)\,(s-j2.75)\,(s+5.7)\,(s+1.3)$

5.9 (a) System stable for $K<666.25$. Oscillations of frequency 4.06 rad/sec when $K=666.25$.
(b) System stable for $23.3<K<35.7$. Oscillations of frequency 1.56 rad/sec when $K=23.3$, and 2.56 rad/sec when $K=35.7$.

5.10 $K=2$; $a=0.75$

5.11 (a) $K<15$ (b) 7.07 rad/sec for $K=15$
(c) Two characteristic roots have time-constants larger than 1 sec.

5.12 (a) Unstable for all K_c (b) For stability, $T_D>\tau$

5.13 (a) $K<30$ (b) $\tau<0.2$ (c) $K<\left(\dfrac{2}{\tau}+10\right)$

5.14 $K_c<(30-25/T_I)$

5.15 $K<(7.5+15K_t)$

6.1 (b)(i) $\omega_n=10$ rad/sec; $\zeta=0.5$; $\omega_d=8.66$ rad/sec
(ii) $t_r=0.242$ sec; $t_p=0.363$ sec; $M_p=16.32\%$; $t_s=0.8$ sec
(iii) $K_p=\infty$; $K_v=10$; $K_a=0$ (iv) $e_{ss}=0$; $e_{ss}=0.1$; $e_{ss}=\infty$

6.2 (a) $K_A=2.5$ (b) $e_{ss}=0.4$

6.3 (a)(i) $e_{ss}=0$ (ii) $e_{ss}=2$ (b) The system of Fig. P6.3b is unstable

6.4 $e_{ss}=7/3$

6.5 (a) $K_A<23.84$ (b) $K_A=11.25$

6.6 (b) $0 < K_I < 3$

6.7 (a) $K_c = 10$; $K_D = 0.09$ (b) ζ is not an accurate estimate of M_p.

6.8 (a) $K_I = 10$ (b) $K_c = 0.41$
(c) $-1 \pm j\,11.14$; $\zeta = 0.09$ (d) ζ approximately represents M_p.

6.9 (a) $T_D = 0.216$ (c) $T_I > 0.0198$

6.10 (a) $\zeta = 0.158$ (b) $K_t = 0.216$; $e_{ss} = 0.316$
(c) $K_t = 0.9$; $K_A = 10$

6.11 (a) $K_1 = 735.39$; $K_2 = 0.31$ (b) $K_p = \infty$; $K_v = 114.9$; $K_a = 0$

6.12 $K = 8$; $K_t = 0.79$

6.13 $M = 79.71$ kg; $B = 182.47$ N/(m/sec); $K = 300$ N/m

6.14 $J = 2.5$ kg-m^2; $B = 40$ N-m/(rad/sec); $K_T = 1000$ N-m/rad

6.15 $\omega(t) = 1.5\pi\,(1 - e^{-0.5t})$ rad/sec; $e_{ss} = 5$ rpm

6.16 $\theta(t) = \dfrac{\pi}{3}\left[1 - 1.1547e^{-2t}\sin\left(3.464t + \dfrac{\pi}{3}\right)\right]$ rad; $M_p = 16.3\%$

6.17 (b) $K_A = 904.5$; $M_p = 0.85\%$; $t_s = 0.0796$ sec (d) $M_p = 0.772\%$; $t_s = 0.08$ sec

6.18 $K_A = 2.67$; fraction of the tachogenerator voltage fedback = 0.024

6.19 (b) $K_A = 1010$; $\zeta = 0.355$; $M_p = 30.33\%$ (c) $K_D = 6.95$; $M_p = 9.5\%$

6.20 (a) $e_{ss} = 0.01/K_A$ (b) $y_{ss} = 0.1/K_A$
(c) Minimum $e_{ss} = 7.81 \times 10^{-3}$; Minimum $y_{ss} = 0.078$

6.21 (a) System-type number = 2 (b) $K_c > 10$; $K_D > 0.1\,K_c$

6.22 $K_1 = 3$; $K_2 = 19.237$

6.23 (i) $K_c = 0.54$; $T_I = 3.75$ min (ii) $K_c = 0.9$; $T_I = 2.81$ min; $T_D = 0.45$ min

6.24 $K = 1$; $\tau = 1.875$; $\tau_D = 1.375$ (a) $K_c = 1.36$ (b) $K_c = 1.23$; $T_I = 4.58$ min

---

7.2 (i) Two roots at $s = -1.1835$; Two roots at $s = -2.8165$
(ii) Three roots at $s = -2$ (iii) Three roots at $s = -3$
(iv) Two roots at $s = -1$; Two roots at $s = -1 + j1.22$; Two roots at $s = -1 - j1.22$
(v) Four roots at $s = -1$

7.3 $K = 1.04$; Closed-loop transfer function

$$= \frac{1.04}{(s + 0.33 + j0.58)(s + 0.33 - j0.58)(s + 2.33)}$$

7.4 $K = 130$; real part of complex pair away from $j\omega$-axis is approximately four times as large as that of the pair near $j\omega$-axis.

7.5 $s_d = -2 + j3.4$; $K = 65$; Third pole at $s = -4$

7.6 $K = 1.128$; oscillations of $\sqrt{5}$ rad/sec when $K = 30$

7.8 $\zeta = 0.82$; $K = 2.1$

7.10 There exists a circular root locus with centre at $\left(\frac{1}{2}, 0\right)$ and the radius equal to $\sqrt{5}/2$.

7.11 $K = 5$; $M_p = 4.3\%$, $t_s = \frac{4}{3}$ sec, $e_{ss} = 11.11\%$
7.12 $K = 14$
7.13 $K = 1.475$
7.14 (a) $K = 10$ (b) $\zeta = 0.4$
7.15 $K = 10.154$; $s_d = -0.75 + j1.3$; Third pole at $s = -4.5$
7.16 $K_t = 0.3427$
7.17 $K_t = 0.449$
7.18 $\alpha = 2.16$; closed-loop poles: $-0.63 \pm j1.09$, -2.75
7.19 $\alpha = 2.8$; closed-loop poles: $-1 \pm j1.732$, -7.
7.20 (c) System is stable for $K > 19.2$; steady-state error to unit-ramp input $= -16/K$.
7.21 Uncompensated system: $K = 7.0$, $K_v = 1.4$, $t_s = 11.6$ sec
Compensated system: $K = 60$, $K_v = 12.0$, $t_s = 12.7$ sec
7.22 $\alpha = 5.3$; $K = 23.2$; third pole at $s = -3.1$
7.23 (c) $K_P = 8$; $K_D = 2$
7.24 $D(s)$ improves transient performance considerably; no effect on steady-state performance
7.28 $-0.33 \pm j0.58$; $K_v = 0.53$
7.30 $K = 820$; $K_v = 4.1$
7.33 (a) $D(s) = 3 + 2s$; $K_p = 3$
7.34 (a) $K = 56$ (b) $t_s = 3.6$ sec; $K_v = 2.07$

7.37 There exists a circular root locus with centre at (2, 0) and the radius equal to $\sqrt{12}$.

8.2 (a) Unstable (b) Stable
8.3 (i) Yes (ii) No (iii) Yes
8.4 (a) Two (b) Two (c) Stable
(d) Stable (e) Nyquist criterion not applicable
(f) Stable
8.5 (i) Stable (ii) Unstable
8.6 (a) Stable for $K < 5/4$ (b) Stable for all K (c) Unstable for all K (d) Stable for $K < 2.65$
8.7 $K > 0.75$
8.8 $K > 6$
8.9 $K > 2$
8.10 (a) $K = 0.385$ (b) Unstable for all values of K
8.11 $\tau_D = 1.2$ sec
8.12 $\omega_g = 6.2$ rad/sec; $\omega_\phi = 15.9$ rad/sec; $\Phi M = 31.7°$; $GM = 5.5$
8.13 $GM = 0.7$; $\Phi M = 10°$
8.14 (a) 16 rad/sec (b) 10.2 rad/sec (c) 10 rad/sec (d) 26 rad/sec
8.15 (a) $\omega_g = 7.86$ rad/sec; ω_ϕ: phase never reaches $-180°$; $\Phi M = 51.8°$; $GM = \infty$
(b) $\omega_g = 6.8$ rad/sec; $\omega_\phi = 10$ rad/sec; $\Phi M = 21.4°$; $GM = 6$ dB
(c) $\omega_g = 9$ rad/sec; ω_ϕ: Phase never reaches $-180°$; $\Phi M = 73.4°$; $GM = \infty$

(d) $\omega_g = 9$ rad/sec; $\omega_\phi = 13.65$ rad/sec; $\Phi M = 22°$; $GM = 4.2$ dB
(e) ω_g: gain never reaches 0 dB; $\omega_\phi = 7$ rad/sec; $\Phi M = \infty$; $GM = 20$ dB
(f) $\omega_g = 3.16$ rad/sec; ω_ϕ: phase never reaches $-180°$; $\Phi M = -33°$: $GM = -\infty$

8.16 (i) Stable system with $\Phi M = 21°$ and $GM = 8$ dB (ii) Unstable system with $\Phi M = -30°$, and $GM = -12$ dB

8.17 (a) $K < 400$ (b) $K < 55$ (c) $K < 1.67$

8.18 (a) $GM = 12$ dB; $\Phi M = 33°$ (b) $GM = 2.5$ dB; $\Phi M = 18°$
(c) $\tau_D = 0.078$ sec

8.19 (a) $\dfrac{4(1+s/2)}{s(1+s/10)}$ (b) $\dfrac{5s}{(1+s/2)(1+s/10)(1+s/30)}$

(c) $\dfrac{0.355(1+s)(1+0.05s)}{s(1+0.025s)}$ (d) $\dfrac{250}{s(1+0.4s)(1+0.025s)}$

(e) $\dfrac{79.6s^2}{(1+2s)(1+s)(1+0.2s)}$

8.20 (a) $\dfrac{31.623s}{(1+s)\left(\frac{1}{5}s+1\right)\left(\frac{1}{20}s+1\right)}$ (b) $\omega_{g1} = 0.0316$ rad/sec

(c) 56.234 rad/sec

8.21 $GM = -2.5$ dB

8.22 $G(s) = \dfrac{5\left(1+\frac{1}{10}s\right)}{s\left(1+\frac{1}{2}s\right)\left[1+\frac{0.6}{50}s+\frac{1}{2500}s^2\right]}$

8.23 $G(s) = \dfrac{0.1}{\left(\frac{1}{3}s+1\right)^2}$

9.4 (a) $K = 475$; $a = 26.2$ (b) $t_s = 0.305$ sec; $\omega_b = 25.1$ rad/sec

9.5 $M_r = 1.11$; $\omega_r = 13.25$ rad/sec; $\omega_b = 24.6$ rad/sec

9.6 $\zeta = 0.01\,\phi_m$; $K = \dfrac{1}{K_t^2}\left[2\times10^{-4}\phi_m^2\,\tau - K_t \pm 2\times10^{-2}\phi_m\sqrt{\tau}\,\sqrt{10^{-4}\phi_m^2\,\tau - K_t}\,\right]$

9.7 $K = \dfrac{1}{G_m}\left(\dfrac{1}{\tau_1}+\dfrac{1}{\tau_2}\right)$

9.8 (a) $\omega_g = 1$ rad/sec; $\Phi M = 59.2°$ (b) $M_p = 9.48\%$; $t_s = 4.76$ sec

9.9 $\Phi M = 50°$; $GM = 24$ dB; $M_p \cong 18\%$

9.10 (a) $\Phi M = 12°$ (b) Reduce the gain by a factor of 3.5 (c) $M_p \cong 18\%$

9.11 $K = 1.826$; $GM = \infty$

9.12 (a) $GM = 3.88$ dB; $\Phi M = 10°$ (b) Gain should be changed by a factor of 0.156
(c) Gain should be changed by a factor of 0.147

9.13 $K = 582.51$; $t_p = 0.19$ sec

9.14 (a) $GM = 5$ dB, $\Phi M = 30°$, $\omega_g = 0.83$ rad/sec
(b) Gain should be reduced by 5 dB
(c) Gain should be increased by 4.8 dB
(d) Gain should be reduced by 3.5 dB

9.15 $K = 37.67$

9.16 (a) $M_p = 33\%$ (b) $M_p = 7.3\%$

9.17 (a) $\Phi M = 40°$ (b) $\Phi M = -3°$; Reduce the gain by a factor of 1.78
(c) Increase in steady-state error as the loop gain is reduced

9.18 (a) $M_r = 1.8$; $\omega_b = 3.61$ rad/sec (b) $M_p = 38.6\%$; $t_s = 5.58$ sec

9.19 (b) $M_r = 1.4$; $\omega_r = 4$ rad/sec (c) $M_p = 26.43\%$; $t_s = 2.14$ sec

9.20 (a) $\omega_g = 8.3$ rad/sec, $\omega_\phi = 14.14$ rad/sec
$GM = 8.2$ dB, $\Phi M = 27.7°$
(b) $M_r = 6.7$ dB, $\omega_r = 9$ rad/sec,
$\omega_b = 13.6$ rad/sec

9.21 $GM = 7$ dB; $\Phi M = 17°$; $M_r = 10$ dB; $\omega_r = 2.75$ rad/sec; $\omega_b = 4.2$ rad/sec

9.22 (a) $\Phi M = 12°$ (b) Gain should be reduced to the value 4/3.5
(c) 0.911 rad/sec (d) $M_p = 18\%$; $t_s = 11.93$ sec

9.23 (a) $M_r = 1.4$; $\omega_r = 6.9$ rad/sec (b) $\zeta = 0.39$; $\omega_n = 8.27$ rad/sec

9.24 (a) $K = 0.54$ (b) $\omega_b = 9.2$ rad/sec

9.25 (a) $K = 0.5$ (b) $K = 0.446$ (c) $K = 0.63$, $\omega_r = 0.5$ rad/sec, $\omega_b = 1$ rad/sec
(d) $K = 1.35$

9.26 $GM = 16.5$ dB; $\Phi M = 59°$
Gain should be increased by a factor of 1.75. The gain compensated system has $GM = 11.6$ dB, $\Phi M = 42.5°$.

9.27 K should be reduced by a factor of 3.5.; $\Phi M = 42.5°$, $M_r = 1.4$ gives $\zeta = 0.387$, $\Phi M = 42.5°$ gives $\zeta = 0.394$

10.1 (a) $GM = 6$ dB; $\Phi M = 17°$ (b) $K_c = 1.2$

10.2 (a) $\omega_g = 4.08$ rad/sec; $\Phi M = 3.9°$, $GM = 1.6$ dB
(b) $\omega_g = 5$ rad/sec; $\Phi M = 37.6°$, $GM = 18$ dB

10.3 (a) $K = 12$
(b) $\Phi M = 15°$; $\omega_b = 5.5$ rad/sec; $M_r = 12$ dB; $\omega_r = 3.5$ rad/sec

10.16 (a) $\Phi M = 0.63°$
(b) $\Phi M = 9.47°$; no effect on steady-state performance

10.17 $K_v = 4.8$

11.2 $T = 0.5$ sec; $\dfrac{U(z)}{E(z)} = \dfrac{2.2[4.1 - 3.9z^{-1}]}{4.01 - 3.99z^{-1}}$

11.3 (b) $u(k) = \dfrac{1 - \dfrac{aT}{2}}{1 + \dfrac{aT}{2}} u(k-1) + \dfrac{K\left(1 + \dfrac{bT}{2}\right)}{1 + \dfrac{aT}{2}} e(k) - \dfrac{K\left(1 - \dfrac{bT}{2}\right)}{1 + \dfrac{aT}{2}} e(k-1)$

11.4 (a) $K_c = 3.75$; $T_I = 5$ min; $T_D = 0.8$ min
(b) $K_c = 3.63$; $T_I = 5.17$ min; $T_D = 0.83$ min

11.5 $K_c = 2.25$; $T_I = 28.33$ sec

11.6 (a) $y(k+1) + \dfrac{1}{2} y(k) = -r(k+1) + 2r(k)$

$$\frac{Y(z)}{R(z)} = \frac{-z + 2}{z + \dfrac{1}{2}}$$

(b) $y(k) = \begin{cases} -1 & ; k = 0 \\ \dfrac{5}{2}\left(-\dfrac{1}{2}\right)^{k-1} & ; k \geq 1 \end{cases}$

(c) $y(k) = \dfrac{2}{3} - \dfrac{5}{3}\left(-\dfrac{1}{2}\right)^k ; k \geq 0$

11.7 $y(k) = 1 + \dfrac{1}{2}\left(\dfrac{1}{\sqrt{2}}\right)^k \left[\sin\dfrac{k\pi}{4} - \cos\dfrac{k\pi}{4}\right]; k \geq 0$

11.8 $y(k) = 3(2)^k - 2; k \geq 0$

11.9 (a) $y(k) = -40\delta(k) + 20\delta(k-1) - 10(0.5)^k + 50(-0.3)^k; k \geq 0$
(b) $y(k) = -16 + (0.56)^k [7.94 \sin(0.468k) + 16 \cos(0.468k)]; k \geq 0$

11.10 (a) $y(k) = -0.833(0.5)^k - 0.41(-0.3)^k + 0.476(-1)^k + 0.769; k \geq 0$
(b) $y(k) = -10k\,(0.5)^k + 2.5(0.5)^k - 6.94(0.1)^k + 4.44: k \geq 0$

11.11 $G(z) = \dfrac{1 - e^{-T}}{z - e^{-T}}$; $y(k) = 1 - e^{-kT}; k \geq 0$

11.12 $\dfrac{Y(z)}{R(z)} = \dfrac{10}{16}\left[\dfrac{z + 0.76}{(z-1)(z-0.46)}\right]$

11.13 $G_{h0}G(z) = 0.0288\left[\dfrac{z+0.92}{(z-1)(z-0.7788)}\right]$; $\dfrac{\theta_L(z)}{\theta_R(z)} = \dfrac{G_{h0}G(z)}{1+G_{h0}G(z)}$

11.14 $\dfrac{Y(z)}{R(z)} = 0.0095\left[\dfrac{z(z+0.92)}{z^3-2.81z^2+2.65z-0.819}\right]$

11.15 $y(k) = 1.02(0.795)^k \sin(0.89k)$; $k \geq 0$

11.16 $y(k) = 0.5[1-(-0.264)^k]\,\mu(k)$

11.17 $K_p = \infty$; $K_v = K_1/K_2$; $K_a = 0$.

11.18 0, 1/3.041, ∞

11.19 Underdamped response with $\zeta = 0.199$ and $\omega_n = 8.93$.

11.21 $0 < K < 2.1$; $K = 0.38$

11.22 (a) $K = 2.3925$ (b) (i) $K = 1.4557$; (ii) $K = 0.9653$

11.23 $0 < K < 0.785$

11.24 (a) $K = 0.88$; 1.33 rad/sec (b) $K = 0.072$; $\tau = 2.3$ sec
(c) $K = 0.18$; $\omega_n = 0.644$ rad/sec

11.25 $0 < A < 3.33$

11.26 (a) $D_1(z) = 13.934\left(\dfrac{z-0.8187}{z-0.1595}\right)$ (b) $K_v = 3$

11.27 $D(z) = 1.91\left(\dfrac{z-0.84}{z-0.98}\right)$

12.1 $x_1 = \theta_M$, $x_2 = \dot{\theta}_M$, x_3 = motor armature current i_a, x_4 = generator field current i_f; $y = \theta_L$

$$\mathbf{A} = \begin{bmatrix} 0 & 1 & 0 & 0 \\ 0 & -0.025 & 3 & 0 \\ 0 & -12 & -190 & 1000 \\ 0 & 0 & 0 & -4.2 \end{bmatrix}; \mathbf{b} = \begin{bmatrix} 0 \\ 0 \\ 0 \\ 0.2 \end{bmatrix}; \mathbf{c} = [0.5\ 0\ 0\ 0]$$

12.2 $$\mathbf{A} = \begin{bmatrix} 0 & 1 & 0 \\ 0 & -1 & 20 \\ 0 & 0 & -5 \end{bmatrix}; \mathbf{b} = \begin{bmatrix} 0 \\ 0 \\ 2.5 \end{bmatrix}; \mathbf{c} = [1\ 0\ 0]$$

12.3 $x_1 = \theta_M$, $x_2 = \dot{\theta}_M$, $x_3 = i_a$

$$\mathbf{A} = \begin{bmatrix} 0 & 1 & 0 \\ 0 & -0.5 & 19 \\ \dfrac{-k_1}{40} & \dfrac{-(k_2+0.5)}{2} & \dfrac{-21}{2} \end{bmatrix}; \mathbf{b} = \begin{bmatrix} 0 \\ 0 \\ \dfrac{k_1}{2} \end{bmatrix}; \mathbf{c} = \begin{bmatrix} \frac{1}{20} & 0 & 0 \end{bmatrix}$$

12.4 $\mathbf{A} = \begin{bmatrix} \dfrac{-B}{J} & \dfrac{K_T}{J} \\ \dfrac{-(k_1 K_t K_c + K_b)}{L_a} & \dfrac{-(R_a + k_2 K_c)}{L_a} \end{bmatrix}$; $\mathbf{b} = \begin{bmatrix} \dfrac{k_1^0 K_c}{L_a} \end{bmatrix}$; $\mathbf{c} = [1 \quad 0]$

12.5 (a) $\bar{\mathbf{A}} = \begin{bmatrix} -11 & 6 \\ -15 & 8 \end{bmatrix}$; $\bar{\mathbf{b}} = \begin{bmatrix} 1 \\ 2 \end{bmatrix}$; $\bar{\mathbf{c}} = [2 \quad -1]$

(b) $= \dfrac{1}{s^2 + 3s + 2}$

12.6 (a) $\mathbf{A} = \begin{bmatrix} 0 & 1 \\ 0 & 0 \end{bmatrix}$; $\mathbf{b} = \begin{bmatrix} 0 \\ 1 \end{bmatrix}$ (b) $\bar{\mathbf{A}} = \begin{bmatrix} 1 & 1 \\ -1 & -1 \end{bmatrix}$; $\bar{\mathbf{b}} = \begin{bmatrix} 0 \\ 1 \end{bmatrix}$

(c) $|\lambda \mathbf{I} - \mathbf{A}| = |\lambda \mathbf{I} - \bar{\mathbf{A}}| = \lambda^2$

12.7 $\mathbf{G}(s) = \dfrac{1}{\Delta} \begin{bmatrix} s(s+3) & s+3 & 1 \\ -1 & s(s+3) & s \\ -s & -1 & s^2 \end{bmatrix}$; $\mathbf{H}(s) = \dfrac{1}{\Delta} \begin{bmatrix} 1 \\ s \\ s^2 \end{bmatrix}$; $\Delta = s^3 + 3s^2 + 1$

12.9 x_1, x_2, x_3: outputs of integrators starting at the right and proceeding to the left.

$\mathbf{A} = \begin{bmatrix} 0 & 1 & 0 \\ 0 & -2 & 1 \\ -2 & 1 & -2 \end{bmatrix}$; $\mathbf{b} = \begin{bmatrix} 0 \\ 0 \\ 1 \end{bmatrix}$; $\mathbf{c} = [2 \quad -2 \quad 1]$

12.10 (a) $G(s) = \dfrac{s+3}{(s+1)(s+2)}$ (b) $G(s) = \dfrac{1}{(s+1)(s+2)}$

12.11 (a) $\mathbf{A} = \begin{bmatrix} -5 & 0.5 & -3.5 \\ 4 & -5 & 0 \\ 0 & 1 & 0 \end{bmatrix}$; $\mathbf{b} = \begin{bmatrix} 0 \\ 0 \\ -1 \end{bmatrix}$; $\mathbf{c} = [0 \; 1 \; 0]$

(b) $G(s) = \dfrac{14}{(s+1)(s+2)(s+7)}$

12.12 (a) x_1 = output of lag $1/(s+2)$; x_2 = output of lag $1/(s+1)$

$\mathbf{A} = \begin{bmatrix} -2 & 1 \\ -1 & -1 \end{bmatrix}$; $\mathbf{b} = \begin{bmatrix} 0 \\ 1 \end{bmatrix}$; $\mathbf{c} = [-1 \quad 1]$; $d = 1$

(b) x_1 = output of lag $1/(s+2)$; x_2 = output of lag $1/s$; x_3 = output of lag $1/(s+1)$

$$\mathbf{A} = \begin{bmatrix} -2 & 1 & 1 \\ -1 & 0 & 0 \\ -1 & 0 & -1 \end{bmatrix}; \mathbf{b} = \begin{bmatrix} 0 \\ 1 \\ 1 \end{bmatrix}; \mathbf{c} = [0 \quad 1 \quad 1]$$

12.13 (i) $\mathbf{A} = \begin{bmatrix} -1 & 0 \\ 0 & -2 \end{bmatrix}; \mathbf{b} = \begin{bmatrix} 1 \\ 1 \end{bmatrix}; \mathbf{c} = [2 \quad -1]$

(ii) $\mathbf{A} = \begin{bmatrix} 0 & 0 & -2 \\ 1 & 0 & -5 \\ 0 & 1 & -4 \end{bmatrix}; \mathbf{b} = \begin{bmatrix} 5 \\ 0 \\ 0 \end{bmatrix}; \mathbf{c} = [0 \quad 0 \quad 1]$

(iii) $\mathbf{A} = \begin{bmatrix} 0 & 1 & 0 \\ 0 & 0 & 1 \\ -6 & -11 & -6 \end{bmatrix}; \mathbf{b} = \begin{bmatrix} 0 \\ 0 \\ 1 \end{bmatrix}; \mathbf{c} = [2 \quad 6 \quad 2]$

12.14 (i) $\mathbf{A} = \begin{bmatrix} 0 & 0 & 0 \\ 1 & 0 & -2 \\ 0 & 1 & -3 \end{bmatrix}; \mathbf{b} = \begin{bmatrix} 1 \\ 1 \\ 0 \end{bmatrix}; \mathbf{c} = [0 \quad 0 \quad 1]$

(ii) $\mathbf{A} = \begin{bmatrix} 0 & 1 & 0 \\ 0 & 0 & 1 \\ -6 & -11 & -6 \end{bmatrix}; \mathbf{b} = \begin{bmatrix} 0 \\ 0 \\ 1 \end{bmatrix}; \mathbf{c} = [1 \quad 0 \quad 0]$

(iii) $\mathbf{\Lambda} = \begin{bmatrix} -1 & 0 & 0 \\ 0 & -2 & 0 \\ 0 & 0 & -3 \end{bmatrix}; \mathbf{b} = \begin{bmatrix} 1 \\ 1 \\ 1 \end{bmatrix}; \mathbf{c} = [-1 \quad 2 \quad 1]; d = 1$

12.15 (a) $\mathbf{A} = \begin{bmatrix} 0 & 1 & 0 \\ 0 & 0 & 1 \\ 0 & -100 & -52 \end{bmatrix}; \mathbf{b} = \begin{bmatrix} 0 \\ 0 \\ 1 \end{bmatrix}; \mathbf{c} = [5000 \quad 1000 \quad 0]$

(b) $\mathbf{\Lambda} = \begin{bmatrix} 0 & 0 & 0 \\ 0 & -2 & 0 \\ 0 & 0 & -50 \end{bmatrix}; \mathbf{b} = \begin{bmatrix} 50 \\ -31.25 \\ -18.75 \end{bmatrix}; \mathbf{c} = [1 \quad 1 \quad 1]$

12.16 (a) $\mathbf{\Lambda} = \begin{bmatrix} -1 & 1 & 0 \\ 0 & -1 & 0 \\ 0 & 0 & -2 \end{bmatrix}$; $\mathbf{b} = \begin{bmatrix} 0 \\ 1 \\ 1 \end{bmatrix}$; $\mathbf{c} = [1 \quad 1 \quad 1]$

(b) $y(t) = 2.5 - 2e^{-t} - 0.5e^{-2t} - te^{-t}$

12.17 $\mathbf{F} = \begin{bmatrix} 0.696 & 0.246 \\ 0.123 & 0.572 \end{bmatrix}$; $\mathbf{g} = \begin{bmatrix} -0.021 \\ 0.747 \end{bmatrix}$; $\mathbf{c} = [2 \quad -4]$; $d = 6$

12.18 $x_1(k) = y(k)$; $x_2(k) = u(k-1)$

$$\mathbf{F} = \begin{bmatrix} 0.3679 & 0.1809 \\ 0 & 0 \end{bmatrix}; \quad \mathbf{g} = \begin{bmatrix} 0.4512 \\ 0 \end{bmatrix}; \quad \mathbf{c} = [1 \quad 0]$$

12.19 (b) $\dfrac{X_1(s)}{x_1^0} = G_{11}(s) = \dfrac{1/2}{s+1} + \dfrac{1/2}{s+3}$; $\dfrac{X_1(s)}{x_2^0} = G_{12}(s) = \dfrac{1/2}{s+1} + \dfrac{-1/2}{s+3}$

$\dfrac{X_2(s)}{x_1^0} = G_{21}(s) = \dfrac{1/2}{s+1} + \dfrac{-1/2}{s+3}$; $\dfrac{X_2(s)}{x_2^0} = G_{22}(s) = \dfrac{1/2}{s+1} + \dfrac{1/2}{s+3}$

$\dfrac{X_1(s)}{U(s)} = H_1(s) = \dfrac{1}{s+1}$; $\dfrac{X_2(s)}{U(s)} = H_2(s) = \dfrac{1}{s+1}$

(c) (i) $\mathbf{x}(t) = \dfrac{1}{2}\begin{bmatrix} e^{-t}(x_1^0 + x_2^0) + e^{-3t}(x_1^0 - x_2^0) \\ e^{-t}(x_1^0 + x_2^0) + e^{-3t}(-x_1^0 + x_2^0) \end{bmatrix}$

(ii) $\mathbf{x}(t) = \begin{bmatrix} 1 - e^{-t} \\ 1 - e^{-t} \end{bmatrix}$

12.20 (a) Asymptotically stable (b) $y(t) = \frac{1}{2} + 2e^{-t} - \frac{3}{2}e^{-2t}$

12.21 (a) $\mathbf{A} = \begin{bmatrix} -6 & 0.5 \\ 4 & -5 \end{bmatrix}$; $\mathbf{b} = \begin{bmatrix} 7 \\ 0 \end{bmatrix}$; $\mathbf{c} = [0 \quad 1]$

(b) $y(t) = \dfrac{28}{3}\left[\frac{1}{4}(1 - e^{-4t}) - \frac{1}{7}(1 - e^{-7t})\right]$

12.22 $\begin{bmatrix} x_1(1) \\ x_2(1) \end{bmatrix} = \begin{bmatrix} 2.7183 - k \\ 2k \end{bmatrix}$ for any $k \neq 0$

12.23 $e^{\mathbf{A}t} = \begin{bmatrix} 2e^{-t} - e^{-2t} & e^{-t} - e^{-2t} \\ 2e^{-2t} - 2e^{-t} & 2e^{-2t} - e^{-t} \end{bmatrix}$; $\mathbf{A} = \begin{bmatrix} 0 & 1 \\ -2 & -3 \end{bmatrix}$

12.26 (i) Controllable but not observable (ii) Controllable but not observable
(iii) Both controllable and observable (iv) Both controllable and observable

12.27 (i) Observable but not controllable (ii) Controllable but not observable
(iii) Neither controllable nor observable
$A = -1$; $b = 1$; $c = 1$

12.28 (i) $G(s) = \dfrac{1}{s+2}$ (ii) $G(s) = \dfrac{s+4}{(s+2)(s+3)}$

The state model is not controllable The state model is not observable

12.29 (a) $\lambda_1 = 1$; $\lambda_2 = -2$; $\lambda_3 = -1$; unstable

(b) $G(s) = \dfrac{1}{(s+1)(s+2)}$; stable

12.30 (a) $\mathbf{A} = \begin{bmatrix} 0 & 1 \\ 0 & -1 \end{bmatrix}$; $\mathbf{b} = \begin{bmatrix} 0 \\ 1 \end{bmatrix}$; $\mathbf{c} = [10 \quad 0]$

(b) $\mathbf{A} = \begin{bmatrix} 0 & 1 & 0 \\ 0 & 0 & 1 \\ 0 & -2 & -3 \end{bmatrix}$; $\mathbf{b} = \begin{bmatrix} 0 \\ 0 \\ 1 \end{bmatrix}$; $\mathbf{c} = [20 \quad 10 \quad 0]$

(c) $\mathbf{A} = \begin{bmatrix} 0 & 0 & 0 \\ 1 & 0 & -2 \\ 0 & 1 & -3 \end{bmatrix}$; $\mathbf{b} = \begin{bmatrix} 20 \\ 10 \\ 1 \end{bmatrix}$; $\mathbf{c} = [0 \quad 0 \quad 1]$

13.1 (a) $k_1 = 74$, $k_2 = 25$, $k_3 = 3$ (b) $\dot{\hat{\mathbf{x}}} = (\mathbf{A} - \mathbf{mc})\ \hat{\mathbf{x}} + \mathbf{b}u + \mathbf{m}y$
$\mathbf{m}^T = [3 \quad 7 \quad -1]$

13.2 (a) $\mathbf{k} = [3 \quad 7 \quad -1]$ (b) $\mathbf{m}^T = [74 \quad 25 \quad 3]$
$\dot{\mathbf{x}} = (\mathbf{A} - \mathbf{bk})\mathbf{x}$

13.3 (a) $\mathbf{A} = \begin{bmatrix} 0 & 9 \\ 1 & 0 \end{bmatrix}$; $\mathbf{b} = \begin{bmatrix} 9 \\ 0 \end{bmatrix}$; $\mathbf{c} = [0 \quad 1]$

(b) $\mathbf{k} = \begin{bmatrix} \frac{2}{3} & 3 \end{bmatrix}$

(c) $\dot{\hat{\mathbf{x}}} = (\mathbf{A} - \mathbf{mc})\ \hat{\mathbf{x}} + \mathbf{b}u + \mathbf{m}y$
$\mathbf{m}^T = [81 \quad 12]$

13.4 (a) $\mathbf{A} = \begin{bmatrix} 0 & 1 \\ -\omega_0^2 & 0 \end{bmatrix}$; $\mathbf{b} = \begin{bmatrix} 0 \\ 1 \end{bmatrix}$; $\mathbf{c} = [1 \quad 0]$

(b) $k_1 = 3\omega_0^2$; $k_2 = 4\omega_0$

(c) $\dot{\hat{\mathbf{x}}} = (\mathbf{A} - \mathbf{mc})\ \hat{\mathbf{x}} + \mathbf{b}u + \mathbf{m}y$

$\mathbf{m}^T = [20\omega_0 \quad 99\omega_0^2]$

13.5 (a) $\mathbf{k} = [29.6 \quad 3.6]$ (b) $\dot{\hat{\mathbf{x}}} = (\mathbf{A} - \mathbf{mc})\,\hat{\mathbf{x}} + \mathbf{b}u + \mathbf{m}y$

$\mathbf{m}^T = [16 \quad 84.6]$

13.6 (a) $\mathbf{A} = \begin{bmatrix} 0 & 1 \\ 0 & 0 \end{bmatrix}$; $\mathbf{b} = \begin{bmatrix} 0 \\ 1 \end{bmatrix}$; $\mathbf{c} = [1 \quad 0]$

(b) $\mathbf{k} = [1 \quad \sqrt{2}]$

(c) $\dot{\hat{\mathbf{x}}} = (\mathbf{A} - \mathbf{mc})\hat{\mathbf{x}} + \mathbf{b}u + \mathbf{m}y$

$\mathbf{m}^T = [5 \quad 25]$

13.7 (a) $k_1 = 4$; $k_2 = 3$; $k_3 = 1$; $N = k_1$ (b) $\mathbf{m}^T = [5 \quad 7 \quad 8]$

13.8 $\mathbf{k} = [-1.4 \quad 2.4 \quad -1.6]$

13.9 $k_1 = a_2/\beta$; $k_2 = (a_1 - \alpha)/\beta$; $N = k_1$

13.10 (a) $\mathbf{k} = [3 \quad 1.5]$

(b) For a unit-step input, the steady-state error in the output is 6/7.

(c) $k_1 = 2$; $k_2 = 1.5$; $k_3 = -3.5$

13.11 $k_1 = -4$; $k_2 = -3/2$; $k_3 = 0$

13.12 $\mathbf{k} = [-0.5 \quad -0.2 \quad 1.1]$

$\mathbf{x}(k+1) = (\mathbf{F} - \mathbf{gk})\mathbf{x}(k)$

13.13 (a) $\mathbf{k} = \begin{bmatrix} \frac{111}{76} & -\frac{18}{19} \end{bmatrix}$ (b) $\hat{\mathbf{x}}\,(k+1) = (\mathbf{F} - \mathbf{mc})\,\hat{\mathbf{x}}\,(k) + \mathbf{g}u(k) + \mathbf{m}\,y(k)$

$\mathbf{m}^T = [8 \quad -5]$

13.14 (a) $\mathbf{F} = \begin{bmatrix} 0 & 1 \\ -0.16 & -1 \end{bmatrix}$; $\mathbf{g} = \begin{bmatrix} 0 \\ 1 \end{bmatrix}$; $\mathbf{c} = [1 \quad 0]$

(b) $k_1 = 0.36$; $k_2 = -2.2$

13.15 (a) $\mathbf{F} = \begin{bmatrix} 1 & 0.1 \\ 0 & 1 \end{bmatrix}$; $\mathbf{g} = \begin{bmatrix} 0.005 \\ 0.1 \end{bmatrix}$ (b) $k_1 = 13$; $k_2 = 3.95$

(c) $\hat{\mathbf{x}}\,(k+1) = (\mathbf{F} - \mathbf{mc})\,\hat{\mathbf{x}}\,(k) + \mathbf{g}u(k) + \mathbf{m}y(k)$

$\mathbf{m}^T = [2 \quad 10]$

13.16 (a) $\mathbf{F} = \begin{bmatrix} 1 & 0.0952 \\ 0 & 0.905 \end{bmatrix}$; $\mathbf{g} = \begin{bmatrix} 0.00484 \\ 0.0952 \end{bmatrix}$; $\mathbf{c} = [1 \quad 0]$

(b) $k_1 = 105.1$; $k_2 = 14.625$

(c) $\hat{\mathbf{x}}(k+1) = (\mathbf{F} - \mathbf{mc})\hat{\mathbf{x}}(k) + \mathbf{g}u(k) + \mathbf{m}y(k)$

$\mathbf{m}^T = [1.9 \quad 8.6]$

13.17 (a) $y(k+1) = 0.368y(k) + 0.632u(k)$

(b) $K = 0.3687$

(c) $K_1 = 0.553$; $K_2 = -2.013$

14.2 $\frac{8M}{\pi}$; 1 rad/sec; $y(t) = \frac{-8M}{\pi} \sin t$

14.3 0.3; 10 rad/sec

14.4 $\Delta < 0.131$

14.6 4.25; $\sqrt{2}$ rad/sec, stable limit cycle

14.7 3.75; 1 rad/sec

14.8 (a) Stable node; (0, 0) point in $(y, \dot{y})$-plane (b) Stable node; (1,0) point in $(y, \dot{y})$-plane

(c) Unstable focus; (2,0) point in $(y, \dot{y})$-plane

14.9 Singularity at (0, 0) is either a stable node or a stable focus, depending upon the magnitudes of a and K. Singular point $(\pi, 0)$ is a saddle point.

14.10 (i) Singularity (1,0) in $(y, \dot{y})$-plane is a centre

(ii) Singularity (1,0) in $(y, \dot{y})$-plane is a stable focus.

14.11 (a) For $-0.1 < x_1 < 0.1$, $\ddot{x}_1 + \dot{x}_1 + 7x_1 = 0$

For $x_1 > 0.1$, $\ddot{x}_1 + \dot{x}_1 + 0.7 = 0$

For $x_1 < -0.1$, $\ddot{x}_1 + \dot{x}_1 - 0.7 = 0$

(b) Isocline equations:

$x_2 = \frac{-7x_1}{m+1}$; $-0.1 < x_1 < 0.1$

$x_2 = \frac{-0.7}{m+1}$; $x_1 > 0.1$

$x_2 = \frac{0.7}{m+1}$; $x_1 < -0.1$

(c) A singular point at the origin

14.12 (a) For $-0.1 < x_1 < 0.1$, $\ddot{x}_1 + \dot{x}_1 = 0$

For $x_1 < -0.1$ $\ddot{x}_1 + \dot{x}_1 + 7(x_1 + 0.1) = 0$

For $x_1 > 0.1$, $\ddot{x}_1 + \dot{x}_1 + 7(x_1 - 0.1) = 0$

(b) Isocline equations:

$m = -1$; $-0.1 < x_1 < 0.1$

$x_2 = \frac{-7x_1 - 0.7}{m+1}$; $x_1 < -0.1$

$$x_2 = \frac{-7x_1 - 0.7}{m+1}; \quad x_1 < -0.1$$

$$x_2 = \frac{-7x_1 + 0.7}{m+1}; \quad x_1 > 0.1$$

(c) Singular points at $(x_1 = \pm 0.1, x_2 = 0)$

14.13 (a) $\ddot{x}_1 + \dot{x}_1 + 0.7 \text{ sgn } x_1 = 0$

(b) Isocline equations:

$$x_2 = \frac{-0.7}{m+1}; x_1 > 0$$

$$x_2 = \frac{0.7}{m+1}; x_1 < 0$$

(c)No singular points

14.14 (a)For $-0.1 < x_1 < 0.1$, $\ddot{x}_1 + \dot{x}_1 = 0$

For $x_1 > 0.1$, $\ddot{x}_1 + \dot{x}_1 + 0.7 = 0$

For $x_1 < -0.1$, $\ddot{x}_1 + \dot{x}_1 - 0.7 = 0$

(b) Isocline equations:

$m = -1; -0.1 < x_1 < 0.1$

$$x_2 = \frac{-0.7}{m+1}; x_1 > 0.1$$

$$x_2 = \frac{0.7}{m+1}; x_1 < -0.1$$

(c) No singular points

14.15 (a) $\ddot{x}_1 + 0.1 \text{ sgn } \dot{x}_1 + x_1 = 0$

(b) Isocline equation:

$$x_2 = \frac{-x_1 - 0.1 \text{ sgn } x_2}{m}$$

(c) Singualar points at $(x_1 = \mp 0.1, x_2 = 0)$

14.16 Steady-state error to unit-step input = – 0.2 rad
Maximum steady-state error = ± 0.3 rad.

14.17 Deadzone helps to reduce system oscillations, and introduces steady-state error

14.18 Saturation has a slowing down effect on the transient.

14.19 Asymptotically stable

14.20 Unstable

14.21 $|x_1| < 1$; origin is the equilibrium state

14.22 Asymptotically stable; origin is the equilibrium state.

Index

MATLAB and Simulink Support

Appendix A

MATLAB, an abbreviation for MATrix LABoratory, is a high-performance language for technical computing. It integrates computation, visualization, and programming in an easy-to-use environment where problems and solutions are expressed in familiar mathematical notation.

The MATLAB family of programs includes the *base program* plus a variety of application-specific solutions called *toolboxes*. Toolboxes are comprehensive collections of MATLAB functions that extend the MATLAB environment to solve particular classes of problems. Together, the base program plus the *Control System Toolbox* provide the capability to use MATLAB for control system analysis and design problems at the level of the text. Whenever MATLAB is referred to in this book, you can interpret that to mean the base program plus the control system toolbox.

Simulink, a companion program to MATLAB, is an interactive system for simulating nonlinear dynamic systems. It is a graphical mouse-driven program that allows you to model a system by drawing a block diagram on the screen and manipulating it dynamically. It is a powerful, comprehensive, and user-friendly software package for simulation studies.

If you are new to MATLAB and Simulink, and want to learn it quickly, start by visiting the web course: MATLAB Modules for Control System Principles and Design [151]. The course has been designed to serve the purpose of giving a 'starting kick' to the students who need to be kicked to action. The course has not been designed as a substitute to the MATLAB manuals. MathWorks [152] provides extensive documentation in both printed and online format to help you learn about and use all the features of MATLAB and Simulink. The online **help** provides task-oriented, and function-reference information. The documentation is also available in PDF format. Visit the website of MathWorks [152].

Our presentation in this appendix has a limited objective of helping the reader refresh his/her knowledge on MATLAB and Simulink. We use MATLAB version 7. For the most part, the material applies to 6x version as well. MATLAB continues to evolve as a software tool. However, the basic operation of MATLAB and its basic capabilities have, more or less, stabilized around the optimum level. Dramatic changes are not expected in near future; the material, therefore, will continue to apply to 7x version as well.

A.1 MATLAB FUNCTIONS FOR CONTROL DESIGN

A.1.1 Models

When a control engineer is given a control problem, often one of the first tasks that he undertakes is the development of the mathematical model of the process to be controlled. We can use first principles of physics to write down a model. Another way is to perform "system identification" via the use of real plant data to produce a model of the system.

For linear time-invariant systems, mathematical model building based on physical laws normally results in a set of (first-order and second-order) differential equations. These equations, when rearranged as a set of first-order differential equations, result in a state-space model of the following form for single-input, single-output (SISO) systems:

$$\begin{aligned} \dot{\mathbf{x}} &= \mathbf{A}\mathbf{x} + \mathbf{b}u \\ y &= \mathbf{c}\mathbf{x} + du \end{aligned} \tag{A.1}$$

where $\mathbf{x}(t)$ is the $n \times 1$ internal state vector, $u(t)$ is the control input and $y(t)$ is the measured output. Overdot represents differentiation with respect to time t.

Complex processes and machines often have several manipulated inputs available to provide this control (multivariable or MIMO system). In many situations, one input affects primarily one output and has only weak effect on other outputs; it becomes possible to ignore weak interactions (coupling) and design controllers under the assumption that one input affects only one output. Input-output pairing to minimize the effect of interactions and application of SISO control schemes to obtain separate controllers for each input-output pair, results in an acceptable performance. This, in fact, amounts to considering the MIMO system as consisting of an appropriate number of separate SISO systems. Coupling effects are considered as disturbances to the separate control systems. Though MATLAB has a provision for both the SISO and MIMO models, we will limit our discussion to SISO models.

For the state-space representation (A.1), the data for the model consists of four matrices. For convenience, the MATLAB provides customized data structure. This is called the **SS** object. This object encapsulates the model data and enables you to manipulate linear time-invariant (LTI) system as single entity, rather than collection of data vectors and matrices.

An LTI object of the type **SS** is created whenever you invoke the construction function **ss**. For example, type

```
>> A = [– 8   – 16   – 6;   1   0   0 ; 0   1   0];
>> b = [1;   0;   0];
>> c = [2   8   6];
>> d = 0;
>> sys = ss(A, b, c, d)
```

and MATLAB responds with

```
a =
                x1          x2          x3
    x1          – 8         – 16        – 6
    x2          1           0           0
    x3          0           1           0
b =
                u1
    x1          1
    x2          0
    x3          0
c =
                x1          x2          x3
    y1          2           8           6
d =
                u1
    y1          0
```

Controllability and observability of a system in state variable form can be checked using the MATLAB functions **ctrb** and **obsv**, respectively. The inputs to the **ctrb** function are the system matrix **A** and the input matrix **b**; the output of **ctrb** function is the controllability matrix **U**. Similarly, the inputs to the **obsv** function are the system matrix **A** and the output matric **c**; the output is observability matrix **V**. The functions **det(U)/rank(U)** and **det(V)/rank(V)** give, respectively, the controllability and observability properties.

Our next step is to make a design model. Since our focus is going to be on frequency-domain design methods, a transfer function model will be required. A transfer function

$$G(s) = \frac{n(s)}{d(s)} \tag{A.2}$$

is characterized by the numerator $n(s)$ and denominator $d(s)$; both polynomials of the Laplace variable s. MATLAB provides LTI object **TF** for transfer functions. The object **TF** is created whenever you invoke the construction function **tf**. For example, for

$G(s) = (8 + 12s + 4s^3)/(17s^5 + 23s^3 + 8s^2 + 6)$, type

```
>> num = [4   0   12   8]; den = [17   0   23   8   0   6];
>> sys = tf(num, den)
```

and MATLAB responds with

Transfer function

$$\frac{\mathbf{4s\ ^\ 3 + 12s + 8}}{\mathbf{17s\ ^\ 5 + 23s\ ^\ 3 + 8s\ ^\ 2 + 6}}$$

Quite often, the transfer function in hand is in zero-pole-gain form,

$$G(s) = \frac{10(s-3)(s+4.5)(s+100)}{(s+40)^3(s+80)}$$

MATLAB provides construction function **zpk** to create **ZPK** object. We can, however, create **TF** object for this transfer function using construction function **tf**.

```
>> r1 = [3; – 4.5; – 100]; r2 = [– 40; – 40; – 40; – 80];
>> num = 10* poly(r1); den = poly(r2);
>> sys = tf(num, den);
```

r1 is a column vector containing the roots of a polynmial. The function **poly(r1)** assembles the polynomial.

Some more examples of construction of **TF** object follow.

$$G(s) = \frac{10(s+2)(s+5)}{(s^2+2s+5)(s+3)}$$

with real as well as complex poles.

```
>> r = [– 2; – 5];
>> num = 10 * poly(r);
>> p = [1 2 5];  q = [1   3];
>> den = conv(p, q);
>> sys = tf(num, den);
```

The function **conv** has been used to multiply two polynomials $p(s) = s^2 + 2s + 5$, and $q(s) = s + 3$.

$$G(s) = \frac{100(5s+1)(15s+1)}{s(3s+1)(10s+1)}$$

is a transfer function in time-constant form.

```
>> n1 = [5   1]; n2 = [15   1];   d1 = [1   0]; d2 = [3   1];
>> d3 = [10   1]; num = 100 * conv(n1, n2);
>> den = conv(d1, conv(d2, d3));
>> sys = tf(num, den);
```

To create the object **TF** directly, use these commands:

```
>> s = tf('s');
>> sys = 100*(5*s+1)*(15*s+1)/[s*(3*s+1)*(10*s+1)];
```

In cases where our knowledge of the system under study is limited, or the theoretical model turns out to be highly complex, the only reliable information on which to base the control design is the experimental data. MATLAB has a provision of creating an LTI object called **FRD** which stores frequency response data (complex frequency response, alongwith a corresponding vector of frequency points) that you obtain experimentally.

MATLAB has the means to perform model conversions. Given the **SS** model ***sys_ss***, the syntax for conversion to **TF** model is

sys_tf = tf(sys_ss)

Common pole-zero factors of the **TF** model must be cancelled before we can claim that we have the transfer function representation of the system. To assist us in pole-zero cancellation, MATLAB provides **minreal** function.

sysr = minreal(sys_tf)

Given the **TF** model **sys_tf**, the syntax for conversion to **SS** model is

sys_ss = ss(sys_tf)

Process transfer function models frequently have dead-time (input-output delay). **TF** object for transfer functions with dead-time can be created using the syntax

sys = tf(num, den, 'InputDelay', value)

For $G(s) = (6.6\, e^{-7s})/(10.9s + 1)$, type

```
>> num = [6.6]; den = [10.9   1];
>> sys = tf(num, den, 'InputDelay', 7);
```

Two cascaded blocks with transfer functions $G_1(s)$ and $G_2(s)$ can be multiplied using the **series** function.

```
sys1 = tf(num1, den1) % G1(s)
sys2 = tf(num2, den2) % G2(s)
sys = series(sys1, sys2) % G1(s)G2(s)
```

or

```
sys = sys1 *sys2
```

If **sys1** and **sys2** are in parallel, then

```
sys = parallel(sys1, sys2) % G1(s) + G2(s)
```

or

```
sys = sys1 + sys2
```

For a negative feedback loop with forward path transfer function $G(s)$ and feedback path transfer function $H(s)$, the function **feedback** results in closed-loop transfer function.

```
sys1 = tf(num1, den1) % G(s)
sys2 = tf(num2, den2) % H(s)
sys = feedback(sys1, sys2) % G(s)/(1 + G(s)H(s))
```

For a unity-feedback system, the closed-loop transfer function is given by

```
sys = feedback(sys1, 1) % G(s)/(1 + G(s))
```

A.1.2 Time Response

For the **SS** object of the model (A.1):

sys = ss(A, b, c, d)

the function **step(sys)** will generate a plot of unit-step response $y(t)$ (with zero initial conditions). The time vector is automatically selected when **t** is not explicitly included in the **step** command.

If you wish to supply the time vector **t** at which the response will be computed, the following command is used.

step(sys, t)

You can specify either a final time **t = Tfinal,** or a vector of evenly spaced time samples of the form

t = 0 : dt : Tfinal

When invoked with left-hand arguments such as

[y,t] = step(sys)
[y,t,X] = step(sys)
y = step(sys, t)

no plot is generated on the screen. Hence it is necessary to use a **plot** command to see the response curves. The vector **y** and matrix **X** contain the output and state response of the system, respectively, evaluated at the computation points returned in the time vector **t** (**X** has as many columns as states and one row for each element in vector **t**).

Other time-response functions of interest to us are:

```
impulse(sys)      % impulse response
initial(sys,x0)   % free response to initial state vector x0
lsim(sys,u,t)     % response to input time history
lsim(sys,u,t,x0)  % in vector u having length (t) rows
```

For the **TF** object of the model (A.2):

sys = tf(num, den)

the function **step(sys)** will generate a unit-step response $y(t)$. The time vector is automatically selected when **t** is not explicitly included in the **step** command. If you wish to supply the time vector **t** at which the response will be computed, the following command is used.

step (sys,t)

When invoked with left-hand arguments such as

[y,t] = step(sys)
y = step(sys,t)

no plot is generated on the screen. Hence it is necessary to use a **plot** command to see the response curve. The vector **y** has one column and one row for each element in time vector **t**.

Other time-response functions of interest to us are:

```
impulse(sys)  % impulse response
lsim(sys,u,t) % response to input time history in vector u having
              % length (t) rows.
```

Place your mouse on any point along a plot line (step, impulse, lsim, initial). Left-clicking on this point opens data with relevant information displayed.

As the nature of the transient response of a control system is dependent upon the system poles only and not on the type of the input, it is sufficient to analyze the transient response to one of the standard test signals; a step is generally used. In specifying the steady-state response characteristics, it is common to specify the steady-state error of the system to one or more of the standard test signals—step, ramp, parabola.

Typical design specifications demand that the system have (when subjected to command/disturbance inputs)

(i) a step response inside some constraint boundaries—specified by settling time, peak overshoot, etc; and

(ii) steady-state error to step/ramp/parabolic input within prescribed limits, under the constraints imposed by physical limitations of the selected plant, actuator, and sensor.

You can analyze the time response using the **GUI** (graphical user interface) for viewing and manipulating response plots of LTI models. For example, **step (sys)** will open a window displaying the step response of the LTI model **sys**. Once initialized, the **GUI** assists you with the analysis of the response by facilitating such functions as zooming into regions of the response plots; calculating response characteristics such as peak response, settling time, rise time, steady-state; toggling the grid on or off the plot; and many other useful features.

Right-click anywhere in the plot region of the step response plot. This opens a menu list in the plot region. Select the **Grid** menu item with left mouse button. A grid for the graph appears. Now right-click again and place the pointer in the **Characteristics** menu item. The submenu items (Peak Response, Settling Time, Rise Time, Steady-State) of the Characteristics menu are displayed. Select **Settling Time** with left mouse button. The settling time marker appears on the graph. Place your mouse on the marker. This opens data with relevant information displayed. To make it persistent, left-click on the marker.

In addition to right-click menus, the GUI provides plot-data markers. Left-click anywhere on a plot line; a data marker appears with the response values of the plot at that point displayed. You can move the data marker along the plot line. Move the mouse pointer over the marker. The pointer becomes a hand. Grab the marker by holding down the left mouse button when the hand appears. Drag the marker with your mouse and release the mouse button at a point of your interest along the plot line. Response values at the selected point are displayed.

You can use the **Property Editor** to customize various attributes of your plot. Move the pointer on the **Properties** menu item to open the editor.

The GUI feature is available with all the time response plots.

A.1.3 Frequency Response

For the **TF** object of the model (A.2):

sys = tf(num, den)

the function **bode(sys)** generates the Bode frequency-response plots. This function automatically selects the frequency values by placing more points in regions where the frequency response is changing quickly. This range is user-selectable using the command **bode(sys,w)**. Since the Bode diagram has log scale, if we choose to specify the frequencies explicitly, it is desirable to generate the vector **w** using the **logspace** function. When invoked with left-hand arguments,

[mag,phase,w] = bode(sys)

[mag,phase] = bod(sys,w)

return the magnitude and phase of frequency response at the frequencies **w**.

nyquist(sys) plots the real and imaginary parts of the frequency response of an arbitrary LTI model **sys**. **nyquist (sys,w)** explicitly specifies the frequency range to be used for the plot. To focus on a particular frequency interval, set **w = {wmin,wmax}**. When invoked with left-hand arguments,

[re,im,w] = nyquist(sys)

[re,im] = nyquist(sys,w)

return the real and imaginary parts of the frequency response at the frequencies **w**.

Sometimes in the course of using the **nyquist** function, we may find that a Nyquist plot looks nontraditional or that some information appears to be missing. It may be necessary, in these cases, to override the automatic scaling and focus in on the $-1 + j0$ point region for stability analysis.

In practice, Nyquist diagrams are commonly plotted on the Nichols coordinate system with rectangular coordinate axes for the phase (in degrees) and the gain (in dB). On the Nichols coordinate system, the critical point for stability becomes (180°, 0dB).

The Nyquist diagram on the Nichols coordinate system can be generated using the **nichols** function. **nichols(sys)** produces a Nyquist plot of the LTI model **sys**. **nichols(sys,w)** explicitly specifies the frequency range to be used for the plot. When invoked with left-hand arguments,

[mag,phase,w] = nichols(sys)

[mag,phase] = nichols(sys,w)

return the magnitude (in dB) and phase (in degrees) of the frequency response at the frequencies **w** (in rad/sec). Nichols chart grid is drawn on the existing plot using **ngrid** function.

Requirements that a control system have a step response inside some constraint boundaries—specified by settling time, peak overshot, etc., can equivalently be represented as requirements that the system have a frequency response satisfying certain constraints specified by gain margin, phase margin, bandwidth, etc. The function **margin** determines gain margin, phase margin, gain crossover frequency, and phase crossover frequency. Resonance peak, resonance frequency, and bandwidth of a closed-loop system may be obtained from the plot generated by **nichols** and **ngrid** functions.

You can analyze the frequency response using the **GUI** (graphical user interface) for viewing and manipulating response plots of LTI models. For example, **nichols (sys)** will open a window displaying the Nichols plot of the LTI system **sys**. Once initialized, the **GUI** assists you with the analysis of the response by facilitating such functions as zooming into regions of response plot; calculating response characteristics such as resonance peak, resonance frequency, bandwidth, stability margins; and many other useful features.

Right-click anywhere in the plot region of the Nichols plot. This opens a menu list in the plot region. Select the **Grid** menu item with left mouse button. A grid for the graph appears. Identify the –3 dB contour on the grid. Zoom in on the region of intersection of this contour with the plot. Click on the point of intersection; hold the mouse button down to read the value of bandwidth.

In addition to right-click menus, the GUI provides plot-data markers. Left-click anywhere on a plot line; a data marker appears with the response values of the plot at that point displayed. You can move the data marker along the plot line. Move the mouse pointer over the marker. The pointer becomes a hand. Grab the marker by holding down the left mouse button when the hand appears. Drag the marker with your mouse and release the mouse button at a point of your interest along the plot line. Response values at the selected point are displayed.

You can use the **Property Editor** to customize various attributes of your plot. Move the pointer on the **Properties** menu item to open the editor.

The GUI feature is available with all the frequency-response plots.

A.1.4 Design

Root Locus: If **sys** models a transfer function

$$G(s) = \frac{n(s)}{d(s)}$$

rlocus adaptively selects a set of positive gains K and produces a smooth plot of the roots of

$$d(s) + Kn(s) = 0$$

Alternatively, **rlocus(sys,K)** uses the user-specified vector **K** of gains to plot the root locus. Left-click anywhere on the root loci to see the relevant information about the locus at that point.

The function **rlocfind** returns the feedback gain associated with a particular set of poles on the root locus. **[K,poles] = rlocfind(sys)** is used for interactive gain selection. The function **rlocfind** puts up a cross hair cursor on the root locus plot that you use to select a particular pole location. The root locus gain associated with this point is returned in **K** and the column vector **poles** contains the closed-loop poles for this gain. To use this command, the root locus must be present in the current figure window.

The function **sgrid/spchart** is used for ω_n and ζ grid on the root locus.

Note that LTI functions are available in figure windows of the commands **margin**, **bode**, **nyquist**, **nichols**, **rlocus**. Left-click anywhere on a particular plot line to see the response values of that plot at that point. You can drag the data marker along a plot line. Also right-click menus are available.

Lag/Lead Design: To form an initial estimate of the complexity of the design problem, sketch frequency response (Bode plot) and root-locus plot with respect to plant gain. Try to meet the specifications with a simple controller of lag/lead variety. Compare a lead network in the forward path to minor-loop feedback structure having direct feedback from velocity sensor, to see which gives a better design.

For design by root-locus method, the design specifications are translated into desired dominant closed-loop poles. Other closed-loop poles are required to be located at a large distance from the $j\omega$-axis. It may be noted that pole-placement methods do not allow the designer to judge how close the system performance is to the best possible. Also, there is lack of visibility into low-frequency disturbance rejection. This can cause many problems: the disturbance rejection may not be optimized, and the plant-parameter variations may cause large closed-loop response variations. Stability margins on Nyquist/Bode plot give a better robustness measure. For this reason, though the specifications on the closed-loop performance are often formulated in time domain, it is worthwhile to convert them into frequency-domain specifications and then design the compensator with frequency-domain methods. Root-locus plots are very impressive analysis tools for systems that have been designed by frequency-domain methods. For example, these plots can be valuable for the analysis of the effects of certain parameter variations on stability.

You can design a compensator using frequency-response MATLAB functions **bode** and **nichols**.

Suppose analog compensator $D(s)$ has been created in MATLAB as **sysc**. The command

```
sysd = c2d(sysc,T,'tustin') % Tustin approximation
                            % T is sampling interval
```

converts the continuous-time system $D(s)$ to discrete-time system using trapezoidal rule for integration. The object **sysc** may be an **SS** object or a **TF** object.

A.1.5 Simulation of Performance of Design

After reaching the best compromise among process modification, actuator and sensor selection, and controller design choice, run a computer model of the feedback system. This model should include important nonlinearities—such as actuator saturation, and parameter variations you expect to find during operation of the system. The simulation will confirm stability and robustness, and allow you to predict the true performance you can expect from the system.

MATLAB provides many Runge Kutta numerical integration routines for solving ordinary differential equations; the function **ode23** usually suffices for our applications. The feedback system is represented by a set of linear/nonlinear state-space equations; the system is coded in an **M-file**, and then **ode** solver function such as **ode23** is applied to solve the system on a given time interval with a particular initial condition vector. Refer [155] for details.

MATLAB's Simulink is better suited for simulation studies in our applications.

More on Design and Performance Analysis: In Chapters 11-14, we have given a brief account of a range of topics on digital control, state variable methods, and nonlinear systems. Detailed account of these topics is available in the companion book [155]. Also included in the companion book is an appendix on MATLAB and Simulink support on these topics. This appendix is available at: http://www.mhhe.com/gopal/dc3e

A.2 MATLAB/Simulink

In the simulation process, the computer is provided with appropriate input data and other information about system structure, operates on this input data and generates output data, which it subsequently displays. Several software packages that have been produced over the last two decades include computer programs that allow these simulation operations. Over the years, these simulation packages have become quite sophisticated, powerful and very "user-friendly". The usefulness and importance of these software packages is undeniable, because they greatly facilitate the analysis and design of control systems. They provide a tremendous tool in the hands of control engineers.

MATLAB/Simulink is one of the most successful software packages currently available, and is particularly suited for work in control. It is a powerful, comprehensive and user-friendly software package for simulation studies. Our objective here is to help the reader gain a basic understanding of this software package by showing how to set up and solve a simulation problem. Interested readers are encouraged to further explore this very complete and versatile mathematical computation package [151, 152].

A very nice feature of Simulink is that it visually represents the simulation process by using *simulation block diagrams*. Especially, functions are represented by "subsystem blocks" that are then interconnected to form a Simulink block diagram that defines the system structure. Once the structure is defined, parameters are entered in the individual subsystem blocks that correspond to the given system data. Some additional simulation parameters must also be set to

govern how the numerical computation will be carried out and how the output data will be displayed. As a matter of fact, the Simulink block diagrams are essentially the same we have used in the text to describe control system structures and signal flow.

Because Simulink is graphical and interactive, we encourage you to jump right in and try it. To help you start using Simulink quickly, we describe here the simulation process though a demonstration example on Microsoft Windows platform with MATLAB version 7, Control Toolbox version 6.1 and Simulink version 6.1.

To start Simulink, enter **simulink** command at the MATLAB prompt. Simulink Library Browser appears which displays tree-structured view of the Simulink block libraries. It contains several nodes; each of these nodes represents a library of subsystem blocks that is used to construct simulation block diagrams. You can expand/collapse the tree by clicking on the ⊞/⊟ boxes beside each node, and block in the block set pan.

Expand the node labeled "Simulink". Subnodes of this node are displayed. Expanding the "Sources" subnode displays a long list of Sources library blocks; contents are displayed in the diagram view. The purpose of the block "Step" is to generate a step function. The block "Constant" generates a specified real or complex value, independent of time. Simply click on any block to learn about its functionality in the description box.

You may now collapse the Sources subnode, and expand the "Sinks" subnode. A list of Sinks library blocks appears. The purpose of block labeled "XY Graph" is to display an X-Y plot of signals using a MATLAB figure window. The block has two scalar inputs; it plots data in the first input (the x direction) against data in the second input (the y direction). The block "Scope" displays its inputs (signals generated during a simulation) with respect to simulation time. The block "To Workspace" transfers the data to MATLAB workspace.

You may now collapse the Sinks subnode and expand the "Continuous" subnode. A list of library blocks corresponding to this subnode appears. The purpose of the "Derivative" block is to output the time derivative of the input. The "State-Space" block implements a linear system whose behaviour is described by a state variable model. The "Transfer Fcn" block implements a transfer function.

The "Discontinuities" subnode has blockset of various nonlinearities: Backlash, Coulomb and Viscous Friction, Deadzone, Relay, Saturation, etc.

The "Math Operations" subnode has several blocks. The block "Sum" generates the sum of inputs. It is useful as an error detector for control system simulations. The "Sign" block indicates the sign of the input (The output is 1 when the input is greater than zero: the output is 0 when the input is equal to zero; and the output is -1 when the input is less than zero).

Expand now the node "Control System Toolbox". The block "LTI system" accepts the continuous and discrete objects as defined in the Control System Toolbox. Transfer functions and state-space formats are supported in this block.

We have described some of the subsystem libraries available that contain the basic building blocks of simulation diagrams. The reader is encouraged to explore the other libraries as well. You can also customize and create your own blocks. For information on creating your own blocks, see the MATLAB documentation on "Writing S-Functions".

We are now ready to proceed to the next step, which is the construction of a simulation diagram. To do this, we need to open a new window. Click the **New** button on the Library Browser's toolbar. A new window opens up that will be used to build up an interconnection of Simulink blocks from the subsystem libraries. This is an "untitled" window; we call it the Simulation Window. We consider here analysis of electromechanical servo system described in Review Example 10.4 (Fig. 10.34).

With the "Sources" subnode of Simulink node expanded, move the pointer and click the block labeled "Step"; while keeping the mouse button pressed down, drag the block and place it inside the Simulation Window, and release the mouse button. We will use "Step" for command inputs. Duplicate "Step" for disturbance inputs.

You can duplicate blocks in a model as follows. While holding down the **Ctrl** key, select the block with the mouse button, then drag it to the new location and release the mouse button.

Drag to the Simulation Window the block labeled "Sum" from the "Math Operations" subnode of Simulink node. Make two more copies of the "Sum" block. Now drag the block labeled "Gain" from "Math Operations" subnode. Make three more copies of this block.

With the "Continuous" subnode expanded, click the block labeled "Transfer Fcn", and drag it to the Simulation Window. Duplicate "Transfer Fcn". Also drag to the Simulation Window "Integrator" block from the "Continuous" subnode.

Drag the blocks "To Workspace" and "Scope" from "Sinks" subnode.

We have now completed the process of dragging subsystem blocks from the appropriate libraries and placing them in the Simulation Window. The next step is to interconnect these subsystem blocks and obtain the structure of simulation block diagram. To do this, we just need to work in the Simulation Window.

The first step is to rearrange the blocks in the Simulation Window in a specified structure. This will require moving a block from one place to another within the Simulation Window. This can be done by clicking inside the block, keeping the mouse button pressed, dragging the block to the new desired location and releasing mouse button.

Select "Gain" block in the feedback path. Press (**Ctrl+R**) to rotate it clockwise by 90°. Repeat rotate step to obtain 180° rotation of this "Gain" block.

Lines are drawn to interconnect these blocks as per the desired structure. A line can connect the output port of one block with the input port of another block. A line can also connect the output port of one block with input ports of many blocks by using branch lines.

To connect the output port of one block to the input port of another block, position the pointer on the first block's output port; the pointer shape changes to a crosshair. Press and hold down the mouse button. Drag the pointer to the second block's input port. You can position the pointer on or near the port; the pointer shape changes to a double crosshair. Release the mouse button. Simulink replaces the port symbols by a connecting line with an arrow showing the direction of signal flow.

A *branch line* is a line that starts from an existing line and carries its signal to the input port of a block. Both the existing line and the branch line carry the same signal. To add a branch line, position the pointer on the line where you want the branch line to start. While holding down the **Ctrl** key, press and hold down the mouse button. Drag the pointer to the input port of the target block, then release the mouse button and the **Ctrl** key.

The branch lines are usually an interconnection of line segments. With the **Ctrl** key pressed, identify the branch point and drag the mouse (horizontally/vertically) to an unoccupied area of the diagram and release the mouse button. An arrow appears on the unconnected end of the line. To add another line segment, position the pointer over the end of the segment and draw another segment.

To move a line segment, position the pointer on the segment you want to move. Press and hold down the left mouse button. Drag the pointer to the desired location and release.

To disconnect a block from its connecting lines, hold down the **Shift** key, then drag the block to a new location. You can insert a block in a line by dropping the block on the line.

You can cancel the effects of an operation by choosing **Undo** from the **Edit** menu of the Simulation Window. You can thus undo the operations of adding/deleting a line/block. Effects of **Undo** command may be reversed by choosing **Redo** from the **Edit** menu.

To delete a block/line, select a block/line to be deleted and choose **Clear** or **Cut** from the **Edit** menu. The **Cut** command writes the block/line into the clipboard, which enables you to **Paste** it into a model. **Clear** command does not enable you to paste the block/line later.

All block names in a model must be unique and must contain at least one character. By default, block names appear below blocks. To edit a block name, click on the block name and insert/delete/write text. After you are done, click the pointer somewhere else in the model, the name is accepted or rejected. If you try to change the name of a block to a name that already exists, Simulink displays an error message.

This gives us a generic diagram because we have not yet specified the parameter values of the blocks. Our next priority is to go into each of these blocks and set the parameters that correspond to our specific system. In addition, we need to set some simulation parameters.

We begin with the command input to the feedback system by double-clicking on the block labeled "Command" in the Simulation Window. A dialog box pops up. We set the parameters: Step time 0, Initial value 0, and Final value 1. The parameter values of the "Disturbance" block are all set to 0 initially, i.e, we set the parameters to obtain the response to command inputs only.

Next we set the "Sum" block. In the dialog box for this block we enter Icon shape: round, and list of signs, + –. This gives us an error detector for negative feedback system.

We set the "Amp gain" to 4.1545, "Torque const" to 0.0952, "Gear ratio" to 1/10.5, and "Back emf const" 0.0952. The "Armature" circuit transfer function is set to $1/(0.01s + 3.086)$, and the "Load" when reflected to motor shaft is represented by $1/(0.000041804s + 0.000475)$.

"To Workspace" block requires variable name and the format. We use **Array** format for our data and enter variable name **Response** in the dialog box.

Finally, we need to set the parameters for the simulation run. We move the pointer to the menu labeled "Simulation", and enter Configuration Parameters: start time, stop time, in the dialog box.

At this point in the simulation process, we have generated the appropriate Simulink block diagram (shown in Fig. A.1) and entered the specific parameters for our system and simulation. We are now ready to execute the program, and have the computer perform the simulation. We move the pointer to the "Simulation" menu and choose "Start". Double-click the "Scope" block to view the simulation result (click "autoscale" on toolbar if required).

You may now execute the following program in MATLAB workspace.

```
figure (1);
plot (tout, Response); grid;
hold on
```

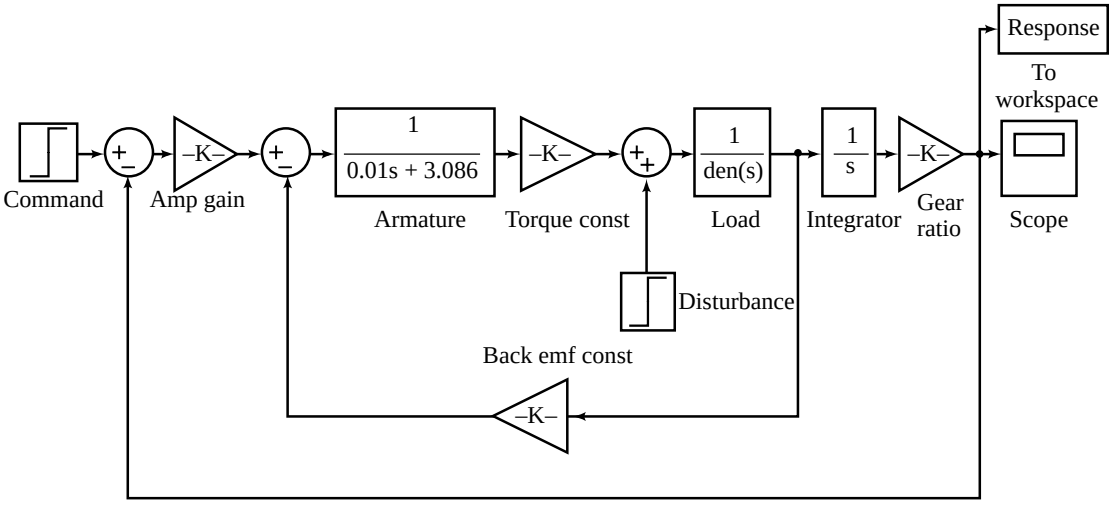

Fig. A.1

We have used an example to show how to enter data and carry out a simulation in the Simulink environment. The reader will agree that this is a very simple process. Download the file **SimulinkFigA1** in MATLAB environment. Double-click each block and study the properties of the block (You may change these properties as per your analysis requirement).

Study/modify simulation parameters, and execute the program.

Problems

Each problem covers an important area of control-system analysis or design. Important MATLAB commands have been included as help to these problems, in the form of scrip files.

Open these files in MATLAB environment. In attempting a problem, the reader can use the MATLAB commands in the script file in an interactive manner, or use the script file as an **M-file**. The description of the MATLAB functions in the Script files can easily be accessed from the **help file** using **help** command.

Simulink files are included as help to some problems. Download the Simulink files from the URL. Open these files in MATLAB environment. Doube-click and study the properties of each block.

Following each problem, one or more what-if's may be posed to examine the effect of variations of the key parameters. Comments to alert the reader to the special features of MATLAB commands are included in the script files to enhance the learning experience. Partial answers to the problems are also included.

A.1 Figure 4.6 shows the model of a heat exchanger control loop. Plot response of the system to unit-step input θ_r, for $K_A = 10$, and for $K_A = 5$.
Comment on the effect of amplifier gain on transient and steady-state accuracy.

A.2 Figure 4.6 shows the model of a heat exchanger control loop. Plot response of the system to unit-step disturbance θ_i, for $K_A = 10$, and for $K_A = 5$.
Comment on the effect of amplifier gain on transient and steady-state accuracy.

A.3 Figure 4.6 shows the model of a heat exchanger control loop. Determine the closed-loop poles of the system. Sketch a pole-zero map and therefrom comment upon stability.

A.4 *Review Example 5.3 revisited.*
A non-unity feedback system has process transfer function

$$G(s) = \frac{K}{s(s+1)}$$

and feedback transfer function

$$H(s) = \frac{1 - Ts}{1 + Ts}$$

What are the combinations of K and T for which the system is stable?

A.5 *The Script PA.4 revisited.*
The MATLAB response to this script shows the stability region for a non-unity feedback system. Take a point in this region and determine the response of the resulting feedback system to a unit-ramp input.

A.6 *Review Example 6.2 revisited.*
A unity-feedback system is characterized by the open-loop transfer function

$$G(s) = \frac{1}{s(0.5s+1)(0.2s+1)}$$

(a) Determine the damping ratio and natural frequency of dominant closed-loop poles.
(b) Determine the error constants K_p, K_v, and K_a.
(c) Determine peak overshoot, time to peak, and settling time of the step response of the feedback system. Are your results different from the ones given in the text? Why?

(Ans: $M_p = 12.1186\%$; $t_p = 3$ sec; $t_s = 4.52$ sec)

A.7 *Examples 6.2 and 6.4 revisited.*
A unity-feedback position control system has open-loop transfer function

$$G(s) = \frac{4500}{s(s+361.2)}$$

Plot step response of the system with a cascade controller $D(s)$ with
(a) $D(s) = 184.1$
(b) $D(s) = 184.1 + 0.324s$
(c) $D(s) = 14.728 + 147.28/s$
Compare the responses for (a) and (b), and those for (a) and (c). Comment upon the effects of derivative and integral control actions.

A.8 *Examples 9.2 and 9.4 revisited.*
A unity-feedback system has open-loop transfer function

$$G(s) = \frac{10}{s(1+0.1s)(1+0.05s)}$$

(a) Determine gain margin, phase margin, gain crossover frequency and phase crossover frequency.
(b) Determine resonance peak, resonance frequency, and bandwidth.
The answers will be slightly different from the ones given in the text. The text answers are based upon Bode plot obtained using asymptotic approximation.

A.9 *Design Example 1 in Section 7.5 revisited.*
A unity-feedback system has open-loop transfer function

$$G(s) = \frac{K}{s(s+1)(s+5)}$$

Relative stability specification calls for a peak overshoot of 14%. Find the value of K to meet this specification and the resulting closed-loop poles. What is the natural frequency of dominant pair of poles?
Using GUI, determine the peak overshoot and settling time of the closed-loop step response.
(Ans: 19%; 9.51 sec)

A.10 *Example 7.8 revisited.*
A unity-feedback system has open-loop transfer function

$$G(s) = \frac{K}{s(s+2)}$$

It is desired that dominant closed-loop poles provide damping ratio $\zeta = 0.5$ and have an undamped natural frequency $\omega_n = 4$ rad/sec. Velocity error constant K_v is required to be greater than 4.
(a) Verify that only gain adjustment can't meet these objectives.
(b) Design a lead compensator to meet the objectives.
(c) Using GUI, determine the peak overshoot and settling time of the lead-compensated system
(Ans: $M_p = 21\%$; $t_s = 0.02$ sec)
(d) Design a lag compensator to meet the objectives (Refer Example 7.10).

A.11 *Example 10.3 revisited.*
A unity-feedback system has open-loop transfer function

$$G(s) = \frac{K}{s(s+1)}$$

It is desired to have the velocity error constant $K_v = 10$. Furthermore, we desire that the phase margin of the system be atleast 45°. Design a phase-lag compensator to achieve these specifications.
Are your results different from the ones given in the text? Why?
Using GUI, determine the peak overshoot and settling time of the lag-compensated system.
(Ans: $M_p = 28\%$; $t_s = 14$ sec)

A.12 *Example 10.1 revisited.*
Repeat Problem A.11 under the constraint that we use phase-lead compensation to achieve the performance specifications. (Ans: $M_p = 29\%$; $t_s = 1.77$ sec)

A.13 *Example 8.16 revisited.*
A unity-feedback system has open-loop transfer function

$$G(s) = \frac{e^{-s\tau_D}}{s(s+1)(s+2)}$$

Determine gain crossover frequency, phase crossover frequency, phase margin and gain margin when (i) $\tau_D = 0$ (ii) $\tau_D = 1$.

A.14 *Example 11.2 revisited.*
For a unity-feedback system with plant transfer function $G(s) = 1/s^2$, show that the cascade compensator $D(s) = 0.81\,(s + 0.2)/(s + 2)$ meets the specifications: $\zeta = 0.7$, $\omega_n = 0.3$. Plot step response of the compensated system. Now discretize the compensator (sampling time $T = 1$ sec) and plot step response of the discretized system with digital compensator. Comment upon the discrepancy with respect to performance achieved using analog design.

A.15 *Example 12.9 revisited*
Show that the Inverted Pendulum described in this example is unstable. Also show that state-feedback

$$u(t) = -\mathbf{k}\,\mathbf{x}(t)$$

$$\mathbf{k} = [-15.4785 \quad -2.9547 \quad -0.0705 \quad -0.2820]$$

stabilizes this system.
For initial conditions

$$\mathbf{x}(0) = [0.1 \quad 0 \quad 0 \quad 0]^T$$

and zero external input, simulate the feedback system.

A.16 *Review Example 10.4 revisited*
In the electromechanical servo system of Fig. 10.34, the compensator

$$D(s) = 17.05(s + 5)/(s + 0.2)$$

(a) Simulate the system for step commands, ramp commands, and step disturbances.
(b) Set the parameters of "Command" and "Disturbance" blocks to 0. Insert a "Step" source at the error point e (refer Fig. 10.34). Connect "To Workspace" block to the output of "Armature" block and study the variation of armature current when error step inputs are given. Determine the range of error for which the armature current does not exceed 5A. For this range of error, determine the range of the amplifier output voltage e_a (Fig. 10.34).

A.17 *Review Example 10.4 revisited*
In the electromechanical servo system of Fig. 10.34, the compensator

$$D(s) = 17.05(s + 5)/(s + 0.2)$$

(a) Simulate the system for step commands of value higher than 0.29 rad.
(b) Insert the saturation nonlinearity block at the output of the "Amp gain" block. Set the parameters of the saturation nonlinearity as per Fig. 10.36. Simulate this system for step comands of values greater than 0.29 rad.
(c) Compare the responses in (a) and (b) for the same value of step command.

Appendix

B

Control Theory Quiz

A set of questions with multiple answer choices is given here. These questions have been designed to capture important aspects of Control Theory covered in the book. For each of these questions, identify the best of the given answer choices. Compare your answers with the master key given at the end of the session. This quiz should serve the purpose of a self-appraisal test for the reader.

1. A linear time-invariant system initially at rest, when subjected to a unit-step input, gives a response $y(t) = te^{-t}$; $t > 0$. The transfer function of the system is

   (A) $\dfrac{1}{(s+1)^2}$ (B) $\dfrac{1}{s(s+1)^2}$ (C) $\dfrac{s}{(s+1)^2}$ (D) $\dfrac{1}{s(s+1)}$

2. The system shown in Fig. Q2 is of
   (A) zero order (B) first order
   (C) second order (D) third order

3. The impulse response of an initially relaxed linear system is $e^{-2t}\mu(t)$ where $\mu(t)$ is a unit step function. To produce a response of $te^{-2t}\mu(t)$, the input must be equal to

   (A) $2e^{-2t}\mu(t)$ (B) $\dfrac{1}{2}e^{-2t}\mu(t)$

   (c) $e^{-2t}\mu(t)$ (D) $e^{-t}\mu(t)$

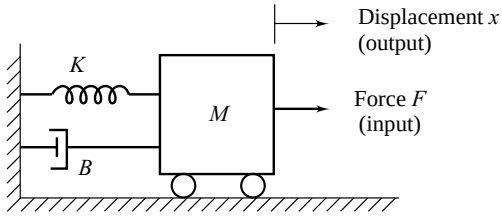

Fig. Q2

4. The step response of a system with transfer function $G(s) = 1/(\tau s + 1)$ attains more than 98% of its final value in time t equal to
   (A) τ (B) 2τ (C) 3τ (D) 4τ

5. The response of the system of Fig. Q5a to an input $r(t) = 8\mu(t)$ is shown in Fig. Q5b. The time-constant τ is equal to
   (A) 0.535 msec (B) 0.32 msec (C) 0.09 msec (D) 11.25 msec

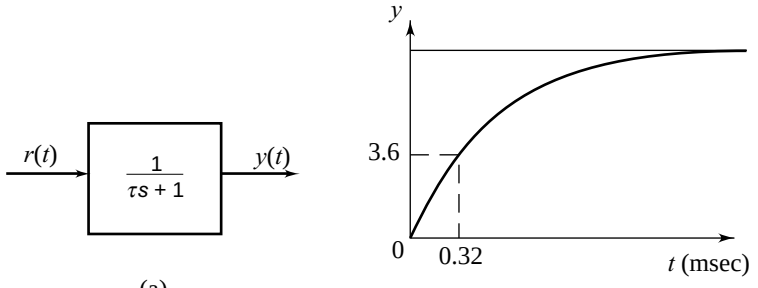

Fig. Q5

6. Closed-loop transfer function of a unity-feedback system is given by $Y(s)/R(s) = 1/(\tau s + 1)$. Steady-state error to unit-ramp input is
   (A) ∞ (B) τ (C) 1 (D) $1/\tau$
7. The series RLC circuit shown in Fig. Q7 is underdamped if
   (A) $\left(\frac{R}{2L}\right)^2 < \frac{1}{LC}$
   (B) $\left(\frac{R}{2L}\right)^2 = \frac{1}{LC}$
   (C) $\left(\frac{R}{2L}\right)^2 > \frac{1}{LC}$
   (D) None of the answers in (A), (B), and (C) is correct

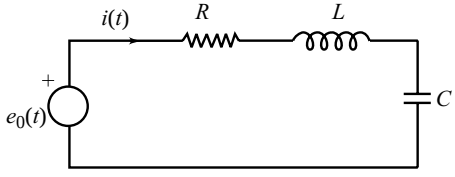

Fig. Q7

8. Closed-loop transfer function of a unity-feedback system is given by $\frac{Y(s)}{R(s)} = \frac{\omega_n^2}{s^2 + 2\zeta\omega_n s + \omega_n^2}$.
   Steady-state error to unit-ramp input is
   (A) ∞ (B) $2\zeta/\omega_n$
   (C) 1 (D) $4/\zeta\omega_n$
9. When two networks shown in Fig. Q9 are cascaded in tandem, the overall transfer function $E_4(s)/E_1(s)$ is
   (A) $H_1(s)\,H_2(s)$ (B) $H_1(s) + H_2(s)$
   (C) $H_1(s)/H_2(s)$ (D) None of the answers in (A), (B), and (C) is correct

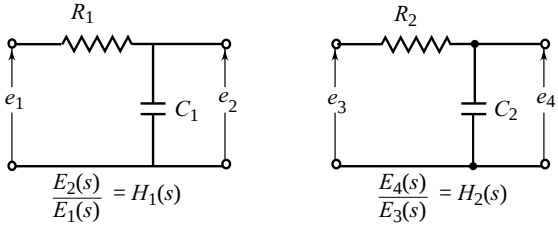

Fig. Q9

10. Dead-time model $e^{-s\tau_D}$ may be approximated by the transfer function
    (A) $\frac{1 - \frac{\tau_D}{2}s}{1 + \frac{\tau_D}{2}s}$ (B) $\frac{1 + \frac{\tau_D}{2}s}{1 - \frac{\tau_D}{2}s}$ (C) $\frac{1 - \tau_D s}{1 + \tau_D s}$ (D) $\frac{1 + \tau_D s}{1 - \tau_D s}$
11. If a system has two real and equal characteristic roots, it is described as
    (A) having no damping (B) being underdamped (C) being critically damped (D) being overdamped
12. If the roots of a characteristic equation are given by $s_{1,2} = -3 \pm j2$, the values of damping ζ and damped natural frequency ω_d are

(A) $\left(\frac{3}{\sqrt{13}}, \sqrt{13}\right)$ (B) $\left(\frac{1}{\sqrt{13}}, 2\right)$ (C) $\left(\frac{1}{\sqrt{13}}, \sqrt{13}\right)$ (D) $\left(\frac{3}{\sqrt{13}}, 2\right)$

13. A liquid-level system comprises two noninteracting tanks which can be represented by two first-order transfer functions in cascade having time constants $\tau_1 = 100$ sec and $\tau_2 = 300$ sec. The inflow $q(t)$ is the input and the level of the second tank is the output. The response of the output height to a step change in flow will be

(A) having no damping (B) underdamped (C) critically damped (D) overdamped

14. An open-loop control system requires an operator to set a motorized valve setting c where $0 < c < 1$, so that two fluids are mixed together. One stream has a constant flow of 10 m^3/hr and the outflowing stream should be 14 m^3/hr. The configuration is shown in Fig. Q14, where motorized valve dynamics are given. The value of valve setting to achieve the desired steady-state outflow is

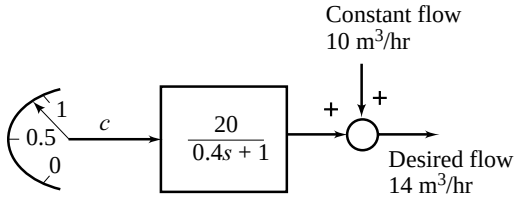

Fig. Q14

(A) 0.2 (B) 0.4

(C) 0.5 (D) 0.7

15. A linear approximation at the operating point ($x^* = 0.5$, $u^* = 1.5$) to $y(x, u) = 2x^2 + xu + u^2$, is

(A) $\delta y = 3.5\ \delta x + 3.5\ \delta u$ (B) $\delta y = 4\ \delta x + 2\ \delta u$

(C) $\delta y = 2\ \delta x + 3\ \delta u$ (D) $\delta y = 4.75\ \delta x + 3.75\ \delta u$

16. In a level control system, the fluid flow is related to the inflow rate by the following transfer function:

$$G(s) = \frac{\text{level } H(s)}{\text{inflow } Q(s)} = \frac{0.75}{2500s + 1}$$

Initially the tank is empty. The inflow control valve is suddenly opened to allow a flow rate of 0.5 m^3/sec into the tank. The level after 2500 sec is

(A) 0.474 m (B) 0.375 m (C) 0.75 m (D) 0.237 m

17. The system of Fig. Q17 is underdamped of

(A) $\frac{K}{M} > \left(\frac{B}{2M}\right)^2$

(B) $\frac{K}{M} = \left(\frac{B}{2M}\right)^2$

(C) $\frac{K}{M} < \left(\frac{B}{2M}\right)^2$

(D) None of the answers in (A), (B) and (C) is correct

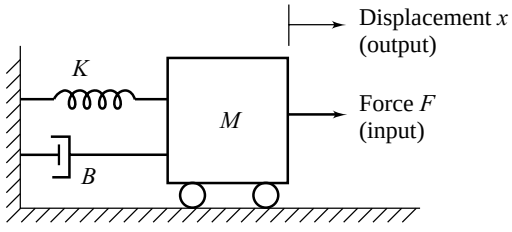

Fig. Q17

18. The damping ratio of the system of Fig. Q18 is

(A) $\frac{1}{2}\frac{1}{\sqrt{BM}}$

(B) $\frac{1}{2}\sqrt{\frac{M}{B}}$

(C) $\frac{1}{2}\sqrt{\frac{B}{M}}$

(D) None of the answers in (A), (B), and(C) is correct.

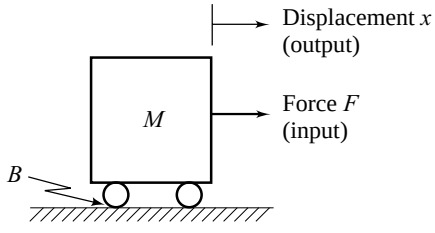

Fig. Q18

19. For a second-order system with damping $\zeta > 1$, the roots of the characteristic equation are
    (A) real but not equal (B) real and equal
    (C) complex conjugate (D) imaginary
20. The plot in Fig. Q20 shows the unit step response of a first-order system. Transfer function of the system is

    (A) $\frac{1}{5s+1}$ (B) $\frac{2}{15s+1}$

    (C) $\frac{2}{3s+1}$ (D) $\frac{1}{15s+1}$

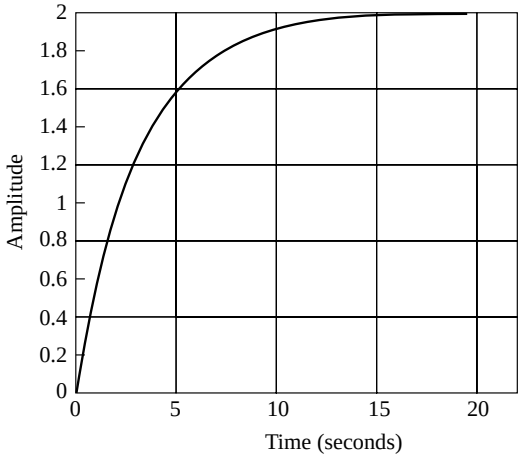

Fig. Q20

21. Three different systems have the following poles: $p_1 = -0.2$, $p_2 = -0.4$, $p_3 = -0.6$. What is the time-constant of the fastest step response?
    (A) 0.2 (B) 0.6
    (C) 1/0.2 (D) 1/0.6
22. Consider the following statements:
    (i) The test signals step, ramp and parabola are not useful for control-system analysis if actual inputs are not step, ramp, and parabola, respectively.
    (ii) Transient and steady-state performance of control systems is adequately given by the response to only one test signal, say step.
    (A) None of the above statements is true (B) Statement (i) is true but statement (ii) is false
    (C) Statement (i) is false but statement (ii) is true (D) Both the statements are true
23. Consider the op amp circuit shown in Fig. Q23. It can be used as
    (A) a lead compensator only (B) a lag compensator only
    (C) either a lead or a lag compensator (D) neither a lead nor a lag compensator

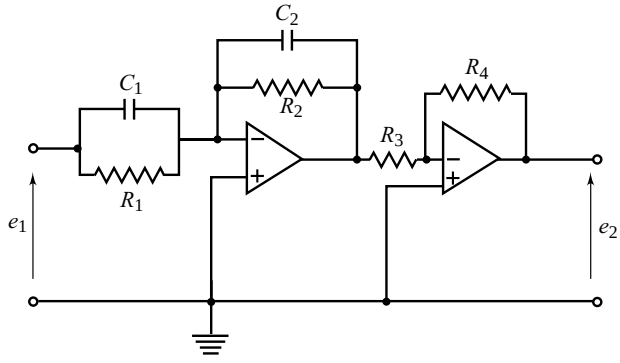

Fig. Q23

24. Consider the block diagram shown in Fig. Q24. The transfer function between $Y(s)$ and $W(s)$ is

    (A) $\frac{D(s)G(s)N(s)}{1+D(s)G(s)H(s)}$ (B) $\frac{N(s)}{1+D(s)G(s)H(s)}$

    (C) $\frac{N(s)}{1-D(s)G(s)H(s)}$ (D) None of the answers in (A), (B), and (C) is correct

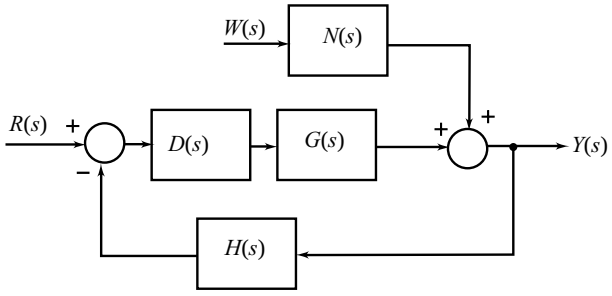

Fig. Q24

25. The gear train shown in Fig. Q25
    (A) reduces the speed and the torque
    (B) increases the speed and the torque
    (C) reduces the speed and increases the torque
    (D) increases the speed and reduces the torque

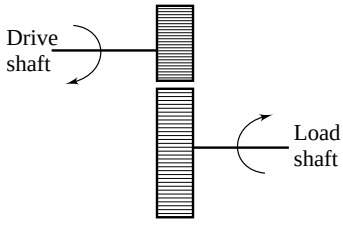

Fig. Q25

26. Effect of back emf in an armature-controlled dc servomotor is
    (A) to increase effective motor friction, thereby reducing motor time-constant
    (B) to increase effective motor friction, thereby increasing motor time-constant
    (C) to increase motor inertia, thereby increasing motor time-constant
    (D) to increase motor inertia, thereby reducing motor time-constant
27. Electrical time-constant of an armature-controlled dc servomotor is
    (A) equal to mechanical time-constant
    (B) smaller than mechanical time-constant
    (C) larger than mechanical time-constant
    (D) None of the answers in (A), (B), and (C) is correct
28. Ratio of the rotor reactance X to the rotor resistance R for a two-phase servomotor
    (A) is equal to that of a normal induction motor
    (B) is less than that of a normal induction motor
    (C) is greater than that of a normal induction motor
    (D) may be less or greater than that of a normal induction motor
29. A rotating load is connected to a field-controlled dc motor with negligible field inductance. A test results in output steady-state speed (ω) of 2 rad/sec when an input voltage (e_f) of 100 V is applied to the motor terminals. Also the test shows that output speed reaches 0.632×2 rad/sec within 0.75 sec. The transfer function $\omega(s)/E_f(s)$ of the motor is

    (A) $\dfrac{0.02}{(0.375s+1)}$ (B) $\dfrac{0.02}{0.75s+1}$ (C) $\dfrac{50}{0.75s+1}$ (D) $\dfrac{50}{(0.375s+1)}$

30. The transfer function from $R(s)$ to $Y(s)$ of the system of Fig. Q30 is

    (A) $\dfrac{s(\tau s+1)}{\tau s^2+(1+KK_2)s+KK_1}$ (B) $\dfrac{K_1 s(\tau s+1)}{\tau s^2+(1+KK_2)s+KK_1}$

    (C) $\dfrac{KK_1}{\tau s^2+(1+KK_2)s+KK_1}$ (D) $\dfrac{s(\tau s+1+KK_2)}{\tau s^2+(1+KK_2)s+KK_1}$

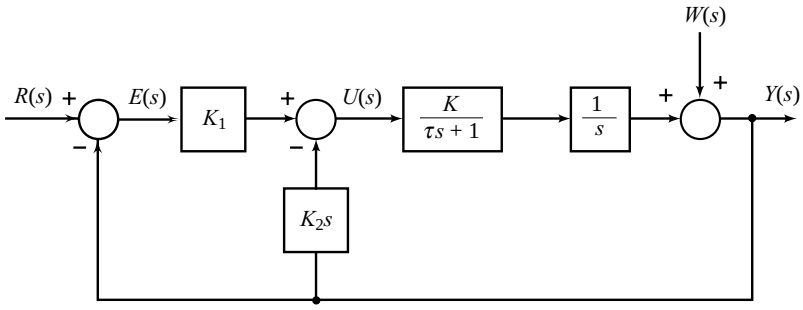

Fig. Q30

31. The transfer function from $W(s)$ to $Y(s)$ of the system of Fig. Q30 is

(A) 1

(B) $\dfrac{s(\tau s+1)}{\tau s^2+(1+KK_2)s+KK_1}$

(C) $\dfrac{KK_1}{\tau s^2+(1+KK_2)s+KK_1}$

(D) None of the answers in (A), (B), and (C) is correct

32. The transfer function between $R(s)$ and $E(s)$ of the system of Fig. Q30 is

(A) $\dfrac{s(\tau s+1+KK_2)}{\tau s^2+(1+KK_2)s+KK_1}$

(B) $\dfrac{s(\tau s+1)}{\tau s^2+(1+KK_2)s+KK_1}$

(C) $\dfrac{KK_1}{\tau s^2+(1+KK_2)s+KK_1}$

(D) $\dfrac{K_1s(\tau s+1)}{\tau s^2+(1+KK_2)s+KK_1}$

33. The transfer function between $R(s)$ and $U(s)$ of the system of Fig. Q30 is

(A) $\dfrac{s(\tau s+1)}{\tau s^2+(1+KK_2)s+KK_1}$

(B) $\dfrac{s(\tau s+1+KK_2)}{\tau s^2+(1+KK_2)s+KK_1}$

(C) $\dfrac{KK_1}{\tau s^2+(1+KK_2)s+KK_1}$

(D) $\dfrac{K_1s(\tau s+1)}{\tau s^2+(1+KK_2)s+KK_1}$

34. Consider the following statements:
   (i) Synchro is a three phase machine.
   (ii) Rotor of synchro transmiter is of dumb bell type while that of control transformer is cylindrical.
   (A) None of the above statements is true
   (B) Statement (i) is true but statement (ii) is false
   (C) Statement (i) is false but statement (ii) is true
   (D) Both the statements are true

35. Consider the following statements:
   (i) AC devices (servomotor, synchro) are normally operated at higher frequencies (400 Hz, for example) and not at 50 Hz.
   (ii) The output of a synchro is demodulated before feeding it to a dc motor for actuation of inertial load.
   (A) None of the above statements is true
   (B) Statement (i) is true but statement (ii) is false
   (C) Statement (i) is false but statement (ii) is true
   (D) Both the statements are true

36. A position control system has a two-loop configuration. The minor loop is a velocity-feedback loop realized through tachogenerator. Consider the following statements:
    (i) The tacho is usually mounted on motor shaft rather than the load shaft.
    (ii) The minor loop is a positive-feedback loop.
    (A) None of the above statements is true
    (B) Statement (i) is true but statement (ii) is false
    (C) Statment (i) is false but statement (ii) is true
    (D) Both the statements are true

37. Feedback control systems are
    (A) insensitive to both forward- and feedback-path parameter changes
    (B) less sensitive to feedback-path parameter changes than to forward-path parameter charges
    (C) less sensitive to forward-path parameter changes than to feedback-path parameter changes
    (D) equally sensitive to forward- and feedback-path parameter charges

38. In the system of Fig. Q38, sensitivity of $M(s) = Y(s)/R(s)$ with respect to parameter K_1 is

    (A) $\dfrac{1}{1+K_1K_2}$

    (B) $\dfrac{1}{1+K_1G(s)}$

    (C) 1

    (D) None of the answers in (A), (B), and (C) is correct

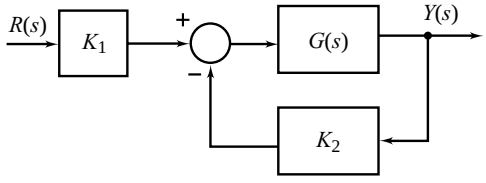

Fig. Q38

39. In the system of Fig. Q38, sensitivity of $M(s) = Y(s)/R(s)$ with respect to parameter K_2 is

    (A) $\dfrac{1}{1+K_2K_1}$

    (B) $\dfrac{1}{1+K_2G(s)}$

    (C) $\dfrac{-K_2G(s)}{1+K_2G(s)}$

    (D) None of the answers in (A), (B), and (C) is correct.

40. A speed control system is represented by the signal flow graph shown in Fig. Q40. The nominal value of the parameter K is 10. Sensitivity of $M(s) = \omega(s)/\omega_r(s)$ to changes in K is

    (A) $\dfrac{s+0.1}{s+11}$

    (B) $\dfrac{s+0.1}{s+0.2}$

    (C) $\dfrac{-0.1}{s+0.2}$

    (D) None of the answers in (A), (B), and (C) is correct.

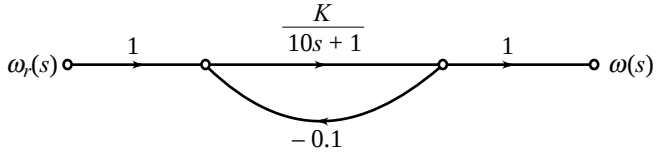

Fig. Q40

41. A speed control system is represented by the block diagram of Fig. Q41. The system is subjected to a step disturbance $W(s)$. $\omega_{ss}^{CL}/\omega_{ss}^{OL}$ (the steady-state speed under closed-loop operation/steady-state speed under open-loop operation) is equal to

(A) 1/2
(B) 1
(C) 2
(D) None of the answers in (A), (B), and (C) is correct

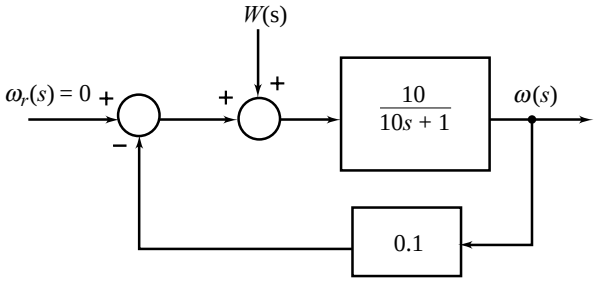

Fig. Q41

42. The time response of the system of Fig. Q42a to an input $r(t) = 10\,\mu(t)$ is shown in Fig. Q42b. The gain K is equal to
(A) 10
(B) 8
(C) 4
(D) None of the answers in (A), (B), and (C) is correct

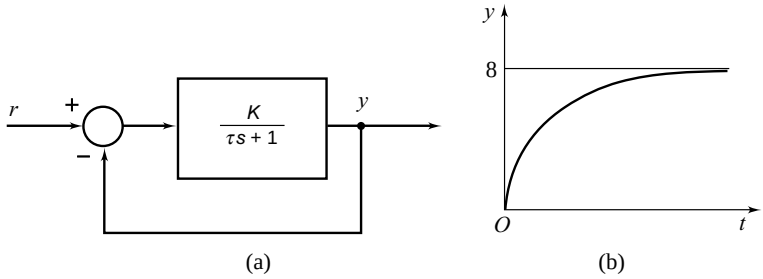

(a) (b)

Fig. Q42

43. An inertial and a frictional load are driven by a dc motor with torque T_M. The dynamic model of the system is

$$T_M(t) = J\frac{d\omega(t)}{dt} + B\omega(t)$$

The steady-state speed of the motor for step input will be doubled when
(A) inertia J is doubled
(B) friction B is doubled
(C) both the inertia J and friction B are doubled
(D) None of the answers in (A), (B), and (C) is correct

44. Consider the following statements:
(i) If an open-loop system is unstable, applying feedback will always improve its stability.
(ii) If an open-loop system is subject to parameter variations, applying feedback will always improve robustness.
Which of the following is the correct answer?
(A) None of the above statements is true
(B) Statement (i) is true but statement (ii) is false
(C) Statement (i) is false but statement (ii) is true
(D) Both the statements are true

45. The characteristic equation of the closed-loop system of Fig. Q45 is
(A) $s^2 + 11s + 10 = 0$
(B) $s^2 + 11s + 130 = 0$
(C) $s^2 + 10s + 120 = 0$
(D) $s^2 + 10s + 12 = 0$

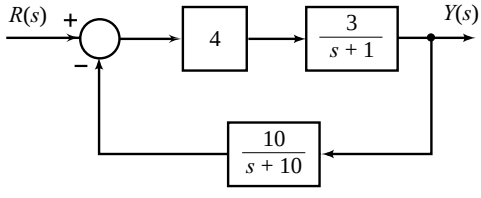

Fig. Q45

46. Which of the following describes the step response of the closed-loop system of Fig. Q46?
    (A) Underdamped
    (B) Critically damped
    (C) Overdamped
    (D) The output does not reach a steady-state value.

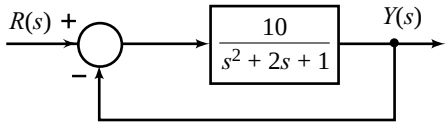

Fig. Q46

47. The system of Fig. Q47 has the steady-state error
    (A) $\frac{1}{1.125}$ (B) $\frac{0.1}{1.125}$
    (C) $\frac{1.1}{1.125}$ (D) None of the answers in (A), (B), and (C) is correct

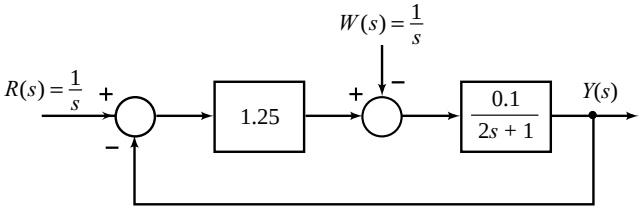

Fig. Q47

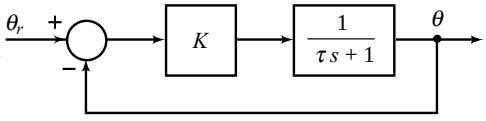

Fig. Q48

48. It is desired that the output θ changes by unit step with zero error at steady state (Fig. Q48). We can achieve it by injecting
    (A) θ_r = unit step (B) θ_r of step size $(1+K)/K$
    (C) θ_r of step size $K/(K+1)$ (D) None of the answers in (A), (B), and (C) is correct
49. Consider the system of Fig. Q49. The steady-state error is zero for
    (A) $K_f = 0$ (B) $K_f = \frac{1}{1.25}$
    (C) $K_f = 1.25$ (D) None of the answers in (A), (B), and (C) is correct

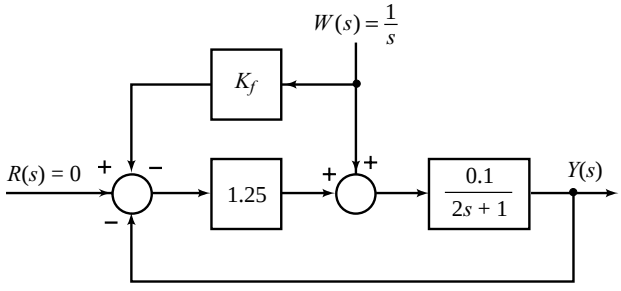

Fig. Q49

50. Sensitivity S_G^M of the closed-loop transfer function $M(s)$ with respect to open-loop transfer function $G(s)$ (Fig. Q50) is
    (A) $\frac{1}{2s^2+(3K_P+1)s+3K_I}$ (B) $\frac{s(2s+1)}{2s^2+(K_P+1)s+3K_I}$
    (C) $\frac{s(2s+1)}{2s^2+(K_P+1)s+K_I}$ (D) $\frac{s(2s+1)}{2s^2+(3K_P+1)s+3K_I}$

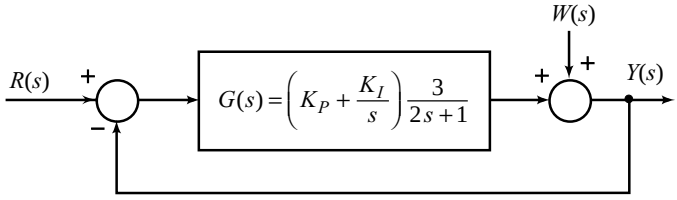

Fig. Q50

51. For what value of K is the time-constant of the system of Fig. Q51 equal to 0.2 seconds?
    (A) $K = 3$ (B) $K = 5$
    (C) $K = 7$ (D) $K = 9$
52. Consider the system of Fig. Q52. The K_P to move the time-constant to one sixth of its open-loop value is
    (A) $\frac{0.333}{2}$ (B) $\frac{0.333}{6}$
    (C) $\frac{6}{0.333}$ (D) $\frac{2}{0.333}$

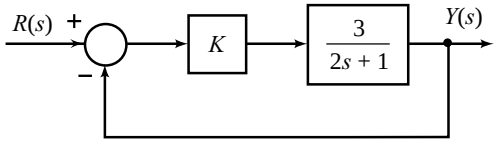

Fig. Q51

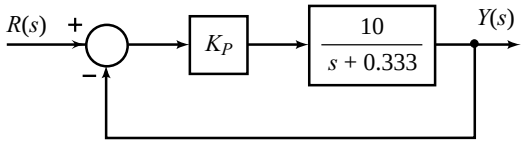

Fig. Q52

53. Consider the system of Fig. Q53. The steady-state offset is zero when K_P is
    (A) zero (B) infinity
    (C) any value of K_P (D) no value of K_P

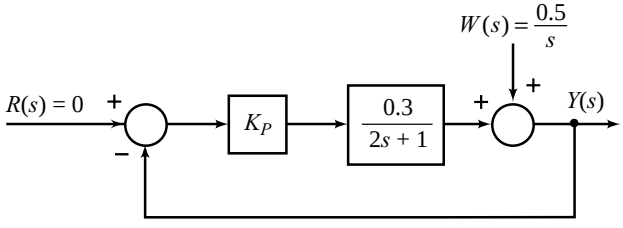

Fig. Q53

54. A proportional controller, K_P, is used with a first-order system $G(s) = K/(\tau s + 1)$ in unity-feedback structure. Increasing K_P will
    (A) increase the time-constant and decrease the steady-state error to step inputs
    (B) decrease the time-constant and decrease the steady-state error to step inputs
    (C) decrease the time-constant and increase the steady-state error to step inputs
    (D) increase the time-constant and increase the steady-state error to step inputs
55. Consider the system of Fig. Q55. K_I that gives critical damping is
    (A) 0.417
    (b) 0.257
    (C) 1
    (D) None of the answers in (A), (B), and (C) is correct

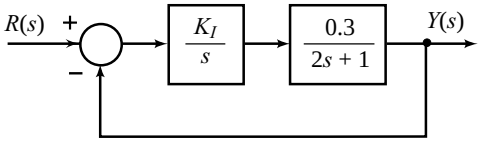

Fig. Q55

56. Consider the system of Fig. Q56. The steady-state offset is zero for
(A) $K_I = 0$ (B) $K_I = \infty$
(C) any value of K_I (D) no value of K_I

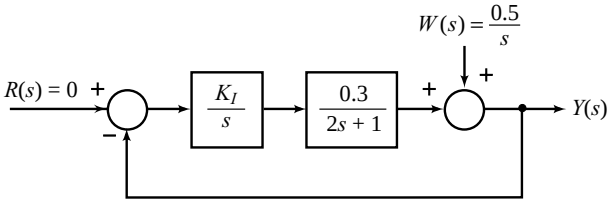

Fig. Q56

57. An integral controller K_I/s is used with a first-order system $G(s) = K/(\tau s + 1)$ in unity-feedback structure. Increasing K_I will
(A) decrease damping with no change in steady-state offset to step commands.
(B) decrease damping with decrease in steady-state offset to step commands.
(C) increase damping with no change in steady-state offset to step commands.
(D) increase damping with decrease in steady-state offset to step commands.

58. The condition that all the roots of the polynomial

$$\Delta(s) = a_0 s^3 + a_1 s^2 + a_2 s + a_3;\ a_i > 0$$

have negative real parts, is given by
(A) $a_1 a_3 > a_0 a_2$ (B) $a_1 a_0 > a_2 a_3$ (C) $a_1 a_2 > a_0 a_3$ (D) $a_2 a_0 > a_1 a_3$

59. Consider the following statements:
(i) All the roots of the polynomial

$$\Delta_1(s) = 3s^4 + 10s^3 + 5s^2 + 2$$

have negative real parts.
(ii) All the roots of the polynomial

$$\Delta_2(s) = s^4 + 4s^3 + 6s^2 + 4s - 5$$

have negative real parts.
Which of the following is the correct answer?
(A) None of the above statements is true
(B) Statement (i) is true but statement (ii) is false
(C) Statement (i) is false but statement (ii) is true
(D) Both the statements are true

60. The characteristic equation of a feedback control system is given by

$$2s^4 + s^3 + 2s^2 + 5s + 10 = 0$$

The number of roots in the right half of s-plane are
(A) zero (B) 1 (C) 2 (D) 3

61. The polynomial

$$\Delta(s) = s^3 + 3s^2 + 2s + 6$$

has
(A) two roots in left half s-plane and one root in right half
(B) two roots in right half s-plane and one root in left half
(C) two roots on $j\omega$-axis of s-plane and one root in right half
(D) two roots on $j\omega$-axis of s-plane and one root in left half.

62. The characteristic equation of a feedback control system is

$$s^3 + \alpha_1 s^2 + \alpha_2 s + K\alpha_2 = 0;\ \alpha_1,\ \alpha_2,\ > 0,$$

where K is a variable positive scalar parameter. The system is stable for all values of K given by

(A) $K > \alpha_2$ (B) $K < \alpha_2$ (C) $K > \alpha_1$ (D) $K < \alpha_1$

63. The open-loop transfer function of a unity feedback system is

$$G(s) = K/[s^2(s + 5)]; \quad K > 0$$

The system is unstable for

(A) $K > 5$ (B) $K < 5$

(C) $K > 0$ (D) All the answers in (A), (B), and (C) are correct

64. A unity feedback system has open-loop transfer function

$$G(s) = K/[s(s + 1)(s + 2)]; \quad K > 0$$

The value of K that results in oscillatory response to step input, is

(A) 2 (B) 6 (C) 20 (D) 60

65. The first two rows of Routh tabulation of a third-order system are

s^3	2	2
s^2	4	4

(A) The characteristic equation has one root in right half s-plane

(B) The characteristic equation has two roots on the $j\omega$-axis at $s = \pm j$

(C) The characteristic equation has two roots on the $j\omega$-axis at $s = \pm 2j$

(D) None of the answers in (A), (B), and (C) is correct

66. Presence of transportion lag in the forward path of a closed-loop control system

(A) decreases margin of stability (B) increases margin of stability

(C) does not affect its margin of stability

67. Consider a unity-feedback system with plant $G(s) = \dfrac{1}{s^2 + s + 1}$ and cascade controller $D(s) = K_P + \dfrac{2}{s}$. The values of K_P for which the system is stable are

(A) $K_P > 0$ (B) unstable for all $K_P > 0$ (C) $K_P > 1$ (D) $K_P > 2$

68. The error function of a feedback system is

$$E(s) = \frac{(s + 0.1)(s + 0.5)}{s(s + 0.1)(s + 0.5) + 0.5(s + 1)}$$

The steady-state value of $e(t)$ is

(A) 0.001 (B) 0.1 (C) 0.01

(D) None of the answers in (A), (B), and (C) is correct

69. Consider the system of Fig. Q69. The steady-state error is less than 2% for step input for

(A) $K_c > 49$ (B) any value of K_c (C) no value of K_c (D) $K_c > 50$

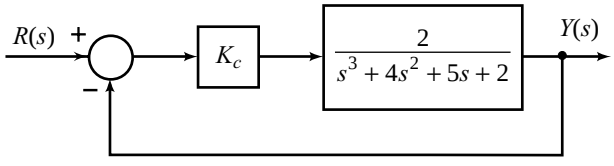

Fig. Q69

70. A unity feedback system has open-loop transfer function $G(s) = 9/[s(s + 3)]$. The system has

(A) damping ratio = 1/2, and natural frequency = 9 (B) damping ratio = 1/6, and natural frequency = 3

(C) damping ratio = 1/6, and natural frequency = 9 (D) damping ratio = 1/2, and natural frequency = 3

71. A unity feedback system has open-loop transfer function $G(s) = 25/[s(s + 6)]$. The time t_p at which the peak of the step-input response occurs, is

(A) 11/7 sec (B) 11/4 sec (C) 11/14 sec (D) 11/28 sec

72. Peak overshoot of step-input response of an underdamped second-order system is explicitly indicative of
(A) settling time (B) rise time (C) natural frequency (D) damping ratio

73. A unity feedback system has open-loop transfer function $G(s) = 25/[s(s + 6)]$. The peak overshoot in the step-input response of the system is approximately equal to
(A) 5% (B) 10% (C) 15% (D) 20%

74. The step-input response of the system of Fig. Q74a is shown in Fig. Q74b. The value of damping ratio of the system is
(A) 0.39 (B) 0.49 (C) 0.59 (D) 0.69

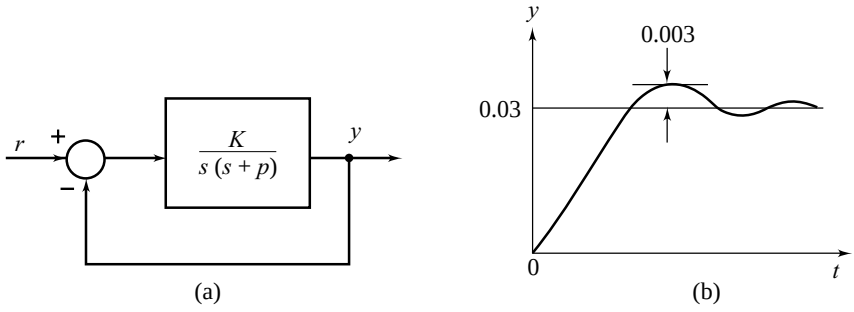

Fig. Q74

75. A unity feedback system with open-loop transfer function $G(s) = 4/[s(s + p)]$ is critically damped. The value of the parameter p is
(A) 4 (B) 3 (C) 2 (D) 1

76. A unity feedback system has open-loop transfer function $G(s)$. The steady-state error is zero for
(A) step input and type-1 $G(s)$ (B) ramp input and type-1 $G(s)$
(C) step input and type-0 $G(s)$ (D) ramp input and type-0 $G(s)$

77. A unity feedback system with forward path transfer function $G(s) = 1/[s^2(s + 1)]$ is subjected to an input $r(t) = K_1 + K_2 t + \frac{1}{2} t^2$. The steady-state error of the system is
(A) infinity (B) 1
(C) zero (D) None of the answers in (A), (B), and (C) is correct

78. Closed-loop transfer function of a unity feedback system is given by

$$\frac{Y(s)}{R(s)} = \frac{1}{\tau s + 1}$$

System K_v is
(A) τ (B) $1/\tau$ (C) 1 (D) ∞

79. Closed-loop transfer function of a unity feedback system is given by

$$\frac{Y(s)}{R(s)} = \frac{\omega_n^2}{s^2 + 2\zeta\omega_n s + \omega_n^2}$$

System K_v is
(A) $\omega_n/2\zeta$ (B) 1 (C) ∞ (D) $2\zeta/\omega_n$

80. Consider the position control system of Fig. Q80. The value of K such that the steady-error is 10° for input $\theta_r = 400t\ \mu(t)$ rad/sec, is
(A) 104.5
(B) 114.5
(C) 124.5
(D) None of the answers in (A), (B), and (C) is correct

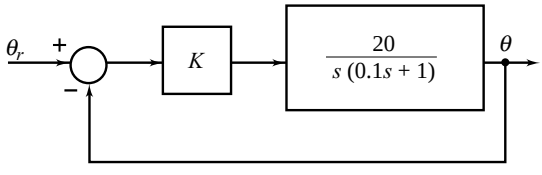

Fig. Q80

81. Consider the speed control system shown in Fig. Q81. Parameter variations occurring during operating conditions cause K_A to modify to $K'_A = 0.9K_A$. The value of K_A that limits the change in steady-state motor speed due to parameter variations to 0.1%, is
(A) 25 (B) 35 (C) 45 (D) 55

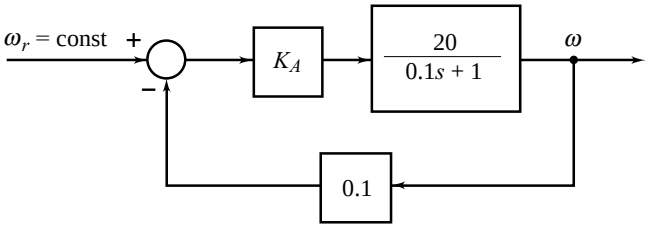

Fig. Q81

82. Derivative error compensation is employed in feedback control systems to
(A) increase the effective damping in the system
(B) decrease the effective damping in the system
(C) improve the steady-state response of the system

83. Tachogenerator feedback is sometimes used in position control systems to
(A) increase the effective damping in the system
(B) decrease the effective damping in the system
(C) improve the steady-state response of the system

84. Integral error compensation is employed in feedback control systems to
(A) improve damping
(B) improve speed of response
(C) reduce steady-state error

85. A temperature control system is found to have zero error to a constant tracking input, and an error of 0.5°C to a tracking input that is linear in time, rising at the rate of 40°C/sec. What is the type number of the system?
(A) 0 (B) 1
(C) 2 (D) Type number cannot be determined from the given information

86. Poles of second-order models with the same damping ratio lie
(A) on the real axis (B) on a radial line from the origin
(C) on the imaginary axis (D) None of the answers in (A), (B), and(C) is correct

87. The percentage overshoot of a second-order system $G(s) = \dfrac{K\omega_n^2}{s^2 + 2\zeta\omega_n s + \omega_n^2}$ to a step input depends only on
(A) the value of the step input (B) the value of the damping ratio
(C) the value of the gain K (D) the parameter ω_n

88. Consider the system of Fig. Q88. Increasing proportional gain will
(A) increase the overshoot and decrease the steady-state error to ramp inputs
(B) decrease the overshoot and increase the steady-state error to ramp inputs
(C) increase the overshoot and increase the steady-state error to ramp inputs
(D) decrease the overshoot and decrease the steady-state error to ramp inputs

89. Consider the system of Fig. Q89. The steady-state offset is zero when
(A) $K_P = \infty$, $K_D = \infty$
(B) $K_P = 0$, K_D = any value
(C) $K_P = \infty$, K_D = any value
(D) no values of K_P and K_D

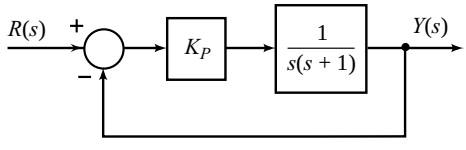

Fig. Q88

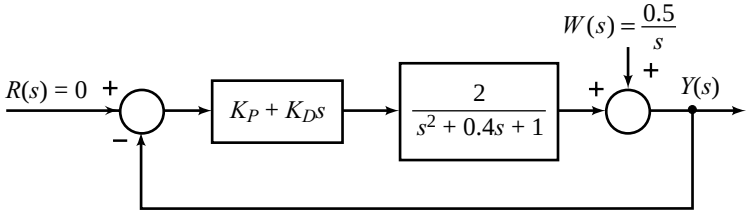

Fig. Q89

90. Consider the system of Fig. Q90. $R(s)$ and $W(s)$ are step signals
    (A) Steady-state error to $R(s)$ is zero and to $W(s)$ is non-zero
    (B) Steady-state error to $R(s)$ is non-zero and to $W(s)$ is zero
    (C) Steady-state error to both $R(s)$ and $W(s)$ is non-zero

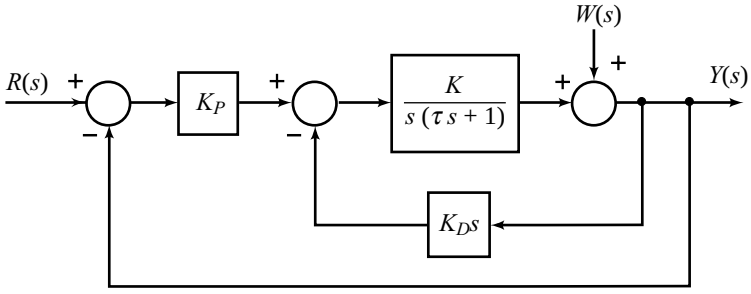

Fig. Q90

91. Consider the system of Fig. Q91. The steady-state error is less than 2% to step inputs for
    (A) any value of K_I
    (B) no values of K_I
    (C) $K_I > 50$
    (D) None of the answers is (A),(B), and (C) is correct

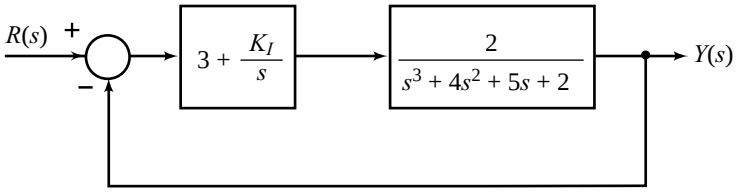

Fig. Q91

92. A unity feedback system has open-loop transfer function $G(s) = 1/s^2$. This uncompensated type-2 system possesses a satisfactory steady-state error for
    (A) step input signals
    (B) ramp input signals
    (C) both the step and ramp input signals
    (D) none of the step and ramp input signals
93. Consider the following statements:
    (i) Many systems are designed for peak overshoot in the range 5–25%.
    (ii) Desired dominant closed-loop poles are usually a complex-conjugate pair.
    (A) None of the above statements is true
    (B) Statement (i) is true but statement (ii) is false
    (C) Statement (i) is false but statement (ii) is true
    (D) Both the statements are true
94. The steady-state error due to step commands can be eliminated from proportional control systems with type-0 plants by

(i) intentionally 'misadjusting' reference input
(ii) introducing integral mode in the controller

(A) None of the above statements is true (B) Statement (i) is true but statement (ii) is false
(C) Statement (i) is false but statement (ii) is true (D) Both the statements are true

95. Consider the following statements:
(i) In a position control system, the integrating effect naturally appears in system plant.
(ii) We do not require integral control for position control systems to obtain zero steady-state error to step disturbances in load.

(A) None of the above statements is true (B) Statement (i) is true but statement (ii) is false
(C) Statement (i) is false but statement (ii) is true (D) Both the statements are true

96. A type-1 plant is changed to type-2 feedback system by the following cascade control action:
(A) PD (B) PI (C) Either PD or PI (D) Neither PD nor PI

97. A unity feedback system has open-loop poles at $s = -2 \pm j2$, $s = -1$, and $s = 0$; and a zero at $s = -3$. The angles made by the root-locus asymptotes with the real axis, and the point of intersection of the asymptotes are, respectively,
(A) (60°, – 60°, 180°) and – 3/2 (B) (60°, – 60°, 180°) and – 2/3
(C) (45°, – 45°, 180°) and – 2/3 (D) (45°, – 45°, 180°) and – 4/3

98. Which of the root locus plots shown in Fig. Q98 is the correct plot for a unity feedback system with open-loop poles at $s = -1 \pm j1$, and a zero at $s = -2$?
(A) Fig. Q98a (B) Fig. Q98b (C) Fig. Q98c (D) Fig. Q98d

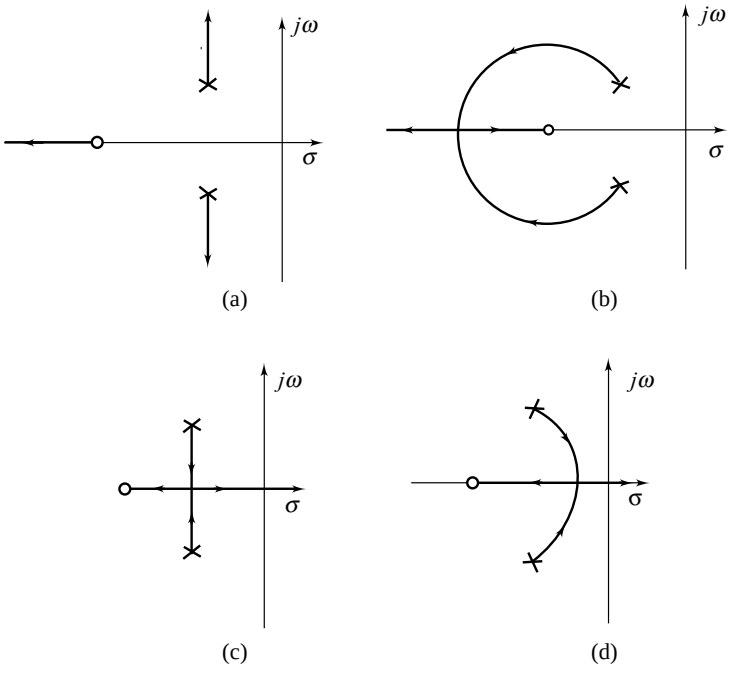

Fig. Q98

99. Which of the root locus plots shown in Fig. Q99 is the correct plot for a unity feedback system with open-loop transfer function $G(s) = K/[s^2(s + 5)]$?
(A) Fig. Q99a (B) Fig. Q99b (C) Fig. Q99c

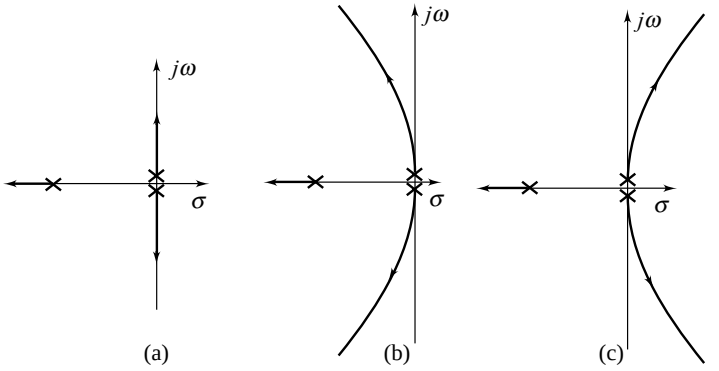

Fig. Q99

100. A unity feedback system has open-loop transfer function $G(s) = K(s+1)(s+2)/[s(s+3)(s+4)]$. For $K = 10$, the closed-loop poles are
   (A) all real and distinct
   (B) one real and two complex conjugate
   (C) all real and repeated
   (D) None of the answers in (A), (B), and (C) is correct

101. Root locus plot of a feedback system as gain K is varied, is shown in Fig. Q101. The system response to step input is non-oscillatory for
   (A) $0 < K < 0.4$
   (B) $0.4 < K < 6$
   (C) $6 < K < \infty$
   (D) None of the answers in (A), (B), and (C) is correct

102. Consider the root locus plot shown in Fig. Q101.
   (i) Adding a zero between $s = -1$ and $s = -2$ would move the root locus to the left.
   (ii) Adding a pole at $s = 0$ would move the root locus to the right.
   Which of the following is the correct answer?
   (A) None of the above statements is true
   (B) Statement (i) is true but statement (ii) is false
   (C) Statement (i) is false but statement (ii) is true
   (D) Both the statements are true

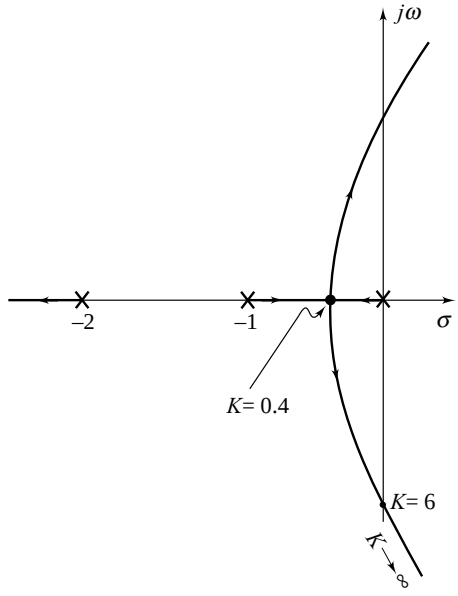

Fig. Q101

103. Consider the root locus plot of unity-feedback system with open-loop transfer function

$$G(s) = \frac{K(s+5)}{s(s+2)(s+4)(s^2+2s+2)}$$

   The meeting point of the asymptotes on the real axis occurs at
   (A) –1.2 (B) – 0.85 (C) – 1.05 (D) – .75

104. Consider the root locus plot of unity-feedback system with open-loop transfer function

$$G(s) = \frac{K(s+5)}{s(s+2)(s+4)(s^2+2s+2)}$$

The break away point of the root loci on the real axis occurs at

(A) – 3 (B) – 4.5

(C) – 5.5 (D) None of the answers is (A), (B), and (C) is correct

105. The transfer function of a lag compensator is

$$D(s) = \frac{1+\alpha\tau s}{1+\tau s}; \tau > 0$$

the value of α is given by

(A) $\alpha = 1$ (B) $\alpha > 1$

(C) $\alpha < 1$ (D) α is any constant

106. The root locus plot of the characteristic equation

$$1 + KF(s) = 0$$

is given in Fig. Q106. The value of K at $s = \pm j1$ is

(A) 4

(B) 1

(C) 10

(D) None of the answers in (A), (B), and (C) is correct

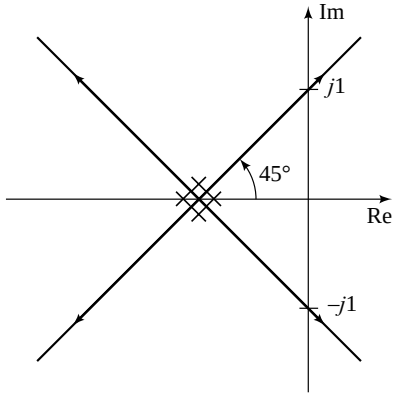

Fig. Q106

107. Consider the following statements:

(i) A lead compensator is nothing but a PD controller with a filter.

(ii) A lag compensator has the characteristics of a PI controller

(A) None of the above statements is true

(B) Statement (i) is true but statement (ii) is false

(C) Statement (i) is false but statement (ii) is true

(D) Both the statements are true

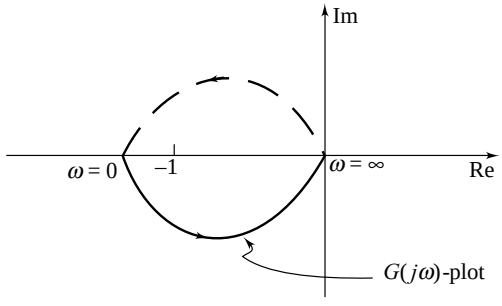

Fig. Q108

108. Figure Q108 shows the Nyquist plot of a unity feedback system having open-loop transfer function $G(s)$ with one pole in right half of s-plane. The feedback system is

(A) stable

(B) unstable

(C) marginally stable

109. Figure Q109 shows the Nyquist plot of a unity feedback system having open-loop transfer function $G(s)$ with one pole in right half of s-plane. The feedback system is

(A) stable (B) unstable

(C) marginally stable

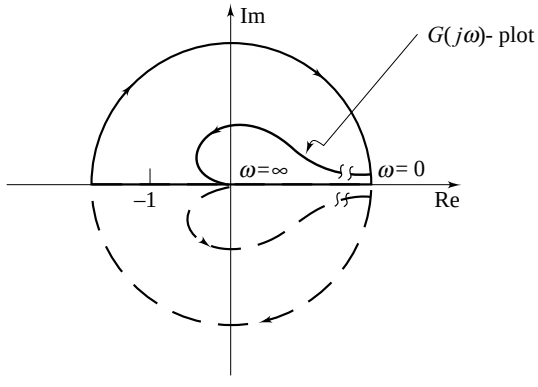

Fig. Q109

110. Polar plot of $G(j\omega) = 1/[j\omega(1 + j\omega\tau)]$

(A) crosses the negative real axis

(B) crosses the negative imaginary axis

(C) crosses the positive imaginary axis

(D) None of the answers in (A), (B), and (C) is correct

111. Which of the polar plots shown in Fig. Q111 is the correct plot for $G(j\omega) = 1/[(j\omega)^2(1 + j\omega\tau)]$?
(A) Fig. Q111a (B) Fig. Q111b (C) Fig. Q111c (D) Fig. Q111d

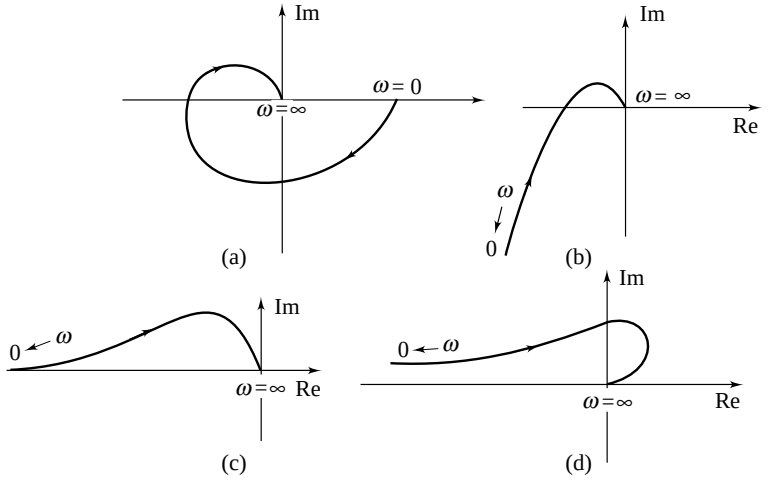

Fig. Q111

112. Which of the Bode asymptotic plots shown in Fig. Q112 is the correct plot for $G(s) = K/[s^2(s + 5)]$?
(A) Fig. Q112a (B) Fig. Q112b (C) Fig. Q112c (D) Fig. Q112d

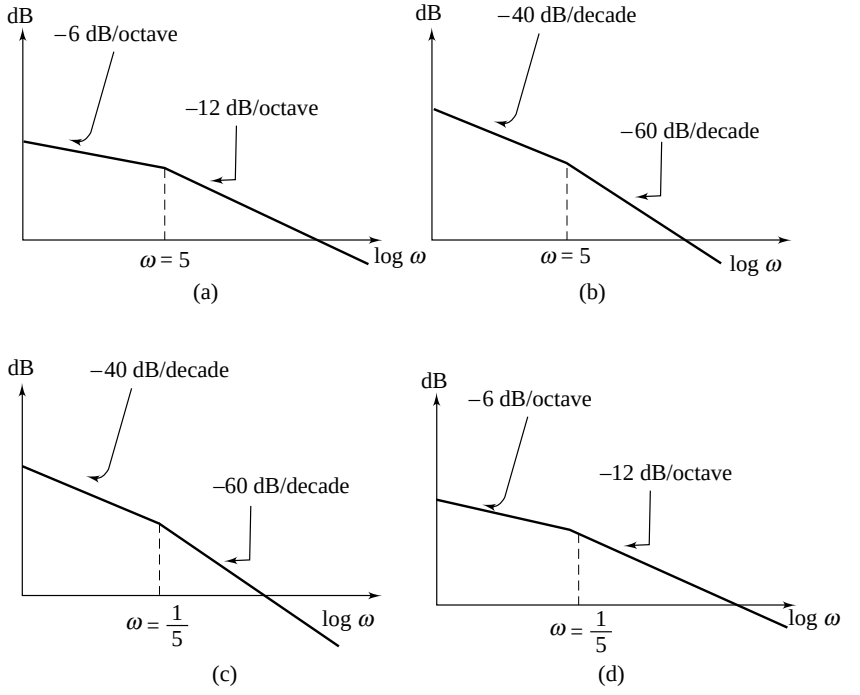

Fig. Q112

113. The Bode asymptotic plot of a transfer function is given in Fig. Q113. There
(A) are no poles at the origin (B) is one pole at the origin (C) are two poles at the origin

114. The Bode asymptotic plot of a transfer function is given in Fig. Q114. The transfer function has
(A) one pole and one zero (B) two poles and one zero (C) one pole and two zeros

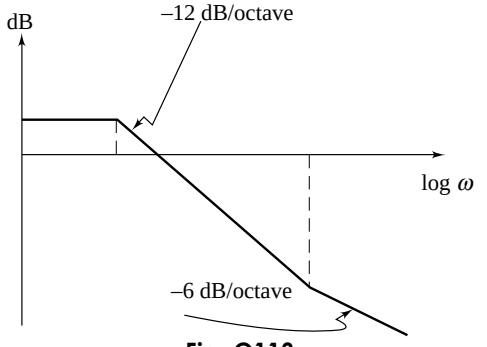

Fig. Q113

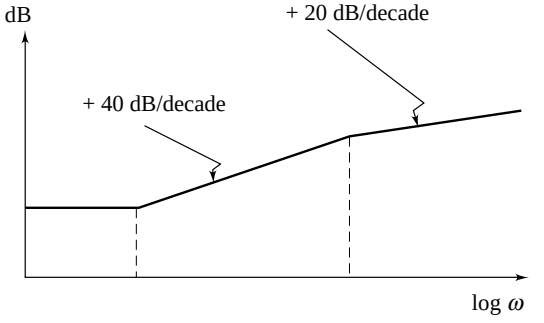

Fig. Q114

115. The minimum-phase transfer function that corresponds to the Bode asymptotic plot shown in Fig. Q115, is

(A) $\frac{1}{2s+1}$ (B) $2s + 1$

(C) $\frac{1}{\frac{1}{2}s+1}$ (D) $\frac{1}{2}s + 1$

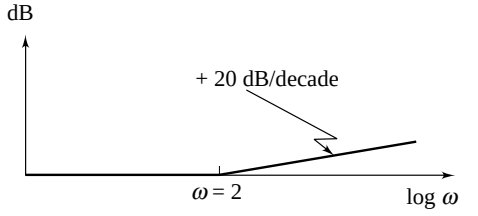

Fig. Q115

116. A unity feedback system has open-loop transfer function $G(s)$. Polar plot of $G(j\omega)$ is shown in Fig. Q116. The gain margin (GM) and the phase margin (ΦM) of the feedback system are

(A) $GM = -0.3$; $\Phi M = 112.33°$
(B) $GM = 0.3$; $\Phi M = 112.33°$
(C) $GM = 3.33$; $\Phi M = 67.67°$
(D) None of the answers in (A), (B), and (C) is correct

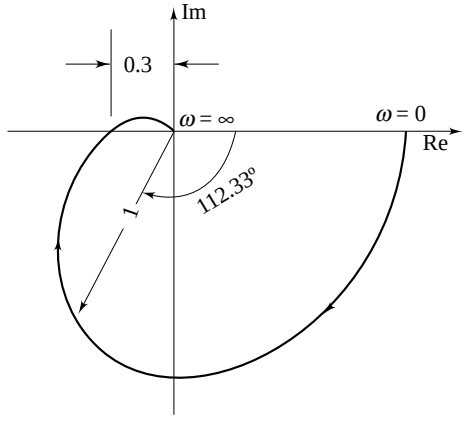

Fig. Q116

117. A unity feedback system has open-loop transfer function $G(s) = K/[s(1 + s\tau)]$. The gain margin of the feedback system is
(A) ∞
(B) 0
(C) 1
(D) None of the answers in (A), (B), and (C) is correct

118. A unity feedback system has open-loop transfer function $G(s)$. Bode plot of $G(j\omega)$ is shown in Fig. Q118. The feedback system has
(A) positive phase margin and negative gain margin
(B) positive phase margin and positive gain margin
(C) negative phase margin and negative gain margin
(D) negative phase margin and positive gain margin

119. The corner frequencies in Bode plot of the transfer function

$$G(s) = \frac{6(s^2 + 10s + 100)}{s^2(50s^2 + 15s + 1)}$$

are
(A) 1,50
(B) 100,1
(C) 10,1
(D) None of the answers in (A), (B), and (C) is correct

120. The low-frequency asymptote in Bode plot of

$$G(s) = \frac{6(s^2 + 10s + 100)}{s^2(50s^2 + 15s + 1)}$$

has a slope of
(A) 0 dB/decade (B) – 20 dB/decade
(C) – 40 dB/decade (D) None of the answers in (A), (B), and (C) is correct

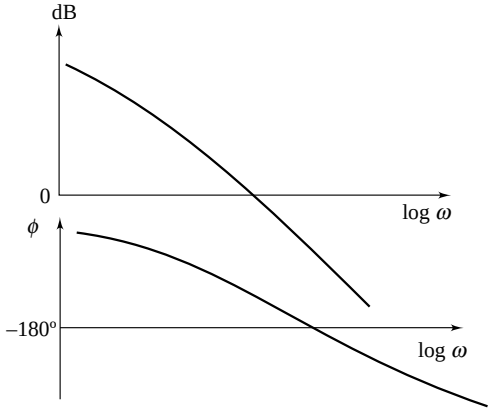

Fig. Q118

121. The high-frequency asymptote in Bode plot of

$$G(s) = \frac{6(s^2 + 10s + 100)}{s^2(50s^2 + 15s + 1)}$$

has a slope of
(A) 0 dB /decade (B) – 20 dB/decade
(C) – 40 dB/decade (D) None of the answers in (A), (B), and(C) is correct

122. If a system's gain is given as $|G(j\omega_0)| = 0$ dB, what will happen to an input signal at the frequency ω_0?
(A) It will be amplified (B) It will be attenuated
(C) There will be no output signal (D) None of the answers in (A), (B), and (C) is correct

123. An engineer applies the input $r(t) = 2\sin t$ to a chemical process and measures the output as $y(t) = 0.4\sin(t - 1.55)$. What are the gain and phase of the system?
(A) (– 14dB, – 89°) (B) (– 8dB, – 1.55°) (C) (–14 dB, – 1.55°) (D) (– 8dB, – 89°)

124. A current to pressure transducer has a gain of – 10 dB and a phase of – 60° at $\omega = 10$ rad/sec. An input signal of $r(t) = 5\cos(10t - \pi/2)$ is injected. What is the output signal?
(A) $1.58\cos(20t - 5\pi/6)$ (B) $1.58\cos(10t - \pi/6)$
(C) $1.58\cos(10t + \pi/6)$ (D) None of the answers in (A), (B), and (C) is correct

125. Bode magnitude plot of a system has – 20 dB gain at low frequencies. The system is
(A) type-0 (B) type-1
(C) type-2 (D) Nothing can be deduced about type number from the given information

126. A PI controller $K_P + K_I/s = 100 + 0.01/s$ has a high-frequency gain of 40dB. The values of K_P and K_I that reduce high-frequency gain to 20dB are (calculations based on asymptote plot in Bode coordinates)
(i) (10,0.01) (ii) (10,0.001)
(A) Both the statements are true (B) Statement (i) is true but (ii) is false
(C) Statement (i) is false but (ii) is true (D) Both the statements are false

127. The frequency response of the system $G(s) = e^{-\tau_D s}/s$ at frequency $\omega = \pi/(2\tau_D)$ gives magnitude and phase of
(A) $2\tau_D/\pi$, – 90° (B) $2\tau_D/\pi$, –180°
(C) $2\tau_D/\pi$,0° (D) None of the answers in (A), (B) and (C) is correct

128. A PD controller has transfer function $(0.1 + 0.01s)$. The frequency at which the magnitude is 20dB is (calculations based on asymptotic plot is Bode coordinates)
(A) 10 (B) 1000 (C) 1 (D) 100

129. Frequency response of a system is given in the following table.

Frequency (rad/sec)	*Gain*	*Phase (deg)*
0.1	5	0
1	1.5	– 90
10	0.25	– 180
100	0.1	– 235

Gain margin is

(A) 4 (B) 0.25 (C) 5 (D) 1.5

130. Frequency response of a system is given in the following table.

Frequency (rad/sec)	*Gain*	*Phase (deg)*
1	10	– 50
10	2	– 100
100	1	– 155
1000	0.1	– 235

Phase margin is

(A) – 25° (B) +25° (C) – 55° (D) +55°

131. Nyquist plot and Bode magnitude plot of two systems are given in Fig. Q131.

(A) Both the systems are type-0
(B) Both the systems are type-1
(C) System I is type-0 and system II is type-1
(D) System II is type-0 and system I is type-1

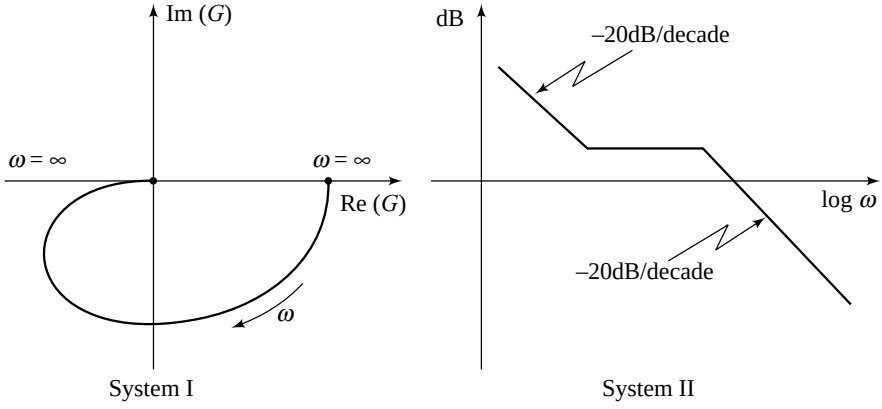

Fig. Q131

132. Consider the following statements for an underdamped second-order system:

(i) Peak overshoot in step-input response reduces as damping is increased from 0.2 to 0.6.
(ii) Resonance peak in frequency response reduces as damping is increased from 0.2 to 0.6.

Which of the following is the correct answer?

(A) None of the above statements is true (B) Statement (i) is true but statement (ii) is false
(C) Statement (i) is false but statement (ii) is true (D) Both the statements are true

133. Undamped natural frequency ω_n and resonance frequency ω_r of a unity feedback system with open-loop transfer function

$$G(s) = \frac{\omega_n^2}{s(s + 2\zeta\omega_n)}\ ;\ \zeta < 1/\sqrt{2}\ ,$$

are related as

(A) $\omega_n = \omega_r$ (B) $\omega_n > \omega_r$

(C) $\omega_n < \omega_r$ (D) None of the answers in (A), (B), and (C) is correct

134. For a unity feedback system with open-loop transfer function $G(s) = \frac{\omega_n^2}{s(s + 2\zeta\omega_n)}$, $\zeta < 0.7$;

(i) phase margin is explicitly indicative of damping ratio;

(ii) resonance peak is explicitly indicative of damping ratio.

Which of the following answers is correct?

(A) None of the above statements is true (B) Statement (i) is true but statement (ii) is false

(C) Statement (i) is false but statement (ii) is true (D) Both the statements are true

135. Open-loop transfer function of a unity feedback system is $G(s) = K/[s(s + 5)]$. The gain K that results in a phase margin of 50° is approximately

(A) 15 (B) 20 (C) 25 (D) 30

136. Consider a unity-feedback system with open-loop transfer function $G(s) = \frac{K}{s(s+1)}$. Increase in gain K will cause:

(A) the gain crossover frequency to reduce (B) the gain crossover frequency to increase

(C) the system to respond more slowly (D) None of the statement in (A), (B), and (C) is correct

137. The closed-loop dynamics of a system is of second-order. To improve the damping, we should

(A) decrease the phase margin (B) increase the phase margin

(C) decrease the gain margin (D) increase the gain margin

138. The vertical axis of the Nichols chart represents

(A) open-loop gain (B) open-loop phase (C) closed-loop gain (D) closed-loop phase

139. M-Contours on the Nichols chart represent

(A) open-loop gain (B) open-loop phase (C) closed-loop gain (D) closed-loop phase

140. Consider the following statements

(i) The resonance peak of the frequency response of $G/(1+G)$ is given by the M-contour on the Nichols chart which is tangent to the Nichols plot of G.

(ii) The resonance peak of the frequency response of $G/(1+G)$ is the peak value of the frequency response of $G/(1+G)$ on Bode magnitude plot.

(A) Both the statements are true (B) Statement (i) is true but (ii) is false

(C) Statement (i) is false but (ii) is true (D) Both the statements are false

141. The closed-loop dynamics of a system is of second-order. The resonance peak of the closed-loop frequency response is related to

(i) overshoot of time response

(ii) damping ratio

(A) Both the statements are true (B) Statement (i) is true but (ii) is false

(C) Statement (i) is false but (ii) is true (D) Both the statements are false

142. The bandwidth of $G/(1+G)$

(i) is the frequency at which the -3 dB M-contour on Nichols chart intersects the Nichols plot of G.

(ii) is the frequency at which the Bode magnitude plot of $G/(1+G)$ has a gain of -3 dB.

(A) Both the statements are true (B) Statement (i) is true but (ii) is false

(C) Statement (i) is false but (ii) is true (D) Both the statements are false

143. A unity-feedback system has open-loop transfer function

$$G(s) = \frac{\omega_n^2}{s\left(s + 2\zeta\omega_n\right)}$$

(i) The peak overshoot of step-input response of $G/(1+G)$ is indicative of damping
(ii) The resonance peak of frequency response of $G/(1+G)$ is indicative of damping.
(A) Both the statements are true (B) Statement (i) is true but (ii) is false
(C) Statement (i) is false but (ii) is true (D) Both the statements are false

144. For the system $1/(s^2 + 0.1s + 1)$, the resonance frequency ω_r and natural frequency ω_n are related as
(A) $\omega_r = \omega_n$ (B) $\omega_r > \omega_n$
(C) $\omega_r < \omega_n$ (D) None of the answers in (A), (B), and (C) is correct

145. Maximum phase-lead of the compensator $D(s) = (0.5s + 1)/(0.05s + 1)$, is
(A) 52° at 4 rad/sec (B) 52° at 10 rad/sec
(C) 55° at 12 rad/sec (D) None of the answers in (A), (B), and (C) is correct

146. In control systems
(i) reduction in bandwidth results in sluggish response;
(ii) reduction in bandwidth results in better signal/noise ratio.
Which of the following is the correct answer?
(A) None of the above statements is true
(B) Statement (i) is true but statement (ii) is false
(C) Statement (i) is false but statement (ii) is true
(D) Both the statements are true

147. Consider the following statements:
(i) Lead compensation is suitable for systems having unsatisfactory transient response. It also provides a limited improvement in steady-state response.
(ii) Lag compensation is suitable for systems with satisfactory transient response but unsatisfactory steady-state response.
Which of the following is the correct answer?
(A) None of the statements is true
(B) Statement (i) is true but statement (ii) is false
(C) Statement (i) is false but statement (ii) is true
(D) Both the statements are true

148. Consider the following statements:
(i) The natural frequency ω_n must be large for good performance; however, bandwidth considerations impose a limit on increasing ω_n.
(ii) When design considerations impose a limit on ω_b, a PD compensator with a filter is suitable.
(A) None of the above statments is true (B) Statement (i) is true but statement (ii) is false
(C) Statement (i) is false but statement (ii) is true (D) Both the statements are true

149. Consider the sampled-data system shown in Fig. Q149. Steady-state error for unit-ramp input is
(A) $\frac{1}{KT}$ (B) $\frac{T}{K}$
(C) $\frac{1}{K}$ (D) None of the answers in (A), (B), and (C) is correct

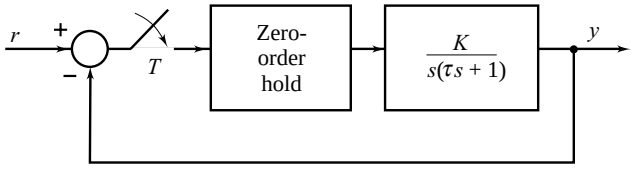

Fig. Q149

150. In a digital control system, selection of a large sampling period
(A) increases the stability margin
(B) decreases the stability margin
(C) has no effect on stability
(D) has an effect on stability that depends on plant parameters

151. In a digital control scheme, selection of a large sampling interval
(A) improves the steady-state performance
(B) deteriorates the steady-state performance
(C) has no effect on steady-state performance
(D) has an effect on steady-state performance that depends on plant parameters

152. In a sampled-data control system, delay introduced by sampling and reconstruction process is approximately equal to
(A) sampling interval
(B) twice the sampling interval
(C) half the sampling interval
(D) None of the answers in (A), (B), and (C) is correct

153. Given a state variable model

$$\dot{\mathbf{x}} = \mathbf{A}\mathbf{x} + \mathbf{b}u$$
$$y = \mathbf{c}\mathbf{x} + du$$

Under the transformation $\mathbf{x} = \mathbf{P}\,\bar{\mathbf{x}}$; $\mathbf{P}$ a constant nonsingular matrix, the model becomes

$$\dot{\bar{\mathbf{x}}} = \bar{\mathbf{A}}\,\bar{\mathbf{x}} + \bar{\mathbf{b}}\,u$$
$$y = \bar{\mathbf{c}}\,\bar{\mathbf{x}} + du$$

(A) $\bar{\mathbf{A}} = \mathbf{P}\mathbf{A}\mathbf{P}^{-1};\ \bar{\mathbf{b}} = \mathbf{P}^{-1}\mathbf{b};\ \bar{\mathbf{c}} = \mathbf{c}\mathbf{P}$
(B) $\bar{\mathbf{A}} = \mathbf{P}^{-1}\mathbf{A}\mathbf{P};\ \bar{\mathbf{b}} = \mathbf{P}^{-1}\mathbf{b};\ \bar{\mathbf{c}} = \mathbf{c}\mathbf{P}$
(C) $\bar{\mathbf{A}} = \mathbf{P}^{-1}\mathbf{A}\mathbf{P};\ \bar{\mathbf{b}} = \mathbf{P}\mathbf{b};\ \bar{\mathbf{c}} = \mathbf{c}\mathbf{P}$
(D) $\bar{\mathbf{A}} = \mathbf{P}^{-1}\mathbf{A}\mathbf{P};\ \bar{\mathbf{b}} = \mathbf{P}\mathbf{b};\ \bar{\mathbf{c}} = \mathbf{c}\mathbf{P}^{-1}$

154. A state variable formulation of a system is given by the equations

$$\begin{bmatrix}\dot{x}_1\\ \dot{x}_2\end{bmatrix} = \begin{bmatrix}-1 & 0\\ 0 & -3\end{bmatrix}\begin{bmatrix}x_1\\ x_2\end{bmatrix} + \begin{bmatrix}1\\ 1\end{bmatrix}u$$

$$y = \begin{bmatrix}1 & 0\end{bmatrix}\begin{bmatrix}x_1\\ x_2\end{bmatrix}$$

The transfer function of the system is

(A) $\dfrac{1}{(s+1)(s+3)}$
(B) $\dfrac{1}{s+1}$
(C) $\dfrac{1}{s+3}$
(D) None of the answers in (A), (B), and (C) is correct

155. A state variable formulation of a system is given by the equations

$$\begin{bmatrix}\dot{x}_1\\ \dot{x}_2\end{bmatrix} = \begin{bmatrix}-1 & 0\\ 0 & -3\end{bmatrix}\begin{bmatrix}x_1\\ x_2\end{bmatrix} + \begin{bmatrix}1\\ 1\end{bmatrix}u;\ x_1(0) = x_2(0) = 0$$

$$y = \begin{bmatrix}1 & 0\end{bmatrix}\begin{bmatrix}x_1\\ x_2\end{bmatrix}$$

The response $y(t)$ to unit-step input is

(A) $1 + e^{-t}$
(B) $\dfrac{1}{3}\,(1 - e^{-3t})$
(C) $1 - e^{-t}$
(D) None of the answers in (A), (B), and (C) is correct

156. The eigenvalues of the matrix

$$\mathbf{A} = \begin{bmatrix} 0 & 1 & 0 \\ 0 & 0 & 1 \\ 0 & -3 & -4 \end{bmatrix}$$

are

(A) 0, – 1, – 3 (B) 0, – 3, – 4

(C) 0, 0, – 4 (D) None of the answers in (A), (B), and (C) is correct

157. Given the system

$$\dot{\mathbf{x}} = \begin{bmatrix} 0 & 0 & -20 \\ 1 & 0 & -24 \\ 0 & 1 & -9 \end{bmatrix} \mathbf{x} + \begin{bmatrix} 3 \\ 1 \\ 0 \end{bmatrix} u$$

$$y = [0 \quad 0 \quad 1]\mathbf{x}$$

The characteristic equation of the system is

(A) $s^3 + 20s^2 + 24s + 9 = 0$

(B) $s^3 + 9s^2 + 24s + 20 = 0$

(C) $s^3 + 24s^2 + 9s + 20 = 0$

(D) None of the answers in (A), (B), and (C) is correct

158. A state variable model of a system is given by

$$\begin{bmatrix} \dot{x}_1 \\ \dot{x}_2 \end{bmatrix} = \begin{bmatrix} 1 & 1 \\ -2 & -1 \end{bmatrix} \begin{bmatrix} x_1 \\ x_2 \end{bmatrix} + \begin{bmatrix} 0 \\ 1 \end{bmatrix} u$$

$$y = [1 \quad 0] \begin{bmatrix} x_1 \\ x_2 \end{bmatrix}$$

The system is

(A) controllable and observable (B) controllable but unobservable

(C) observable but uncontrollable (D) uncontrollable and unobservable

159. The transfer function

$$G(s) = \mathbf{c}(s\mathbf{I} - \mathbf{A})^{-1}\mathbf{b}$$

of the system

$$\dot{\mathbf{x}} = \mathbf{A}\mathbf{x} + \mathbf{b}u$$
$$y = \mathbf{c}\mathbf{x} + du$$

has pole-zero cancellation. The system

(A) is uncontrollable and unobservable (B) is observable but uncontrollable

(C) is controllable but unobservable (D) may be any one of (A), (B), and (C)

160. The transfer function

$$G(s) = \mathbf{c}(s\mathbf{I} - \mathbf{A})^{-1}\mathbf{b}$$

of the system

$$\dot{\mathbf{x}} = \mathbf{A}\mathbf{x} + \mathbf{b}u$$
$$y = \mathbf{c}\mathbf{x} + du$$

has no pole-zero cancellation. The system

(A) is controllable and observable (B) is observable but uncontrollable

(C) is controllable but unobservable (D) may be any one of (A), (B), and (C)

161. Consider the system

$$\mathbf{A} = \begin{bmatrix} 0 & 1 & 0 \\ 0 & 0 & 1 \\ -6 & -11 & -6 \end{bmatrix}; \mathbf{b} = \begin{bmatrix} 0 \\ 0 \\ 1 \end{bmatrix}; \mathbf{c} = [4 \quad 5 \quad 1]$$

The transfer function of the system has pole-zero cancellation. The system is

(A) controllable and observable
(B) uncontrollable and unobservable
(C) controllable but unobservable
(D) observable but uncontrollable

162. Consider the system

$$\mathbf{A} = \begin{bmatrix} 0 & -2 \\ 1 & -3 \end{bmatrix}; \mathbf{b} = \begin{bmatrix} 1 \\ 1 \end{bmatrix}; \mathbf{c} = [0 \quad 1]$$

The transfer function of the system has pole-zero cancellation. The system is

(A) controllable and observable
(B) uncontrollable and unobservable
(C) controllable but unobservable
(D) observable but uncontrollable

163. In a control system design exercise for a marine engine, an engineer is using the state-space framework. The system model is given by

$$\dot{\mathbf{x}} = \begin{bmatrix} 13/6 & 4/3 \\ -4/3 & -7/6 \end{bmatrix} \mathbf{x} + \mathbf{b}u; \mathbf{b} = \begin{bmatrix} 0 \\ 0.5 \end{bmatrix}$$

The engineer decides to experiment with a different method of actuation for the system and this leads to the different input matrix

$$\mathbf{b}_1 = \begin{bmatrix} -1/6 \\ 1/3 \end{bmatrix}$$

(A) Both the systems are controllable
(B) System with input matrix **b** is controllable, and it becomes uncontrollable when **b** is changed to $\mathbf{b}_1$
(C) System with input matrix **b** is uncontrollable and it becomes controllable when **b** is changed to $\mathbf{b}_1$
(D) Both the systems are uncontrollable

164. Given the state variable model {**A**,**b**,**c**} of a single-input, single-output system. The asymptotic stability is determined from

(A) **A**,**b** and **c** matrices
(B) **A** and **b** matrices
(C) **A** and **c** matrices
(D) **A** matrix

Master Key

1. (C)	2. (C)	3. (C)	4. (D)
5. (A)	6. (B)	7. (A)	8. (B)
9. (D)	10. (A)	11. (C)	12. (D)
13. (D)	14. (A)	15. (A)	16. (D)
17. (A)	18. (D)	19. (A)	20. (C)
21. (D)	22. (A)	23. (C)	24. (B)
25. (C)	26. (A)	27. (B)	28. (B)
29. (B)	30. (C)	31. (B)	32. (A)
33. (D)	34. (C)	35. (D)	36. (B)
37. (C)	38. (C)	39. (C)	40. (B)
41. (A)	42. (C)	43. (D)	44. (C)
45. (B)	46. (A)	47. (C)	48. (B)
49. (B)	50. (D)	51. (A)	52. (A)

53. (B) 54. (B) 55. (A) 56. (C)
57. (A) 58. (C) 59. (A) 60. (C)
61. (D) 62. (D) 63. (D) 64. (B)
65. (B) 66. (A) 67. (C) 68. (D)
69. (C) 70. (D) 71. (C) 72. (D)
73. (B) 74. (C) 75. (A) 76. (A)
77. (B) 78. (B) 79. (A) 80. (B)
81. (D) 82. (A) 83. (A) 84. (C)
85. (B) 86. (B) 87. (B) 88. (A)
89. (C) 90. (B) 91. (D) 92. (D)
93. (D) 94. (D) 95. (B) 96. (B)
97. (B) 98. (B) 99. (C) 100. (A)
101. (A) 102. (D) 103. (D) 104. (D)
105. (C) 106. (A) 107. (D) 108. (A)
109. (B) 110. (D) 111. (C) 112. (B)
113. (A) 114. (C) 115. (D) 116. (C)
117. (A) 118. (B) 119. (D) 120. (C)
121. (C) 122. (D) 123. (A) 124. (D)
125. (A) 126. (A) 127. (B) 128. (B)
129. (A) 130. (B) 131. (C) 132. (D)
133. (B) 134. (D) 135. (C) 136. (B)
137. (B) 138. (A) 139. (C) 140. (A)
141. (A) 142. (A) 143. (A) 144. (C)
145. (D) 146. (D) 147. (D) 148. (D)
149. (C) 150. (B) 151. (C) 152. (C)
153. (B) 154. (B) 155. (C) 156. (A)
157. (B) 158. (A) 159. (D) 160. (A)
161. (C) 162. (D) 163. (B) 164. (D)